Department Chemie
Fakultät für Chemie und Pharmazie
Ludwig-Maximilians-Universität München

Energetic Coordination Chemistry: Ligand Design, Materials Syntheses, Characterization and Application

Habilitationsschrift

zur Erlangung der Lehrbefähigung im Fach Anorganische Chemie
an der Fakultät für Chemie und Pharmazie
der Ludwig-Maximilians-Universität München

vorgelegt von

Dr. rer. nat. Jörg Stierstorfer

München, 2023

Eidesstattliche Versicherung:

Diese kumulative Habilitationsschrift wurde eigenständig und ohne unerlaubte Hilfe erarbeitet.

Wörthsee, 15.02.2023

……
Dr. Jörg Stierstorfer

Habilitationskommission:

1. Prof. Dr. Hans-Christian Böttcher
2. Prof. Dr. Andreas Kornath
3. Prof. Dr. Christian Ochsenfeld

Dedicated to my family

Acknowledgment

The results of this habilitation thesis would never be possible without the help, support, and intense input of several kind persons.

- First, I would like to thank my boss Prof. Dr. Thomas M. Klapötke for his longtime support and the opportunity to work on my own research projects while using his research facilities and budget. He is always available for questions, ideas, and new projects but also for problems. It is very pleasant to be a co-founder and co-managing director of the EMTO GmbH.
- Second, I express my grateful thank to all Ph.D. and Master students which were involved in doing the experimental work, intense paper writing, and developing new concepts and ideas. These are Dr. Norbert Szimhardt, Dr. Maximilian Wurzenberger, Marcus Lommel (M.Sc.), Michael Gruhne (M.Sc.), Dr. Moritz Kofen, Simon Endrass (M.Sc.), Markus Rösch (M.Sc.), Jasmin Lechner (M.Sc.), Vanessa Braun (M.Sc.), Tobias Lenz (M.Sc.), Dr. Maximilian Benz, and many more research and bachelor students. Of course, there are/were many more Ph.D. students not directly involved in this research study but making life at university even more enjoyable, for example, Elena Reinhardt, Dr. Niko Fischer and Dr. Dennis Fischer, Maurus Völkl, Chantal von der Heide, Stefan Huber, Alexander Harter, Lukas Bauer and Jan-Willy Cremers.
- Many thanks to several people in the chemistry department at LMU for their support and fellowship, first of all, Mrs. Irene Scheckenbach, Prof. Dr. Konstantin Karaghiosoff, Dr. Peter Mayer, Prof. Dr. Jürgen Evers, Prof. Dr. Lena Daumann, Dr. Habil. Constantin Hoch, Dr. Magdalena Rusan and many more.
- I want to thank some collaboration partners e.g. Dr. Daniel Shem-Tov (Tel-Aviv University), Dr. Davin Piercey (Purdue University), Dr. Rainer Schirra (EMACON-RS), Mr. Joseph Köhler, Dr. Jiri Pachman, Dr. Robert Matyas and Dr. Vojtéch Pelican from Pardubice's university, Dr. Mila Krupka from OZM but also some selected companies which rely on our findings and skills on primary explosives like DetNet South Africa, Astotec, FN Herstal, Diehl Defense, Diehl Aviation and Davey Bickford Enaex.
- Also, I would like to thank my habilitation committee Prof. Dr. Hans-Christian Böttcher, Prof. Dr. Andreas Kornath, and Prof. Dr. Christian Ochsenfeld for their time, suggestions, and input to my habilitation process.
- Especially, all external and internal examiners of this thesis are gratefully acknowledged for their time and efforts. In particular, these are Prof. Dr. Fritz Kühn from the Technical University München (TUM) and Prof. Dr. Florian Kraus from the Philipps-Universität Marburg as well as all Prof. Dr. Hans-Christian Böttcher from the LMU München.
- Last but not least, it is all about family. Thanks to Karin, Romy, and Felix, my parents, and my parents-in-law.

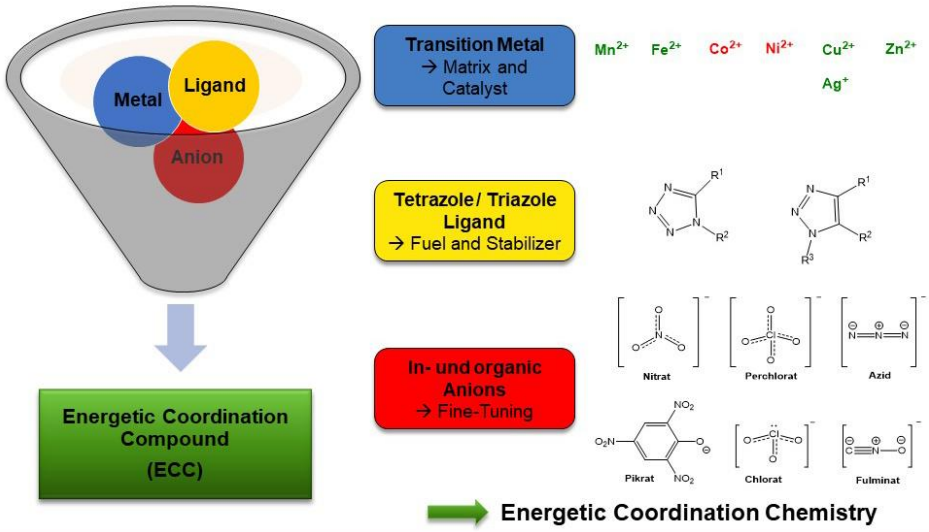
Table of Content

1. Abstract 6
2. Introduction 7
   2.1. Coordination Chemistry involving Transition Metals 7
   2.2. High-Energy Materials 9
      2.2.1. Primary Explosives 11
      2.2.2. Research on new Primary Explosives 14
      2.2.3. Requirements for new Primary Explosives 16
      2.2.4. Laser Ignition of High-Energy Materials and Energetic Coordination Compounds 20
3. Goals and Concept 24
4. Summary 27
5. Outlook 45
6. References 47
7. Appendix 51

1. Abstract

The main goal of this work is the determination and later prediction of structure-property relationships of energetic N-heterocyclic transition metal complexes.

The use of coordination chemistry is a modern approach to obtaining tunable and applicable materials for a large area of applications. Next to pharmaceuticals, catalysts, dyes, MOFs, and other new potential future requests such as molecular switches, *new energetic materials with enhanced safety and performance parameters, and lower toxicity* are still needed. The endless options to construct new energetic coordination compounds (ECCs), generally consisting of metal cations, ligands, and counter-anions, request a systematic investigation of the influence of single components on the final properties of the material. For that reason, this habilitation thesis gathers several hundreds of new compounds based on late 3d transition metals (manganese, iron, cobalt, nickel, copper, zinc) as well as silver(I), triazole or tetrazole ligands as well as oxygen or nitrogen-rich anions (e.g. ClO_4^-, ClO_3^-, N_3^-, $N(NO_2)_2^-$, etc.) are investigated.



From the chemical perspective, the new compounds were characterized (almost always) by means of single crystal X-ray diffraction, elemental analysis, and IR spectroscopy. More importantly, the physico-chemical properties were explored. Thermal analysis was performed using DTA, DSC, and/or TG measurements, impact and friction sensitivities were measured with the BAM drophammer and friction tester, and ESD values were determined by the OZM XSpark10 ESD sensitivity tester. In most cases, the behavior towards flames and hot surfaces was monitored by flame and hot plate tests. With respect to potential applications as primary explosives, hot needle tests, a classical blasting cap, and new laser initiation tests were established. Due to the systematic investigation of this novel class of energetic materials, many new strategies for the construction of future materials could be postulated. These include for example:

- 1-Substituted 5*H*-tetrazoles are much more suitable as ligands in ECCs due to their i) better accessibility, ii) lower sterically demand, and iii) lower toxicity than their 2-substituted isomers;
- Bridging ditetrazoles lead to high thermal resistance;
- The thermal stability of isostructural complexes follows the metal row: $Ni^{2+} > Co^{2+} > Fe^{2+} > Cu^{2+} > Zn^{2+} > Mn^{2+}$;
- Higher heats of formation but also high combined nitrogen-oxygen contents of ligands yield to highly sensitive ligands; ligands with high sensitivity give also sensitive ECCs, but insensitive ligands can also produce highly sensitive complexes;
- The sensitivity of ECCs is extended by the row $ClO_4^- < ClO_3^- < BrO_3^-$;
- Trinitrophenolates are suitable to increase the thermal stability of ECCs.

2. Introduction

2.1. Coordination Chemistry involving Transition Metals

There exist hundreds of textbooks that give a nice overview of the fundamentals of coordination chemistry. In the chemistry bachelor and master classes at LMU in Germany, we recommend for example Riedel &Janiak: Anorganische Chemie,[1] Alsfasser, Janiak, Klapötke & Meyer: Moderne Anorganische Chemie[2], Holleman & Wiberg, Anorganische Chemie [3] or Mortimer & Müller: Chemie[4]
Also, for English readers, there are numerous well-suited textbooks on inorganic chemistry (e.g. Housecroft & Sharpe: Inorganic Chemistry[5]). All contain basic principles of coordination chemistry as well as the d-block elements. Although the present habilitation thesis does not contain advanced concepts of coordination chemistry, it is nevertheless recommended to at least realize topics such as transition elements, coordinative bonding, crystal field theory, and different types of ligands.

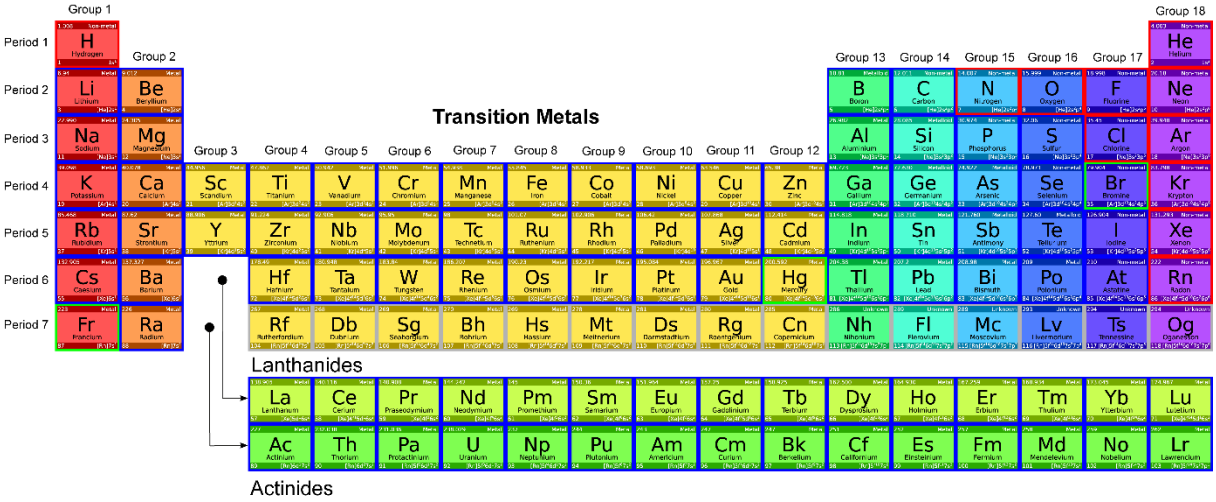


Figure 1. *Periodic table of the elements.*

Long before the first alchemistic activities, several metals were already known and also used. Elemental copper (5000 BC), gold (3400 BC), and silver (BC) are reported to be the oldest applied transition metals.[6] The fascination of these three metals is still alive in 2022, not only in their pure form for electric and electronic devices but also in jewelry and money investment. The abundance of the transition metals strongly differs. While iron is the most common (followed by titanium and manganese) in the earth's crust, rhodium, iridium, osmium, and rhenium are very rare and therefore expensive.[6] Three of the transition metals were not discovered before 1922. These are hafnium (1922), rhenium (1925) and technetium (1937). From an atomic view, the big difference between 3d elements and their precursor from periods 1 and 2, is their occupation of d-orbitals with electrons enabling not only a large variety in oxidation states, magnetic behavior, and colors but also coordination bonds (dative bonding) allowing the multifarious coordination chemistry. Modern coordination chemistry is usually split into two parts: i) Metal-organic compounds in which metal-carbon bonds are present and ii) Werner-type Compounds. Latter ones are named after Alfred Werner, a Swiss chemist, and the first real inorganic Nobel prize winner in 1913. He usually is named the founder of modern complex chemistry because of his correct structures for coordination compounds containing complex ions, in which a central transition metal is surrounded by neutral or anionic ligands. He investigated cobalt(II) ammine chloride isomers by conductivity measurements and the precipitation with silver(I) nitrate and proposed correct structures such as $[Co(NH_3)_4Cl_2]Cl$. After determining the geometry of the complexes, different theories to describe the binding situation were developed (Figure 1). In this figure, a typical Cu^{2+} complex is described because most of the compounds in this thesis are based on copper(II). The first bonding theory was the valance bond theory (VB theory) which simply put the donating electrons of the ligands into

free orbitals of the metal center. In the case of Cu^{2+} the obtained sp^3d^2 hybridization would lead to an optimized octahedral coordination sphere. However, almost all Cu^{2+} complexes follow the Jahn-Teller distortion, which leads to an elongation of the *z* coordination bonds. This effect can be explained by the second bonding theory, which is called crystal field theory (CF Theory). It is an electrostatic model in which ligands are seen as point charges and the tendency of maximum repulsion. In that theory, the degeneracies of electron orbital states are broken. In the case of an octahedral electric field, the d orbitals are split into two stages (called t_{2g} (lower energy) and e_g (higher energy)). By further energy splitting of these groups (e.g. in paramagnetic metals), distortions can be explained. In addition, high- and low-spin complexes can be explained. In simple systems like Cr^{3+}, the gap between t_{2g} and e_g directly corresponds to the absorbed wavelength and therefore to the obtained complementary color of a complex. The last theory invented is the molecular orbital (MO) theory which is able to explain higher-order effects such as non-expected results from UV/VIS and electron pair resonance (EPR) measurements. It not only involves orbitals of the center metals but also those located at the ligands. Also, metal-ligand π (back)-bonding can be described properly.

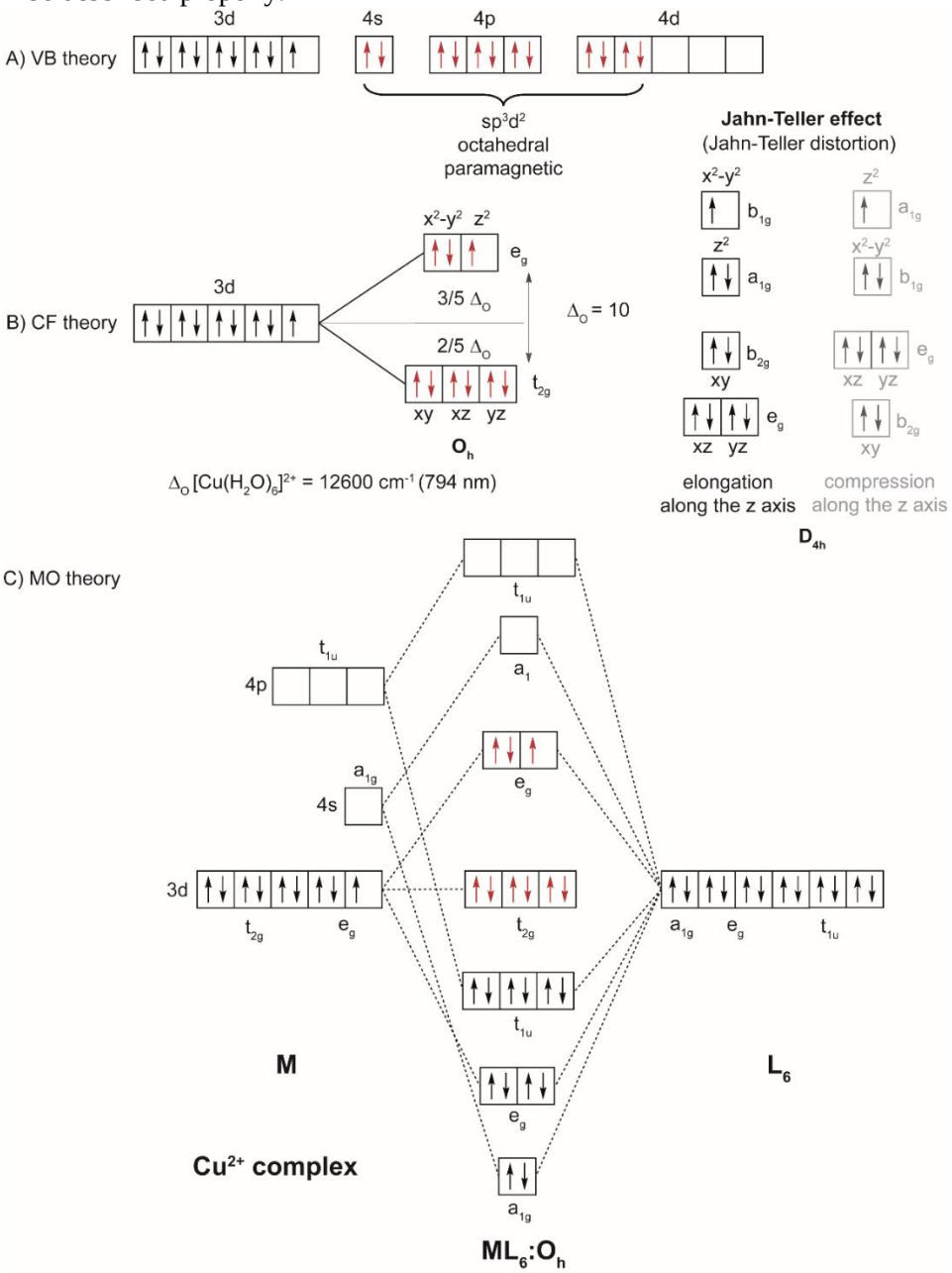


Figure 2. *Three theories that help to describe transition metal complexes and their bonding situation: A) Valance bond (VB) theory; B) Crystal-field (CF) theory and C) Molecular Orbital (MO) theory.*

2.2. High-Energy Materials

Although there exist numerous good introductions toward High-Energy Materials, not only in the collected papers in the appendix but especially in dissertations from the research group of Prof. Dr. Thomas M. Klapötke, (which can be obtained free of charge from the electronic library of the university of Munich (LMU)[7]) a short introduction is given anyway. Here some of my own impressions, experiences, and background information are collected, as well as some definitions and classifications.

The term *energetic materials* nowadays can be misleading and should be further explained. While in the case of this thesis, the term energetic materials is referred to compounds (high-energy materials) that release energy in a rapid non-reversible process, the area of *energy materials* is continuously increasing. These include many different classes of compounds that are related to batteries and supercapacitors, fuel cells, photovoltaics, thermoelectrics, hydrogen generation and storage, solar cells, piezoelectrics, thermoelectrics, photocatalysis, and reversible energy conversion. For the first class of materials oftentimes the abbreviation HEDM (for **h**igh **e**nergetic **d**ense **m**aterials) was used. However, density is also a relative parameter ranging from very low values smaller than 1 g cm^{-3} (e.g. polyethylene and polypropylene) to about 22.5 g cm^{-3} (elemental osmium and iridium) to $3 \cdot 10^{14}$ g cm^{-3} (density of an atom nucleus). As a consequence, the term ***high-energy materials*** has been established during the last years [8,9,10] and should be used in the future to comprise the area of explosives, pyrotechnics, and propellants.

An easy ***general definition of high-energy materials*** is: Metastable materials that are capable to form a large amount of non-reversible energy in the form of heat, work, pressure, sound, or light without the use of external substances (air, water, etc.).

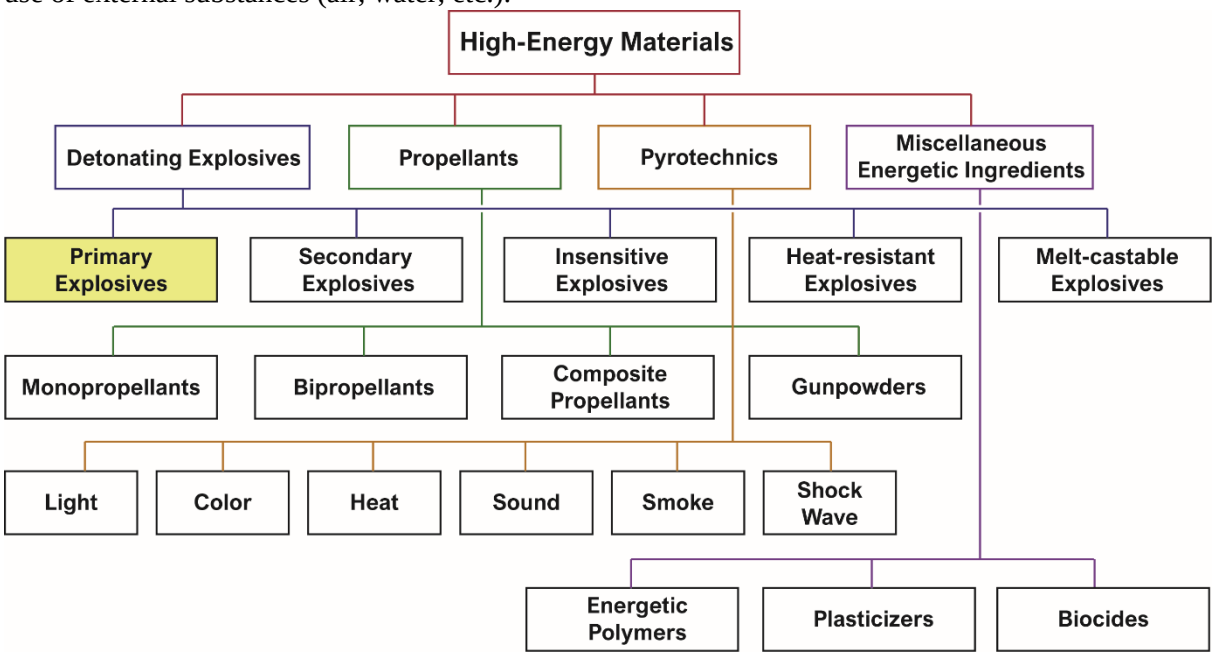


Figure 3. *Classification of High-Energy Materials according to their purpose. The class of primary explosives is marked yellow since most of the compounds in this work belong to it. The research of a safe and green primary explosive is also the main practical goal of this research thesis.*

High-energy materials can be subdivided best according to their purpose and final applications which is shown in Figure 3. In contrast to many previous classification schemes, the area of miscellaneous energetic compounds was added here.
There exist a lot of new research topics which cannot be assigned to the classical subdivisions: explosives, pyrotechnics, and propellants. For example, energetic polymers are desired for all three parts and will never be used alone. In many papers, webpages, and also in Wikipedia [11] *explosives and*

propellants are described as (i) high-explosives for compounds/mixtures which should detonate and (ii) low-explosives for compounds/mixtures which should deflagrate. This might result from the most irregular use and the definition of the word "explosion" in different languages. According to ISO 8421-1, EN 1127-1 an explosion is a sudden oxidation or decomposition reaction under the increase of pressure and/or temperature. However, the speed of reaction is insufficiently described. In the German language, there exists a relatively specific differentiation of the speed of oxidation reaction: *mm/s Verbrennung, cm/s Verpuffung, m/s Deflagration, km/s Detonation*. In the English language, several misleading phrases (civil explosive, industrial explosive, explosive agent, explosive substance, or solely explosives) are used to describe "detonating explosives". The phrase "detonating explosives" is probably the best description for high-explosives or blasting agents with a speed of reaction faster than the speed of sound (343.2 m/s and 1236 km/h). The detonation velocity V_{det}, next to the detonation pressure, is one of the most important values of a detonating explosive. The fundamental Kamlet-Jacobs Equations to calculate these values as well as the demonstration of an ideal explosive (in terms of enthalpy and oxygen balance) are shown in Figure 4.

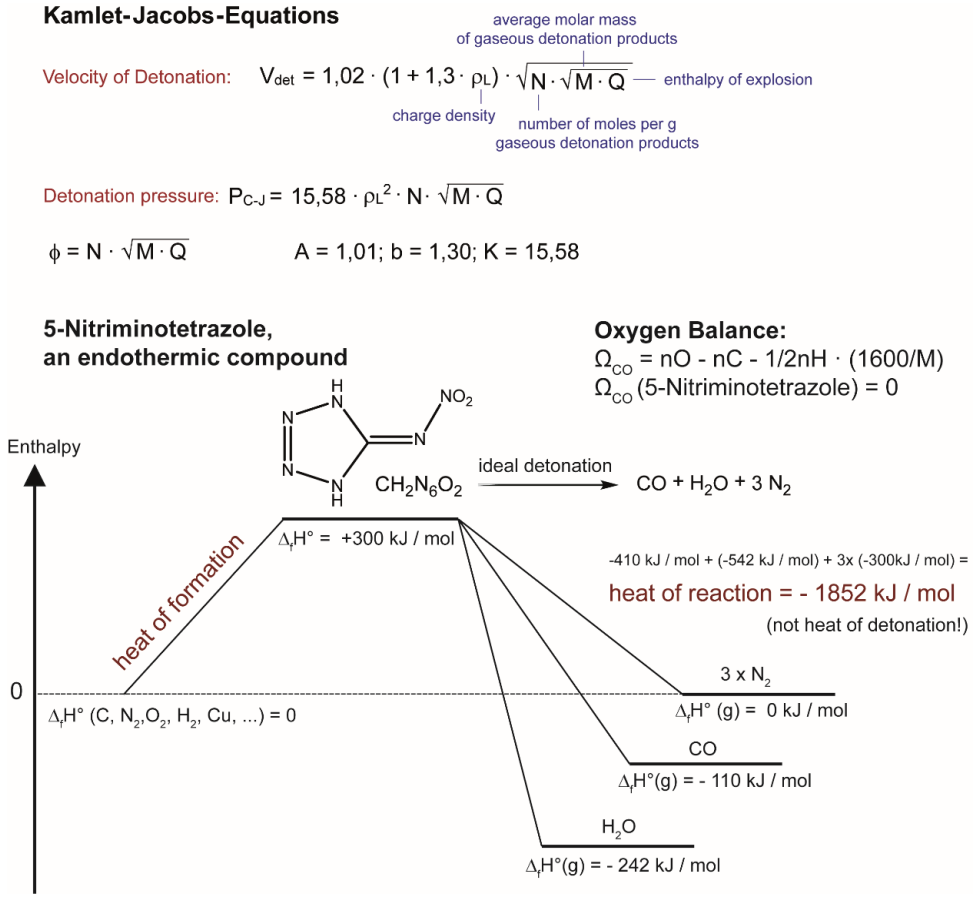


Figure 4. *Kamlet-Jacob's equations, oxygen balance and a view on the enthalpy of 5-nitrimino-tetrazole. It is important to mention that the heat of detonation is given at the temperature of detonation and therefore much lower than the ideal enthalpy of decomposition reaction which is given at room temperature.*

The group of detonating explosives can be subdivided into five sets (Figure 3). Primary explosives (which are the main focus of this work) generally are at the start of an explosive train and are mostly used in lower scales because of their sensitive nature. They must not necessarily show a high detonation velocity. In contrast, the main characteristic of a secondary explosive is its high performance (energy, velocity, and pressure of detonation). They usually consist only of C,H,N,O atoms. To obtain the highest performance they should be balanced to an exothermic N_2, H_2O, and CO formation and possess a high density. An ideal example (5-nitriminotetrazole) is shown in Figure 4. The probably most prominent

examples are PETN (pentaerythritol tetranitrate), RDX (hexogen, cyclo-trimethylene trinitramine), and HMX (octogen, cyclo-tetramethylene tetranitramine). In recent years TKX-50[12], a nitrogen-rich ionic tetrazole-oxide-based explosive, gained a lot of interest, and is commercialized by EURENCO.[13] Most secondary explosives are formulated in polymeric binder systems (e.g. C4: PETN + polyisobutylene) which are also of research interest. TATB (1,3,5-triamino-2,4,6-trinitrobenzene is the most prominent example of an insensitive explosive. They are used in applications where unwanted ignition absolutely must be avoided e.g. in nuclear weapons. Heat-resistant explosives are used for oil and gas exploration at higher temperatures. HNS (hexanitrostilbene, T_{dec}: 320°C) and PYX (picrylaminodinitropyridin, T_{dec}: 360°C) are typical examples. Last but not least melt-casting processes are an easy method to produce detonating charges. TNT (trinitrotoluene, T_{melt}: 80°C) is still the most important and cheapest representative.

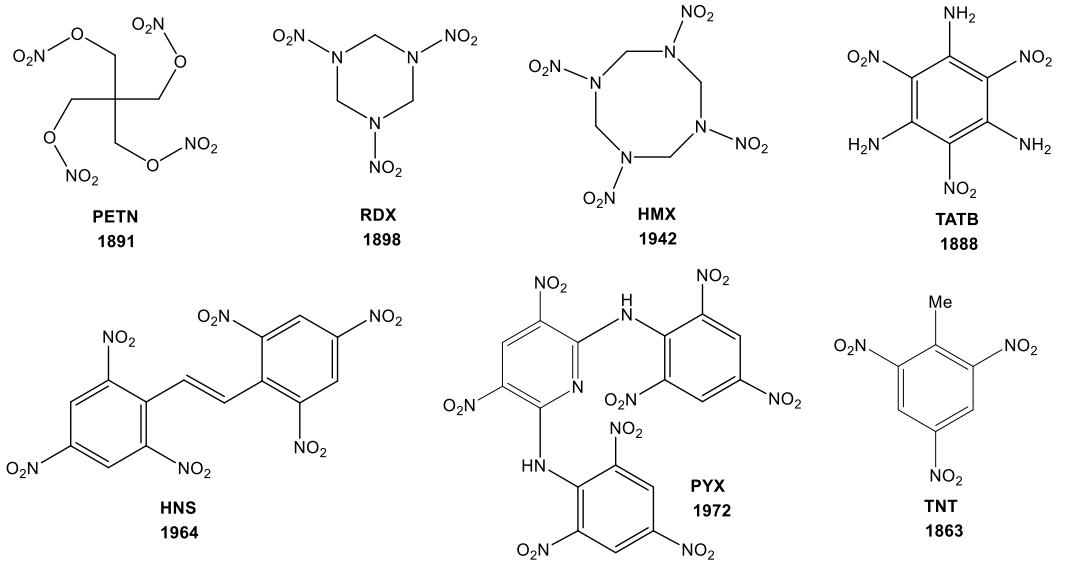


Figure 5. *Prominent and applied secondary explosives and the year of the first description.*

2.2.1. Primary Explosives

Several books and hundreds of research papers can be found on primary explosives. Nevertheless, a short introduction is given to this exciting topic here. One of the best books is *Primary Explosives* (Wiley) written by the experts Dr. Robert Matyas and Dr. Jiri Pachman from the university of Pardubice.[14] Primary explosives are substances that can be activated by a *simple initiation impulse* (SII) such as heat, flame, friction, impact, shock, or laser irradiation (Figure 6)

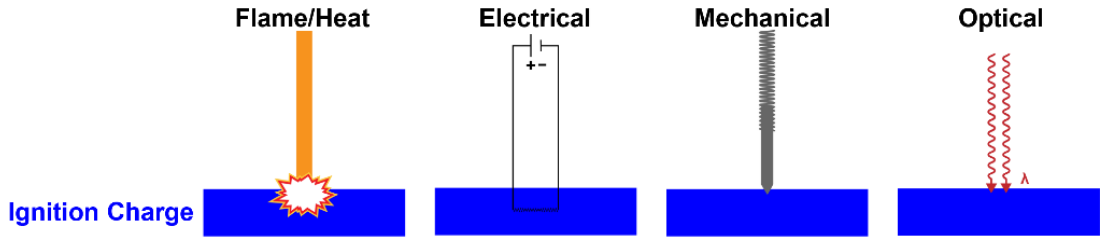


Figure 6. *Most common types of ignitions of primary explosives by a simple initiation impulse.*

Activation leads to a rapid exothermic decomposition reaction (oftentimes resulting in a shock wave). Primary explosives, therefore, are metastable compounds usually showing a low activation barrier. The class of primary explosives can be subdivided into compounds that show immediate detonation so-called *detonants*, and compounds that show a detectable deflagration-to-detonation transition (strongly dependent on confinement and also grain size). The latter group sometimes is called *mercury fulminate type primary explosive*. Oftentimes primary explosives are synonymized with *sensitive explosives*. This should be avoided in my opinion! Depending on the type of "*simple initiating impulse"* the compound

should be as less sensitive as possible to ensure safe handling. Since many primary explosives are triggered by stab initiation (combined impact and friction forces) they have very high sensitivities. The most important sensitivity values for basic research are

- Impact sensitivity (in most western countries measured by the BAM drophammer, according to UN recommendation [15], ranging from 1 J (sometimes 0.1 J) to 100 J). According to the UN recommendations on the transport of dangerous goods the following partitions are defined: < 4 J Extremely sensitive, 4–8 J Very sensitive, 8–36 J Sensitive, >36 J Insensitive)
- Friction sensitivity (usually measured by the BAM friction tester, according to a STANAG 4487 and UN recommendation [15], ranging from 5 N (sometimes 0.1 N) to 360 N. According to the UN recommendations on the transport of dangerous goods the following partitions are defined: Friction: Insensitive >360 N, Less Sensitive = 360 N, Sensitive <360 N and >80 N, Very Sensitive ≤80 N, Extremely Sensitive ≤10 N.

  In reality, most of the known primary explosives and also ECCs within the present thesis are classified as extremely sensitive (!) although it is mostly safe to work with them. Many new high-energy materials have impact sensitivities of <1 J and can nevertheless be handled also in larger scales. More important is the value of friction sensitivity. Here, compounds with values smaller than 5 N should only be handled with great care. Glass-on-glass rubbing but also metal-on-glass rubbing should always be avoided during work on explosives. Investigation of the electrostatic discharge (ESD) sensitivity is important before compounds are synthesized on larger scales. We observed (only) one accidental ignition during the work on more than 500 new sensitive materials. This happened on a very small but very sensitive sample during sensitivity measurements caused by a metal spatula. The risk of accidental ignition by ESD can be minimized by using conducting equipment, earthed shoes, and gloves.

There are two **main tasks for primary explosives**. Either they should reliably generate a
- shock wave for initiation of secondary explosives
or secure
- intense flame output for ignition of other high-energy materials such as high explosives, propellants, or pyrotechnic mixtures.

The difference is shown in Figure 7. It must be noticed that both devices are only examples. The transitions between both are fluent. Every application and all manufacturers have their own setup and compounds or compositions.

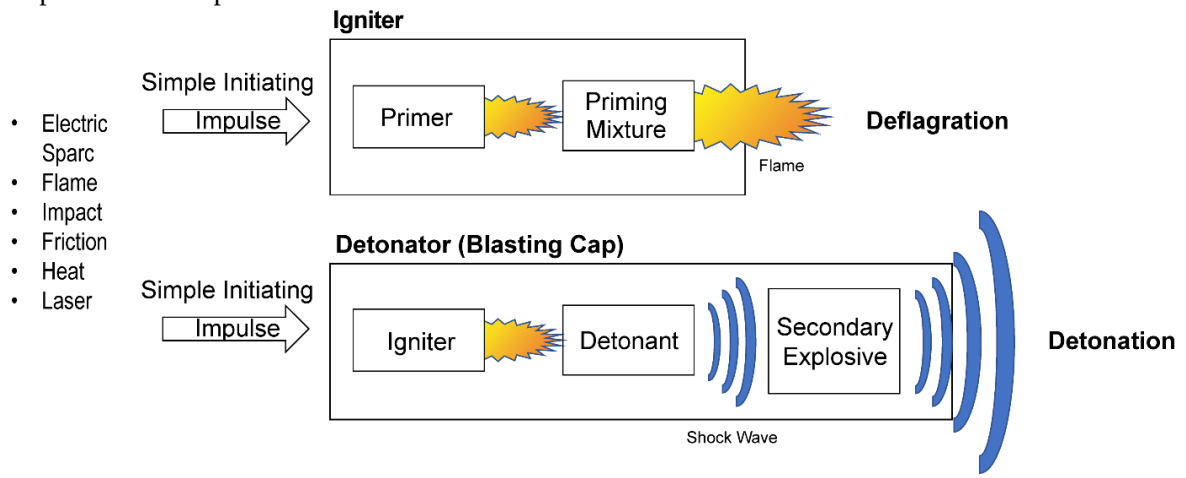


Figure 7. *Illustration of the difference between an igniter (generates flame) and detonator (generates shock wave).*

This illustration should not be confused with blasting caps which are mostly used for civil applications such as in the (surface) mining industry and the deconstruction of buildings, towers, and bridges. There

exist several types of blasting caps e.g. (i) electronic, (ii) electrical, and (iii) non-electrical ones (Figure 8). A very challenging project is the current development of wireless blasting caps.

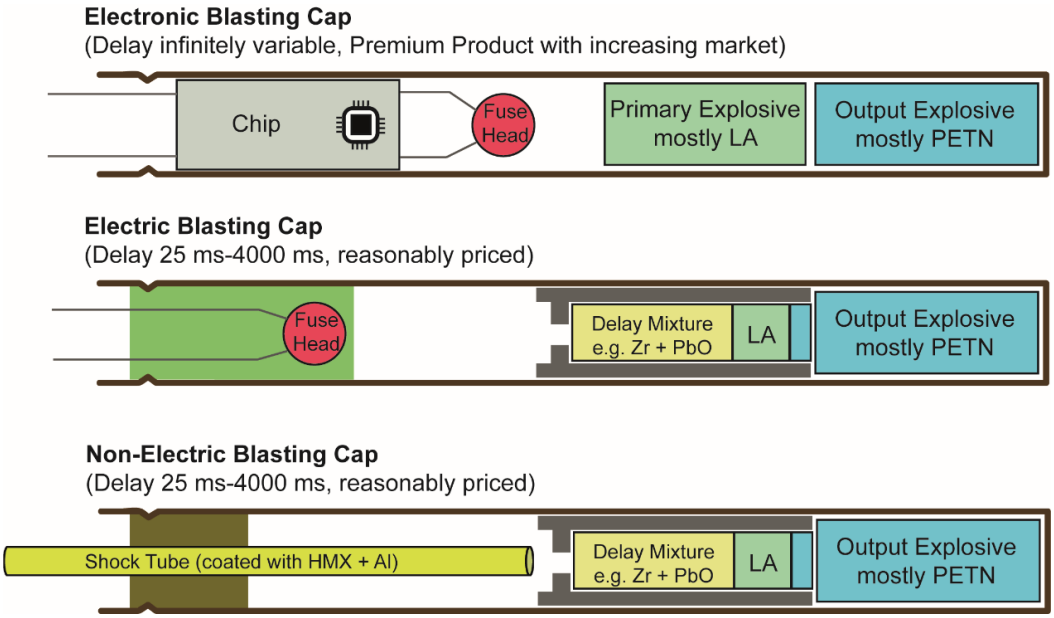


Figure 8. *Illustration of commercially available blasting caps for mostly mining and destruction applications.*

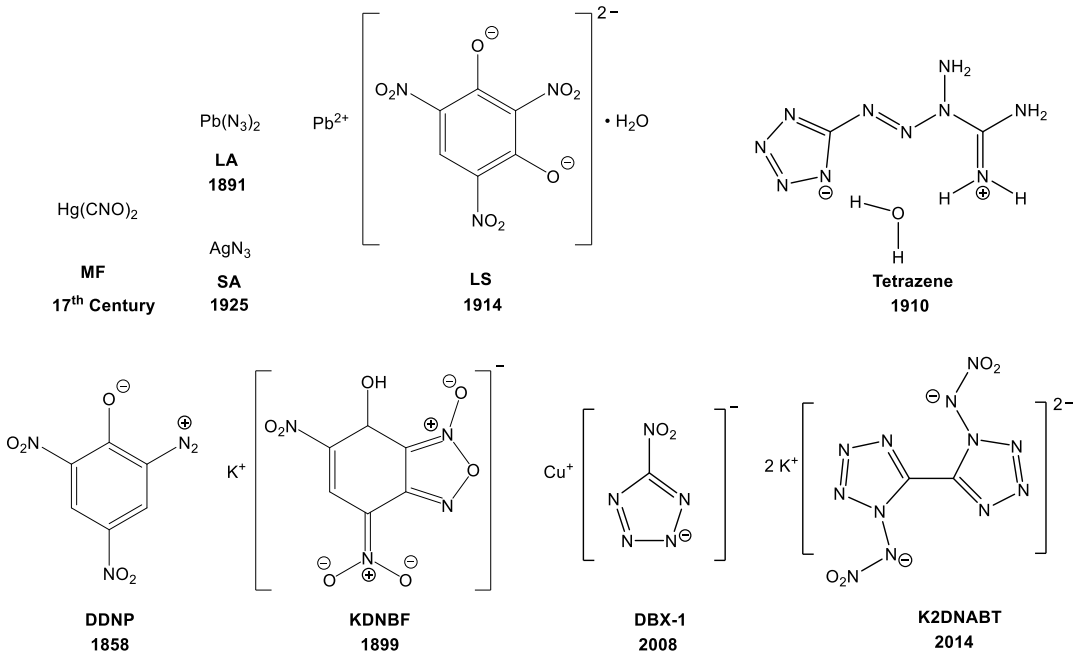


Figure 9. *Examples of primary explosives and the year of their first description as PE.*

Lead(II) azide as a typical primary explosive looks simple and can be used as a detonant by itself. However, there exist numerous different modifications of lead(II) azide (raw, pure, dextrinated, RD1133, desensitized, etc.), and all of them behave differently. The ignition additionally is influenced by the grain size, crystal habit, loading density, type of confinement, temperature, etc..

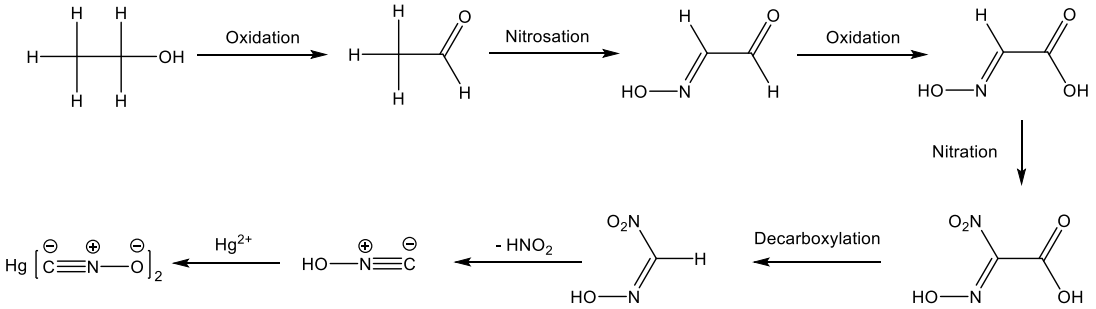
Primer is generally the declaration of the first component in an explosive train. However, a primer must not consist of only one single compound, it also can be a priming composition. Typical *primary explosives* are shown in Figure 9. Known priming mixtures used in percussion primers are gathered in Table 1.

Priming mixtures such as nano-thermites, ZPP (zirconium potassium perchlorate), LA+LS mixture) are used for detonators/blasting caps. The addition of lead styphnate to lead azide positively influences the flame sensitivity, mechanical sensitivity, and compressibility. More prominent is the use of priming mixtures in percussion caps or percussion primers. Percussion primers are used to set off the black powder (historically) or nitrocellulose gun powder in cartridges for firearms or large-caliber guns.

Table 1. *Examples of Priming Compositions used in percussion primers.*[16]

	Primary Explosive	**Secondary Explosive**	**Fuel**	**Oxidizer**	**Sensitizer**
	Initiator	*Booster & Gas Generator*	*Pyrotechnic System*	*Pyrotechnic System*	*Friction Agent*
Dreyse Mix (1828)			Sb_2S_3 (52%)	$KClO_3$ (48%)	
Forsyth Mix (1831)	MF		Sb_2S_3	$KClO_3$	Glass powder
SINOXID (1928)	LS, Tetrazene		Sb_2S_3	$Ba(NO_3)_2$, PbO_2	$CaSi_2$, Glass
FA-956 (1950s)	LS (37%), Tetrazene (4%)	PETN (5%)	Al (7%), Sb_2S_3 (15%)	$Ba(NO_3)_2$ (15%)	
S8 (.50 mix)	LS (38.1%), Tetrazene (2.9%)		Al (4.7%), Sb_2S_3 (4.7%)	$Ba(NO_3)_2$ (40%), PbO_2(4.7%),	$CaSi_2$(4.7%)
SINTOX (1986)	DDNP, Tetrazene		Ti	ZnO_2	
EMTO Research Mix (2020)	$[Cu_2(N_3)_4(dtb)]$, Tetrazene		Al, CuS	$BiONO_3$, CuO	$CaSi_2$

Interestingly the first really widely applied primary explosive, which is mercury fulminate (MF), is formed in a very complex mechanism. The reaction of ethanol, nitric acid, and mercury was studied by Wöhler and the following mechanism was proposed (Scheme 1). *For some papers in this work (e.g. Appendix 19), silver(I) fulminate was prepared. Interestingly, in the beginning, we had strong problems with the synthesis. First, we used silver nitrate for the synthesis in combination with pure ethanol and 65% HNO_3. However, we mostly obtained a colorless powder which was not possible to filtrate. Slight contact with rough surfaces or edges (e.g. during filtration) led to a partial or full detonation of the material. In the end, we applied elemental silver and technical reagents for the synthesis and successful isolation of SF.*



Scheme 1. *Formation of mercury fulminate according to Wöhler*[17] *in the reaction of mercury with ethanol and nitric acid.*

2.2.2. Research on new Primary Explosives

The most important rule in the development of new primary explosives is to start at a very small scale (approximately 50–100 mg). Even 250 mg of a primary explosive, detonated accidentally, can cause serious injuries e.g., blast trauma or when confined, penetration of fragments into your body or eyes. Next to the minimum scale one has to protect yourself. Suitable safety measures are Kevlar gloves and wrist protectors, ear plugs, face visors, earthed shoes, and putting blast shields in front of the reaction,

filtration, or drying setup. The personal distance to the explosive should always be maximized and constant work in the fume hoods under mostly closed windows is desired.
After the first isolation of a potential primary explosive, a few milligrams should always be ignited carefully on a spatula. At best, that should be done twice with a) direct contact with a flame and b) slow heating from below. This first experiment gives a lot of information on the compound isolated e.g., sensitivity, performance, carbon & metal content, etc.). Afterwards the sensitivities towards friction and impact should be checked roughly. A precise measurement of these parameters does not make sense at this stage of characterization, since the purity must be checked first. For reputable scientific research on primary explosives at the best, the following devices are needed.

A) IR spectrometer, to detect specific groups (such as azides, cyanides, acetylides, etc.) and to quickly (re)check (repeated) reaction products.

B) Single crystal X-ray diffractometer, to determine the absolute molecular and crystal structure (including the density) as well as to visualize potential polymorphs.

C) Elemental analysis, to check the bulk purity of a compound including residual inorganic salts and solvents which are sometimes not detectable by NMR spectroscopy for example.

D) Robust thermal analyzer, to determine melting and decomposition temperatures as well as loss of solvents, ligands, and phase transition. It is recommended to start with less than 1 mg (!), otherwise, normal devices built for organic and inorganic chemistry are destroyed very easily. Heating rates of 5 degrees per minute or smaller are desired. A combination of thermo-gravimetry and DSC would be the best option, however, is much more expensive when damaged.

E) BAM drophammer, to determine the sensitivity toward impact. The measurement of a confined sample (in a small steel roller between two stamps) with a specific volume on a BAM drophammer is the most accepted method worldwide. In order to define a lower safety limit, the "1 out of 6 method" is applied, in which the lowest energy is published, at which an audible decomposition takes place during six measurements. At the next lower energy level, six negative experiments were recognized.

E) BAM friction tester, to determine the friction sensitivity. This value is even more important than the impact sensitivity because it is a more realistic scenario. For primary explosives definitely, the setup with lower weights must be used in order to get friction forces between 0.1 and 20 N). Here a defined volume of the sample is placed on a rough porcelain plate and pin.

F) ESD tester, to measure the sensitivity toward electrostatic discharge. Some primary explosives such as LS, SF, ZPP, KDNBF, and K_2DNABT are extremely sensitive toward electrostatic discharge (<1 mJ).

Here it is important to control and note the grain size of the powder/crystals since finer samples are getting much more sensitive in this experiment.

G) Detonation setup, to determine the applicability and performance. Last but not least the primary explosive must somehow be tested for its desired use. In the case of potential detonants for blasting caps. copper tubes filled with PETN fixed on some kind of stable witness plate can be used. A specific amount of primary (5 mg–200 mg) is placed on the secondary and initiated by a Typ A electrical igniter igniter. A hole in the witness plate after the experiment can demonstrate its suitability as a primary explosive for this type of application.

Additionally, there are some other analytic machines, which are very convenient for research on (metal-based) primary explosives:

H) Powder diffractometer, in order to check purities and different polymorph formation.

I) ICP-MS, to determine the metal content of the new compounds.

J) Laser setup, to check the compounds' ignitibility under laser irradiation.

K) NMR spectroscopy, for the characterization of ligands.

L) Ball drop tester, as combined friction and impact sensitivity tester.

M) Microscopes (visible and electron), to check the crystal morphologies.

N) HPLC-MS, to detect intermediates and products in the ligands' synthesis.

In order to get a better feeling for new compounds it is also desirable to carry out the fast and easy **O) Hot-plate test** and **Q) Hot-needle test**. In the first one, the material is heated on a copper plate over a Bunsen burner without any flame contact. Most of the metal-containing primary explosives show a strong and loud fulmination. Hot needle tests simulate the initiation of a PE under slight confinement which is done with cellular tape on some sheets of paper with a red-glowing needle. Detonants show also immediate fulmination.

Last but not least, any kind of toxicity test or simulation is needed to demonstrate better environmental compatibility than currently used lead-containing primary explosives. For that, we have used the **R) Aqueous luminescent bacteria inhibition test** in combination with "vibrio fischeri" bacteria.

Generally, there are very few research groups located at universities worldwide, which work on new primary explosives. This may be a consequence of the high sensitivities of the compounds. However, during the research on all of the new compounds within this habilitation, we had "zero" serious incidents and no injuries. Due to the safety precautions and the growing experience, it is possible to predict the compounds' stability and sensitivity. Smaller incidents arose during the handling of pure copper(II) azide and silver(I) fulminate as well as the complex $[Cu(1\text{-}AT)_6](ClO_3)_2$). In Germany, next to our group, only the company DYNITEC in Troisdorf and DIEHL Defence in Röthenbach is studying new primary explosives. Worldwide there are some active groups in the United States (Purdue University,[18] Los Alamos National Laboratories,[19] ARDEC,[20] Sandia National Laboratories,[21] and Pacific Scientific[22]), at the French-German institute ISL[23] and in China. In the latter country, there is a strongly increasing number of smaller research groups working on primary explosives especially at the Beijing Institute of Technology and at Nanjing University of Science and Technology.[24]

2.2.3. Requirements for new Primary Explosives

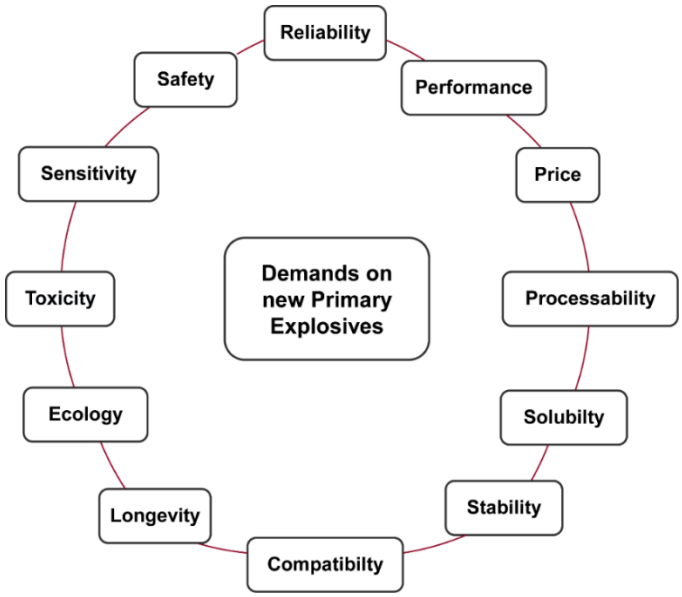


Figure 10. *Industrial requirements for a new primary explosive.*

There are numerous requirements for new Primary Explosives. The task to develop a new candidate for industry processes is equally challenging to register a new pharmaceutical. Let us have a closer look at Figure 10, start on the top and go clockwise.

A) Reliability

This probably is one of the most important aspects. Primary explosives are used as primers in explosive trains. So, the whole train is dependent on a responsible ignition or initiation. A misfire always leads to unwanted complications which could lead to severe hazards and complex disarming. Common examples of failed initiation are aircraft bombs from the 2nd world

war. If not ignited, accidentally years after the shooting, sometimes thousands of people must be evacuated, and streets to be closed to disarm or blast these devices safely.

B) Performance

The performance of secondary explosives is characterized by parameters like detonation energy, pressure, and velocity. In contrast, primary explosives are high performing when they react fast on the simple initiating impulse (detonants: fast initiation to detonation; mercury fulminate type: fast initiation to deflagration to detonation, lead styphnate type: fast initiation to flame output). Secondly, the limited minimum amount to generate the desired output is of great importance. Devices can be built smaller, unnecessary amounts of compounds can be avoided, as well as better reliability can be obtained when using better-performing primary explosives. It is not fully understood whether a higher detonation velocity of primary explosives is also beneficial, however, it seems that booster charges (mostly PETN-based) can be minimized or avoided.

It is very challenging to experimentally measure detonation parameters such as velocity, pressure, temperature, and energy. The detonation velocity usually can be determined by measuring the shock wave velocity inside a detonating charge by the use of optical fibers in a very precise distance and a corresponding detection instrument e.g. OZM Detonation Velocity Tester VOD815.[25] The shock wave can also be monitored by electrical methods using an oscilloscope since the shock front inside a charge generates short conductivity of the sample because of the partly charged and highly mobile "plasma" products. However, charges of primary explosives are usually smaller and shorter than those of secondary explosives and, therefore, it is even harder to perform those measurements. Because of the limited data on primary explosives, the current computer codes such as EXPLO and Cheetah are rather imprecise in the prediction of metal-based primary explosives. In addition, the heat of formation is needed as an input parameter, which is really hard to determine. In bomb calorimetric measurements primary explosives tend to detonate or explode, rather than combust in ideal equations. In the present work, we tried to follow a Russian method [26] which was fitted to metal perchlorate complexes such as BNCP (bis-5-nitrotetrazolato cobalt(III) perchlorate). The detonation velocities were calculated according to the increment method, adapted for ECCs by Prof. Mikhail Ilyushin. Similar to pyrotechnical mixtures, the respective ECC is divided into an explosive part (anion, ligand) and an inactive ultra-dispersed metal additive (copper). The active part was further divided into chemical bonds and structural fragments. Corresponding increment values can be found in the literature,[27] which unfortunately is only available in the Russian language. Some of the values are dependent on the hydrogen and oxygen content of the coordination compound. The summarized values for the single fragments (anions and ligands) are listed in the supplementary information of the corresponding paper (e.g. **Appendix 27**). A calculator for the calculation of ECCs and increments was integrated into the EMTO webpage.[28] For the copper(II) azides complexes the detonation velocities were calculated between 7800 and 8300 m s^{-1}.

C) Price

Unfortunately, the currently used poisonous compounds such as lead(II) azide and lead styphnate can be produced very cheaply. The production costs in Germany of 1 kg of lead azide and lead styphnate are about 1500–2000 €[29]. In comparison to the remaining explosive train and the construction, materials and electronic cost of the remaining devices are much higher, a cheap and easy production is strongly desired especially for mining blasting caps where millions are produced a year.

D) Facile synthesis

The synthesis of primary explosives should not only be safe but also straightforward. Most suitable is a one-step process. At least there should be no sensitive intermediates that must be isolated. So, it is desired that the explosophoric group (e.g. azides, nitrates etc.) is introduced in

the final step. Currently used lead azide is prepared very simple. Batches up to 5 kg are synthesized in one reactor within a couple of hours. In industry lead(II) nitrate or acetate is dissolved in water. The pH value is strictly controlled. For non-military products, oftentimes, dextrin is added. This avoids the formation of needle-like sensitive crystals and forms a round-shaped product. To that solution, a second solution of sodium azide in water is dropped, while the reactor is stirred continuously. The precipitation of lead azide occurs instantly. The crystal shape of the LA of every batch is controlled by optical microscopy. If there are any needles observed, the whole charge is destroyed. Destruction of LA can be carried out by nitrous acid

$$2\ HNO_2 + 2\ N_3^- \rightarrow 3\ N_2 + 2\ NO + 2\ OH^- \quad (\textbf{eq.1})$$

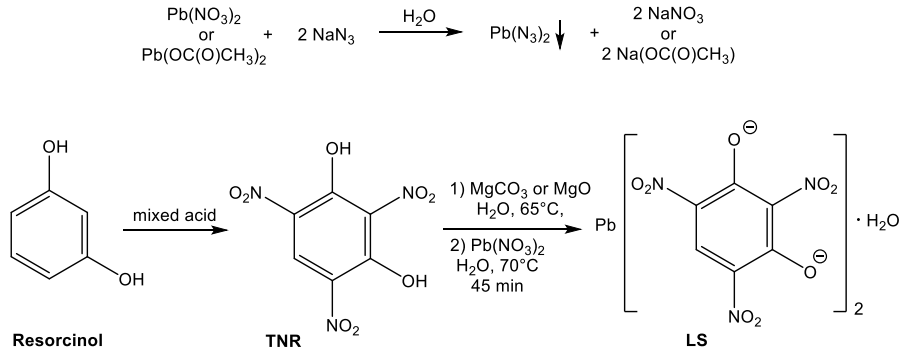
or hypochlorous acid

$$HOCl + 2\ N_3^- \rightarrow 3\ N_2 + Cl^- + OH^- \quad (\textbf{eq.2}).$$

The LA formed is analyzed for its precise composition. The azide content is titrated with ammonium cerium(IV) nitrate solution and the nitrogen gas released is determined volumetrically (equation 3).

$$Pb(N_3)_2(s) + 2(NH_4)_2Ce^{IV}(NO_3)_6 \rightarrow 2Ce^{III}(NO_3)_3 + Pb(NO_3)_2 + 4NH_4NO_3 + 3N_2\,(g) \quad (\textbf{eq.3})$$

The lead content can be determined by titration with EDTA solution or atom-absorption-spectroscopy. If needed lead azide is dissolved by adding ammonium acetate. While military-grade LA e.g. RD1333 contains >98% LA (≈30-50 µm), dextrinated LA for blasting caps contains up to 10% of dextrin.



Scheme 2 *Synthesis of lead azide (LA) and lead(II) styphnate (LS)*

Also lead(II) styphnate monohydrate is formed in a simple manner. In the first step, resorcinol is nitrated to form styphnic acid (trinitro-resorcinate, TNR). Then styphnic acid is deprotonated with basic magnesia to form a well soluble magnesium salt. To that, lead(II) nitrate solution is added und precipitation of lead styphnate as its monohydrate.

E) Processability

The safe synthesis of primary explosives and their steady implementation into applications are extremely important and challenging tasks. Because nearly all primary explosives are loaded volumetrically into their final application their "flowability" is a critical parameter. Flowability means that the PE does not stick to surfaces and slides completely and fast during filling operations. The flowability mostly is dependent on the particle shape. While small plates or needles hardly can be dumped, round balls (<10 µm) can be (mostly) loaded easily. In industry, the balls are not single-crystalline, but consist of many micro-crystalline particles forming a conglomerate. This is supported by the addition of crystallization and phlegmatization agents such as dextrin, carboxy methyl cellulose, SPAN60 (sorbitan monostearate), etc..

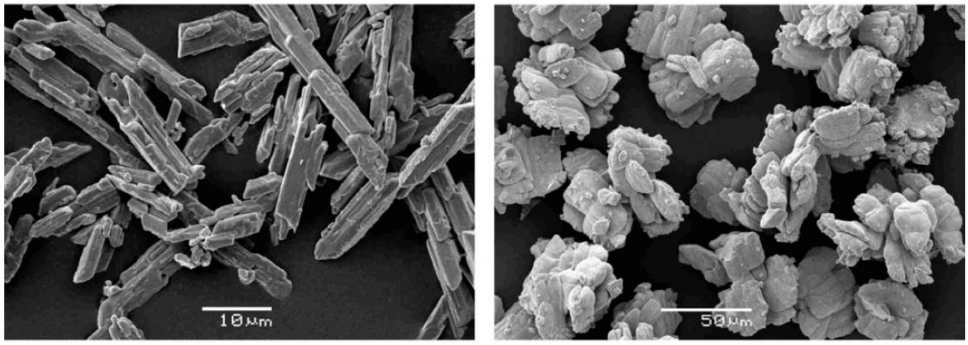


Figure 11 *Left: crystalline lead azide. Right: dextrinated lead azide. Picture taken from reference*[30].

F) Solubility

Primary explosives should be very low soluble in water. This may avoid groundwater pollution on the one hand side. On the other side, water as a non-toxic, non-flammable and cheap media is used to phlegmatize sensitive compounds after manufacturing and during transport. For example, wetted lead azide (10% water) does not show any friction or impact sensitivities. Many primary explosives which belong to the explosives group 1.1S are not allowed to be transported in a dry state. Exceptions can be e.g. transport in small scales in special containers.

G) Stability

Although energetic materials are metastable compounds, their activation energy must be high enough to show long-term stability also at slightly higher temperatures. NATO-related products are tested in a temperature range of −54 to +72 °C. This can be performed by isothermal long-term DSC/DTA or microcalorimetry measurements for example. There also exist numerous models to predict the stability of materials by kinetic models such as Ozawa and Kissinger. These methods are based on heat-rate-depending thermal analysis.

H) Compatibility

Since primary explosives are in contact with other materials such as shells or secondary explosives the compatibility must be investigated. Shells are usually made from copper, brass, stainless steel, or aluminum. Compatibilities can be investigated in detail by a vacuum stability test or microcalorimetry. The simplest method is the thermal analysis e.g. DTA, DSC, or TG of a 1:1 mixture in order to check variations of the critical temperatures.

I) Longevity

Manufacturers of ammunition only guarantee 10 years lifetime. However, most gunpowder and explosives operate reliably also decades later. Metastable materials tend to show certain halftime due to decomposition processes. These can be simulated by molecular dynamic calculations but also followed experimentally e.g. in TG measurements coupled with gas analysis. We use the NETSCH Kinetics Neo software [31] to predict long-term stabilities.

J) Ecology

The effect of new materials and their decomposition products should be harmless to all types of creatures and organisms. Also the production should follow modern sustainability requirements, such as a good atom economy, low energy demands, green solvents, high yields, and non-toxic starting materials, reagents, or byproducts.

K) Toxicity

Since Paracelsus we all should know, everything can be toxic. Nowadays, the precise toxicity and hazards of chemicals to human creatures are more and more explored. REACH is one

approach in the European Union to accommodate the increasing number of new molecules of chemical research. Compounds with a certain level of mutagenicity are nominated as compounds with high concern in the REACH system. Depending on their "system relevance" and support by lobbyists they are finally placed on the REACH list of compounds that should be finally banned. The list of CMR compounds is constantly growing. Cancerogenic, mutagenic, and repro-toxic compounds are probably the most worrying since their toxicity takes effect later than the intake or exposure. As a first step towards the investigation of the toxicity of new compounds, we are performing the luminescent bacteria inhibition test which shows the effect of a soluble compound on the aquatic organism vibrio fischerii. In the second step, promising compounds are sent to biochemistry laboratories for AMES tests with and without metabolic activation. We recommend the company BIENTA (Enamine Biology Services) in Kiew.[32] The AMES test is a bacterial reverse mutation test using amino acid requiring strains of Salmonella typhimurium and Escherichia coli to detect chemical substances that can produce genetic damage and lead to gene mutations. Point mutations are introduced in the histidine (S.typhimurium) or the tryptophan (E.coli) operon, making the tester strains incapable of producing these amino acids. The test detects mutagens, which revert these mutations restoring the functional capability to synthesize histidine or tryptophan. As the result, the revertant bacteria acquire the ability to grow in the absence of the amino acid required by the parent test strain.

L) Sensitivity

There exists a general rule for energetic materials: These materials should be as insensitive as possible. Of course, there are some limitations for primary explosives with respect to their initiation mechanism. Initiation by impact or friction (while also the first one mostly generates friction within the material) needs a specific sensitivity value to ensure reliable activation. It is recommended to look more at the friction values of energetic materials. Impact energies are usually not generated during synthesis, manipulation, or fabrication. Also, the test methods of the impact sensitivities strongly differ in many countries in the world which makes comparison hard and difficult. There is also a significant influence of the consumables which differ in their hardness, stiffness, and roughness. Not only the method can be different, but also the final value determined is given at different positions on the sensitivity curve. In the US mostly the H_{50} is given, where 50% of the experiments show a positive result. Usually, sensitivity values in Germany are given according to the BAM guidelines as their 1 out of 6 value which can be seen as $H_{>16.6}$ value. Although primary explosives are on the lower limit of the sensitivity scale there must be a measurable no-fire level. That means that compounds that show a friction sensitivity lower than 0.1 N are too sensitive for practical use. *Exceptions prove the rule!*

M) Safety

Accidents must be avoided in any case! Accidents can occur during synthesis, filtration, purification, transport, storing, loading, utilization, elaboration, and destruction. As mentioned earlier, synthesis should be performed under automatic-controlled conditions. If not possible, amounts should be kept as small as possible, distance to the materials should be maximized and self-protection should be worn.

2.2.4. Laser Ignition of High-Energy Materials and Energetic Coordination Compounds

Parts of the following paragraph were published as a Wiley book chapter by Stierstorfer, Shem-Tov and Wurzenberger.[33]

As just pointed out, safety and reliability are one of the most important aspects in the development of new primary explosives. One approach is the use of laser diodes as external stimuli to ignite/initiate

high-energy materials. Since laser ignitable compounds must not necessarily have a high sensibility to impact and friction, “safer” compounds are in the focus.

Since the first invention of a practical laser in 1960 by Theodore Maiman, they are nowadays omnipresent and essential in countless areas of daily life ranging from simple light pointers, readers of optical storage media all the way to laser scalpels.[34] Soon after the introduction of laser systems they were successfully used for the initiation of energetic materials by Brish *et al.* and Yang *et al.*.[35,36] Since then much more investigations regarding the laser ignition of energetic materials have been carried out and different test setups using varying initiation mechanisms were investigated. To give a complete overview of all subgenres of laser initiation would go beyond the scope of this chapter and for that, the interested reader is referred to the relevant literature.[37,38,39] Recent advances in the ignition of energetic coordination compounds (ECCs) will be given. Contrary to traditional initiation methods like heat, spark, friction, etc., the laser initiation and ignition of ECCs is probably the most advantageous method of all, since the isolation of the energetic material to electric impulses excludes unintended initiation in most cases. Further benefits over classical initiation techniques are the very short function times (< 1 ms) and the possible utilization of less sensitive ignition charges, which further increases the handling and safety of these substances significantly.[40,41]

Although the concept of energetic coordination compounds was first postulated in the nineties,[42] the investigation of energetic transition metal complexes for their initiation abilities using laser diodes already started in the late eighties with pentaammine(5-cyano-2*H*-tetrazolato)cobalt(III) perchlorate (CP).[43] Due to the use of cyanogen as starting material it was later replaced by tetraammine-*cis*-bis(5-nitro-2*H*-tetrazolato-N^2)cobalt(III) perchlorate (BNCP) (Figure 12).[44]

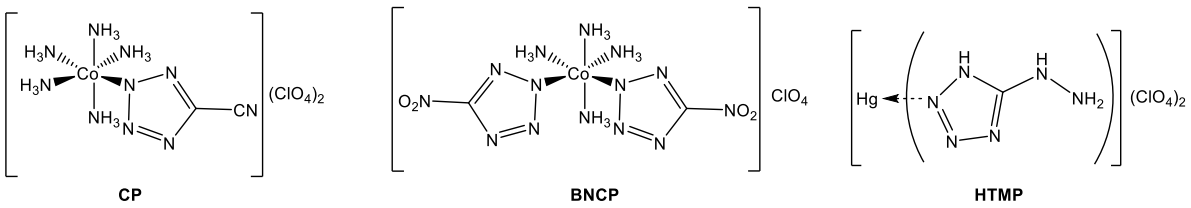
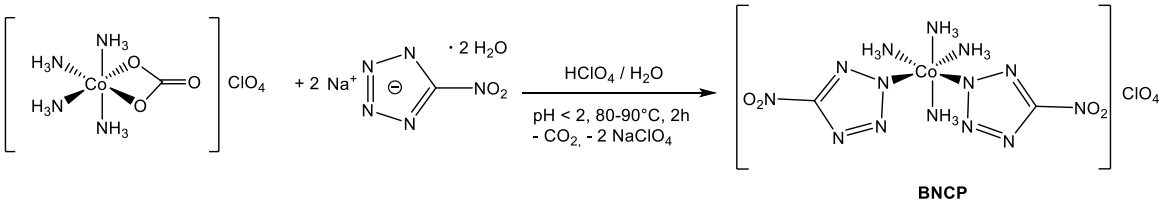


Figure 12. *Molecular structures of CP, BNCP, and HTMP.*

However, also the synthesis of 5-nitrotetrazole and the final cobalt complex BNCP (Scheme 3) is challenging. 5-Nitrotetrazole usually is synthesized by diazotization of 5-aminotetrazole with acidic sodium nitrite solutions. The intermediate 5-diazotetrazole is highly sensitive (!) and often causes micro-detonations when carried out in normal batch reactions. Therefore, the synthesis using micro-flow reactors is preferred meanwhile. BNCP is then synthesized by the reaction of a tetraamine carbonato cobalt perchlorate complex (Scheme 3), however, can sometimes be impurified with the monocoordinated NCP (pentaammine-(5-nitro-2*H*-tetrazolato-N^2)cobalt(III) perchlorate (NCP).



Scheme 3. *Synthesis of BNCP according to literature.*[45]

With the discovery of BNCP and its ignition by laser light, many new ECCs, such as 5-hydrazino-1*H*-tetrazole mercury(II) perchlorate (HTMP), were synthesized and investigated concerning their behavior when irradiated with a laser diode.[23–25] However, many of them suffer from the toxicity of the applied central metals (*e.g.*, nickel, cobalt or mercury are highly toxic or carcinogenic), leading to high demand for new and more eco-friendly materials.

In general, the concept of energetic coordination compounds (please see Chapter 3: Goals and Concepts) is based on three different building blocks: cation, anion, and ligand. The variation of the individual building blocks allows the tailoring of the complexes' physical and chemical properties to meet specific requirements. Therefore, it is possible to control a compounds' energetic nature and adjust its optical characteristics.

The first building block is represented by a transition metal, which mainly comes from the late 3d series (manganese, iron, cobalt, nickel, copper or zinc), but there are also more exotic energetic complexes described, *e.g.*, based on silver,[46] cadmium,[47] gold,[48,49] or mercury.[50] The metal center serves as a catalyst and matrix responsible for the cohesion between all components. The second component is a neutral ligand which mainly functions as a fuel and comes from the family of nitrogen-rich heterocycles, chiefly triazoles and tetrazoles, but also tri- and tetrazine-based molecules can be applied.[51] These ligands possess an extensive number of potential coordination sites and have a highly endothermic character due to their large number of N-N single and N=N double bonds and the associated driving force for the formation of molecular nitrogen N_2. The last component is the anion, which can be used as a fine-tuning agent for the energetic framework. While it former was limited to oxidizing agents (e.g. ClO_x^-) by the postulation of Sinditskii and Serushkin,[42] it was successfully shown within the last years that also other anions such as nitrate or azide can be perfectly applied.[47,52,53] In special occasions the nitrogen-rich molecules can work as both ligand and anion, which narrows the possible tuning opportunities. The most important benefits of ECCs in laser ignition devices is their relatively low energy threshold for an energetic response, which is in most cases drastically lower compared to high explosives.[35,36] In general, primary explosives possess quite low laser initiation thresholds, *e.g.*, $Pb(N_3)_2$ requires solely 11 mJ/cm^2 when using near-infrared laser light (NIR).[54] Furthermore, the sensitivity against laser irradiation highly correlates with the sensitivity against external stimuli and the booster explosive PETN already needs exposure in the range of 1.4–21 J/cm^2, depending on different parameters such as density, light source, or addition of absorbent additives.[55,56,57] Due to the superior characteristics of BNCP, its implementation in optical initiation devices was investigated and, furthermore, many other tetrazole-based coordination compounds were explored regarding their reaction towards laser irradiation beginning of the 21st century.[58] Russian scientists were successfully detonating various complexes based on 5-amino-1*H*-tetrazolate, 5-nitro-2*H*-tetrazolate, 1,5-diamino-1*H*-tetrazole, and 5-hydrazino-1*H*-tetrazole.[50,59] Especially the mercury perchlorate ECC of the latter ligand (5-hydrazino-1*H*-tetrazole-mercury(II) perchlorate, HMPT) shows very high sensitivities towards laser irradiation and was further investigated in the following years.[60,61] Nevertheless, the high toxicity of mercury and its associated ban, which was laid down in the CLRTAP protocol, will prevent future applications in most of the countries of the northern hemisphere.[62] Despite the very fast reaction time (≤ 30 µs) and low energy threshold when irradiated (all fire at 130 µJ) as well as the high-temperature stability (> 230 °C) of BNCP, its relatively high sensitivity against friction (< 5 N) in the range of typical primary explosives thwart the broader use of optical detonators in safe applications.[58] Especially for the use in so-called "in-line-detonators", which can also be used in active protection systems, materials with lower sensitivities are essential for the safe handling of the devices. Therefore, research shifted to complexes with higher carbon content in recent years.[41] In addition, most soluble cobalt salts are classified as toxic, therefore "greener" metals such as iron and copper are under current investigation.

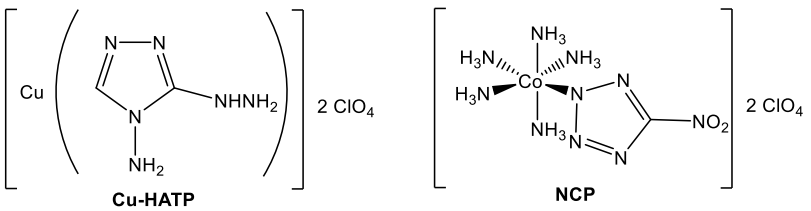
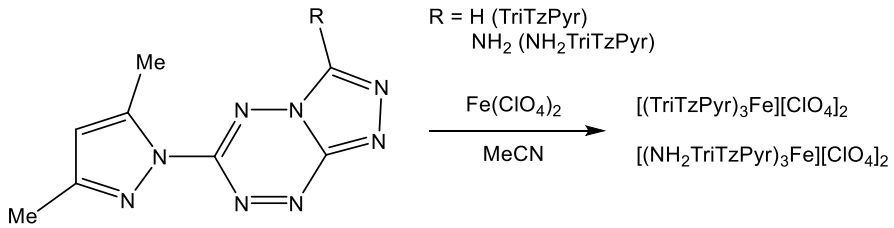


Figure 13. *Molecular structures of Cu-HATP and NCP.*

For optimizing the sensitivities of laser ignitable explosives to an acceptable range, different strategies were applied by scientist all around the world within the last years. In general, it can be stated that optimal properties of new laser ignitable ECCs should achieve similar requirements for a booster explosive (impact sensitivity >4 J, friction sensitivity >80 N), but depending on the application also deviating values are conceivable.[63] Russian scientists, most notably Ilyushin and Tverjanovich from St. Petersburg, investigated several azole-based ECCs within the last years. Beside the already mentioned HTMP with 5-hydrazino-1*H*-tetrazole as ligand, complexes based on the related 3-hydrazino-4-amino-1,2,3-triazole with decreased nitrogen content were investigated.[64] The most promising compound was found in the copper(II) perchlorate complex HATP (Figure 13), which shows the highest sensitivity towards laser mono pulses compared to other metal perchlorate ECCs (Cd^{2+}, Ni^{2+}, Co^{2+}) with a threshold as low as 10 mJ/cm^2. Nevertheless, the sensitivities of HATP are comparable to conventional primary explosives, which can only be reduced when mixing the ECC with polymers.[65,66] Another promising candidate is the BNCP related pentaammine-5-nitrotetrazolato-*N*2-cobalt(III) perchlorate (NCP), which was extensively investigated in recent years.[67,68] Compared to BNCP and to increase the stability against outer stimuli, in NCP one nitrotetrazolate was substituted with an ammine ligand, which results in values comparable to those of the booster explosive PETN.[69] The gravest drawback of NCP is its highly toxic character caused by the cobalt central metal, which is also stated by the authors and a general problem of cobalt compounds.[67,70] Apart from the possible desensitizing effect of polymers, many investigations were conducted regarding the influence towards the initiation threshold when using optical additives especially different carbon modifications, such as graphene,[71] diamond,[72] and fullerene.[68]

While research in Russia focuses on azole-based complexes, US scientist shifted their investigations towards ECCs with different substituted tetrazine ligands in the last years. The group of Chavez synthesized various coordination compounds based on the transition metals nickel, cobalt, copper, as well as iron and investigated the correlation of the metal-ligand charge transfer towards the laser initiation, which was also verified using time-dependent density functional theory studies.[73,74] Whereas they found out it is impossible to initiate nitrate complexes with NIR light,[73,75] they successfully proved, that both the laser initiation threshold (4.5 J/cm^2), as well as the mechanical sensitivity, can be decreased when using iron(II) perchlorate complexes, which is against the usual trend.[76] The most promising materials consist of 6-pyrazolyl-1,2,4-triazolo[4,3-*b*][1,2,4,5]-tetrazine (TriTzPyr) and 3-amino-6-pyrazolyl-1,2,4-triazolo[4,3-*b*][1,2,4,5]-tetrazine ((NH$_2$TriTzPyr) as the ligands yielding the complexes ([(TriTzPyr)$_3$Fe][ClO$_4$]$_2$ and ([(NH$_2$TriTzPyr)$_3$Fe][ClO$_4$]$_2$) (Scheme 4). When using 3-amino-6-(4-nitro-pyrazolyl)-1,2,4-triazolo[4,3-*b*][1,2,4,5]-tetrazine it could also be shown that the threshold is not only conditional from the absorption and explosive properties but also from other factors, such as the density.[77] Furthermore, the complexes can also be successfully applied in optical detonators to detonate PETN.[78]



***Scheme 4**. Synthesis of [(TriTzPyr)$_3$Fe][ClO$_4$]$_2$ and [(NH$_2$TriTzPyr)$_3$Fe][ClO$_4$]$_2$.*

While the first-ever laser initiation experiments of ECCs were already using laser diodes (GaAlAs laser) with a wavelength of 820 nm,[43] most other researchers in Russia, the USA and Germany are using NIR light sources in the range of ~1064 nm, such as Nd:YAG lasers.[50,76] Although several groups in China deal with the investigation of laser irradiation of energetic complexes not many reports can be found in the literature. The few articles that can be found indicate a high level of diversity concerning the different

setups. Similar to other researchers, initiation experiments using a laser wavelength of 1064 nm were carried out with a MOF consisting of cadmium, aqua ligands, and the very prominent bistetrazole-1,1-diolate anion.[79] A very interesting compound is represented by the silver perchlorate complex of 3-amino-1*H*-1,2,4-triazole-5-carbohydrazide, which possesses a high decomposition temperature (230 °C) and sensitivities comparable to PETN. The silver ECC was successfully initiated using a femtosecond laser (λ = 800 nm) with very low energies of 200 mJ.[80 [Nevertheless, the stated "very low delay time" of only 73 ms is probably too slow for laser initiation of energetic complexes and prevents its potential implementation in any application, which normally need function times of < 1ms. The relatively high delay time of the silver compound can be explained with its colorless appearance and the resulting rigorous absorption diminishment. Whereas most other experiments were carried out with single-pulsed irradiation, in this setup continuous exposure with a frequency of 1000 Hz was used and the initiation can be explained by simple heating of the material. In general, the missing absorption of colorless compounds prevents their initiation in single-pulsed laser experiments unless colorants or dyes are added. Another system, which was investigated by several researchers from Xi'an in cooperation with Professor Gozin from Tel Aviv, deals with the initiation of ECCs with a 980 nm laser diode. The nickel(II), cobalt(II), and copper(II) carbohydrazide complexes with nitrate and perchlorate as anion were examined and the delay times further optimized through doping with graphene oxide. In general, the perchlorate materials possess very short delay times in the range of several hundred µs and sensitivities lower than those of PETN.[81] Similar to Chavez *et al.* the results prove the decreased initiation capability of nitrate complexes compared to perchlorate ones. Furthermore, doping with graphene oxide leads to an increase in stability while at the same time the delay times are drastically shortened.

3. Goals and Concept

There are three main goals for the research described in this habilitation work.

A) Synthesis, Characterization and Publication of a large amount **of new energetic coordination compounds (ECCs)** based on late 3d metal salts as well as silver(I) in combination with non-acidic tetrazole and triazole ligands.

B) Generation of a large database of new ECCs in order to compare and especially predict the energetic properties of future materials.

C) Development of an applicable REACH conform new high-energy material that can be transferred into industry processes and applications.

ECCs are composed of three different building blocks: ligand, transition metal, and anion (Figure 14). Especially suitable for the synthesis of energetic materials is the use of nitrogen-rich azoles as ligands, such as non-acidic triazoles and tetrazoles. They possess a strongly endothermic character and act mainly as fuel with the accompanying driving force to decompose into molecular nitrogen. The second building block is represented by the transition metal, which acts as a catalyst and matrix to build up the system. Familiar representatives are silver and metals from the second half of the 3d series (Mn–Zn). Last but not least, the anion functions as a fine-tuning agent for the energetic framework. It is either an oxidizing (*e.g.*, (per)chlorate, nitrate, bromate, polynitrophenolates) or endothermic (*e.g.*, azide, fulminate, dicyanamide) element for further increasing the energy of the resulting substance. By varying the building blocks, the resulting complexes' properties can be easily adapted to specific requirements. Therefore, a straightforward optimization of the desired characteristic, like laser ignition, thermal stability, solubility, and sensitivity, can be achieved.

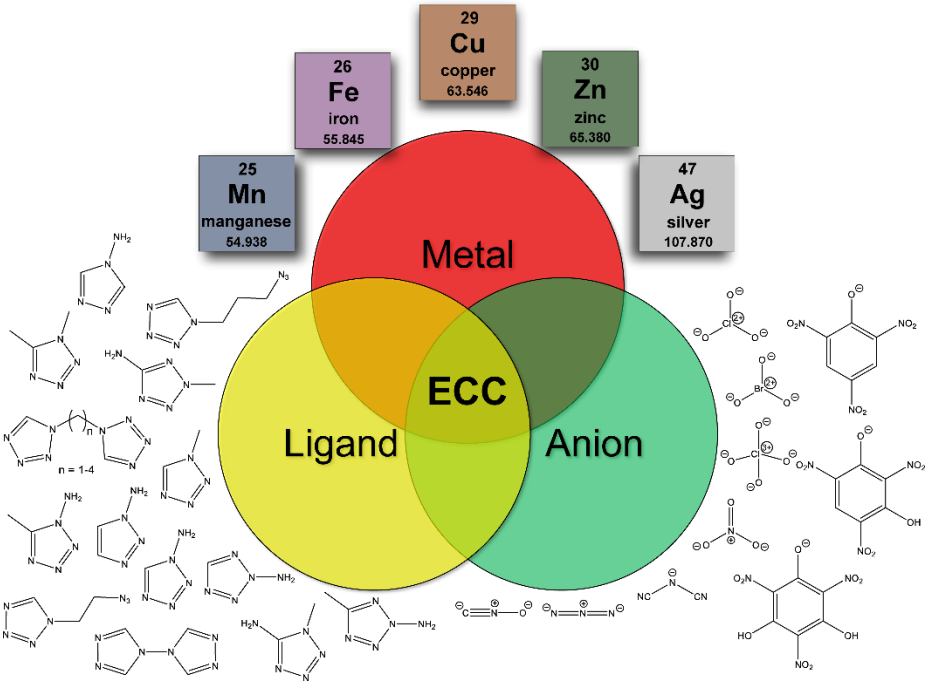


Figure 14. *The concept of energetic coordination compounds and selected components utilized in that habilitation work.*

The synthesis of new ECCs is highly academic, since the collection of different physiochemical properties related on the selection of building blocks, generates useful data. It already started that computers predict suitable target compounds by using large datasets collected in databases. We hope that our new ECCs form a sufficient amount of information that we use artificial intelligence to meet future sustainability demands. Only suitable compounds should be synthesized by the new generation chemists to avoid waste and environmental pollution. "Suitable" is the word of choice to combine the industrial aspects. *Basic research is good, but applied chemistry research is better.*

In the field of high-energy materials, more than 10 years ago the most dominant primary explosives lead(II) azide (LA) and lead styphnate (LS) were added to the REACH "candidate list of substances of very high concern for authorization. Although nearly all companies affected try to circumvent the fact that lead salts are strongly poisonous and try to appeal this decision, one has to expect strong restrictions for LA and LS during the next years. We already synthesized ECCs which are under current industrial investigation as new environmentally benign primary explosives.

We tried to use quickly gained knowledge to mostly concentrate on non-acidic 1-substituted tetrazoles. For better comparison, we mostly involved the simple aromatic 5H-tetrazole moiety. The following tetrazole ligands shown in Figure 15 were part of publications during this work. Many more tetrazole and triazole ligands are under current synthesis and investigation, however, have not been officially described yet.

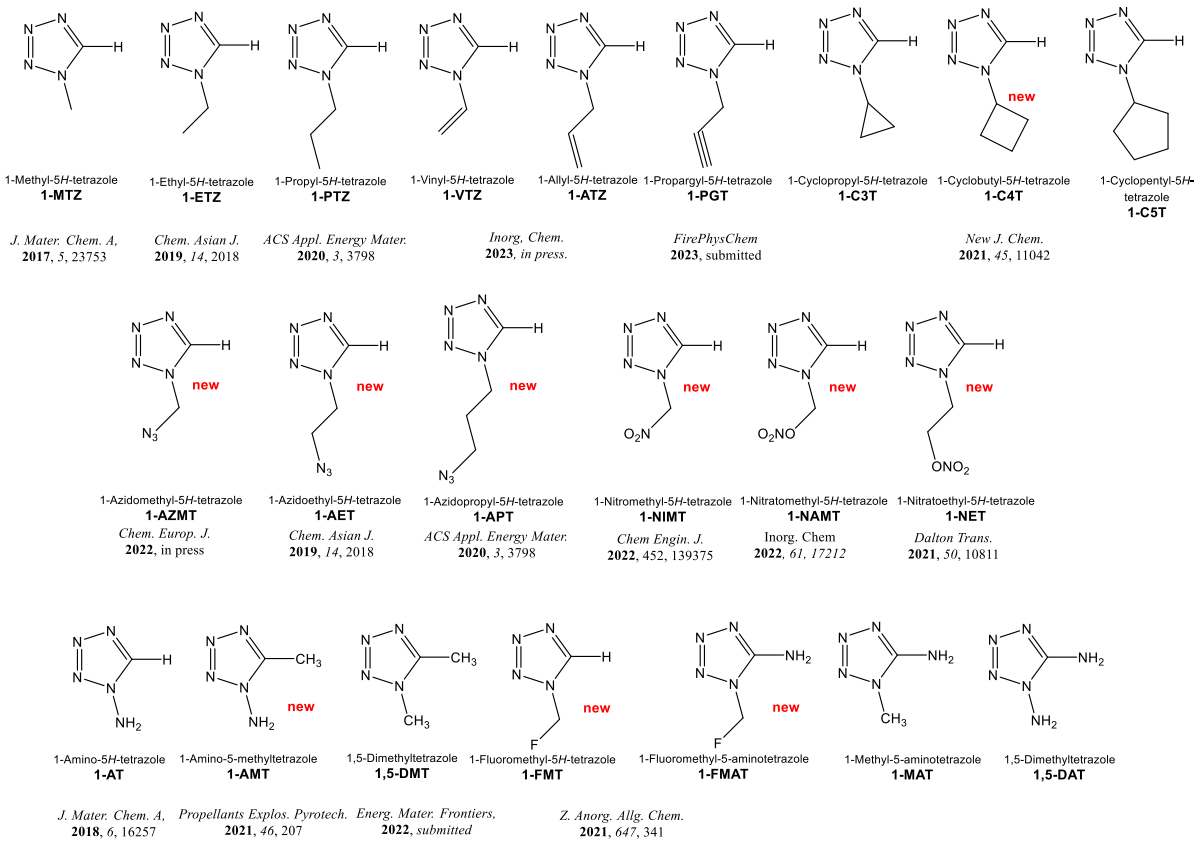


Figure 15. *Tetrazoles involved in this work. Only the 1-substituted derivative is drawn. 2-Substituted tetrazoles were also investigated when achieved by alkyl- or amination reactions as an isomeric main or by-product.*

The used anions follow Figure 16. They have either oxidizing (*e.g.*, (per)chlorate, nitrate, bromate, polynitrophenolates) or reducing (*e.g.*, azide, fulminate, dicyanamide) character. Perchlorate complexes have been synthesized from every ligand, if not already known. Most of the work involving the tetrazolate anions, listed in the last row of Figure 16, are still under investigation and has not been published yet. However, it seems when the right conditions are found, extremely valuable compounds can be achieved.

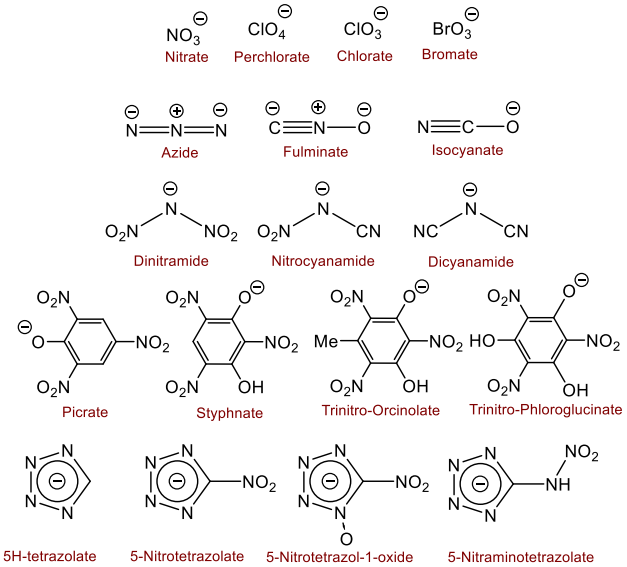


Figure 16. *Representation of anions that were used during this work.*

4. Summary

In this extensive experimental work, hundreds of new compounds were synthesized and characterized. All new ECCs (energetic coordination compounds) are collected in an Excel-based table (not open, available upon request) in which compounds can be sorted according to their building blocks or physico-chemical properties. In total, more than 450 complexes were published, and about hundred are still under investigation, reproduction shows tough or waiting for further candidates to complete meaningful publication. In total 34 papers (Appendix 1 – Appendix 34) have been published in recognized peer-reviewed journals. These are listed in the following and are depicted in the appendix. For every paper supporting information can be retrieved from the internet.

List of papers, only related to this habilitation work:

1. N. Szimhardt, Maximilian H. H. Wurzenberger, A. Beringer, L. J. Daumann, J. Stierstorfer, Coordination chemistry with 1-methyl-5*H*-tetrazole: cocrystallization, laser-ignition, lead-free primary explosives - one ligand, three goals, *J. Mater. Chem. A*, **2017**, *5*, 23753–23765; https://doi.org/10.1039/C7TA07780G
2. N. Szimhardt, J. Stierstorfer, Methylsemicarbazide as Ligand in Late 3d Transition Metal Complexes, *Chem. Europ. J.* **2018**, *24*, 2687–2698. https://doi.org/10.1002/chem.201705030.
3. M. Wurzenberger, N. Szimhardt, J. Stierstorfer, Copper(II) Chlorate Complexes – the Renaissance of a Forgotten and Misjudged Energetic Anion, *J. Am. Chem. Soc.* **2018**, *140*, 3206–3209. https://doi.org/10.1021/jacs.7b13230
4. N. Szimhardt, M. H. H. Wurzenberger, T. M. Klapötke, J. T. Lechner, H. Reichherzer, C. C. Unger, J. Stierstorfer, Highly functional energetic complexes: stability tuning through coordination diversity of isomeric propyl-linked ditetrazoles, *Mater. Chem. A*, **2018**, *6*, 6565–6577. https://doi.org/10.1039/C8TA01412D
5. M. Wurzenberger, N. Szimhardt, J. Stierstorfer, Nitrogen-Rich Copper(II) Bromate Complexes: an Exotic Class of Primary Explosives, *Inorg. Chem.* **2018**, 57, 7940–7949. https://doi.org/10.1021/acs.inorgchem.8b01045
6. N. Szimhardt, M. H. H. Wurzenberger, L. Zeisel, M.S. Gruhne, M. Lommel, Maximization of the Energy Capability Level in Transition Metal Complexes through Application of 1-Amino- and 2-Amino-5H-tetrazole Ligands *J. Mater. Chem. A*, **2018**, *6*, 16257–16272. https://doi.org/10.1039/C8TA06326E
7. N. Szimhardt, M. S. Gruhne, M. Lommel, A. Hess, Maximilian H. H. Wurzenberger, T. M. Klapötke, J. Stierstorfer, 2,2-Bis(5-tetrazolyl)propane as Ligand in Energetic 3d Transition Metal Complexes, *Z. Anorg. Allg. Chem.* **2019**, *645*, 354–361. https://doi.org/10.1002/zaac.201800288
8. L. Zeisel N. Szimhardt, Maximilian H. H. Wurzenberger, T. M. Klapötke, J. Stierstorfer, 2-Methyl-substituted monotetrazoles in copper(II) perchlorate complexes: manipulating coordination chemistry and derived energetic properties, *New. J. Chem.* **2019**, *43*, 609–616. https://doi.org/10.1039/c8nj05375h
9. N. Szimhardt, M. H. H. Wurzenberger, P. Spieß, T. M. Klapötke, J. Stierstorfer, Potassium *N*-Nitramino-5*H*-tetrazolates - Powerful Green Primary Explosives with High Initiation Capabilities, *Propellants Explos. Pyrotech.* **2018**, *43*, 1203–1209. https://doi.org/10.1002/prep.201800221
10. Maximilian H. H. Wurzenberger, Michael S. Gruhne, Marcus Lommel, Norbert Szimhardt, Thomas M. Klapötke, Jörg Stierstorfer, Comparison of 1-Ethyl-5H-tetrazole and 1-Azidoethyl-5H-tetrazole as Ligands in Energetic Transition Metal Complexes, *Chem. Asian J.* **2019**, *14*, 2018–2028. https://doi.org/10.1002/asia.201900269.

11. N. Szimhardt, Maximilian H. H. Wurzenberger, L. Zeisel, M. S. Gruhne, M. Lommel, T. M. Klapötke, J. Stierstorfer, 1-AminoTriazole Transition-Metal Complexes as Laser-Ignitable and Lead-Free Primary Explosives, *Chem. Eur.J.* **2019**, *25*, 1963–1974. https://doi.org/10.1002/chem.201803372

12. M. H. H. Wurzenberger, B. R. G. Bissinger, M. Lommel, M. S. Gruhne, N. Szimhardt, J. Stierstorfer, Synthesis and Comparison of Copper(II) Complexes with various N-Aminotetrazole Ligands Involving Trinitrophenol Anions, *New J. Chem.* **2019**, *43*, 18193–18202. https://doi.org/10.1039/C9NJ03937F.

13. M. S. Gruhne, M. Lommel, M. H. H. Wurzenberger, N. Szimhardt, T. M. Klapötke, J. Stierstorfer, OZM Ball Drop Impact Tester (BIT-132) vs. BAM Standard Method-a Comparative Investigation, *Propellants Explos. Pyrotech.* **2020**, *45*, 147–153. https://doi.org/10.1002/prep.201900286

14. M. H. H. Wurzenberger, J. T. Lechner, M. Lommel, T. M. Klapötke, J. Stierstorfer, Salts of Picramic Acid – Nearly forgotten temperature-resistant energetic materials, *Propellants Explos. Pyrotech.* **2020**, *45*, 898–907. https://doi.org/10.1002/prep.201900402

15. M. H. H. Wurzenberger, S. M. J. Endraß, M. Lommel, T. M. Klapötke, J. Stierstorfer, Comparison of 1-Propyl-5*H*-tetrazole and 1-Azidopropyl-5*H*-tetrazole as Ligands for Laser Ignitable Complexes, *ACS Appl. Energy Mater.* **2020**, 3, 4, 3798–3806. https://doi.org/10.1021/acsaem.0c00229

16. M. H. H. Wurzenberger, J. T. Lechner, J. Stierstorfer, Copper(II) Dicyanamide Complexes with *N*-Substituted Tetrazole Ligands – Energetic Polymers with Moderate Sensitivities, *ChemPlusChem* **2020**, *85*, 769– 775. http://doi.org/10.1002/cplu.202000156.

17. a) M. H. H. Wurzenberger, M. Lommel, M. S. Gruhne, N. Szimhardt, J. Stierstorfer, Refinement of Copper(II) Azide with 1-Alkyl-5H-tetrazoles: Adaptable Energetic Complexes, *Angew. Chem. Int. Ed.* **2020**, *59*, 12367–12370 https://doi.org/10.1002/anie.202002823. b) M. H. H. Wurzenberger, M. Lommel, M. S. Gruhne, N. Szimhardt, J. Stierstorfer, Veredelung von Kupfer(II)-azid mittels 1-Alkyl-5*H*-tetrazolen: Leistungsfähige energetische Komplexverbindungen, *Angew. Chem.* **2020**, *132*, 12466–12469. https://doi.org/10.1002/ange.202002823.

18. M. H. H. Wurzenberger, V. Braun, M. Lommel, T. M. Klapötke, J. Stierstorfer, Closing the Gap: Synthesis of Three Isomeric N,N-Ditetrazolymethane Ligands and Their Coordination Proficiency in Adaptable Laser Responsive Copper(II) and Sensitive Silver(I) Complexes, *Inorg. Chem.* **2020**, *59*, 10938−10952. https://dx.doi.org/10.1021/acs.inorgchem.0c01403.

19. M. H. H. Wurzenberger, M. Gruhne, M. Lommel, V. Braun, N. Szimhardt, J. Stierstorfer, Taming the Dragon: Complexation of Silver Fulminate with Nitrogen-Rich Azole Ligands, *Inorg. Chem.* **2020**, *59*, 17875–17879. https://doi.org/10.1021/acs.inorgchem.0c03027

20. M. Reichel, M. H. H. Wurzenberger, M. Lommel, M. Kofen, B. Krumm, J. Stierstorfer, K. Karaghiosoff, *N*-Fluoromethylated (Amino)Tetrazoles: Manipulating Thermal and Energetic Properties, *Z. Anorg. Allg. Chem.* **2021**, *Z. Anorg. Allg. Chem.* 2021, 647, 341–349. https://doi.org/10.1002/zaac.202000341

21. M. H. H. Wurzenberger, M. S. Gruhne, M. Lommel, J. Stierstorfer, 1-Amino-5-methyltetrazole in Energetic 3 d Transition Metal Complexes – Ligand Design for Future Primary Explosives, *Propellants Explos. Pyrotech.* **2021**, *46*, 207–213. https://doi.org/10.1002/prep.202000179

22. M. S. Gruhne, M. Lommel, M. H. H. Wurzenberger, T. M. Klapötke, J. Stierstorfer, Investigation of Ethylenedinitramine as a Versatile Building Block in Energetic Salts, Cocrystals, and Coordination Compounds, *Inorg. Chem.* **2021**, *60*, 4816−4828. https://doi.org/10.1021/acs.inorgchem.0c03752

23. M. S. Gruhne, M. H. H. Wurzenberger, M. Lommel, J. Stierstorfer, A Smart Access to the Dinitramide Anion – The Use of Dinitraminic Acid for the Preparation of Energetic

Coordination Compounds, *Chem. Europ. J.* **2021**, 27, 9112–9123. https://doi.org/10.1002/chem.202100747

24. M. Wurzenberger, V. Braun, V. Weippert, J. Stierstorfer, Tailoring the properties of 3d transition metal complexes with different N-cycloalkyl-substituted tetrazoles, *New J. Chem.* **2021**, *45*, 11042–11050. https://doi.org/10.1039/D1NJ01675J
25. M. Gruhne, T. Lenz, M. Rösch, M. Lommel, M. H. H. Wurzenberger, T. M. Klapötke, J. Stierstorfer, Nitratoethyl-5H-tetrazoles: Improving Oxygen Balance through Application of Organic Nitrates in Energetic Coordination Compounds, *Dalton Trans*. **2021**, *50*, 10811–10825, https://doi.org/10.1039/D1DT01898A.
26. M. Gruhne, M. Benz, T. Lorenzen, T. Lenz, T. M. Klapötke, J. Stierstorfer, Hybridization of Dinitramide and Dicyanamide: Evaluation of Nitrocyanamide in Energetic Salts and Coordination Compounds, *Cryst. Growth Des.*, **2022**, *22*, 200–212. https://doi.org/10.1021/acs.cgd.1c00858
27. M. H. H. Wurzenberger, M. Gruhne, N. Szimhardt, M. Lommel, J. Stierstorfer, Advancement and Stabilization of Copper(II) Azide by the Use of Triazole- and Tetrazole Ligands – Enhanced Primary Explosives, *Mater. Adv*. **2022**, *3*, 579–591. https://doi.org/10.1039/D1MA00588J
28. J. T. Lechner, T. M. Klapötke, J. Stierstorfer, Synthesis, Characterization and Derivatives of Iso-Picramic Acid, *Propellants. Explos. Pyrotech.* **2022**, *47*, e2021002. https://doi.org/10.1002/prep.202100205
29. T. M. Klapötke, M. Kofen, L. Schmidt, J. Stierstorfer, Maximilian H. H. Wurzenberger, 1-(Azidomethyl)-5H-tetrazole – a Powerful New Ligand for Highly Energetic Coordination Compounds, *Chemistry Eur. J.* **2022**, *28*, e202200492. https://doi.org/10.1002/chem.202200492
30. M. Kofen, A. G. Harter, T. M. Klapötke, J. Stierstorfer, 1,5-Dimethyltetrazole as a ligand in energetic $3d^5$ to $3d^{10}$-metal coordination compounds, Energetic Materials Frontiers, **2022**, 3, 111–121. https://doi.org/10.1016/j.enmf.2022.07.004
31. M. Kofen, V. Braun, S. M. J. Endraß, T. M. Klapötke, J. Stierstorfer, 1-(Nitratomethyl)-5H-tetrazole: A Highly Sensitive Ligand with Improved Oxygen Balance for Laser-Ignitable Coordination Compounds, *Inorg. Chem.* **2022**, *61*, 17212–17225. https://doi.org/10.1021/acs.inorgchem.2c02805
32. M. Kofen, T. M. Klapötke, J. Stierstorfer, Energetic Coordination Compounds of late 3d metals with 1N-(Nitromethyl)-5H-tetrazole, a ligand with astonishing properties from the rare class of N-nitromethyl azoles, *Chemical Engineering Journal*, **2022**, *452*, 139375. https://doi.org/10.1016/j.cej.2022.139375
33. S. M. J. Endraß, A. Neuer, T. M. Klapötke, J. Stierstorfer, Trinitro-orcinolate and Trinitro-resorcinate – Sensitivity Trends in Nitroaromatic Energetic Materials, *ChemistrySelect*, **2022**, *7*, e202203140. https://doi.org/10.1002/slct.202203140
34. M. Rösch, M. Gruhne, M. Lommel, S.M. J. Endraß, J. Stierstorfer, The Adjustability of Physicochemical Properties: Comparison of 1-Vinyl-5H-tetrazole and 1-Allyl-5H-tetrazole as Ligands in 3d Metal Energetic Coordination Compounds (ECC), *Inorg. Chem.* **2023**, in press. https://doi.org/10.1021/acs.inorgchem.2c03624

For the preparation of the ECCs the following ligands were synthesized, partly shown in Figure 15. These are: 1-azidomethyl-5*H*-tetrazole, 1-azidoethyl-5*H*-tetrazole, 1-azidopropyl-5*H*-tetrazole, 1-nitromethyl-5*H*-tetrazole, 1-nitratomethyl-5*H*-tetrazole, 1-nitratoethyl-5*H*-tetrazole, 1-cyclobutyl-5*H*-tetrazole, 1-fluoromethyl-5*H*-tetrazole, 1-fluoromethyl-5-amino-tetrazole, 1-amino-5-methyl-tetrazole; and known ligands: 1-methyl-5*H*-tetrazole, 1-ethyl-5*H*-tetrazole, 1-propyl-5*H*-tetrazole, 1-vinyl-5*H*-tetrazole, 1-allyl-5*H*-tetrazole, 1-propargyl-5*H*-tetrazole, 1-cyclopropyl-5*H*-tetrazole, 1-cyclopentyl-

5*H*-tetrazole, 1-amino-5*H*-tetrazole, 1-propargyl-5*H*-tetrazole, 1,5-dimethyl-tetrazole, 1-methyl-5-amino-tetrazole, and 1,5-diaminotetrazole.
In many cases, we also obtained the 2-substituted isomer e.g. 2-methyl-5*H*-tetrazole, 2-amino-5*H*-tetrazole, 2-methyl-5-amino-tetrazole, 2-propargyl-5H-tetrazole, etc.
In addition, the diacidic ligand 2,2-bis(5-tetrazolyl)propane was used (Appendix 7) to synthesize low sensitive (often hydrated) complexes.
In Appendix 2, methylsemicarbazide was used as an easily accessible (95% yield) non-tetrazole ligand. The ligand itself showed no toxicity toward vibrio fischerii and yielded more than 20 complexes with thermal decomposition points around 180°C. The highest sensitivity in this study was measured for the copper(II) perchlorate complex.
In Appendix 11, the two *N*-substituted aminotriazoles 1-amino-1,2,3-triazole (1-ATRI) and 1-amino-1,2,4-triazole (1-A-1,2,4-TRI) (Figure 17) were prepared by a simple one-step synthesis starting from the respective triazoles (1,2,3- or 1,2,4-triazole) and the conventional amination reagent hydroxylamine-*O*-sulfonic acid (HOSA). Although a multitude of 4-ATRI complexes have been reported in the literature, the overall goal of this study was to further increase the energy content of complexes by employing more endothermic ligands and thus produce useful new lead-free primary explosives. Here 14 new complexes composed of two isomeric aminotriazoles, four metals (Mn, Fe, Cu, and Zn), and seven different anions were presented. The majority of the synthesized complexes could be laser-ignited and showed different behavior that could be correlated with the measured sensitivities. Not only the high positive heat of formation of 1-ATRI is an explanation for the extreme powerful resulting complexes when used as a ligand. Positive initiation capability tests, which were not expected from our previous experiences, were observed for example for the dihydrate (!) ($[Cu(H_2O)_2(1\text{-ATRI})_4](ClO_4)_2$) and also a zinc complex ($[Zn(1\text{-ATRI})_6](ClO_4)_2$).

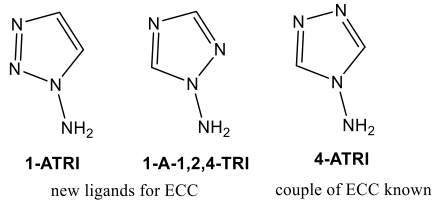


Figure 17. *Three different isomeric amino-triazoles which can be used as ligands for ECCs.*

In general, we wanted to focus on 1-substituted (5-nonsubstituted) tetrazoles because of their simple structure and potential derivatization capabilities in order to generate a large dataset of a simple and useful main structure. In one paper (Appendix 8) we only presented 2-substituted tetrazoles as ligands in transition metal complexes. However, after careful evaluation of many examples, we decided not longer to investigate the 2-substituted tetrazoles because they show

(i) larger sterically hindrance and the tendency of included coordinated water;

(ii) no selective synthesis;

(iii) lower yields;

(iv) lower melting and vaporization temperatures;

(v) higher toxicity values in the LBIT (luminescent bacterial inhibition test). The latter fact could also be observed for the resulting complexes, in which 2-substituted tetrazoles (e.g. mono-tetrazoles such as 1/2-methyl-5*H*-tetrazole but also bridging ditetrazoles such as 1,1-dtp, 1,2-dtp, and 2,2-dtp) were coordinated.

(vi) lower heat of formations (Figure 18).

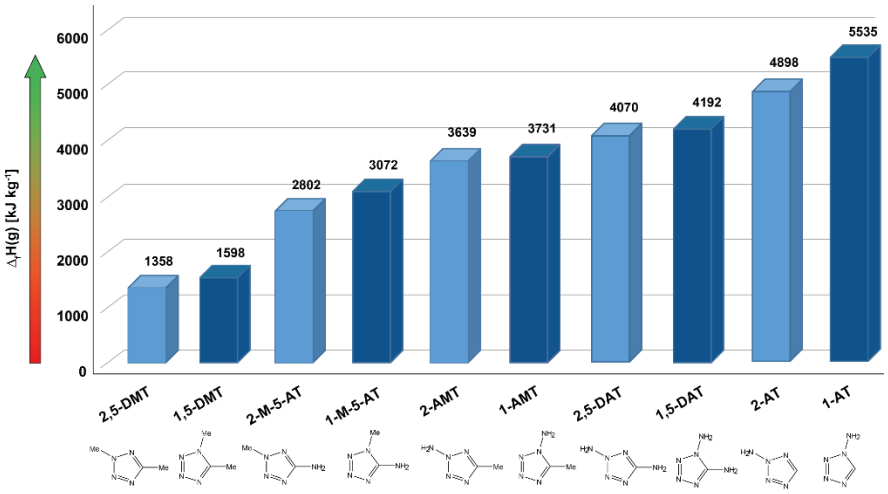
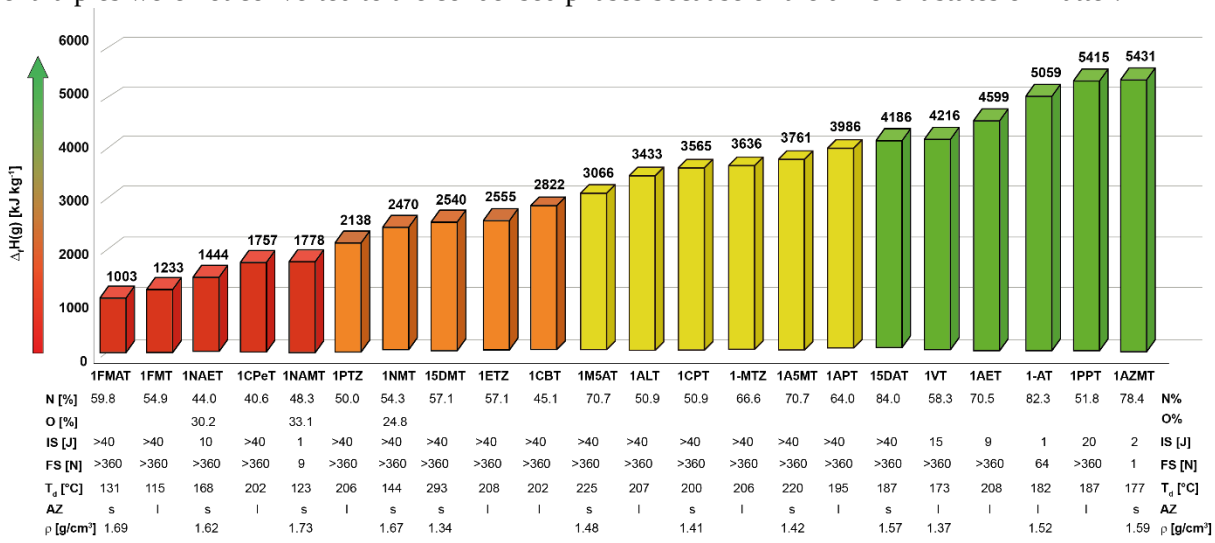


Figure 18. *Comparison of the gas-phase heat of formation of selected corresponding 1- and 2-substituted tetrazoles.*

This is a main finding that 2-substituted 5*H*-tetrazoles seem to be more toxic and lower in heat of formation.

The used 1-substituted 5H-tetrazoles were investigated toward their heat of formation (HOF) in order to see the influence on the resulting physico-chemical properties of the prepared ECCs. Because of the low precision of the bomb calorimeter in the research group, we decided to calculate all HOF by the same quantum-chemical method. The electronic energies obtained by the CBS-4M method were converted to gas phase enthalpies of formation using the atomization method. For better comparison, the gas phase enthalpies of formation given in Figure 19 are given in the mass-related unit kJ/kg. The enthalpies were not converted to the condensed phases because of the different states of matter.



	1FMAT	1FMT	1NAET	1CPeT	1NAMT	1PTZ	1NMT	15DMT	1ETZ	1CBT	1M5AT	1ALT	1CPT	1-MTZ	1A5MT	1APT	15DAT	1VT	1AET	1-AT	1PPT	1AZMT	
N [%]	59.8	54.9	44.0	40.6	48.3	50.0	54.3	57.1	57.1	45.1	70.7	50.9	50.9	66.6	70.7	64.0	84.0	58.3	70.5	82.3	51.8	78.4	N%
O [%]			30.2		33.1		24.8																O%
IS [J]	>40	>40	10	>40	1	>40	>40	>40	>40	>40	>40	>40	>40	>40	>40	>40	>40	15	9	1	20	2	IS [J]
FS [N]	>360	>360	>360	>360	9	>360	>360	>360	>360	>360	>360	>360	>360	>360	>360	>360	>360	>360	>360	64	>360	1	FS [N]
T_d [°C]	131	115	168	202	123	206	144	293	208	202	225	207	200	206	220	195	187	173	208	182	187	177	T_d [°C]
AZ	s	l	s	l	s	l	s	s	l	l	s	l	s	l	s	l	s	l	l	l	l	s	AZ
ρ [g/cm³]	1.69		1.62		1.73		1.67	1.34			1.48		1.41		1.42		1.57	1.37		1.52		1.59	ρ [g/cm³]

Figure 19 *Comparison of the gas-phase heat of formation of the used ligands and selected physico-chemical properties, oxygen and nitrogen contents, state of matter and X-ray density (if solid). Ligands: 1FMAT (1-fluoromethyl-5-amino-tetrazole), 1FMT (1-fluoromethyl-5H-tetrazole). 1NAET (1-nitratoethyl-5H-tetrazole), 1CPeT (1-cyclopentyl-5H-tetrazole), 1NAMT (1-nitratomethyl-5H-tetrazole), 1PTZ (1-propyl-5H-tetrazole), 1NMT (1-nitromethyl-5H-tetrazole), 15DMT (1,5-dimethyltetrazole), 1ETZ (1-ethyl-5H-tetrazole), 1CBT (1-cyclobutyl-5H-tetrazole), 1M5AT (1-methyl-5H-tetrazole), 1ALT (1-allyl-5H-tetrazole), 1CPT (1-cyclopropyl-5H-tetrazole), 1-MTZ (1-methyl-5-methyltetrazole), 1APT (1-azidopropyl-5H-tetrazole), 1A5MT (1-amino-5-methyltetrazole), 15DAT (1,5-diaminotetrazole), 1VT (1-vinyl-5H-tetrazole), 1AET (1-azidoethyl-5H-tetrazole), 1-AT (1-amino-5H-tetrazole), 1PPT (1-propargyl-5H-tetrazole), 1AZMT (1-azidomethyl-5H-tetrazole).*

From that comparison a couple of trends can be stated:

(i) 5*H*-tetrazoles show a higher HOF than 5-aminotetrazoles.

(ii) The longer the carbon chain, the lower the HOF.

(iii) The nitrogen content cannot be correlated with the HOF. Unsaturated carbon chains such as vinyl and propargyl yield to highly positive HOF.

(iv) The nitrogen content cannot be correlated to the sensitivities. The explosophoric nitrato group yield highly sensitive ligands.

(v) Many of the ligands are insensitive towards friction and impact.

(vi) The highest impact sensitivity was measured for the ligands 1-amino-5*H*-tetrazole and 1-nitratomethyl-5*H*-tetrazole. The highest friction sensitivity was observed for 1-azidomethyl-5H-tetrazole. Liquid compounds generally show less friction sensitivity.

(vii) Nitrato-groups at the carbon chain lower the temperature of decomposition.

(viii) The highest decomposition temperatures were measured for the disubstituted tetrazoles 1,5-dimethyltetrazole (293°C), 1-methyl-5-aminotetrazole (225°C) and 1-amino-5-methyltetrazole (220°C).

(ix) Fluorine atoms in the side chain drastically decrease the HOF.

(x) Nitro- and nitrato-groups show an increase in density.

By using the following reaction equation, we were able to synthesize a series of homoleptic copper(II) perchlorate complexes (Figure 20).

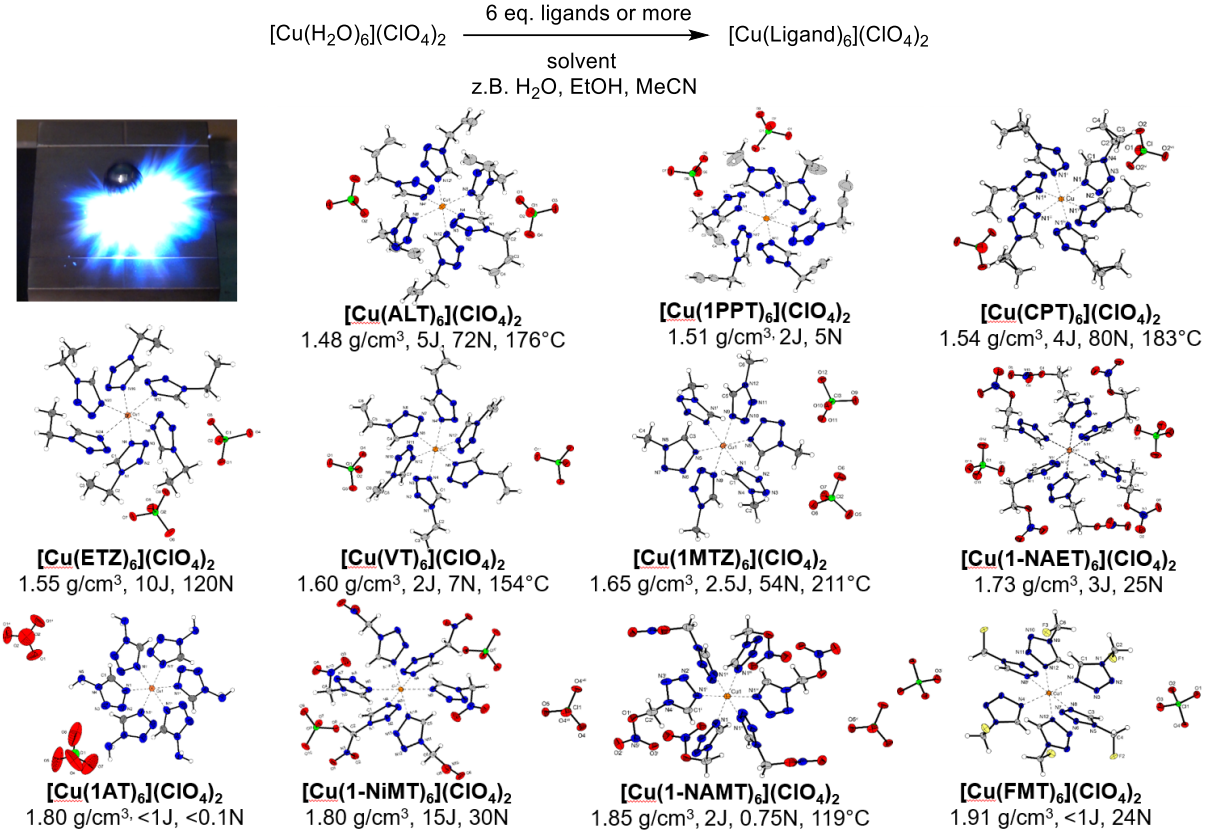


Figure 20. *Homoleptic copper(II) perchlorate complexes (measured by single-crystal XRD) listed according to increasing densities with given X-ray densities and sensitivity values and selected decomposition temperatures.*

From Figure 20 can be concluded that the sensitivity of the ligands cannot be correlated to the sensitivities of the complexes. Also, insensitive ligands such as 1-fluormethy-5H-tetrazole yielded extremely sensitive perchlorate complexes. Longer carbon chains lead complexes with a lower density. The highest density was observed for the fluoromethyl complex $[Cu(FMT)_6](ClO_4)_2$. More bulky side chains as well as disubstituted tetrazoles could not be coordinated six fold around copper(II). The remaining coordination sides are filled with aqua ligands (Figure 21).

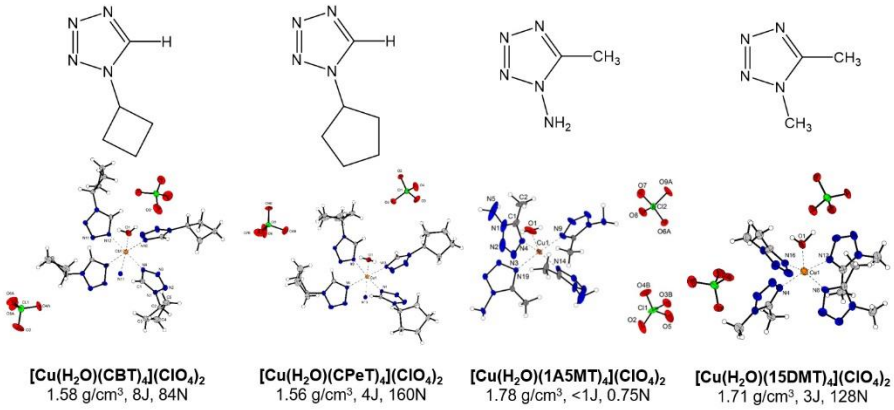
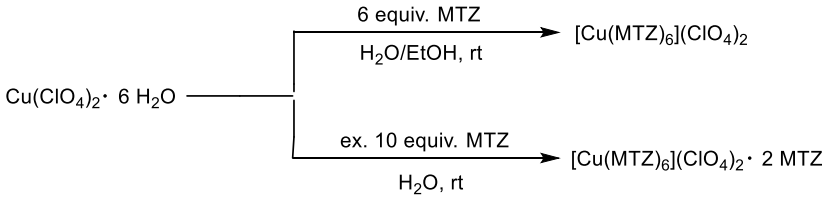


Figure 21. *Copper(II) perchlorate complexes based on disubstituted 1,5-tetrazoles or more bulky side chains at nitrogen atom N1 yield to coordination of aqua ligands.*

Cocrystallization (Appendix 1)

Cocrystallization of the endothermic ligands (complex + 2 eq. ligand) led in the case of the 1-MTZ study in most cases to a decrease in sensitivities toward mechanical stimuli while maintaining its highly energetic character and is therefore an excellent concept for the desensitization of energetic coordination compounds. Cocrystallization is strongly dependent on the stoichiometry of the ligand and was unfortunately not possible for most of the used ligands during work on this habilitation.



Scheme 5. *Formation of hexakis(1-methyltetrazole) copper(II) perchlorate with and without inclusion of 2 eq. of 1-MTZ ligand.*

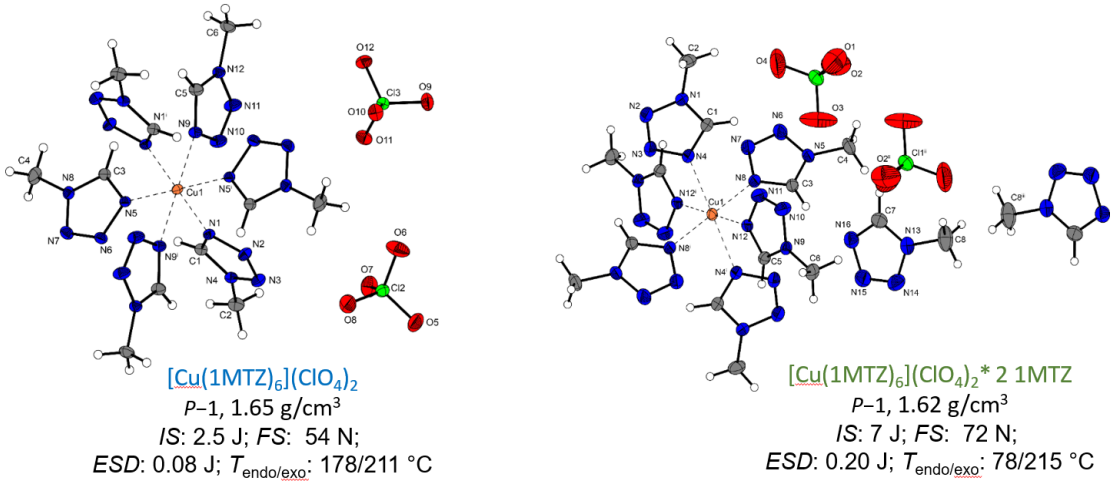
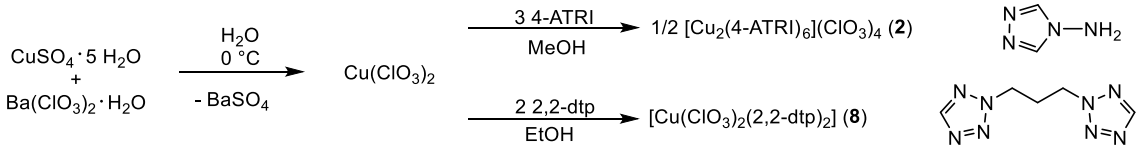


Figure 22. *Molecular moieties and energetic properties of hexakis(1-methyltetrazole) copper(II) perchlorate with and without inclusion of 2 eq. of 1-MTZ ligand.*

Chlorate Complexes (Appendix 3)

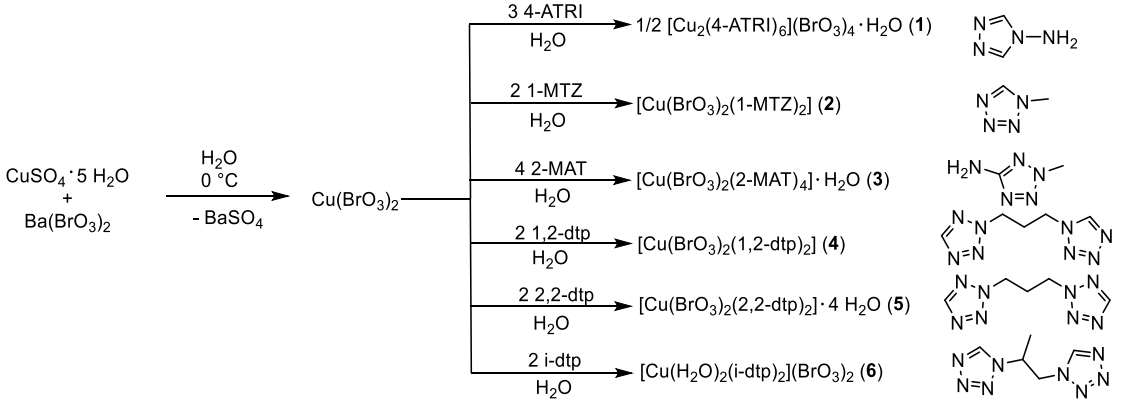
A straightforward and low-cost synthetic route toward modern energetic copper(II) chlorate complexes was demonstrated according to Scheme 6. The aminotriazole complex **2** as well as the 2,2-dtp complex show promising energetic properties. Easy ignition by heat was proven by the hot needle and hot plate tests. In addition, the primary explosives **2** and **8** showed excellent initiation capabilities toward the secondary PETN indicated by positive deflagration to detonation transitions. The use of alkyl-bridged ditetrazoles with longer chain lengths leads to an improvement of the mechanical sensitivities while maintaining its highly energetic character. Toxicity measurements using *vibrio fischeri* showed a lower toxicity in comparison to the analogous perchlorate complex and confirmed the higher environmental friendliness of chlorate compounds. Detonations during the laser ignition experiments of almost every single compound demonstrated the great suitability of chlorate complexes in future laser initiation systems.



Scheme 6. *Synthesis of two selected copper(II) chlorate complexes starting from copper(II) sulfate and barium chlorate. (**2**: IS: 1J, FS<5N, 186°C (dec.); **8**: IS: 1J, FS<5N, 176°C (dec.))*

Bromate Complexes (Appendix 5)

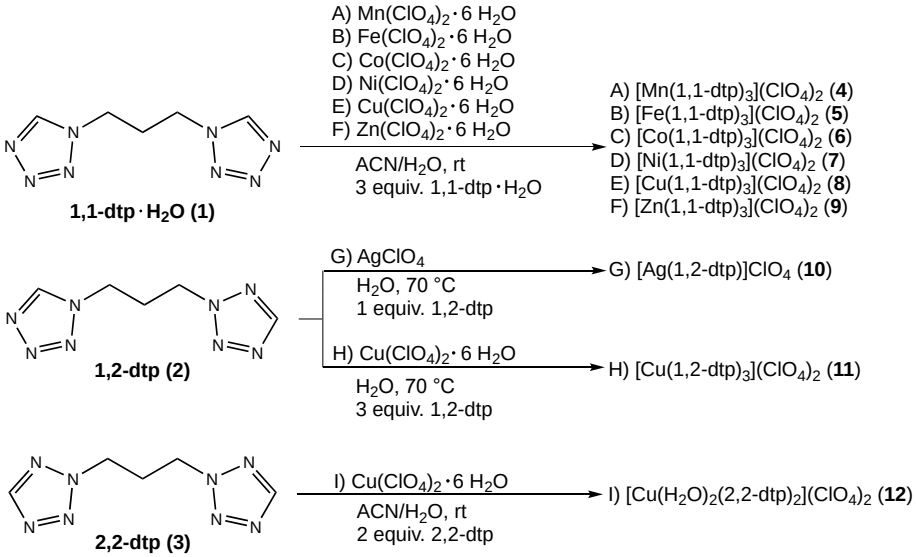
The six synthesized and investigated copper(II) bromate compounds (Scheme 7) with azole ligands represent a considerable contribution to the coordination chemistry in general and in particular to ECCs, due to the enormous lack in literature regarding this topic. The displayed synthesis of the complexes is a straightforward and low-cost synthetic route toward modern lead-free primary explosives with promising performance characteristics. The simple complexation of $Cu(BrO_3)_2$ with different nitrogen-rich ligands based on tri- and tetrazole derivatives assures the formation of energetic compounds with high densities. Most of the compounds were received in decent yields (57–85 %) directly from the mother liquor in the form of single crystals suitable for X-ray diffraction. Most of the compounds showed exothermic decomposition temperatures above 135 °C in thermal stability measurements by DTA. In comparison to the analogous perchlorate and chlorate complexes, ECC **2** showed a lower environmentally hazardousness toward aquatic life in toxicity assessments using *vibrio fischeri*, which proves the higher environmental friendliness of bromate compounds. Also, the energetic behavior was more impressive than the corresponding chlorate complexes. Within the preliminary analysis of decomposition gases, no HBr and Br_2 formation was observed in the mass spectra. Detonations during laser ignition experiments of nearly every single compound revealed the great capability of copper(II) bromate complexes in future laser initiation systems.



Scheme 7. *Synthesis of several copper(II) bromate-based complexes starting from copper(II) sulfate and barium bromate.*

Coordination of propyl-linked ditetrazoles (Appendix 4)

Three isomeric ditetrazolylpropanes (1,3-di(tetrazol-1-yl)propane (1,1-dtp), 1-(tetrazol-1-yl)-3-(tetrazol-2-yl)propane (1,2-dtp) and 1,3-di(tetrazol-2-yl)propane (2,2-dtp), differing, only in the nitrogen substitution pattern at the tetrazole, were prepared and purified in a straightforward one-step synthesis through alkylation of 1,5*H*-tetrazole. Obtained endothermic *N*-propyl linked ditetrazoles were exhaustively characterized by various methods including toxicity assessments, X-ray studies and heteronuclear ^{15}N NMR spectroscopy. Toxicity determinations toward aquatic life of the free uncoordinated ligands together with the promising related copper(II) perchlorate complexes showed that 1-alkylated species are less toxic than their 2-alkylated isomers. Laser initiation experiments with 1,2-di(tetrazol-5-yl)ethane (1,1-dte) based transition metal(II) complexes have shown promising results in the past but were too sensitive for any application. As a logical consequence, ditetrazolylpropane ligands with higher carbon contents especially the *N1*,*N1*-substituted ditetrazole (1,1-dtp) were now implemented into the corresponding coordination compounds in order to increase the stability of the new energetic materials. The present contribution covers the synthesis, characterization and comparison of 12 new eco-friendly energetic coordination compounds (ECCs) based on three different isomeric propyl-linked ditetrazoles, which differ drastically in their coordination pattern. Complexation of the ligands leads to intramolecular reorientation of the ditetrazole molecules and enables the formation of polymeric chains. Synthesized coordination compounds consist of a first-row transition metal(II) (Mn, Fe, Co, Ni, Cu, Zn), several different anions (ClO_4^-, TNR^{2-}, $CDNM^-$, DN^-) and one of the three isomeric ditetrazoles. In order to form thermally stable materials, non-volatile bridging bidentate ditetrazole ligands were implemented into the complexes to establish highly stable multidimensional polymeric structures (MOFs). Through this strategy extraordinary exothermic decomposition temperatures could be achieved for all complexes up to a very impressive 297 °C for compound **7**. The highest sensitivities were measured for cobalt(II) perchlorate complex **6**. Laser initiation tests, which were performed at a wavelength of 915 nm showed detonations for the most promising iron(II) and copper(II) complexes **5**, **8**, **11**, **12** at the lowest configurable laser setup energy input (0.2 mJ). The successful initiations proved the suitability of these high performing and thermal stable candidates for future laser initiation systems, which can be easily synthesized from inexpensive chemicals in a simple, inexpensive and upscalable reaction.



Scheme 8. *Synthesis of the metal(I,II) perchlorate complexes based on different propyl-linked ditetrazole ligands.*

Reduction of the amount of carbon atoms in the linker of ditetrazolyl-alkanes (Appendix 18)

While complexes with 1,1-dte were already known from our research group in previous times, the synthesis of the methyl bridged tetrazoles was of high interest. For the first time the nitrogen-rich compounds di(tetrazol-1-yl)methane (1,1-dtm), (tetrazol-1-yl)(tetrazol-2-yl)methane (1,2-dtm), and di(tetrazol-2-yl)methane (2,2-dtm) were synthesized by the reaction of triethylammonium 5*H*-

tetrazolate with dibromomethane in a one-step reaction. The coordination behavior of the three ligands was studied in detail leading to 15 new energetic coordination compounds (ECCs) based on silver(I) and copper(II) as well as different oxidizing anions (nitrate, perchlorate, picrate, styphnate, and trinitrophloroglucinate). Especially the copper perchlorate complexes involving 1,2-dtm and 2,2-dtm show very good initiation capabilities of PETN. The overall crystal structures reveal a high degree of diversity for the coordination of the three different isomers. Due to the potential bridging character of the ligands, most of the complexes form polymeric structures with differing dimensionality. However, especially compared to other 5*H*-ditetrazolyl ligands, dtm ligands have comparatively often a terminal coordination behavior, which is highly influencing the polymeric structures and even leading in some cases to the formation of complex monomers. Moreover, exceptional coordination spheres, like a 5-fold bounding of 2,2-dtm to silver(I) nitrate or a distorted pentagonal bipyramidal geometry around Cu^{2+} in the copper nitrate 2,2-dtm ECC, can be observed.

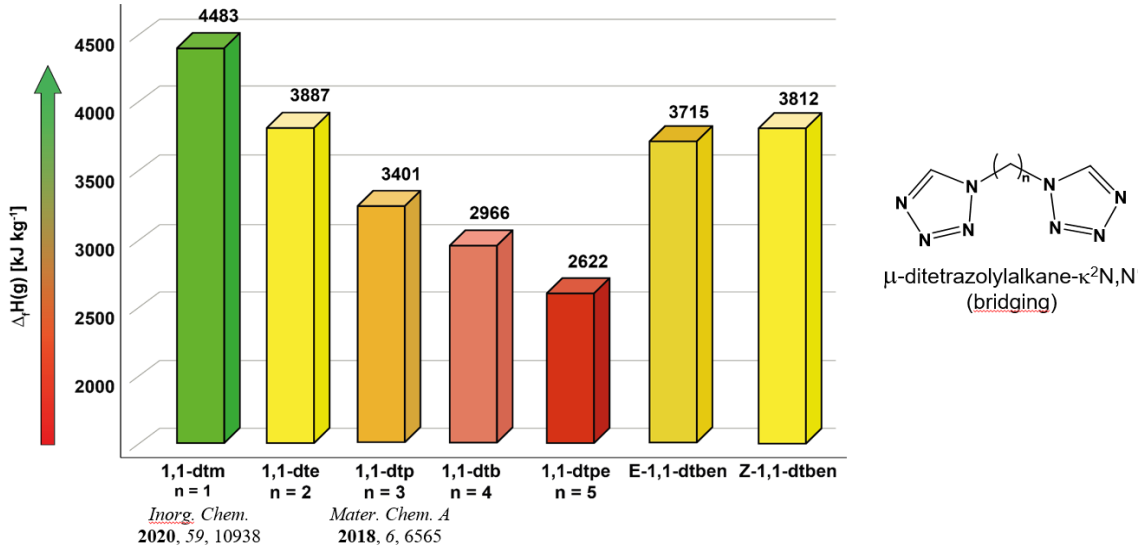


Figure 23. *Gas phase heat of formation of 1,1-ditetrazolyl-alkanes showing the influence of the growing linking carbon chain.*

Application of 1-amino- and 2-amino-5*H*-tetrazole ligands (Appendix 6)

Two isomeric amino-5*H*-tetrazoles (1-amino-5*H*-tetrazole (1-AT) and 2-amino-5*H*-tetrazole (2-AT)) with sensitivities already in the range of primary explosives were synthesized in a simple one step reaction starting from 1,5*H*-tetrazole and the commercially available amination reagent hydroxylamine-*O*-sulfonic acid (HOSA). The obtained isomeric mixture was purified by column chromatography, preventing the highly risky distillation mentioned in the literature and yielded the products in satisfying yields. Due to the great potential of 1-AT as ligand in powerful energetic transition metal(II) complexes, a selective, upscalable and isomerically pure route toward this highly endothermic compound has been developed. The received nitrogen-rich aminoazoles were comprehensively characterized by diverse analytical methods enclosing heteronuclear ^{15}N NMR spectroscopy, X-ray studies and toxicity determinations. The toxicity assessments toward aquatic organisms revealed the non-toxicity of both heterocycles. These *N*-aminoazoles have been incorporated in metal complexes resulting in a tremendous performance increase releasing several of the most energetic coordination compounds synthesized up to 2020. The paper features the preparation, analysis and evaluation of 20 new lead, nickel and cobalt-free energetic complexes. The synthesized complexes can be prepared by an easy upscalable and low-cost synthetic route. The strategy of energetic coordination compounds (ECCs), which enables the fine-tuning of the optical and energetic properties through easy change of the building blocks (metal, anion and ligand) has proved once again its suitability in the difficult and challenging research area of lead-free primary explosives. The synthesis of the metal(II) perchlorate coordination compounds based on 2-amino-5*H*-tetrazole were highly dependent on the reaction conditions like stoichiometry or solvent system and yielded either aqua complexes or co-crystallized species. Laser

initiation experiments executed with NIR light at a wavelength of 915 nm showed fast deflagration-to-detonation transitions at extremely low energy thresholds for most of the coordination compounds and destroyed large parts of the laser setup due to the destructive power of the complexes. The initiation capability toward pentaerythritol tetranitrate (PETN) filled copper shell detonators was tested for several selected complexes (hot plate and hot needle experiments) and demonstrated the enormous potential of the synthesized complexes as lead-free primary explosive replacements. Interestingly also the nitrate complex 9 was able to act as a really detonating primary explosive which is caused by the highly endothermic 1-aminotetrazole ligand.

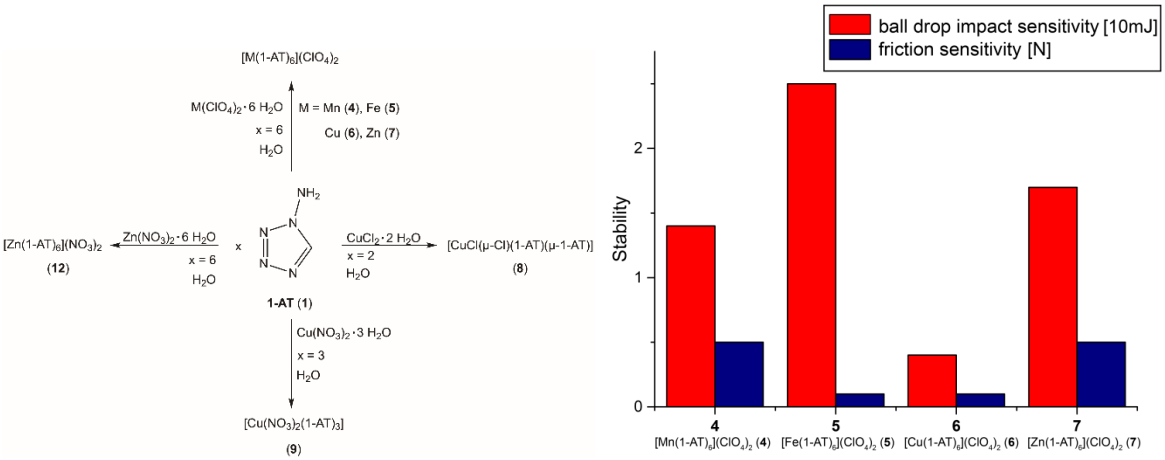


Figure 24. *Left: Synthesis of selected transition metal(II) complexes based on 1-amino-5H-tetrazole (1-AT) as ligand. Right: Comparison of the ball drop impact and friction sensitivities of the metal(II) 1-AT perchlorates.*

Increasing carbon chain length and azido-derivatives (Appendix 10 Appendix 15 & Appendix 29)

It could be demonstrated that the carbon chain length of the ligand in monosubstituted tetrazoles shows an tremendous influence on the final complexes. This could be shown on the three ligands 1-methyl-5*H*-tetrazole, 1-ethyl-5*H*-tetrazole and 1-propyl-5*H*-tetrazole but more exciting on the azido functionalized ligands 1-azidomethyl-5*H*-tetrazole (Appendix 29), azidoethyl-5*H*-tetrazole (Appendix 10) and azidopropyl-5*H*-tetrazole (Appendix 15) (Figure 25). Latter three were all new, so also their complexes. Especially the exploration of the synthesis of 1-azidomethyl-5*H*-tetrazole (AzMT), which took more than two years, was very challenging. This ligand not only shows the highest heat of formation but also the highest sensitivities. All resulting complexes were observed to show extreme sensitivity values. While the 2-azidoethyl ligand showed balanced properties (performance vs. sensitivities) the azido-propyl ligand can be used for the formation of low sensitive ECCs which are possible candidates for future laser explosive applications, avoiding the use of lead-containing and very dangerous primary explosives.

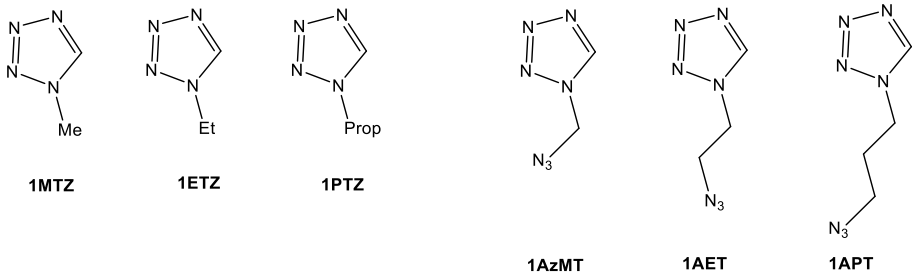


Figure 25 *1-methyl-5H-tetrazole, 1-ethyl-5H-tetrazole, 1-propyl-5H-tetrazole, 1-azidomethyl-5H-tetrazole, 1-azidoethyl-5H-tetrazole and 1-azidopropyl-5H-tetrazole*

Metal complexes with different *N*-cycloalkyl-substituted tetrazoles (Appendix 24)
Three ligands, 1-cyclopropyl-5*H*-tetrazole (C_3tz), 1-cyclobutyl-5*H*-tetrazole (C_4tz), and 1-cyclo-pentyl-5*H*-tetrazole (C_5tz), were synthesized. In order to tune the energetic properties of new energetic coordination compounds, the ligands were incorporated in 19 complexes based on various central metal atoms (Cu^{2+}, Fe^{2+}, Mn^{2+}, Zn^{2+}) and a variety of anions, such as nitrates, azides, and (per)chlorates. Compared to the open chain ligand, 1-propyl-5*H*-tetrazole, the C_3tz-based complexes show increased energetic properties while at the same time similar thermal stabilities. These results prove the benefits of cycloalkyl-substituted tetrazole ligands with higher ring strain and their ability to adjust the properties of the resulting complexes. Furthermore, a new iron(ii) SCO complex was synthesized and investigated with regard to the correlation between the spin-state change of a transition metal complex and its crystal structure. At $T_{1/2}$ = 172 K, an HS-LS spin-crossover transition could be observed accompanied by a visible color change from violet to colorless. The successful characterization of this ECC revealed an interesting candidate for future SCO research, and it was possible to determine the crystal structure of both the HS and the LS species.

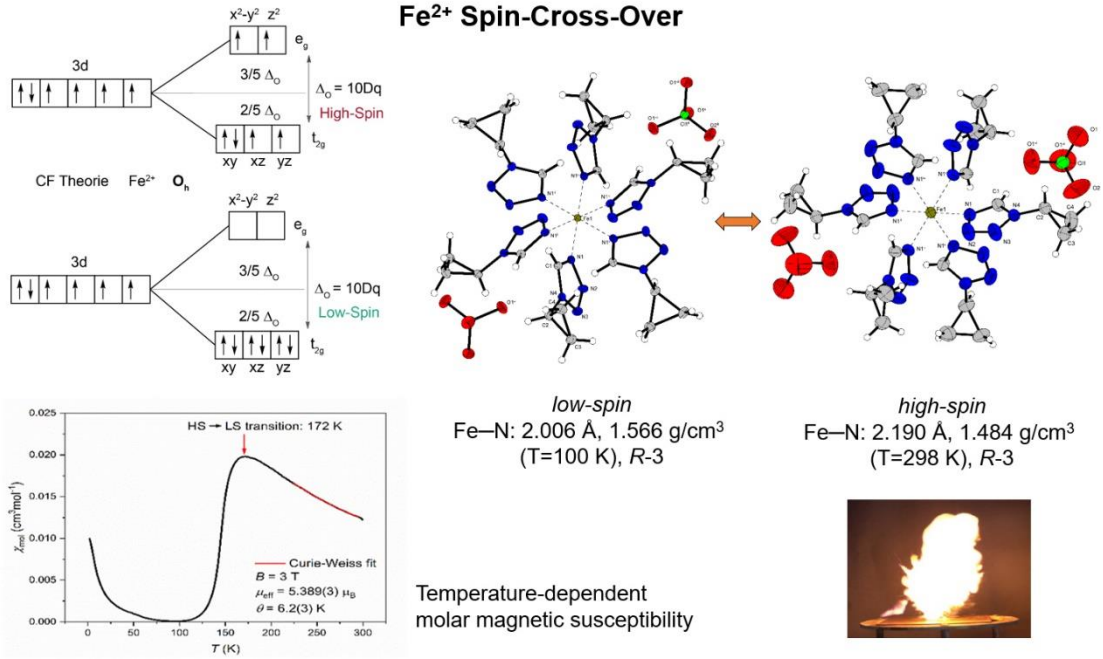


Figure 26. *Fe^{2+} Spin-Cross-Over in hexakis-(1-cyclopropyl)-tetrazole copper(II) perchlorate $[Cu(C_3Tz)_6](ClO_4)_2$.*

Comparison of 1-vinyl-5*H*-tetrazole and 1-allyl-5*H*-tetrazole as ligands in ECCs (Appendix 34)
The goal of the present study has been the preparation of the nitrogen-rich neutral ligands 1-VTZ and 1-ATZ (**2**) and their incorporation into ECCs aiming for green primary explosives capable of replacing LA and LS. Of particular interest was the investigation of the influence of the alkenyl chain lengthening by comparing analogous ECCs based on 1-VTZ and 1-ATZ Besides, the influence of the increased endothermicity by introducing an unsaturated C—C bond (1-ETZ *vs.* 1-VTZ and 1-PTZ *vs.* 1-ATZ) is discussed. Lengthening of the alkenyl chain leads to increased thermal stability (1-VTZ: 173 °C (T_{dec}), 1-ATZ: 207 °C (T_{dec}) and decreased impact sensitivity (1-VTZ: 15 J, 1-ATZ: > 40J) of the uncoordinated ligands. For the first time, it was possible to obtain a single crystal structure of 1-VTZ. In all cases, the introduction of an additional carbon atom increased the thermal stability and decreased the complex sensitivity toward various mechanical stimuli. Furthermore, the synthesized ligands 1-VTZ (**1**) and 1-ATZ (**2**) and their ECCs are put in relation to already published *N*1-substituted C_2-derived and C_3-derived tetrazole-based ECCs, respectively. Comparison of $[Cu(1\text{-}VTZ)_6](ClO_4)_2$ with the literature known $[Cu(1\text{-}ETZ)_6](ClO_4)_2$ proves that the introduction of an unsaturated bond leads to more sensitive and less thermally stable ECCs. The same observation is made in the case of $[Cu(1\text{-}ATZ)_6](ClO_4)_2$ (**11**) and $[Cu(1\text{-}PTZ)_6](ClO_4)_2$.

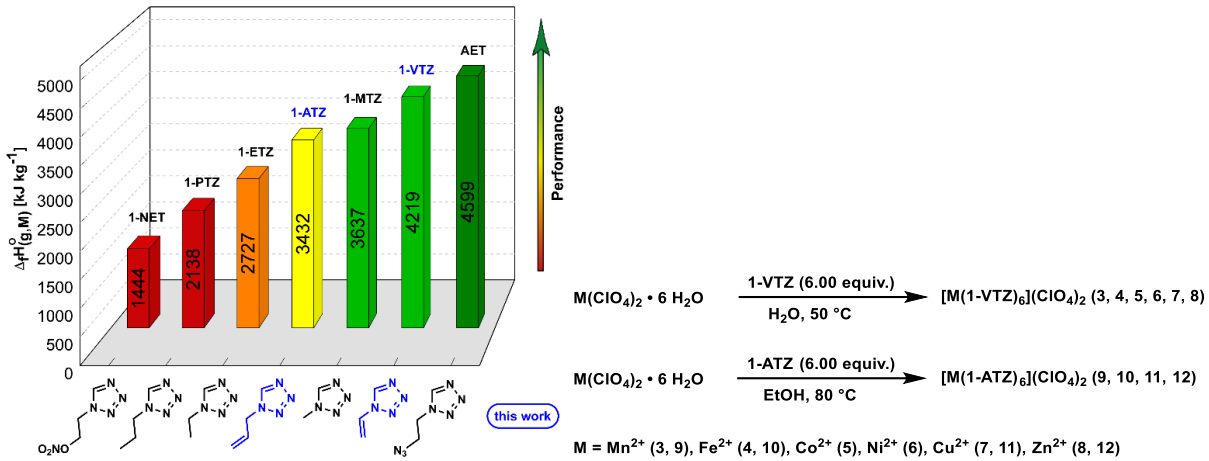
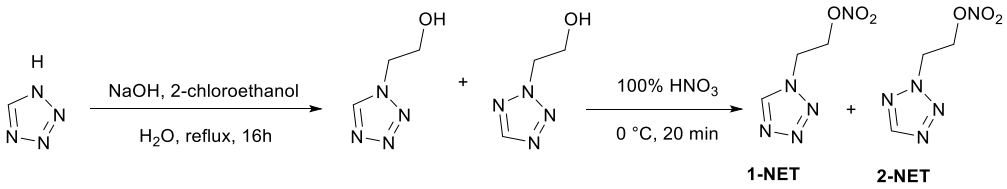


Figure 27. *Left: Comparison of the calculated gas-phase enthalpies of formation for various monotetrazole derivatives. Right: Selected reactions towards the corresponding ECCs.*

Nitratoethyl-tetrazoles, 1-nitratomethyl-tetrazole, and 1-nitromethyl-tetrazole as ligands (Appendix 25, Appendix 31 & Appendix 32)



Scheme 9. *Synthesis of 1-NET (1-nitratoethyl-5H-tetrazole) and 2-NET (2-nitratoethyl-5H-tetrazole).*

The tetrazole derivatives were subsequently used for the preparation of 22 different metal (Mn, Cu, Zn, and Ag) complexes. Only acetonitrile and water were used as green solvents, with both the ligands and the resulting ECCs exhibiting a desirable poor solubility in water. Especially the copper (II) nitrate complex $[Cu(1\text{-}NET)_3(NO_3)_2]$ (196 °C) and the trinitrophenolate based complexes $[Cu(1\text{-}NET)_2(PA)_2]$ (197 °C) and $[Cu(1\text{-}NET)_2(TNR)]$ (195°C) showed very good thermal stabilities, which are outstanding especially for organic nitrates. The improved oxygen balance due to this functional group, as well as the deflagration reactions of the compounds during hot plate and hot needle tests, reveal that these compounds can be considered as burn rate catalysts like basic copper nitrate (BCN). However, due to their energetic properties, they simultaneously improve the performance of the mixture. The laser ignition experiments showed that non-classical routes of initiation are also possible for the majority of these additives. However, for classical use as detonating primary explosives, the overall performance is too low. Therefore it was suggested to synthesize the nitratomethy-derivatives.

The synthesis of 1-(nitratomethyl)-5*H*-tetrazole (1-NAMT) was possible by the nitration of the literature known isomeric mixture of 1- and 2-(hydroxymethyl)-5*H*-tetrazole with acetyl nitrate in moderate yield (21 %) (Scheme 10). Differential thermal analysis observed a rather low thermal stability of the 1-NAMT ligand (119 °C) (lowest value of all ligands investigated). BAM sensitivity measurements revealed a high impact (<1 J) and friction (9 N) sensitivity, both in the range of typical primary explosives. 1-NAMT was used as ligand for the formation of seven energetic coordination compounds of copper(II) chlorate, perchlorate, nitrate, trinitro phloroglucinolate, styphnate, picrate and trinitro-orcinolate. For all ECCs an extremely high impact sensitivity of <1 – 2 J was observed, while the chlorate, perchlorate and nitrate compounds exhibited increased friction sensitivities (0.4–5 N) compared to pure 1-NAMT. Interestingly, the formation of ECCs containing the trinitrophenolate anions led to a drastic increase (> 50°C) of the thermal stability of 1-NAMT. The compounds are less suitable

than the corresponding 1-nitratoethyl ones, discussed before, because of their hard accessibility, high sensitivities but rather worse DDT behavior.

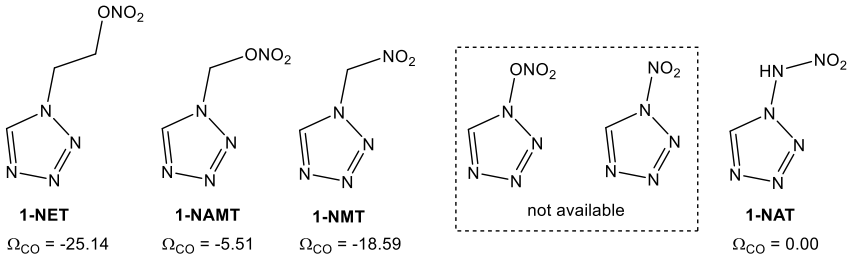
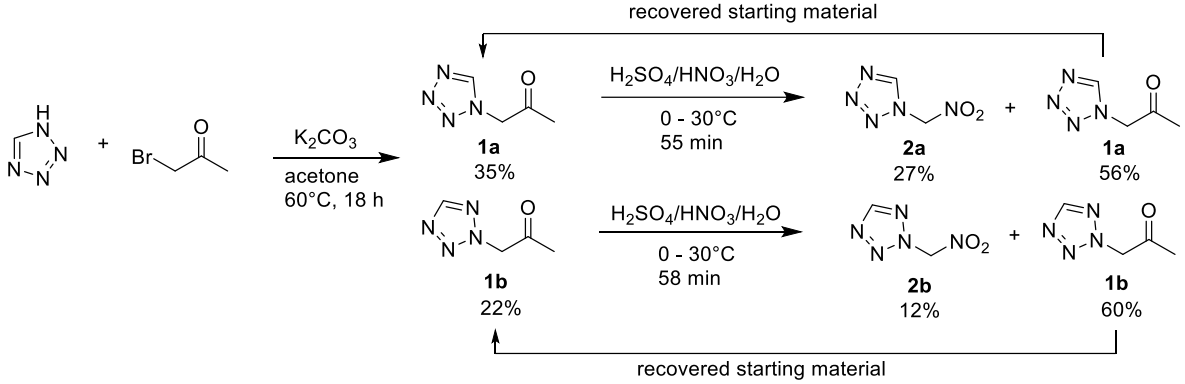


Figure 28. *Comparison of oxygen balances between selected 1-substituted-tetrazole containing a nitro moiety.*

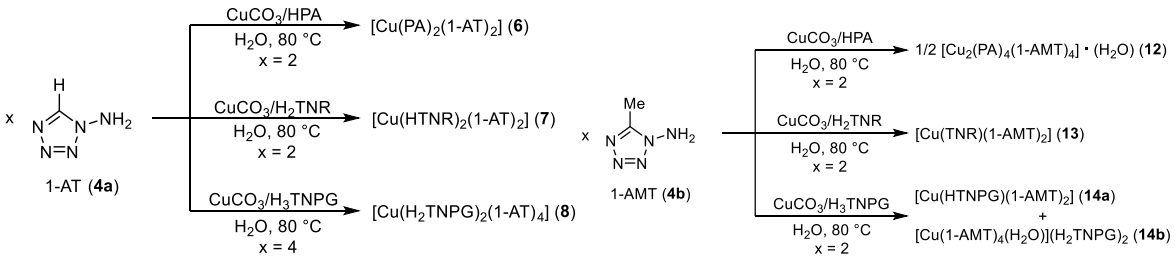
The nitrogen-rich 1-(nitromethyl)-5*H*-tetrazole (1-NMT) and 2-(nitromethyl)-5*H*-tetrazole (2-NMT) were synthesized for the first time, representing the fourth and fifth ever synthesized *N*-nitrometyl azoles. 1-NMT was applied as a ligand for energetic coordination compounds of copper(II) chlorate, nitrate, and perchlorate, as well as perchlorates of iron(II), nickel(II) and zinc(II). Like 1-NMT, the sensitivities towards impact and friction were measured, revealing a drastic increase in sensitivity compared to the pure ligand but still being significantly more stable than the ECCs based on 1-(azidomethyl)-5*H*-tetrazole and 1-(nitratomethyl)-5*H*-tetrazole.



Scheme 10. *Synthesis of 1- and 2-(nitromethyl)-5H-tetrazole (1-NMT, 2-NMT) starting from 1,5H-tetrazole and bromoacetone.*

Nitrophenolates (Appendix 12)

Meanwhile the influence of more complex anions were investigated. The use of picric acid, styphnic acid (trinitro-resorcinol) and trinitro-phloroglucinate and later trinitro-orcinolate (methyl-trinitro-resorcinate yielded ECCs with lower performance but better thermo stability. This may be a reason of lower heat of formations and arising nitro-nitro interactions. These findings were combined with the comparison of 1-amino-5*H*-tetrazole with its methylated 1-amino-5-methyl-derivative (and also the 2-subst. isomers) in Appendix 12. It could be demonstrated that 5-methyl-1/2-amino ligands tend to form complexes with higher thermal stability and lower sensitivity. The most promising compound in that study was the 1-AMT-based copper(II) styphnate (**13**).



Scheme 11. *Synthesis of ECCs based on 1-AT and 1-AMT in combination with trinitro-phenolates.*

Trinitro-orcinolate and its comparison to trinitro-resorcinate (Appendix 33)

This work has provided 17 new compounds, among which eleven were characterized by low-temperature X-ray diffraction analysis. This analysis gave an interesting insight in the coordination behavior of trinitro-orcinolate compared to the anions of styphnic acid. Surprisingly, the investigation of the physiochemical properties showed, that despite the lower enthalpy of formation, trends towards an increased impact sensitivity and lower thermal stability of the trinitro-orcinolates can be observed. The sensitivities towards friction, in contrast, seem to be lower compared to the respective styphnates. While the high sensitivities towards impact, that were observed for most trinitro-orcinolates, excludes them from application as a primary explosive, utilization as a replacement of lead styphnate or as a sensitizer in priming mixtures might be considered.

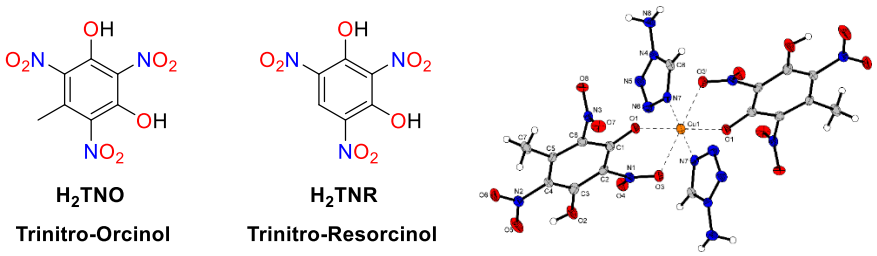
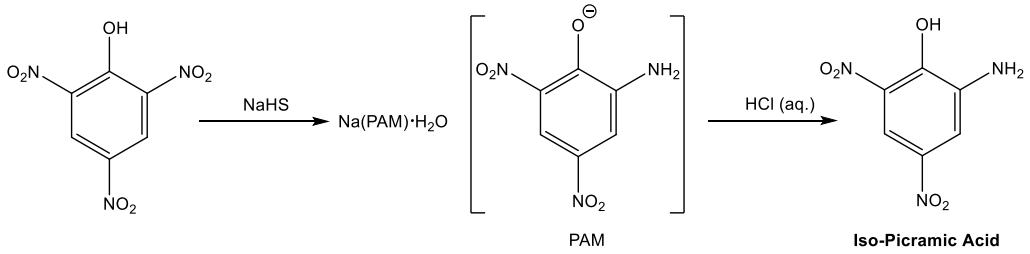


Figure 28. *Drawing of trinitro-orcinol and styphnic acid as well as the structural molecular moiety of [Cu(1-AT)$_2$(HTNO)$_2$] with the typical coordination behavior.*

Picramic acid (HPAM) and iso-picramic acid (Appendix 14 & Appendix 28)

Picramic acid (HPAM) was also investigated as a potential building block in ECCs. Unfortunately salts of picramic acids are very low soluble. 14 salts were published, amongst others also Zn(PAM)$_2$·2H$_2$O and Cu(PAM)$_2$·2H$_2$O, however, no classical ECCs with a tetrazole ligand, could be synthesized.



Scheme 12. *Synthesis of sodium picramate monohydrate and representation of the PAM anion.*

Also, the iso-picramic acid was synthesized and investigated (Appendix 28). Because iso-picramic acid shows a zwitterionic structure, most of the reactions to transform the -NH$_3$ group failed and oftentimes iso-DDNP was obtained as the product. The amine could successfully converted to a 5*H*-tetrazole substituent which shows very similar energetic parameters. However, the compound could not be used as a ligand for classical ECCs. Moreover some selected ionic compounds of iso-picramic acid were synthesized, but we could not manage to include the anion in copper(II) based ECCs.

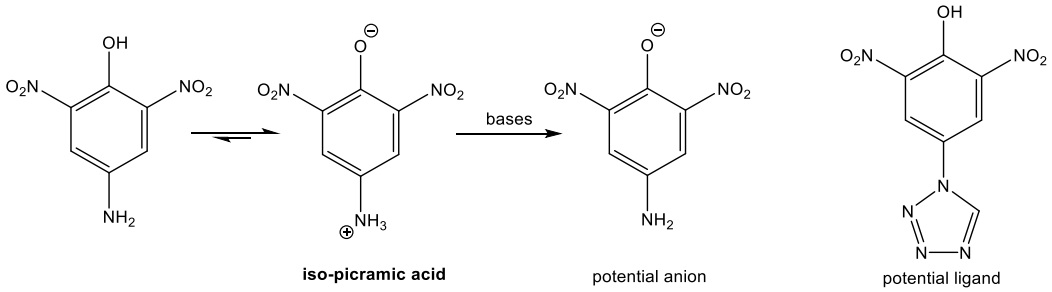


Figure 29. *Formula of iso-picramic acid, iso-picramate and 2,4-dinitro-4-tetrazol-1-yl-phenole.*

Dicyanamides, Nitro-cyanamide and Dinitramide (Appendix 16, Appendix 23 & Appendix 26)
Figure 30 shows the dicyanamide, nitro-cyanamide and dinitramide anions which were applied for new ECCs.

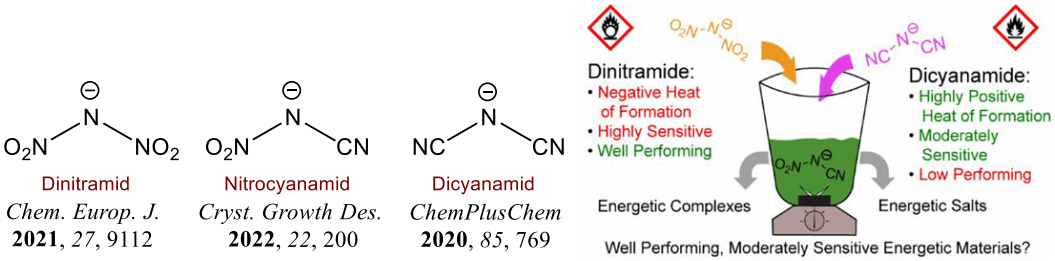


Figure 30. *Amides with the electron-withdrawing NO_2 and CN groups and the TOC graphic of the nitrocyanamide paper which summarizes euphemized the results from these anions.*

While NO_2 groups are known to increase the energetic properties due to a better oxygen-balance, cyano groups are known to significantly increase the heat of formation. Another difference is the ability to participate in coordination. Calculation of the gas-phase enthalpy of different mono-negatively charged anions is shown in Figure 31. In contrast to dinitramide (−1195 kJ/kg), the dicyanamide is formed strongly endothermic (1852 kJ/kg).

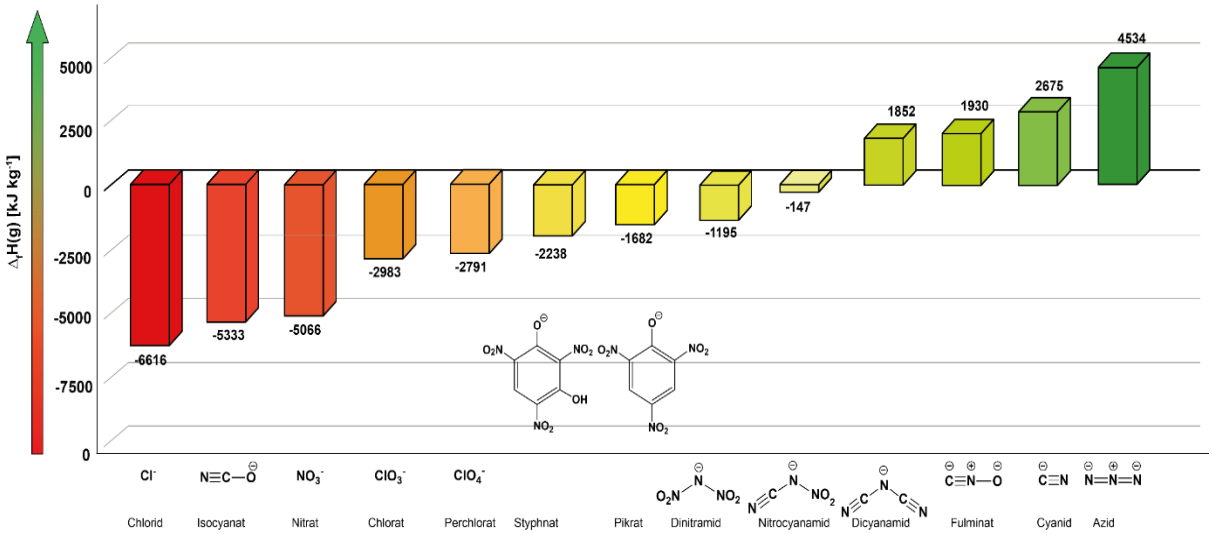


Figure 31. *Calculated (CBS4M & atomization method) gas phase heat of formation of selected anions (mono-negativ charged) within this thesis.*

The coordination participation of the anions is shown in the following Figure 32 on the ECCs involving 1-MTZ and 1,1-dte.

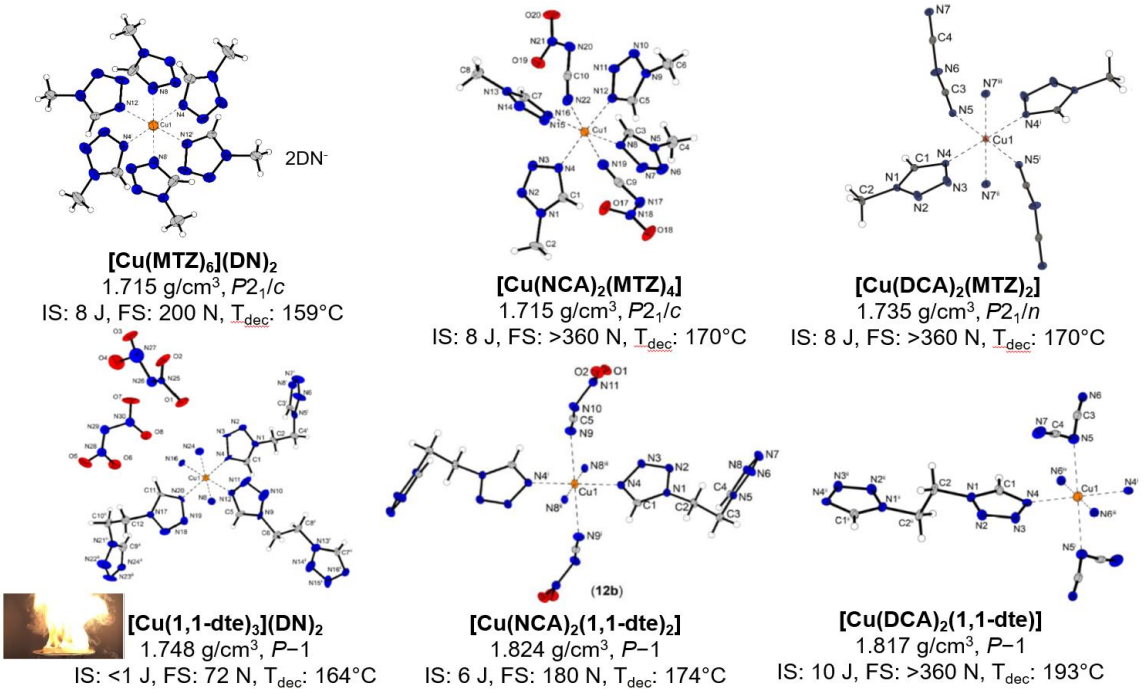
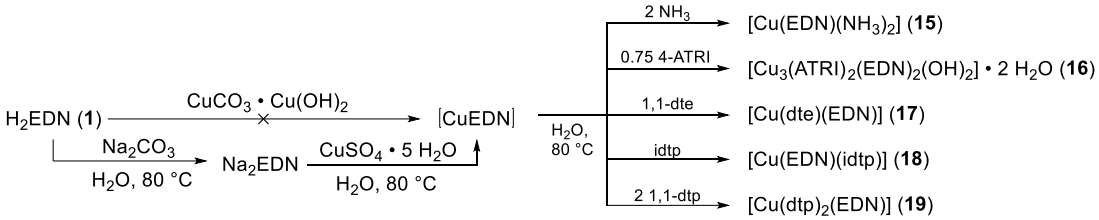


Figure 32. *Coordination behavior of the DN, NCA and DCA anions. The dinitramide anion does not participate in copper(II) coordination. In the case of nitro-cyanamide the axial positions are taken from the NC-group, while in the case of dicyanamide four positions are blocked by the NC groups.*

Ethylenedinitramine as an anion in ECCs (Appendix 22)

Ethylenedinitramine (H_2EDN) was prepared in a simple manner and with a high overall yield by direct nitration of 2-imidazolidinone using 100% HNO_3 at 0 °C and subsequent hydrolysis in water at 100 °C. The versatility of H_2EDN allows its application as starting material for a broad range of different materials. H_2EDN was successfully applied in the concept of energetic coordination compounds (ECCs) resulting in five copper(II) and two silver(I) complexes. The prepared ECCs show slower DDT and are more interesting as laser-ignitable primary explosives than as classical detonants.



Scheme 13. *In situ preparation of copper(II) ethylenedinitramide and preparation of some copper(II) based ECCs.*

Copper(II) azide complexes (Appendix 17 & Appendix 27)

Probably the most useful complexes for replacement of lead(II) azide were synthesized by complexation of copper(II) azide. This group of new complexes were also filed as a patent[82], which was also the fundament of two industrial projects involving our start-up EMTO GmbH. The obtained compounds are mostly very low soluble in water and show fast DDT. Within these experiments the formation of round-shaped flowable materials with manageable sensitivities was most challenging. This was accomplished by the (i) strong control of the order of addition (rate and stirring controlled) and (ii) the addition of binder and coagulation reagents such as dextrin, polysorbates or carboxmethylcellulose. Simple examples are shown in Figure 33.

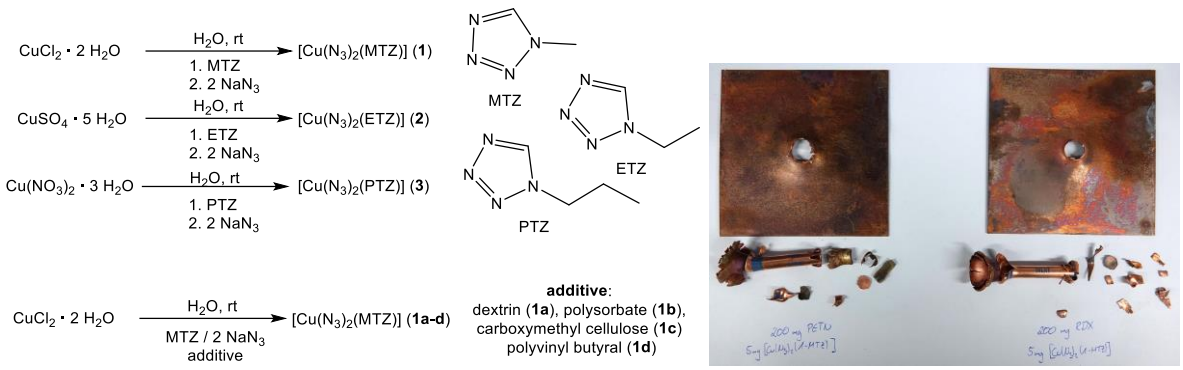


Figure 33. *Left: Syntheses of pure copper(II) azide complexes with 1-MTZ, 1-ETZ and 1-PTZ ligands and phlegmatized compounds. Right: PETN and RDX initiation test results using only 5 mg of [Cu(N3)2(1MTZ)].*

Complexes of silver fulminate (Appendix 19)

We successfully synthesized seven new silver fulminate complexes based on different neutral nitrogen-rich azole ligands. All ECCs show fascinating coordination behavior with cluster formation and argentophilic interactions close to the shortest reported Ag–Ag distances. The resulting compounds possess manageable sensitivities, and ligands with bridging character increased the thermal stability up to 215 °C. The possible synthesis of the complex $[Ag_4(CNO)_4(2,2\text{-dtp})]$ in a one-pot reaction from elemental silver, ethanol, nitric acid, and ligand in high yields avoids the isolation of pure SF and opens the field to a safe synthesis of SF complexes, which could be used as a potential replacement for LS.

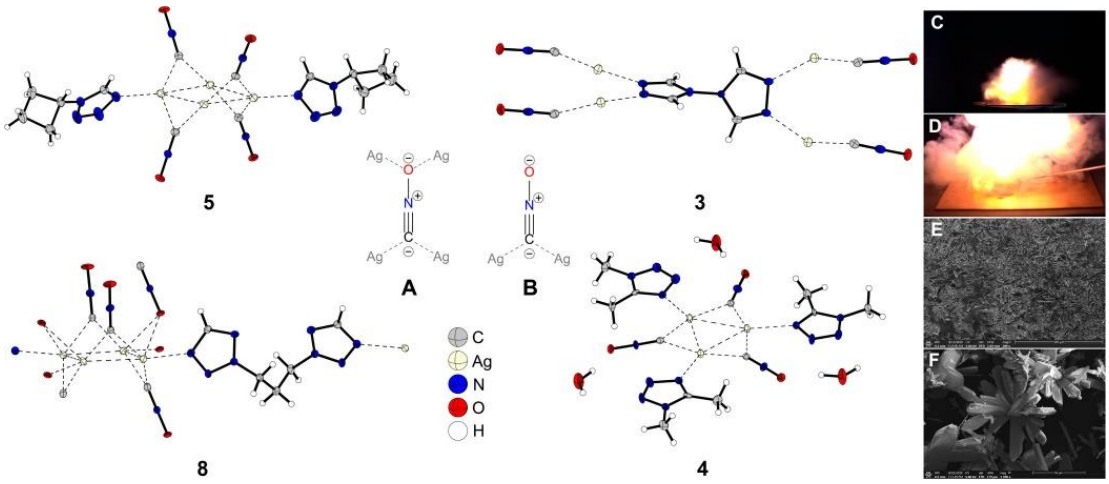


Figure 34. *Different bridging modes A and B of the fulminate anion and molecular units of silver fulminate complexes **3–5** as well as the extended molecular unit of **8**. Ellipsoids are set to the 50% probability level. Physicochemical properties: (C) detonation of the ECC **3** during the hot plate test; (D) deflagration of 3 during the hot needle test; (E) SEM image of decomposed AgCNO (200× enlargement); (F) SEM image of complex **8** (1200× enlargement).*

Ball drop impact tester (BIT-132) (Appendix 13)

The BIT-132 Ball drop impact tester from OZM Research was used to evaluate the sensitivity of more than 16 well-known, sensitive energetic materials. In addition, the BAM standard methods were used to determine sensitivities for all compounds. As shown by the examples of lead styphnate and lead azide, it is impossible to correlate the most recent BIT results with the data obtained using the BAM drop hammer (1 of 6). This is a result of the different test set-ups and therefore different ignition types. A closer correlation between the sensitivity to friction and ball drop impact sensitivity was observed. It is assumed that a combination of friction and impact is exerted on the substance by the spin of a falling steel ball. Furthermore, it was found that there is a strong coherence between the particle size and the

sensitivity towards BDIS of the compounds. Smaller particle sizes clearly showed more sensitivity, which is in strong contradiction to earlier assumptions that larger crystal sizes lead to drastically higher sensitivities. For the well-known explosives PETN, RDX, FOX-7 and TKX-50 no ignitions could be observed at certain grain sizes.
So the current BIT has limited suitability for characterization of secondary explosives. However, the device is perfectly suitable for testing primary explosives. Interestingly within our test series HMTD showed the highest sensitivity values (Figure 35).

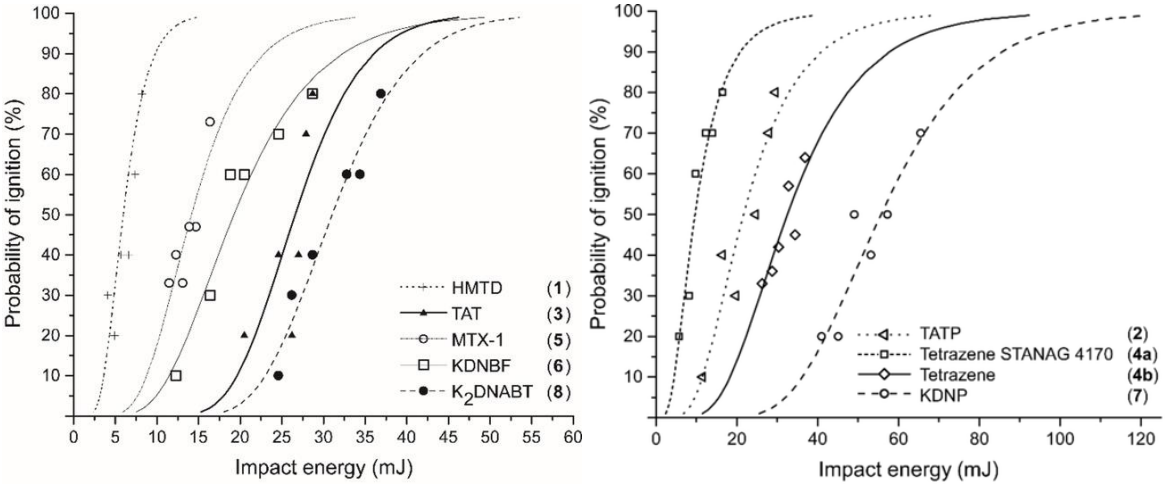


Figure 35. *Probit curves of prominent explosives measured at the BIT-132 from OZM.*

5. Outlook

Based on the findings, during the last years, a couple of valuable strategies in order to prepare the next generation of *green, safe and high performing ECCs* could be developed. Since these materials have enormous potential for being applied in the future in numerous devices, of course, not a single target compound will be presented here. We would like to continue and research towards all the building blocks of the ECCs: a) new ligands, b) new metals, c) new anions.

A wish list of new nitrogen- (and oxygen)-rich ligands is presented in Figure 36. Some of the proposed ligands are under current investigation, probably some of them will never be successfully prepared. Although the compounds are small and simple, their preparation is extremely challenging and needs strong synthetical skills.

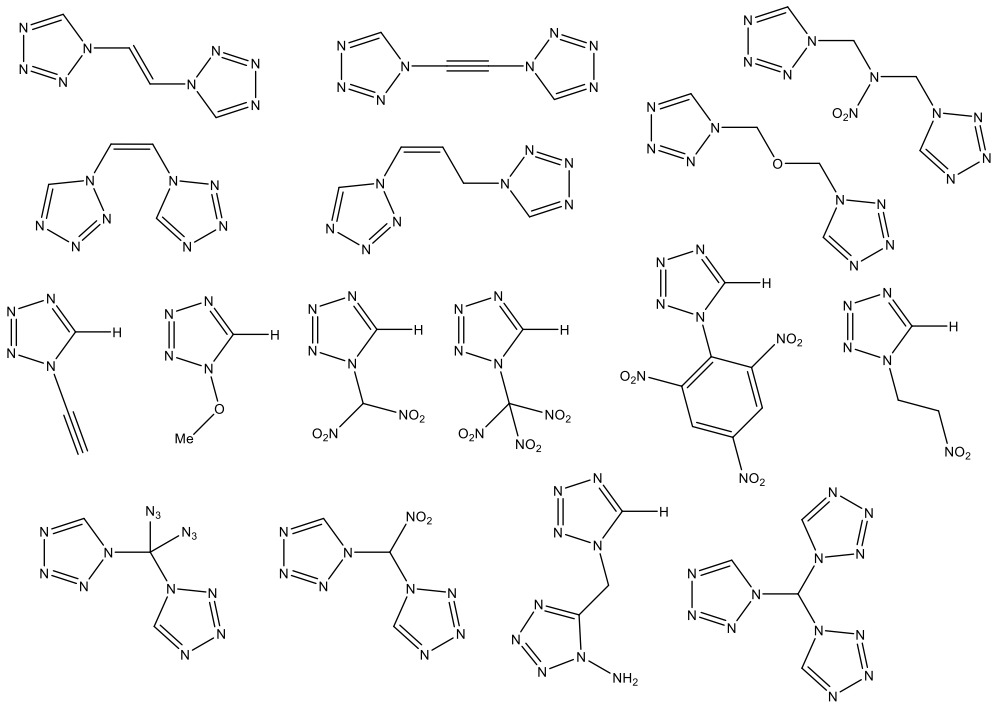


Figure 36. *New proposed ligands for future green, safe and high-performing ECCs.*

In addition, we would like to extend this chemistry to further metals and oxidation states. Copper(I) was not really in the focus yet. With respect to toxicity, bismuth(III) is described to be a valuable candidate. For academic reasons also further, noble transition metals such as gold, platinum, iridium, palladium and rhenium would be desirable in order to synthesize the "most noble explosive on earth". Palladium is described to form a hydrolytically non-water-soluble azide which could be a platform to further investigate.
Ignition by magnetic stimuli could also be eligible. Also, the use of low-energy photodiodes as an ignition method is supposed. For that reason, ligands with a different configuration should be synthesized to use e.g. the trans/cis transition for exothermic decomposition of the ECCs.

Regarding the anions, it is proposed to focus e.g. on acetylides (C_2^{2-} and HC_2^-) as anions with extremely high positive heats of formation (Figure 37). In addition, amino-nitro-phenolates could be a class of anions that form extremely temperature-stable ECCs. Not only as a contribution to the outstanding work of Prof. Wolfgang Beck at the LMU, the chemistry of fulminates (CNO^-) should be continued. Fulminate complexes of e.g. zinc(II) and copper (I/II) would be highly interesting and energetic.

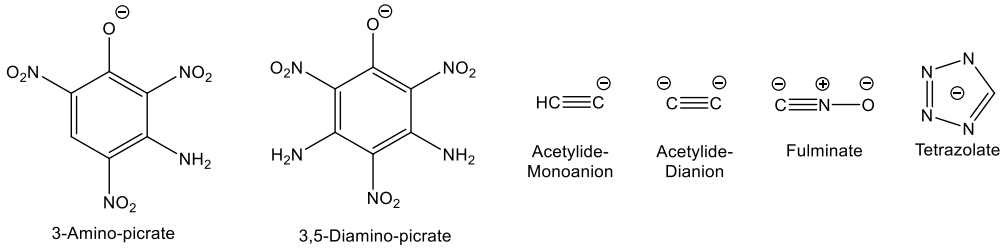


Figure 37. *Anions of future implementation in ECCs.*

So there exist numerous possibilities to prepare new ECCs in the future. We also would like to investigate the properties of heteroleptic (two or more different ligands at one metal center) and mixed anionic (containing two different anion, e.g. picrate + azide) complexes. However, not only the synthesis of new materials will be in the focus, also the modification of crystals (habit, size, flowability) and complying with the concepts of green chemistry is of constantly increasing interest.

6. References

1 E. Riedel, C. Janiak, *Anorganische Chemie*, de Gruyter Studium, 10th ed., **2022**.

2 E. Riedel, R. Alsfasser, C. Janiak, T. M. Klapötke, *Moderne Anorganische Chemie*, de Gryter, 3th ed., **2007**.

3 A. F. Holleman, N. Wiberg, *Anorganische Chemie*, Band 1&2, de Gruyter, **2016**

4 C. E. Mortimer, U. Müller, *Chemie: Das Basiswissen der Chemie*, Thieme, 13th edn, **2019**.

5 C. E. Houscroft, A. G. Sharpe, *Inorganic Chemistry*, Pearson, 5th edn, **2018**.

6 C. J. Jones, *d- and f-Block Chemistry*, *in Basic Concepts in Chemistry*, Wiley-Interscience, **2001**. https://doi.org/10.1039/9781847550682

7 https://edoc.ub.uni-muenchen.de/ (31.01.2023)

8 J. P. Agrawal, *High Energy Materials: Propellants, Explosives and Pyrotechnics*, Wiley-VCH, **2010**.

9 E.-C. Koch, *High Explosives, Propellants, Pyrotechnics*, 2nd edition, De Gruyter, **2021**.

10 T. M. Klapötke, *Chemistry of High-Energy Materials*, 5th edition, De Gruyter, **2022**.

11 https://en.wikipedia.org/wiki/Explosive (18.11.2022).

12 N. Fischer, D. Fischer, T. M. Klapötke, D. G. Piercey, J. Stierstorfer, *J. Mater. Chem.* **2012**, *22*, 20418–20422.

13 https://www.edrmagazine.eu/eurenco-looks-at-new-future-energetic-materiel (18.11.2022).

14 R. Matyás, J. Pachman, *Primary Explosives*, Springer, Springer Heidelberg New York Dordrecht London, **2013**, DOI 10.1007/978-3-642-28436-6.

15 Recommendations on the Transport of Dangerous Goods (ST/SG/AC.10/11/Rev.7)

16 M. Lommel, Bachelor thesis, Ludwig Maximilian University Munich (LMU), 2018.

17 R. Matyáš, J. Pachman, Chapter Fulminates, in Primary Explosives, Springer, 2012, pp 37–70

18 M. L. Gettings, M. T. Thoenen, E. F. C. Byrd, J. J. Sabatini, M. Zeller, D. G. Piercey, *Chem. Eur. J.* **2020**, *26*, 14530–14535

19 T.-Ai D. Nguyen, Ja. M. Veauthier, G. F. Angles-Tamayo, D. E. Chavez, E. Lapsheva, T. W. Myers, T. R. Nelson, E. J. Schelter, *J. Am. Chem. Soc.* **2020**, *142*, 4842−4851

20 N. Mehta, K. Oyler, G. Cheng, A. Shah, J. Marin, K. Yee, Primary Explosives, *Z. Anorg. Allg. Chem.* **2014**, *640*, 1309–1313.

21 https://www.sandia.gov/working-with-sandia/technology-deployment-centers/explosive-components-facility-ecf/ (18.11.2022).

22 J. W. Fronabarger, M. D. Williams, W. B. Sanborn, D. A. Parrish, M. Bichay, *Propellants, Explosives, Pyrotechnics*, **2011**, *36*, 459-470.

23 M. Comet, C. Martin, M. Klaumünzer, F. Schnell, D. Spitzer, *Appl. Phys. Lett.* **2015**, *107*, 243108.

24 A) Dan Chen, HongweiYang, Zhenxin Yi, Hualin Xiong, Lin Zhang, Shunguan Zhu. Guangbin Cheng, *Angew. Chem. Int. Ed.* **2018**, *57*, 2081–2084. b) C. Lei, H. Yang, G. Cheng, *ACS Appl. Mater. Interfaces* **2022**, *14*, 39091−39097,

25 http://www.ozm.cz (31.01.2023).

26 M. A. Ilyushin, A. V. Smirnov, A. A. Kotomin, I. V. Tselinskii, *Energ. Mater. 1994*, 2, 16–20.

27 Н.Ю. Сугак, С.В. Мочалов, РАСЧЕТ ВЗРЫВЧАТЫХ ХАРАКТЕРИСТИК ВВ, БТИ АлтГТУ, Бийск, 2013.

28 http://emto.eu/software/ecc-calculator/ (31.01.2023).

29 R. Schirra, *privat communication*, EMACON-RS, Dr. Rainer Schirra, Lohmar / Germany

30 R. Matyás, J. Selesovsky , T. Musil, *Journal of Hazardous Materials*, **2012**, *213–214*, 236– 241

31 NETZSCH Kinetics Neo software, version 2.5.0.1, 2021.

32 https://enamine.net/ (31.01.2023).

33 M. H. H. Wurzenberger, D. Shem-Tov, J. Stierstorfer, *Chapter 4: Laser Ignition of Energetic Transition Metal Complexes*, in M. Gozin, L. L. Fershtat, *Nitrogen-Rich Energetic Material*, Wiley-VCH, **2023**.

34 T. H. Maiman, Stimulated Optical Radiation in Ruby. *Nature* **1960**, *187*, 492–494.

35 A. A. Brish, I. A. Galeeva, B. N. Zaitsev, E. A. Sbimev, L. V. Tararinstev, *Fiz. Goreniya Vzryva* **1966**, *2*, 132–133.

36 L. C. Yang, V. J. Menichelli, *Appl. Phys. Lett.* **1971**, *19*, 473–475.

37 S. R. Ahmad, M. Cartwright in *Laser Ignition of Energetic Materials*, John Wiley & Sons, Ltd, Chichester, **2015**.

38 Y. Tverjanovich, A. Tverjanovich, A. Averyanov, M. Panov, M. Ilyshin, M. Balmakov in *Progress in Photon Science – Recent Advances*, Springer Nature Switzerland, Cham, **2019**.

39 M. W. Leeuw, A. J. T. Rooijers, A. C. van der Steen in *Advances in Chemical Reaction Dynamics*, D. Reidel Publishing Company, Dordrecht, **1986**.

40 H. Moulard (Institut Franco-Allemand de Recherches de Saint-Louis), EP 1067357B1, France, **1999**.

41 M. Joas, U. Deisenroth (IBD Deisenroth Eng GmbH), DE 102016120539A1, Germany, **2016**.

42 V. P. Sinditskii, V. V. Serushkin, *Def. Sci. J.* **1996**, *46*, 371–383.

43 S. C. Kunz, F. J. Salas, *Proceedings of the 13th International Pyrotechnics Seminar* **1988**, 505–523.

44 J. A. Merson, F. J. Salas, J. G. Harlan, *Proceedings of the 19th International Pyrotechnics Seminar* **1994**, 191–206.

45 A. Y. Zhilin, M. A. Ilyushin, I. V. Tselinskii, A. S. Brykov, *Russ. J. Appl. Chem.* **2001**, *74*, 99–102.

46 Q. Sun, X. Li, Q. Lin, M. Lu, *J. Mater. Chem. A* **2019**, *7*, 4611–4618.

47 J.-G. Xu, S.-J. Lin, X.-Z. Li, H.-F. Wu, J. Lu, W.-F. Wang, J. Chen, F.-K. Zheng, G.-C. Guo, *Chem. Eng. J.* **2020**, *390*, 124587.

48 G. Steinhauser, J. Evers, S. Jakob, T. M. Klapötke, G. Oehlinger, *Gold Bull.* **2008**, *41*, 305–317.

49 T. M. Klapötke, B. Krumm, J.-C. Galvez-Ruiz, H. Nöth, *Inorg. Chem.* **2005**, *44*, 9625–9627.

50 M. A. Ilyushin, I. V. Tselinsky, I. A. Ugryumov, A. Y. Zhilin, A. S. Kozlov, *6th New Trends in Research of Energetic Materials Seminar* **2003**, 146–152.

51 D. E. Chavez, S. K. Hanson, R. J. Scharff, J. M. Veauthier, T. M. Myers (Los Alamos National Security LLC), US 20160031767 A1, USA, **2015**.

52 M. H. H. Wurzenberger, M. S. Gruhne, M. Lommel, V. Braun, N. Szimhardt, J. Stierstorfer, *Inorg. Chem.* **2020**, *59*, 17875–17879.

53 M. H. H. Wurzenberger, M. Lommel, M. S. Gruhne, N. Szimhardt, J. Stierstorfer, *Angew. Chem. Int. Ed.* **2020**, *59*, 12367–12370.

54 V. M. Lisitsyn, V. N. Tsipilev, G. Damamme, D. Malis, *Combust. Explos. Shock Waves* **2011**, *47*, 591–600.

55 A. M. Renlund, P. L. Stanton, W. M. Trott, *Proceedings of the 9th International Detonation Symposium* **1989**, 1118−1127.

56 D. L. Paisley, *Proceedings of the 9th International Detonation Symposium* **1989**, 1110−1117.

57 B. P. Aduev, D. R. Nurmukhametov, R. I. Furega, A. A. Zvekov, A. V. Kalenskii, *Russ. J. Phys. Chem. B* **2013**, *7*, 453−456.

58 H. Scholles, R. Schirra, H. Zoellner, *Proceeding of the 42nd International Pyrotechnics Seminar* **2016**, 422–428.

59 A. Y. Zhilin, M. A. Ilyushin, I. V. Tselinskii, A. S. Kozlov, I. S. Lisker, *Russ. J. Appl. Chem.* **2003**, *76*, 572–576.

60 S. I. Gerasimov, M. A. Ilyushin, V. A. Kuz'min, *Tech. Phys. Lett.* **2015**, *41*, 338–340.

61 S. I. Gerasimov, M. A. Ilyushin, I. V. Shugalei, A. V. Smirnov, Z. V. Kapitonenko, *Russ. J. Gen. Chem.* **2017**, *87*, 3156–3159.

62 https://unece.org/, (30 March 2021).

63 NATO Allied Ordnance Publication 7, 2nd ed., June, **2003**.

64 M. A. Ilyushin, I. V. Tselinsky, I. A. Bachurina, A. V. Chernay, *10th New Trends in Research of Energetic Materials Seminar* **2007**, 165–182.

65 A. V. Chernai, V. V. Sobolev, V. A. Chernai, M. A. Ilyushin, A. Dlugashek, *Combust. Explos. Shock Waves* **2003**, *39*, 335–339.

66 M. A. Ilyushin, A. A. Kotomin, S. A. Dushenok, *Russ. J. Phys. Chem. B* **2019**, *13*, 119–138.

67 A. S. Tverjanovich, A. O. Aver'yanov, M. A. Ilyshin, Yu. S. Tverjanovich, A. V. Smirnov, *Russ. J. Appl. Chem.* **2015**, *88*, 226–231.

68 M. A. Ilyushin, A. S. Tver'yanovich, Yu. S. Tver'yanovich, G. O. Abdrashitov, A. O. Aver'yanov, M. D. Bal'makov, *Glass Phys. Chem.* **2018**, *44*, 120–122.

69 A. S. Tverjanovich, G. O. Abdrashitovh, A. O. Averyanovh, M. A. Ilyshinh, A. V. Smirnovh, Yu. S. Tveryanovich, *Int. J. Energ. Mater. Chem. Propul.* **2016**, *15*, 113–122.

70 R. Danzeisen, D. L. Williams, V. Viegas, M. Dourson, S. Verberckmoes, A. Burzlaff, *Toxicol. Sci.* **2020**, *174*, 311–325.

71 A. V. Kuzmenko, A. S. Tverjanovich, M. A. Ilyushin, Yu. S. Tveryanovich, *J. Energ. Mater.* **2019**, *37*, 420–432.

72 M. A. Ilyushin, I. A. Ugryumov, V. Yu. Dolmatov, M. V. Veretennikova (Zakrytoe aktsionernoe obshchestvo "Almaznyj Tsentr"), RU 2309139C2, Russia, **2004**.

73 T. W. Myers, D. E. Chavez, S. K. Hanson, R. J. Scharff, B. L. Scott, J. M. Veauthier, R. Wu, *Inorg. Chem.* **2015**, *54*, 8077–8086.

74 A. E. Sifain, J. A. Bjorgaard, T. W. Myers, J. M. Veauthier, D. E. Chavez, O. V. Prezhdo, R. J. Scharff, S. Tretiak, *J. Phys. Chem. C* **2016**, *120*, 28762−28773.

75 T. W. Myers, K. E. Brown, D. E. Chavez, R. J. Scharff, J. M. Veauthier, *Eur. J. Inorg. Chem.* **2016**, 3178–3183.

76 T. W. Myers, J. A. Bjorgaard, K. E. Brown, D. E. Chavez, S. K. Hanson, R. J. Scharff, S. Tretiak, J. M. Veauthier, *J. Am. Chem. Soc.* **2016**, *138*, 4685–4692.

77 T. W. Myers, K. E. Brown, D. E. Chavez, R. J. Scharff, J. M. Veauthier, *Inorg. Chem.* **2017**, *56*, 2297–2303.

78 K. E. Brown, T. W. Myers, C. Snyder, S. A. Clarke, *Proceedings of the Conference of the American Physical Society Topical Group on Shock Compression of Condensed Matter* **2017**, 100008.

79 Q. Zhang, D. Chen, H. Li (Institute of Chemical Materials, China Academy of Engineering Physics), CN 112280055 A, China, **2020**.

80 T. Wang, Q. Zhang, H. Deng, L. Shang, D. Chen, Y. Li, S. Zhu, H. Li, *ACS Appl. Mater. Interfaces* **2019**, *11*, 41523−41530.

81 Q.-L. Yan, P.-J. Liu, A.-F. He, J.-K. Zhang, Y. Ma, H.-X. Hao, F.-Q. Zhao, M. Gozin, *Chem. Eng. J.* **2018**, *338*, 240−247.

82 T. M. Klapötke, J. Stierstorfer, N. Szimhardt, M. H. H. Wurzenberger, *EP 18151497.7*; application date: January 12th, **2018**.

7. Appendix

Peer Reviewed Paper published on Energetic Coordination Chemistry:

1. Coordination chemistry with 1-methyl-5*H*-tetrazole: cocrystallization, laser-ignition, lead-free primary explosives – one ligand, three goals 53

2. Methylsemicarbazide as Ligand in Late 3d Transition Metal Complexes 67

3. Copper(II) Chlorate Complexes – the Renaissance of a Forgotten and Misjudged Energetic Anion 80

4. Highly functional energetic complexes: stability tuning through coordination diversity of isomeric propyl-linked ditetrazoles 85

5. Nitrogen-Rich Copper(II) Bromate Complexes: an Exotic Class of Primary Explosives ... 99

6. Maximization of the Energy Capability Level in Transition Metal Complexes through Application of 1-Amino- and 2-Amino-5H-tetrazole Ligands 110

7. 2,2-Bis(5-tetrazolyl)propane as Ligand in Energetic 3d Transition Metal Complexes 128

8. 2-Methyl-substituted monotetrazoles in copper(II) perchlorate complexes: manipulating coordination chemistry and derived energetic properties 137

9. Potassium *N*-Nitramino-5*H*-tetrazolates - Powerful Green Primary Explosives with High Initiation Capabilities 146

10. Comparison of 1-Ethyl-5H-tetrazole and 1-Azidoethyl-5H-tetrazole as Ligands in Energetic Transition Metal Complexes 154

11. 1-AminoTriazole Transition-Metal Complexes as Laser-Ignitable and Lead-Free Primary Explosives 166

12. Synthesis and Comparison of Copper(II) Complexes with various N-Aminotetrazole Ligands Involving Trinitrophenol Anions 179

13. OZM Ball Drop Impact Tester (BIT-132) vs. BAM Standard Method-a Comparative Investigation 190

14. Salts of Picramic Acid – Nearly forgotten temperature-resistant energetic materials 198

15. Comparison of 1-Propyl-5*H*-tetrazole and 1-Azidopropyl-5*H*-tetrazole as Ligands for Laser Ignitable Complexes 209

16. Copper(II) Dicyanamide Complexes with *N*-Substituted Tetrazole Ligands – Energetic Polymers with Moderate Sensitivities 219

17. Refinement of Copper(II) Azide with 1-Alkyl-5H-tetrazoles: Adaptable Energetic Complexes 227

18. Closing the Gap: Synthesis of Three Isomeric N,N-Ditetrazolymethane Ligands and Their Coordination Proficiency in Adaptable Laser Responsive Copper(II) and Sensitive Silver(I) Complexes 232

19. Taming the Dragon: Complexation of Silver Fulminate with Nitrogen-Rich Azole Ligands 248

20. *N*-Fluoromethylated (Amino)Tetrazoles: Manipulating Thermal and Energetic Properties 254

21. 1-Amino-5-methyltetrazole in Energetic 3d Transition Metal Complexes – Ligand Design for Future Primary Explosives 264

22. Investigation of Ethylenedinitramine as a Versatile Building Block in Energetic Salts, Cocrystals, and Coordination Compounds 273

23. A Smart Access to the Dinitramide Anion – The Use of Dinitraminic Acid for the Preparation of Energetic Coordination Compounds 287

24. Tailoring the properties of 3d transition metal complexes with different N-cycloalkyl-substituted tetrazoles 300

25. Nitratoethyl-5H-tetrazoles: Improving Oxygen Balance through Application of Organic Nitrates in Energetic Coordination Compounds 310

26. Hybridization of Dinitramide and Dicyanamide: Evaluation of Nitrocyanamide in Energetic Salts and Coordination Compounds 326

27. Advancement and Stabilization of Copper(II) Azide by the Use of Triazole- and Tetrazole Ligands – Enhanced Primary Explosives 340

28. Synthesis, Characterization and Derivatives of Iso-Picramic Acid 354

29. 1-(Azidomethyl)-5H-Tetrazole: A Powerful New Ligand for Highly Energetic Coordination Compounds 365

30. 1,5-Dimethyltetrazole as a ligand in energetic 3d5 to 3d10-metal coordination compounds 378

31. 1-(Nitratomethyl)-5H-tetrazole: A Highly Sensitive Ligand with Improved Oxygen Balance for Laser-Ignitable Coordination Compounds 390

32. Energetic Coordination Compounds of late 3d metals with 1N-(Nitromethyl)-5H-tetrazole, a ligand with astonishing properties from the rare class of N-nitromethyl azoles 405

33. Trinitro-orcinolate and Trinitro-resorcinate – Sensitivity Trends in Nitroaromatic Energetic Materials 406

34. The Adjustability of Physicochemical Properties: Comparison of 1-Vinyl-5*H*-tetrazole and 1-Allyl-5*H*-tetrazole as Ligands in 3d Metal Energetic Coordination Compounds (ECC) ... 414

35. Curriculum Vitae 435

36. Bibliography 437

37. List of Lecture Activities 451

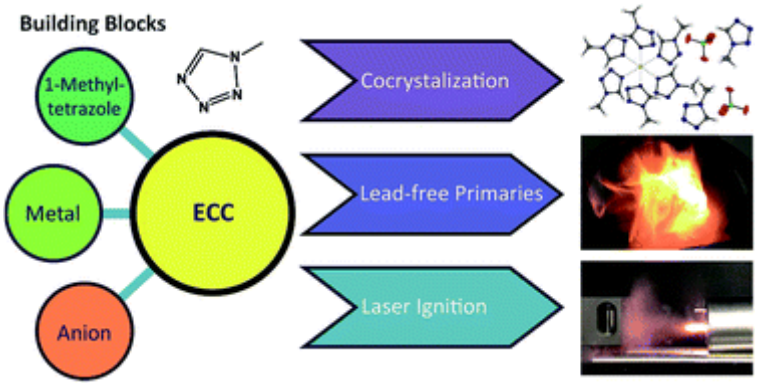
Appendix 1

Coordination chemistry with 1-methyl-5*H*-tetrazole: cocrystallization, laser-ignition, lead-free primary explosives – one ligand, three goals

N. Szimhardt, M. H. H. Wurzenberger, A. Beringer, L. J. Daumann, J. Stierstorfer

J. Mater. Chem. A, **2017**, *5*, 23753–23765

https://doi.org/10.1039/C7TA07780G



Supplementary Information:
https://www.rsc.org/suppdata/c7/ta/c7ta07780g/c7ta07780g1.pdf

Published on 19 October 2017. Downloaded by Ludwig Maximilians Universitaet Muenchen on 2/16/2022 7:53:54 AM.

Journal of Materials Chemistry A

PAPER

View Article Online
View Journal | View Issue

Check for updates

Cite this: J. Mater. Chem. A, 2017, 5, 23753

Coordination chemistry with 1-methyl-5*H*-tetrazole: cocrystallization, laser-ignition, lead-free primary explosives – one ligand, three goals†‡

Norbert Szimhardt, Maximilian H. H. Wurzenberger, Andreas Beringer, Lena J. Daumann and Jörg Stierstorfer*

Received 4th September 2017
Accepted 19th October 2017

DOI: 10.1039/c7ta07780g

rsc.li/materials-a

The synthesis and characterization of 1-methyl-5*H*-tetrazole (**1**, MTZ) from 1,5*H*-tetrazole and methyl iodide is achieved. This neutral ligand was evaluated for its use in energetic transition metal complexes. The formation of complexes is a valuable concept because of their easy synthesis and the large number of possible combinations: (i) metal, (ii) ligand, and (iii) anion. A series of 31 new complexes based on MTZ as the ligand was prepared in order to tune their optical properties and sensitivity values by using seven different metals (Mn^{2+}, Fe^{2+}, Co^{2+}, Ni^{2+}, Cu^{2+}, Zn^{2+}, and Ag^{+}) and six different anions (chloride, nitrate, perchlorate, cyanodinitromethanide, picrate, and styphnate). This variation allows tailoring of the energetic properties of the desired molecule toward *e.g.* suitable primary explosives or laser-ignitable materials. Obtained compounds were characterized by low temperature single crystal X-ray diffraction, IR spectroscopy, elemental analysis and thermal analysis (DTA, DSC and TGA). The sensitivities toward external stimuli (impact, friction and electrostatic discharge) were determined according to the Bundesamt für Materialforschung und -prüfung (BAM) standard methods. These complexes have been characterized in laser ignition experiments and as new primary explosives. UV-vis measurements of selected complexes were carried out to get a possible insight into the laser initiation mechanism. For the first time a large number of compounds with sensitivities ranging from insensitive to very sensitive were synthesized to give a wide range of new materials for different possible applications.

Introduction

Lead styphnate and lead azide were put on the candidate list of authorization (substances of very high concern, Annex XIV) for the REACH (Registration, Evaluation, Authorization and Restriction of Chemicals)[1] regulations in 2011 due to their high toxicity. Almost certainly, the two compounds will be strictly regulated or banned. Therefore; research into possible lead-free replacements is strongly needed.

The use of endothermic ligands, such as tetrazoles and triazoles, in coordination compounds has been growing over the past few years with multiple uses in the field of inorganic chemistry.[2,3] Specifically, these complexes have applications as metal–organic frameworks (MOFs),[4] spin crossover systems[5] and energetic materials.[6]

Crystalline compounds containing two or more different species – including hydrates, solvates, coordinating and non-coordinating ligands – are defined as cocrystals and have an increasing number of applications as molecular semiconductors, advanced pharmaceuticals and optical materials.[7] In the field of energetic materials, cocrystallization can be used for enhancing the density and the detonation/combustion performance or to lower the mechanical sensitivities.[8] Regarding energetic complexes, this concept has recently been described with 1,2-di(1*H*-tetrazol-5-yl)ethane as the ligand.[9] In this work, the neutral ligand itself has been used as a cocrystallized species for the first time to increase the stability of energetic complexes.

Coordination compounds of iron(II), in particular bearing alkylated tetrazole ligands like 1-methyl-5*H*-tetrazole (**1**), are some of the most investigated compounds in spin crossover systems.[10] Perchlorate and tetrafluoroborate iron(II) alkyltetrazole coordination compounds exhibited two different lattice sites for the central metals with a spin transition from high spin (hs) to low spin (ls) at a specific temperature.[11] Metastable long-lived hs and ls states on both sides can be induced through

University of Munich (LMU), Department of Chemistry, Butenandtstr. 5–13, D-81377, Germany. E-mail: jstch@cup.uni-muenchen.de; Fax: +49 89 2180 77007

† Dedicated to John W. Fronabarger on the occasion of his 90th birthday. Parts of this work were presented at the 48th International Annual Conference 2017 of the Fraunhofer ICT in Karlsruhe (Germany).

‡ Electronic supplementary information (ESI) available: X-ray diffraction; IR spectroscopy of **3**, **6–10**, **17** and **23**; DTA plots of **1–10**, **12–14**, **27** and **29–37**; thermal gravimetric analysis of **4**, **9**, **17** and **24**; column diagrams of the complexes **15–26**; hot plate and hot needle tests; laser ignition tests; UV-vis spectra of **15**, **20–27**, **31** and **36**; experimental part. CCDC 1566359–1566386. For ESI and crystallographic data in CIF or other electronic format see DOI: 10.1039/c7ta07780g

This journal is © The Royal Society of Chemistry 2017

Published on 19 October 2017. Downloaded by Ludwig Maximilians Universitaet Muenchen on 2/16/2022 7:53:54 AM.

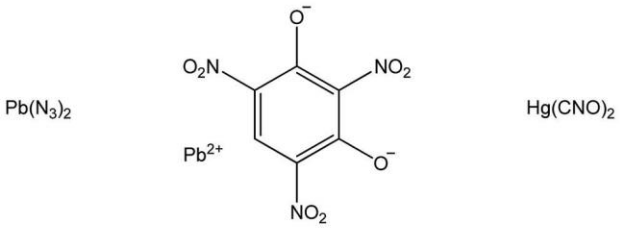


Chart 1 Commonly used primary explosives: lead(II) azide, lead(II) styphnate and mercury(II) fulminate.

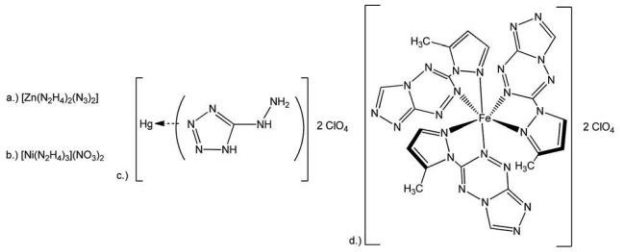


Chart 2 Energetic coordination compounds (ECCs): (a) $[Zn(N_2H_4)_2(N_3)_2]$[16] and (b) $[Ni(N_2H_4)_3](NO_3)_2$ [17] as possible replacements for lead containing primaries; (c) 5-hydrazino-1*H*-tetrazole-mercury(II) perchlorate (old generation of laser ignitable explosives)[25] and (d) $[Fe(TriTzPyr)_3](ClO_4)_2$ (new generation of laser ignitable explosives).[22]

irradiation with green or red light, which makes spin crossover compounds interesting for uses in liquid crystals, gel phases and molecular switches.[12]

In terms of energetic materials, transition metal complexes have been proposed for numerous applications.[13] Ordinarily used primary explosives, such as lead(II) azide, lead(II) styphnate and, in former times, mercury(II) fulminate (Chart 1), have led to significant contamination of the environment.[14,15] Energetic coordination compounds (ECCs) containing nitrogen-rich tetrazole ligands with high positive heats of formation and low or non-toxic metals like copper, zinc or iron can be used as substitutes for currently used primary explosives containing toxic heavy metals (Chart 2a and b).[6,16–18]

The use of laser initiation systems is also becoming more attractive as a strategy for replacing sensitive primary explosives.[19] Instead of using very sensitive compounds for igniting secondary explosives, relatively insensitive energetic materials are ignited directly by laser irradiation. The ignition can be triggered by using high power lasers or with lower energies by adding small amounts of light absorbing materials to energetic materials, like carbon black or chemical dyes.[20] However, promising ECCs, using transition metals as the central atom (for example Cu^{2+}, Co^{2+}, Ni^{2+} or Fe^{2+}) and tetrazole ligands, have been reported in the literature that are ignitable by laser irradiation without the addition of dyes (Chart 2d).[21,22] The most prominent examples include pentaammine(5-cyano-2*H*-tetrazolate)cobalt(III) perchlorate (CP),[23] tetraammine-*cis*-bis(5-nitro-2*H*-tetrazolato-N^2)cobalt(III) perchlorate (BNCP)[24] and 5-hydrazino-1*H*-tetrazolemercury(II) perchlorate (HTMP, Chart 2c).[25] Although they were initiated by laser ignition, they proved to be too sensitive for any application. The research of insensitive replacements is still of interest.

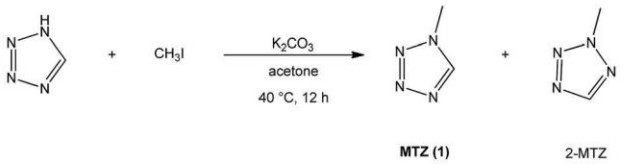
1-Methyl-5*H*-tetrazole (**1**) was first synthesized in 1910 by reaction of methylisocyanide with hydrazoic acid by Oliveri-Nandalá.[26] The ligand has a high nitrogen content of 66.63% and can be easily synthesized at low cost. The resulting driving force of producing nitrogen gas out of N–N single or N=N double bonds makes it promising as a ligand in combination with oxidizing anions for ECCs. Until now, the compound has only been described in relation to EPR studies,[27] spin transition complexes[10–12,28], and pyrotechnic[29]/propellant compositions.[30] Therefore, in this paper, efforts have been made to utilize MTZ as a neutral ligand to generate new energetic complexes with promising properties as (laser-ignitable) primary explosives or cocrystallized coordination compounds.

Results and discussion

Synthesis

The nitrogen-rich heterocycle 1-methyl-5*H*-tetrazole (**1**, MTZ) can be synthesized in various ways. One route is the cycloaddition reaction of sodium azide with triethyl orthoformate and methylamine in acetic acid under reflux.[31] Another route is the nucleophilic methylation of 1*H*-tetrazole with a methylating agent such as methyl iodide. The methylation reaction reported here was carried out in acetone at 40 °C under reflux using potassium carbonate as a base, according to a modified literature procedure (Scheme 1).[32] The methylation leads to an isomeric mixture of 1-methyl-5*H*-tetrazole (**1**) and 2-methyl-5*H*-tetrazole. The desired product can be isolated from this mixture either by flash column chromatography or distillation. Filtration of the reaction mixture followed by distillation (MTZ: 90 °C, 0.01 mbar, 2-methyltetrazole: 40 °C, 12 mbar) of the organic residue resulted in the isolation of product **1** with a yield of 48%. The side product 2-methyl-5*H*-tetrazole was obtained with a yield of 23%.

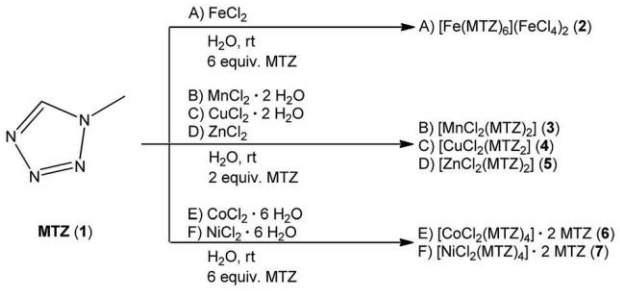
The divalent transition metal complexes **2–13** and **15–26** were prepared by combining solutions of 1-methyl-5*H*-tetrazole (**1**) and metal(II) salts with the respective stoichiometries at room temperature (Schemes 2–4). Water was chosen as a non-flammable, low-volatility and cheap reaction medium because of the good solubility of both the metal(II) salts and the tetrazole ligand in this solvent. In order to obtain crystalline materials, a minimal amount of solvent was used. An iron(II) tetrachloridoferrate(III) coordination compound **2** with iron in two different oxidation states was synthesized analogously to the literature known spin crossover tetrabromidoferrate(II) complex



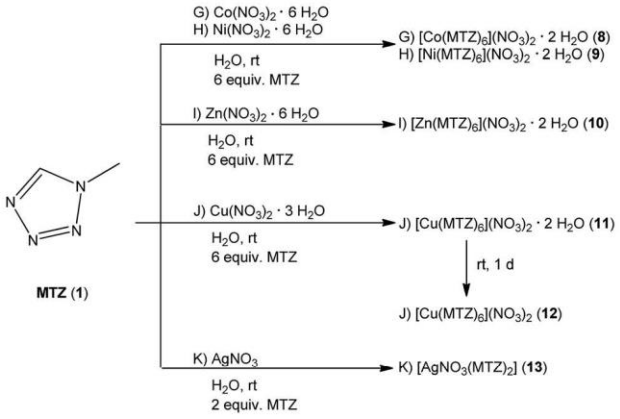
Scheme 1 Synthesis of 1-methyl-5*H*-tetrazole (**1**, MTZ).

This journal is © The Royal Society of Chemistry 2017

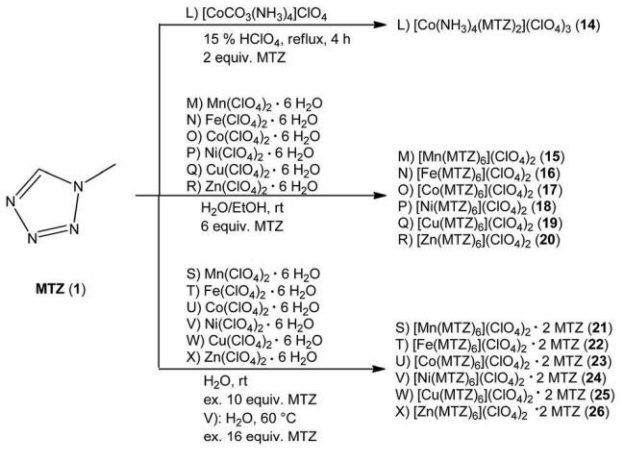
Published on 19 October 2017. Downloaded by Ludwig Maximilians Universitaet Muenchen on 2/16/2022 7:53:54 AM.



Scheme 2 Synthesis of the metal(II) chloride based MTZ complexes **2–7** with different metal centers.



Scheme 3 Synthesis of selected metal nitrate based MTZ complexes **8–13** with different metal centers.



Scheme 4 Synthesis of the energetic perchlorate coordination compounds **14–26**.

of 1-methyl-5*H*-tetrazole.[12] Ethanol was used for recrystallization of **2** and as a co-solvent in the synthesis of the perchlorate complexes **15–20** to achieve better crystallization. Complexes **4** and **5** have already been described in the literature and were synthesized to fill the gaps in the physico-chemical analytics.[33,34] The cobalt(II) and nickel(II) chlorido coordination compounds **6** and **7** crystallized, in contrast to **3–5** and the literature reported $CoCl_2$ and $NiCl_2$ complexes, with four coordinating and two cocrystallized non-coordinating MTZ molecules. The nickel(II) chlorido complex **7** precipitated as a powder and single crystals could not be obtained by recrystallization. On comparison of the infrared spectra of **3**, **6** and **7**, and elemental analysis a complex formula of $[NiCl_2(MTZ)_4] \cdot 2$MTZ is proposed for the coordination compound **7** (Fig. S20‡).

The ligand has no acidic proton, which enables the integration of the neutral tetrazole ligand to assemble cationic or neutral complexes with oxidizing anions like nitrates, perchlorates, cyanodinitromethanides (CDNM), picrates (PA) or trinitroresorcinates (HTNR). The incorporation of these oxidizing anions leads to more sensitive and powerful energetic materials that are possible alternatives for lead free laser ignitable primary explosives.

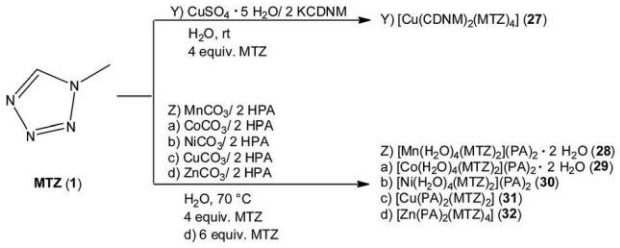
Compound **11** lost the crystal water molecules and its crystallinity overnight, in contrast to **8–10**, and was analyzed in its anhydrous form **12**. The colored reaction mixtures were left for crystallization until a precipitate appeared. The majority of the complexes were obtained in satisfactory yields directly from the mother liquor as single crystals suitable for X-ray diffraction within a few hours or days. Unfortunately compound **14** precipitated as an amorphous powder in a low yield of 18% and despite considerable recrystallization efforts single crystals could not be obtained.

The complex was synthesized by treatment of carbonato tetraamine(III) perchlorate with two equivalents of **1** in 15% perchloric acid for 4 h under reflux according to a modified procedure of an analogous compound.[35] The compound was filtered off, washed with a small amount of ethanol and dried in air.

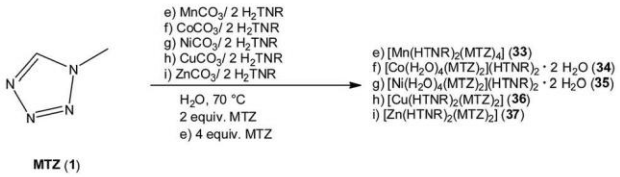
All perchlorate complexes were obtained without inclusion of aqua ligands or water solvent molecules, which results in a higher performance. The synthesis of the perchlorate complexes is strongly dependent on the quantity of the ligand added and yields either a structure where all MTZ ligands are bound to the metal ions (**15–20**) or a complex unit with two additional cocrystallized tetrazoles (**21–26**) when an excess of the ligand is used. Both species can be clearly distinguished through infrared spectroscopy.[32] This is illustrated exemplarily for the cobalt(II) perchlorate complexes **17** and **23** in Fig. S22.‡ In addition to an intense stretching vibration around 1106 cm^{-1} stemming from the perchlorate counter ions, a characteristic ring vibration of the bound MTZ ligand around 965 cm^{-1} is observed in the spectra of both **17** and **23**. The free ligand as well as complex **23** exhibits a stretch in the spectra at around 997 cm^{-1} stemming from in plane ring vibrations in free MTZ.[32] The C–H vibration can be detected at 3100 cm^{-1} in the free ligand and complex **23** spectra, respectively, while the bound MTZ ligand in **23** and **17** does occur at slightly higher wavenumbers (3147 cm^{-1}).

The corresponding metal(II) precursors for the complexes **27–37** were prepared and used *in situ* by simple acid–base reactions between metal(II) carbonates and picric/styphnic acid or metathesis reactions. The aqueous solutions of the corresponding precursors were then reacted with ligand **1** (Schemes

Published on 19 October 2017. Downloaded by Ludwig Maximilians Universitaet Muenchen on 2/16/2022 7:53:54 AM.



Scheme 5 Formation of the complexes **27–32** with varying metal centers and anions (CDNM = cyanodinitromethanide, HPA = picric acid, and PA = picrate).



Scheme 6 Synthesis of the metal(II) based styphnate complexes **33–37**.

5 and 6). In some cases non-stoichiometric amounts of the ligand were used to increase the yield or purity of the respective compounds. All complexes crystallized within several minutes (copper(II) picrate and styphnate compounds) or days and were obtained directly from the mother liquor in reasonable yields (60–86%). Crystals were filtered off, washed with cold ethanol when necessary to remove unreacted starting materials and dried in air, resulting in suitable samples for X-ray diffraction. Due to the high solubility of compound **33** in ethanol, no purification step was performed. In the case of the manganese(II) picrate complex **28** unfortunately only a few X-ray suitable single crystals could be picked between the unreacted starting material and the powder bulk material with unknown composition. The attempted synthesis of the coordination compound in sufficient amounts failed and only the crystal structure could be determined which is shown in the ESI (Fig. S12‡).

Crystal structures

All complexes (except **4**, **5**, **7–9**, **12**, **14** and **16**) were characterized using low temperature single crystal X-ray diffraction. Details of the crystal structures of complexes **3**, **11**, **15**, **17**, **18**, **20**, **21**, **23–26**, **28–30**, **32** and **34–37** are given in the ESI‡ together with the measurement and refinement data. The single crystals of the cobalt(II) and nickel(II) nitrate complexes **8** and **9** were measured to give an indication of the most likely structures. Finalization of the dataset was not possible because of the strongly disordered moieties and the related weak diffractions. The complexes **8** and **9** exhibit the same coordination environment and were therefore compared with **10** by infrared spectroscopy to confirm its structure (Fig. S21‡). The crystal structures were uploaded to the CSD database[36] and can be obtained free of charge with the CCDC no. 1566368 (**2**), 1566362 (**3**), 1566371 (**6**), 1566381 (**10**), 1566384 (**11**), 1566379 (**13**), 1566370 (**15**), 1566366 (**17**), 1566363 (**18**), 1566364 (**19**), 1566361 (**20**), 1566359 (**21**), 1566380 (**22**), 1566382 (**23**), 1566385 (**24**), 1566386 (**25**), 1566360 (**26**), 1566378 (**27**), 1566377 (**28**), 1566376 (**29**), 1566372 (**30**), 1566375 (**31**), 1566383 (**32**), 1566373 (**33**), 1566367 (**34**), 1566374 (**35**), 1566365 (**36**), 1566369 (**37**). The bond lengths and angles of the coordinating and non-coordinating MTZ rings in the investigated complexes are in the typical range of tetrazole ligands and similar to the non-coordinating ligand **1**.[37,38] The tetrazole ligand is therefore not discussed in detail in any of the following compounds. Coordination to the metal centers always takes place by the N4 nitrogen atom of 1-methyl-5*H*-tetrazole (**1**). Except compound **13**, all complexes with MTZ show an octahedral coordination sphere. This can be explained by the low steric hindrance of the ligand.

$[Fe(MTZ)_6](FeCl_4)_2$ (**2**) contains iron in the oxidation states +II and +III. It crystallizes in the form of yellow blocks in the trigonal space group $\bar{P}3$ with one formula unit per unit cell and a calculated density of 1.747 g cm^{-3} at 123 K. The molecular unit consists of six asymmetric unit cells with an octahedrally coordinated iron(II) center, which is bonded to six MTZ ligands (Fe1–N1 = 2.010(13) Å, ∠(N1–Fe1–N1^{i}) = 88.68(6)°). The second iron(III) atom is tetrahedrally coordinated by four chlorido-ligands (Fe2–Cl1 = 2.203(5) Å, ∠(Cl2–Fe2–Cl1^{vii}) = 109.49(2)°, (Cl1^{vi}–Fe2–Cl1^{vii}) = 109.46(2)°) forming the tetrachloridoferrate(III) counteranion (Fig. 1).

The cobalt(II) chlorido complex $[CoCl_2(MTZ)_4]\cdot 2MTZ$ (**6**) crystallizes in the form of yellow blocks in the monoclinic space group $P2_1/c$ with two formula units per unit cell and a calculated density of 1.617 g cm^{-3} at 123 K. In comparison to literature reported tetrazole containing complexes, most of the investigated compounds show low densities, which can be attributed to the low density of MTZ itself.[39] The molecular unit contains two cocrystallized non-coordinating MTZ molecules, which are stabilized by non-covalent interactions and an octahedrally coordinated cobalt(II) cation. The metal(II) center is coordinated (Fig. 2) by two chlorido ligands in axial positions and by four

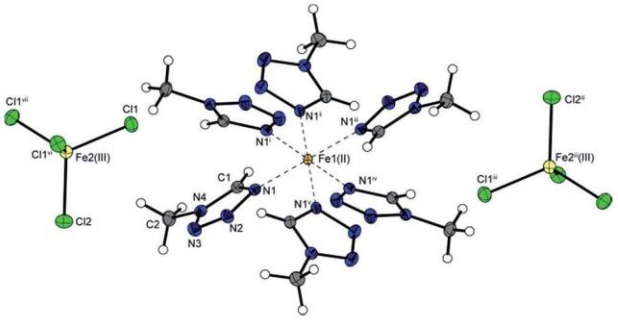


Fig. 1 Molecular unit of $[Fe(MTZ)_6](FeCl_4)_2$ (**2**). Thermal ellipsoids of non-hydrogen atoms in all structures are set to the 50% probability level. Selected bond lengths (Å): Fe1–N1 2.010(13), Fe2–Cl2 2.185(8), and Fe2–Cl1 2.202(5); selected bond angles (°): N1–Fe1–N1^{i} 88.68(6), N1–Fe1–N1^{ii} 91.32(6), Cl2–Fe2–Cl1^{vi} 109.49(2), and Cl1^{vi}–Fe2–Cl1^{vii} 109.46(2). Symmetry codes: (i) $y, -x+y, 1-z$; (ii) $-y, x-y, z$; (iii) $x-y, x, 1-z$; (iv) $-x+y, -x, z$; (v) $-x, -y, 1-z$; (vi) $-x+y, 1-x, z$; (vii) $1-y, 1+x-y, z$.

This journal is © The Royal Society of Chemistry 2017

Published on 19 October 2017. Downloaded by Ludwig Maximilians Universitaet Muenchen on 2/16/2022 7:53:54 AM.

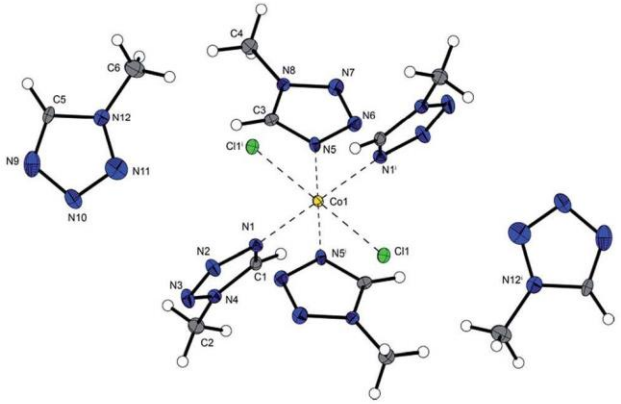


Fig. 2 Molecular unit of $[CoCl_2(MTZ)_4]\cdot 2MTZ$ (**6**). Selected bond lengths (Å): Co1–N1 2.143(6), Co1–N5 2.161(6), and Co1–Cl1 2.443(2); selected bond angles (°): Cl1–Co1–N1 89.52(2), Cl1–Co1–N5 90.48(2), and N1–Co1–N5 87.7(2). Symmetry code: (i) $-x, 1-y, -z$.

MTZ molecules in a plane (Co1–N1 = 2.143(6) Å, Co1–N5 = 2.161(6) Å, and Co1–Cl1 = 2.443(2) Å). The deviation of the ideal coordination sphere is marginal ($\angle$(N1–Co1–N1) = 89.52(2)°, $\angle$(Cl11–Co1–N5) = 90.48(2)°, $\angle$(N1–Co1–N5) = 87.7(2)°).

The complexes **10** (colorless block) and **11** (blue block) with nitrate counter ions crystallize isotypically in the triclinic space group $P\bar{1}$ with two formula units per unit cell showing almost the same metric (see Table S1 in the ESI‡) and densities: **10**: 1.608 g cm^{-3} and **11**: 1.626 g cm^{-3} at 123 K.

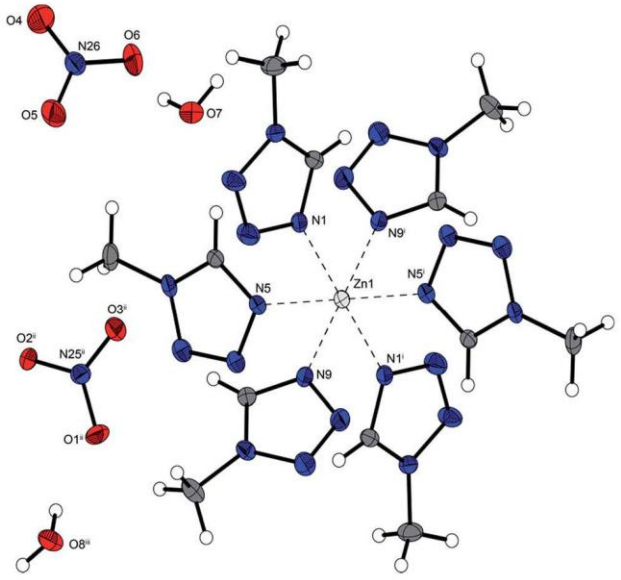


Fig. 3 Molecular unit of $[Zn(MTZ)_6](NO_3)_2\cdot 2H_2O$ (**10**). Selected bond lengths (Å): Zn1–N5 2.139(2), Zn1–N1 2.166(2), Zn1–N9 2.185(2), O2–N25 1.257(3), O3–N25 1.250(3), and O4–N26 1.223(4); selected bond angles (°): N5–Zn1–N1 88.91(8), N5^{i}–Zn1–N1 91.09(8), N5–Zn1–N9^{i} 91.77(8), N5^{i}–Zn1–N9^{i} 88.23(8), N1–Zn1–N9^{i} 89.51(8), N1^{i}–Zn1–N9^{i} 90.49(8), O3–N25–O2 120.0(2), O1–N25–O2 119.8(2), O4–N26–O5 120.6(3), O4–N26–O6 119.8(3), and O5–N26–O6 119.5(3). Symmetry codes: (i) $2-x, 2-y, -z$; (ii) $2-x, 1-y, 1-z$.

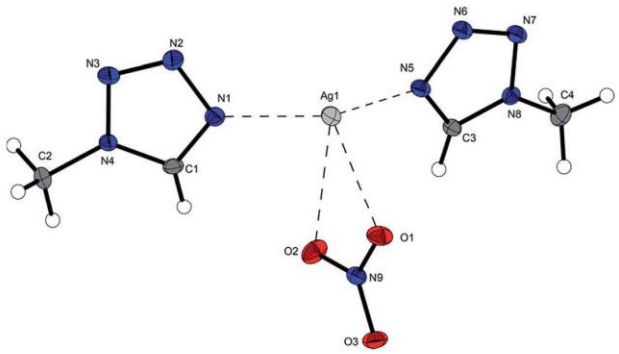


Fig. 4 Molecular unit of $[AgNO_3(MTZ)_2]$ (**13**). The fifth ligand from an adjacent nitrate was omitted for clarity. Selected bond lengths (Å): Ag1–N1 2.233(3), Ag1–N5 2.255(3), Ag1–O1 2.544(3), Ag1–O3^{i} 2.545(3), Ag1–O2 2.719(3), O1–N9 1.251(4), O2–N9 1.257(5), and O3–N9 1.252(4); selected bond angles (°): N1–Ag1–N5 137.76(12), N1–Ag1–O1 111.85(11), N5–Ag1–O1 95.09(11), N1–Ag1–O3^{i} 119.23(11), N5–Ag1–O3^{i} 95.82(11), O1–Ag1–O3^{i} 81.30(10), O1–N9–O3 120.7(3), O1–N9–O2 119.6(3), and O3–N9–O2 119.7(3). Symmetry codes: (i) $1+x, y, z$; (ii) $-1+x, y, z$.

Both metal(II) centers have an octahedral coordination sphere with six MTZ ligands (Fig. 3 and S2‡). As expected, the d^9-ion copper(II) ion in **11** shows Jahn–Teller distortion along its axial coordination sphere. In comparison, the respective zinc(II) complex exhibits a nearly undistorted coordination sphere and the six surrounding MTZs are nearly undistorted (Zn1–N5 = 2.139(2) Å, Zn1–N1 = 2.166(2) Å, $\angle$(N5^{i}–Zn1–N9^{i}) = 88.23(8)°, $\angle$(N1–Zn1–N9^{i}) = 89.51(8)°).

The silver(I) complex **13** crystallizes in the monoclinic space group $P2_1/c$ with four formula units per unit cell and a calculated density of 2.112 g cm^{-3} at 123 K. Every silver(I) center is penta-coordinated by two MTZ ligands and two bridging nitrates (Fig. 4).

The nitrato ligand binds through all of its three oxygen atoms. In addition to a bidentate coordination mode to one silver(I) cation, the nitrato ligand is also bound in a monodentate fashion to a second silver(I) ion, bridging the two cations and forming polymeric chains along the *a* axis (Fig. 5). The distances between silver(I) and oxygen (Ag1–O1 = 2.544(3) Å, Ag1–O3^{i} 2.545(3) Å, and Ag1–O2 2.719(3) Å) are longer than the silver(I) nitrogen distances (Ag1–N1 = 2.233(3) Å and Ag1–N5 = 2.255(3) Å).

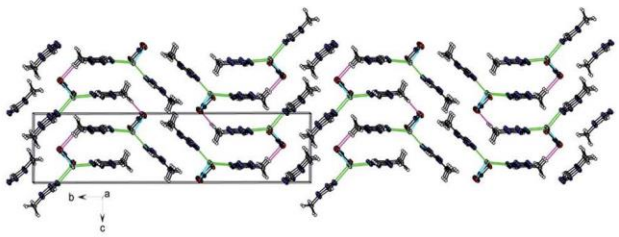


Fig. 5 View of the structure of **13** along the *a* axis (Ag–O bonds = cyan; Ag–N bonds = green). Stabilization through non-classical hydrogen bonds (C–H···N and C–H···O; C–H···O hydrogen bonds = purple) and hydrophobic interactions between the methyl groups.

Published on 19 October 2017. Downloaded by Ludwig Maximilians Universitaet Muenchen on 2/16/2022 7:53:54 AM.

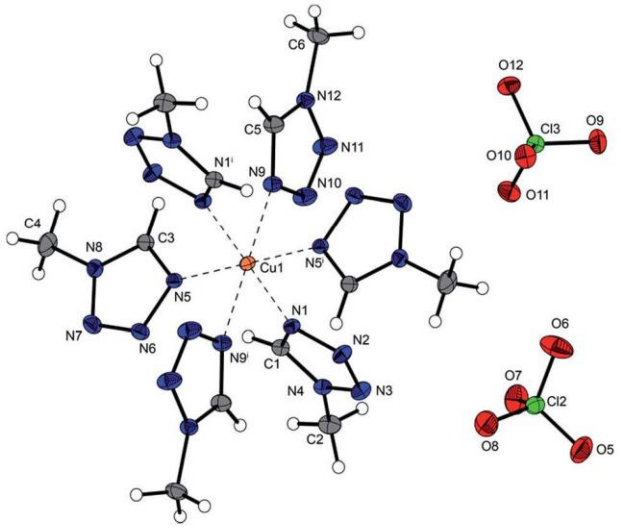


Fig. 6 Complex unit of $[Cu(MTZ)_6](ClO_4)_2$ (**19**). Selected bond lengths (Å): Cu1–N1 2.035(2), Cu1–N5 2.014(2), Cu1–N9 2.401(2), and Cl2–O5 1.437(2); selected bond angles (°): N1–Cu1–N5 89.83(2), N1–Cu1–N9 91.04(2), N5–Cu1–N9 89.54(2), and O5–Cl2–O6 109.32(2). Symmetry codes: (i) $-x, 2-y, -z$; (ii) $1-x, -y, 1-z$; (iii) $1-x, 1-y, 1-z$; (iv) $-x, 1-y, -z$.

The complexes with perchlorate counter ions **15**/**20** and **17**/**18** crystallize isotypically in monoclinic and trigonal space groups (**15**: $P2_1/n$, 1.582 g cm^{-3} (Fig. S3‡); **17**: $\bar{R}3$, 1.614 g cm^{-3} (Fig. S4‡); **18**: $\bar{R}3$, 1.629 g cm^{-3} (Fig. S5‡); **20**: $P2_1/n$, 1.635 g cm^{-3} at 123 K (Fig. S6‡)). The blue copper(II) perchlorate compound **19** is the only complex that crystallizes in the triclinic space group $\bar{P}1$ with two formula units per unit cell and a calculated density of 1.645 g cm^{-3} at 123 K, which is the highest of all perchlorates. Its molecular motif is illustrated in Fig. 6. Each metal(II) center contains an octahedral surrounding and is connected to six tetrazole ligands. As already observed in the coordination environment of the cation in **11**, the copper(II) center shows a Jahn–Teller distortion caused by the d^9-configuration (Cu1–N1 2.035(2) Å, Cu1–N5 2.014(2) Å, and Cu1–N9 2.401(2) Å).

New perchlorate species **21–26** of the investigated metals(II) were obtained after using an excess of the tetrazole ligand during the synthesis. The complexes with two cocrystallized tetrazoles crystallize isotypically in the triclinic space group $\bar{P}1$ with one formula unit per unit cell and similar densities. However, their densities increase in the order of Mn^{2+} (1.590 g cm^{-3}; 123 K) < Fe^{2+} (1.592 g cm^{-3}; 173 K) < Co^{2+} (1.612 g cm^{-3}, 143 K) < Ni^{2+} (1.621 g cm^{-3}; 143 K) < Cu^{2+} (1.623 g cm^{-3}; 143 K) < Zn^{2+} (1.630 g cm^{-3}; 123 K). The molecular structure of complex **22** is shown in Fig. 7 and used exemplarily for all complexes.

Again, two additional non-coordinating MTZ molecules could be cocrystallized. Six regular tetrazole ligands are surrounding the transition metal(II) centers in octahedral arrangements and interact hydrophobically and through non-classical hydrogen bonds with the cocrystallized compounds.

The cyanodinitromethanide complex **27** crystallizes in the form of blue blocks in the triclinic space group $\bar{P}1$ with one formula unit per unit cell and a calculated density of 1.746 g cm^{-3} at 123 K.

The molecular unit is built up of two asymmetric unit cells. The octahedral complex (Fig. 8), with four MTZ ligands in a plane (Cu1–N8 = 2.002(16) Å, Cu1–N1 = 2.019(19) Å, ∠(N8^i–Cu1–N7^i) = 88.54(6)°, ∠(N1^i–Cu1–N7^i) = 90.72(7)°), shows

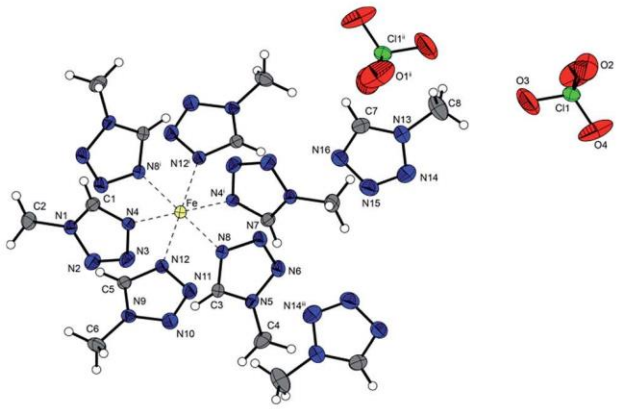


Fig. 7 Complex unit of $[Fe(MTZ)_6](ClO_4)_2 \cdot 2MTZ$ (**22**). Selected bond lengths (Å): Fe1–N12 2.181(2), Fe1–N4 2.183(2), Fe1–N8 2.194(2), and Cl1–O4 1.405(4); selected bond angles (°): N12–Fe1–N4 89.53(8), N12^i–Fe1–N4 90.48(8), O1–Cl1–O4 108.1(2), N12–Fe1–N8^i 91.61(8), N12^i–Fe1–N8^i 88.39(8), N4–Fe1–N8^i 89.63(8), N4^i–Fe1–N8^i 90.37(8), and N12^i–Fe1–N8 91.61(8). Symmetry codes: (i) $-x, -y, 1-z$; (ii) $1-x, 1-y, -z$; (iii) $1-x, 1-y, 1-z$.

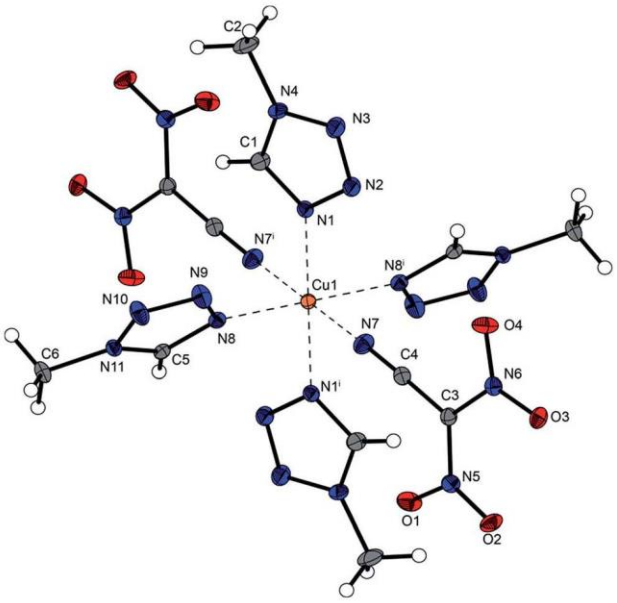


Fig. 8 Molecular unit of $[Cu(CDNM)_2(MTZ)_4]$ (**27**). Selected bond lengths (Å): Cu1–N8 2.002(16), N6–C3 1.399(2), N7–C4 1.151(3), Cu1–N1 2.019(19), C3–C4 1.407(3), Cu1–N7 2.412(18), N5–C3 1.394(3), O2–N5 1.238(2), and O4–N6 1.243(3); selected bond angles (°): N8–Cu1–N1^i 91.31(7), N8^i–Cu1–N1^i 88.69(7), N8–Cu1–N7^i 91.46(6), N1^i–Cu1–N7^i 90.72(7), N1–Cu1–N7^i 89.28(7), N8–Cu1–N7 88.54(6), O3–N6–O4 122.53(17), O3–N6–C3 122.02(18), O4–N6–C3 115.45(16), C1–N1–N2 106.45(18), N5–C3–N6 124.47(17), N5–C3–C4 117.23(16), and N7–C4–C3 178.0(2). Symmetry code: (i) $1-x, -y, -z$.

This journal is © The Royal Society of Chemistry 2017

Published on 19 October 2017. Downloaded by Ludwig Maximilians Universitaet Muenchen on 2/16/2022 7:53:54 AM.

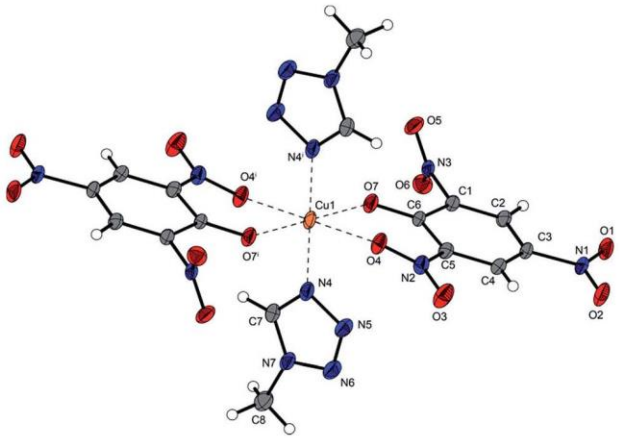


Fig. 9 Molecular unit of the copper(II) picrate complex **31**. Selected bond lengths (Å): Cu1–N4 2.001(3), Cu1–O4 2.354(2), and Cu1–O7 1.929(2); selected bond angles (°): O4–Cu1–N4 91.63(9), O7–Cu1–N4 91.07(9), and O4–Cu1–O7 79.32(9). Symmetry code: (i) $1-x, 1-y, -z$.

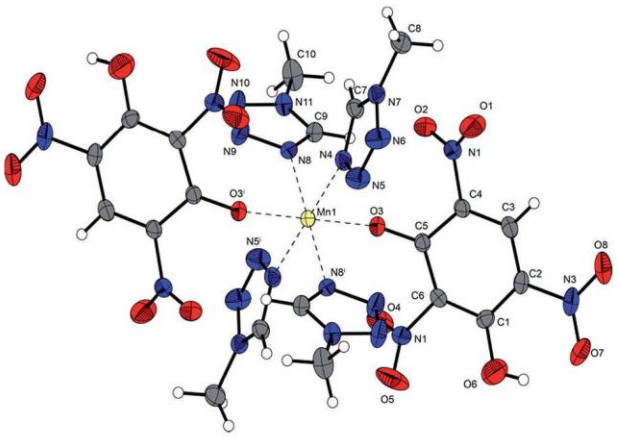


Fig. 10 Molecular unit of $[Mn(HTNR)_2(MTZ)_4]$ (**33**). Selected bond lengths (Å): Mn1–O3 2.156(2), Mn1–N4 2.250(3), and Mn1–N8 2.239(3); selected bond angles (°): O3–Mn1–N4 93.04(9), O1–Mn1–N8 85.42(11), and N4–Mn1–N8 92.18(10). Symmetry code: (i) $-x, 2-y, -z$.

elongation along the axial positions, which are occupied by two cyanodinitromethanide anions (Cu1–N7 = 2.412(18) Å). The structure of the CDNM anion is comparable to literature values.[40]

The manganese(II) **28** and cobalt(II) **29** picrate complexes crystallize isotypically in the monoclinic space group $P2_1/c$ with two formula units per unit cell and calculated densities of 1.746 g cm^{-3} at 123 K for **28** and 1.786 g cm^{-3} at 173 K for **29**. Their molecular units consist of two asymmetric units, containing one MTZ ligand, two aqua ligands, one crystal water and one non-coordinating picrate counteranion (Fig. S12/13‡). The same monoclinic space group $P2_1/c$ could be observed for the nickel(II) picrate complex **30** (1.757 g cm^{-3} at 123 K), which shows a different molecular composition with no crystallized water molecules, and two aqua and four MTZ ligands (Fig. S14‡). Among the metal(II) picrate complexes, only the copper(II) **31** and zinc(II) **32** complexes crystallize water-free in monoclinic space groups (**31**: $P2_1/c$; **32**: $P2_1/n$) with two formula units per unit cell and calculated densities of 1.828 g cm^{-3} at 123 K for **31** and 1.724 g cm^{-3} at 173 K for **32**.

In comparison to the other picrate compounds discussed so far, the trinitrophenolate counter anions coordinate bidentately to the copper(II) (*via* the nitro- and deprotonated phenolate-groups) and monodentately to the zinc(II) metal cations in **31**/**32**. The remaining coordination sites of the octahedron are occupied by two methyltetrazole ligands in **31** (Fig. 9) and by four tetrazoles in **32** (Fig. S15‡). The octahedral geometry of **31** shows deviations to the ideal 90° angle caused by the fixed structure of the picrate anion and its Jahn–Teller distortion along the O4–Cu1–O4^{i} axis ($\angle$(O4–Cu1–N4) = 91.63(9)°, $\angle$(O7–Cu1–N4) = 91.07(9)°, $\angle$(O4–Cu1–O7) = 79.32(9)°).

The manganese(II) styphnate complex **33** interestingly crystallizes isotypically to the zinc(II) picrate complex **32** with almost the same density (1.732 g cm^{-3} at 123 K) but with different anionic ligands, and is depicted in Fig. 10.

The cobalt(II) **34** and nickel(II) **35** styphnate complexes (Fig. S16 and S17‡) crystallize isotypically to each other and to the picrate complexes **28**/**29**. A similar situation can be observed for complex **36**, which exhibits a similar coordination sphere to **31** with analogous cell parameters but with styphnates instead of picrates (Fig. S18‡). The zinc(II) complex **37** has the same sum formula as compound **36**, but crystallizes in the triclinic space group $P\bar{1}$ and with a different metal center (Fig. S19‡).

Sensitivities and thermal stability

Thermal measurements of highly energetic and sensitive complexes are very challenging since larger quantities (>2 mg) can damage the instrument seriously. On the other hand endothermic signals may not be detected properly when using an insufficient amount. Endothermic events like dehydration, melting or loss of cocrystallized/coordinating MTZ molecules, as well as other critical temperatures of the described compounds were measured with a heating rate of β = 5 °C min^{-1} *via* differential thermal analysis, differential scanning calorimetry or by thermal gravimetric analysis. The measured onset temperatures are summarized in Tables 1 and 2. Details of the DTA plots of complexes **1–10**, **12–14**, **27** and **29–37** are given in the ESI.‡ Most of the complexes have exothermic decomposition events higher than or close to 200 °C, which is in the range of the uncoordinated ligand **1** ($T_{exo.}$: 206 °C). However, endothermic decompositions *e.g.* loss of water or the ligand have been observed partly at lower temperatures. Both nitrate complexes **12** and **13**, which decompose exothermically at relatively low temperatures of 160 °C (**12**) and 119 °C (**13**), showed the lowest thermal stabilities of all investigated compounds. Comparing them to the other coordination compounds bearing the same metal ion, but different anions, no general trend regarding their decomposition temperatures could be observed.

Exceptional endothermic events during the DTA measurements could be observed for the complexes (**4**, **5**, **9**, **19**, **20**, **32**,

Published on 19 October 2017. Downloaded by Ludwig Maximilians Universitaet Muenchen on 2/16/2022 7:53:54 AM.

Table 1 Thermal stability measurements of 1–10 and 11–20 by DTA[a]

	$T_{endo1.}$[b] (°C)	$T_{endo2.}$[b] (°C)	$T_{exo.}$[c] (°C)
MTZ (1)	39	—	206
$[Fe(MTZ)_6](FeCl_4)_2$ (2)	—	—	236
$[MnCl_2(MTZ)_2]$ (3)	—	—	234
$[CuCl_2(MTZ)_2]$ (4)	185	—	199
$[ZnCl_2(MTZ)_2]$ (5)	184	—	204
$[CoCl_2(MTZ)_4]\cdot 2MTZ$ (6)	66	—	206
$[NiCl_2(MTZ)_4]\cdot 2MTZ$ (7)	106	—	199
$[Co(MTZ)_6](NO_3)_2\cdot 2H_2O$ (8)	—	—	199
$[Ni(MTZ)_6](NO_3)_2\cdot 2H_2O$ (9)	86	166	194
$[Zn(MTZ)_6](NO_3)_2\cdot 2H_2O$ (10)	50–75[d]	—	196
$[Cu(MTZ)_6](NO_3)_2$ (12)	—	—	160
$[AgNO_3(MTZ)_2]$ (13)	—	—	119
$[Co(NH_3)_4(MTZ)_2](ClO_4)_3$ (14)	—	—	201
$[Mn(MTZ)_6](ClO_4)_2$ (15)	—	—	223
$[Fe(MTZ)_6](ClO_4)_2$ (16)	—	—	213
$[Co(MTZ)_6](ClO_4)_2$ (17)	—	—	253
$[Ni(MTZ)_6](ClO_4)_2$ (18)	—	—	271
$[Cu(MTZ)_6](ClO_4)_2$ (19)	178	—	211
$[Zn(MTZ)_6](ClO_4)_2$ (20)	196	—	221

[a] Onset temperatures at a heating rate of 5° min^{-1}. [b] Endothermic peak, which indicates melting, dehydration or loss of coordinating/cocrystallized MTZ molecules. [c] Exothermic peak, which indicates decomposition. [d] Weight loss detected by TGA.

Table 2 Thermal stability measurements of 21–27 and 29–37 by DTA[a]

	$T_{endo1.}$[b] (°C)	$T_{endo2.}$[b] (°C)	$T_{exo.}$[c] (°C)
$[Mn(MTZ)_6](ClO_4)_2\cdot 2MTZ$ (21)	105	—	216
$[Fe(MTZ)_6](ClO_4)_2\cdot 2MTZ$ (22)	111	—	215
$[Co(MTZ)_6](ClO_4)_2\cdot 2MTZ$ (23)	107	—	210
$[Ni(MTZ)_6](ClO_4)_2\cdot 2MTZ$ (24)	93	—	207
$[Cu(MTZ)_6](ClO_4)_2\cdot 2MTZ$ (25)	78	—	206
$[Zn(MTZ)_6](ClO_4)_2\cdot 2MTZ$ (26)	108	—	212
$[Cu(CDNM)_2(MTZ)_4]$ (27)	—	—	201
$[Co(H_2O)_4(MTZ)_2](PA)_2\cdot 2H_2O$ (29)	61[d]	79[d]	248
$[Ni(H_2O)_4(MTZ)_2](PA)_2$ (30)	106	—	211
$[Cu(PA)_2(MTZ)_2]$ (31)	—	—	226
$[Zn(PA)_2(MTZ)_4]$ (32)	92	—	212
$[Mn(HTNR)_2(MTZ)_4]$ (33)	141	—	202
$[Co(H_2O)_4(MTZ)_2](HTNR)_2\cdot 2H_2O$ (34)	70	80	200
$[Ni(H_2O)_4(MTZ)_2](HTNR)_2\cdot 2H_2O$ (35)	86	105	227
$[Cu(HTNR)_2(MTZ)_2]$ (36)	—	—	231
$[Zn(HTNR)_2(MTZ)_2]$ (37)	—	—	214

[a] Onset temperatures at a heating rate of 5° min^{-1}. [b] Endothermic peak, which indicates melting, dehydration or loss of coordinating/cocrystallized MTZ molecules. [c] Exothermic peak, which indicates decomposition. [d] Measured by DSC.

and 33) and were further investigated by thermal gravimetric analysis (Fig. 11 and S27‡). The free ligand 1, which has a relatively low melting point of 39 °C, shows a continuous weight loss at elevated temperatures until its exothermic decomposition temperature is reached. This fact can be attributed to its high vapour pressure and could be a possible explanation for

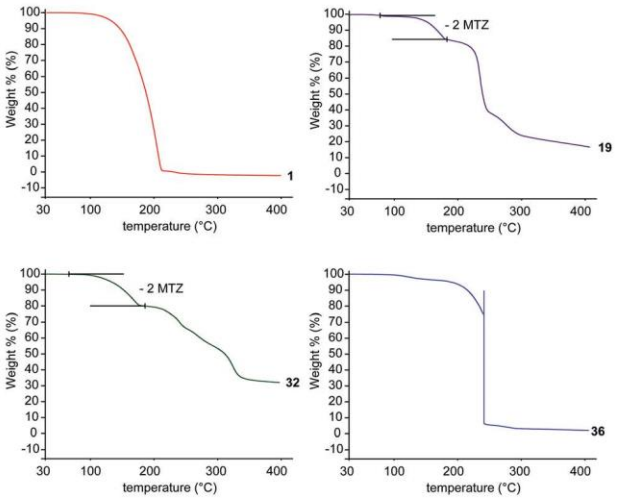


Fig. 11 TGA measurements (5° min^{-1}) of the selected compounds.

the observed endothermic peaks in the DTA plots for the above-mentioned complexes. Comparable phenomena have been reported in the literature.[41,42] The endothermic loss of two coordinating MTZ molecules in the complexes 19 and 32 leads most likely to an intermediate species, which decomposes at a later stage exothermically (similar to compounds 20 and 33). Various decomposition paths and mechanisms are possible. The tendency of vaporization of the ligands and the relative bond strength of the coordinating tetrazoles are strongly dependent on the metal ($MnCl_2$ (3) *vs.* $CuCl_2$ (4)/$ZnCl_2$ (5)), anion ($Ni(NO_3)_2$ (9) *vs.* $Ni(ClO_4)_2$ (18)) and the corresponding coordination environment of the complexes. For example, the monodentate picrate complex 32 disintegrates in two stages (loss of two ligands followed by an exothermic event) whereas the bidentate styphnate complex 36 decomposes in only one single stage.

The thermal stability of the metal(II) MTZ perchlorate complexes (Fig. 12) increases in the following order: Cu^{2+} (211 °C) < Fe^{2+} (213 °C) < Zn^{2+} (221 °C) < Mn^{2+} (223 °C) < Co^{2+} (253 °C) < Ni^{2+} (271 °C). For previous compounds a similar trend has been reported in the literature.[43] The cocrystal perchlorate complexes 21–26 (Fig. 13) as well as the chlorides 6/7 lose their cocrystallized MTZ molecules in the range between 66–111 °C

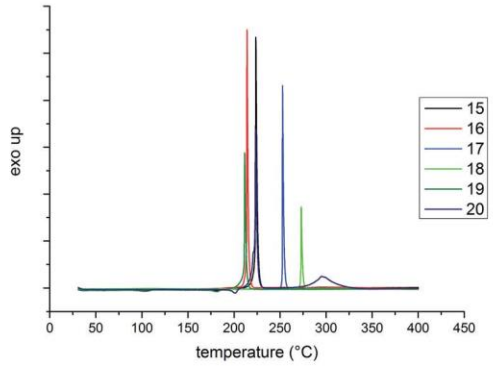


Fig. 12 DTA plots (5° min^{-1}) of the perchlorate complexes 15–20.

This journal is © The Royal Society of Chemistry 2017

Published on 19 October 2017. Downloaded by Ludwig Maximilians Universitaet Muenchen on 2/16/2022 7:53:54 AM.

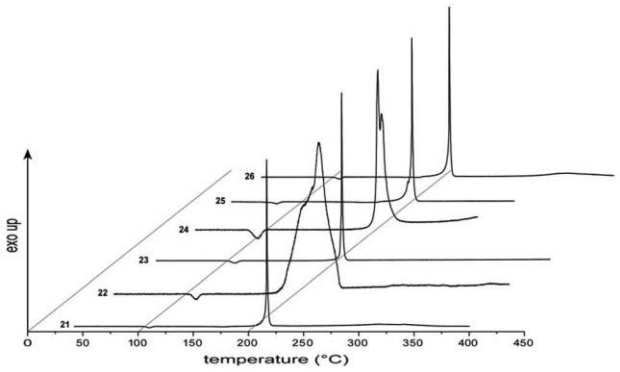


Fig. 13 DTA plots (5° min^{-1}) of the perchlorate cocrystal compounds **21–26**.

Table 3 Sensitivities toward impact, friction and ESD of **1**, **3–10**, **12–27** and **29–37**

	IS[a] (J)	FS[b] (N)	ESD[c] (J)	Grain size (μm)
1	>40	>360	1.50	<100
3	>40	>360	1.50	100–500
4	>40	>360	1.30	500–1000
5	>40	>360	1.50	<100
6	>40	>360	1.00	<100
7	>40	>360	0.80	<100
8	>40	>360	1.50	<100
9	>40	324	1.50	100–500
10	>40	>360	0.40	100–500
12	>40	>360	1.50	100–500
13	40	160	0.15	<100
14	9	160	0.036	<100
15	7	120	0.08	<100
16	1	60	0.10	<100
17	3	60	0.50	<100
18	5	60	0.10	<100
19	2.5	54	0.08	<100
20	10	120	0.25	<100
21	7	216	0.46	100–500
22	10	120	0.40	100–500
23	10	80	0.13	500–1000
24	6	192	0.20	<100
25	7	72	0.20	500–1000
26	10	144	0.60	100–500
27	4	324	1.50	100–500
29	>40	>360	1.00	100–500
30	>40	>360	1.50	100–500
31	4	>360	0.30	500–1000
32	15	>360	0.25	100–500
33	15	288	0.20	100–500
34	25	>360	0.23	100–500
35	25	>360	0.15	<100
36	2	160	1.50	100–500
37	4	240	0.80	500–1000

[a] Impact sensitivity according to the BAM drophammer (method 1 of 6). [b] Friction sensitivity according to the BAM friction tester (method 1 of 6). [c] Electrostatic discharge sensitivity (OZM ESD tester); impact: insensitive > 40 J, less sensitive ≥ 35 J, sensitive ≥ 4 J, very sensitive ≤ 3 J; friction: insensitive > 360 N, less sensitive = 360 N, sensitive < 360 N and > 80 N, very sensitive ≤ 80 N, extremely sensitive ≤ 10 N. According to the UN Recommendations on the Transport of Dangerous Goods.

and are slightly less temperature stable than their corresponding perchlorate compounds **15–20**. The aqua ligand and crystal water containing complexes can be dehydrated after heating as demonstrated by an endothermic peak in the DTA/DSC plots or by weight loss during the TGA measurements.

The sensitivities toward impact, friction and electrostatic discharge for the compounds were determined according to BAM standards. In addition, the compounds have been classified in accordance with the "UN Recommendations on the Transport of Dangerous Goods" using the measured values. An overview of the sensitivities is given in Table 3. The uncoordinated ligand **1** has sensitivities greater than 40 J, greater than 360 N for friction and an ESD value of 1.50 J and can therefore be classified as insensitive. The chloride complexes **3–8** are insensitive toward impact, friction and ESD. Introduction of oxidizing anions like nitrates, cyanodinitromethanides, picrates or styphnates increases the sensitivity against impact, friction and ESD under most circumstances (impact: 2–40 J; friction: 160–360 N; ESD: 0.13–1.50 J). All water-free complexes with trinitrobenzene-derivatives as anions are more sensitive toward mechanical stimuli compared with their crystal water or aqua ligand containing analogs. The perchlorate complexes **14–26** are sensitive toward impact (1–10 J) and vary from sensitive to very sensitive against friction (54–216 N). The stability toward impact of the $[M^{II}(MTZ)_6](ClO_4)_2$ complexes (Fig. S28‡) decreases in the order: Zn^{2+} (10 J) < Mn^{2+} (7 J) < Ni^{2+} (5 J) < Co^{2+} (3 J) < Cu^{2+} (2.5 J) < Fe^{2+} (1 J) and in the following order toward friction: Zn^{2+} (120 N) ≈ Mn^{2+} (120 N) < Ni^{2+} (60 N) ≈ Co^{2+} (60 N) ≈ Fe^{2+} (60 N) < Cu^{2+} (54 N). Similar trends have been observed

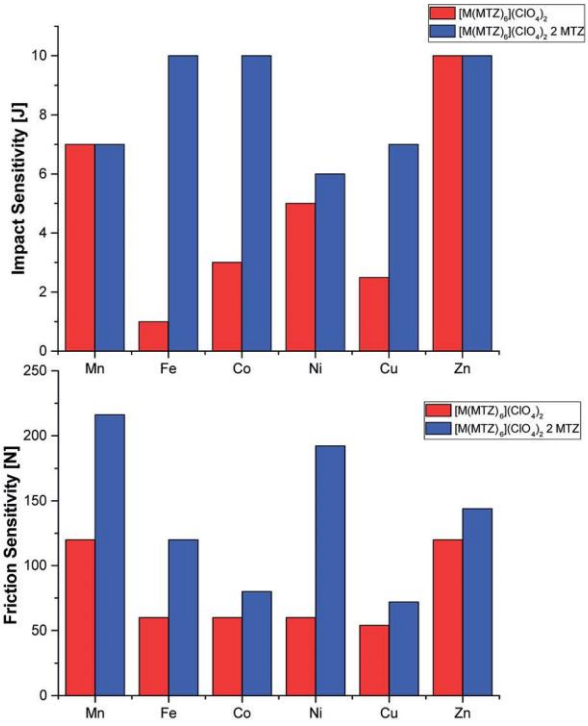


Fig. 14 Comparison of the impact and friction sensitivities of both the metal perchlorates with and without cocrystallization of 1-methyl-5*H*-tetrazole (**1**).

Published on 19 October 2017. Downloaded by Ludwig Maximilians Universitaet Muenchen on 2/16/2022 7:53:54 AM.



Fig. 15 Moment of deflagration of compound **16** during the hot needle tests (left) and hot plate test (right).

in the literature in correlation with energetic metal(II) diaminotetrazole perchlorate complexes.[44] Cocrystallization of the nitrogen-rich ligand (**21–26**) leads in most cases to a decrease in sensitivities toward mechanical stimuli in comparison to the related perchlorate complexes (Fig. S29‡) while maintaining its highly energetic character and is therefore a great concept for the desensitization of energetic complexes (Fig. 14).

Hot needle and hot plate tests of the investigated compounds **16**, **19** and **25** showed deflagrations (Fig. 15 and S30–S33‡). The samples were fixed on a copper plate using adhesive tape. Detonation of the compound typically indicates a valuable primary explosive. The safe and practicable hot plate test shows only the behavior of the unconfined sample toward fast heating on a copper plate. It does not necessarily allow any conclusions on a compound's capability as a primary explosive.

Toxicity

The toxicity of the uncoordinated free ligand 1-methyl-5*H*-tetrazole (**1**) was determined together with the most promising perchlorate complexes **16**, **19** and **25** using the known luminescence bacteria inhibition test in aqueous media.[45] The luminescent marine bacterium Vibrio fischeri NRRL-B-11177, which is part of the commercially available bioassay system LUMIStox, is a representative species for other aquatic organisms and therefore a valuable indicating device when it comes to groundwater contamination. The half maximal effective concentration EC_{50} of these compounds was determined after an incubation time of 30 min. This toxicological parameter is defined as the concentration of the investigated compound, at which the bioluminescence of the bacteria strain is halved after a certain exposure time (*e.g.* 15 or 30 min) and then compared to the original bioluminescence of the sample before being treated. With EC_{50} (30 min) values of 5.45 g L^{-1} for the free tetrazole **1** and 1.66 g L^{-1} for the iron(II) perchlorate complex **16**, both compounds can be considered as non-toxic (toxicity level after 30 min incubation: very toxic < 0.10 g L^{-1}; toxic 0.10–1.00 g L^{-1}; non-toxic > 1.00 g L^{-1}).[46] As expected, the copper(II) perchlorate compounds showed half maximum effective concentrations of 0.13 g L^{-1} for **19** and 0.26 g L^{-1} for **25**. Therefore, both complexes have to be classified as toxic, which is not surprising, due to the known toxicity of copper compounds toward microorganisms.[47]

Laser initiation

Chavez *et al.* and our group showed that iron(II) and copper(II) perchlorate complexes with suitable ligands can be initiated in laser ignition experiments.[22,48] These compounds could be potential candidates for laser ignition systems in the future. About 15 mg of the carefully pestled complex to be investigated was filled into a transparent plastic cap, pressed with a pressure force of 1 kN and sealed with a UV-curing adhesive. The laser initiation experiments were carried out with a 45 W InGaAs laser diode operating in the single-pulsed mode. The diode was connected to an optical fiber with a core diameter of 400 μm and a cladding diameter of 480 μm. The optical fiber was coupled *via* a SMA type connecter directly to the laser and to a collimator. This collimator was linked to an optical lens, which was positioned in its focal distance (f = 29.9 mm) to the sample. The lens

Table 4 Results of the laser ignition tests[a]

	7 A	8 A	9 A	10 A
14	—	—	deflag.	—
15	—	—	—	x
16	dec.	—	—	deflag.
17	—	—	—	x
18	—	—	—	deflag.
19	det.	—	—	det.
20	—	—	—	x
22	—	—	—	deflag.
24	—	—	—	deflag.
25	deflag.	deflag.	—	—
27	—	dec.	—	—
31	—	—	—	dec.
36	—	—	—	deflag.
37	—	—	—	x

[a] (—: not tested, x: no ignition, dec.: decomposition, deflag.: deflagration, det.: detonation). Operating parameters: current I = 7–10 A; voltage U = 4 V; theoretical maximal output power P_{max} = 45 W; theoretical energy E_{max} = 26–60 mJ; wavelength λ = 915 nm; pulse length τ = 15 ms.

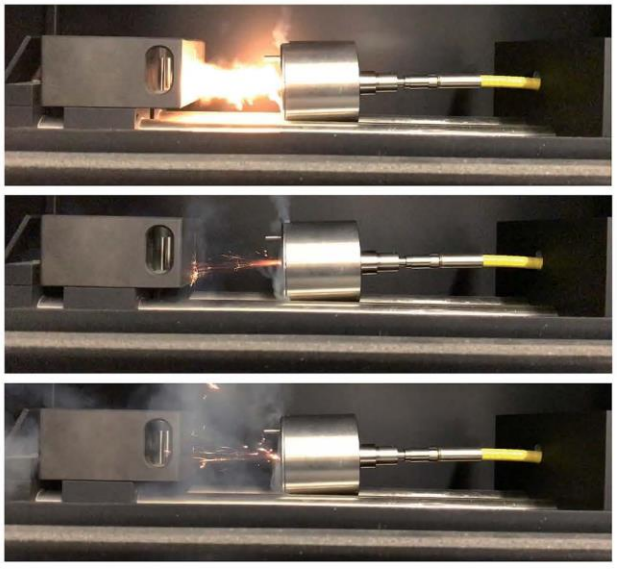


Fig. 16 Moment of deflagration of compound **22** shown as a sequence.

This journal is © The Royal Society of Chemistry 2017

Published on 19 October 2017. Downloaded by Ludwig Maximilians Universitaet Muenchen on 2/16/2022 7:53:54 AM.

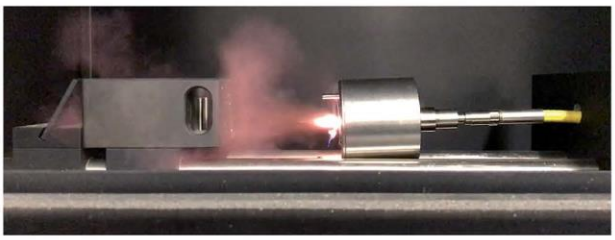


Fig. 17 Moment of detonation of complex $[Cu(MTZ)_6](ClO_4)_2$ (**19**).

was protected from the explosive by a sapphire glass. Only complexes with sensitivities in the range of PETN (IS: ≥2.5 J, FS: ≥54 N) were tested in laser initiation experiments. These compounds show slightly increased sensitivities toward mechanical stimuli but are still safe to handle. The confined samples were irradiated at a wavelength of 915 nm, a pulse length of 15 ms, a varying current of 7–10 A and a voltage of 4 V, which together results in an approximate energy output of 26–60 mJ. The investigated compounds (**14–20**, **22**, **24**, **25**, **27**, **31**, **36**, and **37**) showed different responses to the laser irradiation depending on the used metal(II) and anion.

The results of these tests are summarized in Table 4. No reaction was observed for the complexes **15**, **17**, **19** and **37** under the employed laser parameters. The other compounds could be initiated showing decompositions for **27**/**31**, deflagrations for **14**, **16**, **19**, **22**, **24**, **25** and **36** (Fig. 16 and S34–S38‡) and detonation of compound **19** (Fig. 17). The complexes exhibit different laser initiation thresholds at comparable sensitivities toward mechanical stimuli. The two cocrystallized MTZ molecules in **25** cause a higher initiation threshold in comparison to **19**, which is expressed in a higher required energy input. These results correlate with their observed sensitivities and the conclusion of a higher stability of the cocrystals. Consequently, copper(II) complex **19** represents a promising compound with manageable sensitivities, which can be initiated easily by using a laser at low initiation energies.

UV-vis spectroscopy

The solid state UV-vis spectra for the complexes **14–27**, **31** and **36** were collected in the wavelength range of 350–1000 nm in order to get a better understanding of the laser ignition process. Observed optical properties are summarized in Table 5. The step in the absorption intensity at 800 nm in the spectra is caused by a detector change. The UV-vis spectra exhibit only a qualitative character. Selected complexes of different metal centers are exemplarily shown in Fig. 18.

The coordination compounds had absorptions in the UV, visible and near-infrared region typical for the corresponding transition metals. These transitions can be assigned to the characteristic d–d-transitions and correlate with the complementary colors. As expected, the d^5 manganese(II) and d^{10} zinc(II) complexes showed no absorptions in the measured range and are illustrated together with the cocrystallized perchlorate compounds in the ESI (Fig. S39‡). The cocrystals diverged only minimally from their regular analogues. In addition, the copper(II) cyanodinitromethanide and trinitrobenzene derivative complexes **27**, **31** and **36** also have strong absorptions ranging from the UV to the visible region of the electromagnetic spectrum (Fig. S40‡). These observations indicated the expected presence of additional electronic transitions in these compounds caused by the coordinating anions (n–π*: 358 (**27**); 380 (**31**); 404 (**36**) nm).

Table 5 Optical properties of **14–27**, **31** and **36**

	M	Color	$\lambda_{d\text{-}d}$[a]	$\lambda_{915}/\lambda_{d\text{-}d}$[b]
14	Co^{III} (ls)	Orange	463	0.14
15	Mn^{II}	Colorless	—	—
16	Fe^{II} (hs)	Colorless	887	0.99
17	Co^{II}	Orange	464, 960	0.64
18	Ni^{II}	Purple	536, 883	0.75
19	Cu^{II}	Blue	663	0.46
20	Zn^{II}	Colorless	—	—
21	Mn^{II}	Colorless	—	—
22	Fe^{II} (hs)	Colorless	883	0.99
23	Co^{II}	Orange	467, 961	0.59
24	Ni^{II}	Purple	547, 904	0.84
25	Cu^{II}	Blue	676	0.42
26	Zn^{II}	Colorless	—	—
27	Cu^{II}	Blue	358[c], 612	0.53
31	Cu^{II}	Green	380[c], 630	0.74
36	Cu^{II}	Green	404[c], 657	0.69

[a] Absorption intensity maximum wavelength, which can be assigned to electron d–d excitations in the measured range of 350–1000 nm. [b] Quotient of the absorption intensity at the laser wavelength and the intensity at the d–d absorption wavelength. [c] n–π* transitions.

The laser initiation mechanism is still not fully understood.[49] Many different reaction pathways (*e.g.* electronically or thermally) are imaginable. Simply regarding the absorption of the complexes at the laser wavelength of 915 nm as shown in Fig. 18 and Table 5, one might derive a direct correlation with the performed laser ignition. In contrast to this, the examined Co(II) compound **17**, which clearly absorbs in the corresponding region, showed no reaction after exposure to laser irradiation. For MTZ complexes of iron(II) it is well known that the structure in the crystal as well as the counterion (*e.g.* ClO_4^-, BF_4^-, PF_6^- or $CF_3SO_3^-$) can have a profound effect on for example the spin

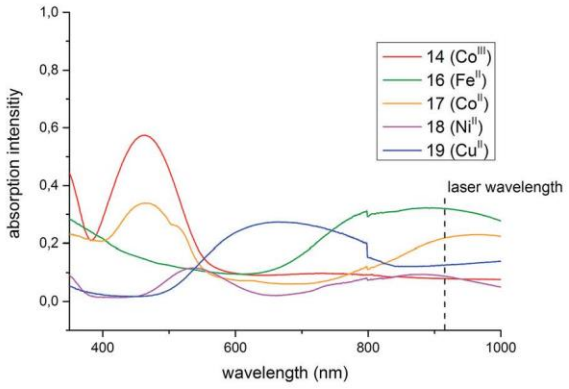


Fig. 18 UV-vis spectra in the solid state of selected complexes.

Published on 19 October 2017. Downloaded by Ludwig Maximilians Universitaet Muenchen on 2/16/2022 7:53:54 AM.

crossover properties.[50] It is possible that not only the absorption properties but also subtle changes in the geometry or crystal packing influence the susceptibility of the complexes to laser ignition. The underlying initiation processes likely depend on multiple different parameters. Based on the presented results, a general tendency has been observed that the examined compounds are more likely to deflagrate/detonate by applying laser irradiation if they exhibit high mechanical sensitivities. Due to the fact that the ligands influence the laser initiation process, as well as the process itself has not been clarified yet, future investigation will be necessary to fully understand the laser initiation of energetic materials.

Conclusions

The nitrogen-rich heterocycle 1-methyl-5*H*-tetrazole (**1**, MTZ) was synthesized in an one-pot synthesis by methylation of 1,5*H*-tetrazole. The resulting isomeric mixture was purified by distillation and yielded the desired product in a yield of 48%. In order to develop new laser-ignitable and environmentally benign primary explosives, diverse energetic coordination compounds were synthesized and characterized. The present energetic transition metal complexes are built up by the nitrogen-rich ligand 1-methyl-5-tetrazole, transition metals (Mn, Fe, Co, Ni, Cu, Zn and Ag) and oxidizing anions such as perchlorate, nitrate, cyanodinitromethanide, picrate and styphnate. The synthetic route to these complexes is simple, low-cost and fulfills environmental requirements. 31 new coordination compounds, based on MTZ as the monodentate ligand, were prepared and comprehensively characterized. Thermal analysis by DTA showed thermal stabilities with exothermic decomposition temperatures higher than or equal to 200 °C for most of the complexes (except **12** and **13**). Extraordinary endothermic events such as loss of MTZ and water during the DTA measurements were further investigated by thermal gravimetric analysis. Interesting results in terms of the decomposition pathways of selected compounds were achieved. In addition, X-ray crystal structures were determined for 28 complexes to get better insight into the interesting and challenging complex units showing (except for **13**) octahedral coordination spheres. To explore the structural diversity and to tailor the optical and energetic properties of these complexes, seven different metals and seven different ligands/counter-anions (Cl, NH_3, NO_3, ClO_4, CDNM, PA, and HTNR) were used. Preparation of the metal perchlorate complexes **15**–**20** was strongly dependent on the stoichiometry of the ligand and yielded complex units without and with (**21**–**26**) two co-crystallized tetrazoles. Cocrystallization of the endothermic MTZ molecule leads in most cases to a decrease in sensitivities toward mechanical stimuli while maintaining its highly energetic character and is therefore an excellent concept for the desensitization of energetic coordination compounds. Environmentally benign iron and copper complexes **16**, **19** and **25** were also evaluated for use as primary explosives by hot needle tests, hot plate tests and toxicity assessments. Laser ignition experiments, which were carried out at a wavelength of 915 nm and a pulse length of 15 ms showed detonation of compound **16** (IS: 2.5 J, FS: 54 N, $T_{exo.}$: 211 °C). The successful initiation makes **16** a promising candidate for future laser initiation systems.

Conflicts of interest

There are no conflicts to declare.

Acknowledgements

This work was financially supported by the Ludwig-Maximilian University of Munich (LMU). The authors want to thank Mr Stefan Huber for sensitivity measurements, Florian Binder for experimental contributions, Ms Cornelia Unger for toxicity assessments and Mr Josh Bauer for proofreading. In addition, the authors are indebted to Prof. Thomas M. Klapötke and gratefully acknowledge his financial and technical support.

Notes and references

1 https://echa.europa.eu/de/candidate-list-table, accessed August 2017.
2 G. Bélanger-Chabot, S. M. Kaplan, P. Deokar, N. Szimhardt, R. Haiges and K. O. Christe, *Chem.–Eur. J.*, 2017, **23**, 13087–13099.
3 Y. Tang, S. Dharavath, G. H. Imler, D. A. Parrish and J. M. Shreeve, *Chem.–Eur. J.*, 2017, **23**, 9185–9191.
4 J.-S. Qin, S.-J. Bao, P. Li, W. Xie, D.-Y. Du, L. Zhao, Y.-Q. Lan and Z.-M. Su, *Chem.–Asian J.*, 2014, **9**, 749–753.
5 A. Rudavskyi, R. W. A. Havenith, R. Broer, C. de Graaf and C. Sousa, *Dalton Trans.*, 2013, **42**, 14702–14709.
6 S. Li, Y. Wang, C. Qi, X. Zhao, J. Zhang, S. Zhang and S. Pang, *Angew. Chem., Int. Ed.*, 2013, **52**, 14031–14035.
7 T. Friščić and W. Jones, *Cryst. Growth Des.*, 2009, **3**, 1621–1637.
8 J. Zhang and J. M. Shreeve, *CrystEngComm*, 2016, **18**, 6124–6133.
9 J. Evers, I. Gospodinov, M. Joas, T. M. Klapötke and J. Stierstorfer, *Inorg. Chem.*, 2014, **53**, 11749–11756.
10 A. F. Stassen, O. Roubeau, I. F. Gramage, J. Linarès, F. Varret, I. Mutikainen, U. Turpeinen, J. G. Haasnoot and J. Reedijk, *Polyhedron*, 2001, **20**, 1699–1707.
11 T. Buchen, P. Poganiuch and P. Gütlich, *J. Chem. Soc., Dalton Trans.*, 1994, **15**, 2285–2288.
12 O. Roubeau, M. Evangelisti and E. Natividad, *Chem. Commun.*, 2012, **48**, 7604–7606.
13 O. S. Bushuyev, P. Brown, A. Maiti, R. H. Gee, G. R. Peterson, B. L. Weeks and L. J. Hope-Weeks, *J. Am. Chem. Soc.*, 2012, **134**, 1422–1425.
14 T. M. Klapötke, *Chemistry of High-Energy Materials*, Walter de Gruyter, Berlin, Boston, 2nd edn, 2012.
15 M. A. Ilyushin, I. V. Tselinsky and I. V. Shugalei, *Cent. Eur. J. Energ. Mater.*, 2012, **9**, 293–327.
16 B.-D. Wu, L. Yang, S.-W. Wang, T.-L. Zhang, J.-G. Zhang, Z.-N. Zhou and K.-B. Yu, *Z. Anorg. Allg. Chem.*, 2011, **637**, 450–455.
17 Z. Shunguan, W. Youchen, Z. Wenyi and M. Jingyan, *Propellants, Explos., Pyrotech.*, 1997, **22**, 317–320.

This journal is © The Royal Society of Chemistry 2017

Published on 19 October 2017. Downloaded by Ludwig Maximilians Universitaet Muenchen on 2/16/2022 7:53:54 AM.

18 K. A. McDonald, S. Seth and A. J. Matzger, *Cryst. Growth Des.*, 2015, **15**, 5963–5972.
19 T. W. Myers, K. E. Brown, D. E. Chavez, R. J. Scharff and J. M. Veauthier, *Eur. J. Inorg. Chem.*, 2016, **2016**, 3178–3183.
20 X. Fang and S. R. Ahmad, *Cent. Eur. J. Energ. Mater.*, 2016, **13**, 103–115.
21 M. Joas, T. M. Klapötke and N. Szimhardt, *Eur. J. Inorg. Chem.*, 2014, **2014**, 493–498.
22 T. W. Myers, J. A. Bjoorgard, K. E. Brown, D. E. Chavez, S. K. Hanson, R. J. Scharff, S. Tretiak and J. M. Veauthier, *J. Am. Chem. Soc.*, 2016, **138**, 4685–4692.
23 S. C. Kunz and F. J. Salas, *Proc. Int. Pyrotech. Semin.*, 1988, **13**, 505–523.
24 J. A. Merson, F. J. Salas and J. G. Harlan, *Proc. Int. Pyrotech. Semin.*, 1994, **19**, 191–206.
25 Y.-H. Zhu, D.-L. Sheng, B. Yang, L.-K. Chen and F.-E. Ma, *Hanneng Cailiao*, 2009, **17**, 169–172.
26 (*a*) E. Oliveri-Nandalà and B. Alagna, *Atti Reale Accad. Lincei*, 1910, **19**, 228–231; (*b*) E. Oliveri-Nandalà and B. Alagna, *Chem. Zentralbl.*, 1910, **1**, 1794–1795.
27 P. E. M. Wijnands, J. S. Wood, J. Reedijk and W. J. A. Maaskant, *Inorg. Chem.*, 1996, **35**, 1214–1222.
28 T. Buchen, D. Schollmeyer and P. Gütlich, *Inorg. Chem.*, 1996, **35**, 155–161.
29 J. J. Sabatini, J. M. Raab, R. K. Hann, R. Damavarapu and T. M. Klapötke, *Chem.–Asian J.*, 2012, **7**, 1657–1663.
30 Q. Yang, S. Chen, G. Xie and S. Gao, *J. Hazard. Mater.*, 2011, **197**, 199–203.
31 P. N. Gaponik, M. M. Degtyarik, A. S. Lyakhov, V. E. Matulis, O. A. Ivashkevih, M. Quesada and J. Reedijk, *Inorg. Chim. Acta*, 2005, **358**, 3949–3957.
32 P. L. Franke, J. G. Haasnoot and A. P. Zuur, *Inorg. Chim. Acta*, 1982, **59**, 5–9.
33 N. C. Baenzinger and R. J. Schultz, *Inorg. Chem.*, 1971, **10**, 661–667.
34 L. S. Ivashkevich, A. S. Lyakhov, D. O. Ivashkevich, M. M. Degtyarik and P. N. Gaponik, *Zh. Neorg. Khim.*, 2005, **50**, 82–86.
35 A. Zhilin, M. Ilyushin, I. Tselinksi, A. Kozlov and N. Kuz'mina, *Russ. J. Appl. Chem.*, 2002, **75**, 1849–1851.
36 ESI.‡
37 L. Wiehl, *Acta Crystallogr., Sect. B: Struct. Sci.*, 1993, **49**, 289–303.
38 M. H. Palmer and S. Parsons, *Acta Crystallogr., Sect. B: Struct. Sci.*, 1996, **52**, 2818–2822.
39 M. Freis, T. M. Klapötke, J. Stierstorfer and N. Szimhardt, *Inorg. Chem.*, 2017, **56**, 7936–7947.
40 B. Klewe, *Acta Chem. Scand.*, 1972, **26**, 1921–1930.
41 K. C. Patil, *J. Chem. Sci.*, 1986, **96**, 459–464.
42 R. A. F. Sherriff and A. K. Galwey, *J. Chem. Soc. A*, 1967, 1705–1708.
43 M. Joas, PhD thesis, Ludwig-Maximilians Universität, München, 2014.
44 K. Wang, D. Zeng, J.-G. Zhang, Y. Cui, T.-L. Zhang, Z.-M. Li and X. Jin, *Dalton Trans.*, 2015, **44**, 12497–12501.
45 G. I. Sunahara, S. Dodard, M. Sarrazin, L. Paquet, G. Ampleman, S. Thiboutot, J. Hawari and A. Y. Renoux, *Ecotoxicol. Environ. Saf.*, 1998, **39**, 185–194.
46 C. J. Cao, M. S. Johnson, M. M. Hurley and T. M. Klapötke, *JANNAF J. Propuls. Energet.*, 2012, vol. 5, pp. 41–51.
47 V. Ochoa-Herrera, G. Léon, Q. Banihani, J. A. Field and R. Sierra-Alvarez, *Sci. Total Environ.*, 2011, **380**, 412–413.
48 M. Joas, T. M. Klapötke, J. Stierstorfer and N. Szimhardt, *Chem.–Eur. J.*, 2013, **19**, 9995–10003.
49 E. D. Aluker, A. G. Krechetov, A. Y. Mitrofanov, D. R. Nurmukhametov and M. M. Kuklja, *J. Phys. Chem. C*, 2011, **115**, 6893–6901.
50 M. Halcrow, *Polyhedron*, 2007, **26**, 3523–3576.

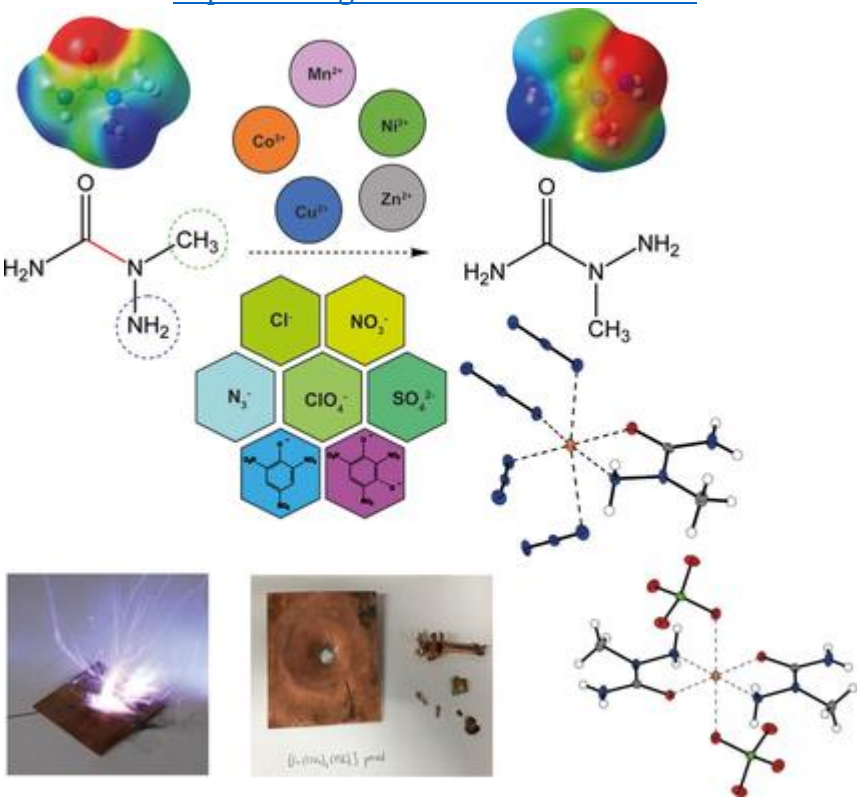
Appendix 2

Methylsemicarbazide as Ligand in Late 3d Transition Metal Complexes

N. Szimhardt, J. Stierstorfer

Chem. Europ. J. **2018**, *24*, 2687–2698.

https://doi.org/10.1002/chem.201705030



Supplementary Information:
https://chemistry-europe.onlinelibrary.wiley.com/action/downloadSupplement?doi=10.1002%2Fchem.201705030&file=chem201705030-sup-0001-misc_information.pdf

ChemPubSoc Europe

DOI: 10.1002/chem.201705030

CHEMISTRY
A European Journal
Full Paper

Transition Metal Chemistry |Hot Paper|

Methylsemicarbazide as a Ligand in Late 3d Transition Metal Complexes

Norbert Szimhardt and Jörg Stierstorfer*[a]

Abstract: Most ignition and initiation systems nowadays still contain poisonous chemicals such as lead styphnate and lead azide but also chromates and other compounds of high concern. Therefore, methylsemicarbazide (**1**, MSC), which can be prepared in a one-step reaction and in an extraordinary high yield of 95%, has been evaluated as ligand in energetic coordination compounds. For the first time 25 new transition metal complexes (Mn^{2+}, Ni^{2+}, Co^{2+}, Cu^{2+}, and Zn^{2+}) using methylsemicarbazide (**1**) as the ligand were prepared and comprehensively analyzed by, for example, XRD, IR, EA, UV/Vis and DSC/DTA/TGA. Many show a strong energetic character, which can be tuned by using different anions such as Cl^-, SO_4^{2-}, NO_3^-, ClO_4^-, picrate or styphnate. Selected compounds were additionally evaluated as lead-free primary explosives in initiation tests (nitropenta filled detonators) and in laser ignition systems. Especially compound **7** showed very promising results during these tests and could be a potential candidate for future applications.

Introduction

The investigation of energetic coordination compounds (ECC) is one of the most useful strategies in discovering new environmentally benign materials for ignition and initiation mixtures.[1–4] Ignition implies the release and transfer of energy in the form of heat, flame or subsonic shock waves. This is required for many different applications such as ammunition or in gas generators (e.g., airbags, oxygen candles). Igniters mostly contain a complex mixture of an inorganic pyrotechnic mixture or thermite as well as a weak primary explosive (often lead styphnate (LS) or diazodinitrophenol (DDNP)) and a sensitizer (often tetrazene).[5] Owing to their high toxicity and the related pollution of the environment, research into possible replacements is strongly needed.[6–8] Various requirements have to be fulfilled when synthesizing suitable candidates. The compound should not only be non-toxic and environmentally friendly but also be easily produced. Depending on the application, the mixtures can be ignited by impact, friction, light, electric impulses or heat. In contrast, initiation mixtures produce hypersonic shock waves, which are able to set off secondary explosives. Until the early 20th century, mercury fulminate (MF), first applied by Alfred Nobel, was the initiator of choice (Figure 1).[9] Nowadays, usually lead azide (LA) or silver azide are used. Initiation compositions are used, for example, in millions of commercial detonators for the mining industry but also in nearly all military warheads.

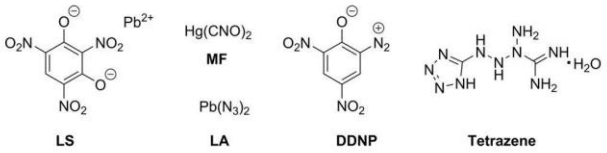


Figure 1. Molecular structures of lead styphnate (LS), mercury fulminate (MF), lead azide (LA), diazoniumdinitrophenolate (DDNP) and tetrazene.

The use of late first row transition metals (Mn^{2+}, Fe^{2+}, Co^{2+}, Ni^{2+}, Cu^{2+}, Zn^{2+}) is a good compromise for: i) availability, ii) price, iii) density, iv) toxicity (only for Mn^{2+}, Fe^{2+}, Cu^{2+} and Zn^{2+}), and v) the coordination ability to nitrogen-rich ligands because of low oxophilicity. Useful ECC contain: a) a metal cation, b) nitrogen-rich ligands and c) coordinating or non-coordinating anions (either oxygen-rich such as NO_3^-, ClO_4^-, $N(NO_2)_2^-$ or nitrogen-rich such as N_3^-, tetrazolates or triazolates). Various combinations have been described in the literature.[10] Highly energetic and sensitive complexes are formed by the combination of hydrazine derivatives (hydrazine, monomethylhydrazine, dimethylhydrazine, semicarbazide (SC), carbohydrazide (CHZ) but also *N*-amino-azoles) as the ligand with nitrate or perchlorate transition metal salts.[11,12] One of the most prominent ECC of this type is NHN (nickel hydrazine nitrate) which has also successfully been tested in detonators but contains very toxic nickel(II).[13]

Carbohydrazide (CHZ), which belongs to the group of carbazides was first synthesized 1894 by Curtius and Heidenreich who obtained the compound by the reaction of diethyl carbonate with hydrazine.[14] Since then, many carbazide-based compounds have been reported (prominent examples in Figure 2 a) with manifold uses for example as precursor of

[a] *N. Szimhardt, Dr. J. Stierstorfer*
Department of Chemistry, Ludwig Maximilian University of Munich
Butenandtstr. 5–13, 81377 Munich (Germany)
E-mail: jstch@cup.uni-muenchen.de
Homepage: http://www.hedm.cup.uni-muenchen.de

Supporting information, including X-ray data, IR spectra, DTA plots, UV/Vis spectra, experimental methods, and the ORCID numbers for the authors of this article can be found under https://doi.org/10.1002/chem.201705030.

© 2018 Wiley-VCH Verlag GmbH & Co. KGaA, Weinheim

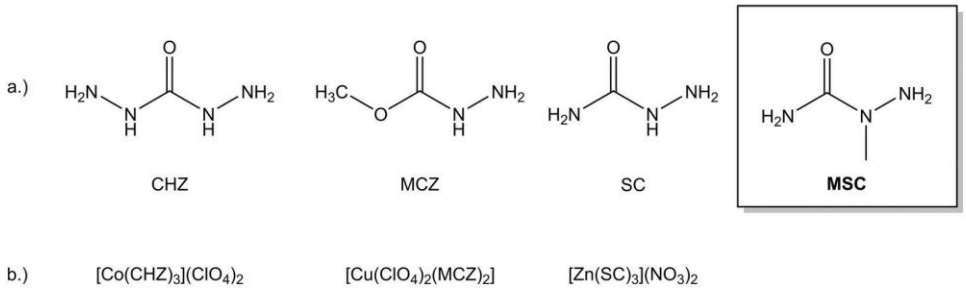


Figure 2. a) Overview of selected carbazides; b) energetic coordination compounds (ECCs) with different carbazide ligands and transition metals.[20]

drugs[15] and herbicides.[16] Also various coordination compounds were synthesized using carbazide ligands (Figure 2b) which are proposed to be interesting energetic materials.[17] Especially some of them with possible application as primary explosives[18] and partly also ignitable by laser irradiation (Figure 2b).[19]

Some of the described CHZ and SC compounds are too sensitive for any potential use. To decrease the sensitivity, we synthesized methylsemicarbazide (**1**, MSC) as a new ligand for ECC. MSC has a higher carbon content and has been shown to be an outstanding ligand for the preparation of new energetic material complexes with tunable sensitivities and promising properties.

Results and Discussion

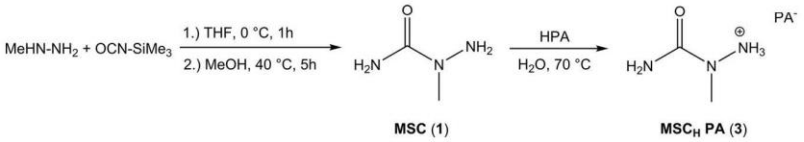
Synthesis

The title compound methylsemicarbazide (**1**) can be prepared mainly in two routes starting from different reactants. One way is the reaction of sodium cyanate with methylhydrazine in hydrochloric acid at 0 °C overnight followed by chromatographic purification.[21] Another route is the high-yielding reaction of commercially available trimethylsilylisocyanate with methylhydrazine carried out in dry THF (Scheme 1) at a temperature of 0 °C.[22] Due to the very hygroscopic character of (trimethylsilyl)isocyanate, the reaction mixture was held constant under nitrogen atmosphere. Addition of methanol and heating to 40 °C for 5 hours led to the isolation of **1** with a high yield of 95%. The acid-base reaction of **1** with picric acid in boiling water resulted in X-ray suitable crystals of the protonated picrate salt **3**.

Methylsemicarbazide (**1**) bears no acidic proton, which allows the inclusion of the neutral molecule to form complex cations or neutral metal coordination compounds with endothermic (e.g., azides) or oxidizing anions like nitrates, perchlorates, picrates (PA) or trinitroresorcinates (HTNR). The selective integration of these anions results in energetic coordination compounds with adjustable sensitivity and performance.

The coordination compounds **4–28** were prepared by the simple reaction of transition metal(II) salts with corresponding equivalents of methylsemicarbazide (**1**) as ligand in water at room or elevated temperatures (Table 1). Due to the good solubility of the resulting complexes only small quantities of solvents were used. In some cases specific amounts of co-solvents like ethanol or acid were added to the reaction mixture to get better crystallization behavior, improved yields or higher purities. The concentration of acid used as co-solvent is significant for the formation of the complexes. Excessive amounts of acid, especially for the perchlorate complexes can cause protonation of the methyl hydrazine moiety and associated blocking of a coordination site. In this context methylsemicarbazidium perchlorate (**2**) was observed. Another observation was the hydrolysis of methylsemicarbazide (**1**) in too strongly acidic media, which is detected by decomposition products like ammonium perchlorate. Also, in case of the cobalt(II) chloride complexes, two different species have been observed when using varying concentrations of acid. These are the blue water-free compound (**16**) from concentrated hydrochloric acid and a red diaqua complex (**17**) from diluted 2 M acid.

The synthesis of the zinc(II) perchlorate complexes **11** and **12** strongly depends on the stoichiometry of added ligand and yields two different coordination compounds with two or three ligands coordinating to the zinc(II) metal center, respectively. The corresponding metal(II) salts for the complexes **19–28** were synthesized in situ by reaction of metal(II) carbonates and picric/styphnic acid at 70 °C in water. The colored reaction mixtures were left for crystallization until a solid appeared. All products were filtered off, washed with cold ethanol to remove unreacted starting materials when necessary and dried, overnight, in air. Most of the compounds were obtained in yields of 28–97% directly from the mother liquor in form of



Scheme 1. Applied synthesis of methylsemicarbazide (**1**) and its protonated picrate salt (**3**).

© 2018 Wiley-VCH Verlag GmbH & Co. KGaA, Weinheim

Table 1. Synthesis of transition metal complexes **4–28** with methylsemicarbazide.

Metal Salt + Ligand $\xrightarrow[\text{Solvent}]{\text{co-Anion}}$ Product
Conditions

Metal salt	Ligand	Co-anion	Solvent	Conditions	Product	No.
$CuSO_4 \cdot 5H_2O$	2 MSC		H_2O	RT	$[Cu(H_2O)_2(MSC)_2]SO_4$	**4**
$CuCl_2 \cdot 2H_2O$	2 MSC		H_2O, 15% HCl	RT	$[CuCl_2(MSC)_2]$	**5**
$Cu(NO_3)_2 \cdot 3H_2O$	2 MSC		H_2O, EtOH	RT	$[Cu(NO_3)_2(MSC)_2]$	**6**
$Cu(ClO_4)_2 \cdot 6H_2O$	2 MSC		H_2O, 70% $HClO_4$	RT	$[Cu(ClO_4)_2(MSC)_2]$	**7**
$CuSO_4 \cdot 5H_2O$	1 MSC	2 NaN_3	H_2O	60 °C, 5 min	$[Cu(N_3)_2(MSC)_2]$	**8**
$ZnCl_2$	2 MSC		H_2O	RT	$[ZnCl_2(MSC)_2]$	**9**
$Zn(NO_3)_2 \cdot 6H_2O$	2 MSC		H_2O, EtOH	RT	$[Zn(NO_3)_2(MSC)_2]$	**10**
$Zn(ClO_4)_2 \cdot 6H_2O$	2 MSC		H_2O	RT	$[Zn(H_2O)_2(MSC)_2](ClO_4)_2$	**11**
$Zn(ClO_4)_2 \cdot 6\ H_2O$	3 MSC		H_2O	RT	$[Zn(MSC)_3](ClO_4)_2 \cdot H_2O$	**12**
$MnCl_2 \cdot 2H_2O$	2 MSC		H_2O	RT	$[MnCl_2(MSC)_2]$	**13**
$Mn(NO_3)_2 \cdot 4H_2O$	2 MSC		H_2O	RT	$[Mn(NO_3)_2(MSC)_2]$	**14**
$Mn(ClO_4)_2 \cdot 6H_2O$	2 MSC		H_2O	RT	$[Mn(H_2O)_2(MSC)_2](ClO_4)_2$	**15**
$CoCl_2 \cdot 6H2O$	2 MSC		H_2O, conc. HCl	RT	$[CoCl_2(MSC)_2]$	**16**
$CoCl_2 \cdot 6H_2O$	2 MSC		H_2O, 2 M HCl	RT	$[Co(H_2O)_2(MSC)_2]Cl_2$	**17**
$Ni(ClO_4)_2 \cdot 6H_2O$	3 MSC		H_2O	50 °C, 5 min	$[Ni(MSC)_3](ClO_4)_2$	**18**
$CuCO_3$	2 MSC	2 HPA	H_2O	70 °C, 5 min	$[Cu(PA)_2(MSC)_2]$	**19**
$ZnCO_3 \cdot 3Zn(OH)_2$	12 MSC	2 HPA	H_2O	70 °C, 5 min	$[Zn(MSC)_3](PA)_2$	**20**
$MnCO_3$	2 MSC	2 HPA	H_2O	70 °C, 5 min	$[Mn(PA)_2(MSC)_2]$	**21**
$CoCO_3 \cdot H_2O$	2 MSC	2 H_2TNR	H_2O	70 °C, 5 min	$[Co(PA)_2(MSC)_2]$	**22**
$NiCO_3 \cdot 2Ni(OH)_2 \cdot 4H_2O$	9 MSC	2 H_2TNR	H_2O	70 °C, 5 min	$[Ni(MSC)_3](PA)_2$	**23**
$CuCO_3$	2 MSC	2 H_2TNR	H_2O	70 °C, 5 min	$[Cu(H_2O)_2(MSC)_2](HTNR)_2$	**24**
$ZnCO_3 \cdot 3Zn(OH)_2$	8 MSC	2 H_2TNR	H_2O	70 °C, 5 min	$[Zn(H_2O)_2(MSC)_2](HTNR)_2$	**25**
$MnCO_3$	2 MSC	2 H_2TNR	H_2O	70 °C, 5 min	$[Mn(HTNR)_2(MSC)_2]$	**26**
$CoCO_3 \cdot H_2O$	2 MSC	2 H_2TNR	H_2O	70 °C, 5 min	$[Co(H_2O)_2(MSC)_2](HTNR)_2$	**27**
$NiCO_3 \cdot 2Ni(OH)_2 \cdot 4H_2O$	6 MSC	2 H_2TNR	H_2O	70 °C, 5 min	$[Ni(H_2O)_2(MSC)_2](HTNR)_2$	**28**

suitable crystals for X-ray determination within hours or days (details are conducted in the experimental part in the Supporting Information). Only complexes **20** and **23** precipitated as amorphous powders after the addition of the ligand and all recrystallization attempts failed. A complex formula based on elemental analysis of $[M^{II}(MSC)_3](PA)_2$ is proposed for compounds **20** and **23**. The majority of the coordination compounds were isolated water-free (without crystal water molecules or aqua ligands) which leads to a higher performance and thermal stability of the compounds. All compounds, except **2** and **16**, could be synthesized and characterized in larger quantities. For the perchlorate salt **2** and the cobalt(II) chlorido complex **16**, unfortunately, only a few single crystals could be picked between unreacted starting material, decomposition products and powder bulk material with unknown constitution. Therefore, only the crystal structures of **2** and **16** could be determined which are shown in the Supporting Information. The attempted syntheses of iron(II) and (III) as well as Ag^{I} complexes were unsuccessful.

Crystal structures

The structures of all complexes (except **20** and **23**) were determined by low temperature crystal X-ray diffraction. Details on the crystal structures of compounds **5**, **6**, **9**, **19**, **21**, **24**, **25**, **27** are given in the Supporting Information together with the measurement and refinement data. Single crystals of the zinc(II), manganese(II) and nickel(II) perchlorate complexes **11**, **12**, **15** and **18** were measured to give an indication of the most likely composition. An adequate refinement of the data set was not possible because of the strongly disordered moieties, however elemental analysis confirmed its preliminary observed structures. The coordination compounds **11**/**15** and **20**/**23** exhibit the same coordination environment and their infrared absorptions were therefore compared by infrared spectroscopy (Figure S11/12 in the Supporting Information) The crystal structures were deposited to the CSD database.[23]

Methylsemicarbazide (**1**) crystallizes in the monoclinic space group $P2_1/n$ with four formula units per unit cell and a calculated density of 1.288 g cm^{-3} at 173 K. Selected bond distances and angles of the molecule are given in Figure 3. The C–O [1.249(2) Å), C1–N1 (1.346(2) Å) and N–N (1.414(2) Å] bonds are comparable to values found in carbohydrazide and urea. Lengthening of the C–O double bond comes along with shorter C–N and N–N single bond distances and confirms the conjugation of these atoms.[24,25] In addition, stabilization of the molecular structure is generated through strong intermolecular hydrogen bonds formed between the carbonyl function and the neighboring amino groups (N1-H1B···O1 0.93(2), 2.02(2), 2.9428(19) Å, 172(17)°; N3-H3A···O1 0.947(18), 2.052(18), 2.9920(19) Å, 171.7(15)°, N3-H3B···O1 0.91(2), 2.25(2), 3.148(2) Å, 172.5(16)°). These observations are consistent with the almost planar geometry of the molecule (∡(N3-N2-C1-N1) = −5.8(2)°; ∡(C2-N2-C1-O1) = 6.9(2)°).

As described above, parent compound **1** can be protonated under certain acidic conditions. Protonation takes place on the NH_2 group of the methylhydrazine functional group and causes a reorientation of half of the molecule. The salts show

© 2018 Wiley-VCH Verlag GmbH & Co. KGaA, Weinheim

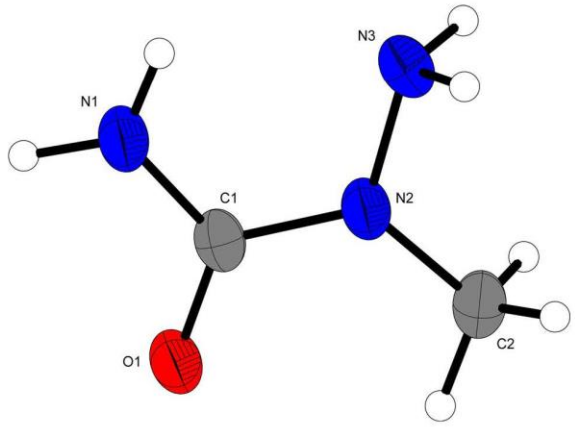


Figure 3. Molecular structure of methylsemicarbazide (**1**). Thermal ellipsoids of non-hydrogen atoms in all structures are set to the 50% probability level. Selected bond lengths (Å): O1–C1 1.249(2), N1–C1 1.346(2), N2–N3 1.414(2), N2–C1 1.349(2), N2–C2 1.445(2); selected bond angles (°): N3-N2-C1 117.81(2), N1-C1-N2 117.26(2), N3-N2-C2 119.20(2), O1-C1-N1 121.40(2), C1-N2-C2 122.26(2), O1-C1-N2 121.28(2); selected torsion angles (°): N3-N2-C1-N1 −5.8(2), C2-N2-C1-O1 6.9(2).

significantly higher densities in comparison to the neutral molecule (**2**: 1.734 g cm^{-3} (123 K); **3**: 1.750 g cm^{-3} (143 K) vs. 1.288 g cm^{-3} (173 K) for **1**). The perchlorate compound **2** crystallizes in the monoclinic space group $P2_1/c$ with sixteen formula units per unit cell. On the other hand, the picrate salt **3** crystallizes in the triclinic space group $P\bar{1}$ with two molecules in the unit cell. Structural parameters and the molecular structures of both salts are shown in Figure 4. Salt formation had no significant influence on the bond distances but rather on the planarity of the methysemicarbazinium cation with a torsion angle of ∡(C2-N2-C1-N3) = −30.1(6)° in **3**.

The bond distances and most angles of the coordinating MSC ligands in the examined coordination compounds are similar to the non-coordinated ligand **1**. The carbazide ligand is therefore not investigated or discussed in more detail in any of the compounds crystal structures outlined below. Methylsemicarbazide (**1**) is bidentate and coordinates through the carbonyl oxygen and amino-methylhydrazine nitrogen atom to

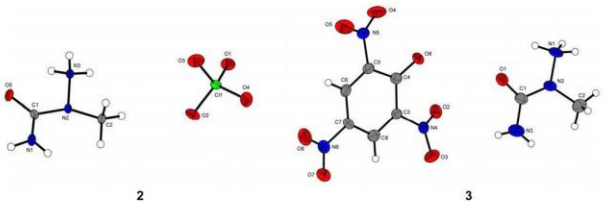


Figure 4. Molecular moieties of the MSC salts **2** (left) and **3** (right). Selected bond lengths (Å): **2**: N1–C1 1.325(4), N2–N3 1.430(3), N2–C2 1.464(4), N2–C1 1.386(4), C1–O5 1.238(4) Cl1–O1 1.438(2); **3**: N1–N2 1.446(5), N2–C1 1.405(5), N2–C2 1.457(6), N3–C1 1.322(6), C1–O1 1.228(6); selected bond angles (°): **2**: N3-N2-C1 111.3(2), N3-N2-C2 112.9(2), C1-N2-C2 124.2(2), O1-C1-N1 125.1(3), O1-C1-N2 118.0(3); **3**: N1-N2-C1 110.5(3), N1-N2-C2 112.9(3), C1-N2-C2 122.9(2), O1-C1-N2 119.7(4), O1-C1-N3 124.3(4); selected torsion angle (°): **3**: C2-N2-C1-N3 −30.1(6).

the transition metal. A reorientation of the MSC molecule, already described in the salts **2** and **3**, can be observed in the complexes (Figure 5). All complexes show a (more or less) octahedral coordination sphere, which can be explained by the low steric hindrance of the ligand.

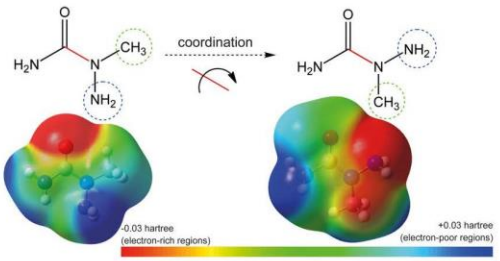


Figure 5. Reorientation of the MSC molecule after coordination or salt formation and depiction of the calculated (B3LYP/6-31G(d,p)) electrostatic potentials (3D isosurface of electron density) of **1** and its coordinated form.

The copper(II) sulfate complex **4** crystallizes in the form of blue rods in the monoclinic space group $P2_1/c$ with four formula units per unit cell and a calculated density of 1.857 g cm^{-3} at 123 K. The molecular unit shown in Figure 6 consists of a octahedrally surrounded copper(II) center with two aqua ligands along the Jahn–Teller distorted axial axis (Cu1–O8 = 2.495(3) Å) and two bidentaly connected MSC ligands in a plane (Cu1–O5 = 1.934(3), Cu1–N2 = 1.977(4) Å, ∡(O5-Cu1-N2) = 83.28(1)°, ∡(O5-Cu1-N2^{i}) = 96.73(12)°). All complexes described here show higher densities than the non-coordinating MSC molecule itself.

Complexes **5** (copper(II), green block, Figure S1 in the Supporting Information), **9** (zinc(II), colorless block, Figure S2) and **16** (cobalt(II), blue block) with coordinating chlorido ligands crystallize in the monoclinic space group $P2_1/c$ with two formula units per unit cell showing similar densities (**5**: 1.838 g cm^{-3}

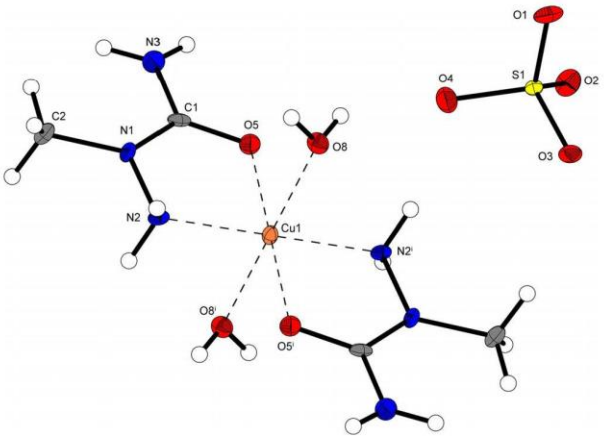


Figure 6. Molecular unit of $[Cu(H_2O)_2(MSC)_2]SO_4$ (**4**). Selected bond lengths (Å): Cu1–O5 1.934(3), Cu1-O8 2.495(3), Cu1–N2 1.977(4), S1–O1 1.467(3); selected bond angles (°): O5-Cu1-O8 88.03(11), O5-Cu1-N2 83.28(12), O8-Cu1-N2 90.26(12), O5-Cu1-O8^{i} 91.97(11), O5-Cu1-N2^{i} 96.73(12), O1-S1-O2 109.77(16). Symmetry code: (i) −x, −y, −z.

© 2018 Wiley-VCH Verlag GmbH & Co. KGaA, Weinheim

at 123 K; **9**: 1.799 g cm^{-3} and **16**: 1.791 g cm^{-3} at 123 K). The remaining complex **13** with coordinating chlorido ligands and manganese(II) transition metal center (colorless block, Figure S3) also crystallizes in a monoclinic space group ($P2_1/n$) with four formula units per unit cell and exhibits a calculated density of 1.765 g cm^{-3} at 173 K. Every metal(II) center, as illustrated for compound **16** (Figure 7), shows an octahedral surrounding with two chloridos and two methylsemicarbazides.

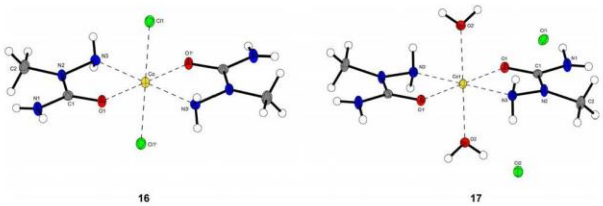


Figure 7. Complex units of compound **16** (left) and **17** (right). Selected coordination distances (Å): **16**: Co–Cl1 2.4935(6), Co1–O1 2.0396(16), Co1–N3 2.140(2); **17**: Co1–O2 2.1016(17), Co1–N3 2.138(2), Co1–O3 2.0505(16); selected bond angles (°): **16**: Cl1-Co-O1 88.48(5), Cl1-Co-N3 91.22(7), Cl1-Co-O1^{i} 91.53(5), Cl1-Co-N3^{i} 88.78(7), O1-Co-N3 78.46(8), O1-Co-N3^{i} 101.54(8); **17**: O2-Co1-O1 91.09(2), O2-Co1-N3 88.67(2), O1-Co1-N3 78.06(2), N3-Co1-O1 101.94(2). Symmetry codes: **16**: (i) 1−*x*, −*y*, 1−*z*; **17**: (i) 1−*x*, 1−*y*, 1−*z*.

On the contrary, the cobalt(II) chloride complex **17** is composed of two aqua ligands and two MSC ligands. The chlorides act only as counter-anions (Figure 7). It crystallizes in the monoclinic space group $P2_1/n$ with four formula units per unit cell and has a calculated density of 1.735 g cm^{-3} at 123 K.

The copper(II) and manganese(II) nitrato complexes **6**/**14** crystallize isotypically in the triclinic space group $P\bar{1}$ with one formula unit per unit cell (**6**: blue block, 1.873 g cm^{-3}; **14**: colorless block, 1.752 g cm^{-3} at 173 K). The colorless zinc(II) nitrato compound **10** crystallizes in the monoclinic space group $P2_1$ with two formula units per unit cell and a calculated density of 1.860 g cm^{-3} (123 K). Each metal(II) cation is bonded to two nitrato ligands in axial positions and two MSC ligands in equatorial positions. As expected, the d^9-copper(II) center shows Jahn–Teller distortion (elongation in axial direction). Their molecular motifs are illustrated in Figures 8 and S4 in the Supporting Information.

From an energetic perspective the most interesting copper(II) perchlorate complex **7** is octahedrally coordinated by two perchlorato ligands in Jahn–Teller distorted axial positions and by two chelating MSC ligands in a plane (Figure 9). It crystallizes in the form of blue blocks in the monoclinic space group $P2_1/c$ with two formula units per unit cell and the highest calculated density of 2.055 g cm^{-3} at 123 K of all complexes described here.

Copper(II) azido complex **8** crystallizes in the form of green needles in the monoclinic space group $P2_1/c$ with four formula units per unit cell and a calculated density of 2.016 g cm^{-3} at 123 K. Every copper(II) center is hexa-coordinated by one chelating MSC molecule and four bridging azido ligands forming polymeric chains. It is the only octahedral complex with just one methylsemicarbazide ligand coordinating to the metal(II) center. Due to the d^9-induced Jahn–Teller distortion, elongation

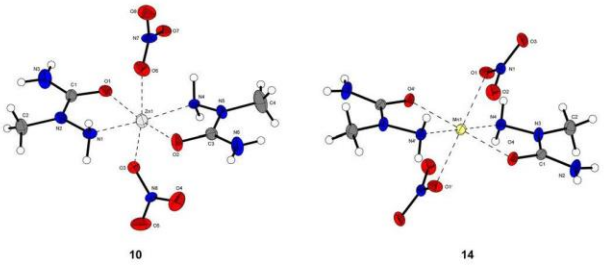


Figure 8. Molecular units of compounds **10** (left) and **14** (right). Selected coordination distances (Å): **10**: Zn1–O1 2.061(6), Zn1–O2 2.046(6), Zn1–O3 2.145(9), Zn1–O6 2.351(9), Zn1–N1 2.073(10), Zn1–N4 2.092(9); **14**: Mn1–O1 2.2176(17), Mn1–N4 2.268(2), Mn1–O4 2.1392(15); selected bond angles (°): **10**: O1-Zn1-O2 169.2(4), O1-Zn1-O3 88.7(3), O1-Zn1-O6 85.8(3), O1-Zn1-N1 78.9(4), O1-Zn1-N4 100.5(3), O2-Zn1-O3 102.0(4), O2-Zn1-O6 83.5(4), O2-Zn1-N1 99.5(4), O2-Zn1-N4 80.3(4), O3-Zn1-O6 172.5(3), O3-Zn1-N1 87.9(4), O3-Zn1-N4 97.1(3), O6-Zn1-N1 86.1(4), O6-Zn1-N4 89.0(3), N1-Zn1-N4 175.0(4); **14**: O1-Mn1-O4 89.53(5), O1-Mn1-N4 83.80(7), O1-Mn1-O4^{i} 90.47(5), O1-Mn1-N4^{i} 96.20(7), O4-Mn1-N4 73.24(6), O4-Mn1-N4^{i} 106.76(6). Symmetry code: **14**: (i) 2−*x*, −*y*, 2−*z*.

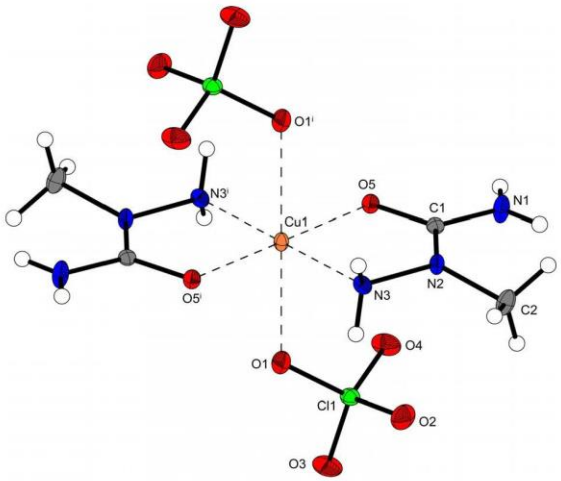


Figure 9. Complex unit of the highly energetic complex $[Cu(ClO_4)_2(MSC)_2]$ (**7**). Selected bond lengths (Å): Cu1–O1 2.4730(16), Cu1–O5 1.9257(15), Cu1–N3 1.994(2), Cl1–O1 1.4472(16); selected bond angles (°): O1-Cu1-O5 91.41(6), O1-Cu1-N3 90.07(7), O1-Cu1-O5^{i} 88.59(6), O1-Cu1-N3^{i} 89.93(7), O5-Cu1-N3 82.83(8), O5-Cu1-N3^{i} 97.17(8), O1-Cl1-O2 108.57(11). Symmetry code: (i) 2−*x*, −*y*, 1−*z*.

along the axial sites can be observed, which are occupied by azido ligands (Cu1–N6^{ii} = 2.636(3), Cu1–N9^{i} = 2.479(2) Å). The coordination environment of the copper(II) cation is depicted in Figure 10a and shows the small deviation of the ideal coordination sphere caused by the fixed structure of the azidos and the MSC ligand (∡(O1-Cu1-N3) = 81.52(7)°, ∡(N3-Cu1-N6^{ii}) = 78.03(10)°). Various coordination and bridging modes of the azido ligands (1,1; 1,3; 1,1,3; 1,1,1 etc.) are possible and known in literature.[26] The azido ligand N4-N5-N6 connects two copper(II) centers through *cis* 1,3-coordination, whereas *trans*-1,3-coordination can be observed for the second azido equivalent N7-N8-N9 (Figure 10b). This end-on binding situation causes similar bond lengths and almost linear bond

© 2018 Wiley-VCH Verlag GmbH & Co. KGaA, Weinheim

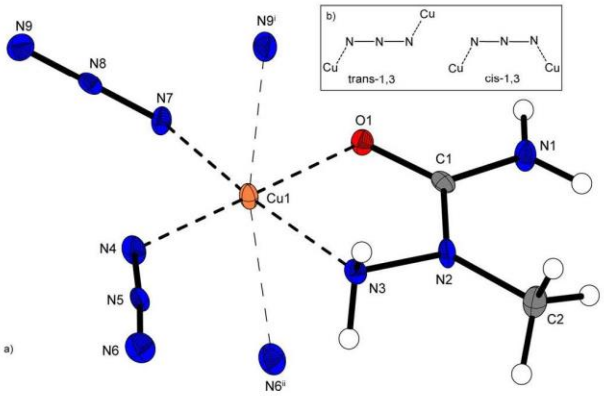


Figure 10. a) Depiction of the octahedral coordination environment of the copper(II) cation in **8**. Selected bond lengths (Å): Cu1–O1 1.957(2), Cu1–N3 2.012(3), Cu1–N4 1.963(3), Cu1–N7 1.988(2), Cu1–N6^{ii} 2.636(3), Cu1–N9^{i} 2.479(2), N4–N5 1.204(3), N5–N6 1.162(3), N7–N8 1.195(3), N8–N9 1.160(4); selected bond angles (°): O1-Cu1-N3 81.52(9), O1-Cu1-N4 179.24(9), O1-Cu1-N7 88.72(9), O1-Cu1-N6^{ii} 85.14(9), O1-Cu1-N9^{i} 86.59(9), N3-Cu1-N4 99.15(10), N3-Cu1-N7 169.26(10), N3-Cu1-N6^{ii} 78.03(10), N3-Cu1-N9^{i} 92.01(10), N4-Cu1-N7 90.58(10), N4-Cu1-N6^{ii} 94.63(11), N4-Cu1-N9^{i} 93.75(11), N6^{ii}-Cu1-N7 96.77(9), N7-Cu1-N9^{i} 91.88(9), N6^{ii}-Cu1-N9^{ii} 167.88(8), N4-N5-N6 176.4(3), N7-N8-N9 179.6(3). Symmetry codes: (i) 2.5−x, −0.5+y, 0.5−z; (ii) 1.5−x, 0.5+y, 0.5−z; b) Observed coordination modes of the azido ligand in **8**.

angles within the azido groups (N4–N5 = 1.204(3), N5–N6 = 1.162(3), N7–N8 = 1.195(3), N8–N9 = 1.160(4) Å, ∡(N4-N5-N6) = 176.4(3)°, ∡(N7-N8-N9) = 179.6(3)°).

The water-free copper(II) **19** (green block), manganese(II) **21** (yellow block) and cobalt(II) **22** (orange block) picrate complexes crystallize isotypically to each other in the triclinic space group $P\bar{1}$ with one formula unit per unit cell exhibiting very similar calculated densities (**19**: 1.885 g cm^{-3} at 123 K; **21**: 1.825 g cm^{-3} and **22**: 1.866 g cm^{-3} at 143 K) and cell dimensions. Their molecular unit consist of two chelating MSC ligands and two picrate ligands in axial positions (Figures 11 and S5, S6 in the Supporting Information). The picrate anion binds through its deprotonated phenolate-group to the transition metal(II) in a monodentate way causing shortening of the

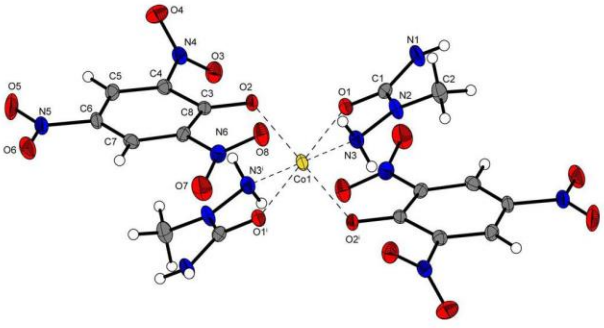


Figure 11. Molecular unit of the cobalt(II) picrate complex **22**. Selected bond lengths (Å): Co1–O1 2.0664(15), Co1–O2 2.1136(13), Co1–N3 2.115(2); selected bond angles (°): O1-Co1-O2 90.36(6), O1-Co1-N3 77.42(7), O1-Co1-O2^{i} 89.64(5), O1-Co1-N3^{i} 102.58(7), O2-Co1-N3 89.26(7), O2-Co1-N3^{i} 90.74(7). Symmetry code: (i) 1−x, 1−y, −z.

MSC bond angle due to the steric hindrance of the trinitrobenzene derivative [∡(O1-Co1-N3) = 77.42(7)°].

In comparison to the picrate compounds discussed so far, the styphnate counter-anions do not coordinate to the transition metals(II) in compounds **24**/**25** and **27**/**28**, which crystallize isotypically in the triclinic space group $P\bar{1}$ with one formula unit per unit cell and analogous cell parameters. Their densities increase in the row of Ni^{2+} (1.844 g cm^{-3}; 173 K) < Co^{2+} (1.852 g cm^{-3}; 123 K) < Zn^{2+} (1.866 g cm^{-3}, 123 K) < Cu^{2+} (1.880 g cm^{-3}; 173 K). The molecular unit of the complexes illustrated in Figure 12 and in the Supporting Information are built up by two aqua ligands, two MSC ligands and two non-

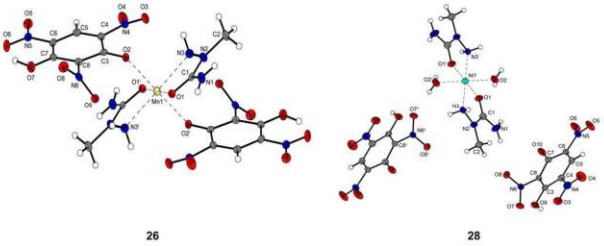


Figure 12. Complex units of compounds **26** (left) and **28** (right). Selected coordination distances (Å). **26**: Mn1–O1 2.1426(15), Mn1–O2 2.1949(15), Mn1–N3 2.266(2); **28**: Ni1–N3 2.060(3), Ni1–O1 1.9923(15), Ni1–O2 2.143(2); selected bond angles (°): **26**: O1-Mn1-O2 90.51(6), O1-Mn1-N3 73.19(7), O1-Mn1-O2^{i} 89.46(6), O1-Mn1-N3^{i} 106.81(7), O2-Mn1-N3 91.45(7), O1^{i}-Mn1-O2 89.49(6), O2-Mn1-N3^{i} 88.55(7); **28**: O1-Ni1-O2^{i} 91.30(8), O1-Ni1-N3^{i} 99.43(8), O2-Ni1-N3 85.23(9), O2-Ni1-N3^{i} 94.78(9), O1^{i}-Ni1-O2^{i} 88.70(8), O1^{i}-Ni1-N3^{i} 80.57(8). Symmetry codes: **26**: (i) 1−x, 1−y, −z; **28**: (i) −x, −y, 1−z; (ii) 1−x, 1−y, 1−z.

coordinating styphnates. The space group $P\bar{1}$ could also be determined for the water-free manganese(II) picrate complex **26** (1.892 g cm^{-3} at 123 K), which shows a different molecular composition with no aqua ligands, but two coordinating styphnate ligands instead (Figure 12). A similar situation that was found for the picrates with distortion along the MSC bond angle can also be observed for the styphnate coordination compounds. Each copper(II) complex in **19** and **24** shows Jahn–Teller distortion with longer axial bond distances.

Sensitivities and thermal stability

Thermal stability measurements of highly sensitive coordination compounds are very challenging because quantities larger than about 2 mg can damage the instrument seriously. On the other hand, endothermic signals such as melting, vaporization, dehydration or loss of ligand may not be detected properly when using an inadequate amount. Approximately 1 mg of the compounds were measured with a heating rate of 5 °C min^{-1} using differential thermal analysis (DTA) and/or by thermal gravimetric analysis (TGA). Critical temperatures are given as onset temperatures and are summarized in Table 2. Additional details on the DTA plots of **6–8**, **11**, **12**, **15** and **18** are given in the Supporting Information. The majority of the investigated compounds have exothermic decomposition events higher or close to 180 °C. Losses of water or ligands ex-

© 2018 Wiley-VCH Verlag GmbH & Co. KGaA, Weinheim

Table 2. Thermal stability measurements of **1**, **3–15** and **17–28** by DTA.

	$T_{endo1.}$ [°C][a]	$T_{endo2.}$ [°C][a]	$T_{exo.}$ (°C)[b]
MSC (**1**)	60	111	–
MSC_H PA (**3**)	–	–	166
$[Cu(H_2O)_2(MSC)_2]SO_4$ (**4**)	144	–	156
$[CuCl_2(MSC)_2]$ (**5**)	146	–	166
$[Cu(NO_3)_2(MSC)_2]$ (**6**)	–	–	147
$[Cu(ClO_4)_2(MSC)_2]$ (**7**)	–	–	186
$[Cu(N_3)_2(MSC)]$ (**8**)	–	–	121
$[ZnCl_2(MSC)_2]$ (**9**)	171	–	186
$[Zn(NO_3)_2(MSC)_2]$ (**10**)	183	–	208
$[Zn(H_2O)_2(MSC)_2](ClO_4)_2$ (**11**)	114	–	231
$[Zn(MSC)_3](ClO_4)_2{\cdot}H_2O$ (**12**)	123	187	333
$[MnCl_2(MSC)_2]$ (**13**)	107	189	209
$[Mn(NO_3)_2(MSC)_2]$ (**14**)	169	–	208
$[Mn(H_2O)_2(MSC)_2](ClO_4)_2$ (**15**)	96	–	234
$[Co(H_2O)_2(MSC)_2]Cl_2$ (**17**)	99	259	266
$[Ni(MSC)_3](ClO_4)_2$ (**18**)	252	–	258
$[Cu(PA)_2(MSC)_2]$ (**19**)	–	–	179
$[Zn(MSC)_3](PA)_2$ (**20**)	–	–	190
$[Mn(PA)_2(MSC)_2]$ (**21**)	–	–	190
$[Co(PA)_2(MSC)_2]$ (**22**)	–	–	211
$[Ni(MSC)_3](PA)_2$ (**20**)	–	–	217
$[Cu(H_2O)_2(MSC)_2](HTNR)_2$ (**24**)	119	–	179
$[Zn(H_2O)_2(MSC)_2](HTNR)_2$ (**25**)	134	–	195
$[Mn(HTNR)_2(MSC)_2]$ (**26**)	–	–	184
$[Co(H_2O)_2(MSC)_2](HTNR)_2$ (**27**)	155	–	205
$[Ni(H_2O)_2(MSC)_2](HTNR)_2$ (**28**)	172	–	193

Onset temperatures at a heating rate of 5° min^{-1}. [a] Endothermic peak, which indicates melting, vaporization, dehydration or loss of coordinating MSC molecules. [b] Exothermic peak, which indicates decomposition.

pressed by endothermic decomposition points have been observed partly at lower temperatures. Methylsemicarbazide (**1**) showed no exothermic decomposition event in the measured range of 25–400 °C but had indeed two endothermic points. Compound **1** first melts (60 °C) and vaporizes afterwards at temperatures above 110 °C, which was determined by constant weight loss during TGA (Figure 13). This behavior could be a possible explanation for the exceptional endothermic peaks observed for **5**, **9**, **10**, **12–14**, **17** and **18** during DTA measurements. Endothermic loss of coordinating MSC molecules could lead to the formation of intermediate species, which decompose in an exothermic manner at later stages. Numerous decomposition paths and mechanisms are possible. Similar phenomena have already been described in the literature.[27–29] The ligand vaporization tendency and the relating bond strengths are strongly influenced by the metal $[Zn(ClO_4)_2$ (**12**) vs. $Ni(ClO_4)_2$ (**18**), Figure S12 in the Supporting Information], anion $[Cu(NO_3)_2$ (**6**) vs. $Cu(ClO4)_2$ (**19**), Figure S12] and the corresponding coordination environment ($Zn(ClO_4)_2$, (**11**) vs. (**12**)). The copper(II) azido (Figure 13) and nitrato complexes **6** and **8**, which decompose exothermically at low temperatures of 121 °C (**8**) and 147 °C (**6**) showed the lowest thermal stabilities of all investigated coordination compounds. Comparing them to the other complexes bearing different anions, but the same metal ion, the decomposition temperatures increase in the following order: N_3^- (121 °C) < NO_3^- (146 °C) < SO_4^{2-} (156 °C) < Cl^- (166 °C) < PA^- (179 °C) ≈ $HTNR^-$ (179 °C) < ClO_4^- (186 °C). This

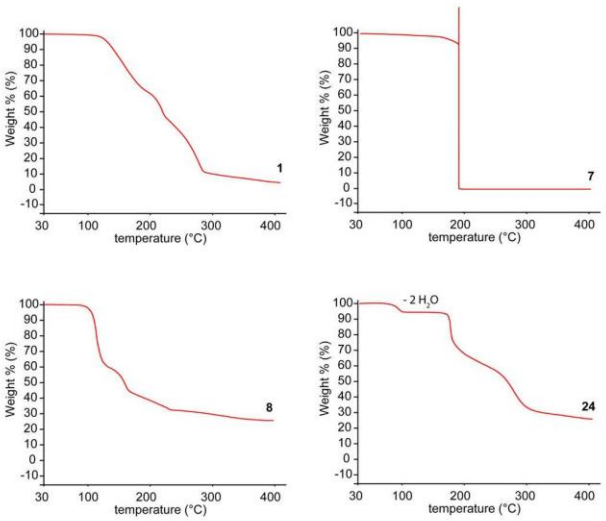


Figure 13. TGA measurements of the free ligand **1** and selected complexes at a heating rate of 5° min^{-1}.

general trend underlines the importance and correlation of the decomposition temperature with the anion and coordination environment.

The water-free metal(II) MSC picrate coordination compounds showed relatively high thermal stabilities ranging from 179 °C for **19** up to 217 °C for **23** (Figure 14). Their exothermic decomposition temperatures increase in the following order: Cu^{2+} (179 °C) < Zn^{2+} (190 °C) ≈ Mn^{2+} (190 °C) < Co^{2+} (211 °C) < Ni^{2+} (217 °C). For previous complexes analogous trends have been observed.[30]

Most of the styphnate complexes showed similar thermal stabilities in comparison with the picrates but crystallized in different complex structures. Instead of coordinating trinitrobenzene derivative ligands, complexes with two aqua molecules were obtained. Dehydration indicated by an endothermic peak in the DTA plots (see Figures 15 and 16 for thermal stabilities and DTA plots, respectively) can be achieved by heating

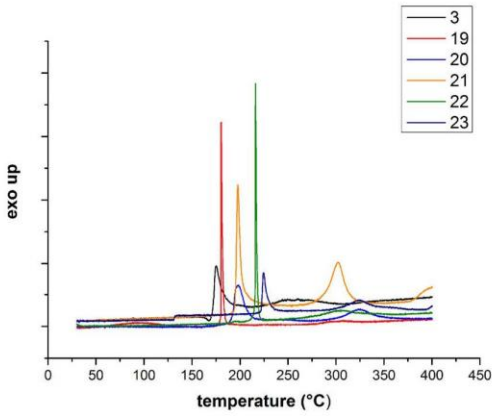


Figure 14. DTA plot (5° min^{-1}) comparison of the picrate compounds **3** and **19–23**.

© 2018 Wiley-VCH Verlag GmbH & Co. KGaA, Weinheim

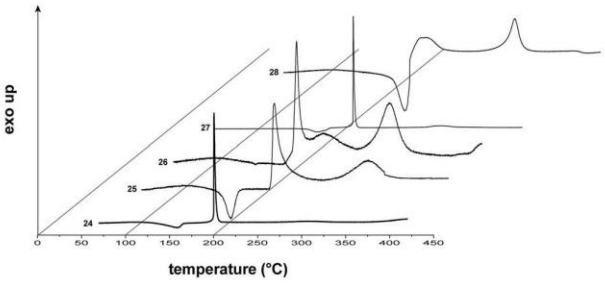


Figure 15. DTA plots (5° min^{-1}) of the styphnate complexes **24–28**.

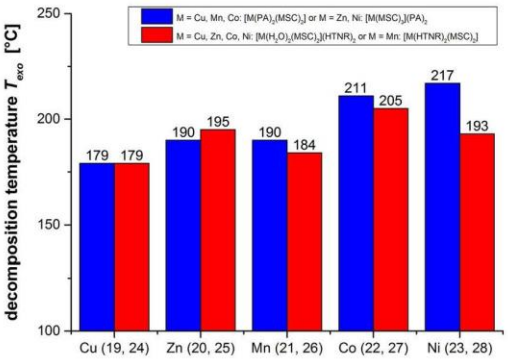


Figure 16. Comparison of the exothermic decomposition temperatures of picrate complexes with styphnate coordination compounds.

shown through weight loss during the TGA measurements (Figure 13).

The sensitivities toward impact, friction and electrostatic discharge for the compounds were determined according to BAM standards. In addition, the compounds have been classified in accordance to the "UN Recommendations on the Transport of Dangerous Goods" using the measured values. An overview of the sensitivities is given in Table 3. The uncoordinated free ligand **1** can be considered as "insensitive" with values greater than 40 J for impact, greater than 360 N for friction and an ESD value of 1.50 J. For complete energetic categorization of compound **1**, we calculated the enthalpy of formation to be −205 kJ mol^{-1}.[31] So the compound is formed exothermically in contrast to the condensed phase heat of formation of monomethylhydrazine (54.1 kJ mol^{-1}).[32]

The sulfate, chloride and nitrate complexes are insensitive against impact, friction and ESD (except compound **6**, which is sensitive toward friction). In most cases, substitution of these anions with perchlorates, azides, picrates or styphnates causes higher sensitivities toward impact, friction and ESD (impact: 2–40 J, friction: 24–360 N; ESD: 0.07–1.50 J). All water-free compounds with coordinating picrates or styphnates are more sensitive toward mechanical stimuli than their aqua ligand-containing analogs. Compound **7**, which behaves like a primary explosive, can be classified as very sensitive toward impact and friction, but it is still safe to handle, which makes it a very suitable initiating substance. The sensitivity toward impact of the $[M^{II}(PA)_2(MSC)_2]/[M^{II}(MSC)_3](PA)_2$ complexes (Figure 17) increases in the order: $Cu^{2+} < Zn^{2+} < Ni^{2+} < Mn^{2+} < Co^{2+}$ and in the following order toward friction: $Cu^{2+} \approx Ni^{2+} < Zn^{2+} < Mn^{2+} < Ni^{2+}$. Incorporation of aqua ligands in the styphnate complexes **24**/**25** and **27**/**28** leads to an increase in stability toward mechanical stimuli but decreases its energetic character compared to the relating water-free picrate complexes (Figure 17).

Table 3. Sensitivities toward impact, friction and ESD of **1**, **3–12**, **14–15** and **17–28**.

Compound	IS [J][a]	FS [N][b]	ESD [J][c]	Grain size [μm]
1	>40	>360	1.50	<100
3	>40	160	0.65	<100
4	>40	>360	1.50	<100
5	>40	>360	1.50	<100
6	>40	324	1.50	<100
7	2	24	0.07	<100
8	10	>360	1.50	<100
9	>40	>360	1.50	<100
10	>40	>360	1.50	<100
11	>40	160	0.30	<100
12	25	>360	0.60	<100
14	40	>360	1.25	<100
15	10	216	1.00	<100
17	>40	>360	1.50	<100
18	10	<60	0.10	<100
19	30	>360	0.30	<100
20	10	360	1.00	<100
21	9	288	0.55	<100
22	5	288	0.30	<100
23	10	>360	0.75	<100
24	>40	>360	0.40	<100
25	>40	>360	1.00	<100
26	25	324	0.60	<100
27	>40	>360	1.50	<100
28	>40	>360	1.50	<100

[a] Impact sensitivity according to the BAM drophammer (method 1 of 6). [b] Friction sensitivity according to the BAM friction tester (method 1 of 6). [c] Electrostatic discharge sensitivity (OZM ESD tester); Impact: insensitive >40 J, less sensitive ≥35 J, sensitive ≥4 J, very sensitive ≤3 J; friction: insensitive >360 N, less sensitive = 360 N, sensitive <360 N and >80 N, very sensitive ≤80 N, extremely sensitive ≤10 N. According to the UN Recommendations on the Transport of Dangerous Goods.

Hot needle and hot plate tests of the most promising compound **7** showed a sharp deflagration in both tests (Figure 18). The sample was fixed on a copper plate underneath adhesive tape and initiated by a red hot needle. Strong deflagration or detonation of the compound usually indicates a valuable primary explosive. The safe and straightforward hot plate test shows only the behavior of the unconfined sample toward fast heating on a copper plate. It does not necessarily allow any conclusions on a compound's capability as a suitable primary explosive.

Based on the positive results of the hot needle and hot plate tests, the initiation capability of compound **7** toward pentaerythritol tetranitrate (PETN) as secondary explosive was investigated. A copper shell with a diameter of 7 mm and length of 88 mm was filled with 200 mg sieved PETN (grain size 100–500 μm) and pressed with a weight of 8 kg. 50 mg of the primary explosive was subsequently loosely filled on top of the main charge. To examine the influence of pressing of the

© 2018 Wiley-VCH Verlag GmbH & Co. KGaA, Weinheim

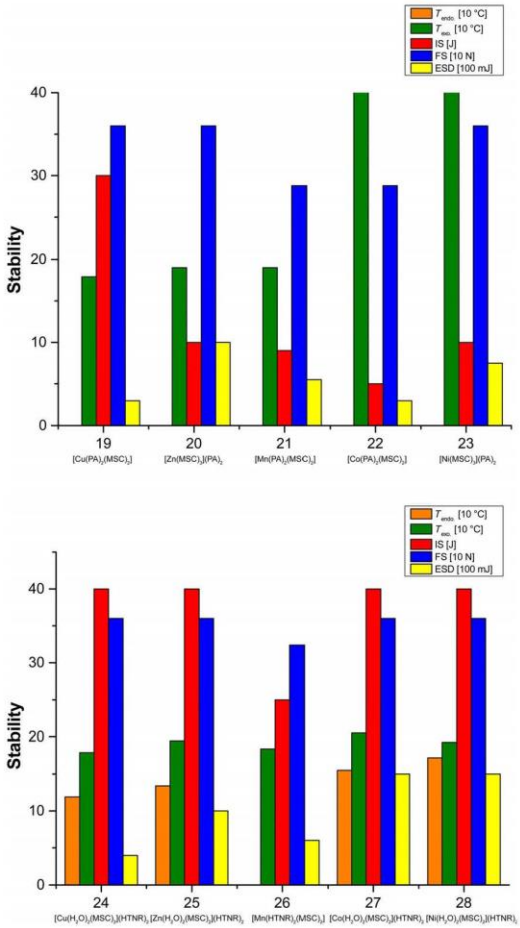


Figure 17. Stabilities of the picrate and styphnate coordination compounds **19**–**28**.



Figure 18. Moment of deflagration of compound **7** during the hot needle test (left) and hot plate test (right).

primary explosive on the initiation capability, two experiments were conducted with (a) and without pressing (b). The shell was sealed by an insulator, placed in a retaining ring, which was soldered to a copper witness plate with a thickness of 1 mm and finally initiated by a type A electrical igniter (Figure 19).

A positive test is indicated by a hole in the copper plate and fragmentation of the shell caused by a deflagration-to-detonation transition (DDT) of the secondary explosive. In the case of compound **7**, two different results are observed depending on the pressing of the sample and the related loading density (Figure 20). A negative test, represented by a nearly undamaged copper plate, was obtained after loosely filling the primary into the shell. Pressing of the sample on top of the main charge led to a positive result and complete detonation of PETN proofed by a hole in the plate.



Figure 19. Schematic test setup (left); copper shell and plate before the initiation capability test (right).

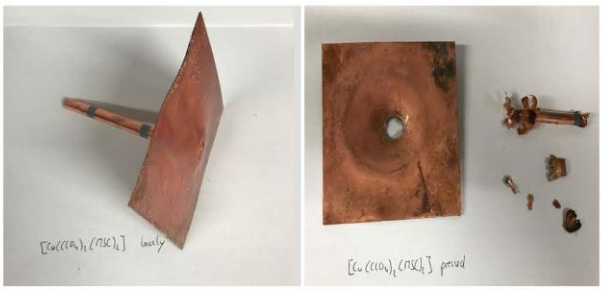


Figure 20. Negative (left) and positive (right) results of the PETN initiation tests.

Toxicity

The toxicity of compound **1** was determined using the known luminescence marine bacterium *Vibrio fischeri* to estimate the potential toxicological impact of the corresponding complexes.[33] With a value of 1.48 g L^{-1} for the half maximal effective concentration EC_{50} after 30 min, the compound can be considered as non-toxic (toxicity level after 30 min incubation: very toxic $<$0.10 g L^{-1}; toxic 0.10–1.00 g L^{-1}; non-toxic $>$1.00 g L^{-1}).[34]

Laser initiation

In recent years, more and more research groups all over the world have been working intensively on new laser ignitable energetic materials.[3,35,36] The laser initiation shows many advantages compared to conventional methods like mechanical stimuli or heat and investigated compounds do not require high sensitivities toward the customary stimuli. Consequently, laser ignitable explosives with high performance, high thermal stability and no impact on the environment can be used as insensitive but powerful energetic materials to allow much safer handling and prevent undesired initiations. About 15 mg of the carefully pestled complex to be investigated were filled into a transparent plastic cap, pressed with a pressure force of

© 2018 Wiley-VCH Verlag GmbH & Co. KGaA, Weinheim

1 kN and sealed by a UV-curing adhesive. The laser initiation experiments were carried out with a 45 W InGaAs laser diode operating in the single-pulsed mode. The diode was connected to an optical fiber with a core diameter of 400 μm and a cladding diameter of 480 μm. The optical fiber was coupled by a SMA-type connecter directly to the laser and to a collimator. This collimator was linked to an optical lens, which was positioned in its focal distance (f=29.9 mm) to the sample. The lens was protected from the explosive by a sapphire glass. The confined samples were irradiated at a wavelength of 915 nm, a voltage of 4 V and varying parameters regarding pulse length (0.1 ms or 15 ms) and current (8 A or 9 A). The combined current and pulse length result in an approximately energy output of 0.20 mJ (0.1 ms/8 A) and 34 mJ (15 ms/9 A). Only selected compounds with promising properties (**7**, **8** and **18**) were tested toward laser irradiation and showed different responses depending on the used metal(II) and anion. A summary of the test results is given in Table 4. All investigated complexes could be initiated showing detonations for **7** and **18** (Figure 21) and decomposition for compound **8** under the applied laser parameters.

Table 4. Results of the laser ignition tests.[a]

Compound	0.1 ms/8 A	15 ms/9 A
7	det.	–
8	dec.	–
18	*x*	det.

[a] –: not tested, *x*: no ignition, dec.: decomposition, deflag.: deflagration, det.: detonation. Operating parameters: current I=8–9 A; voltage U=4 V; theoretical maximal output power P_{max}=45 W; theoretical energy E_{max}=0.20–34 mJ; wavelength λ=915 nm; pulse length τ=0.1–15 ms.

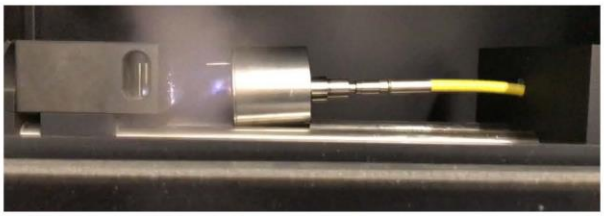


Figure 21. Moment of detonation of compound **7**.

Different laser initiation thresholds could be observed for the complexes expressed by varying outcomes and required energy inputs. Copper(II) complex **7** detonated at the lowest possible initiation energy configurable in the settings of the laser device. The compound exhibits slightly increased sensitivities against mechanical stimuli but is still safe to handle and therefore a promising candidate for future laser ignition systems.

UV/Vis spectroscopy

To get a deeper insight into the laser initiation mechanism of energetic materials solid state UV/Vis spectra for the coordination compounds **7**, **8** and **18** were recorded in the wavelength region 350–1000 nm (Figure 22). In addition, the influence of

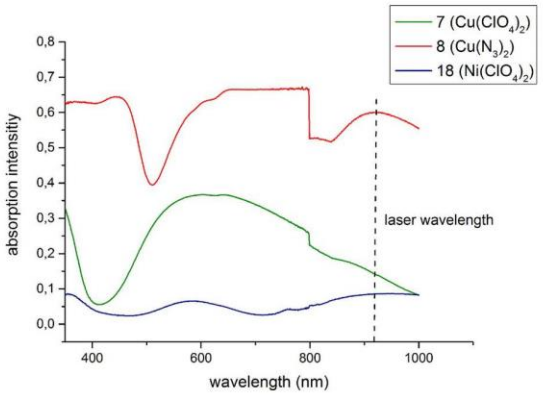


Figure 22. UV/Vis spectra in the solid state of complexes **7**, **8** and **18**. The step in the absorption intensity at 800 nm in the spectra is caused by a detector change. The UV/Vis spectra have only qualitative character.

different anions on the absorption for copper(II) complexes was investigated and compared to each other (Figure S13 in the Supporting Information). An overview of the observed optical properties is given in Table 5.

Table 5. Optical properties of **4**–**8**, and **18**.

	M	Color	$\lambda_{d\text{-}d}$[a]	$\lambda_{915}/\lambda_{d\text{-}d}$[b]
4	Cu^{II}	blue	646	0.51
5	Cu^{II}	blue	642	0.51
6	Cu^{II}	blue	603	0.46
7	Cu^{II}	blue	602	0.40
8	Cu^{II}	green	786	0.89
18	Ni^{II}	blue	581 952	0.98

[a] Absorption intensity maximum wavelength, which can be assigned to electron d–d excitations in the measured range of 350–1000 nm. [b] Quotient of the absorption intensity at the laser wavelength and the intensity at the d–d absorption wavelength.

All analyzed complexes showed characteristic absorptions in the near-infrared, visible and UV region correlating with their observed complementary colors. Depending on the transition metal (Cu^{2+} vs. Ni^{2+}) or coordination environment (blue $Cu(ClO_4)_2$ (**7**) vs. green $Cu(N_3)_2$ (**8**)) different d–d transitions can be found. As expected, the blue copper(II) complexes **4**–**7** differ only minimally from each other, which can be explained by their similar coordination environment.

The nature of the laser ignition process (e.g., thermally, electronically or combined) and the related requirements of compounds to be laser ignitable are still not fully understood.[37]

© 2018 Wiley-VCH Verlag GmbH & Co. KGaA, Weinheim

Looking at the absorption intensity of the coordination compounds at the irradiated wavelength of 915 nm (Figure 22), one could possibly derive a direct connection to the performed laser ignition because all complexes could be initiated. However, the laser initiation capability depends not only on the absorption but also on multiple other factors like crystal structure or the coordination environment.[29] It can be concluded that deflagration or detonation of the complexes after exposure to laser irradiation occurs possibly if the compounds possess high mechanical sensitivities. Considering the influence of the metal, anion and ligand on the laser initiation process, as well as that the mechanism itself has not been clarified yet, future investigations will be needed to fully understand the laser initiation of energetic materials.

Conclusions

Methylsemicarbazide (**1**, MSC), a methyl derivative of semicarbazide and member of the prominent carbazide family, was prepared in a facile one-step reaction by treatment of trimethylsilylisocyanate with methylhydrazine in a high yield of 95%. Toxicity determination showed no toxicity of **1** toward aquatic life, which makes it a suitable candidate as ligand in environmental benign complexes for various applications. In comparison to hydrazine and methylhydrazine as ligands (both show high toxicities), significantly less sensitive compounds are obtained which might be a reason of the negative heat of formation ($-205\ kJ\,mol^{-1}$) of **1**. In the present extensive study, 25 new coordination compounds, with **1** as the ligand, were synthesized and investigated. Coordination causes intramolecular rotation of the bidentate ligand and leads to an increase in density in comparison to the free compound **1**. Obtained complexes are composed of a 3d transition metal (Mn, Co, Ni, Cu, Zn), methylsemicarbazide and varying anions (SO_4^{2-}, Cl^-, NO_3^-, ClO_4^-, N_3^-, picrates, styphnates). Attempts using Fe^{II} and Fe^{III} salts failed. The concept of energetic coordination compounds (ECC), which are obtained by including nitrate, perchlorate, nitrophenolates and azide anions, is a brilliant, inexpensive and simple strategy to find new laser-ignitable and eco-friendly primary explosives. Energetic and optical properties can be easily adjusted by variation of the building blocks (metal, ligand, anion). Most of the complexes showed exothermic decomposition temperatures higher or close to 180 °C during differential thermal analysis (DTA) measurements. Thermal gravimetric analysis (TGA) of selected compounds gave new insights into possible decomposition pathways at elevated temperatures. Highest stabilities toward temperature were observed for nickel(II) and cobalt(II) complexes, whereas the highest stabilities toward physical stress for manganese(II) and zinc(II) complexes. Additionally, low temperature X-ray structure elucidation for 22 compounds was achieved and allowed the correlation between crystal structure and mechanical stabilities (e.g., the bridging azido ligand in the low-performing copper(II) complex **8** vs. the highly sensitive perchlorato complex **7**). All investigated picrate complexes crystallized waterfree and showed higher sensitivities in comparison to their diaqua containing styphnate analogs. Compound **7** has a high thermal stability (186 °C) and shows manageable sensitivities for a primary explosive. Further investigation in a PETN filled copper shell proofed its suitability as lead-free alternative. The successful ignition (observing detonation) of PETN makes copper(II) complex **7** to an interesting candidate for future primary explosive applications. It can be prepared by a simple, low-cost and upscalable reaction. Also, non-classical initiation tests by laser irradiation at a wavelength of 915 nm showed detonation of complex **7** after irradiation at the lowest applicable energy input of the laser setup (0.2 mJ).

Acknowledgements

We acknowledge the financial support provided by the Ludwig–Maximilian University of Munich (LMU). The authors also want to thank Mr. Stefan Huber for sensitivity measurements, Mrs. Cornelia Unger for toxicity assessments, Mr. Josh Bauer for proofreading and Mrs. Chantal von der Heide for contribution. In addition, the authors are indebted to Prof. Thomas M. Klapötke and gratefully acknowledge his financial and technical support.

Conflict of interest

The authors declare no conflict of interest.

Keywords: coordination chemistry · laser ignition · methylsemicarbazide · primary explosives · transition metal complexes

[1] T. W. Myers, K. E. Brown, D. E. Chavez, R. J. Scharff, J. M. Veauthier, *Inorg. Chem.* **2017**, *56*, 2297–2303.
[2] S. Seth, K. A. McDonald, A. J. Matzger, *Inorg. Chem.* **2017**, *56*, 10151–10154.
[3] M. Freis, T. M. Klapötke, J. Stierstorfer, N. Szimhardt, *Inorg. Chem.* **2017**, *56*, 7936–7947.
[4] S. Li, Y. Wang, C. Qi, X. Zhao, J. Zhang, S. Zhang, S. Pang, *Angew. Chem. Int. Ed.* **2013**, *52*, 14031–14035; *Angew. Chem.* **2013**, *125*, 14281–14285.
[5] K. D. Oyler, in *Green Energetic Materials*, Wiley, **2014**, pp. 103–132.
[6] Y. Tang, C. He, L. A. Mitchell, D. A. Parrish, J. M. Shreeve, *Angew. Chem. Int. Ed.* **2016**, *55*, 5565–5567; *Angew. Chem.* **2016**, *128*, 5655–5657.
[7] D. G. Piercey, D. E. Chavez, B. L. Scott, G. H. Imler, D. A. Parrish, *Angew. Chem. Int. Ed.* **2016**, *55*, 15315–15318; *Angew. Chem.* **2016**, *128*, 15541–15544.
[8] R. Haiges, K. O. Christe, *Inorg. Chem.* **2013**, *52*, 7249–7260.
[9] R. Matyáš, J. Pachman, in *Primary Explosives*, Springer, Heidelberg **2013**.
[10] M. A. Ilyushin, I. V. Tselinsky, I. V. Shugalei, *Cent. Eur. J. Energ. Mater.* **2012**, *9*, 293–327.
[11] M. Joas, T. M. Klapötke, J. Stierstorfer, N. Szimhardt, *Chem. Eur. J.* **2013**, *19*, 9995–10003.
[12] J. Zhang, Y. Du, K. Dong, H. Su, S. Zhang, S. Li, S. Pang, *Chem. Mater.* **2016**, *28*, 1472–1480.
[13] B. Hariharanath, K. S. Chandrabhanu, A. G. Rajendran, M. Ravindran, C. B. Kartha, *Def. Sci. J.* **2006**, *56/3*, 383–389.
[14] T. Curtius, K. Heidenreich, *Chem. Ber.* **1894**, *27*, 55.
[15] M. B. Labib, P. F. Lamie, *Med. Chem. Res.* **2016**, *25*, 2607–2618.
[16] R. J. W. Cremlyn, J. L. Turner, *J. Chem. Soc. C* **1970**, 2629–2631.
[17] W.-C. Tong, J.-C. Liu, Q.-Y. Wang, L. Yang, T.-L. Zhang, *Z. Anorg. Allg. Chem.* **2014**, *640*, 2991–2997.
[18] a) V. P. Sinditskii, A. E. Fogelz'ang, M. D. Dutov, V. V. Serushkin, S. P. Yarkov, B. S. Svetlov, *Zh. Neorg. Khim.* **1986**, *31*, 1759–1765; b) V. P. Sinditskii, A. E. Fogelz'ang, M. D. Dutov, V. I. Sokol, V. V. Serushkin, B. S.

© 2018 Wiley-VCH Verlag GmbH & Co. KGaA, Weinheim

Svetlov, M. A. Porai-Koshits, *Zh. Neorg. Khim.* **1987**, *32*, 1944–1949; c) M. B. Talawar, A. P. Agrawal, J. S. Chhabra, S. N. Asthana, *J. Hazard. Mater.* **2004**, *113*, 57–65.

[19] M. Joas, T. M. Klapötke, *Propellants Explos. Pyrotech.* **2015**, *40*, 246–252.

[20] C. Sitong, G. Weiming, Z. Bo, Z. Tonglai, Y. Li, *Polyhedron* **2016**, *117*, 110–116.

[21] X. Fu, F. He, Y. Li, L. Liu, Y. Mi, Y.-C. Xu, G. Xun, Z. Yu, J. Y. Zhang, M. Dai, Heterocyclic hydrazone compounds as c-Met tyrosine kinase inhibitors and their preparation and use in the treatment of cancer and inflammation, WO2011018454A1, Novartis AG, Basel, **2011**.

[22] A. Shibayama, R. Kajiki, M. Kobayashi, T. Mitsunari, A. Nagamatsu, Preparation of 6-acyl-1,2,4-triazine-3,5-dione derivatives as herbicides, WO2012002096A1, Kumiai Chemical Industry Co., Ltd., Japan, Ihara Chemical Industry Co., Ltd., **2012**.

[23] CCDC 1534424 (**1**), 1534443 (**2**), 1574510 (**3**), 153442 (**4**), 153442 (**5**), 153442 (**6**), 153442 (**7**), 153442 (**8**), 1580445 (**9**), 1534421 (**10**), 1534435 (**13**), 1534440 (**14**), 1534429 (**16**), 1534441 (**17**), 1534429 (**19**), 1574511 (**21**), 1574509 (**22**), 1534442 (**24**), 1534434 (**25**), 1534437 (**26**), 1534420 (**27**), and 1534423 (**28**) contain the supplementary crystallographic data for this paper. These data are provided free of charge by The Cambridge Crystallographic Data Centre.

[24] P. Domiano, M. A. Pellinghelli, A. Tiripicchio, *Acta Crystallogr. Sect. B* **1972**, *28*, 2495–2498.

[25] J. E. Worsham, Jr., H. A. Levy, S. W. Peterson, *Acta Crystallogr.* **1957**, *10*, 319–323.

[26] A. Cabort, B. Therrien, K. Bernauer, G. Süss-Fink, *Inorg. Chim. Acta* **2003**, *349*, 78–84.

[27] K. C. Patil, *J. Chem. Sci.* **1986**, *96*, 459–464.

[28] R. A. F. Sherriff, A. K. Galwey, *J. Chem. Soc. A* **1967**, 1705–1708.

[29] N. Szimhardt, M. H. H. Wurzenberger, A. Beringer, L. Daumann, J. Stierstorfer, *J. Mater. Chem. A* **2017**, *5*, 23753–23765.

[30] M. Joas, PhD thesis; Ludwig–Maximilians Universität München, **2014**.

[31] a) CBS-4M was applied for the electronic enthalpy; atomization method for conversion to gas phase enthalpy of formation and Trouton's rule for computing the sublimation enthalpy; b) T. Altenburg, T. M. Klapötke, A. Penger, J. Stierstorfer, *Z. Anorg. Allg. Chem.* **2010**, *636*, 463–471.

[32] NIST http://webbook.nist.gov/cgi/cbook.cgi?ID=C302012&Mask=1E9F, Accessed October 2017.

[33] G. I. Sunahara, S. Dodard, M. Sarrazin, L. Paquet, G. Ampleman, S. Thiboutot, J. Hawari, A. Y. Renoux, *Ecotoxicol. Environ. Saf.* **1998**, *39*, 185–194.

[34] C. J. Cao, M. S. Johnson, M. M. Hurley, T. M. Klapötke, *JANNAF J. Propuls. Energet.* **2012**, *5*, 41–51.

[35] T. W. Myers, J. A. Bjorgaard, K. E. Brown, D. E. Chavez, S. K. Hanson, R. J. Scharff, S. Tretiak, J. M. Veauthier, *J. Am. Chem. Soc.* **2016**, *138*, 4685–4692.

[36] M. A. Ilyushin, I. V. Tselinksi, *Zh. Prikl. Khim.* **2000**, *73*, 1233–1240.

[37] E. D. Aluker, A. G. Krechetov, A. Y. Mitrofanov, D. R. Nurmukhametov, M. M. Kuklja, *J. Phys. Chem. C* **2011**, *115*, 6893–6901.

Manuscript received: October 23, 2017
Accepted manuscript online: December 1, 2017
Version of record online: January 31, 2018

 © 2018 Wiley-VCH Verlag GmbH & Co. KGaA, Weinheim

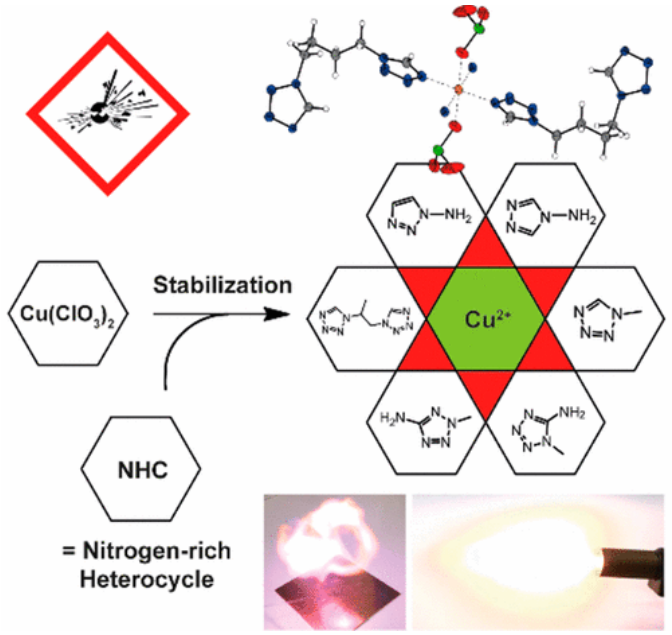
Appendix 3

Copper(II) Chlorate Complexes – the Renaissance of a Forgotten and Misjudged Energetic Anion

M. Wurzenberger, N. Szimhardt, J. Stierstorfer

J. Am. Chem. Soc. **2018**, *140*, 3206–3209.

https://doi.org/10.1021/jacs.7b13230



Supplementary Information:
https://pubs.acs.org/doi/suppl/10.1021/jacs.7b13230/suppl_file/ja7b13230_si_001.pdf

JACS
JOURNAL OF THE AMERICAN CHEMICAL SOCIETY
Cite This: J. Am. Chem. Soc. 2018, 140, 3206−3209
Communication
pubs.acs.org/JACS

Copper(II) Chlorate Complexes: The Renaissance of a Forgotten and Misjudged Energetic Anion

Maximilian H. H. Wurzenberger, Norbert Szimhardt, and Jörg Stierstorfer*

Department of Chemistry, Ludwig Maximilian University Munich, 81377 München, Germany

Supporting Information

ABSTRACT: A convenient synthetic route toward new copper(II) chlorate complexes with potential use in modern advanced ignition or initiation systems is described. Obtained compounds were not only accurately characterized (XRD, IR, UV/Vis EA and DTA) but also investigated for their energetic character (sensitivities, initiation capability and laser ignition). The copper 4-aminotriazolyl chlorate complex showed excellent initiation of PETN, while also being thermally stable and safe to handle. Solid-state UV−Vis measurements were performed to get a possible insight toward the laser initiation mechanism. In contrast to expectations, the presented copper(II) chlorate energetic coordination compounds show manageable sensitivities that can be tamed or boosted by the appropriate choice of nitrogen-rich ligands.

Downloaded via LMU MUENCHEN on February 16, 2022 at 07:55:53 (UTC).
See https://pubs.acs.org/sharingguidelines for options on how to legitimately share published articles.

The use of chlorates is still ever-present in everyday life with applications in bleach (both $NaClO_3$ and $KClO_3$ are responsible for the production of ClO_2 in elemental chlorine-free bleaching processes), oxygen candles (for aircrafts or submarines), herbicides and even medicine (e.g., $Al(ClO_3)_3$ in mouth washes against mild inflammation in the pharynx due to its astringent effect).[1] The mixture of approximately 65−80 w% potassium chlorate together with 20−35 w% red phosphorus in one of the most spectacular and sensitive formulations, called the Armstrong's mixture (Figure 1A), can cause disastrous accidents. The composition tends to spontaneous ignite when mixed or grinded. It is used in matches, fireworks, toy cap guns and earlier in primers and guns. It has nearly been completely replaced due to corrosion issues. Also, the risk of misuse is high and may lead to accidents through incorrect handling.[2] Mixtures containing chlorates with different reducing agents such as sugar, metal powders, saw dust, carbon black or graphite are extremely dangerous.[3] Chlorates possess a high oxidation potential (performance), are thermally stable (T_{dec} $NaClO_3$: 255 °C, $KClO_3$: 368 °C) and show low toxicities (LD_{50} ($NaClO_3$) 1200 mg kg^{-1}).[4] Investigations by the European Food Safety Authority showed that the potency of chlorate to the human body is 10 times lower compared with perchlorate and only chronic exposure over a long time period could cause inhibition of the thyroid iodine uptake.[5] The ongoing use of lead containing priming mixtures and the accompanied environmental accumulation holds a high ecological risk. Finally, lead styphnate and lead azide, the most commonly used substances in primer mixtures, were put on the candidate list of authorization (substances of very high concern, Annex XIV) during the REACH (Registration, Evaluation, Authorization and Restriction of Chemicals)[6] regulations in 2011 due to their high toxicity. This could lead to prohibition or restriction of the compounds, which makes research into possible alternatives very important.[7]

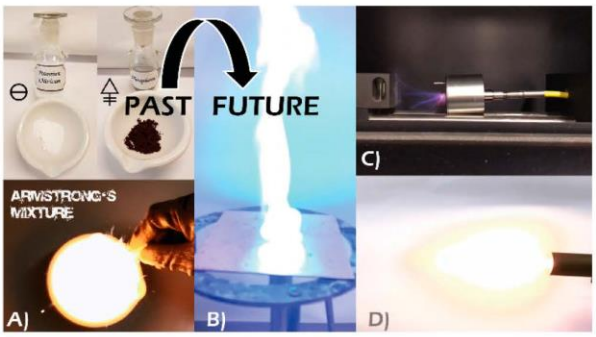


Figure 1. Old versus new: (A) Armstrong's mixture containing potassium chlorate and red phosphorus; (B) hot plate test showing blue light emission during the decomposition from copper(II) chlorates; (C) laser ignition of a copper(II) chlorate complex 8; (D) smokeless muzzle flash of a new ignition mixture.

The described approach herein for the replacement of lead containing primary explosives is the use of energetic copper(II) chlorate complexes, which were stabilized and tuned with different endothermic nitrogen-rich ligands. Interestingly, very few copper(II) complexes using chlorate as the counteranion or ligand have been described in literature. These include ammonia, a few primary amines, ethylenediamine and 4-amino-1,2,4-triazole (4-ATRI).[8] However, crystal structures and sensitivities have not been reported and energetic investigations are limited to their decomposition temperatures. This may be a consequence of the poor accessibility toward copper(II) chlorate, which is not commercially available, exists with variable water contents (4−6 H_2O) and is highly hygroscopic.[9] Although perchlorates are stronger oxidizers, the reduction of chlorates is favored, leading to an easier initiation.[10] The higher reactivity can also be explained by the missing shielding of the chlorine(+V) atom. The difficult main goal in the synthesis of metal chlorate complexes is the stabilization of the desired products. For that reason, neutral tri- and tetrazole derivatives were utilized, which are either commercially available or easy to synthesize.[11] The next

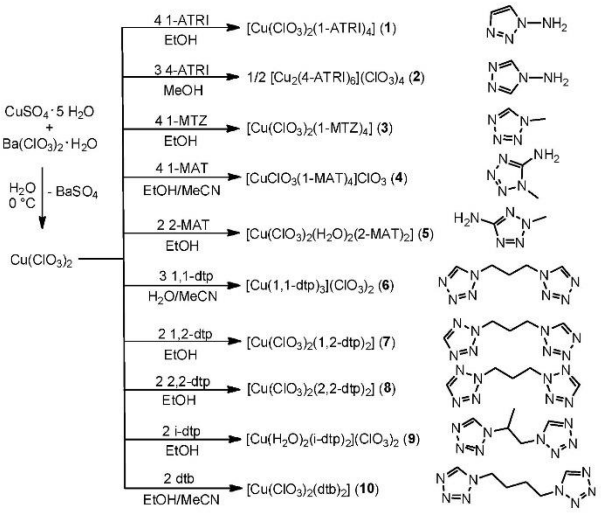
Received: December 21, 2017
Published: February 16, 2018

ACS Publications © 2018 American Chemical Society

DOI: 10.1021/jacs.7b13230
J. Am. Chem. Soc. 2018, 140, 3206−3209

challenge we faced was the difficult access to copper(II) chlorate, which was solved by a simple metathesis reaction exploiting the precipitation of barium sulfate as the driving force (Scheme 1). Due to the high hygroscopicity of copper(II)

Scheme 1. Synthesis of the Complexes 1−10 Starting from Copper(II) Sulfate and Barium Chlorate[a]



[a]Overview of used nitrogen-rich ligands: 1-ATRI: 1-amino-1,2,3-triazole; 4-ATRI: 4-amino-1,2,4-triazole; 1-MTZ: 1-methyltetrazole; 1-MAT: 1-methyl-5-aminotetrazole; 2-MAT: 2-methyl-5-aminotetrazole; 1,1-dtp: 1,3-di(tetrazol-1-yl)propane; 1,2-dtp: 1-(tetrazol-1-yl)-3-(tetrazol-2-yl)propane; 2,2-dtp: 1,3-di(tetrazol-2-yl)propane; i-dtp: 1,1′-(propane-1,2-diyl)bis(tetrazole); dtb: 1,4-di(tetrazol-1-yl)butane.

chlorate, freshly prepared alcoholic solutions (except **6**) of copper(II) chlorate were combined with respective stoichiometric amounts of the ligands dissolved in organic solvents (MeOH, EtOH, MeCN).

All compounds were analyzed by low temperature single crystal X-ray diffraction. Figure 2 shows six different coordination modes in the complexes with no (**2**, **6** and **9**), one (**4**) and two (**5** and **8**) coordinating chlorato ions. The most favored mode in this study is the octahedral coordination

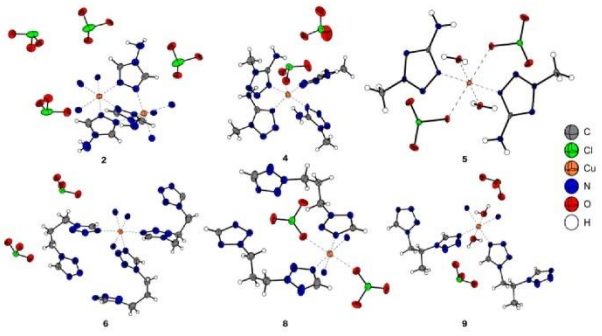


Figure 2. Different coordination modes of copper(II) chlorate complexes $[Cu_2(4\text{-ATRI})_6](ClO_3)_4$ (**2**), $[CuClO_3(1\text{-MAT})_4]ClO_3$ (**4**), $[Cu(ClO_3)_2(H_2O)_2(2\text{-MAT})_2]$ (**5**), $[Cu(1,1\text{-dtp})_3](ClO_3)_2$ (**6**), $[Cu(ClO_3)_2(2,2\text{-dtp})_2]$ (**8**) and $[Cu(H_2O)_2(i\text{-dtp})_2](ClO_3)_2$ (**9**) determined by low temperature X-ray diffraction. Ellipsoids are drawn at the 50% probability level.[12]

sphere with two coordinating chlorato ligands surrounding the copper(II) metal center. Also, an extraordinary square pyramidal coordination in compound **4** with both a coordinating chlorato ligand and a nonbinding chlorate counteranion was observed. Monodentate ligands such as 1-ATRI, 1-MTZ, and 2-MAT lead to the formation of closed octahedral coordination spheres in the complexes **1** and **3**−**5**. Whereas 4-ATRI and the propyl-linked ditetrazole isomers are bidentate and form 1D polymeric chains by coordinating between the same copper(II) cation in compounds **2** and **6**−**9**. A different situation can be found in complex **10**, where each butyl ligand bridges two different center metals forming 2D polymeric networks. Though complexes **2** and **6** are the only presented compounds with copper(II) ions exclusively coordinated by six nitrogen donors, the coordination sphere of **5** shows the greatest variety with two aqua, chlorato and tetrazole ligands each. The molecular unit of **2** consists of two different crystallographic center atoms, both showing a Jahn−Teller distortion. Whereas Cu1 exhibits a rare compressed coordination sphere with shorter axial Cu−N-bonds compared to the equatorial ones, the stretched coordination environment of Cu2 is composed of longer axial and shorter equatorial Cu−N-bonds. In contrast, the copper(II) centers in complex **6** show no distortion at all, possessing six Cu−N-bond lengths of almost the same distance.

For the determination of the compounds' deflagration to detonation transition (DDT) capability the hot plate test, hot needle test and plate dent test (Figure 3) were performed. The

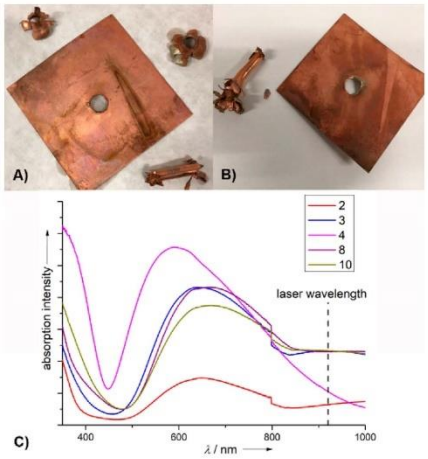


Figure 3. Positive PETN initiation test of compound **2** (A) and **8** (B); (C): solid-state UV−Vis measurements which were correlated to the laser initiation experiments.

most promising compounds in terms of performance and thermal stability are complexes **2** and **8**. Their physicochemical properties are summarized in Table 1 and compared with that of lead azide. The sensitivities toward mechanical stimuli are comparable to those observed for $Pb(N_3)_2$, whereas the susceptibility against electrostatic discharge is lower, making them safer to handle. The compounds possess both good densities and thermal stabilities.

Copper(II) chlorate complexes **2** and **8** were tested in copper shell initiation tests and showed positive DDTs toward the secondary explosive PETN (Figure 3A,B). In the laser ignition tests (Figure 1C), all complexes, except diaqua compound **9**,

DOI: 10.1021/jacs.7b13230
J. Am. Chem. Soc. 2018, 140, 3206−3209

Table 1. Physicochemical Properties of Compounds 2 and 8 Compared to Lead Azide[15]

	2	8	$Pb(N_3)_2$[15]
Formula	$C_{12}H_{24}Cl_4Cu_2N_{24}O_{12}$	$C_{10}H_{16}Cl_2CuN_{16}O_6$	PbN_6
FW [g mol^{-1}]	965.37	590.79	291.24
$\rho_{calc.}$ [g cm^{-3}] (T [K])	1.964 (143)	1.821 (173)	4.8
IS [J][a]	1	1	2.5–4
FS [N][b]	<5	<5	0.1–1
ESD [mJ][c]	15	50	6–12
T_{dec} [°C][d]	186	176	320–360

[a]Impact sensitivity according to the BAM drophammer (methods 1 of 6). [b]Friction sensitivity according to the BAM friction tester (methods 1 of 6). [c]Electrostatic discharge sensitivity (OZM ESD tester). [d]Temperature of decomposition indicated by exothermic event according to DTA (onset temperatures at a heating rate of 5 °C min^{-1}).

showed a detonation differing in the required energy input between 0.17–25.5 mJ. However, UV–Vis measurements showed that the complexes only exhibit moderate absorption in the laser wavelength area (Figure 3C). Complex **2** cannot be compared with its perchlorate analogue since no energetic properties were explored.[13] Comparing **8** to the corresponding perchlorate complex (4-ATRI as ligand), a higher decomposition temperature (250 °C), and a significantly lower density can be observed. It shows a higher friction sensitivity (8.8 N) and was positive in PETN initiation tests.[14]

The toxicity measurements, using luminescent marine bacterium *Vibrio fischeri* NRRL-B-11177, for compound **3** and comparison with the corresponding copper(II) perchlorate complex, recently published by our group,[16] prove the lower toxicity toward aquatic life of chlorate compounds.

In conclusion, we demonstrated a straightforward and low-cost synthetic route toward energetic copper(II) chlorate complexes. Complexation of $Cu(ClO_3)_2$ assures stabilization and tuning of the energetic character by the simple selection of different nitrogen-rich ligands based on tri- and tetrazole derivatives. In the course of this work, ten new coordination compounds were successfully synthesized and comprehensively compared with each other. All ten ligands lead to a disappearance of the high hygroscopy of pure copper(II) chlorate. For the first time, X-ray crystal structures of all compounds were determined and the previously predicted structure of **2**[8c] successfully proven. Thermal stability measurements by DTA showed exothermic decomposition temperatures above 150 °C for most of the compounds. Easy ignition by heat was proven by the hot needle and hot plate tests. In addition, the most promising primary explosives **2** and **8** showed excellent initiation capabilities toward the secondary PETN indicated by positive deflagration to detonation transitions. The use of alkyl-bridged ditetrazoles with longer chain lengths leads to an improvement of the mechanical sensitivities while maintaining a highly energetic character. This could be a promising concept for desensitization of energetic (copper(II) chlorate) complexes in the future. Toxicity measurements using *Vibrio fischeri* of compound **3** showed a lower toxicity in comparison to the analogous perchlorate complex and confirmed the higher environmental friendliness of chlorate compounds. During the laser ignition experiments, detonation of almost every compound was observed and demonstrated the great suitability of chlorate complexes in future laser initiation systems.

■ ASSOCIATED CONTENT

Supporting Information

The Supporting Information is available free of charge on the ACS Publications website at DOI: 10.1021/jacs.7b13230.

Experimental procedure and general methods; results and discussion; synthesis; crystal structures; sensitivities and thermal stability; laser ignition tests; UV–Vis spectroscopy; initiation capability tests; toxicity; X-ray diffraction; IR spectroscopy; references (PDF)

Data for X-ray data for compounds **1–10** (CIF)

■ AUTHOR INFORMATION

Corresponding Author

*jstch@cup.uni-muenchen.de

ORCID

Norbert Szimhardt: 0000-0001-6722-2562

Jörg Stierstorfer: 0000-0002-2105-1275

Notes

The authors declare no competing financial interest.

■ ACKNOWLEDGMENTS

Financial support of this work by the Ludwig-Maximilian University of Munich (LMU). The authors thank Prof. Dr. Thomas M. Klapötke for providing the research facilities but also for invaluable scientific input.

■ REFERENCES

(1) (a) Holleman, A. F.; Wiberg, E.; Wiberg, N. *Lehrbuch der Anorganischen Chemie*; de Gruyter: Berlin, 2007; pp 469–470. (b) Bruchhausen, F. v. *Hagers Handbuch der pharmazeutischen Praxis*; Springer Verlag: Berlin, 1995; pp 171. (c) Glasner, A.; Weidenfeld, L. *J. Am. Chem. Soc.* **1952**, *74*, 2464–2467.

(2) Kosanke, K. L.; Kosanke, B. J. *Selected Pyrotechnic Publications of K. L. and B. J. Kosanke, Part 4 (1995 Through 1997)*; Journal of Pyrotechnis: Whitewater, 1999; pp 42–43.

(3) Hofmann, K. A. In *Anorganische Chemie*; 21st ed., Hofmann, U., Rüdorff, W., Eds.; Springer Verlag: Berlin, 2013; pp 447.

(4) www.sigmaaldrich.com (accessed November 6, 2017).

(5) European Food Safety Authority (EFSA). *EFSA J.* **2015**, *13*, 4135–4238.

(6) https://echa.europa.eu/de/candidate-list-table (accessed November 6, 2017).

(7) (a) Zhang, J.; Dharavath, S.; Shreeve, J. M.; Mitchell, L. A.; Parrish, D. A. *J. Am. Chem. Soc.* **2016**, *138*, 7500–7503. (b) Myers, T. W.; Bjorgaard, J. A.; Brown, K. E.; Chavez, D. E.; Hanson, S. K.; Scharff, R. J.; Tretiak, S.; Veauthier, J. M. *J. Am. Chem. Soc.* **2016**, *138*, 4685–4692. (c) Landenberger, K. B.; Bolton, O.; Matzger, A. J. *J. Am. Chem. Soc.* **2015**, *137*, 5074–5079. (d) Ilyushin, M. A.; Tselinsky, I. V.; Shugalei, I. V. *Cent. Eur. J. Energy Mater.* **2012**, *9*, 293–327. (e) Petrie,

DOI: 10.1021/jacs.7b13230
J. Am. Chem. Soc. 2018, 140, 3206–3209

M. A.; Sheehy, J. A.; Boatz, J. A.; Rasul, G.; Prakash, G. K. S.; Olah, G. A.; Christe, K. O. *J. Am. Chem. Soc.* **1997**, *119*, 8802−8808. (f) Mi, Z.; Chen, S.; Jing, Z.; Yang, L.; Zhang, T. *Eur. J. Inorg. Chem.* **2016**, *2016*, 3978−3983. (g) Klapötke, T. M.; Petermayer, C.; Piercey, D. G.; Stierstorfer, J. *J. Am. Chem. Soc.* **2012**, *134*, 20827−20836.

(8) (a) Amiel, J. *Compt. rend.* **1934**, *199*, 51−53. (b) Amiel, J. *Compt. rend.* **1934**, *199*, 201−203. (c) Sinditskii, V. P.; Vernidub, T. Y.; Fogel'zang, A. E.; Zueva, N. A. *Izv. Vyssh. Uchebn. Zaved., Khim. Khim. Tekhnol.* **1991**, *34*, 15−19.

(9) (a) Blackburn, A. C.; Gallucci, J. C.; Gerkin, R. E. *Acta Crystallogr., Sect. B: Struct. Sci.* **1991**, *47*, 474−479. (b) Perry, D. L.; Phillips, S. L. In *Handbook of Inorganic Compounds*, 1st ed.; Perry, D. L., Phillips, S. L., Eds.; CRC Press: Boca Raton, 1995; pp 139.

(10) Brown, G. M.; Gu, B. In *Perchlorate Environmental Occurrence, Interactions and Treatment*, 1st ed.; Gu, B., Coates, J. D., Eds.; Springer Verlag: New York, 2006; pp 17−47.

(11) (a) https://www.abcr.de/startseite/ (accessed October 26, 2017). (b) van Koningsbruggen, P. J.; Garcia, Y.; Kahn, O.; Fournès, L.; Kooijman, H.; Spek, A. L.; Haasnoot, J. G.; Moscovici, J.; Provost, K.; Michalowicz, A.; Renz, F.; Gütlich, P. *Inorg. Chem.* **2000**, *39*, 1891−1900. (c) van Koningsbruggen, P. J.; Garcia, Y.; Kooijman, H.; Spek, A. L.; Haasnoot, J. G.; Kahn, O.; Linares, J.; Codjovi, E.; Varret, F. *J. Chem. Soc., Dalton Trans.* **2001**, *4*, 466−471.

(12) Selected X-ray data: **2**: *C*2/*m*, *a* 13.5622(16) Å, *b* 15.5713(18) Å, *c* 7.7338(15) Å, *β* 91.559(12)°, *V* 1632.6(4) Å^3, *Z* 4, *ρ* 1.964 g cm^{-3}; **4**: $P2_1/n$, *a* 13.1028(10) Å, *b* 10.7288(8) Å, *c* 16.2265(14) Å, *β* 95.036(7)°, *V* 2272.3(3) Å^3, *Z* 4, *ρ* 1.832 g cm^{-3}; **5**: $P\bar{1}$, *a* 6.5617(3) Å, *b* 7.5260(4) Å, *c* 9.0097(4) Å, *α* 111.762(2)°, *β* 98.711(2)°, *γ* 104.197(2)°, *V* 385.81(3) Å^3, *Z* 1, *ρ* 2.000 g cm^{-3}; **6**: $P\bar{3}c1$, *a* 10.9642(2) Å, *c* 14.3772(4) Å, *V* 1496.78(8) Å^3, *Z* 2, *ρ* 1.711 g cm^{-3}; **8**: *C*2/*c*, *a* 14.6638(7) Å, *b* 8.9883(5) Å, *c* 16.3538(8) Å, *β* 90.324(5)°, *V* 2155.44(19) Å^3, *Z* 4, *ρ* 1.821 g cm^{-3}; **9**: *C*2/*c*, *a* 15.0672(5) Å, *b* 9.0113(3) Å, *c* 17.5426(6) Å, *β* 97.696(3)°, *V* 2360.39(14) Å^3, *Z* 4, *ρ* 1.764 g cm^{-3}.

(13) Bronisz, R. *Eur. J. Inorg. Chem.* **2004**, *18*, 3688−3695.

(14) Cudziło, S.; Nita, M. *J. Hazard. Mater.* **2010**, *177*, 146−149.

(15) Meyer, R.; Köhler, J.; Homburg, A. *Explosives*; Wiley-VCH: Weinheim, 2002; pp 196−197.

(16) Szimhardt, N.; Wurzenberger, M. H. H.; Beringer, A.; Daumann, L.; Stierstorfer, J. *J. Mater. Chem. A* **2017**, *5*, 23753−23765.

DOI: 10.1021/jacs.7b13230
J. Am. Chem. Soc. 2018, 140, 3206−3209

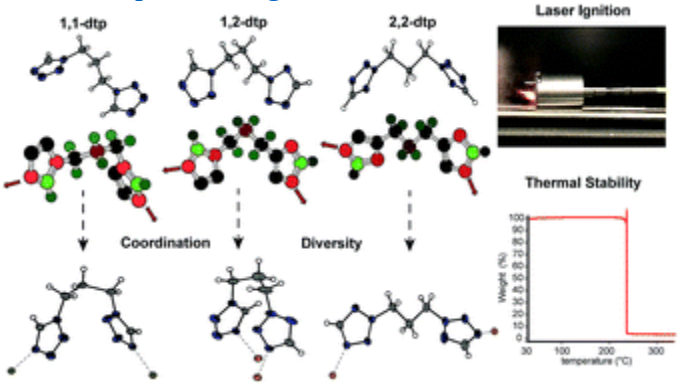
Appendix 4

Highly functional energetic complexes: stability tuning through coordination diversity of isomeric propyl-linked ditetrazoles

N. Szimhardt, M. H. H. Wurzenberger, T. M. Klapötke, J. T. Lechner, H. Reichherzer, C. C. Unger, J. Stierstorfer

Mater. Chem. A, **2018**, *6*, 6565–6577.

https://doi.org/10.1039/C8TA01412D



Supplementary Information:
https://www.rsc.org/suppdata/c8/ta/c8ta01412d/c8ta01412d1.pdf

Published on 08 March 2018. Downloaded by Ludwig Maximilians Universitaet Muenchen on 2/16/2022 7:58:20 AM.

Journal of Materials Chemistry A

PAPER

View Article Online
View Journal | View Issue

Check for updates

Cite this: J. Mater. Chem. A, 2018, 6, 6565

Highly functional energetic complexes: stability tuning through coordination diversity of isomeric propyl-linked ditetrazoles†

Norbert Szimhardt, Maximilian H. H. Wurzenberger, Thomas M. Klapötke, Jasmin T. Lechner, Hannes Reichherzer, Cornelia C. Unger and Jörg Stierstorfer *

Currently used primary explosives suffer not only from various drawbacks like insidious sensitivities toward mechanical stimuli and electrostatic discharge, but also from environmental concerns largely attributed to toxic lead compounds. These issues can directly be related to higher risk during processing and handling of these sensitive materials. In this research, 12 new lead-free energetic coordination compounds (ECCs) based on three isomeric propyl-linked ditetrazoles as ligands with moderate sensitivities are described, which can be initiated reliably and safely by irradiation with near infrared light (NIR). Excellent thermal stabilities for all complexes up to an outstanding decomposition temperature of 297 °C for compound 7 could be achieved through the formation of stable polymeric networks. The optical and energetic properties of these complexes can easily be customized by variation of various building blocks like different transition metals (Mn^{2+}, Fe^{2+}, Ni^{2+}, Co^{2+}, Cu^{2+}, Zn^{2+}, and Ag^{+}) and anions (perchlorate, styphnate, cyanodinitromethanide and dinitramide) and for the first time by the use of three different isomeric ditetrazole ligands. 1,3-Di(tetrazol-1-yl)propane (1,1-dtp), 1-(tetrazol-1-yl)-3-(tetrazol-2-yl) propane (1,2-dtp) and 1,3-di(tetrazol-2-yl)propane (2,2-dtp) were prepared in a convenient and straightforward one-step alkylation reaction of 1,5*H*-tetrazole. The obtained compounds were extensively characterized by *e.g.* XRD, IR, EA, UV/Vis and DTA. In addition, the sensitivities toward external stimuli (impact, friction and electrostatic discharge) were determined according to Bundesamt für Materialforschung und -prüfung (BAM) standard methods. Iron(II) **5** and copper(II) perchlorate complexes **8**, **11** and **12** show promising characteristics and could be potential candidates for possible applications in the future.

Received 9th February 2018
Accepted 8th March 2018

DOI: 10.1039/c8ta01412d

rsc.li/materials-a

Introduction

The first tetrazole compound mentioned in the literature, 1-phenyl-1*H*-tetrazole-5-carbonitrile, was accidentally synthesized by the Swedish chemist J. A. Bladin in 1885 at the University of Uppsala.[1] Since then numerous compounds based on this five-membered heterocycle have been prepared and extensively characterized.[2–4] Particularly in the challenging field of coordination chemistry, tetrazole ligands have proven to be versatile components that form a large number of functional materials.[5,6] These compounds show promise in many different applications such as molecular magnetism in spin-crossover systems,[7,8] porous metal–organic frameworks (MOFs) for potential gas storage,[9] and possible use as energetic materials such as secondary and primary explosives.[10,11]

The spin crossover (SCO) phenomenon, wherein the spin state of the compound alters in consequence of an external stimulus (specific temperature, pressure or light irradiation), has attracted considerable attention in recent years.[12] Especially iron(II) complexes, but also other transition metals with d^4 to d^7 electronic configuration coordinated by alkylated mono- and di-tetrazoles (Chart 1a) in combination with various counter-

University of Munich (LMU), Department of Chemistry, Butenandtstr. 5–13, D-81377, Germany. E-mail: jstch@cup.uni-muenchen.de; Fax: +49 89 2180 77007

† Electronic supplementary information (ESI) available: IR spectroscopy of **1–15**; X-ray diffraction; DTA plots of **1–3**, **8** and **10–15**; column diagrams of complexes **8** and **11–15**; hot plate and hot needle tests; laser ignition tests; UV-Vis spectra of **4**, **9**, **10** and **13–15**; experimental part and general methods. CCDC 1816637 (**1**), 1816632 (**2**), 1816943 (**3**), 1816628 (**4**), 1816635 (**5**), 1816627 (**6**), 1816626 (**8**), 1816629 (**9**), 1816630 (**10**), 1816636 (**11**), 1816633 (**12**), 1816631 (**14**) and 1816634 (**15**). For ESI and crystallographic data in CIF or other electronic format see DOI: 10.1039/c8ta01412d

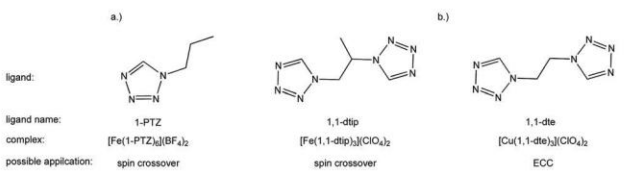


Chart 1 Overview of selected mono- and di-tetrazole ligands in combination with different metal salts proposed as: (a) spin crossover compounds or (b) ECCs.[19–21]

Published on 08 March 2018. Downloaded by Ludwig Maximilians Universitaet Muenchen on 2/16/2022 7:58:20 AM.

anions like ClO_4^- and BF_4^-, showed this behavior. The phenomenon appears as a result of the interaction between the electron–electron repulsion and the dependence of the ligand-field strength on the metal to ligand distance.[13] The complexes showed two different lattice sites for the metal centers with a spin transition (hs to ls) depending on the applied temperature. The emission of electromagnetic waves with wavelengths in the green or red region can initiate metastable long-lived hs and ls states on both sides, which makes these compounds attractive for use as molecular switches or in liquid crystals.[14] In contrast to magnetic properties, very little is known of transition metal complexes in association with energetic materials (Chart 1b), although these compounds could indeed solve two basic problems of current primary explosives: high toxicity and high sensitivity. Toxic compounds like lead azide and lead styphnate are still the main components in most priming compositions today. Due to their potential risk to the human health and the environment, many scientists from around the world are searching for alternatives with partly different approaches.[15–18]

Possible solutions comprise the use of non-toxic and sensitive: (a) neutral,[22,23] (b) ionic[24,25] or (c) coordination compounds (Chart 2).[26–28] Energetic coordination compounds (ECCs) fulfill most of the desired requirements (low-cost, high yields, good compatibilities, low environmental impact, low toxicities, *etc.*) and are therefore promising candidates for future applications in the field of high energy density materials.[29–31]

Energetic complexes hold great potential in the area of optical initiation, which offers various benefits over conventional systems (electrical, mechanical, and thermal).[32] The risk of accidental initiation by unintended impulses (impact, friction, and ESD) can be minimized through the application of less sensitive explosives (Chart 2d) with the consequence of an easier processing and handling of these materials.[33] A further advantage of laser ignition is a shorter response time toward initiation pulses after irradiation by NIR, which allows safer and more reliable initiation of the materials.[34]

Many recently developed primary explosives are struggling to meet the desired criteria regarding thermostability, which are particularly important for special applications in industry (*e.g.* mining and oil drilling).[35] Especially complex monomers without extended structures suffer from low thermal stabilities, which can most likely be attributed to a high vapor pressure of the ligands in combination with relatively weak coordination bonds.[6]

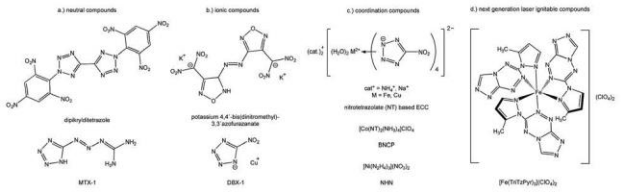


Chart 2 Different synthetic approaches in order to replace lead containing primary explosives through: (a) neutral,[22,23] (b) ionic,[24,25] (c) coordination compounds,[26–28] (d) new generation of laser ignitable explosives.[33]

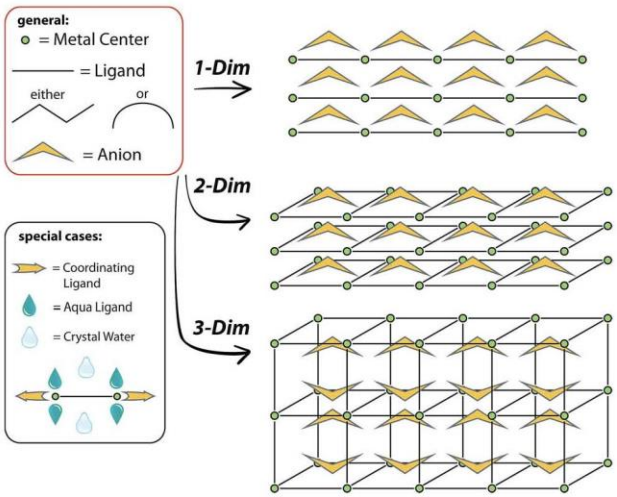


Fig. 1 Concept of thermostability in energetic coordination compounds (ECCs) achieved through the assembly of multidimensional (1D, 2D or 3D) polymeric networks (MOFs) based on bidentate bridging ditetrazole ligands.

In order to overcome the lack of thermal stability, modifications and further developments were made and bidentate bridging tetrazole ligands were incorporated into ECCs to build stable multidimensional (1D, 2D or 3D) polymeric networks (MOFs, Fig. 1). In the past, investigations of the physicochemical properties of these tetrazole based energetic complexes as well as toxicological studies toward aquatic life have proven the great suitability of these ligands.[6,17] For this purpose, three different isomeric propyl linked ditetrazoles prepared in a convenient one step reaction were selected, which until now, have only been described in correlation with magnetic studies in spin transition experiments.[36,37] Desired physicochemical properties of the compounds were easily adjusted by variation of the metal and the anion and for the first time by application of different isomers with varying complexation patterns resulting in great coordination diversity. In this contribution, reasonable efforts have been made to use these nitrogen-rich ligands as building blocks for the preparation of new energetic coordination polymers with desired characteristics, such as thermal stability and laser-ignitibility.

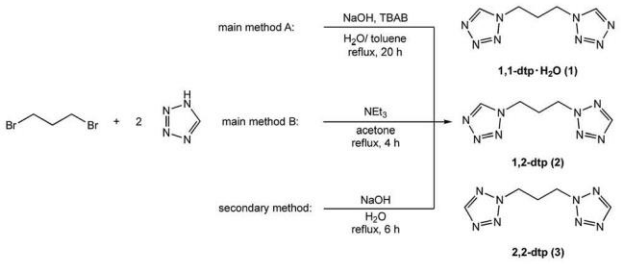
Results and discussion

Synthesis

Various synthetic pathways toward tetrazole derivatives have been reported in the literature providing an easy access to this class of compounds.[38] One commonly used route starts from primary amine precursors and enables the preparation of *N*1-substituted tetrazoles free of other regioisomers.[39,40] Corresponding amines cyclize after treatment with sodium azide and triethyl orthoformate under acidic conditions in a [2+3] cycloaddition reaction. However, the synthesis of 1,3-di(tetrazol-1-yl) propane (1,1-dtp) *via* this conventional route fails and isolation of the desired compound is not possible. Therefore, two

This journal is © The Royal Society of Chemistry 2018

Published on 08 March 2018. Downloaded by Ludwig Maximilians Universitaet Muenchen on 2/16/2022 7:58:20 AM.



Scheme 1 Preparation of propyl-linked ditetrazole isomers **1–3** *via* different synthetic pathways.

synthetic protocols have been developed, including the nucleophilic substitution reaction of 1,3-dibromopropane with sodium 5*H*-tetrazolate under various conditions.[36,37] However, this alkylation method affords an isomeric mixture containing not only 1,1-dtp but also *N*2-substituted 1,3-di(tetrazol-2-yl) propane (**3**, 2,2-dtp) and mixed *N*1,*N*2-substituted 1-(tetrazol-1-yl)-3-(tetrazol-2-yl)propane (**2**, 1,2-dtp). Latter two heterocycles, which have already been described in the literature, cannot be synthesized directly.[41–43] Therefore, an extensive investigation was carried out on the synthesis, purification and isolation of all three isomers from one reaction mixture by different preparative strategies (Scheme 1). After the evaluation and comparison of these methods, information regarding the influence of a phase transfer catalyst, varying solvents, organic/inorganic bases and a differing work-up on the reaction products (yield and ratio) was obtained and is summarized in Table 1. All syntheses examined used 1,5*H*-tetrazole as the starting material, which was deprotonated to the corresponding tetrazolate salt by sodium hydroxide (main method A and secondary method) or by triethylamine (main method B) and further reacted with the alkylating agent 1,3-dibromopropane in a nucleophilic substitution reaction. In contrast to other described syntheses using solely acetone or water as the solvent, method A included the use of a phase transfer catalyst (TBAB = tetrabutylammonium bromide) in combination with a water/toluene solvent mixture to facilitate the dispersion of the reactants. Heating of the reaction mixtures to reflux for a certain time period was accompanied by the formation of the associated bromide salts (sodium bromide or triethylammonium bromide), which were separated later during the work-up process. The separation of the crude material was accomplished through flash column chromatography on silica gel partly and through extraction and addition of different organic solvents (main method B and secondary method) based on the different polarities of the three isomers. Further details on the work-up procedures can be found in the Experimental section.

The highest overall yield was observed for method A with a value of 71%, followed by 66% for method B and only 17% for the secondary method. A possible explanation for the low yield of the secondary method could be an incomplete reaction of the starting materials due to the poor solubility of the reactants in water and losses during the work-up. The selectivity of alkylation is mainly dominated by the electronic structure of the substituents at the heterocycle and favors the formation of mixed *N*1,*N*2-substituted ditetrazole **2**. The distinction of the obtained isomers can easily be made by infrared spectroscopy (Fig. S1†) and ^{1}H and ^{13}C NMR spectroscopy. In addition, proton coupled ^{15}N NMR or two dimensional ^{1}H, ^{15}N NMR HMBC spectroscopy can be applied (Fig. 2).

Various coordination compounds based on 1,2-di(tetrazol-5-yl)ethane (1,1-dte) as the ligand have shown promising results during laser initiation experiments in the past but were too sensitive for any application.[17] In order to increase the stability, ditetrazolylpropane ligands with higher carbon contents were used for the synthesis of new complexes in this contribution. The main focus was put on the analogous *N*1,*N*1-substituted ditetrazole (1,1-dtp), which has been proven to be an extraordinary ligand for the preparation of new energetic materials. Our synthetic concept includes the formation of neutral coordination compounds or complex cations with integrated oxidizing anions like perchlorates, trinitrorescorcinates (TNRs), cyanodinitromethanides or dinitramides enabled through the incorporation of neutral non-acidic ligands. Copper(II) perchlorate containing energetic coordination compounds have shown to be very promising in laser initiation experiments and were synthesized in combination with three different propyl-linked ditetrazoles.[44]

The synthesis of coordination compounds **4–12** was achieved *via* combination of the associated metal(I,II) perchlorate salts and the respective ditetrazole ligands **1–3** in the corresponding stoichiometries at room temperature (Scheme 2). The exclusive use of water as the solvent in the synthesis of **4–9** leads to the precipitation of compound **1** among the desired complexes due

Table 1 Overview of the different methods, associated yields and isomer ratios

	Main method A	Main method B	Secondary method
Base	NaOH	NEt_3	NaOH
Solvent	Water/toluene	Acetone	Water
Temp./time	Reflux/20 h	Reflux/4 h	Reflux/6 h
Phase transfer cat.	TBAB	—	—
Work-up	Column chromatography	Desorption/column chromatography	Extraction/column chromatography
1,1-dtp·H_2O	12%	9%	8%
1,2-dtp	41%	33%	6%
2,2-dtp	18%	24%	3%
Overall yield	71%	66%	17%

Published on 08 March 2018. Downloaded by Ludwig Maximilians Universitaet Muenchen on 2/16/2022 7:58:20 AM.

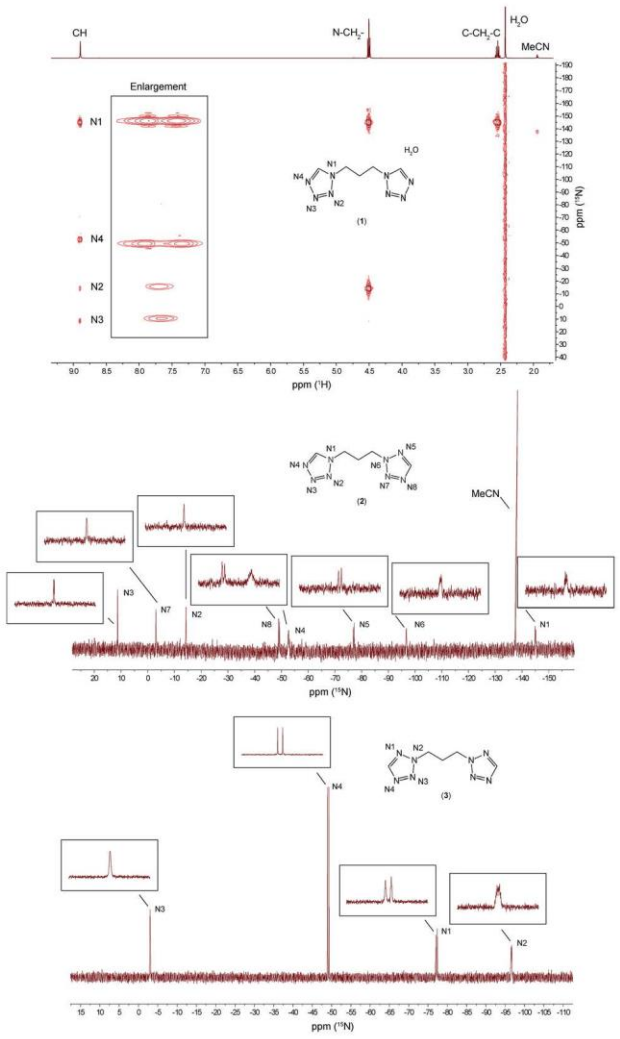
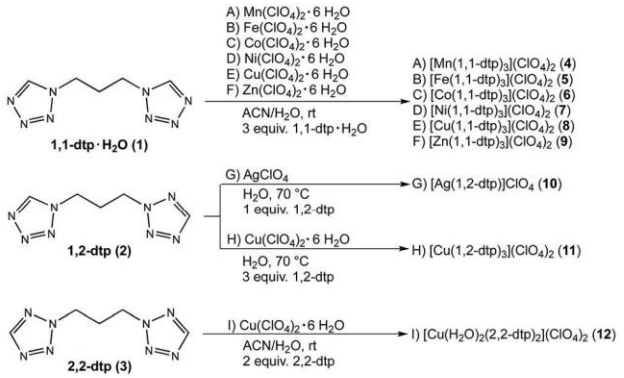


Fig. 2 Two dimensional ^{1}H, ^{15}N HMBC NMR spectrum of **1** and proton coupled ^{15}N NMR spectra of **2** and **3**.

to the low solubility of **1** in water. In order to increase the solubility of the organic alkylated heterocycles, a mixture of water and acetonitrile was chosen as the solvent and only small quantities were used to ensure fast crystallization of the desired complexes.

Coordination compounds **5** and **7** have already been described in relation to the SCO phenomenon and were prepared to close their physico-chemical gaps.[37] In addition, an intensive investigation and characterization of their energetic character has been conducted. All compounds (except **7**) were analyzed by single crystal diffraction. Nickel(II) perchlorate complex **7** precipitated, in contrast to the isotypic 1,1-dtp coordination compounds, as an amorphous powder and all recrystallization attempts failed to achieve single crystals. After the comparison of the infrared spectra of **4–9** and elemental analysis, a complex composition of $[Ni(1,1.dtp)_3](ClO_4)_2$ can be presumed for coordination compound **7**, analogous to the other perchlorate complexes (Fig. S2†).

The nitrogen-rich compound 1-(tetrazol-1-yl)-3-(tetrazol-2-yl) propane (**2**), which has been successfully inserted into the



Scheme 2 Synthesis of metal(I,II) perchlorate complexes **4–12** based on different propyl-linked ditetrazole ligands.

silver(I) and copper(II) perchlorate complexes (**10** and **11**), was used for the first time as a ligand in transition metal complexes. Each complex exhibits different absorptions in the infrared spectra showing a bidentate (**11**) or a tetradentate (**10**) complexation of the metal centers (Fig. S3†). The attempted preparation of silver(I) complexes with ligands **1** and **3** was unsuccessful.

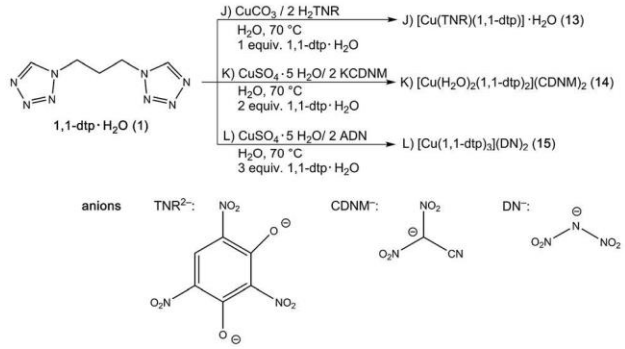
The majority of the complexes could be achieved without crystal water or aqua ligand inclusion. This has a significant influence on the stability and performance of the compounds leading to more powerful molecules. Complex **12** crystallizes, in contrast to the reported copper(II) perchlorate coordination compound, as a diaqua species, which contains only two dtp ligands independent of the stoichiometry applied (2 equiv. *vs.* 3 equiv.).[42] A possible explanation could be the formation of a kinetic ($[Cu(2,2\text{-dtp})_3](ClO_4)_2$) complex first, which reacts slowly with the solvent molecules to form a thermodynamic product ($[Cu(H_2O)_2(2,2\text{-dtp})_2](ClO_4)_2$). The copper(II) perchlorate complexes described here can easily be distinguished through IR spectroscopy due to the varying complexation manner of the three ditetrazole ligands (Fig. S4†). In particular, 2,2-dtp containing complexes have shown to crystallize primarily with solvent molecules, lowering the performance of the desired energetic material and making them unsuitable for any application.[42,43]

The commercially unavailable metal(II) salt precursors for the preparation of coordination compounds **13–15** were synthesized *in situ* through metathesis or straightforward acid–base reaction between copper(II) carbonate and styphnic acid (H_2TNR) at 70 °C in water. The corresponding precursors were then reacted with ditetrazole ligand **1** (Scheme 3) and the lower solubility of the complexes was used as the driving force. Coordination compound **13** precipitated unintentionally as double deprotonated styphnate and crystal water containing complex immediately after the addition of the ligand. Due to the low performance of the complex, no other trinitrobenzene containing anion (*e.g.* picrate) has been employed in the other complexes.

All described coordination compounds were left undisturbed for crystallization and were isolated by filtration after a solid material appeared from the mother liquor in the form of single crystals within hours or days (except nickel(II) complex **7**).

This journal is © The Royal Society of Chemistry 2018

Published on 08 March 2018. Downloaded by Ludwig Maximilians Universitaet Muenchen on 2/16/2022 7:58:20 AM.



Scheme 3 Formation of copper(II) coordination compounds **13–15** with varying anions (TNR^{2-} = trinitroresorcinate, $CDNM^-$ = cyanodinitromethanide, and DN^- = dinitramide; IR spectra illustrated in Fig. S5†).

The products were received in reasonable yields (35–89%) after washing with ice-cold ethanol to remove unreacted materials when necessary and drying in air overnight.

Crystal structures

The structure of all compounds including ligands and complexes (except **7**) was determined by low temperature X-ray diffraction. In contrast to the literature, ditetrazole **3** could be solidified through controlled freezing with liquid nitrogen and subsequent thawing to room temperature. The ligand stayed crystalline and single crystal blocks suitable for X-ray diffraction could be measured. Compound **7** emerged in the form of an amorphous powder making single crystal experiments impossible. All central atoms, except the silver(I) metal ion in complex **10**, show an octahedral coordination sphere where the complexation to the metal ion takes place through the N4 and N8 nitrogen atoms of the ditetrazolylpropanes. The chelation of the ligand is prevented through the rigidity of the propyl chains, which disables the generation of complex monomers and leads to the formation of polymeric structures with varying dimensions by bridging between the metal centres. Poor quality single crystals of complex **13** were measured to get an indication of the most likely appearance of the structure. An appropriate finalization of the data set was not possible due to the strongly disordered moieties and the related weak diffractions. Nonetheless, elemental analysis in combination with infrared spectroscopy (Fig. S5†) validated its temporarily observed structure. Details of the crystal structures of complexes **4**, **5**, **6**, **9**, and **13** are given in the ESI† together with the measurement and refinement data of all compounds. The crystal structures were deposited in the CSD database[45] and can be obtained free of charge with the CCDC no. 1816637 (**1**), 1816632 (**2**), 1816943 (**3**), 1816628 (**4**), 1816635 (**5**), 1816627 (**6**), 1816626 (**8**), 1816629 (**9**), 1816630 (**10**), 1816636 (**11**), 1816633 (**12**), 1816631 (**14**), and 1816634 (**15**).†

Compound **1** crystallizes as a monohydrate in the form of colorless blocks in the orthorhombic space group *Pbca* with eight formula units per unit cell and a calculated density of 1.439 g cm^{-3} at 173 K. One of the tetrazole rings stands in *gauche* (C1, N1–N4) orientation while the other stands in *anti* (C5, N5–N8) conformation to the propyl function (Fig. 3), similar to the situation found in an anhydrous compound reported in the literature.[36] The bond lengths of the propyl chain (C2–C3 1.5189(19) Å and C3–C4 1.5184(17) Å) are in the typical range of C–C single bonds and the distances in the tetrazole rings (N1–C1 1.3293(16) Å, N1–C2 1.4620(15) Å, N4–C1 1.3092(16) Å, N1–N2 1.3505(14) Å, N2–N3 1.2901(16) Å and N3–N4 1.3673(15) Å) are comparable to those of other 1-substituted tetrazoles.[46]

Nitrogen-rich ligand **2** crystallizes in the form of colorless blocks in the monoclinic space group $P2_1/n$ with four formula units per unit cell and a calculated density of 1.462 g cm^{-3} at 173 K. Ligand **2** shows, in contrast to compound **1**, a *gauche* conformation of both tetrazole rings to the propyl group with analogous bond lengths in the ring (C1, N1–N4) and the propyl bridge (Fig. 4). In comparison to the other tetrazole moiety, only minor deviations can be observed in the bond lengths for the *N*2-substituted heterocycle (N5–C5 1.3249(15) Å, N6–C4 1.4655(14) Å, N8–C5 1.3376(15) Å, N5–N6 1.3265(13) Å, N6–N7 1.3177(12) Å and N7–N8 1.3239(13) Å).

*N*2,*N*2-substituted ditetrazole ligand **3** crystallizes in the form of colorless blocks in the monoclinic space group $P2_1/c$ with four formula units per unit cell and a calculated density of 1.474 g cm^{-3} at 143 K. The ligand shows unlike compounds **1** and 1,2-dtp an *anti* conformation of both tetrazole heterocycles to the alkyl bridge but with similar bond lengths in the ring and chain (Fig. 5).

The coordination of the ditetrazole causes a reorientation of the ligands and is shown in Fig. 6. The bond lengths of the coordinating ligands in the investigated complexes are in the same range as that of uncoordinated ditetrazole compounds **1–3** and are not discussed in detail in any of the following ECCs.

The octahedrally coordinated metal(II) perchlorate complexes of heterocycle **1** (**4–6**, **8** and **9**) all crystallize

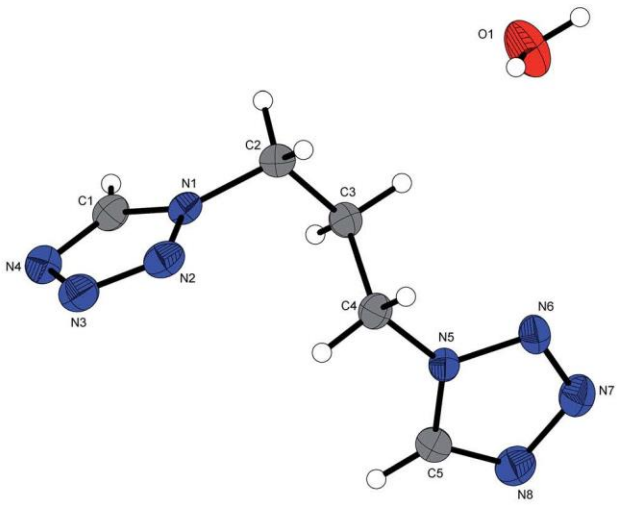


Fig. 3 Molecular unit of 1,1-dtp·H_2O (**1**). Thermal ellipsoids of non-hydrogen atoms in all structures are set to the 50% probability level. Selected bond angles (°): C2–C3–C4 112.12(11), N1–C2–C3 111.38(11), and N5–C4–C3 110.96(10).

Published on 08 March 2018. Downloaded by Ludwig Maximilians Universitaet Muenchen on 2/16/2022 7:58:20 AM.

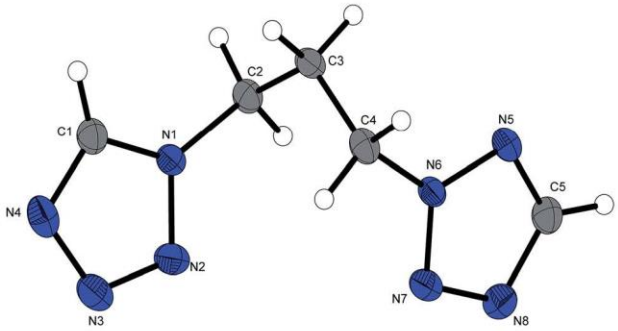


Fig. 4 Molecular unit of 1,2-dtp (**2**). Selected bond lengths(Å): C2–C3 1.5204(17), C3–C4 1.5181(16), N1–C1 1.3308(14), N1–C2 1.4670(14), N4–C1 1.3070(16), N1–N2 1.3453(13), N2–N3 1.2932(14), and N3–N4 1.3620(15); selected bond angles (°): C2–C3–C4 114.57(9), N1–C2–C3 112.19(9), and N6–C4–C3 111.93(9).

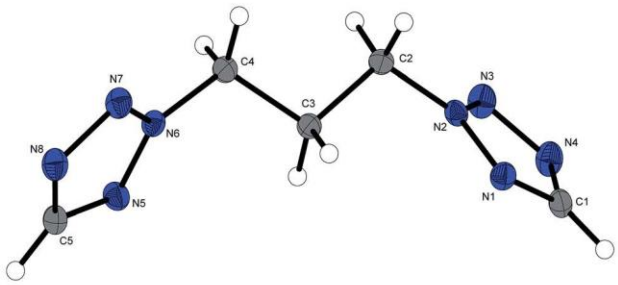


Fig. 5 Molecular unit of 2,2-dtp (**3**). Selected bond lengths(Å): C2–C3 1.5209(15), C3–C4 1.5164(15), N1–C1 1.3260(16), N2–C2 1.4593(14), N6–C4 1.4590(15), N1–N2 1.3252(14), N2–N3 1.3200(14), and N3–N4 1.3237(14); selected bond angles (°): C2–C3–C4 107.96(8), N2–C2–C3 112.05(8), and N6–C4–C3 112.19(8).

isotypically in the trigonal space group $P\bar{3}c1$ with two formula units per unit cell showing almost the same metric with varying densities between 1.656 (**4**) and 1.754 g cm^{-3} (**5**) (Mn: 1.656 (173 K); Fe: 1.754 (123 K); Co: 1.712 (173 K); Cu: 1.721 (123 K); and Zn: 1.747 (123 K) g cm^{-3}). Interestingly the expected Jahn–Teller distortion, typical of d^9 electron configuration, cannot be observed in the structure of copper(II) complex **8** (Fig. 7).

Compared to the free ligand, both tetrazole rings are in *gauche* conformation to the propyl chain enabling the formation of

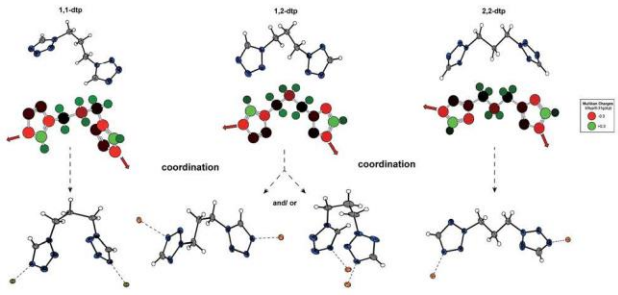


Fig. 6 Reorientation of the ditetrazoles after complexation (except complex **10**) together with the calculated (B3LYP/6-31G(d,p)) Mulliken charges of the uncoordinated dtp ligands.

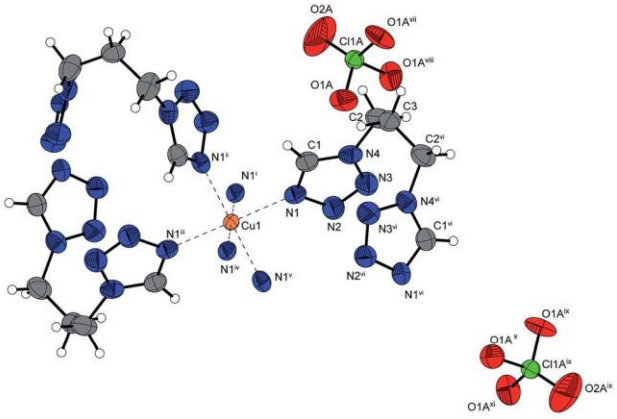


Fig. 7 Copper(II) coordination environment of $[Cu(1,1\text{-dtp})_3](ClO_4)_2$ (**8**). Selected bond length (Å): Cu–N1 2.131(2); selected bond angles (°): N1–Cu1–N1^{i} 89.33(9), N1–Cu1–N1^{iii} 180.00, and N1–Cu1–N1^{iv} 90.68(9). Symmetry codes: (i) $y, -x+y, 1-z$; (ii) $x-y, x, 1-z$; (iii) $-x, -y, 1-z$; (iv) $-y, x-y, z$; (v) $-x+y, -x, z$; (vi) $-x, -x+y, 1.5-z$; (vii) $-x+y, 1-x, z$; (viii) $1-y, 1+x-y, z$; (ix) $1+x-y, 1-y, 1.5-z$; (x) $y, x, 1.5-z$; (xi) $1-x, -x+y, 1.5-z$.

polymeric chains made of transition metals(II), where the central atoms are connected by bridging ditetrazole units (Fig. S6–9†). In all perchlorate 1,1-dtp structures the central methylene units of the propylene bridges and also the perchlorate anions are heavily disordered and had to be refined as split positions.

d^{10} metal(I) perchlorate **10** is the only complex that shows a tetrahedral coordination sphere. The compound crystallizes in the form of colorless blocks in the monoclinic space group $P2_1/c$ with four formula units per unit cell and a calculated density of 2.267 g cm^{-3} at 123 K, the highest density observed among all compounds. The silver(I) cation is bonded to only one neutral tetradentately (N1, N4, N7, and N8) coordinating ditetrazole (Fig. 8).

The *N*1-substituted tetrazole bridges through its N3 and N4 donor atoms, whereas the 2-substituted ring binds with the N1 and N4 atoms. Compared to the free uncoordinated ligand, both rings maintain their *gauche* conformation to the propyl chain and each ditetrazolylpropane bridges between four

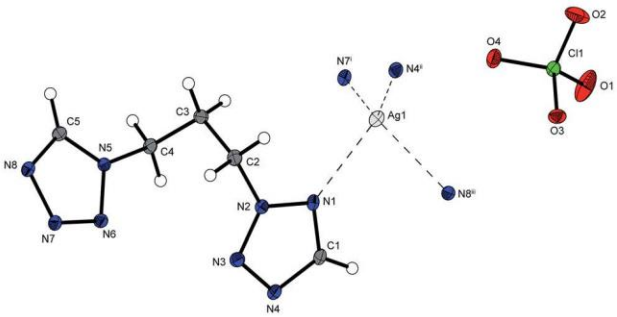


Fig. 8 Silver(I) coordination environment of $[Ag(1,2\text{-dtp})]ClO_4$ (**10**). Selected bond lengths (Å): Ag1–N1 2.435(2), Ag1–N4^{ii} 2.264(2), Ag1–N7^{i} 2.265(2), and Ag1–N8^{iii} 2.365(2); selected bond angles (°): N1–Ag1–N7^{i} 105.96(6), N1–Ag1–N8^{iii} 83.91(6), and N1–Ag1–N4^{ii} 109.10(6). Symmetry codes: (i) $-x, 0.5+y, 0.5-z$; (ii) $x, 1.5-y, -0.5+z$; (iii) $-1+x, 1.5-y, -0.5+z$.

This journal is © The Royal Society of Chemistry 2018

Published on 08 March 2018. Downloaded by Ludwig Maximilians Universitaet Muenchen on 2/16/2022 7:58:20 AM.

different silver(I) atoms (Fig. 9a and b) building a three-dimensional polymeric network with incorporated non-coordinating perchlorate anions (Fig. 9c and d).

Complex **11** with 1.693 g cm^{-3} at 123 K shows the lowest density among all copper(II) complexes. It crystallizes in the form of blue rods in the triclinic space group $P\bar{1}$ with two formula units per unit cell and shows every type of conformation (*gauche*/*gauche*; *gauche*/*anti*; and *anti*/*anti*), in comparison to free ligand **2**. The complex has an octahedral coordination sphere with six coordinating tetrazoles building a three-dimensional polymeric network and shows, in contrast to **8**, the expected Jahn–Teller distortion along the axial direction (Fig. 10). The inconsistent conformations of the ligand are accompanied by a loss of density.

Diaqua complex **12** illustrated in Fig. 11 crystallizes in the form of blue blocks in the monoclinic space group $P2_1/c$ with two formula units per unit cell and a calculated density of 1.765 g cm^{-3} at 233 K. The substitution of one ditetrazole through two aqua ligands leads to a slightly higher density in comparison to compounds **8** (ρ = 1.721 g cm^{-3}) and **11** (ρ = 1.693 g cm^{-3}). Every tetrazole ring of the 2,2-dtp ligand is similar to the uncoordinated compound in *anti* conformation to the propyl chain linking the copper(II) metal center to four other metal ions. The oxygen atoms in axial positions prevent the formation of a 3D-polymeric structure leading to two dimensional layers with two non-coordinating perchlorate counteranions.

The molecular unit of compound **14** consists of two non-coordinating cyanodinitromethanide counterions and one copper(II) cation, which is coordinated by two axial aqua ligands and four tetrazoles in a plane corresponding to two 1,1-dtps

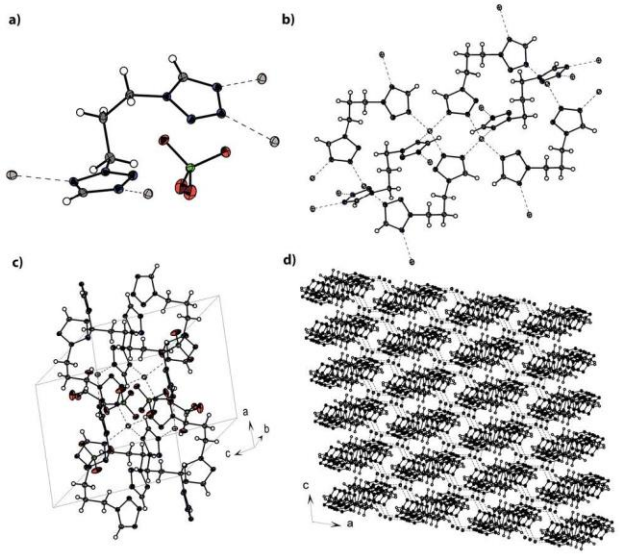


Fig. 9 Coordination in [Ag(1,2-dtp)]ClO_4 (**10**): (a) formula unit with the linkage of the ligand between the metal(I) cations; (b) bridging pattern of tetradentately coordinating tetrazole **2** (with the omission of the perchlorate anions for better clarity); (c) unit cell with 4 formula units; (d) metal–organic framework (MOF) depicted along the *b* axis (without perchlorate anions).

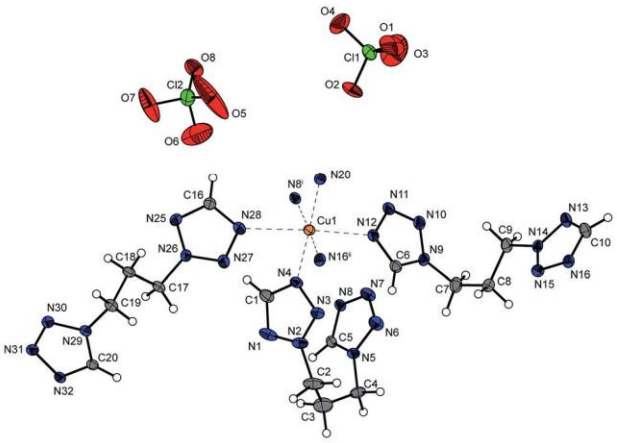


Fig. 10 Coordination environment of [Cu(1,2-dtp)$_3$]$(ClO_4)_2$ (**11**). Selected bond lengths (Å): Cu1–N4 2.043(4), Cu1–N8 2.020(4), Cu1–N12 2.316(4), Cu1–N16 2.011(3), Cu1–N20 2.031(4), and Cu1–N28 2.483(5); selected bond angles (°): N4–Cu1–N12 90.9(2), N4–Cu1–N8 94.1(2), and N4–Cu1–N16 87.7(2). Symmetry codes: (i) 1 − *x*, −*y*, 1 − *z*; (ii) 2 − *x*, −*y*, 1 − *z*.

(Fig. 12). Compared to the perchlorate complexes of 1,1-dtp, the ligands maintain the conformation with one tetrazole ring in the *gauche* and one in the *anti* position to the propyl chain preventing the bonding of two additional nitrogen atoms to the metal center. As already observed for compound **12**, the replacement of one ditetrazole through two aqua ligands in **14** leads to a small increase in density (1.761 g cm^{-3}). The one-dimensional polymeric complex crystallizes in the form of blue blocks in the triclinic space group $P\bar{1}$ with two formula units per unit cell.

Similar to complex **8**, the octahedral coordination sphere of anhydrous compound **15** consists of six tetrazole rings with two

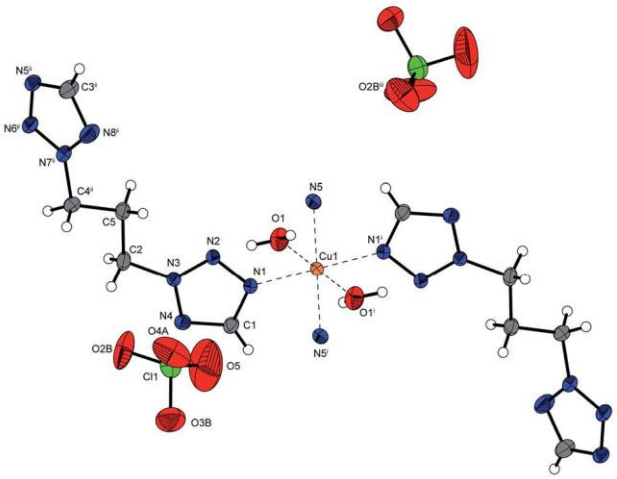


Fig. 11 Copper(II) coordination environment of [Cu(H_2O)$_2$(2,2-dtp)$_2$]$(ClO_4)_2$ (**12**). Selected bond lengths (Å): Cu1–O1 2.294(2), Cu1–N1 2.0214(19), and Cu1–N5 2.0317(19); selected bond angles (°): O1–Cu1–N1 90.00(8), O1–Cu1–N5 92.60(9), and N1–Cu1–N5 89.52(8). Symmetry codes: (i) 1 − *x*, −*y*, 1 − *z*; (ii) 2 − *x*, 0.5 + *y*, 1.5 − *z*; (iii) 1 − *x*, −0.5 + *y*, 1.5 − *z*.

Published on 08 March 2018. Downloaded by Ludwig Maximilians Universitaet Muenchen on 2/16/2022 7:58:20 AM.

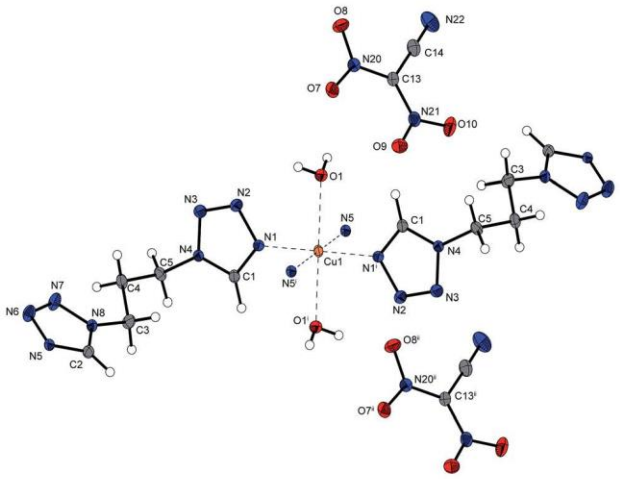


Fig. 12 Copper(II) coordination environment of $[Cu(H_2O)_2(1,1\text{-dtp})_2](CDNM)_2$ (**14**). Selected bond lengths (Å): Cu1–O1 2.3298(15), Cu1–N1 2.0107(15), and Cu1–N5 2.0241(15); selected bond angles (°): O1–Cu1–N1 94.98(6), O1–Cu1–N5 89.50(6), and N1–Cu1–N5 90.18(6). Symmetry codes: (i) $1-x, 1-y, 1-z$; (ii) $-1+x, y, z$.

non-coordinating dinitramide counterions in the molecular unit (Fig. 13). All rings are in *anti* conformation to the propyl chain, which enables the linkage of one transition metal to six other copper(II) ions and leads to a tightly packed three-dimensional network with a density of 1.711 g cm^{-3}. The complex crystallizes in the form of blue platelets in the monoclinic space group $C2/c$ with 8 formula units per unit cell.

Sensitivities and thermal stability

Endothermic signals such as melting, dehydration or loss of aqua ligands, as well as other critical temperatures of all compounds were investigated by differential thermal analysis (DTA) with a heating rate of $\beta = 5$ °C min^{-1}. The determined onset temperatures are listed in Table 2. DTA plots and additional details of coordination compounds **1–3**, **8** and **10–15** are displayed in Fig. S11–13 in the ESI.† The ditetrazole ligands melt at 45 °C (2,2-dtp), 50 °C (1,2-dtp) and 126 °C (1,1-dtp). Higher melting points are observed when more *N*1 substitution is present at the heterocycle, which is in accordance with the literature.[47] All complexes (except **10** and **15**) show excellent exothermic decomposition temperatures with values greater than 210 °C. The thermal stabilities of the investigated compounds exceed in most cases the temperatures observed for the uncoordinated ligands. The silver(I) perchlorate **10** and copper(II) dinitramide **15** complexes show the lowest exothermic decomposition temperatures among all examined compounds with values of 186 °C (**10**) and 154 °C (**15**), respectively. The poor stability of dinitramide containing compounds against heat is a well-known issue and has already been described in literature.[48]

The observation of endothermic signals, which indicate melting, dehydration or loss of aqua ligands for compounds **1–3** and **12–14**, match perfectly with the described structural composition. The outstanding thermal stabilities of most complexes can be explained by the formation of extended structures (MOFs) and the related strengthening of the scaffold within the coordination compounds. In contrast, complex monomers based on relatively volatile ligands suffer from a high vaporization tendency resulting in earlier decomposition after reaching the critical temperature.[6] Therefore, two selected complexes **6** and **8** were investigated by thermal gravimetric analysis (TGA, Fig. 14). The theory of a higher stability of coordination polymers could be confirmed. Both polymeric compounds showed no weight loss until decomposition during heating. The exothermic decomposition temperatures of metal(II) 1,1-dtp perchlorate complexes **4–9**, depicted in Fig. 15, rise

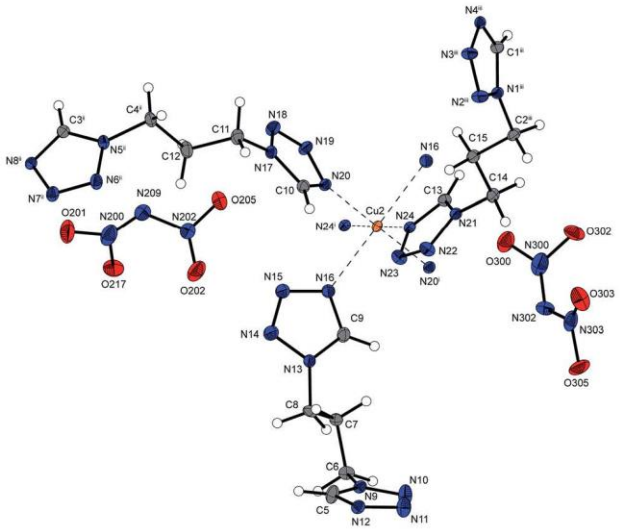


Fig. 13 Coordination environment of anhydrous copper(II) dinitramide complex **15**. Selected bond lengths (Å): Cu2–N16 2.3861(16), Cu2–N20 2.0437(14), and Cu2–N24 2.004(2); selected bond angles (°): N16–Cu2–N20 85.55(6), N16–Cu2–N24 90.87(7), and N20–Cu2–N24 88.81(7). Symmetry codes: (i) $-x, 1-y, -1-z$; (ii) $x, y, -1+z$; (iii) $-0.5-x, 0.5-y, -1-z$.

Table 2 Thermal stability measurements of **1–15** by DTA [a]

	$T_{endo.}$ [b] (°C)	$T_{exo.}$ [c] (°C)
1,1-dtp·H_2O (**1**)	68 ($-H_2O$), 126	205
1,2-dtp (**2**)	50	212
2,2-dtp (**3**)	45	246
$[Mn(1,1\text{-dtp})_3](ClO_4)_2$ (**4**)	—	243
$[Fe(1,1\text{-dtp})_3](ClO_4)_2$ (**5**)	—	234
$[Co(1,1\text{-dtp})_3](ClO_4)_2$ (**6**)	—	255
$[Ni(1,1\text{-dtp})_3](ClO_4)_2$ (**7**)	—	297
$[Cu(1,1\text{-dtp})_3](ClO_4)_2$ (**8**)	—	231
$[Zn(1,1\text{-dtp})_3](ClO_4)_2$ (**9**)	—	253
$[Ag(1,2\text{-dtp})]ClO_4$ (**10**)	—	185
$[Cu(1,2\text{-dtp})_3](ClO_4)_2$ (**11**)	—	222
$[Cu(H_2O)_2(2,2\text{-dtp})_2](ClO_4)_2$ (**12**)	132 ($-H_2O$)	257
[Cu(TNR)(1,1-dtp)]·H_2O (**13**)	88 ($-H_2O$)	248
$[Cu(H_2O)_2(1,1\text{-dtp})_2](CDNM)_2$ (**14**)	93 ($-H_2O$)	212
$[Cu(1,1\text{-dtp})_3](DN)_2$ (**15**)	—	153

[a] Onset temperatures at a heating rate of 5 °C min^{-1}. [b] Endothermic peak, which indicates melting, dehydration or loss of aqua ligands. [c] Exothermic peak, which indicates decomposition.

This journal is © The Royal Society of Chemistry 2018

Published on 08 March 2018. Downloaded by Ludwig Maximilians Universitaet Muenchen on 2/16/2022 7:58:20 AM.

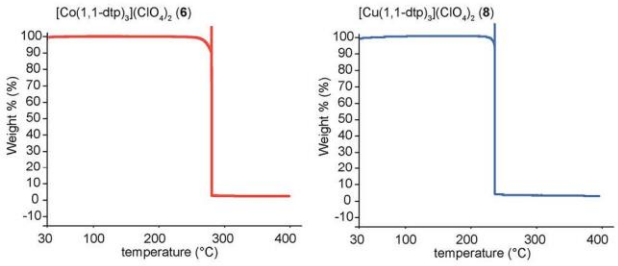


Fig. 14 TGA measurements of the selected coordination compounds **6** and **8** at a heating rate of 5 °C min^{-1}.

in the following order: Cu^{2+} (231 °C) < Fe^{2+} (234 °C) < Mn^{2+} (243 °C) < Zn^{2+} (253 °C) < Co^{2+} (255 °C) < Ni^{2+} (297 °C). A similar trend has been described in literature for metal(II) perchlorate complexes bearing 1-methyl-5*H*-tetrazole as a ligand.[6]

The nitrogen substitution pattern of the ditetrazoles has a strong influence on the exothermic decomposition temperature, which can be observed for uncoordinated ligands **1–3** and their corresponding copper(II) perchlorate complexes (Fig. S12†). Comparing the 1,1-dtp complexes with copper(II) as metal, but varying anions, showed again the relevance and dependency of different coordination environments for the thermal stability (Fig. S13†).

The sensitivities toward impact and friction were measured according to BAM standard methods together with the electrostatic discharge sensitivity for all compounds. Furthermore, the compounds have been categorized in compliance with the "UN Recommendations on the Transport of Dangerous Goods" using the determined values. An outline of the sensitivities is given in Table 3. Uncoordinated ditetrazole ligands **1–3** can be described as "insensitive" with values greater than 40 J for impact and greater than 360 N for friction and ESD values between 0.15 and 1.50 J. All perchlorate complexes **4–12** (except **10** with a value of 8 J) can be considered as very sensitive against impact (1–3 J) and vary from sensitive to very sensitive toward friction (16–288 N).

Table 3 Sensitivities toward impact, friction and ESD of **1–15**[a]

	IS[b] (J)	FS[c] (N)	ESD[d] (J)
1	>40	>360	1.35
2	>40	>360	1.50
3	>40	>360	0.15
4	3	216	0.30
5	2	72	0.10
6	1	18	0.08
7	3	120	0.20
8	1	54	0.33
9	1	288	0.20
10	8	16	0.15
11	1.5	18	0.10
12	1.5	64	0.30
13	10	>360	0.50
14	10	>360	0.50
15	3	>360	0.70

[a] Determined at a grain size < 100 μm. [b] Impact sensitivity according to the BAM drophammer (method 1 of 6). [c] Friction sensitivity according to the BAM friction tester (method 1 of 6). [d] Electrostatic discharge sensitivity (OZM ESD tester); impact: insensitive > 40 J, less sensitive ≥ 35 J, sensitive ≥ 4 J, and very sensitive ≤ 3 J; friction: insensitive > 360 N, less sensitive = 360 N, sensitive < 360 N and > 80 N, very sensitive ≤ 80 N, and extremely sensitive ≤ 10 N. According to the UN Recommendations on the Transport of Dangerous Goods.

The application of metal(II) salts with oxidizing anions like trinitroresorcinates, cyanodinitromethanides or dinitramides in combination with endothermic ligands usually caused intensified sensitivities toward various stimuli like impact, friction and ESD (impact: 3–10 J; friction: >360 N; ESD: 0.50–0.70 J). The inclusion of crystal water molecules or aqua ligands on the other hand lowered the performance and predominantly led to a lower sensitivity. The sensitivity toward impact of the $[M^{II}(1,1\text{-dtp})_3](ClO_4)_2$ coordination compounds (Fig. 16) increases in the following order: Mn^{2+} (3 J) ≈ Ni^{2+} (3 J) < Fe^{2+} (2 J) < Zn^{2+} (1 J) ≈ Cu^{2+} (1 J) ≈ Co^{2+} (1 J) and in the following order against friction: Zn^{2+} (288 N) < Mn^{2+} (216 N) < Ni^{2+} (120 N) < Fe^{2+} (72 N) < Cu^{2+} (54

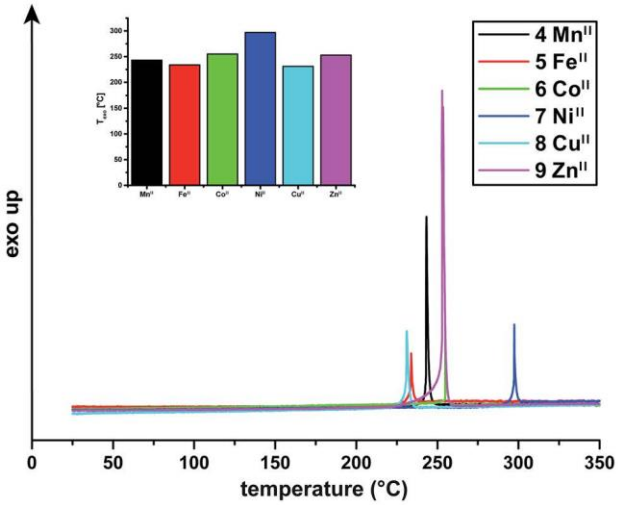


Fig. 15 DTA plot (5 °C min^{-1}) comparison of 1,1-dtp containing metal(II) perchlorate complexes **4–9**.

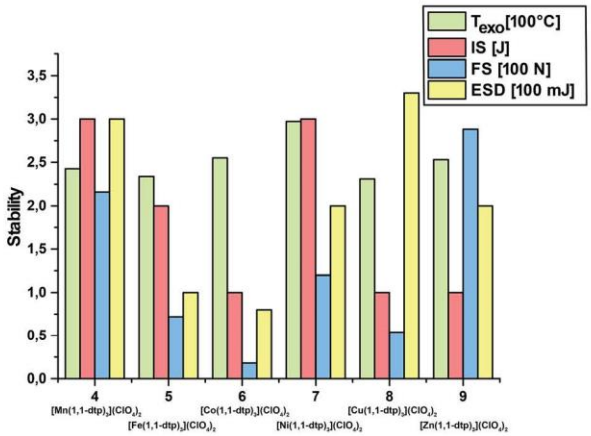


Fig. 16 Comparison of the stabilities of 1,1-dtp containing metal(II) perchlorate complexes **4–9**.

Published on 08 March 2018. Downloaded by Ludwig Maximilians Universitaet Muenchen on 2/16/2022 7:58:20 AM.

N) < Co^{2+} (18 N). Comparable results have been described in the literature in connection with 1,5-diaminotetrazole and 1-methyl-5*H*-tetrazole containing ECCs.[6,49] In addition, fine-tuning of the stability of the complexes can be achieved through an appropriate choice of the implemented dtp ligands or oxygen-rich anions (Fig. S14 and S15†). The presented copper(II) perchlorate complexes show promising characteristics by having manageable sensitivities, which makes them highly suitable as laser ignitable substances in modern initiation devices.

Initiation capability tests by using a hot plate and hot needle were performed for the most promising compounds **8**, **11** and **12**. All investigated complexes showed deflagrations in both tests and no detonations indicating that they are valuable compounds with moderate sensitivities and performances for laser ignition experiments (Fig. 17 and S16–18†). More details on the procedures can be found in the Experimental section.

Toxicity assessment

In order to determine the toxicological impact of complexes with isomeric propyl-linked ditetrazoles, the uncoordinated free ligands (**1**, **2** and **3**), as well as their corresponding copper(II) complexes (**8**, **11** and **12**) were tested. The toxicity determinations were carried out with a LUMI-Stox 300 spectrometer obtained from HACH LANGE GmbH, as described by the provider. A ten-point dilution series was prepared according to DIN/EN/ISO 11348 (without the G1 level) with a known weight of the compounds and a 2% NaCl stock solution.[50] The measurements were performed at a temperature of 15 °C starting with the determination of the bioluminescence of untreated reactivated *Vibrio fischeri* NRRL-B-11177 bacterial strains. The bioluminescence is again determined after exposure times of 15 and 30 minutes with a specific amount of the component. At the concentration level where the bioluminescence is decreased by 50%, the EC_{50} (effective concentration) value is obtained. Compounds can be classified as non-toxic according to their EC_{50} values (non-toxic > 1.00 g L^{-1}; toxic 0.10–1.00 g L^{-1}; very toxic < 0.10 g L^{-1}).[51]

As shown in Table 4, the half-maximum effective concentrations of the propyl-linked ditetrazoles vary considerably. Compound **1** has an EC_{50} value of 10.30 g L^{-1} after 30 minutes and can be considered as non-toxic. It is interesting to note that in contrast to ligand **1**, isomeric compounds **2** (0.84 g L^{-1}) and **3** (0.36 g L^{-1}) show increased toxicities by having only a slightly different substitution pattern. Similar values have been observed for all copper(II) complexes, which is not surprising due to their known toxicity toward microorganisms.[52] It also becomes apparent that ditetrazole **3** and complexes containing this ligand are more toxic toward *Vibrio fischeri*. Copper(II) compound **12** is the most toxic complex, even though it forms complexes with two aqua ligands and two ditetrazole ligands instead of three ditetrazole ligands (compounds **8** and **11**). Furthermore, the toxicity values of **8**, **11** and **12** are in a proportional range of other copper(II) perchlorate complexes, but they are slightly less toxic compared to already known 1-methyl-5*H*-tetrazole analogues.[6] This could lead to a general trend that 2-alkylated 5-*H*-tetrazoles are more toxic than their 1-alkylated analogues.

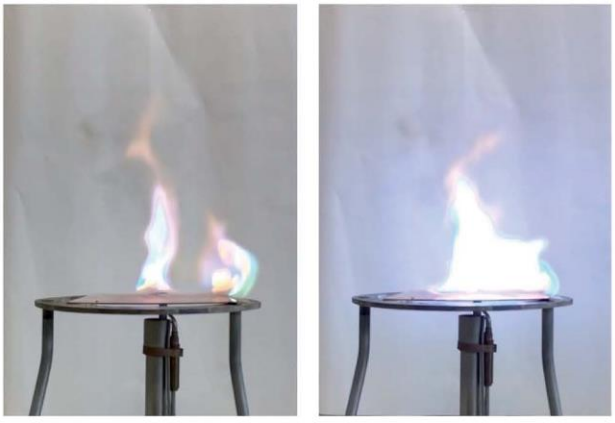


Fig. 17 Moment of deflagration of compound **8** during the hot plate test shown as a sequence.

Laser ignition tests

Over the past few years, many new laser ignitable materials based on energetic coordination compounds have been explored and developed by several researchers all over the world.[33,53–55] Initiation by a laser has various benefits in comparison to classical ignition methods like thermal initiation (bridge wire) or mechanical stimuli (*e.g.* stab initiation). Since high sensitivities against usual stimuli are no longer needed, almost insensitive highly energetic compounds can be used, which can reduce undesired initiations and allow safer processing. The "green" laser ignitable explosives presented in this study feature all desired characteristics like high performance, superior thermal stability, moderate sensitivities and no environmental impact. Approximately 15 mg of the carefully pestled complex to be investigated was filled into a transparent plastic cap (PC), pressed with a pressure force of 1 kN and sealed with a UV-curing adhesive. The laser initiation experiments were performed with a 45 W InGaAs laser diode operating in the single-pulse mode. The diode is attached to an optical fiber with a core diameter of 400 μm and a cladding diameter of 480 μm. The optical fiber is connected *via* a SMA type connecter directly to the laser and to a collimator. This collimator is coupled to an optical lens, which was positioned at its focal distance (f = 29.9 mm) from the sample. The lens is shielded from the explosive by a sapphire glass. The confined samples were irradiated at

Table 4 Experimental EC_{50} values for uncoordinated free ligands **1–3** in comparison to their respective copper(II) perchlorate complexes **8**, **11** and **12**

Compound	EC_{50} (15 min) [g L^{-1}]	EC_{50} (30 min) [g L^{-1}]
1,1-dtp·H_2O (**1**)	13.90	10.30
1,2-dtp (**2**)	0.81	0.79
2,2-dtp (**3**)	0.36	0.36
$[Cu(1,1\text{-dtp})_3](ClO_4)_2$ (**8**)	0.44	0.35
$[Cu(1,2\text{-dtp})_3](ClO_4)_2$ (**11**)	0.64	0.44
$[Cu(H_2O)_2(2,2\text{-dtp})_2](ClO_4)_2$ (**12**)	0.34	0.28

This journal is © The Royal Society of Chemistry 2018

Published on 08 March 2018. Downloaded by Ludwig Maximilians Universitaet Muenchen on 2/16/2022 7:58:20 AM.

a wavelength of 915 nm, a voltage of 4 V, a current of 8 A and varying pulse lengths (0.1 ms or 15 ms). The combined current and pulse length result in an energy output of about 0.20 mJ (0.1 ms/8 A) and 30 mJ (15 ms/8 A). Only selected complexes with promising characteristics and moderate sensitivities were tested showing different behaviors upon laser irradiation depending on the metal(II)/anion combination. An overview of the experimental results is given in Table 5.

Zinc(II) complex **9** was the only compound investigated, which showed no reaction after laser irradiation. All other complexes examined could be initiated showing decompositions for **7**/**14**, deflagrations for **13**/**15** and detonations for **5**, **6**, **8**, **11** and **12** (Fig. 18 and S19–22†). Various laser initiation thresholds could be observed for the varying coordination compounds, which exhibit similar sensitivities toward mechanical stimuli, but showed different responses under the employed laser settings. Iron(II) and copper(II) perchlorate complexes **5**, **8**, **11** and **12** detonated at the lowest possible initiation energy available in the parameters of the laser device and could be promising candidates in future laser initiation systems based on their outstanding initiation capabilities and highly practicable sensitivities.

UV-Vis spectroscopy

The solid-state UV-Vis spectra of all coordination compounds **4–15** were recorded in the wavelength region of 350–1000 nm to acquire a better understanding and get a deeper insight into the laser initiation process (Fig. 17 and S23†). Observed optical characteristics are collected and listed in Table 6. The investigated complexes showed characteristic transitions in the near-infrared, visible and UV regions responsible for the complementary colours and typical of the related transition metal. The observed absorptions can be primarily designated to the d–d transitions of the corresponding metals and are largely dependent on the inserted metal(II), anion and ligand (Fig. 19).

As assumed initially, no absorptions could be observed for d^5 manganese(II) compound **4** and the two d^{10} complexes with zinc(II) **9** and silver(I) **10**. Additional strong n–π^* transitions from the UV to the blue visible region (Fig. S23†) could be detected in copper(II) complexes **13–15** caused by the nitro group containing anions (trinitroresorcinate, cyanodinitromethanide, and dinitramide).

Many uncertainties of the fundamental basis of the laser initiation process (*e.g.* electronical, thermal or combined) have not been clarified yet and are still questionable.[34,56,57] Solely

Table 5 Results of the laser ignition tests[a]

	0.1 ms/8 A	1 ms/8 A	15 ms/8 A
5	det.	–	–
6	x	x	det.
7	–	–	dec.
8	det.	–	–
9	–	–	x
11	det.	–	–
12	det.	–	–
13	–	–	deflag.
14	–	–	dec.
15	–	–	deflag.

[a] (–: not tested, x: no ignition, dec.: decomposition, deflag.: deflagration, det.: detonation). Operating parameters: current $I = 8$ A; voltage $U = 4$ V; theoretical maximal output power $P_{max} = 45$ W; theoretical energy $E_{max} = 0.20$–30 mJ; wavelength $\lambda = 915$ nm; pulse length $\tau = 0.1$–15 ms.



Fig. 18 Moment of detonation of complex $[Fe(1,1\text{-dtp})_3](ClO_4)_2$ (**5**) in the laser initiation experiment.

Table 6 Observed optical characteristics of **4–15**

	M	Color	$\lambda_{d\text{-}d}$[a]	$\lambda_{915}/\lambda_{d\text{-}d}$[b]
4	Mn^{II}	Colorless	—	—
5	Fe^{II} (hs)	Yellow	893	0.97
6	Co^{II}	Orange	468, 982	0.61
7	Ni^{II}	Purple	547, 891	0.84
8	Cu^{II}	Blue	701	0.30
9	Zn^{II}	Colorless	—	—
10	Ag^{I}	Colorless	—	—
11	Cu^{II}	Blue	688	0.48
12	Cu^{II}	Blue	654	0.63
13	Cu^{II}	Green	390[c], 696	1.00
14	Cu^{II}	Blue	389[c], 624	0.51
15	Cu^{II}	Blue	377[c],630	0.41

[a] Absorption intensity maximum wavelength, which can be assigned to electron d–d excitations in the measured range of 350–1000 nm. [b] Quotient of the absorption intensity at the laser wavelength and the intensity at the d–d absorption wavelength. [c] n–π^* transitions.

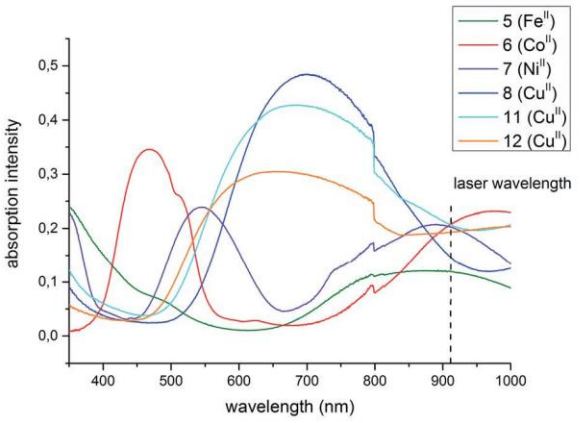


Fig. 19 UV-Vis spectra in the solid state of the selected complexes. The step in the absorption intensity at 800 nm in the spectra is caused by a detector change. The UV-Vis spectra have only qualitative character.

Published on 08 March 2018. Downloaded by Ludwig Maximilians Universitaet Muenchen on 2/16/2022 7:58:20 AM.

looking at the absorption of the coordination compounds at the laser wavelength of 915 nm one could conclude a possible direct interrelationship with the laser initiation capability once all complexes could be ignited. The initiation ability of energetic materials by a laser depends not only on the absorption at the relevant wavelength but also on other factors like the electronic structure or the metal center surrounding. It can be assumed that the reaction of the coordination compounds after irradiation by laser light may occur when energetic materials exhibit high sensitivities toward mechanical stimuli. Future studies are necessary to gain further insights into the laser initiation process, which should cover the effect of the compound composition (metal, anion or ligand) and investigate the nature of the mechanism.

Conclusions

Three isomeric ditetrazolylpropanes (1,3-di(tetrazol-1-yl)propane (1,1-dtp)), 1-(tetrazol-1-yl)-3-(tetrazol-2-yl)propane (**2**, 1,2-dtp) and 1,3-di(tetrazol-2-yl)propane (**3**, 2,2-dtp), differing only in the nitrogen substitution pattern at the tetrazole, were prepared and purified in a straightforward one-step synthesis through alkylation of 1,5*H*-tetrazole. Different synthetic strategies were applied and the influence of various preparative parameters on the reaction product composition was systematically investigated. The analysis and comparison of these procedures resulted in deep insights into the effect on the yield and ratio of the isomers from different solvent systems and various organic/inorganic bases, and the influence of a phase transfer catalyst and a distinct work-up method. The obtained endothermic *n*-propyl linked ditetrazoles were exhaustively characterized by various methods including toxicity assessments, X-ray studies and heteronuclear ^{15}N NMR spectroscopy. Toxicity determinations toward aquatic life of the free uncoordinated ligands together with the promising related copper(II) perchlorate complexes showed that 1-alkylated species are less toxic than their 2-alkylated isomers moreover, no tested complex is considered as very toxic. The concept of ECCs is an excellent, fair and simple approach in order to find environmentally friendly primary explosives or materials applicable for laser ignition experiments with reasonable sensitives. Laser initiation experiments with 1,2-di(tetrazol-5-yl)ethane (1,1-dte) based transition metal(II) complexes have shown promising results in the past but were too sensitive for any application. As a logical consequence, ditetrazolylpropane ligands with higher carbon contents especially *N*1,*N*1-substituted ditetrazole (1,1-dtp) were now incorporated into the corresponding coordination compounds in order to increase the stability of the new energetic materials. The present contribution covers the synthesis, characterization and comparison of 12 new eco-friendly energetic coordination compounds (ECCs) based on three different isomeric propyl-linked ditetrazoles, which differ drastically in their coordination pattern. The complexation of the ligands leads to intramolecular reorientation of the ditetrazole molecules and enables the formation of polymeric structures. The optical as well as energetic properties of the highly functional complexes were accurately tuned by the careful selection of the varying metal(II) salts and also the appropriate choice of the isomers. The synthesized coordination compounds consist of a first-row transition metal(II) (Mn, Fe, Co, Ni, Cu, and Zn), several different anions (ClO_4^-, TNR^2, CDNM, and DN) and one of the three isomeric ditetrazoles. Approaches utilizing Ag(I) as the metal center failed with the exception of coordination compound **10** with 1,2-dtp as a ligand. In order to form thermally stable materials, non-volatile bridging bidentate ditetrazole ligands were incorporated into the complexes to establish highly stable multidimensional polymeric structures (MOFs). Through this strategy extraordinary exothermic decomposition temperatures could be achieved for all complexes up to a very impressive 297 °C for compound **7**, which were partly checked and confirmed by thermal gravimetric analysis (TGA). The powerful water-free nature of the majority of the energetic complexes was revealed through single crystal X-ray experiments of all compounds (except complex **7**), which allowed interesting correlations between the crystal structures and their stabilities toward mechanical stress (highest sensitivities for cobalt(II) perchlorate complex **6**). Laser initiation tests, which were performed at a wavelength of 915 nm, showed detonations for the most promising iron(II) and copper(II) complexes **5**, **8**, **11**, and **12** at the lowest configurable laser setup energy input (0.2 mJ). The successful initiations proved the suitability of these high performance and thermally stable candidates for future laser initiation systems, which can be easily synthesized from inexpensive chemicals in a simple, inexpensive and upscalable reaction.

Conflicts of interest

There are no conflicts to declare.

Acknowledgements

Financial support of this work by the Ludwig-Maximilian University of Munich (LMU) and the Office of Naval Research (ONR) under grant no. ONR.N00014-16-1-2062 is acknowledged. The authors want to thank Mr Stefan Huber for sensitivity measurements, Mr Josh Bauer for proofreading and Prof. Dr Konstantin Karaghiosoff for the measurement of various ^{15}N NMR spectra.

Notes and references

1 F. R. Benson, *Chem. Rev.*, 1947, **41**, 1–61.
2 R. Haiges and K. O. Christe, *Inorg. Chem.*, 2013, **52**, 7249–7260.
3 H. Xue, H. Gao, B. Twamley and J. n. M. Shreeve, *Chem. Mater.*, 2007, **19**, 1731–1739.
4 T. M. Klapötke, J. Stierstorfer and A. U. Wallek, *Chem. Mater.*, 2008, **20**, 4519–4530.
5 O. Sengupta and P. S. Mukherjee, *Inorg. Chem.*, 2010, **49**, 8583–8590.
6 N. Szimhardt, M. H. H. Wurzenberger, A. Beringer, L. J. Daumann and J. Stierstorfer, *J. Mater. Chem. A*, 2017, **5**, 23753–23765.
7 C. M. Grunert, J. Schweifer, P. Weinberger, W. Linert, K. Mereiter, G. Hilscher, M. Müller, G. Wiesinger and P. J. van Koningsbruggen, *Inorg. Chem.*, 2004, **43**, 155–165.

This journal is © The Royal Society of Chemistry 2018

Published on 08 March 2018. Downloaded by Ludwig Maximilians Universitaet Muenchen on 2/16/2022 7:58:20 AM.

8 R. Bronisz, *Inorg. Chem.*, 2005, **44**, 4463–4465.
9 P. Cui, Y.-G. Ma, H.-H. Li, B. Zhao, J.-R. Li, P. Cheng, P. B. Balbuena and H.-C. Zhou, *J. Am. Chem. Soc.*, 2012, **134**, 18892–18895.
10 M. Joas, T. M. Klapötke and N. Szimhardt, *Eur. J. Inorg. Chem.*, 2014, **2014**, 493–498.
11 M. H. V. Huynh, M. D. Coburn, T. J. Meyer and M. Wetzler, *Proc. Natl. Acad. Sci. U. S. A.*, 2006, **103**, 10322–10327.
12 Z. Wu, J. F. Justo, C. R. S da Silva, S. de Gironcoli and R. M. Wentzcovitch, *Phys. Rev. B: Condens. Matter Mater. Phys.*, 2009, **80**, 014409.
13 G. Aromí, L. A. Barrios, O. Roubeau and P. Gamez, *Coord. Chem. Rev.*, 2011, **255**, 485–546.
14 O. Roubeau, M. Evangelisti and E. Natividad, *Chem. Commun.*, 2012, **48**, 7604–7606.
15 T. M. Klapötke, *Chemistry of High-Energy Materials*, Walter de Gruyter, Berlin, Boston, 2nd edn, 2012.
16 J.-G. Xu, C. Sun, M.-J. Zhang, B.-W. Liu, X.-Z. Li, J. Lu, S.-H. Wang, F.-K. Zheng and G.-C. Guo, *Chem. Mater.*, 2017, **29**, 9725–9733.
17 T. Liu, X. Qi, K. Wang, J. Zhang, W. Zhang and Q. Zhang, *New J. Chem.*, 2017, **41**, 9070–9076.
18 G.-H. Tao, D. A. Parrish and J. n. M. Shreeve, *Inorg. Chem.*, 2012, **51**, 5305–5312.
19 L. Wiehl, *Acta Crystallogr., Sect. B: Struct. Sci.*, 1993, **49**, 289–303.
20 P. J. van Koningsbruggen, Y. Garcia, O. Kahn, L. Fournes, H. Kooijman, A. L. Spek, J. G. Haasnoot, J. Moscovici, K. Provost, A. Michalowicz, F. Renz and P. Guetlich, *Inorg. Chem.*, 2000, **39**, 1891–1900.
21 M. Joas, PhD thesis, Ludwig-Maximilians Universität München, 2014.
22 J. Koehler, Low-polluting pyrotechnic composition, AT410315B, 2003.
23 J. W. Fronabarger, M. D. Williams, A. G. Stern and D. A. Parrish, *Cent. Eur. J. Energ. Mater.*, 2016, **13**, 33–52.
24 Y. Tang, C. He, L. A. Mitchell, D. A. Parrish and J. n. M. Shreeve, *Angew. Chem., Int. Ed.*, 2016, **55**, 5565–5567.
25 J. W. Fronabarger, M. D. Williams, W. B. Sanborn, J. G. Bragg, D. A. Parrish and M. Bichay, *Propellants, Explos., Pyrotech.*, 2011, **36**, 541–550.
26 M. H. V. Huynh, M. A. Hiskey, T. J. Meyer and M. Wetzler, *Proc. Natl. Acad. Sci. U. S. A.*, 2006, **103**, 5409–5412.
27 A. Y. Zhilin, M. A. Ilyushin, I. V. Tselinskii, A. S. Kozlov and I. S. Lisker, *Russ. J. Appl. Chem.*, 2003, **76**, 572–576.
28 Z. Shunguan, W. Youchen, Z. Wenyi and M. Jingyan, *Propellants, Explos., Pyrotech.*, 1997, **22**, 317–320.
29 Q. Zhang and J. n. M. Shreeve, *Angew. Chem., Int. Ed.*, 2014, **53**, 2540–2542.
30 S. Zhang, Q. Yang, X. Liu, X. Qu, Q. Wei, G. Xie, S. Chen and S. Gao, *Coord. Chem. Rev.*, 2016, **307**, 292–312.
31 S. Li, Y. Wang, C. Qi, X. Zhao, J. Zhang, S. Zhang and S. Pang, *Angew. Chem., Int. Ed.*, 2013, **52**, 14031–14035.
32 M. Freis, T. M. Klapötke, J. Stierstorfer and N. Szimhardt, *Inorg. Chem.*, 2017, **56**, 7936–7947.
33 T. W. Myers, J. A. Bjorgaard, K. E. Brown, D. E. Chavez, S. K. Hanson, R. J. Scharff, S. Tretiak and J. M. Veauthier, *J. Am. Chem. Soc.*, 2016, **138**, 4685–4692.
34 S. R. Ahmad and M. Cartwright, Laser Ignition – Practical Considerations, in *Laser Ignition of Energetic Materials*, John Wiley & Sons, Ltd, 2014, pp. 247–268.
35 A. Cohen, Y. Yang, Q.-L. Yan, A. Shlomovich, N. Petrutik, L. Burstein, S.-P. Pang and M. Gozin, *Chem. Mater.*, 2016, **28**, 6118–6126.
36 D. Müller, C. Knoll, B. Stöger, W. Artner, M. Reissner and P. Weinberger, *Eur. J. Inorg. Chem.*, 2013, **2013**, 984–991.
37 M. Weselski, M. Książek, J. Kusz, A. Białońska, D. Paliwoda, M. Hanfland, M. F. Rudolf, Z. Ciunik and R. Bronisz, *Eur. J. Inorg. Chem.*, 2017, **2017**, 1171–1179.
38 S. J. Wittenberger, *Org. Prep. Proced. Int.*, 1994, **26**, 499–531.
39 P. L. Franke, J. G. Haasnoot and A. P. Zuur, *Inorg. Chim. Acta*, 1982, **59**, 5–9.
40 P. N. Gaponik, V. P. Karavai and Y. V. Grigoriev, *Khim. Geterotsikl. Soedin.*, 1985, **11**, 1521–1524.
41 A. Białońska and R. Bronisz, *Tetrahedron*, 2008, **64**, 9771–9779.
42 R. Bronisz, *Eur. J. Inorg. Chem.*, 2004, 3688–3695.
43 R. Bronisz, *Inorg. Chem.*, 2007, **46**, 6733–6739.
44 J. Evers, I. Gospodinov, M. Joas, T. M. Klapötke and J. Stierstorfer, *Inorg. Chem.*, 2014, **53**, 11749–11756.
45 Crystallographic data for the structures have been deposited with the Cambridge Crystallographic Data Centre.†
46 M. H. Palmer and S. Parsons, *Acta Crystallogr.*, 1996, **52**, 2818–2822.
47 P. N. Gaponik, M. M. Degtyarik, A. S. Lyakhov, V. E. Matulis, O. A. Ivashkevich, M. Quesada and J. Reedijk, *Inorg. Chim. Acta*, 2005, **358**, 3949–3957.
48 J. Zhang, Y. Du, K. Dong, H. Su, S. Zhang, S. Li and S. Pang, *Chem. Mater.*, 2016, **28**, 1472–1480.
49 K. Wang, D. Zeng, J.-G. Zhang, Y. Cui, T.-L. Zhang, Z.-M. Li and X. Jin, *Dalton Trans.*, 2015, **44**, 12497–12501.
50 Wasserbeschaffenheit - Bestimmung der Hemmwirkung von Wasserproben auf die Lichtemission von Vibrio Fischeri (Leuchtbakterientest), DIN EN ISO, 2009, 11348–2.
51 C. J. Cao, M. S. Johnson, M. M. Hurley and T. M. Klapötke, *JANNAF J. Propuls. Energet.*, 2012, **5**, 41–51.
52 V. Ochoa-Herrera, G. Leon, Q. Banihani, J. A. Field and R. Sierra-Alvarez, *Sci. Total Environ.*, 2011, **412–413**, 380–385.
53 T. W. Myers, D. E. Chavez, S. K. Hanson, R. J. Scharff, B. L. Scott, J. M. Veauthier and R. Wu, *Inorg. Chem.*, 2015, **54**, 8077–8086.
54 M. A. Ilyushin and I. V. Tselinskii, *Zh. Prikl. Khim.*, 2000, **73**, 1233–1240.
55 N. Szimhardt and J. Stierstorfer, *Chem.–Eur. J.*, 2018, **24**, 2687–2698.
56 E. D. Aluker, A. G. Krechetov, A. Y. Mitrofanov, D. R. Nurmukhametov and M. M. Kuklja, *J. Phys. Chem. C*, 2011, **115**, 6893–6901.
57 T. W. Myers, K. E. Brown, D. E. Chavez, R. J. Scharff and J. M. Veauthier, *Inorg. Chem.*, 2017, **56**, 2297–2303.

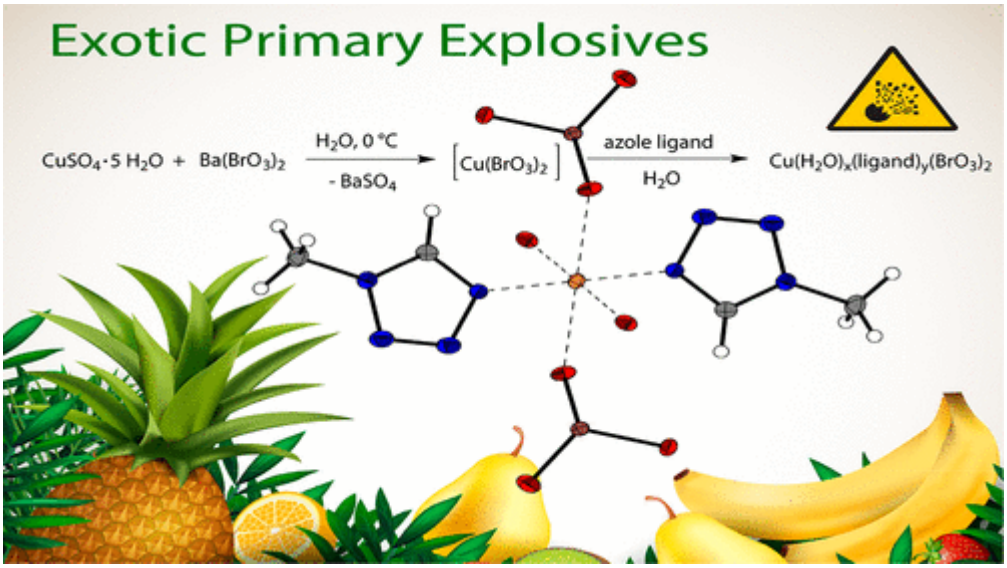
Appendix 5

Nitrogen-Rich Copper(II) Bromate Complexes: an Exotic Class of Primary Explosives

M. Wurzenberger, N. Szimhardt, J. Stierstorfer

Inorg. Chem. **2018**, 57, 7940–7949.

https://doi.org/10.1021/acs.inorgchem.8b01045



Supplementary Information:
https://pubs.acs.org/doi/suppl/10.1021/acs.inorgchem.8b01045/suppl_file/ic8b01045_si_001.pdf

Inorganic Chemistry
Cite This: Inorg. Chem. 2018, 57, 7940−7949
Article
pubs.acs.org/IC

Nitrogen-Rich Copper(II) Bromate Complexes: an Exotic Class of Primary Explosives†

Maximilian H. H. Wurzenberger, Norbert Szimhardt, and Jörg Stierstorfer*

Department of Chemistry, Ludwig Maximilian University of Munich, Butenandtstraße 5−13, Haus D, D-81377 Munich, Germany

Supporting Information

ABSTRACT: Because of the ongoing very challenging search for potential replacements of the currently used toxic lead-based primary explosives, new synthetic strategies have to be developed. In particular, the smart concept of energetic coordination compounds (ECC) has proven to hold great potential to solve this difficult and complex problem. The herein-described approach combines the exotic and neglected class of copper(II) bromate ECC with different environmentally friendly nitrogen-rich heterocycles, which exhibit the energetic properties of powerful primary explosives. The concept is the simple adjustment of the energetic properties of the complexes through alteration of the corresponding azoles. Six new copper(II) bromate complexes with reasonable sensitivities are featured in this study, which were synthesized in a practical and straightforward fashion, assured through easy access to copper(II) bromate obtained by metathesis reaction. Obtained compounds were comprehensively characterized through various analytical methods such as low-temperature X-ray diffraction, IR spectroscopy, and elemental analysis. Their sensitivities toward impact and friction were assessed through BAM standard techniques, together with their sensitivity against electrostatic discharge. Evaluation of the energetic properties of the newly synthesized compounds included examination of the respective thermal stabilities by differential thermal analysis. Furthermore, the complexes were tested regarding their behavior toward laser irradiation. Additionally, to receive insight into a possible correlation between the laser-investigated compounds' optical absorption and their ability to ignite by exposure to laser irradiation, UV−vis−near-IR spectra were recorded.



1. INTRODUCTION

Energetic materials include a wide range of chemical compounds and can be classified into four main subgroups: primary explosives, secondary explosives, pyrotechnics, and propellants.[1] In contrast to the high-performing secondary explosives, primaries embody compounds showing a very fast deflagration-to-detonation transition (DDT) after being initiated by a nonexplosive simple initiation impulse.[1,2] The most commonly used primary explosives nowadays are lead styphnate (LS) and lead azide (LA), two compounds that possess highly toxic potential toward human and nature.[3,4] To avoid exposure of toxic chemicals during the utilization and manufacturing of lead-containing primaries, modern research in the field of primary explosives focuses on the synthesis of new green compounds while maintaining the desired properties of LS and LA (Chart 1).[5−10]

From all energetic characteristics, the previously discussed sensitivities are of high importance as well as high decomposition temperature and chemical and physical stability during long-term storage.[2] Moreover, to enable the substitution of commonly used compounds, the required synthesis of a new primary explosive should include as few as possible reaction steps and ought to be compatible with conventional materials (detonators, secondaries, and blasting caps).[2]

One promising approach to obtaining green primary explosives includes the synthesis of energetic coordination compounds (ECC), a strategy that has gained increased attention in recent years.[7,17−20] Regarding the numerous parameters (metal center, ligand system, and counterion) that can be modified, the specific properties of a desired compound can be tailored incrementally toward the final target. In that manner, copper(II) bears great potential considering previous investigations,[19,21] and, therefore, was examined extensively in combination with bromate as the anion in the course of this work. Besides the tedious search for possible replacements of LS and LA, recently, the research on primary explosives focused on laser-ignitable compounds.[22] In contrast to the conventional methods of initiation through impact, friction, and electrostatic discharge, this new initiation method bears encouraging potential because of the circumstance that examined compounds do not require high sensitivities toward the customary stimuli.[23] Consequently, laser-ignitable energetic materials with high performance, high thermal stability, and an uncritical impact on the environment can be used as insensitive but powerful charges to allow much safer handling

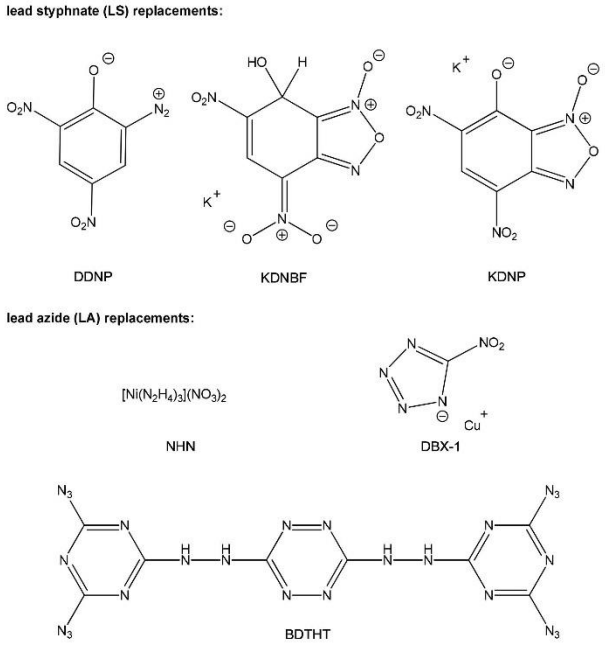
Received: April 17, 2018
Published: June 21, 2018

ACS Publications © 2018 American Chemical Society

DOI: 10.1021/acs.inorgchem.8b01045
Inorg. Chem. 2018, 57, 7940−7949

Downloaded via LMU MUENCHEN on February 16, 2022 at 07:58:24 (UTC).
See https://pubs.acs.org/sharingguidelines for options on how to legitimately share published articles.

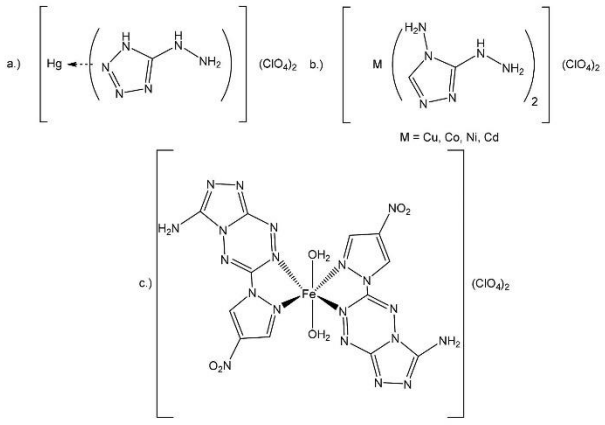
Chart 1. Molecular Structures of Possible LS and LA Replacements[a]



[a]DDNP = diazoniumdinitrophenolate,[11] KDNBF = potassium dinitrobenzofuroxan,[12] KDNP = 5,7-dinitro-[2,1,3]-benzoxadiazol-4-olate 3-oxide,[13] NHN = nickel(II) hydrazine nitrate,[14] DBX-1 = copper(I) nitrotetrazolate,[15] and BDTHT = 3,6-bis(2-(4,6-diazido-1,3,5-triazin-2-yl)hydrazinyl)-1,2,4,5-tetrazine.[16]

and to prevent undesired initiations.[22] On the basis of the idea of primary explosives in the form of coordination compounds, Zhilin et al. isolated several very promising complexes in the early 2000s (Chart 2a,b), including the well-known *cis*-bis(5-nitro-2*H*-tetrazolato-*N*2)cobalt(III) perchlorate and 5-hydrazino-1*H*-tetrazolemercury(II) perchlorate.[24−27] On the basis of these promising results, several research groups were starting to examine laser-sensitive ECC for future applications in military and civil areas.[28−30]

Chart 2. Different Laser-Ignitable Coordination Compounds[a]



[a](a) 5-Hydrazino-1*H*-tetrazolemercury(II) perchlorate,[26] (b) 3-hydrazino-4-amino-1,2,4-triazole-based metal(II) perchlorates,[27] or (c) $[(H_2NTriTz^{NO_2}Pyr)_2Fe(H_2O)_2](ClO_4)_2$.[31]

Bromates, particularly in the form of alkali salts, can be found in many different industrial processes (food production, synthetic reagents, dyeing, cosmetics, etc.) and are therefore an integral part of our daily life. While the use of alkali bromates ($NaBrO_3$ and $KBrO_3$) is rather common, the investigation of transition-metal bromates is relatively poor, especially with copper(II). Their high thermal stabilities,[32] exceptional performances, and relatively low prices make alkali bromates promising candidates in explosive mixtures. The latter fact led to the development of manageable potassium bromate containing concrete cracking agents and airbag-gas-generating compositions, as well as the invention of detectors for bromate-containing explosive mixtures.[33−35] Because of the strong oxidizing power of bromates and their high redox reactivity, mixtures with fuels or reducing agents have to be handled with great care. In particular, compositions with sulfur or organic compounds, such as dinitrotoluene or malonic acid, are highly unstable and tend to self-ignite within hours.[36]

Only a very few copper(II) complexes [including complexes with ammonia, primary amines, 4-amino-1,2,4-triazole (4-ATRI)] using bromate as the counteranion are known in the literature so far.[37,38] However, none of them was investigated for its crystal structure or has been described in relation to energetic materials. One of the very few, literature-reported examples uses the compound as a source for in situ generated Cu^IBr and as an alternative oxidizer (BrO_3^- vs ClO_4^-) in blue-light-emitting pyrotechnics.[39] The current contribution covers, as a further development of our recently published copper(II) chlorate complexes, analogous bromate-containing compounds with sensitivities in the range of primary explosives.[40] Obtained exceptional copper(II) bromate coordination compounds could be initiated by laser irradiation and their energetic character precisely tailored through the application of different nitrogen-donating azole-based ligands.

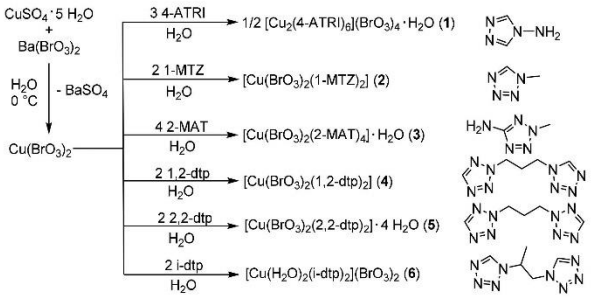
2. RESULTS AND DISCUSSION

2.1. Synthesis. Copper(II) bromate is poorly accessible, not commercially available, and exists with variable water contents (2−6 H_2O).[41,42] Therefore, the driving force of barium sulfate precipitation was utilized to synthesize copper(II) bromate stoichiometrically in situ as an intermediate for further reaction with the ligands (Scheme 1) through metathesis of copper(II) sulfate and barium bromate. All ligands used were commercially available or were synthesized according to the literature. Because of the very good solubility of the used nitrogen-rich azoles and copper(II) bromate, a minimum amount of water was chosen as the reaction medium for the synthesis of ECC **1**−**6**. As a result, the compounds often contain crystal water or aqua ligands. All attempts to change the reaction media to organic solvents led to decomposition of bromate to bromide because of its high redox activity [redox potential of E^0 = 1.45 V (to BrO^-); pH = 0], which is even slightly higher than that of perchlorate or chlorate [E^0 = 1.43 V (to ClO^-)].[43]

Most of the compounds were received in decent yields (57−85%) directly from the mother liquor in the form of single crystals suitable for X-ray diffraction. Only the compound $[Cu_2(4\text{-ATRI})_6](BrO_3)_4{\cdot}H_2O$ (**1**) was isolated as a light-blue powder, and crystal growth was achieved through layering and very slow formation at the phase boundary.

DOI: 10.1021/acs.inorgchem.8b01045
Inorg. Chem. 2018, 57, 7940−7949

Scheme 1. Synthesis of Complexes 1–6 Starting from Copper(II) Sulfate and Barium Bromate[a]



[a]Overview of the nitrogen-rich ligands used: 4-ATRI = 4-amino-1,2,4-triazole; 1-MTZ = 1-methyltetrazole; 2-MAT = 2-methyl-5-amino-tetrazole; 1,2-dtp = 1-(tetrazol-1-yl)-3-(tetrazol-2-yl)propane; 2,2-dtp = 1,3-di(tetrazol-2-yl)propane; i-dtp = 1,1′-(propane-1,2-diyl)bis-(tetrazole).

All coordination compounds were filtered off, washed with small amounts of cold water, and dried in air. The complexes can easily be distinguished by IR spectroscopy (Figures S1 and S2) because of the different coordination modes of the anions and the water molecules or through the absence of crystal water.

2.2. Crystal Structures. All complexes were characterized by low-temperature single-crystal X-ray diffraction. The crystal structures were uploaded to the CSD database[44] and can be obtained free of charge as CCDC 1836542 (**1**), 1836543 (**2**), 1836539 (**3**), 1836540 (**4**), 1836537 (**5**), 1836541 (**6**), 1836544 (**7**), 1836538 (**8**). The bond lengths and angles of the coordinating ligands in the analyzed complexes are in the typical range of the tetrazole and triazole ligands and nearly the same as in the noncoordinating ligands.[45−47] The ligands are therefore not part of the discussion in any of the following coordination compounds. All copper(II) bromate complexes show octahedral coordination with a Jahn−Teller distortion along the axial coordination sphere. In general, copper(II) bromate complexes tend to crystallize with water as solvent molecules [**1**, $[Cu(BrO_3)_2(2\text{-MAT})_4]\cdot H_2O$ (**3**), and $[Cu(BrO_3)_2(2,2\text{-dtp})_2]\cdot 4H_2O$ (**5**)] or in the form of aqua ligands {$[Cu(H_2O)_2(i\text{-dtp})_2](BrO_3)_2$ (**6**) and $[Cu(H_2O)_2(en)_2](BrO_3)_2$ (**7**)}. Only the bridging bromato anions in compounds $[Cu(BrO_3)_2(1\text{-MTZ})_2]$ (**2**) and $[Cu(BrO_3)_2(1,2\text{-dtp})_2]$ (**4**) prevented the inclusion of aqua molecules.

The monohydrated complex **1** is the only one presented with copper(II) ions exclusively coordinated by nitrogen atoms. It crystallizes in the form of blue blocks in the monoclinic space group *C*2/*c* with four formula units per unit cell and a calculated density of 2.299 g cm^{-3} at 143 K. The molecular unit contains two different copper(II) cations (Figure 1), and each is octahedrally coordinated by six triazole ligands. Both central atoms show a Jahn−Teller distortion, whereas the axial Cu−N bonds of Cu1 are shorter compared with those of Cu2. Three ligands are bridging between the same two copper(II) atoms and form polymeric chains.

2 shows the highest density (2.491 g cm^{-3} at 143 K) of all bromate complexes and crystallizes in the form of blue plates in the monoclinic space group $P2_1/c$ with two formula units per unit cell. The bromate anions in **2** are now coordinating to the transition-metal(II) center in comparison to compound **1**

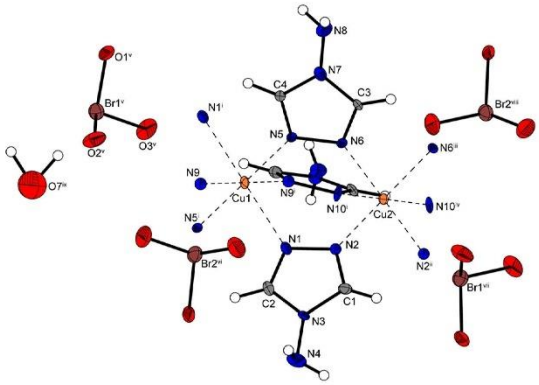


Figure 1. Copper(II) coordination environment of **1**. Thermal ellipsoids of non-hydrogen atoms in all structures are set to the 50% probability level. Selected bond lengths (Å): Cu1−N1 2.298(6), Cu1−N5 2.052(6), Cu1−N9 2.022(7), Cu2−N2 2.019(6), Cu2−N6 2.036(6), Cu2−N10^{i} 2.408(7). Selected bond angles (deg): N1−Cu1−N5 88.6(2), N1−Cu1−N9 88.8(2), N5−Cu1−N9 89.7(2), N2−Cu2−N6 91.4(2), N2−Cu2−N10^{i} 89.7(2), N6−Cu2−N10^{i} 88.0(2). Symmetry codes: (i) −*x*, −*y*, 1 − *z*; (ii) −*x*, *y*, 1.5 − *z*; (iii) −*x*, *y*, 1.5 − *z*; (iv) *x*, −*y*, 0.5 + *z*; (v) −1.5 + *x*, 0.5 + *y*, *z*; (vi) 0.5 − *x*, −0.5 − *y*, 1 − *z*; (vii) 0.5 + *x*, −0.5 − *y*, 0.5 + *z*; (viii) 0.5 − *x*, 0.5 + *y*, 1.5 − *z*; (ix) −1 + *x*, *y*, *z*.

(Figure 2). Each of the bromato ligands is bridging between two different metal(II) atoms, building up polymeric 2D layers.

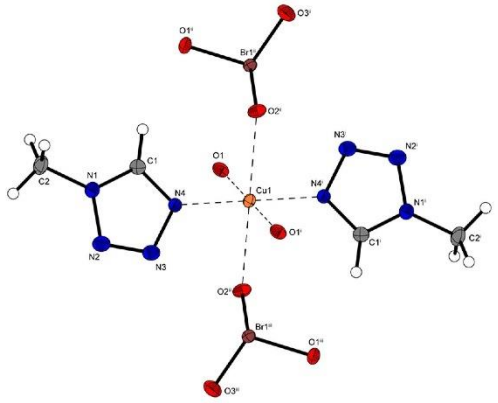


Figure 2. Copper(II) coordination environment of **2**. Selected bond lengths (Å): Cu1−O1 2.009(2), Cu1−O2^{ii} 2.346(2), Cu1−N4 1.987(3). Selected bond angles (deg): O1−Cu1−N4 90.71(10), O1−Cu1−O2^{ii} 87.89(8), O2^{ii}−Cu1−N4 89.80(9). Symmetry codes: (i) −*x*, 2 − *y*, −*z*; (ii) −*x*, 0.5 + *y*, 0.5 − *z*; (iii) *x*, 1.5 − *y*, −1.5 + *z*.

The monodentate ligand 2-MAT leads to the formation of a closed octahedral coordination sphere in complex **3**. It crystallizes in the form of green blocks in the monoclinic space group $P2_1/c$ with four formula units per unit cell and exhibits the lowest density (1.983 g cm^{-3} at 143 K) of all compounds. The molecular unit consists of one copper(II) cation (Figure 3), coordinated by two bromato and four tetrazole ligands together with an additional crystal water molecule. In contrast to compound **2**, the bromatos are only coordinating to one copper(II) central atom; therefore, the formation of polymeric structures does not occur. The water-free compound **4** crystallizes in the form of blue blocks in the monoclinic space group $P2_1/c$ with two formula units per unit

DOI: 10.1021/acs.inorgchem.8b01045
Inorg. Chem. 2018, 57, 7940−7949

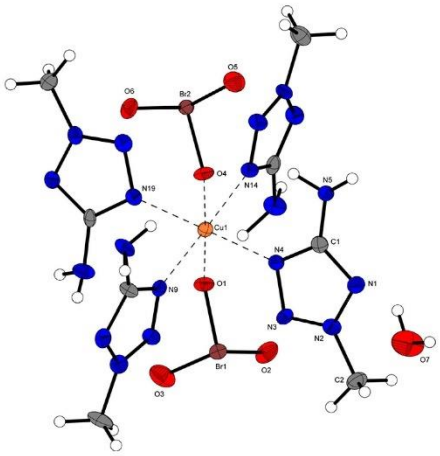


Figure 3. Molecular unit of **3**. Selected bond lengths (Å): Cu1−O1 2.367(4), Cu1−O4 2.381(4), Cu1−N4 2.018(5), Cu1−N9 2.057(5), Cu1−N14 2.043(5), Cu1−N19 2.033(5). Selected bond angles (deg): O1−Cu1−N9 88.57(17), O4−Cu1−N9 90.95(17), N4−Cu1−N9 91.08(19), N4−Cu1−N14 89.84(19).

cell and a calculated density of 2.142 g cm^{-3} at 130 K. The molecular unit is built up by one copper(II) cation (Figure 4),

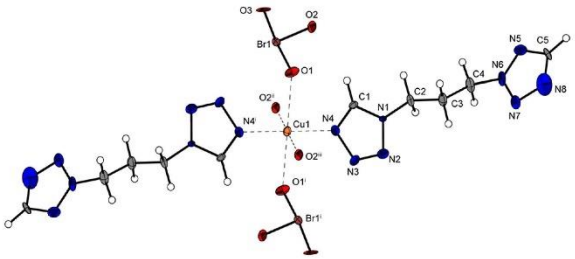


Figure 4. Copper(II) coordination environment of **4**. Selected bond lengths (Å): Cu1−O1 2.352(11), Cu1−O2^{ii} 2.033(12), Cu1−N4 1.976(12). Selected bond angles (deg): O1−Cu1−N4 90.9(5), O1−Cu1−O2^{ii} 96.2(4), O2^{ii}−Cu1−N4 90.4(5). Symmetry codes: (i) 2 − *x*, −*y*, −*z*; (ii) *x*, −0.5 − *y*, −0.5 + *z*; (iii) 2 − *x*, 0.5 + *y*, 0.5 − *z*.

two coordinating ligands in equatorial positions, and two bridging bromato anions. The ditetrazole ligands are only connected with the 1-substituted tetrazole ring, while the 2-substituted ring is not coordinating at all. Similar to complex **2**, every bromato is bridging between two different copper(II) atoms, building up polymeric 2D layers.

5 crystallizes in the form of blue blocks in the triclinic space group $P\bar{1}$ with one formula unit per unit cell and a calculated density of 2.002 g cm^{-3} at 143 K. The molecular unit is composed of a copper(II) cation (Figure 5) with two coordinating bromato ligands in the axial positions, two 2,2-dtp ligands in the plane, and four noncoordinating crystal water molecules. In contrast to compounds **2** and **3**, the bromates are not bridging, but two neutral ligands are linking between two central metals, building up polymeric chains.

The diaqua coordination compound **6** crystallizes in the form of blue blocks in the monoclinic space group $C2/c$ with four formula units per unit cell and a calculated density of 1.989 g cm^{-3} at 143 K. In contrast to the other aqua complexes, the water molecules act as ligands whereas the bromate counterions are not coordinating. The molecular unit

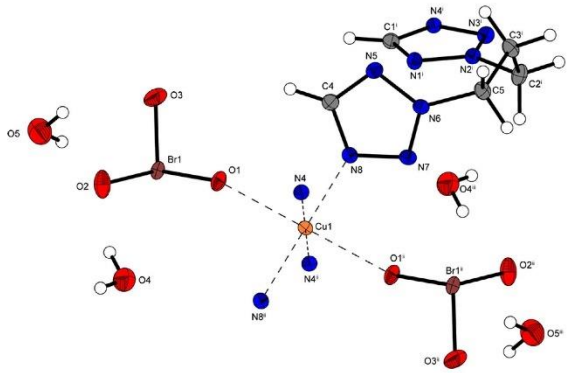


Figure 5. Copper(II) coordination environment of **5**. Selected bond lengths (Å): Cu1−O1 2.3200(13), Cu1−N4 2.0042(15), Cu1−N8 2.0335(15). Selected bond angles (deg): O1−Cu1−N4 93.85(5), O1−Cu1−N8 86.72(5), N4−Cu1−N8 91.38(6). Symmetry codes: (i) 3 − *x*, −*y*, 2 − *z*; (ii) 2 − *x*, −*y*, 2 − *z*; (iii) 1 − *x*, 1 − *y*, 2 − *z*.

contains one central metal(II) (Figure 6) with two aqua ligands in axial positions, two equatorial ditetrazole molecules,

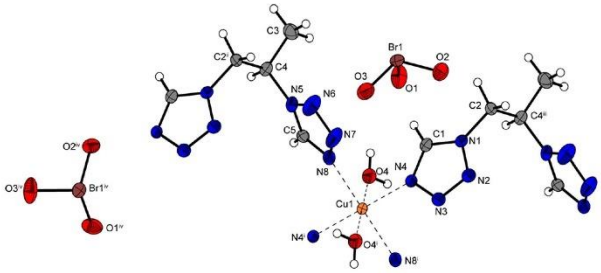
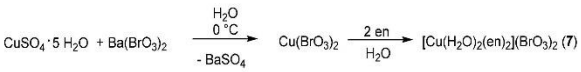


Figure 6. Copper(II) coordination environment of **6**. Selected bond lengths (Å): Cu1−O4 2.258(2), Cu1−N4 2.030(2), Cu1−N8 2.078(2). Selected bond angles (deg): O4−Cu1−N4 91.46(9), O4−Cu1−N8 85.56(9), N4−Cu1−N8 89.45(9). Symmetry codes: (i) 2 − *x*, 2 − *y*, 1 − *z*; (ii) 0.5 + *x*, −0.5 + *y*, *z*; (iii) −0.5 + *x*, 0.5 + *y*, *z*; (iv) 0.5 + *x*, 0.5 − *y*, −0.5 + *z*.

and two noncoordinating counterions. Analogously to complex **5**, the ligands are bridging between the copper(II) ions, building up polymeric chains.

Amiel described the synthesis of one of the first ever copper(II) bromate complexes with ethylenediamine (en) as the ligand in 1935 (Scheme 2). He suggested a monoclinic

Scheme 2. Synthesis of the Reinvestigated Complex 7



space group for the obtained violet compound with a formula of $(BrO_3)_2Cu(en)_2(H_2O)$.[37] This compound was reinvestigated by single-crystal X-ray diffraction.

The reinvestigation of this compound (Figure 7) verifies indeed a monoclinic space group ($P2_1/c$) for compound **7**. Two chelating en molecules in the equatorial position and two aqua ligands in the axial position are building up closed octahedral coordination spheres around the copper(II) center with noncoordinating bromate counteranions in the molecular unit. The diaqua coordination compound crystallizes in the

DOI: 10.1021/acs.inorgchem.8b01045
Inorg. Chem. 2018, 57, 7940−7949

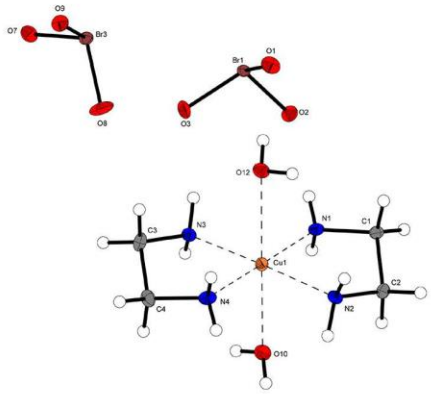


Figure 7. Molecular unit of 7. Selected bond lengths (Å): Cu1–N1 2.000(4), Cu1–N2 2.027(3), Cu1–N3 2.014(4), Cu1–N4 1.995(4), Cu1–O10 2.555(4), Cu1–O12 2.551(3). Selected bond angles (deg): N1–Cu1–N2 84.82(16), N1–Cu1–N3 94.90(16), N1–Cu1–N4 179.17(17), N1–Cu2–O10 83.98(15), N1–Cu2–O12 92.00(15).

form of purple blocks with six formula units per unit cell and a calculated density of 2.201 g cm^{-3} at 143 K.

The ligands highly influence the coordination mode of the bromate counterions. This affinity can also be observed in the various hydrates of copper(II) bromate. In $[Cu(BrO_3)_2(H_2O)_2]$, the coordination sphere around the metal(II) center is built up of four bridging bromato and two aqua ligands.[41] Blackburn et al. published the crystal structure of $[Cu(H_2O)_6](BrO_3)_2$ with noncoordinating anions, and the up-to-now unknown structure of $[Cu(BrO_3)_2(H_2O)_4]$ (**8**), measured in the course of this work, shows coordination but no linking of the bromato ligands.[42] The tetraaqua form of copper(II) bromate (**8**) crystallizes in the form of blue blocks in the orthorhombic space group *Pbca* with four formula units per unit cell and a calculated density of 2.975 g cm^{-3} at 143 K. Similar to complexes **3** and **5**, the coordination sphere around the copper(II) atom contains nonbridging bromato ligands in the axial positions and four extra equatorial aqua ligands (Figure 8).

2.3. Sensitivities and Thermal Stability. For the investigation of endothermic events, like dehydration or melting, and for determination of the thermal stabilities, differential thermal analysis (DTA) measurements with a heating rate of β = 5 °C min^{-1} were performed. The sensitivities of the complexes toward electric discharge as well as against impact and friction have been determined according to BAM standards, and all compounds were classified in accordance with the U.N. recommendations on the transport of dangerous goods.[48] An overview of the physicochemical properties of all compounds is given in Table 1. The sensitivities toward mechanical stress are comparable to those for LS and LA, whereas the susceptibility against electrostatic discharge sensitivity (ESD) is lower, making them more secure.[49]

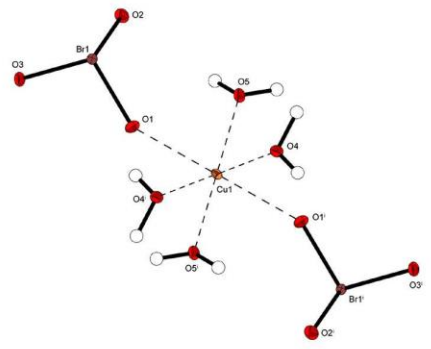


Figure 8. Molecular unit of 8. Selected bond lengths (Å): Cu1–O1 2.399(2), Cu1–O4 1.9572(19), Cu1–O5 1.9520(19). Selected bond angles (deg): O1–Cu1–O4 88.94(7), O1–Cu1–O5 95.11(7), O4–Cu1–O5 89.07(8). Symmetry code: (i) 1 − *x*, −*y*, 1 − *z*.

The only endothermic occasions occurred during heating of coordination compounds **5** and **6** (Figure 9C) were the loss of their crystal water (**5**) or aqua (**6**) ligands at 103 and 129 °C, respectively. The loss of crystal water molecules after heating in compounds **1** and **3** leads to instability of the whole molecule and results therefore in exothermic decomposition. One possible explanation of the higher thermal stability of compounds **5** and **6** could be the formation of water-free species that decompose at a later stage. Nevertheless, stable water-free products of **5** and **6** could not be obtained through dehydration. All ECCs have an exothermic decomposition temperature above 130 °C, except complex **3**, which possesses a very low thermal stability of 92 °C due to the loss of crystal water. The highest temperature stability (169 °C) shows the water-free 2D polymer **2**. The general trend becoming apparent is that bridging bromatos lead to crystallization of anhydrous complexes with higher thermal stabilities. Determination of the compounds' DDT capability by hot-plate and hot-needle testing (Figure 9A,B) was performed. Hot-needle tests were conducted by fixation of the sample underneath adhesive tape on a copper plate, followed by penetration with a red-heated needle. A compound's detonation typically indicates a valuable primary explosive, whereas the safe and practicable hot-plate test shows the performance of the unconfined sample toward fast heating on a copper plate. It does not necessarily allow any conclusions on a compound's capability as a primary explosive. All compounds, except complex **1**, showed deflagration in both tests. While the water-free compound **2** shows relatively high-temperature stability and only weak DDT, it is the other way around with compound **1**, possessing a great DDT but a low decomposition temperature.

2.4. Laser Ignition Tests and UV–Vis Measurements. The laser ignition tests were performed with a single-pulsed 45 W InGaAs laser diode in the single-pulsed mode. The diode was coupled directly to an optical fiber with a core diameter of 400 μm and a cladding diameter of 480 μm. The optical fiber was linked via a SMA-type connecter directly to the laser and to a collimator. The collimator, in turn, was connected to an optical lens, which was stationed in its focal distance (f = 29.9 mm) to the sample. The lens was shielded from the explosive with sapphire glass. Transparent polycarbonate percussion caps were filled with approximately 25 mg of the compound, pressed with a pressure force of 1 kN, and sealed by a UV-curing adhesive. The confined samples were irradiated at a wavelength of 915 nm, a varying current of 7–8 A, a voltage of 4 V, and a varying pulse length of 0.10–15 ms, which combined the results in an approximate energy output of 0.17–30 mJ. The results of the laser experiments, which are classified in decomposition, deflagration, or detonation according to the generated sound, are summarized in Table 2.

DOI: 10.1021/acs.inorgchem.8b01045
Inorg. Chem. 2018, 57, 7940–7949

Table 1. Physicochemical Properties of Compounds 1–6 as Well as LS and LA[50]

	IS [J][a]	*FS* [N][b]	*ESD* [mJ][c]	T_{endo} [°C][d]	T_{exo} [°C][e]	grain size [μm]
1	2	<5	25		137	<100
2	1	<5	60		169	100–500
3	2	<5	90		92	100–500
4	<1	10	150		146	100–500
5	8	108	260	103	150	100–500
6	1	40	150	129	146	100–500
LS	2.5–5	1.5	0.02–1.0	115	275–280	
LA	2.5–4	0.1–1	6–12		320–360	

[a]Impact sensitivity according to the BAM drophammer (method 1 of 6). [b]Friction sensitivity according to the BAM friction tester (method 1 of 6). [c]Electrostatic discharge sensitivity (OZM ESD tester). [d]Endothermic peak indicating dehydration or loss of aqua ligands according to DTA (onset temperatures at a heating rate of 5 °C min^{-1}). [e]Exothermic peak indicating decomposition according to DTA (onset temperatures at a heating rate of 5 °C min^{-1}).

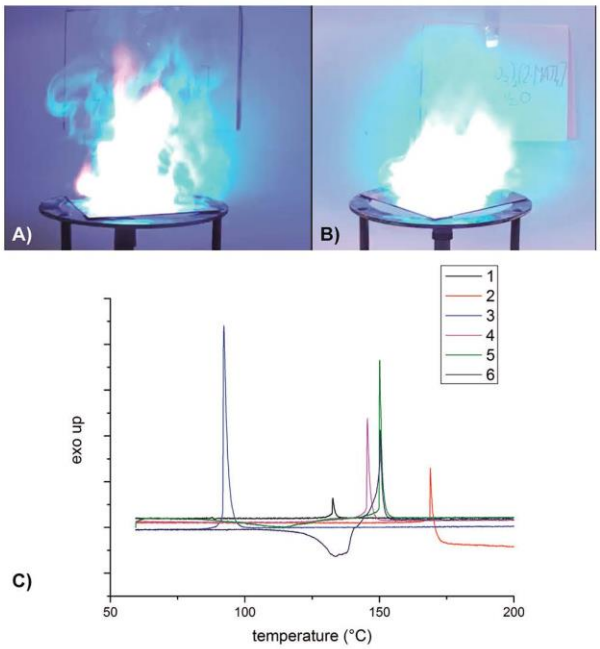


Figure 9. Hot-plate test of compounds **2** (A) and **3** (B). (C) DTA plots (5 °C min^{-1}) of complexes **1–6** shown in the range of 50–200 °C.

Table 2. Results of the Laser Ignition Tests of Compounds 1–6

	1	2	3	4	5	6
E_{max} [mJ]	0.17	30.0	0.20	0.17	5.10	2.55
outcome[a]	det.	det.	det.	det.	dec.	det.

[a]det. = detonation; dec = decomposition. Operating parameters: current I = 7–8 A; voltage U = 4 V; theoretical maximal output power P_{max} = 45 W; wavelength λ = 915 nm; pulse length τ = 0.10–15 ms.

All complexes, except tetraaqua compound **5**, showed a detonation (Figure 10A,B) differing in the required energy input between 0.17 and 2.55 mJ. Compared to LA[51] (3–30 mJ cm^{-2}) and LS[52] (1.3 J cm^{-2}), the ignition of most of the ECCs is possible with lower energy input, although the results are difficult to compare because of their different setups. These results correlate with the observed sensitivities and make copper(II) bromate complexes promising compounds for laser ignition with low initiation energies.

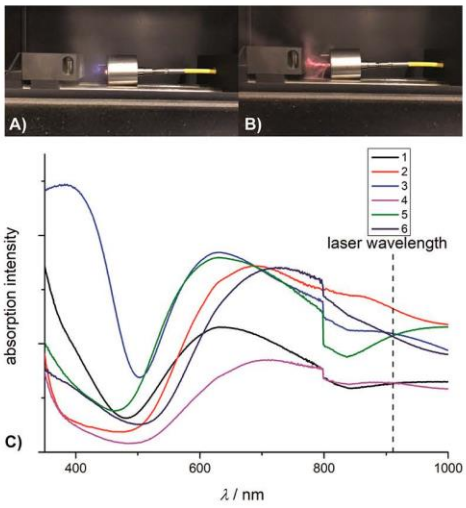


Figure 10. Positive laser initiation tests of compounds **2** (A) and **6** (B). (C) Solid-state UV–vis measurements that were correlated with the laser-initiation experiments.

In order to gain insight toward the laser-initiation mechanism, solid-state UV–vis measurements were performed in the range of 350–1000 nm for all complexes (Figure 10C). The step in the absorption intensity at 800 nm in the spectra is caused by a detector change. The UV–vis spectra exhibit only qualitative character.

Because of the characteristic d–d transitions, the spectra show absorptions in the UV, visible, and near-IR regions typical for copper(II) compounds. The mechanism for laser initiation is still not fully understood, and many pathways, such as electronic or thermal, are imaginable.[53] Because of the different coordination spheres, no conclusions can be drawn about the influence of the metal–ligand bond energy toward the color of the compounds. Compound **3**, the only green copper(II) bromate complex, shows absorption maxima close to 400 and 600 nm. All other copper(II) bromate complexes show absorption maxima close to 350 and 600 nm with only minor deviations among each other. All complexes show only minor absorptions at the laser wavelength of 915 nm. The excitation at 915 nm could be a conceivable explanation for the initiation. The process of laser ignition probably depends on multiple parameters, and more investigations are necessary for a better understanding of the laser-initiation mechanism in the future.

DOI: 10.1021/acs.inorgchem.8b01045
Inorg. Chem. 2018, 57, 7940–7949

2.5. Toxicity Determination and Mass Spectrometry (MS) of Decomposition Gases. The commercially available bioassay system LUMIStox test (luminescent marine bacterium *Vibrio fischeri* NRRL-B-11177), which measures the toxicity in aqueous media, is a valuable indicating device when it comes to groundwater contamination. The half-maximal effective concentration EC_{50} of these compounds was determined after an incubation time of 30 min (the toxicity level after 30 min of incubation: very toxic, <0.10 g L^{-1}; toxic, 0.10−1.00 g L^{-1}; nontoxic, >1.00 g L^{-1}).[54] With an EC_{50} (30 min) value of 0.21 g L^{-1} for compound **2**, it has to be considered as toxic, which is not surprising, because of the known toxicity of copper(II) compounds toward microorganisms.[55] Compared to the corresponding copper(II) chlorate and perchlorate complex, recently published by our group,[56,40] with EC_{50} values of 0.19 and 0.13 g L^{-1}, respectively, the lower toxicity toward aquatic life of bromate compounds is proven.

For analysis of the gaseous decomposition products, a sample of approximately 40 mg of compound **2** was heated to 200 °C in a nitrogen gas flow and the formed gases were detected with a Cirrus3-XD quadrupole mass spectrometer (Figure 11). The spectra show the formation of oxygen (32), CO_2 (44), and small amounts of water (18). No formation of toxic Br_2 or HBr was observed.

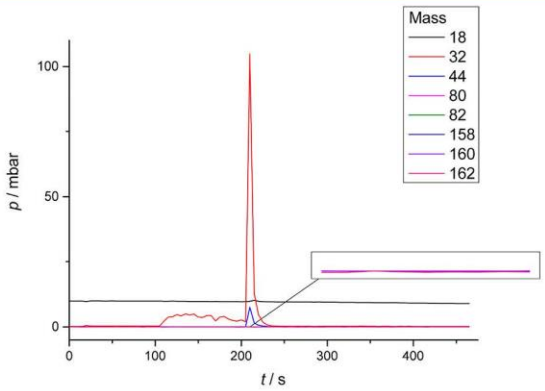


Figure 11. Results of the MS gas analysis of the decomposition products of compound **2**.

3. CONCLUSION

We demonstrated the next step in the development toward environmentally benign perchlorate-free ECCs with our exclusive concept of using bromate anions as "exotic" oxidizing species. The six newly synthesized and investigated copper(II) bromate compounds with azole ligands represent a considerable contribution to the coordination chemistry in general and in particular to ECC because of the enormous lack of literature regarding this topic. The displayed synthesis of the complexes is a straightforward and low-cost synthetic route toward modern lead-free primary explosives with promising performance characteristics. The simple complexation of $Cu(BrO_3)_2$ with different nitrogen-rich ligands based on tri- and tetrazole derivatives assures the formation of energetic compounds with high densities. The trend of inclusion of water into many of the structures can hardly be explained by the average oxophilicity of copper(II); however, it can be prevented by the formation of 2D polymeric layers caused by bridging bromato ligands. X-ray studies of all compounds gave insight into the fascinating coordination variety of copper(II) bromate complexes highly depending on the ligands used. The compositions of complexes **1**−**6** were confirmed by elemental analysis and are in accordance with the crystal structures observed. In addition, the X-ray structure of the up-to-now unknown tetrahydrate of copper(II) bromate **8** could successfully be determined and the previously predicted structures of **1**[38] and **7**[37] proven wrong. Most of the compounds showed exothermic decomposition temperatures above 135 °C in thermal stability measurements by DTA. In comparison to the analogous perchlorate and chlorate complexes, ECC **2** showed a lower environmental hazardousness toward aquatic life in toxicity assessments using *V. fischeri*, which proves the higher environmental friendliness of bromate compounds. Within preliminary analysis of decomposition gases, no HBr and Br_2 formation was observed in the MS spectra. Detonations during laser-ignition experiments of nearly every single compound revealed the great capability of copper(II) bromate complexes in future laser-initiation systems.

4. EXPERIMENTAL SECTION

All chemicals and solvents were employed as received (Sigma-Aldrich, Fluka, Acros, and ABCR). ^1H and ^{13}C NMR spectra were recorded with neat solids as samples at ambient temperature using a JEOL Eclipse 270, JEOL EX 400, or JEOL Eclipse 400 instrument. The chemical shifts quoted in parts per million in the text refer to typical standards such as tetramethylsilane (^1H and ^{13}C). Dehydration, melting, and decomposition temperatures of the described compounds were measured through DTA with an OZM Research DTA 552-Ex instrument. The samples were measured in a range of 25−400 °C at a heating rate of 5 °C min^{-1}. IR spectra were measured with pure samples on a PerkinElmer BXII FT-IR system with a Smith DuraSampler IR II diamond attenuated total reflectance instrument. Determination of the carbon, hydrogen, nitrogen, and sulfur contents was carried out by combustion analysis using an an Elementar Vario El analyzer (the nitrogen values determined are often lower than the calculated ones because of their explosive behavior). UV−vis spectra were recorded in the solid state using a Varian Cary 500 spectrometer in the wavelength range of 350−1000 nm. Impact sensitivity tests were carried out according to STANAG 4489[57] modified instruction[58] using a BAM (Bundesanstalt für Materialforschung) drophammer.[59] Friction sensitivity tests were carried out according to STANAG 4487[60] modified instruction[60,61] using the BAM friction tester. The classification of the tested compounds results from the "U.N. Recommendations on the Transport of Dangerous Goods".[62] Additionally, all compounds were tested for their sensitivity toward electrical discharge using the Electric Spark Tester ESD 2010 EN.S7.[63] Liquid-dried luminescent bacteria of the strain *V. fischeri* NRRL-B-11177 provided by the HACH LANGE GmbH were used for the luminescent bacteria inhibition test to determine their toxicity toward aquatic organisms according to a modified procedure.[64] All of the obtained coordination compounds were washed with cold water, dried overnight in air, and used for analytics without further purification.

Caution! *All investigated compounds are potentially explosive energetic materials, which show partly increased sensitivities toward various stimuli (e.g., elevated temperatures, impact, friction, or electrostatic discharge). Therefore, proper security precautions (safety glass, face shield, earthed equipment and shoes, leather coat, Kevlar gloves, Kevlar sleeves, and ear plugs) have to be applied while synthesizing and handling the described compounds. Especially compound* ***1*** *must be handled with great care!*

General Procedure for the Preparation of Complexes 1−7. Copper(II) sulfate pentahydrate (62.4 mg, 0.25 mmol) and barium bromate (98.3 mg, 0.25 mmol), each dissolved in 5 mL of water, were combined and stirred mechanically for 10 min, and the precipitated

DOI: 10.1021/acs.inorgchem.8b01045
Inorg. Chem. 2018, 57, 7940−7949

barium sulfate was filtered off. The aqueous filtrate was dried under reduced pressure and the obtained copper(II) bromate dissolved in 2 mL of water. Stoichiometric amounts of the ligand dissolved in 1 mL of water were added under stirring. The reaction mixtures were left to crystallize, and the solids were filtered off, washed with cold water (2 mL), and dried in air. Only one single crystal of compound **7** was picked for X-ray determination experiments, and the complex was not further analyzed. The up-to-now unknown structure of **8** was picked out of a complex solution, which was left for crystallization as a single crystal, and a pure product for further investigation was not obtained.

$[Cu_2(4\text{-ATRI})_6](BrO_3)_4 \cdot H_2O$ (1). Compound **1** was isolated as a light-blue precipitate. Yield: 116 mg (0.20 mmol, 80%). Single-crystal growth was achieved by overlaying an aqueous solution (8 mL) of copper(II) bromate with an ethanolic solution (8 mL) of 4-ATRI, separated by a mixture (4 mL) of water/ethanol (50/50). After 7 days, blue rods suitable for X-ray determination were obtained.

DTA (5 °C min^{-1}) onset: 137 °C (exothermic). IR (ATR, cm^{-1}): $\tilde{\nu}$ 3545 (vw), 3250 (m), 3208 (w), 3153 (m), 3126 (m), 3089 (m), 3063 (m), 3018 (w), 2965 (w), 1644 (w), 1631 (w), 1553 (w), 1539 (w), 1491 (vw), 1424 (vw), 1396 (w), 1373 (w), 1321 (vw), 1222 (m), 1207 (w), 1095 (m), 1085 (m), 1050 (m), 1007 (w), 992 (w), 979 (w), 913 (w), 890 (w), 818 (s), 808 (s), 783 (vs), 761 (vs), 693 (w), 679 (w), 622 (vs). Elem anal. Calcd for $C_{12}H_{26}Br_4Cu_2N_{24}O_{13}$ (1161.29): C, 12.41; H, 2.26; N, 28.95. Found: C, 12.78; H, 2.28; N, 28.64. BAM drophammer = 2 J; friction tester = <5 N; ESD = 25 mJ (at grain size <100 μm).

$[Cu(BrO_3)_2(1\text{-MTZ})_2]$ (2). Blue platelike crystals of complex **2** were obtained within 5 days and were suitable for X-ray determination. Yield: 89.4 mg (0.18 mmol, 73%).

DTA (5 °C min^{-1}) onset: 169 °C (exothermic). IR (ATR, cm^{-1}): $\tilde{\nu}$ 3143 (m), 3034 (w), 1762 (vw), 1522 (m), 1472 (w), 1304 (w), 1202 (m), 1178 (vw), 1109 (m), 1066 (w), 1036 (w), 1003 (w), 883 (m), 862 (vs), 788 (s), 726 (s), 708 (s), 686 (vs), 652 (s). Elem anal. Calcd for $C_4H_8Br_2CuN_8O_6$ (487.51): C, 9.85; H, 1.65; N, 22.99. Found: C, 10.11; H, 1.81; N, 23.13. BAM drophammer = 1 J; friction tester = <5 N; ESD = 60 mJ (at grain size 100−500 μm).

$[Cu(BrO_3)_2(2\text{-MAT})_4] \cdot H_2O$ (3). Green blocks suitable for X-ray determination of the monohydrated complex **3** crystallized within 3 days. Yield: 106 mg (0.14 mmol, 58%).

DTA (5 °C min^{-1}) onset: 92 °C (exothermic). IR (ATR, cm^{-1}): $\tilde{\nu}$ 3359 (m), 3317 (m), 3306 (m), 3223 (m), 3174 (w), 3020 (w), 2962 (w), 1629 (m), 1606 (m), 1557 (s), 1439 (m), 1422 (m), 1383 (w), 1345 (w), 1333 (w), 1195 (m), 1132 (w), 1103 (w), 1075 (w), 1023 (w), 803 (vs), 760 (vs), 749 (vs), 680 (m), 670 (w), 631 (m), 571 (w). Elem anal. Calcd for $C_8H_{22}Br_2CuN_{20}O_7$ (733.75): C, 13.10; H, 3.02; N, 38.18. Found: C, 13.13; H, 2.95; N, 38.37. BAM drophammer = 2 J; friction tester = <5 N; ESD = 90.0 mJ (at grain size 100−500 μm).

$[Cu(BrO_3)_2(1,2\text{-dtp})_2]$ (4). Blue blocklike crystals of the water-free compound **4** were isolated within 7 days and were suitable for X-ray determination. Yield: 96.9 mg (0.14 mmol, 57%).

DTA (5 °C min^{-1}) onset: 146 °C (exothermic). IR (ATR, cm^{-1}): $\tilde{\nu}$ 3144 (m), 1764 (w), 1741 (m), 1571 (w), 1516 (m), 1466 (m), 1457 (m), 1446 (m), 1396 (w), 1381 (m), 1366 (m), 1301 (w), 1287 (m), 1198 (m), 1180 (m), 1141 (m), 1134 (m), 1108 (w), 1059 (w), 1031 (m), 1015 (m), 1008 (m), 886 (m), 860 (s), 786 (s), 751 (m), 727 (s), 713 (s), 700 (vs), 677 (m), 654 (s). Elem anal. Calcd for $C_{10}H_{16}Br_2CuN_{16}O_6$ (679.70): C, 17.67; H, 2.37; N, 32.97. Found: C, 17.20; H, 2.47; N, 32.51. BAM drophammer = <1 J; friction tester = 10 N; ESD = 150 mJ (at grain size 100−500 μm).

$[Cu(BrO_3)_2(2,2\text{-dtp})_2] \cdot 4H_2O$ (5). The four-crystal water-containing complex **5** crystallized within 7 days in the form of blue blocks suitable for X-ray determination. Yield: 113 mg (0.15 mmol, 60%).

DTA (5 °C min^{-1}) onset: 103 °C (loss of water), 150 °C (exothermic). IR (ATR, cm^{-1}): $\tilde{\nu}$ 3524 (w), 3441 (w), 3367 (w), 3151 (w), 3125 (w), 3014 (w), 2985 (vw), 2970 (vw), 2945 (vw), 1741 (vw), 1737 (vw), 1652 (vw), 1623 (w), 1608 (w), 1573 (vw), 1512 (w), 1488 (w), 1474 (w), 1464 (w), 1447 (w), 1438 (w), 1382 (w), 1373 (w), 1359 (w), 1322 (w), 1306 (w), 1285 (w), 1254 (vw), 1209 (w), 1199 (w), 1187 (w), 1172 (m), 1153 (m), 1137 (m), 1101 (m), 1086 (m), 1076 (w), 1059 (w), 1031 (m), 1021 (m), 1012 (w), 982 (w), 936 (w), 890 (vw), 861 (w). Elem anal. Calcd for $C_{10}H_{24}Br_2CuN_{16}O_{10}$ (751.76): C, 15.98; H, 3.22; N, 29.81. Found: C, 16.46; H, 3.36; N, 31.06. BAM drophammer = 8 J; friction tester = 108 N; ESD = 260 mJ (at grain size 100−500 μm).

$[Cu(H_2O)_2(i\text{-dtp})_2](BrO_3)_2$ (6). Product **6** was received within 8 days in the form of blue blocks suitable for X-ray determination. Yield: 152 mg (0.21 mmol, 85%).

DTA (5 °C min^{-1}) onset: 129 °C (loss of water followed by decomposition). IR (ATR, cm^{-1}): $\tilde{\nu}$ 3357 (w), 3267 (w), 3151 (w), 3116 (w), 3016 (w), 2986 (w), 2945 (vw), 2776 (vw), 2661 (vw), 1741 (vw), 1652 (w), 1571 (vw), 1512 (w), 1489 (w), 1437 (m), 1391 (w), 1376 (w), 1360 (w), 1321 (vw), 1304 (w), 1287 (w), 1211 (w), 1187 (m), 1173 (m), 1160 (w), 1127 (w), 1100 (m), 1086 (m), 1039 (m), 1031 (w), 1011 (m), 990 (w), 916 (w), 891 (w), 840 (s), 782 (vs), 753 (s), 719 (w), 675 (m), 665 (m), 632 (m), 532 (vw). Elem anal. Calcd for $C_{10}H_{20}Br_2CuN_{16}O_8$ (715.73): C, 16.78; H, 2.82; N, 31.31. Found: C, 16.91; H, 2.92; N, 31.81. BAM drophammer = 1 J; friction tester = 40 N; ESD = 150 mJ (at grain size 100−500 μm).

■ ASSOCIATED CONTENT

Supporting Information

The Supporting Information is available free of charge on the ACS Publications website at DOI: 10.1021/acs.inorgchem.8b01045.

X-ray diffraction and IR spectroscopy of **1**−**6** (PDF)

Accession Codes

CCDC 1836537−1836544 contain the supplementary crystallographic data for this paper. These data can be obtained free of charge via www.ccdc.cam.ac.uk/data_request/cif, or by emailing data_request@ccdc.cam.ac.uk, or by contacting The Cambridge Crystallographic Data Centre, 12 Union Road, Cambridge CB2 1EZ, UK; fax: +44 1223 336033.

■ AUTHOR INFORMATION

Corresponding Author

*E-mail: jstch@cup.uni-muenchen.de (J.S.). Fax: +49 89 2180 77007. Web page: http://www.cup.lmu.de/ac/stierstorfer/.

ORCID

Norbert Szimhardt: 0000-0001-6722-2562

Jörg Stierstorfer: 0000-0002-2105-1275

Notes

The authors declare no competing financial interest.

†Parts of this work were presented at the 21st International Seminar "New Trends in Research of Energetic Materials" in Pardubice, Czech Republic.

■ ACKNOWLEDGMENTS

Financial support of this work by the Ludwig-Maximilian University of Munich and the Office of Naval Research under Grant ONR.N00014-16-1-2062 is gratefully acknowledged. Prof. Thomas M. Klapötke is thanked for great financial support and indispensable scientific assistance. The authors additionally thank Cornelia Unger for her great contribution in the form of toxicity assessments.

■ REFERENCES

(1) Klapötke, T. M. *Chemistry of High-Energy Materials*, 3rd ed.; Walter De Gruyter, Berlin/Boston, 2015.

(2) Brinck, T. *Green Energetic Materials*, 1st ed.; John Wiley & Sons: Chichester, U.K., 2014.

(3) Fairhall, L. T.; Jenrette, W. V.; Jones, S. W.; Pritchard, E. A. The toxicity of lead azide. *Public Health Rep.* **1943**, *58*, 607−617.

(4) Gidlow, D. A. Lead toxicity. *Occup. Med.* **2015**, *65*, 348−356.

DOI: 10.1021/acs.inorgchem.8b01045
Inorg. Chem. 2018, 57, 7940−7949

(5) Haiges, R.; Christe, K. O. Energetic High-Nitrogen Compounds: 5-(Trinitromethyl)-2*H*-tetrazole and -tetrazolates, Preparation, Characterization, and Conversion into 5-(Dinitromethyl)tetrazoles. *Inorg. Chem.* **2013**, *52*, 7249−7260.
(6) Huynh, M. H. V.; Coburn, M. D.; Meyer, T. J.; Wetzler, M. Green primary explosives: 5-Nitrotetrazolato-*N*2-ferrate hierarchies. *Proc. Natl. Acad. Sci. U. S. A.* **2006**, *103*, 10322−10327.
(7) Xu, J.-G.; Sun, C.; Zhang, M.-J.; Liu, B.-W.; Li, X.-Z.; Lu, J.; Wang, S.-H.; Zheng, F.-K.; Guo, G.-C. Coordination Polymerization of Metal Azides and Powerful Nitrogen-Rich Ligand toward Primary Explosives with Excellent Energetic Performances. *Chem. Mater.* **2017**, *29*, 9725−9733.
(8) Liu, T.; Qi, X.; Wang, K.; Zhang, J.; Zhang, W.; Zhang, Q. Green primary energetic materials based on N-(3-nitro-1-(trinitromethyl)-1*H*-1,2,4-triazol-5-yl)nitramide. *New J. Chem.* **2017**, *41*, 9070−9076.
(9) Tang, Y.; He, C.; Mitchell, L. A.; Parrish, D. A.; Shreeve, J. n. M. Potassium 4,4'-Bis(dinitromethyl)-3,3'-azofurazanate: A Highly Energetic 3D Metal-Organic Framework as a Promising Primary Explosive. *Angew. Chem., Int. Ed.* **2016**, *55*, 5565−5567.
(10) He, P.; Wu, L.; Wu, J.; Wang, Q.; Li, Z.; Gozin, M.; Zhang, J. Green Energetic Nitrogen-Rich Salts of 1,1'-Dinitramino-5,5'-bistetrazolate. *Chem. - Eur. J.* **2017**, *23*, 11159−11168.
(11) Clark, L. V. Diazodinitrophenol, a Detonating Explosive. *Ind. Eng. Chem.* **1933**, *25*, 663−669.
(12) Spear, R. J.; Norris, W. P. Structure and properties of the potassium hydroxide-dinitrobenzofuroxan adduct (KDNBF) and related explosive salts. *Propellants, Explos., Pyrotech.* **1983**, *8*, 85−88.
(13) Fronabarger, J. W.; Williams, M. D.; Sanborn, W. B.; Parrish, D. A.; Bichay, M. KDNP − A Lead Free Replacement for Lead Styphnate. *Propellants, Explos., Pyrotech.* **2011**, *36*, 459−470.
(14) Shunguan, Z.; Youchen, W.; Wenyi, Z.; Jingyan, M. Evaluation of a New Primary Explosive: Nickel Hydrazine Nitrate (NHN) complex. *Propellants, Explos., Pyrotech.* **1997**, *22*, 317−320.
(15) Fronabarger, J. W.; Williams, M. D.; Sanborn, W. B.; Bragg, J. G.; Parrish, D. A.; Bichay, M. DBX-1-A Lead Free Replacement for Lead Azide. *Propellants, Explos., Pyrotech.* **2011**, *36*, 541−550.
(16) Chen, D.; Yang, H.; Yi, Z.; Xiong, H.; Zhang, L.; Zhu, S.; Cheng, G. $C_8N_{26}H_4$: An Environmentally Friendly Primary Explosive with High Heat of Formation. *Angew. Chem., Int. Ed.* **2018**, *57*, 2081−2084.
(17) Ilyushin, M. A.; Aleksandrova, M. A.; Bachurina, I. V.; Smirnov, A. V.; Tselinskii, I. V. Synthesis and properties of an energetic complex pentaamminecobalt (III) perchlorate, with 4-amino-1,2,4-triazole as ligand. *Russ. J. Appl. Chem.* **2010**, *83*, 92−96.
(18) Chen, S.; Guo, W.; Bi, Y.; Zhang, T. Synthesis and Properties of $[Cd(HTRTR)_2(H_2O)_4](HTNR)_2$ as an Energetic Complex. *Z. Anorg. Allg. Chem.* **2016**, *642*, 761−765.
(19) Talawar, M. B.; Agrawal, A. P.; Asthana, S. N. Energetic coordination compounds: Synthesis, characterization and thermolysis studies on bis-(5-nitro-2H-tetrazolato-N2)tetraammine cobalt (III) perchlorate (BNCP) and its new transition metal (Ni/Cu/Zn) perchlorate analogues. *J. Hazard. Mater.* **2005**, *120*, 25−35.
(20) Szimhardt, N.; Wurzenberger, M. H. H.; Klapötke, T. M.; Lechner, J. T.; Reichherzer, H.; Unger, C.; Stierstorfer, J. Highly functional energetic complexes: stability tuning through coordination diversity of isomeric propyl-linked ditetrazoles. *J. Mater. Chem. A* **2018**, *6*, 6565−6577.
(21) Evers, J.; Gospodinov, I.; Joas, M.; Klapötke, T. M.; Stierstorfer, J. Cocrystallization of Photosensitive Energetic Copper(II) Perchlorate Complexes with the Nitrogen-rich Ligand 1,2-Di(1*H*-tetrazol-5-yl)ethane. *Inorg. Chem.* **2014**, *53*, 11749−11756.
(22) Ahmad, S. R.; Cartwright, M. Laser Ignition—Practical Considerations. *Laser Ignition of Energetic Materials*; John Wiley & Sons, Ltd., 2014; pp 247−268.
(23) Schirra, R.; Zöllner, H. A fast low-energy optical detonator. *Proceedings of the 42nd International Pyrotechnics Seminar*, Grand Junction, CO, July 10−15, 2016; IPSUSA, 2016; pp 422−428.
(24) Zhilin, A. Y.; Ilyushin, M. A.; Tselinskii, I. V.; Brykov, A. S. Synthesis of a high-energy-capacity compound, cis-tetraamminebis(5-nitro-2*H*-tetrazolato-N2)cobalt(III) perchlorate. *Russ. J. Appl. Chem.* **2001**, *74*, 99−102.
(25) Zhilin, A. Y.; Ilyushin, M. A.; Tselinskii, I. V.; Kozlov, A. S.; Lisker, I. S. High-energy-capacity cobalt(III) tetrazolates. *Russ. J. Appl. Chem.* **2003**, *76*, 572.
(26) Ilyushin, M. A.; Tselinsky, I. V.; Ugryumov, I. A.; Zhilin, A. Y.; Kozlov, A. S. Coordination complexes as inorganic primary explosives. *Proceedings of the 6th Seminar on New Trends in Research of Energetic Materials*, Pardubice, Czech Republic, Apr 22−24, 2003; University of Pardubice, 2003; pp 146−152.
(27) Ugryumov, I. A.; Ilyushin, M. A.; Tselinskii, I. V.; Kozlov, A. S. Synthesis and properties of photosensitive complex perchlorates of d metals with 3(5)-hydrazino-4-amino-1,2,4-triazole as ligand. *Russ. J. Appl. Chem.* **2003**, *76*, 439−441.
(28) Myers, T. W.; Brown, K. E.; Chavez, D. E.; Scharff, R. J.; Veauthier, J. M. Correlating the Structural, Electronic, and Explosive Sensitivity Properties of CuII Tetrazine Complexes. *Eur. J. Inorg. Chem.* **2016**, *2016*, 3178−3183.
(29) Myers, T. W.; Bjorgaard, J. A.; Brown, K. E.; Chavez, D. E.; Hanson, S. K.; Scharff, R. J.; Tretiak, S.; Veauthier, J. M. Energetic Chromophores: Low-Energy Laser Initiation in Explosive Fe(II) Tetrazine Complexes. *J. Am. Chem. Soc.* **2016**, *138*, 4685−4692.
(30) Joas, M. Ph.D. Thesis, Ludwig-Maximilians Universität München, München, Germany, 2014.
(31) Myers, T. W.; Brown, K. E.; Chavez, D. E.; Scharff, R. J.; Veauthier, J. M. Laser Initiation of Fe(II) Complexes of 4-Nitropyrazolyl Substituted Tetrazine Ligands. *Inorg. Chem.* **2017**, *56*, 2297−2303.
(32) Yoffe, D.; Frim, R.; Ukeles, S. D.; Dagani, M. J.; Barda, H. J.; Benya, T. J.; Sanders, D. C. Bromine Compounds. In *Ullmann's Encyclopedia of Industrial Chemistry*, 7th ed.; Elvers, B., Ed.; Wiley-VCH Verlag: Weinheim, Germany, 2013; pp 27−28.
(33) Yoshinaga, S.; Matsumoto, M.; Nagaishi, T. Reaction among potassium bromate, aluminium and dinitrotoluene. *Kogyo Kayaku* **1979**, *40*, 101−108.
(34) Yoshida, T. Air bag gas generating composition. U.S. Patent 5,898,126A, 1999.
(35) Menzel, R. E. Method for detecting trace explosives using photoluminescence. U.S. 7,910,376B2, 2011.
(36) Urben, P. G. *Bretherick's Handbook of Reactive Chemical Hazards*, 8nd ed.; Elsevier: Amsterdam, The Netherlands, 2017; pp 69−70.
(37) Amiel, J. Complex cupric perchlorates and bromates with primary amines. *Compt. rend.* **1935**, *200*, 672−674.
(38) Sinditskii, V. P.; Vernidub, T. Y.; Fogel'zang, A. E.; Zueva, N. A. Coordination compounds of 4-amino-1,2,4-triazole with metal chlorates, bromates and nitrates. *Izv. Vyssh. Uchebn. Zaved., Khim. Khim. Tekhnol.* **1991**, *34*, 15−19.
(39) Juknelevicius, D.; Karvinen, E.; Klapötke, T. M.; Kubilius, R.; Ramanavicius, A.; Rusan, M. Copper(I) Bromide: An Alternative Emitter for Blue-Colored Flame Pyrotechnics. *Chem. - Eur. J.* **2015**, *21*, 15354−15359.
(40) Wurzenberger, M. H. H.; Szimhardt, N.; Stierstorfer, J. Copper(II) Chlorate Complexes − the Renaissance of a Forgotten and Misjudged Energetic Anion. *J. Am. Chem. Soc.* **2018**, *140*, 3206−3209.
(41) Markin, V. N.; Rozhdestvenskaya, I. V.; Fedosova, O. I. Crystal structure of copper bromate dihydrate ($Cu(BrO_3)_2 \cdot 2H_2O$). *Vestn. Leningr. Univ., Ser. 4: Fiz., Khim.* **1985**, *1*, 104−107.
(42) Blackburn, A. C.; Gallucci, J. C.; Gerkin, R. E. Structure of hexaaquacopper(II) bromate. *Acta Crystallogr., Sect. C: Cryst. Struct. Commun.* **1991**, *47*, 2019−2023.
(43) Holleman, A. F.; Wiberg, E.; Wiberg, N. *Lehrbuch der Anorganischen Chemie*; de Gruyter: Berlin, 2007; pp 464−474.
(44) Crystallographic data for the structures have been deposited with the Cambridge Crystallographic Data Centre. Copies of the data can be obtained free of charge upon application to The Director, CCDC, 12 Union Road, Cambridge CB2 1EZ, UK (fax

DOI: 10.1021/acs.inorgchem.8b01045
Inorg. Chem. 2018, 57, 7940−7949

int.code_(1223)336-033; e-mail for inquiry fileserv@ccdc.cam.ac.uk; e-mail for deposition deposit@ccdc.cam.ac.uk).
(45) Wiehl, L. Structures of hexakis(1-propyltetrazole)iron(II) bis(tetrafluoroborate), $[Fe(CHN_4C_3H_7)_6](BF_4)_2$, hexakis(1-methyltetrazole)iron(II) bis(tetrafluoroborate), $[Fe(CHN_4CH_3)_6](BF_4)_2$, and the analogous perchlorates. Their relation to spin crossover behavior and comparison of Debye-Waller factors from structure determination and Moessbauer spectroscopy. *Acta Crystallogr., Sect. B: Struct. Sci.* **1993**, *49*, 289−303.
(46) van Koningsbruggen, P. J.; Garcia, Y.; Kahn, O.; Fournès, L.; Kooijman, H.; Spek, A. L.; Haasnoot, J. G.; Moscovici, J.; Provost, K.; Michalowicz, A.; Renz, F.; Gütlich, P. Synthesis, Crystal Structure, EXAFS, and Magnetic Properties of Catena [μ-Tris(1,2-bis(tetrazol-1-yl)propane-*N*1,*N*1')iron(II)] Bis(perchlorate). First Crystal Structure of an Iron(II) Spin-Crossover Chain Compound. *Inorg. Chem.* **2000**, *39*, 1891−1900.
(47) Romanenko, G. V.; Savelieva, Z. A.; Podberezskaya, N. V.; Larionov, S. V. Structure of the Cu(II) chloride complex with 4-amino-1,2,4-triazole $Cu(C_2H_4N_4)Cl_2$. *J. Struct. Chem.* **1997**, *38*, 171−176.
(48) Impact: insensitive, >40 J; less sensitive, ≥35 J; sensitive, ≥4 J; very sensitive, ≤3 J. Friction: insensitive, >360 N; less sensitive, 360 N; sensitive, <360 and >80 N, very sensitive, ≤80 N, extremely sensitive, ≤10 N. According to the U.N. Recommendations on the Transport of Dangerous Goods, + indicates not safe for transport.
(49) Meyer, R.; Köhler, J.; Homburg, A. *Explosives*, 5th ed.; Wiley-VCH Verlag: Weinheim, Germany, 2002; pp 196−197.
(50) Meyer, R.; Köhler, J.; Homburg, A. *Explosives*; Wiley-VCH: Weinheim, Germany, 2002; pp 196−197.
(51) Hagan, J. T.; Chaudhri, M. M. Low energy laser initiation of single crystals of β-lead azide. *J. Mater. Sci.* **1981**, *16*, 2457−2466.
(52) de Yon, L.; Nguyen, T.; Waschl, J. *Laser ignition of explosives, pyrotechnics and propellants*; Defence Science and Technology Organization, 1995.
(53) Aluker, E. D.; Krechetov, A. G.; Mitrofanov, A. Y.; Nurmukhametov, D. R.; Kuklja, M. M. Laser Initiation of Energetic Materials: Selective Photoinitiation Regime in Pentaerythritol Tetranitrate. *J. Phys. Chem. C* **2011**, *115*, 6893−6901.
(54) Cao, C. J.; Johnson, M. S.; Hurley, M. M.; Klapötke, T. M. In Vitro Approach to Rapid Toxicity Assessment of Novel High-Nitrogen Energetics. *JANNAF J. Propuls. Energet.* **2012**, *5*, 41−51.
(55) Ochoa-Herrera, V.; Léon, G.; Banihani, Q.; Field, J. A.; Sierra-Alvarez, R. Toxicity of copper(II) ions to microorganisms in biological wastewater treatment systems. *Sci. Total Environ.* **2011**, *412-413*, 380−385.
(56) Szimhardt, N.; Wurzenberger, M. H. H.; Beringer, A.; Daumann, L.; Stierstorfer, J. Coordination chemistry with 1-methyl-5*H*-tetrazole: cocrystallization, laser-ignition, lead-free primary explosives - one ligand, three goals. *J. Mater. Chem. A* **2017**, *5*, 23753−23765.
(57) NATO standardization agreement (STANAG) on explosives, impact sensitivity tests, no. 4489, first ed., Sept 17, 1999.
(58) WIWEB-Standardarbeitsanweisung 4-5.1.02, Ermittlung der Explosionsgefährlichkeit, hier der Schlagempfindlichkeit mit dem Fallhammer, Nov 8, 2002.
(59) http://www.bam.de, accessed Apr 2018.
(60) NATO standardization agreement (STANAG) on explosive, friction sensitivity tests, no. 4487, first ed., Aug 22, 2002.
(61) WIWEB-Standardarbeitsanweisung 4-5.1.03, Ermittlung der Explosionsgefährlichkeit oder der Reibeempfindlichkeit mit dem Reibeapparat, Nov 8, 2002.
(62) Impact: insensitive, >40 J; less sensitive, ≥35 J; sensitive, ≥4 J; very sensitive, ≤3 J. Friction: insensitive, >360 N; less sensitive, 360 N; sensitive, <360 and > 80 N; very sensitive, ≤80 N, extremely sensitive, ≤10 N. According to the U.N. Recommendations on the Transport of Dangerous Goods, + indicates not safe for transport.
(63) http://www.ozm.cz, accessed Apr 2018.
(64) Scharf, R. Ph.D. Thesis, Ludwig-Maximilians Universität München, München, Germany, 2016.

DOI: 10.1021/acs.inorgchem.8b01045
Inorg. Chem. 2018, 57, 7940−7949

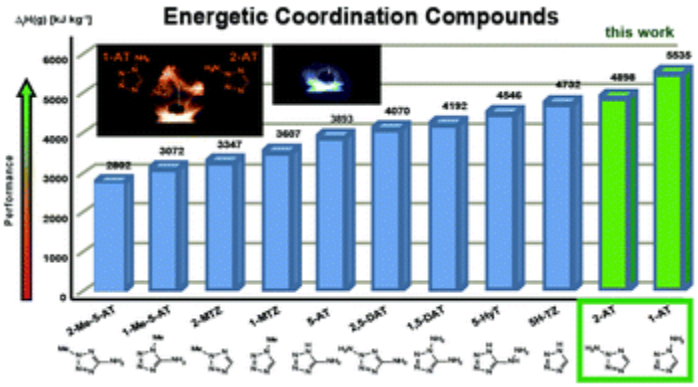
Appendix 6

Maximization of the Energy Capability Level in Transition Metal Complexes through Application of 1-Amino- and 2-Amino-5H-tetrazole Ligands

N. Szimhardt, M. H. H. Wurzenberger, L. Zeisel, M.S. Gruhne, M. Lommel, J. Stierstorfer

J. Mater. Chem. A, **2018**, *6*, 16257–16272.

https://doi.org/10.1039/C8TA06326E



Supplementary Information:
https://www.rsc.org/suppdata/c8/ta/c8ta06326e/c8ta06326e1.pdf

Published on 06 August 2018. Downloaded by Ludwig Maximilians Universitaet Muenchen on 2/16/2022 7:59:25 AM.

Journal of Materials Chemistry A

PAPER

View Article Online
View Journal | View Issue

Check for updates

Cite this: J. Mater. Chem. A, 2018, 6, 16257

Maximization of the energy capability level in transition metal complexes through application of 1-amino- and 2-amino-5*H*-tetrazole ligands†

Norbert Szimhardt, Maximilian H. H. Wurzenberger, Lukas Zeisel, Michael S. Gruhne, Marcus Lommel and Jörg Stierstorfer*

Toxic lead compounds (especially lead azide and lead styphnate), reliable but highly harmful compounds, still dominate the field of primary explosives used in most ignition and initiation systems to this day. Therefore, an extensive investigation into energetic materials with similar performance and minimized toxicity led to the very promising strategy of developing energetic coordination compounds (ECC). For the first time in literature, two isomeric amino-5*H*-tetrazoles with sensitivities already in the range of primaries, which could be obtained *via* practicable, easily scalable synthesis, proved to be very promising new energetic ECC ligands. By variation of the respective isomer (1-AT, 2-AT), metal(II) center (Mn^{II}, Fe^{II}, Cu^{II}, Zn^{II}) and the corresponding counter-anion (Cl^-, NO_3^-, ClO_3^-, ClO_4^-, styphnate, trinitrophloroglucinate) desired properties could be tailored gradually, yielding 20 new, highly energetic and easily accessible transition metal(II) complexes. In addition to comprehensive characterization by XRD, IR, EA, solid-state UV/Vis, DTA and TGA, BAM standard sensitivity measurements as well as ESD and ball drop impact sensitivities were determined. Classical initiation tests (nitropenta filled detonator) validated the present approach to be extraordinarily promising for potential use in advanced initiation systems. Beyond successfully achieving set goals in terms of sensitivity and toxicity, investigated complexes match or even outperform lead-based primaries' high performance and, more importantly, do not necessarily depend on initiation by mechanical stimuli. Laser irradiation of the received primary explosives with near-infrared light (NIR) yielded initiation reliably and safely, further extending their potential for future applications.

Received 2nd July 2018
Accepted 3rd August 2018

DOI: 10.1039/c8ta06326e

rsc.li/materials-a

In recent years, the demand for "green" chemicals, with respect to the invention, design and application of chemical products and processes, has grown continuously with the objective of reducing or eliminating the use and generation of hazardous substances.[1] The wide and fast expanding field of "green" chemicals comprises biodegradable plastics, bio-based polymers and environmentally friendly explosives from different portfolios of sustainable, eco-sufficient materials feasible of outclassing products based on petroleum feedstock or toxic heavy metals such as lead, mercury, barium and others.[2] Interaction between the chemical industry and academic research plays a key part in this social and economic evolution and the eventual success of green and sustainable materials. A guideline relevant to applied research in this area is the candidate list of substances of very high concern for authorization (Annex XIV) from the REACH (Registration, Evaluation, Authorization and Restriction of Chemicals) regulations.[3]

The REACH regulations were established in June 2007 as a European Union-wide project to reduce the amount of harmful or at least suspected-to-be-harmful chemicals to which European citizens were exposed to in their everyday life. In fact, REACH is not restricted to industrial processes, and also covers the chemicals used in everyday products such as paint, cleaning products or personal hygiene articles.[4] ECHA (European Chemicals Agency) uses this decree to hold the chemical industry responsible for collecting information about their manufactured chemicals, while also assessing their hazards and potential risk to the environment. Based on the simple "one substance, one registration" principle manufacturers and

Department of Chemistry, Ludwig Maximilian University of Munich, Butenandtstr. 5-13, D-81377 Munich, Germany. E-mail: jstch@cup.uni-muenchen.de; Web: http://www.cup.lmu.de/ac/stierstorfer/; http://www.hedm.cup.uni-muenchen.de; Fax: +49-89-2180-77492

† Electronic supplementary information (ESI) available: Compounds overview; IR spectroscopy of **1–9**, **12**, and **16–23**; DTA plots of **1–3**, **8**, **9**, **12** and **16–23**; column diagrams of the complexes **18–23**; hot plate and hot needle tests; initiation capability tests; laser ignition tests; UV-Vis spectra of **18**, **19**, **21**, and **23**; experimental part and general methods. CCDC 1834855 (**1**), 1834849 (**3**), 1834847 (**5**), 1834859 (**6**), 1834851 (**7**), 1834845 (**8**), 1834844 (**9**), 1834853 (**10**), 1834852 (**12**), 1834858 (**13**), 1834857 (**14**), 1834854 (**15**), 1834842 (**16**), 1834843 (**17**), 1834841 (**18**), 1834856 (**19**), 1834846 (**20**), 1834848 (**21**), 1834850 (**22**) and 1838980 (**23**). For ESI and crystallographic data in CIF or other electronic format see DOI: 10.1039/c8ta06326e

Published on 06 August 2018. Downloaded by Ludwig Maximilians Universitaet Muenchen on 2/16/2022 7:59:25 AM.

importers register their chemicals in conjunction with each other for later evaluation to clarify if these registered chemicals bear any risk to the environment or health.[5] The subsequent authorization process ensures that substances of very high concern (SVHCs) are gradually replaced with other less dangerous and less harmful alternatives – if possible and readily available. As soon as the committee or the commission reaches an agreement that the addition of a SVHC to the candidate list is reasonable, the substance is added to the database.[6]

One of the many candidates mentioned on this list are lead azide and lead styphnate, which are widely used as primary explosives. A total of 31 lead containing compounds appear on the REACH list, with all of them being suspected to be toxic for reproduction and some also to be carcinogenic (*e.g.* lead chromate since 2009).[7] As lead azide and lead styphnate are mainly used in small arm ammunition for military and commercial applications (mining, deconstruction works, *etc.*), there is a strong drive for substitution of these currently used-primary explosives. Scientists in many countries from all over the world are therefore looking for possible alternatives and replacements.[8–14] Thought must be given to many different factors (fast deflagration-to-detonation transition (DDT), compatibility, energetic properties *etc.*) during the design, the synthesis and evaluation of potential new primary explosives. The most important characteristics for suitable candidates include the sensitivities, the chemical and physical stability, low toxicity, low price, high performance and practicabilities according to industrial needs (Fig. 1). The concept of energetic coordination compounds (ECC), containing nitrogen rich ligands with low or non-toxic metals (*e.g.* Mn, Fe, Cu, Zn), stands out from other competing strategies and fulfills all of the desired criteria.[15–17] One of the biggest advantages of this promising approach is that the simple adjustment of one of the three building blocks (metal, ligand, anion) allows exact tailoring of the complexes in regard to the physico-chemical properties. Another important benefit of energetic coordination compounds, making them highly promising and suitable candidates for potential future applications, is their ignitability by optical methods like laser irradiation.[18,19] This approach offers various advantages in comparison to conventional initiation methods like short function times or the high isolation toward other stimuli.[20]

In particular endothermic tetrazoles have proven themselves in the past as very promising ligands in energetic complexes.[21–23] Their energetic character can easily be modified by various methods such as alteration of the functional groups (alkyl chains, nitro groups, nitramine units, hydrazinyl derivatives, attached tetrazoles *etc.*) or their substitution pattern (*N*1-substituted *vs.* *N*2-substituted *vs.* *C*5-substituted).[15,24] Many coordination compounds are well-known with different tetrazole ligands but surprisingly no complexes have been prepared up to date with two of the most energetic and powerful neutral ligands, 1-amino-5*H*-tetrazole (**1**, 1-AT) and 2-amino-5*H*-tetrazole (**2**, 2-AT, Fig. 2).[25–31] These two isomers, which proved to be non-toxic toward aquatic organisms (see 2.5) and have an incorporated hydrazine function ($N_{Tetrazole}$–NH_2) exhibit an outstandingly high nitrogen content of 82.33% and were described almost 50 years ago for the first time in 1966 and 1969

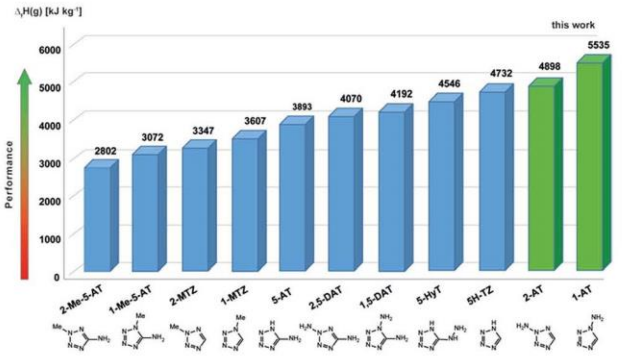


Fig. 2 Comparison of the per unit mass calculated enthalpies of formation for various monotetrazoles shows the highest values for 1- and 2-amino-5*H*-tetrazole. Gas phase enthalpies of formation were calculated using the atomization method ($\Delta_f H^0_{(g,M)} = H_{(M)} - \Sigma H^0_{(A)} + \Sigma \Delta_f H^0_{(A)}$) using Gaussian09 computed CBS-4M electronic enthalpies.

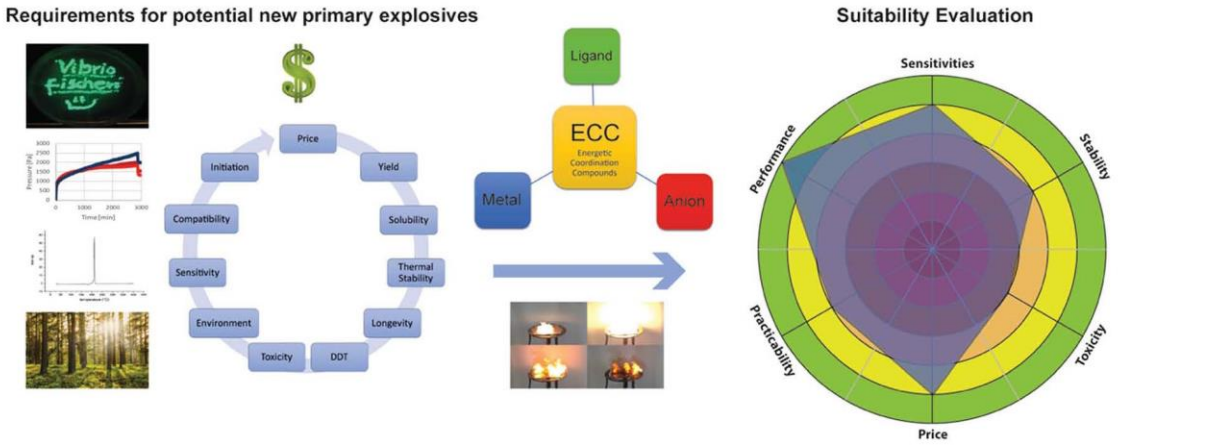


Fig. 1 List of requirements to be met for new potential primary explosives, which are compiled in our suitability evaluation diagram.

 This journal is © The Royal Society of Chemistry 2018

Published on 06 August 2018. Downloaded by Ludwig Maximilians Universitaet Muenchen on 2/16/2022 7:59:25 AM.

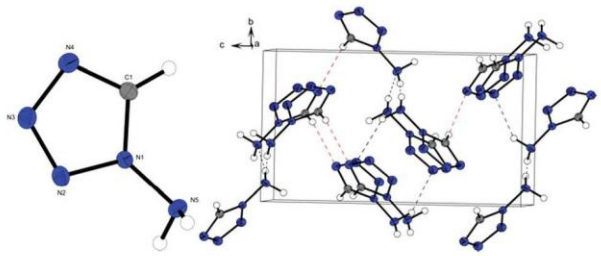


Fig. 4 Molecular unit (left) and unit cell (right) of 1-AT (**1**). Thermal ellipsoids of non-hydrogen atoms in all structures are set to the 50% probability level. Selected bond lengths (Å): N1–C1 1.3256(18), N1–N5 1.4000(17), N1–N2 1.3441(15), N2–N3 1.2986(19), N3–N4 1.370(2), N4–C1 1.3128(19); selected bond angles (°): N2–N1–N5 123.21(11), N2–N1–C1 109.17(11), N5–N1–C1 127.54(12), N1–N2–N3 105.71(11), N2–N3–N4 110.82(12), N3–N4–C1 105.18(12).

units per unit cell and a calculated density of 1.963 g cm^{-3} at 173 K. The distances between the ring atoms lie within the range of partial double bonds and the torsion angle C1–N1–N2–N3 is very close to 0° (C1–N1–N2–N3 −0.5(2)°). Moreover, every bond length besides the N1–N2 distance is slightly shorter in the non-coordinating tetrazole ring of **3**. In addition to these results, the aromaticity of the heterocycle is proved by the bond angles amongst the ring atoms. The bond distance between the amine's and the adjacent ring nitrogen is close to those of the tetrazole's π-system. In regard to the *N*2's sp^2-hybridization as part of an aromatic heterocycle, the bond angles between *N*5, *N*1 and the neighboring ring atoms are close to be the ideal 120°. The interesting conclusion, that the whole aminotetrazolium cation appears as one plane molecule when including the amino group at *N*5, can be made based on the torsion angle N5–N2–N3–N4 which almost amounts to 180° (N5–N2–N3–N4 = 175.03(15)°). Due to the previously mentioned sp^2-hybridization of the atoms of this aromatic heterocycle, the hydrogen atoms at N4 and C1 are part of the molecule's plane. On the other hand, the hydrogen atoms of the sp^3-hybridized N5 are both orientated toward in the same direction. The perchlorate counter-ion of the tetrazolium cation is only marginally distorted exhibiting typical Cl–O bond distances and bond angles based on their tetrahedral molecular structure (Fig. 5). In summary, the resulting structural parameters almost exclusively match data quoted in literature of similar tetrazolium perchlorate salts.[39]

The bond lengths and angles of the coordinating ligands in the complexes analyzed are in the same range as in the non-coordinating ligand **1** and are therefore not part of the discussion in any of the following coordination compounds.

The metal(II) perchlorate compounds of 1-AT (**4–7**) all crystallize isotypically in the trigonal space group $P\bar{3}$ with densities between 1.736 (**4**) and 1.918 g cm^{-3} (**6**) (Mn: 1.736 g cm^{-3} (143 K); Fe: 1.766 g cm^{-3} (173 K); Cu: 1.918 g cm^{-3} (173 K); Zn: 1.783 g cm^{-3} (173 K)). All complexes consist of two distinguishable metal centers with one exhibiting an ideal coordination polyhedron and the other being slightly distorted. Six nitrogen-rich ligands are bound to each metal(II) center and the perchlorate counter-anions are non-coordinating (Fig. 6 and S6–8†).

In each case, the three dimensional stability is guaranteed by several hydrogen bonds represented in Table S6,† exemplarily illustrated for complex [Fe(1-AT)$_6$](ClO$_4$)$_2$ (**5**). The unit cell of **5** is depicted in Fig. 7 illustrating the two-dimensional packing in view along the crystallographic *c*-axis. The comparison of the investigated perchlorate complexes with 1-amino-5*H*-tetrazole as the coordinating ligand shows no major differences besides the Jahn–Teller distorted Cu2 center in **6** (Fig. S7†) and the previously mentioned densities. Notwithstanding, one might recognize the slight differences regarding the bond coordination distances between the ligands and the respective metal(II) center. While all complexes show disordered perchlorate anions, the manganese(II) compound **4** additionally possesses strong disorders in the heterocyclic ligands (Fig. S6†).

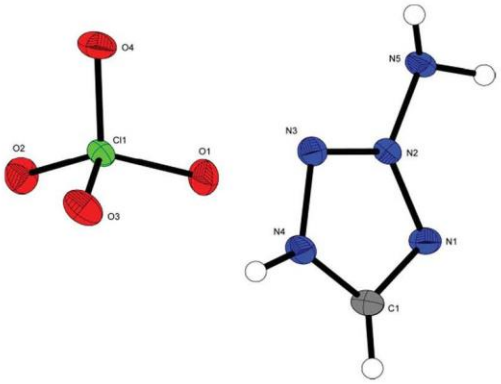


Fig. 5 Molecular unit of 2-AT$_H$ ClO$_4$ (**3**). Selected bond lengths (Å): Cl1–O1 1.4369(14), N1–C1 1.318(2), N1–N2 1.333(2), N2–N3 1.289(2), N2–N5 1.369(2), N3–N4 1.331(2), N4–C1 1.322(2); selected bond angles (°): O1–Cl1–O3 109.82(8), O2–Cl1–O4 108.65(8), N2–N1–C1 101.68(14), N1–N2–N3 116.77(15), N1–N2–N5 121.17(15), N2–N3–N4 101.33(15), N3–N4–C1 110.89(15), N1–C1–N4 109.33(15).

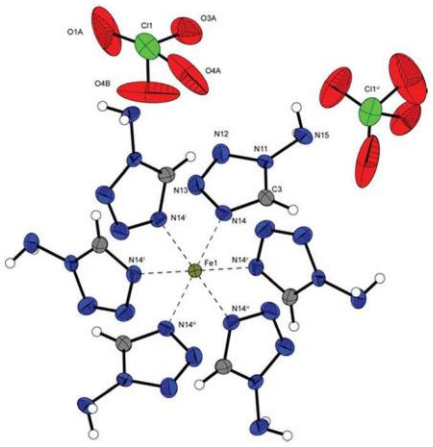


Fig. 6 Molecular unit of complex [Fe(1-AT)$_6$](ClO$_4$)$_2$ (**5**). Selected bond length (Å): Fe1–N14 2.185(3); selected bond angles (°): N14–Fe1–N14^{vii} 88.88(11), N14–Fe1–N14^{iii} 91.12(12). Symmetry codes: (i) 1 − *y*, *x* − *y*, *z*; (ii) 1 − *x* + *y*, 1 − *x*, *z*; (iii) −*x*, −*y*, −*z*; (iv) *x* − *y*, *x*, −*z*; (v) −*x* + *y*, −*x*, *z*; (vi) −*y*, *x* − *y*, *z*; (vii) *y*, −*x* + *y*, −*z*.

This journal is © The Royal Society of Chemistry 2018

Published on 06 August 2018. Downloaded by Ludwig Maximilians Universitaet Muenchen on 2/16/2022 7:59:25 AM.

respectively.[32,33] Several recently published energetic coordination compounds based on 1-methyl-5*H*-tetrazole as the ligand show a deficit in energetic performance.[15] Substitution of the methyl group by an amino group tremendously increases the energy content of the molecule due to the additional N–N single bond (Fig. 2). The highly endothermic character and the resulting driving force of nitrogen gas formation, makes these tetrazoles exceptional great ligands, which show potential in combination with oxygen-rich anions as primary explosives.

The obtained compounds easily outperform commonly used-primaries like lead azide or lead styphnate through the maximization of the energy content in the resulting transition metal complexes.

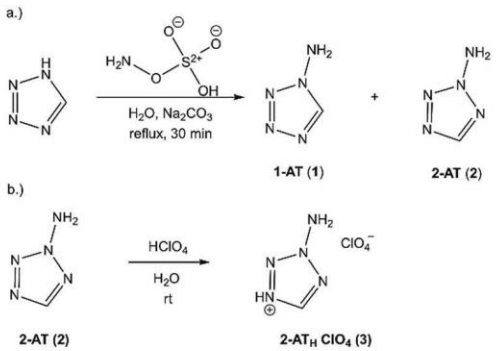
In this comprehensive study, considerable efforts have been made to implement the highly endothermic ligands 1-amino-5*H*-tetrazole (**1**) and 2-amino-5*H*-tetrazole (**2**) into a large number of promising coordination compounds, which show great potential for possible future applications (optical and classical initiation systems).

Results and discussion

Synthesis

CAUTION! All investigated compounds are potentially explosive energetic materials (the majority of the compounds lie in the range of primary explosives), which show partly increased sensitivities toward various stimuli (*e.g.* elevated temperatures, impact, friction or electrostatic discharge). Therefore, proper security precautions (safety glasses, face shield, earthed equipment and shoes, leather jacket, Kevlar gloves, Kevlar sleeves and ear plugs) have to be worn while synthesizing and handling the described compounds. Especially the very sensitive compounds **4–7** and **18–23** must be handled with great care! An excess of ligand **2** has to be applied during the synthesis of complex **18** in order to prevent the formation of unisolable side species (most likely a diperchlorato or hexacoordinated tetrazole complex), which tends to spontaneous violent decomposition during crystallization.

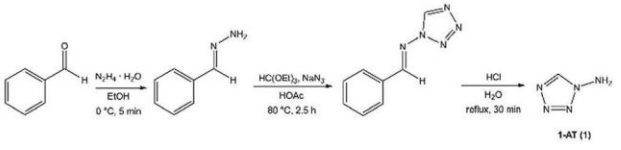
In principle, the preparation of 1-amino-5*H*-tetrazole (**1**) can be achieved *via* two different synthetic protocols. One way is the amination of 1,5*H*-tetrazole, reported in 1969 for the first time, which leads to an isomeric mixture of compound **1** and 2-amino-5*H*-tetrazole (**2**) as a side product.[33] As of today, unfortunately no direct synthetic path has been developed for this isomer, which in comparison to compound **1**, is surprisingly more sensitive. The amination reaction of the *in situ* generated sodium tetrazolate proceeds *via* a nucleophilic substitution mechanism and has been performed with the well-known amination reagent hydroxylamine-*O*-sulfonic acid (HOSA) in water under reflux and a constantly readjusted pH value of 7–8 according to a modified literature procedure (Scheme 1).[33,34] Instead of the very dangerous separation by distillation of the isomeric mixture obtained, a much safer and more efficient purification by flash column chromatography (EtOAc/DCM 5 : 1) on silica gel was developed. The two isomers could be isolated in yields of 27% for compound **1** and 19% for the nitrogen-rich ligand **2**. The relatively low yields can most likely



Scheme 1 (a) Synthesis of 1-amino-5*H*-tetrazole (**1**) and 2-amino-5*H*-tetrazole (**2**) by amination of 1,5*H*-tetrazole by hydroxylamine-*O*-sulfonic acid (HOSA). (b) Synthesis of 2-amino-5*H*-tetrazolium perchlorate (**3**).

be attributed to the electron-poor character of the aromatic heterocycle and its related low nucleophilicity. Treatment of the two amino-5*H*-tetrazoles **1** and **2** with aqueous diluted acids (HNO_3 and $HClO_4$) resulted in ionic liquids and were therefore investigated in more detail. The only exception was the protonated 2-amino-5*H*-tetrazolium perchlorate salt (**3**), which crystallized within 5 days and has been comprehensively characterized (Scheme 1).

1-Amino-5*H*-tetrazole (**1**) can be prepared (overall yield: 32%), in contrast to compound **2**, directly and isomerically pure *via* a simple and upscalable three-step synthesis (Scheme 2). In the first step, one amino group of the hydrazine molecule is protected as benzhydrazone by treatment with benzaldehyde in a condensation reaction. Particular attention should be given to the low reaction temperature, the sequence of starting materials added and the reaction time to prevent formation of a further reaction to the bisbenzhydrazone. The next step entails the ring closure of the remaining free amino group of benzhydrazone in a [3 + 1 + 1] cyclization with triethyl orthoformate and sodium azide carried out at 80 °C for 2.5 h under acidic conditions. The resulting tetrazole immediately precipitates in the form of a yellow-orange solid right after pouring into water. The benzyl protection group is cleaved almost quantitatively in the last reaction step under acidic conditions with hydrochloric acid and the resulting benzaldehyde was removed using the rotary evaporator at elevated temperatures under vacuum. This reaction step has been greatly improved and simplified in comparison to literature-reported procedures where water steam



Scheme 2 Selective and isomerically pure preparation of 1-amino-5*H*-tetrazole (**1**) in a three-step reaction starting from benzaldehyde and hydrazine monohydrate.

Published on 06 August 2018. Downloaded by Ludwig Maximilians Universitaet Muenchen on 2/16/2022 7:59:25 AM.

distillation and distillation under vacuum are applied to remove the emerging benzaldehyde.[32,35]

Both isomers can easily be differed by infrared spectroscopy (Fig. S1†) or proton and carbon NMR spectroscopy. Furthermore, two dimensional ^{1}H, ^{15}N NMR HMBC or proton coupled ^{15}N NMR spectroscopy can be performed (Fig. 3).

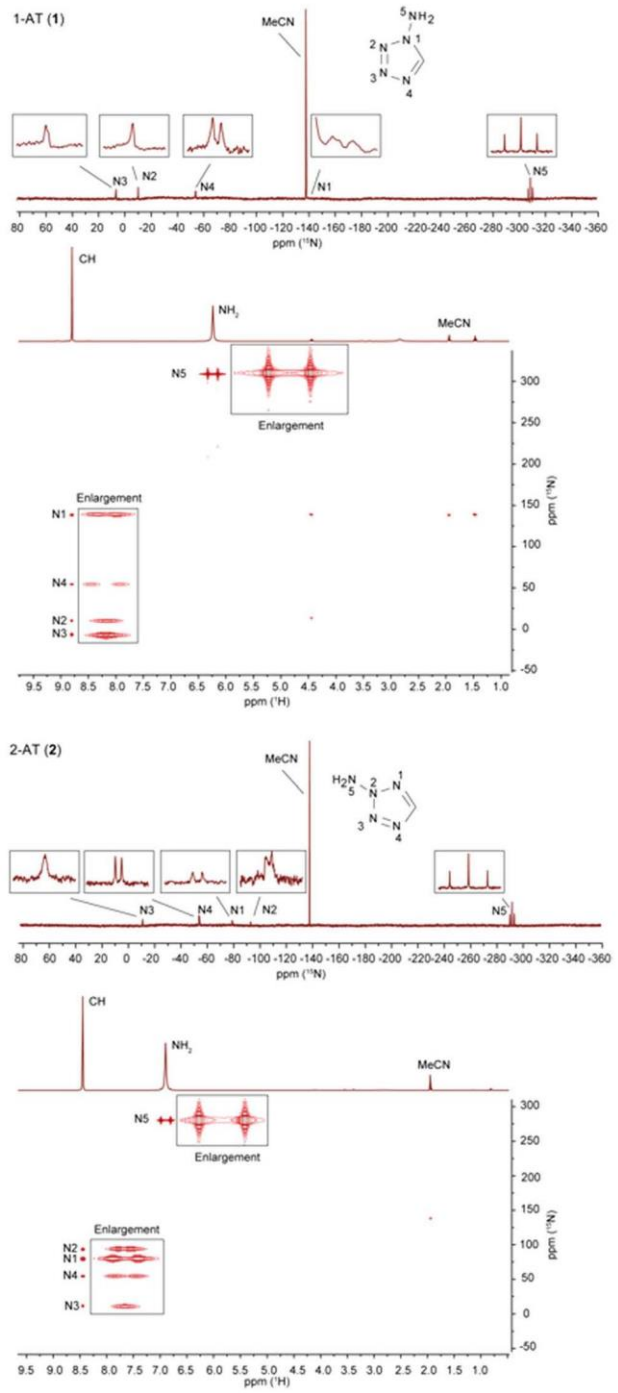


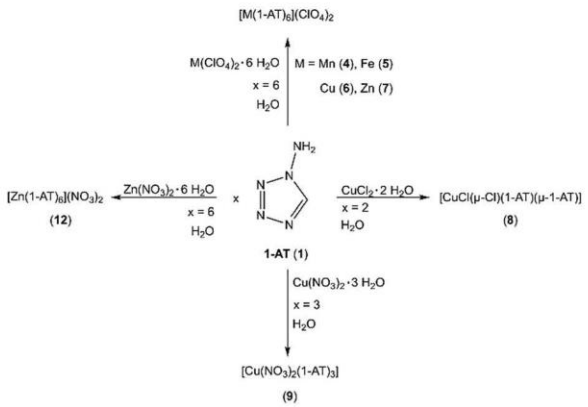
Fig. 3 Proton coupled ^{15}N NMR spectra and two dimensional ^{1}H, ^{15}N-HMBC NMR spectra of **1** and **2**.

A large number of complexes based on various monotetrazoles like 1,5-diaminotetrazole or 1-methyl-5*H*-tetrazole have been described in literature but have insufficient power for any possible application as a primary explosive.[16,30] Owing to this lack of power and to maximize the energetic performance, new transition metal complexes were synthesized with even more powerful endothermic ligands.

Our synthetic strategy comprises the preparation of cationic or neutral complex units to increase the energetic character of the coordination compounds and to ensure the integration of oxidizing anions, facilitated through the application of neutral basic nitrogen-rich ligands. In addition, the influence on the coordination sphere and the physico-chemical properties were investigated by alteration of the tetrazole isomers while maintaining the metal(II) and anion building blocks. The synthesis of the divalent transition metal(II) complexes **4–9** and **12** was accomplished through combination of aqueous solutions of the relevant metal(II) salts and the ligand **1** in the corresponding stoichiometries at room temperature (Scheme 3).

Water has been selected as the green solvent for all reaction mixtures to ensure slow crystallization of the desired complexes and because of the good solubilities of the ligands and the transition metal(II) salt starting materials in this solvent system. All coordination compounds crystallized with decent yields (32–79%) without inclusion of aqua ligands or crystal water molecules resulting in a higher performance of the complexes. The exclusive use of ethanol as solvent instead of water leads to precipitation of the complexes in most cases in the form of amorphous powders.

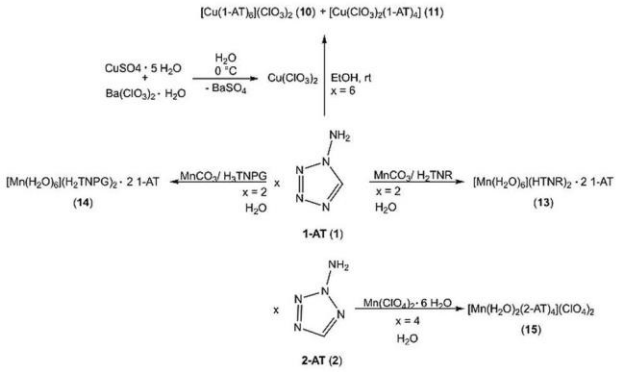
Analogous to our recently published work, an ethanolic solution of copper(II) chlorate was reacted with 1-amino-5*H*-tetrazole (**1**) in order to synthesize the corresponding copper(II) chlorate coordination compound (Scheme 4).[36] After a few days and evaporation of the solvent, two different crystalline species appeared from the reaction mixture, which could be picked and handled while still wet. X-ray diffraction analysis revealed a complex species with six coordinating 1-AT ligands (**10**, Fig. S9†) and a species with four 1-AT ligands and two coordinating chlorato anions (**11**, Fig. S10†). All attempts to dry the



Scheme 3 Synthesis of the transition metal(II) complexes **4–9** and **12** based on 1-amino-5*H*-tetrazole (**1**) as ligand.

This journal is © The Royal Society of Chemistry 2018

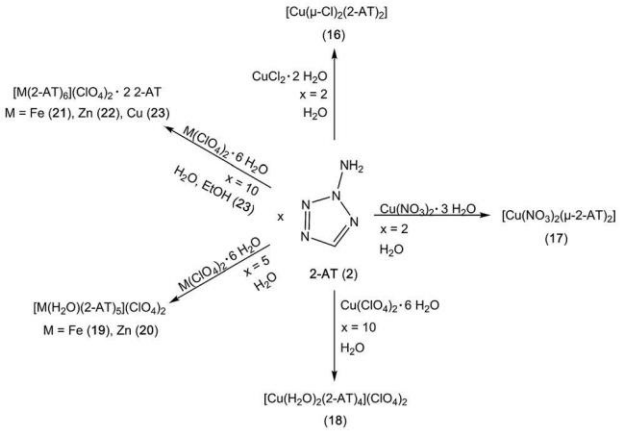
Published on 06 August 2018. Downloaded by Ludwig Maximilians Universitaet Muenchen on 2/16/2022 7:59:25 AM.



Scheme 4 Formation of complexes **10**, **11** and **13–15** with varying metal(II) centers, anions and ligands.

compounds for further characterization failed due to the extreme sensitivity and resulted in violent detonations. Unfortunately, only a few single crystals suitable for X-ray diffraction of the manganese(II) complexes **13–15** (Scheme 4) could be isolated in between amorphous bulk material with indefinite composition and unreacted starting materials.

Therefore, only their X-ray crystal structures, which are shown in the ESI† can be presented. All attempted syntheses to achieve a pure elemental analysis of the complexes were unsuccessful. The 2-amino-5*H*-tetrazole (**2**) based coordination compounds **16–23** (Scheme 5) were synthesized in analogy to their 1-substituted isomers (easily distinguishable by IR, Fig. S3†) through a straightforward reaction of the corresponding metal(II) salts in the necessary stoichiometries in water or ethanol at room temperature. An excess of ligand **2** had to be applied during the synthesis of complex **18** in order to prevent the formation of an unisolable side species (most likely a diperchlorato or hexacoordinated tetrazole complex), which tended to spontaneous violent decomposition during crystallization. It should also be noted, that the use of six equivalents of **2** instead of five during the synthesis of the complexes **19–20**



Scheme 5 Synthesis of selected energetic coordination compounds **16–23** based on 2-amino-5*H*-tetrazole (**2**) as ligand in combination with different metal(II) salts.

leads to the same monoaqua species and has no influence on the composition of the resulting coordination compounds. The preparation of the metal(II) perchlorate complexes **18–23** yields for each metal(II) salt two different species depending largely on the applied stoichiometry and solvent system. In addition to the aqua ligand containing coordination compounds **18–20**, complex units with two additional cocrystallized aminotetrazoles **21–23** can be isolated when an excess of ligand is used. Both species can easily be detected and distinguished from each other by IR spectroscopy (Fig. S4/5†). In the case of the copper(II) perchlorate complexes **18**/**23**, the solvent system plays an important role in the formation of the relevant complexes. Water leads to the diaqua species **18**, whereas ethanol as solvent results in the formation of the cocrystallized compound **23**.

All coordination compounds were directly obtained from the mother liquor and crystallized in satisfactory yields with exception of the cocrystallized species. The crystalline materials, all suitable for X-ray diffraction, were filtered off, washed with a small amount of ice-cold ethanol when necessary in order to remove unreacted starting materials and were then dried in air overnight.

Crystal structures

The nitrogen-rich ligand **1**, the perchlorate salt **3** and all complexes were characterized by low temperature single crystal X-ray diffraction. In contrast to ligand **2**, 1-amino-5*H*-tetrazole (**1**) could be solidified through controlled freezing with liquid nitrogen. Its low melting point of 5 °C (ref. 35) allowed the picking of a single crystal at 0 °C for X-ray determination. The measurements of compound **4** and **11** showed considerable structural disorders within the tetrazole rings as well as in the perchlorate (**4**) and chlorate (**11**) anions. Nevertheless, they allow the identification of the complexes' composition. Elemental analysis and infrared spectra comparison (Fig. S2†) verified the analogous structure of **4** as in the other isotypic hexakis(1-amino-5*H*-tetrazole) metal(II) perchlorate complexes **5–7**. The high degree of disorder observed for the copper(II) chlorate complex **11** unfortunately allowed only an isotropic illustration (Fig. S10†) of the molecular structure. All complexes, except compound **9**, show an octahedral coordination sphere of the metal(II) center. Complexation of the ligands **1** and **2** always takes place through the N4 nitrogen atom of the tetrazole ring, except for compounds **8** and **19** which show bidentate aminotetrazole ligands. The crystal datasets were uploaded to the CSD database.†[37]

Compound **1** crystallizes in the form of colorless rods in the orthorhombic space group $P2_12_12_1$ with four formula units per unit cell and a calculated density of 1.515 g cm^{-3} at 143 K. All non-hydrogen atoms lie within a plane with torsion angles close to 0° (C1–N1–N2–N3 0.31(15)°, N5–N2–C1–N1 1.59(1)° and N2–N1–C1–N4 0.12(16)°) and show bond lengths as well as angles comparable to those of other 1-substituted tetrazole compounds (Fig. 4).[38]

The perchlorate salt **3**, crystallizes in the form of colorless blocks in the monoclinic space group $P2_1/n$ with four formula

Published on 06 August 2018. Downloaded by Ludwig Maximilians Universitaet Muenchen on 2/16/2022 7:59:25 AM.

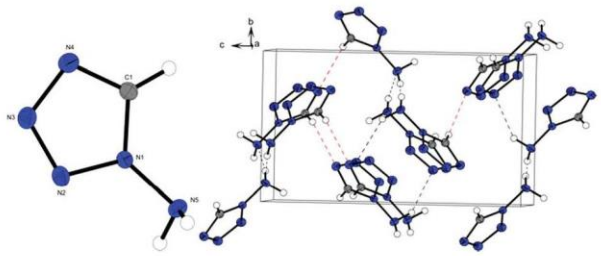


Fig. 4 Molecular unit (left) and unit cell (right) of 1-AT (**1**). Thermal ellipsoids of non-hydrogen atoms in all structures are set to the 50% probability level. Selected bond lengths (Å): N1–C1 1.3256(18), N1–N5 1.4000(17), N1–N2 1.3441(15), N2–N3 1.2986(19), N3–N4 1.370(2), N4–C1 1.3128(19); selected bond angles (°): N2–N1–N5 123.21(11), N2–N1–C1 109.17(11), N5–N1–C1 127.54(12), N1–N2–N3 105.71(11), N2–N3–N4 110.82(12), N3–N4–C1 105.18(12).

units per unit cell and a calculated density of 1.963 g cm^{-3} at 173 K. The distances between the ring atoms lie within the range of partial double bonds and the torsion angle C1–N1–N2–N3 is very close to 0° (C1–N1–N2–N3 −0.5(2)°). Moreover, every bond length besides the N1–N2 distance is slightly shorter in the non-coordinating tetrazole ring of **3**. In addition to these results, the aromaticity of the heterocycle is proved by the bond angles amongst the ring atoms. The bond distance between the amine's and the adjacent ring nitrogen is close to those of the tetrazole's π-system. In regard to the *N*2's sp^2-hybridization as part of an aromatic heterocycle, the bond angles between *N*5, *N*1 and the neighboring ring atoms are close to be the ideal 120°. The interesting conclusion, that the whole aminotetrazolium cation appears as one plane molecule when including the amino group at *N*5, can be made based on the torsion angle N5–N2–N3–N4 which almost amounts to 180° (N5–N2–N3–N4 = 175.03(15)°). Due to the previously mentioned sp^2-hybridization of the atoms of this aromatic heterocycle, the hydrogen atoms at N4 and C1 are part of the molecule's plane. On the other hand, the hydrogen atoms of the sp^3-hybridized N5 are both orientated toward in the same direction. The perchlorate counter-ion of the tetrazolium cation is only marginally distorted exhibiting typical Cl–O bond distances and bond angles based on their tetrahedral molecular structure (Fig. 5). In summary, the resulting structural parameters almost exclusively match data quoted in literature of similar tetrazolium perchlorate salts.[39]

The bond lengths and angles of the coordinating ligands in the complexes analyzed are in the same range as in the non-coordinating ligand **1** and are therefore not part of the discussion in any of the following coordination compounds.

The metal(II) perchlorate compounds of 1-AT (**4–7**) all crystallize isotypically in the trigonal space group $P\bar{3}$ with densities between 1.736 (**4**) and 1.918 g cm^{-3} (**6**) (Mn: 1.736 g cm^{-3} (143 K); Fe: 1.766 g cm^{-3} (173 K); Cu: 1.918 g cm^{-3} (173 K); Zn: 1.783 g cm^{-3} (173 K)). All complexes consist of two distinguishable metal centers with one exhibiting an ideal coordination polyhedron and the other being slightly distorted. Six nitrogen-rich ligands are bound to each metal(II) center and the perchlorate counter-anions are non-coordinating (Fig. 6 and S6–8†).

In each case, the three dimensional stability is guaranteed by several hydrogen bonds represented in Table S6,† exemplarily illustrated for complex [Fe(1-AT)$_6$](ClO$_4$)$_2$ (**5**). The unit cell of **5** is depicted in Fig. 7 illustrating the two-dimensional packing in view along the crystallographic *c*-axis. The comparison of the investigated perchlorate complexes with 1-amino-5*H*-tetrazole as the coordinating ligand shows no major differences besides the Jahn–Teller distorted Cu2 center in **6** (Fig. S7†) and the previously mentioned densities. Notwithstanding, one might recognize the slight differences regarding the bond coordination distances between the ligands and the respective metal(II) center. While all complexes show disordered perchlorate anions, the manganese(II) compound **4** additionally possesses strong disorders in the heterocyclic ligands (Fig. S6†).

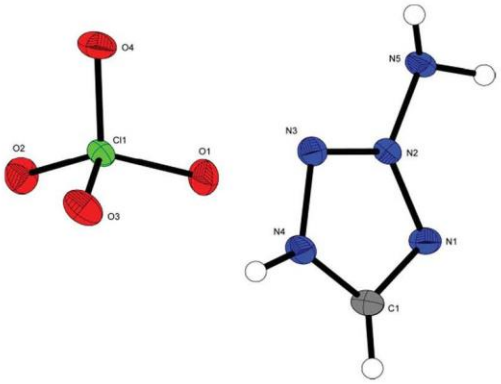


Fig. 5 Molecular unit of 2-AT$_H$ ClO$_4$ (**3**). Selected bond lengths (Å): Cl1–O1 1.4369(14), N1–C1 1.318(2), N1–N2 1.333(2), N2–N3 1.289(2), N2–N5 1.369(2), N3–N4 1.331(2), N4–C1 1.322(2); selected bond angles (°): O1–Cl1–O3 109.82(8), O2–Cl1–O4 108.65(8), N2–N1–C1 101.68(14), N1–N2–N3 116.77(15), N1–N2–N5 121.17(15), N2–N3–N4 101.33(15), N3–N4–C1 110.89(15), N1–C1–N4 109.33(15).

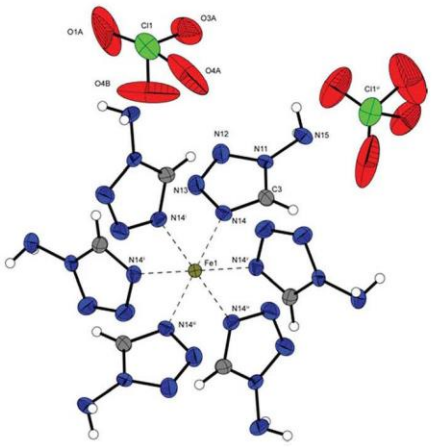


Fig. 6 Molecular unit of complex [Fe(1-AT)$_6$](ClO$_4$)$_2$ (**5**). Selected bond length (Å): Fe1–N14 2.185(3); selected bond angles (°): N14–Fe1–N14^{vii} 88.88(11), N14–Fe1–N14^{iii} 91.12(12). Symmetry codes: (i) $1-y, x-y, z$; (ii) $1-x+y, 1-x, z$; (iii) $-x, -y, -z$; (iv) $x-y, x, -z$; (v) $-x+y, -x, z$; (vi) $-y, x-y, z$; (vii) $y, -x+y, -z$.

This journal is © The Royal Society of Chemistry 2018

Published on 06 August 2018. Downloaded by Ludwig Maximilians Universitaet Muenchen on 2/16/2022 7:59:25 AM.

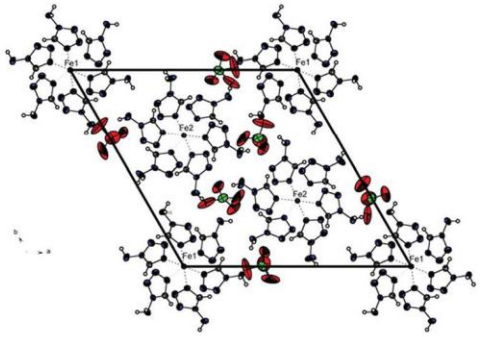


Fig. 7 Unit cell of $[Fe(1\text{-}AT)_6](ClO_4)_2$ (**5**) in the direction of view along the *c*-axis.

The copper(II) chloride coordination compounds of 1-AT and 2-AT both crystallize in the form of green blocks in similar monoclinic space groups $P2_1/n$ (**8**) and $P2_1/c$ (**16**) with four and two formula units per unit cell respectively. The calculated densities at 173 K vary only slightly (2.146 g cm^{-3} (**8**) and 2.177 g cm^{-3} (**16**) respectively). The two complexes show completely different coordination spheres, which are highly dependent on the inserted ligand. 2-Amino-5*H*-tetrazole acts as a monodentate ligand in complex **16** with bridging chlorido ligands, which are responsible for the assembly of 1D polymeric chains. The 1-AT ligand instead shows a bidentate behavior in compound **8** leading to the formation of 2D polymeric layers. The copper(II) center of **8** is octahedrally coordinated and bridged to polymeric planes over two chlorido and two 1-amino-5*H*-tetrazole ligands (Fig. 8). The equatorial positions are occupied by one bridging and one terminal equivalent of each, the chlorido and the 1-amino-5*H*-tetrazole ligand, generating a plane. The coordination octahedron exhibits a Jahn–Teller distortion along the $Cl2^{ii}$–Cu1–N5 axis with N5 being part of the second bridging equivalent of **8**. Moreover, the structure of the complex is close to an ideal octahedron with the maximum deviation of the bond angles between two *cis*-ligands from 90° being 5.76° and of two *trans*-ligands from 180° being 4.41°. In contrast, the molecular unit of **16** consists of four bridging chlorido and two terminal 2-amino-5*H*-tetrazole ligands forming an octahedral coordination sphere (Fig. 8). Once again, the d^9-copper center shows a significant Jahn–Teller distortion along the $Cl1\text{–}Cu\text{–}Cl1^{iv}$ axis. The equatorial coordination sites are occupied by two bridging chlorido ligands and the remaining two equivalents of 2-AT building up an almost ideal plane. Considering the findings that the bond angles between ligands in *cis* positions are close to the ideal 90° and angles amongst molecules coordinating *trans* to each other are exclusively 180°, the coordination polyhedron shows multiple signs of being an ideal octahedron, despite the previously discovered distortions in regard to the bond lengths.

Analogous to the chlorido complexes, the copper(II) nitrate coordination compounds **9** and **17** show a completely different metal(II) coordination environment. In contrast to **8** and **16**, 1-AT now behaves monodentately, a fact leading to the formation of closed coordination spheres, whereas the bidentate behavior of 2-AT causes the building-up of 2D polymeric layers. The very interesting copper(II) nitrate complex **9** crystallizes in the form of blue rods in the monoclinic space group *Cc* with four formula units per unit cell and a calculated density of 1.968 g cm^{-3} at 173 K. Despite the usually observed octahedral copper(II) coordination sphere with significant Jahn–Teller distortion, compound **9** consists of a sevenfold coordinated metal(II) center leading to the coordination polyhedron of an unusual pentagonal-like bipyramid (Fig. 9). The equatorial positions are occupied by two chelating nitrate anions and one equivalent of **1** forming a distinctly deformed plane. The ideal properties of a pentagonal bipyramid prescribe the bond angles between the equatorial ligands to be 72° – a requirement, which is definitely not fulfilled for the investigated complex due to the nitrate anion's fixed structure. In addition, the axis through the two-

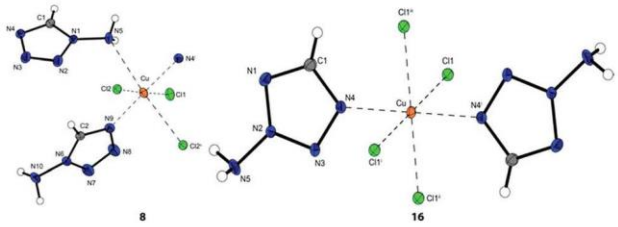


Fig. 8 Copper(II) coordination environments of $[CuCl(\mu\text{-}Cl)(1\text{-}AT)(\mu\text{-}1\text{-}AT)]$ (**8**) (left) and $[Cu(\mu\text{-}Cl)_2(2\text{-}AT)_2]$ (**16**) (right). Selected bond lengths (Å) of **8**: Cu1–Cl1 2.2854(6), Cu1–Cl2 2.3122(6), Cu1–N9 2.0113(19), Cu1–N5 2.725(2); selected bond angles (°) of **8**: Cl1–Cu1–Cl2 177.96(2), Cl2–Cu1–N5 93.90(5), N5–Cu1–Cl1 84.55(5), N9–Cu1–Cl1 90.78(5), Cl2–Cu1–N9 90.64(5). Symmetry codes of **8**: (i) 0.5 + *x*, 1.5 − *y*, 0.5 + *z*; (ii) 1.5 + *x*, 1.5 − *y*, 1.5 + *z*. Selected bond lengths (Å) of **16**: Cu–Cl1 2.8124(6), Cu–N4 2.0422(19); selected bond angles (°) of **16**: Cl1–Cu–N4 90.25(5), $Cl1\text{–}Cu\text{–}Cl1^{ii}$ 91.30(2), $Cl1^{iv}\text{–}Cu\text{–}N4$ 89.76(5), $Cl1^{ii}\text{–}Cu\text{–}N4$ 88.84(6). Symmetry codes of **16**: (i) 2 − *x*, 2 − *y*, −*z*; (ii) *x*, 1 + *y*, *z*; (iii) 2 − *x*, 1 − *y*, −*z*; (iv) *x*, −1 + *y*, *z*.

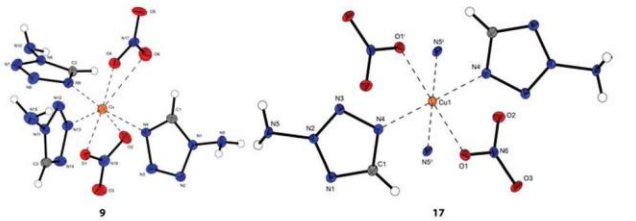


Fig. 9 Molecular unit of $[Cu(NO_3)_2(1\text{-}AT)_3]$ (**9**) (left) and the copper(II) coordination environment of $[Cu(NO_3)_2(\mu\text{-}2\text{-}AT)_2]$ (**17**) (right). Selected bond lengths (Å) of **9**: Cu–O1 1.987(3), Cu–O2 2.637(3), Cu–O4 1.990(3), Cu–O6 2.742(4), Cu–N13 2.287(4), Cu–N4 2.003(4), Cu–N9 1.999(4); selected bond angles (°) of (**9**): N4–Cu–N9 162.97(13), O1–Cu–O2 54.03(11), O1–Cu–N13 84.56(13), O2–Cu–O6 80.11(10), O4–Cu–O6 51.81(11), O4–Cu–N13 89.95(13), O1–Cu–N4 92.57(15), O1–Cu–N9 88.03(14), O2–Cu–N4 82.95(12), O2–Cu–N9 83.65(12), O4–Cu–N4 90.25(14), O4–Cu–N9 90.85(14), O6–Cu–N4 87.65(14), O6–Cu–N9 79.72(13). Selected bond lengths (Å) of (**17**): $Cu1\text{–}N5^{ii}$ 2.4208(16), Cu1–O1 2.0339(12), Cu1–N4 1.9831(16); selected bond angles (°) of (**17**): $O1\text{–}Cu1\text{–}N4$ 87.42(6), $O1\text{–}Cu1\text{–}N5^{ii}$ 81.45(5), $O1\text{–}Cu1\text{–}N5^{iv}$ 98.55(5). Symmetry codes of (**17**): (i) −*x*, −*y*, −*z*; (ii) 0.5 + *x*, 0.5 − *y*, 0.5 + *z*; (iii) 0.5 − *x*, 0.5 + *y*, 0.5 − *z*; (iv) 0.5 − *x*, −0.5 + *y*, 0.5 − *z*.

Published on 06 August 2018. Downloaded by Ludwig Maximilians Universitaet Muenchen on 2/16/2022 7:59:25 AM.

remaining amino-5*H*-tetrazole ligands in axial positions is crooked, differing considerably from the ideal 180°. Another deviation from the perfect pentagonal bipyramid can be observed regarding the bond angles between axial and equatorial ligands partially varying by up to 10° from the expected 90°. The nitrate complex **17** crystallizes in the form of blue plates in the monoclinic space group $P2_1/n$ with two formula units per unit cell and a calculated density of 2.169 g cm^{-3} at 173 K. This coordination compound consists of an octahedrally coordinated copper(II) center including a straight, Jahn–Teller distorted N5^{ii}–Cu1–N5^{iv} axis between the axial 2-AT ligands (Fig. 9). The equatorial positions of **17** are occupied by the remaining two equivalents of **2** and the coordinating nitrate anions building up an almost ideal plane. Every bond angle of *cis* coordinating axial or equatorial ligands in **17** slightly differs from the ideal 90°.

The spatial order of the investigated copper(II) nitrate complex (**17**) reveals some very interesting observations: each of the coordinating 2-amino-5*H*-tetrazole ligands possesses bridging characteristics and thus causes cross-linking of adjacent copper(II) centers.

The extremely sensitive copper(II) perchlorate complex **18** is the only compound which crystallizes in the tetragonal space group $P4_2/n$ with two formula units per unit cell and a calculated density of 1.947 g cm^{-3} at 173 K. Once again, the Jahn–Teller distortion along the O1–Cu–O1^{iii} axis induces significant deviations between the coordination distances of axial and equatorial ligands (Fig. 10). The four equatorial 2-AT ligands form a crooked plane, a fact that causes the bond angles between axial and equatorial ligands to slightly differ from the ideal 90°. On the other hand, the angles between *cis* amino-5*H*-tetrazole ligands in the plane almost perfectly conform to 90°. The angles amongst two equatorial ligands coordinating *trans* to each other are also influenced by the obliqueness of the N1–N1^{iii}–N1^{ii}–N1^{i} plane (N1–Cu–N1^{ii} 177.77(12)°). The analogous manganese(II) complex **15** crystallizes in the form of colorless blocks in the triclinic space group $P\bar{1}$ with two formula units per unit cell and a calculated density of 1.897 g cm^{-3} at 173 K. Compared to compound **18** the Mn–N bonds are slightly longer than the Cu–N ones with simultaneous shorter Mn–O bonds (Fig. S14†).

The coordination polyhedrons built up by five equivalents of **2** are completed by one aqua ligand forming an octahedral coordination sphere around the respective metal center (Fig. 11 and S17†). In both complexes, the M^{2+}–N distances are significantly longer than the particular M^{2+}–O coordination distances between the metal(II) center and the aqua ligands. Regarding the bond angles of the metal(II) centers, it becomes clear that there is no major distortion to be observed. Nevertheless, none of the bond angles of either of these perchlorate compounds conform the ideal values of 90° for *cis* coordinating ligands and 180° for molecules coordinating *trans* to each other. The isotypic complexes **19** and **20**, two coordination isomers containing an iron(II) (**19**) or alternatively a zinc(II) (**20**) metal center both crystallize in the form of colorless blocks in the triclinic space group $P\bar{1}$ with two formula units per unit cell and calculated densities of 1.855 g cm^{-3} (**19**) and 1.884 g cm^{-3} (**20**) at 173 K. On an additional note, the perchlorate counter-anions containing Cl2 are significantly distorted.

The investigated complexes **21–23**, all including cocrystallized 2-amino-5*H*-tetrazole, crystallize in the triclinic space group $P\bar{1}$ with two formula units per unit cell and calculated densities between 1.784 g cm^{-3} (**21**) and 1.815 g cm^{-3} (**23**) (Fe: 1.784 g cm^{-3} (173 K); Cu: 1.815 g cm^{-3} (143 K); Zn: 1.812 g cm^{-3} (173 K)). In comparison to the very similar coordination compounds **19** and **20**, once again, no major differences regarding the structural parameters, besides the substitution of the aqua ligand by one additional equivalent of **2**, could be observed.

The cocrystallized 2-AT molecules show no considerable deviations from the previously examined coordinating **2** referring to the bond lengths and bond distances. The octahedral

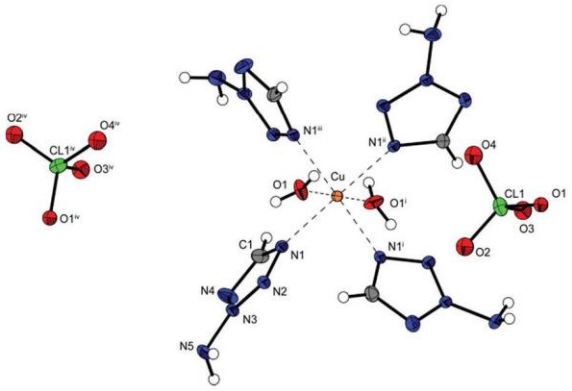


Fig. 10 Molecular unit of $[Cu(H_2O)_2(2\text{-}AT)_4](ClO_4)_2$ (**18**). Selected bond lengths (Å): Cu–O1 2.311(4), Cu–N1 2.025(2); selected bond angles (°): N1–Cu–N1^{ii} 177.77(12), O1–Cu–N1 91.11(9), N1–Cu–N1^{iii} 90.02(8). Symmetry codes: (i) y, 0.5 − x, 0.5 − z; (ii) 0.5 − x, 0.5 − y, z; (iii) 0.5 − y, x, 0.5 − z; (iv) 1 − y, −0.5 + x, −0.5 + z.

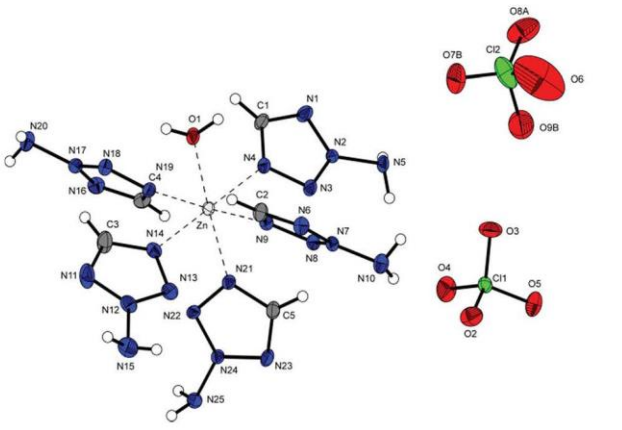


Fig. 11 Molecular unit of $[Zn(H_2O)(2\text{-}AT)_5](ClO_4)_2$ (**20**). Selected bond lengths (Å): Zn–O1 2.083(3), Zn–N4 2.146(3), Zn–N9 2.197(3), Zn–N14 2.147(3), Zn–N19 2.166(3), Zn–N21 2.160(3); selected bond angles (°): O1–Zn–N21 176.80(11), N4–Zn–N14 177.92(11), O1–Zn–N4 87.56(12), O1–Zn–N9 86.13(11), O1–Zn–N14 91.08(12), O1–Zn–N19 89.52(11), N4–Zn–N9 90.45(11), N4–Zn–N19 90.29(11), N4–Zn–N21 89.63(11), N9–Zn–N14 87.89(11).

This journal is © The Royal Society of Chemistry 2018

Published on 06 August 2018. Downloaded by Ludwig Maximilians Universitaet Muenchen on 2/16/2022 7:59:25 AM.

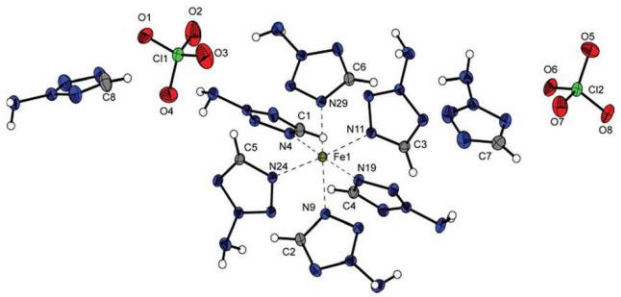


Fig. 12 Molecular unit of $[Fe(2\text{-}AT)_6](ClO_4)_2 \cdot 2$ 2-AT (**21**). Selected bond lengths (Å): Fe1–N4 2.2191(16), Fe1–N9 2.1618(16), Fe1–N11 2.2135(16), Fe1–N19 2.1868(16), Fe1–N24 2.2157(16), Fe1–N29 2.1629(16); selected bond angles (°): N4–Fe1–N19 175.41(6), N4–Fe1–N9 89.38(6), N4–Fe1–N11 86.35(6), N4–Fe1–N24 91.91(6), N24–Fe1–N29 90.62(6).

coordination spheres of the d^{10} and d^6 metal centers zinc(II) and iron(II) show no Jahn–Teller distortion but differ slightly from the ideal octahedron (Fig. 12 and S18†). Nevertheless, the d^9 copper(II) center possesses a typical Jahn–Teller distortion along the axial Cu–N bonds (Fig. S19†). The coordination distances between the metal(II) center and the coordinating ligand are roughly within the same range as for the compounds **19** and **20** but appear to be somewhat longer than in the previous cases. All perchlorate counter-anions show no significant distortion.

Powder diffraction

Due to the possible formation of different species or polymorphs, X-ray powder diffraction measurements were carried out in addition to elemental analysis to ensure the purity of the bulk material. Fig. 13 shows the powder diffraction patterns for the compounds **5**, **6**, **9** and **17**. The results prove the purity of the nitrogen-rich coordination compounds. Small deviations between the measured and the calculated data sets can be observed in all diffractograms and are caused by the temperature differences between the single crystal and powder diffraction experiments. The larger differences in the intensities for the iron(II) and copper(II) complexes **5** and **6** can be attributed to the heavy disorders in the perchlorate moieties (Fig. 13(A) and (B)).

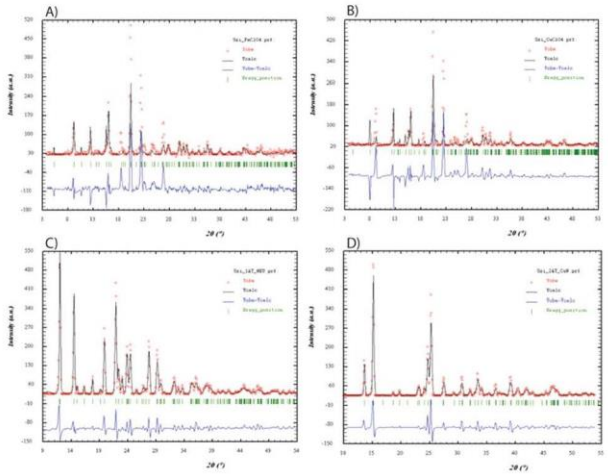


Fig. 13 Powder diffraction experiments (comparison of the measured and calculated data) for the complexes **5** (A), **6** (B), **9** (C) and **17** (D).

Scanning electron microscopy (SEM) and energy dispersive X-ray spectroscopy (EDX)

Since sensitivity data are strongly dependent on the grain size and crystal habitus (microscope images S20–25), scanning electron microscopy and energy dispersive X-ray spectroscopy were performed to explore the compounds' morphology but also the chemical composition. The results of the measurements for compounds **5**, **6**, **9** and **17** are shown in Fig. 14–17.

The iron(II) perchlorate complex **5** forms up to 200 μm-sized blocks beside plate-like crystals. Aside from insignificant trace amounts of silicon, the EDX spectrum did not show any other atoms present in the complex.

Complex **6**, illustrated in Fig. 15 reveals the consistency of the block-like crystals except for small spikes. Compared to compound **5**, no other elements, which are not included in the complex composition, can be observed in the EDX spectrum.

The SEM image of complex **15** exposes an amorphous constitution in comparison to its microscope images. The phase-purity is confirmed by the EDX spectrum.

Compound **17** shows a plate-like morphology and compared to nitrate complex **9** a lower content of carbon and nitrogen, which is consistent with the chemical compositions of the two coordination compounds.

Sensitivities and thermal stability

The behavior of all compounds toward heating in a certain range was investigated by differential thermal analysis (DTA) at a heating rate of $\beta = 5$ °C min^{-1}. The observed endothermic events (melting, dehydration or loss of coordinating/cocrystallized AT ligands) as well as other critical temperatures are listed in Table 1. DTA plots of the compounds **1–3**, **8**, **9**, **12**, **16–23**, and additional information regarding the thermal stabilities can be found in the Fig. S27–30 in the ESI.†

In accordance with our previous findings and literature reports, higher vaporization temperatures $T_{vap.}$,[34] (and melting temperatures) in combination with lower exothermic decomposition temperatures can be observed for 1-AT and 2-AT, and the more *N*1 substitution pattern is existent at the tetrazole.[40,43] Both tetrazoles are liquids under ambient conditions and start to vaporize slowly at certain temperatures until both compounds reach their respective exothermic decomposition stages and deflagrate, as the TGA plot of both ligands clearly

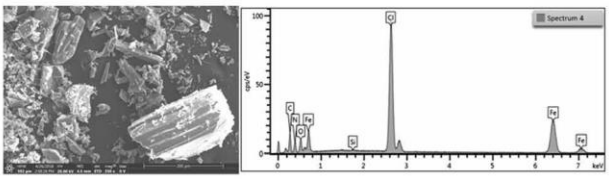


Fig. 14 SEM image (350× magnitude) and EDX spectrum of compound **5**.

Published on 06 August 2018. Downloaded by Ludwig Maximilians Universitaet Muenchen on 2/16/2022 7:59:25 AM.

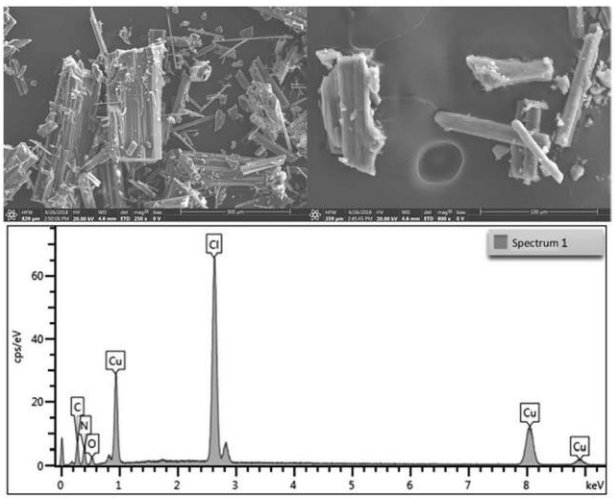


Fig. 15 SEM images (250× magnitude (left) and 800× magnitude-(right)) and EDX spectrum of compound **6**.

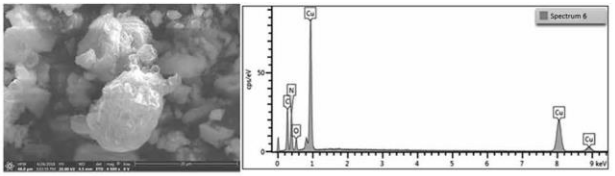


Fig. 16 SEM image (4500× magnitude) and EDX spectrum of compound **9**.

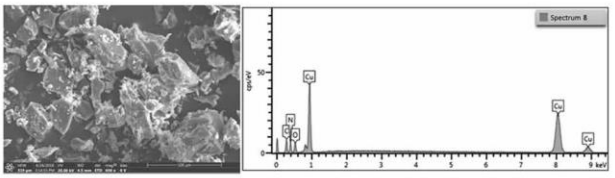


Fig. 17 SEM image (650× magnitude) and EDX spectrum of compound **17**.

illustrates (Fig. S26†). The thermal stabilities of most of the investigated compounds lie in the satisfying range of 175–180 °C (except **3**). Nevertheless, the lowest decomposition temperatures can be observed for the 2-amino-5*H*-tetrazolium perchlorate salt (**3**, $T_{exo.} = 122$ °C) and for the copper(II) nitrato complexes **9** ($T_{exo.} = 161$ °C) and **17** ($T_{exo.} = 157$ °C). Notably the poor thermal stabilities for the nitrato coordination compounds **9** and **17** are not surprising and a known issue in the literature.[15]

Relatively high thermal stabilities have been determined for the water-free 1-AT based metal(II) perchlorate complexes (Fig. 18), which increase in the following order Cu^{II} ($T_{exo.} = 174$ °C) < Fe^{II} ($T_{exo.} = 187$ °C) < Zn^{II} ($T_{exo.} = 189$ °C) < Mn^{II} ($T_{exo.} = 195$ °C). Analogical complexes with 1-methyl-5*H*-tetrazole instead of 1-amino-5*H*-tetrazole (methyl *vs.* amino group) showed, interestingly exactly the same tendency, which could possibly be a useful indicator during the planning and design of

Table 1 Thermal stability measurements of **1–9**, **12**, and **16–23** by DTA[a]

	$T_{endo.}$[b] (°C)	$T_{exo.}$[c] (°C)
1-AT (**1**)	—	182
2-AT (**2**)	—	197
2-AT_HClO_4 (**3**)	122	122
$[Mn(1\text{-}AT)_6](ClO_4)_2$ (**4**)	—	195
$[Fe(1\text{-}AT)_6](ClO4)_2$ (**5**)	—	187
$[Cu(1\text{-}AT)_6](ClO_4)_2$ (**6**)	—	174
$[Zn(1\text{-}AT)_6](ClO_4)_2$ (**7**)	—	189
$[CuCl(\mu\text{-}Cl)(1\text{-}AT)(\mu\text{-}1\text{-}AT)]$ (**8**)	—	175
$[Cu(NO_3)_2(1\text{-}AT)_3]$ (**9**)	—	161
$[Zn(1\text{-}AT)_6](NO_3)_2$ (**12**)	115	180
$[Cu(\mu\text{-}Cl)_2(2\text{-}AT)_2]$ (**16**)	—	171
$[Cu(NO_3)_2(\mu\text{-}2\text{-}AT)_2]$ (**17**)	—	157
$[Cu(H_2O)_2(2\text{-}AT)_4](ClO_4)_2$ (**18**)	110	173
$[Fe(H_2O)(2\text{-}AT)_5](ClO4)_2$ (**19**)	—	159
$[Zn(H_2O)(2\text{-}AT)_5](ClO_4)_2$ (**20**)	132	200
$[Fe(2\text{-}AT)_6](ClO_4)_2 \cdot 2\text{-}AT$ (**21**)	106	169
$[Zn(2\text{-}AT)_6](ClO_4)_2 \cdot 2\text{-}AT$ (**22**)	96	192
$[Cu(2\text{-}AT)_6](ClO_4)_2 \cdot 2\text{-}AT$ (**23**)	108	157

[a] Onset temperatures at a heating rate of 5 °C min^{-1}. [b] Endothermic peak, which indicates melting, dehydration, or loss of coordinating/cocrystallized AT ligands. [c] Exothermic peak, which indicates decomposition.

future high-temperature stable energetic complexes.[15] Dehydration (complex **18** and **20**) or loss of co-crystallized 2-amino-5*H*-tetrazoles during heating of **21–23** indicated by endothermic signals strongly agree with the identified X-ray crystal structures. Drying of the iron(II) monoaqua complex **19** is not possible and leads to an unstable intermediate, which detonates immediately without significant endothermic signal.

An exceptional endothermic peak could be detected during the DTA measurement of the zinc(II) nitrate coordination compound **12** and was therefore investigated into more detail

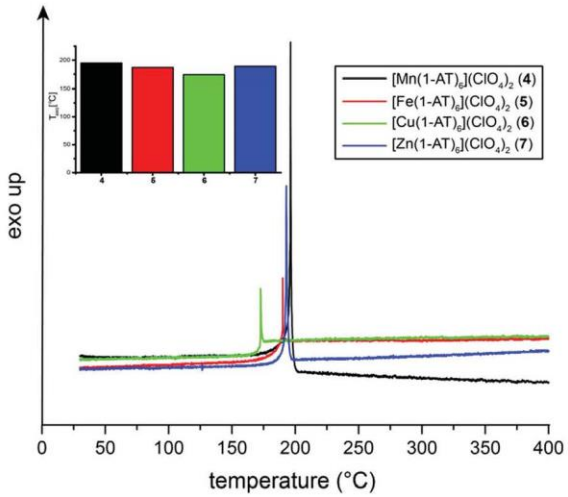


Fig. 18 Comparison of the thermal stabilities ($\beta = 5$ °C min^{-1}) of the 1-AT containing metal(II) perchlorate complexes **4–7**.

This journal is © The Royal Society of Chemistry 2018

Published on 06 August 2018. Downloaded by Ludwig Maximilians Universitaet Muenchen on 2/16/2022 7:59:25 AM.

by thermal gravimetric analysis together with complex **4** as reference sample (Fig. 19).

While no change in weight after heating has been detected for the manganese(II) complex **4** until it decomposes, a gradual loss of coordinating 1-AT molecules beginning at 110 °C up to its decomposition point for coordination complex **12** can be observed. It can be assumed that this endothermic loss leads to the formation of an intermediate species, which later decomposes exothermically.[41]

By comparison of complexes with the same transition metal(II) but with varying AT isomers or anions (except **9** and **17**), no general trend regarding their exothermic decomposition temperatures can be drawn.

The sensitivities toward impact and friction were assessed according to BAM standard methods (1 of 6) together with the electrostatic discharge sensitivity for all compounds. In addition, the compounds have been categorized in accordance with the "UN Recommendations on the Transport of Dangerous Goods" using the determined sensitivities. An overview of the sensitivities is given in Table 2. The ligands as well as all complexes have to be considered as very sensitive to all applied stimuli (impact, friction and ESD) and should therefore be categorized as primary explosives. The majority of the synthesized coordination compounds can even be described as "extremely sensitive" with values smaller than 10 N against friction. Implementation of non-oxidizing chlorido anions into the complexes lowered the performance on the one hand but on the other hand led to a desensitization of the coordination compounds.

The sensitivity against ball drop impact is a very realistic and safety–relevant parameter for compounds with a potential industrial application. Therefore, and in order to get a better understanding of their stability, the sensitivity toward ball drop impact has been determined for the very promising water-free $[M^{II}(1\text{-AT})_6](ClO_4)_2$ coordination compounds **4–7** and the copper(II) nitrato complex **9** (Fig. 20). An overview of the experimental results is given in Table 3.

The sensitivity (Fig. 21) of the 1-AT perchlorate complexes against ball drop impact rises in the following order Fe^{2+} (25 mJ) < Zn^{2+} (16 mJ) < Mn^{2+} (14 mJ) < Cu^{2+} (<4 mJ) and in the following order toward friction Zn^{2+} (0.5 N) ~ Mn^{2+} (0.5 N) < Fe^{2+} (<0.1 N) ~ Cu^{2+} (<0.1 N).

The implementation of oxidizing anions like nitrates or perchlorates into the nitrogen-rich coordination compounds, in comparison to halides, generally leads to increased sensitivities toward mechanical stimuli (Fig. 22).

The same trend can be observed when **2** is applied as a ligand instead of **1**. Therefore, exact tailoring of the desired optical and energetic properties can be easily accomplished by variation of the corresponding coordination environment, facilitating the synthesis of a wide range of different materials (Fig. S31/32†).

Table 2 Sensitivities toward impact, friction, and ESD of **1–9**, **12** and **16–23** compared to lead styphnate and lead azide[42,a]

Compound	IS[b] (J)	FS[c] (N)	ESD[d] (mJ)
1[e]	<1	64	—
2[e]	<1	36	—
3	<1	0.2	10
4	<1	0.5	11[f]
5	<1	<0.1	12
6	<1	<0.1	5
7	<1	0.5	12
8	3	60	50
9	3	2.25	10
12	<1	6	620[f]
16	<2	40	10
17	<1	2	10
18	1	0.4	10
19	1.5	0.15	10
20	1.5	0.5	10
21	<1	0.1	25
22	2	0.2	30
23	1	<0.2	1.2[f]
Lead styphnate[g]	2.5–5	1.5	0.02–1.0
Lead azide[g]	2.5–4	0.1–1	6–12

[a] Determined at a grain size of <100 μm were **3**, **6**, **8**, **9**, **16**, **17**, and **20**. The sensitivities of the remaining complexes were determined at grain sizes between 100 and 500 μm. [b] Impact sensitivity according to the BAM drop hammer test (method 1 of 6). [c] Friction sensitivity according to the BAM friction tester (method 1 of 6). [d] Electrostatic discharge sensitivity (OZM ESD tester); impact: insensitive > 40 J, less sensitive ≥ 35 J, sensitive ≥ 4 J, very sensitive ≤ 3 J; friction: insensitive > 360 N, less sensitive = 360 N, sensitive < 360 N and > 80 N, very sensitive ≤ 80 N, extremely sensitive ≤ 10 N. As per the UN Recommendations on the Transport of Dangerous Goods. [e] From ref. 34. [f] Measured on our new OZM Electric Spark XSpark10 device. [g] From ref. 42.

Primary explosive suitability evaluation

Hot plate and hot needle tests of the most promising compounds were carried out in order to evaluate their applicability as suitable primary explosives (Fig. 23/24 and S33–48†)

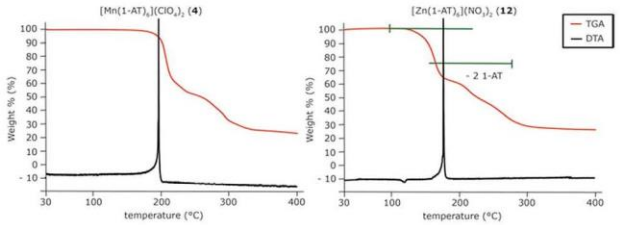


Fig. 19 TGA measurements ($\beta = 5$ °C min^{-1}) of selected compounds **4** and **12**.



Fig. 20 Moment of detonation of compounds **6** and **9** during the ball drop impact test.

Published on 06 August 2018. Downloaded by Ludwig Maximilians Universitaet Muenchen on 2/16/2022 7:59:25 AM.

Table 3 Ball drop impact sensitivities for **4–7** and **9**[a]

	4	5	6	7	9
IS (mJ)	14	25	<4	16	6

[a] Ball drop impact sensitivity determined with the 1 of 6 method in accordance with the MIL-STD 1751A (method 1016). For the testing a 30 mg sample size, a drop weight of a 0.500-inch diameter steel ball (m = 8.35 g) and a steel ball guidance track, which rose 32-inches vertically from a steel base were used.

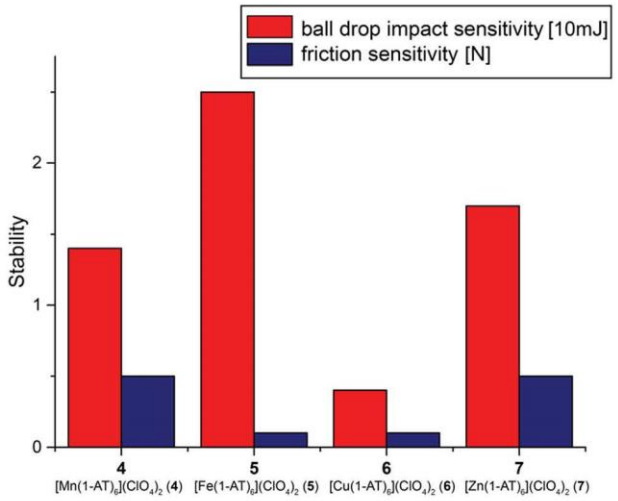


Fig. 21 Comparison of the ball drop impact and friction sensitivities of the metal(II) 1-AT perchlorates **4–7**.

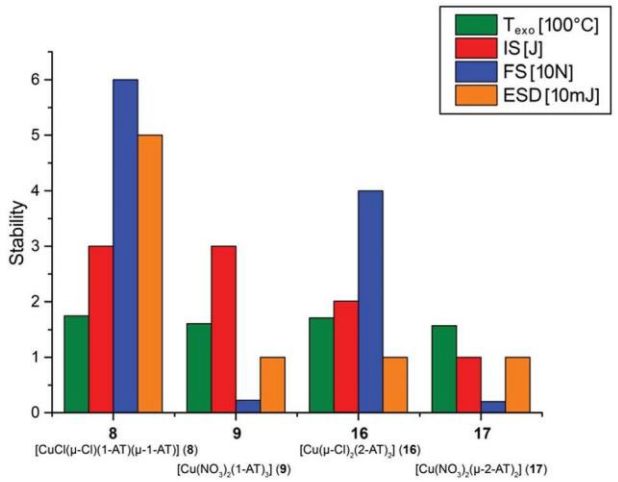


Fig. 22 Stabilities of the copper(II) chlorido and nitrato complexes **8**/**9** and **16**/**17** based on the isomeric amino-5*H*-tetrazoles.

and to observe their behavior toward fast heating with and without confinement. An outline of the experimental results is given in Table 4. All compounds showed strong detonations during the tests, which was indicated by the heavy deformations



Fig. 23 Moment of detonation of compound **22** during the hot needle (HN) initiation shown in sequence.



Fig. 24 Moment of detonation of complex **22** during the hot plate (HP) test shown in sequence.

Table 4 Overview of the hot plate and hot needle test results for **3–7**, **9**, **12**, and **17–23**[a]

Compound	HP	HN	Compound	HP	HN
3	det.	det.	**17**	def.	def.
4	det.	def.	**18**	det.	det.
5	det.	det.	**19**	det.	det.
6	det.	det.	**20**	det.	det.
7	def.	det.	**21**	det.	def.
9	def.	def.	**22**	det.	det.
12	def.	def.	**23**	det.	det.

[a] def.: deflagration; det.: detonation.

of the used copper plate and needles which were used in the analysis (except **9**, **12**, and **17**, which deflagrated only sharply).

On the basis of the positive results of the hot needle and hot plate tests, which gave a first indication of its suitability as a primary explosive, the initiation capability for most of the promising compounds toward pentaerythritol tetranitrate (PETN) as the main charge in copper shells was explored (Fig. 25). Additional details on the test procedures can be found in the Experimental section of the ESI.†

Positive initiation tests caused by a DDT of PETN indicated by a hole in the witness plate and fragmentation of the copper shell (Fig. 26 and S49–52†) were observed for **3**, **5**, **6**, **9**, **17–19**, and **21–23**.

Energetic coordination compounds bearing nitrates as anions are usually unable to initiate common secondary



Fig. 25 PETN initiation capability test setup.

This journal is © The Royal Society of Chemistry 2018

Published on 06 August 2018. Downloaded by Ludwig Maximilians Universitaet Muenchen on 2/16/2022 7:59:25 AM.

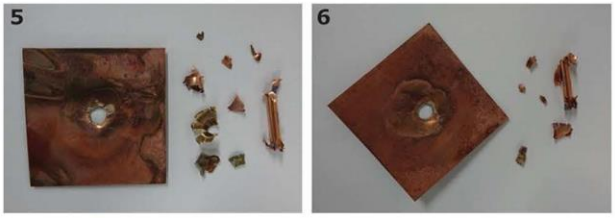


Fig. 26 Positive PETN initiation tests for the coordination compounds **5** and **6**.

Table 5 Results of PETN initiation tests of **3–7**, **9** and **17–23**[a]

Compound	Initiation	Compound	Initiation
3	pos.	**18**	pos.
4	neg.	**19**	pos.
5	pos.	**20**	neg.
6	pos.	**21**	pos.
7	neg.	**22**	pos.
9	pos.	**23**	pos.
17	pos.		

[a] pos.: positive; neg.: negative.

explosives, due to their lack of performance. Thus, it is even more astounding that both copper(II) nitrate complexes **9** and **17**, which show great promise for the future, were able to initiate PETN. Negative test results, indicated by intact copper shells and plates were surprisingly obtained for the perchlorate complexes **4**, **7** and **20**. An overview of the test results can be found in Table 5.

Toxicity

In order to evaluate the toxicity of the synthesized complexes, the toxicological impact on aquatic organisms of the two uncoordinated nitrogen-rich ligands **1** and **2** was measured using the commonly known luminescence marine bacterium *Vibrio fischeri* NRRL-B-11177 strain.[43] Both tetrazoles can be classified as non-toxic (toxicity level after 30 min exposure: very toxic < 0.10 g L^{-1}; toxic 0.10–1.00 g L^{-1}; non-toxic > 1.00 g L^{-1}) with half the maximal effective concentration values EC_{50} of 4.58 g L^{-1} for **1** and 3.87 g L^{-1} for **2** determined after an incubation time of 30 minutes. The values obtained lie within the range of 1-methyl-5*H*-tetrazole, the methylated analogue of 1,5*H*-tetrazole,[15] and confirm the recently observed trend of higher toxicities for 2-substituted tetrazoles in comparison to their 1-substituted isomers.[44]

Laser initiation

The optical initiation of energetic materials has received considerable attention in the last decades and a lot of research has been done from many scientists all over the world.[18,44–46] Laser initiation has several advantages over classical ignition methods (thermal or mechanical) and could therefore be of great interest for industrial applications (*e.g.* laser ignitable ammunition or optical detonators).[20] All here investigated

Table 6 Laser initiation test results[a]

Compound	0.15 mJ	0.17 mJ	26 mJ
5	det.	—	det.
6	det.	—	det.
9	det.	det.	—
16	—	—	✗
17	✗	det.	—
18	✗	det.	—
19	det.	—	—
21	det.	—	—
23	✗	det.	—

[a] (—: not tested, ✗: no ignition, dec.: decomposition, deflag.: deflagration, det.: detonation). Operating parameters: current I = 6–7 A; voltage U = 4 V; theoretical maximal output power P_{max} = 45 W; theoretical energy E_{max} = 0.15–26 mJ; wavelength λ = 915 nm; pulse length τ = 0.1–15 ms.

compounds suffer from their increased sensitivities toward mechanical stimuli making them highly suitable for application as lead-free primaries but unfortunately not for any use in laser ignition systems. Therefore, the focus of this contribution was placed on more academic questions like the laser ignitibility of the complexes at different energy thresholds. Only selected colored coordination compounds showed a response to laser irradiation differing in the required energy input depending on the isomer/metal(II)/anion combination. A summary of the performed experiments is given in Table 6. More details on the experimental setup can be found in the ESI.† All complexes investigated except the copper(II) chloride complex **16** detonated heavily under the employed settings resulting in deformations of the sample holder and destruction of the optical lens and sapphire glass due to the extreme powerful nature of the complexes (Fig. 27 and S53–57†). The complexes exhibited similar initiation thresholds and could be ignited at the lowest applicable initiation energy settable in the parameters of the laser. Even the very sensitive copper(II) nitrate complexes **9** and **17** were successfully be initiated and are therefore one of the rare examples of laser-ignitable nitrate complexes in literature.[47,48]

UV-Vis spectroscopy

The UV-Vis spectra in the solid state, illustrated in Fig. 28 and S58,† were measured for selected laser-ignitable complexes in the range of 350–1000 nm with regard to any possible correlation between the laser ignitability and the absorption of the

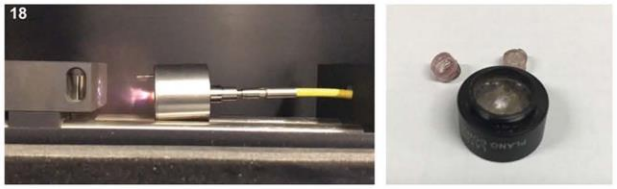


Fig. 27 Moment of detonation of complex **18** (left) and destroyed lens and sample holder (right) caused by the tremendous shockwave.

Published on 06 August 2018. Downloaded by Ludwig Maximilians Universitaet Muenchen on 2/16/2022 7:59:25 AM.

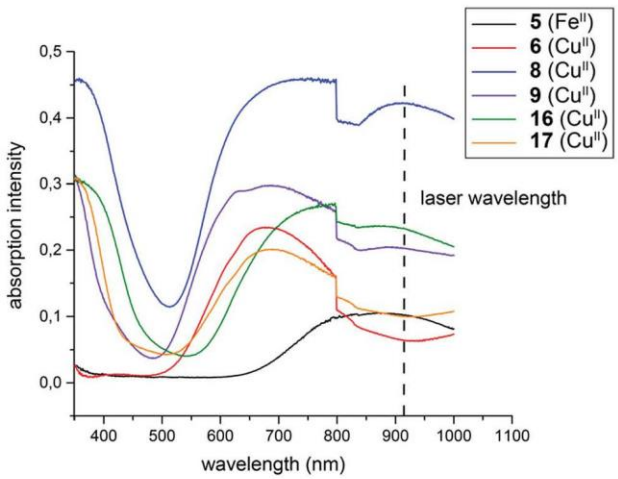


Fig. 28 Solid state UV-Vis spectra of selected copper(II) and iron(II) complexes. The step in the absorption intensity at 800 nm is caused by a detector change. The UV-Vis spectra have only qualitative character.

Table 7 Measured optical properties of complexes **5**, **6**, **8**, **9**, **16**, **17**–**19**, **21** and **23**

Compound	M	Color	λ_{d-d}[a]	$\lambda_{915}/\lambda_{d-d}$[b]
5	Fe^{II} (hs)	Yellowish	871	0.97
6	Cu^{II}	Blue	677	0.27
8	Cu^{II}	Green	768	0.92
9	Cu^{II}	Blue	686	0.68
16	Cu^{II}	Green	796	0.63
17	Cu^{II}	Blue	689	0.50
18	Cu^{II}	Blue	647	0.37
19	Fe^{II} (hs)	Yellowish	868	0.95
21	Fe^{II} (hs)	Yellowish	795	0.93
23	Cu^{II}	Blue	655	0.35

[a] Absorption intensity maximum wavelength, which can be assigned to electron d–d transitions in the measured range of 350–1000 nm. [b] Quotient of the absorption intensity at the laser wavelength and the intensity at the d–d absorption wavelength.

compounds at the corresponding wavelength. The investigated optical properties of the complexes are compiled and summarized in Table 7. The examined energetic coordination compounds showed typical absorptions in the NIR, visible and ultra-violet region resulting from the corresponding d–d transitions, which are highly dependent on the implemented 3d metal(II), anion and isomeric ligand. The exact mechanism of the underlying laser initiation process (*e.g.* thermal, electronical) is still questionable and has not been understood completely.[49,50]

All investigated complexes show a moderate absorption in the laser wavelength region of 915 nm, which could be a possible explanation for the laser ignitibility of the coordination compounds since none of the colorless complexes (Mn^{II} or Zn^{II}) could be initiated. The laser ignitibility is not only linked to its absorption behavior but also to several other parameters like the coordination sphere of the corresponding transition metal(II) or its electronic configuration. One plausible explanation of the laser ignitibility of the complexes and imaginable initiation pathway could be the formation of several hot spots in the material caused by photothermal excitations after irradiation. It should be emphasized that contrary to literature assumings, complexes bearing the nitrate anion could be ignited.[47]

Additional studies in the future should be carried out to obtain further information regarding the initiation process, which should cover the influence of the complexes' structure and the type of the mechanism.

Conclusions

Two isomeric amino-5*H*-tetrazoles (1-amino-5*H*-tetrazole (**1**, 1-AT) and 2-amino-5*H*-tetrazole (**2**, 2-AT)) with sensitivities already in the range of primary explosives were synthesized in a simple one step reaction starting from 1,5*H*-tetrazole and the commercially available amination reagent hydroxylamine-*O*-sulfonic acid (HOSA). The obtained isomeric mixture was purified by column chromatography, preventing the highly risky distillation mentioned in the literature and yielded the products in satisfying yields. Due to the great potential of 1-AT as ligand in powerful energetic transition metal(II) complexes, a selective, upscalable and isomerically pure route toward this highly endothermic compound has been developed. The received nitrogen-rich aminoazoles were comprehensively characterized by diverse analytical methods enclosing heteronuclear ^{15}N NMR spectroscopy, X-ray studies and toxicity determinations. The toxicity assessments toward aquatic organisms revealed the non-toxicity of both heterocycles. Transition metal(II) complexes based on 1-methyl-5*H*-tetrazole as ligand have shown great promise in the past but had not enough power to be appropriate candidates as lead-free primary explosives. As obvious and logical consequence, *N*-aminoazoles with a higher nitrogen content exhibiting the powerful outer N–N single bond have been incorporated into the equivalent complexes resulting in a tremendous performance increase releasing several of the most energetic coordination compounds synthesized so far. The present study features the preparation, analysis and evaluation of 20 new lead, nickel and cobalt-free energetic complexes, which are built-up by two isomeric aminotetrazoles, four different metals and six varying anions. The synthesized complexes, which show a great coordination sphere diversity depending on the inserted components, can be prepared by an easy upscalable and low-cost synthetic route. The strategy of energetic coordination compounds (ECC), which enables the fine-tuning of the optical and energetic properties through easy change of the building blocks (metal, anion and ligand) has proved once again its suitability in the difficult and challenging research area of lead-free primary explosives. The synthesis of the metal(II) perchlorate coordination compounds based on 2-amino-5*H*-tetrazole were highly dependent on the reaction conditions like stoichiometry or solvent system and yielded either aqua complexes or co-crystallized species. Single X-ray studies in combination with powder diffraction and electron microscopy of the auspicious and mostly water-free complexes gave interesting insights and

This journal is © The Royal Society of Chemistry 2018

Published on 06 August 2018. Downloaded by Ludwig Maximilians Universitaet Muenchen on 2/16/2022 7:59:25 AM.

allowed correlations between the observed structure and their sensitivity against mechanical stimuli. After comparing all compounds, the following trends can be formulated: (i) iron(II) and copper(II) complexes are more sensitive than manganese(II) and zinc(II) coordination compounds; (ii) the more oxidizing the anion, the more sensitive the compound; (iii) complexes with 1-AT are more sensitive than those with 2-AT, which can be attributed to the anhydrous nature of those. Laser initiation experiments executed with NIR light at a wavelength of 915 nm showed fast deflagration-to-detonation transitions at extremely low energy thresholds for most of the coordination compounds and destroyed large parts of the laser setup due to the destructive power of the complexes. The initiation capability toward pentaerythritol tetranitrate (PETN) filled copper shell detonators was tested for several pre-selected complexes (hot plate and hot needle experiments) and demonstrated the enormous potential of the synthesized complexes as lead-free primary explosive replacements. Besides the lead-free, but not completely environmentally friendly perchlorate compounds, the nitrato complexes show excellent properties and can therefore be considered as promising primary explosive candidates.

Conflicts of interest

The authors declare no conflict of interest.

Acknowledgements

Financial support of this work by the Ludwig-Maximilian University of Munich (LMU). The authors would like to thank Prof. Dr Thomas M. Klapötke for not only providing the research facilities but also for his scientific support. In addition, the authors would like to thank Prof. Dr Konstantin Karaghiosoff for the measurement of various ^{15}N NMR spectra, Prof. Dr Jürgen Evers for the recording of several X-ray powder diffractions, Mrs Cornelia Unger for toxicity assessments as well as Jasmin Lechner, Alexander Kremsmair and Philipp Spiess for their great contribution to this work.

Notes and references

1 T. D. Ngo, M. Nofar, M. T. Ton-That, M. Sepehr, W. Hu and J. Denault, *Presented in part at the 68th Annu. Tech. Conf. – Soc. Plast. Eng.*, Orlando, May, 2010.
2 A. K. Mohanty, M. Misra and L. T. Drzal, *J. Polym. Environ.*, 2002, **10**, 19.
3 SVHC identification, https://echa.europa.eu/substances-of-very-high-concern-identification-explained, accessed March, 2018.
4 Understanding REACH, https://echa.europa.eu/regulations/reach/understanding-reach, accessed March, 2018.
5 REACH evaluation, https://echa.europa.eu/regulations/reach/evaluation, accessed March, 2018.
6 SVHC identification, https://echa.europa.eu/substances-of-very-high-concern-identification-explained, accessed March, 2018.
7 SVHC list, https://echa.europa.eu/candidate-list-table, accessed March, 2018.
8 J. W. Fronabarger, M. D. Williams, W. B. Sanborn, J. G. Bragg, D. A. Parrish and M. Bichay, *Propellants, Explos., Pyrotech.*, 2011, **36**, 541.
9 Y. Tang, C. He, L. A. Mitchell, D. A. Parrish and J. n. M. Shreeve, *Angew. Chem., Int. Ed.*, 2016, **55**, 5565.
10 R. Haiges and K. O. Christe, *Inorg. Chem.*, 2013, **52**, 7249.
11 D. Chen, H. Yang, Z. Yi, H. Xiong, L. Zhang, S. Zhu and G. Cheng, *Angew. Chem., Int. Ed.*, 2018, **57**, 2081.
12 J.-G. Xu, C. Sun, M.-J. Zhang, B.-W. Liu, X.-Z. Li, J. Lu, S.-H. Wang, F.-K. Zheng and G.-C. Guo, *Chem. Mater.*, 2017, **29**, 9725.
13 M. H. V. Huynh, M. A. Hiskey, D. E. Chavez, D. L. Naud and R. D. Gilardi, *J. Am. Chem. Soc.*, 2005, **127**, 12537.
14 M. H. V. Huynh, M. D. Coburn, T. J. Meyer and M. Wetzler, *Proc. Natl. Acad. Sci. U. S. A.*, 2006, **103**, 10322.
15 N. Szimhardt, M. H. H. Wurzenberger, A. Beringer, L. J. Daumann and J. Stierstorfer, *J. Mater. Chem. A*, 2017, **5**, 23753.
16 Q. Zhang and J. n. M. Shreeve, *Angew. Chem., Int. Ed.*, 2014, **53**, 2540.
17 K. A. McDonald, S. Seth and A. J. Matzger, *Cryst. Growth Des.*, 2015, **15**, 5963.
18 T. W. Myers, J. A. Bjorgaard, K. E. Brown, D. E. Chavez, S. K. Hanson, R. J. Scharff, S. Tretiak and J. M. Veauthier, *J. Am. Chem. Soc.*, 2016, **138**, 4685.
19 I. A. Ugryumov, M. A. Ilyushin, I. V. Tselinskii and A. S. Kozlov, *Russ. J. Appl. Chem.*, 2003, **76**, 439.
20 R. Schirra and H. Zöllner, *Presented in part at the 42nd International Pyrotechnics Seminar*, Colorado, July, 2016.
21 A. Y. Zhilin, M. A. Ilyushin, I. V. Tselinskii, A. S. Kozlov and N. E. Kuz'mina, *Russ. J. Appl. Chem.*, 2002, **75**, 1849.
22 K. Karaghiosoff, T. M. Klapötke and C. M. Sabaté, *Chem. - Eur. J.*, 2009, **15**, 1164.
23 M. A. Ilyushin, I. V. Bachurina, A. V. Smirnov, I. V. Tselinsky and I. V. Shugalei, *Cent. Eur. J. Energ. Mater.*, 2009, **7**, 33.
24 P. N. Gaponik, M. M. Degtyarik, A. S. Lyakhov, V. E. Matulis, O. A. Ivashkevich, M. Quesada and J. Reedijk, *Inorg. Chim. Acta*, 2005, **358**, 3949.
25 A. Hahma and E. Karvinen, *EU Pat.*, 2450329A2, Diehl BGT Defence GmbH & Co. KG, 2012.
26 A. Y. Zhilin, M. A. Ilyushin, I. V. Tselinskii, A. S. Kozlov and I. S. Lisker, *Russ. J. Appl. Chem.*, 2003, **76**, 572.
27 A. V. Smirnov, M. A. Ilyushin and I. V. Tselinskii, *Russ. J. Appl. Chem.*, 2004, **77**, 794.
28 J. G. Zhang, J. Y. Li, Y. Zang, Y. J. Shu, T. L. Zhang, L. Yang and P. P. Power, *Z. Anorg. Allg. Chem.*, 2010, **636**, 1147.
29 M. H. V. Huynh, *WIPO Pat.*, 2008143724A2, Los Alamos National Security LLC, 2008.
30 M. H. V. Huynh, *US Pat.*, 20080200688A1, Los Alamos National Security LLC, 2008.
31 K. Wang, D. Zeng, J.-G. Zhang, Y. Cui, T.-L. Zhang, Z.-M. Li and X. Jin, *Dalton Trans.*, 2015, **44**, 12497.
32 I. Hagedorn and H. D. Winkelmann, *Chem. Ber.*, 1966, **99**, 850.

Published on 06 August 2018. Downloaded by Ludwig Maximilians Universitaet Muenchen on 2/16/2022 7:59:25 AM.

33 R. Raap, *Can. J. Chem.*, 1969, **47**, 3677.
34 T. M. Klapötke, D. G. Piercey and J. Stierstorfer, *Dalton Trans.*, 2012, **41**, 9451.
35 P. N. Gaponik and V. P. Karavai, *Khim. Geterotsikl. Soedin.*, 1983, **6**, 841.
36 M. H. H. Wurzenberger, N. Szimhardt and J. Stierstorfer, *J. Am. Chem. Soc.*, 2018, **140**, 3206.
37 Crystallographic data for the structures have been deposited with the Cambridge Crystallographic Data Centre.†
38 M. H. Palmer and S. Parsons, *Acta Crystallogr.*, 1996, **52**, 2818–2822.
39 T. M. Klapötke, C. M. Sabate and J. Stierstorfer, *Z. Anorg. Allg. Chem.*, 2016, **634**, 1867.
40 P. N. Gaponik, M. M. Degtyarik, A. S. Lyakhov, V. E. Matulis, O. A. Ivashkevich, M. Quesada and J. Reedijk, *Inorg. Chim. Acta*, 2005, **358**, 3949.
41 N. Szimhardt and J. Stierstorfer, *Chem.–Eur. J.*, 2017, **24**, 2687.
42 R. Meyer, J. Köhler and A. Homburg, *Explosives*, Wiley-VCH, Weinheim, 5th edn, 2002.
43 G. I. Sunahara, S. Dodard, M. Sarrazin, L. Paquet, G. Ampleman, S. Thiboutot, J. Hawari and A. Y. Renoux, *Ecotoxicol. Environ. Saf.*, 1998, **39**, 185.
44 N. Szimhardt, M. H. H. Wurzenberger, T. M. Klapötke, J. T. Lechner, H. Reichherzer, C. C. Unger and J. Stierstorfer, *J. Mater. Chem. A*, 2018, **6**, 6565.
45 T. W. Myers, K. E. Brown, D. E. Chavez, R. J. Scharff and J. M. Veauthier, *Inorg. Chem.*, 2017, **56**, 2297.
46 M. A. Ilyushin and I. V. Tselinskii, *Zh. Prikl. Khim.*, 2000, **73**, 1233.
47 T. W. Myers, K. E. Brown, D. E. Chavez, R. J. Scharff and J. M. Veauthier, *Eur. J. Inorg. Chem.*, 2016, 3178.
48 T. W. Myers, D. E. Chavez, S. K. Hanson, R. J. Scharff, B. L. Scott, J. M. Veauthier and R. Wu, *Inorg. Chem.*, 2015, **54**, 8077.
49 S. R. Ahmad and M. Cartwright, *Laser Ignition of Energetic Materials*, John Wiley & Sons, Hoboken, 2014.
50 E. D. Aluker, A. G. Krechetov, A. Y. Mitrofanov, D. R. Nurmukhametov and M. M. Kuklja, *J. Phys. Chem. C*, 2011, **115**, 6893.

This journal is © The Royal Society of Chemistry 2018

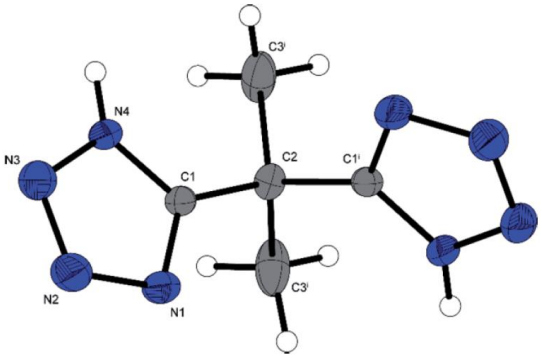
Appendix 7

2,2-Bis(5-tetrazolyl)propane as Ligand in Energetic 3d Transition Metal Complexes

N. Szimhardt, M. S. Gruhne, M. Lommel, A. Hess, Maximilian H. H. Wurzenberger, T. M. Klapötke, J. Stierstorfer

Z. Anorg. Allg. Chem. **2019**, *645*, 354–361.

https://doi.org/10.1002/zaac.201800288



Supplementary Information:
https://onlinelibrary.wiley.com/action/downloadSupplement?doi=10.1002%2Fzaac.201800288&file=zaac201800288-sup-0001-SupMat.pdf

Journal of Inorganic and General Chemistry
ZAAC
Zeitschrift für anorganische und allgemeine Chemie
DOI: 10.1002/zaac.201800288
ARTICLE

2,2-Bis(5-tetrazolyl)propane as Ligand in Energetic 3d Transition Metal Complexes

Norbert Szimhardt,[a] Michael S. Gruhne,[a] Marcus Lommel,[a] Andreas Hess,[a] Maximilian H. H. Wurzenberger,[a] Thomas M. Klapötke,[a] and Jörg Stierstorfer*[a]

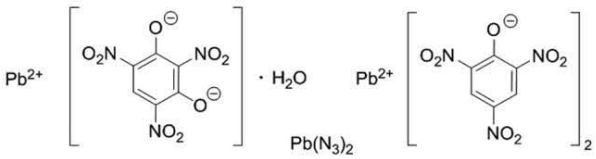
Dedicated to Prof. Dr. Thomas F. Fässler on the Occasion of his 60th Birthday

Abstract. This contribution covers the preparation and characterization of 2,2-bis(5-tetrazolyl)propane (5-DTP) (**1**). The bridged bitetrazole is used as a neutral nitrogen-rich ligand in 3d transition metal(II) based complexes for the first time and can be synthesized via [2+3] cycloaddition from sodium azide and dimethylmalononitrile. The combination with different anions (e.g., perchlorate, nitrate, sulfate, and chloride) yields materials with widely varying physicochemical properties. The obtained coordination compounds were characterized using low-temperature single-crystal X-ray diffraction (except **14**), IR spectroscopy, elemental analysis, and DTA (except **16**). The sensitivities toward external stimuli (impact and friction) were determined according to the Bundesamt für Materialforschung und -prüfung (BAM) standard methods together with its sensitivities against electrostatic discharge (except **16**). Complexes **10** and **14** were characterized in laser ignition experiments. For determination of the compounds' deflagration to detonation transition (DDT) capability, hot plate and hot needle tests were performed for the zinc(II) and copper(II) perchlorate complexes.

Introduction

In the context of high toxicity and increasing environmental hazards, the commonly used primary explosives lead styphnate (**LS**) and lead azide (**LA**) (Chart 1) have been added to the candidate list of authorization (substances of very high concern, Annex XIV) during the REACH (Registration, Evaluation, Authorization, and Restriction of Chemicals) regulations in 2011.[1] Consequently, research into lead-free replacements, with lower impact on our environment, is inevitable.

Investigations into coordination compounds, comprising endothermic nitrogen-rich ligands such as tetrazoles and triazoles, a late 3d transition metal and a coordinating or non-coordinating anion, demonstrated promising properties suitable for a wide range of applications, more particularly as metal-organic frameworks (MOFs),[2] spin crossover systems,[3] and energetic materials.[4] Polynuclear branched tetrazole systems can be considered as analogs to multibasic carboxylic acids concerning the complex-forming activity with metal ions. Investigations into the coordination ability of late 3d transition metals resulted in a preference for the heterocyclic derivatives.[5] Specifically, carboxyl groups are substituted by tetrazol-5-yl fragments,[6] showing similarities in acidities, abilities to form intermolecular hydrogen bonds, and electron-withdrawing effects.[7]



LS LA LP

Chart 1. Commonly used primary explosives: lead(II) styphnate (LS), lead(II) azide (LA), and lead(II) picrate (LP).

On this basis, the biological activity of tetrazoles was newly interpreted. N–H-unsubstituted and 1,5-disubstituted tetrazole rings are metabolically stable and can serve as bioisostere for amide and carboxy groups in modified amino acids. An increasing use as biologically active oligo- and polypeptides can be found.[8,9] The already mentioned ability to form hydrogen bonds is comparable with those of purine and pyrimidine bases.[10] Involvement of two nitrogen atoms of the heterocycle in intermolecular hydrogen bonding opens up the possibility of multicenter intermolecular interactions, especially with hydrogen atoms of the active site of enzymes.[7]

Therefore, tetrazoles have a strong position in the pharmaceutical market as drugs. With medicinal applications ranging from hypotensive action,[11] antimicrobial, anti-inflammatory,[12] antifungal,[13] and antiviral activities.[14,15] Selected pharmaceuticals are exemplarily shown in Chart 2.

* Dr. J. Stierstorfer
E-Mail: jstch@cup.uni-muenchen.de
Homepage: http://www.hedm.cup.uni-muenchen.de
[a] Department of Chemistry
Ludwig-Maximilian-University of Munich
Butenandtstr. 5–13
81377 Munich, Germany
Supporting information for this article is available on the WWW under **http://dx.doi.org/10.1002/zaac.201800288** or from the author.

 © 2019 WILEY-VCH Verlag GmbH & Co. KGaA, Weinheim

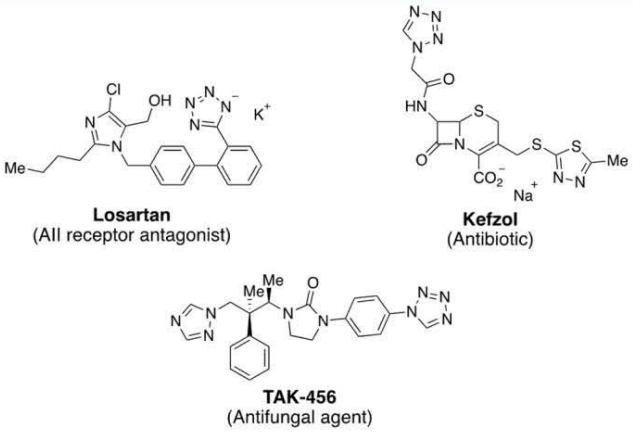


Chart 2. Tetrazole-based pharmaceutical products.

Apart from this, tetrazole derivatives offer tremendous potential as endothermic ligands in environmentally benign energetic coordination compounds (ECC), to some extent ignitable by laser irradiation.[16,17] The first published laser initiation experiments date back to the late sixties by analyzing samples of LA, RDX, Tetryl, and PETN.[18–20] Investigations were performed by utilizing two laser-type systems, more particularly a ruby laser (λ = 694 nm)[21] and a neodymium laser (λ = 1060 nm) operating in the Q-switch mode.[20] Owing to the relatively large size of the used solid-state lasers, practical applications were limited. Due to the commercial availability of laser diodes, new options regarding initiation and ignition of energetic materials arose.[21] With common ignition methods (flame, heat, mechanical stimuli, or shock),[22] existing disadvantages like unintended initiation can be excluded by isolation of the energetic material to electric impulses. Nevertheless, shorter function times and the use of less sensitive ignition charges (impact sensitivity $\geq$ 3 J, friction sensitivity $\geq$ 80 N, T_{dec} $\geq$ 180 °C) increase the safety and handling of these compounds significantly. Recent investigations stated the high sensitivity of energetic coordination compounds toward laser irradiation, which predicts excellent suitability for laser ignitable initiation systems.[16,17] In consideration of initiation abilities, energetic transition metal complexes investigations were started with pentaamine(5-cyano-2*H*-tetrazolate)cobalt(III) perchlorate (CP, Chart 3) and its subsequent replacement tetraamine-cis-bis(5-nitro-2*H*-tetrazolato-*N*2)-cobalt(III) perchlorate (BNCP, Chart 3) applying a GaAlAs diode laser.[23,24] Despite positive initiation by laser ignition, both compounds still suffer from increased sensitivities, restricting their applicability. Since then, several coordination compounds, comprising various ligands and central metal atoms, have been synthesized and investigated regarding applications in laser ignitable initiation systems.[25–29]

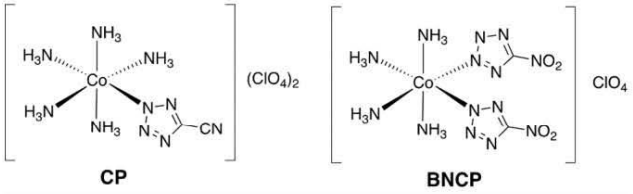


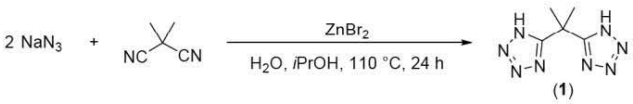
Chart 3. Molecular structures of CP and BNCP.

An extensive series of late 3d transition metal(II) based energetic coordination compounds using bis(1*H*-tetrazol-5-yl)ethane, and its methylene bridged analog bis(1*H*-tetrazol-5-yl)methane as nitrogen-rich ligands were presented by our research group. Due to the increased sensitivities, derivatization (e.g., alkylation) was of interest in order to increase the stability and decrease the sensitivity of the compounds.[26,30] In this contribution, a large series of energetic complexes consisting of 2,2-bis(5-tetrazolyl)propane (5-DTP), which has been used for the first time in literature, were examined and their physicochemical properties explored. The synthesized complexes consist of a late 3d transition metal(II) as center, 5-DTP as ligand, and coordinating or non-coordinating anions (nitrate, perchlorate, chloride, or sulfate).

Results and Discussion

Synthesis

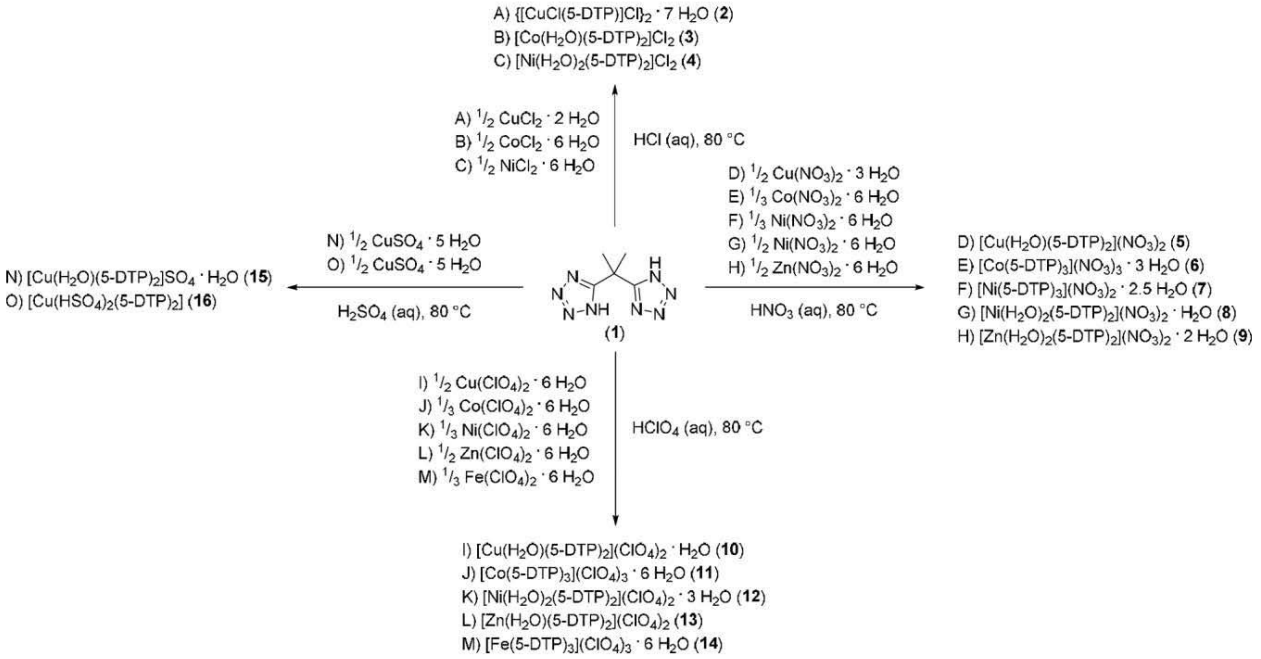
The nitrogen-rich ligand 2,2-bis(5-tetrazolyl)propane (5-DTP) (**1**) could be obtained in a yield of 55 % by [2+3] cycloaddition reaction using dimethylmalononitrile and sodium azide as reactants (Scheme 1). According to a literature procedure,[31] the starting materials and zinc(II) bromide as catalyst were partially dissolved in water, while propan-2-ol was added to increase the solubility. The reaction mixture was refluxed at a constant reaction temperature of 110 °C to prevent decomposition of dimethylmalononitrile at higher temperatures. After 24 h, the suspension was acidified with 2 M hydrochloric acid to dissolve the precipitate. After extraction with ethyl acetate and recrystallization from water the product was obtained in the form of colorless crystals.



Scheme 1. Synthesis of 2,2-bis(5-tetrazolyl)propane (**1**).

In comparison to the very sensitive copper(II) perchlorate complexes based on 5-DTM as ligand, compounds based on 5-DTP are supposed to show a higher tolerance toward mechanical stimuli.[30] The transition metal(II) complexes **2**–**16** were prepared by combining solutions of stoichiometric amounts of 2,2-bis(5-tetrazolyl)propane (**1**) as ligand and metal(II) salts in the corresponding acid at 80 °C (Scheme 2). Due to the acidic character of the ligand, diluted acids were used as the solvent for the reaction in order to prevent precipitation of the corresponding metal(II) tetrazolate salts. This strategy ensures the incorporation of the neutral nitrogen-rich ligand to build up cationic or neutral complexes with non-oxidizing anions like chlorides or sulfates and oxidizing ones like nitrates or perchlorates to produce more promising energetic materials as possible alternatives for toxic heavy metal based primary explosives. The central metal atoms of the complexes **6**, **11**, and **14** were oxidized through perchloric acid, resulting in the oxidation state +III of cobalt and iron.

 © 2019 WILEY-VCH Verlag GmbH & Co. KGaA, Weinheim



Scheme 2. Synthesis of 5-DTP complexes **2**–**16** with different central metal(II) or metal(III) atoms and chloride, nitrate, perchlorate and sulfate as anions.

The reaction mixtures were left for a few days or weeks until crystalline material could be obtained. All compounds could be achieved in the form of X-ray suitable crystals directly from the mother liquor. Unfortunately, only a few single crystals could be picked of complex **16** beside compounds with unknown composition, which allowed no further characterization of the compound. Regarding complexes based on nickel(II) nitrate, two different species could be isolated, depending on the amount of ligand used. The products were filtered off and dried in air.

No further purification step was necessary to get pure products in satisfying to high yields (36–82 %). IR spectra were measured for every compound except **16** and are available in the Supporting Information (Figures S1–S4).

Crystal Structures

All complexes were characterized using low-temperature single-crystal X-ray diffraction. Finalization of the data set for complexes **6**, **7**, **11**, **12**, and **14** was not possible because of the strongly disordered moieties and the related weak diffractions. Nonetheless, the elemental analysis in combination with infrared spectroscopy validated their temporarily observed structures. Details of the crystal structures of complexes **6**, **11**, and **16** as well as measurement and refinement data are given in the Supporting Information. The crystal datasets were uploaded to the CSD database.[32] The atomic distances and angles of the coordinating ligand 5-DTP are nearly the same as in the non-coordinating compound and are consequently not discussed.[31]

5-DTP (**1**) crystallizes in the orthorhombic space group *Fdd*2 with eight formula units per unit cell and a calculated density of 1.437 g·cm^{-3} at 173 K (Figure 1). The molecular unit is built up by two asymmetric units and shows two planar tetrazole rings [<(N1–N2–N3–N4) = –0.08(18)°, <(C1–N1–N2–N3) = –0.59(18)°] substituted and connected by an isopropane molecule. As expected, the nitrogen–nitrogen and nitrogen–carbon distances lie in a typical range of literature reported tetrazole compounds and are between single and double bonds.[33,34]

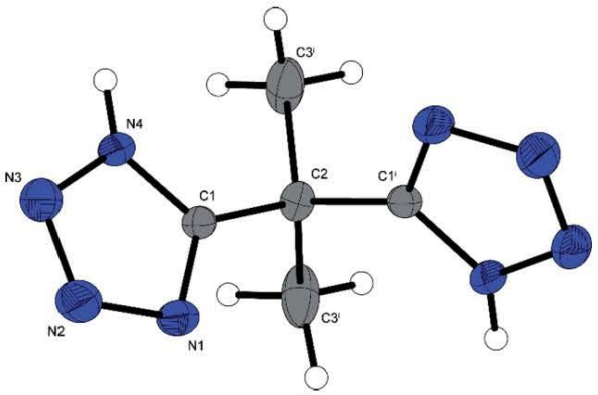


Figure 1. Molecular unit of 2,2-bis(5-tetrazolyl)propane (**1**). Selected bond lengths /Å: C1–C2 1.507(18), C1–N1 1.320(18), N1–N2 1.363(19), N2–N3 1.290(19), N3–N4 1.343(18), N4–C1 1.334(17), C2–C3^{i} 1.532(2); selected bond angles /°: C1–C2–C1^{i} 108.10(14), C3^{i}–C2–C3^{i} 110.20(16), C1–N1–N2 106.39(12), N1–N2–N3 110.10(14), N2–N3–N4 106.70(12), N3–N4–C1 109.00(11). Symmetry code: (i) –x, –y, z.

Compound **2** crystallizes in the monoclinic space group $P2_1/n$ with four formula units per unit cell and a calculated density of 1.596 g·cm^{-3} at 173 K. The complex has a profoundly distorted trigonal bipyramidal coordination sphere

 © 2019 WILEY-VCH Verlag GmbH & Co. KGaA, Weinheim

with a chlorido ligand and two coordinating ditetrazoles (Figure 2). The possible reason for the distortion could be the fixed structure of the nitrogen-rich ligand. The distance between the central copper(II) atom and the chloride is in a typical range for trigonal bipyramidal coordinated chlorido ligands.[35]

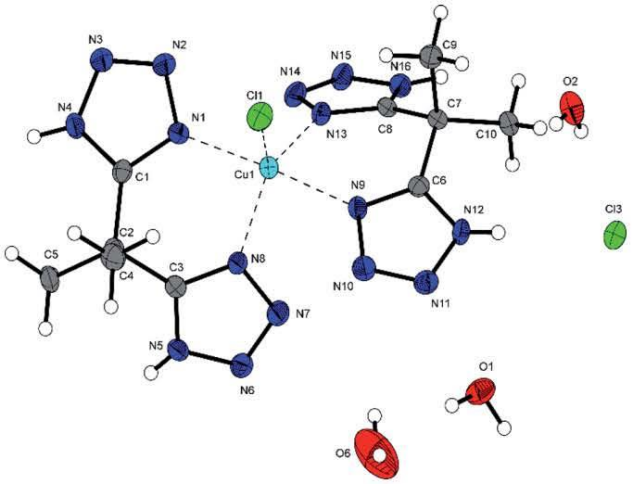


Figure 2. Selection of the molecular unit of $\{[CuCl(5\text{-}DTP)_2]Cl\}_2 \cdot 7\ H_2O$ (**2**). Selected bond lengths /Å: Cu1–N9 1.979(12), Cu1–N1 1.982(4), Cu1–N8 2.050(12), Cu1–N13 2.158(12), Cu1–Cl1 2.293(14); selected bond angles /°: N9–Cu1–N1 175.9(12), N9–Cu1–N8 91.01(5), N1–Cu1–N8 84.97(12), N9–Cu1–N13 84.56(5), N1–Cu1–N13 95.87(11), N8–Cu1–N13 106.5(5), N9–Cu1–Cl1 91.98(5), N1–Cu1–Cl1 91.29(12), N8–Cu1–Cl1 132.9(5), N13–Cu1–Cl1 120.6(5).

The cobalt(II) chloride complex **3**, with a calculated density of 1.678 g·cm^{-3} at 173 K, crystallizes in the monoclinic space group *P2/c* with two formula units per unit cell. The molecular unit is built up by two asymmetric unit cells (Figure 3). The central cobalt(II) atom is octahedrally coordinated by two *cis* aqua ligands and two twisted 5-DTP molecules on the opposite side in nearly the same distance from the metal(II). The coordination as well as the bond lengths, and angles are similar to the cobalt(II) chloride complex with bis(1*H*-tetrazol-5-yl)methane as ligand instead, however, the aqua ligands are *trans* coordinated.[30]

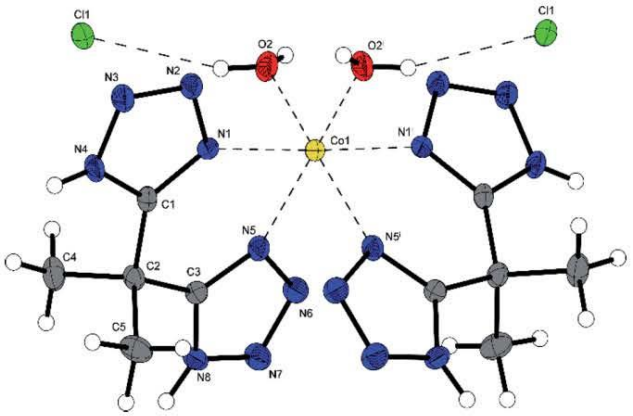


Figure 3. Molecular unit of $[Co(H_2O)_2(5\text{-}DTP)_2]Cl_2$ (**3**). Selected bond lengths /Å: Co1–O2 2.072(2), Co1–N1 2.106(2), Co1–N5 2.132(2); selected bond angles /°: $O2^i$–Co1–O2 97.10(9), O2–Co1–$N1^i$ 89.63(8), O2–Co1–N1 88.74(8), $N1^i$–Co1–N1 177.54(7), $O2^i$–Co1–N5 169.26(9), O2–Co1–N5 90.42(9), $N1^i$–Co1–N5 99.00(8), N1–Co1–N5 82.85(8), $O2^i$–Co1–$N5^i$ 90.42(9), O2–Co1–$N5^i$ 169.26(9), N5–Co1–$N5^i$ 83.22(8). Symmetry code: (i) 1–x, y, 0.5–z.

Coordination compound **4** crystallizes in the monoclinic space group *P2/n* with four formula units per unit cell and a calculated density of 1.683 g·cm^{-3} at 173 K (Figure 4). Complex **4** shows a similar coordination sphere like the cobalt(II) based complex **3** with two asymmetric unit cells per molecular unit and an octahedron built up by two aqua ligands and two chelating 5-DTP units.

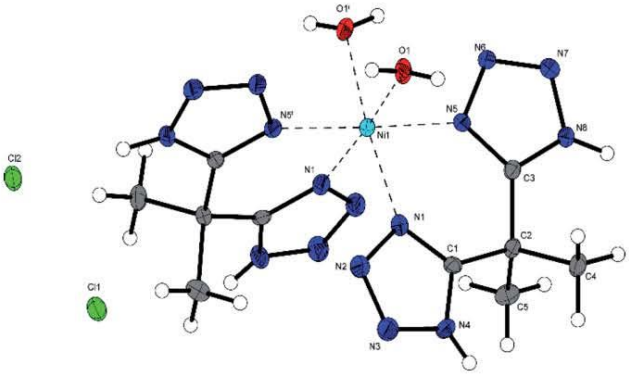


Figure 4. Molecular unit of $[Ni(H_2O)_2(5\text{-}DTP)_2]Cl_2$ (**4**). Selected bond lengths /Å: Ni1–N5 2.049 (2), Ni1–O1 2.070(22), Ni1–N1 2.071(22); selected bond angles /°: N5–Ni1–$N5^i$ 177.84(9), N5–Ni1–O1 89.81(10), N5–Ni1–$O1^i$ 88.64(10), O1–Ni1–$O1^i$ 88.15(10), N5–Ni1–N1 85.09(9), $N5^i$–Ni1–N1 96.48(9), O1–Ni1–N1 92.35(10), $O1^i$–Ni1–N1 173.70(10), N5–Ni1–$N1^i$ 96.48(9), N1–Ni1–$N1^i$ 87.84(10). Symmetry code: (i) 1.5–x, y, 0.5–z.

$[Cu(H_2O)(5\text{-}DTP)_2](NO_3)_2$ (**5**) crystallizes in the monoclinic space group $P2_1/c$ with four formula units per unit cell and a calculated density of 1.808 g·cm^{-3} at 173 K. The central copper(II) atom is surrounded by one aqua ligand and two 5-DTP. Compared to the trigonal bipyramidal coordinated copper(II) chloride complex **2**, a distorted square pyramidal structure with an aqua ligand in axial position and 5-DTP ligands in a plane (Figure 5) can be observed.

Two *cis* coordinating aqua ligands and two *cis* chelating 5-DTP form the octahedral nickel(II) complex **8**, which crystallizes in the monoclinic space group *P2/c* with four formula units per unit cell and a calculated density of 1.719 g·cm^{-3} at 173 K (Figure 6). The molecular unit is built up by two asymmetric unit cells.

Compound **9** (Figure 7) crystallizes in the form of colorless rods in the triclinic space group $P\bar{1}$ with one formula unit per unit cell and a calculated density of 1.736 g·cm^{-3} at 173 K. The molecular unit is built up by two asymmetric unit cells. The central zinc(II) atom is octahedrally surrounded by two aqua ligands, and two chelating 5-DTP ligands. The analogous zinc(II) complex with bis(1*H*-tetrazol-5-yl)methane as ligand instead of 5-DTP, shows nearly the same coordination sphere.[30]

The perchlorate complex **10** crystallizes in the monoclinic space group *C2/c* with eight formula units per unit cell and a calculated density of 1.848 g·cm^{-3} at 173 K. An aqua ligand in

 © 2019 WILEY-VCH Verlag GmbH & Co. KGaA, Weinheim

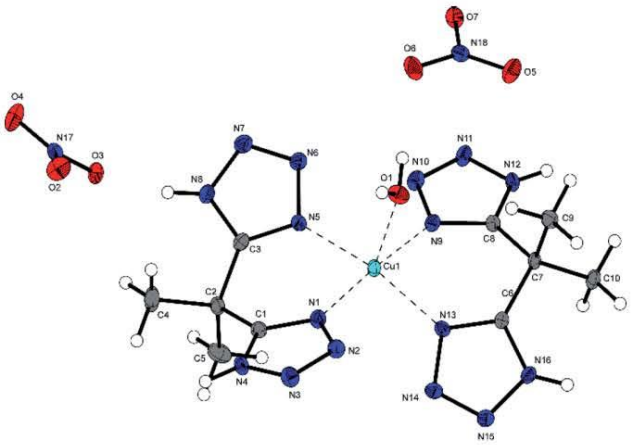


Figure 5. Molecular unit of $[Cu(H_2O)(5\text{-DTP})_2](NO_3)_2$ (**5**). Selected bond lengths /Å: Cu1–N13 1.985(19), Cu1–N5 1.986(19), Cu1–N1 2.002(19), Cu1–N9 2.034(19), Cu1–O1 2.198(2); selected bond angles /°: N13–Cu1–N5 166.20(8), N13–Cu1–N1 92.60(8), N5–Cu1–N1 84.81(8), N13–Cu1–N9 84.59(8), N5–Cu1–N9 97.07(8), N1–Cu1–N9 175.45(8), N13–Cu1–O1 100.87(8), N5–Cu1–O1 92.92(8), N1–Cu1–O1 98.41(8), N9–Cu1–O1 85.66(8).

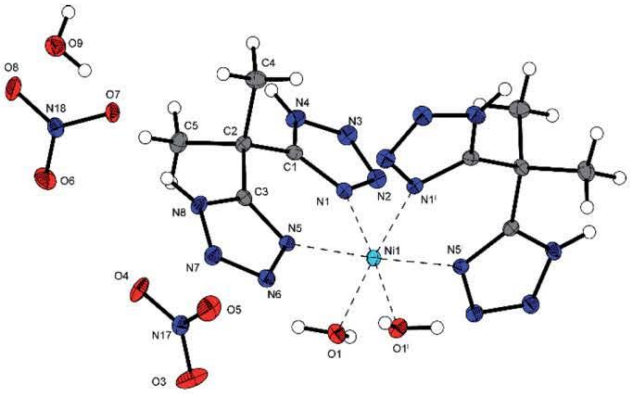


Figure 6. Molecular unit of $[Ni(H_2O)_2(5\text{-DTP})_2](NO_3)_2{\cdot}H_2O$ (**8**). Selected bond lengths /Å: Ni1–N5 2.052(18), Ni1–N1 2.075(2), Ni1–O1 2.080(18); selected bond angles /°: $N5^i$–Ni1–N5 176.38(6), $N5^i$–Ni1–N1 92.05(7), N5–Ni1–N1 85.41(7), N5–Ni1–O1 90.22(7), N1–Ni1–O1 91.52(75), N1–Ni1–$N1^i$ 91.05(80), $N5^i$–Ni1–O1 92.42(72), N5–Ni1–O1 90.22(72), N1–Ni1–O1 91.52(8). Symmetry codes: (i) 1–x, y, 0.5–z.

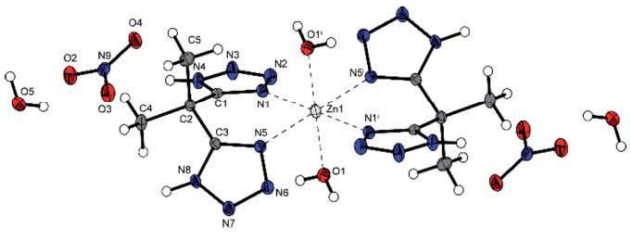


Figure 7. Molecular unit of $[Zn(H_2O)_2(5\text{-DTP})_2](NO_3)_2{\cdot}2\ H_2O$ (**9**). Selected bond lengths /Å: Zn1–N5 2.131(2), Zn1–N1 2.145(19), Zn1–O1 2.149(2); selected bond angles /°: $N5^i$–Zn1–N1 97.13(8), N5–Zn1–N1 82.87(8), N5i–Zn1–O1 91.37(9), N5–Zn1–O1 88.63(9), N1–Zn1–O1 86.85(8), $N1^i$–Zn1–O1 93.15(8). Symmetry code: (i) –x, –y, 2–z.

axial position and two 5-DTP ligands in a plane are forming a distorted square-pyramidal coordination sphere (Figure 8). Independently of the counter anion, copper(II) complexes with 5-DTP prefer pentacoordinate structures, illustrated by compound **2** and **5**, in contrast to bis(1*H*-tetrazol-5-yl)methane based complexes, forming octahedral shaped coordination spheres.[30]

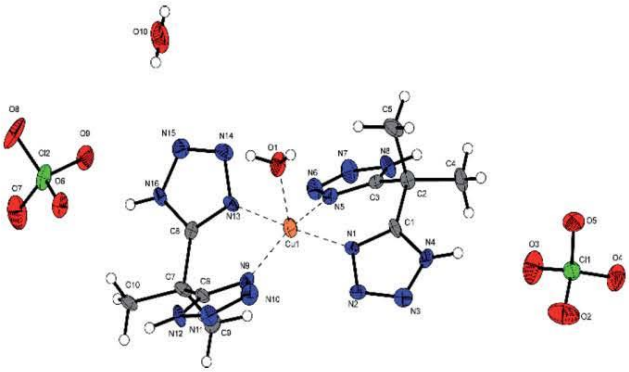


Figure 8. Molecular unit of $[Cu(H_2O)(5\text{-DTP})_2](ClO_4)_2{\cdot}H_2O$ (**10**). Selected bond lengths /Å: Cu1–O1 2.254(5), Cu1–N5 1.979(6), Cu1–N1 1.988(7), Cu1–N9 2.024(6), Cu1–N13 1.983(7); selected bond angles /°: N5–Cu1–N1 87.0(3), N1–Cu1–N9 97.7(3), N9–Cu1–N13 86.2(3), N13–Cu1–N5 89.4(3), O1–Cu1–N5 107.8(2), O1–Cu1–N13 89.7(2), N9–Cu1–N5 158.9(3), N1–Cu1–N13 176.1(3).

The zinc(II) complex **13** (Figure 9) crystallizes in the form of colorless rods in the monoclinic space group *I*2 with two formula units per unit cell and a calculated density of 1.807 g·cm^{-3} at 173 K. The molecular unit is built up by two asymmetric unit cells. Similar to previously discussed copper(II) complexes, compound **13** shows a pentacoordinate central metal(II). Again, already observed for complex **2**, a trigonal bipyramidal coordination sphere is formed.

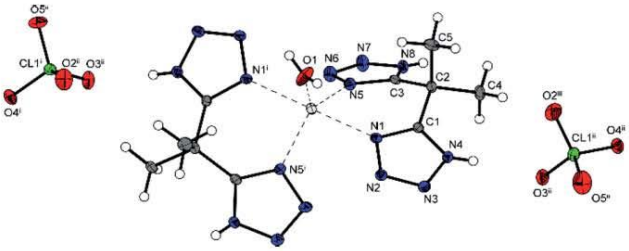


Figure 9. Molecular unit of $[Zn(H_2O)(5\text{-DTP})_2](ClO_4)_2$ (**13**). Selected bond lengths /Å: Zn–N1 2.170(3), Zn–N5 2.024(3), Zn–O1 1.990(4); selected bond angles /°: N1–Zn–N5 84.85(13), N1–Zn–$N5^i$ 95.51(13), O1–Zn–N1 89.67(8), O1–Zn–N5 122.79(8), $N5^i$–Zn–N5 114.43(12), N1–Zn–$N1^i$ 179.35(12). Symmetry codes: (i) –x, y, 2–z; (ii) –0.5+x, –0.5+y, 0.5+z; (iii) 0.5+x, 0.5+y, –0.5+z.

The pentacoordinate complex **15** crystallizes in the form of blue needles in the monoclinic space group $P2_1/c$ with four formula units per unit cell and a calculated density of 1.776 g·cm^{-3} at 133 K (Figure 10). The structure is rather square pyramidal with an aqua ligand in axial position and two 5-DTP ligands in a plane, but could also be treated as highly disordered trigonal bipyramidal with the same configuration

 © 2019 WILEY-VCH Verlag GmbH & Co. KGaA, Weinheim

observed for complex **13** and copper(II) instead of zinc(II) as transition metal(II).

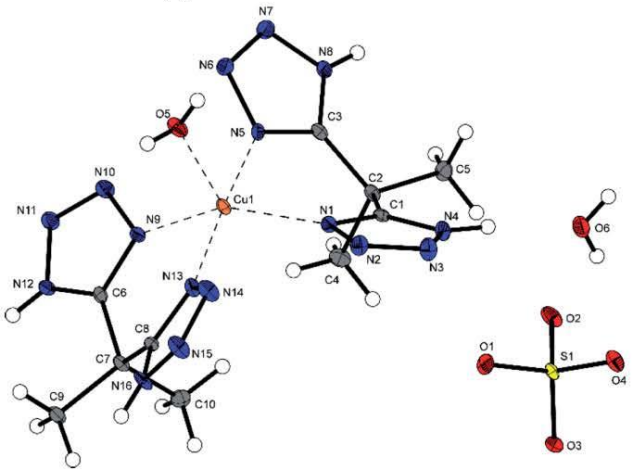


Figure 10. Molecular unit of $[Cu(H_2O)(5\text{-DTP})_2]SO_4{\cdot}H_2O$ (**15**). Selected bond lengths /Å: Cu1–N13 1.989(3), Cu1–N5 1.991(3), Cu1–N1 2.022(3), Cu1–N9 2.038(3), Cu1–O5 2.066(3); selected bond angles /°: N13–Cu1–N5 175.12(11), N13–Cu1–N1 92.99(11), N5–Cu1–N1 85.33(11), N13–Cu1–N9 85.09(11), N5–Cu1–N9 93.68(11), N1–Cu1–N9 145.34(11), N13–Cu1–O5 94.54(12), N5–Cu1–O5 90.33(12), N1–Cu1–O5 114.50(11), N9–Cu1–O5 100.14(11).

Sensitivities and Thermal Stabilities

The thermal stabilities of all compounds were determined by differential thermal analysis (DTA) with a heating rate of β = 5 K·min^{-1} (Table 1). DTA plots are available in the Supporting Information (Figures S8–S10). Most of the complexes show decomposition temperatures comparable to the free ligand **1** (250 °C) or even higher. Especially the chloride (**2** and **3**), sulfate (**15**), perchlorate (**10**, and **13**), and the nitrate complexes (**5** and **6**) exhibit very high exothermic decomposition temperatures (225–293 °C). The other nitrate and perchlorate compounds (**7**–**9**, **12**, and **14**) are less stable toward heat (163–206 °C).

Table 1. Thermal stability measurements of **1**–**15** by DTA [a].

Compound	$T_{endo1.}$ [b] /°C	$T_{endo2.}$ [b] /°C	$T_{exo.}$ [c] /°C
$C_5H_8N_8$ (**1**)	235	–	235
2	92	–	259
3	194	–	253
4	207	–	207
5	172	–	293
6	125	–	267
7	–	–	203
8	126	–	163
9	107	–	170
10	138	168	251
11	88	–	206
12	159	–	190
13	–	–	256
14	145	–	176
15	162	188	225

a) Onset temperature at a heating rate of 5 K·min^{-1}. b) Endothermic peak, which indicates melting, vaporization, dehydration, or loss of aqua ligands. c) Exothermic peak, which indicates decomposition.

The sensitivities toward impact, friction, and electrostatic discharge were investigated for all complexes **2**–**15** and the corresponding free ligand **1**. An overview is given in Table 2. The free ligand **1** is, according to UN standards, "insensitive" toward friction and electrostatic discharge with values greater than 360 N for friction and greater than 1.50 J for ESD, but "sensitive" toward impact (25 J).[36] The chloride and sulfate complexes **2**–**4** and **15** with coordinating 5-DTP are "insensitive" toward impact (≥ 40 J), friction (> 360 N) and electrostatic discharge (≥ 0.75 J). Substitution of chloride by nitrate (**5**–**9**) increases the sensitivities. Values of 5–10 J for impact, ≥ 324 N for friction and ≥ 0.15 J for ESD were measured. Replacing nitrate by perchlorate (**10**–**14**) decreases, as expected, the stability toward impact (< 1–12.5 J), friction (10–72 N), and ESD (0.065–0.50 J), whereby some complexes, such as compound **10** and **13**, are very sensitive toward impact, but still practicable without substantial risk.

Table 2. Sensitivities toward impact, friction, and ESD of **1**–**15**.

Compound	IS [d] /J	FS [e] /N	ESD [f] /J
1 [b]	30	> 360	1.50
2 [b]	> 40	> 360	1.50
3 [c]	> 40	> 360	1.50
4 [c]	> 40	> 360	1.50
5 [a]	8	360	1.50
6 [b]	10	> 360	1.50
7 [c]	5	324	1.50
8 [b]	10	360	0.15
9 [b]	40	> 360	0.20
10 [c]	3	10	0.065
11 [c]	12.5	72	0.50
12 [c]	20	216	0.75 [g]
13 [a]	2	20	0.20
14 [b]	< 1	15	0.10
15 [b]	> 40	> 360	0.75

a) Determined at a grain size < 100 µm. b) Determined at a grain size 100–500 µm. c) Determined at a grain size 500–1000 µm. d) Impact sensitivity according to the BAM Drophammer (method 1 of 6). e) Friction sensitivity according to the BAM friction tester (method 1 of 6). f) Electrostatic discharge sensitivity (OZM ESD tester). g) Electrostatic discharge sensitivity (OZM Electric Spark XSpark10).

Hot plate and hot needle tests of the most promising compounds **10** and **13** were performed to get an insight into the compounds' behavior during fast heating with and without confinement. For both tested compounds, only deflagrations could be observed during hot plate as well as hot needle tests (Figure 11, Figures S11 and S12, Supporting Information).

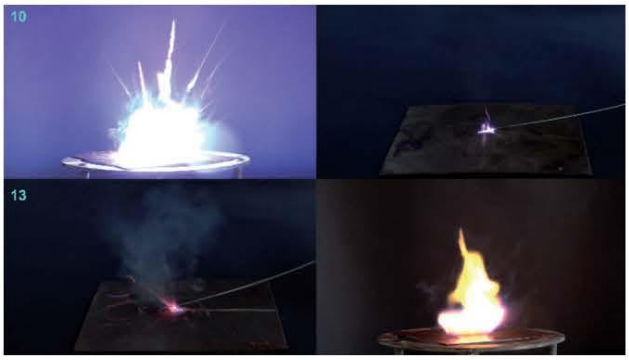


Figure 11. Upper side: moment of deflagration of **10** during the hot plate and hot needle test. Bottom side: deflagration of complex **13** during hot needle and hot needle test.

© 2019 WILEY-VCH Verlag GmbH & Co. KGaA, Weinheim

Laser Ignition Experiments

Laser ignition is a modern way of initiation of energetic materials, which shows various advantages over classical approaches. Cobalt(III) amine complexes have shown good results in laser ignition tests, as well as some copper(II) complexes in the past.[32,37] The confined samples of **10** and **14** were irradiated at a wavelength of 915 nm, a pulse length of 15 ms (1 ms for **10**), a current of 7 A for **10**, 9 A for **14**, and a voltage of 4 V, which results in an approximately energy output of 0.7–37.5 mJ. Other compounds were not tested due to their low sensitivities toward other initiation impulses and the consequently expected negative laser ignition test. An overview of the results is given in Table 3. UV/Vis spectra of **10**, **13**, and **14** were measured in liquid in the corresponding acid. Details on the measurement and spectra are available in the Supporting Information (Figure S13)

Table 3. Results of the laser ignition tests [a].

	I /A	τ /ms	Result
10	7	1	det.
10	7	15	det.
14	9	15	deflag.

a) det. = detonation; deflag. = deflagration. Operating parameters: current I = 7–9 A, voltage U = 4 V; theoretical output power P_{max} = 45 W; theoretical energy E_{max} = 0.70–37.5 mJ; wavelength λ = 915 mm; pulse length τ = 1–15 ms.

The copper(II) perchlorate complex **10** detonated under both applied energy inputs, whereas compound **14** showed only a deflagration during the laser ignition experiment (Figure 12). The copper(II) complex is, therefore, a valuable photosensitive energetic coordination compound with manageable sensitivities and holds great promise for possible future applications.

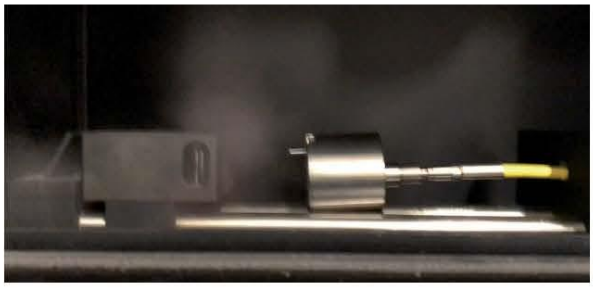


Figure 12. Moment of detonation of complex **10** during the laser initiation experiment.

Conclusions

The nitrogen-rich ligand 2,2-bis(5-tetrazolyl)propane (5-DTP) (**1**) was synthesized in high purity and characterized by multinuclear NMR spectroscopy (^{1}H, ^{13}C). Furthermore, **1** was investigated by X-ray diffraction, elemental analysis, IR spectroscopy, differential thermal analysis together with its sensitivities toward various stimuli (impact, friction, ESD). The aim of this work was to develop new photosensitive and environmentally friendly primary explosives by combining different transition metal(II) salts with the prepared nitrogen-rich ligand. The synthetic route toward these new energetic coordination compounds is simple, cost-efficient, and environmentally benign. All newly synthesized coordination compounds except **16** were characterized by IR spectroscopy, elemental analysis, DTA and sensitivity measurements. The X-ray crystal structure of 15 complexes could be determined to get an insight into the fascinating coordination behavior. Adjustment of the optical and energetic properties could be achieved through the variation of the anion (chloride, nitrate, sulfate, or perchlorate) and the late 3d transition metals. The compounds show captivating structures, building distorted coordination spheres caused by the chelating ligand. Most of the complexes show good thermal stabilities. Especially the most interesting coordination compounds **10** and **13** possess very high exothermic decomposition temperatures above 250 °C, while both show manageable sensitivities toward impact, friction, and ESD. Furthermore, copper(II) compound **10** (IS: 3 J, FS: 10 N, ESD: 0.065 J) was successfully initiated in laser experiments with a very low energy input of only 0.7 mJ, making it to a promising candidate as laser ignitable explosive.

Supporting Information (see footnote on the first page of this article): X-ray data, IR spectra, DTA plots, UV/Vis spectra, experimental methods.

Acknowledgements

Financial support of this work by the Ludwig-Maximilian University of Munich (LMU) and the Office of Naval Research (ONR) under grant no. ONR.N00014–16–1-2062 is acknowledged. The authors want to thank *Florian Binder* for his great contribution to this work.

Keywords: Coordination chemistry; Laser ignition; 2,2-Bis(5-tetrazolyl)propane; Primary explosives; Transition metal complexes

References

[1] https://echa.europa.eu/de/candidate-list-Table, accessed May **2018**.
[2] Q. Jun-Sheng, B. Shao-Juan, L. Peng, X. Wei, D. Dong-Ying, Z. Liang, L. Ya-Qian, S. Zhong-Min, *Chem. Asian J.* **2014**, *9*, 749–753.
[3] A. Rudavskyi, R. W. A. Havenith, R. Broer, C. de Graaf, C. Sousa, *Dalton Trans.* **2013**, *42*, 14702–14709.
[4] L. Shenghua, W. Yuan, Q. Cai, Z. Xiuxiu, Z. Jichuan, Z. Shaowen, P. Siping, *Angew. Chem. Int. Ed.* **2013**, *52*, 14031–14035.
[5] V. Y. Zubarev, E. V. Bezklubnaya, A. K. Pyartman, R. E. Trifonov, V. A. Ostrovskii, *Chem. Heterocycl. Compd.* **2003**, *39*, 1317–1325.
[6] V. Y. Zubarev, R. E. Trifonov, V. V. Poborchii, V. A. Ostrovskii, *Chem. Heterocycl. Compd.* **2006**, *42*, 469–474.
[7] V. A. Ostrovskii, R. E. Trifonov, E. A. Popova, *Russ. Chem. Bull.* **2012**, *121*, 768–780.
[8] G. R. Marshall, D. J. Kuster, Y. Che, *Methods Mol. Biol.* **2009**, *575*, 123–158.
[9] R. J. Herr, *Bioorg. Med. Chem.* **2002**, *10*, 3379–3393.
[10] R. Trifonov, M. Trukhnitskaya, A. Tarkhanova, I. Vikhrova, V. Ostrovskii, *Russ. J. Org. Chem.* **2006**, *42*, 1059–1062.

 © 2019 WILEY-VCH Verlag GmbH & Co. KGaA, Weinheim

[11] B. Le Bourdonnec, E. Meulon, S. Yous, J.-F. Goossens, R. Houssin, J.-P. Hénichart, *J. Med. Chem.* **2000**, *43*, 2685–2697.
[12] J. R. Anacona, P. Alvarez, *Transition Met. Chem.* **2002**, *27*, 856–860.
[13] C. N. S. S. P. Kumar, D. K. Parida, A. Santhoshi, A. K. Kota, B. Sridhar, V. J. Rao, *MedChemComm* **2011**, *2*, 486–492.
[14] A. D. Abell, G. J. Foulds, *J. Chem. Soc. Perkin Trans. 1* **1997**, 2475–2482.
[15] B. C. H. May, A. D. Abell, *J. Chem. Soc. Perkin Trans. 1* **2002**, 172–178.
[16] M. Joas, T. M. Klapötke, J. Stierstorfer, N. Szimhardt, *Chem. Eur. J.* **2013**, *19*, 9995–10003.
[17] T. W. Myers, J. A. Bjorgaard, K. E. Brown, D. E. Chavez, S. K. Hanson, R. J. Scharff, S. Tretiak, J. M. Veauthier, *J. Am. Chem. Soc.* **2016**, *138*, 4685–4692.
[18] A. A. Brish, B. N. Zaitsev, E. A. Sbitnev, L. V. Tatarintsev, *Fiz. Goreniya Vzryva* **1966**, *2*, 132–133.
[19] A. A. Brish, B. N. Zaitsev, E. A. Sbitnev, L. V. Tatarintsev, *Fiz. Goreniya Vzryva* **1969**, *5*, 475–480.
[20] L. C. Yang, V. J. Menichelli, *Appl. Phys. Lett.* **1971**, *19*, 473–475.
[21] E. S. Hafenrichter, B. Marshall, K. J. Fleming, Fast Laser Diode Ignition of CP and BNCP, in *Proceedings of the 29th International Pyrotechnics Seminar*, Westminster, CO, July 14–19, **2002**; IPSUSA, **2002**; pp 787–793.
[22] P. W. Cooper, *Explosives Engineering*, Wiley-VCH: Weinheim, **1996**.
[23] S. C. Kunz, F. J. Salas, Diode Laser Ignition of High Explosives and Pyrotechnics, in *Proceedings of the 13th International Pyrotechnics Seminar*, Grand Junction, CO, July 11–15, 1988; IIT Research Insitute: Chicago, IL, 1988; pp 505–523.
[24] J. A. Merson, F. J. Salas; J. G. Harlan, The Development of Laser ignited Deflagaration-to-Detonation Transition (DDT) Detonators and Pyrotechnic Actuators, in *Proceedings of the 19th International Pyrotechnics Seminar*, Christchurch, New Zealand, Feb 20–25, 1994; IPS, 1994; pp 191–206.
[25] A. Y. Zhilin, M. A. Ilyushin, I. V. Tselinskii, A. S. Kozlov, I. S. Lisker, *Russ. J. Appl. Chem.* **2003**, *76*, 572–576.
[26] J. Evers, I. Gospodinov, M. Joas, T. M. Klapötke, J. Stierstorfer, *Inorg. Chem.* **2014**, *53*, 11749–11756.
[27] A. Y. Zhilin, M. A. Ilyushin, I. V. Tselinskii, A. S. Brykov, *Russ. J. Appl. Chem.* **2001**, *74*, 99–102.
[28] A. V. Smirnov, M. A. Ilyushin, I. V. Tselinskii, *Russ. J. Appl. Chem.* **2004**, *77*, 794–796.
[29] T. W. Myers, K. E. Brown, D. E. Chavez, R. J. Scharff, J. M. Veauthier, *Eur. J. Inorg. Chem.* **2016**, *2016*, 3178–3183.
[30] M. Freis, T. M. Klapötke, J. Stierstorfer, N. Szimhardt, *Inorg. Chem.* **2017**, *56*, 7936–7947.
[31] Z. P. Demko, K. B. Sharpless, *J. Org. Chem.* **2001**, *66*, 7945–7950.
[32] Crystallographic data (excluding structure factors) for the structures in this paper have been deposited with the Cambridge Crystallographic Data Centre, CCDC, 12 Union Road, Cambridge CB21EZ, UK. Copies of the data can be obtained free of charge on quoting the depository numbers CCDC-1850236 (**1**), CCDC-1850244 (**2**), CCDC-1850246 (**3**), CCDC-1850239 (**4**), CCDC-1850243 (**5**), CCDC-1850238 (**8**), CCDC-1850237 (**9**), CCDC-1850245 (**10**), CCDC-1850242 (**13**), CCDC-1850241 (**15**), and CCDC-1850240 (**16**) (Fax: +44-1223-336-033; E-Mail: deposit@ccdc.cam.ac.uk, http://www.ccdc.cam.ac.uk).
[33] D. Chand, D. A. Parrish, J. M. Shreeve, *J. Mater. Chem. A* **2013**, *1*, 15383–15389.
[34] C. A. K. Diop, M. F. Mahon, K. C. Molloy, L. Ooi, P. R. Raithby, M. M. Venter, S. J. Teat, *CrystEngComm* **2002**, *4*, 462–466.
[35] J. Brugger, D. C. McPhail, J. Black, L. Spiccia, *Geochim. Cosmochim. Acta* **2001**, *65*, 2691–2708.
[36] Impact: insensitive >40 J, less sensitive ≥ 35 J, sensitive ≥ 4 J and very sensitive ≤ 3J; friction: insensitive >360 N, less sensitive = 360 N, sensitive <360 N and >80 N, very sensitive ≤ 80 N and extremely sensitive ≤ 10 N. According to the UN Recommendations on the Transport of Dangerous Goods.
[37] A. Y. Zhilin, M. A. Ilyushin, I. V. Tselinskii, A. S. Kozlov, N. E. Kuz′mina, *Russ. J. Appl. Chem.* **2002**, *75*, 1849–1851.

Received: July 2, 2018
Published online: September 11, 2018

 © 2019 WILEY-VCH Verlag GmbH & Co. KGaA, Weinheim

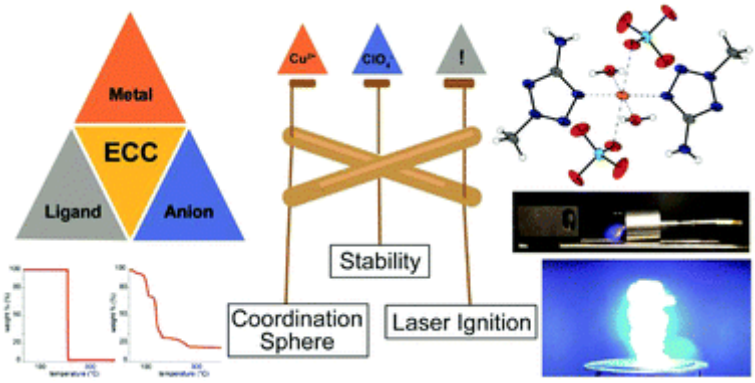
Appendix 8

2-Methyl-substituted monotetrazoles in copper(II) perchlorate complexes: manipulating coordination chemistry and derived energetic properties

L. Zeisel N. Szimhardt, Maximilian H. H. Wurzenberger, T. M. Klapötke, J. Stierstorfer

New. J. Chem. **2019**, *43*, 609–616.

https://doi.org/10.1039/c8nj05375h



Supplementary Information:
https://www.rsc.org/suppdata/c8/nj/c8nj05375h/c8nj05375h1.pdf

Published on 27 November 2018. Downloaded by Ludwig Maximilians Universitaet Muenchen on 2/16/2022 8:00:53 AM.

NJC

PAPER

View Article Online
View Journal | View Issue

Check for updates

Cite this: *New J. Chem.*, 2019, **43**, 609

2-Methyl-substituted monotetrazoles in copper(II) perchlorate complexes: manipulating coordination chemistry and derived energetic properties†‡

Lukas Zeisel, Norbert Szimhardt, Maximilian H. H. Wurzenberger, Thomas M. Klapötke and Jörg Stierstorfer *

Received 23rd October 2018,
Accepted 26th November 2018

DOI: 10.1039/c8nj05375h

rsc.li/njc

A proposed correlation between coordination chemistry and deduced energetic properties (thermal behaviour, and sensitivities towards mechanical and optical stimuli) of copper(II) complexes is investigated. Starting from a system comprising $Cu(ClO_4)_2$ and either of the ligands 2-methyl-5-aminotetrazole (**1**, 2-MAT) or 2-methyl-5*H*-tetrazole (**2**, 2-MTZ), typically altered parameters like the metal(II) centre, ligand, or counterion were predefined. Instead, solely slight changes in ligand concentration and the solvent system were implemented in order to provide an insight into structure–property relationships of energetic coordination compounds (ECC) of this type. As a result, five highly energetic complexes $[Cu(H_2O)_2(2\text{-MAT})_4](ClO_4)_2\cdot H_2O$ (**3**), $[Cu(H_2O)_2(2\text{-MAT})_4](ClO_4)_2$ (**4**), $[Cu(H_2O)_2(2\text{-MAT})_4](ClO_4)_2\cdot 2$ 2-MAT (**5**), $[Cu(ClO_4)_2(H_2O)_2(2\text{-MAT})_2]$ (**6**), and $[Cu(H_2O)_2(2\text{-MTZ})_4](ClO_4)_2$ (**7**) were synthesized and, except for **5**, elaborately characterized. Besides structural elucidation *via* X-ray diffraction, NIR-spectroscopy, differential thermal analysis (DTA), standard sensitivity measurements (impact, friction, and electrostatic discharge), UV/vis-spectroscopy, and optical initiation experiments were conducted to deduce a precise relationship between coordination chemistry and the consequential energetic characteristics of these complexes.

Introduction

Dominated by the oxidation states +I and +II, copper exhibits diverse coordination chemistry. Especially the d^9 Cu^{II} cation is commonly applied in many areas of chemistry as the metal center of coloring agents,[1] insecticides,[2,3] catalysts,[4] and metalloproteins.[5] In most of these cases, copper(II)'s coordination chemistry is influenced by oxygen- and nitrogen-donating ligands, typically forming square planar, tetrahedral and, predominantly, octahedral coordination environments.[3]

In recent years, the growing field of energetic coordination compounds (ECC) has greatly benefited from promising Cu^{II} complexes. Due to the urgent necessity of substituting commonly applied, toxic primary explosives like lead azide and lead styphnate, an approach using significantly less toxic transition metal complexes appeared to be highly encouraging.[6]

Department of Chemistry, Ludwig Maximilian University Munich, Butenandtstrasse 5–13, Haus D, D-81377 Munich, Germany. E-mail: jstch@cup.uni-muenchen.de

† Dedicated to Prof. Dr Ingo-Peter Lorenz on the occasion of his 75th birthday.

‡ Electronic supplementary information (ESI) available: Experimental and general methods, X-ray diffraction, IR spectroscopy, DTA plots, TGA plots of **1–4**, hot plate and hot needle tests, and laser ignition tests. CCDC 1850124 (**3**), 1850121 (**4**), 1850122 (**5**), 1850120 (**6**) 1850123 (**7**). For ESI and crystallographic data in CIF or other electronic format see DOI: 10.1039/c8nj05375h

In recent years, seminal reports from Shreeve,[7] Myers,[8] and Klapötke[9] set the stage for future applications of ECC. In targeting novel transition metal complexes with auspicious properties (convenient accessibility, thermal stability, and safe initiation), a consistently implemented general approach has emerged: starting from a desired transition metal cation with the corresponding counter-anion, energetic ligands, as well as the applied reaction conditions, offer precise tailoring of the desired characteristics.[7–9] Whereas variation of parameters like the ligand, metal centre, and anion tend to distinctly influence the coordination chemistry and the complexes' properties, additional fine tuning towards desired attributes might be achieved by accurately controlling the applied reaction conditions. While initial experiments in this direction have already led to sought results, a comprehensive report is still anticipated until today.[9b–12]

In regard to previously applied ligand systems, mostly nitrogen-rich, endothermic heterocycles were considered.[7–16] Among others, mono-substituted tetrazoles like the highly energetic 1,5-diaminotetrazole (1,5-DAT), 1-amino-5*H*-tetrazole (1-AT) and 2-amino-5*H*-tetrazole (2-AT) as well as 1-methyl-5*H*-tetrazole (1-MTZ) and 1-methyl-5-aminotetrazole (1-MAT) were investigated as ligands in ECC (Chart 1).[10,13,14] Hereby, the obtained transition metal complexes proved to be highly energetic, readily

Published on 27 November 2018. Downloaded by Ludwig Maximilians Universitaet Muenchen on 2/16/2022 8:00:53 AM.

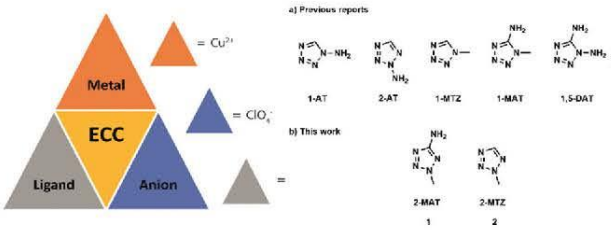
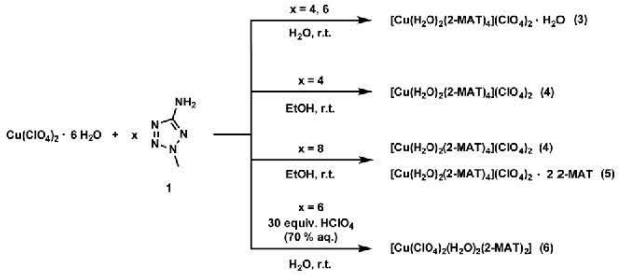


Chart 1 Precedents and current work using energetic monotetrazoles in ECC.



Scheme 1 Synthesis of complexes **3–6** using 2-methyl-5-aminotetrazole (**1**).

synthesized and partially exhibited auspicious properties as laser-ignitable primary explosives.[10,13]

Based on these results, the present work aims for a deeper insight into the possibility of precisely manipulating an ECC's coordination chemistry and the resulting energetic properties (sensitivities, thermal properties, and laser initiation) by solely modifying the reaction conditions (ligand concentration, solvent, and additives) in hand. Predefinitions for the applied systems included copper(II) as metal species, perchlorate counter-anions and, as an extension to previously published reports, 2-methyl-5-aminotetrazole (**1**, 2-MAT, $\Delta_f H^0_{(g)}$ = 2802 kJ kg^{-1})[17] and 2-methyl-5*H*-tetrazole (**2**, 2-MTZ, $\Delta_f H^0_{(g)}$ (2-MTZ) = 3347 kJ kg^{-1})[17] as endothermic ligands. Both nitrogen-rich heterocycles are expected to allow comparison to the respective 1-substituted tetrazoles and their energetic metal complexes. While recently published results from Szimhardt *et al.* provide a comprehensive study of 1-MTZ and its transition metal complexes,[10] only a few examples of 1-MAT ECC have been reported alongside a range of corresponding tetrazolium salts.[18–20] Moreover, and in relation to related, tremendously sensitive 2-aminotetrazole complexes,[13] 2-MAT and 2-MTZ incorporating ECC are proposed to combine efficient optical initiation with enhanced stability towards mechanical stimuli, thus allowing safe handling of these materials.

Results and discussion

Synthesis

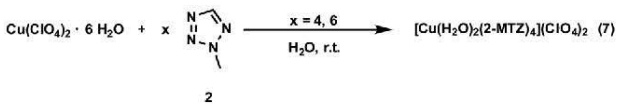
Initially, nitrogen-rich ligand **1** was synthesized *via* a convenient, single step reaction using commercially available 5-aminotetrazole as a starting material (see Scheme S1, ESI‡). Due to the tautomerization of 1,5*H*-tetrazole, the dimethylsulfate-mediated methylation step provided the desired ligand alongside 1-methyl-5-aminotetrazole in a ratio of 3 : 4. With the targeted 2-MAT in hand, initial investigations concerning its coordination chemistry were accessed (Scheme 1).

The performed reactions were carried out at ambient temperature by slowly adding pre-dissolved ligand to a solution of copper(II) perchlorate. By solely applying a minimal amount of solvent, the crystallization process at room temperature could be accelerated. Thereby received solids were filtered off, washed with cold ethanol and dried in air, not requiring further purification.

As a starting point, 6 and 4 equivalents of 2-MAT were applied to an aqueous solution of $Cu(ClO_4)_2$ aiming for a frequently observed hexacoordinate copper(II) center.[10,21] In contrast to that and regardless of the applied ligand concentration, the present reaction provided $[Cu(H_2O)_2(2\text{-MAT})_4](ClO_4)_2 \cdot H_2O$ (**3**) in 52% yield after four days of crystallization. Proceeding from these preliminary results, the utilization of a solvent with decreased polarity was tested. Using ethanol as the reaction medium and 4 equiv. of the ligand indeed led to the isolation of a new complex **4**. Nevertheless and despite successfully preventing the incorporation of cocrystallized water, $[Cu(H_2O)_2(2\text{-MAT})_4](ClO_4)_2$ (**4**) simultaneously retained the actual coordination sphere with two coordinating aqua ligands. To further extend this condition screening, an increased 2-MAT concentration (8 equivalents) was introduced while maintaining ethanol as the solvent. As a result and immediately after combining the ligand and copper(II) perchlorate, a light green precipitate occurred. After filtration, preliminary characterization of the residue by IR spectroscopy confirmed the formation of a previously unknown complex $[Cu(H_2O)_2(2\text{-MAT})_4](ClO_4)_2 \cdot 2$ 2-MAT (**5**) alongside ECC **4**. Since conducted attempts of clean isolation or purification of **5** proved to be unsuccessful, further characterization was impeded. Interestingly, the earlier collected filtrate of the present reaction once again provided **4** after crystallization for six days. A final attempt of interfering with the previously observed coordination chemistry of this system was to apply concentrated perchloric acid. According to reported syntheses, this approach promised a water-free ECC with enhanced energetic characteristics by substituting aqua ligands with coordinating perchlorate counter-anions.[22] Unfortunately, charging the aqueous reaction mixture with 30 equivalents of $HClO_4$ led to complex **6**, which still exhibited coordinating aqua ligands (yield: 76%). In contrast to previously obtained ECC, the coordination sphere of $[Cu(ClO_4)_2(H_2O)_2(2\text{-MAT})_2]$ indeed comprises two copper(II) associated perchlorato anions while solely exhibiting two equivalents of the nitrogen-rich ligand **1**. A possible and reoccurring explanation for a decrease of coordinating tetrazole ligands might be the protonation and simultaneous elimination of an N-coordination site.[9f,12] In comparison to that, the corresponding 1-methyl-5-aminotetrazole exhibited low solubility in water, thus leading to the reoccurring precipitation of the ligand.[19] Moreover, and whenever ligand crystallization could be prevented, collected X-ray data of isolated crystals repeatedly proved the simultaneous presence of multiple ECC species.[19]

 This journal is © The Royal Society of Chemistry and the Centre National de la Recherche Scientifique 2019

Published on 27 November 2018. Downloaded by Ludwig Maximilians Universitaet Muenchen on 2/16/2022 8:00:53 AM.



Scheme 2 Formation of the copper(II) perchlorate complex **7**.

Conclusively, 2-methyl-5*H*-tetrazole (2-MTZ) was investigated as a comparative example for additional 2-substituted monotetrazoles (Scheme 2). The ligand itself was accessed *via* a straightforward two-step reaction starting from basic building blocks (see Scheme S2, ESI‡). Once again, tautomerization led to a significant decrease in the yield of 2-MTZ due to the formation of isomeric 1-methyl-5*H*-tetrazole (1-MTZ) (1-MTZ/2-MTZ = 2 : 1).

When being applied to an aqueous solution of copper(II) perchlorate, 2-MTZ exhibits remarkable similarity to the previously investigated 2-MAT. In comparison to complexes **3** and **4**, $[Cu(H_2O)_2(2\text{-MTZ})_4](ClO_4)_2$ (**7**), which was isolated from the mother liquor after one day (yield: 73%), features almost equivalent coordination chemistry under identical reaction conditions. Moreover, and in contrast to the 2-MAT system, a change of solvent (ethanol) or stoichiometry (x = 4, 6, and 10) exclusively led to the same product **7**. Whenever the metal(II) center was altered (Fe^{2+}, Zn^{2+}, and Mn^{2+}) no crystallization of a potential ECC was achieved. Interestingly, and in accordance with previous reports, 2-substituted tetrazoles as ligands appear to consistently promote the incorporation of aqua ligands.[18b,21] Reasons for this could be the steric hindrance of six tetrazoles coordinating to the transition metal or the thermodynamically and kinetically preferred formation of more inert complexes. However, further studies including thermodynamic calculations are needed for the future.

Crystal structures

Since each of the obtained complexes was obtained as single crystals, structural characterization was conducted using low temperature X-ray diffraction. Measurement and refinement data are provided in the ESI.‡ Additionally, details of the obtained crystal structures were deposited in the CSD database and can be obtained free of charge from the CCDC: 1850124 (**3**), 1850121 (**4**), 1850122 (**5**), 1850120 (**6**), and 1850123 (**7**).‡[23] In terms of the observed coordination geometry, the examined copper(II) centres provided Jahn–Teller distorted octahedra, which consistently exhibited N4-coordinating ligands. Considering calculated electrostatic potentials at the respective ligand's binding sites (Fig. 1), the highest electron density of both 2-MAT and 2-MTZ occurs at the tetrazole's carbon-adjacent nitrogen N4, thus explaining the observed coordination behaviour observed by X-ray diffraction and additionally conducted IR spectroscopy (see ESI,‡ Fig. S1).

Ahead of the comprehensive analysis of received crystal structures it should be stated that structural data of coordinating 2-MAT and 2-MTZ consistently resemble corresponding, literature-known X-ray data of the respective non-coordinating ligand or comparable ECC and are therefore not discussed any further.[24,25]

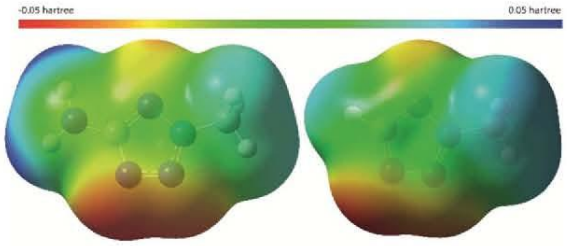


Fig. 1 Calculated (B3LYP/6-31G(d,p)) electrostatic potentials (3D isosurface of electron density) of 2-MAT (**1**, left) and 2-MTZ (**2**, right).

The first of the obtained complexes, $[Cu(H_2O)_2(2\text{-MAT})_4](ClO_4)_2{\cdot}H_2O$ (**3**), crystallizes in the form of blue blocks in the monoclinic space group $C2/c$ with 16 formula units per unit cell and a calculated density of 1.669 g cm^{-3} at 173 K. The Jahn–Teller distorted, octahedral copper(II) coordination sphere comprises two axial aqua and four equatorial 2-MAT ligands (Fig. 2) forming a slightly tilted O–Cu–O axis and a marginally distorted plane, respectively.

In addition to these observations in regard to the structure of a single complex unit, the three-dimensional topology of this compound reveals interesting stacking patterns (Fig. 3).

When viewing along the crystallographic b-axis, a chain pattern with alternating components can be observed. In addition to this ABAB pattern, whose ECC-layers are aligned along the crystallographic c-axis, equally oriented planes of perchlorate anions and cocrystallized water function as H-bond-mediating linkers between adjacent complex layers (Table 1). The aggregation of complexes to said layers equally benefits from intermolecular hydrogen bonding. In addition to that, viewing along the c-axis reveals a similar, but even more complex picture. While exhibiting the same ABAB pattern in between distinguishable chains, B lines further reveal an intrinsic CDCD motif along b.

Crystals of **4** have been isolated in the form of blue blocks in the monoclinic space group $P2_1$ with two formula units per unit

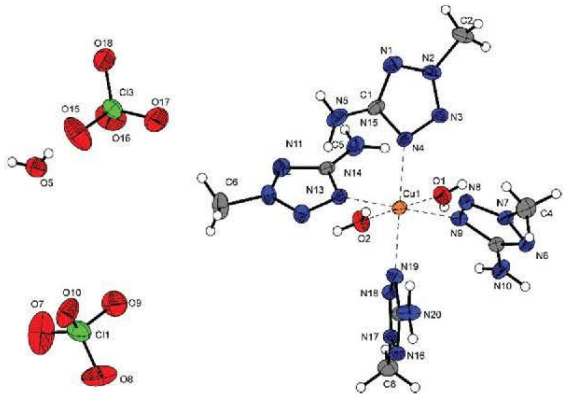


Fig. 2 Molecular unit of complex **3**. Thermal ellipsoids of non-hydrogen atoms in all structures are set to the 50% probability level. Selected bond lengths (Å): O1–Cu1 2.430(6), O2–Cu1 2.363(5), Cu1–N14 2.014(5), Cu1–N19 2.004(4), Cu1–N4 2.003(4), and Cu1–N9 2.008(5); selected bond angles (°): O1–Cu1–O2 177.2(2), N4–Cu1–O1 86.95(19), N4–Cu1–O2 93.91(18), N4–Cu1–N9 91.07(19), N4–Cu1–N14 88.89(19), N14–Cu1–O1 92.9(2), and N9–Cu1–O1 87.2(2).

Published on 27 November 2018. Downloaded by Ludwig Maximilians Universitaet Muenchen on 2/16/2022 8:00:53 AM.

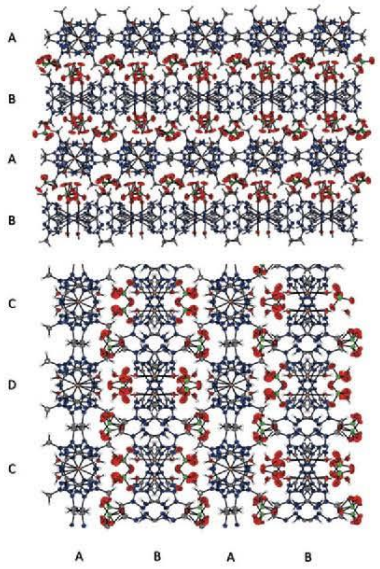


Fig. 3 Structure of **3** with the direction of view along the crystallographic *b*- (top) and *c*-axis (bottom).

Table 1 Lengths and angles of selected hydrogen bonds in **3**

D–H···A	*d*(D–H) [Å]	*d*(H···A) [Å]	*d*(D···A) [Å]	∠D–H···A [°]
N5–H5···N16	0.88	2.27	3.03	144.0
O3–H31···O6	0.83	1.89	2.71	173.6
N15–H15B···O9	0.88	2.57	2.96	107.0
N10–H10A···O9	0.88	2.17	3.02	163.0

cell and a calculated density of 1.788 g cm ^{3} at 173 K. The molecular unit consists of four 2-MAT and two aqua ligands once again resulting in an octahedral coordination sphere (Fig. 4). The corresponding perchlorate anions are non-coordinating. Regarding the appearance of the coordination polyhedron it becomes obvious that there is yet again a Jahn–Teller distortion to be observed along an axis that connects the copper(II) center with the two aqua ligands in axial positions. Considering these first observations it becomes clear that the structural parameters of **4** are almost identical to those of the previously discussed compound **3** with four 2-MAT ligands in the plane. The only significant differences such as the space group and the cell volume are caused by the absence of crystal water molecules. Another slight alteration can be observed regarding the bond angles between the coordinating ligands and copper(II), especially among the aqua and 2-MAT ligands. In the case of **4**, the bond angles approach the 90° of an ideal octahedron.

Crystallizing in the space group $P\bar{1}$, ECC **5** comprises two formula units per unit cell and has a calculated density of 1.699 g cm ^{3} at 173 K. The observed octahedral coordination sphere makes up the molecular unit including four 2-MAT and two aqua ligands. In addition, two equivalents of ligand **1** have been found as cocrystallized species (Fig. 5). Due to the reoccurring Jahn–Teller effect, the bond lengths along the tilted distortion axis O1–Cu1–O2 are significantly longer than those of the metal and the equatorial ligands. Since the equatorial 2-MAT-organized plane is not situated perpendicular on the O1–Cu1 and O2–Cu1 axes, a noticeable deviation from ideal flatness is observed.

As the final representative of the 2-MAT derived complexes, **6** crystallizes in the form of blue rods in the monoclinic space group $P2_1/n$ with two formula units per unit cell and a remarkably high calculated density of 1.997 g cm ^{3} at 173 K. Two asymmetric unit cells make up the molecular unit. The latter consists of a copper(II) center, and two aqua, two perchlorato, and two 2-MAT ligands forming a Jahn–Teller distorted, octahedral coordination sphere (Fig. 6).

The resulting polyhedron is made up of three straight axes which are caused by the fact that the two ligands of each kind coordinate *trans* to one another. The remaining four ligands are

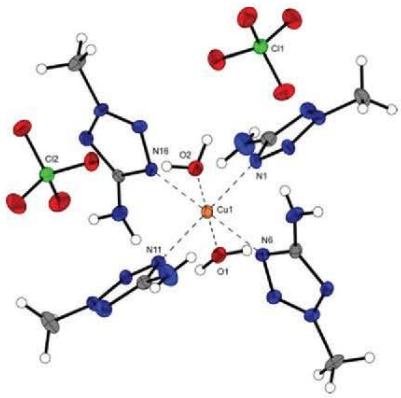


Fig. 4 Molecular unit of $[Cu(H_2O)_2(2\text{-MAT})_4](ClO_4)_2$ (**4**). Selected bond lengths (Å): O1–Cu1 2.417(5), O2–Cu1 2.397(5), N1–Cu1 1.999(5), N6–Cu1 2.049(6), N11–Cu1 2.000(5), and N16–Cu1 2.065(6); selected bond angles (°): O1–Cu1–O2 179.34(19), N1–Cu1–O1 87.6(2), N1–Cu1–O2 91.9(2), N6–Cu1–O1 88.2(2), N6–Cu1–O2 92.2(2), N16–Cu1–O1 90.85(19), and N16–Cu1–O2 88.8(2).

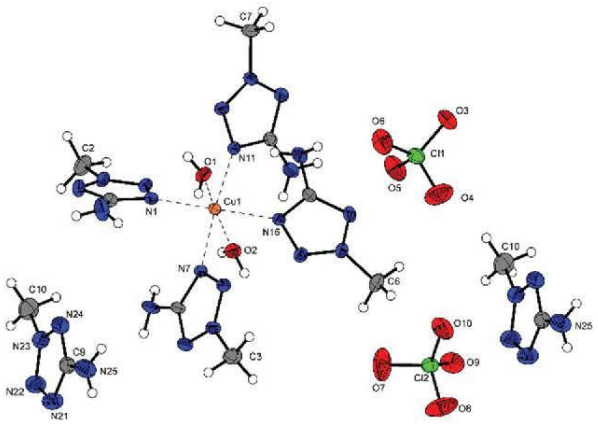


Fig. 5 Molecular unit of $[Cu(H_2O)_2(2\text{-MAT})_4](ClO_4)_2{\cdot}2$ 2-MAT (**5**). Selected bond lengths (Å): O1–Cu1 2.385(2), O2–Cu1 2.501(2), N1–Cu1 2.006(2), N7–Cu1 2.004(2), N11–Cu1 2.020(2), and N16–Cu1 2.000(2); selected bond angles (°): O1–Cu1–O2 173.44(7), N1–Cu1–O1 93.38(8), N1–Cu1–O2 92.11(8), N7–Cu1–O2 85.43(8), N16–Cu1–O2 85.14(8), N7–Cu1–N16 88.68(9), N11–Cu1–N16 86.82(9), N1–Cu1–N16 176.71(9), and N7–Cu1–N11 175.13(9); symmetry codes: (i) $1-x, 1-y, 1-z$, and (ii) $-x, 2-y, 1-z$.

 This journal is © The Royal Society of Chemistry and the Centre National de la Recherche Scientifique 2019

Published on 27 November 2018. Downloaded by Ludwig Maximilians Universitaet Muenchen on 2/16/2022 8:00:53 AM.

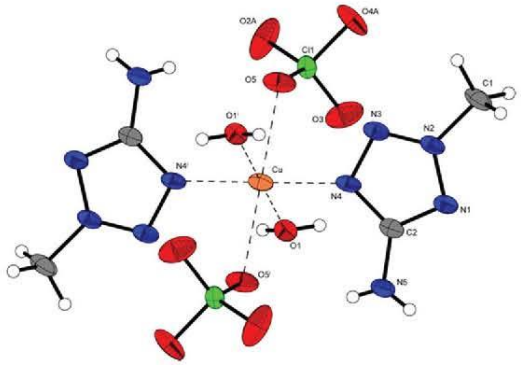


Fig. 6 Molecular unit of $[Cu(ClO_4)_2(H_2O)_2(2\text{-MAT})_2]$ (**6**). Selected bond lengths (Å): Cu1–O5 2.443(3), Cu1–N4 1.998(3), and Cu1–O1 1.960(3); selected bond angles (°): O1–Cu1–O5 96.32(10), O1–Cu1–O5^{i} 83.69(10), O1–Cu1–N4 90.59(12), O1–Cu1–N4^{i} 89.41(12), and O5–Cu1–O5^{i} 180.00; symmetry code: (i) $2 - x, -y, -z$.

located in an ideal plane with bond lengths between the metal(II) center and the respective ligand being expectedly shorter than along the O5–Cu1–O5^{i} axis. Another significant deviation from an ideal octahedron can be observed regarding the bond angles between axial ligands and coordinating molecules in the equatorial plane. Lastly, the molecular structure of **7** was investigated. In analogy to complex **6**, $[Cu(H_2O)_2(2\text{-MTZ})_4](ClO_4)_2$ crystallizes in the monoclinic space group $P2_1/n$ ($Z = 2$), while exhibiting a significantly lower calculated density at 173 K (1.702 g cm^{-3}). As stated beforehand, the obtained crystal structure displays a remarkable resemblance to the molecular structures of **3** and **4** (Fig. 7). Nevertheless, copper(II)–aqua distances along the Jahn–Teller distorted O1–Cu–O1^{i} axis proved to be distinguishably shorter. Despite this deviation, measured torsion angles consistently exhibit values close to those of an ideal octahedron.

Thermal properties and sensitivities

Following the structural characterization of the received complexes, energetic properties in terms of thermal stability and sensitivities towards mechanical stimuli were investigated.

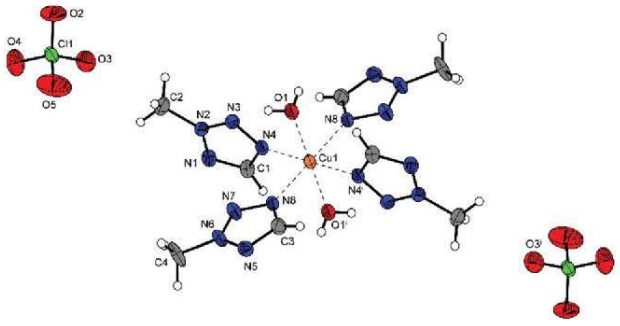


Fig. 7 Molecular unit of $[Cu(H_2O)_2(2\text{-MTZ})_4](ClO_4)_2$ (**7**). Selected bond lengths (Å): Cu1–O1 2.300(3), Cu1–N4 2.023(2), and Cu1–N8 2.029(2); selected bond angles (°): O1–Cu1–N4 93.15(11), O1–Cu1–N8 88.31(11), O1–Cu1–O1^{i} 180.00, N4–Cu1–N8 88.11(9), O1^{i}–Cu1–N8 91.69(11), and N4–Cu1–N4^{i} 180.00; symmetry code: (i) $1 - x, -y, 2 - z$.

Thereby conducted differential thermal analysis (DTA, heating rate: β = 5 °C min^{-1}, see Table 2, Fig. S5, ESI‡) provided a distinct differentiation between uncoordinated ligands **1** and **2** and the obtained ECC. While the nitrogen-rich ligands 2-MAT (**1**) and 2-MTZ (**2**) both exhibit high thermal stability in the measured range of 25–400 °C, the corresponding copper(II) complexes each show exothermic decomposition temperatures from 171 °C (**4**) to 240 °C (**7**). Endothermic events observed for both ligands are assumed to be caused either by melting (T_{endo1} (**1**)) or evaporation of the compound (T_{endo2} (**1**), T_{endo1} (**2**), see corresponding TGA plots, Fig. S6, ESI‡). Whereas the loss of cocrystallized water in the DTA measurement of **4** solely marginally influences the determined exothermic decomposition temperature, it seems possible that in **3** a slow decomposition starts before the onset temperature of 176 °C. In the case of the structurally analogous complexes **3**, **4**, and **7**, endothermic events which are most likely caused by evaporation of cocrystallized or coordinated water were detected in an expectedly narrow range (125 °C (**3**), 110 °C (**4**), and 115 °C (**7**)). To gain a better understanding of this partial ECC decomposition prior to the actual exothermic event, thermal gravimetric analysis was implemented for ECC **3**, **4** (see ESI,‡ Fig. S6), and $[Cu(H_2O)_2(2\text{-MTZ})_4](ClO_4)_2$ (**7**) (Fig. 8).

Whereas TGA plots of **3** and **4** (see ESI,‡ Fig. S6) show an almost continuous loss of the compounds' mass between 100 and 250 °C and no sharp mass decrease at the decomposition temperature, the corresponding plot of **7** exhibits distinct disintegration events. Affirmatively, the observed mass loss starting below 100 °C (5.67%) can be assigned to the loss of present aqua ligands and refers to the first endothermic event (115 °C) during the DTA measurement. Moreover, T_{endo2} (DTA: 208 °C) was confirmed by a matching 26.5% mass loss during

Table 2 Thermal stability measurements of **1–4**, **6**, and **7** by DTA[a]

Compound	T_{endo1}[b] [°C]	T_{endo2}[b] [°C]	T_{exo}[c] [°C]
1	104	252	—
2	152	—	—
3	125	—	176
4	110	—	171
6	—	—	192
7	115	208	240

[a] Onset temperatures at a heating rate of $\beta = 5$ °C min^{-1}. [b] Endothermic peak, which indicates melting, dehydration, or loss of coordinating or cocrystallized molecules. [c] Exothermic peak, indicating decomposition.

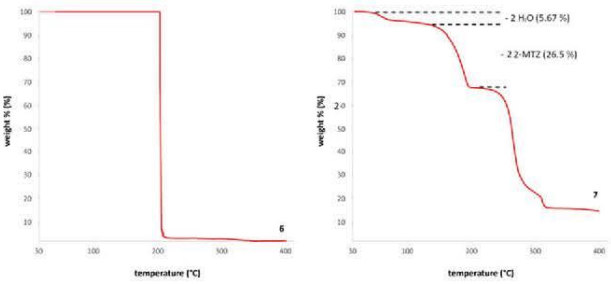


Fig. 8 TGA measurements (5 °C min^{-1}) of **6** and **7**.

Published on 27 November 2018. Downloaded by Ludwig Maximilians Universitaet Muenchen on 2/16/2022 8:00:53 AM.

the TGA measurement, a fact that presumably is effected by ligand evaporation. The final step of decomposition is identified by an exothermic event at the remarkably high temperature of 240 °C. Lastly, complex **6**, which exhibited two copper(II)–perchlorato bonds, proved to similarly disintegrate at high, but slightly lower temperatures without indicating an event of endothermic decomposition (Table 2 and Fig. 8). In order to explain this rather unusual observation, one might consult the complex's coordination chemistry: contrary to complexes **3**, **4**, **5**, and **7**, coordinating aqua ligands are in the plane and exhibit significantly shortened ($\approx$0.4 Å) copper–aqua bond lengths which presumably lead to aggravated dissociation. Additionally, the sharp mass loss observed during TGA measurements further proves ECC **6** remains in its distinct composition until being exposed to its decomposition temperature (Fig. 8). Resulting from the observed thermal properties, the incorporation of cocrystallized water and the introduction of coordinating perchlorato anions cause a measurable increase in thermal stability.[10,22]

Regarding the investigated compounds' sensitivities towards mechanical stimuli, **1** and **2** both can be classified as insensitive according to UN standards (impact: >40 J, friction: >360 N). In contrast to that, introducing the highly oxidizing perchlorate anion and a coordination site like copper(II) once more proves the potential of the ECC approach due to the formation of distinctly more sensitive compounds (Table 3). Considering the series of 2-MAT based copper(II) complexes, one might recognize the tendency that with decreasing content of water, more specifically the loss of the cocrystallized species, the resulting complexes show increased sensitivities (**3** *vs.* **4** and **6**).[10] Unfortunately, proceeding from this initial proposition, ECC **4**, **6**, and **7** each exhibit sensitivities at the lower end of the measuring range. As a result, a quantitative evaluation of sought structure–property relationships most likely is prevented by possibly varying fractal characteristics and particle sizes.[26] Moreover, the correlation between sensitivities and molecular structure is proposed to be dependent on multiple factors like oxygen balance (OB),[27] the electronic band gap,[28] molecular electrostatic potentials,[29] and dissociation energies of critical bonds.[30] Nevertheless, complex **6**, which exhibits the lowest nitrogen ("propellant") content and the OB closest to 0 represents the overall most sensitive compound in terms of impact and friction and can be compared to the analogous chlorate complex.[18b] ECC **4**, which, in comparison to structurally equivalent **7**, incorporates the less energetic ligand, displays a higher nitrogen content and exhibits the highest sensitivities towards impact and electrostatic discharge. Conducted hot plate and hot needle tests for each of the characterized ECC showed sharp deflagration events (see ESI,‡ Fig. S9–S14).

Table 3 Sensitivities towards the external stimuli impact, friction, and ESD

Compound	IS[a] [J]	FS[b] [N]	ESD[c] [mJ]	Grain size [μm]
1	>40	>360	1500	100–500
2	>40	>360	—	100–500
3	5	30	260	500–1000
4	<1	24	20	<100
6	2	2.2	150	<100
7	5	5	50	100–500

[a] Impact sensitivity according to the BAM drophammer (method 1 of 6). [b] Friction sensitivity according to the BAM friction tester (method 1 of 6). [c] Electrostatic discharge sensitivity (OZM ESD tester); impact: insensitive >40 J, less sensitive ≥35 J, sensitive ≥4 J, very sensitive ≤3 J; friction: insensitive >360 N, less sensitive = 360 N, sensitive <360 N and >80 N, very sensitive ≤80 N, extremely sensitive ≤10 N. According to the UN Recommendations on the Transport of Dangerous Goods.

Optical initiation and UV-vis spectroscopy

In addition to the well-established initiation of energetic compounds *via* mechanical and thermal stimuli, recent developments in this field dealt with the neglected sensitivities of these species towards optical initiation.[10,21,31] Until today, a broad range (Mn, Fe, Co, Ni, Cu, and Zn) of 3d transition metal complexes and energetic materials have been successfully initiated *via* laser irradiation while an unambiguous mechanistic proposal is still awaited. On one hand, common suggestions discuss a photochemical initiation mechanism through an excitation–relaxation process during which photonic energy is translated to the decomposition-initiating vibrational energy.[9c,32] Additionally, a reoccurring proposal deals with a photothermal mechanism, during which photonic energy is directly converted into lattice heat and vibrational energy, which according to the "hot-spot"-theory further leads to decomposition of the material.[10,32b] To investigate the optical sensitivities of **3**–**7** and a possible coherence with either of the proposed initiation mechanisms, laser initiation experiments were conducted along with UV-vis spectroscopy (Table 4 and Fig. 9). The distinction between deflagration and detonation was made by means of acoustic output and high-speed recordings (Fig. S7, ESI‡).

While each of the investigated ECC showed a reaction resulting from the applied conditions, solely perchlorato ligand incorporating complex **6**, as well as the 2-MTZ complex **7**, detonated in the course of the experiment.

While **3** exhibited sharp deflagration upon laser irradiation, **4** solely decomposed without any sign of an exothermic reaction. Resulting from that, an unambiguous confirmation of either of the proposed initiation mechanisms (photochemical or thermal) remains anticipated. In contrast to the literature, the comparably strong response of the least sensitive compound **3**

Table 4 Results of laser ignition tests[a] and UV-vis spectroscopy

Compound	Reaction	Color	$\lambda_{d\ d}$[b]	OD(λ_{915})/OD($\lambda_{d\ d}$)[c]
3	deflag.	Blue	613	0.39
4	dec.	Blue	620	0.37
6	det.	Blue	658	0.46
7	det.	Blue	681	0.34

[a] dec.: decomposition, deflag.: deflagration, det.: detonation. Operating parameters: current I = 7 A; voltage U = 4 V; theoretical maximal output power P_{max} = 45 W; theoretical energy E_{max} = 0.17 mJ; wavelength λ = 915 nm; pulse length τ = 0.1 ms. [b] Absorption intensity maximum wavelength, which can be assigned to electron d–d excitations in the measured range of 350–1000 nm. [c] Quotient of the absorption intensity at the laser wavelength and the intensity at the d–d absorption wavelength.

 This journal is © The Royal Society of Chemistry and the Centre National de la Recherche Scientifique 2019

Published on 27 November 2018. Downloaded by Ludwig Maximilians Universitaet Muenchen on 2/16/2022 8:00:53 AM.

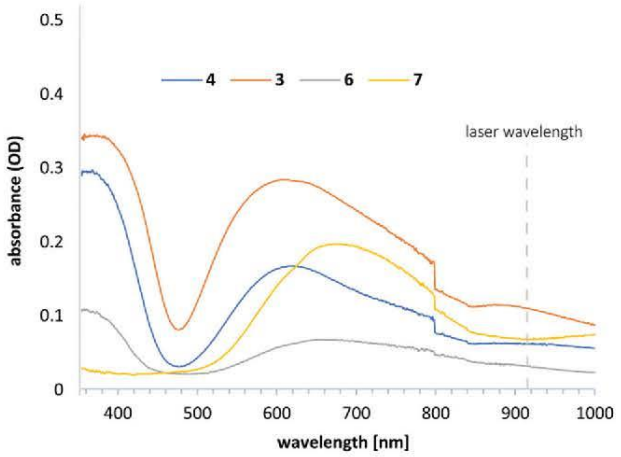


Fig. 9 Solid state UV/vis spectra of selected copper(II) and iron(II) complexes. The step in the absorption intensity at 800 nm is caused by a detector change. The UV-vis spectra have only qualitative character.

towards optical stimuli suggests no distinct correlation between mechanical and optical sensitivites, further being proved by the observed difference between **4** and **7**.[10,12,21] Furthermore, an obvious coherence between thermal properties (see Table 2) and optical initiation is equally prohibited since **6** and **7**, which proved to be highly thermally stable, gave the most violent responses upon laser irradiation (see ESI,‡ Fig. S7). Regarding the densities of the complexes and their outcome in the initiation tests, no general trend can be observed. Whereas compound **6** shows the highest density and a positive result in the experiments, complex **3** with the lowest one gives a stronger response to irradiation than compound **4**. Conducted solid state UV/vis measurements, which solely provide qualitative information, equally lack unequivocal trends (Fig. 9). To begin with, the spectra of **3** and **4**, both reacting noticably differently during laser experiments, are almost identical in terms of the observed d–d-transitions (613 and 620 nm) and curve shape. Moreover, the detected absorbance of the applied radiation (915 nm) solely corresponds to a fraction of the d–d-transition's maximum (see Table 4). Resulting from these conclusions, a desired correlation between coordination chemistry and optical sensitivity once again remained unfulfilled. Based on the previously noted, vague but highly relevant impact of fractal characteristics and the overall inconclusive current state of research in the field of laser-ignitable ECC, further investigations remain indispensable.

Conclusions

In summary, a series of energetic copper(II) perchlorate complexes were successfully synthesized and characterized by manipulating the present coordination chemistry through adjusting the parameters of the solvent, stoichiometry, acidity, and the applied 2-substituted tetrazole ligand. In regard to the 2-MAT complexes $[Cu(H_2O)_2(2\text{-}MAT)_4](ClO_4)_2 \cdot H_2O$ (**3**), $[Cu(H_2O)_2(2\text{-}MAT)_4](ClO_4)_2$ (**4**) and $[Cu(ClO_4)_2(H_2O)_2(2\text{-}MAT)_2]$ (**6**), a decrease of the compound's water content as well as the incorporation of perchlorato ligands led to a rough increase of thermal stability and overall sensitivity. Inconsistencies, especially in regard to measured sensitivities and laser ignitability, might be attributed to fractal characteristics and particle sizes. Introducing a new nitrogen-rich ligand with increased energetic character (2-MTZ, **2**) results in novel patterns of the examined properties despite identical coordination chemistry (**7** *vs.* **4**). In the present case, higher thermal stability was accompanied by an increase in optical and friction sensitivity and a simultaneous decrease of ESD and impact sensitivities. Consequently, the present report provides lead-off insights into the correlation of an ECC's coordination chemistry and derived energetic properties, while future investigations might further develop observed patterns. Moreover, the obtained complexes, especially **6** and **7**, indeed meet targeted properties including exceptionally high thermal stability, decreased mechanical sensitivities in comparison to the 2-aminotetrazole ECC and retained laser ignitability. Therefore, both conveniently synthesized ECC represent promising candidates for being applied in future ignition (optical or mechanical) systems.

Conflicts of interest

There are no conflicts to declare.

Acknowledgements

Financial support of this work by the Ludwig Maximilian University of Munich (LMU) and the Office of Naval Research (ONR) under grant no. ONR.N00014-16-1-2062 is acknowledged. Furthermore, the authors want to thank Mr Michael Gruhne and Mr Marcus Lommel for their great help with the sensitivity determinations.

Notes and references

1 (*a*) E. Platania, N. L. W. Streeton, H. Kutzke, A. Karlsson, E. Uggerud and N. H. Andersen, *Vib. Spectrosc.*, 2018, **97**, 66–74; (*b*) S. Bette, R. K. Kremer, G. Eggert and R. E. Dinnebier, *Dalton Trans.*, 2018, **47**, 8209–8220.

2 (*a*) F. Brunel, N. E. El Gueddari and B. M. Moerschbacher, *Carbohydr. Polym.*, 2013, **92**, 1348–1356; (*b*) S. Chandraleka and G. Chandramohan, *Int. J. ChemTech Res.*, 2014, **6**, 5450–5457.

3 R. R. Conry, Copper: Inorganic & Coordination Chemistry, *Encyclopedia of Inorganic Chemistry*, John Wiley & Sons, Ltd., 1st edn, 2006.

4 (*a*) H.-J. Zhang, A. W. Schuppe, S.-T. Pan, J.-X. Chen, B.-R. Wang, T. R. Newhouse and L. Yin, *J. Am. Chem. Soc.*, 2018, **140**, 5300–5310; (*b*) S. B. Thorpe, J. A. Calderone and W. L. Santos, *Org. Lett.*, 2012, **14**, 1918–1921; (*c*) P. C. Roest, N. W. M. Michel and R. A. Batey, *J. Org. Chem.*, 2016, **81**, 6774–6778.

5 (*a*) P. L. Holland and W. B. Tolman, *Coord. Chem. Rev.*, 1999, **190–192**, 855–869; (*b*) W. L. Nettles, H. Song, E. R. Farquhar, N. C. Fitzkee and J. P. Emerson, *Inorg. Chem.*, 2015, **54**(12),

Published on 27 November 2018. Downloaded by Ludwig Maximilians Universitaet Muenchen on 2/16/2022 8:00:53 AM.

5671–5680; (*c*) C. A. Blasie and J. M. Berg, *J. Am. Chem. Soc.*, 2003, **125**, 6866–6867.

6 T. M. Klapötke, *Chemistry of High-Energy Materials*, Walter de Gruyter, Berlin, Boston, 2nd edn, 2012.

7 (*a*) G.-H. Tao, D. A. Parrish and J. M. Shreeve, *Inorg. Chem.*, 2012, **51**, 5305–5312; (*b*) R. P. Singh, R. D. Verma, D. T. Meshri and J. M. Shreeve, *Angew. Chem., Int. Ed.*, 2006, **45**, 3584–3601; (*c*) Q. Zhang and J. M. Shreeve, *Angew. Chem., Int. Ed.*, 2014, **53**, 2540–2542.

8 (*a*) T. W. Myers, D. E. Chavez, S. K. Hanson, R. J. Scharff, B. L. Scott, J. M. Veauthier and R. Wu, *Inorg. Chem.*, 2015, **54**, 8077–8086; (*b*) T. W. Myers, K. E. Brown, D. E. Chavez, R. J. Scharff and J. M. Veauthier, *Inorg. Chem.*, 2017, **56**, 2297–2303; (*c*) T. W. Myers, J. A. Bjorgaard, K. E. Brown, D. E. Chavez, S. K. Hanson, R. J. Scharff, S. Tretiak and J. M. Veauthier, *J. Am. Chem. Soc.*, 2016, **138**, 4685–4692.

9 (*a*) M. Friedrich, J. C. Gálvez-Ruiz, T. M. Klapötke, P. Mayer, B. Weber and J. J. Weigand, *Inorg. Chem.*, 2005, **44**, 8044–8052; (*b*) G. Geisberger, T. M. Klapötke and J. Stierstorfer, *Eur. J. Inorg. Chem.*, 2007, 4743–4750; (*c*) M. Joas, T. M. Klapötke, J. Stierstorfer and N. Szimhardt, *Chem. – Eur. J.*, 2013, **19**, 9995–10003; (*d*) M. Joas, T. M. Klapötke and N. Szimhardt, *Eur. J. Inorg. Chem.*, 2014, 493–498; (*e*) M. Joas and T. M. Klapötke, *Z. Anorg. Allg. Chem.*, 2014, **640**, 1886–1891; (*f*) T. M. Klapötke, P. C. Schmid, J. Stierstorfer and N. Szimhardt, *Z. Anorg. Allg. Chem.*, 2016, **642**, 383–389.

10 N. Szimhardt, M. H. H. Wurzenberger, A. Beringer, L. J. Daumann and J. Stierstorfer, *J. Mater. Chem. A*, 2017, **5**, 23753–23765.

11 J. Evers, I. Gospodinov, M. Joas, T. M. Klapötke and J. Stierstorfer, *Inorg. Chem.*, 2014, **53**, 11749–11756.

12 N. Szimhardt and J. Stierstorfer, *Chem. – Eur. J.*, 2018, **24**, 2687–2698.

13 N. Szimhardt, M. H. H. Wurzenberger, L. Zeisel, M. S. Gruhne, M. Lommel and J. Stierstorfer, *J. Mater. Chem. A*, 2018, **6**, 16257–16272.

14 (*a*) Y. Cui, T.-L. Zhang, J.-G. Zhang, L. Yang, X.-C. Hu and J. Zhang, *J. Mol. Struct.*, 2008, **889**, 177–185; (*b*) Y. Cui, J. Zhang, T. Zhang, L. Yang, J. Zhang and X. Hu, *J. Hazard. Mater.*, 2008, **160**, 45–50.

15 A. V. Smirnov, M. A. Ilyushin and I. V. Tselinskii, *Russ. J. Appl. Chem.*, 2004, **77**, 794–796.

16 Y. Xu, W. Liu, D. Li, H. Chen and M. Lu, *Dalton Trans.*, 2017, **46**, 11046–11052.

17 Gas phase enthalpies of formation were calculated using the atomization method ($\Delta_f H^0_{(g,M)} = H_{(M)} - \Sigma H^0_{(A)} + \Sigma \Delta_f H^0_{(A)}$) using Gaussian09 computed CBS-4M electronic enthalpies.

18 (*a*) A. Y. Zhilin, M. A. Ilyushin, I. V. Tselinskii, A. S. Kozlov and N. E. Kuz'mina, *Russ. J. Appl. Chem.*, 2002, **75**, 1849–1851; (*b*) M. H. H. Wurzenberger, N. Szimhardt and J. Stierstorfer, *J. Am. Chem. Soc.*, 2018, **140**, 3206–3209.

19 H. Radies, *Synthesis and Characterization of Energetic Transition Metal–Tetrazolate Complexes*, Diploma thesis, Ludwig Maximilian University of Munich, 2006.

20 (*a*) K. Karaghiosoff, T. M. Klapötke, P. Mayer, C. M. Sabaté, A. Penger and J. M. Welch, *Inorg. Chem.*, 2008, **47**, 1007–1019; (*b*) T. M. Klapötke and J. Stierstorfer, *Eur. J. Inorg. Chem.*, 2008, 4055–4062; (*c*) T. M. Klapötke and C. M. Sabaté, *Eur. J. Inorg. Chem.*, 2008, 5350–5366.

21 N. Szimhardt, M. H. H. Wurzenberger, T. M. Klapötke, J. T. Lechner, H. Reichherzer, C. C. Unger and J. Stierstorfer, *J. Mater. Chem. A*, 2018, **6**, 6565–6577.

22 M. Freis, T. M. Klapötke, J. Stierstorfer and N. Szimhardt, *Inorg. Chem.*, 2017, **56**, 7936–7947.

23 Crystallographic data for the structures have been deposited. with the Cambridge Crystallographic Data Centre.‡

24 J. H. Bryden, *Acta Crystallogr.*, 1956, **9**, 874–878.

25 (*a*) P. N. Gaponik, M. M. Degtyarik, A. S. Lyakhov, V. E. Matulis, O. A. Ivashkevich, M. Quesada and J. Reedijk, *Inorg. Chim. Acta*, 2005, **358**, 3949–3957; (*b*) E. J. van den Huevel, P. L. Franke, G. C. Verschoor and A. P. Zuur, *Acta Crystallogr.*, 1983, **39**, 337–339.

26 (*a*) X. Song, Y. Wang, C. An, X. Guo and F. Li, *J. Hazard. Mater.*, 2008, **159**, 222–229; (*b*) Y. Wang, X. Song, D. Song, W. Jiang, H. Liu and F. Li, *Propellants, Explos., Pyrotech.*, 2011, **36**, 505–512.

27 C. B. Storm, J. R. Stine and J. F. Kramer, *Chem. Phys. Energ. Mater.*, 1990, **309**, 605–639.

28 W. Zhu and H. Xiao, *Struct. Chem.*, 2010, **21**, 657–665.

29 P. Politzer and J. S. Murray, *J. Mol. Model.*, 2015, **21**, 25.

30 D. Mathieu, *Ind. Eng. Chem. Res.*, 2017, **56**, 8191–8201.

31 (*a*) M. T. Greenfield, S. D. McGrane, C. A. Bolme, J. A. Bjorgaard, T. R. Nelson, S. Tretiak and R. J. Scharff, *J. Phys. Chem. A*, 2015, **119**, 4846–4855; (*b*) A. E. Sifain, J. A. Bjorgaard, T. W. Myers, J. M. Veauthier, D. E. Chavez, O. V. Prezhdo, R. J. Scharff and S. Tretiak, *J. Phys. Chem. C*, 2016, **120**, 28762–28773; (*c*) E. D. Aluker, A. G. Krechetov, A. Y. Mitrofanov, D. R. Nurmukhametov and M. M. Kuklja, *J. Phys. Chem. C*, 2011, **115**, 6893–6901.

32 (*a*) D. D. Dlott and M. D. Fayer, *J. Chem. Phys.*, 1990, **92**, 3798–3812; (*b*) E. D. Aluker, A. S. Zverev, A. G. Krechetov, A. Yu. Mitrofanov, A. O. Terentyeva and A. V. Tupitsyn, *Russ. J. Phys. Chem. B*, 2014, **8**, 687–691.

 This journal is © The Royal Society of Chemistry and the Centre National de la Recherche Scientifique 2019

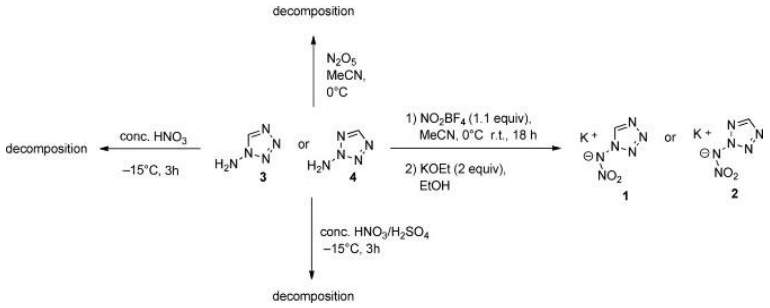
Appendix 9

Potassium *N*-Nitramino-5*H*-tetrazolates - Powerful Green Primary Explosives with High Initiation Capabilities

N. Szimhardt, M. H. H. Wurzenberger, P. Spieß, T. M. Klapötke, J. Stierstorfer

Propellants Explos. Pyrotech. **2018**, *43*, 1203–1209.

https://doi.org/10.1002/prep.201800221



Supplementary Information:
https://onlinelibrary.wiley.com/action/downloadSupplement?doi=10.1002%2Fprep.201800221&file=prep201800221-sup-0001-misc_information.pdf

Full Paper

Propellants, Explosives, Pyrotechnics

DOI: 10.1002/prep.201800221

Potassium *N*-Nitramino-5*H*-Tetrazolates – Powerful Green Primary Explosives with High Initiation Capabilities

Norbert Szimhardt,[a] Maximilian H. H. Wurzenberger,[a] Philipp Spieß,[a] Thomas M. Klapötke,[a] and Jörg Stierstorfer*[a]

Abstract: Since the nowadays used lead-based primary explosives, lead azide, picrate and styphnate suffer from various environmental and toxic issues, there is a great need for new green materials. Therefore, two highly promising lead-free primary explosives potassium 1-(*N*-nitramino)-5*H*-tetrazolate (**1**, 1-KNAT) and potassium 2-(*N*-nitramino)-5*H*-tetrazolate (**2**, 2-KNAT) have been synthesized and characterized. Both isomers show superior energetic performance, initiation capability and were comprehensively analyzed by low-temperature X-ray diffraction, IR, multinuclear NMR spectroscopy, elemental analysis, and DTA. Sensitivity determinations toward impact, friction, and electrostatic discharge revealed its highly powerful, but also sensitive character. In addition, their potential as lead-free primaries were evaluated in initiation tests of PETN or RDX filled detonators confirming their great suitability as lead-free primary explosives.

Keywords: Lead-free Primary Explosives · Tetrazoles · Structure Elucidation · Nitramines · Potassium Salts

1 Introduction

In the field of high energy density materials (HEDM), the challenge has always been to find an ideal balance between high performance and molecular stability. By combining synthetic and theoretical studies, various strategies for the design of new energetic materials have become established [1–4]. However, driven by mounting demands for environmental sustainability and superior performance, considerable research is now focused on promoting the generation of eco-friendly and safe HEDM [2,5,6]. At least since the REACH (Registration, Evaluation, Authorization, and Restriction of Chemicals) [7] regulation in 2011, the restriction or even the prohibition of lead azide (LA) and lead styphnate (LS), which have been put on the candidate list, seems very likely in future. During the research for green primary explosives for both military and civilian purposes, metal-organic compounds have received considerable attention [8–10]. The formation of energetic salts seems to be extremely useful for triggering the individual behavior because of a crystal package and a pronounced cation-anion packing [11]. Among the alkali cations, potassium is considered the best as it combines environmental safety, good coordination, high availability, and low costs [12]. Up to now, several promising potassium-based primaries have been reported and investigated as potential substitutes for the commonly used lead-containing primary explosives (Chart 1) [13–17]. KDBNF is currently widely used in lead-free primer and igniter systems [17]. With KDNP in comparison, the temperature stability could be further improved, whereby also suitable properties for application as possible LS alternative could be shown [13]. In 2014, Fischer *et al.* reported K_2DNABT, a highly powerful green primary explosive, which combined good thermal stability and initiation capability, but shows increased sensitivity issues [14]. With the introduction of the nitramino group, the detonation properties and ease of salt formation could be significantly enhanced [18]. Nevertheless, a seven-step synthesis reduces the usability for industrial processes in order to replace the easily accessible lead compounds. From this point of view, a simpler and shorter synthesis would be very desirable.

Mentally separating the symmetrical K_2DNABT system into two molecules, leads to a mononitraminotetrazolate, which is noticeably easier to synthesize and shows comparable energetic parameters to the parent dinitraminotetrazolate compound. Almost two decades ago, first approaches to synthesize the silver and ammonium salts of 1-(*N*-nitramino)-5*H*-tetrazolate and 2-(*N*-nitramino)-5*H*-tetrazolate salts have been reported using alkyl nitrates as the nitrating reagent [19]. The salts were hardly characterized and suffer from an extreme lack of data (XRD, NMR spectroscopy, sensitivities, etc.). In order to close this gap and due to the expected enormous sensitivity of the silver salts and the probably undesirable good solubility of the ammonium salts, the previously unknown environmentally friendly po-

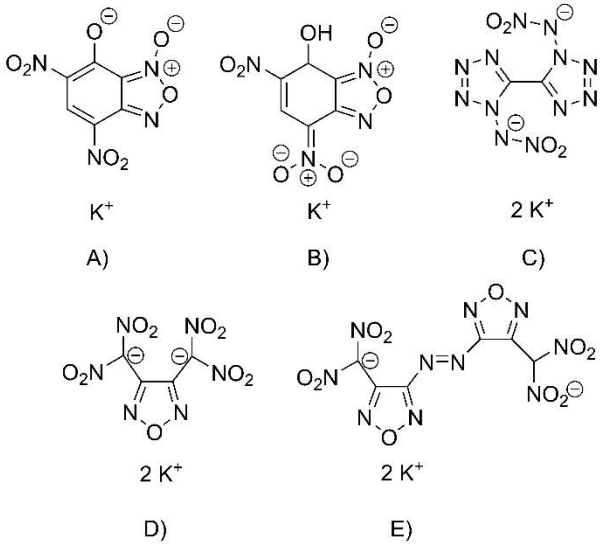
[a] *N. Szimhardt, M. H. H. Wurzenberger, P. Spieß, T. M. Klapötke, J. Stierstorfer*
Department of Chemistry, Energetic Materials Research
Ludwig Maximilian University
Butenandtstr. 5–13 (D), 81377 München (Germany)
**e-mail: jstch@cup.uni-muenchen.de*

Supporting information for this article is available on the WWW under https://doi.org/10.1002/prep.201800221

 © 2018 Wiley-VCH Verlag GmbH & Co. KGaA, Weinheim

15214087, 2018, 12, Downloaded from https://onlinelibrary.wiley.com/doi/10.1002/prep.201800221 by Ludwig-Maximilians-Universität, Wiley Online Library on [29/12/2022]. See the Terms and Conditions (https://onlinelibrary.wiley.com/terms-and-conditions) on Wiley Online Library for rules of use; OA articles are governed by the applicable Creative Commons License

tassium salts were selected as target molecules. Therefore, in our continuing efforts toward environmentally benign materials, we have now prepared and characterized the manageable potassium salts 1-KNAT (**1**) and the corresponding isomeric 2-KNAT (**2**) by an alternative synthetic route. Both compounds show promising energetic and physicochemical properties competitive with those of LA.



2 Experimental Section

More information on the general methods and synthesis of the starting compounds can be found in the Supporting Information.

Caution! All investigated compounds are highly powerful energetic materials, which show increased sensitivities toward various stimuli (e.g. elevated temperatures, impact, friction, or electrostatic discharge). Although no hazards occurred, proper security precautions (safety glasses, face shield, earthed equipment and shoes, leather jacket, Kevlar gloves, Kevlar sleeves, and ear plugs) have to be worn while synthesizing and handling the described compounds.

2.1 General Procedure for the Potassium *N*-Nitramino-5*H*-Tetrazolates 1 and 2

Under nitrogen atmosphere, the corresponding amino-5*H*-tetrazole was dissolved in dry acetonitrile and cooled to 0 °C. NO_2BF_4 was added portion wise, and after complete addition, the ice bath was removed. After stirring overnight, acetonitrile was removed under reduced pressure. The obtained residue was dissolved in a small amount of EtOH and one equivalent of KOEt dissolved in EtOH was added under ice cooling. Colorless precipitation was observed, filtered off, and a second equivalent KOEt in EtOH was added to the filtrate under the same cooling conditions. After filtration, the slightly yellow residue was washed with cold EtOH to obtain the corresponding potassium nitramino-5*H*-tetrazolate. The obtained solid material was further dried overnight at 110 °C.

2.2 Potassium 1-(*N*-Nitramino)-5*H*-Tetrazolate (1)

Following the general procedure 1-amino-5*H*-tetrazole (0.50 g, 5.80 mmol), dissolved in acetonitrile (20 mL), reacts with NO_2BF_4 (0.85 g, 7.00 mmol) to obtain **1** in form of a colorless solid (0.63 g, 3.80 mmol, 64 %). Single crystals suitable for X-ray diffraction were obtained by recrystallization from acetonitrile.

DTA (5 °C min^{-1}): onset: 180 °C (exothermic decomposition after melting); IR (ATR, cm^{-1}): $\tilde{\nu}$ = 3136 (m), 1676 (w), 1572 (w), 1500 (w), 1480 (vw), 1463 (m), 1410 (m), 1384 (s), 1306 (vs), 1276 (s), 1198 (m), 1176 (m), 1161 (s), 1105 (m), 1092 (s), 1007 (m), 957 (m), 925 (w), 891 (m), 867 (s), 820 (w), 775 (s), 725 (m), 725 (m), 717 (m), 687 (w), 654 (s), 535 (w), 472 (w), 453 (m); ^{1}H NMR (DMSO-d_6, 25 °C, ppm) δ: 9.18 (s, 1H, C–*H*); ^{13}C NMR (DMSO-d_6, 25 °C, ppm) δ: 142.2 (s, 1C, *C*N$_4$); ^{14}N NMR (DMSO-d_6, 25 °C, ppm): δ = 4.2 (N6); ^{15}N NMR (DMSO-d_6, 25 °C, ppm): δ 2.8 (d, $^3J_{N-H}$ = 2.8 Hz, N3), −4.9 (s, N6), −14.3 (d, $^3J_{N-H}$ = 0.8 Hz, N2), −54.3 (d, $^2J_{N\ H}$ = 12.2 Hz, N4), −116.1 (d, $^2J_{N\ H}$ = 8.4 Hz, N1), −122.7 (s, N5); EA: ($CHKN_5O_2$, 167.98) calc.: C 7.14, H 0.60, N 49.98 %; found: C 7.40, H 0.89, N 47.02 %; ball drop impact tester: < 4 mJ; BAM drophammer: < 1 J; friction tester: < 0.1 N; ESD: 0.89 mJ (at grain size < 100 μm).

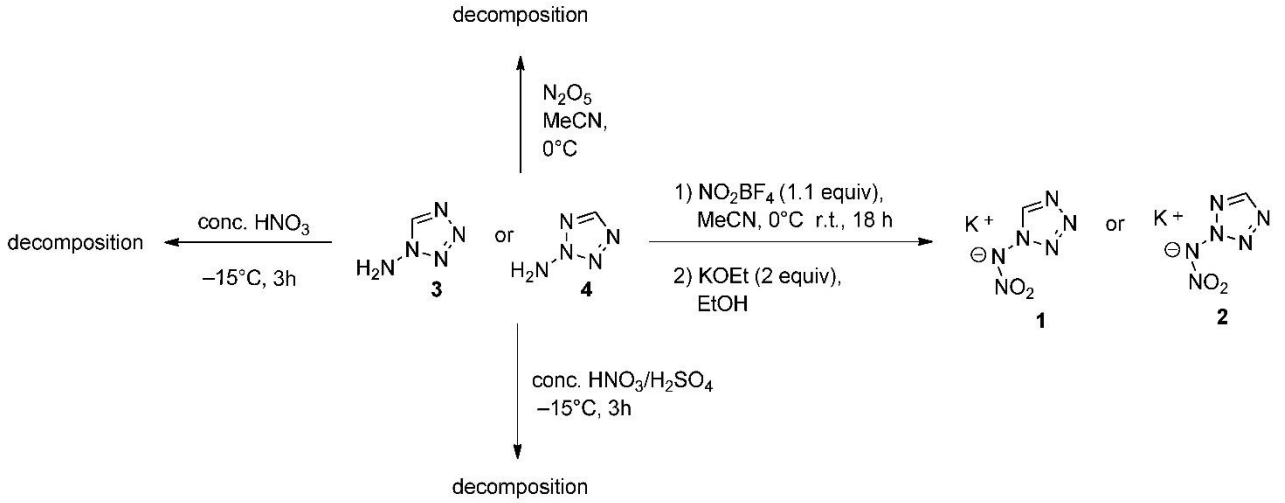
2.3 Potassium 2-(*N*-Nitramino)-5*H*-Tetrazolate (2)

Following the general procedure 2-amino-5*H*-tetrazole (0.82 g, 7.50 mmol) dissolved in 20 mL acetonitrile, reacts with NO_2BF_4 (1.40 g, 10.5 mmol) to obtain **2** as a yellowish solid (0.77 g, 4.60 mmol, 48 %). Single crystals suitable for X-ray diffraction were obtained by recrystallization from acetonitrile.

DTA (5 °C min^{-1}): 176 °C (exothermic decomposition after melting); IR (ATR, cm^{-1}): $\tilde{\nu}$ = 3136 (w), 1814 (vw), 1572 (vw), 1505 (vw), 1481 (w), 1423 (s), 1371 (w), 1334 (s), 1272 (vs), 1262 (vs), 1220 (s), 1166 (m), 1130 (s), 1030 (s), 1009 (m), 1006 (m), 1003 (m), 910 (m), 892 (s), 778 (m), 730 (w), 705 (m), 677 (m), 677 (m); ^{1}H NMR (DMSO-d_6, 25 °C, ppm) δ: 8.77 (s, 1H, –*C*H); ^{13}C NMR (DMSO-d_6, 25 °C, ppm) δ: 151.3 (s, 1 C, *C*N4); ^{14}N NMR (DMSO-d_6, 25 °C, ppm): δ = −3.1 (N6); ^{15}N NMR (DMSO-d_6, 25 °C, ppm) δ: −4.00 (s, N6), −7.8 (d, $^3J_{N-H}$ = 1.5 Hz, N3), −54.4 (d, $^2J_{N\ H}$ = 12.4 Hz, N4), −76.2 (d, $^3J_{N\ H}$ = 7.1 Hz, N2), −76.8 (d, $^2J_{N\ H}$ = 14.4 Hz, N1), −113.1 (s, N5); EA: ($CHKN_5O_2$, 167.98) calc.: C 7.14, H 0.60, N 49.98 %; found: C 7.65, H 0.78, N 45.29 %; ball drop impact tester: < 4 mJ; BAM drophammer: 5 J; friction tester: < 0.1 ; ESD: 8.2 mJ (at grain size < 100 μm).

 © 2018 Wiley-VCH Verlag GmbH & Co. KGaA, Weinheim

15214087, 2018, 12, Downloaded from https://onlinelibrary.wiley.com/doi/10.1002/prep.201800221 by Ludwig-Maximilians-Universität, Wiley Online Library on [29/12/2022]. See the Terms and Conditions (https://onlinelibrary.wiley.com/terms-and-conditions) on Wiley Online Library for rules of use; OA articles are governed by the applicable Creative Commons License



Scheme 1. Different reaction routes using various nitration reagents starting from 1-amino-5*H*-tetrazole and 2-amino-5*H*-tetrazole.

3 Results and Discussion

3.1 Synthesis

The starting materials 1-amino-5*H*-tetrazole and 2-amino-5*H*-tetrazole have been synthesized according to literature modified procedures (more details can be found in the SI). Several direct nitration procedures of 1-amino-5*H*-tetrazole and 2-amino-5*H*-tetrazole with N_2O_5, 100% nitric acid and mixed acids have been approached in order to synthesize **1** and **2** in a more convenient way but were unfortunately unsuccessful (Scheme 1). During the addition step or further by quenching the acid mixtures, gas evolution could be observed. The gas evolution is a reliable indicator for decomposition of the starting material, which can be attributed to the relatively labile N–N bonds of 1-amino-5*H*-tetrazole and 2-amino-5*H*-tetrazole, which break under these harsh reaction conditions, releasing nitrogen gas. This work, deals with the successful nitration with the mild nitration reagent NO_2BF_4, as an alternative method described in the literature [19]. The corresponding salts **1** and **2** were obtained by the stoichiometric addition of potassium ethanolate, after the previous precipitation of KBF_4. Unfortunately, NO_2BF_4 is a relatively expensive reagent and decomposes under hydrolysis fuming on air. This complicates the storage and practicability of NO_2BF_4. Hence, further research into other nitration methods using inexpensive reagents is highly desirable in order to compete with existing inexpensive lead compounds concerning the production for industrial purposes. By protecting the weak point, the amino group of the aminotetrazoles with a protecting group (e.g. carbamate functionality), harsh nitration conditions might be tolerated without observed decomposition. The addition of an excess of base might cleave the nitrated aminotetrazoles and could give access to the potassium salts. Further research studies in this area should be carried out to make these compounds economically attractive. As the used starting material 1-amino-5*H*-tetrazole is accessible through a selective synthetic route from standard feedstock without distillation or column chromatography, compound **1** indicates a great potential to compete in industrial purposes with existing used primaries.

The structural and molecular composition of **1** and **2** were confirmed by elemental analysis, X-ray diffraction, IR, and multinuclear NMR spectroscopy (^1H, ^{13}C, ^{14}N, and ^{15}N). Both isomers can easily be differentiated by NMR and IR analysis (Figure S1). Six nitrogen resonances were observed in each proton coupled ^{15}N NMR spectrum of **1** and **2** (Figure 1).

3.2 Crystal Structures

Low-temperature X-ray diffraction was used to characterize **1** and **2**. The crystal structures were uploaded to the CSD database and can be obtained free of charge with the CCDC no. 1849956 (**1**) and 1849957 (**2**). Details to the measurement and refinement data are given in the SI. Compound **1** crystallizes in the form of colorless blocks in the monoclinic space group $P2_1/c$ with a density of 1.973 g cm^{-1} (143 K) and four molecules per unit cell. The molecular structure and coordination environment around the potassium cation of **1** are shown in Figures 2 and 3. The alkali metal is sevenfold coordinated by four different 1-nitraminotetrazolates, which bind with atoms N3, N4, O1, or O2.

Compound **2** is shown in Figure 4 and crystallizes in the form of colorless rods in the orthorhombic space group *Pbca* with eight formula units per unit cell and a calculated density of 1.983 g cm^{-1} (143 K). The densities of both iso-

 © 2018 Wiley-VCH Verlag GmbH & Co. KGaA, Weinheim

15214087, 2018, 12, Downloaded from https://onlinelibrary.wiley.com/doi/10.1002/prep.201800221 by Ludwig-Maximilians-Universität, Wiley Online Library on [29/12/2022]. See the Terms and Conditions (https://onlinelibrary.wiley.com/terms-and-conditions) on Wiley Online Library for rules of use; OA articles are governed by the applicable Creative Commons License

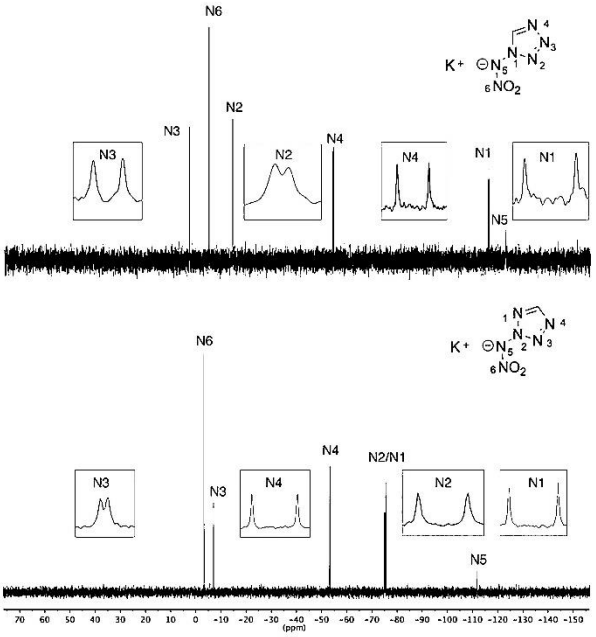


Figure 1. Proton-coupled ^{15}N NMR spectra of compound **1** and **2**.

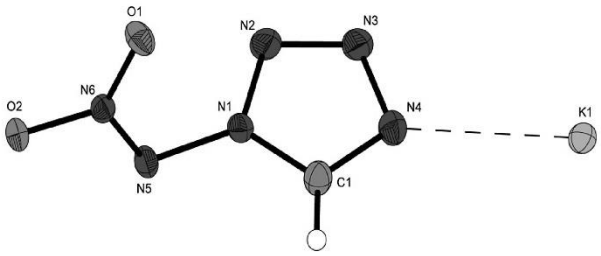


Figure 2. Molecular structure of **1**. Thermal ellipsoids of non-hydrogen atoms in all structures are set to the 50% probability level. Selected bond lengths (pm): C1–H1 92.8(16), N1–C1 133.0(2), N4–C1 131.5(2), N3–N4 136.65(18), N2–N3 129.8(2), N1–N2 134.70(17), 140.47(19), N5–N6 131.81(18), N1–N5 140.5(19), O1–N6 124.70(15), O2–N6 127.10(17).

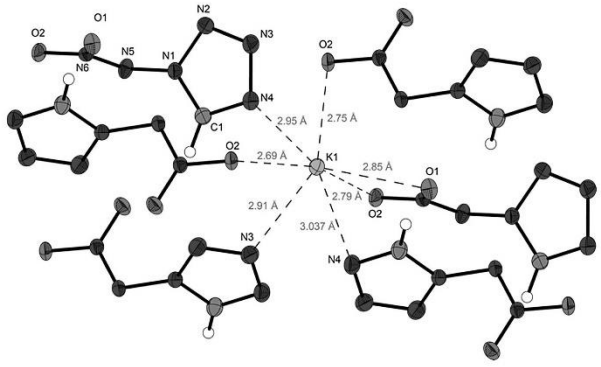


Figure 3. Coordination environment of the potassium cation in **1**.

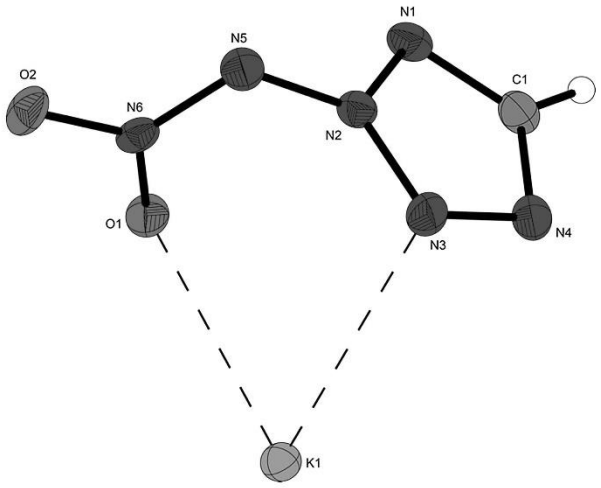


Figure 4. Molecular structure of **2**. Selected bond lengths (pm): C1–H1 94.7(17), N1–C1 132.1(2), N4–C1 134.11(19), N1–N2 132.50(17), N2–N3 131.75(17), N2–N5 139.37 (17), N3–N4 132.14(18), N5–N6 133.40(17), O1–N6 124.94(15), O2–N6 124.46(16).

mers are slightly lower in comparison to K_2DNABT (2.172 g cm^{-3} (100 K)) [14]. In both molecules, the nitro groups are twisted by 109.12° (**1**) and 108.06° (**2**) out of the ring plane, while N5 is almost planar to the tetrazole ring. A comparison of the bond lengths shows that the bond length in **1** between N5 and N6 is slightly shorter with 131.8 pm than in **2** (133.4 pm). These values lie between N–N single and double bonds [20], which reflects the electron-withdrawing effect of the nitro group on the amide moiety. The weakest bond in both molecules is between N1–N5 with 140.5 pm (**1**) and 139.4 pm (**2**). (Further details on the crystal structure can be found in the Supporting Information.)

3.3 Scanning Electron Microscopy (SEM) and Energy-Dispersive X-Ray Spectroscopy (EDX)

Scanning electron microscopy in combination with energy dispersive X-ray spectroscopy was used to determine the morphology, grain size and chemical composition, which can strongly influence the observed sensitivities performed.

Due to the simpler synthesis, the associated lower costs and the more promising characteristics of compound **1** compared to **2**, only this salt was measured by SEM and EDX. Compound **1** shows the consistency of small tubes with cavities (Figure 5). Aside from insignificant trace amounts of silicon, the EDX spectrum only shows elements which are actually present in the molecular structure. No contamination of fluorine or boron was detected.

 © 2018 Wiley-VCH Verlag GmbH & Co. KGaA, Weinheim

15214087, 2018, 12, Downloaded from https://onlinelibrary.wiley.com/doi/10.1002/prep.201800221 by Ludwig-Maximilians-Universität, Wiley Online Library on [29/12/2022]. See the Terms and Conditions (https://onlinelibrary.wiley.com/terms-and-conditions) on Wiley Online Library for rules of use; OA articles are governed by the applicable Creative Commons License

3.4 Physicochemical Properties

Since all materials investigated are highly energetic compounds, their physicochemical properties were explored. The thermal behavior of compound **1** and **2** was investigated using DTA (Figure 6). Violent detonations could be observed for 1 ant 180 °C, and 176 °C for compund 2, after melting of both compounds. The decomposition peak of compound 2 is relatively broad due to the small amount of substance used for the measurement.

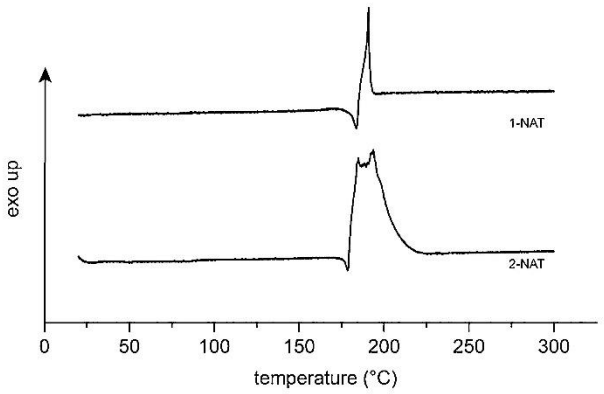


Figure 6. DTA plots of compound **1** and **2**.

To evaluate the potential of **1** and **2** as suitable green primary explosives, the sensitivities toward impact, friction, electrostatic discharge next to thermal stability and detonation performance were investigated (Table 1). The friction, impact, and electrostatic sensitivities of **1** and **2** are comparable to those of LA and K_2DNABT [14]. The measured friction and ball drop impact sensitivities correspond to the lowest possible determinable values for the equipment used, which underlines the highly sensitive nature of these synthesized compounds. Interestingly, and to our surprise, compound **2** was slightly less sensitive toward impact than **1**. The detonation parameters of **1** and **2** were calculated using the latest EXPLO5 6.04 computer code [21]. Both compounds have very high positive heats of formation, as shown in Table 1.

Table 1. Explosive and detonation parameters of **1** and **2** in comparison to K_2DNABT and LA.

Formula	**1** $CHKN_6O_2$	**2** $CHKN_6O_2$	K_2DNABT [14] $C_2K_2N_{12}O_4$	$Pb(N_3)_2$ [22] N_6Pb
IS[a] [J]	<1	5	1	2.4–4
FS[b] [N]	<0.1	<0.1	<0.1	0.1–1.0
ESD[c] [mJ]	0.9	8.2	<0.1	<5.0
BDIS	<4[o]	<4[o]	31.1[p]	53.3[q]
Ω_{CO2}[d] [%]	−6.2	−6.2	−4.8	−11.0
T_{dec}[e] [°C]	180	176	200	320–360
δ[f] [g cm^{-3}]	1.928	1.938	2.172	4.80[n]
$\Delta_f H°$[g] [kJ mol^{-1}]	93.4	77.9	326.4	450.1[n]
$\Delta_f U°$[h] [kJ kg^{-1}]	621.7	529.6	1035.6	1574.9[n]
EXPLO5 6.04 values:				
$-\Delta_{ex}H°$[i] [kJ kg^{-1}]	4616	4526	4959	1575
T_{det}[j] [K]	3259	3209	3417	3285
P_{CJ}[k] [GPa]	25.0	25.1	32.5	34.9
V_{det}[l] [ms^{-1}]	7858	7882	8691	6077
V_0[m] [dm^3 kg^{-1}]	410	409	485	252

[a] Impact sensitivity (BAM drop-hammer (1 of 6)). [b] Friction sensitivity (BAM friction tester (1 of 6)). [c] Electrostatic discharge device (OZM research). [d] Oxygen balance (Ω = (xO − 2yC − 1/2zH) M/1600). [e] Onset temperatures measured by DTA (β = 5 °C min^{-1}). [f] X-ray densities converted to RT. [g] Calculated enthalpy of formation. [h] Calculated energy of formation. [i] Heat of explosion. [j] Temperature of detonation. [k] Detonation pressure. [l] Detonation velocity. [m] Gas volume after detonation (assuming only gaseous products). [n] from EXPLO5 database. [o] ball drop impact sensitivity determined with the OZM ball drop tester applying the 1 of 6 method in accordance with the MIL-STD 1751A (method 1016). [p] E_{50} ball drop impact sensitivity determined with the OZM ball drop tester applying the Probit method with 10 trials at 6 different heights. [q] E_{50} ball drop impact sensitivity of dextrinated LA [22].

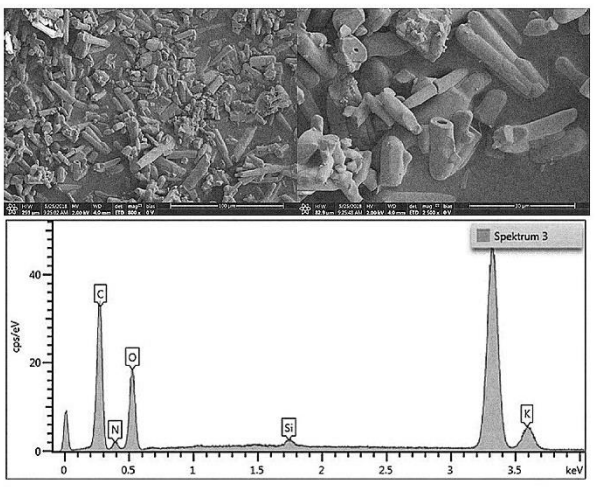


Figure 5. SEM image (800× magnitude (left) and 2500× magnitude (right)) and EDX spectrum of compound **1**.

As expected, the enthalpy of formation and energy of formation values are lower than for the double potassium salt K_2DNABT [14]. The nitramino-5*H*-tetrazolate isomers outperform easily lead azide in performance parameters such as heat of explosion, detonation velocity and gas volume after detonation [22]. Nevertheless, the values are still below those of K_2DNABT, which can be attributed to the higher density and higher heat of formation. The value for the temperature of detonation is in the range of lead azide. From the point of view of detonation pressure, both isomers exhibit detonation pressures 10 GPa lower than for lead azide and 7,5 GPa lower than for K_2DNABT.

In order to determine the compounds' deflagration to detonation transition (DDT) capability, hot needle (HN) and hot plate (HP) tests were performed (Figure 7). The HN test

 © 2018 Wiley-VCH Verlag GmbH & Co. KGaA, Weinheim

15214087, 2018, 12, Downloaded from https://onlinelibrary.wiley.com/doi/10.1002/prep.201800221 by Ludwig-Maximilians-Universität, Wiley Online Library on [29/12/2022]. See the Terms and Conditions (https://onlinelibrary.wiley.com/terms-and-conditions) on Wiley Online Library for rules of use; OA articles are governed by the applicable Creative Commons License

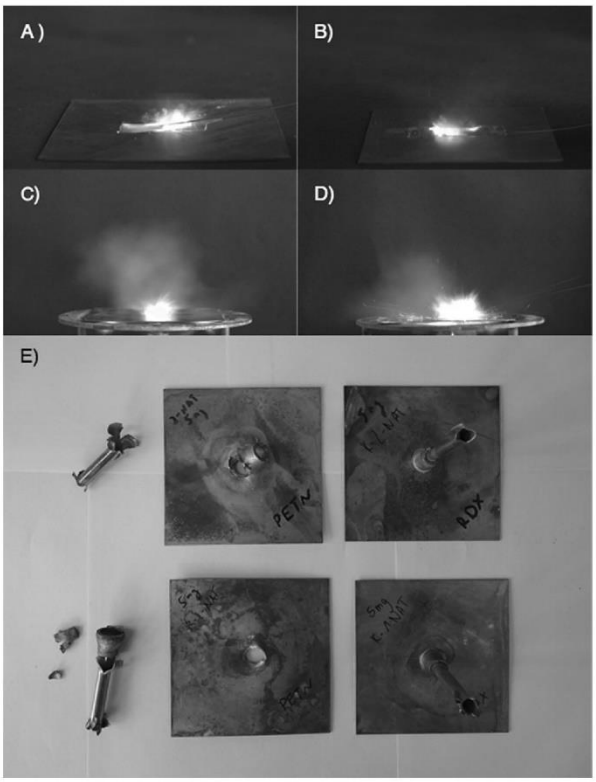


Figure 7. A) and B) HN test of **1** and **2**; C) and D) HP test of **1** and **2**; E) Positive PETN (left) and RDX (right) initiation tests with 5 mg of compound **1** (bottom) and **2** (top).

was performed by the fixation of each compound underneath adhesive tape. The following penetration of **1** and **2** with a red-heated needle resulted in a vast detonation, which indicates their great potential as valuable primary explosives. The safe and straightforward HP test shows the behavior of the unconfined samples toward fast heating. Both compounds detonated also violently during the hot plate test with a slight bending of the plates.

3.5 Toxicity

To estimate the potential environmental impact of compound **1** and **2**, toxicity measurements were carried out using the luminesce marine bacterium *Vibrio fischeri* [23]. Our studies show that, after a time period of 30 min 85% of the bacteria were unaffected at a concentration of 1.60 g L^{-1} (**1**) and 1.61 g L^{-1} (**2**). Due to the extreme non-toxicity of the compounds, no reasonably EC_{50} value could be determined with the dilution series used. Nevertheless, with values clearly over 1.00 g L^{-1}, both compounds can be considered as non-toxic (toxicity level after 30 min incubation: very toxic <0.10 g L^{-1}, toxic 0.10–1.00 g L^{-1}, non-toxic >1.00 g L^{-1}) [24].

4 Conclusions

Potassium 1-(*N*-nitramino)-5*H*-tetrazolate (**1**, 1-KNAT) and its isomeric counterpart potassium 2-(*N*-nitramino)-5*H*-tetrazolate (**2**, 2-KNAT), two new promising primary explosives, could by synthesized through direct nitration of 1-amino-5*H*-tetrazole and 2-amino-5*H*-tetrazole and subsequent addition of potassium ethanolate in a one-step reaction. The potassium salts that could be prepared by an alternative route compared to the literature-known ammonium and silver salts represent a good compromise between solubility, sensitivity, performance, and environmental compatibility. Since the compounds known from literature have been very poorly analyzed, this work carries out an extensive analytical study of the two potassium salts in order to close this gap. Both compounds were characterized by low-temperature X-ray diffraction and showed, unfortunately, a slightly lower density compared to K_2DNABT. In addition, the compounds were analyzed by vibrational (IR) and multinuclear NMR spectroscopy, as well as by EA. To identify impurity residues and to investigate the morphology, grain size and crystal habit of **1**, the latter was measured with scanning electron microscopy and energy dispersive X-ray spectroscopy. Thermal stability measurements by DTA showed satisfying exothermic decomposition temperatures around 180 °C. The measured sensitivities toward friction and impact, underline the highly sensitive character of the two isomers while remaining safe to handle. The calculations of the energetic properties of 1-KNAT and 2-KNAT, show their excellent performance in comparison to lead azide, outperforming LA in several important parameters. Easy thermal initiation was proven by hot plate and hot needle tests and an excellent secondary explosive initiation capability was observed. Only 5 mg of the two compounds were sufficient to initiate PETN and RDX reliably. Toxicity measurements using *Vibrio fischeri* showed the non-toxic character of the environmentally benign potassium salts. 1-KNAT can be considered as a promising lead-free green primary explosive for potential future initiation systems due to its simpler synthesis (starting material is more easily accessible) and better sensitivity values compared to **2**.

Acknowledgements

We acknowledge the financial support of this work, which was provided by the Ludwig Maximilian University of Munich (LMU) and the Office of Naval Research (ONR) under grant no. ONR.N00014-16-1-2062. The authors also want to thank Marcus Lommel and Michael Gruhne for their help in sensitivity measurements tests, Jasmin Lechner for her help in initiation tests, Cornelia Unger for toxicity assessments and Josh Bauer for contribution.

 © 2018 Wiley-VCH Verlag GmbH & Co. KGaA, Weinheim

15214087, 2018, 12, Downloaded from https://onlinelibrary.wiley.com/doi/10.1002/prep.201800221 by Ludwig-Maximilians-Universität, Wiley Online Library on [29/12/2022]. See the Terms and Conditions (https://onlinelibrary.wiley.com/terms-and-conditions) on Wiley Online Library for rules of use; OA articles are governed by the applicable Creative Commons License

References

[1] P. E. Eaton, R. L. Gillardi, M. X. Zhang, Polynitrocubanes: Advanced High-Density, High-Energy Materials, *Adv. Mater.* **2000**, *12*, 1143–1148.

[2] T. M. Klapötke, C. Petermayer, D. G. Piercey, J. Stierstorfer, 1,3-Bis(nitroimido)-1,2,3-triazolate Anion, the N-Nitroimide Moiety, and the Strategy of Alternating Positive and Negative Charges in the Design of Energetic Materials, *J. Am. Chem. Soc.* **2012**, *134*, 20827–20836.

[3] K. B. Landenberger, O. Bolton, A. J. Matzger, Energetic-Energetic Cocrystals of Diacetone Diperoxide (DADP): Dramatic and Divergent Sensitivity Modifications via Cocrystallization, *J. Am. Chem. Soc.* **2015**, *137*, 5074–5079.

[4] H. Gao, J. M. Shreeve, *Chem. Rev.* **2011**, Azole-Based Energetic Salts, *111*, 7377–7436.

[5] J. Zhang, L. A. Mitchell, D. A. Parrish, J. M. Shreeve, Enforced Layer-by-Layer Stacking of Energetic Salts towards High-Performance Insensitive Energetic Materials, *J. Am. Chem. Soc.* **2015**, *137*, 10532–10535.

[6] T. Yongxing, Y. Hongwei, W. Bo, J. Xuehai, L. Chunxu, C. Guangbin, Synthesis and Characterization of a Stable, Catenated N11 Energetic Salt, *Angew. Chemie Int. Ed.* **2013**, *52*, 4875–4877.

[7] https://echa.europa.eu/de/candidate-list-table (Acessed April **2018**)

[8] M. H. V Huynh, M. D. Coburn, T. J. Meyer, M. Wetzler, Green primary explosives: 5-Nitrotetrazolato-N^2-ferrate hierarchies, *Proc. Natl. Acad. Sci.* **2006**, *103*, 10322 LP-10327.

[9] L. Shenghua, W. Yuan, Q. Cai, Z. Xiuxiu, Z. Jichuan, Z. Shaowen, P. Siping, 3D Energetic Metal-Organic Frameworks: Synthesis and Properties of High Energy Materials, *Angew. Chemie Int. Ed.* **2013**, *52*, 14031–14035.

[10] J. Qin, J. Zhang, M. Zhang, D. Du, J. Li, Z. Su, Y. Wang, S. Pang, S. Li, Y. Lan, A Highly Energetic N-Rich Zeolite-Like Metal-Organic Framework with Excellent Air Stability and Insensitivity, *Adv. Sci.* **2015**, *2*, 1500150.

[11] M. Armand, F. Endres, D. R. MacFarlane, H. Ohno, B. Scrosati, Ionic-liquid materials for the electrochemical challenges of the future, *Nat. Mater.* **2009**, *8*, 621.

[12] L. Zhai, X. Fan, B. Wang, F. Bi, Y. Li, Y. Zhu, A green high-initiation-power primary explosive: synthesis, 3D structure and energetic properties of dipotassium 3,4-bis(3-dinitromethylfurazan-4-oxy)furazan, *RSC Adv.* **2015**, *5*, 57833–57841.

[13] J. W. Fronabarger, M. D. Williams, W. B. Sanborn, D. A. Parrish, M. Bichay, KDNP – A Lead Free Replacement for Lead Styphnate, *Propellants Explos. Pyrotech.* **2011**, *36*, 459–470.

[14] D. Fischer, T. M. Klapötke, J. Stierstorfer, Potassium 1,1′-Dinitramino-5,5′-bistetrazolate: A Primary Explosive with Fast Detonation and High Initiation Power, *Angew. Chem. Int. Ed.* **2014**, *53*, 1–5.

[15] Y. Tang, C. He, L. A. Mitchell, D. A. Parrish, J. M. Shreeve, Potassium 4,4′-Bis(dinitromethyl)-3,3′-azofurazanate: A Highly Energetic 3D Metal-Organic Framework as a Promising Primary Explosive, *Angew. Chemie Int. Ed.* **2016**, *55*, 5565–5567.

[16] H. Chunlin, J. M. Shreeve, Potassium 4,5-Bis(dinitromethyl)furoxanate: A Green Primary Explosive with a Positive Oxygen Balance, *Angew. Chemie Int. Ed.* **2015**, *55*, 772–775.

[17] D. E. G. Jones, H. T. Feng, R. C. Fouchard, Kinetic Studies of the Thermal Decomposition of KDNBF, a Primer for Explosives, *J. Therm. Anal. Calorim.* **2000**, *60*, 917–926.

[18] P. Yin, D. A. Parrish, J. M. Shreeve, Energetic Multifunctionalized Nitraminopyrazoles and Their Ionic Derivatives: Ternary Hydrogen-Bond Induced High Energy Density Materials, *J. Am. Chem. Soc.* **2015**, *137*, 4778–4786.

[19] M. A. Ilyushin, A. N. Terpigorev, I. V. Tselinskii, Effect of Isomeric Structure of (N-Nitramino)tetrazoles on the Properties of Theirs Salts, *Russ. J. Gen. Chem.* **1999**, *69*, 1645–1657.

[20] A. F. Hollemann, E. Wiberg, *Lehrbuch der Anorganischen Chemie*, 101st Edition, de Gruyter, New York, **1999**.

[21] M. Sućeska, EXPLO5 Version 6.04 Users' Guide. Zagreb, Croatia: OZM; **2018**.

[22] a) R. Meyer, J. Köhler, A. Homburg, In *Explosives*, Wiley-VCH: Weinheim, **2002**, p. 196–197; b) Military Standard 1751A (MIL-STD-1751A): safety and performance tests for qualification of explosives (high explosives, propellants and pyrotechnics), method 1016, Dec. 11, **2001**.

[23] G. I. Sunahara, S. Dodard, M. Sarrazin, L. Paquet, G. Ampleman, S. Thiboutot, J. Hawari, A. Y. Renoux, *Ecotoxicol. Environ. Saf.* **1998**, *39*, 185 – 194.

[24] C. J. Cao, M. S. Johnson, M. M. Hurley, T. M. Klapötke, *JANNAF J. Propuls. Energet.* **2012**, *5*, 41–51.

Received: July 10, 2018
Revised: September 11, 2018
Published online: October 22, 2018

 © 2018 Wiley-VCH Verlag GmbH & Co. KGaA, Weinheim

15214087, 2018, 12, Downloaded from https://onlinelibrary.wiley.com/doi/10.1002/prep.201800221 by Ludwig-Maximilians-Universität, Wiley Online Library on [29/12/2022]. See the Terms and Conditions (https://onlinelibrary.wiley.com/terms-and-conditions) on Wiley Online Library for rules of use; OA articles are governed by the applicable Creative Commons License

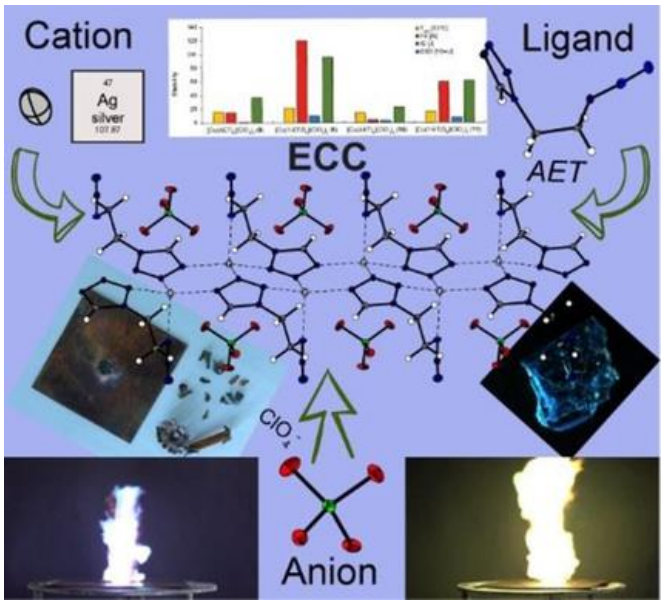
Appendix 10

Comparison of 1-Ethyl-5H-tetrazole and 1-Azidoethyl-5H-tetrazole as Ligands in Energetic Transition Metal Complexes

M. H. H. Wurzenberger, M. S. Gruhne, M. Lommel, N. Szimhardt, T. M. Klapötke, J. Stierstorfer

Chem. Asian J. **2019**, *14*, 2018–2028.

https://doi.org/10.1002/asia.201900269



Supplementary Information:
https://onlinelibrary.wiley.com/action/downloadSupplement?doi=10.1002%2Fasia.201900269&file=asia201900269-sup-0001-misc_information.pdf

ACES Asian Chemical Editorial Society

DOI: 10.1002/asia.201900269

CHEMISTRY AN ASIAN JOURNAL Full Paper

Comparison of 1-Ethyl-5*H*-tetrazole and 1-Azidoethyl-5*H*-tetrazole as Ligands in Energetic Transition Metal Complexes

Maximilian H. H. Wurzenberger, Michael S. Gruhne, Marcus Lommel, Norbert Szimhardt, Thomas M. Klapötke, and Jörg Stierstorfer*[a]

Abstract: Energetic coordination compounds (ECC) based on 3d or 4d transition metals show promising characteristics to be used as potential replacements for highly toxic lead-containing primary explosives. Herein we report the synthesis of 12 new ECC based on 1-azidoethyl-5*H*-tetrazole (AET) or 1-ethyl-5*H*-tetrazole (1-ETZ) as nitrogen-rich ligands as well as various central metals (Cu^{2+}, Fe^{2+}, Zn^{2+}, Ag^{+}) and anions such as perchlorate and nitrate. The influence of the increased endothermicity by adding an additional azide group was studied by comparing analogous ECC based on AET and 1-ETZ. Furthermore, the compounds were extensively analyzed by XRD, IR, EA, solid-state UV/Vis, and DTA as well as their sensitivities toward impact and friction were determined with BAM standard techniques, together with their sensitivity against electrostatic discharge. The sensitivities were compared with the one toward ball drop impact measurements. Classical initiation tests (nitropenta filled detonators) and ignition by laser irradiation highly prove the potential use of the most promising compounds in lead-free initiation systems.

Introduction

Ever since the discovery of the azide anion by Curtius in 1890,[1] the ongoing azide chemistry has fascinated several generations of chemists. Today almost every single element from the periodic table has been combined to build up covalent and ionic azides. The combination of simple main-group and transition metals with the azide anion has provided one high point in this chemistry together with the well-deserved reputation for the explosive behavior.[2] Among easily available and industrial useful ionic azides, lead azide (LA) and sodium azide are the most prominent examples. Nowadays, NaN_3, as the cheapest azide source, is indispensable in many chemical transformations like substitutions or addition reactions in synthetic organic chemistry. Additionally, sodium azide was also found in previous airbag systems.[3] Covalently bonded and ionic azides, in particular, heavy metal azides, are known as thermally decomposable and, in part, explosive classes of compounds. LA is one of the most commonly used primary explosives in both industrial and military applications. However, alternatives, so-called green primary explosives, are in great demand to prevent the considerable, highly toxic lead contamination in military training grounds. Over 95% of all missile launches, shooting, and explosions within the police forces or military are done exclusively for training purposes in "friendly" areas,[4] leading to an ongoing research for new and more eco-friendly energetic materials.[5–10]

Since the discovery of phenyl azide in 1864,[11] azido organic compounds have attracted the attention of chemists due to their unique characteristics. The initial postulation of Curtius and Hantzsch for the structural determination of organic azides suggested a cyclic 1*H*-triazirine structure. Later, however, this hypothesis was rapidly revised in favor of the linear structure (Scheme 1).[1,12–14] The chemical diversity of many organic azides can be explained on the basis of the physicochemical properties by a consideration of the polar mesomeric structures.[15,16]

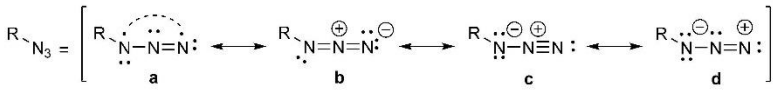
The mesomeric structures **c** and **d**, proposed by Pauling,[17,18] compellingly explain the reactivity in 1,3-dipolar cycloadditions and the decomposition of azides to form nitrenes under the elimination of nitrogen gas. The reactivity of the azide functionality in terms of nucleophilicity (nucleophilic attack of N1) and electrophilicity (nucleophilic attack on N3) can be deduced from the basis of structure **d**. From a thermodynamic standpoint, the azide group is a structural fragment, which shows a high positive heat of formation and adding about 364 $kJ\,mol^{-1}$ of endothermicity to a hydrocarbon compound.[19] Additionally, the azide groups exhibit an environmentally friendly balance, as nitrogen gas is produced as an exclusive smokeless combustion product. Therefore, organic azides are potential candidates for the use in high energetic materials like binders, hypergolic ionic liquids, plasticizers and additives (Figure 1).[2,20–23]

Due to the smokeless gas evolution, the major application nowadays is found in gas generators. Besides these utilizations of organic azides, the use in primary explosives is especially promising. Nitrogen-rich molecules are considered as prime candidates for "green" energetic materials[24–27] since the main combustion product is molecular dinitrogen and the materials

[a] M. H. H. Wurzenberger, M. S. Gruhne, M. Lommel, Dr. N. Szimhardt, Prof. Dr. T. M. Klapötke, Dr. J. Stierstorfer
Department of Chemistry
Ludwig-Maximilian-University of Munich
Butenandtstr. 5–13, 81377 Munich (Germany)
E-mail: jstch@cup.uni-muenchen.de
Homepage: http://www.hedm.cup.uni-muenchen.de

Supporting information and the ORCID identification number(s) for the author(s) of this article can be found under: https://doi.org/10.1002/asia.201900269.

© 2019 Wiley-VCH Verlag GmbH & Co. KGaA, Weinheim



Scheme 1. Mesomeric structures of covalent bonded azide.

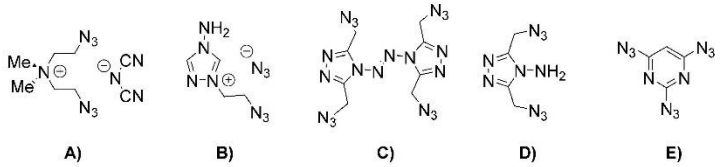


Figure 1. Representative examples for energetic organic compounds: hypergolic ionic liquids (bis(2-azidoethyl)dimethylammonium dicyanamide (**A**) and 1-(2-azidoethyl)-4-amino-1,2,4-triazolium azide (**B**)), energetic plasticizers (3,3′,5,5′-tetra(azidomethyl)-4,4′-azo-1,2,4-triazole (**C**) and 4-amino-3,5-di(azidomethyl)-1,2,4-triazole (**D**)), or an energetic additive in nanotubes (2,4,6-triazidopyrimidine (**E**)).

exhibit desirable performance characteristics in high explosives due to their high positive heat of formation.

In this paper, we demonstrate the increasing performance of ECC by solely substituting one proton of the alkyl rest of 1-ethyl-5*H*-tetrazole with an azide group. The AET based transition metal complexes were both investigated toward their usability as lead-free primary and laser ignitable explosives. In addition, they were compared to their analogous ECC with unsubstituted 1-ETZ as nitrogen-rich ligand.

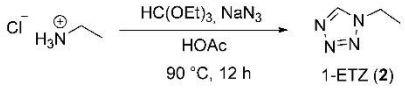
Results and Discussion

Synthesis

Over three decades ago, the synthesis of 1-azidoethyl-5*H*-tetrazole was published for the first time by Gaponik et al..[28] The only reported complex is based on copper(II) chloride as metal salt and was only investigated for its crystal structure.[29] For synthesizing ligand **1** a two-step reaction, starting from a simple and cheap feedstock was performed (Scheme 2).

The first target molecule was 2-azidoethylamine hydrochloride, which is less volatile than the neutral compound and for which several syntheses are already reported in literature.[30,31] 2-Chloroethylamine hydrochloride was reacted with sodium azide in water to form the intermediate in quantitative yield. The crude hydrochloride salt was converted in a [3+1+1] cyclization to the corresponding substituted alkyl tetrazole **1** by applying an excess of triethyl orthoformate and sodium azide in glacial acetic acid at elevated temperature. For the isolation of the nitrogen-rich ligand, the crude was filtrated, extracted with ethyl acetate and subjected to column chromatography leading to a yellowish oil in acceptable 33% yield over two-steps. The physical state of **1** can be explained by previous reports showing the liquefying effect of the azidoethyl functionality.[2]

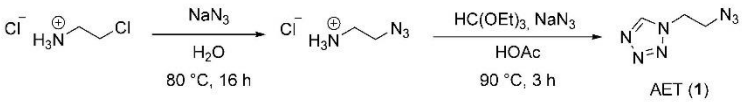
With 1-ethyl-5*H*-tetrazole (**2**), another ethyl-substituted 5*H*-tetrazole derivative is used for the synthesis of nitrogen-rich ECC in this work. The ligand can be obtained via the same selective pathway (Scheme 3) as mentioned above.[28] The



Scheme 3. Selective route for the synthesis of 1-ethyl-5*H*-tetrazole (**2**).

[3+1+1] ring closure reaction again is performed, using triethyl orthoformate, sodium azide, and glacial acetic acid at 80 °C for 12 h. After filtration and extraction using ethyl acetate, the product was received in a satisfying yield of 75%. Both tetrazole derivatives can easily be characterized by IR spectroscopy (Figure S1), proton and carbon NMR spectroscopy. Additionally, two dimensional ^{1}H, ^{15}N NMR HMBC or proton-coupled ^{15}N NMR spectroscopy can be performed (Figure 2 and 3).

As mentioned, a large number of complexes based on various mono-tetrazoles (e.g. 1-methyl- or 1-amino-*5H*-tetrazole) have been described in literature, either having insufficient power or are way too sensitive for practical use.[32,33] In order to maximize the performance, ligand **1** is applied in the formation of new transition metal complexes, whereas the use of ligand **2** is a promising opportunity for reaching the middle course between both demands. The absence of acidic protons in both ligands allows their inclusion in neutral metal coordination compounds with oxidizing anions like nitrates, perchlorates, picrates (PA), styphnates (TNR) or 2,4,6-trinitro-3,5-dihydroxyphenolates (H_2TNPG). The selective integration of these anions in combination with one of the two ligands and different metal(I) or metal(II) cations, results in energetic coordina-



Scheme 2. Synthesis of 1-azidoethyl-5*H*-tetrazole (**1**) starting from 2-chloroethylamine hydrochloride.

© 2019 Wiley-VCH Verlag GmbH & Co. KGaA, Weinheim

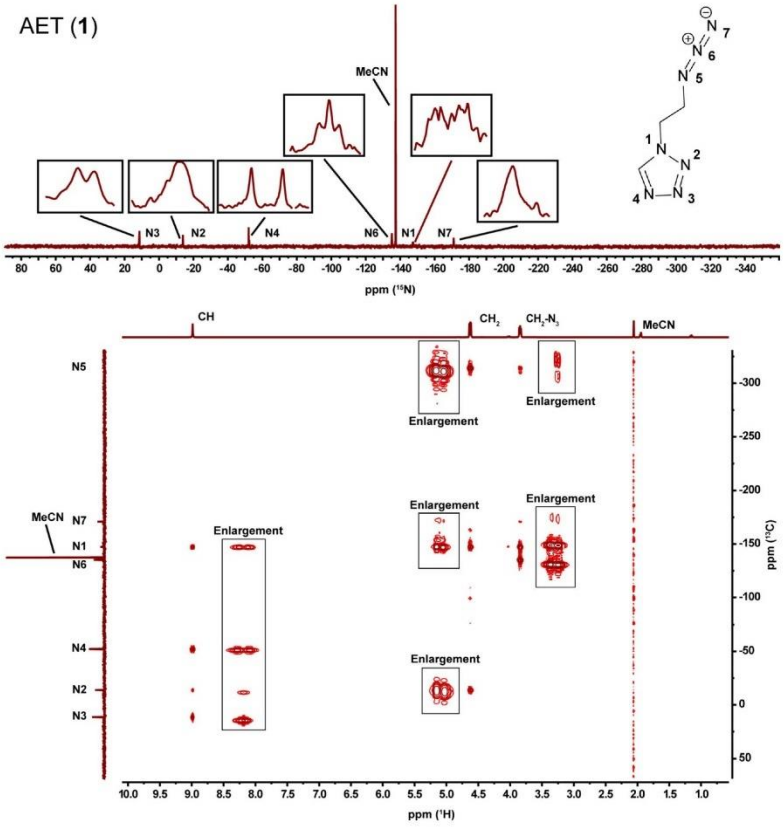
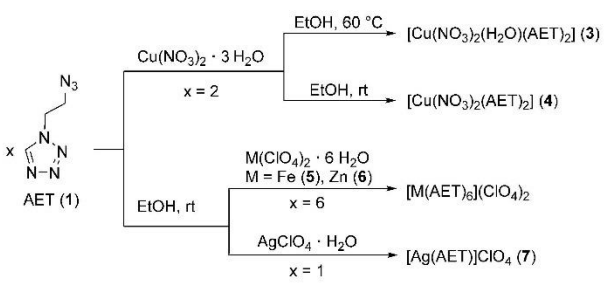


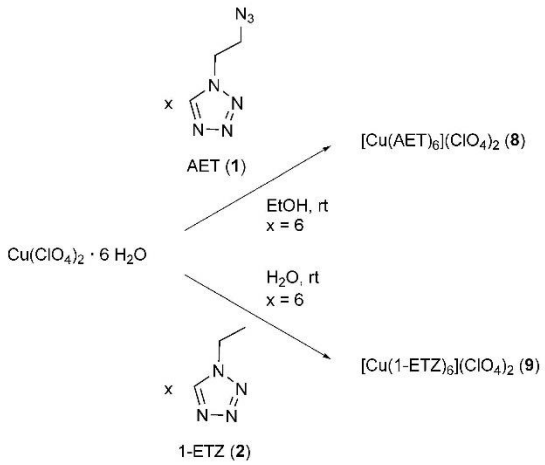
Figure 2. Proton coupled ^{15}N NMR spectra and two dimensional ^{1}H, ^{15}N-HMBC NMR spectra of **1**. ^{15}N NMR (MeCN-d_3, 25 °C): $\delta = 11.4$ (N3, d, $^{2}J_{N-H} = 3.0$), −13.9 (N2), −52.2 (N4, d, $^{2}J_{N\ H} = 12.1$ Hz), −135.2 (N6, t, $^{2}J_{N\ H} = 3.3$ Hz), −147.4 (N1, d, $^{2}J_{N\ H} = 7.3$ Hz), −171.1 ppm (N7).

tion compounds with adjustable sensitivities and performance parameters. The formation of the coordination compounds **3**–**9** was achieved through the combination of ethanolic solutions of the relevant metal(I) or metal(II) salts and the ligand in stoichiometric amounts at r.t. or elevated temperatures in case of compound **3** (Scheme 4 and 5). Water and ethanol as solvent were chosen because of their non-toxic character and the good solubility of the ligand and the metal salts. Except coordination compound **3**, every complex crystallized without inclusion of water molecules. Complex **4** has only been obtained as a side species of **3**, making a further characterization impossible. Copper(II) chlorate complexes based on ligand **1** and **2** have been synthesized analogously to our recently published work (Scheme 6).[34]

Due to the commercial unavailability of the copper(II) starting materials of the compounds **12**–**14**, an acid-base reaction



Scheme 4. Synthesis of the nitrato complexes **3** and **4** together with the perchlorate complexes **5**–**7**.



Scheme 5. Synthesis of the copper(II) perchlorate complexes **8** and **9**.

© 2019 Wiley-VCH Verlag GmbH & Co. KGaA, Weinheim

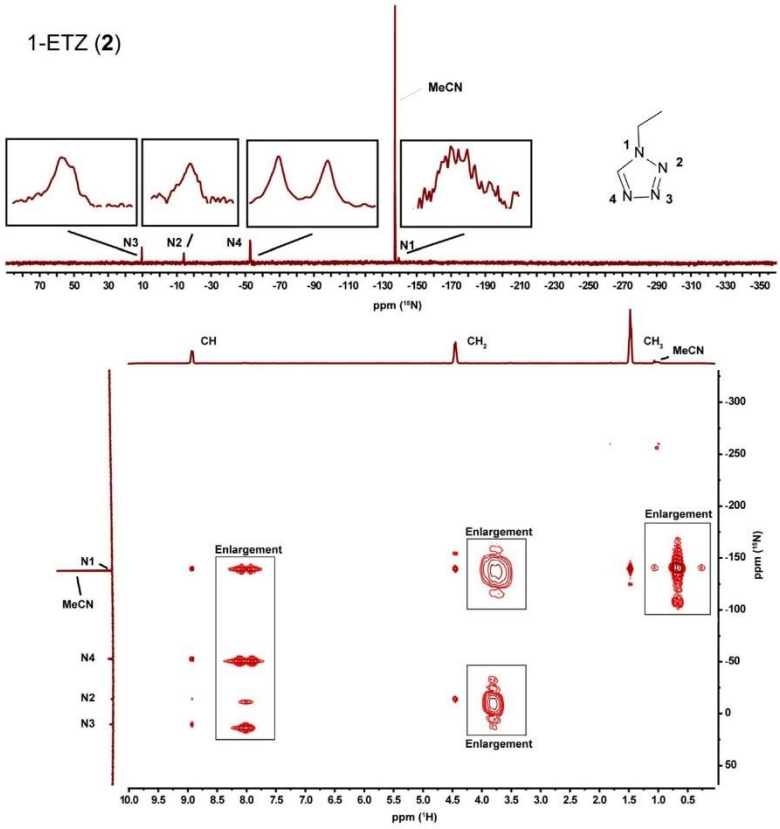
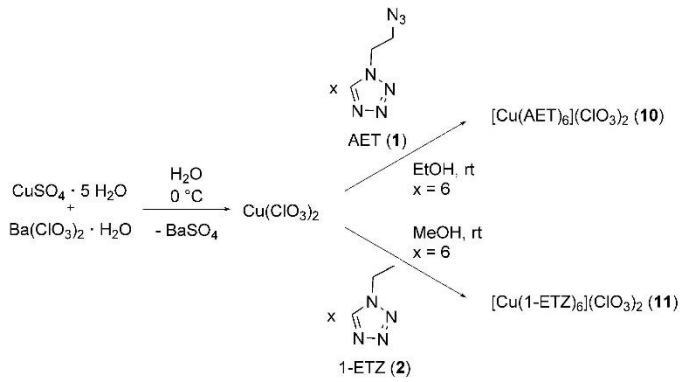
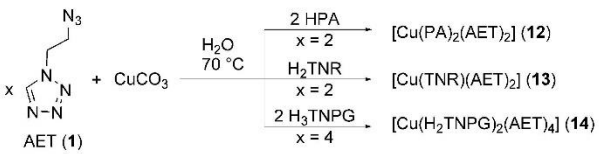


Figure 3. Proton coupled ^{15}N NMR spectra and two dimensional ^{1}H, ^{15}N-HMBC NMR spectra of **2**. ^{15}N NMR (MeCN-d_3, 25 °C): $\delta = 10.4$ (N3), −14.1 (N2), −52.8 (N4, d, $^{2}J_{N\,H} = 12.2$ Hz), −139.5 (N1).



Scheme 6. Synthesis of the chlorate complexes **10** and 11.



Scheme 7. Synthesis of the nitroaromatic coordination compounds **12**–**14**.

had to be applied, starting from the respective 2,4,6-trinitrophenol derivatives and copper(II) carbonate in water at 70 °C. Filtration and treating with ligand **1** yielded the respective coordination compound (Scheme 7).

Potential precipitates during the addition of the ligand are dissolved by dropwise addition of water. Single crystals suitable for X-Ray diffraction were obtained directly from the mother liquor within a day. The filtration step after the acid-base reaction toward **12**–**14** turned out to be indispensable for elemental analysis pure products because traces of unreacted copper(II) carbonate cannot be removed by washing with cold ethanol after crystallization. All coordination compounds were obtained directly from the mother liquor and crystallized in satisfactory yields (38–87 %). The crystalline materials were filtered off, washed with small amounts of ice-cold ethanol and dried in air overnight. Single crystals suitable for X-ray diffraction of every compound except **5**, **8**, **9** and **10** were also obtained directly from the mother liquor. Crystals of the remaining coordination compounds were obtained after recrystallization from water.

© 2019 Wiley-VCH Verlag GmbH & Co. KGaA, Weinheim

Crystal Structures

The crystal structures of the ligands 1-azidoethyl-5*H*-tetrazole (**1**) and 1-ethyl-5*H*-tetrazole (**2**) are not described in literature. Due to their liquid state at r.t. and very low melting points, single crystals of those molecules were not obtained.

Therefore, single-crystal X-ray diffraction studies of all complexes were performed. Details on the crystal structures of compound **9** and **11** together with the measurement and refinement data of all complexes are given in the Supporting Information (Table S1–3 and Figure S5–7). The crystal datasets were uploaded to the CSD database[35] and can be obtained free of charge with the CCDC 1898402 (**3**), 1898401 (**4**), 1898397 (**5**), 1898400 (**7**), 1898399 (**9**), 1898541 (**11**), 1898395 (**12**), 1898398 (**13**), 1898396 (**14**). All metal(II) (per)chlorate complexes show octahedral coordination spheres around the central metals built up by six molecules of ligand **1** or **2** (Figure 5, S5 and S6). Unfortunately, compounds **6**, **8** and **10** could only be measured at r.t. and are therefore highly disordered. Finalization of the datasets was impossible but the measurements allowed an insight into the complexes' composition, which were confirmed by elemental analysis and IR spectroscopy (Figure S2–4). In all complexes, except compound **7**, both tetrazole derivatives coordinate to the central metals exclusively through their heterocyclic N4 nitrogen atoms. ECC **3** shows a rather uncommon sevenfold-bonded copper(II) cation (Figure 4) and complex **7**, with Ag–N bond lengths between 2.323(3) and 2.538(3) Å, possesses distorted tetrahedrally coordinated silver ions.

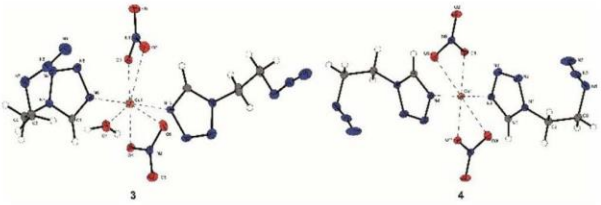


Figure 4. Molecular units of $[Cu(NO_3)_2(H_2O)(AET)_2]$ (**3**) and $[Cu(NO_3)_2(AET)_2]$ (**4**). Selected bond lengths (Å) of **3**: Cu1–N6 1.997(5), Cu1–N13 1.981(5); selected bond angles (°) of **3**: O1-Cu1-O2 52.15(15), O1-Cu1-O4 178.70(16), O1-Cu1-O5 127.78(15), O1-Cu1-N6 91.55(19), O1-Cu1-N13 88.86(19), O2-Cu1-O4 127.13(15), O2-Cu1-O5 78.29(14), O4-Cu1-O5 51.98(15), O4-Cu1-N13 92.32(19), O5-Cu1-O7 137.21(17), O5-Cu1-N6 98.24(17), O5-Cu1-N13 79.86(17), O7-Cu1-N6 92.5(2), O7-Cu1-N13 89.6(2), N6-Cu1-N13 177.85(19). Selected bond lengths (Å) of **4**: Cu–O1 1.9837(14), Cu1–O3 2.6497(18), Cu1–N4 1.971(2); selected bond angles (°) of **4**: O1-Cu1-O3 53.54(6), O1-Cu1-N4 89.96(7), O1-Cu1-O1^{i} 180.00, O1-Cu1-O3^{i} 126.46(6); symmetry code of **4**: (i) 1−*x*, 2−*y*, 1−*z*.

The copper(II) nitrato complex (**3**) crystallizes in the form of blue plates in the triclinic space group *P*-1 with two formula units per unit cell and a calculated density of 1.834 g cm^{-3} at 143 K. The sevenfold coordination environment of the copper(II) center consists of two chelating nitrato, one aqua, and two AET ligands. The nitrates are functioning as bidentate nitrato-ligands, resulting in a longer (2.734 Å) and a shorter (1.971 Å) Cu–O bond. Overall, the unusual amount of five ligands together with the extended sevenfolded coordination sphere results in three clearly longer Cu–O bonds (O2–Cu1 2.734(5) Å, O5–Cu1 2.734(5) Å O7–Cu1 2.337(5) Å), including the aqua ligand. The anhydrous nitrato complex **4** crystallizes in the form of blue blocks in the monoclinic space group $P2_1/c$ with two formula units per unit cell. The calculated density is 1.895 g cm^{-3} at 173 K. The closed octahedral coordination sphere again includes two chelating nitrato and two AET ligands (Figure 4). The nitrato ligands are located in the equatorial and axial positions, whereas ligand **1** exclusively occupies equatorial positions. In consequence of the bidentate character of the nitrate, the bond angles are highly distorted from the ideal bond angle of 90°. A comparison of the complexes **3** and **4** shows, that the addition of a water ligand leads to a simple extension of the coordination sphere from a sixfold highly symmetric complex to a sevenfolded coordinated complex without any symmetry. In case of an extended coordination sphere, it is not surprising that in complex **3** the bond distances between the coordinating ligands and the copper(II) center are longer than the bond distances reported for the water-free compound **4**. Additionally, the torsion angle between the oxygens of one nitrate ligand is shortened from 53.54° (**4**) to 52.15° (**3**). The formation of a sevenfolded coordination sphere is a behavior, already observed for 1*H*-substituted tetrazole derivatives in copper(II) nitrato complexes with similar bond lengths around the central metal.[33]

The metal(II) perchlorate complexes **5**, **6** and **8** all crystallize isotypically in the monoclinic space group $P2_1/c$ with similar cell parameters and densities. Unfortunately, compounds **6** and **8** could only be measured at r.t. and therefore the ethyl azide moieties are highly disordered. The unit cell of **5** is built up by two formula units and possesses a calculated density of 1.648 g cm^{-3} at 128 K. The iron(II) central atom is surrounded by six molecules of ligand **1** (Figure 5) with similar Fe1–N bond lengths. Both perchlorate anions are non-coordinating.

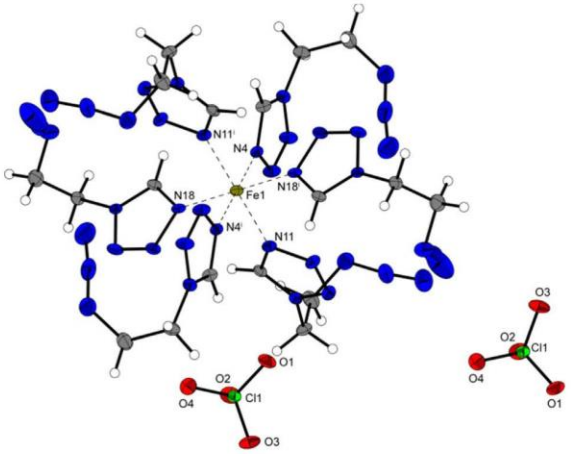


Figure 5. Molecular unit of $[Fe(AET)_6](ClO_4)_2$ (**5**). Selected bond lengths (Å): Fe1–N4 1.990(4), Fe1–N11 1.996(4), Fe–N18 1.977(5); selected bond angles (°): N11-Fe1-N11^{i} 180.00, N4-Fe1-N11 89.17(16), N18-Fe1-N18^{i} 180.00, N4-Fe1-N18^{i} 89.96(16), N4-Fe1-N4^{i} 180.00, N11-Fe1-N18 89.41(18); symmetry code: −*x*, −*y*, −*z*.

© 2019 Wiley-VCH Verlag GmbH & Co. KGaA, Weinheim

The silver(I) complex **7** crystallizes in the form of colorless needles in the triclinic space group *P*-1 and consists of two formula units per unit cell. With a calculated density of 2.470 g cm^{-3} at 173 K, the complex possesses the highest one of all compounds (Figure 6). In contrast to all other complexes based on

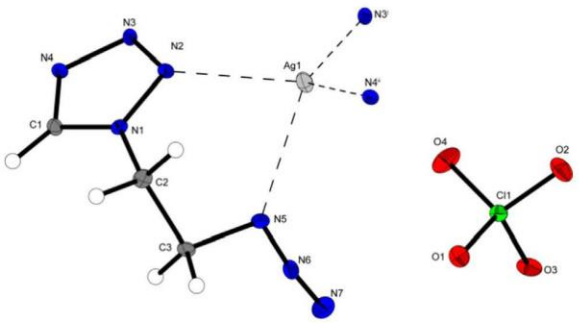


Figure 6. Coordination environment of [Ag(AET)]ClO_4 (**7**). Selected bond lengths (Å): Ag1–N2 2.420(3), Ag1–N4^{i} 2.323(3), Ag1–N3^{ii} 2.331(3); selected bond angles (°): N2-Ag1-N4^{i} 122.84(10), N2-Ag1-N3^{ii} 111.68(11), N4^{i}-Ag1-N5 86.06(11), N3^{ii}-Ag1-N5 133.85(10); symmetry codes: (i) $-x$, $1-y$,$1-z$; (ii) $1+x$, y, z.

AET, the ligand coordinates with four different coordination sides, in particular, the nitrogen atoms N2, N3, N4, and N5. This is resulting in the formation of one-dimensional polymeric chains (Figure 7). For the first time, the azide functionality of the ligand **1** is involved in the coordination bonding, with an astonishing long bond of Ag1-N5 (2.538 Å). With its bond angles (N3^{ii}-Ag-N4^{i} = 122.84°, N2-Ag1-N5 = 77.31°), the tetrahedral formed by compound **7** strongly differs from the perfect angles of 109.47°. This deviation can be explained by the perchlorate anions located above and underneath the layers of silver ions and their interaction with these.

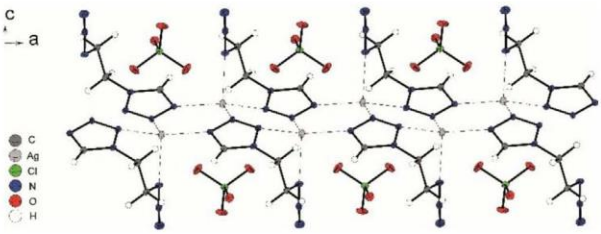


Figure 7. Segment of the polymeric chain of **7**, formed by tetrazole rings linking between three different silver atoms.

The coordination compound **12** crystallizes in the form of green plates in the monoclinic space group $P2_1/c$ with two formula units per unit cell. The complex possesses a calculated density of 1.815 g cm^{-3} at 143 K. The coordination sphere is built up by two equatorial arranged AET ligands and two molecules of picrate (Figure 8). The anions are acting as bidentate ligands, coordinating over the deprotonated hydroxy group and by another oxygen atom of one of the nitro groups. The

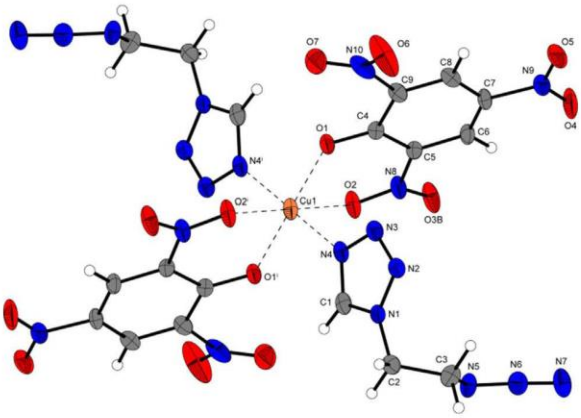


Figure 8. Molecular unit of [Cu(PA)$_2$(AET)$_2$] (**12**). Selected bond lengths (Å): Cu1–O1 1.931(4), Cu1–O2 2.334(3), Cu1–N4 1.997(4); selected bond angles (°): O1-Cu1-O1^{i} 180.00, O1-Cu1-O2 79.35(14), O1-Cu1-N4 91.62(17); symmetry code: (i) $-x$, $1-y$, $-z$.

latter occupy axial positions leading to a typical Jahn–Teller distortion along the O2-Cu1-O2^{i} axis.

The styphnate complex **13** shows a similar density (1.803 g cm^{-3} at 143 K) to compound **12** and crystallizes in the triclinic space group *P*-1 with two formula units per unit cell (Figure 9).

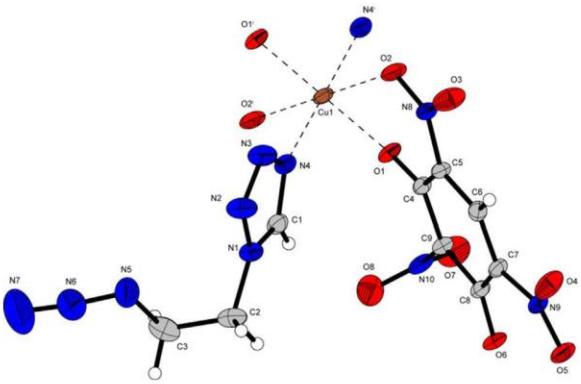


Figure 9. Coordination environment of [Cu(TNR)(AET)$_2$] (**13**). Selected bond lengths (Å): Cu1–O1 1.9266(16), Cu1–O2 2.3431(17), Cu1–N4 2.0115(19); selected bond angles (°): O1-Cu1-O1^{i} 180.00, O1-Cu1-O2 80.65(7), O1-Cu1-N4 88.92(7); symmetry code: (i) $2-x$, $-y$, $2-z$.

Both hydroxy groups of styphnic acid are deprotonated leading to the formation of a trinitroresorcinate anion, which is coordinating to two different copper(II) cations by chelating each with one nitro and one phenolate oxygen. The Jahn–Teller-distortion along the O2-Cu1-O2^{i} is formed by two weaker bonded nitro groups of two different anions. Similar to silver complex **7**, **13** forms one-dimensional polymeric chains, which are however not caused by bridging ligands but by the fourfold coordinating anion (Figure S7). Coordination compound **14** crystallizes in the triclinic space group *P*-1 with only one formula unit per unit cell and a calculated density of

© 2019 Wiley-VCH Verlag GmbH & Co. KGaA, Weinheim

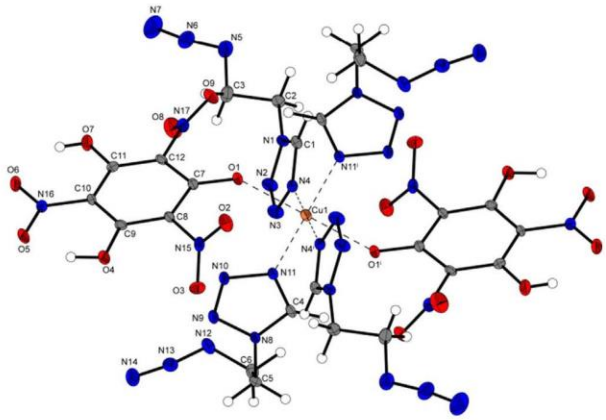


Figure 10. Unit cell of coordination compound $[Cu(H_2TNPG)_2(AET)_4]$ (**14**). Selected bond lengths (Å): Cu1–O1 2.345(2), Cu1–N4 2.027(3), Cu1–N11 1.983(3); selected bond angles (°): O1-Cu1-N4 89.97(11), O1-Cu1-N11 95.31(11), O1-Cu1-O1^{i} 180.00, N4-Cu1-N11 89.59(11); symmetry code: (i) $1-x$, $-y$, $1-z$.

1.766 g cm^{-3} at 143 K. In contrast to nitroaromatic compound **13**, the anions are only single deprotonated and solely coordinating with the phenolate group (Figure 10). The remaining equatorial positions are occupied by four instead of two molecules of ligand **1**. Again, the Jahn–Teller-distortion can be observed along the O-Cu-O axis.

Sensitivities and thermal stability

The behavior of all compounds, except the side-product **4**, was investigated in differential thermal analysis (DTA). The measurements were performed in the range from 25–400 °C at a heating rate of $\beta = 5$ °C min^{-1}. Critical points are given as onset temperatures. The observed endothermic events (melting, dehydration or loss of coordinating ligand), as well as exothermic events, are listed in Table 1. DTA-plots of the compounds **1–3** and **5–14** are available in Figure S12–15 in the SI.

The exothermic decomposition temperature reported for ligand **1** is in accordance with our findings, whereas for ligand **2** no data is available.[28] The exothermic decomposition temperatures of most of the investigated compounds are above 150 °C, except **10** (T_{exo} = 146 °C) and **14** (T_{exo} = 121 °C). The relatively low thermal stabilities of the nitrato compound **3** (T_{exo} = 152 °C), as well as the chlorate complexes, are a known issue, resulting from the metal salt, the coordination compounds are based on and is already reported in literature.[32,33] Besides its low point of exothermic decomposition, the nitrato complex (**3**) is the only compound showing two endothermic signals (T_{endo1} = 94 °C, T_{endo2} = 121 °C), indicating melting, followed by the loss of coordinating aqua ligand (proofed by TGA). Other endothermic events of compounds **6** and **8–11** can also be assigned to their respective melting points, which were also observed during heating of the respective compounds in hot plate tests. In order to examine the endothermic events more closely, some of the compounds were further investigated by thermal gravimetric analysis (Figure S15). Except **3**, none of the compounds based on ligand **1** showed significant loss of mass until their exothermic decomposition points. Copper(II) complexes comprising 1-ETZ (**2**) show similar to the methyl-substituted analogous compounds evaporation of the ligand before their exothermic decomposition.[32] In the row of 2,4,6-trinitroaromatic based copper(II) complexes, the thermal stability decreases with increasing number of hydroxy groups, with **14** (T_{exo} = 121 °C) showing the lowest stability of all investigated compounds.

The highest exothermic decomposition temperature was observed for the copper(II) perchlorate complex **9** (T_{exo} = 210 °C), based on ligand **2**, showing an exothermic signal 52 °C higher than the analogous coordination compound based on ligand **1** (**8**: T_{exo} = 158 °C). The same can be observed for the two comparable chlorate complexes (Figure 11). This trend is confirmed,

Table 1. Overview of the compounds' thermal stability,[a] sensitivities toward various external stimuli and results of hot plate (HP) and hot needle (HN) tests compared to lead azide.

Compound	$T_{endo.}$ [°C][b]	$T_{exo.}$ [°C][c]	IS[d] [J]	FS[e] [N]	ESD[f] [mJ]	BDIS[g] [mJ]	HP[h]	HN[h]
AET (**1**)	–	193	9	>360	n.d.	n.d.	n.d.	n.d.
1-ETZ (**2**)	–	208	>40	>360	n.d.	n.d.	n.d.	n.d.
$[Cu(NO_3)_2(H_2O)(AET)_2]$ (**3**)	94, 121	152	10	108	840	n.d.	def.	def.
$[Fe(AET)_6](ClO_4)_2$ (**5**)	–	151	3	3.75	65–0	<4	det.	det.
$[Zn(AET)_6](ClO_4)_2$ (**6**)	159	196	15	40	368	20	def.	def.
$[Ag(AET)]ClO_4$ (**7**)	–	165	<1	0.6	65.0	<4	det.	det.
$[Cu(AET)_6](ClO_4)_2$ (**8**)	135	158	<1	15	368	12	def.	det.
$[Cu(1\text{-}ETZ)_6](ClO_4)_2$ (**9**)	172	210	10	120	960	n.d.	def.	def.
$[Cu(AET)_6](ClO_3)_2$ (**10**)	77	146	2.5	4	226	29	def.	det.
$[Cu(1\text{-}ETZ)_6](ClO_3)_2$ (**11**)	111	158	7	60	608	n.d.	def.	def.
$[Cu(PA)_2(AET)_2]$ (**12**)	–	183	3	252	226	>200	def.	def.
$[Cu(TNR)(AET)_2]$ (**13**)	–	177	<1	240	123	>200	def.	def.
$[Cu(H_2TNPG)_2(AET)_4]$ (**14**)	–	121	1.5	84	608	>200	def.	def.
$Pb(N_3)_2$[37]	–	320-360	2.5-4	0.1–1.0	7.00	n.d.	n.d	n.d

[a] Onset temperature at a heating rate of 5 °C min^{-1} measured by DTA; [b] Endothermic peak, which indicates melting, vaporization, dehydration, or loss of aqua ligands; [c] Exothermic peak, which indicates decomposition. [d] Impact sensitivity according to the BAM drophammer (method 1 of 6). [e] Friction sensitivity according to the BAM friction tester (method 1 of 6). [f] Electrostatic discharge sensitivity (OZM Electric Spark XSpark10, method 1 of 6). [g] Ball drop impact sensitivity determined with the 1 of 6 method in accordance with the MIL-STD 1751A (method 1016). [h] def.: deflagration; det.: detonation.

© 2019 Wiley-VCH Verlag GmbH & Co. KGaA, Weinheim

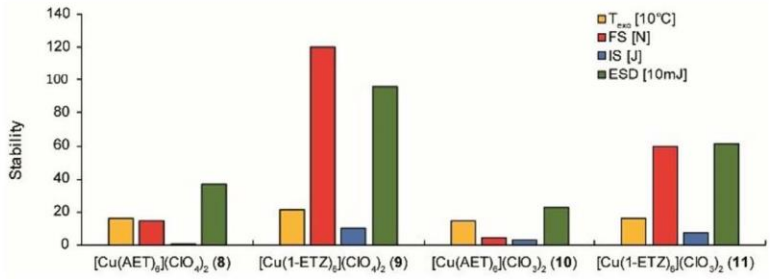


Figure 11. Comparison of the sensitivities and thermal stability of the chlorate and perchlorate complexes based on the ligands **1** and **2**, confirming the lower stability of chlorate compounds toward external stimuli.

looking at the temperatures evaluated for the respective ligand (**1**: $T_{exo}=193\,^{\circ}C$; **2**: $T_{exo}=208\,^{\circ}C$) and is guessed to be caused by the azido function of ligand **1**.

A general trend within the row of the investigated 3d perchlorate coordination compounds shows higher exothermic decomposition temperatures with an increasing atomic number ($Fe^{2+}<Cu^{2+}<Zn^{2+}$), which is in conflict (Cu^{2+}-based complexes being less stable than Fe^{2+}) with our prior findings for 1*H*-substiuted tetrazoles (Figure 11).[32] Interestingly, compounds **6** and **9** even show slightly higher exothermic decomposition temperatures ($T_{exo}=196\,^{\circ}C$ and $210\,^{\circ}C$, respectively) than the corresponding ligand.

The sensitivities toward impact (IS) and friction (FS) were assessed according to BAM standard methods (1 of 6) together with the electrostatic discharge sensitivity (ESD) for all compounds. In addition, all complexes have been categorized in accordance with the "UN Recommendations on the Transport of Dangerous Goods" using the determined sensitivities.[36] An overview of the sensitivities is given in Table 1. Because sensitivity data are highly affected by the crystal morphology, the compounds' grain size and habitus were investigated using light microscopy. The data are represented in the supplementary information (Figure S8–11).

The free ligand **2** is the only investigated compound to be ranked as insensitive with its high stability toward friction and impact. In contrast to that, ligand **1** has to be classified as sensitive because of its sensitivity of 9 J toward impact, whereas it is insensitive toward friction. No measurements regarding electrostatic discharge could be performed due to the physical state of both ligands. The highest stability toward impact of all ECC (15 J, sensitive) is possessed by the only zinc coordination compound **6**, which has to be considered as very sensitive because of its friction sensitivity. Comparing the perchlorate complexes reveals, that all have to be considered as very sensitive (**6**, **8**) or even extremely sensitive (**5**, **7**), except compound **9**, which is stated as sensitive, also possessing the highest stability toward friction of all investigated perchlorates. The sensitivity toward impact of the ECC based on perchlorate and AET increases in the following order: Zn^{2+} (15 J) $<Fe^{2+}$ (3 J) $<Cu^{2+}$ (<1 J) $\approx Ag^{+}$ (<1 J) and in the following order against friction: Zn^{2+} (40 N) $<Cu^{2+}$ (15 N) $<Fe^{2+}$ (3.75 N) $<Ag^{+}$ (0.6 N) (Figure 12). Again these results contradict earlier observations.[32,33]

Compounds **8–11** show comparable trends to external stimuli as in thermal experiments. Complexes based on ligand **1** are more sensitive (**8** and **10** are both ranked as extremely sensitive) than those of compound **2** (both sensitive) and the copper(II) chlorate complexes are less stable (**11**) or at least show similar sensitivities (**10**) compared to the analogous perchlorate ones (Figure 11), which is in accordance to our previous findings.[34] The nitroaromatic derivatives **12–14** possess one of the highest stabilities of all complexes toward friction, but due to their sensitivities toward impact, they are all ranked as very sensitive (Figure S17).

Because of the realistic terms of testing, sensitivity toward ball drop impact (BDIS) was also determined for the most sensitive complexes **5–8**, and **10** (Figure S18). Due to the high discrepancy of **12–14** regarding the sensitivities toward impact

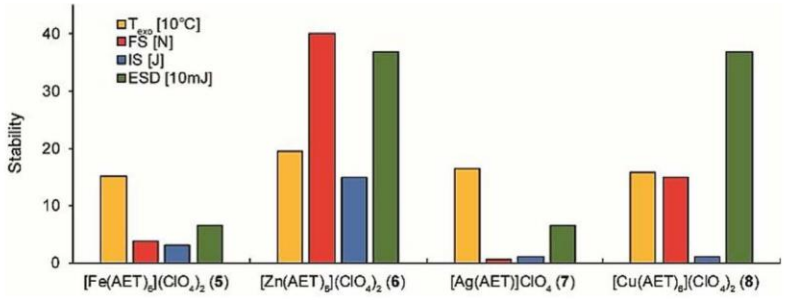


Figure 12. Comparison of the thermal stabilities together with the sensitivities toward various stimuli of the perchlorate coordination compounds **5–8**, showing that the silver compound is the most sensitive and the zinc one is the most insensitive one.

© 2019 Wiley-VCH Verlag GmbH & Co. KGaA, Weinheim

and friction according to BAM standard methods, ball drop experiments were carried out for those compounds too. In the case of the perchlorate complexes it becomes clear that low stability to friction (**7** < **5** < **8** < **6**) is accompanied by a higher sensitivity to BDIS (**7** ~ **5** < **8** < **6**) and that the impact sensitivity in the drophammer experiments (**7** ~ **8** < **5** ≪ < **6**) is less significant. The same trend can be observed for the nitroaromatic compounds **12–14**.

Primary explosive suitability evaluation and laser initiation

For an insight into the behavior toward fast heating with and without confinement and for gaining an overall insight in their applicability as a primary explosive, hot plate and hot needle tests were performed for every investigated coordination compound (Table 1, Figure 13 and S19–30). Except the chlorate and perchlorate complexes **5**, **7**, **8** and **10**, which at least showed detonations during one of the tests, every other compound only deflagrated.

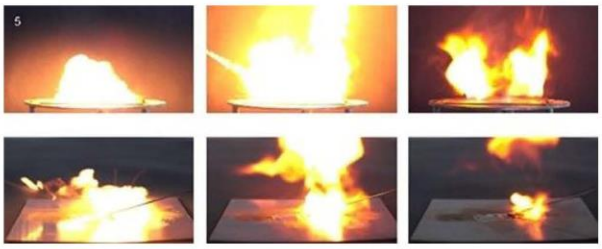


Figure 13. Hot plate test (top) and hot needle test (bottom) of the iron(II) perchlorate complex **5**, shown as a sequence.

The most promising compounds were tested in initiation capability tests with nitropenta (PETN) as the main charge. Further information on the test setup can be found in the General Methods of the Supporting Information. Positive tests, indicated by a hole in the copper witness plate and fragmentation of the shell, caused by a positive deflagration-to-detonation transition (DDT) toward the secondary explosive, were observed for **5** and **7**. [Ag(AET)]ClO_4 (**7**) is representing one of the rare ECC with silver as central metal being able to initiate PETN (Figure 14). Tests concerning the copper(II) and zinc(II) perchlorate compound **6** and **8** did in our test not result in a positive DDT.

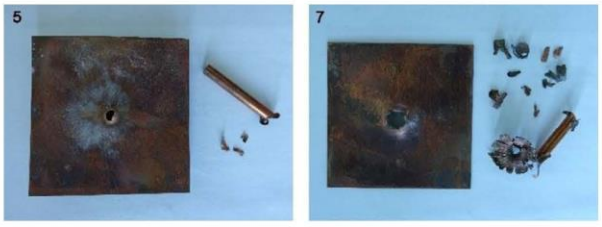


Figure 14. Positive results of the initiation capability tests toward PETN of compounds **5** and **7**.

Nowadays used primary explosives like LA or LS suffer, besides their toxicity, from their high sensitivity toward mechanical stimuli.[25] In classical initiation devices, which are based on mechanical stimuli, these properties are mandatory, but with the ability to be initiated by laser irradiation they are no longer required. This circumstance is responsible for the great interest that the field has gained in recent years.[38,39] Possible industrial applications like optical detonators or laser ignitable ammunition are already under current research.[40,41] Based on latest results concerning the laser ignition of ECC, this work focused only on the colored compounds **3**, **5** and **8–14**.[33] Further information for the applied setup can be found in the Supporting Information. All complexes showed reaction toward laser irradiation (Table 2), which strongly differed by the applied ligand and anion system.

Table 2. Results of the laser initiation experiments.[a]

Compound	0.17 mJ	25.5 mJ	30 mJ	111 mJ
3	–	–	deflag.	–
5	–	deflag.	det.	–
8	deflag.	det.	–	–
9	–	–	dec.	–
10	det.	det.	–	–
11	–	–	dec.	–
12	–	–	–	dec.
13	–	–	dec.	–
14	–	dec.	–	–

[a] –: not tested, dec.: decomposition, deflag.: deflagration, det.: detonation. Operating parameters: current I = 7–12 A; voltage U = 4 V; theoretical maximal output power P_{max} = 45 W; theoretical energy E_{max} = 0.17–111 mJ; wavelength λ = 915 nm; pulse length τ = 0.1–20 ms.

As already recognized during hot plate and hot needle tests, coordination compounds based on the more energetic ligand **1** tend way more likely to show detonations than compounds based on ligand **2**. The use of nitrate or aromatic anions is leading to deflagrations only, whereas, in case of ligand **1**, the use of chlorates and perchlorates leads to detonations (Figure 15 and S31–37).

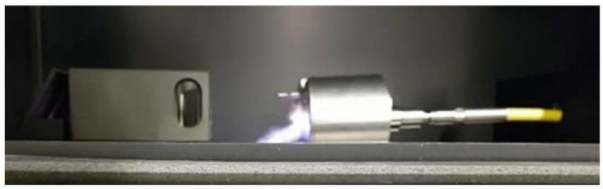


Figure 15. Detonation of the copper(II) perchlorate complex **8** during laser initiation test.

UV/Vis spectroscopy

Regarding the mechanism of laser initiation, UV/Vis spectra (Figure S38 and S39) of all tested compounds were recorded in the solid-state and analyzed in detail at the laser operating wavelength of 915 nm. A summary of the optical properties of

© 2019 Wiley-VCH Verlag GmbH & Co. KGaA, Weinheim

the measured compounds is given in Table S4. The observed absorption in the near infrared, visible and ultra-violet region results from the d-d transitions, based on the respective central metal and its interaction with the ligand and anion. Nevertheless, the process of initiation via laser irradiation (e.g. thermal, electrochemical) has still not been understood completely and is therefore of high importance and strongly investigated.[42,43] All complexes show moderate absorption behavior at the laser wavelength of 915 nm. This could be a possible explanation for the ignitability via laser irradiation since the colorless zinc and silver perchlorate compounds **6** and **7** could not be ignited. Besides the absorption in the desired area, other factors are important concerning laser initiation, like the corresponding metal or its electron configuration. Therefore, future studies should aim at the initiation process, in particular, the influence of the complexes' structure and the mechanism behind the initiation.

Conclusions

The nitrogen-rich ligands 1-azidoethyl-5*H*-tetrazole (**1**, AET) and 1-ethyl-5*H*-tetrazole (**2**, 1-ETZ), which can be synthesized in straightforward, green and cost-effective manners were successfully applied in coordination compounds and analyzed by two dimensional ^{1}H, ^{15}N HMBC NMR. Copper, iron, zinc, and silver salts of common anions like perchlorate or nitrate were used together with rather unusual ones like picrate, styphnate, trinitrophloroglucinate or chlorate. All of the synthesized coordination compounds, except byproduct **4**, were characterized in detail. By introducing the azide function into the ligand system, the performance of the ECC can be significantly increased. While the sensitivities of compounds **9** and **11** (based on 1-ETZ (**2**)) lie in the range of secondary explosives, most of the ECC based on ligand **1** are primary explosives. The iron (**5**) and silver (**7**) perchlorate compounds were both positive tested to initiate PETN. Especially **5** with its manageable sensitivities and nontoxic central metal could be a candidate of future interest. During laser ignition experiments coordination compound **5** as well as the copper compounds **8** and **10** showed detonations at energies between 0.17 mJ and 30.0 mJ making them promising candidates as green laser ignitable explosives. The comparison of the impact sensitivities determined by drophammer and ball drop reveals a higher similarity of the BDIS to FS than IS.

Acknowledgements

Financial support of this work by the Ludwig-Maximilian University of Munich (LMU). The authors would like to thank Prof. Dr. Konstantin Karaghiosoff for the measurement of various ^{15}N NMR spectra, Antonia Stadler for proofreading and Valentin Bockmair as well as Philipp Spieß for their great contribution to this work.

Conflict of interest

The authors declare no conflict of interest.

Keywords: copper(II) · energetic coordination compounds · energetic materials · explosives · laser ignition · tetrazoles

[1] T. Curtius, *Ber. Dtsch. Chem. Ges.* **1890**, *23*, 3033–3041.
[2] S. Schneider, T. Hawkins, M. Rosander, J. Mills, A. Brand, L. Hudgens, G. Warmoth, A. Vij, *Inorg. Chem.* **2008**, *47*, 3617–3624.
[3] J. Haase in *Organic Azides: Syntheses and Applications, Vol. 1* (Eds.: S. Bräse, K. Banert), Wiley, Hoboken, **2010**, pp. 29–48.
[4] T. M. Klapötke, N. Mehta, *Propellants Explos. Pyrotech.* **2014**, *39*, 7–8.
[5] J. C. Bennion, N. Chowdhury, J. W. Kampf, A. J. Matzger, *Angew. Chem. Int. Ed.* **2016**, *55*, 13118–13121; *Angew. Chem.* **2016**, *128*, 13312–13315.
[6] S. I. Gerasimov, M. A. Ilyushin, I. V. Shugalei, A. V. Smirnov, Z. V. Kapitonenko, *Russ. J. Gen. Chem.* **2017**, *87*, 3156–3159.
[7] H. Wei, J. Zhang, J. M. Shreeve, *Chem. Asian J.* **2015**, *10*, 1130–1132.
[8] D. E. Chavez, D. A. Parrish, L. Mitchell, G. H. Imler, *Angew. Chem. Int. Ed.* **2017**, *56*, 3575–3578; *Angew. Chem.* **2017**, *129*, 3629–3632.
[9] C. Qi, R. Zhang, X. Zhang, Y. Li, Y. Wang, S. Pang, *Chem. Asian J.* **2011**, *6*, 1456–1462.
[10] K. O. Christe, D. A. Dixon, M. Vasiliu, R. Haiges, B. Hu, *Propellants Explos. Pyrotech.* **2019**, *44*, 263–266.
[11] P. Griess, *J. Chem. Soc.* **1865**, *18*, 268–272.
[12] A. Hantzsch, *Ber. Dtsch. Chem. Ges.* **1933**, *66*, 1349–1354.
[13] M. N. Glukhovtsev, R. D. Bach, L. Laiter, *Int. J. Quantum Chem.* **1997**, *62*, 373–384.
[14] T. Curtius, *J. Prakt. Chem.* **1894**, *50*, 275–294.
[15] G. L'Abbé, *Chem. Rev.* **1969**, *69*, 345–363.
[16] E. F. V. Scriven, K. Turnbull, *Chem. Rev.* **1988**, *88*, 297–368.
[17] L. O. Brockway, L. Pauling, *Proc. Natl. Acad. Sci. USA* **1933**, *19*, 860–867.
[18] L. Pauling, L. O. Brockway, *J. Am. Chem. Soc.* **1937**, *59*, 13–20.
[19] M. A. Petrie, J. A. Sheehy, J. A. Boatz, G. Rasul, G. K. Surya Prakash, G. A. Olah, K. O. Christe, *J. Am. Chem. Soc.* **1997**, *119*, 8802–8808.
[20] Y. Tang, J. M. Shreeve, *Chem. Eur. J.* **2015**, *21*, 7285–7291.
[21] D. Kumari, K. D. B. Yamajala, H. Singh, R. R. Sanghavi, N. A. Shri, K. Raju, S. Banerjee, *Propellants Explos. Pyrotech.* **2013**, *38*, 805–809.
[22] C. Ye, H. Gao, J. A. Boatz, G. W. Drake, B. Twamley, J. M. Shreeve, *Angew. Chem. Int. Ed.* **2006**, *45*, 7262–7265; *Angew. Chem.* **2006**, *118*, 7420–7423.
[23] Y.-H. Joo, H. Gao, Y. Zhang, J. M. Shreeve, *Inorg. Chem.* **2010**, *49*, 3282–3288.
[24] Y. H. Ding, S. Inagaki, *Chem. Lett.* **2003**, *32*, 304–305.
[25] T. M. Klapötke in *High Energy Density Materials, Vol. 1*, Springer, Berlin/Heidelberg, **2007**, pp. 85–122.
[26] J. Giles, *Nature* **2004**, *427*, 580–581.
[27] P. Singh Rajendra, R. D. Verma, D. T. Meshri, J. M. Shreeve, *Angew. Chem. Int. Ed.* **2006**, *45*, 3584–3601; *Angew. Chem.* **2006**, *118*, 3664–3682.
[28] P. N. Gaponik, V. P. Karavai, Y. V. Grigor'ev, *Khim. Geterotsikl. Soedin.* **1985**, *21*, 1255–1258.
[29] D. O. Ivashkevich, A. S. Lyakhov, P. N. Gaponik, A. N. Bogatikov, A. A. Govorova, *Acta Crystallogr. Sect. E* **2001**, *57*, m335–m337.
[30] Y. Guo, H. Liu, M. Xu, *Hecheng Huaxue* **2011**, *19*, 299–303.
[31] A. Riechers, A. Grauer, S. Ritter, B. Sperl, T. Berg, B. König, *J. Mol. Recognit.* **2010**, *23*, 329–334.
[32] N. Szimhardt, M. H. H. Wurzenberger, A. Beringer, L. J. Dauman, J. Stierstorfer, *J. Mater. Chem. A* **2017**, *5*, 23753–23765.
[33] N. Szimhardt, M. H. H. Wurzenberger, L. Zeisel, M. S. Gruhne, M. Lommel, J. Stierstorfer, *J. Mater. Chem. A* **2018**, *6*, 16257–16272.
[34] M. H. H. Wurzenberger, N. Szimhardt, J. Stierstorfer, *J. Am. Chem. Soc.* **2018**, *140*, 3206–3209.
[35] CCDC 1898402 (**3**), 1898401 (**4**), 1898397 (**5**), 1898400 (**7**), 1898399 (**9**), 1898541 (**11**), 1898395 (**12**), 1898398 (**13**), 1898396 (**14**) contain the supplementary crystallographic data for this paper. These data can be obtained free of charge from The Cambridge Crystallographic Data Centre.

© 2019 Wiley-VCH Verlag GmbH & Co. KGaA, Weinheim

[36] Impact: insensitive > 40 J, less sensitive ≥ 35 J, sensitive ≥ 4 J, very sensitive ≤ 3 J; Friction: insensitive > 360 N, less sensitive = 360 N, sensitive < 360 N and > 80 N, very sensitive ≤ 80 N, extremely sensitive ≤ 10 N. According to the UN Recommendations on the Transport of Dangerous Goods, (+) indicates not safe for transport.
[37] T. M. Klapötke in *Energetic Materials Encyclopedia, Vol. 1*, Walter De Gruyter, Berlin/Boston, **2018**, pp. 275–277.
[38] T. W. Myers, J. A. Bjorgaard, K. E. Brown, D. E. Chavez, S. K. Hanson, R. J. Scharff, S. Tretiak, J. M. Veauthier, *J. Am. Chem. Soc.* **2016**, *138*, 4685–4692.
[39] T. W. Myers, K. E. Brown, D. E. Chavez, R. J. Scharff, J. M. Veauthier, *Inorg. Chem.* **2017**, *56*, 2297–2303.
[40] R. Schirra, H. Zöllner, *Proc. Int. Pyrotech. Semin.* **2016**, *42*, 422–428.
[41] H. Lebreton, D. Cazajous, S. Larue, *Proc. Int. Pyrotech. Semin.* **2015**, *41*, 1–6.
[42] S. R. Ahmad, M. Cartwright in *Laser Ignition of Energetic Materials*, Wiley, Hoboken, **2015**, pp. 17–29.
[43] E. D. Aluker, A. G. Krechetov, A. Y. Mitrofanov, D. R. Nurmukhametov, M. M. Kukja, *J. Phys. Chem. C* **2011**, *115*, 6893–6901.

Manuscript received: February 22, 2019
Revised manuscript received: April 1, 2019
Accepted manuscript online: April 3, 2019
Version of record online: May 8, 2019

© 2019 Wiley-VCH Verlag GmbH & Co. KGaA, Weinheim

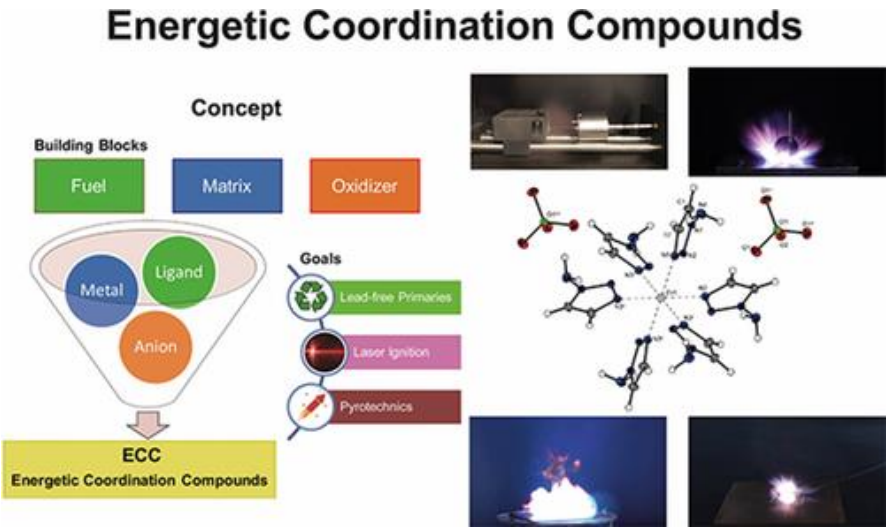
Appendix 11

1-AminoTriazole Transition-Metal Complexes as Laser-Ignitable and Lead-Free Primary Explosives

N. Szimhardt, Maximilian H. H. Wurzenberger, L. Zeisel, M. S. Gruhne, M. Lommel, T. M. Klapötke, J. Stierstorfer

Chem. Eur.J. **2019**, *25*, 1963–1974.

https://doi.org/10.1002/chem.201803372



Supplementary Information:
https://chemistry-europe.onlinelibrary.wiley.com/action/downloadSupplement?doi=10.1002%2Fchem.201803372&file=chem201803372-sup-0001-misc_information.pdf

ChemPubSoc Europe

DOI: 10.1002/chem.201803372

CHEMISTRY A European Journal Full Paper

Check for updates

Energetic Coordination Compounds | *Hot Paper*

1-AminoTriazole Transition-Metal Complexes as Laser-Ignitable and Lead-Free Primary Explosives

Norbert Szimhardt, Maximilian H. H. Wurzenberger, Lukas Zeisel, Michael S. Gruhne, Marcus Lommel, Thomas M. Klapötke, and Jörg Stierstorfer*[a]

Abstract: This unique complex study describes two isomeric aminotriazoles as auspicious nitrogen-rich ligands for energetic coordination compounds (ECCs) to replace the commonly used highly poisonous and environmentally harmful lead-based primary explosives. The triazoles were obtained by easily scalable and convenient synthetic routes starting solely from commercially available starting materials. 1-Amino-1,2,3-triazole (**1**, 1-ATRI) and, for the first time, 1-amino-1,2,4-triazole (**2**, 1A-1,2,4-TRI) were employed as ligands to form highly energetic transition-metal(II) complexes. The desired characteristics could be altered successively by using various nonpoisonous metal(II) centers (Cu^{2+}, Mn^{2+}, Fe^{2+}, and Zn^{2+}) and anions (Cl^-, NO_3^-, ClO_3^-, ClO_4^-, picrate, styphnate, 2,4,6-trinitro-3-hydroxyphenolate, and 2,4,6-trinitro-3,5-dihydroxyphenolate). The 14 synthesized coordination compounds were characterized comprehensively by XRD, IR and UV/Vis spectroscopy, elemental analysis, and differential thermal and thermogravimetric analyses. Ball-drop impact, electrostatic discharge (ESD), and mechanical (impact and friction) sensitivities were determined according to BAM standard methods. In addition to laser ignition experiments, selected ECCs were evaluated in classical secondary explosive initiation tests (detonators filled with pentaerythritol tetranitrate (nitropenta)), which revealed their enormous potential and proved them to be very attractive for future applications in explosives.

Introduction

The demanding field of energetic materials can be roughly divided into four main areas: 1) primary explosives, 2) secondary explosives, 3) propellants, and 4) pyrotechnics.[1] The majority of the currently used explosives, or at least their degradation products, exhibit enormous toxicity towards human life and the environment, thereby making research into green alternatives indispensable.[2–4] Especially in the field of primary explosives, there is an urgent need for the development of these alternatives, as extremely toxic lead compounds, namely lead azide and lead styphnate, are still in use.[5–7] Both compounds, which have been added to the Registration, Evaluation, Authorisation and Restriction of Chemicals (REACH) candidate list, are the main components of various ignition systems, such as primers or detonators, which are of great importance in ammunition and warheads as well as in civilian areas such as mine construction.[8]

A very promising strategy for countering the issues mentioned above is the synthesis of energetic transition-metal complexes based on endothermic azole ligands.[9–12] The most significant advantage of this concept is the possible alteration of the three different components, namely 1) the metal, 2) the anion, and 3) the ligand, which allows an exact adjustment of the optical and energetic properties (Figure 1). In recent years, a large number of different combinations have been reported in the literature.[13,14] Another benefit of this approach, in addition to the ease of manufacture, includes the possibility of moving away from toxic heavy metals like lead or mercury to more environmentally friendly alternatives such as copper, iron, manganese, or zinc, which exhibit significantly lower toxicity.[15] In particular, the selection of these transition metals is a good compromise between price, availability, and environmental compatibility.

Compounds or mixtures can be ignited by various methods or ignition sources, such as mechanical stimuli, light, electricity, or heat, depending on the application. In particular, initiation by laser irradiation, which has several advantages over classical initiation methods, has made considerable progress recently.[16–21] Compared with conventional initiation methods, the number of unwanted ignitions could be reduced by using less mechanically sensitive compounds that instead react preferably upon optical excitation. Energetic coordination compounds (ECCs) based on azole ligands such as tetrazoles or triazoles have so far shown promising results both in the field of laser-

[a] *Dr. N. Szimhardt, M. H. H. Wurzenberger, L. Zeisel, M. S. Gruhne, M. Lommel, Prof. Dr. T. M. Klapötke, Dr. J. Stierstorfer*
Department of Chemistry
Ludwig Maximilian University of Munich
Butenandtstr. 5–13, 81377 Munich (Germany)
E-mail: jstch@cup.uni-muenchen.de
Homepage: http://www.hedm.cup.uni-muenchen.de

*Supporting information and the ORCID identification number(s) for the author(s) of this article can be found under: https://doi.org/10.1002/chem.201803372: IR spectra of **1–16**, X-ray diffraction detail, TGA plot of the zinc(II) perchlorate complex **13**, DTA plots of **1–9** and **14–16**, column diagrams of the complexes **3–9**, hot-plate and hot-needle tests, laser ignition test of complex **16**, general methods and experimental details.*

© 2019 Wiley-VCH Verlag GmbH & Co. KGaA, Weinheim

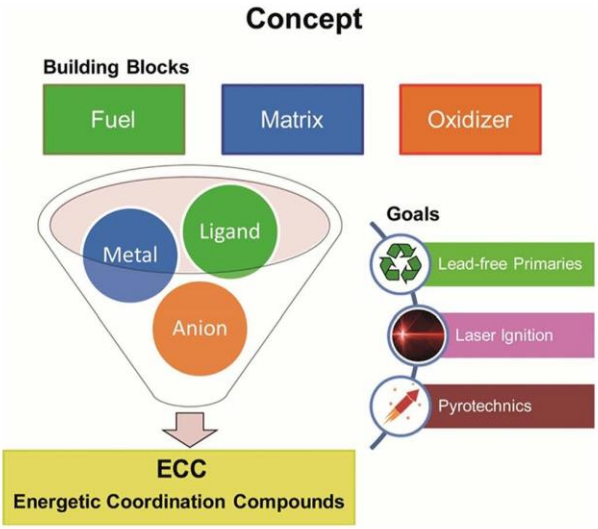


Figure 1. Concept of energetic coordination compounds (ECCs) based on the three building blocks.

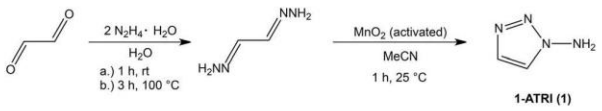
ignitable energetic materials and lead-free primary explosives.[22] Triazole complexes in particular, the energetic character of which can be adapted by isomerism (1,2,3-triazoles vs. 1,2,4-triazoles) or functionalization (nitrogen or carbon substitution), have been discussed in relation to a large number of different potential fields of application such as metal organic frameworks for gas storage or optical devices.[23] Of exceptional interest are ligands that incorporate the hydrazine function to increase their endothermic character, and consequently the energy content of complexes. The literature contains a multitude of interesting 4-amino-1,2,4-triazole coordination compounds, but until now no complexes have been synthesized with the 1-amino isomer nor the more energetic 1-amino-1,2,3-triazole analogue (Figure 2).[24,25] Both ligands exhibit a relatively high nitrogen content (66.63%) and have been known for almost half a century.[26,27]

The majority of the known triazole complexes do not have the necessary power to be considered as potential primary explosives or laser-ignitable compounds. To further increase the energy content of complexes, 1-amino-1,2,3-triazole (**1**, 1-ATRI) and 1-amino-1,2,4-triazole (**2**, 1-A-1,2,4-TRI) were used as ligands. In particular, 1-ATRI, which contains four nitrogen atoms in a row, shows a highly endothermic character (Figure 2) and can be synthesized by straightforward amination or oxidation reactions. The ligand shows excellent complexation behavior, and the resulting ECCs confirmed their tremendous potential during laser ignition and nitropenta (pentaerythritol tetranitrate) initiation tests.

Results and Discussion

Synthesis

1-Amino-1,2,3-triazole (**1**) can be synthesized by different methods. On the one hand by amination of 1,2,3-triazole, which unfortunately leads to a mixture of isomers, and on the other hand by a two-step synthesis, which leads directly to the desired isomerically pure product (Scheme 1). Freshly precipitated manganese dioxide has the ability to promote intramolecular cyclization of organic molecules through oxidation.[28,29] To obtain the mild oxidizing agent MnO_2 in its activated form, Mn^{II} salts are treated with MnO_4^- in a redox reaction in an alkaline milieu (Scheme 2a). The bis-hydrazone key intermediate can be prepared by the condensation of hydrazine hydrate and glyoxal (Scheme 1).[30] This reaction occurs twice, once at each carbonyl function of the dialdehyde. It may be that only one carbonyl group of glyoxal reacts, which decreases the yield of the reaction by contamination. Possible impurities of the reaction are removed by recrystallization from ethanol.



Scheme 1. Isomerically pure two-step synthesis of 1-ATRI (**1**) starting from the commercially available starting materials hydrazine hydrate and glyoxal.

The subsequent intramolecular cyclization reaction of the intermediate can be formulated as concerted electron shifts be-

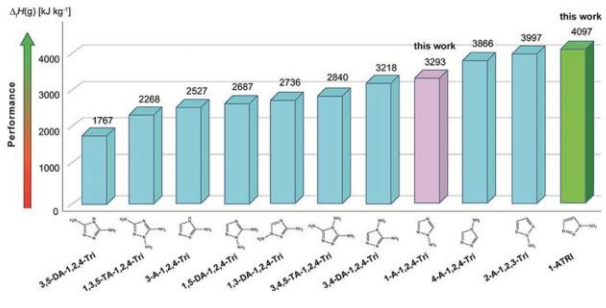
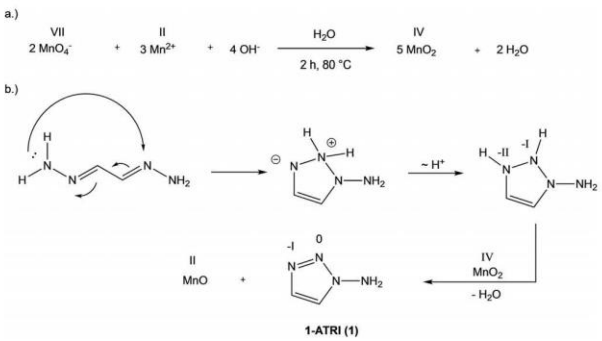


Figure 2. Comparison of the per-unit-mass-calculated gas-phase enthalpies of formation for several different triazoles. Enthalpies of formation were calculated by the atomization method ($\Delta_f H^\circ_{(g,M)} = H_{(M)} - \Sigma H^\circ_{(A)} + \Sigma \Delta_f H^\circ_{(A)}$) using CBS-4M based electronic enthalpies.



Scheme 2. a) Synthesis of activated manganese dioxide and b) proposed mechanism for the formation of 1-ATRI (**1**).

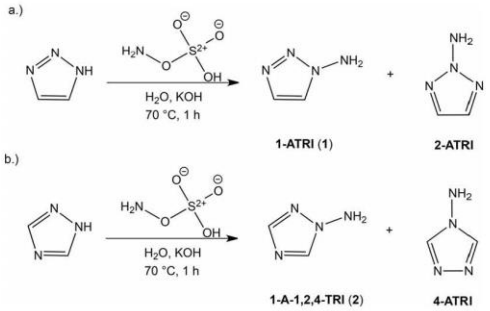
© 2019 Wiley-VCH Verlag GmbH & Co. KGaA, Weinheim

tween the atoms of this molecule and is realized in acetonitrile at room temperature (Schemes 1 and 2b).[31] One possible mechanism of this patent procedure could take place in the following way: The lone pair from one primary amine nucleophilically attacks the nitrogen of the more distant imine group and the two electrons that form the nitrogen–carbon double bond relocate to provide a carbon–carbon double bond. Finally, the remaining carbon–nitrogen double bond is converted into a single bond, with the two electrons shifting to the adjacent nitrogen atom. The resulting unstable five-membered ring, in particular the N2 and N3 atoms, is oxidized by the mild oxidizing agent $Mn^{IV}O_2$ to form the stable 1-ATRI (**1**), $Mn^{II}O$, and water (Scheme 2b).

The ability of activated MnO_2 to perform the discussed oxidation reaction turns out to be highly dependent on the time frame between its precipitation and its application in the reaction. Already 4 days after its preparation, this mild oxidation agent was unable to promote the cyclization of 1-ATRI in reasonable yields. Moreover, the excess of the oxidizing MnO_2 partially leads to the further oxidation of two equivalents of **1** to the associated azo compound. Due to the major contamination of the reaction product and its high viscosity, a proper crystallization of compound **1** at low temperatures turned out to be rather challenging. The crystallized solids were constantly enclosed by the remaining viscous oil, which could not be separated through filtration. Because 1-ATRI (**1**) turned out to be low-melting, sublimation of the obtained reaction product at 80 °C proved to be the most convenient way to purify the synthesized compound. The triazole was isolated in the form of colorless crystals. To increase the yield of the reaction (33%), variation of the reaction conditions with respect to the MnO_2/glyoxal/bis-hydrazone molar ratio, the reaction time, and the temperature seemed to be important. Although increasing the temperature resulted in decreasing yields, a longer reaction time and higher molar ratios of MnO_2/glyoxal/bis-hydrazone led to even more of the desired product.[30]

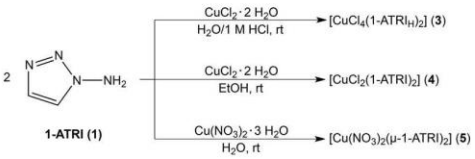
An alternative reaction pathway leads to the preparation of 1-ATRI (**1**) and 1-A-1,2,4-TRI (**2**). The respective potassium triazolate generated in situ was treated with the common amination reagent hydroxylamine-*O*-sulfonic acid (HOSA) in water at a temperature of 70 °C in analogy to a standard literature procedure (Scheme 3).[32,33] The respective isomeric mixture obtained was then purified by column chromatography (EtOAc/EtOH, 9:1) on silica gel to yield 1-ATRI (19%) and by vacuum sublimation (80 °C, 1.5×10^{-2} mbar) to isolate 1-A-1,2,4-TRI (31%). Possible explanations for the relatively low yields are the formation of an isomeric mixture, the weak nucleophilic character of the starting material, the sensitivity of the amination reagent toward hydrolysis, and the sensibility to fluctuations in pH.

Because a large number of complexes based on 4-aminotriazole have already been reported in the literature, this work aimed to increase the energy content of these coordination compounds further by utilizing 1-ATRI (**1**) as the ligand (Figure 2). Our concept for synthesizing promising primary explosives involves the preparation of cationic or neutral complex units to assure the inclusion of anionic oxidizing agents



Scheme 3. Synthesis of a) 1-ATRI (**1**) and b) 1-A-1,2,4-TRI (**2**) by amination of the corresponding triazoles.

(e.g., nitrate or perchlorate). This could be realized through the blocking of the acidic triazole sites by amino units as functional groups. Complexes **3–5** and **10–14** (which are easy to differentiate by IR spectroscopy, see Figures S1 and S3 in the Supporting Information) were synthesized by mixing aqueous or ethanolic solutions of the metal(II) salts and ligand **1** in the respective stoichiometry at room temperature (Schemes 4 and 6). Immediately after the addition of all the reactants during the synthesis of the copper(II) chloride complex, a green solid precipitated from solution, most likely compound **4**, which was dissolved again by the addition of hydrochloric acid. Addition of the acid resulted in the isolation of the rare tetrachlorido triazolium species **3**.

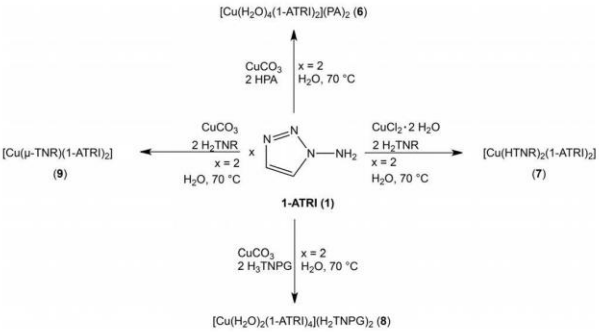


Scheme 4. Synthesis of the 1-ATRI-based copper(II) complexes **3–5**.

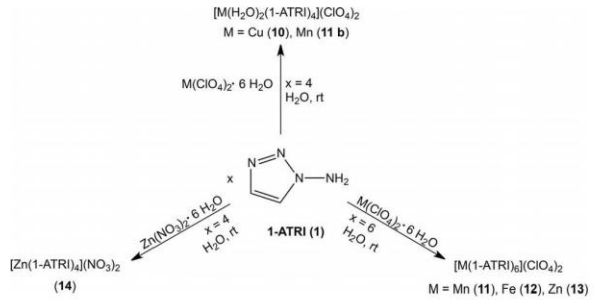
The commercially unavailable metal(II) salt starting materials employed for the synthesis of the complexes **6–9** were prepared by simple acid/base or metathesis reactions in water and subsequently treated with the nitrogen-rich ligand **1** (Scheme 5). The reaction of styphnic acid (2,4,6-trinitroresorcinol, H_2TNR) with **1** and a copper(II) source (copper(II) chloride vs. copper(II) carbonate) is highly pH dependent and resulted either in the isolation of a complex with a single (**7**) or double (**9**) deprotonated anion (distinguishable by IR spectroscopy, see Figure S2 in the Supporting Information). Particular attention should be paid to compound **8**, which, to the best of our knowledge, is the first of its type, because no copper(II) complexes with trinitrophloroglucinol (H_3TNPG)-based anions have been reported in the literature so far.

The preparation of manganese(II) perchlorate complexes was highly sensitive to the stoichiometry applied and coordinated species with either four (**11b**) or six (**11**) 1-ATRI ligands were furnished (Scheme 6). The copper(II) perchlorate (**10**) and zinc(II) nitrate (**14**) complexes, on the other hand, were ob-

© 2019 Wiley-VCH Verlag GmbH & Co. KGaA, Weinheim



Scheme 5. Formation of the copper(II) 1-ATRI picrate (PA), 2,4,6-trinitro-3-hydroxyphenolate (HTNR), 2,4,6-trinitro-3,5-dihydroxyphenolate (H_2TNPG), and styphnate (TNR) transition-metal(II) complexes **6**–**9**.

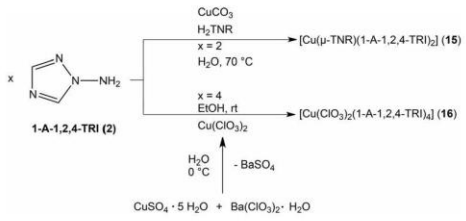


Scheme 6. Synthesis of complexes **10**–**14** with different metal(II) centers and anions.

tained with four coordinating 1-ATRI ligands, hexa-coordinated by two H_2O and four 1-ATRI ligands.

For better comparison and classification of the complexes, the isomer 1-A-1,2,4-TRI (**2**) was also investigated as a ligand. Thus, selected complexes with copper(II) styphnate (**15**) and chlorate (**16**) were prepared analogously to their related 1-ATRI homologues (Scheme 7).[22] However, the attempted synthesis of a copper(II) perchlorate complex yielded, unfortunately, no single crystalline product.

Although water was selected as the solvent to assure slow crystallization, the majority of the complexes crystallized (except **4**) in satisfactory yields (23–91 %) without aqua ligands (except **6**, **8**, and **10** and **11 b**) or the inclusion of crystal water, which results in a higher performance of the complexes. Therefore, only the water-free complex **11** and not the diaqua species **11 b** was characterized. Using ethanol instead of water led in most cases to the precipitation of the desired products due to the low solubility of the coordination compounds.



Scheme 7. Preparation of the energetic coordination compounds **15** and **16** based on 1-amino-1,2,4-triazole.

Crystal structures

The crystal structure of 1-ATRI (**1**) has already been described in the literature, whereas that of 1A-1,2,4-TRI (**2**) is hitherto unknown.[31] Therefore, single-crystal X-ray diffraction studies of ligand **2** and all of the complexes, except compound **4**, were performed. Details of the crystal structures of compounds **6**, **11**, **11 b**, and **13**–**15** are given in the Supporting Information together with the measurement and refinement data.[34] Both triazole ligands coordinate to the central metals through their heterocyclic nitrogen atoms in all the complexes. Additionally, the amino group of ligand **1** is coordinated in compound **5**. All the central metals show an octahedral coordination sphere except for in complex **14**, which is tetrahedrally coordinated.

Ligand **2** crystallizes in the form of colorless blocks in the monoclinic space group *P*2/*c* with eight formula units per unit cell and a calculated density of 1.420 g cm^{-3} at 150 K. All the non-hydrogen atoms of 1-A-1,2,4-TRI (**2**) lie in a plane, which is confirmed by the torsion angles (C2-N2-N3-C1 0.5(2)°, N1-N2-C2-N4 178.0(2)°, and C2-N4-C1-N3 0.2(3)°). The ligand shows comparable bond lengths and angles to those of 1-ATRI (**1**; Figure 3).[31]

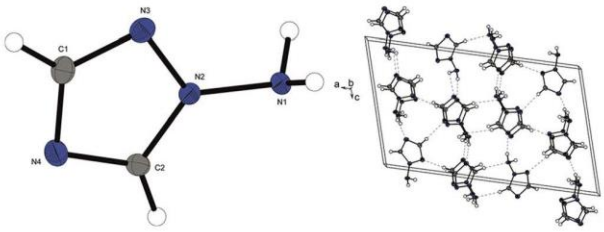


Figure 3. Molecular unit, packing and hydrogen bonding of 1A-1,2,4-TRI (**2**). Selected bond lengths [Å]: N1–N2 1.400(3), N2–N3 1.365(3), N2–C2 1.322(3), N3–C1 1.317(3), N4–C1 1.356(3), N4–C2 1.328(3); selected bond angles [°]: N1-N2-N3 123.17(18), N1-N2-C2 126.3(2), N3-N2-C2 110.47(19), N2-N3-C1 101.61(19), C1-N4-C2 102.43(19).

1-Amino-1,2,3-triazole (**1**) was protonated during the synthesis of compound **3** under the applied acidic conditions. The resulting tetrachlorido copper(II) complex crystallizes in the form of green blocks in the triclinic space group $P\bar{1}$ with one formula unit per unit cell and a calculated density of 2.038 g cm^{-3} at 173 K. Two asymmetric unit cells form the molecular unit, which consists of four chlorido ligands and two equivalents of 1-amino-1,2,3-triazolium that form an octahedral coordination sphere around the copper(II) center (Figure 4). As expected, the d^9 copper(II) shows a strong Jahn–Teller distortion along the N2-Cu1-N2^i axis with the nitrogen–copper(II) bond lengths being impressively long. The remaining four coordination positions are occupied by four chlorido ligands forming a vertical plane that is not perpendicular to the N2-Cu1-N2^i axis.

© 2019 Wiley-VCH Verlag GmbH & Co. KGaA, Weinheim

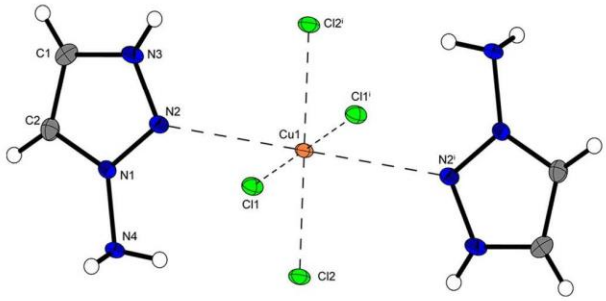


Figure 4. Molecular unit of $[CuCl_4(1\text{-ATRI}_H)_2]$ (**3**). Selected bond lengths [Å]: Cu1–N2 2.799(2), Cu1–Cl1 2.2835(7), Cu1–Cl2 2.2818(7); selected bond angles [°]: Cl1-Cu1-N2 84.49(5), Cl2-Cu1-N2 91.62(5), Cl1-Cu1-Cl2 89.68(2). Symmetry code: (i) $-x$, $2-y$, $-z$.

The nitrato complex **5** is the only compound with bridging 1-ATRI ligands. The nitrogen-rich molecules coordinate through the amino group as well as one heterocyclic nitrogen atom, leading to the formation of 2D polymeric layers. The compound crystallizes in the form of blue rods in the monoclinic space group $P2_1/n$ with two formula units per unit cell and a calculated density of 2.165 g cm^{-3} at 173 K. This coordination compound consists of a copper(II) center with an octahedral coordination sphere that shows Jahn–Teller-distorted axial nitrato ligands along the O1-Cu1-O1^{i} axis (Figure 5). The four equatorial positions of the coordination polyhedron are occupied by ligand **1** in an ideal plane. Although the bond angles between the equatorial ligands are almost 90° in each case, the axis formed by the nitrato anions runs obliquely through the N1^{iii}-N4-N1^{ii}-N4^{i} plane. Detailed descriptions of the polymeric structure (see Figure S5) and the hydrogen bonds (Table S5) are given in the Supporting Information.

Depending on the starting materials, two different complexes formed from copper(II), ligand **1**, and single- or double-deprotonated trinitroresorcinate as counter anion can be synthesized (Figure 6). 2,4,6-Trinitro-3-hydroxyphenolate leads to the formation of a closed octahedral coordination sphere (**7**), whereas with the styphnate bridging ligand as counter anion 1D polymeric chains (**9**) are formed. Both compounds differ

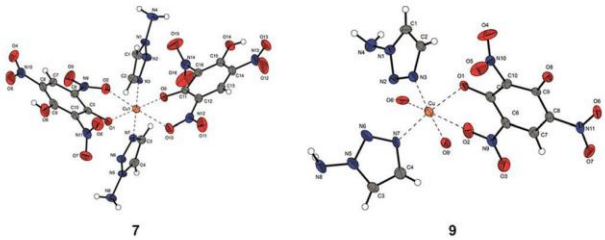


Figure 6. Molecular unit of compound **7** (left) and coordination environment of copper(II) in **9** (right). Selected bond lengths [Å] for **7**: Cu1–O1 1.947(3), Cu1–O2 2.329(3), Cu1–N7 1.977(3); for **9**: Cu1–O2 2.440(4), Cu1–O1 1.951(3), Cu1–N3 1.981(4), Cu1–N7 1.981(4); selected bond angles [°] for **7**: O1-Cu1-O2 82.11(12), O9-Cu1-O10 78.55(12), O1-Cu1-N7 90.65(15), O2-Cu1-N7 87.00(13), O9-Cu1-N3 92.60(15), O10-Cu1-N3 88.29(13), O10-Cu1-N7 92.71(13), O1-Cu1-O9 178.54(13); for **9**: O2-Cu1-O6^{ii} 161.56(13), O8^{ii}-Cu1-N3 173.16(17), O1-Cu1-O2 75.67(14), O6^{ii}-Cu1-O8^{ii} 79.21(14), O1-Cu1-N3 86.90(16), O2-Cu1-N7 99.20(15), O2-Cu1-O8^{ii} 84.09(14), O8^{ii}-Cu1-N7 88.37(17). Symmetry codes for **9**: (i) $-x$, $0.5+y$, $0.5-z$; (ii) $-x$, $-0.5+y$, $0.5-z$.

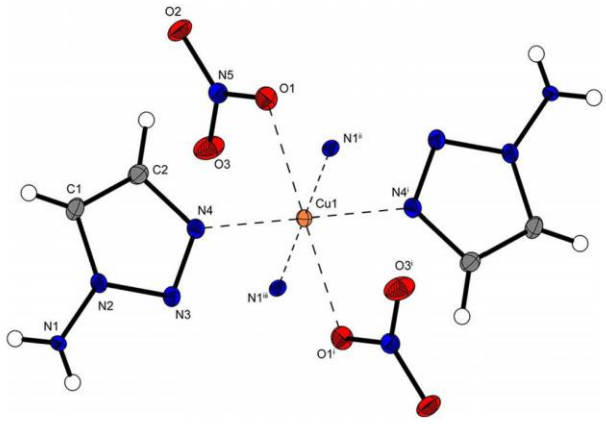


Figure 5. Coordination environment of $[Cu(NO_3)_2(\mu\text{-}1\text{-ATRI})_2]$ (**5**). Selected bond lengths [Å]: Cu1–O1 2.3738(16), Cu1–N4 1.9946(17), Cu1–N1^{ii} 2.092(3); selected bond angles [°]: N1^{ii}-Cu1-N4 90.03(8), O1^{iii}-Cu1-N4 92.43(6), O1-Cu1-N1^{iii} 93.58(7), O1-Cu1-N1^{ii} 86.42(7), O1-Cu1-N4 87.57(6). Symmetry codes: (i) $-x$, $-y$, $-z$; (ii) $1.5+x$, $0.5-y$, $1.5+z$; (iii) $-0.5-x$, $0.5+y$, $-0.5-z$; (iv) $-0.5-x$, $-0.5+y$, $-0.5-z$.

only slightly in their densities (1.842 g cm^{-3} for **7** and 1.876 g cm^{-3} for **9** at 173 K) and crystallize in similar space groups $P2_1$ and $P2_1/c$. Both complexes possess an octahedral coordination sphere with two equivalents of ligand **1** and deprotonated hydroxy groups in the equatorial positions. The Jahn–Teller-distorted axial coordination sites are occupied by the oxygen atoms of two nitro groups. Given the fixed structures of the counter anions, it becomes clear why the coordination polyhedrons of the investigated complexes are significantly distorted. Complex **15**, formed from copper(II) styphnate and ligand **2**, is analogous to compound **9**, and its crystal structure can be found in Figure S10 in the Supporting Information.

Copper(II) complex **8** crystallizes in the form of green blocks in the triclinic space group $P\bar{1}$ with one formula unit per unit cell and a calculated density of 1.840 g cm^{-3} at 173 K. In contrast to compounds **7** and **9**, the counter anion 2,4,6-trinitro-3,5-dihydroxyphenolate does not participate in the coordination sphere, which consists of four equatorial 1-ATRIs and two axial aqua ligands (Figure 7). Once again, the complex monomers show a Jahn–Teller distortion along the O1-Cu-O1^{i} axis.

The perchlorate complexes of ligand **1** form two different species with the transition-metal(II) cations. They crystallize either as water-free hexakis(1-amino-1,2,3-triazole) compounds or as tetrakis(1-amino-1,2,3-triazole) complexes with two aqua ligands (Figure 8). Within both forms, the complexes are isotypic and exhibit similar cell dimensions. The dihydrates **10** and **11b** crystallize in the triclinic space group $P\bar{1}$ with one formula unit per unit cell and differ only slightly in their densities (Cu: 1.810 g cm^{-3} (173 K); Mn: 1.721 g cm^{-3} (173 K)). The octahedral coordination spheres consist of four equivalents of **1** and two axial water molecules. Also, the d^9 copper(II) in com-

© 2019 Wiley-VCH Verlag GmbH & Co. KGaA, Weinheim

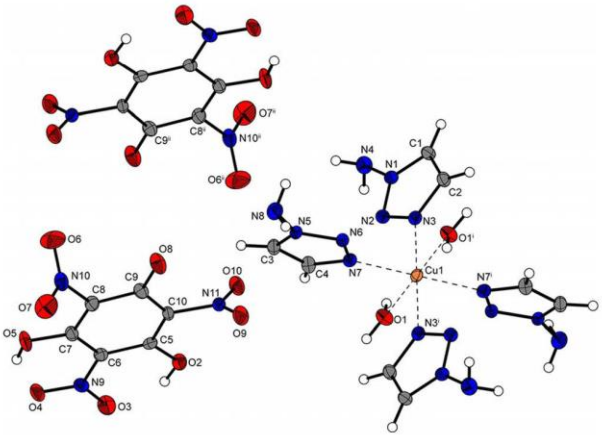


Figure 7. Molecular unit of compound **8**. Selected bond lengths [Å]: Cu1–O1 2.3287(16), Cu1–N3 2.0051(17), Cu1–N7 2.0407(16); selected bond angles [°]: O1-Cu1-N3 87.43(6), O1-Cu1-N7 88.49(6), N3-Cu1-N7 88.80(7). Symmetry codes: (i) 2−*x*, −*y*, −*z*; (ii) 2−*x*, 1−*y*, 1−*z*.

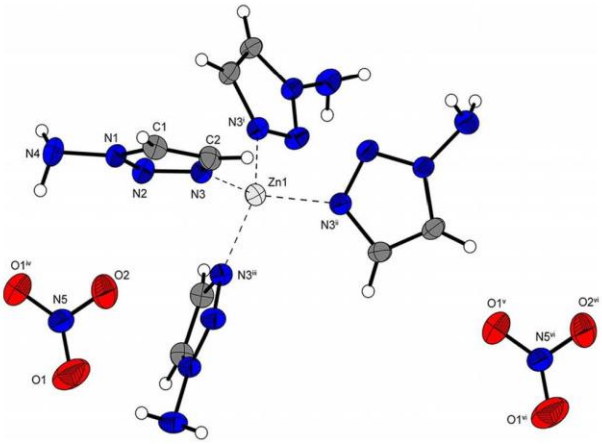


Figure 9. Molecular unit of the zinc(II) nitrate complex **14**. Selected bond length [Å]: Zn1–N3 1.9879(17); selected bond angles [°]: N3-Zn1-N3^{i} 112.25(7), N3-Zn1-N3^{ii} 104.06(7). Symmetry codes: (i) 0.25−*y*, 0.25+*x*, 0.25−*z*; (ii) −0.25+*y*, 0.25−*x*, 0.25−*z*; (iii) −*x*, 0.5−*y*, *z*; (iv) −*x*, 0.5−*y*, *z*; (v) 0.5−*x*, −*y*, −0.5+*z*; (vi) 0.5+*x*, −0.5+*y*, −0.5+*z*.

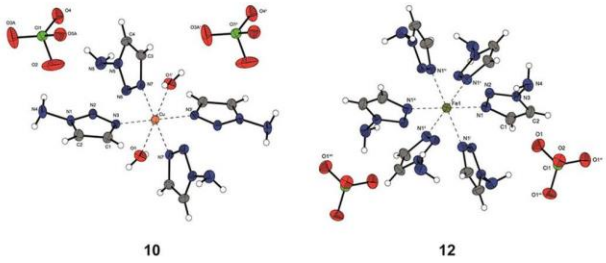


Figure 8. Molecular units of compounds **10** (left) and **12** (right). Selected bond lengths [Å] for **10**: Cu–O1 2.357(3), Cu–N3 2.020(2), Cu–N7 2.032(2); for **12**: Fe1–N1 2.2011(17); selected bond angles [°] for **10**: O1-Cu-N3 87.01(10), O1-Cu-N7 92.13(9), N3-Cu-N7 90.69(9), O1-Cu-N3^{i} 92.99(10); for **12**: N1-Fe1-N^{ii} 92.86(8), N1-Fe1-N^{v} 87.14(17). Symmetry codes for **10**: (i) 2−*x*, −*y*, −*z*; for **12**: (i) 0.67+*x*−*y*, 0.33+*x*, 0.33−*z*; (ii) 1−*y*, 1+*x*−*y*, *z*; (iii) 0.67−*x*, 1.33−*y*, 0.33−*z*; (iv) −*x*+*y*, 1−*x*, *z*; (v) −0.33+*y*, 0.33−*x*+*y*, 0.33−*z*; (vi) −*y*, −*y*, *z*; (vii) −*x*+*y*, −*x*, *z*; (viii) 1+*x*, +*y*, *z*.

pound **10** shows a Jahn–Teller distortion along the O1-Cu1-O1^{i} axis, which causes significantly higher copper(II)–oxygen coordination distances in comparison with those of the respective copper(II)– and manganese(II)–nitrogen atoms. The equatorial positions of the coordination polyhedrons form an ideal plane. The water-free complexes **11–13** crystallize in the trigonal space group $R\bar{3}$ with three formula units per unit cell and similar densities (Mn: 1.673 g cm^{-3} (143 K); Fe: 1.697 g cm^{-3} (123 K); Zn: 1.740 g cm^{-3} (133 K)). The molecular units consist of six-coordinate metal(II) centers and noncoordinating perchlorate counter anions, and the octahedral coordination sphere is only slightly distorted.

The zinc(II) compound $[Zn(1\text{-ATRI})_4](NO_3)_2$ (**14**) is the only tetrahedral complex (Figure 9). It crystallizes in the form of colorless blocks in the tetragonal space group $I4_1/a$ with four formula units per unit cell and a calculated density of 1.768 g cm^{-3} at 173 K. The complex is built up of four triazole ligands with N-Zn-N bond angles differing only slightly from the perfect tetrahedral angle of 109.47° and noncoordinating counter anions.

In contrast to the perchlorate compounds **10–13** discussed above, the chlorate counter anions in compound **16** coordinate to the copper(II) center. Compound **16** crystallizes in the triclinic space group $P\bar{1}$ with one formula unit per unit cell and a calculated density of 1.888 g cm^{-3} at 143 K. The molecular unit of the complex, illustrated in Figure 10, is built up of two axial chlorato and four equatorial triazole ligands. The compound shows again a typical Jahn–Teller distortion along the O1-Cu1-O1^{i} axis.

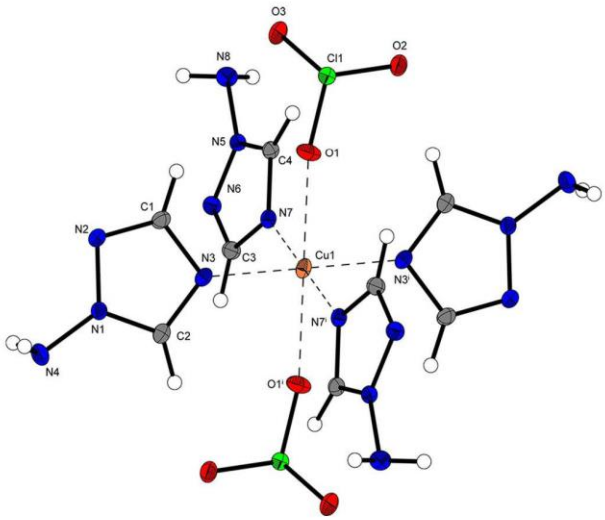


Figure 10. Complex unit of compound **16**. Selected bond lengths [Å]: Cu1–O1 2.497(2), Cu1–N3 2.000(2), Cu1–N7 1.998(2); selected bond angles [°]: O1-Cu1-N3 87.05(8), O1-Cu1-N7 91.58(8), N3-Cu1-N7 88.94(9). Symmetry code: (i) 2−*x*, −*y*, −*z*.

© 2019 Wiley-VCH Verlag GmbH & Co. KGaA, Weinheim

Scanning electron microscopy (SEM) and energy-dispersive X-ray spectroscopy (EDX)

To determine the morphologies and chemical compositions of the compounds, scanning electron microscopy experiments in combination with energy-dispersive X-ray spectroscopy were performed. The results of the measurements, exemplarily conducted for compounds **10** and **12**, are shown in Figures 11 and 12. Also, the grain sizes and crystal habits were examined by microscope imaging (see Figure S11–S15 in the Supporting Information), because both can strongly influence the sensitivity data of the compounds.

Figure 11 confirms the plate-like crystal habits of complex **10**. The plates can form blocks with sizes up to 300 μm. No elements other than those included in the complex composition can be observed in the EDX spectrum, which indicates the purity of the compound.

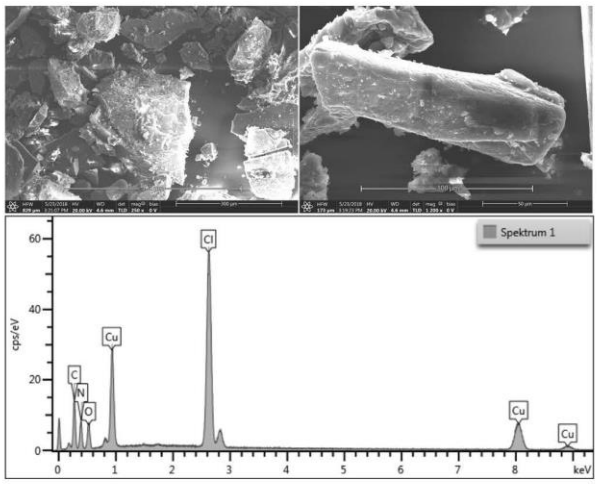


Figure 11. SEM images (250× magnitude (left, scale 500 μm) and 1200× magnitude (right, 100 μm)) and EDX spectrum of compound **10**.

The iron(II) perchlorate compound **12** forms blocks with sizes up to 300 μm beside small needle-like crystals (Figure 12). Compared with complex **10**, a higher content of non-oxygen atoms can be observed, which is consistent with the chemical compositions of the two coordination compounds. Besides insignificant trace amounts of sulfur, the EDX spectrum did not show any atoms other than those present in the complex.

Sensitivities and thermal stability

All the compounds were investigated by differential thermal analysis (DTA) at a heating rate of 5 °C min^{-1}. The observed decomposition temperatures as well as endothermic events (melting, dehydration, or loss of coordinating 1-ATRI ligands) are listed in Table 1.

The DTA plots of the compounds **1–9** and **14–16** as well as additional information regarding the thermal stabilities can be found in Figures S17–S19 in the Supporting Information. For a closer examination of the endothermic events, thermal gravimetric analysis (TGA) was performed on both ligands as well as complexes **11**, **13**, and **14** (Figure 13 and Figure S16). Compounds **1** and **2** both possess melting points at 39 °C and the TGA measurements reveal constant loss of the ligands until their exothermic decomposition temperatures at 267 and 222 °C, respectively. Compared with 4-amino-1,2,4-triazole (4-ATRI), the two ligands show lower melting points, but 1-ATRI is slightly more thermally stable. Both zinc(II) complexes show endothermic events in the DTA. The nitrate compound **14** shows the loss of two ligands during the TGA experiment (Figure 13) before it decomposes, whereas the perchlorate

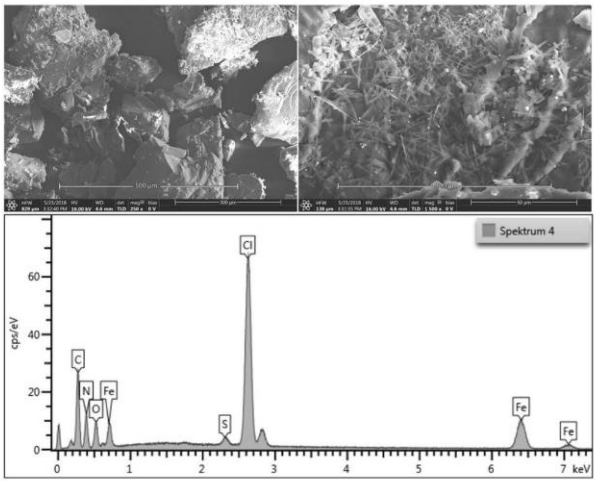


Figure 12. SEM images (250× magnitude (left, scale 500 μm) and 1500× magnitude (right, scale 100 μm)) and EDX spectrum of compound **12**.

Table 1. Thermal stability measurements[a] for compounds **1–16** and 4-ATRI by DTA.

	T_{endo1} [°C][b]	T_{endo2} [°C][b]	T_{exo} [°C][c]
1-ATRI (**1**)	39	267	267
1-A-1,2,4-TRI (**2**)	39	222	222
4-ATRI	80	–	261
$[CuCl_4(1\text{-}ATRI_H)_2]$ (**3**)	148	–	148
$[CuCl_2(1\text{-}ATRI)_2]$ (**4**)	165	–	165
$[Cu(NO_3)_2(\mu\text{-}1\text{-}ATRI)_2]$ (**5**)	–	–	167
$[Cu(H_2O)_4(1\text{-}ATRI)_2](PA)_2$ (**6**)	66	–	188
$[Cu(Htnr)_2(1\text{-}ATRI)_2]$ (**7**)	–	–	177
$[Cu(H_2O)_2(1\text{-}ATRI)_4](H_2TNPG)_2$ (**8**)	123	–	153
$[Cu(\mu\text{-}tnr)(1\text{-}ATRI)_2]$ (**9**)	–	–	194
$[Cu(H_2O)_2(1\text{-}ATRI)_4](ClO_4)_2$ (**10**)	–	–	167
$[Mn(1\text{-}ATRI)_6](ClO_4)_2$ (**11**)	161	–	194
$[Fe(1\text{-}ATRI)_6](ClO_4)_2$ (**12**)	–	–	166
$[Zn(1\text{-}ATRI)_6](ClO_4)_2$ (**13**)	91	–	188
$[Zn(1\text{-}ATRI)_4](NO_3)_2$ (**14**)	134	–	188
$[Cu(\mu\text{-}tnr)(1\text{-}A\text{-}1,2,4\text{-}TRI)_2]$ (**15**)	–	–	237
$[Cu(ClO_3)_2(1\text{-}A\text{-}1,2,4\text{-}TRI)_4]$ (**16**)	–	–	132

[a] Onset temperatures at a heating rate of 5 °C min^{-1}. [b] Endothermic peak, which indicates melting, vaporization, dehydration, or loss of coordinating 1-ATRI molecules. [c] Exothermic peak, which indicates decomposition.

© 2019 Wiley-VCH Verlag GmbH & Co. KGaA, Weinheim

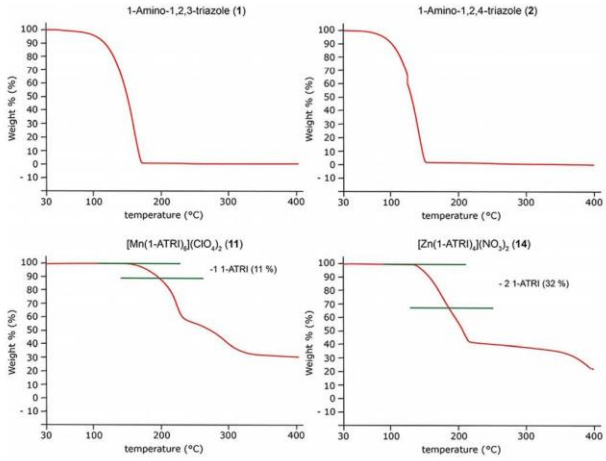


Figure 13. TGA measurements of the free ligands **1** and **2** as well as the selected complexes **11** and **14** acquired at a heating rate of 5 °C min^{-1}.

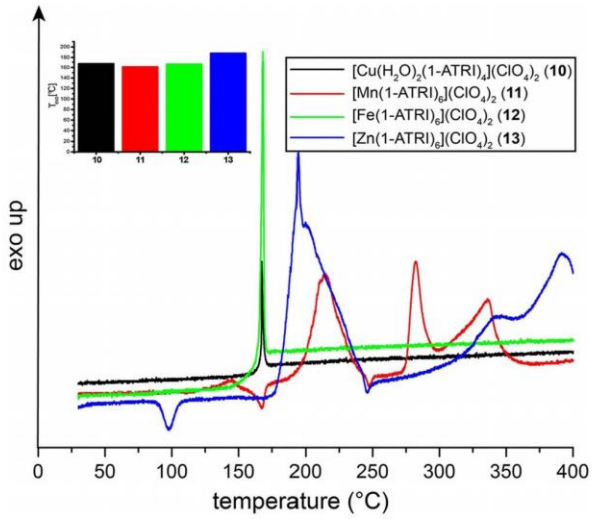


Figure 14. DTA plots (5 °C min^{-1}) of the perchlorate compounds **10**–**13**.

complex **13** shows no loss of mass, which proves its thermal stability, and exhibits a melting point at 134 °C (see Figure S16). Similarly to **14**, compound **11** exhibits the loss of one ligand before its thermal decomposition. The endothermic events of the aqua complexes **6** and **8** indicate the formation of stable water-free compounds during heating, whereas for the diaqua complex **10**, the water molecules are necessary for the stability of the crystal structure.

With the exception of **15**, all of the investigated compounds show exothermic decomposition events at temperatures lower than the uncoordinated ligands. But still, most of the compounds (except **3**, **8**, and **16**) show excellent exothermic thermal decomposition temperatures between 165 (**4**) and 237 °C (**15**). The very good thermal stabilities of **9** and **15** can be explained by the formation of polymeric structures, whereas the exceptionally low thermal stability of chlorate complex **16** is consistent with our former observations for the copper(II) chlorate complex with 1-ATRI as ligand ($[Cu(ClO_3)_2(1\text{-ATRI})_4]$).[22]

The perchlorate-based metal(II) complexes **10**–**13** possess relatively high thermal stabilities (Figure 14), which increase in the order Fe^{II} ($T_{exo.}$ = 166 °C) ≈ Cu^{II} ($T_{exo.}$ = 167 °C) < Zn^{II} ($T_{exo.}$ = 188 °C) < Mn^{II} ($T_{exo.}$ = 194 °C). Analogous complexes with 1-methyl-5*H*-tetrazole or 1-amino-5*H*-tetrazole interestingly show almost the same trend, which could be a useful indicator for the design of future energetic complexes with high-temperature stability.[35] Compared with the copper(II) perchlorate complex of 4-ATRI with a decomposition temperature of 250 °C,[36] it becomes clear that the formation of closed octahedral coordination spheres with the absence of polymeric structures leads to a significant decrease in thermal stability. Interestingly, the nitrate complexes **5** and **14**, which usually show lower thermal stabilities, exhibit the same decomposition temperatures as the analogous perchlorate complexes.[36]

The sensitivities toward impact and friction were explored according to BAM standard methods (1 of 6). Additionally, the electrostatic discharge (ESD) sensitivities were determined and the data obtained were categorized in accordance with the "UN Recommendations on the Transport of Dangerous Goods". An overview of the sensitivities can be found in Table 2.

The free ligand **2** as well as dichlorido compound **4** and picrate complex **6** can be considered as "insensitive" toward impact and friction, whereas ligand **1** is "less sensitive" toward impact. Compared with complex **4**, tetrachlorido compound **3** is slightly less stable. The perchlorate compounds are "extremely sensitive" to both impact and friction, whereas the

Table 2. Sensitivities toward impact, friction, and ESD for compounds **1**–**16**.[a]

Compound	IS [J][b]	FS [N][c]	ESD [J][d]
1	35	>360	1.50
2	>40	>360	1.50
3	35	216	1.40
4	>40	>360	0.70
5	<1	30	0.10
6	>40	>360	1.22
7	1.5	80	0.04
8	2	160	0.30
9	3	60	0.05
10	1	0.45	0.10
11	3	10	0.06
12	1.5	2	0.04
13	3	6.75	0.07
14	6	45	0.70
15	30	240	0.09
16	<1	23	0.01

[a] Determined at a grain size of 100–500 μm except for **4**, **6**, **7**, **10**, and **16** (**4**, **16**: <100 μm; **6**, **7**, **10**: 500–1000 μm). [b] Impact sensitivity according to the BAM drop-hammer method (method 1 of 6). Insensitive >40 J, less sensitive ≥35 J, sensitive ≥4 J, very sensitive ≤3 J, as per the UN Recommendations on the Transport of Dangerous Goods. [c] Friction sensitivity according to the BAM friction tester (method 1 of 6). Insensitive >360 N, less sensitive 360 N, sensitive <360 N and >80 N, very sensitive ≤80 N, extremely sensitive ≤10 N, as per the UN Recommendations on the Transport of Dangerous Goods. [d] Electrostatic discharge sensitivity (OZM ESD tester).

© 2019 Wiley-VCH Verlag GmbH & Co. KGaA, Weinheim

copper(II) nitrato and chlorate complexes show the lowest stability toward impact, they are only "very sensitive" toward friction. The use of less oxidizing anions such as styphnate or 2,4,6-trinitro-3,5-dihydroxyphenolate leads to stabilization of the complexes toward applied friction and impact stimuli (see Figure S21 in the Supporting Information). Comparison of the complexes with (nitrate) and without (chloride) oxidizing anions reveals the destabilization of the nitrate complexes and concomitant enhancement of the performance (see Figure S20). The stability of the perchlorate complexes toward friction and impact increases in the order $Cu^{2+} < Fe^{2+} < Zn^{2+} \leq Mn^{2+}$ (Figure 15).

The most promising compounds **6**, **10–13**, and **16**, were tested in ball-drop impact experiments (Figure 16) to gain a better insight into their behavior against external stimuli. The measured sensitivities (Figure 17) of the perchlorate complexes toward ball-drop impact, summarized in Table 3, are consistent with the values observed for drop-hammer impact and friction, although unfortunately no explanation can be given for the high stability of **11**.

To gain an initial indication of the suitability of the most promising complexes (**5**, **10–14**, and **16**) as primary explosives and their behavior toward rapid heating, hot-plate and hot-needle tests were carried out (Figures 18 and 19 and Figures S22–S32 in the Supporting Information). An overview of the experimental results is compiled in Table 4. All the investigated compounds showed sharp deflagrations during the tests

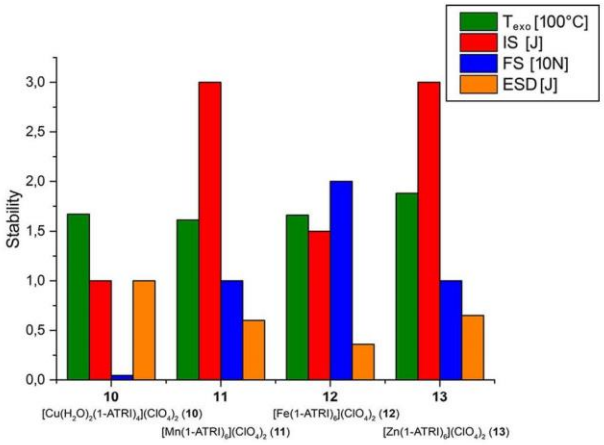


Figure 15. Stabilities of the perchlorate coordination compounds **10–13**.

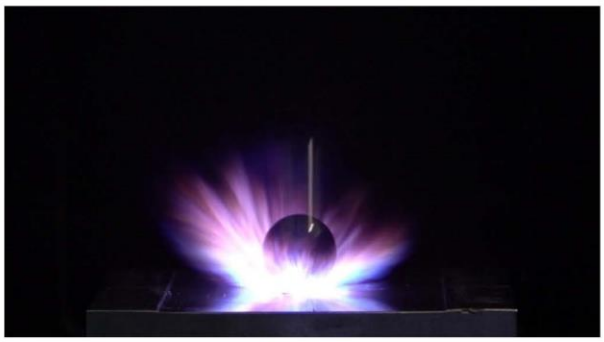


Figure 16. Moment of detonation of complex **10**.

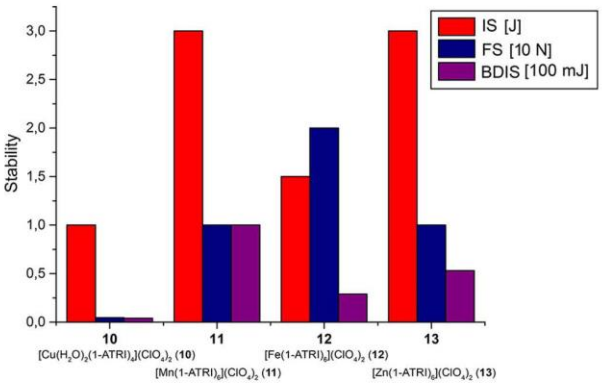


Figure 17. Comparison of the impact (drop hammer) and friction sensitivities with the ball-drop impact sensitivities (BDISs) of the metal(II) perchlorate complexes **10–13**.

Table 3. Ball-drop impact sensitivities for **6**, **10–13**, and **16**.[a]

	6	10	11	12	13	16
BDIS [mJ]	66	<4	>100	29	53	8

[a] Ball-drop impact sensitivity determined by the OZM ball-drop test applying the 1 of 6 method in accordance with the MIL-STD 1751A (method 1016). For the testing, a 30 mg sample size, a steel ball drop weight with a diameter of 0.500 inch ($m = 8.35$ g), and a steel ball guidance track, which rises 32 inches vertically from a steel base, were used.

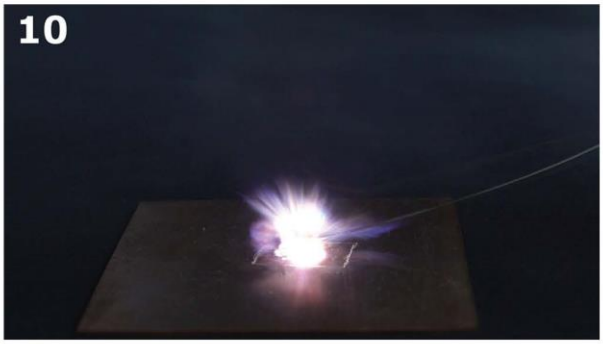


Figure 18. Moment of detonation of copper(II) complex **10** during the hot-needle (HN) test (right: deformed needle).



Figure 19. Deflagration of the coordination compound **10** during the hot-plate (HP) test (images shown in sequence).

© 2019 Wiley-VCH Verlag GmbH & Co. KGaA, Weinheim

Table 4. Summary of the hot-plate (HP) and hot-needle (HN) test results for **5**, **10**–**14**, and **16**.[a]

Compound	HP	HN	Compound	HP	HN
5	def.	def.	**13**	def.	def.
10	def.	det.	**14**	def.	def.
11	def.	def.	**16**	def.	def.
12	def.		def.		

[a] def.: deflagration; det.: detonation.

except for the powerful compound **10**, which detonated during the hot-needle test and deformed the used needle (Figure 18).

After performing the hot-plate and hot-needle tests, the initiation capability of the complexes toward nitropenta (PETN) as the main charge in copper shells was investigated. Further information on the test setup can be found in the General Methods of the Supporting Information.

Positive tests, indicated by a hole in the copper witness plate and fragmentation of the shell caused by a deflagration-to-detonation transition (DDT) of the secondary explosive PETN, were only observed for the very promising complexes **10** and **13** (Figure 20). Negative tests, represented by an undamaged copper plate and shell, were obtained for the other tested compounds (**5**, **11**, **12**, **14**, and **16**).

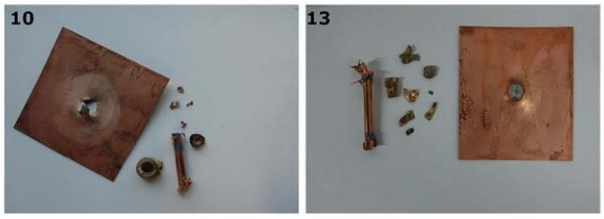


Figure 20. Positive nitropenta (PETN) initiation tests for the metal(II) perchlorate complexes **10** and **13**.

Toxicity

The toxicity toward aquatic organisms of the nitrogen-rich triazole **1** was determined by using the known luminescence marine bacterium *Vibrio fischeri* NRRL-B-1177 strain to predict the possible toxicological impact of the relevant coordination compounds.[37] With a half-maximal effective concentration (EC_{50}) value of 3.11 g L^{-1} after 30 min, the compound can practically be considered as non-toxic (toxicity level after 30 min incubation: very toxic <0.10 g L^{-1}, toxic 0.10–1.00 g L^{-1}, nontoxic >1.00 g L^{-1}).[38]

Laser initiation

Energetic materials can be ignited by a variety of different initiation methods (e.g., mechanical, heat, electrical). In particular, the initiation by optical means such as laser has attracted increasing attention in recent years.[13,20] Most of the ignition mechanisms currently in use still involve traditional techniques due to their great simplicity. Nevertheless, more and more applications based on optical initiation are coming onto the market, as this method has some advantages over conventional methods.[18,39] Because a photothermal and not a photochemical mechanism can be assumed, only selected colored compounds were tested. The observed behavior toward laser irradiation correlates to a large extent with the observed sensitivities and varies widely depending on the metal, ligand, and anion combination, which allows precise tailoring of the compounds to the requirements of future systems. Decompositions could be observed for the complexes **6**–**9**, deflagrations for **5**, **15**, and **16**, and detonations for the metal(II) perchlorate compounds **10** and **12** (Figure 21 and Figure S33 in the Supporting Information). The complexes could all be ignited with the low energies applied, which underlines the fact that these compounds are highly suitable for use as explosives. A detailed overview of the results is given in Table 5. Further details on sample preparation and experimental setup can be found in the Supporting Information.

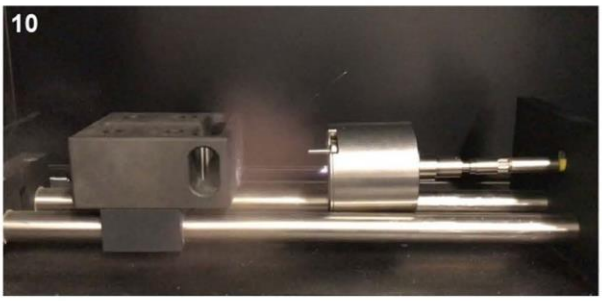


Figure 21. Moment of detonation of the coordination compound **10**.

Table 5. Laser ignition test results.[a]

Compound	Reaction	Compound	Reaction
5	def.	**10**	det.
6	dec.	**12**	det.
7	dec.	**15**	def.
8	dec.	**16**	def.
9		dec.	

[a] dec.: decomposition; def.: deflagration; det.: detonation. Operating parameters: current $I=7$ A, voltage $U=4$ V, theoretical maximal output power $P_{max}=45$ W, theoretical energy $E_{max}=0.17$ mJ, wavelength $\lambda=915$ nm, pulse length $\tau=0.1$ ms.

UV/Vis spectroscopy

Solid-state UV/Vis spectra of the laser-ignitable compounds were recorded in the range of 350–1000 nm to investigate a possible correlation between absorption and laser ignitability (Figure 22). The measured optical properties of the compounds are summarized in Table 6. The investigated compounds have characteristic absorptions in the NIR, visible, and UV ranges resulting from typical d–d transitions, which are strongly depen-

© 2019 Wiley-VCH Verlag GmbH & Co. KGaA, Weinheim

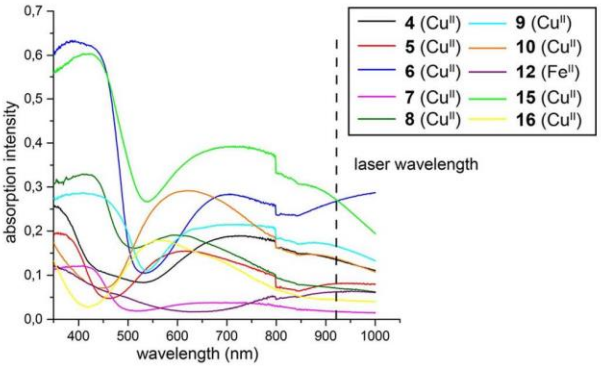


Figure 22. Solid-state UV/Vis spectra of selected complexes.

Table 6. Optical properties of **4–10**, **12**, **15**, and **36**.

Compound	M	Color	$\lambda_{d\text{-}d}$[a] [nm]	$A_{915}/A_{d\text{-}d}$[b]
4	Cu^{II}	green	737	0.72
5	Cu^{II}	blue	617	0.52
6	Cu^{II}	green	393,[c] 708	0.94
7	Cu^{II}	green	408,[c] 737	0.47
8	Cu^{II}	green	408,[c] 595	0.38
9	Cu^{II}	green	408,[c] 711	0.78
10	Cu^{II}	blue	618	0.48
12	Fe^{II}	colorless	950	0.97
15	Cu^{II}	green	410,[c] 732	0.70
16	Cu^{II}	violet	565	0.25

[a] Absorption wavelength of maximum intensity, which can be assigned to electron d–d excitations in the measured range of 350–1000 nm. [b] Quotient of the absorption intensity at the laser wavelength and the intensity at the d–d absorption wavelength. [c] n–π^* transitions.

dent on the coordination sphere and the respective metal, anion, and ligand.

The exact mechanism still remains unclear.[40] However, it is assumed that compounds with increased absorption in the laser wavelength range generate photothermally induced hot spots and are therefore rather laser-ignitable. Nevertheless, further mechanistic studies are needed to gain a full understanding of the mechanism. Additional strong n–π^* absorption bands ranging from the UV up to the visible blue region can be observed for the copper(II) complexes **6–9** and **15**, which are most likely derived from the trinitrobenzene anions.

Conclusions

The two N^1-substituted aminotriazoles 1-amino-1,2,3-triazole (**1**, 1-ATRI) and 1-amino-1,2,4-triazole (**2**, 1-A-1,2,4-TRI) were prepared by a simple one-step synthesis starting from the respective triazoles (1,2,3- or 1,2,4-triazole) and the conventional amination reagent hydroxylamine-*O*-sulfonic acid (HOSA). The resulting isomeric mixtures were then purified by simple column chromatography or vacuum sublimation to yield the desired products in satisfactory yields. Due to the enormous potential of 1-ATRI as a ligand in high-energetic coordination compounds, a scalable, cheap, and isomerically pure two-step synthesis was elaborated. The ligands 1-ATRI and 1-A-1,2,4-TRI were extensively characterized by multinuclear NMR spectroscopy and XRD and their toxicities were determined, with 1-ATRI showing nontoxic character toward aquatic organisms. Although a multitude of 4-ATRI complexes have been reported in the literature, the overall goal of this work was to further increase the energy content of complexes by employing more endothermic ligands and thus produce useful new lead-free primary explosives. The present work involved the synthesis, characterization, and evaluation of 14 new complexes composed of two isomeric aminotriazoles, four metals (Mn, Fe, Cu, and Zn), and seven different anions. The complexes, with a very interesting variety of coordination spheres, were synthesized by a scalable and cost-effective route. The concept of energetic coordination compounds (ECCs), which allows fine-tuning by varying the individual components, has once again revealed its great potential in addressing the problems of lead-free primary explosives and laser ignition. X-ray diffraction studies in combination with SEM and microscope imaging of the most promising complexes has provided fascinating insights and allowed correlations between structure and the observed sensitivities to be identified. The majority of the synthesized complexes could be laser-ignited and showed different behavior that could be correlated with the measured sensitivities. Positive initiation capability tests ($[Cu(H_2O)_2(1\text{-ATRI})_4](ClO_4)_2$ and $[Zn(1\text{-ATRI})_6](ClO_4)_2$) with PETN-loaded copper tube detonators underlined the enormous potential of single complexes as alternatives to lead-free primary explosives.

Acknowledgements

Financial support of this work by the Ludwig-Maximilian University of Munich (LMU) and the Office of Naval Research (ONR, grant no. ONR.N00014-16-1-2062) is acknowledged. The authors would like to thank Mrs. Cornelia Unger for toxicity assessments as well as Jasmin Lechner and Alexander Kremsmair for their great contributions.

Conflict of interest

The authors declare no conflict of interest.

Keywords: amines · energetic coordination compounds · explosives · nitrogen heterocycles · transition metals

[1] T. M. Klapötke, *Chemistry of High-Energy Materials, 3rd ed.*, Walter de Gruyter, Berlin/Boston, **2015**.
[2] E. C. Johnson, J. J. Sabatini, D. E. Chavez, R. C. Sausa, E. F. C. Byrd, L. A. Wingard, P. E. Guzman, *Org. Process Res. Dev.* **2018**, *22*, 736–740.
[3] Y. Tang, C. He, G. H. Imler, D. A. Parrish, J. M. Shreeve, *J. Mater. Chem. A* **2018**, *6*, 5136–5142.
[4] G. Bélanger-Chabot, S. M. Kaplan, P. Deokar, N. Szimhardt, R. Haiges, K. O. Christe, *Chem. Eur. J.* **2017**, *23*, 13087–13099.
[5] D. Chen, H. Yang, Z. Yi, H. Xiong, L. Zhang, S. Zhu, G. Cheng, *Angew. Chem. Int. Ed.* **2018**, *57*, 2081–2084; *Angew. Chem.* **2018**, *130*, 2103–2106.

© 2019 Wiley-VCH Verlag GmbH & Co. KGaA, Weinheim

[6] J. W. Fronabarger, M. D. Williams, W. B. Sanborn, J. G. Bragg, D. A. Parrish, M. Bichay, *Propellants Explos. Pyrotech.* **2011**, *36*, 541 – 550.
[7] D. Fischer, T. M. Klapötke, J. Stierstorfer, N. Szimhardt, *Chem. Eur. J.* **2016**, *22*, 4966 – 4970.
[8] https://echa.europa.eu/de/regulations/reach/understanding-reach, Accessed June **2018**.
[9] Q. Zhang, J. M. Shreeve, *Angew. Chem. Int. Ed.* **2014**, *53*, 2540 – 2542; *Angew. Chem.* **2014**, *126*, 2574 – 2576.
[10] K. A. McDonald, S. Seth, A. J. Matzger, *Cryst. Growth Des.* **2015**, *15*, 5963 – 5972.
[11] J.-G. Xu, C. Sun, M.-J. Zhang, B.-W. Liu, X.-Z. Li, J. Lu, S.-H. Wang, F.-K. Zheng, G.-C. Guo, *Chem. Mater.* **2017**, *29*, 9725 – 9733.
[12] M. Joas, T. M. Klapötke, J. Stierstorfer, N. Szimhardt, *Chem. Eur. J.* **2013**, *19*, 9995 – 10003.
[13] T. W. Myers, J. A. Bjorgaard, K. E. Brown, D. E. Chavez, S. K. Hanson, R. J. Scharff, S. Tretiak, J. M. Veauthier, *J. Am. Chem. Soc.* **2016**, *138*, 4685 – 4692.
[14] W. Shan, W. Qianyou, F. Xiao, W. Bo, Y. Li, *Adv. Mater.* **2017**, *29*, 1701898.
[15] N. Szimhardt, J. Stierstorfer, *Chem. Eur. J.* **2018**, *24*, 2687 – 2698.
[16] A. Y. Zhilin, M. A. Ilyushin, I. V. Tselinskii, A. S. Kozlov, I. S. Lisker, *Russ. J. Appl. Chem.* **2003**, *76*, 572 – 576.
[17] Y.-H. Zhu, D.-L. Sheng, B. Yang, L.-K. Chen, F.-E. Ma, *Hanneng Cailiao* **2009**, *17*, 169 – 172.
[18] R. Schirra, H. Zöllner, *Proceedings of the 42nd International Pyrotechnics Seminar*, Grand Junction, CO, July 10 – 15, 2016 **2016**, 422 – 428.
[19] M. H. V. Huynh, M. D. Coburn, T. J. Meyer, M. Wetzler, *Proc. Natl. Acad. Sci. USA* **2006**, *103*, 10322 – 10327.
[20] M. A. Ilyushin, I. V. Tselinsky, I. V. Shugalei, *Cent. Eur. J. Energ. Mater.* **2012**, *9*, 293 – 327.
[21] T. W. Myers, K. E. Brown, D. E. Chavez, R. J. Scharff, J. M. Veauthier, *Eur. J. Inorg. Chem.* **2016**, 3178 – 3183.
[22] M. H. H. Wurzenberger, N. Szimhardt, J. Stierstorfer, *J. Am. Chem. Soc.* **2018**, *140*, 3206 – 3209.
[23] O. Kahn, C. J. Martinez, *Science* **1998**, *279*, 44 – 48.
[24] M. A. Ilyushin, M. A. Aleksandrova, I. V. Bachurina, A. V. Smirnov, I. V. Tselinskii, *Russ. J. Appl. Chem.* **2010**, *83*, 92 – 96.
[25] S. Cudziło, M. Nita, *J. Hazard. Mater.* **2010**, *177*, 146 – 149.
[26] S. Hauptmann, H. Wilde, K. Moser, *Tetrahedron Lett.* **1967**, 3295 – 3297.
[27] J. De Mendoza, M. L. Castellanos, J. P. Fayet, M. C. Vertut, J. Elguero, *J. Chem. Res. Synop.* **1980**, 50 – 51.
[28] F. Grande, A. Brizzi, A. Garofalo, F. Aiello, *Tetrahedron* **2013**, *69*, 9951.
[29] F. Aiello, A. Garofalo, F. Grande, *Tetrahedron* **2010**, *66*, 274.
[30] K. Shigeno, T. Ono, M. Tanaka, S. Yamada, T. Asao, EP0727418B1, **1999**.
[31] G. Kaplan, G. Drake, K. Tollison, L. Hall, T. Hawkins, *J. Heterocycl. Chem.* **2005**, *42*, 19 – 27.
[32] H.-X. Hu, H.-X. Niu, Y. Wang, Y.-C. Li, S.-P. Pang, *Mater. Res. Innovations* **2014**, *18*, 1127 – 1131.
[33] G. Laus, W. Kloetzer, *Synthesis* **1989**, 269 – 272.
[34] CCDC 1847945 (**2**), 1847943 (**3**), 1847948 (**5**), 1847946 (**6**), 1847952 (**7**), 1847944 (**8**), 1847951 (**9**), 1847947 (**10**), 1847949 (**11**), 1847939 (**11b**), 1847941 (**12**), 1847950 (**13**), 1847942 (**14**), 1847940 (**15**), and 1848019 (**16**) contain the supplementary crystallographic data for this paper. These data are provided free of charge by The Cambridge Crystallographic Data Centre.
[35] N. Szimhardt, M. H. H. Wurzenberger, A. Beringer, L. J. Daumann, J. Stierstorfer, *J. Mater. Chem. A* **2017**, *5*, 23753 – 23765.
[36] S. Cudziło, M. Nita, *J. Hazard. Mater.* **2010**, *177*, 146 – 149.
[37] G. I. Sunahara, S. Dodard, M. Sarrazin, L. Paquet, G. Ampleman, S. Thiboutot, J. Hawari, A. Y. Renoux, *Ecotoxicol. Environ. Saf.* **1998**, *39*, 185 – 194.
[38] C. J. Cao, M. S. Johnson, M. M. Hurley, T. M. Klapötke, *JANNAF J. Propuls. Energet.* **2012**, *5*, 41 – 51.
[39] H. Lebreton, D. Cazajous, S. Larue, *Proc. Int. Pyrotech. Semin.* **2015**, *41st*, 1 – 6.
[40] E. D. Aluker, A. G. Krechetov, A. Y. Mitrofanov, D. R. Nurmukhametov, M. M. Kuklja, *J. Phys. Chem. C* **2011**, *115*, 6893 – 6901.

Manuscript received: July 2, 2018
Accepted manuscript online: August 24, 2018
Version of record online: October 22, 2018

© 2019 Wiley-VCH Verlag GmbH & Co. KGaA, Weinheim

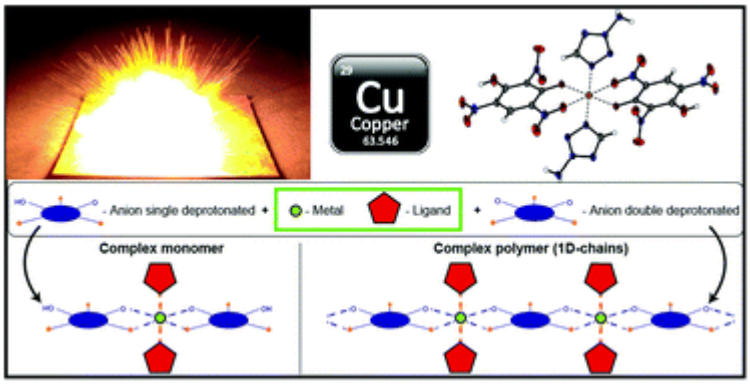
Appendix 12

Synthesis and Comparison of Copper(II) Complexes with various N-Aminotetrazole Ligands Involving Trinitrophenol Anions

M. H. H. Wurzenberger, B. R. G. Bissinger, M. Lommel, M. S. Gruhne, N. Szimhardt, J. Stierstorfer

New J. Chem. **2019**, *43*, 18193–18202.

https://doi.org/10.1039/C9NJ03937F



Supplementary Information:
https://www.rsc.org/suppdata/c9/nj/c9nj03937f/c9nj03937f1.pdf

Published on 28 October 2019. Downloaded by Ludwig Maximilians Universitaet Muenchen on 2/16/2022 8:04:02 AM.

NJC

PAPER

View Article Online
View Journal | View Issue

Check for updates

Cite this: *New J. Chem.*, 2019, **43**, 18193

Synthesis and comparison of copper(II) complexes with various *N*-aminotetrazole ligands involving trinitrophenol anions†‡

Maximilian H. H. Wurzenberger, Benjamin R. G. Bissinger, Marcus Lommel, Michael S. Gruhne, Norbert Szimhardt and Jörg Stierstorfer *

Received 30th July 2019,
Accepted 28th October 2019

DOI: 10.1039/c9nj03937f

rsc.li/njc

Due to the ongoing research on lead-free energetic materials, two different ligand systems (1-amino-5*H*-tetrazole (1-AT), 2-amino-5*H*-tetrazole (2-AT), 1-amino-5-methyltetrazole (1-AMT), and 2-amino-5-methyltetrazole (2-AMT)) were applied for the synthesis of 12 new energetic coordination compounds (ECC) with copper(II) as the central metal. Different anions based on trinitrophenols (picric acid (HPA), styphnic acid (H_2TNR), and trinitrophloroglucinol (H_3TNPG)) were used for the specifical tuning of the energetic and physico-chemical properties of the complexes. Through the choice of ligand, the characteristics of the resulting products can be easily adjusted either towards sensitive primary explosives usable for classical initiation setups or towards laser-ignitable explosives with decreased sensitivities. The ECC were extensively characterized by *e.g.*, X-ray diffraction (XRD), elemental analysis (EA), IR, differential thermal analysis (DTA), and UV/vis. In addition, the most promising compounds were analyzed by TGA and in classical initiation tests using nitropenta (PETN). Furthermore, the sensitivities towards external stimuli (impact, friction, and electrostatic discharge) were determined by standard methods and the influence of the anions towards them was investigated. Compounds [Cu(TNR)(1-AMT)$_2$] and [Cu(HTNPG)(1-AMT)$_2$] both possess appropriate sensitivities as well as thermal stabilities above 200 °C and show promising results to be used as potential lead azide replacements. In addition, all ECC were irradiated with a near infrared light (NIR) laser diode leading to different responses.

Introduction

The energetic character of many nitroaromatic compounds derives from the oxidation of the carbon-backbone and the circumstance that these substances combine both the fuel (C–H backbone) and the oxidizer (nitro groups) within one molecule. As a result of this, selected polynitroaromatics can be used as explosives, most notably trinitrotoluene (TNT).[1] A close structural relative of TNT is picric acid (HPA, **1**) (Chart 1), which was discovered in the form of its potassium salt by Johann Glauber in 1742.[2]

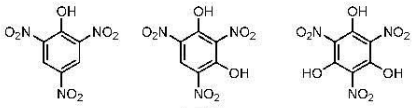


Chart 1 Trinitrophenols picric acid (**1**), styphnic acid (**2**) and trinitrophloroglucinol (**3**).

The compound was obtained *via* treatment of wool or horn with HNO_3 and has since been applied as a dye for silk, and, due to its intensely bitter taste and tinctorial power, as a replacement for hops in beer. However, it wasn't until more than 100 years later that German chemist Hermann Sprengel demonstrated that picric acid could be brought to detonation, and therefore filed the related patents. Following this, HPA replaced black powder in nearly all military applications.[2–4]

Styphnic acid (H_2TNR, **2**) and 2,4,6-trinitrophloroglucinol (H_3TNPG, **3**) derive structurally from picric acid and have a wide history of military applications together with their metal salts. The most prominent is lead styphnate (LS), a rather sensitive and highly toxic primary explosive. Together with lead

Department of Chemistry, Ludwig Maximilian University of Munich, Butenandtstr. 5-13, D-81377 Munich, Germany. E-mail: jstch@cup.uni-muenchen.de; Web: http://www.cup.lmu.de/ac/stierstorfer/, http://www.hedm.cup.uni-muenchen.de; Fax: +49-89-2180-77492

† Parts of this work were presented at the 22nd Seminar on New Trends in Research of Energetic Materials 2019 at the University of Pardubice (Czech Republic).

‡ Electronic supplementary information (ESI) available: Compound overview; IR spectroscopy; X-ray diffraction; TGA plots of **6**, **8**, **11–13**, and **16**; DTA plots of **4b**, **5b**, and **6–17**; column diagrams of the complexes; hot plate and hot needle tests; laser ignition tests; UV-vis spectra of **6–14a** and **15–17**; experimental part and general methods. CCDC 1934798–1934813. For ESI and crystallographic data in CIF or other electronic format see DOI: 10.1039/c9nj03937f

Published on 28 October 2019. Downloaded by Ludwig Maximilians Universitaet Muenchen on 2/16/2022 8:04:02 AM.

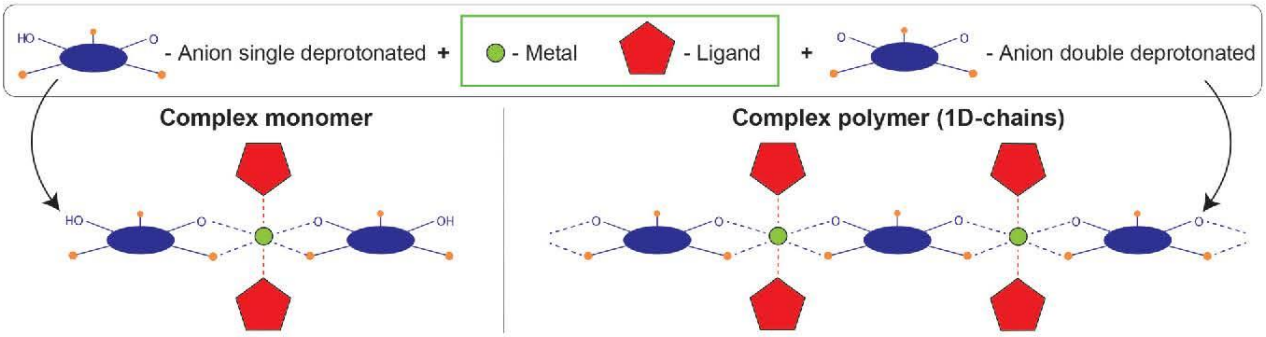


Fig. 1 Schematic overview of the formation of either complex monomers (left) or polymeric structures (right) caused by the deprotonation level of the nitroaromatic anions.

azide (LA), LS has been employed since the beginning of the 20th century and was originally developed as a replacement for mercury fulminate.[2,5] One major drawback of the highly acidic compounds **1**–**3** is their potential to corrode metal shells, along with the formation of the corresponding highly sensitive metal salts. This process significantly lowers the manageability of such explosives and is known to have caused fatal accidents.[6]

With LA and LS still being the most predominantly used primary explosives *e.g.*, in small arms ammunition, people in frequent contact with firearms and commercial applications (mining, deconstruction works, *etc.*) are at high risk of chronic damage due to heavy metal poisoning. A recent study revealed elevated blood lead levels in regular visitors of shooting ranges, accredited to the discharge of lead upon firing a gun. The adverse health effects associated with shooting are especially critical to women and children, relating to the impact on future generations.[7] In order to reduce or even prevent the use of toxic explosives, scientists all around the world are focusing on the development of new substances with superior properties.[8–15] One very promising concept for replacing toxic primary explosives which has gained increasing attention in recent years is focused on the laser ignition of energetic materials. By combining the right building blocks, this approach could ensure lifelong economic efficiency with environmentally friendly disposal management. At the same time, it can increase safety by allowing the application of less sensitive explosives.[16] 3D Metal coordination compounds with trinitrophenolates of **1**–**3** as counteranions are known in the literature for only a few tetrazole derivatives, especially TNPG-based anions are rather uncommon. Copper(II) complexes have a unique position among these described compounds since in every single example the anions coordinate to the central metal and thus in almost all cases anhydrous compounds are obtained. Especially, the nitroaromatic complexes based on Mn(II), Co(II), Ni(II) and Zn(II) have a high tendency to incorporate aqua ligands, crystal water molecules or even both of them.[17–23] Another characteristic of styphnic acid and trinitrophloroglucinol is their ability to work either as singly or multiply deprotonated anions and it has also been shown that within one ligand system both cases can be obtained. A great advantage of the twofold deprotonation of trinitrophenols is their potential to bridge different metal centres. In contrast, abstraction of a single proton usually leads to complex monomers (Fig. 1).[24]

The linking of the anions allows the formation of polymeric structures with varying properties such as increased thermal stabilities.

Recently, our research group published several of the most powerful ECC available, based on 1-amino-5*H*-tetrazole (1-AT) and 2-amino-5*H*-tetrazole (2-AT), in combination with highly oxidizing anions such as perchlorate and nitrate.[25] Some of the most auspicious of these candidates combine excellent energetic properties with good thermal stabilities and low environmental toxicities, however, the highly endothermic aminotetrazole ligands and oxidizing anions induce extreme sensitivities to various mechanical stimuli. This diminishes their applicability as primary explosives in classical, as well as optical initiation systems. To manage the excessive energetic capacities and sensitivities of 1-AT and 2-AT based ECC, we replaced the common anions nitrate and perchlorate with nitroaromatic mono- and dianions of **1**–**3**. Furthermore, an additional methyl group was introduced at the 5-position of the ligands (1-amino-5-methyltetrazole (1-AMT) and 2-amino-5-methyltetrazole (2-AMT)) to further stabilize the system by lowering the enthalpies of formation (Fig. 2).

This extensive study describes the effect of various *N*-amino-tetrazole ligands on nitroaromatic copper(II) complexes and

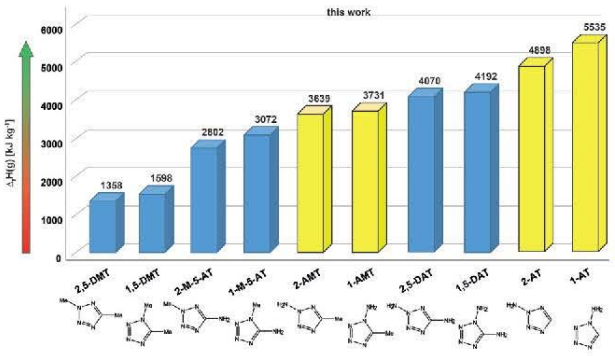


Fig. 2 Comparison of the calculated enthalpies of formation for several *N*-substituted monotetrazoles showing decreased values for AMT ligands compared to AT. Gas phase enthalpies of formation were calculated using the atomization method ($\Delta_f H^0_{(g,M)} = H_{(M)} - \sum H^0_{(A)} + \sum \Delta_f H^0_{(A)}$) using Gaussian09 computed CBS-4M electronic enthalpies.

 This journal is © The Royal Society of Chemistry and the Centre National de la Recherche Scientifique 2019

Published on 28 October 2019. Downloaded by Ludwig Maximilians Universitaet Muenchen on 2/16/2022 8:04:02 AM.

their selective potential to be used as either laser ignitable explosives or as classical lead-free primary explosives for the initiation of PETN (nitropenta). Furthermore, the influence of the level of deprotonation as well as the number of hydroxy groups in the anions towards the properties of the ECC is compared.

Results and discussion

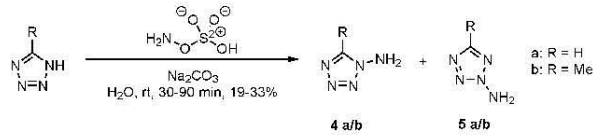
Synthesis

1-AMT (**4b**) and 2-AMT (**5b**) were prepared in accordance with the synthesis[25] of **4a** and **5a** *via* nucleophilic amination of commercially available 5-methyl-1*H*-tetrazole with hydroxylamine-*O*-sulfonic acid under basic conditions, giving the isomers **4b** and **5b** in 33% and 25% yield, respectively (Scheme 1). Due to the positive inductive effect of the additional methyl group, which increases the nucleophilicity of the electron-poor heterocycle, the overall yield of the reaction could be increased compared to the amination of unsubstituted tetrazole (58% *vs.* 46%).

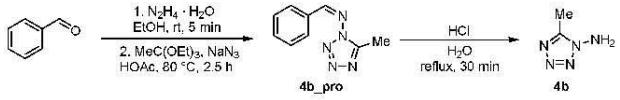
In analogy to **4a**, 1-AMT can be obtained directly and isomerically pure *via* a simple and scalable three-step reaction.[25] The synthesis is initiated by the condensation of benzaldehyde and hydrazine hydrate, followed by [3+1+1] cyclization with sodium azide and triethyl orthoacetate, which generates the 5-methyltetrazole-moiety (**4b_pro**). Cleavage under acidic conditions followed by water steam distillation furnishes the ligand **4b** in a relatively low yield of 18% (Scheme 2).

The isomers **4b** and **5b** can easily be differentiated by IR (Fig. S1, ESI‡) or by ^{1}H and ^{13}C NMR spectroscopy. Furthermore, proton coupled ^{15}N NMR measurements were performed for both compounds (Fig. 3 and 4).

The synthesis of ECC **6**–**17** starts with the *in situ* generation of the copper(II) salt of the required trinitrophenol, which is



Scheme 1 Synthesis of aminotetrazole ligands **4** and **5** by amination of 1*H*-tetrazole with hydroxylamine-*O*-sulfonic acid (HOSA).



Scheme 2 Selective synthesis of 1-amino-5-methyltetrazole (1-AMT, **4b**).

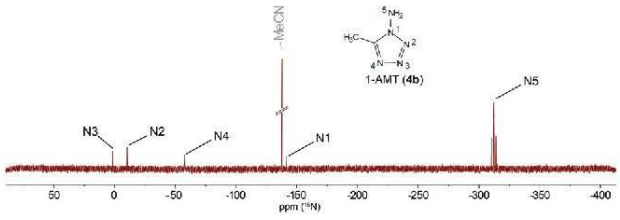


Fig. 3 Proton coupled ^{15}N NMR spectra of **4b**.

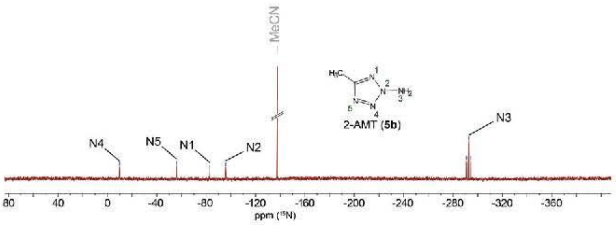
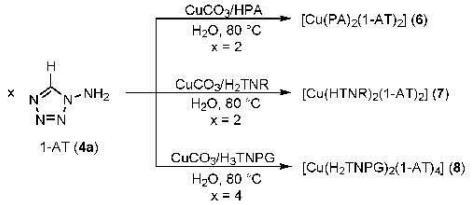


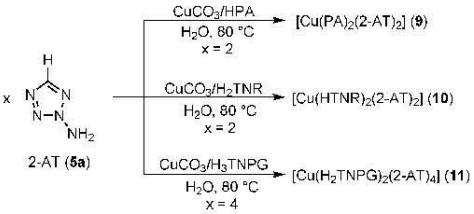
Fig. 4 Proton coupled ^{15}N NMR spectra of **5b**.

achieved by reaction of copper(II) carbonate with the respective acid **1**–**3** in aqueous medium at elevated temperatures. In the case of amino-5*H*-tetrazole derivates, each of the performed syntheses was carried out by slow addition of an aqueous solution of the ligand to the respective solution of metal(II) salt at 80 °C (Schemes 3 and 4). After continuous stirring of the particular reaction mixture, the solutions were left for crystallization at room temperature. After a few days, the compounds were filtered off, washed with ethanol and dried in air. This synthetic strategy can easily be performed on a large scale and the products can be isolated almost quantitatively if the solvent of the reaction mixture is removed by rotary evaporation.

Synthesis of the analogous AMT-based complexes **12**–**17** proceeded identically (Schemes 5 and 6), the only noteworthy divergence being the immediate precipitation of green and brown solids during the synthesis of compounds **13** and **14a**, respectively. Both compounds form polymeric structures that arise from the twofold deprotonation of the corresponding anions (**13**: styphnate, **14a**: 5-hydroxy-2,4,6-trinitroresorcinate) leading to bridging between different central metals, which significantly reduces their water solubility. All other isolated AMT-complexes were obtained after crystallisation from the mother liquor within a few days. After formation, the products were filtered off, washed with ethanol and dried in air. Even though final products **13** and **14a** are formed of only one

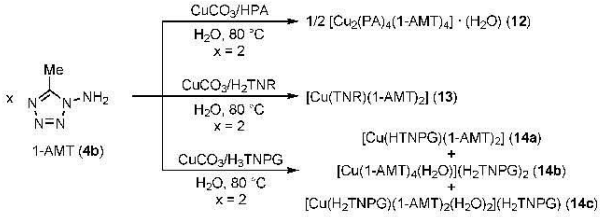


Scheme 3 Synthesis of copper(II) picrate, 3-hydroxy-2,4,6-trinitrophenolate and 3,5-dihydroxy-2,4,6-trinitrophenolate complexes **6**–**8** of 1-AT (**4a**).

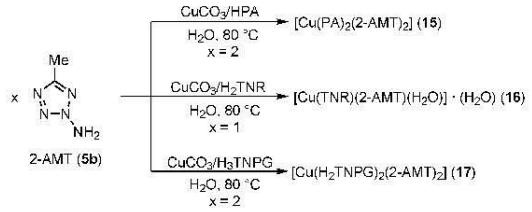


Scheme 4 Synthesis of the ECC **9**–**11** based on 2-amino-5*H*-tetrazole (2-AT, **5a**).

Published on 28 October 2019. Downloaded by Ludwig Maximilians Universitaet Muenchen on 2/16/2022 8:04:02 AM.



Scheme 5 Synthesis of copper(II) picrate (PA), styphnate (TNR) and 2,4,6-trinitrophloroglucol-based (HTNPG/H_2TNPG) complexes of 1-amino-5-methyltetrazole (1-AMT, **4b**).



Scheme 6 Synthesis of ECC **15–17** based on 2-amino-5-methyltetrazole (2-AMT, **5b**).

equivalent of the corresponding anions, for complete reaction of copper(II) carbonate twice the amount of free acid is required. Interestingly, the formation of a second (**14b**) and a third (**14c**) species during the reaction of copper(II) carbonate, trinitrophloroglucinol and 1-AMT was observed.

Single crystal experiments reveal the composition of two different aqua complexes $[Cu(1\text{-}AMT)_4(H_2O)](H_2TNPG)_2$ (**14b**) and $[Cu(H_2TNPG)(1\text{-}AMT)_2(H_2O)_2](H_2TNPG)$ (**14c**) with only singly deprotonated anions (3,5-dihydroxy-2,4,6-trinitrophenolate). The dark green needles of **14a** crystallised quickly from the filtrate and accumulated on the inner walls of the crystallisation vessel. Contrary to **14a**, however, **14b** turned out to be extremely water-soluble, which prevented the execution of further analytical investigation, because sufficient amounts could not be isolated. Similar to **14b**, **14c** is highly water soluble and some single crystals could only be obtained after complete desiccation of the filtrate of **14a**. To the best of our knowledge, **14b** and **14c** are the first copper(II) complexes with non-coordinating counteranions based on trinitrophenols of **1–3**.

Compared to the anhydrous compounds **6–11** it becomes clear that the AMT ligands slightly increase the hydrophilicity of the formed products and thus the formation of complexes with aqua ligands (**14b** and **14c**), crystal water molecules (**12**) or even both of them (**16**) can partly be observed.

Crystal structures

Nitrogen-rich ligand **4b** and its precursor **4b_pro**, as well as all ECC, were investigated by low-temperature single crystal X-ray diffraction. In contrast to their 1-amino isomers, 2-AT (**5a**) and 2-AMT (**5b**) were not able to be crystallised, even when subjected to liquid nitrogen. The crystal structure of ligand **4a** has already been published;[25] the results of the crystallographic analysis of **4b_pro** (Fig. S4, ESI‡) are given in the ESI,‡ together with the measurement and refinement data of all experiments (Tables S1–S4, ESI‡).

The crystal datasets were uploaded to the CSD database[26] and can be obtained free of charge with the CCDC 1934808 (**4_pro**), 1934810 (**4b**), 1934799 (**6**), 1934801 (**7**), 1934798 (**8**), 1934809 (**9**), 1934811 (**10**), 1934812 (**11**), 1934806 (**12**), 1934805 (**13**), 1934803 (**14a**), 1934807 (**14b**), 1934813 (**14c**), 1934800 (**15**), 1934802 (**16**), and 1934804 (**17**). All complexes, except side species **14b**, show octahedral coordination spheres around the copper(II) central cations with typical Jahn–Teller distortions along the axial O–Cu–O axes. In every structure, the ligands are solely coordinated through the N4 nitrogen atom of the tetrazole rings. In almost all compounds electrostatic intermolecular interactions can be observed, leading to specific orientations of the nitro groups of the phenolate anions. Normally the nitro groups of the trinitrophenols are aligned with the aromatic system, while nitro–nitro interactions between different anions twist one or two of the functional groups in the complexes. This perpendicular arrangement of nitro groups enables the electrostatic interaction of the vertical π-orbital with the oxygen atom of a second nitro group. The distances O_{Nitro}–π$(N)_{Nitro}$ in the crystal structures lie in the typical range of nitro–nitro interactions described in the literature.[27]

Similar to **4a**,[25] tetrazole **4b** crystallises in the orthorhombic space group $P2_12_12_1$ with four formula units per unit cell and a slightly lower calculated density of 1.420 g cm^{-3} at 143 K. This relatively significant difference in density arises from the presence of the methyl group in **4b**, preventing closer packing due to the increased steric hindrance (Fig. 5). It crystallises in the form of colourless blocks and all non-hydrogen atoms lie within a plane with torsion angles close to 0° (C1–N1–N2–N3 1.25(15)°, N5–N1–C1–C2 −2.2(2)°, and N2–N1–C1–N4 −1.13(16)°). The bond angles and lengths lie within the range of typical values for tetrazole compounds and differ only slightly from 1-AT.

Picrate compounds **6** (green platelets) and **12** (green blocks) crystallise in similar monoclinic space groups $P2_1/c$ and $P2_1/n$ with calculated densities of 1.952 g cm^{-3} and 1.786 g cm^{-3} at 143 K, respectively. The slightly distorted octahedral coordination spheres – **12** shows a stronger deviation than **6** – around the

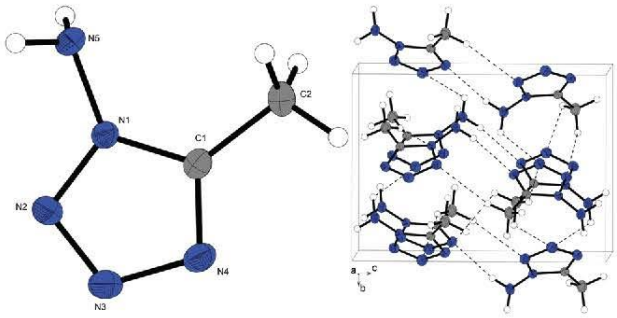


Fig. 5 Molecular unit (left) and unit cell (right) of 1-AMT (**4b**). Thermal ellipsoids of nonhydrogen atoms in all structures are set to the 50% probability level. Selected bond lengths (Å): N1–N2 1.3482(16), N1–N5 1.3908(17), N1–C1 1.3341(18), N2–N3 1.2959(19), N3–N4 1.3648(19), N4–C1 1.3206(19); selected bond angles (°): N2–N1–N5 123.54(11), N2–N1–C1 109.92(12), N5–N1–C1 126.53(12), N3–N4–C1 106.14(12), N4–C1–C2 127.78(13).

Published on 28 October 2019. Downloaded by Ludwig Maximilians Universitaet Muenchen on 2/16/2022 8:04:02 AM.

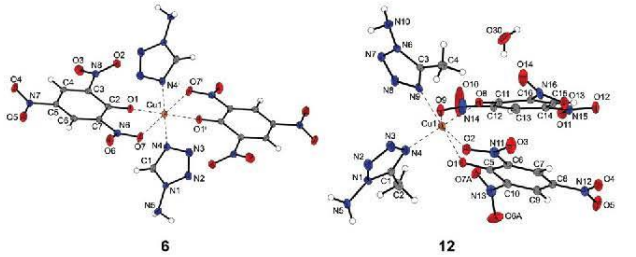


Fig. 6 Molecular unit of $[Cu(PA)_2(1\text{-}AT)_2]$ (**6**) (left) and segment of the unit cell of $[Cu_2(PA)_4(1\text{-}AMT)_4]\cdot H_2O$ (**12**) (right). Selected bond lengths (Å) of **6**: Cu1–O1 1.918(3), Cu1–O7 2.338(3), Cu1–N4 2.010(3); selected bond angles (°) of **6**: O1–Cu1–O7 78.92(10), O1–Cu1–N4 90.18(12), O7–Cu1–N4 86.01(11). Symmetry code of **6**: (i) $2 - x, -y, 2 - z$. Selected bond lengths (Å) of **12**: Cu1–O2 2.467(3), Cu1–O8 1.946(3), Cu1–N4 1.972(3), Cu1–N9 1.995(3); selected bond angles (°) of **12**: O1–Cu1–O2 74.07(11), O1–Cu1–N4 90.31(13), O1–Cu1–N9 171.19(13), N4–Cu1–N9 89.82(14).

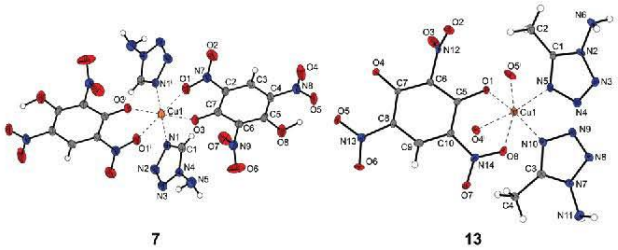


Fig. 7 Molecular unit of $[Cu(HTNR)_2(1\text{-}AT)_2]$ (**7**) (left) and the copper(II) coordination environment of $[Cu(TNR)(1\text{-}AMT)_2]$ (**13**) (right). Selected bond lengths (Å) of **7**: Cu1–O1 2.316(3), Cu1–O3 1.962(2), Cu1–N1 1.998(3); selected bond angles (°) of **7**: O1–Cu1–O3 81.17(10), O1–Cu1–N1 87.63(12), O3–Cu1–N1 90.00(11). Symmetry code of **7**: (i) $2 - x, 1 - y, 1 - z$. Selected bond lengths (Å) of **13**: Cu1–O1 1.958(5), Cu1–O8 2.515(6), Cu1–N5 1.994(6), Cu1–N10 2.010(6); selected bond angles (°) of **13**: O1–Cu1–O8 72.54(16), O1–Cu1–N5 86.0(2), O1–Cu1–N10 167.1(2), N5–Cu1–N10 94.7(2). Symmetry code of **13**: (i) $1 - x, 2 - y, 0.5 + z$.

copper(II) central cations in both crystal structures show similar compositions. The central metals are surrounded by two monodentate tetrazole ligands and two chelating picrate anions. $[Cu(PA)_2(1\text{-}AT)_2]$ (**6**) represents a centrosymmetric unit in itself with *trans* coordinating 1-AT ligands, while in $[Cu_2(PA)_4(1\text{-}AMT)_4]\cdot H_2O$ (**12**) the pairs of ligand molecules and picrate anions each occupy adjacent coordination sites (Fig. 6). The molecular unit of picrate **12** is a dimer consisting of two of the previously described asymmetric units and an additional crystal water molecule, where the coordinating picrate anions are facing each other in the centre of the unit and are twisted against each other at angles of approximately 90°.

Complexes **7** and **13**, based on 2,4,6-trinitroresorcinol, crystallise in the monoclinic and orthorhombic space groups $P2_1/c$ and $Pna2_1$ as green platelets and needles, respectively. Their calculated densities of 1.905 g cm^{-3} and 1.887 g cm^{-3} at 143 K vary only slightly. Except for the crystal water molecule, the compounds' chemical building blocks and the arrangement of those are comparable to those of the analogue picrate complexes **6** and **12**. ECC **7** forms complex monomers with a highly symmetrical structure, in which 1-AT and anionic 3-hydroxy-2,4,6-trinitrophenolate ligands oppose each other.

In fact, both coordinating molecules of 1-AT lie in the same plane and are aligned perfectly parallel, the singly deprotonated anions span two parallel planes. In 1-AMT-based compound **13** the pairs of ligand molecules and styphnate anions again occupy adjacent coordination sites (Fig. 7). The twofold deprotonation of styphnic acid in **13** leads to the formation of 1D-polymeric chains, in which each dianion bridges between two copper(II) centres. The monoanions existent in **7** are not suitable for linking between metal centres as they only possess a single coordination site, and thus two of them are required per formula unit.

Comparing the styphnate complexes **7** and **13** with the analogous trinitrophloroglucinol-based compounds, it becomes clear that the complexation of the central metal is different in the case of **8** and almost identical for **14a**. They crystallise in the monoclinic space group $P2_1/n$ (**8**) as green-yellow rods and orthorhombic space group $Pna2_1$ (**14a**) as brown needles with calculated densities of 1.928 g cm^{-3} (173 K) and 1.891 g cm^{-3} (143 K), respectively. The crystal structure of **8** is composed of four neutral 1-AT ligands and two 3,5-dihydroxy-2,4,6-trinitrophenolate monoanions around octahedrally coordinated copper(II) centres. The singly deprotonated anions are monodentate and are building up the Jahn–Teller distorted along the axial O1–Cu–O1^{i} axis (Fig. 8). All equatorial positions are occupied by tetrazole derivatives, which form hydrogen bonds with their amino function to nitro groups of the anions and tetrazole rings of neighbouring complex monomers. The primary species obtained from copper(II) carbonate, trinitrophloroglucinol and 1-AMT, $[Cu(HTNPG)(1\text{-}AMT)_2]$ (**14a**), crystallises isotypically to **13** with similar cell axes, density, and cell volume. Again, the double deprotonation leads to higher distortion and the formation of polymeric 1D chains. The coordination polymer is otherwise almost identical to **13**.

The side species **14b** and **14c** both crystallise as green rods in monoclinic space groups ($P2_1/c$ and $P2_1/n$) with calculated densities of 1.798 g cm^{-3} (143 K) and 1.948 g cm^{-3} (111 K), respectively. While **14b** shows a rare square pyramidal coordination sphere around the copper(II) centre, the coordination sphere of **14c** is a

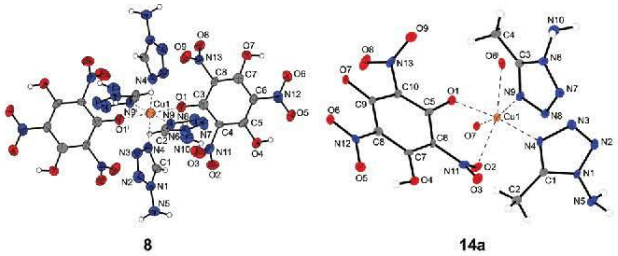
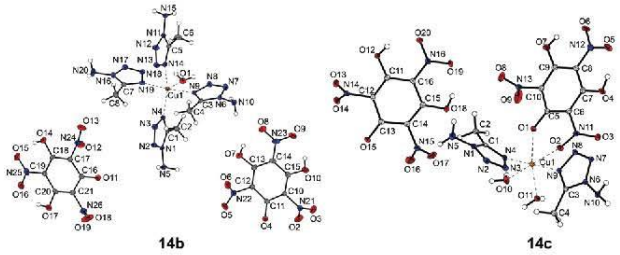


Fig. 8 Molecular unit of $[Cu(H_2TNPG)_2(1\text{-}AT)_4]$ (**8**) (left) and the copper(II) coordination environment of $[Cu(HTNPG)(1\text{-}AMT)_2]$ (**14a**) (right). Selected bond lengths (Å) of **8**: Cu1–O1 2.348(4), Cu1–N4 2.015(5), Cu1–N9 1.986(5); selected bond angles (°) of **8**: O1–Cu1–N4 87.64(17), O1–Cu1–N9 96.28(17), N4–Cu1–N9 91.1(2). Symmetry code of **8**: (i) $1 - x, 1 - y, 1 - z$. Selected bond lengths (Å) of **14a**: Cu1–O1 1.933(4), Cu1–O2 2.252(5), Cu1–N4 1.985(6), Cu1–N9 2.007(6); selected bond angles (°) of **14a**: O1–Cu1–O2 81.56(18), O1–Cu1–N4 171.7(2), O1–Cu1–N9 90.8(2), N4–Cu1–N9 95.5(2). Symmetry code of **14a**: (i) $1 - x, 1 - y, -0.5 + z$.

Published on 28 October 2019. Downloaded by Ludwig Maximilians Universitaet Muenchen on 2/16/2022 8:04:02 AM.

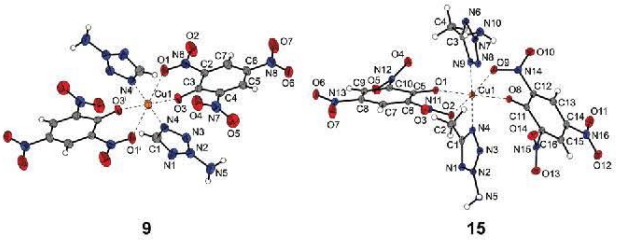


14b 14c

Fig. 9 Molecular units of side species $[Cu(1\text{-}AMT)_4(H_2O)](H_2TNPG)_2$ (**14b**) (left) and $[Cu(H_2TNPG)(1\text{-}AMT)_2(H_2O)_2](H_2TNPG)$ (**14c**) (right). Selected bond lengths (Å) of **14b**: Cu1–O1 2.230(3), Cu1–N4 2.000(3), Cu1–N9 2.005(3), Cu1–N14 1.997(3), Cu1–N19 1.997(3); selected bond angles (°) of **14b**: O1–Cu1–N4 103.93(12), O1–Cu1–N9 87.27(12), N4–Cu1–N9 92.78(12), N4–Cu1–N14 149.23(11), N4–Cu1–N19 92.08(12), N9–Cu1–N19 174.14(12). Selected bond lengths (Å) of **14c**: Cu1–O1 1.9934(15), Cu1–O11 2.0671(17), Cu1–N4 1.9784(16), Cu1–N9 1.9856(16); selected bond angles (°) of **14c**: O1–Cu1–O2 74.84(6), O1–Cu1–O10 107.90(6), O1–Cu1–O11 163.97(6), O1–Cu1–N4 88.60(7), O1–Cu1–N9 91.36(7), N4–Cu1–N9 179.38(7).

highly distorted octahedron. In contrast to **14a**, **14b** possesses non-coordinating anions and, similar to **8**, **11** and **17**, the TNPG-based monoanions are present as 3,5-dihydroxy-2,4,6-trinitrophenolates stacked on top of each other. They form hydrogen bonds to amino groups of neighbouring tetrazole ligands and typical nitro–nitro interactions between each other. The coordination sphere around the copper(II) central metal in **14b** is composed of one aqua and four ligand molecules of 1-AMT (Fig. 9). The water molecule represents the tip of the pyramid with a slightly longer Cu–O bond (2.230 Å) compared to the Cu–N bonds (1.997–2.005 Å). To minimise steric hindrance, pairs of opposing tetrazole ligands are arranged with the methyl groups facing in alternating directions and the two heterocycles are slightly angled, leading to a distorted plane of coordinating nitrogen atoms (N14–N4–N9–N19 23.7(1)°). The molecular unit of **14c** consists of one non-coordinating and one chelating monoanion, as well as two aqua and two tetrazole ligands. Interestingly, the Jahn–Teller distortion along the O2–Cu1–O10 axis shows one very long Cu–O bond (Cu1–O2 2.4665(14)), while the second is only slightly elongated (Cu1–O10 2.1604(16)).

Even though the coordination environments of the copper(II) centres of picrate complexes **9** and **15** are almost identical and show similar densities (**9**: 1.905 g cm^{-3} @ 173 K; **15**: 1.860 g cm^{-3} @ 143 K), they crystallise in fundamentally different space groups. $[Cu(PA)_2(2\text{-}AT)_2]$ (**9**) crystallises as green needles in the monoclinic $P2_1/c$ and $[Cu(PA)_2(2\text{-}AMT)_2]$ (**15**) as green blocks in the triclinic space group $P\bar{1}$. The equatorial positions are occupied by deprotonated hydroxyl groups and two *trans* coordinating aminotetrazole ligands. In the case of 2-AT based complex **9**, the two heterocycles are aligned anti-parallel, whereas, in complex **15**, the 2-AMT molecules are roughly mirrored in the equatorial plane. The axial positions are occupied by two nitro functions of the picrate anion (Fig. 10). Whereas **9**, similar to picrate complex **6**, shows highly symmetric coordination of the ligands, compound **15** possesses a greater deviation from the perfect octahedron. It is the only



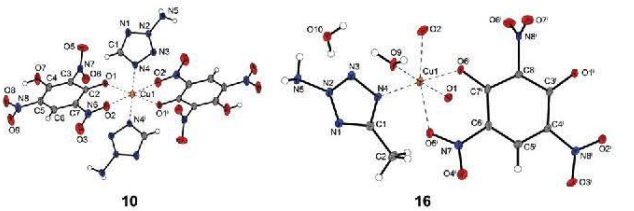
9 15

Fig. 10 Molecular unit of $[Cu(PA)_2(2\text{-}AT)_2]$ (**9**) (left) and $[Cu(PA)_2(2\text{-}AMT)_2]$ (**15**) (right). Selected bond lengths (Å) of **9**: Cu1–O1 2.321(2), Cu1–O3 1.941(2), Cu1–N4 1.982(3); selected bond angles (°) of **9**: O1–Cu1–O3 80.03(9), O1–Cu1–N4 87.69(10), O3–Cu1–N4 92.42(10). Symmetry code of **9**: (i) $-x, 1-y, 1-z$. Selected bond lengths (Å) of **15**: Cu1–O1 1.933(2), Cu1–O2 2.335(2), Cu1–N4 2.003(2); selected bond angles (°) of **15**: O1–Cu1–O2 80.73(8), O1–Cu1–N4 89.67(9), O2–Cu1–N4 88.15(9).

AMT-based compound with methyl groups pointing in the same direction, leading to higher steric hindrance (N4–Cu1–N9 172.08(10)°) and thus lower symmetry.

Styphnate compound **10** shows an almost identical composition to its 1-AT isomer **7** and crystallises in the triclinic space group $P\bar{1}$ with a calculated density of 1.864 g cm^{-3} at 173 K in the form of green blocks. Its 5-methyltetrazole analogue **16** crystallises as green rods in the monoclinic space group $P2_1/c$ with a calculated density of 1.949 g cm^{-3} at 143 K. The only similarity with its 1-AMT analogue **13** is the formation of polymer strands due to the twofold deprotonation of the anion. However, complex **16** only contains one neutral heterocycle and an additional aqua ligand, which are located *cis* to each other (Fig. 11). Also, a molecule of crystal water is present in **16**, which is fixed inside the structure by four hydrogen bonds.

3,5-Dihydroxy-2,4,6-trinitrophenolate complexes **11** and **17** both crystallise as green blocks in the triclinic space group $P\bar{1}$ with similar calculated densities of 1.909 g cm^{-3} (173 K) and 1.939 g cm^{-3} (143 K), respectively. Again, **11** shows an identically constructed coordination sphere to 1-AT isomer **8** with four 2-AT ligands in the equatorial plane and monodentate H_2TNPG monoanions in axial positions. Compared to **11**, the octahedron in complex **17** consists only of two tetrazole ligands, and once again



10 16

Fig. 11 Molecular unit of $[Cu(HTNR)_2(2\text{-}AT)_2]$ (**10**) (left) and extended molecular unit of $[Cu(TNR)(2\text{-}AMT)(H_2O)]\cdot H_2O$ (**16**) (right). Selected bond lengths (Å) of **10**: Cu1–O1 1.9410(12), Cu1–O2 2.3932(13), Cu1–N4 1.9858(14); selected bond angles (°) of **10**: O1–Cu1–O2 78.44(5), O1–Cu1–N4 88.72(6), O2–Cu1–N4 88.65(5). Symmetry code of **10**: (i) $-x, 2-y, -z$. Selected bond lengths (Å) of **16**: Cu1–O1 1.941(2), Cu1–O2 2.284(2), Cu1–O9 1.968(2), Cu1–N4 2.005(2); selected bond angles (°) of **16**: O1–Cu1–O2 82.20(8), O1–Cu1–O9 176.78(9), O1–Cu1–N4 90.48(8), O2–Cu1–N4 92.83(9), O9–Cu1–N4 92.70(10). Symmetry code of **16**: (i) $1-x, -0.5+y, 0.5-z$.

 This journal is © The Royal Society of Chemistry and the Centre National de la Recherche Scientifique 2019

Published on 28 October 2019. Downloaded by Ludwig Maximilians Universitaet Muenchen on 2/16/2022 8:04:02 AM.

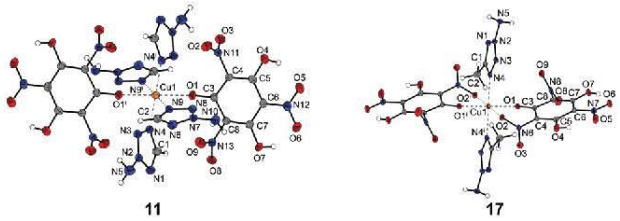


Fig. 12 Molecular unit of $[Cu(H_2TNPG)_2(2\text{-}AT)_4]$ (**11**) (left) and $[Cu(H_2TNPG)_2(2\text{-}AMT)_2]$ (**17**) (right). Selected bond lengths (Å) of **11**: Cu1–O1 2.3614(18), Cu1–N4 2.007(2), Cu1–N9 2.0101(19); selected bond angles (°) of **11**: O1–Cu1–N4 88.38(7), O1–Cu1–N9 95.38(7), N4–Cu1–N9 89.16(9). Symmetry code of **11**: (i) $1 - x, 1 - y, -z$. Selected bond lengths (Å) of **17**: Cu1–O1 1.9180(19), Cu1–O2 2.354(2), Cu1–N4 2.022(3); selected bond angles (°) of **17**: O1–Cu1–O2 81.50(9), O1–Cu1–N4 91.12(10), O2–Cu1–N4 92.03(10). Symmetry code of **17**: (i) $-x, 1 - y, -z$.

two H_2TNPG monoanions, which are in this case chelating (Fig. 12). The presence of the anions as 3,5-dihydroxy-2,4,6-trinitrophenolate (like in **8**, **11**, **14b**, and **14c**) is preventing the bridging between different copper(II) centres.

Sensitivities and thermal stability

Ligands **4b** and **5b**, as well as energetic complexes **6**–**17**, with the exception of side-products **14b** and **14c**, were subjected to differential thermal analysis (DTA) by heating at a constant rate of $\beta = 5$ °C min^{-1} in the temperature range of 25–400 °C. Critical points, such as dehydration, loss of a coordinating ligand or decomposition, are listed in Table 1 and are given as onset temperatures. The DTA plots can be found in the ESI‡ (Fig. S18–S30). All investigated compounds exhibit exothermic decomposition temperatures above 170 °C. Five of the examined ECC (**9**, **10**, **13**, **14a**, and **17**) even surpass a decomposition temperature of 200 °C. Styphnate **13**, the compound with the highest decomposition temperature of all investigated complexes (T_{exo} = 212 °C) derives its high thermal stability from its polymeric structure. A similar case can be observed in ECC **14a** (T_{exo} = 202 °C) with bridging trinitrophenolate anions. However, the relatively low decomposition temperature of the only other 2-AMT-based coordination polymer **16** (T_{exo} = 172 °C) can be explained by the presence of aqua ligands and crystal water molecules. The loss of both (T_{endo} = 122 °C and 160 °C) destabilises the crystal structure, leading to a lower exothermic decomposition temperature. Comparison of the 1-AMT complexes to those featuring 5*H*-tetrazole ligands reveals higher exothermic stabilities for the methyltetrazole based compounds. In the case of the 2-amino isomers, it is the other way round. The ECC based on 2-AT are thermally more stable than the analogous 2-AMT complexes. Apart from **16**, an endothermic peak is only observed in the DTA plot of **11** and is caused by the evaporation of coordinating 2-AT ligands. More detailed investigations using thermal gravimetric analysis (TGA) reveals the loss of two tetrazole derivatives (≙18.4%) starting at 135 °C (Fig. 13).

TGA measurements of ECC **6**, **8**, **11**–**13** and **16** clearly show the loss of water molecules in **12** and **16** and no significant mass loss in the other measured compounds, which proves their thermal stability up to the corresponding exothermic decomposition points (Fig. S17, ESI‡).

Due to the fact that the crystal morphology has a high effect on sensitivities as well as performance parameters (*e.g.*, a higher sensitivity against ESD with decreasing crystal size[30]), the compounds' grain size and habit were determined by light microscopy (Fig. S5 and S16, ESI‡). The sensitivities towards impact (IS) and friction (FS) of the compounds were determined according to BAM standard techniques (1 of 6) and they

Table 1 Data of thermal stability measurements by DTA,[a] as well as sensitivities towards various external stimuli and results of hot plate (HP) and hot needle (HN) experiments of **4a-5b** and **6–17**

	T_{endo}[b] (°C)	T_{exo}[c] (°C)	IS[d] (J)	FS[e] (N)	ESD[f] (mJ)	BDIS[g] (mJ)	HP[h]	HN[h]
1-AT (**4a**)	—	182[23]	<1[28]	64[28]	n.d.	n.d.	n.d.	n.d.
2-AT (**5a**)	—	197[23]	<1[28]	36[28]	n.d.	n.d.	n.d.	n.d.
1-AMT (**5b**)	—	190	>40	360	n.d.	n.d.	n.d.	n.d.
2-AMT (**5b**)	—	176	35	>360	n.d.	n.d.	n.d.	n.d.
$[Cu(PA)_2(1\text{-}AT)_2]$ (**6**)	—	178	4	120	50	207	def.	def.
$[Cu(HTNR)_2(1\text{-}AT)_2]$ (**7**)	—	186	1.5	48	16	14	def.	def.
$[Cu(H_2TNPG)_2(1\text{-}AT)_4]$ (**8**)	—	193	3.5	20	90	14	def.	def.
$[Cu(PA)_2(2\text{-}AT)_2]$ (**9**)	—	203	3	128	60	>207	def.	def.
$[Cu(HTNR)_2(2\text{-}AT)_2]$ (**10**)	—	206	3	48	20	55	def.	def.
$[Cu(H_2TNPG)_2(2\text{-}AT)_4]$ (**11**)	135	176	2	24	100	14	def.	def.
$[Cu_2(PA)_4(1\text{-}AMT)_4]\cdot H_2O$ (**12**)	—	190	2	168	88	>207	def.	def.
$[Cu(TNR)(1\text{-}AMT)_2]$ (**13**)	—	212	2	16	6.3	10	def.	def.
$[Cu(HTNPG)(1\text{-}AMT)_2]$ (**14a**)	—	202	1	7	4.9	8	def.	det.
$[Cu(PA)_2(2\text{-}AMT)_2]$ (**15**)	—	176	2.5	108	37	>207	def.	def.
$[Cu(TNR)(2\text{-}AMT)(H_2O)]\cdot H_2O$ (**16**)	122, 160	172	2.5	38	840	69	def.	def.
$[Cu(H_2TNPG)_2(2\text{-}AMT)_2]$ (**17**)	—	202	2	20	8.2	41	def.	def.
$Pb(N_3)_2$[29]		320–360	2.5–4.0	0.1–1.0	7.0	n.d.	det.	det.
PETN[29]	141–143	163–170	3.0–4.2	73	60	n.d.	def.	def.

[a] Onset temperatures at a heating rate of 5 °C min^{-1}. [b] Endothermic peak, which indicates melting, dehydration or loss of coordinating molecules. [c] Exothermic peak, which indicates decomposition. [d] Impact sensitivity according to the BAM drophammer (method 1 of 6). [e] Friction sensitivity according to the BAM friction tester (method 1 of 6). [f] Electrostatic discharge sensitivity (OZM Electric XSpark10) (method 1 of 6). [g] Ball drop impact sensitivity determined with method 1 of 6 in accordance with MIL-STD 1751A (method 1016). [h] def.: deflagration, det.: detonation, dec.: decomposition.

Published on 28 October 2019. Downloaded by Ludwig Maximilians Universitaet Muenchen on 2/16/2022 8:04:02 AM.

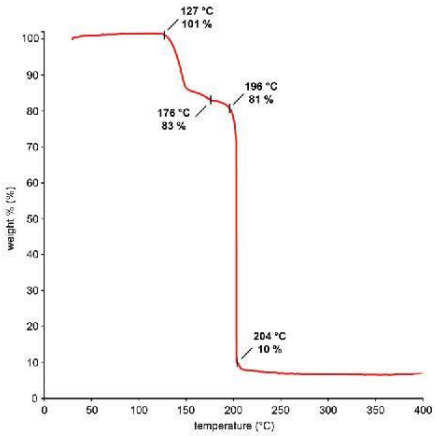


Fig. 13 TGA plot of **11** showing the loss of two aminotetrazole ligands starting at 127 °C followed by the decomposition of the compound.

have been classified in accordance with the "UN Recommendations on the Transport of Dangerous Goods".[31] Furthermore, the electrostatic discharge sensitivity (ESD) of all isolated ECC was analysed and all measurement data are summarised in Table 1. Comparing the free ligands, it becomes clear that the additional methyl group in 1-AMT and 2-AMT is drastically increasing the stability of the aminotetrazole derivatives against external stimuli. Concerning the impact sensitivity, all ECC show similar values against impact and except **6** and **8** ("sensitive") have to be classified as "very sensitive". In the case of FS, a clear trend is observable, revealing an increase of the sensitivity with the number of hydroxy groups of the anion (Fig. 14 and Fig. S31–S33, ESI‡), leading to the general trend: PA (all friction "sensitive") < TNR ("very sensitive") ≤ TNPG ("very sensitive" or even "extremely sensitive" (**14a**)). Due to the more realistic conditions during ball drop impact sensitivity (BDIS) measurements, ECC **6–17** were all tested and show a similar trend in comparison to the determined FS. This confirms our previous findings[22] that the sensitivity against ball drop impact shows a higher correlation with FS than with IS. Interestingly, ECC **13** and **14a**, based on a less sensitive ligand, both show the most sensitive values against external stimuli. The multiple deprotonations of nitroaromatic anions lead not only to higher thermal stability but also to increased sensitivities. This concept can be used for the synthesis and design of sensitive but thermally stable primary explosives for classical initiation devices.

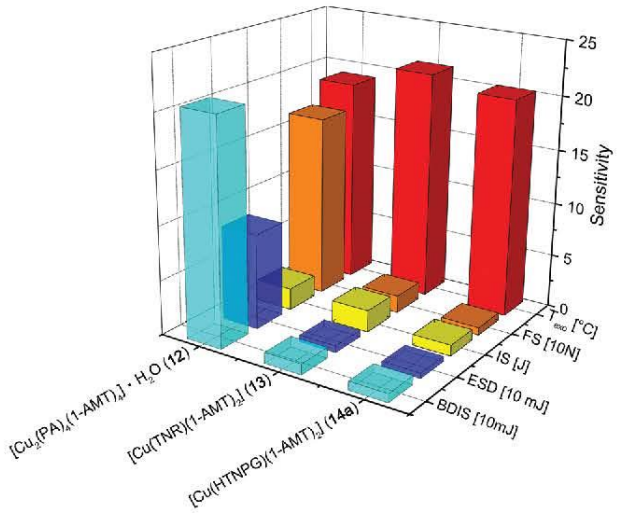


Fig. 14 Comparing the sensitivities against external stimuli of the ECC **12–14a**.

Primary explosive suitability evaluation

In order to get an insight into the compounds' behaviour against fast heating with and without confinement, hot plate (HP) and hot needle (HN) tests were performed with all ECC (Fig. 15 and Fig. S34–S47, ESI‡), except for side species **14b** and **14c**. The results are displayed in Table 1 and furthermore allow a preliminary evaluation of their applicability to be used for the initiation of energetic materials. The most promising compounds in these tests have been found to be the 1-AMT-based copper(II) styphnate (**13**) and 5-hydroxy-2,4,6-trinitroresorcinate (**14a**) complexes, which showed either sharp deflagrations or even detonations in this setup.

For their potential use as lead-free primary explosives, both compounds were tested towards their capability of initiating pentaerythritol tetranitrate (PETN). Therefore, 200 mg of the booster explosive was loaded into a copper shell and the test substance was filled on top (Fig. 16).

More details on the test setup can be found in the General methods of the ESI.‡ Positive transfer of the detonation wave from the primary explosive towards PETN is indicated by a hole in the copper witness plate and fragmentation of the shell. Both compounds were able to initiate nitropenta; whereas **13** worked in our standard setup with pressed PETN, **14a** was only successful in combination with uncompressed PETN (Fig. 16). Due to the known fact that unconfined PETN requires much lower energies than the compressed one,[30] **13** is the more powerful primary explosive compared to **14a**. Additionally, **13** shows a 10 °C higher thermal stability and is slightly less sensitive towards

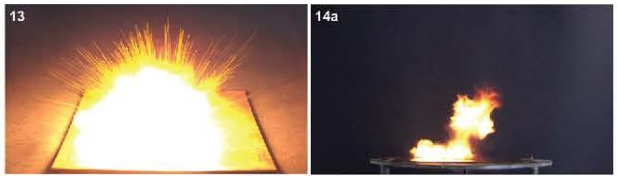


Fig. 15 Moments of deflagration of **13** (left) during hot needle and **14a** (right) during hot plate tests.



Fig. 16 Schematic setup of the PETN initiation capability test (left) as well as positive results of ECC **13** (middle) and **14a** (right).

 This journal is © The Royal Society of Chemistry and the Centre National de la Recherche Scientifique 2019

Published on 28 October 2019. Downloaded by Ludwig Maximilians Universitaet Muenchen on 2/16/2022 8:04:02 AM.

Table 2 Results of the laser initiation experiments[a]

E_{max} [mJ]	0.17	0.20	0.24	3.00	25.5	30.0	36.0
6	dec.	dec.	—	—	—	—	dec.
7	def.	—	—	—	det.	—	—
8	def.	—	—	def.	—	—	—
9	dec.	dec.	—	—	—	—	dec.
10	def.	def.	—	—	def.	—	—
11	def.	—	—	—	—	def.	det.
12	—	—	—	—	—	dec.	dec.
13	—	—	—	—	dec.	—	dec.
14a	neg.	—	dec.	—	—	dec.	—
15	—	dec.	—	—	—	—	dec.
16	—	—	—	dec.	—	dec.	—
17	dec.	dec.	—	—	—	—	—

[a] Not tested; neg.: no reaction; dec.: decomposition; def.: deflagration; det.: detonation. Operating parameters: voltage U = 4 V; wavelength λ = 915 nm; current I = 7–9 A; pulse length τ = 0.1–15 ms; theoretical maximal output power P_{max} = 45 W; theoretical energy E_{max} = 0.17–36.0 mJ.

all tested external stimuli (IS, FS, ESD, and BDIS) making its manageability safer.

Laser initiation experiments

The most tremendous benefits of laser initiation over classical ignition methods (thermal or mechanical) are the applicability of less sensitive compounds and the resulting lower risk of unintended ignition.[16] Therefore, this research area has gained increasing interest within the energetic material community and a lot of investigations were performed.[17,20,32–34] All complexes, except **14b** and **14c**, were irradiated with an InGaAs laser diode working in single-pulse mode. Details of the applied test setup can be found in the ESI.‡ All examined ECC showed a reaction towards the laser irradiation, differing in the intensity of the outcome (Table 2 and Fig. S48–S59, ESI‡). The most interesting compounds in this investigation are the ones showing both decreased impact and friction sensitivities ($\geq$3 J, $\geq$48 N), which are close to the values of PETN.[29]

These values pose slightly increased sensitivities towards mechanical stimuli but still allow safe handling of the material. Interestingly, all complexes based on AMT ligands solely exhibit decomposition or no reaction at all, regardless of the energy they are irradiated with. In the case of the aminotetrazole compounds, the picrates display the same outcome, whereas the HTNR- and H_2TNPG-based ECC deflagrate at lower energies or can even be detonated (**7** and **11**) when irradiated with higher values. Comparing the more sensitive compounds (**7**, **8**, **11**, **13**, **14a**, and **17**), it becomes clear that the most sensitive ones (**13**, **14a** and **17**) and also the most energetic ones in classical initiation tests (**13** and **14a**) show lower performance in this setup, which is not in accordance with our previous findings.[17,20,22]

UV-vis spectroscopy

UV-vis spectra in the solid state were recorded for the examined ECC **6–17**, except **14b** and **14c**, in the range of 350–1000 nm (Fig. S60–S63, ESI‡), to reveal any possible correlation between the absorption intensity and wavelength of the laser diode. The discovered optical properties of the complexes are summarised in Table 3. All ECC show characteristic transitions in the near infrared, visible and UV regions, as well as moderate to very strong absorption at a laser wavelength of 915 nm. The observed absorptions can mainly be assigned to the d–d transitions of the copper(II) centres. In accordance with previous investigations, the positive reaction towards laser irradiation could be explained by the imaginable formation of several hot spots within the compounds caused by photothermal excitation after irradiation.[16] Interestingly, there is no trend between the absorption intensity at the laser wavelength and the resulting outcome of the irradiation.

Table 3 Summary of the discovered optical properties of the examined ECC **6–17**

Compound	M	Colour	$\lambda_{d\ d}$[a]	$\lambda_{915}/\lambda_{d\ d}$[b]
6	Cu(II)	Green	405	0.45
7	Cu(II)	Green	410	0.65
8	Cu(II)	Green-yellow	356	0.35
9	Cu(II)	Green	424	0.43
10	Cu(II)	Green	412	0.52
11	Cu(II)	Green	437	0.56
12	Cu(II)	Green	431	0.64
13	Cu(II)	Green	459	0.57
14a	Cu(II)	Brown	409	0.53
15	Cu(II)	Green	426	0.68
16	Cu(II)	Green	610	0.97
17	Cu(II)	Green	388	0.40

[a] Absorption intensity maximum wavelength in the observed range of 350–1000 nm, which can be assigned to electron d–d transitions. [b] Quotient of the absorption intensity at the laser wavelength and the intensity at the d–d absorption wavelength.

Conclusions

In this extensive study, the nitrogen-rich ligands 1-amino- (**4a**, 1-AT) and 2-amino-5*H*-tetrazole (**5a**, 2-AT) as well as 1-amino- (**4b**, 1-AMT) and 2-amino-5-methyltetrazole (**5b**, 2-AMT) were successfully applied for the synthesis of new copper(II) complexes. It could be demonstrated that ligands **4b** and **5b** tend to form complexes with higher thermal stability and lower sensitivity. The crystal structures of 16 (12 main products, 2 side species, one ligand, and one precursor) compounds were elucidated by low-temperature single crystal X-ray diffraction and compared in detail. Especially the use of anions based on trinitrophloroglucinol offers a wide range of different complexes with various as well as interesting coordination modes. Furthermore, like styphnic acid, it allows the formation of polymeric structures through the multiple deprotonation of its hydroxy groups, which is accompanied by an increase in thermal stability. Interestingly, the ECC based on the more energetic and more sensitive AT-ligands show better stabilities against external stimuli, such as impact and friction, than the analogous compounds containing AMT derivatives. Whereas complexes **13** and **14a** were able to successfully initiate nitro-penta, **7**, **8**, **10**, and **11** show promising results during the laser ignition experiments. Due to their deflagrations at already 0.17 mJ they are interesting candidates for future laser ignition devices, while **13** and **14a** could be potential replacements for lead azide in classic initiation devices. The low performances of the AMT complexes when irradiated with NIR wavelengths

Published on 28 October 2019. Downloaded by Ludwig Maximilians Universitaet Muenchen on 2/16/2022 8:04:02 AM.

indicate that systems based on copper(II) and nitroaromatic anions with these are not very suitable for laser initiation or need substantially higher energies.

Conflicts of interest

There are no conflicts to declare.

Acknowledgements

Financial support of this work from the Ludwig-Maximilian University of Munich (LMU). The authors would like to thank Prof. Dr Thomas M. Klapötke for his scientific support as well as for providing his research facilities and, furthermore, Prof. Dr Konstantin Karaghiosoff for measuring the ^{15}N NMR spectra. Andreas Bartonek and Jasmin Lechner are given thanks for their great contribution to this work.

Notes and references

1 T. M. Klapötke, *Chemistry of High-Energy Materials*, De Gruyter, Berlin/Boston, 4th edn, 2017.
2 J. Akhavan, *The Chemistry of Explosives*, Royal Society of Chemistry, Cambridge, 2nd edn, 2004.
3 H. Sprengel, *The Discovery of Picric Acid (Melinite, Lyddite) "As a Powerful Explosive" and of Cumulative Detonation with its Bearing on wet Gun Cotton*, Eyre & Spottiswoode, London, 2nd edn, 1903.
4 H. Sprengel, *Br. Pat.*, #901, 1871.
5 J. S. Wallace, *Chemical Analysis of Firearms, Ammunition, and Gunshot Residue*, CRC Press, Boca Raton, 1st edn, 2008.
6 J. P. Agrawal and R. D. Hodgson, *Organic Chemistry of Explosives*, John Wiley & Sons, Hoboken, 1st edn, 2007.
7 M. A. S. Laidlaw, G. Filippelli, H. Mielke, B. Gulson and A. S. Ball, *Environ. Health*, 2017, **16**, 34.
8 R. V. Kent, T. P. Vaid, J. A. Boissonnault and A. J. Matzger, *Dalton Trans.*, 2019, **48**, 7509.
9 Y. Liu, G. Zhao, Y. Tang, J. Zhang, L. Hu, G. H. Imler, D. A. Parrish and J. M. Shreeve, *J. Mater. Chem. A*, 2019, **7**, 7875.
10 E. C. Johnson, E. J. Bukowski, J. J. Sabatini, R. C. Sausa, E. F. C. Byrd, M. A. Garner and D. E. Chavez, *ChemPlusChem*, 2019, **84**, 319.
11 Q. Sun, X. Li, Q. Lin and M. Lu, *J. Mater. Chem. A*, 2019, **7**, 4611.
12 A. A. Larin, N. V. Muravyev, A. N. Pivkina, K. Y. Suponitsky, I. V. Ananyev, D. V. Khakimov, L. L. Fershtat and N. N. Makhova, *Chem. – Eur. J.*, 2019, **25**, 4225.
13 R. Haiges and K. O. Christe, *Dalton Trans.*, 2015, **44**, 10166.
14 J.-G. Xu, X.-Z. Li, H.-F. Wu, F.-K. Zheng, J. Chen and G.-C. Guo, *Cryst. Growth Des.*, 2019, **19**, 3934.
15 J.-G. Xu, C. Sun, M.-J. Zhang, B.-W. Liu, X.-Z. Li, J. Lu, S.-H. Wang, F.-K. Zheng and G.-C. Guo, *Chem. Mater.*, 2017, **29**, 9725.
16 S. R. Ahmad and M. Cartwright, *Laser Ignition of Energetic Materials*, John Wiley & Sons, Ltd., Hoboken, 1st edn, 2015.
17 N. Szimhardt, M. H. H. Wurzenberger, A. Beringer, L. J. Daumann and J. Stierstorfer, *J. Mater. Chem. A*, 2017, **5**, 23753.
18 Y. Cui, T. L. Zhang, J. G. Zhang, L. Yang, J. Zhang and X. Hu, *Propellants, Explos., Pyrotech.*, 2008, **33**, 437.
19 Y. Cui, J. G. Zhang, T. L. Zhang, L. Yang, Y. Zhang and Y. J. Shu, *Chin. J. Chem.*, 2008, **26**, 2029.
20 N. Szimhardt, M. H. H. Wurzenberger, T. M. Klapötke, J. T. Lechner, H. Reichherzer, C. C. Unger and J. Stierstorfer, *J. Mater. Chem. A*, 2018, **6**, 6565.
21 Y. G. Bi, Y. A. Feng, Y. Li, B. D. Wu and T. L. Zhang, *J. Coord. Chem.*, 2015, **68**, 181.
22 M. H. H. Wurzenberger, M. S. Gruhne, M. Lommel, N. Szimhardt, T. M. Klapötke and J. Stierstorfer, *Chem. – Asian J.*, 2019, **14**, 2018.
23 Y. Cui, J. G. Zhang, T. L. Zhang, L. Yang, J. Zhang and X. Hu, *J. Hazard. Mater.*, 2008, **160**, 45.
24 N. Szimhardt, M. H. H. Wurzenberger, L. Zeisel, M. S. Gruhne, M. Lommel, T. M. Klapötke and J. Stierstorfer, *Chem. – Eur. J.*, 2019, **25**, 1963.
25 N. Szimhardt, M. H. H. Wurzenberger, L. Zeisel, M. S. Gruhne, M. Lommel and J. Stierstorfer, *J. Mater. Chem. A*, 2018, **6**, 16257.
26 Crystallographic data for the structures has been deposited with the Cambridge Crystallographic Data Centre. Copies of the data can be obtained free of charge on application to The Director, CCDC, 12 Union Road, Cambridge CB2 1EZ, UK {Fax: int.code_(1223)336-033; e-mail for inquiry: fileserv@ccdc.cam.ac.uk; e-mail for deposition: {deposit@ccdc.cam.ac.uk}.
27 M. Daszkiewicz, *CrystEngComm*, 2013, **15**, 10427.
28 T. M. Klapötke, D. G. Piercey and J. Stierstorfer, *Dalton Trans.*, 2012, **41**, 9451.
29 T. M. Klapötke, *Energetic Materials Encyclopedia*, 1st edn, De Gryter, Berlin/Boston, 2018.
30 R. Matyáš and J. Pachman, *Primary Explosives*, Springer, Berlin, 1st edn, 2013.
31 Impact: insensitive > 40 J, less sensitive ≥ 35 J, sensitive ≥ 4 J, very sensitive ≤ 3 J; friction: insensitive > 360 N, less sensitive = 360 N, sensitive < 360 N and > 80 N, very sensitive ≤ 80 N, extremely sensitive ≤ 10 N. According to the UN Recommendations on the Transport of Dangerous Goods.
32 D. E. Chavez, S. K. Hanson, R. J. Scharff, J. M. Veauthier and T. W. Myers, *US Pat.*, 20160031767A1, Triad National Security LLC, 2015.
33 S. I. Gerasimov, M. A. Ilyushin, I. V. Shugalei, A. V. Smirnov and Z. V. Kapitonenko, *Russ. J. Gen. Chem.*, 2017, **87**, 3156.
34 W. Guo, L. Wu, N. He, S. Chen, W. Zhang, R. Shen and Y. Ye, *Laser Part. Beams*, 2018, **36**, 29.

 This journal is © The Royal Society of Chemistry and the Centre National de la Recherche Scientifique 2019

Appendix 13

OZM Ball Drop Impact Tester (BIT-132) vs. BAM Standard Method-a Comparative Investigation

M. S. Gruhne, M. Lommel, M. H. H. Wurzenberger, N. Szimhardt, T. M. Klapötke, J. Stierstorfer

Propellants Explos. Pyrotech. **2020**, *45*, 147–153.

https://doi.org/10.1002/prep.201900286



Supplementary Information:
https://onlinelibrary.wiley.com/action/downloadSupplement?doi=10.1002%2Fprep.201900286&file=prep201900286-sup-0001-misc_information.pdf

Full Paper

Propellants, Explosives, Pyrotechnics

DOI: 10.1002/prep.201900286

OZM Ball Drop Impact Tester (BIT-132) vs. BAM Standard Method – a Comparative Investigation

Michael S. Gruhne,[a] Marcus Lommel,[a] Maximilian H. H. Wurzenberger,[a] Norbert Szimhardt,[a] Thomas M. Klapötke,*[a] and Jörg Stierstorfer*[a]

Abstract: Safety, performance, cost efficient synthesis and toxicity are the most important aspects of modern explosives. Sensitivity measurements are performed in accordance with different protocols all around the world. Sometimes the BAM drop hammer does not accurately reflect the sensitivity of an energetic material, in particular the sensitivity of primary explosives. Therefore, we present here preliminary results obtained using the novel ball drop tester (BIT-132), manufactured by OZM research, following MIL-STD-1751 A (method 1016). The ball drop impact sensitivity tester is a device in which a free-falling steel ball is dropped onto an unconfined sample, and is expected to produce more realistic results than the currently commonly used BAM method. The results obtained using the probit analysis were compared to those from the BAM drop hammer and friction tester. The following sensitive explosives were investigated: HMTD, TATP, TAT, Tetrazene, MTX-1, KDNBF, KDNP, K_2DNABT, Lead Styphnate Monohydrate, DBX-1, Nickel(II) Hydrazine Nitrate, Silver Acetylide, AgN_3, $Pb(N_3)_2$ RD-1333, AgCNO, and $Hg(CNO)_2$.

Keywords: Impact Sensitivity · Ball Drop · Primary Explosives · Safety · Probit Method

1 Introduction

In the field of applicable energetic materials chemistry, the safe handling of explosives is as important as a tailored performance or an economic synthesis. Nowadays, theoretical calculations based on quantum chemical models or structural relationships are possible and allow an estimation of the sensitivity of an energetic material toward mechanical or electrostatic stimuli [1].

Nevertheless, the experimental determination of sensitivities cannot be replaced by calculations, since many reliable calculations focus on a limited set of CHNO-based compounds and are based on empirical data. Unfortunately, sensitivity measurements are performed and evaluated using different methods all over the world, making comparisons of the sensitivity values difficult. The method for impact sensitivity testing which is recommended by the UN is the BAM (Bundesanstalt für Materialforschung und -prüfung) drop hammer, and has therefore become the most frequently used standard measuring method [2]. Besides its major advantages, some particular aspects must be taken into account when using the BAM drop hammer. The substance is placed between two steel cylinders enclosed by a steel guide, and a weight is dropped onto the steel cylinders from variable heights which may lead to an ignition. This ignition scenario facilitates the interpretation of the testing outcome, but it doesn't correspond to realistic conditions as the setup could cause hot spots during impact, leading to ignition [3]. An ignition could also be induced by adiabatic compression of the air trapped between the two cylinders [4].

An alternative method which can be used is the ball drop impact tester (BIT) in accordance with MIL-STD-1751 A, method 1016 [5]. Similar ball drop impact testing devices are mostly used in the US. In this method, a free-falling steel ball is dropped onto an unconfined layer of substance. This testing scenario takes more realistic circumstances into account, e.g. the slight spin of the ball when hitting the sample [6]. This enables an alternative, more realistic result, to be obtained which allows a simpler and more reliable ignition mechanism and therefore safer handling of energetic materials. The lack of uniformity of results, especially regarding ball drop impact sensitivities, (e.g. energy, force, height, etc.) and different evaluation procedures (E_{50}, no-fire-level, 1-out-of-10, etc.) are problems that urgently needed to be addressed. Consequently, an intensive study ap-

[a] *M. S. Gruhne, M. Lommel, M. H. H. Wurzenberger, N. Szimhardt, T. M. Klapötke, J. Stierstorfer*
Department of Chemistry
Ludwig-Maximilian University of Munich
Butenandtstr. 5–13, 8137 Munich (Germany)
**e-mail: tmk@cup.uni-muenchen.de*
jstch@cup.uni-muenchen.de
Homepage: http://www.hedm.cup.uni-muenchen.de

Supporting information for this article is available on the WWW under https://doi.org/10.1002/prep.201900286

© 2019 The Authors. Published by Wiley-VCH Verlag GmbH & Co. KGaA. This is an open access article under the terms of the Creative Commons Attribution Non-Commercial NoDerivs License, which permits use and distribution in any medium, provided the original work is properly cited, the use is non-commercial and no modifications or adaptations are made.

plying the BIT method to the most common sensitive energetic materials under uniform testing conditions was long overdue [7,8,9]. In order to obtain the largest possible data set, the probit method is used as the evaluation method of choice [10].

In this work, a variety of different sensitive energetic materials were chosen in order to compare the ball drop impact sensitivities. The selected primary explosives included a range of typical, commercially used ones such as tetrazene (**4a**, **4b**), KDNBF (**6**), lead styphnate monohydrate (LS, **9a**, **9b**), nickel(II) hydrazine nitrate (NHN, **11**), AgN_3 (SA, **13a**, **13b**), $Pb(N_3)_2$ RD-1333 (LA, **14**), AgCNO (SF, **15**)), and mercury fulminate (MF, **16**). In addition, several homemade explosives such as HMTD (**1**), TATP (**2**) and silver acetylide (**12**) were chosen, as well as a series of potential green primary explosives (TAT (**3**), MTX-1 (**5**), KDNP (**7**), K_2DNABT (**8**), and DBX-1 (**10**)).

2 Experimental Section

CAUTION! *All of the compounds which were investigated are potentially explosive energetic materials, which show increased sensitivities toward various stimuli (e.g. elevated temperatures, impact, friction or electrostatic discharge). Therefore, proper safety precautions (safety glasses, face shield, earthed equipment and shoes, leather jacket, Kevlar gloves, Kevlar sleeves and ear plugs) must be worn while synthesizing and handling these compounds.*

Each compound that was tested was synthesized on a 1.5–3 g batch size, depending on the sensitivity of the compound and its bulk density. This should guarantee that all measurements could be carried out from the same batch. The crystal shapes and sizes were established using light microscopy, and the results - together with the particle size distributions - are shown in Figures S16–17 and Table S17.

2.1 Synthesis of the Explosives

Common primary explosives were synthesized according to standard literature procedures. The organic peroxides **1** and **2** were prepared by the reaction of hexamine (**1**) or acetone (**2**) with hydrogen peroxide under acid catalysis [11,12]. Compound **3** was precipitated from a mixture of acetone and water by the reaction of cyanuric chloride and sodium azide [13]. Tetrazene (**4b**) was synthesized by dissolving aminoguanidine bicarbonate in acetic acid and further reaction with sodium nitrite [14]. Compound **5** was obtained by treating tetrazene with sodium nitrite [15]. Compound **6** was obtained using a two-step synthesis, in which picryl chloride was reacted with sodium azide and potassium carbonate [16]. The reaction of 3-bromo-2,4,6-trinitroanisole with potassium azide and diethyl carbonate resulted in compound **7** [17].

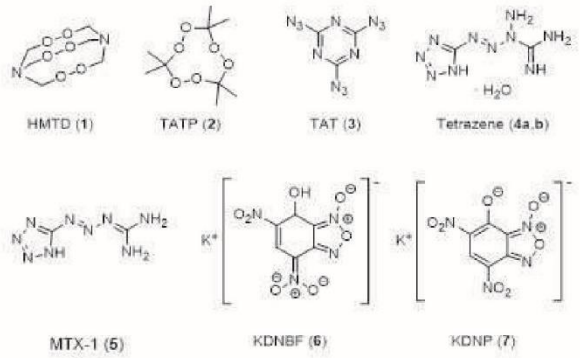


Chart 1. Prepared primary explosives **1**–**7**.

The 1,1′-Dinitramino-5,5′-bistetrazole salt **8** was prepared from hydrazine and diethyl carbonate according to WO 2018209366 A2 [18]. Dissolving an aqueous solution of styphnic acid in magnesium oxide and subsequent reaction with lead(II) nitrate yielded compound **9b** [19]. Compound **10** was obtained by conversion of sodium 5-nitrotetrazolate dihydrate into the copper(I) salt [20]. The nickel complex **11** was prepared by adding hydrazine hydrate to nickel nitrate [21]. Silver acetylide (**12**) was synthesized by passing acetylene through silver nitrate solution in aqueous ammonia [22]. Silver azide (**13b**) was synthesized by a simple metathesis reaction starting from sodium azide and silver nitrate [23]. The fulminate salts **15** and **16** were obtained by dissolving the respective metal in nitric acid and then pouring the reaction mixture onto ethanol [21,24].

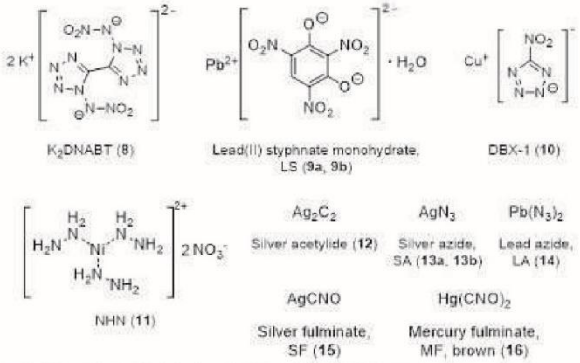


Chart 2. Synthesized primary explosives **8**–**16**.

Compounds **4a**, **9a**, **13a**, and **14** were provided by DynITEC GmbH Germany, whereas **4b**, **9b**, and **13b** were synthesized in the lab according to literature procedures.

2.2 Sensitivity Measurements

The ball drop experiments were carried out using the BIT-132 ball drop impact tester (OZM Research, Czech Republic) [25] following MIL-STD-1751 A (method 1016) [5]. A steel ball (0.50–2.00 inch, 8.35–534.70 g) is rolled of a steel guid-

 © 2019 The Authors. Published by Wiley-VCH Verlag GmbH & Co. KGaA

ance and dropped onto the explosive compound with a certain spin.

The sample layer was prepared as follows: The explosive compound was placed onto a steel target platform using a 30 mm^3 volumetric spoon. The sample was then spread out on the platform, resulting in a homogenous layer of 0.33 mm height (Figure 2). Steel balls with diameters of 0.50 inch (1.27 cm, 8.35 g) and 0.75 inch (1.91 cm, 28.20 g) were used. For every steel ball, a different steel ball guide was used to ensure a proper drop [26].



Figure 1. OZM BIT-132 (left side) and its release mechanism (right side).

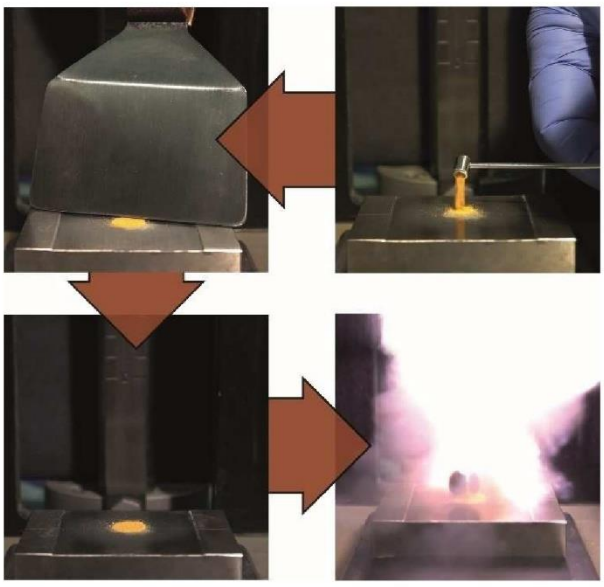


Figure 2. Stepwise sample preparation.

Any visual observation of decomposition was considered a positive result. After each trial, the remaining material was disposed of and the target block loaded with a freshly prepared layer. The steel balls were replaced for each substance. The impact energy was calculated from the product of the drop height, the mass of the steel ball used during the experiment and the gravitational constant. The initial drop height was chosen after several preliminary attempts, in which the height was determined at which the majority of the tests were positive. The probit analysis was used to evaluate the results [9]. The probability of ignition of each compound was determined using 6 test heights, with 10–15 trials at each height. The probabilities obtained were expressed as probits and the linear regression between probits and natural logarithms of the impact energy was performed. The sensitivity curve was obtained by backward transformation of the regression line into the probability-impact energy coordinates. Details of the 1 of 6 method that was used when a probit analysis wasn't possible, can be found in the general methods in the Supporting Information.

Additionally, the impact and friction sensitivities were determined according to the BAM (Bundesanstalt für Materialforschung) standard methods. The impact sensitivity tests were performed according to STANAG 4489 [27] with a modified instruction [28] using a BAM drop hammer [2]. Steel guide rings and steel cylinders for BAM drop hammers were obtained from OZM Research, Czech Republic [24]. The impact energy was calculated as explained above for the ball drop device. Friction sensitivity tests were performed according to STANAG 4487 [29] with a modified instruction [30] using a BAM friction tester [2]. Porcelain plates and pins were obtained from OZM Research, Czech Republic [24]. The friction force was calculated using the lever rule. The limiting values of the impact energy and friction force were determined in accordance with the method recommended by the UN for testing impact and friction sensitivities (1 of 6 method), according to ST/SG/AC.10/11/Rev.6 (s. 13.4.2.3.3) [31].

3 Results and Discussion

A key factor influencing the results was the type of steel ball used for each measurement. For compounds **4**, **5**, **11** and **16**, a smaller ball size at the same energy did not result in complete detonation or deflagration of the sample, and only a slight crackling was observed. This complicated the interpretation of a positive result by acoustic signals. It is assumed that the deflagration to detonation transition (DDT), shockwave sensitivity or critical diameter of each substance is an essential factor. This circumstance also influences any visual evaluation, since remaining substance does not necessarily indicate a negative test in every case.

The use of larger steel balls solves the problem, since the larger surface area of the bigger steel ball enables a larger amount of material to react, making evaluation clearer. However, larger steel balls tend to mask the sound of the detonating sample due to the louder impact noise. In addition, the use of the larger steel ball dusts the solid that would remain after a negative test, making visual evaluation nearly impossible.

Sensitivity measurements were carried out as described for each primary explosive. Standard deviations of the associated E_{50}, and $E_{16.6}$ values can be found in the supporting information (Table S1), together with plots of the results of each individual compound (Figure S1–15). In addition, detailed data on the results of each substance can be found in the Tables S2–S16.

In addition to primary explosives, some high explosives were also investigated. An evaluation with the probit method was not possible for any of these cases. In addition to the problems mentioned above with respect to the ignition of substances, a strong grain size dependence was observed. PETN, RDX and TKX-50 could be ignited only using the smallest grain sizes which were obtained after flash crystallization or sieving. Larger grain sizes showed lower impact sensitivities. In the case of FOX-7, no ignition was observed at all. Due to this behavior, we decided to investigate these substances in more detail in future work.

During the characterization of each metal azide (**13**, **14**), variations in the sensitivity were observed. A proper probit analysis leading to reliable sensitivity data was not possible. Extending the test setup, for example the number of test heights and the number of tests per selected height, is assumed to correct statistical variations in compounds **13** and **14**.

In the case of silver fulminate (**15**), no probit evaluation was possible because a no-fire-level could not be determined. The Ball Drop Impact Sensitivity (BDIS) of these compounds was determined using the 1 of 6 method.

The results of the sensitivity measurements are shown in Table 1 together with the sensitivity data determined using BAM standard methods. In order to compare the substances examined with probit analysis to those compounds for which it was not possible, the 16.6% ignition probability values of these substances were calculated. This corresponds approximately to the probability level represented by the 1 of 6 method.

The probit method was successfully used for the evaluation of the BDIS of compounds **1**–**12** and **16**. The respective E_{50}, and $E_{16.6}$ values together with the sensitivity values according to BAM, as well as the particle size distributions are compiled in Table 1.

The diagrams shown in Figures 3 and 5 and 6 are combined according to their respective slopes. Figures 3 and 4 show the curves with the highest gradients. Compound **4b** was placed in Figure 4 to give a better comparison of the influence of the manufacturing process and the particle size of tetrazene. The improvised explosive HMTD (**1**) is the most sensitive compound investigated by the probit method ($E_{16.6}$ = 4 mJ). It is assumed that silver fulminate is even more sensitive, since a probit-based analysis was not possible. The $E_{16.6}$ level is even closer to the lowest measurement limit (1 of 6 = ≤ 4 mJ).

Table 1. Sensitivity data of the compounds **1**–**16**.

Compound		Ball drop impact sensitivity (mJ) E_{50}	$E_{16.6}$	BAM friction sensitivity 1 of 6 (N)	BAM impact sensitivity 1 of 6 (J)	Particle size dist. (µm)
HMTD	(**1**)	6	4	0.3	1.5	50–200
TATP	(**2**)	18	13	0.4	≤ 1	< 30
TAT	(**3**)	27	21	0.3	≤ 1	50–300
Tetrazene STANAG 4170	(**4a**)	10	5	2.5 (> 7[c])	1.5 (> 1[c])	< 30
Tetrazene	(**4b**)	33	21	2.5	1.5	400–1000
MTX-1	(**5**)	14	10	2	2	< 30
KDNBF	(**6**)	19	13	2	1.5	< 30
KDNP	(**7**)	56	40	12	3	< 30
K_2DNABT	(**8**)	31	25	≤ 0.1	≤ 1	500–1500
LS STANAG 4170	(**9a**)	28	19	1 (> 0.5[c])	7 (1.75[c])	40–140
LS	(**9b**)	22	15	0.45	8	< 30
DBX-1	(**10**)	39	21	≤ 0.1	≤ 1	< 30
NHN	(**11**)	175	134	15	20	< 30
Silver acetylide	(**12**)	29	14	≤ 0.1	≤ 1	50–150
AgN_3 STANAG 4170	(**13a**)	n.d.[a]	29[b]	≤ 0.1 (≤ 0.1[c])	≤ 1 (> 2.25[c])	< 10
AgN_3	(**13b**)	n.d.[a]	29[b]	≤ 0.1	3	< 30
$Pb(N_3)_2$ RD-1333	(**14**)	n.d.[a]	37[b]	≤ 0.1 (≤ 0.1[c])	4 (> 1.75[c])	< 30–50
AgCNO	(**15**)	n.d.[a]	≤ 4	≤ 0.1[c]	5	100–200
$Hg(CNO)_2$, brown	(**16**)	21	16	2.5	2.5	50–300

[a] No probit analysis possible. [b] Determined by 1 of 6 method. [c] Sensitivity data according to supplier.

 © 2019 The Authors. Published by Wiley-VCH Verlag GmbH & Co. KGaA

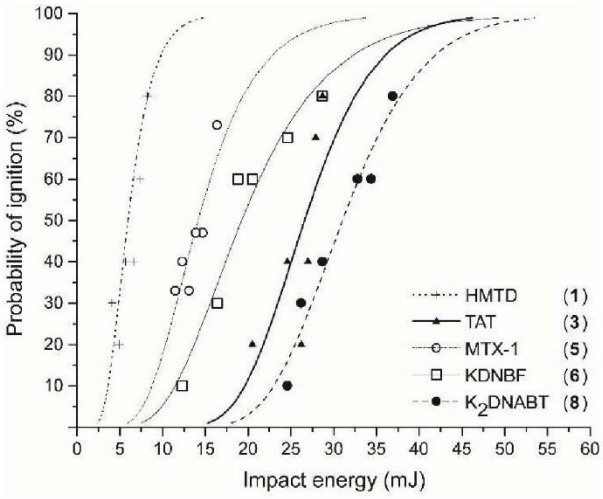


Figure 3. Probit curves of compounds **1**, **3**, **5**, **6**, and **8**.

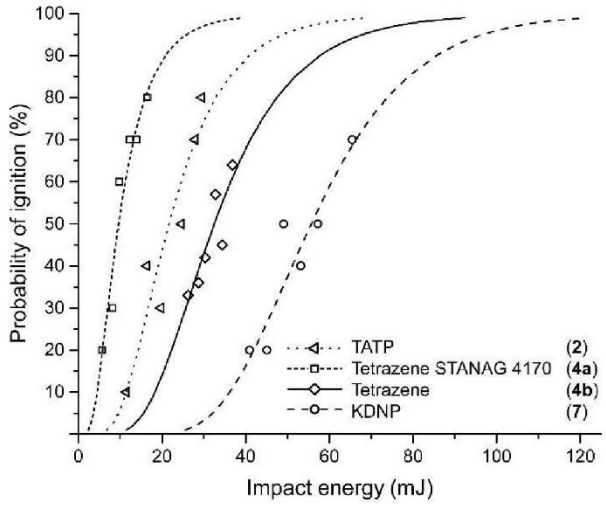


Figure 4. Probit curves of compounds **2**, **4a**, **4b**, and **7**.

However, this observation is only partly consistent with the sensitivity data according to BAM, as silver fulminate (**15**) has an unexpectedly high tolerance to impact (FS: 0.3 N (**1**), ☒ 0.1 N (**15**); IS: 1.5 J (**1**), 5 J (**15**)). Among the curves shown in Figure 3, K_2DNABT (**8**) has the highest $E_{16.6}$ value (25 mJ). This is in strong contrast to the extreme sensitivity data determined with the BAM standard methods (< 0.1 N, < 1J). The same applies to TAT (**3**), which has a similar $E_{16.6}$ value (21 mJ) at very low friction and impact sensitivities according to BAM (FS: 0.3 N, IS: ☒ 1J).

In case of tetrazene (**4**), larger crystals show the same sensitivity toward friction (**4a**: FS: 2.5 N vs. **4b**: FS: 2.5 N), while in the case of lead styphnate monohydrate (**9**) the trend indicated by the ball drop impact tester was confirmed for the friction sensitivity (**9a**: FS: 1 N, $E_{16.6}$: 19 mJ vs. **9b**: FS: 0.45 N, $E_{16.6}$: 15 mJ). Identical sensitivity data were observed for both types of silver azide (**13a**, **13b**). This observation fits with expectations since both compounds have approximately the same particle size, whereby the commercial product **13a** consists of agglomerates of smaller particles (Figure 7).

With regard to the measured data (Table 1), however, these grain sizes do not seem to have any influence on the sensitivity toward mechanical manipulation. Nickel(II) hydrazine nitrate (**11**) turned out to be the most insensitive compound according to BAM (FS: 15 N, IS: 20 J). The data determined using the ball drop impact tester in this case agrees with the $E_{16.6}$ of 134 mJ.

Regarding lead styphnate monohydrate (**9**) and the already mentioned silver fulminate (**15**), a significantly higher

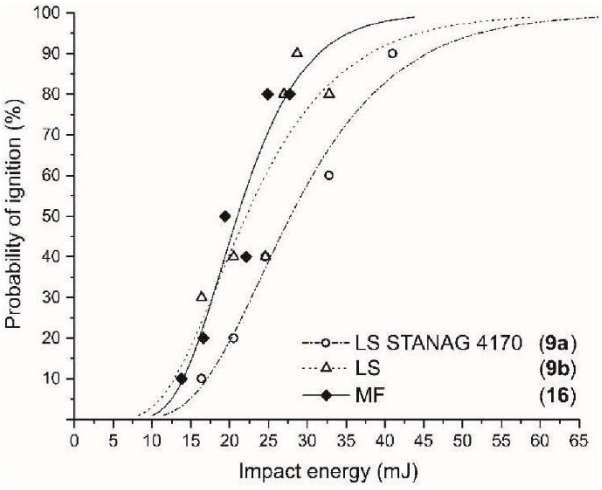


Figure 5. Probit curves of compounds **9a**, **9b**, and **16**.

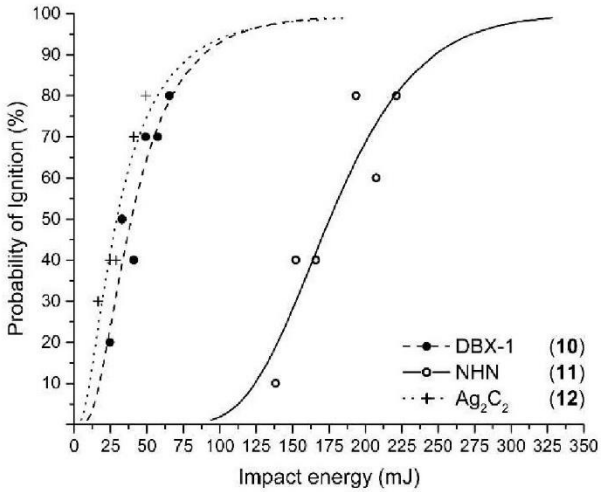


Figure 6. Probit curve determined for compounds **10**–**12**.

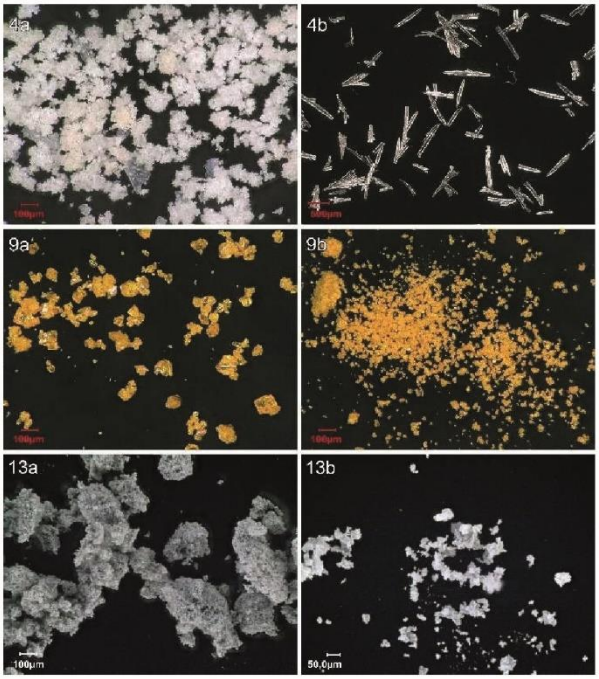


Figure 7. Different crystal shapes and particle size distributions of the compounds Tetrazene (**4**), Lead-styphnate Monohydrate (**9**), and Silver Azide (**13**).

discrepancy between the ball drop impact sensitivities and impact sensitivities according to BAM was observed (**9a**: $E_{16.6}$: 19 mJ, IS: 7 J; **9b**: $E_{16.6}$: 15 mJ, IS: 8 J). It is assumed that grain size effects play a major role here. In addition, a comparison with literature values again reveals the problem of comparing sensitivity values. According to *Köhler*, lead styphnate monohydrate possesses an impact sensitivity of 2.5–5 J [32, 33].

The United States Army Material Command reported an impact sensitivity of 3.4 J for the Picatinny Arsenal apparatus, as well as 0.17 J determined using the Bureau of Mines apparatus. [34] In both cases, no conclusions can be drawn about the measured particle size distribution, which is known to have a large influence on the results. Regarding the data by *Köhler*, no reference to the measuring instrument is given. This lack of a uniform specification of the measuring methodology also leaves open whether the results presented are E_{50}, no-fire or BAM 1 of 6 values.

A general relationship between both of the impact sensitivity testing methods was not found. It was generally observed that low BDIS values are accompanied by low friction sensitivity data. (Figure 8) The only significant exception was KDNP (**7**). At low BDIS values, KDNP (**7**) shows a lower sensitivity to friction, which is comparable to that of NHN (**11**) (**7**: $E_{16.6}$: 40 mJ, FS: 12 N; **11**: $E_{16.6}$: 134 mJ, FS: 15 N).

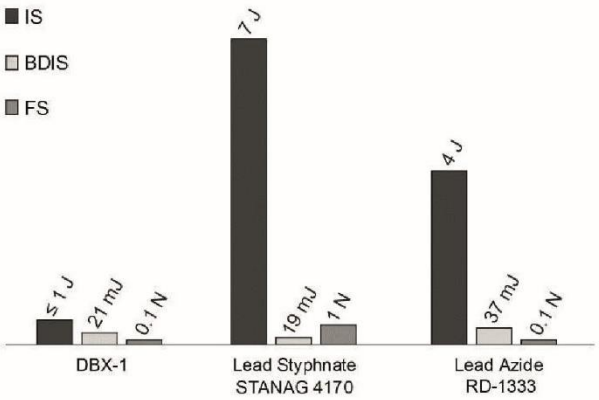


Figure 8. Comparison of the sensitivity data of compounds **9a** and **14**.

4 Conclusion

The BIT-132 Ball drop impact tester from OZM Research was used to evaluate the sensitivity of well-known, sensitive energetic materials. In addition, the BAM standard methods were used to determine sensitivities for all compounds. The sensitivity data obtained using the BIT-132 apparatus was evaluated using a probit analysis. In cases where this was not possible, the BAM 1 of 6 method was applied.

As shown by the examples of lead styphnate and lead azide, it is impossible to correlate the most recent BIT results with the data obtained using the BAM drop hammer (1 of 6). This is a result of the different test set-ups and therefore different ignition types. A closer correlation between the sensitivity to friction and ball drop impact sensitivity was observed. It is assumed that a combination of friction and impact is exerted on the substance by the spin of a falling steel ball.

Furthermore, it was found that there is a strong coherence between the particle size and the sensitivity towards BDIS of the compounds. Smaller particle sizes clearly showed more sensitivity, which is in strong contradiction to earlier assumptions that larger crystal sizes lead to drastically higher sensitivities. For the well-known explosives PETN, RDX, FOX-7 and TKX-50 o ignitions could be observed at certain grain sizes. So the current BIT has limited suitability for characterization of secondary explosives.

The authors would suggest the use of balls with a constant diameter and different densities. The 0.75 inch or the 1.00 inch ball, which were used in the set-up described in this work, are preferred for evaluating primary explosives.

Since most of the above problems do not apply to the testing of primary explosives, the device is perfectly suitable for testing primary explosives.

 © 2019 The Authors. Published by Wiley-VCH Verlag GmbH & Co. KGaA

Acknowledgements

Financial support of this work by the Ludwig-Maximilian University of Munich (LMU), and the Office of Naval Research (ONR) under grant no. ONR.N00014-16-1-2062 is gratefully acknowledged. The authors would like to thank OZM Research for the cooperation on the development of explosive equipment and testing devices. The authors would also like to thank Dr. Constantin Hoch for recording images with the microscope. In addition, the authors would like to thank Dr. Manuel Joas (DynITEC GmbH) for providingAgN_3 STANAG 4170, LS STANAG 4170, RD-1333 and Tetrazene STANAG 4170. We also would like to thank Dr. Davin Piercey and Mr. Maurus Völkl for their guidance during the synthesis of some of the primary explosives, as well as Maximilian Benz and Dr. Marc Bölter for the synthesis of several high explosives.

References

[1] M. H. Keshavarz, T. M. Klapötke, *The Properties of Energetic Materials, Sensitivity, Physical and Thermodynamic Properties*, 1st Ed., De Gruyter, Berlin, Boston, **2018**, pp 91–94.
[2] BAM, http://www.bam.de, (accessed August 2019).
[3] J. G. Reynolds, P. C. Hsu, G. A. Hust, S. A. Strout, H. K. Springer, Hot Spot Formation in Mock Materials in Impact Sensitivity Testing by Drop Hammer, *Propellants Explos. Pyrotech.* **2017**, *42*, 1303–1308.
[4] S. M. Walley, J. E. Field, R. A. Biers, W. G. Proud, D. M. Williamson, A. P. Jardine, The Use of Glass Anvils in Drop-Weight Studies of Energetic Materials, *Propellants Explos. Pyrotech.* **2015**, *40*, 351–365.
[5] United States Military Standard 1751 A (MIL-STD-1751 A), Safety and performance tests for qualification of explosives (high explosives, propellants and pyrotechnics), Method 1016, **2001**.
[6] B. D. Pollock, R. F. Gentner, *Impact Sensitivity of Wetted Primary Explosives as Determined by the Ball Drop Test*, Picatinny Arsenal, Dover, NJ, **1972**.
[7] N. Szimhardt, M. H. H. Wurzenberger, L. Zeisel, M. S. Gruhne, M. Lommel, T. M. Klapötke, J. Stierstorfer, 1-AminoTriazole Transition-Metal Complexes as Laser-Ignitable and Lead-Free Primary Explosives, *Chem. Eur. J.* **2018**, *24*, 1–13.
[8] N. Szimhardt, M. H. H. Wurzenberger, L. Zeisel, M. S. Gruhne, M. Lommel, J. Stierstorfer, Maximization of the energy capability level in transition metal complexes through application of 1-amino- and 2-amino-5*H*-tetrazole ligands, *J. Mater. Chem. A* **2018**, *6*, 16257–16272.
[9] a) M. H. H. Wurzenberger, M. S. Gruhne, M. Lommel, N. Szimhardt, T. M. Klapötke, J. Stierstorfer, Comparison of 1-Ethyl-5*H*-tetrazole and 1-Azidoethyl-5*H*-tetrazole as Ligands in Energetic Transition Metal Complexes, *Chem. Asian J.* **2019**, *14*, 2018–2028; b) N. Szimhardt, M. H. H. Wurzenberger, P. Spiess, T. M. Klapötke, J. Stierstorfer, Potassium *N*-Nitramino-5*H*-Tetrazolates-Powerful Green Primary Explosives with High Initiation Capabilities, *Propellants Explos. Pyrotech.* **2018**, *43*, 1203–1209.
[10] C. I. Bliss, The Method of Probits, *Science* **1934**, *79*, 38–39.
[11] W. P. Schaefer, J. T. Fourkas, B. G. Tiemann, Structure of Hexamethylene Triperoxide Diamine, *J. Am. Chem. Soc.* **1985**, *107*, 2461–2463.
[12] O. Reany, M. Kapon, M. Botoshansky, E. Keinan, Rich Polymorphism in Triacetone-Triperoxide, *Cryst. Growth Des.* **2001**, *9*, 3661–3670.
[13] E. Ott, E. Ohse, Zur Kenntnis einfacher Cyan- und Cyanurverbindungen. 11. Über das Cyanurtriazid, (C_3N_{12}), *Ber. Dtsch. Chem. Ges.* **1921**, *2*, 179–186.
[14] T. Urbański, *Chemistry and Technology of Explosives*, Vol. 3, Pergamon Press, Oxford, **1967**, p 206–209.
[15] J. W. Fronabarger, M. D. Williams, A. G. Stern, D. A. Parrish, MTX-1-A Potential Replacement for Tetrazene in Primers, *Cent. Eur. J. Energ. Mat.* **2016**, *13*, 33–52.
[16] Mehilal, A. K. Skider, S. Pawar, N. Skider, Synthesis, characterisation, thermal and explosive properties of 4,6-dinitrobenzofuroxan salts, *J. Hazard. Mater.* **2002**, *90*, 221–227.
[17] J. W. Fronabarger, M. D. Williams, W. B. Sanborn, D. A. Parrish, M. Bichay, KDNP-A Lead Free Replacement for Lead Styphnate, *Propellants Explos. Pyrotech.* **2011**, *36*, 459–470.
[18] E. L. Muller, T. M. Klapoetke, J. Stierstorfer, M. F. Boelter, M. Voelkl, *Explosive compound and method of manufacturing same*, WO Patent 2018209366 A2, DetNet South Africa (Pty.) Ltd., Modderfontein, South Africa **2018**.
[19] T. Urbański, *Chemistry and Technology of Explosives*, Vol. 3, Pergamon Press, Oxford, **1967**, pp 213–215.
[20] J. W. Fronabarger, M. D. Williams, W. B. Sanborn, J. G. Bragg, D. A. Parrish, M. Bichay, DBX-1-A Lead Free Replacement for Lead Azide, *Propellants Explos. Pyrotech.* **2011**, *36*, 541–550.
[21] S. G. Zhu, Y. C. Wu, W. Y. Zhang, J. G. Mu, Evaluation of a New Primary Explosive: Nickel Hydrazine Nitrate (NHN) complex, *Propellants Explos. Pyrotech.* **1997**, *22*, 317–320.
[22] R. Matyas, J. Selesovsky, T. Musil, Sensitivity to friction for primary explosives, *J. Hazard. Mater.* **2012**, *213–214*, 236–241.
[23] T. Urbański, *Chemistry and Technology of Explosives*, Vol. 3, Pergamon Press, Oxford, **1967**, pp 182–184.
[24] T. Pasinszki, M. Krebsz, B. Hajgato, Cycloaddition reactions of ICNO, *Chem. Phys. Lett.* **2009**, *473*, 343–347.
[25] OZM, http://www.ozm.cz, (accessed August 2019).
[26] OZM Research: Ball Drop Impact Test BIT-132, Instruction Manual, Rev. No. 1/17, **2017**.
[27] NATO standardization agreement (STANAG) on explosives, impact sensitivity tests, no. 4489, 1st ed., Sept. 17, **1999**.
[28] WIWEB-Standardarbeitsanweisung 4-5.1.02, Ermittlung der Explosionsgefährlichkeit, hier der Schlagempfindlichkeit mit dem Fallhammer, Nov. 8, **2002**.
[29] NATO standardization agreement (STANAG) on explosive, friction sensitivity tests, no. 4487, 1st ed., Aug. 22, **2002**.
[30] WIWEB-Standardarbeitsanweisung 4-5.1.03, Ermittlung der Explosionsgefährlichkeit oder der Reibeempfindlichkeit mit dem Reibeapparat, Nov. 8, **2002**.
[31] UN Model Regulation: Recommendations on the Transport of Dangerous Goods-Manual of Tests and Criteria, section 13.4.2.3.3, **2015**.
[32] T. M. Klapötke, *Energetic Materials Encyclopedia*, 1st Ed., De Gruyter, Berlin, Boston, **2018**, pp 278–279.
[33] R. Meyer, J. Köhler, A. Homburg, *Explosives*, 7th Ed., Wiley-VCH, Weinheim, **2016**, pp. 206–207.
[34] AMC Pamphlet Engineering Design Handbook: Explosive Series Properties of Explosives of Military Interest, Headquarters, U. S. Army Materiel Command, January **1971**.

Manuscript received: August 19, 2019
Revised manuscript received: September 3, 2019
Version of record online: October 30, 2019

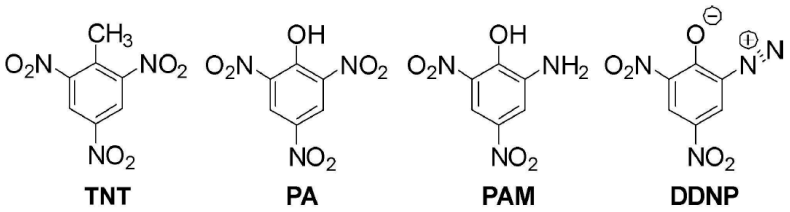
Appendix 14

Salts of Picramic Acid – Nearly forgotten temperature-resistant energetic materials

M. H. H. Wurzenberger, J. T. Lechner, M. Lommel, T. M. Klapötke, J. Stierstorfer

Propellants Explos. Pyrotech. **2020**, *45*, 898–907.

https://doi.org/10.1002/prep.201900402



Supporting Information:
https://onlinelibrary.wiley.com/action/downloadSupplement?doi=10.1002%2Fprep.201900402&file=prep201900402-sup-0001-misc_information.pdf

Full Paper

Propellants, Explosives, Pyrotechnics

DOI: 10.1002/prep.201900402

Salts of Picramic Acid – Nearly Forgotten Temperature-Resistant Energetic Materials

Maximilian H. H. Wurzenberger,[a] Jasmin T. Lechner,[a] Marcus Lommel,[a] Thomas M. Klapötke,[a] and Jörg Stierstorfer*[a]

Dedicated to Dr. Klaus Römer on the Occasion of his 80th Birthday

Abstract: Thermally stable explosives are becoming more and more important nowadays due to their important role in the oil and mining industry. The requirements of these explosives are constantly changing. Picramate-based compounds are poorly investigated towards their energetic properties as well as sensitivities. In this work, 13 different salts of picramic acid were synthesized as potential energetic materials with high thermal stability in a simple one-step reaction and compared with commercially used lead picramate. The obtained compounds were extensively characterized by e. g. XRD, IR, EA, DTA, and TGA. In addition, the sensitivities towards impact and friction were determined with the BAM drop hammer and the BAM friction tester. Also, the electrostatic discharge sensitivity was explored. Calculations of the energetic performance of selected compounds were carried out with the current version of EXPLO5 code. Therefore, heats of formation were computed and X-ray densities were converted to room temperature. Some of the synthesized salts show promising characteristics with high exothermic decomposition temperatures. Especially, the water-free rubidium, cesium, and barium salts **5**, **6** and **10** with decomposition temperatures of almost 300 °C could be promising candidates for future applications.

Keywords: Picramic Acid · Energetic Materials · Energetic Salts · Thermally Stable Explosives · Nitroaromatic Compounds

1 Introduction

The field of energetic materials is manifold and can be divided into several subgroups, such as propellants, primary or high explosives, which is leading to numerous and diverse applications [1–3]. Especially, due to the increased environmental awareness, there are many research groups around the world working on the development of ever more efficient molecules. The new compounds should, if possible, be less toxic and harmful to the environment than current molecules and at the same time also cheaper to produce [4–6]. Various strategies exist for designing new energetic materials, like increasing the energy of a molecule by ring or cage strain. Another approach is the synthesis of nitrogen-rich compounds, which release a lot of energy during their decomposition, due to their large endothermic heat of formation. The third strategy is the combination of fuel (carbon-backbone) and oxidizer (nitro groups) in one molecule. Various examples for this concept are displayed in Chart 1, with 2,4,6-trinitrotoluene (TNT) being the most favorite one, since it was the most commonly used explosive in World War I and is still used in explosive charges today [2, 7].

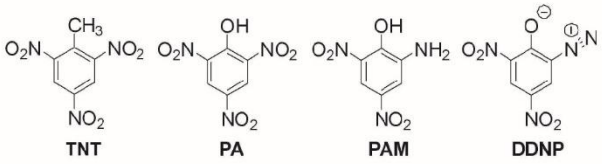


Chart 1. Chemical structures of 2,4,6-trinitrotoluene (TNT), 2,4,6-trinitrophenol (PA), 2-amino-4,6-dinitrophenol (PAM), and diazodinitrophenol (DDNP).

Another famous representative of this group is picric acid (PA), which replaced black powder at the end of the 19th century in military applications [8]. Later it was substituted by TNT itself because it caused undesired formations of very sensitive

[a] *M. H. H. Wurzenberger, J. T. Lechner, M. Lommel, T. M. Klapötke, J. Stierstorfer*
Department of Chemistry
Ludwig-Maximilian University of Munich
Butenandtstr. 5–13, 81377 Munich (Germany)
**e-mail: jstch@cup.uni-muenchen.de*
Homepage: http://www.hedm.cup.uni-muenchen.de

Supporting information for this article is available on the WWW under https://doi.org/10.1002/prep.201900402

© 2020 The Authors. Published by Wiley-VCH Verlag GmbH & Co. KGaA. This is an open access article under the terms of the Creative Commons Attribution License, which permits use, distribution and reproduction in any medium, provided the original work is properly cited.

metal salts in grenades and mines [2, 9]. A rather uncommon representative is 2-amino-4,6-dinitrophenol, also known as picramic acid (PAM), which can be obtained by partial reduction of PA with sodium hydrogen sulfide, ammonium sulfide or hydrazine. PAM is known for its explosive character but the neutral compound and the associated sodium salt are more familiar as ingredients for 'henné' color in hair and skin colorants [10–12]. Indeed, picramic acid and some of its soluble salts are more well-known as precursors for the synthesis of diazodinitrophenol (DDNP), an efficient heavy metal-free primary explosive [10, 13].

In 1961 Glowiak *et al.* demonstrated, based on lead picrate and lead picramate, that the replacement of a nitro group by an amino group leads to an increase in thermal stability with simultaneously reduced impact sensitivity [14]. This was also confirmed by J. P. Agrawal, who developed some approaches to increase the thermal stability of energetic molecules. He particularly emphasized the concepts 'salt formation' and 'introduction of amino groups' [1]. Agrawal *et al.* examined the energetic characteristics of iron(II), cobalt(II), nickel(II), copper(II), silver(I), zinc(II), cadmium(II), and mercury(I) picramate [15–17]. A few years later, Srivastava and Agrawal investigated titanium(IV), zirconium(IV) and thorium(IV) as well as palladium(IV) and uranium(IV) picramate [18, 19]. All metal picramates showed energetic properties but are only partly investigated, except lead picramate, which is the only salt used for industrial applications nowadays, especially in fuse head compositions of electric detonators [20, 21].

Accordingly, alkali and alkaline earth picramates, as well as ammonium picramate, could be promising thermally stable energetic compounds. In this work, these compounds were synthesized as well as their energetic properties studied and compared. A few already known salts were re-investigated in detail, due to the lack of analytical data in literature.

2 Experimental Section

Caution! *All investigated compounds are energetic materials and some of them show increased sensitivities towards various stimuli (e.g. elevated temperatures, impact, friction or electronic discharge). Although no hazards occurred, proper security precautions (safety glasses, face shield, earthed equipment and shoes, leather jacket, Kevlar sleeves, and earplugs) have to be worn while synthesizing and handling the described compounds.*

More information on the general methods and syntheses of compounds **2–15** can be found in the Supporting Information.

3 Results and Discussion

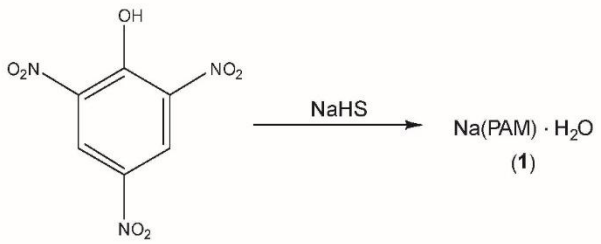
3.1 Synthesis

Sodium picramate monohydrate (**1**) was available in sufficient quantities in the research group and can be synthesized according to a literature procedure (Scheme 1) [22]. It was used as starting material to prepare picramic acid (**2**) (Scheme 2) by straightforward protonation with hydrochloric acid.

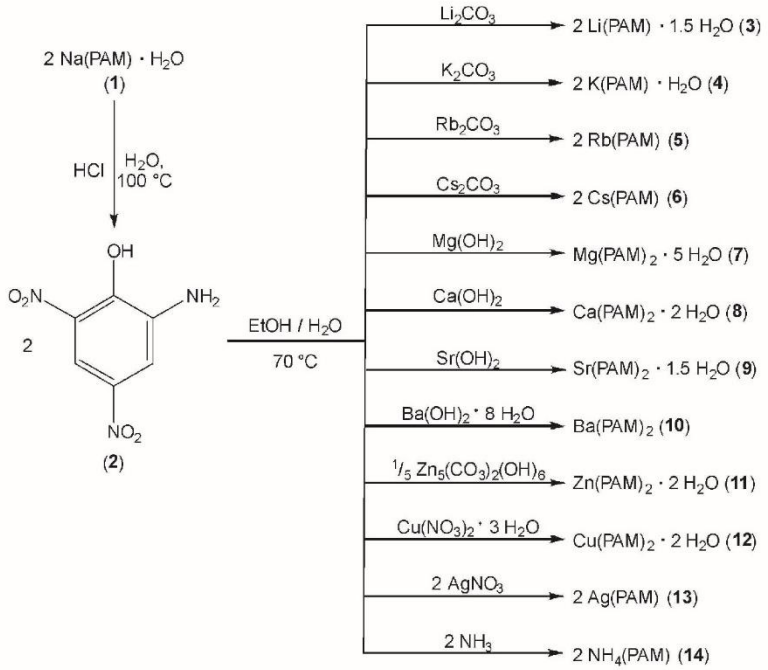
The isolated picramic acid (**2**) was further reacted in simple metathesis reactions to the corresponding salts **3–14**. It was dissolved in ethanol and a metal salt of the desired cation in water was added (Scheme 2), which led in all cases to a darkening of the solution. For a successful synthesis, an alkaline milieu had to be ensured during the whole reaction. For obtaining the alkali salts of picramic acid, the corresponding carbonates were used. Compounds **3–6** were filtered off after crystallization of sufficient amounts during evaporation of the solvent in air. For the syntheses of the alkaline earth salts **7–10** the corresponding metal hydroxides were used. Magnesium picramate (**7**) was obtained as pentahydrate in the form of single crystals suitable for X-ray diffraction experiments. The remaining alkaline earth salts could only be isolated as microcrystalline solids, due to their low solubility. For the synthesis of zinc(II) picramate (**11**), basic zinc(II) carbonate was used. The low solubility of $Zn(PAM)_2$ leads to the immediate precipitation of the product after mixing of the solutions. Similar circumstances were observed during the synthesis of silver(I) and copper(II) picramates (**12** and **13**), starting from the corresponding nitrate salts. Single crystals of **11** and **12** were obtained by layering aqueous solution of the nitrate salts with ethanolic solutions of HPAM to ensure slow formation at the phase boundary.

The yields can be increased by evaporation of the remaining mother liquor.

Ammonium picramate (**14**) was received by the addition of aqueous ammonia to the solution of picramic acid. After evaporation of the solvent, **14** was obtained as crystalline material. In case of lead picramate (**15**), the reaction of the free acid with a soluble lead salt did not lead to the formation of the desired product. Instead, sodium picramate



Scheme 1. Synthesis of sodium picramate (**1**, Na(PAM)).

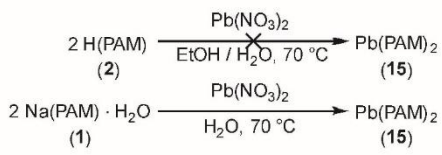


Scheme 2. Reaction scheme for the synthesis of the energetic salts **3**–**14**.

(**1**) was utilized as starting material (Scheme 3) leading to the direct precipitation of lead picramate.

3.2 Crystal Structures

Until today only the crystal structures of the free acid, as well as the potassium salt, were measured at room-temperature and published as private communications [23,24]. Therefore, low-temperature single-crystal X-ray diffraction experiments of compounds **1**–**7**, **10 b**, **11**, **12**, and **14** were performed. The crystal structures have been uploaded to the CSD database and are available under the CCDC numbers 1965957 (**1**), 1965965 (**2**), 1965964 (**3**), 1965963 (**4**), 1965958 (**5**), 1965966 (**6**), 1965967 (**7**), 1965960 (**10 b**), 1965962 (**11**), 1965959 (**12**), and 1965961 (**14**). Due to the very low solubility of pure barium picramate (**10**), it was only possible to obtain single crystals from saturated DMSO solutions. This led to the incorporation of both, DMSO and water solvent molecules (**10 b**). Details on the measurement and refinement data of all structures are given in the SI (Table S1–3).



Scheme 3. Reaction scheme for the preparation of lead picramate (**15**).

The neutral compound **2** crystallizes in the form of red blocks in the triclinic space group *P*-1 with a density of 1.730 g cm^{-3} (123 K) and four molecules per unit cell. The bond lengths are in the typical range of comparable compounds and all non-hydrogen atoms, except the oxygens of the nitro groups, are within one plane (Figure 1). Latter ones are only slightly twisted out of the benzol layer.

Compared to the parent compound **2**, the deprotonation and interaction with the cations in all other compounds are leading to a shortening of the C–O and elongation of the C–N bonds of the amino groups. The only exception is cesium salt **6** with a contraction of both bonds. The nitro groups in all structures show bonds with almost the same lengths and only vary in the level of twisting out of the benzol plane.

Except of **3** (*P*-1), all alkali salts are crystallizing in monoclinic space groups (**1**: *Pc*; **4**/**5**: $P2_1/c$; **6**: *C*2/*c*) with increasing densities (Li: 1.707 g cm^{-3} (121 K) < Na: 1.791 g cm^{-3} (127 K) < K: 1.837 g cm^{-3} (135 K) < Rb: 2.226 g cm^{-3} (122 K) < Cs: 2.526 g cm^{-3} (135 K)) in terms of atomic number. A similar trend can be observed in terms of the coordination sphere around the cations: Li: CN = 4/5, Na: CN = 6, K: CN = 9, Rb: CN = 9, Cs: CN = 12. This is also influencing the polymeric structures. While lithium compound **3** is building up dimers consisting of two asymmetric units, sodium, (**1**) as well as potassium (**4**) picramate, are forming 2D polymeric layers and the rubidium (**5**), as well as cesium (**6**) salt, consist as 3D networks.

 © 2020 The Authors. Published by Wiley-VCH Verlag GmbH & Co. KGaA

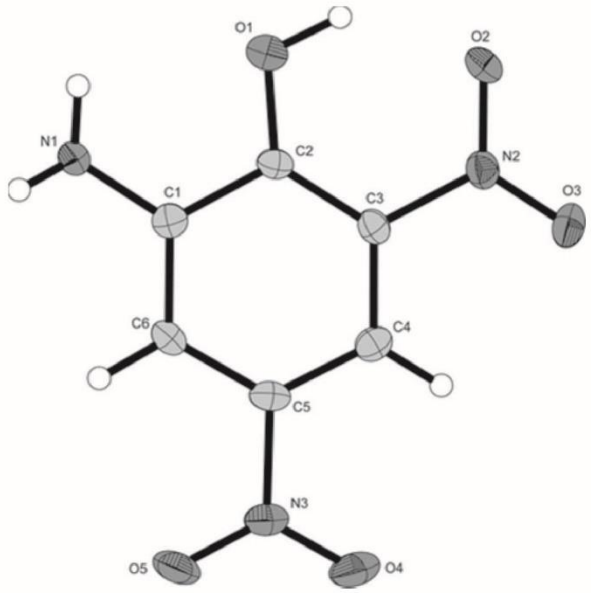


Figure 1. Molecular structure of **2**. Thermal ellipsoids of non-hydrogen atoms in all structures are set to the 50% probability level. Selected bond lengths (pm): C1–N1 135.5(2), C2–O1, 133.1(2), C3–N2 145.3(2), N2–O2 124.4(2), N2–O3 122.0(2), C5–N3 146.4(2), N3–O4 122.5(2), N3–O5 122.4(2), C1–C2 141.9(2), C2–C3 139.9(2), C3–C4 139.5(2), C4–C5 137.6(3), C5–C6 139.5(2), C6–C1 139.4(2).

The dimeric structure of **3** consists of two asymmetric units containing two different lithium ions (Figure 2). While Li1 shows a rather uncommon fivefold coordination by two chelating PAM anions and one additional aqua ligand, Li2 is tetrahedrally coordinated by one amino and one nitro group as well as two water molecules. Furthermore, the two inner anions each are bridging between three cations and the outer two are only coordinating to one lithium ion.

Similar to compound **3**, which crystallizes as sesquihydrate, sodium (**1**) and potassium (**4**) picramate are also present as mono- and sesquihydrate, respectively (Figure 3).

The only water-free alkaline salts are Rb(PAM) (**5**) and Cs(PAM) (**6**) (Figure 4). Magnesium picramate (**7**) crystallizes as pentahydrate in the form of brown rods in the monoclinic space group $P2_1/c$ with a density of 1.735 g cm^{-3} (109 K) and two molecules per unit cell. There are two different coordinated magnesium cations present, which are both octahedrally coordinated. Mg1 is chelated by two PAM anions and two monodentate aqua ligands, whereas Mg2 is solely bounded by aqua ligands. The unit cell is completed with two non-coordinating water molecules and picramate anions with a significantly twisted nitro group (Figure 5).

Recrystallization of water-insoluble $Ba(PAM)_2$ (**10**) from DMSO gave single crystals of **10b** and leads to the incorporation of water as well as solvent molecules. It crystallizes in the form of red rods in the monoclinic space group $P2_1/n$ and a density of 1.949 g cm^{-3} (127 K). The barium cation is elevenfold coordinated by two anions and one aqua as well as DMSO ligand. The molecular unit is completed by one crystal water molecule (Figure 6).

The zinc(II) (**11**) and copper(II) (**12**) salts of picramic acid crystallize isotypically in the triclinic space group *P*-1 with similar cell axes and volume as well as comparable densities. Both compounds show an octahedral coordination sphere around the central metal, whereas the two aqua ligands occupy the axial positions and two chelating anions are in equatorial positions (Figure 7). Furthermore, a typical Jahn-Teller distortion can be observed along the O6–Cu1–O6^{i} axis.

Ammonium picramate (**14**) crystallizes as anhydrous salt in the form of orange platelets in the monoclinic space group $P2_1/c$ with four molecules per unit cell (Figure 8). It possesses the lowest density (1.693 g cm^{-3}@104 K) of all compounds.

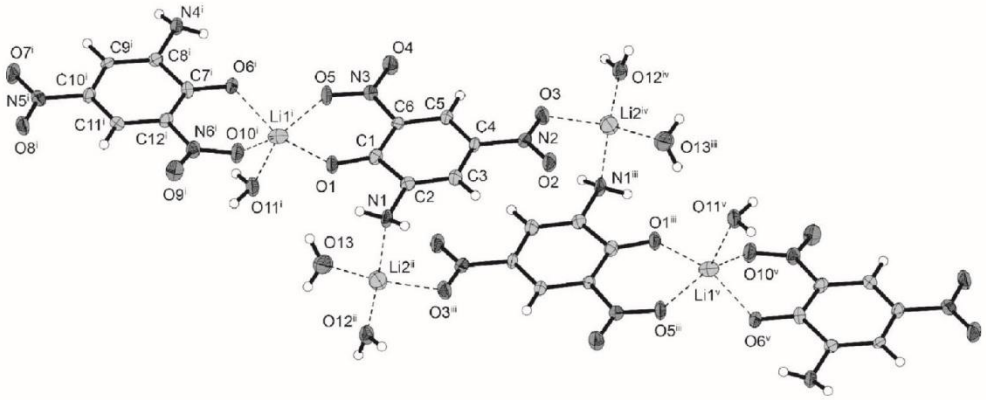


Figure 2. Dimeric structure of **3**. Selected bond lengths (pm): Li1^{i}–O1 190.4(8), Li1^{i}–O5 205.0(8), Li1^{i}–O6^{i} 196.5(8), Li1^{i}–O10^{i} 206.2(8), Li1^{i}–O11^{i} 202.7(9), Li2^{ii}–O3^{iii} 201.8(8), Li2^{ii} –O12^{ii} 184.8(9), Li2^{ii} –O13 190.3(9). Symmetry codes: i) 1−x, 1−y, −z; ii) x, −1 + y; iii) −x, −y, 1−z; iv) −x, 1−y, 1−z; v) −1 + x, −1 + y, 1 + z.

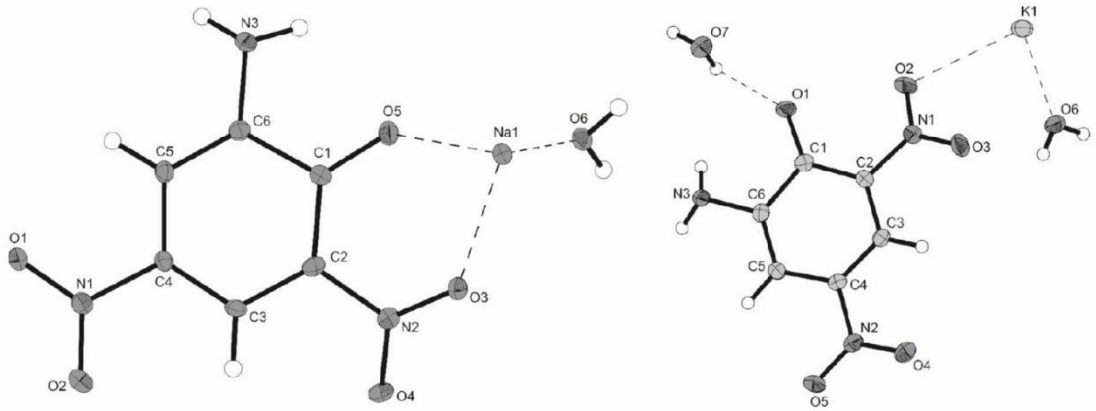


Figure 3. Molecular structure of **1** (left) and extended molecular structure of **4** (right). Selected bond lengths (pm) of **1**: Na1–O3 245.0(6), Na1–O5 232.5(6), Na1–O6 235.9(7). Selected bond lengths (pm) of **4**: K1–O2 281.33(15), K1–O3 295.71(16) K1–O6 273.64(16).

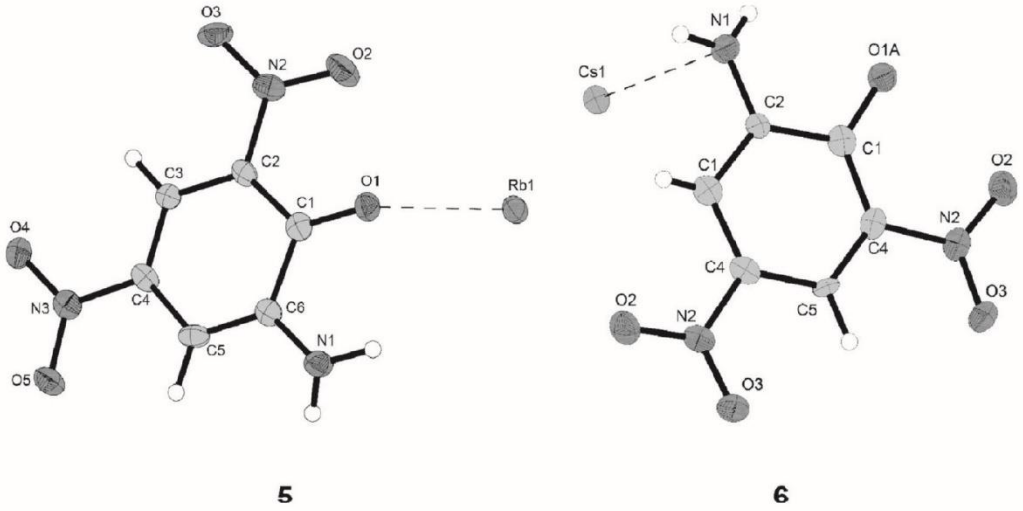


Figure 4. Molecular structure of **5** (left) and **6** (left). Selected bond length (pm) of **5**: Rb1–O1 280.3(3). Selected bond length (pm) of **6**: Cs1–N1 343.47(9).

3.3 Physiochemical Properties

The physicochemical properties of all compounds, except **10 b**, were investigated and therefore thermal stability measurements were performed as well as their sensitivities towards external stimuli were determined. Furthermore, calculations of the heat of formations of **2** and **14** were made using the EXPLO5 code.

Potassium picramate (**4**), which crystallizes as sesquihydrate, seems to lose half a crystal water molecule when stored at ambient conditions. Elemental analysis as well as thermogravimetric analyses only show the presence of one molecule of water.

3.3.1 Thermal Analysis

The exothermic decomposition temperatures determined via differential thermal analysis (DTA) are listed in Table 1 together with the obtained sensitivity values. The DTA measurements were performed with a linear heating rate of $\beta = 5\,^{\circ}C\,min^{-1}$ from 30 °C to 400 °C and critical events are given as onset temperatures. The plots of the measurements can be seen in Figure 9 and S5–7. Both sodium salt **1** and picramic acid (**2**) show an endothermic event at 174 and 175 °C, respectively. Whereas **1** first loses its crystal water and decomposes afterwards at 292 °C, the neutral compound **2** melts shortly before it shows an exothermic decomposition at 217 °C. In general, it can be seen that all

 © 2020 The Authors. Published by Wiley-VCH Verlag GmbH & Co. KGaA

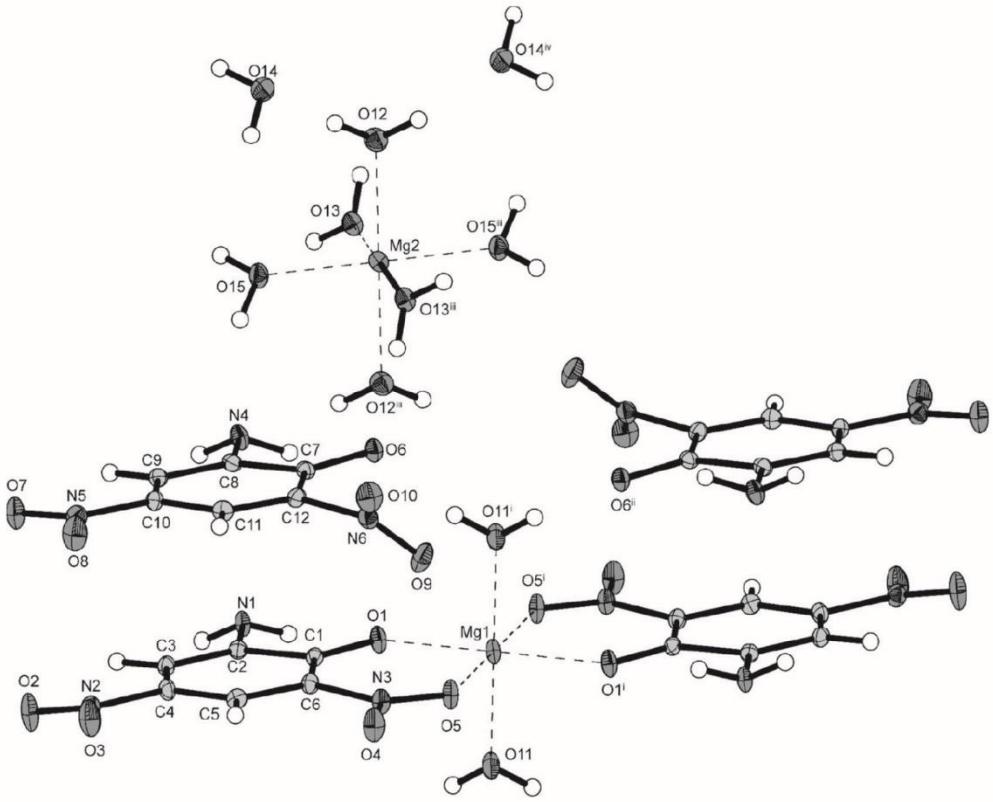


Figure 5. Molecular structure of **7**. Selected bond lengths (pm): Mg1–O1 197.29(13), Mg1–O5 210.23(13), Mg1–O11 202.39(15), Mg2–O12 205.88(14), Mg2–O13 207.10(14), Mg2–O15 205.93(13). Symmetry codes: i) 2−x, −y, −z; ii) 1−x, −y, −z; iii) 1−x, −y, 1−z; iv) −x, −y, −z.

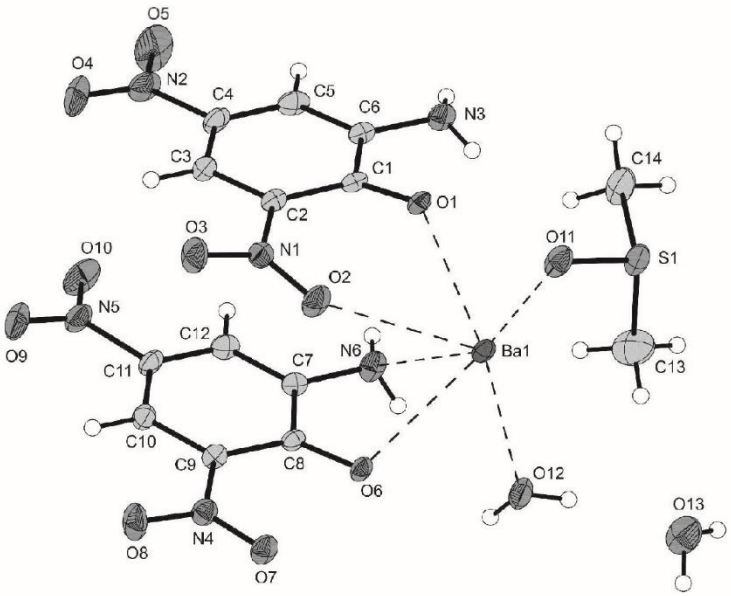


Figure 6. Molecular structure of **10b**. Selected bond lengths (pm): Ba1–O1 267.4(2), Ba1–O2 308.0(2), Ba1–O6 283.3(2), Ba1–O11 268.7(2), Ba1–O12 280.0(3), Ba1–N6 305.1(3).

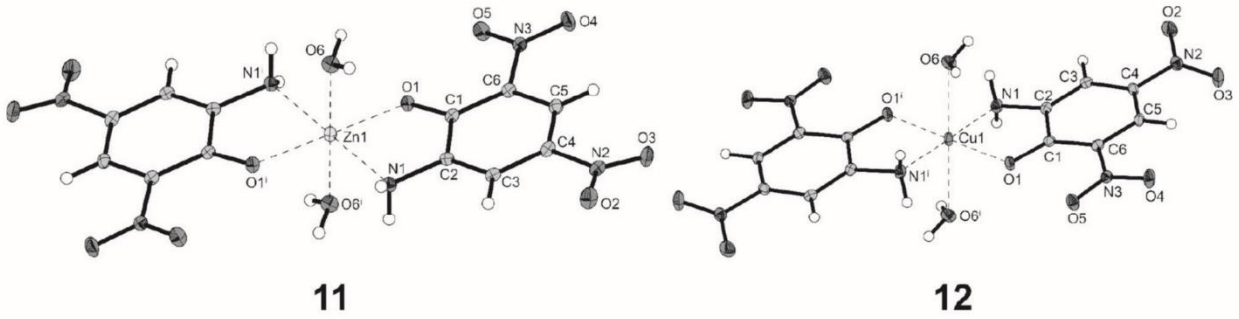


Figure 7. Molecular structures of **11** (left) and **12** (right). Selected bond lengths (pm) of **11**: Zn1–O1 207.15(16), Zn1–O6 218.70(18), Zn1–N1 211.7(2). Selected bond lengths (pm) of **12**: Cu1–O1 196.81(12), Cu1–O6 243.54(15), Cu1–N1 201.15(15). Symmetry code of **11**: 1−x, 2−y, 1−z. Symmetry code of **12**: 1−x, 1−y, −z.

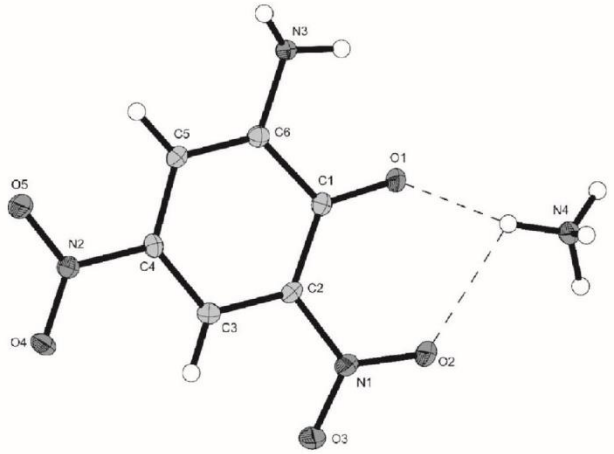


Figure 8. Molecular structure of **14**. Selected bond lengths (pm): C1–O1 126.97(17), C2–N1 144.30(18), N1–O2 123.06(17), N1–O3 123.36(17), C4–N2 143.23(18), N2–O4 123.41(15), N2–O5 124.85(16), C6–N3 139.77(18).

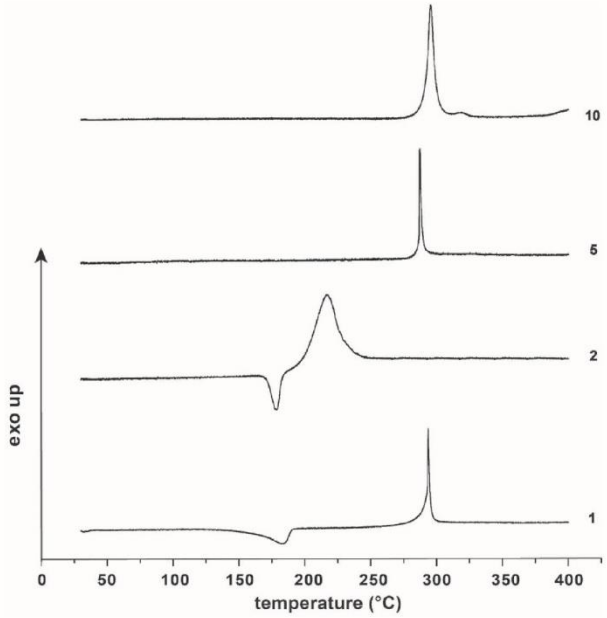


Figure 9. DTA plots of compounds **1**, **2**, **5**, and **10**.

exothermic decomposition temperatures, except the one of **13**, are all above 200 °C. Furthermore, the alkali, alkaline earth and zinc(II) picramates are even close to 300 °C, which makes those compounds to interesting energetic compounds for high-temperature applications.

The water containing compounds **3**, **7**, **8**, and **11** also show endothermic events between 79 and 223 °C, which can be matched to the loss of water. Interestingly, for the other hydrates (**4**, **9**, and **12**) no loss of water can be detected in the DTA measurements, indicating a too low sensibility of the device for minor endothermic events. Similar to picramic acid (**2**), the ammonium salt shows an endothermic event at 182 °C, that can be assigned to a melting, which was also observed during melting-point measurements. In the case of NH_4(PAM), it is directly followed by an exothermic decomposition at 209 °C (Figure S7). The relatively low thermal stability of silver picramate (**13**), is in accordance with observations made before, describing the constant decomposition starting above 120 °C [16].

Due to the difficulties in detecting the loss of water in some compounds and to further investigate the occurring endothermic events, thermogravimetric analyses (TGA) were performed. In the TGA measurements, it was heated with a heating rate of $\beta = 5\,°C\,min^{-1}$ from 30 °C to 400 °C.

In sodium picramate (**1**) the loss of 7.5 wt% can be clearly seen around 174 °C, which perfectly fits the mass of one crystal water molecule. The temperature is in accordance with the endothermic signal occurring in the DTA measurement. The same can be observed for compound **3** with a mass loss of 11 wt% at 105 °C conforming to the presence of a sesquihydrate. Due to the absence of crystal water molecules in **6** and **15**, loss of mass only can be seen at the corresponding decomposition points of the compounds (Figure 10). Similar trends can be observed for all other picramates (Figure S8–10). Special cases can be ob-

 © 2020 The Authors. Published by Wiley-VCH Verlag GmbH & Co. KGaA

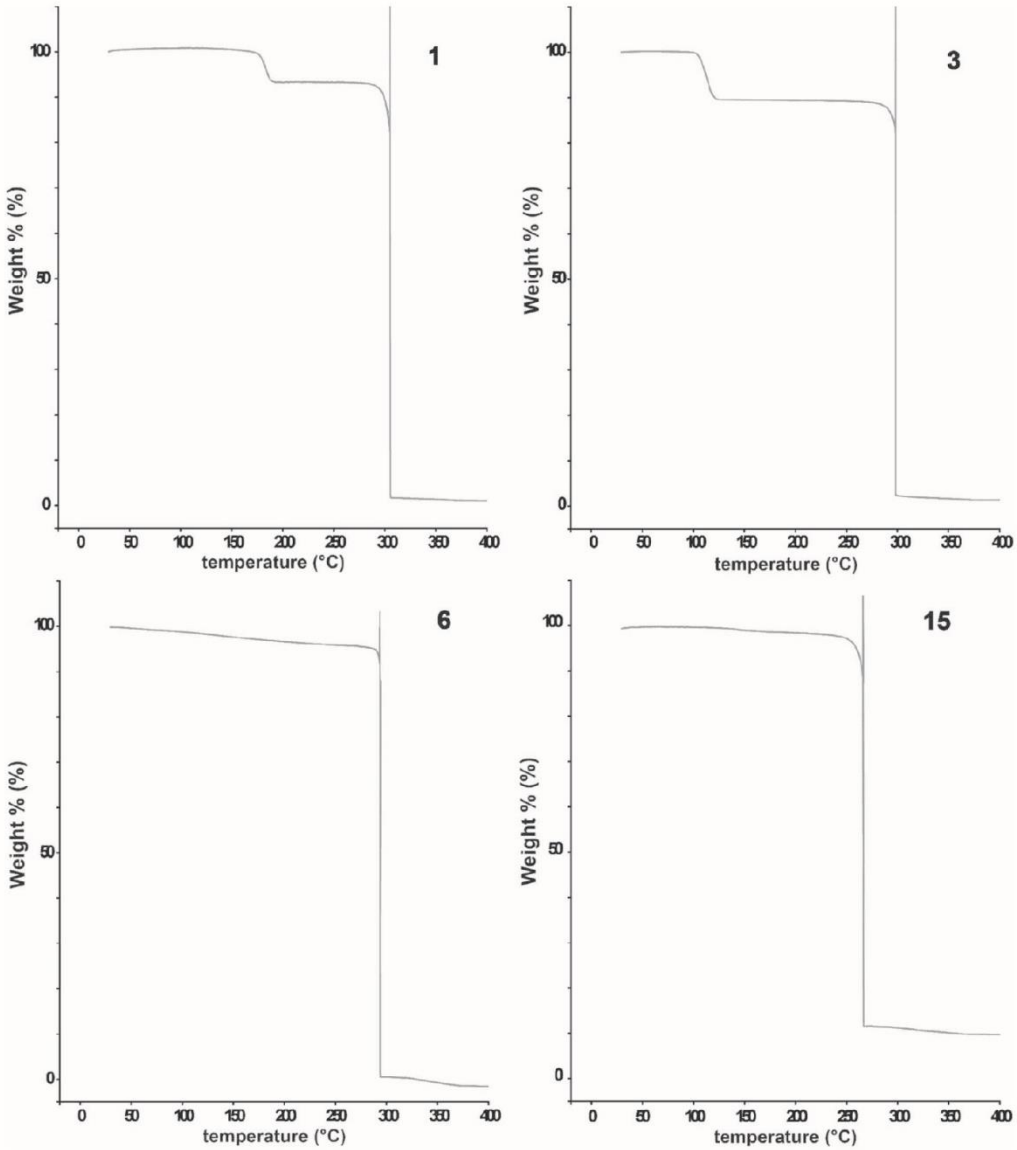


Figure 10. TGA plot of compounds **1**, **3**, **6**, and **15**.

served in substances **4** and **10**, whose compositions were verified by EA, IR, and thermal measurements. Usually, potassium salts are present as anhydrates whereas barium compounds often exist as hydrates. Therefore, both are rare examples in literature.

K(PAM)·H_2O (**4**) which shows no endothermic event during DTA measurements (Figure S5) clearly shows the loss of water till 90 °C in the TGA. When drying 4 for 24 h at 100 °C, an anhydrous substance is obtained, which immediately begins to absorb water under ambient conditions.

3.3.2 Sensitivities and Energetic Properties

Except for **10 b**, all compounds were tested towards their sensitivities against impact, friction as well as electrostatic discharge (Table 1). Lead picramate (**15**) is by far the most sensitive salt of all, with values of a primary explosive (< 1 J, 16 N). Comparing the friction sensitives, the other picramates can be classified as insensitive (> 360 N) according to the UN Recommendations on the Transport of Dangerous Goods. The only exceptions are **6** and **13** with sensitivities of 360 N (less sensitive).

In case of impact sensitivity only compounds **2**, **3**, **7**, **11**, and **13** are ranked as insensitive, whereas **9** and **10** are less

Table 1. Thermal stability measurements by DTA[a] as well as sensitivities towards impact, friction, and ESD of **1–15**.[b]

	T_{exo}[c] (°C)	IS[d] (J)	FS[e] (N)	ESD[f] (mJ)
Na(PAM)·H_2O (**1**)	292	20	> 360	> 1500
HPAM (**2**)	217	> 40	> 360	840
Li(PAM)·1.5 H_2O (**3**)	295	> 40	> 360	1080
K(PAM)·H_2O (**4**)	295	10	> 360	960
Rb(PAM) (**5**)	286	9	> 360	540
Cs(PAM) (**6**)	287	10	360	450
$Mg(PAM)_2$·5 H_2O (**7**)	275	> 40	> 360	630
$Ca(PAM)_2$·2 H_2O (**8**)	300	10	> 360	740
$Sr(PAM)_2$·1.5 H_2O (**9**)	288	40	> 360	227
$Ba(PAM)_2$ (**10**)	291	40	> 360	840
$Zn(PAM)_2$·2 H_2O (**11**)	293	> 40	> 360	250
$Cu(PAM)_2$·2 H_2O (**12**)	252	30	> 360	270
Ag(PAM) (**13**)	156	> 40	360	480
NH_4(PAM) (**14**)	209	20	> 360	740
$Pb(PAM)_2$ (**15**)	259	< 1	16	0.33

[a] Onset temperatures at a heating rate of 5 °C min^{-1}. [b] Determined at a grain size < 100 µm. [c] Exothermic peak, which indicates decomposition. [d] Impact sensitivity according to the BAM drop hammer (method 1 of 6). [e] Friction sensitivity according to the BAM friction tester (method 1 of 6). [f] Electrostatic discharge sensitivity (OZM ESD tester); impact: insensitive > 40 J, less sensitive≙ 35 J, sensitive≙ 4 J, and very sensitive≙ 3 J; friction: insensitive > 360 N, less sensitive = 360 N, sensitive < 360 N and > 80 N, very sensitive≙ 80 N, and extremely sensitive≙ 10 N. According to the UN Recommendations on the Transport of Dangerous Goods.

sensitive. All other compounds are in the range between 9 J (**5**) and 30 J (**12**) and are therefore sensitive. The observed sensitivity of picramic acid (34 J) could not be verified in our tests. The stark contrast of the lead salt compared to all other investigated salts cannot really be explained in detail yet.

Hot needle (HN) and hot plate (HP) tests of compounds **10** and **15** prove the energetic character of the water-free picramates salts (Table 2).

Whereas barium picramate shows deflagrations in both setups (Figure 11), slight confinement of $Pb(PAM)_2$ is already leading to detonations (Figure 12).

For a better classification with already used explosives, important detonation parameters of **2** and **14** were calculated using the EXPLO5 code [25]. It can be seen that **14** is comparable to TNT with values close to it (Table 3).

As seen in Figure S11, only sodium and lithium compounds **1** and **3** could be used as potential flame colorants. Especially lithium picramate is producing an intensive red flame. All other salts show very little to no coloring, which can be explained by their low solubility.

Table 2. Hot needle and hot plate tests of **10** and **15**.

	HN[a]	HP[a]
$Ba(PAM)_2$ (**10**)	def.	def.
$Pb(PAM)_2$ (**15**)	det.	def.

[a] def.: deflagration; det.: detonation.

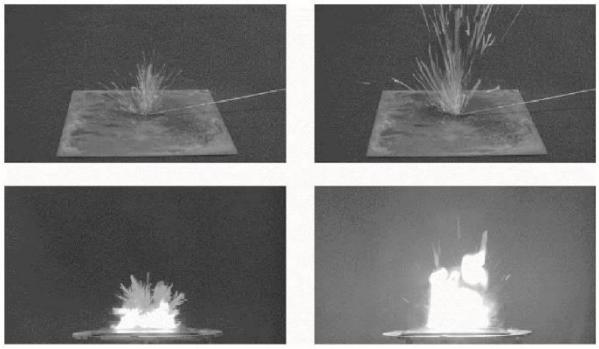


Figure 11. Hot needle (top) and hot plate (bottom) tests of compound **10**.



Figure 12. Hot needle (top) and hot plate (bottom) tests of compound **15**.

Table 3. EXPLO5 6.05.02 values of **2** and **14** compared to TNT.

	H(PAM) (**2**)	NH_4(PAM) (**14**)	TNT
1[a] [g cm^{-3}]	1.69	1.64	1.65
Ω_{CO_2}[b] [%]	−76.33	−81.42	−73.96
~ $_fH°$[c] [kJ mol^{-1}]	−1299	−1267	−261
~ $_fU°$[d] [kJ kg^{-1}]	−1202	−1146	−171
−~ $_{ex}H°$[e] [kJ kg^{-1}]	−3362	−3346	−4427
T_{det} [K]	2555	2423	3222
P_{CJ}[f] [GPa]	1.63	1.68	1.94
V_{det}[g] [m s^{-1}]	6546	6780	6824
V_0[h] [L kg^{-1}]	644	729	633

[a] Measured X-ray densities converted to RT. [b] Oxygen balance (Ω = (xO–2yC–1/2zH)M/1600). [c] Calculated enthalpy of formation at 298.15 K. [d] Calculated energy of formation at 298.15 K. [e] Heat of explosion. [f] Detonation pressure. [g] Detonation velocity. [h] Volume of detonation gases (assuming only gaseous products).

 © 2020 The Authors. Published by Wiley-VCH Verlag GmbH & Co. KGaA

4 Conclusion

In this work, 14 salts of picramic acid were prepared with simple one-step acid-base reactions whereupon 11 of them were characterized by low-temperature X-ray diffraction. All intensively colored compounds (mostly red) are easily accessible by the reaction of picramic acid with the corresponding bases in hot water/ethanol and were obtained with good yields. Surprisingly, all of the investigated compounds are far less sensitive than lead(II) picramate. The calculation of the ammonium salt showed that its performance is in the range of TNT while possessing a higher decomposition temperature. Most of the metal salts show very high thermal stabilities of up to 300 °C. Especially the water-free barium picramate could be of future interest, due to its low solubility, high stability and energetic performance.

Acknowledgements

For financial support of this work by Ludwig Maximilian University (LMU), the Office of Naval Research (ONR) under grant no. ONR N00014-19-1-2078 and the Strategic Environmental Research and Development Program (SERDP) under contract no. W912HQ19 C0033 are gratefully acknowledged. The authors would like to thank Mr. Othmar Janowitz for the inspiration to investigate this topic and Dr. Peter Mayer for helping with X-ray crystal structure analysis. In addition, the authors would like to thank Mr. Moritz Kofen and Mr. Michael Gruhne for their great contribution to this work.

References

[1] J. P. Agrawal, *High Energy Materials: Propellants, Explosives and Pyrotechnics*, 1st ed., Wiley-VCH, Weinheim, **2010**.
[2] T. M. Klapötke, *Chemistry of High-Energy Materials*, 5th ed., Walter De Gruyter, Berlin, Boston, **2019**.
[3] T. M. Klapötke, *Energetic Materials Encyclopedia*, 1st ed., Walter De Gruyter, Berlin, Boston, **2018**.
[4] E. C. Johnson, E. J. Bukowski, J. J. Sabatini, R. C. Sausa, E. F. C. Byrd, M. A. Garner, D. E. Chavez, Bis(1,2,4-oxadiazolyl) Furoxan: A Promising Melt-Castable Eutectic Material of Low Sensitivity, *ChemPlusChem* **2019**, *84*, 319–322.
[5] L. L. Fershtat, N. N. Makhova, 1,2,5-Oxadiazole-Based High-Energy-Density Materials: Synthesis and Performance, *ChemPlusChem* **2020**, *85*, 13—42, doi: 10.1002/cplu.201900542.
[6] J. Zhang, Q. Zhang, T. T. Vo, D. A. Parrish, J. M. Shreeve, Energetic Salts with π-Stacking and Hydrogen-Bonding Interactions Lead the Way to Future Energetic Materials, *J. Am. Chem. Soc.* **2015**, *137*, 1697–1704.
[7] J. P. Agrawal, R. D. Hodgson, *Organic Chemistry of Explosives*, 1st ed., Wiley-VCH, Weinheim **2006**.
[8] H. Sprengel, *The Discovery of Picric Acid (Melinite, Lyddite) „As a Powerful Explosive" and of Cumulative Detonation with its Bearing on wet Gun Cotton*, 2nd ed., Eyre & Spottiswoode, London, **1903**.
[9] R. Matyáš, J. Pachman, *Primary Explosives*, 1st ed., Springer, Berlin, Heidelberg, **2013**.
[10] J. Köhler, R. Meyer, A. Homburg, *Explosivstoffe*, 10th ed., Wiley-VCH, Weinheim, **2008**.
[11] M. Nicoletti, C. Frezza, L. Tomassini, M. Serafini, A. Bianco, Detection of picramic acid and picramates in henné products by NMR Spectroscopy, *Nat. Prod. Res.* **2019**, *33*, 2073–2078.
[12] L. C. Becker, W. F. Bergfeld, D. V. Belsito, C. D. Klaassen, J. G. Jr Marks, R. C. Shank, T. J. Slaga, P. W. Snyder, F. A. Andersen, Amended Safety assessment of Sodium Picramate and Picramic Acid, *Int. J. Toxicol.* **2009**, *28*, 205–216.
[13] Z. Yang, Y. Liu, D. Liu, L. Yan, J. Chen, Synthesis and characterization of spherical 2-diazo-4,6-dinitrophenol (DDNP), *J. Hazard. Mat.* **2010**, *177*, 938–943.
[14] B. Glowiak, Thermochemical interpretation of explosive properties. I. Nitro derivatives of phenols, *Chem. Stosowana* **1961**, *5*, 575–598.
[15] S. P. Agrawal, J. P. Agrawal, Chemistry of metal picramates. I. Picramates of iron, cobalt, and nickel, *Indian J. Chem.* **1969**, *7*, 1264–1267.
[16] S. P. Agrawal, J. P. Agrawal, Chemistry of Metal Picramates – Part II (Copper and Silver), *Def. Sci. J.* **1970**, *20*, 237–248.
[17] S. P. Agrawal, B. D. Agrawal, Chemistry of zinc, cadmium, and mercury picramates, *Indian J. Chem.* **1972**, *10*, 1106–1107.
[18] R. S. Srivastava, S. P. Agrawal, H. N. Bhargava, Chemistry of Titanium, Zirconium and Thorium Picramates, *Propellants Explos. Pyrotech.* **1976**, *1*, 101–103.
[19] S. Srivastava, S. P. Agrawal, H. N. Bhargava, Synthesis, Characterization and Explosive Properties of Picramates of Palladium and Uranium, *Kogyo Kayaku* **1979**, *40*, 38–42.
[20] S. R. Yoganarasimhan, G. O. Reddy, S. Achar, Mass spectral and thermal studies on explosion of lead salts of picramic acid and 2,4-dinitrophenol, *J. Energ. Mater.* **1992**, *10*, 151–171.
[21] N. Orbovic, A. C. Luco, M. Bozovic, Production of Exploding Materials for Electro Explosive Devices, *Propellants Explos. Pyrotech.* **2008**, *33*, 271–278.
[22] L. Molard, J. Vaganay, Manufacture of picramic acid and of sodium picramate, *Meml. Poudres* **1957**, *39*, 123–136.
[23] H. Adolf, A. L. Rheingold, M. B. Allen, CCDC 1215579 **1996**.
[24] M. A. Menelaou, N. H. Fischer, F. R. Fronczek, CCDC 125117 **1999**.
[25] M. Sućeska, EXPLO5 Version 6.05.02, Zagreb, **2018**.

Manuscript received: December 3, 2019
Revised manuscript received: February 3, 2020
Version of record online: April 3, 2020

 © 2020 The Authors. Published by Wiley-VCH Verlag GmbH & Co. KGaA

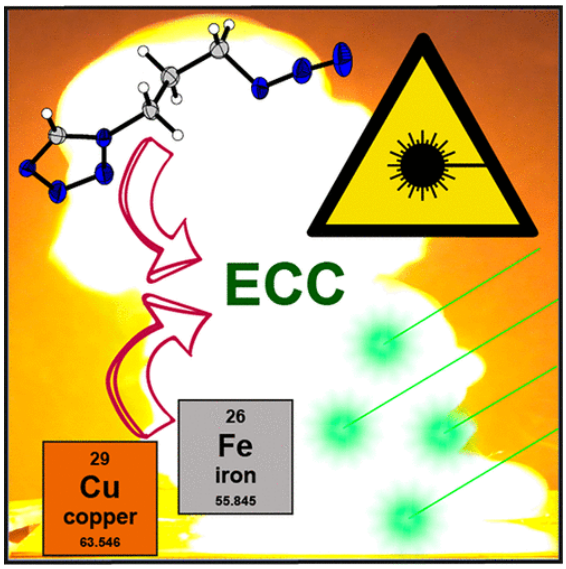
Appendix 15

Comparison of 1-Propyl-5*H*-tetrazole and 1-Azidopropyl-5*H*-tetrazole as Ligands for Laser Ignitable Complexes

M. H. H. Wurzenberger, S. M. J. Endraß, M. Lommel, T. M. Klapötke, J. Stierstorfer

ACS Appl. Energy Mater. **2020**, 3, 4, 3798–3806.

https://doi.org/10.1021/acsaem.0c00229



Supplementary Information:
https://pubs.acs.org/doi/suppl/10.1021/acsaem.0c00229/suppl_file/ae0c00229_si_001.pdf

ACS APPLIED ENERGY MATERIALS

www.acsaem.org Article

Comparison of 1-Propyl-5*H*-tetrazole and 1-Azidopropyl-5*H*-tetrazole as Ligands for Laser Ignitable Energetic Materials

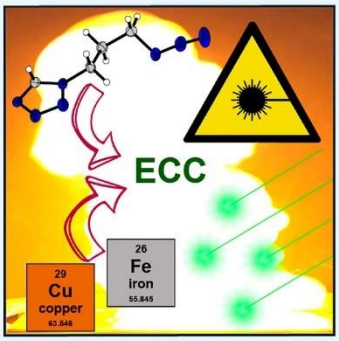
Maximilian H. H. Wurzenberger, Simon M. J. Endraß, Marcus Lommel, Thomas M. Klapötke, and Jörg Stierstorfer*

Cite This: *ACS Appl. Energy Mater.* 2020, 3, 3798−3806 Read Online

ACCESS | Metrics & More | Article Recommendations | Supporting Information

Downloaded via LMU MUENCHEN on February 16, 2022 at 08:04:18 (UTC).
See https://pubs.acs.org/sharingguidelines for options on how to legitimately share published articles.

ABSTRACT: Laser ignitable explosives are potential candidates in future applications for replacing toxic and very sensitive primary explosives, which are used in current devices. In this study, the literature unknown ligand 1-azidopropyl-5*H*-tetrazole (APT, **1**) was synthesized for the first time and applied in energetic coordination compounds (ECC). The complexes are based on different 3d transition metals (Mn^{2+}, Fe^{2+}, Cu^{2+}, and Zn^{2+}) as well as various oxidizing anions (NO_3^-, ClO_4^-, and ClO_3^-) and were tested toward their capability as laser ignitable explosives. Furthermore, analogous complexes based on the literature known ligand 1-propyl-5*H*-tetrazole (PT, **2**) were investigated for comparing the influence of the additional azide group toward the performance of the ECC. Toxicity measurements using *Vibrio fischeri* and the decreased sensitivities prove their usability as safer laser ignitable explosive with lower toxicities compared to currently used explosives.



KEYWORDS: *laser ignition, tetrazole ligands, energetic coordination compounds, nitrogen heterocycles, structure elucidation*

1. INTRODUCTION

Since Theodore Maiman invented the first practical laser in 1960, they have become nowadays ubiquitous and indispensable in countless areas of daily life. They can be found in simple light pointers, readers of optical storage media, and all the way to laser scalpels.[1] A rather unconventional application are laser ignition systems, which could be used in new combustion engines with higher efficiency or in next-generation rocket engines. The latter one would prevent the utilization of highly toxic hydrazine and dinitrogen tetroxide and allows the usage of "green" nonhypergolic propellants, which are getting initiated when irradiated with a laser diode.[2,3] Lasers are already being used for the initiation or ignition of energetic materials and are attracting increasing attention in this field of research (Figure 1).[4−7]

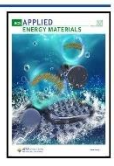
In general, a lot of research from scientists all around the world is undertaken to improve the disadvantages of conventional initiator systems, such as introducing less toxic materials.[8−11] In contrast to traditional initiation methods (spark, friction, heat, etc.), laser ignition and initiation is probably the most beneficial method of all, since the isolation of the energetic material from electric impulses excludes unintended initiation in most cases. Further advantages over classical initiation methods are the very short function times (<1 ms) and the possible application of less sensitive and lead-free ignition charges, which increase the safety and handling of these compounds significantly. The investigation of energetic transition metal complexes for their initiation abilities started with pentaammine(5-cyano-2*H*-tetrazolate)cobalt(III) perchlorate (CP) and its promising replacement tetraammine-*cis*-bis(5-nitro-2*H*-tetrazolato-N^2)cobalt(III) perchlorate (BNCP).[12,13] Since then, various coordination compounds with varying ligands and metal centers have been synthesized and tested in applications of laser irradiation.[14−16] To overcome the toxicities and the high sensitivities of CP and BNCP, the ligand 1-azidopropyl-5*H*-tetrazole (APT, **1**) has been synthesized and used as nitrogen-rich ligand for laser ignitable ECC with decreased sensitivities.

2. RESULTS AND DISCUSSION

2.1. Synthesis. For the synthesis of the new ligand 1-azidopropyl-5*H*-tetrazole (**1**), a simple two-step synthesis was performed similar to that of 1-azidoethyl-5*H*-tetrazole (Scheme 1).[17]

The starting material 3-chloropropylamine hydrochloride is a cheap commercially available molecule, which can be reacted

Received: February 5, 2020
Accepted: March 17, 2020
Published: March 17, 2020



ACS Publications © 2020 American Chemical Society

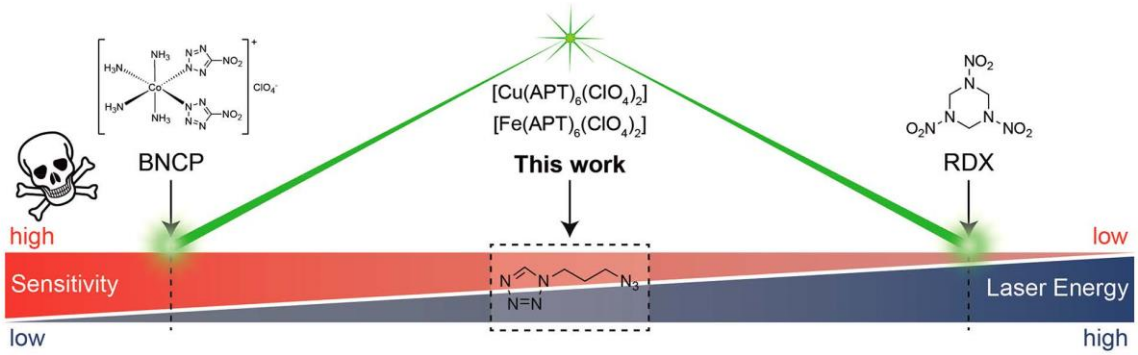
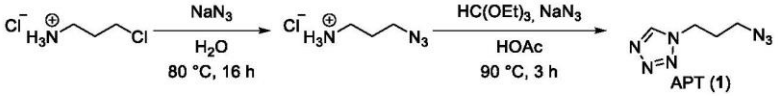


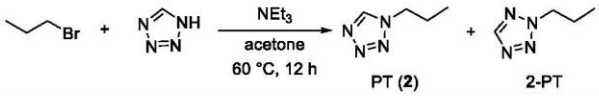
Figure 1. Conflict between sensitivities and ignitability of explosives. Well-balanced laser ignitable compounds (**6** and **7**) from this work can be placed in between.

Scheme 1. Synthesis of 1-Azidopropyl-5*H*-tetrazole (1)



in nearly quantitative yields to the corresponding azide with an excess of NaN_3. A [3 + 1 + 1] cyclization of the intermediate together with triethyl orthoformate and sodium azide in acetic acid is leading to the target molecule in a good overall yield of 60% over two steps. APT can also be synthesized in a one-pot reaction, avoiding the isolation and purification of the intermediate. The second heterocyclic ligand, 1-propyl-5*H*-tetrazole (**2**), was synthesized based on a modified literature procedure by the substitution of 1-bromopropane with 1,5*H*-tetrazole.[18] The deprotonation of tetrazole with triethylamine and following reaction with the bromoalkane led to the formation of an isomeric mixture of PT and 2-PT in an overall yield of 70% (Scheme 2). Isomeric pure PT was obtained after column chromatography with ethyl acetate (31%).

Scheme 2. Synthesis of 1-Propyl-5*H*-tetrazole (2)



The successful synthesis of **1** and **2** can easily be proven by infrared (IR) (Figure S1) as well as proton and carbon NMR spectroscopy. Also, two-dimensional ^{1}H, ^{15}N-HMBC or proton-coupled ^{15}N NMR are particularly suitable (Figures 2 and 3). In the case of APT (**1**), it is important to perform both types of measurements. Normally, ^{1}H, ^{15}N-HMBC is much faster and more sensitive compared to normal proton-coupled ^{15}N NMR; on the other hand, the terminal nitrogen of the azide group is almost invisible with this method (Figure 2, bottom).

Because of the absence of acidic protons in **1** and **2**, they both can be used as neutral ligands in coordination compounds. By the combination of different oxidizing anions (nitrate, chlorate, and perchlorate) with various 3d transition metal cations (Mn^{2+}, Fe^{2+}, Cu^{2+}, and Zn^{2+}), the characteristics and performances of the resulting ECC can be tuned toward the desired properties. For the synthesis of ECC **3**–**12**, ethanolic solutions of **1** or **2** were combined with the respective metal(II) salts, dissolved either in ethanol (**3** and **4**) or acetonitrile (**5**–**12**) (Schemes 3 and 4). The reaction mixtures were stirred for 10 min at ambient (**10**–**12**) or elevated (**4**–**9**) temperatures and left in air for crystallization. At room temperature, the reaction of copper(II) nitrate with APT produced two different complexes. It was possible to pick crystals of an anhydrous compound ($[Cu(NO_3)_2(APT)_2]$, **3**) and a monohydrate species ($[Cu(NO_3)_2(H_2O)(APT)_2]$, **4**) out of one reaction vessel. The latter one was able to be synthesized specifically when increasing the reaction temperature to 60 °C.

While the metal(II) perchlorate salts for coordination compounds **5**–**8**, **10**, and **11** are commercially available, copper(II) chlorate for the syntheses of **9** and **12** was obtained by a simple metathesis reaction. All complexes were obtained within days up to several weeks (10 weeks for complex **12**) as crystalline materials in very low to very good yields (12–84%).

2.2. Crystal Structures. The crystal structures of $[Fe(PT)_6](ClO_4)_2$ (**10**) and $[Cu(PT)_6](ClO_4)_2$ (**11**) are already known in the literature, and therefore no low-temperature single-crystal X-ray diffraction experiments were performed on those.[19,21] All other compounds were measured, but similar to the already mentioned difficulties for determining the structure of **10**, the crystals of the chlorate and perchlorate compounds are highly intergrown, and cutting of them led to the introduction of many defects. Only in the case of manganese(II) perchlorate complex **5** was one good single crystal of sufficient size for finalizing the data set obtained. In all other cases, except copper(II) nitrate species **3** and **4**, the measurements only allowed an insight into the compositions of the compounds. They all show an octahedral coordination sphere around the central metals consisting of six tetrazole ligands and noncoordinating anions. The structures' compositions were verified by elemental analysis and IR spectra (Figures S1–S3). The measurement and refinement data of complexes **3**–**5** are given in the Supporting Information (Table S1), and the data sets were uploaded to the CSD database (CCDC 1980874 (**3**), 1980875 (**4**), and 1980876 (**5**)). The ligands are exclusively coordinating through their heterocyclic N4 nitrogen atoms in all structures. The side species **3** crystallizes in the triclinic space group *P*−1 with two

https://dx.doi.org/10.1021/acsaem.0c00229
ACS Appl. Energy Mater. 2020, 3, 3798−3806

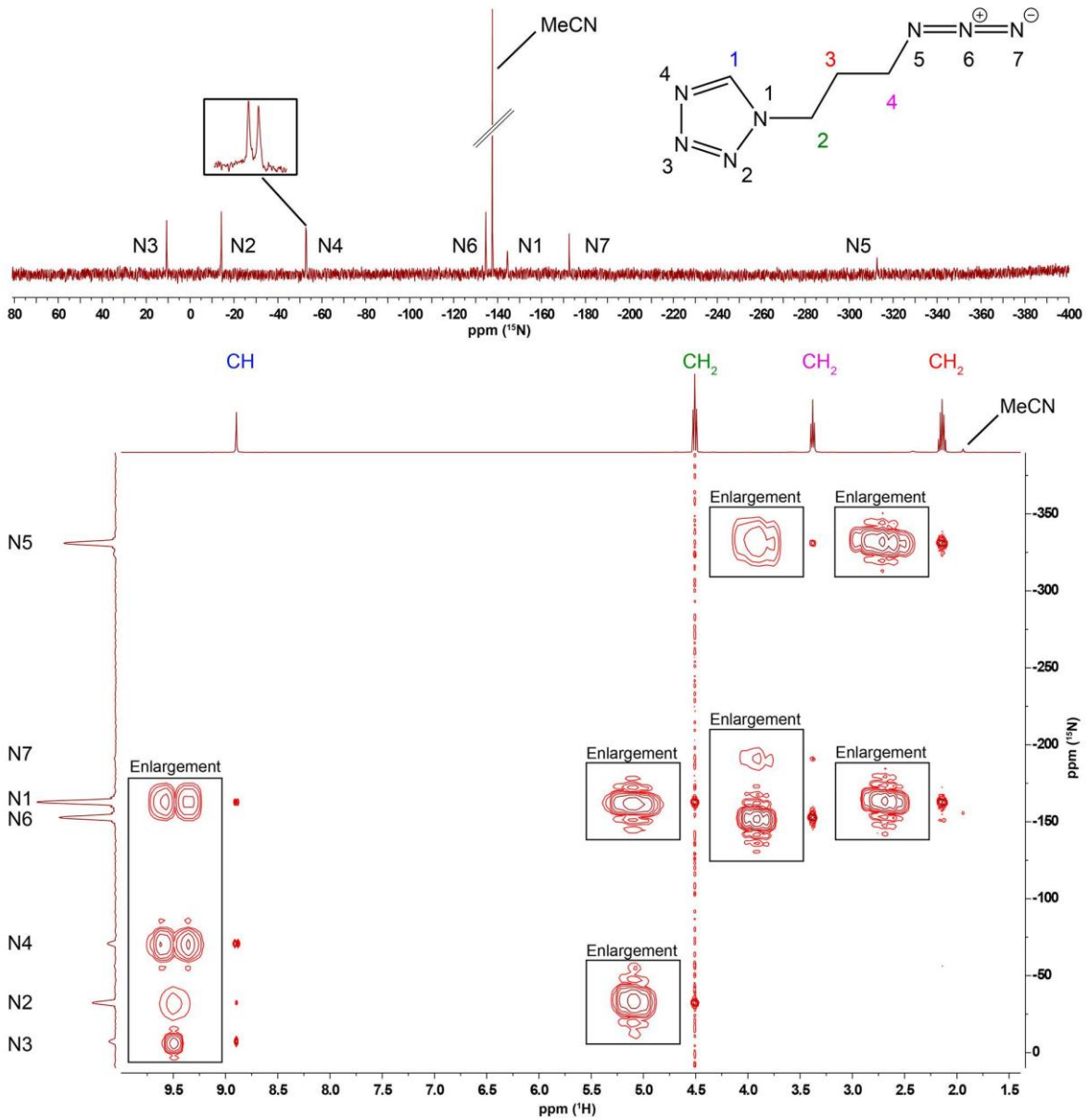


Figure 2. Proton coupled ^{15}N NMR spectra (top) and two-dimensional ^{1}H, ^{15}N-HMBC NMR spectra (bottom) of **1**. ^{15}N NMR (MeCN-d_3, 25 °C): δ = 10.7 (N3, s), −14.2 (N2, s), −52.8 (N4, d, J_{N-H} = 11.9 Hz), −134.6 (N6, s), −144.4 (N1, s), −172.6 (N7, s), −312.7 ppm (N5, s).

formula units per unit cell and a calculated density of 1.732 g cm^{-3} at 134 K. The octahedral coordination sphere around the copper atom is built up by two chelating nitrato and two APT ligands (Figure 4).

Because of the typical Jahn−Teller distortion along the O2−Cu1−O2^{i} axis and the sterical hindrance of the anionic ligands, there is a strong deviation of the perfect octahedron. The monohydrate of **3**, complex **4**, shows a similar density (1.713 g cm^{-3} (134 K)) and crystallizes in the monoclinic space group *I*2/*a* with four formula units per unit cell. The addition of the aqua ligand leads to a simple extension of the coordination sphere from an octahedron to a rather uncommon capped trigonal-prismatic molecular geometry around the copper central metal (Figure 5).

Similar to compound **3**, the manganese(II) perchlorate complex **5** crystallizes in the triclinic space group *P*−1 and possesses a relatively low density of 1.534 g cm^{-3} at 131 K with two formula units per unit cell. The complex is built up by six APT ligands around the central metal with similar Mn−N bond lengths (2.239(2)−2.264(2) Å) and two noncoordinating perchlorate anions (Figure 6).

2.3. Sensitivities and Thermal Stability. All compounds, except side species **3**, were investigated by differential thermal analysis (DTA), and additionally, thermal gravimetric analyses (TGA) were performed to further examine the critical onset temperatures (e.g., melting or dehydration as well as exothermic decomposition) from the DTA experiments (Figure 7 and Figures S4−S8). All values from the DTA experiments are given in Table 1 together with the compounds'

https://dx.doi.org/10.1021/acsaem.0c00229
ACS Appl. Energy Mater. 2020, 3, 3798−3806

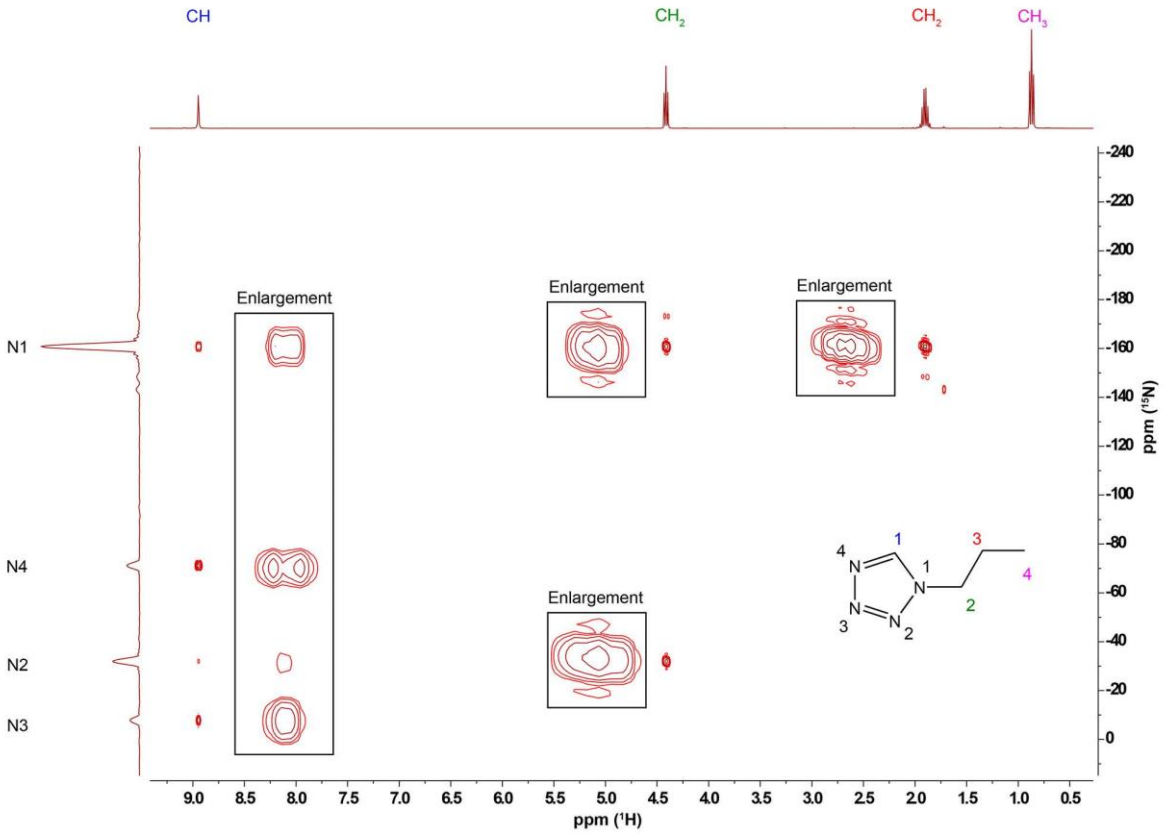
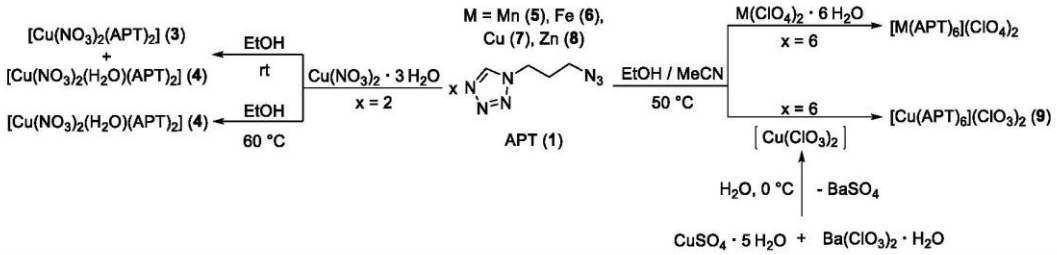
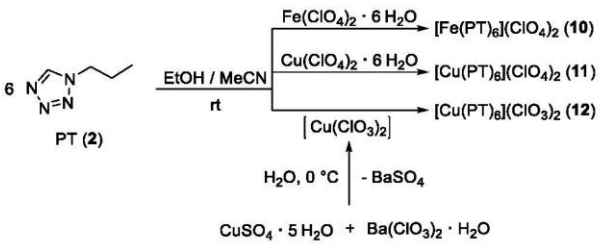


Figure 3. Two-dimensional ^{1}H, ^{15}N-HMBC NMR spectra of **2**.

Scheme 3. Synthesis of ECC 3–9 Based on Ligand 1



Scheme 4. Synthesis of ECC 10–12 Based on Ligand 2



stability against various external stimuli, such as impact, friction, and electrostatic discharge.

Comparing the values of the pure nitrogen-rich ligands, it becomes clear that both are insensitive against impact as well as friction (>40 J; > 360 N) and that the azide substituent has only a slightly destabilizing effect toward heat resistance (**1**: 195°; **2**: 206 °C). Because of the liquid state of both molecules, it was not possible to perform ESD measurements. All ECC, except **6**, show exothermic decomposition temperatures above 150 °C whereas complexes **5** and **11** even exceed the ones of their corresponding ligands (208 and 209 °C, respectively). In the row of perchlorate complexes, the temperature stability is increasing in the following order: Fe^{2+} < Cu^{2+} < Zn^{2+} < Mn^{2+}, which is in accordance with previous findings.[17] Comparing analogous complexes based on the different ligands APT and PT, the clear trend of higher stability for compounds based on **2** is observable. While the free nitrogen-rich molecules only show a difference of 11 °C, the iron(II) and copper(II) perchlorate composed complexes deviate 56 and 44 °C, respectively. Whereas the metal centers in **6** and **7** seem to catalyze the decomposition of the azide-containing ligand, the relatively low stability of the chlorate complexes **9** and **12** can be attributed to the anion, which is known in the literature.[16] The endothermic event in ECC **4**

https://dx.doi.org/10.1021/acsaem.0c00229
ACS Appl. Energy Mater. 2020, 3, 3798–3806

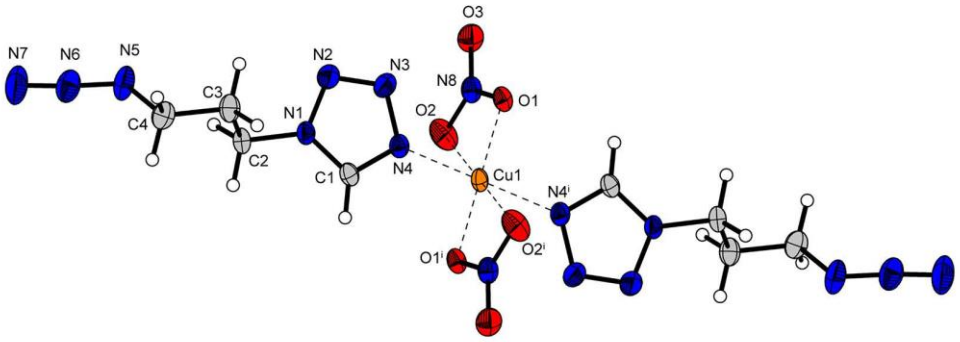


Figure 4. Molecular unit of side species $[Cu(NO_3)_2(APT)_2]$ (**3**). Selected bond lengths (Å): Cu1–O1 1.974(2), Cu1–O2 2.625(3), and Cu1–N4 1.988(3); selected bond angles (deg): O1–Cu1–O2 53.90(7), O1–Cu1–N4 90.24(10), O1–Cu1–$O1^i$ 180.00, and O1–Cu1–$O2^i$ 126.10(7); symmetry code: $2 - x, -y, -z$.

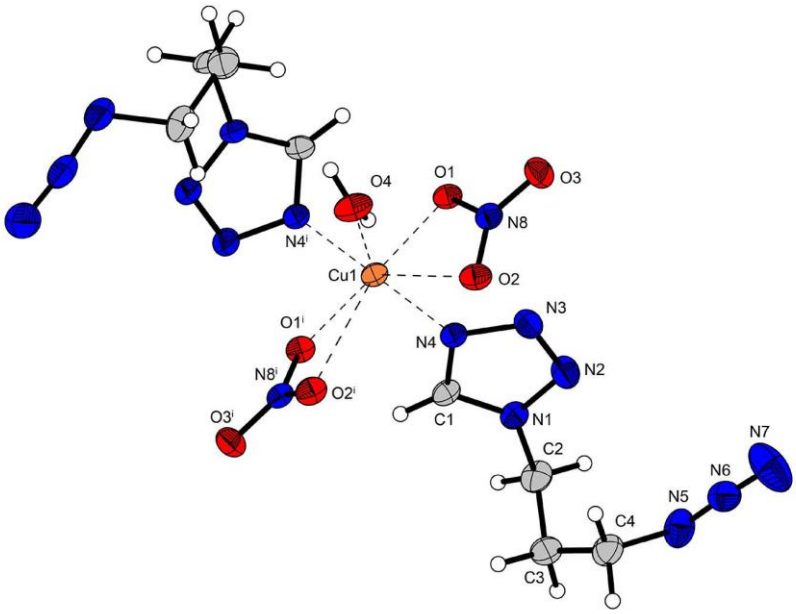


Figure 5. Molecular unit of $[Cu(NO_3)_2(H_2O)(APT)_2]$ (**4**). Selected bond lengths (Å): Cu1–O1 1.9830(12), Cu1–O2 2.7675(12), Cu1–O4 2.348(2), and Cu1–N4 1.9865(14); selected bond angles (deg): O1–Cu1–O2 51.42(4), O1–Cu1–O4 88.56(3), O1–Cu1–N4 91.81(5), O1–Cu1–$O1^i$ 177.12(5), O1–Cu1–$O2^i$ 131.41(4), and O2–Cu1–O4 138.81(3); symmetry code: $0.5 - x, y, -z$.

can be assigned to the loss of the aqua ligand, which is also confirmed by TGA (Figure 7).

All other complexes do not show alterations in weight at the endothermic events, revealing the presence of melting points. Especially remarkable is the high temperature difference between melting and decomposition of compounds **5** and **9** with values of 86 °C, making them potential melt castable explosives.

The sensitivities of all compounds toward impact (IS) and friction (FS) were determined according to BAM standard methods (1 of 6) together with the electrostatic discharge sensitivity (ESD). In addition, the compounds have been classified in accordance with the "UN Recommendations on the Transport of Dangerous Goods" by using the determined sensitivities.[22] Whereas nitrate complex **4** is insensitive against impact and sensitive against friction, all other APT-based ECC show increased sensitivities. Except for zinc(II) compound **8** (9.0 J), their impact sensitivity is in the range of lead azide as well as PETN, and therefore they have to be classified as very sensitive (**6**, **7**, **9**) or sensitive (**5**). Compared to the primary explosive $Pb(N_3)_2$, they all possess higher stability against friction close to the values of PETN. Their safer handling is finally proven by their ESD sensitivities, which are all above the ones of lead azide and nitropenta. The absence of the azide function in complexes **10**–**12** is significantly increasing the stability compared to the APT-based analogues, which is leading to their classification as sensitive materials.

2.4. Energetic Performance and Laser Initiation. To get an insight into the compounds' energetic performance, hot plate (HP) and hot needle (HN) tests were performed. While the HP test only reveals the behavior of the unconfined samples against fast heating on a copper plate, the ECC are fixed under adhesive tape during HN tests. All PT-based complexes only decomposed in both setups, whereas the azide compounds showed deflagrations with varying intensity depending on the combination of central metal and anion (Figure 8 and Figures S9–S13). The weakest output possesses nitrate compound **4** followed by the (per)chlorate ECC **5**, **8**,

https://dx.doi.org/10.1021/acsaem.0c00229
ACS Appl. Energy Mater. 2020, 3, 3798–3806

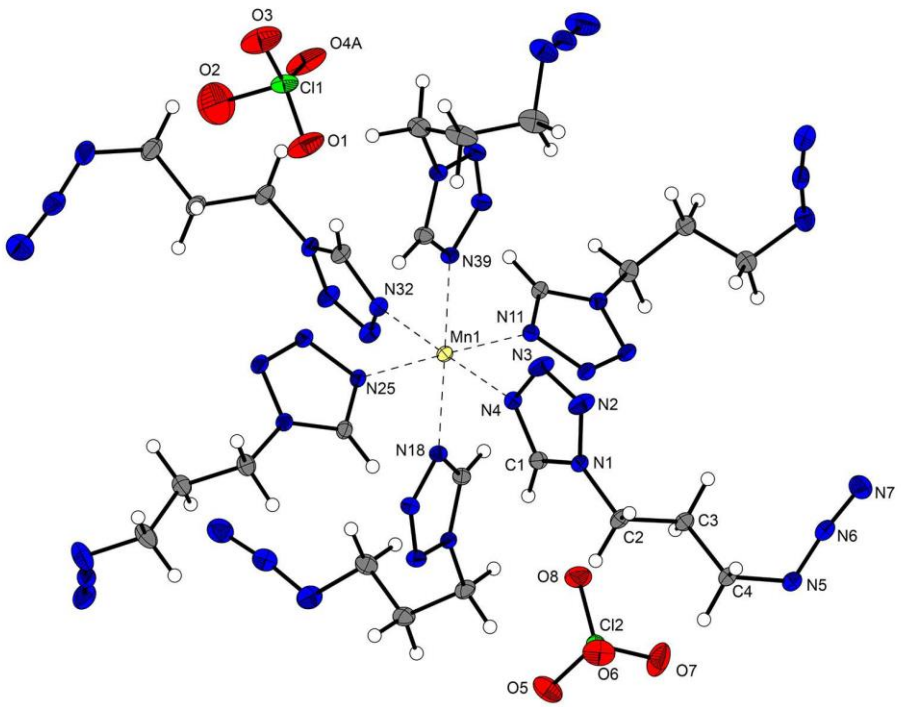


Figure 6. Molecular unit of $[Mn(APT)_6](ClO_4)_2$ (**5**). Selected bond lengths (Å): Mn1−N4 2.249(2), Mn1−N11 2.239(2), Mn−N18 2.264(2), Mn1−N25 2.249(2), Mn1−N32 2.239(2), and Mn−N39 2.254(2); selected bond angles (deg): N4−Mn1−N11 89.75(8), N4−Mn1−N18 87.61(8), N4−Mn1−N25 90.05(8), and N4−Mn1−N32 178.86(9).

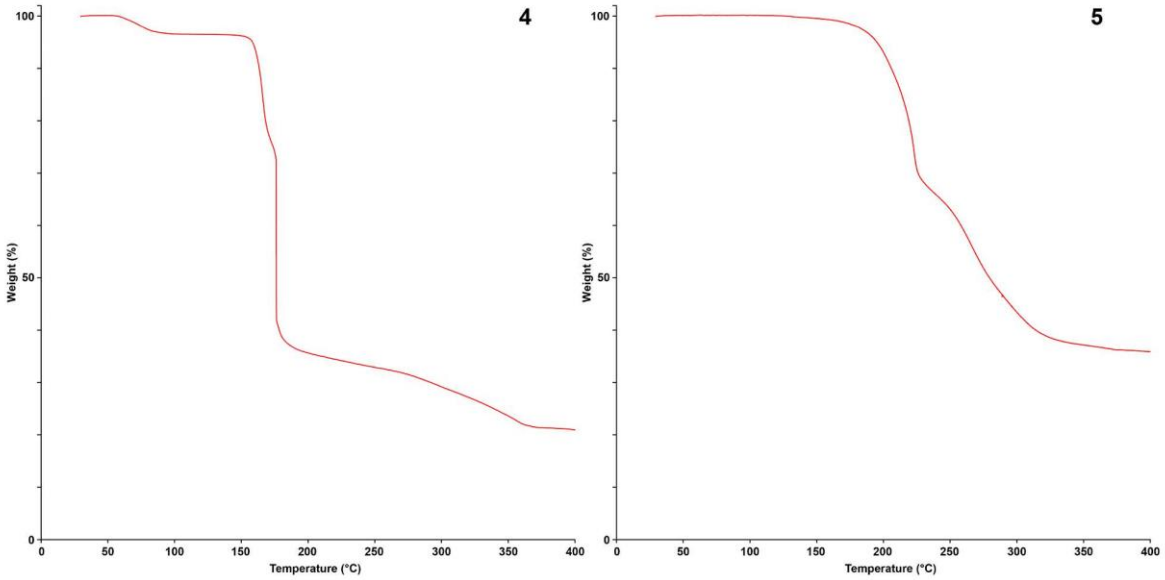


Figure 7. TGA plots of ECC **4** and **5** revealing the loss of the aqua ligand in $[Cu(NO_3)_2(H_2O)(APT)_2]$ (**4**) and the presence of melting point in $[Mn(APT)_6](ClO_4)_2$ (**5**).

and **9**. A very strong deflagration is shown by the iron(II) compound **6**.

For testing the usability of the ECC as laser ignitable explosives, they were irradiated with a 45 W InGaAs laser diode working in the single-pulse mode and a wavelength of 915 nm. Approximately 25 mg of all colored compounds (colorless substances **5**, **8**, and **10** cannot be ignited in our setup) was filled in transparent plastic caps, pressed with a pressure force of 1 kN, and sealed with a UV-curing adhesive. The samples were placed in the focal distance (f = 29.9 mm) of an optical lens, which was linked to a collimator. The collimator itself was coupled via a SMA type connector and an optical fiber (core diameter of 400 μm and cladding diameter of 480 μm) to the laser diode. The confined samples were irradiated with a voltage of 4 V and a varying current (7−20 A) as well as pulse length (1−20 ms), which together resulted in

https://dx.doi.org/10.1021/acsaem.0c00229
ACS Appl. Energy Mater. 2020, 3, 3798−3806

Table 1. Thermal Stability[a] and Sensitivities to External Stimuli of Compounds 1, 2, and 4−12 Compared to the Ones of Lead Azide and PETN[21]

	T_{endo}[b] [°C]	T_{exo}[c] [°C]	IS[d] [J]	F[e]S [N]	ESD[f] [mJ]
APT (**1**)		195	>40	>360	n.d.
PT (**2**)		206	>40	>360	n.d.
$[Cu(NO_3)_2(H_2O)(APT)_2]$ (**4**)	70	155	>40	96	422
$[Mn(APT)_6](ClO_4)_2$ (**5**)	122	208	4.5	60	368
$[Fe(APT)_6](ClO_4)_2$ (**6**)		146	2.5	28	317
$[Cu(APT)_6](ClO_4)_2$ (**7**)	115	165	2.5	32	368
$[Zn(APT)_6](ClO_4)_2$ (**8**)		183	9.0	80	422
$[Cu(APT)_6](ClO_3)_2$ (**9**)	65	151	2.5	24	>1500
$[Fe(PT)_6](ClO_4)_2$ (**10**)		202	25	192	1220
$[Cu(PT)_6](ClO_4)_2$ (**11**)	174	209	30	240	>1500
$[Cu(PT)_6](ClO_3)_2$ (**12**)	111	152	>40	168	960
PETN	141−143	180−210	3.0−4.2	60−80	60
$Pb(N_3)_2$		320−360	2.5−4.0	0.1−1.0	7.0

[a]DTA onset temperatures at a heating rate of 5 °C min^{-1}. [b]Endothermic peak indicating melting or dehydration. [c]Exothermic peak indicating decomposition. [d]Impact sensitivity according to the BAM drophammer (method 1 of 6). [e]Friction sensitivity according to the BAM friction tester (method 1 of 6). [f]Electrostatic discharge sensitivity (OZM Electric Spark XSpark10; method 1 of 6).

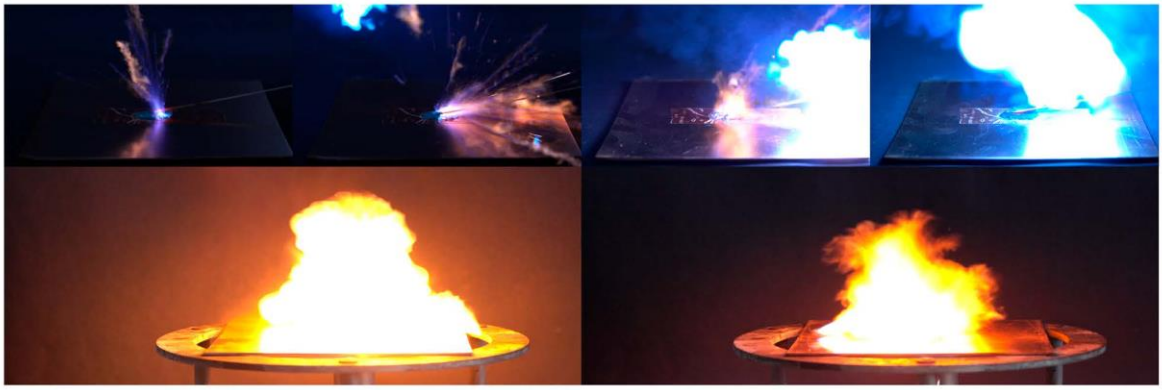


Figure 8. Top: HN test of copper(II) perchlorate complex **7** shown as a sequence. Bottom: deflagration of iron (**6**, left) and copper (**7**, right) compounds during the HP test.

an energy output of 2.00−68.0 mJ. All tested compounds showed a reaction to the laser irradiation (Table 2) varying in the strength of the output (Figure 9 and Figures S14−S17). While copper(II) chlorate and perchlorate complexes of APT already show a deflagration at very low energies (2 mJ), iron compound **6** must be irradiated with higher power for the same output. ECC **7** can even be detonated with further increased energy levels. Nitrate compound **4** has in common with perchlorate complexes **11** and **12** that they only decompose under the generation of smoke when initiated with a laser pulse. They even show the same output with energies above 150 mJ.

Table 2. Outcome of the Laser Initiation Experiments at Different Energy Levels[a]

	E_{max} [mJ]				
	2.00	25.5	30.0	51.0	68.0
$[Cu(NO_3)_2(H_2O)(APT)_2]$ (**4**)			dec	dec	dec
$[Fe(APT)_6](ClO_4)_2$ (**6**)		dec	def	def	
$[Cu(APT)_6](ClO_4)_2$ (**7**)	def		def	det	
$[Cu(APT)_6](ClO_3)_2$ (**9**)	def		def		def
$[Cu(PT)_6](ClO_4)_2$ (**11**)			dec	dec	dec
$[Cu(PT)_6](ClO_3)_2$ (**12**)			dec	dec	dec

[a]dec: decomposition, def: deflagration, det: detonation. Operating parameters: voltage U = 4 V; wavelength λ = 915 nm; current I = 7−20 A; pulse length τ = 1−20 ms; theoretical maximal output power P_{max} = 45 W; theoretical energy E_{max} = 2.00−68.0 mJ.

The ECC initiated in the laser experiments were investigated in solid state UV−vis measurements concerning a possible correlation between the absorption of the complexes at the laser wavelength and their laser ignitability (Figure 10). The optical properties are summarized in Table 3 and clearly show typical d−d transitions of the corresponding 3d transition metal. All measured ECC show moderate absorptions in the range of the operating laser wavelength.

It is noticeable that there is no observable difference between the complexes which showed a positive outcome in the laser initiation experiments (**6**, **7**, **9**) and those that were tested negative (**4**, **11**, **12**). But in fact, **6**, **7**, and **9** are more sensitive compared to the other compounds. This and the fact that the colorless compounds **5**, **8**, and **10** do not show any reaction in the setup lead to the explanation that the initiation ability by a laser not only depends on the absorption at the relevant wavelength but also on other factors like the metal center surrounding and sensitivities toward mechanical stimuli. In accordance with previous results, the formation of several hot spots by photothermal excitation when irradiated is

https://dx.doi.org/10.1021/acsaem.0c00229
ACS Appl. Energy Mater. 2020, 3, 3798−3806

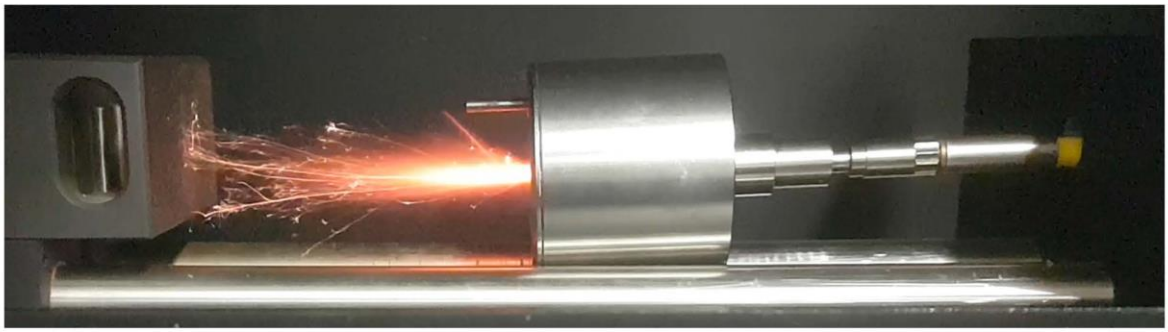


Figure 9. Deflagration of $[Fe(APT)_6](ClO_4)_2$ (**6**) during the laser experiments.

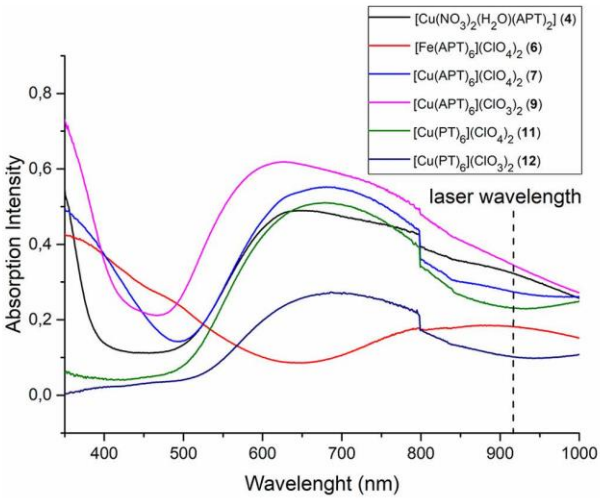


Figure 10. Solid state UV−vis spectra of ECC tested in the laser ignition experiments. The spectra have only qualitative character, and the step at 800 nm is caused by a detector change.

Table 3. Measured Optical Properties of Colored ECC

compound	color	λ_{d-d} [a]	$\lambda_{915}/\lambda_{d-d}$ [b]
$[Cu(NO_3)_2(H_2O)(APT)_2]$ (**4**)	blue	350	0.59
$[Fe(APT)_6](ClO_4)_2$ (**6**)	yellowish	350	0.43
$[Cu(APT)_6](ClO_4)_2$ (**7**)	blue	680	0.50
$[Cu(APT)_6](ClO_3)_2$ (**9**)	blue	350	0.48
$[Cu(PT)_6](ClO_4)_2$ (**11**)	blue	678	0.45
$[Cu(PT)_6](ClO_3)_2$ (**12**)	blue	686	0.37

[a]Absorption intensity maximum wavelength, which can be assigned to electron d−d transition in the measured range of 350−1000 nm. [b]Quotient of absorption intensity at the laser wavelength and the intensity at the d−d absorption wavelength.

assumed and a certain energetic character is necessary for the deflagration or detonation of the ECC.[23,24]

2.5. Toxicity. The toxicities of the uncoordinated free ligand 1-azidopropyl-5*H*-tetrazole (**1**) and iron(II) perchlorate complex **6** were investigated by using the common luminescence bacteria inhibition test in aqueous media.[25] Details of the measurements are given in the Supporting Information. With values of 0.28 g L^{-1} for the free tetrazole **1** and 0.84 g L^{-1} for the iron(II) perchlorate complex **6**, both compounds have to be considered as toxic. The toxicity of APT (**1**) is comparable to the ones of commonly used secondary explosive RDX (EC_{50} (30 min) = 0.24 g L^{-1}),[26] whereas ECC **6** is 3 times less toxic.

3. CONCLUSION

For the first time in the literature, it was possible to synthesize the nitrogen-rich molecule 1-azidopropyl-5*H*-tetrazole (**1**, APT). It was successfully applied as ligand in energetic coordination compounds. The synthesis can be performed in a straightforward, green as well as cost-effective approach and furthermore avoids the isolation of intermediate species. ^{1}H, ^{15}N-HMBC NMR proved to be very useful for assigning all tetrazole nitrogens. For the comparison with **1**, the literature-known ligand 1-propyl-5*H*-tetrazole (**2**, PT) and three complexes consisting of it were synthesized and compared to the APT analogues. All investigated ECC are based on less or nontoxic 3d transition metals (Mn, Fe, Cu, and Zn) and oxidizing anions like nitrate, chlorate, or perchlorate. All synthesized complexes, except side product **3**, were comprehensively characterized, and especially their energetic character was investigated in detail. Compared to commonly used primary explosives such as lead azide, they possess higher stability against friction, which allows safer handling of those compounds. With the ignitability of the complexes **6** and **7** based on iron(II) and copper(II) perchlorate in single-pulse laser experiments making them to possible candidates for future laser explosive applications, avoiding the use of lead-containing and very dangerous primary explosives.

■ ASSOCIATED CONTENT

Supporting Information

The Supporting Information is available free of charge at https://pubs.acs.org/doi/10.1021/acsaem.0c00229.

Compounds overview; IR spectroscopy of **1**, **2**, and **4**−**12**; X-ray diffraction; DTA plots of **1**, **2**, and **4**−**12**; TGA plots of **6**−**12**; hot plate and hot needle tests; laser initiation tests of **4**, **9**, **11**, and **12**; experimental part and general methods; references (PDF)

■ AUTHOR INFORMATION

Corresponding Author

Jörg Stierstorfer − *Department of Chemistry, Ludwig Maximilian University Munich 81377 München, Germany;* orcid.org/0000-0002-2105-1275; Email: jstch@cup.uni-muenchen.de

Authors

Maximilian H. H. Wurzenberger – *Department of Chemistry, Ludwig Maximilian University Munich 81377 München, Germany*

Simon M. J. Endraß – *Department of Chemistry, Ludwig Maximilian University Munich 81377 München, Germany*

Marcus Lommel – *Department of Chemistry, Ludwig Maximilian University Munich 81377 München, Germany*

Thomas M. Klapötke – *Department of Chemistry, Ludwig Maximilian University Munich 81377 München, Germany;* orcid.org/0000-0003-3276-1157

Complete contact information is available at: https://pubs.acs.org/10.1021/acsaem.0c00229

Notes

The authors declare no competing financial interest.

■ ACKNOWLEDGMENTS

We gratefully acknowledge the financial support of this work by the Ludwig-Maximilian University (LMU), the Office of Naval Research (ONR) under Grant ONR N00014-19-1-2078, and the Strategic Environmental Research and Development Program (SERDP) under Contract W912HQ19C0033. The authors also thank Prof. Dr. Konstantin Karaghiosoff for the measurement of the ^{15}N NMR spectra, Miss Cornelia Unger for toxicity assessments, Miss Antonia Stadler for proofreading, and Miss Marina Schönherr for her great contribution to this work.

■ REFERENCES

(1) Maiman, T. H. Stimulated Optical Radiation in Ruby. *Nature* **1960**, *187*, 493−494.

(2) Manfletti, C. Laser Ignition of an Experimental Cryogenic Reaction and Control Thruster: Ignition Energies. *J. Propul. Power* **2014**, *30*, 952−961.

(3) Weinrotter, M.; Kopecek, H.; Wintner, E. Laser ignition of engines. *Laser Phys.* **2005**, *15*, 947−953.

(4) Zhilin, A. Y.; Ilyushin, M. A.; Tselinskii, I. V.; Brykov, A. S. Synthesis of a high-energy-capacity compound, cis-tetraamminebis(5-nitro-2H-tetrazolato-N2)cobalt(III) perchlorate. *Russ. J. Appl. Chem.* **2001**, *74*, 99−102.

(5) Myers, T. W.; Bjorgaard, J. A.; Brown, K. E.; Chavez, D. E.; Hanson, S. K.; Scharff, R. J.; Tretiak, S.; Veauthier, J. M. Energetic Chromophores: Low-Energy Laser Initiation in Explosive Fe(II) Tetrazine Complexes. *J. Am. Chem. Soc.* **2016**, *138*, 4685−4692.

(6) Zhang, H.; Wu, L.; Hu, P.; Guo, W.; Zhang, W.; Ye, Y.; Shen, R. Launch and impact characteristics of typical multi-layered flyers driven by ns-pulsed laser. *Opt. Laser Technol.* **2019**, *120*, 105709.

(7) Wang, T.; Zhang, Q.; Deng, H.; Shang, L.; Chen, D.; Li, Y.; Zhu, S.; Li, H. Evolution of Oxidizing Inorganic Metal Salts: Ultrafast Laser Initiation Materials Based on Energetic Cationic Coordination Polymers. *ACS Appl. Mater. Interfaces* **2019**, *11*, 41523−41530.

(8) Zhang, J.; Zhang, J.; Imler, G. H.; Parrish, D. A.; Shreeve, J. M. Sodium and Potassium 3,5-Dinitro-4-hydropyrazolate: Three-Dimensional Metal-Organic Frameworks as Promising Super-heat-resistant Explosives. *ACS Appl. Energy Mater.* **2019**, *2*, 7628−7634.

(9) Kent, R. V.; Vaid, T. P.; Boissonnault, J. A.; Matzger, A. J. Adsorption of tetranitromethane in zeolitic imidazolate frameworks yields energetic materials. *Dalton Trans.* **2019**, *48*, 7509−7513.

(10) Baxter, A. F.; Martin, I.; Christe, K. O.; Haiges, R. Formamidinium Nitroformate: An Insensitive RDX Alternative. *J. Am. Chem. Soc.* **2018**, *140*, 15089−15098.

(11) Tang, Y.; He, C.; Imler, G. H.; Parrish, D. A.; Shreeve, J. M. Aminonitro Groups Surrounding a Fused Pyrazolotriazine Ring: A Superior Thermally Stable and Insensitive Energetic Material. *ACS Appl. Energy Mater.* **2019**, *2*, 2263−2267.

(12) Kunz, S. C.; Salas, F. J. Diode laser ignition of high explosives and pyrotechnics. *Proceedings of the 13th International Pyrotechnics Seminar* **1988**, 505−523.

(13) Merson, J. A.; Salas, F. J.; Harlan, J. G. The development of a laser ignited deflagration-to-detonation (DDT) detonators and pyrotechnic actuators. *Proceedings of the 19th International Pyrotechnics Seminar* **1994**, 191−206.

(14) Myers, T. W.; Brown, K. E.; Chavez, D. E.; Scharff, R. J.; Veauthier, J. M. Correlating the Structural, Electronic, and Explosive Sensitivity Properties of CuII Tetrazine Complexes. *Eur. J. Inorg. Chem.* **2016**, *2016*, 3178−3183.

(15) Smirnov, A. V.; Ilyushin, M. A.; Tselinskii, I. V. Synthesis of Cobalt(III) Ammine Complexes as Explosives for Safe Priming Charges. *Russ. J. Appl. Chem.* **2004**, *77*, 794−796.

(16) Wurzenberger, M. H. H.; Szimhardt, N.; Stierstorfer, J. Copper(II) Chlorate Complexes: The Renaissance of a Forgotten and Misjudged Energetic Anion. *J. Am. Chem. Soc.* **2018**, *140*, 3206−3209.

(17) Wurzenberger, M. H. H.; Gruhne, M. S.; Lommel, M.; Szimhardt, N.; Klapötke, T. M.; Stierstorfer, J. Comparison of 1-Ethyl-5H-tetrazole and 1-Azidoethyl-5H-tetrazole as Ligands in Energetic Transition Metal Complexes. *Chem. - Asian J.* **2019**, *14*, 2018−2028.

(18) Gaponik, P. N.; Degtyarik, M. M.; Lyakhov, A. S.; Matulis, V. E.; Ivashkevich, O. A.; Quesada, M.; Reedijk, J. Bis(2-methyltetrazole)dichlorocopper(II) is a layered coordination polymer built from dinuclear chloro-bridged Cu units linked by bridging tetrazoles. The first structurally and magnetically characterized complex of 2-monosubstituted tetrazoles. *Inorg. Chim. Acta* **2005**, *358*, 3949−3957.

(19) Wiehl, L. Structures of hexakis(1-propyltetrazole)iron(II) bis(tetrafluoroborate), $[Fe(CHN_4C_3H_7)_6](BF_4)_2$, hexakis(1-methyltetrazole)iron(II) bis(tetrafluoroborate), $[Fe(CHN_4CH_3)_6](BF_4)_2$, and the analogous perchlorates. Their relation to spin crossover behavior and comparison of Debye-Waller factors from structure determination and Moessbauer spectroscopy. *Acta Crystallogr., Sect. B: Struct. Sci.* **1993**, *49*, 289−303.

(20) Mills, A. M.; Spek, A. L.; Stassen, A. F.; Haasnoot, J. G.; Reedijk, J. Private Communication CCDC 637921, 2007.

(21) Klapötke, T. M. *Energetic Materials Encyclopedia*; Walter De Gruyter: Berlin, 2018.

(22) Impact: insensitive >40 J, less sensitive ≥35 J, sensitive ≥4 J, very sensitive ≤3 J. Friction: insensitive >360 N, less sensitive = 360 N, sensitive <360 N and >80 N, very sensitive ≤80 N, extremely sensitive ≤10 N. According to the UN Recommendations on the Transport of Dangerous Goods.

(23) Wurzenberger, M. H. H.; Bissinger, B. R. G.; Lommel, M.; Gruhne, M. S.; Szimhardt, N.; Stierstorfer, J. Synthesis and comparison of copper(II) complexes with various N-aminotetrazole ligands involving trinitrophenol anions. *New J. Chem.* **2019**, *43*, 18193−18202.

(24) Szimhardt, N.; Wurzenberger, M. H. H.; Klapötke, T. M.; Lechner, J. T.; Reichherzer, H.; Unger, C. C.; Stierstorfer, J. Highly functional energetic complexes: stability tuning through coordination diversity of isomeric propyl-linked ditetrazoles. *J. Mater. Chem. A* **2018**, *6*, 6565−6577.

(25) Sunahara, G. I.; Dodard, S.; Sarrazin, M.; Paquet, L.; Ampleman, G.; Thiboutot, S.; Hawari, J.; Renoux, A. Y. Development of a soil extraction procedure for ecotoxicity characterization of energetic compounds. *Ecotoxicol. Environ. Saf.* **1998**, *39*, 185−194.

(26) Fischer, D.; Klapötke, T. M.; Reymann, M.; Stierstorfer, J. Dense Energetic Nitraminofurazanes. *Chem. - Eur. J.* **2014**, *20*, 6401−6411.

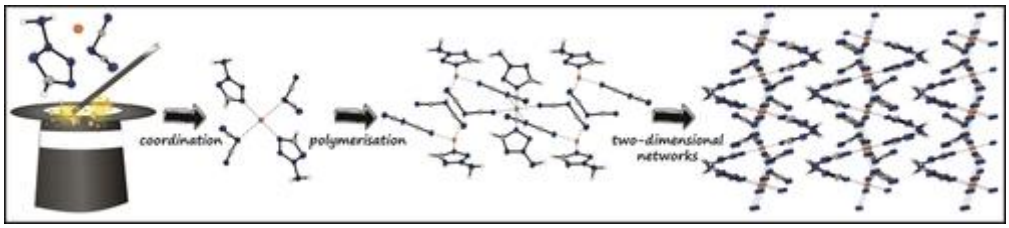
Appendix 16

Copper(II) Dicyanamide Complexes with *N*-Substituted Tetrazole Ligands – Energetic Polymers with Moderate Sensitivities

M. H. H. Wurzenberger, J. T. Lechner, J. Stierstorfer

ChemPlusChem **2020**, *85*, 769–775.

http://doi.org/10.1002/cplu.202000156



Supplementary Information:
https://chemistry-europe.onlinelibrary.wiley.com/action/downloadSupplement?doi=10.1002%2Fcplu.202000156&file=cplu202000156-sup-0001-misc_information.pdf

Check for updates
Chemistry Europe
European Chemical Societies Publishing

Copper(II) Dicyanamide Complexes with *N*-Substituted Tetrazole Ligands – Energetic Coordination Polymers with Moderate Sensitivities

Maximilian H. H. Wurzenberger, Jasmin T. Lechner, and Jörg Stierstorfer*[a]

Following the useful concept of energetic coordination compounds (ECC), copper(II) dicyanamide was used as a building block for the synthesis of eight new complexes. As ligands, six different *N*-substituted tetrazoles were applied, leading to the formation of high-nitrogen containing complexes. The obtained compounds were characterized in detail by single crystal as well as powder XRD, IR, EA, DTA, and TGA. In addition, the sensitivities towards impact and friction were determined with BAM standard techniques as well as the sensitivity towards electrostatic discharges. All compounds show moderate sensitivities ($IS > 6$, $FS > 80$ N) and energetic properties but differ in their polymeric structures forming polymeric chains or layers up to 3D networks.

Introduction

The dicyanamide moiety belongs to the class of cyanamides, which have manifold applications and are used as precursors or intermediates in industry. Sodium dicyanamide (NaDCA) can be easily obtained by reacting cyanamide with cyanogen chloride and sodium hydroxide.[1]

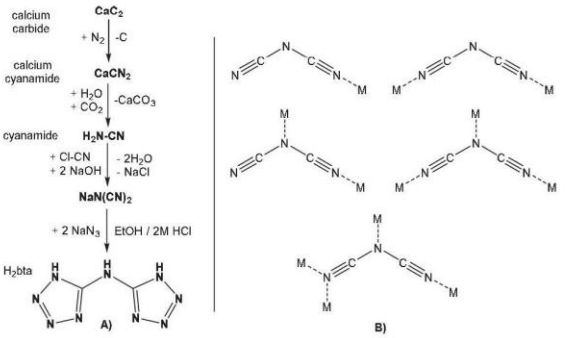


Chart 1. A) Synthesis of the di-heterocyclic compound bis(tetrazolyl)amine H_2bta starting from sodium dicyanamide (NaDCA), which can be produced from calcium carbide; **B)** Different coordination modes of the DCA anion reported in the literature.[2]

Dicyanamides can be used as starting materials for the synthesis of many different materials such as heterocycles, ionic liquids or transition metal complexes.[3] An interesting heterocycle with regards to its very high nitrogen content on the one hand side and its perfect stability and facile accessibility on the other hand side is 5,5'-bis(1*H*-tetrazol-5-yl)amine (H_2bta). It can easily be prepared by a one-step reaction starting with NaDCA (Chart 1 **A**)). The neutral compound and its metal salts were discussed for different applications, especially for the use as energetic materials, e.g. as burn rate modifiers due to their moderate sensitivities.[4] Another important use of the DCA anion is its application in transition metal complexes. Due to its manifold coordination modes and bridging character it can connect between several metal centers forming polymeric compounds with unique features (Chart 1 **B**)).[2] An innumerable amount of complexes mainly based on 3d transition metals are discussed in literature for different applications such as magnetic switches.[5] Besides the commonly used central metals copper and cobalt there can also be found more exotic ones, like silver or uranium.[6]

In the past, strong oxidizing anions such as nitrate or perchlorate were often used for the synthesis of energetic coordination compounds (ECC). The obtained complexes are powerful compounds with great performance but also come along with high sensitivities making their handling considerably more difficult.[7] In recent years, the focus of new energetic compounds shifted strongly towards substances that are safer to use and therefore possess decreased sensitivities.[8] For the synthesis of novel ECC, we focused on small anions with positive heat of formation ($\triangle H_f$). Most of the anions such as (per)chlorate, nitrate, etc. are formed exothermically in the gas phase (Figure 1). In contrast cyanide, fulminate, azide, and dicyanamide have different positive calculated $\triangle H_f$'s and allow therefore the tuning of the desired properties.

In the case of copper(II) complexes the choices are considerably narrowed. Both, fulminates and cyanides are leading to the reduction to Cu^+, while copper azides are extremely sensitive and dangerous to handle. The optimal compromise for the synthesis of energetic copper complexes with moderate sensitivities is thus the dicyanamide anion

[a] *M. H. H. Wurzenberger, J. T. Lechner, Dr. J. Stierstorfer*
Department of Chemistry
University of Munich (LMU)
Butenandtstrasse 5–13, 81377 München (Germany)
E-mail: jst@cup.uni-muenchen.de

Supporting information for this article is available on the WWW under https://doi.org/10.1002/cplu.202000156

© 2020 The Authors. Published by Wiley-VCH Verlag GmbH & Co. KGaA. This is an open access article under the terms of the Creative Commons Attribution License, which permits use, distribution and reproduction in any medium, provided the original work is properly cited.

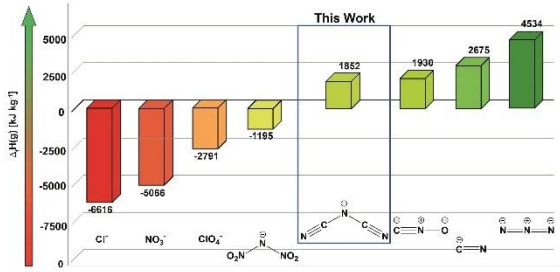


Figure 1. Comparison of the calculated gas-phase enthalpies of formation[9] for several simple negatively charged anions showing positive heat of formation for the DCA anion.

showing a moderate positive heat of formation. For the DCA anion, both the pure copper(I) and copper(II) salts are stable at ambient conditions.[10] While many copper(II) dicyanamide complexes were investigated, nitrogen-rich representatives are very rare in literature. Solely the 1,5-diaminotetrazole compound is mentioned as an energetic combustion catalyst for propellant systems, indicating their potential as possible ECC.[11] Therefore, in this work, new copper(II) coordination polymers based on dicyanamide and tetrazole ligands were synthesized and their energetic properties investigated.

Results and Discussion

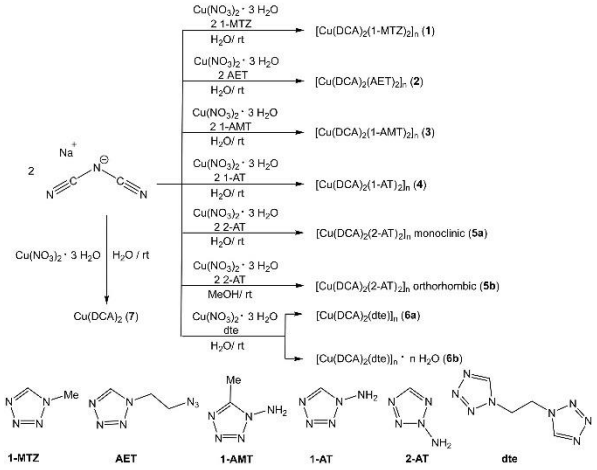
Synthesis

The copper(II) dicyanamide compounds were synthesized using six different tetrazole ligands and started with a metathesis reaction. Therefore, the corresponding copper(II) nitrate complexes were generated *in situ* and further reacted with aqueous sodium dicyanamide solutions (Scheme 1). The used ligands were available in the research group and prepared according to literature known syntheses.[12] All eight complexes possess polymeric structures due to the bridging nature of the DCA anion and therefore crystallize quickly after the synthesis.

During the synthesis of **6a**, sometimes the formation of a second species in very small traces was observed. The side-species **6b** represents a monohydrate of **6a** and is the only water-containing compound. All other complexes were obtained as anhydrous substances. Similar to **6b** only some single-crystals of complex **3** were able to be obtained. Therefore, both compounds could not be further characterized. The pure copper(II) dicyanamide (**7**) was obtained as the main product during the attempted synthesis of **3** and as the only product when 2-amino-5-methyltetrazole was applied as ligand.

Crystal Structures

All compounds were characterized by low-temperature single-crystal X-ray diffraction and details on the measurement and



Scheme 1. Syntheses of the coordination compounds **1**–**6** and the pure copper(II) salt **7** (**top**). Structures of the used ligands (bottom). 1-MTZ: 1-methyl-5*H*-tetrazole; AET: 1-azidoethyl-5*H*-tetrazole; 1-AMT: 1-amino-5-methyltetrazole; 1-AT: 1-amino-5*H*-tetrazole; 2-AT: 2-amino-5*H*-tetrazole; dte: 1,2-di(tetrazol-1-yl)ethane.

refinement data are given in the Supporting Information (Table S1–3).[13]

In all eight complexes, the central Cu^{2+} cations are octahedrally coordinated and show typical d^9 Jahn-Teller distortions. Due to the bridging dicyanamide anion, all structures are multidimensional. The spatial structures of compounds **1**, **2** and **3** with the ligands 1-MTZ (**1**), AET (**2**) and 1-AMT (**3**) are quite similar. The copper atoms are all coordinated by two tetrazole ligands in equatorial positions and four bridging dicyanamido anions. The MTZ complex **1** is crystalizing in the monoclinic space group $P2_1/n$ and compounds **2** and **3** in the triclinic space group $P\bar{1}$ (Figure 2). They show comparable densities between 1.735 and 1.772 g cm^{-3}.

In all three cases, the bridging leads to the formation of one-dimensional chains (Figure 3), which are caused by the binding of the two outer nitrogen atoms of the DCA to the central metals. Two anions each bridging between the same two cations. The heterocycles all bind to the copper via the N4 atom which is located next to the carbon atom. The bond lengths between the Cu1and the N4 atom are almost the same for all three complexes. The copper complex **4** with **1**-AT as ligand has a nearly similar coordination environment as the previously described complexes **1**–**3**. The central copper atom is coordinated by two 1-AT ligands via N4, and 4 DCA anions again via the outer two nitrogen atoms (Figure 4). It crystallizes in the monoclinic space group $P2_1/c$ with two formula units per unit cell and a calculated density of 1.860 g cm^{-3} at 143 K.

However, the compounds differ in their polymeric structure. While in complexes **1**–**3** the dicyanamide anions are bridging always between the same two central metals, the four DCAs in compound **4** link to four different copper cations. This creates a two-dimensional polymeric layer (Figure 5).

The coordination polymers of copper(II) dicyanamide with 2-aminotetrazole can be obtained in two different polymorphs

© 2020 The Authors. Published by Wiley-VCH Verlag GmbH & Co. KGaA

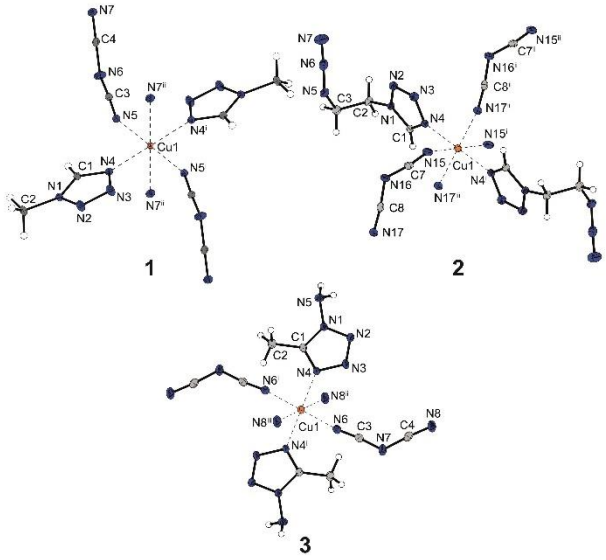


Figure 2. Copper(II) coordination environment of **1** (top left), **2** (top right) and **3** (bottom). Thermal ellipsoids of non-hydrogen atoms in all structures are set to the 50% probability level. Selected bond lengths of **1** (Å): Cu1–N4 2.0179(13), Cu1–N5 1.9892(14), Cu1–N7^{ii} 2.4717(14). Selected bond angels of **1** (°): N4–Cu1–N5 89.07(6), N4–Cu1–N4^{i} 180.00, N4–Cu1–N7^{ii} 85.17(5). Symmetry codes of **1**: i) 1-x, 1-y, 1-z; ii) x, −1 + y, z; iii) 1-x, 2-y, 1-z. Selected bond lengths of **2** (Å): Cu1–N4 2.013(2), Cu1–N15 2.459(2), Cu1–N17^{ii} 1.991(2). Selected bond angels of **2** (°): N4–Cu1–N15 90.28(8), N4–Cu1–N4^{i} 180.00, N4–Cu1–N17^{ii} 90.83(9). Symmetry codes of **2**: i) 2-x, −y, 1-z; ii) −1 + x, y, z; iii) 3-x, −y, 1-z. Selected bond lengths of **3** (Å): Cu1–N4 2.0459(16), Cu1–N6 1.944(2), Cu1–N8^{ii} 2.544(2). Selected bond angels of **3** (°): N4–Cu1–N6^{i} 90.55(8), N4–Cu1–N4^{i} 180.00, N4–Cu1–N8^{ii} 89.23(6). Symmetry codes of **3**: i) −x, −y, −z; ii) −1 + x, y, z; iii) 1-x, −y, −z.

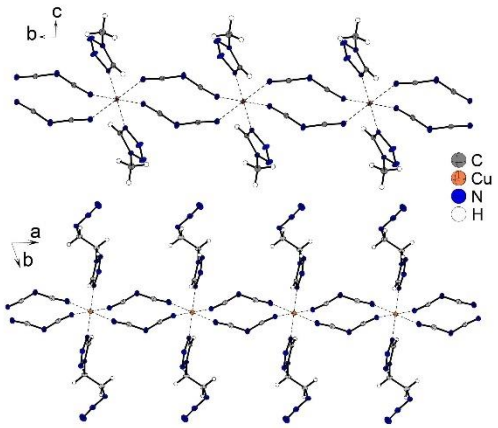


Figure 3. One-dimensional polymeric structure of **1** (top) and **2** (bottom).

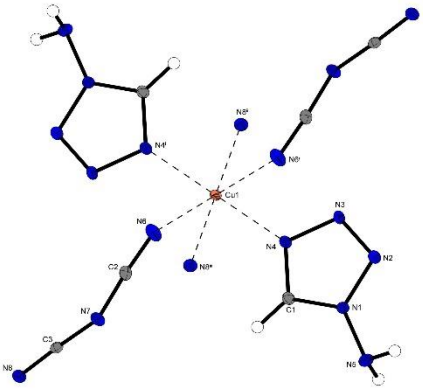


Figure 4. Copper(II) coordination environment of **4**. Selected bond lengths (Å): Cu1–N4 2.0191(12), Cu1–N6 2.3986(14), Cu1–N8^{ii} 1.9884(14). Selected bond angels (°): N4–Cu1–N6^{i} 90.69(5), N4–Cu1–N4^{i} 180.00, N4–Cu1–N8^{iii} 89.55(5). Symmetry codes: i) x, 2-y, −z; ii) x, 0.5 + y, −0.5-z; iii) x, 1.5-y, 0.5 + z.

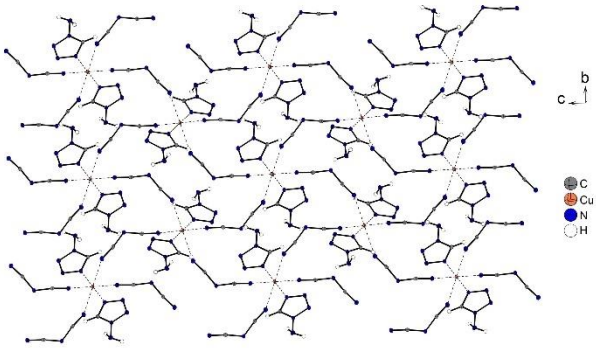


Figure 5. Two-dimensional polymeric structure of **4**, view along the *a* axis.

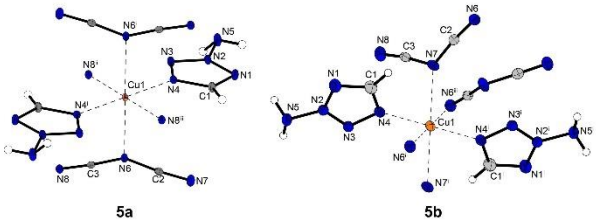


Figure 6. Copper(II) coordination environment of **5a** (left) and of **5b** (right). Selected bond lengths of **5a** (Å): Cu1–N4 2.0321(14), Cu1–N6 2.4280(13), Cu1–N8^{ii} 1.9803(14). Selected bond angels of **5a** (°): N4–Cu1–N6^{i} 92.51(5), N4–Cu1–N4^{i} 180.00, N4–Cu1–N8^{iii} 89.13(5). Symmetry codes of **5a**: i) −x, 1-y, 1-z; ii) x, 1.5−y, 0.5 + z; iii) −x, −0.5 + y, 0.5-z. Selected bond lengths of **5b** (Å): Cu1–N4 2.0311(18), Cu1–N6^{ii} 1.956(2), Cu1–N7 2.464(2). Selected bond angels of **5b** (°): N4–Cu1–N6^{ii} 89.77(8), N4–Cu1–N4^{i} 180.00, N4–Cu1–N7 86.19(7). Symmetry codes of **5b**: i) 1-x, 1-y, −z; ii) −0.5 + x, 0.5-y, −z; iii) 1.5-x, 0.5 + y, z.

5a and **5b**. Similar to **4**, both compounds show a coordination structure with the copper central atom bound to two 2-AT ligands via the N4 atom. Furthermore, four dicyanamide anions bind to the Cu(II), but this time each via one outer and the middle nitrogen atom. While **5a** crystallizes in a monoclinic space group ($P2_1/c$), **5b** is present in an orthorhombic one (*Pbca*; Figure 6. Interestingly, they show a difference in density of about 0.1 g cm^{-3}, whereby **5a** has 1.858 g cm^{-3} at 127 K and **5b** 1.757 g cm^{-3} at 143 K.

Both compounds show a comparable coordination behavior with the dicyanamido ligands linking the central metals to four different copper atoms forming two-dimensional polymers. Upon closer examination, it becomes clear that the only

© 2020 The Authors. Published by Wiley-VCH Verlag GmbH & Co. KGaA

difference between the two is the arrangement of the tetrazole ligands. While in **5b** the heterocycles of one side all point to the same side in **5a** they alternate, allowing a denser packing and explaining the higher density (Figure 7).

Compared to the other complexes, the structures of **6a** and **6b** are outstanding due to the insertion of an additional bridging ligand. The anhydrous compound **6a** crystallizes in the triclinic space group *P*−1 with a density of 1.817 g cm ^{3} (110 K) and the monohydrate in the monoclinic space group *C*2/*c* with a slightly lower density (1.752 g cm ^{3} @ 127 K). In both cases, the central metals are coordinated by two tetrazoles and four DCA nitrogen atoms. Like in **5a** and **5b**, the anions are binding with one outer and the middle nitrogen atom. The molecular unit of **6b** is completed by an additional crystal water molecule (Figure 8).

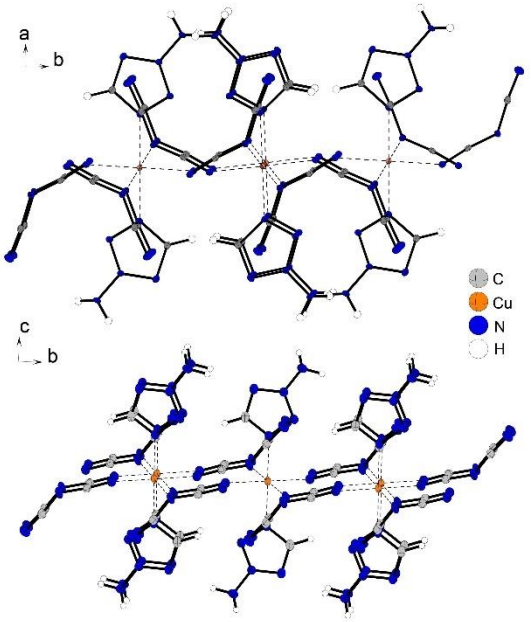


Figure 7. Two-dimensional polymeric structure of **5a** (top) and **5b** (bottom).

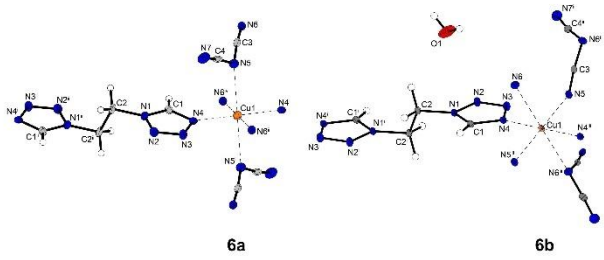


Figure 8. Copper(II) coordination environment of **6a** (left) and of **6b** (right). Selected bond lengths of **6a** (Å): Cu1–N4 2.027(3), Cu1–N5 2.438(3), Cu1–N6^{iii} 1.958(3). Selected bond angels of **6a** (°): N4–Cu1–N5^{i} 93.14(12), N4–Cu1–N4^{i} 180.00, N4–Cu1–N6^{iv} 90.82(13). Symmetry codes of **6a**: i) 2-x, −y, −z; ii) 2-x, −1-y, 1-z; iii) 1-x, −y, −z; iv) 1 + x, y, z. Selected bond lengths of **6b** (Å): Cu1–N4 2.0094(14), Cu1–N5 1.9619(14), Cu1–N6 2.4851(15). Selected bond angels of **6b** (°): N4–Cu1–N6 86.20(5), N4–Cu1–N4^{iii} 180.00, N4–Cu1–N5^{iii} 90.22(6). Symmetry codes of **6b**: i) −x, −y, 1-z; ii) x, 1-y, 0.5 + z; iii) 0.5-x, 0.5-y, 1-z.

Nevertheless, **6b** is not just simply the monohydrate of **6a**. A closer examination of the crystal structures reveals the difference of **6a** forming a two-dimensional and **6b** a three-dimensional structure. Similar to compounds **1**–**3**, in **6a** two anions each are bridging between the same two central metals leading to the formation of polymeric chains. The additional linking of the ditetrazolyl ligand is causing an enhancement of the dimension to polymeric layers (Figure 9).

The dte ligand is also increasing the dimension in complex **6b**, but here the DCA anions are already forming 2D-layers, similar to complex **5a** and **5b**. This results in a three-dimensional polymeric structure of **6b** (Figure 10). The structure favors the storage of water, which is why **6b** crystallizes as monohydrate.

Physiochemical Properties

All synthesized compounds, except **3** and **6b**, were investigated regarding their thermal properties and sensitivities towards external stimuli. In order to check the isomeric purity of compounds **5a** and **5b**, they were further investigated by powder X-ray diffraction.

Thermal Analysis

Compounds **1**, **2**, **4**, **5a**, **5b**, and **6a** were characterized by differential thermal analysis (DTA) with a linear heating rate of

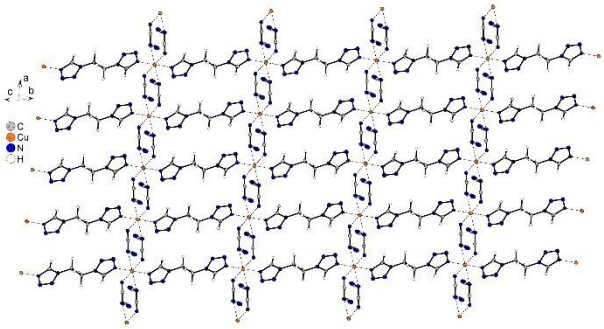


Figure 9. Two-dimensional polymeric structure of **6a**.

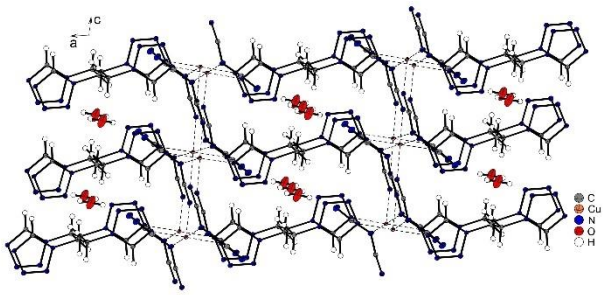


Figure 10. View along the *b* axis of three-dimensional polymeric structure of **6b**.

© 2020 The Authors. Published by Wiley-VCH Verlag GmbH & Co. KGaA

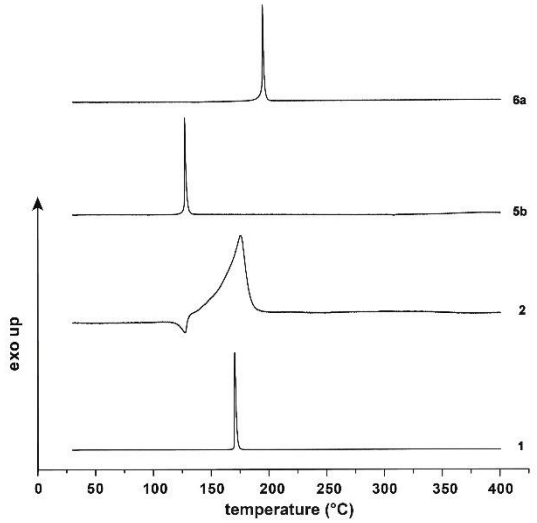


Figure 11. DTA plots of compounds **1**, **2**, **5b** and **6a**.

Table 1. Thermal stability measurements by DTA[a], as well as sensitivities towards impact, friction and ESD of compounds **1**–**7**.[b]

	T_{exo}[c] (°C)	IS[d] (J)	FS[e] (N)	ESD[f] (mJ)
1	170	8	>360	>1500
2	131	6	192	1500
4	141	6	144	1350
5a	129	9	80	540
5b	126	9	80	540
6a	193	10	>360	1220
7	254	40	>360	630

[a] Onset temperatures at a heating rate of 5 °C min^{-1}. [b] Determined at a grain size <100 µm. [c] Exothermic peak, which indicates decomposition. [d] Impact sensitivity according to the BAM drop hammer (method 1 of 6). [e] Friction sensitivity according to the BAM friction tester (method 1 of 6). [f] Electrostatic discharge sensitivity (OZM XSpark10 ESD tester); impact: insensitive >40 J, less sensitive ≥35 J, sensitive ≥4 J, and very sensitive ≤3 J; friction: insensitive >360 N, less sensitive =360 N, sensitive <360 N and >80 N, very sensitive ≤80 N, and extremely sensitive ≤10 N. According to the UN Recommendations on the Transport of Dangerous Goods.

ß = 5 °C min^{-1} in the range of 30 to 400 °C. The DTA plots are shown in Figures 11 and S3.

The experiments (Table 1) reveal that all complexes possess lower decomposition points (126–193 °C) compared to pure Cu $(DCA)_2$ (254 °C). Furthermore, compound **2** is the only one showing an endothermic event right before its decomposition. Closer examination using thermogravimetric analysis (TGA) proves the compounds' stability up to their corresponding exothermic decomposition temperatures, revealing a melting point for complex **2** at 126 °C (Figures 12 and S4).

Sensitivities

Except for **3** and **6b**, the energetic properties of all compounds were investigated. The sensitivities towards impact, friction, and electrostatic discharge are summarized in Table 1. The impact sensitivities are in the range of 6–10 J and therefore, the complexes have to be classified as sensitive according to the UN Recommendations on the Transport of Dangerous Goods. Only the salt **7** is classified as less sensitive with a value of 40 J.

Concerning the friction sensitivities, compounds **1**, **6a** and **7** can be classified as insensitive (>360 N). In contrast, complexes **2**, **4**, **5a** and **5b** have to be classified as sensitive, with values between 80 N (**5a**, **5b**) and 192 N (**2**). It can be seen that the energetic character of pure copper(II) dicyanamide is getting increased through the coordination of nitrogen-rich ligands. Interestingly the two different polymorphs **5a** and **5b** do not show major aberrations in their energetic properties.

Powder diffraction

For a more detailed investigation, compounds **5a** and **5b** were applied to X-ray powder diffraction measurements (Figure 13).

Small variations in the orthorhombic species **5b** can be attributed to the temperature differences of single-crystal and powder X-ray diffraction. Therefore, it is possible to synthesize **5b** isomerically pure. However, in the case of **5a** contamination with the second polymorph are observable and further research is necessary for selective synthesis of it.

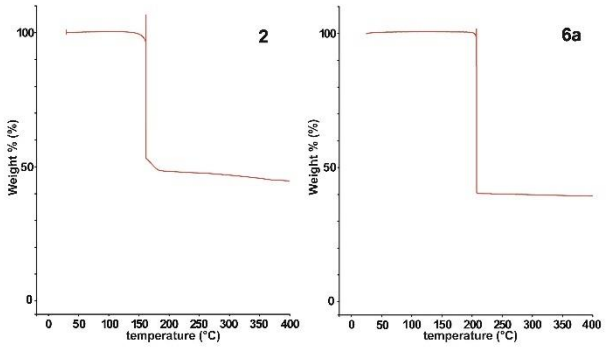


Figure 12. TGA plots of compounds **2** and **6a**.

Conclusion

In this work, eight new nitrogen-rich copper(II) dicyanamide complexes based on *N*-substituted tetrazole ligands were synthesized. Due to the good coordination behavior of dicyanamide, they can all be obtained without the inclusion of water. Only the formation of a 3D-polymeric side-species allows the inclusion of guest solvent molecules. All complexes were investigated by low-temperature single-crystal X-ray experiments and their polymeric structure examined in detail. The energetic properties and thermal behavior of the low water-soluble six ECC were determined and showed moderate sensitivities (*IS* >6, *FS* >80 N). This allows the safe handling of

© 2020 The Authors. Published by Wiley-VCH Verlag GmbH & Co. KGaA

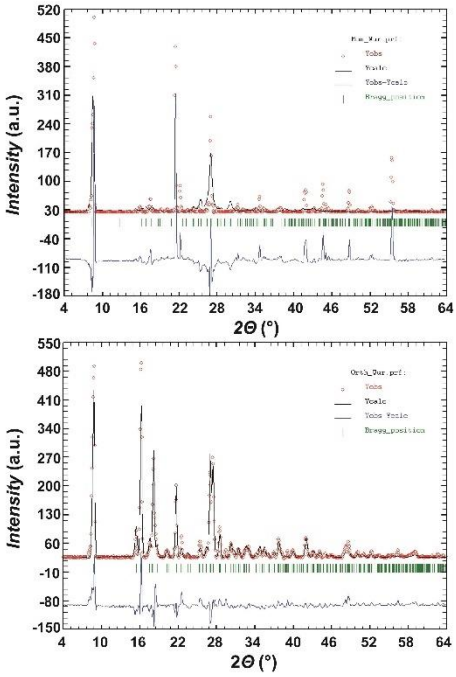


Figure 13. Powder diffraction experiments (comparison (blue) of the measured (red) and calculated (black) data) of compounds **5a** (top) and **5b** (bottom).

the complexes, which could be used as potential energetic additives e.g. burn rate catalysts. Also, a non-energetic use as magnetic switches could be possible. Especially compounds **4** and **5b** show promising properties for the use as energetic metal-organic frameworks (EMOF).

Experimental Section

Caution! All investigated compounds are energetic materials, which partly show increased sensitivities towards various stimuli (e.g. elevated temperatures, impact, friction or electronic discharge). Although no incidents occurred, proper security precautions (safety glasses, face shield, earthed equipment and shoes, leather jacket, Kevlar sleeves, and earplugs) have to be worn while synthesizing and handling the described compounds.

Detailed information on chemicals, syntheses, as well as analytical data and methods of **1**–**6** can be found in the Supplementary Information.

General procedure for the preparation of copper(II) dicyanamide complexes (**1**–**5a** and **6a**): To a solution of copper(II) nitrate trihydrate (60.4 mg, 0.25 mmol, 1 eq) in water (1 mL) the corresponding ligand (**1**: 1-methyl-5*H*-tetrazole (42.0 mg, 0.5 mmol, 2 eq); **2**: 1-azidoethyl-5*H*-tetrazole (69.6 mg, 0.5 mmol, 2 eq); **3**: 1-amino-5-methyltetrazole (49.6 mg, 0.5 mmol, 2 eq); **4**: 1-amino-5*H*-tetrazole (42.5 mg, 0.5 mmol, 2 eq); **5a**: 2-amino-5*H*-tetrazole (42.5 mg, 0.5 mmol, 2 eq); **6a**: 1,2-di(tetrazol-1-yl)ethane (41.55 mg, 0.25 mmol, 1 eq)) was added. After stirring for a minute, an aqueous solution (1 mL) of sodium dicyanamide (44.5 mg, 0.5 mmol, 2 eq) was added, the mixture was stirred for one more minute at room temperature and left for crystallization. After formation of the crystalline products, the compounds were filtered off, washed with cold ethanol and dried in air. All compounds were obtained in the form of single crystals suitable for X-ray diffraction.

Acknowledgements

For financial support of this work by Ludwig-Maximilian University (LMU). The authors would like to thank especially Prof. Dr Thomas M. Klapötke for providing facilities and great scientifc support, Prof. Dr Jürgen Evers for the X-ray powder diffraction experiments, Dr. Peter Mayer for helping with X-ray crystal structure analysis and Mr. Marcus Lommel for his great contribution to this work.

Conflict of Interest

The authors declare no conflict of interest.

Keywords: bridging ligands · copper · dicyanamides · energetic materials · nitrogen heterocycles

[1] T. Güthner, B. Mertschenk in *Cyanamides. Ullmann's Encyclopedia of Industrial Chemistry*, Wiley-VCH, Weinheim, **2006**.
[2] J. L. Manson, T. Lancaster, S. J. Blundell, Y. Qiu, J. Singleton, P. Sengupta, F. L. Pratt, J. Kang, C. Lee, M.-H. Whangbo, *Polyhedron* **2010**, *29*, 514–520.
[3] a) A. M. Kini, U. Geiser, H. H. Wang, K. D. Carlson, J. M. Williams, W. K. Kwok, K. G. Vandervoort, J. E. Thompson, D. L. Stupka, D. Jung, M. Whangbo , *Inorg. Chem.* **1990**, *29*, 2555–2557; b) T. Chivers, D. Gates, X. Li, I. Manners, M. Parvez, *Inorg. Chem.* **1999**, *38*, 70–76; c) N. Delgado-Mellado, J. García, F. Rodríguez, R. D. Rogers, *ChemPlusChem* **2019**, *84*, 872–881; d) S. R. Batten, P. Jensen, B. Moubaraki, K. S. Murray, *Chem. Commun.* **2000**, *23*, 2331–2332; e) Y.-H. Joo, H. Gao, Y. Zhang, J. M. Shreeve, *Inorg. Chem.* **2010**, *49*, 3282–3288; f) Z. Jalový, Z. Padělková, R. Jirásko, R. Matyáš, M. Holčapek, O. Němec, M. Novotná, L. Mišková, *Polyhedron* **2012**, *44*, 88–100; g) O. Reckeweg, A. Schulz, F. J. DiSalvo, *Z. Naturforsch. B* **2013**, *68*, 296–300; h) J. G. Díaz, A. G. Albor, E. V. Jaime, V. Vrábel, J. Kozísek , *Acta Crystallogr. Sect. E* **2012**, *68*, 89–90.
[4] a) M. Dahan, E. Komarala, L. Fadeev, A. K. Chinnam, A. Shlomovich, S. Lipstman, S. P. Padi, H. Haustein, M. Gozin, B. A. Rosen , *J. Mater. Chem. A* **2019**, *7*, 141–149; b) J. Lavoie, C.-F. Petre, P.-Y. Paradis, C. Dubois, *Propellants Explos. Pyrotech.* **2017**, *42*, 149–157; c) T. M. Klapötke, P. Mayer, J. Stierstorfer, J. J. Weigand, *J. Mater. Chem.* **2008**, *18*, 5248–5258.
[5] a) M. Havastijova, J. Kohout, H. Köhler, G. Ondrejovic, *Z. Anorg. Allg. Chem.* **1988**, *566*, 111–120; b) J. Carranza, J. Sletten, F. Lloret, M. Julve, *Inorg. Chim. Acta* **2004**, *357*, 3304–3316; c) R. Sen, A. Bhattacharjee, P. Gütlich, Y. Miyashita, K.-I. Okamoto, S. Koner, *Inorg. Chim. Acta* **2009**, *362*, 4663–4670; d) G. A. van Albada, M. G. van der Horst, S. J. Teat, P. Gamez, O. Roubeau, I. Mutikainen, U. Turpeinen, J. Reedijk, *Polyhedron* **2009**, *28*, 1541–1545; e) J. Kozísek, J. G. Díaz, A. G. Albor , *Acta Crystallogr. Sect. E* **2007**, *63*, 125–126; f) M. Biswas, G. M. Rosair, G. Pilet, S. Mitra, *Inorg. Chim. Acta* **2007**, *360*, 695–699; g) J. Ding, H. Ge, Y. Zhang, B. Li, Y. Zhang, *J. Mol. Struct.* **2006**, *782*, 143–149.
[6] a) K. E. Bessler, L. L. Romualdo, V. M. Deflon, *Z. Anorg. Allg. Chem.* **2000**, *626*, 1942–1945; b) M.-J. Crawford, A. Ellern, K. Karaghiosoff, F. Martin, P. Mayer, *Inorg. Chem.* **2010**, *49*, 2674–2683.
[7] a) T. W. Myers, J. A. Bjorgaard, K. E. Brown, D. E. Chavez, S. K. Hanson, R. J. Scharff, S. Tretiak, J. M. Veauthier , *J. Am. Chem. Soc.* **2016**, *138*, 4685–4692; b) Q. Zhang, J. M. Shreeve, *Angew. Chem.* **2014**, *126*, 2574–2576; *Angew. Chem. Int. Ed.* **2014**, *53*, 2540–2542; c) Q. Zhang, J. M. Shreeve, *Angew. Chem. Int. Ed.* **2014**, *53*, 2540–2542; *Angew. Chem.* **2014**, *126*, 2574–2576; d) N. Szimhardt, M. H. H. Wurzenberger, L. Zeisel, M. S. Gruhne, M. Lommel, J. Stierstorfer, *J. Mater. Chem. A* **2018**, *6*, 16257–16272.

© 2020 The Authors. Published by Wiley-VCH Verlag GmbH & Co. KGaA

[8] a) E. C. Johnson, J. J. Sabatini, D. E. Chavez, L. A. Wells, J. E. Banning, R. C. Sausa, E. F. C. Byrd, J. A. Orlicki , *ChemPlusChem* **2020**, *85*, 237–239; b) L. M. Foroughi, R. A. Wiscons, D. R. Du Bois, A. J. Matzger, *Chem. Commun.* **2020**, *56*, 2111–2114; c) Ł. Gutowski, W. Trzciński, M. Szala, *ChemPlusChem* **2018**, *83*, 87–91; d) B. Wang, H. Xiong, G. Cheng, H. Yang, *ChemPlusChem* **2018**, *83*, 439–447; e) L. L. Fershtat, N. N. Makhova, *ChemPlusChem* **2020**, *85*, 13–42.

[9] Gas phase enthalpies of formation were calculated using the atomization method ($\Delta_f H^0_{(g,M)} = H_{(M)} - \Sigma H^0_{(A)} + \Sigma \Delta_f H^0_{(A)}$) using Gaussian09 computed CBS-4 M electronic enthalpies.

[10] a) O. Reckeweg, R. E. Dinnebier, A. Schulz, B. Blaschkowski, C. Schneck, T. Schleid, *Z. Naturforsch. B: Anorg. Chem. Org. Chem.* **2017**, *72*, 159–165; b) Q. Rayée, P. T. Nguyen, T. Segato, M.-P. Delplancke-Ogletree, T. Doneux, C. Buess-Herman, *J. Electroanal. Chem.* **2018**, *819*, 331–337.

[11] Z. Li, T. Zhang, J. Zhang, L. Wang, Y. Zhong (Beijing Institute Tech), CN 201910821846, China **2019**.

[12] a) P. N. Gaponik, M. M. Degtyarik, A. S. Lyakhov, V. E. Matulis, O. A. Ivashkevih, M. Quesada, J. Reedijk, *Inorg. Chim. Acta* **2005**, *358*, 3949–3957; b) M. H. H. Wurzenberger, M. S. Gruhne, M. Lommel, N. Szimhardt, T. M. Klapötke, J. Stierstorfer, *Chem. Asian J.* **2019**, *14*, 2018–2028; c) K. Sakai, J. P. Anselme, *Org. Prep. Proced. Int.* **1975**, *7*, 61–65; d) R. Raap, *Can. J. Chem.*, **1969**, *47*, 3677; e) P. J. v. Koningsbruggen, Y. Garcia, G. Bravic, D. Chasseau, O. Kahn, *Inorg. Chim. Acta* **2001**, *326*, 101–105.

[13] CCDC 1986804 (**1**), 1986806 (**2**), 1986801 (**3**), 1986805 (**4**), 1986800 (**5a**), 1986803 (**5b**), 1986802 (**6a**) and 1986807 (**6b**) contains the supplementary crystallographic data for this paper. These data can be obtained free of charge from The Cambridge Crystallographic Data Centre.

Manuscript received: March 2, 2020
Revised manuscript received: March 20, 2020
Accepted manuscript online: March 23, 2020

© 2020 The Authors. Published by Wiley-VCH Verlag GmbH & Co. KGaA

Appendix 17

Refinement of Copper(II) Azide with 1-Alkyl-5H-tetrazoles: Adaptable Energetic Complexes

M. H. H. Wurzenberger, M. Lommel, M. S. Gruhne, N. Szimhardt, J. Stierstorfer

Angew. Chem. Int. Ed. **2020**, *59*, 12367–12370

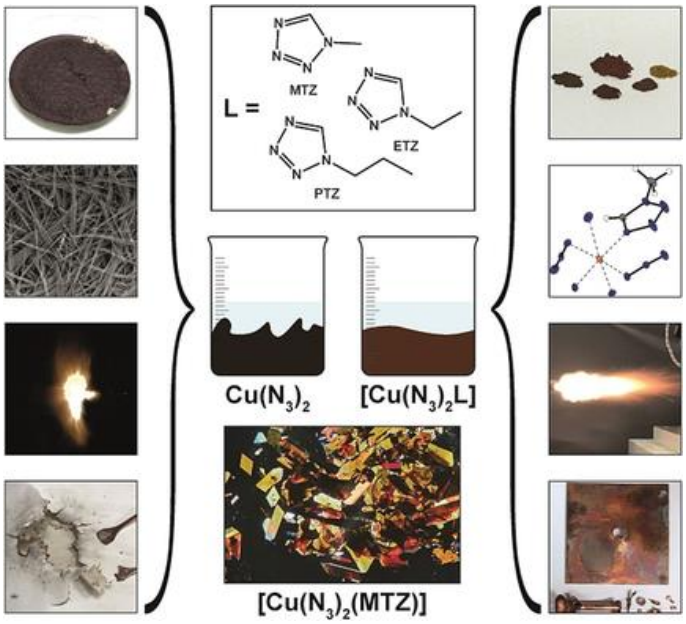
https://doi.org/10.1002/anie.202002823.

Veredelung von Kupfer(II)-azid mittels 1-Alkyl-5*H*-tetrazolen: Leistungsfähige energetische Komplexverbindungen

M. H. H. Wurzenberger, M. Lommel, M. S. Gruhne, N. Szimhardt, J. Stierstorfer,

Angew. Chem. **2020**, *132*, 12466–12469.

https://doi.org/10.1002/ange.202002823.



Supplementary Information:
https://onlinelibrary.wiley.com/action/downloadSupplement?doi=10.1002%2Fanie.202002823&file=anie202002823-sup-0001-misc_information.pdf

How to cite: *Angew. Chem. Int. Ed.* **2020**, *59*, 12367–12370
International Edition: doi.org/10.1002/anie.202002823
German Edition: doi.org/10.1002/ange.202002823

Explosives

Refinement of Copper(II) Azide with 1-Alkyl-5*H*-tetrazoles: Adaptable Energetic Complexes

*Maximilian H. H. Wurzenberger, Marcus Lommel, Michael S. Gruhne, Norbert Szimhardt, and Jörg Stierstorfer**

In memory of Rolf Huisgen

Abstract: *A concept for stabilizing highly sensitive and explosive copper(II) azide with 1-N-substituted tetrazoles is described. It was possible to stabilize the system by the use of highly endothermic, nitrogen-rich ligands. The sensitivities of the resulting energetic copper coordination compounds can be tuned further by variation of the alkyl chain of the ligands and by phlegmatization of the complexes with classical additives during the synthesis. It is demonstrated, using the compound based on 1-methyl-5H-tetrazole ([$Cu(N_3)_2$(MTZ)], **1**) that this class of complexes can be applied as a potential replacement for both lead azide (LA) and lead styphnate (LS). The complex was extensively investigated according to its chemical (elemental analysis, single-crystal and powder X-ray diffraction, IR spectroscopy, scanning electron microscopy) and physico-chemical properties (differential thermal analysis, sensitivities towards impact, friction, and electrostatic discharge) compared to pure copper(II) azide.*

The azide anion (N_3^-) has attracted the attention of chemists worldwide for centuries. While some are scared because of its high nitrogen content and consequent explosive character, others are attracted for the same reason. Due to their highly versatile nature, azides are not only commonly used in organic synthesis and pharmaceutics but also in energetic materials such as in airbags, propellants, and explosives.[1] In recent years, numerous new pentazolate (N_5^-) derivatives synthesized by selective C–N bond cleavage of pentazoles using mCPBA and iron glycinate generated excitement in the field.[2] The first compound of these five-membered heterocycles was described by Huisgen and Ugi. It was detected after a 1,3-dipolar cycloaddition (Huisgen reaction) of a benzene diazonium chloride and lithium azide.[3] A further current global interest is the replacement of lead-containing explosives, particularly lead azide and lead styphnate, with safer and less toxic energetic materials.[4] Various metal salts have been described as substitutes, mainly silver azide and rarely copper azides, although only cupric $Cu(N_3)_2$ (and not cuprous CuN_3) might be of practical interest. However, both azides are extremely sensitive towards impact and friction. Furthermore, $Cu(N_3)_2$ is decomposed by mineral acids as well as bases and slowly forms basic cupric azides (e.g. $Cu(N_3)_2 \cdot x\,Cu(OH)_2$ ($x = 1$–3) and $Cu(N_3)_2 \cdot 8\,CuO$) when exposed to humidity (Figure S18 in the Supporting Information).[5]

In this work, a procedure is described for the syntheses of nitrogen-rich copper(II) azide complexes involving 5*H*-tetrazoles. This concept is explained using three ligands exemplarily (1-methyl-5*H*-tetrazole (MTZ), 1-ethyl-5*H*-tetrazole (ETZ), and 1-propyl-5*H*-tetrazole (PTZ)). Moreover, many different tetrazoles, as well as triazoles, are potential candidates. The application of these compounds yielded two independent patents,[6] which can be discussed and described scientifically. In general, it is known that metal azides (e.g. Mn, Nb, Ti, Zr, Hf, V, W, and Mo) can be stabilized with nitrogen donor ligands, although only some complexes of $Cu(N_3)_2$ have been reported in the literature and are rarely discussed as energetic materials.[7]

For the preparation of energetic coordination compounds (ECC) based on copper(II) azide, the implementation of nitrogen-rich ligands leads to the blockage of one coordination site, resulting in stabilization in comparison to the pure metal azide (Figure 1).

The azide anion is extremely toxic to the environment and all life forms, but its effect on the ecological system depends strongly on the compounds' solubility. High water solubility implies a potent absorption through the skin and mucous membranes, leading to serious consequences for even relatively small amounts (≈ 10 mg).[8] Copper(II) azide was chosen as the main building block due to the expected low solubility of the obtained compounds, resulting in a low risk to the environment. The driving force for the synthesis of the copper(II) azide complexes is the instantaneous precipitation of the compounds after the addition of sodium azide. To prevent the formation of pure copper(II) azide, an aqueous solution of sodium azide was slowly added to in situ generated complexes of soluble copper(II) salts with ligands (Scheme 1). The tetrazoles were synthesized starting from the corresponding alkyl amines or bromides.[9] The addition of sodium azide led to the products' formation as brown precipitates in very good yields (90–93%). The suspensions were mechanically stirred for 10 min, filtered off, washed with water as well as ethanol, and dried in air. Single crystals suitable for X-ray

[*] M. H. H. Wurzenberger, M. Lommel, M. S. Gruhne, Dr. N. Szimhardt, Dr. J. Stierstorfer
Department of Chemistry, University of Munich (LMU)
Butenandtstrasse 5–13 (D), 81377 München (Germany)
E-mail: jst@cup.uni-muenchen.de
Supporting information and the ORCID identification number(s) for the author(s) of this article can be found under: https://doi.org/10.1002/anie.202002823.

© 2020 The Authors. Published by Wiley-VCH Verlag GmbH & Co. KGaA. This is an open access article under the terms of the Creative Commons Attribution License, which permits use, distribution and reproduction in any medium, provided the original work is properly cited.

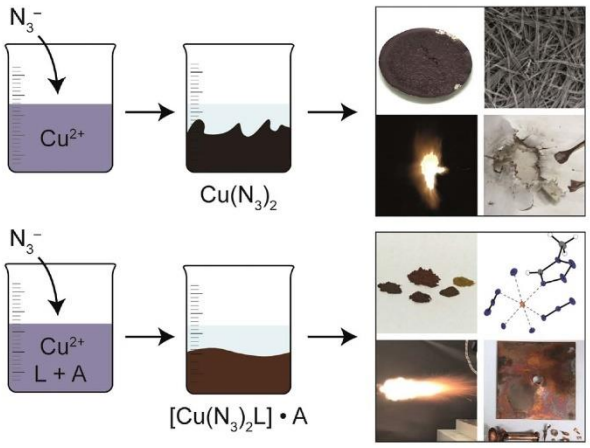
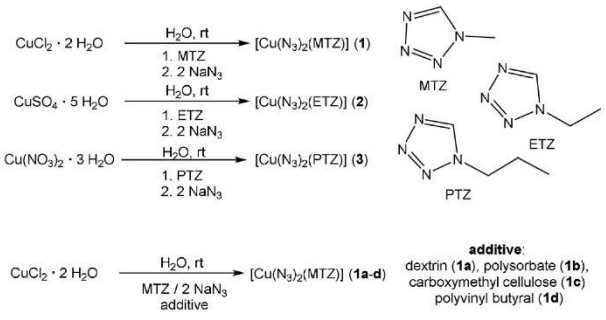


Figure 1. Top: Addition of azide to an aqueous solution of copper(II) leads to instant precipitation of copper azide. Safe handling is almost impossible as the material shows characteristics of a contact explosive. Bottom: Addition of azide to an aqueous solution of copper(II), ligand (L), and additive (A) leads to precipitation of a copper(II) azide complex. The resulting compound can be safely applied as primary explosive.



Scheme 1. Syntheses of selected tetrazole complexes **1–3** as pure and as phlegmatized compounds **1a–1d**.

diffraction were obtained by layering concentrated aqueous and ethanolic solutions to ensure slow formation at the phase boundary. It is also possible to phlegmatize the energetic coordination compounds by using common additives such as carboxymethyl cellulose during the synthesis according to modified literature procedures.[10]

All compounds show a similar coordination behavior and therefore $[Cu(N_3)_2(MTZ)]$ (**1**) is discussed exemplarily for all three presented complexes. The other structures can be found in the Supporting Information (Figures S3 and S4). Compound **1** crystallizes in the form of red-brown plates in the monoclinic space group $P2_1/c$ with four formula units per unit cell and a calculated density of 2.036 g cm^{-3} at 123 K.[11] The molecular unit consists of one copper(II) central cation coordinated by one MTZ ligand in equatorial position and five azido anions (Figure 2A). The two different bridging modes of the azides (Figure 2C) favor the formation of 2D layers (Figure 2B). Two of three equatorial counterions bridge between the same two central metals (N4) and the

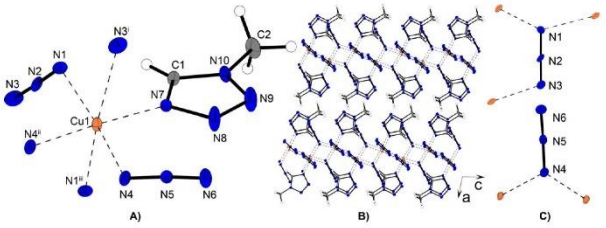


Figure 2. A) Copper(II) coordination environment of $[Cu(N_3)_2(MTZ)]$ (**1**). Selected bond lengths (Å): Cu1–N1 2.013(3), Cu1–N3^{i} 2.563(5), Cu1–N4 2.003(3), Cu1–N7 1.996(3); selected bond angles (°): N1–Cu1–N4 171.74(12), N1–Cu1–N7 90.96(12), N1–Cu1–N3^{i} 84.99(15), N4–Cu1–N7 96.59(13). Symmetry codes: (i) $-x$, $0.5+y$, $0.5-z$; (ii) $-x$, $1-y$, $1-z$; (iii) $-x$, $-0.5+y$, $0.5-z$. B) Polymeric structure of **1** caused by bridging anions along the *b* and *c* axes, leading to the formation of 2D layers stacked above each other along the *a* axis. C) Two different coordination modes of the azide anions in **1**.

other three azides link three different copper(II) atoms (N1 and N3).

Even though no difficulties were encountered during the synthesis or handling of the ECC, pure $[Cu(N_3)_2(MTZ)]$ (**1**) must be classified as very sensitive and does not possess a no-fire-level against impact and friction stimuli according to standard BAM methods. Compared to pure $Cu(N_3)_2$, which shows capricious properties when handled and can even explode when slightly touched (Figure S20), compound **1** can be easily controlled.

For even safer handling and regulation of the particle size in powder form, the compound can be phlegmatized during crystallization. For the stabilization of complex **1**, the commonly used additives dextrin (**1a**), polysorbate 80 (**1b**), carboxymethyl cellulose (**1c**), and polyvinyl butyral (**1d**) were used. The phlegmatization has no significant effect on the exothermic decomposition points but in every case a more or less successful desensitization is evident. The most effective additive is carboxymethyl cellulose (**1c**), leading to sensitivities of 2 J and 0.75 N, which are in the range of those of LA and LS (Table 1). Another approach for reducing the sensitivities of copper(II) azide complexes is the usage of tetrazole ligands with longer alkyl chains at the N1 position. The elongation of the alkyl chain to an ethyl substituent decreases the friction sensitivity to 4.5 N (**2**) and the further extension with a propyl rest to 10 N (**3**). A similar proportionality can be observed for the electrostatic discharge (ESD) values.

Due to the possible formation of different species, elemental analysis may represent only an average value. Confirmation of the purity of the bulk material was therefore exemplarily achieved through powder diffraction measurements of compounds **1** and **2** (Figure S5). Scanning electron microscopy (SEM) was performed to investigate the compounds' morphology and to further examine the influence of the phlegmatization on the crystal habitus and size. It can be seen that the pure copper azide forms agglomerates made of very fine, intergrown crystalline fibers, which are the reason for its high mechanical sensitivity. Pure complex **1** shows a distribution of crystallites. The different additives used for phlegmatization make it possible to tune the crystal morphol-

 © 2020 The Authors. Published by Wiley-VCH Verlag GmbH & Co. KGaA, Weinheim

Table 1: Thermal stability and sensitivities against external stimuli of pure complexes **1–3** and phlegmatized **1** compared to pure cupric azide as well as commercially used lead azide (LA) and lead styphnate (LS).[12]

Cmpd.	T_{exo}[a]	*IS* [J][b]	*FS* [N][c]	*ESD* [mJ][d]
$Cu(N_3)_2$	205	$\ll 1$[5]	$\ll 0.1$	< 0.28
1	148	< 1	< 0.1	0.79
2	134	3	4.5	33
3	148	2.5	10	112
1a	148	< 1	0.40	8.3
1b	149	1.5	0.60	3.9
1c	150	2	0.75	0.54
1d	151	4	0.45	0.33
LA	320–360	2.5–4.0	0.1–1.0	6.0–12
LS	275–280	2.5–5.0	0.5–1.5	0.02–1.0

[a] Temperature of decomposition indicated by exothermic event according to DTA (onset temperatures at a heating rate of 5 °C min^{-1}). [b] Impact sensitivity according to the BAM drop hammer (method 1 of 6). [c] Friction sensitivity according to the BAM friction tester (method 1 of 6). [d] Electrostatic discharge sensitivity (OZM XSpark10 ESD tester).

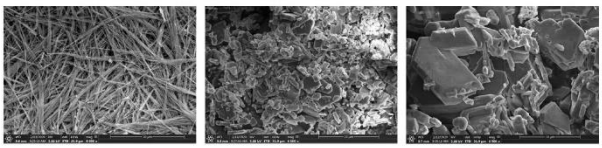


Figure 3. SEM images of $Cu(N_3)_2$ (8000× enlargement), pure complex **1** (6500× enlargement) and dextrinated **1a** (6500× enlargement).



Figure 4. Positive PETN (left) and RDX (right) initiation tests with 5 mg of the coordination compound **1**.



Figure 5. Components for the preparation of lead-free percussion caps based on $[Cu(N_3)_2(MTZ)]$ (**1**) (left and middle) and moment of ignition thereof (right).

ogy (plate- or needle-like) and corresponding size distribution (Figure 3 and Figures S6–S11).

For use as a potential LA replacement, ECC **1** was tested in classical initiation capability tests. Therefore, 200 mg of the common secondary explosives pentaerythritol tetranitrate (PETN) and 1,3,5-trinitro-1,3,5-triazinane (RDX) was pressed into copper shells and initiated with either pure complex **1** or the most promising phlegmatized complex (**1c**). Further information on the test setup can be found in the Supporting Information (Figure S14). As little as 5 mg of compound **1** is able to initiate RDX reliably, making the compound an extremely efficient initiating substance (Figure 4). The initiating properties of **1** far outstrip those of recently published green primary explosives with claimed outstanding initiation efficiency.[13] The phlegmatized complex **1c** (50 mg) also showed positive results in initiating both PETN and RDX (Figure S15).

Apart from its intended use as a potential replacement for lead azide, **1** can also serve as a replacement for lead styphnate for the use in priming mixtures (PM). Since the beginning of the 20th century, LS has been one of the most commonly used primary explosives in PM, which are applied to produce a flame instead of a detonation and are mostly utilized in percussion caps.[5] Complex **1** was used for the preparation of a lead-free PM, which was compared to a commercially available one based on lead styphnate. The PM consisted of 15 % $[Cu(N_3)_2(MTZ)]$ as well as 85 % of a mixture made up of barium nitrate, aluminum, antimony trisulfide, and PETN. The created flame is sufficient for the inflammation of propellant powder (Figure 5). The resulting time–pressure curve generated with a 7.62 NATO cartridge filled with nitrocellulose powder shows an ideal gradient (Figure S17 and Table S3). The sensitivities of the new PM are similar to values of a commercial mixture (Table S2).

Finally, it was successfully shown that copper(II) azide can be stabilized with *N*-substituted tetrazole ligands and the sensitivities can be adjusted by the choice of ligand or phlegmatization during the synthesis. The resulting complexes are manageable energetic materials, which can be used as potential lead-free primary explosives.

Acknowledgements

This work was supported financially by Ludwig-Maximilian University (LMU). We thank especially Prof. Dr. Thomas M. Klapötke for providing his research facilities, Prof. Dr Jürgen Evers for the recording of the X-ray powder diffraction, Dr. Steffen Schmidt for investigating compounds by SEM, and Simon Endraß for his great contribution to this work. We also thank Dr. Manuel Joas for helpful discussions as well as Cornelia Unger and Esra Soner for proofreading of the manuscript.

 © 2020 The Authors. Published by Wiley-VCH Verlag GmbH & Co. KGaA, Weinheim

Conflict of interest

The authors declare no conflict of interest.

Keywords: azides · copper complexes · nitrogen heterocycles · phlegmatization · X-ray diffraction

[1] S. Bräse, C. Gil, K. Knepper, V. Zimmermann, *Angew. Chem. Int. Ed.* **2005**, *44*, 5188–5240; *Angew. Chem.* **2005**, *117*, 5320–5374.

[2] a) Y. Xu, Q. Wang, C. Shen, Q. Lin, P. Wang, M. Lu, *Nature* **2017**, *549*, 78–81; b) C. Zhang, C. Sun, B. Hu, C. Yu, M. Lu, *Science* **2017**, *355*, 374–376.

[3] R. Huisgen, I. Ugi, *Angew. Chem.* **1956**, *68*, 705–706.

[4] a) J. C. Bennion, N. Chowdhury, J. W. Kampf, A. J. Matzger, *Angew. Chem. Int. Ed.* **2016**, *55*, 13118–13121; *Angew. Chem.* **2016**, *128*, 13312–13315; b) A. A. Larin, N. V. Muravyev, A. N. Pivkina, K. Yu. Suponitsky, I. V. Ananyev, D. V. Khakimov, L. L. Fershtat, N. N. Makhova, *Chem. Eur. J.* **2019**, *25*, 4225–4233; c) G. Bélanger-Chabot, M. Rahm, R. Haiges, K. O. Christe, *Angew. Chem. Int. Ed.* **2015**, *54*, 11730–11734; *Angew. Chem.* **2015**, *127*, 11896–11900.

[5] R. Matyáš, J. Pachman in *Primary Explosives*, Springer, Heidelberg, **2013**, pp. 96–100.

[6] a) H. Zöllner, M. Joas, R. Schirra, K. Kaplan (DynITEC GmbH), WO 2018011134A1, Germany, **2018**; b) T. Klapötke, J. Stierstorfer, M. H. H. Wurzenberger, N. Szimhardt (EMTO GmbH), WO 2019134867A1, Germany, **2019**.

[7] a) A. Hinz, M. Köckerling, *ChemistrySelect* **2017**, *2*, 9654–9657; b) J.-C. Liu, D.-G. Fu, J.-Z. Zhuang, C.-Y. Duana, X.-Z. You, *J. Chem. Soc. Dalton Trans.* **1999**, 2337–2342; c) P.-P. Liu, A.-L. Cheng, N. Liu, W.-W. Sun, E.-Q. Gao, *Chem. Mater.* **2007**, *19*, 2724–2726; d) R. Haiges, R. J. Buszek, J. A. Boatz, K. O. Christe, *Angew. Chem. Int. Ed.* **2014**, *53*, 8200–8205; *Angew. Chem.* **2014**, *126*, 8339–8344; e) T. Saal, P. Deokar, K. O. Christe, R. Haiges, *Eur. J. Inorg. Chem.* **2019**, 2388–2391; f) T. Saal, P. Deokar, K. O. Christe, R. Haiges, *Dalton Trans.* **2019**, *48*, 806–813.

[8] J. J. Jobelius, H.-D. Scharff in *Ullmann's Encyclopedia of Industrial Chemistry*, 7th ed. (Ed.: B. Elvers), Wiley-VCH, Weinheim, **2012**, pp. 97–101.

[9] a) P. N. Gaponik, V. P. Karavai, Y. V. Grigor'ev, *Chem. Heterocycl. Compd.* **1985**, *21*, 1255–1258; b) P. N. Gaponik, M. M. Degtyarik, A. S. Lyakhov, V. E. Matulis, O. A. Ivashkevich, M. Quesada, J. Reedijk, *Inorg. Chim. Acta* **2005**, *358*, 3949–3957.

[10] T. Costain, F. B. Wells, in *Technology of the inorganic azides* (Eds.: H. D. Fair, Walker R. F.), Plenum Press, New York, **1977**, pp. 11–54.

[11] Selected X-ray data: red-brown plate, monoclinic, $P2_1/c$, $a=11.4746(7)$, $b=6.1867(3)$, $c=10.8165(5)$ Å, $\beta=100.078(5)°$, $V=756.01(7)$ Å^3, $Z=4$, $\rho=2.036$ g cm^{-3}, $wR2=10.69\%$, $S=1.06$, CCDC 1985252 contains the supplementary crystallographic data for this paper. These data can be obtained free of charge from The Cambridge Crystallographic Data Centre.

[12] a) J. Köhler, R. Meyer, A. Homburg in *Explosivstoffe*, Wiley-VCH, Weinheim, **2008**; b) T. M. Klapötke in *Energetic Materials Encyclopedia*, Walter De Gruyter, Berlin, Boston, **2018**; c) M. S. Gruhne, M. Lommel, M. H. H. Wurzenberger, N. Szimhardt, T. M. Klapötke, J. Stierstorfer, *Propellants Explos. Pyrotech.* **2020**, *45*, 147–153.

[13] a) W. Huang, Y. Tang, G. H. Imler, D. A. Parrish, J. M. Shreeve, *J. Am. Chem. Soc.* **2020**, *142*, 3652–3657; b) M. Deng, Y. Feng, W. Zhang, X. Qi, Q. Zhang, *Nat. Commun.* **2019**, *10*, 1339.

Manuscript received: February 24, 2020
Accepted manuscript online: April 1, 2020
Version of record online: April 21, 2020

 © 2020 The Authors. Published by Wiley-VCH Verlag GmbH & Co. KGaA, Weinheim

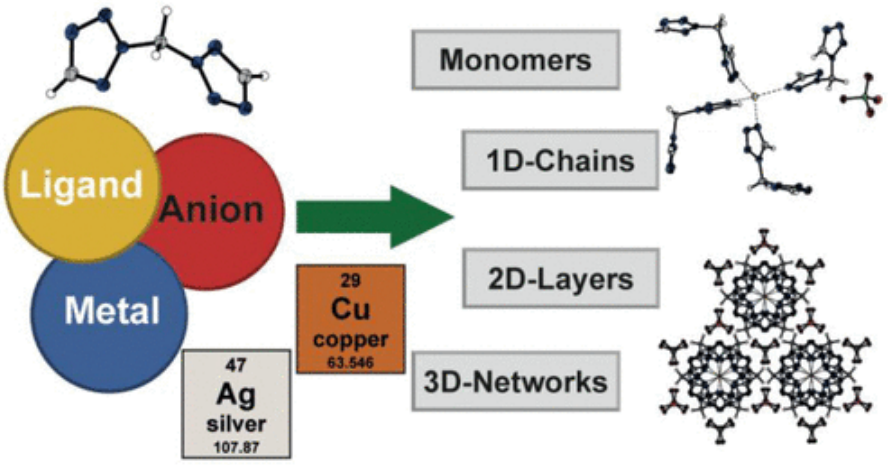
Appendix 18

Closing the Gap: Synthesis of Three Isomeric N,N-Ditetrazolymethane Ligands and Their Coordination Proficiency in Adaptable Laser Responsive Copper(II) and Sensitive Silver(I) Complexes

M. H. H. Wurzenberger, V. Braun, M. Lommel, T. M. Klapötke, J. Stierstorfer

Inorg. Chem. **2020**, *59*, 10938−10952.

https://dx.doi.org/10.1021/acs.inorgchem.0c01403.



Supplementary Information:
https://pubs.acs.org/doi/suppl/10.1021/acs.inorgchem.0c01403/suppl_file/ic0c01403_si_001.pdf

Inorganic Chemistry

pubs.acs.org/IC Article

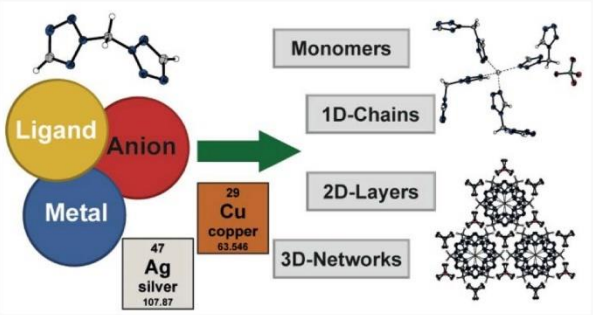
Closing the Gap: Synthesis of Three Isomeric *N,N*-Ditetrazolymethane Ligands and Their Coordination Proficiency in Adaptable Laser Responsive Copper(II) and Sensitive Silver(I) Complexes

Maximilian H. H. Wurzenberger, Vanessa Braun, Marcus Lommel, Thomas M. Klapötke, and Jörg Stierstorfer*

Cite This: *Inorg. Chem.* 2020, 59, 10938−10952 Read Online

ACCESS | Metrics & More | Article Recommendations | Supporting Information

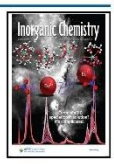
ABSTRACT: *N,N*-Substituted ditetrazolylalkanes are widely used molecules in the field of coordination chemistry and are known with different alkyl chain lengths. The missing fragment within this row is presented by the elementary methylene-bridged ditetrazoles. The three different isomers (di(tetrazol-1-yl)methane (1,1-dtm, **1**), (tetrazol-1-yl)(tetrazol-2-yl)methane (1,2-dtm, **2**), and di-(tetrazol-2-yl)methane (2,2-dtm, **3**)) were synthesized in a convenient one-step reaction. All of them were successfully incorporated as neutral ligands in 15 new energetic coordination compounds (ECC) based on Cu^{2+} and Ag^{+} as well as different anions (nitrate, picrate (PA), styphnate (TNR), trinitrophlor-oglucinate (TNPG), and perchlorate) revealing an extraordinary coordination behavior of the ligands compared to other 5*H*-ditetrazolylalkanes. All compounds were extensively characterized using single-crystal X-ray diffraction experiments, infrared spectroscopy (IR), elemental analysis (EA), and differential thermal analysis (DTA). Furthermore, the sensitivities were determined using standard techniques, and Hirshfeld surface calculations of the ligands were applied to explain their significant divergences to external stimuli. The ECC possess very good exothermic decomposition temperatures up to 242 °C. The ignition of all colored complexes was tested in laser experiments, and two copper(II) perchlorate compounds showed promising results in classic initiation capability tests using pentaerythritol tetranitrate (PETN).



INTRODUCTION

Since the discovery of tetrazoles by Baldin in 1885, its derivatives continue to attract the attention of chemists, and there is still a growing worldwide research interest in this field of nitrogen-rich chemistry.[1] The scope of tetrazole-based compounds is manifold and ranges from medicinal chemistry to molecular electronics to energetic materials.[2] However, it took until 1985 for the very first 5*H*-ditetrazolylalkane to be synthesized by Gaponik et al., namely 1,2-di(tetrazol-1-yl)ethane (dte; Chart 1B).[3] Another 15 years later the first-ever complex based on this class of molecules (idtp; Chart 1B) was reported in the literature.[4] Since then the chemistry of 5*H*-ditetrazolylalkanes rapidly grew, and due to the resulting unique properties, they were incorporated as neutral ligands in myriad numbers of transition metal complexes.[5] In general, the *N*1,*N*1-substituted ligands can be easily and isomerically pure obtained by [3+1+1] cyclization reactions starting from the corresponding diamino compounds.[3] They are reported for chain lengths with 2−10 and 12 carbon atoms and can all be incorporated as neutral ligands in coordination compounds. Most of them were used in combination with iron(II) tetrafluoroborate, perchlorate, or hexafluorophosphate as spin-crossover systems in magnetic studies.[6] It is a known fact that the yields during the ligand syntheses drastically drop for compounds with an odd-numbered chain length between the two tetrazole substituents.[7] Another approach for synthesizing *N*-substituted ditetrazoly-lalkanes deals with the reaction of the corresponding dihaloalkanes with tetrazolates. This synthetic pathway results in an isomeric mixture of the symmetrically *N*1,*N*1- and *N*2,*N*2- as well as asymmetrically *N*1,*N*2-substituted molecules (Chart 1 A)). Although this technique further increases the variability of possible ligands and new coordination compounds, it is rather uncommon in the literature.[8]

Received: May 15, 2020
Published: July 13, 2020

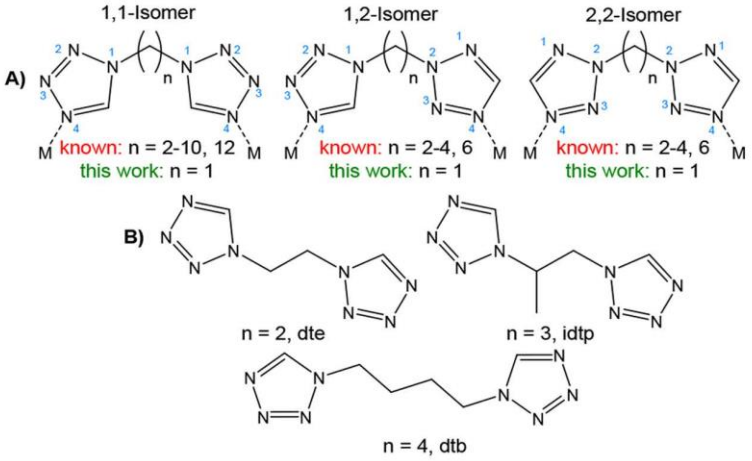


Downloaded via LMU MUENCHEN on February 16, 2022 at 08:05:49 (UTC).
See https://pubs.acs.org/sharingguidelines for options on how to legitimately share published articles.

ACS Publications © 2020 American Chemical Society

https://dx.doi.org/10.1021/acs.inorgchem.0c01403
Inorg. Chem. 2020, 59, 10938−10952

Chart 1. A) Literature Known 5*H*-Ditetrazolylalkanes and Their Bridging Behavior in Transition Metal Complexes and B) Most Commonly Used Ligands[9]



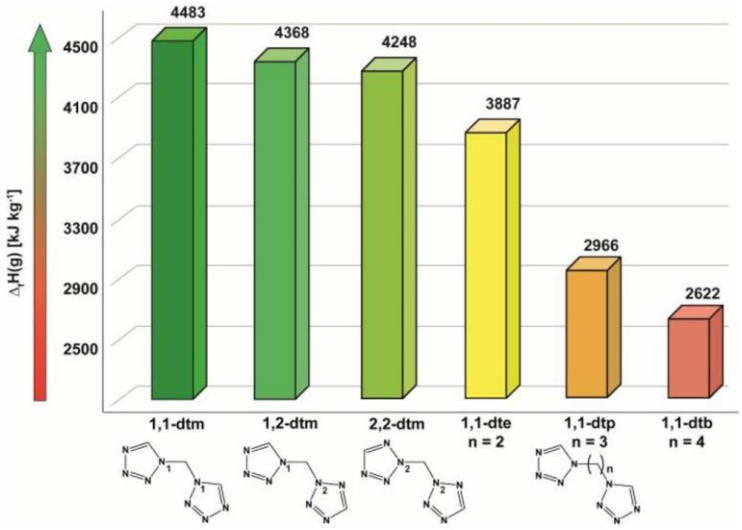


Figure 1. Overview of several calculated gas phase enthalpies of formation for *N*,*N*-disubstituted ditetrazoles showing increased values for the ditetrazolyl-methane ligands. Enthalpies of formation were calculated using the atomization method ($\Delta_f H^0_{(g,M)} = H_{(M)} - \Sigma H^0_{(A)} + \Sigma \Delta_f H^0_{(A)}$) using Gaussian09 computed CBS-4 M electronic enthalpies.

As already mentioned, complexes based on 5*H*-ditetrazolylalkane ligands are known for a variety of different transition metals as well as anions and are discussed for diverse applications, especially as spin crossover materials or molecular magnetics.[10] However, it should not be forgotten that these tetrazoles occasionally show high heat of formations and are potential energetic materials. As expected, the heat of formation increases with shorter alkane bridges, which is shown in Figure 1. Especially their transition metal complexes based on (per)-chlorates and azides can easily be applied as explosives, making their use in the nonenergy field more difficult or even dangerous.[11] Lead azide (LA) and lead styphnate (LS) are still dominating the field of primary explosives in both military and industrial applications. Due to their high toxicity, both were added to the candidate list of authorization (substances of very high concern, Annex XIV) for the REACH (Registration, Evaluation, Authorization and Restriction of Chemicals) regulations in 2011.[12] In addition, executed firing and missile trainings in "friendly" areas are leading to a strong demand for less toxic primary explosives to reduce the contamination with lead.[13] In recent years, the concept of energetic coordination compounds (ECC) has received increasing attention. It allows easy tuning of the energetic performance as well as other properties, (e.g., optical or thermal) of the products by simply exchanging one of the building blocks.[14] The evolving requirements for energetic materials, such as reduced toxicity, safer handling, and easy synthesis, have highly influenced the research of scientists around the world.[15]

For closing the gap in this highly suitable class of ligands, we report on the first synthesis of methylene bridged *N*,*N*-substituted ditetrazoles. These ligands, consisting of the shortest possible alkyl chain, were successfully incorporated in new ECC and show a fascinating coordination diversity. Due to the increased heat of formations compared to other ditetrazoles, they allow the enormous increase of the energetic performance of the resulting complexes. Following the concept of energetic

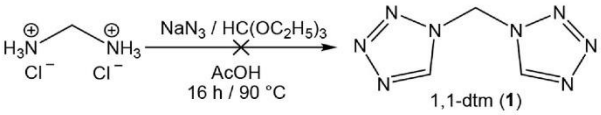
https://dx.doi.org/10.1021/acs.inorgchem.0c01403
Inorg. Chem. 2020, 59, 10938−10952

coordination compounds, the sensitivities and properties of ECC can be easily adjusted by exchanging either the anions or central metals.

SYNTHESIS AND ANALYSIS OF THE PURE LIGANDS

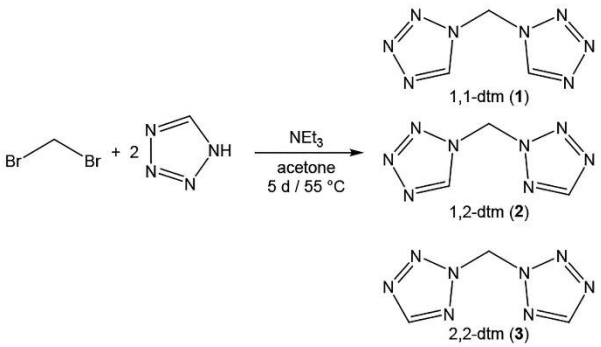
As already mentioned above, there are two common methods for the syntheses of *N*-substituted ditetrazolylalkanes either starting from the corresponding diamine (also hydrochlorides) or dihaloalkanes. Analogous to the synthesis of 1,3-di(tetrazol-1-yl)propane, no product could be obtained during the selective regioisomeric reaction toward **1** staring from methylenediamine dihydrochloride (Scheme 1).[16] Therefore, dibromomethane

Scheme 1. Failed Attempt for the Selective Synthesis of 1



was reacted with *in situ* generated triethylammonium tetrazolate according to a slightly modified literature procedure.[17] This nucleophilic substitution reaction is leading to an isomeric mixture of **1**–**3** in an overall yield of 28% (Scheme 2). The

Scheme 2. Synthesis of Isomers 1–3 Starting from Dibromomethane, 1,5*H*-Tetrazole, and Triethylamine



relatively low amount of product could be explained by the steric hindrance of two tetrazole rings bounded to the same carbon atom, also extending the reaction time to 5 days. It was not possible to increase the yields when using diiodomethane instead of dibromomethane or switching to synthetic protocols based on phase-transfer catalyst or different bases (NaOH, KOH). The three different isomers can be easily separated by flash column chromatography on silica gel using a gradient of pentane and ethyl acetate. The pure compounds were obtained in differing yields of 7% (**1**), 12% (**2**), and 9% (**3**).

The different isomers can easily be distinguished by IR spectroscopy (Figure S1) as well as ^{1}H and ^{13}C NMR spectroscopy. Also, the very useful two-dimensional ^{1}H–^{15}N-HMBC method was applied, which drastically decreases the measurement time compared to normal ^{15}N NMR spectroscopy (Figures 2–4). The free ligands **1**–**3** crystallize in monoclinic ($P2_1/c$; **1**) or orthorhombic space groups ($Fdd2$; **2** and **3**) with comparable densities (1.605 g cm^{-3} (**2**) < 1.632 g cm^{-3} (**3**) < 1.637 g cm^{-3} (**1**)). The bond lengths are in the typical range of *N*,*N*′-substituted ditetrazoles, and all angles around the methylene bridges are close to the one of a perfect tetrahedron (Figure 5).[4]

Comparing the onset temperatures of the three ligands **1**–**3** during DTA experiments, it becomes clear that **3** is the thermally most stable one (184 °C), followed by **1** (152 °C) and **2** (138 °C). They all show an endothermic event, which can be attributed to their melting points (proven by TGA measurements (Figure 6)), whereas **1** decomposes immediately afterward. The same trend for the decomposition temperatures can also be observed in all ECC when comparing the ones based on the same central metals and anions. Interestingly, coordination to metal centers yields in most cases to a significant increase of the resulting decomposition temperatures.

The sensitivities toward both, impact and friction, of the free ligands increase in the following order: **1** (8 J, >360 N) < **2** (2 J, 168 N) < **3** (1.5 J, 84 N). Hirshfeld surface and fingerprint analysis supports the trend of increasing sensitivity. In all three ligands, strong attracting intermolecular N–H bonds are present, explaining the overall stability of the high nitrogen containing molecules (Figure 7). **3** bears a decreased amount of N–H interactions in the crystal and increased repulsive N–N

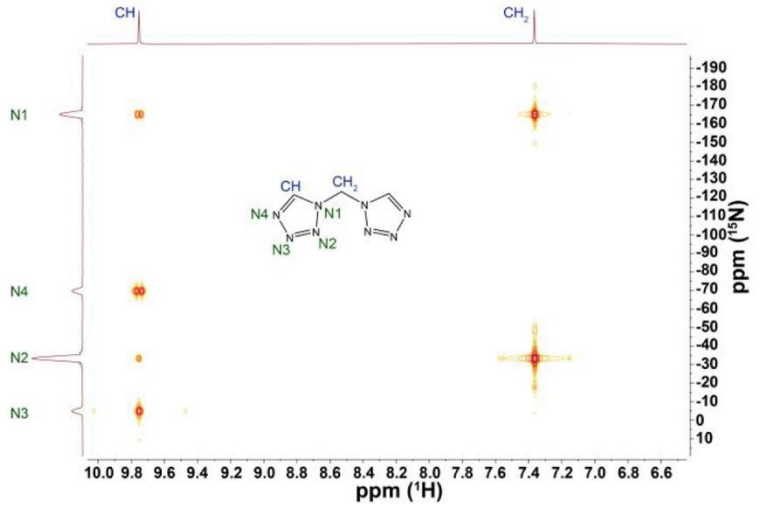


Figure 2. Two-dimensional ^{1}H–^{15}N-HMBC NMR spectra of **1** (DMSO-d_6, 25 °C): δ = −4.7 (N3), −33.2 (N2), −69.6 (N4), −165.1 ppm (N1).

https://dx.doi.org/10.1021/acs.inorgchem.0c01403
Inorg. Chem. 2020, 59, 10938–10952

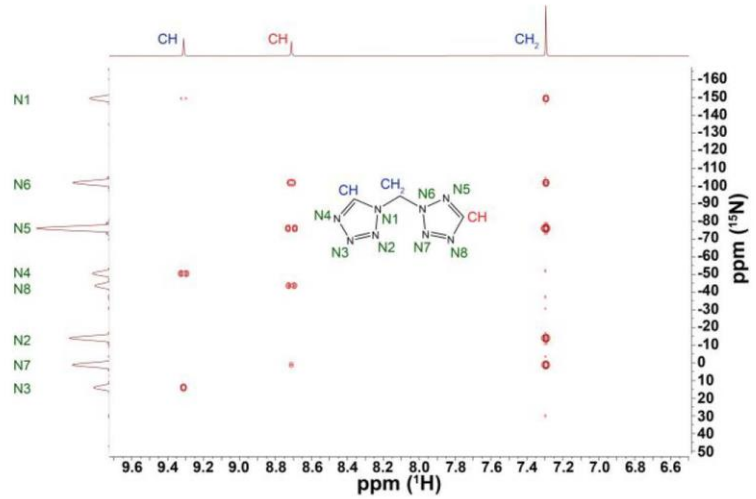


Figure 3. Two-dimensional $^{1}H-^{15}N$-HMBC NMR spectra of **2** (MeCN-d_3, 25 °C): δ = 14.2 (N3), 1.3 (N7), −14.0 (N2), −43.7 (N8), −50.4 (N4), −76.2 (N5), −102.0 (N6), −149.7 ppm (N1).

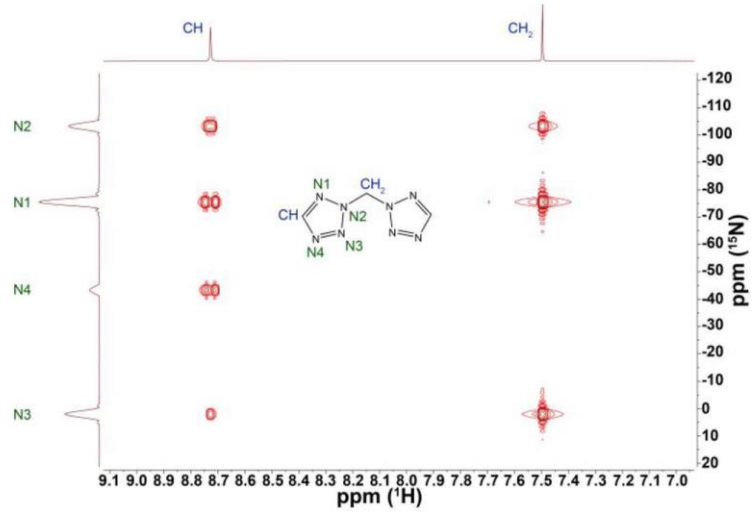


Figure 4. Two-dimensional $^{1}H-^{15}N$-HMBC NMR spectra of **3** (MeCN-d_3, 25 °C): δ = 2.1 (N3), −43.3 (N7), −75.4 (N4), 10.7 (N1), −103.2 ppm (N2).

and H−H interactions. The resulting decrease in intermolecular hydrogen bonding is a known cause for destabilization.[18] Ligand **2**, whose sensitivity lies between the ones of **1** and **3**, shows a very similar distribution of attracting (N−H) and repulsive (N−N, H−H) interactions as **1**, according to fingerprint analysis. Nevertheless, the slightly higher sensitivity is explained by the distribution of present H−H bonds. Even though the amount of repulsive H−H interactions remains nearly the same, they are now promoted as the hydrogen atoms are approaching at a closer distance, pictured by an H−H-spike to the lower left of the fingerprint plot (Figure 7, red surface). With regard to temperature stability, the compounds behave contradictory to the Hirshfeld analysis, and no explanation can be given so far. For a better comparison with known explosives, important detonation parameters of **1**−**3** were calculated using the EXPLO5 code and compared with the ones of TNT (Table 1).[19] Compound **2** shows interesting properties as a melt-cast explosive.

SYNTHESIS OF THE COORDINATION COMPOUNDS

In general, the 5*H*-ditetrazolyl ligands in transition metal complexes show a bridging character leading to the formation of polymeric structures. There are only a few coordination compounds reported in the literature where they act as terminal ligands, either in the presence of bridging anions or in mixed systems, containing both bridging and terminal ligands.[20] During the synthesis of ECC based on the different isomers **1**−**3**, it becomes clear that the nitrogen-rich molecules are often present as terminal ligands. Therefore, the first attempts were performed with 4 (silver(I) complexes) or 6 (copper(II) complexes) equiv. of ligand, and after determining the compositions, the compounds were synthesized using the exact ratio of metal salt to ligand. Except for Ag^{+} and Cu^{2+}, perchlorate salts of the eco-friendly Mn^{2+}, Fe^{2+}, and Zn^{2+} cations were used for the syntheses of coordination compounds, but in all cases only starting material could be obtained.

https://dx.doi.org/10.1021/acs.inorgchem.0c01403
Inorg. Chem. 2020, 59, 10938−10952

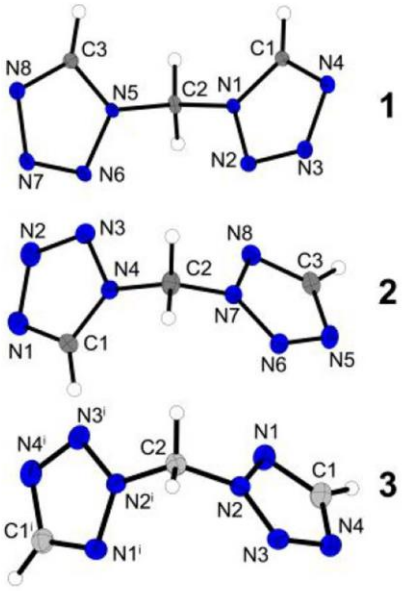


Figure 5. Crystal structures of **1**–**3**. Thermal ellipsoids of non-hydrogen atoms in all structures are set to the 50% probability level. Selected bond lengths of **1** (Å): N1–N2 1.3502(15), N1–C1 1.3377(19), N1–C2 1.4546(19). Selected bond angles of **1** (deg): N2–N1–C1 108.47(11), N2–N1–C2 121.24(11), N1–C2–N5 111.27(11). Selected bond lengths of **2** (Å): N3–N41.347(3), N4–C1 1.328(4), N4–C2 1.453(3). Selected bond angles of **2** (deg): N3–N4–C1 108.5(2), N3–N4–C2 120.1(2), N4–C2–N7 110.2(2). Selected bond lengths of **3** (Å): N1–N2 1.327(2), N1–C1 1.320(2), N2–C2 1.451(2). Selected bond angles of **3** (deg): N1–N2–N3 114.24(13), N1–N2–C2 122.99(12), N2–C2–N2^{i} 110.07(19). Symmetry code of **3**: (i) $-x$, $1-y$, z.

For synthesizing silver complexes **4**–**8**, both starting materials were dissolved in a mixture of water/acetonitrile and stirred for 5 min at room temperature after combining both solutions (Scheme 3). While standing in air the compounds started to crystallize within minutes to 1 day. The attempted synthesis of a silver(I) perchlorate complex based on 2,2-dtm led to the decomposition of the starting materials, which also occurred in the dark. In the case of the copper(II) complexes **9**–**18**, it is highly important to use the right solvents and reaction temperatures, to prevent the formation of aqua species (**9**–**12**) or amorph compounds with an unclear composition (**13**–**18**) (Schemes 4 and 5). **9** is the only copper(II) nitrate-based ECC, which could be isolated without any starting material residues or side species. It crystallized from the reaction solution within 5 days after combining the dissolved metal salt and ligand. When reacting the ditetrazoles with copper(II) perchlorate in water, different aqua complexes were obtained. Changing the solvents to organic ones allows the precipitations of the anhydrous compounds. Single crystals were obtained from the mother liquors after filtration. Complexes **10**–**12** can also be crystallized within 1 h when using ethanol as solvent at 80 °C and adding water dropwise until the precipitates are completely dissolved. For the first step of the syntheses of nitroaromatic complexes **13**–**18**, basic copper(II) carbonate was reacted with 2 equiv. of the corresponding acid to ensure complete conversion.

Even in the case of ECC **14** with the presence of a double-deprotonated anion, 2 equiv. of styphnic acid had to be used. The dissolved ligands were added dropwise at elevated temperatures to the *in situ* synthesized copper(II) trinitrophenolates, and the corresponding complexes were obtained as single crystals within some hours. Due to the low yields of **3** during the ligand synthesis and the high water content of the nitroaromatic complexes, no ECC based on this combination were attempted. Some of the complexes **13**–**18** show endothermic events during DTA measurements. Drying these compounds at 100 °C overnight resulted in anhydrous powders, which rapidly incorporate water again under ambient conditions.

■ CRYSTAL STRUCTURES OF THE ECC

All ECC were investigated by single-crystal X-ray diffraction experiments. The details of the crystal structures of compounds **15**, **17**, and **18**, as well as the measurements and refinement data of all structures, can be found in the SI (Tables S1–S5 and Figures S5 and S6).[21] The bond lengths as well as angles of the coordinating ditetrazoles in all complexes are comparable to the ones of the free ligands and are therefore not further discussed. The nitrogen-rich molecules solely bind via the N4 atoms of their heterocycles and, interestingly, in some cases only coordinate with one of the two tetrazole substituents.

Whereas all silver complexes, except **6**, show a 4-fold coordination around the central metal, the copper(II) compounds, except nitrate ECC **9**, possess an octahedral coordination sphere. The three silver nitrate complexes (**4**–**6**) all show different compositions with varying metal to ligand ratios explaining the differences in their density. While **4** crystallizes in the triclinic space group $P-1$ with a density of 2.112 g cm^{-3} (131 K), **5** and **6** are present in orthorhombic ($Pna2_1$) and monoclinic (Ia) space groups, respectively. With the highest ligand content, **5** also possesses the lowest density (1.886 g cm^{-3} @ 108 K), whereas it is the other way around for **6**

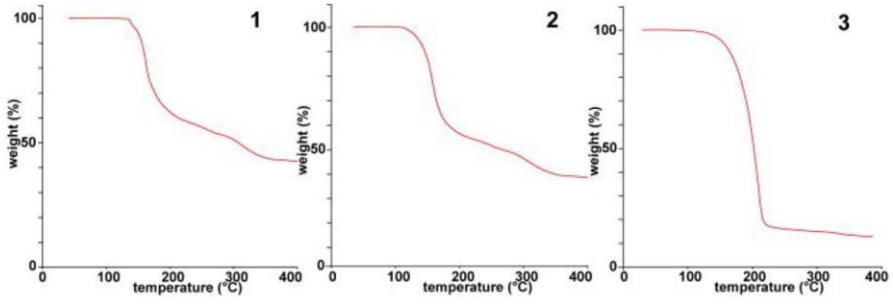


Figure 6. TGA plots of the dtm ligands revealing their stability up to the corresponding exothermic decomposition temperatures.

https://dx.doi.org/10.1021/acs.inorgchem.0c01403
Inorg. Chem. 2020, 59, 10938–10952

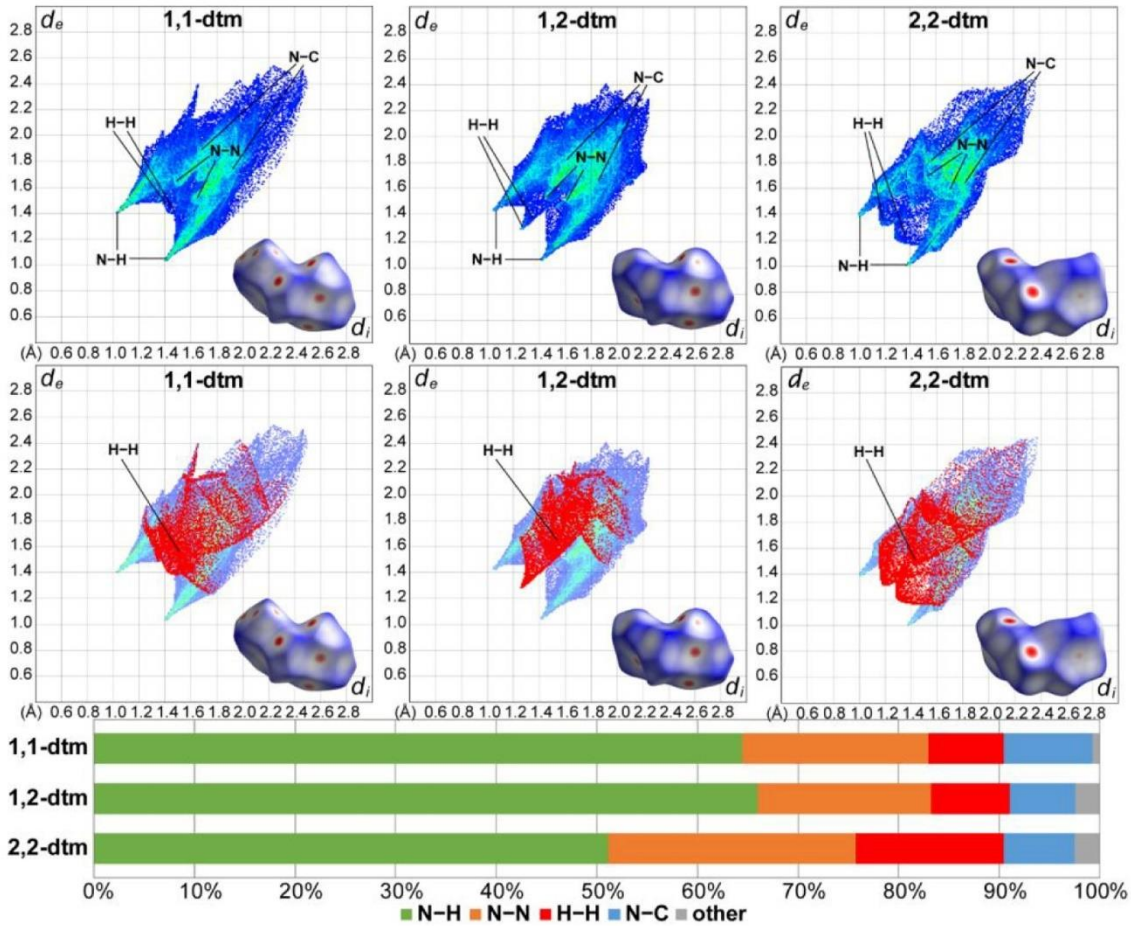


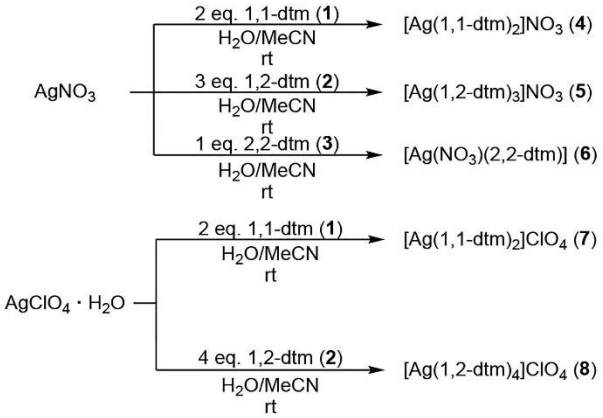
Figure 7. Two-dimensional fingerprint plots of the free ligands **1**–**3** together with their Hirshfeld surfaces. The atomic contacts percentage contribution to the Hirshfeld surface can be obtained from the bar chart.

Table 1. EXPLO5 6.05.02 Values of 1–3 Compared to TNT

	1	2	3	TNT
ρ^a [g cm^{-3}]	1.59	1.57	1.59	1.65
$\Omega_{CO_2}{}^b$ [%]	−84.14	−84.14	−84.14	−73.96
$\Delta_f H^{\circ c}$ [kJ mol^{-1}]	621	599	588	−261
$\Delta_f U^{\circ d}$ [kJ kg^{-1}]	4178	4035	3962	−171
$-\Delta_{ex} H^{\circ e}$ [kJ kg^{-1}]	4076	3938	3866	4427
T_{det} [K]	2850	2793	2752	3222
$P_{CJ}{}^f$ [GPa]	20.9	19.9	20.5	1.94
$V_{det}{}^g$ [m s^{-1}]	7829	7672	7749	6824
$V_0{}^h$ [L kg^{-1}]	776	777	775	633

[a]Measured X-ray densities converted to RT. [b]Oxygen balance (Ω = (xO−2yC−1/2zH)M/1600). [c]Calculated enthalpy of formation at 298.15 K. [d]Calculated energy of formation at 298.15 K. [e]Heat of explosion. [f]Detonation pressure. [g]Detonation velocity. [h]Volume of detonation gases (assuming only gaseous products).

Scheme 3. Synthesis of Silver Nitrate and Perchlorate Complexes 4–8

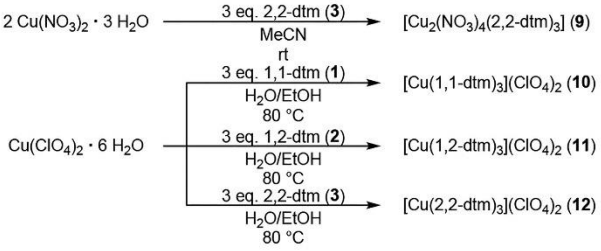


showing the highest density (2.404 g cm^{-3} @ 122 K) of all compounds. The molecular unit of ECC **4** consists of one silver cation, two coordinating ligands, and a nonbinding nitrate anion (Figure 8). The 4-fold coordination sphere around the central metal is caused by the bridging of the ligands between the same cations, leading to the formation of polymeric chains. The geometry can be described as an extended linear coordination. The N4–Ag1–N12 axis with Ag–N bond lengths of 2.254(4) Å gets bent by the elongated bounding (2.593(4) Å) of two more nitrogen atoms from linking ligands to an angle of 157.21(13)°.

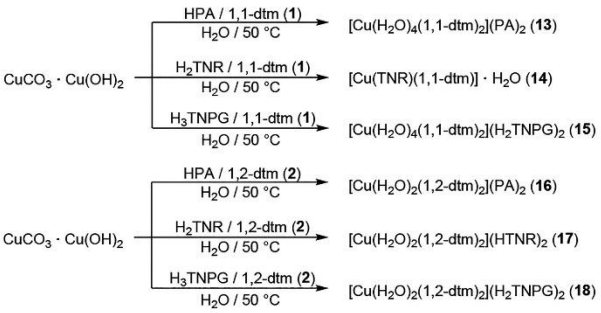
Like **4**, the silver cation in complex **5** is 4-fold coordinated by tetrazole rings, and the anion is not coordinating. In contrast, the geometry can be described as a strongly distorted tetrahedron

https://dx.doi.org/10.1021/acs.inorgchem.0c01403
Inorg. Chem. 2020, 59, 10938−10952

Scheme 4. Synthesis of Copper(II) Nitrate and Perchlorate Complexes 9–12



Scheme 5. Synthesis of Trinitroaromatic Complexes 13–18



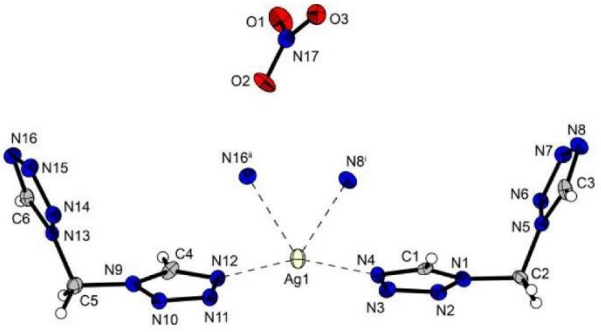


Figure 8. Silver(I) coordination environment of nitrate complex **4**. Selected bond lengths (Å): Ag1–N4 2.254(4), Ag1–N16^{ii} 2.593(4). Selected bond angles (deg): N4–Ag1–N8^{i} 84.83(12), N8^{i}–Ag1–N16^{ii} 78.86(13). Symmetry codes: (i) $-x$, $1-y$, $-z$; (ii) $1-x$, $-y$, $1-z$.

with a smaller deviation of the Ag–N bond lengths (2.261(3)–2.386(3) Å). The three different ligands present in the unit cell, all show a diverse coordination behavior. Whereas one of them is binding with both heterocycles to two different silver cations, the other two are only single coordinating, one with the 1*N*- and the second with the 2*N*-substituted ring (Figure 9). The linking of one ligand, in turn, leads to the formation of a polymeric structure in the form of a chain. Like in coordination compound **4**, the geometry around the silver cation in complex **6** can be described as an extended linear structure. The ligand is connecting two central metals (Ag1–N4 2.231(5) Å and Ag1–N8^{ii} 2.211(7) Å), and the elongated bounding of three oxygen atoms (2.542(5)–2.734(5) Å) is bending the N4–Ag1–N8^{ii} axis to 148.89(19)°, which is even stronger than in compound **4**. Interestingly, in this structure the nitrato anion is not only chelating one cation but also bridging to another one, leading to an uncommon 5-fold coordination sphere around the silver(I) central metal (Figure 10). The double linking of the

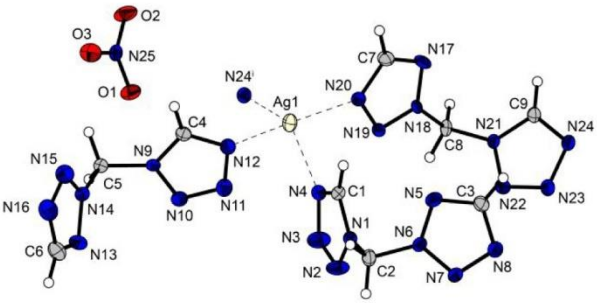


Figure 9. Silver(I) coordination environment of nitrate complex **5**. Selected bond lengths (Å): Ag1–N4 2.386(3), Ag1–N12 2.336(3), Ag1–N20 2.261(3). Selected bond angles (deg): N4–Ag1–N12 108.62(9), N4–Ag1–N20 99.66(9), N12–Ag1–N20 114.87(10), N20–Ag1–N24^{i} 135.69(10). Symmetry code: (i) $1-x$, $-y$, $-0.5+z$.

two different ligands is building a 2D-polymeric network (Figure 11).

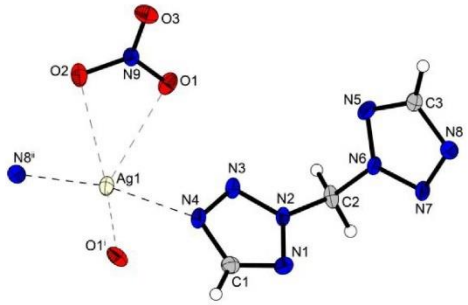


Figure 10. Silver(I) coordination environment of nitrate complex **6**. Selected bond lengths (Å): Ag1–O1 2.712(5), Ag1–O1^{i} 2.542(5), Ag1–O2 2.734(5). Selected bond angles (deg): O1–Ag1–O2 46.80(15), O1–Ag1–N4 78.82(16), O2–Ag1–N4 123.89(15). Symmetry codes: (i) $0.5+x$, $-y$, z; (ii) x, y, $-1+z$.

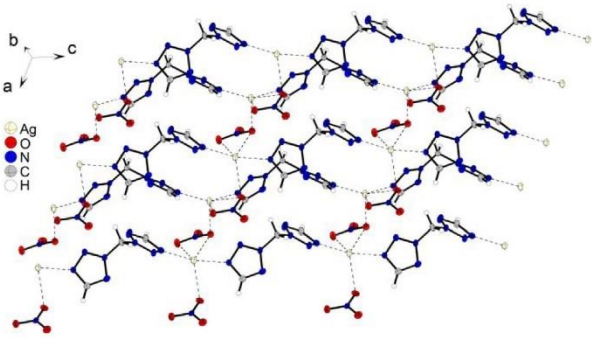


Figure 11. Polymeric structures of **6**.

The perchlorate complexes **7** and **8** show similar coordination geometries to the one of **4**. The linear structures are highly deviating from the ideal 180° by the elongated bonding of additional tetrazole ligands. Whereas the ligands in **7** are both bridging and leading to the formation of polymeric chains, the four ligands in **8** are solely coordinating with one of their rings building up complex monomers (Figure 12). Again, the different composition of the ligand/metal ratio is highly influencing the density. **7** crystallizes with a density of 2.190 g cm^{-3} at 128 K in the triclinic space group $P-1$. The higher ligand content in **8**,

https://dx.doi.org/10.1021/acs.inorgchem.0c01403
Inorg. Chem. 2020, 59, 10938–10952

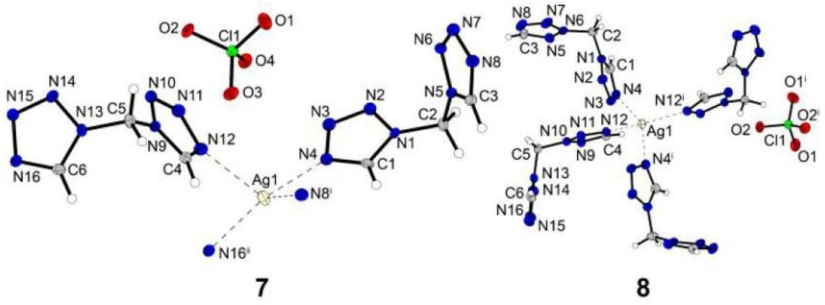


Figure 12. Coordination environment of perchlorate compound **7** and molecular unit of **8**. Selected bond lengths of **7** (Å): Ag1–N4 2.260(2), Ag1–N12 2.581(2), Ag1–N8^{i} 2.612(2), Ag1–N16^{ii} 2.259(2). Selected bond angles of **7** (deg): N4–Ag1–N12 114.85(8), N4–Ag1–N8^{i} 83.40(8), N4–Ag1–N16^{ii} 153.50(8). Symmetry codes of **7**: (i) 1–*x*, –*y*, 1–*z*; (ii) –*x*, 1–*y*, –*z*. Selected bond lengths of **8** (Å): Ag1–N4 2.419(2), Ag1–N12 2.3036(19). Selected bond angles of **8** (deg): N4–Ag1–N12 95.66(7), N4–Ag1–N4^{i} 99.92(7), N12–Ag1–N12^{i} 145.79(8). Symmetry code of **8**: (i) 0.5–*x*, *y*, 0.5–*z*.

which is crystallizing in the monoclinic space group $P2/n$, causes a lower density of 1.901 g cm^{-3} at 111 K.

Copper(II) nitrate complex **9** crystallizes as blue blocks in the monoclinic space group $I2/a$ with four formula units per unit cell and a calculated density of 1.945 g cm^{-3} at 109 K. The molecular unit is composed of a dimer of central metals bridged by one ligand. Each of the two copper(II) cations is further connected by a pair of ligands to the next dimeric unit, leading to the formation of polymeric chains. Apart from the three coordination sides occupied by nitrogen atoms, the coordination sphere is completed by two chelating nitrato ligands. The resulting molecular geometry around the copper central metal is a strongly disordered pentagonal bipyramid, which is very uncommon for copper(II) (Figure 13).

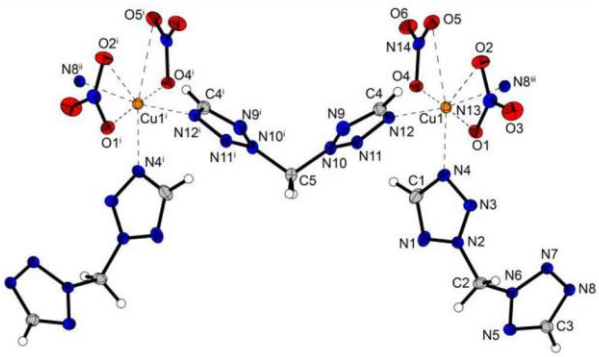


Figure 13. Copper(II) coordination environment of dimeric compound **9**. Selected bond lengths (Å): Cu1–O1 1.9927(14), Cu1–O2 2.7352(16), Cu1–O4 1.9570(14), Cu1–N4 2.2444(16), Cu1–N12 2.0286(16). Selected bond angles (deg): O1–Cu1–O2 52.05(5), O1–Cu1–O4 177.48(6), O1–Cu1–O5 130.04(5), O1–Cu1–N4 89.27(6), O1–Cu1–N12 85.95(6), O1–Cu1–N8^{iii} 90.03(6). Symmetry codes: (i) 0.5–*x*, *y*, 1–*z*; (ii) –0.5+*x*, –*y*, 1+*z*; (iii) 1–*x*, –*y*, –*z*.

The copper(II) perchlorate complexes **10**–**12** all show the same composition of their molecular units with three coordinating ligands, each linking between two copper(II) centers and two noncoordinating anions (Figures 14–16).

Complexes **10** and **11** crystallize in monoclinic space groups ($C2/c$ and $P2_1/n$, respectively), and **12** is present in the hexagonal space group $P6_3/m$ (**12a**) as well as the trigonal one $P\bar{3}c1$ (**12b**). While the ECC possess the same compositions,

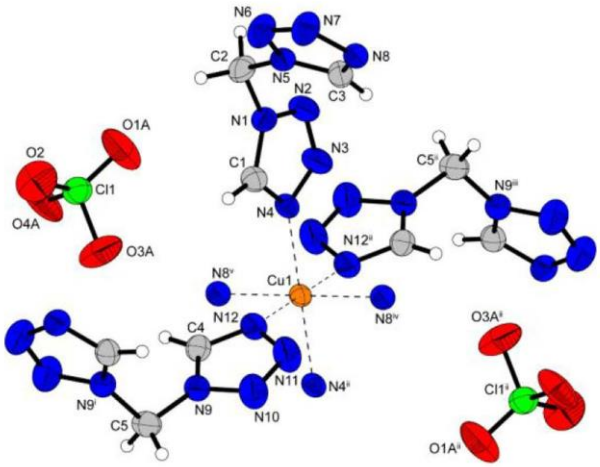


Figure 14. Extended molecular structure of copper(II) perchlorate complex **10**. Selected bond lengths (Å): Cu1–N4 2.0378(19), Cu1–N12 2.313(2), Cu1–N8^{iv} 2.071(2). Selected bond angles (deg): N4–Cu1–N12 91.30(8), N4–Cu1–N4^{ii} 180.00, N4–Cu1–N8^{iv} 91.66(8). Symmetry codes: (i) –*x*, *y*, 0.5–*z*; (ii) 0.5–*x*, 0.5–*y*, 1–*z*; (iii) 0.5+*x*, 0.5–*y*, 0.5+*z*; (iv) –*x*, 1–*y*, 1–*z*; (v) 0.5+*x*, –0.5+*y*, *z*.

they highly differ in their polymeric structure because of the different bridging modes of the ligands. **10** and **11** are forming similar 3D networks by the connection of one central metal to four other ones. In **10**, pairs of equatorial ligands are bridging between the same two copper(II) cations building up polymeric chains. Each ligand in the axial position is linking to another chain, and the strands are twisted at around 90° to each other leading to the formation of 3D-polymeric structures. A similar case can be observed in **11** with the only exception that pairs of one axial and one equatorial ligand are building up chains and the remaining equatorial ligands are responsible for the further linking. Whereas **10** and **11** are forming higher polymeric structures, both polymorphs of **12** are present as 1D chains. In **12a** as well as **12b**, three ligands are bridging between the same two copper(II) cations facilitating the formation of single strands. The only difference in the structures is the arrangement of the two tetrazole rings within the ligand molecules. Whereby in **12a** the carbon atoms are pointing in the same direction, they are opposite in **12b**. This affects the copper–copper distances within the chains (**12a**: ~8.3 Å; **12b**: ~7.5 Å) and is therefore

https://dx.doi.org/10.1021/acs.inorgchem.0c01403
Inorg. Chem. 2020, 59, 10938–10952

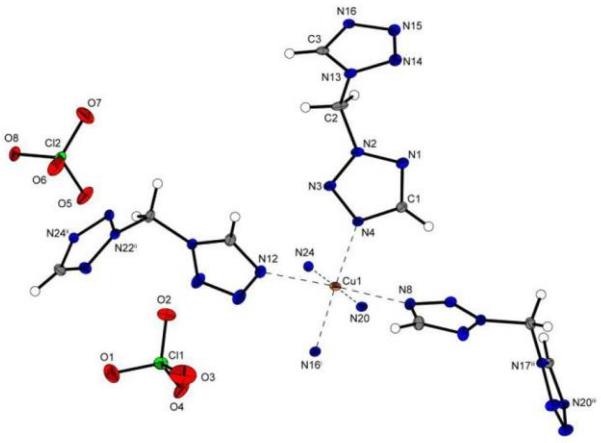


Figure 15. Extended molecular structure of copper(II) perchlorate complex **11**. Selected bond lengths (Å): Cu1–N4 2.0084(18), Cu1–N8 2.445(2), Cu1–N24 2.0398(18). Selected bond angles (deg): N4–Cu1–N8 89.59(7), N4–Cu1–N12 92.93(7), N8–Cu1–N12 177.15(6). Symmetry codes: (i) 0.5+*x*, 0.5−*y*, 0.5+*z*; (ii) −*x*, 1−*y*, 1−*z*; (iii) 1−*x*, −*y*, 1−*z*.

also influencing the compounds' densities (**12a**: 1.913 g cm^{-3}; **12b**: 2.003 g cm^{-3}).

In both cases, the polymeric chains are conjoined over hydrogen bonds and the interaction with the perchlorate anions (Figure 17). The nitroaromatic complexes **13** and **15** based on **1** show a similar buildup. In both cases, the copper(II) central metals are coordinated by four aqua and two ditetrazole ligands, which are only binding with one of their heterocycles. The complex monomers are completed by two noncoordinating and single-deprotonated anions (Figures 18 and S5). Each anion is forming hydrogen bonds to two of the aqua ligands.

In contrast to **13** and **15**, a double-deprotonated anion and bridging ligand is present in **14**. This is leading on the one side to a chelating effect and on the other side also to a linking of the styphnate between two copper(II) cations. The molecular unit is completed by an additional crystal water molecule (Figure 19).

The bridging of tetrazole and styphnate ligands is leading to the formation of polymeric chains. The crystal water molecules are embedded within holes of the chain and show interactions with noncoordinating nitro groups twisted from the ring plane (Figure 20). The polymeric structure is also increasing the density of **14** (1.973 g cm^{-3} @103 K) compared to **13** and **15** (1.757 g cm^{-3} @119 K and 1.810 g cm^{-3} @122 K, respectively). Complexes **16**–**18** crystallize in triclinic (*P*−1 (**16**)) or monoclinic (*C*2/*c* (**17**) and $P2_1/n$ (**18**)) space groups and show a similar buildup. The molecular units consist of one central atom with two aqua as well as two bridging ligands of **2** and two single-deprotonated, noncoordinating anions (Figures 21, S6, and S7). The main difference of the three complexes is the level of Jahn–Teller distortion along the N5^{ii}–Cu–N5^{iii} (**16**), O1–Cu–O1^{i} (**17**), and N4–Cu–N4^{i} (**18**) axis.

Like **13** and **15**, the anions in **16**–**18** are forming hydrogen bonds to the aqua ligands. The bridging of the ligands is reducing the number of water molecules and leading to the formation of polymeric chains in all three structures (Figure 22).

THERMAL STABILITY AND SENSITIVITY MEASUREMENTS

The three ligands and all complexes were examined with respect to their thermal behavior in differential thermal analysis (DTA), and their stability against external stimuli (impact (IS), friction (FS), electrostatic discharge (ESD), and ball drop impact (BDIS) sensitivities) was determined. All values are summarized in Table 2 together with the compounds' outcome in the hot needle and hot plate tests. The DTA experiments were performed with a heating rate of β = 5 °C min^{-1} in the range of 35–400 °C, and the critical points, such as melting, dehydration, or exothermic decomposition, are given as onset temperatures. Except for **4**, **5**, and **18**, all complexes show a higher thermal stability than the respective ligand. The highest decomposition temperatures are achieved by copper(II) perchlorate complexes **10**–**12** as well as styphnate compound **14**, which all exceed 200 °C and **12** is even close to 250 °C (242 °C). Silver nitrate complexes **4** and **5** possess the lowest thermal stability (136 and 124 °C, respectively) as well as **18** with 136 °C (Figure 23).

Interestingly, no endothermic event can be observed for the water containing compounds **14** and **18**. Therefore, they were further investigated using thermal gravimetric analysis (TGA). The measurements clearly reveal the slow evaporation of the crystal water molecule in **14** before the compound decomposes, whereas in **18** no evaporation can be detected (Figure 24). This and the relatively low decomposition temperature (136 °C) lead to the assumption that the complex stability immediately breaks down when the aqua ligands start to evaporate. The determined

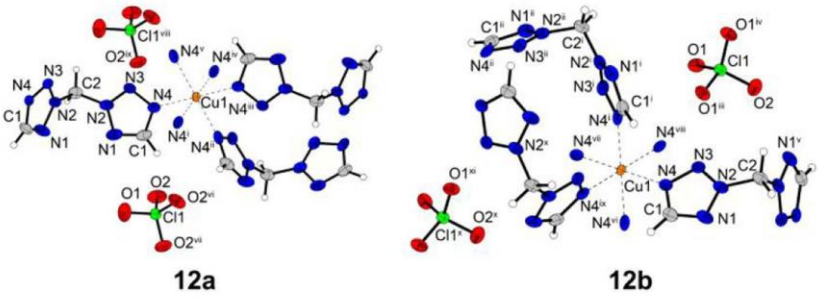


Figure 16. Copper(II) coordination environments of the two different polymorphs of **12**. Selected bond length of **12a** (Å): Cu1–N4 2.131(3). Selected bond angles of **12a** (deg): N4–Cu1–N4^{i} 88.37(11), N4–Cu1–N4^{iii} 180.00, N4–Cu1–N4^{iv} 91.63(11). Symmetry codes of **12a**: (i) −*y*, *x*−*y*, *z*; (ii) *x*−*y*, *x*, −*z*; (iii) −*x*, −*y*, −*z*; (iv) *y*, −*x*+*y*, −*z*; (v) −*x*+*y*, −*x*, *z*; vi) −*x*+*y*, −1−*x*, *z*; vii) −1−*y*, −1+*x*−*y*, *z*; viii) *x*, 1+*y*, *z*; ix) −1−*y*, *x*−*y*, *z*. Selected bond length of **12b** (Å): Cu1–N2 2.133(2). Selected bond angles of **12b** (deg): N4–Cu1–N4^{vi} 90.86(11), N4–Cu1–N4^{vii} 180.00, N4^{vi}–Cu1–N4^{vii} 89.14(11). Symmetry codes of **12b**: (i) *y*, −*x*+*y*, −*z*; (ii) *x*, *x*−*y*, −0.5+*z*; (iii) 1−*x*+*y*, 1−*x*, *z*; (iv) 1−*y*, *x*−*y*, *z*; (v) *y*, *x*, 0.5−*z*; vi) −*y*, *x*−*y*, *z*; vii) −*x*, −*y*, −*z*; viii) −*x*+*y*, −*x*, *z*; ix) *x*−*y*, *x*, −*z*; x) −*x*+*y*, *y*, −0.5+*z*; xi) −*y*, 1−*x*, −0.5+*z*.

https://dx.doi.org/10.1021/acs.inorgchem.0c01403
Inorg. Chem. 2020, 59, 10938−10952

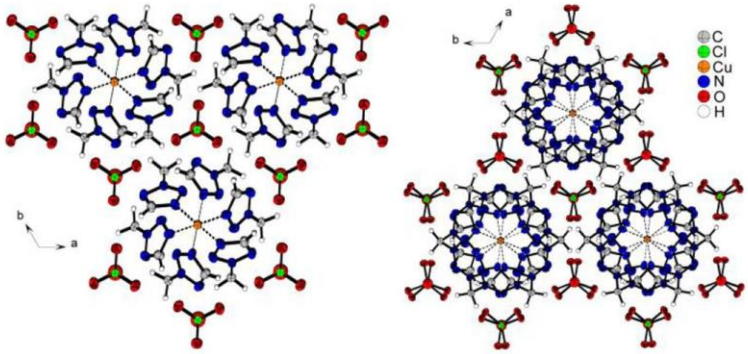


Figure 17. Polymeric structures of **12a** with parallel and **12b** with antiparallel arranged tetrazole rings viewed along the *c* axis.

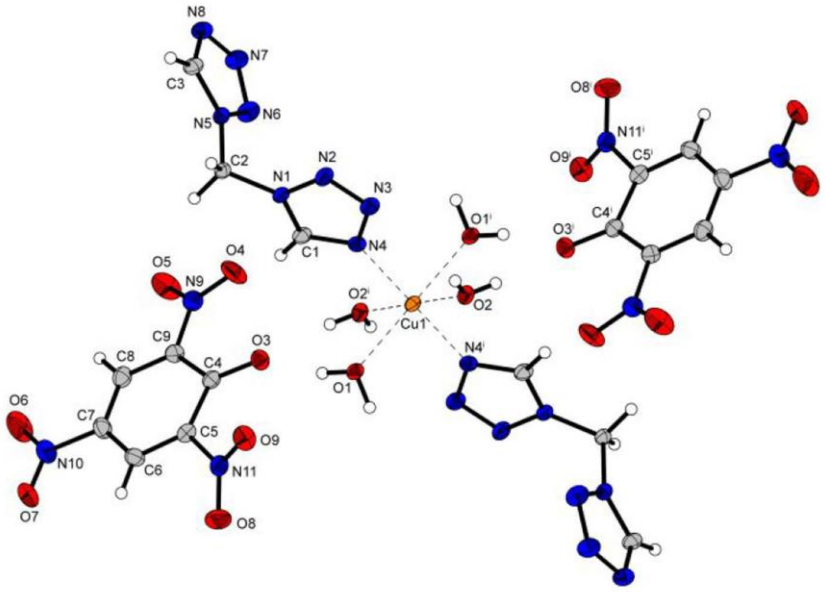


Figure 18. Molecular unit of picrate complex **13**. Selected bond lengths (Å): Cu1−O1 2.3139(18), Cu1−O2 2.003(2), Cu1−N4 2.002(2). Selected bond angles (deg): O1−Cu1−O2 92.46(7), O1−Cu1−N4 85.98(7), O1−Cu1−O1ⁱ 180.00. Symmetry code: (i) 1−*x*, −*y*, −*z*.

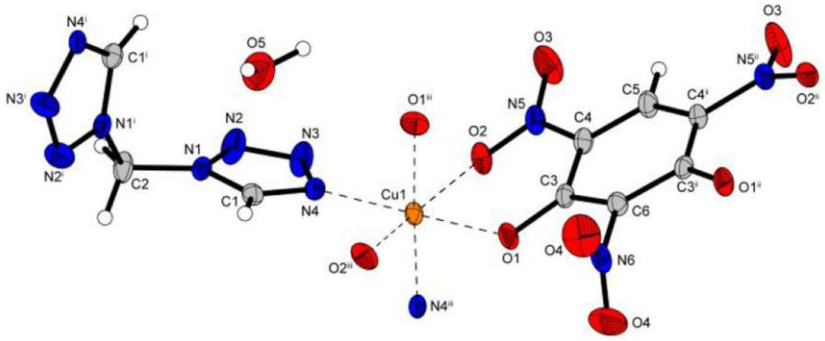


Figure 19. Copper(II) coordination environments of styphnate compound **14**. Selected bond lengths (Å): Cu1−O1 1.9380(15), Cu1−O2 2.2690(15), Cu1−N4 2.0084(17). Selected bond angles (deg): O1−Cu1−O2 82.43(6), O1−Cu1−N4 177.66(7), O2−Cu1−N4 99.16(6). Symmetry codes: (i) 1.75−*x*, 0.75−*y*, *z*; (ii) 0.25−*x*, *y*, 0.25−*z*; (iii) 0.75−*x*, 0.75−*y*, *z*.

sensitivities have been used to classify the compounds in accordance with the "UN Recommendations on the Transport of Dangerous Goods".[23] In general, all complexes must be ranked as sensitive (**4**, **13**, **15**, and **17**) or very sensitive toward impact, and the only two coordination compounds which are insensitive toward friction are the picrate complexes **13** and **16**. Except for **15** (very sensitive), all other trinitrophenolates can be classified as sensitive toward friction. While the copper(II) perchlorate complexes **10**−**12** are extremely sensitive toward friction (0.75−1 N), **9** and all silver compounds can be

https://dx.doi.org/10.1021/acs.inorgchem.0c01403
Inorg. Chem. 2020, 59, 10938−10952

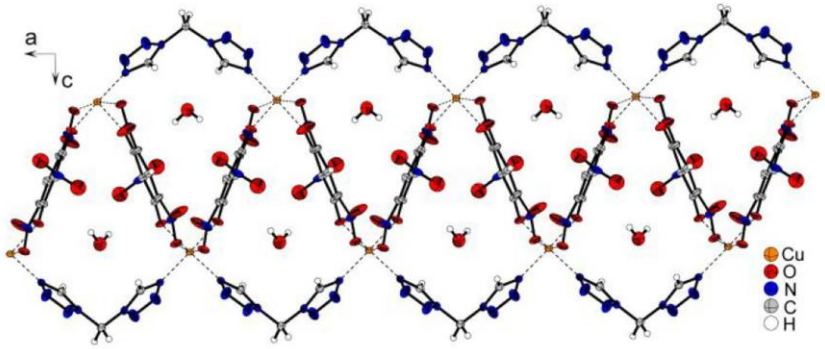


Figure 20. Polymeric structure of **15** view along the *b* axis.

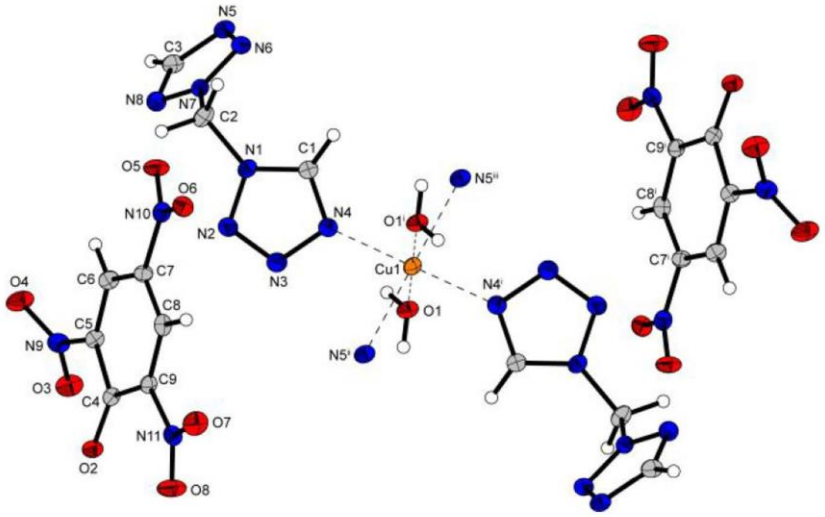


Figure 21. Copper(II) coordination environment of complex **16**. Selected bond lengths (Å): Cu1−O1 1.9778(19), Cu1−N4 2.015(3), Cu1−N5^{ii} 2.362(3). Selected bond angles (deg): O1−Cu1−N4 90.41(9), O1−Cu1−N5^{iii} 91.53(9), N4−Cu1−N5^{iii} 89.61(11). Symmetry codes: (i) 2−*x*, 1−*y*, −*z*; (ii) 1+*x*, *y*, *z*; (iii) 1−*x*, 1−*y*, −*z*.

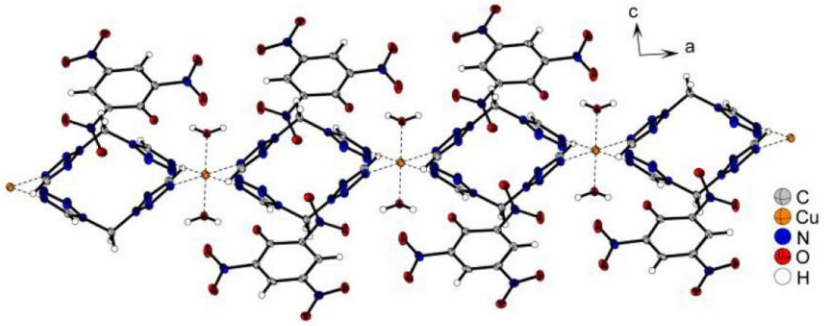


Figure 22. Polymeric structure of **16** viewed along the *b* axis.

categorized as sensitive (**4** and **5**) or very sensitive (**6**−**9**). Comparing the BDIS, which gives more realistic test conditions,[22b] it becomes clear that especially the perchlorate ECC but also compounds **9** and **15** are even more sensitive than LA.

■ ENERGETIC PERFORMANCE AND INITIATION TESTS

For getting insight into the energetic behavior of the compounds, hot plate (HP) and hot needle (HN) tests of all complexes were performed (Table 2, Figures 25 and S12−S17).

While the HP test only shows the performance of the unconfined samples during fast heating, the HN test allows an insight of their confined manners and therefore their potential use as primary explosives. All nitroaromatic compounds show

https://dx.doi.org/10.1021/acs.inorgchem.0c01403
Inorg. Chem. 2020, 59, 10938−10952

Table 2. Summary of the Compounds' Thermal Stability,[a] Sensitivities toward Various External Stimuli and Results of Hot Plate (HP) and Hot Needle (HN) Tests Compared to LA[22]

compound	T_{endo} (°C)[b]	T_{exo} (°C)[c]	IS (J)[d]	FS (N)[e]	ESD (mJ)[f]	BDIS (mJ)[g]	HP[h]	HN[h]
1,1-dtm (**1**)	145	152	8	>360	480	n.d.	n.d.	n.d.
1,2-dtm (**2**)	96	138	2	168	181	n.d.	n.d.	n.d.
2,2-dtm (**3**)	58	184	1.5	84	160	n.d.	n.d.	n.d.
$[Ag(1,1\text{-dtm})_2]NO_3$ (**4**)	132	136	4	144	450	>200	def.	dec.
$[Ag(1,2\text{-dtm})_3]NO_3$ (**5**)	113	124	2	108	540	124	def.	def.
$[Ag(NO_3)(2,2\text{-dtm})]$ (**6**)	166	186	3	36	380	124	def.	def.
$[Ag(1,1\text{-dtm})_2]ClO_4$ (**7**)		163	<1	30	1080	28	def.	def.
$[Ag(1,2\text{-dtm})_4]ClO_4$ (**8**)	132	140	<1	50	226	20	def.	def.
$[Cu_2(NO_3)_4(2,2\text{-dtm})_3]$ (**9**)		198	1.5	30	>1500	16	def.	def.
$[Cu(1,1\text{-dtm})_3](ClO_4)_2$ (**10**)		230	<1	0.75	42	12	def.	def.
$[Cu(1,2\text{-dtm})_4](ClO_4)_2$ (**11**)		215	1.5	1	47	<4	det.	det.
$[Cu(2,2\text{-dtm})_4](ClO_4)_2$ (**12**)		242	<1	0.75	37	<4	det.	def.
$[Cu(H_2O)_4(1,1\text{-dtm})_2](PA)_2$ (**13**)	108	185	6	>360	840	>200	dec.	dec.
$[Cu(TNR)(1,1\text{-dtm})]\cdot H_2O$ (**14**)		236	2	192	188	66	def.	dec.
$[Cu(H_2O)_4(1,1\text{-dtm})_2](H_2TNPG)_2$ (**15**)	74	196	4	48	960	16	def.	dec.
$[Cu(H_2O)_2(1,2\text{-dtm})_2](PA)_2$ (**16**)	122	159	1	>360	750	>200	dec.	dec.
$[Cu(H_2O)_2(1,2\text{-dtm})_2](HTNR)_2$ (**17**)	132	156	7	144	1500	>200	def.	dec.
$[Cu(H_2O)_2(1,2\text{-dtm})_2](H_2TNPG)_2$ (**18**)		136	1.5	128	1350	>200	def.	dec.
$Pb(N_3)_2$		320–360	2.5–4	0.1–1.0	7	37	det.	det.

[a]Onset temperature at a heating rate of 5 °C min^{-1} measured by DTA. [b]Endothermic peak, which indicates melting, dehydration, or loss of aqua ligands. [c]Exothermic peak, which indicates decomposition. [d]Impact sensitivity according to the BAM drop hammer (method 1 of 6). [e]Friction sensitivity according to the BAM friction tester (method 1 of 6). [f]Electrostatic discharge sensitivity (OZM Electric Spark XSpark10). [g]Ball drop impact sensitivity determined with the 1 of 6 method in accordance with the MIL-STD 1751A (method 1016). [h]Abbreviations: dec., decomposition; def., deflagration; det., detonation.

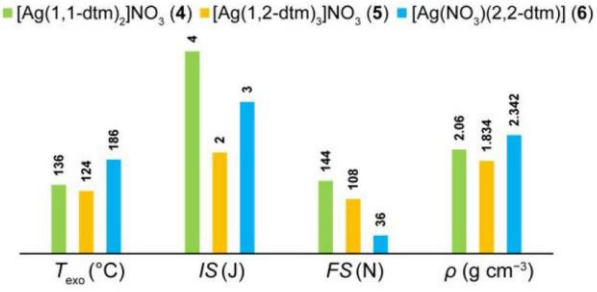


Figure 23. Comparison of the sensitivities and thermal stability of the silver nitrate complexes as well as dependency of the densities (recalculated to room temperature) on ligand content.

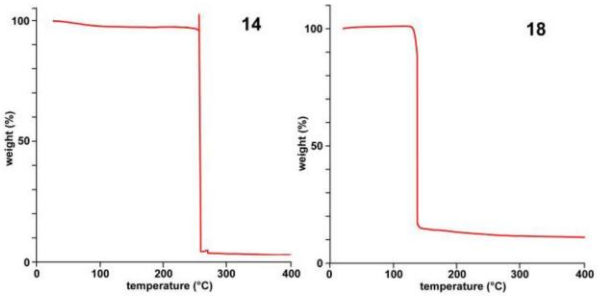


Figure 24. TGA plots of compounds **14** and **18**.

decompositions or weak deflagrations during both tests, which is not surprising due to the presence of aqua ligands or crystal water molecules. Remarkably, all silver complexes possess only poor energetic performances with rather weak deflagrations or even decompositions (**4**) during the experiments. In contrast, the copper(II) perchlorate ECC show detonations or strong

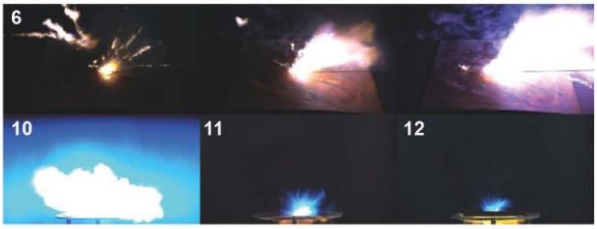


Figure 25. Top: HN test of nitrate compound **6** shown as a sequence; bottom: moments of deflagration (**10**) or detonation (**11** and **12**) of copper(II) perchlorate complexes during the HP tests.

deflagrations, which makes them possible candidates for the initiation of secondary or booster explosives.

Therefore, the three complexes **10**–**12** were investigated in classical initiation capability tests with PETN (nitropenta) as the main charge. Details on the setup can be found in the Supporting Information. Compounds **11** and **12** were able to cause a positive deflagration-to-detonation transition (DDT) toward the booster explosive, which is indicated by a hole in the copper witness plate and fragmentation of the shell (Figure 26). In contrast, no positive results were achieved (even in the case of using unpressed PETN) when **10** was applied as primary explosive.

Furthermore, all colored ECC **9**–**18** were tested in laser ignition experiments using an InGaAs laser diode working in the single-pulse mode. The results are in accordance with our previous findings, and details of the test setup are given in the SI.[24] All nitroaromatic complexes solely show decomposition when irradiated associated with the generation of smoke (Figure 27). The application of a 20 mJ beam on **9** leads to a strong deflagration, whereas the perchlorate complexes **10**–**12** show very strong detonations with an energy input of only 0.2 mJ.

https://dx.doi.org/10.1021/acs.inorgchem.0c01403
Inorg. Chem. 2020, 59, 10938−10952



Figure 26. Positive results of the initiation capability tests toward PETN of compounds **11** (left) and **12** (right).

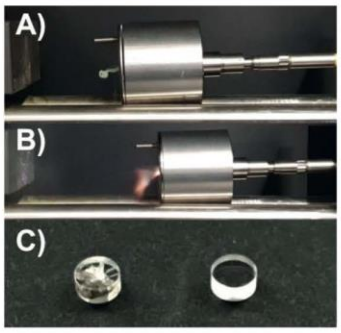


Figure 27. Results of the laser initiation tests: A) decomposition of picrate complex **13**; B) moment of deflagration of nitrate compound **9**; and C) comparison of destroyed (left) sapphire glass with a new one (right) after detonation of **10**.

Compound **10** detonated violently resulting in the destruction of the sapphire glass, which usually protects the laser lens.

CONCLUSION

For the first time the nitrogen-rich compounds di(tetrazol-1-yl)methane (1,1-dtm, **1**), (tetrazol-1-yl)(tetrazol-2-yl)methane (1,2-dtm, **2**), and di(tetrazol-2-yl)methane (2,2-dtm, **3**) were synthesized by the reaction of triethylammonium 5*H*-tetrazolate with dibromomethane in a one-step reaction and exhaustively characterized, e.g., using two-dimensional $^{1}H-^{15}N$-HMBC NMR spectroscopy, X-ray studies (**2**: 1.605 g cm^{-3}, *Fdd*2) < **3**: 1.632 g cm^{-3}, *Fdd*2 < (**1**) 1.637 g cm^{-3}, $P2_1/c$), and Hirshfeld surface calculations. The coordination behavior of the three ligands was studied in detail leading to 15 new energetic coordination compounds (ECC) based on silver(I) and copper(II) as well as different oxidizing anions (nitrate, perchlorate, picrate, styphnate, and trinitrophloroglucinate). The appropriate selection of central metal, anion, and dtm isomer allowed the accurate tuning of the compounds' properties. The combination of the ligands with copper(II) perchlorate results in the formation of powerful and thermally highly stable primary explosives with very efficient performance. Especially ECC **11** and **12** show very good initiation capabilities of PETN. The utilization of nitrate as a building block is increasing the stability toward external stimuli and in the case of **9** allows its use as a laser ignitable explosive with decreased sensitivities. Interestingly, in most cases, complex formation improves thermal stability compared to pure ligands. The crystal structures reveal a high degree of diversity for the coordination of the three different isomers. Due to the potential bridging character of the ligands, most of the complexes form polymeric structures with differing dimensionality. However, especially compared to other 5*H*-ditetrazolyl ligands, **1**–**3** have comparatively often a terminal coordination behavior, which is highly influencing the polymeric structures and even leading in some cases to the formation of complex monomers. Moreover, exceptional coordination spheres, like a 5-fold bounding to silver(I) in complex **6** or a distorted pentagonal bipyramidal geometry around Cu^{2+} in ECC **9**, can be observed.

ASSOCIATED CONTENT

Supporting Information

The Supporting Information is available free of charge at https://pubs.acs.org/doi/10.1021/acs.inorgchem.0c01403.

Experimental part and general methods IR spectroscopy X-ray diffraction DTA plots, hot plate and hot needle tests, and initiation capability tests (PDF)

Accession Codes

CCDC 1988633–1988651 contain the supplementary crystallographic data for this paper. These data can be obtained free of charge via www.ccdc.cam.ac.uk/data_request/cif, or by emailing data_request@ccdc.cam.ac.uk, or by contacting The Cambridge Crystallographic Data Centre, 12 Union Road, Cambridge CB2 1EZ, UK; fax: +44 1223 336033.

AUTHOR INFORMATION

Corresponding Author

Jörg Stierstorfer – *Department of Chemistry, University of Munich (LMU), 81377 München, Germany;* orcid.org/0000-0002-2105-1275; Email: jstch@cup.uni-muenchen.de

Authors

Maximilian H. H. Wurzenberger – *Department of Chemistry, University of Munich (LMU), 81377 München, Germany;* orcid.org/0000-0002-5494-9903

Vanessa Braun – *Department of Chemistry, University of Munich (LMU), 81377 München, Germany;* orcid.org/0000-0003-0215-8576

Marcus Lommel – *Department of Chemistry, University of Munich (LMU), 81377 München, Germany;* orcid.org/0000-0003-1765-0248

Thomas M. Klapötke – *Department of Chemistry, University of Munich (LMU), 81377 München, Germany;* orcid.org/0000-0003-3276-1157

Complete contact information is available at: https://pubs.acs.org/10.1021/acs.inorgchem.0c01403

Notes

The authors declare no competing financial interest.

ACKNOWLEDGMENTS

Financial support of this work by Ludwig-Maximilian University (LMU), the Office of Naval Research (ONR) under grant no. ONR N00014-19-1-2078, and the Strategic Environmental Research and Development Program (SERDP) under contract no. W912HQ19C0033 is gratefully acknowledged. The authors would also like to thank Prof. Dr. Konstantin Karaghiosoff for the measurement of the two-dimensional $^{1}H-^{15}N$-HMBC NMR spectra and Sebastian Hagenrainer for his great contribution to this work.

REFERENCES

(1) (a) Butler, R. N. Tetrazoles. *Compr. Heterocycl. Chem.* **1984**, *5*, 791–838. (b) Ostrovskii, V. A.; Koldobskii, G. I.; Trifonov, R. E. Tetrazoles. *Compr. Heterocycl. Chem. III.* **2008**, *6*, 257–423.

(2) Ostrovskii, V. A.; Popova, E. A.; Trifonov, R. E. Developments in Tetrazole Chemistry (2009−16). *Adv. Heterocycl. Chem.* **2017**, *123*, 1−62.
(3) Gaponik, P. N.; Karavai, V. P.; Grigor'ev, Yu. V. Synthesis of 1-substituted tetrazoles by heterocyclization of primary amines, ethyl orthoformate and sodium azide. *Khim. Geterotsikl. Soedin.* **1985**, *11*, 1521−1524.
(4) van Koningsbruggen, P. J.; Garcia, Y.; Kahn, O.; Fournes, L.; Kooijman, H.; Spek, A. L.; Haasnoot, J. G.; Moscovici, J.; Provost, K.; Michalowicz, A.; Renz, F.; Gütlich, P. Synthesis, Crystal Structure, EXAFS, and Magnetic Properties of Catena [μ-Tris(1,2-bis(tetrazol-1-yl)propane-N4,N4′)iron(II)] Bis(perchlorate). First Crystal Structure of an Iron(II) Spin-Crossover Chain Compound. *Inorg. Chem.* **2000**, *39*, 1891−1900.
(5) Yu, J.-H.; Mereiter, K.; Hassan, N.; Feldgitscher, C.; Linert, W. Designed Assemblies of Metal Halo and Pseudohalo Coordination Polymers with Bridging 1-Substituted Ditetrazoles. *Cryst. Growth Des.* **2008**, *8*, 1535−1540.
(6) (a) Schweifer, J.; Weinberger, P.; Mereiter, K.; Boca, M.; Reichl, C.; Wiesinger, G.; Hilscher, G.; van Koningsbruggen, P. J.; Kooijman, H.; Grunert, M.; Linert, W. catena-[μ-Tris(1,2-bis(tetrazol-1-yl)-ethane-N4,N4′)iron(II)] bis(tetrafluoroborate): synthesis, structure, spectroscopic and magnetic characterization of a chain-type coordination polymer spin-crossover compound. *Inorg. Chim. Acta* **2002**, *339*, 297−306. (b) Absmeier, A.; Bartel, M.; Carbonera, C.; Jameson, G. N. L.; Weinberger, P.; Caneschi, A.; Mereiter, K.; Létard, J.-F.; Linert, W. Both Spacer Length and Parity Influence the Thermal and Light-Induced Properties of Iron(ii) α,ω-Bis(tetrazole-1-yl)alkane Coordination Polymers. *Chem. - Eur. J.* **2006**, *12*, 2235−2243. (c) Grunert, C. M.; Schweifer, J.; Weinberger, P.; Linert, W. Structure and Physical Properties of [μ-Tris(1,4-bis(tetrazol-1-yl)butane-N4,N4′)iron(II)] Bis(hexafluorophosphate), a New Fe(II) Spin-Crossover Compound with a Three-Dimensional Threefold Interlocked Crystal Lattice. *Inorg. Chem.* **2004**, *43*, 155−165.
(7) Absmeier, A.; Bartel, M.; Carbonera, C.; Jameson, G. N. L.; Werner, F.; Reissner, M.; Caneschi, A.; Létard, J.-F.; Linert, W. Mutual Influence of Spacer Length and Noncoordinating Anions on Thermal and Light-Induced Spin-Crossover Properties of Iron(II)−α,ω-Bis-(tetrazol-1-yl)-alkane Coordination Polymers. *Eur. J. Inorg. Chem.* **2007**, *2007*, 3047−3054.
(8) (a) Białońska, A.; Bronisz, R. High Spin and Spin-Crossover Two-Dimensional Coordination Polymers Containing FeII(tetrazol-2-yl)4(solv)2 (solv = Ethanol, Acetonitrile) Cores Linked by Flexible/Elastic Spacers. *Inorg. Chem.* **2010**, *49*, 4534−4542. (b) Bronisz, R. Synthesis and structure of {[Zn(1,2-di(1,2,3,4-tetrazol-2-yl)ethane)3](ClO4)-2}n. The first coordination polymer based on 2-substituted tetrazole. *Inorg. Chim. Acta* **2002**, *340*, 215−220. (c) Białońska, A.; Bronisz, R. Role of Fe-N-C Geometry Flip-Flop in Bistability in Fe(tetrazol-2-yl)4(C2H5CN)2-Type Core Based Coordination Network. *Inorg. Chem.* **2012**, *51*, 12630−12637. (d) Bronisz, R. 1,4-Di(1,2,3,4-tetrazol-2-yl)butane as a precursor of new 2D and 3D coordination polymers of Cu(II). *Inorg. Chim. Acta* **2004**, *357*, 396−404.
(9) (a) van Koningsbruggen, P. J.; Garcia, Y.; Kooijman, H.; Spek, A. L.; Haasnoot, J. G.; Kahn, O.; Linares, J.; Codjovi, E.; Varret, F. A new 3-D polymeric spin transition compound: [tris(1,4-bis-(tetrazol-1-yl)butane-N1,N1)iron(II)] bis(perchlorate). *J. Chem. Soc., Dalton Trans.* **2001**, *4*, 466−471. (b) Baldé, C.; Sylla, M. S.; Desplanches, C.; Chastanet, G. Bis(3-nitro-1-(trinitromethyl)-1H-1,2,4-triazol-5-yl)-methanone: An Applicable and Very Dense Green Oxidizer. *Polyhedron* **2019**, *159*, 84−92.
(10) (a) van Koningsbruggen, P. J.; Garcia, Y.; Bravic, G.; Chasseau, D.; Kahn, O. Crystal structure and physical properties of the new linear chain compound [Cu(1,2-bis(tetrazol-1-yl)ethane)3](ClO4)2. *Inorg. Chim. Acta* **2001**, *326*, 101−105. (b) Liu, P.-P.; Cheng, A.-L.; Liu, N.; Sun, W.-W.; Gao, E.-Q. Toward Tuning the Bulk Magnetic Behaviors of Metal-Azido Materials by Organic Pillars. *Chem. Mater.* **2007**, *19*, 2724−2726. (c) Liu, P.-P.; Wang, Y.-Q.; Tian, C.-Y.; Peng, H.-Q.; Gao, E.-Q. Nickel(II) and copper(II) coordination polymers with 1,2-bis(tetrazol-1-yl)ethane and thiocyanate: Structure, supramolecular isomerism and magnetism. *J. Mol. Struct.* **2009**, *920*, 459−465. (d) Knoll, C.; Müller, D.; Seifried, M.; Giester, G.; Welch, J. M.; Artner, W.; Hradil, K.; Reissnere, M.; Weinberger, P. Cooperativity in spin crossover materials as ligand's responsibility − investigations of the Fe(II) − 1,3-bis((1H-tetrazol-1-yl)methyl)bicyclo[1.1.1]pentane system. *Dalton Trans.* **2018**, *47*, 5553−5557.
(11) (a) Xu, J.-G.; Li, X.-Z.; Wu, H.-F.; Zheng, F.-K.; Chen, J.; Guo, G.-C. Substitution of Nitrogen-Rich Linkers with Insensitive Linkers in Azide-Based Energetic Coordination Polymers toward Safe Energetic Materials. *Cryst. Growth Des.* **2019**, *19*, 3934−3944. (b) Joas, M.; Deisenroth, U. Detonators, especially for use with an optical detonator, based on 1,1′-(1,2-ethanediyl)bis-1H-tetrazole) complexes. DE 102016120539 A1 20180503, 2018. (c) Wurzenberger, M. H. H.; Szimhardt, N.; Stierstorfer, J. Copper(II) Chlorate Complexes: The Renaissance of a Forgotten and Misjudged Energetic Anion. *J. Am. Chem. Soc.* **2018**, *140*, 3206−3209. (d) Xu, J.-G.; Lin, S.-J.; Li, X.-Z.; Wu, H.-F.; Lu, J.; Wang, W.-F.; Chen, J.; Zheng, F.-K.; Guo, G.-C. Energetic azide-based coordination polymers: Sensitivity tuning through diverse structural motifs. *Chem. Eng. J.* **2020**, *390*, 124587.
(12) https://echa.europa.eu/de/candidate-list-table (accessed June 2020).
(13) Klapötke, T. M.; Mehta, N. Lead-free Primary Explosives. *Propellants, Explos., Pyrotech.* **2014**, *39*, 7−8.
(14) (a) Myers, T. W.; Bjorgaard, J. A.; Brown, K. E.; Chavez, D. E.; Hanson, S. K.; Scharff, R. J.; Tretiak, S.; Veauthier, J. M. Energetic Chromophores: Low-Energy Laser Initiation in Explosive Fe(II) Tetrazine Complexes. *J. Am. Chem. Soc.* **2016**, *138*, 4685−4692. (b) Sun, Q.; Li, X.; Lin, Q.; Lu, M. Dancing with 5-substituted monotetrazoles, oxygen-rich ions, and silver: Towards primary explosives with positive oxygen balance and excellent energetic performance. *J. Mater. Chem. A* **2019**, *7*, 4611−4618. (c) Zhang, Q.; Shreeve, J. M. Metal-Organic Frameworks as High Explosives: A New Concept for Energetic Materials. *Angew. Chem., Int. Ed.* **2014**, *53*, 2540−2542. (d) Ilyushin, M. A.; Kotomin, A. A.; Dushenok, S. A. Energy-Saturated Metal Complexes. *Russ. J. Phys. Chem. B* **2019**, *13*, 119−138.
(15) (a) Landenberger, K. B.; Bolton, O.; Matzger, A. J. Energetic-Energetic Cocrystals of Diacetone Diperoxide (DADP): Dramatic and Divergent Sensitivity Modifications via Cocrystallization. *J. Am. Chem. Soc.* **2015**, *137*, 5074−5079. (b) Larin, A. A.; Muravyev, N. V.; Pivkina, A. N.; Suponitsky, K. Yu; Ananyev, I. V.; Khakimov, D. V.; Fershtat, L. L.; Makhova, N. N. Assembly of Tetrazolylfuroxan Organic Salts: Multipurpose Green Energetic Materials with High Enthalpies of Formation and Excellent Detonation Performance. *Chem. - Eur. J.* **2019**, *25*, 4225−4233. (c) Barton, L. M.; Edwards, J. T.; Johnson, E. C.; Bukowski, E. J.; Sausa, R. C.; Byrd, E. F. C.; Orlicki, J. A.; Sabatini, J. J.; Baran, P. S. Impact of Stereo- and Regiochemistry on Energetic Materials. *J. Am. Chem. Soc.* **2019**, *141*, 12531−12535. (d) Baxter, A. F.; Martin, I.; Christe, K. O.; Haiges, R. Formamidinium Nitroformate: An Insensitive RDX Alternative. *J. Am. Chem. Soc.* **2018**, *140*, 15089−15098.
(16) Müller, D.; Knoll, C.; Stöger, B.; Artner, W.; Reissner, M.; Weinberger, P. A Modified Synthetic Pathway for the Synthesis of so far Inaccessible N1-Functionalized Tetrazole Ligands - Synthesis and Characterization of the 1D Chain-Type Spin Crossover Compound [Fe(3ditz)3](BF4)2. *Eur. J. Inorg. Chem.* **2013**, *2013*, 984−991.
(17) Szimhardt, N.; Wurzenberger, M. H. H.; Klapötke, T. M.; Lechner, J. T.; Reichherzer, H.; Unger, C. C.; Stierstorfer, J. Highly functional energetic complexes: stability tuning through coordination diversity of isomeric propyl-linked ditetrazoles. *J. Mater. Chem. A* **2018**, *6*, 6565−6577.
(18) (a) Zhang, J.; Zhang, Q.; Vo, T. T.; Parrish, D. A.; Shreeve, J. M. Energetic Salts with π-Stacking and Hydrogen-Bonding Interactions Lead the Way to Future Energetic Materials. *J. Am. Chem. Soc.* **2015**, *137*, 1697−1704. (b) Liu, Y.; Zhao, G.; Yu, Q.; Tang, Y.; Imler, G. H.; Parrish, D. A.; Shreeve, J. M. Bis(3-nitro-1-(trinitromethyl)-1H-1,2,4-triazol-5-yl)methanone: An Applicable and Very Dense Green Oxidizer. *J. Org. Chem.* **2019**, *84*, 16019−16026.
(19) Sućeska, M. *EXPLO5*, Version 6.05.02; Zagreb, 2018.

https://dx.doi.org/10.1021/acs.inorgchem.0c01403
Inorg. Chem. 2020, 59, 10938−10952

(20) (a) Gao, E.-Q.; Liu, P.-P.; Wang, Y.-Q.; Yue, Q.; Wang, Q.-L. Complex long-range magnetic ordering behaviors in anisotropic cobalt(II)-azide multilayer systems. *Chem. - Eur. J.* **2009**, *15*, 1217−1226. (b) Quesada, M.; Kooijman, H.; Gamez, P.; Sánchez Costa, J.; van Koningsbruggen, P. J.; Weinberger, P.; Reissner, M.; Spek, A. L.; Haasnoot, J. G.; Reedijk, J. [Fe(μ-btzmp)2(btzmp)2](ClO4)2: a doubly-bridged 1D spin-transition bistetrazole-based polymer showing thermal hysteresis behaviour. *Dalton Trans.* **2007**, *6*, 5434−5440. (c) Wurzenberger, M. H. H.; Szimhardt, N.; Stierstorfer, J. Nitrogen-Rich Copper(II) Bromate Complexes: an Exotic Class of Primary Explosives. *Inorg. Chem.* **2018**, *57*, 7940−7949. (d) Liu, P.-P.; Cheng, A.-L.; Yue, Q.; Liu, N.; Sun, W.-W.; Gao, E.-Q. Cobalt(II) coordination networks dependent upon the spacer length of flexible bis(tetrazole) ligands. *Cryst. Growth Des.* **2008**, *8*, 1668−1673.

(21) CCDC 1988649 (**1**), 1988643 (**2**), 1988633 (**3**), 1988648 (**4**), 1988639 (**5**), 1988636 (**6**), 1988647 (**7**), 1988642 (**8**), 1988637 (**9**), 1988644 (**10**), 1988651 (**11**), 1988640 (**12a**), 1988638 (**12b**), 1988650 (**13**), 1988641 (**14**), 1988634 (**15**), 1988635 (**16**), 1988646 (**17**), and 1988645 (**18**) contain the supplementary crystallographic data for this paper. These data are provided free of charge by The Cambridge Crystallographic Data Centre.

(22) (a) Klapötke, T. M. *Energetic Materials Encyclopedia*; De Gruyter: Berlin/Boston, 2018; DOI: 10.1515/9783110442922. (b) Gruhne, M. S.; Lommel, M.; Wurzenberger, M. H. H.; Szimhardt, N.; Klapötke, T. M.; Stierstorfer, J. OZM Ball Drop Impact Tester (BIT-132) vs. BAM Standard Method-a Comparative Investigation. *Propellants, Explos., Pyrotech.* **2020**, *45*, 147−153.

(23) Impact: insensitive > 40 J, less sensitive ≥ 35 J, sensitive ≥ 4 J, very sensitive ≤ 3 J. Friction: insensitive > 360 N, less sensitive = 360 N, sensitive < 360 N and > 80 N, very sensitive ≤ 80 N, extremely sensitive ≤ 10 N. According to the UN Recommendations on the Transport of Dangerous Goods.

(24) Wurzenberger, M. H. H.; Gruhne, M. S.; Lommel, M.; Szimhardt, N.; Klapötke, T. M.; Stierstorfer, J. Comparison of 1-Ethyl-5H-tetrazole and 1-Azidoethyl-5H-tetrazole as Ligands in Energetic Transition Metal Complexes. *Chem. - Asian J.* **2019**, *14*, 2018−2028.

https://dx.doi.org/10.1021/acs.inorgchem.0c01403
Inorg. Chem. 2020, 59, 10938−10952

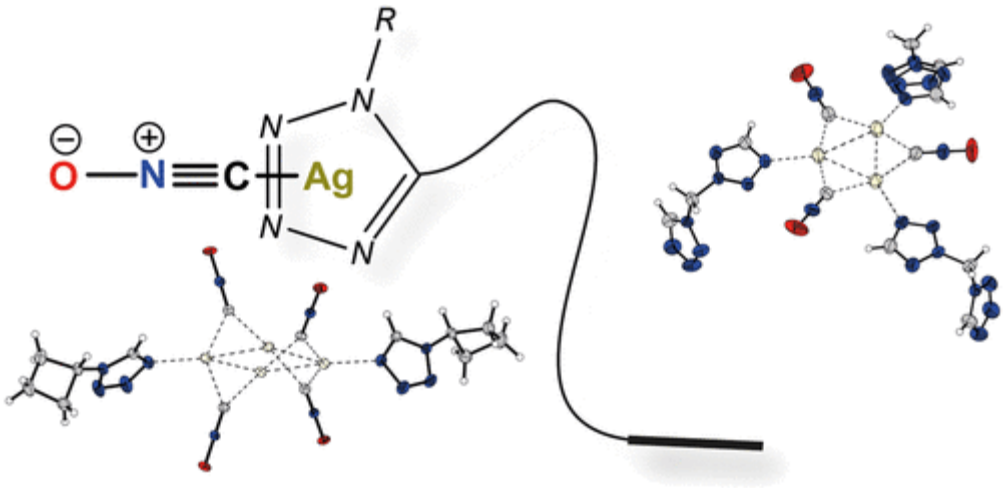
Appendix 19

Taming the Dragon: Complexation of Silver Fulminate with Nitrogen-Rich Azole Ligands

M. H. H. Wurzenberger, M. Gruhne, M. Lommel, V. Braun, N. Szimhardt, J. Stierstorfer

Inorg. Chem. **2020**, *59*, 17875–17879.

https://doi.org/10.1021/acs.inorgchem.0c03027



Supplementary Information:
https://pubs.acs.org/doi/suppl/10.1021/acs.inorgchem.0c03027/suppl_file/ic0c03027_si_001.pdf

Inorganic Chemistry

pubs.acs.org/IC Communication

Taming the Dragon: Complexation of Silver Fulminate with Nitrogen-Rich Azole Ligands

Maximilian H. H. Wurzenberger, Michael S. Gruhne, Marcus Lommel, Vanessa Braun, Norbert Szimhardt, and Jörg Stierstorfer*

Cite This: *Inorg. Chem.* 2020, 59, 17875−17879 Read Online

ACCESS | Metrics & More | Article Recommendations | Supporting Information

ABSTRACT: The almost ancient and very sensitive silver fulminate (SF), which was involved in the establishment of fundamental chemical concepts, was desensitized for the first time with different nitrogen-rich triazoles and tetrazoles, yielding SF complexes $[Ag_x(CNO)_x(N\text{-Ligand})_y]$ (x = 1−4; y = 1−3). These were accurately characterized (X-ray diffraction, scanning electron microscopy, IR, elemental analysis, differential thermal analysis, and thermogravimetric analysis) and investigated concerning their energetic character. The highly energetic coordination compounds suddenly show, in contrast to SF, sensitivities in a manageable range and are therefore safer to handle. In particular, compounds $[Ag_4(CNO)_4(BTRI)]$ [**3**; BTRI = 4,4′-bis(1,2,4-triazole)] and $[Ag_4(CNO)_4(2,2\text{-dtp})]$ [**8**; 2,2-dtp = 1,3-di(tetrazol-1-yl)propane] show values in the range of desired lead styphnate alternatives with similar energetic performances. The crystal structure experiments reveal silver cluster formation in all complexes with distinct argentophilic interactions close to 2.77 Å. Furthermore, it was possible to synthesize **8** in a one-pot reaction, avoiding the isolation of highly sensitive SF.

During a time when alchemy turned into chemistry and attempts were made to transmute elements into gold and silver, the first fulminates were born. The history of fulminates dates back at least to the 17th century, when the unintentional synthesis of mercury fulminate (MF) by Kunckel led to a severe explosion.[1] This incident demonstrates the highly sensitive nature that all fulminates have in common and that is affected by the type of bonding (ionic vs covalent) within the compounds.[2] The explosive characteristics are also responsible for the compounds' designation, which is derived from the Latin word "fulminare", which means "to strike with lightning".[3] Since the first isolation of MF, the most common compound of this class, by Howard in 1799, several famous chemists have investigated fulminates (e.g., Liebig, Gay-Lussac, Kekulé, Pauling, Huisgen, Beck, and many more), which has led to breakthrough discoveries such as the concept of isomerism.[4] Besides the acquisition of fundamental comprehensions and its use for military applications, MF has played a crucial role for peaceful purposes. It enabled, for the first time, the detonation of safely manageable dynamite at the end of the 19th century, thus facilitating civil engineering in general as well as allowing megaprojects such as construction of the Panama Canal (Figure 1A).[1,5]

Except for MF, the only other readily accessible metal fulminate, starting from the corresponding metal, nitric acid, and ethanol, is represented by its silver salt. Silver fulminate (SF) is an extremely dangerous primary explosive (especially toward electrostatic discharge) that can even explode during filtration or underwater and that is therefore too sensitive for almost any application (this corresponds with our experiences!).[6] To the best of our knowledge, the only application of SF is in "bang snaps", also called "snap dragons" (Figure 1B).

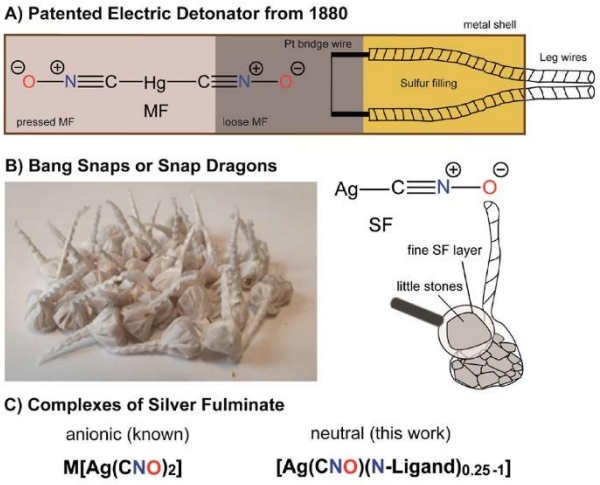
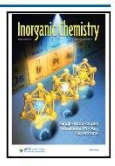


Figure 1. (A) MF in detonators for dynamite initiation. (B) SF for bang snaps. (C) Complexation of SF.

Small amounts of SF, which coats tiny stones that are wrapped in thin paper, instantly detonate when dropped.

Nevertheless, it was intensively examined by Liebig, who was able to handle up to 100 g of this compound. This not only led

Received: October 12, 2020
Published: December 3, 2020

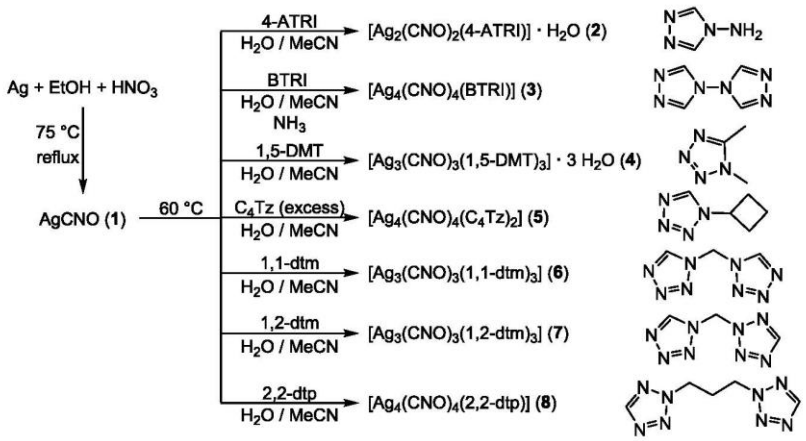


Downloaded via LMU MUENCHEN on February 16, 2022 at 08:07:05 (UTC).
See https://pubs.acs.org/sharingguidelines for options on how to legitimately share published articles.

ACS Publications © 2020 American Chemical Society

https://dx.doi.org/10.1021/acs.inorgchem.0c03027
Inorg. Chem. 2020, 59, 17875−17879

Scheme 1. Synthesis of SF and Its Conversion to Practical ECCs[a]



[a]Overview of the azole ligands used: 4-ATRI, 4-amino-1,2,4-triazole; BTRI, 4,4′-bis(1,2,4-triazole); 1,5-DMT, 1,5-dimethyltetrazole; C_4Tz, 1-cyclobutyltetrazole; 1,1-dtm, di(tetrazol-1-yl)methane; 1,2-dtm, (tetrazol-1-yl)(tetrazol-2-yl)methane; 2,2-dtp, 1,3-di(tetrazol-2-yl)propane.

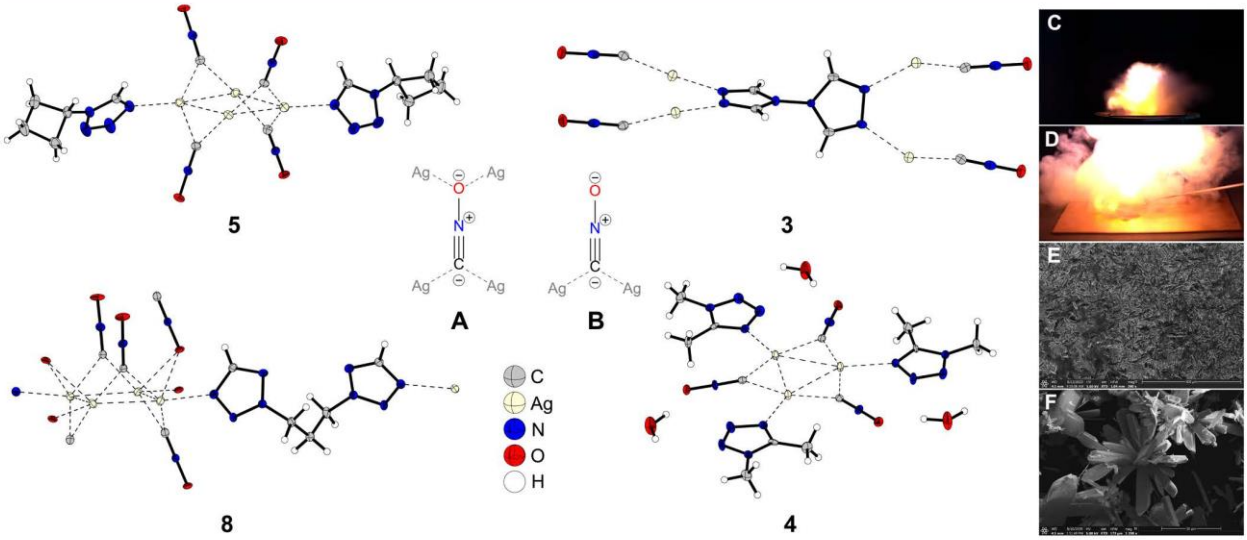


Figure 2. Different bridging modes **A** and **B** of the fulminate anion and molecular units of **3**–**5** as well as the extended molecular unit of **8**. Ellipsoids are set to the 50% probability level.[29] Physicochemical properties: (C) detonation of the ECC **3** during the hot plate test; (D) deflagration of **3** during the hot needle test; (E) SEM image of decomposed AgCNO (200× enlargement); (F) SEM image of complex **8** (1200× enlargement).

to the perfection of his well-known carbon, hydrogen, and nitrogen analysis but also proved his exceptional abilities and great skills.[7] He was also the first one who investigated simple fulminato complexes such as $K[Ag(CNO)_2]$ (Figure 1C).

Soon, several more compounds followed, which were discovered by Nef,[8] Wöhler and Martin,[9] and Wieland.[10] Despite their explosive and sensitive character, all of these complexes had in common that they did not receive much attention regarding their coordination behavior at that time. More detailed examinations on the complexing nature of the CNO^- anion were carried out by Beck, whose work with metal fulminates was extensive.[11] For the first time, it was also possible to obtain nonexplosive and thermally stable fulminato complexes by using large-volume cations.[12] Completely unknown in the literature are fulminate complexes with nitrogen-donor ligands, and especially rare are single-crystal X-ray diffraction (XRD) investigations of fulminate compounds. In recent years, the concept of energetic coordination compounds (ECC) gained increasing interest among scientists worldwide, and various reports set the stage for their future applications.[13−18] Herein, we report the first-ever SF complexes based on nitrogen-rich azole ligands. Following the concept of ECC, highly sensitive SF was combined with (highly) endothermic nonacidic triazole and tetrazole ligands. The incorporation reveals practicable ECC with very diverse and interesting coordination spheres compared to pure SF. Therefore, AgCNO was synthesized according to our preferred literature procedure, which starts with elementary silver, nitric acid, and absolute ethanol.[19] SF was further reacted with readily obtained azole ligands.[20−22] The reaction conditions are highly dependent on the ligand systems used, and all compounds were obtained as colorless solids with satisfactory to very good yields (56−89%). All ECC can be stored at ambient conditions and do not show any evidence for

https://dx.doi.org/10.1021/acs.inorgchem.0c03027
Inorg. Chem. 2020, 59, 17875−17879

Table 1. Summary of the Compounds' Thermal Stability[a], Sensitivities toward Various External Stimuli, and Results of Hot Plate (HP) and Hot Needle (HN) Tests Compared to SF and LS

compound	T_{endo} (°C)[b]	T_{exo} (°C)[c]	IS (J)[d]	FS (N)[e]	ESD (mJ)[f]	BDIS (mJ)[g]	HP[h]	HN[h]
AgCNO (**1**)		196	5[19]	≤0.1[19]	≤0.28	≤4[19]	det.	det.
$[Ag_2(CNO)_2(4\text{-ATRI})]\cdot H_2O$ (**2**)	64, 89	187	>40	>360	>1000	>200	def.	dec.
$[Ag_4(CNO)_4(BTRI)]$ (**3**)		215	5	10	2.5	55	det.	def.
$[Ag_3(CNO)_3(1,5\text{-DMT})_3]\cdot 3H_2O$ (**4**)	82	138	>40	>360	740	>200	def.	dec.
$[Ag_4(CNO)_4(C_4Tz)_2]$ (**5**)		133	20	84	7.3	>200	det.	def.
$[Ag_3(CNO)_3(1,1\text{-dtm})_3]$ (**6**)		152	6	72	25	28	def.	def.
$[Ag_3(CNO)_3(1,2\text{-dtm})_3]$ (**7**)		144	7	64	203	41	def.	def.
$[Ag_4(CNO)_4(2,2\text{-dtp})]$ (**8**)		177	8	1	0.7	8	det.	det.
LS[19,30]		275–280	2.5–5	0.5–1.5	0.02–1	15	det.	det.

[a]Onset temperature at a heating rate of 5 °C min^{-1} measured by differential thermal analysis. [b]Endothermic peak, which indicates melting or dehydration. [c]Exothermic peak, which indicates decomposition. [d]Impact sensitivity according to the BAM drop hammer (method 1 of 6). [e]Friction sensitivity according to the BAM friction tester (method 1 of 6). [f]Electrostatic discharge sensitivity (OZM Electric Spark XSpark10). [g]Ball drop impact sensitivity determined with the 1 of 6 method in accordance with MIL-STD 1751A (method 1016). [h]dec. = decomposition; def. = deflagration; det. = detonation.

decomposition. However, safety precautions (such as Kevlar gloves, face shields, ear protection, etc.) must be applied when handling pure SF and its complexes. Complexes **2**, **4**, and **6**–**8** can easily be crystallized by dissolving AgCNO in a solution of the appropriate amount of ligand in acetonitrile/water (50:50). Whereas the ECC **5** can be synthesized in the same solvent system using an excess of ligand to prevent the formation of pure SF, the coordination compound **2** can be crystallized by adding some drops of aqueous ammonia to the reaction mixture (Scheme 1).

When SF is added to the dissolved ligands in a relatively small amount of solvent, complexes **2**, **6**, and **8** can also be precipitated from the reaction solution, which has to be stirred for 15 (**6** and **8**) to 45 min (**2**). Interestingly, the ECC **8** can be synthesized in a one-pot reaction, avoiding isolation of the highly sensitive SF. Therefore, elemental silver is reacted with nitric acid, and 1,3-di(tetrazol-2-yl)propane (2,2-dtp) dissolved in ethanol is added, which results in the formation of a colorless precipitate (most probably the corresponding silver nitrate complex). When heated with stirring, the solid dissolves around 70 °C, and the typical formation (gas generation accompanied by the precipitation of an off-white solid) of SF occurs. However, instead of pure AgCNO, the corresponding ECC **8** is formed in a very high yield of 89%. All ECC were investigated by single-crystal XRD experiments. Pure SF occurs in two different polymorphic forms, an orthorhombic one as well as a trigonal one.[23] In both cases, coordination of the fulminate anions can be described as a bridging of the terminal carbon and oxygen atoms (Figure 2, **A**) with shorter Ag–C bond lengths (~2.2 Å) compared to the Ag–O ones, leading to 3D polymeric structures. Because some of the Ag–O distances are longer than 2.7 Å, the linking of the anion is better represented as being in mode **B** or between that of **A** and **B**. The addition of nitrogen-donor ligands to SF reveals very diverse and worthwhile coordination chemistry. The same two main coordination modes can be observed in the ECC **2**–**8** (Figures 2 and S3–S9 and Tables S1 and S2). While all structures have the bridging behavior of the fulminate carbon atom between two silver cations in common (Ag–C–Ag = 77–91°), in compounds **2**–**4**, **6**, and **7**, no Ag–O interactions are observed at all. The Ag–O distances in the ECC **5** and **8** are in the range of 2.49–3.01 Å, with most of them above 2.6 Å, which indicates rather weak bonding between them. In all structures, the clear presence of Ag–Ag interactions is observable. These argentophilic interactions are defined as sub van der Waals contacts (<3.44 Å) and have gained increasing attention within the last years.[24−27] The closest Ag–Ag distance with 2.7705(5) Å can be found in the ECC **8**, which is very close to the shortest reported argentophilic interaction [2.7599(3) Å].[28] The ECC **4**, **6**, and **7** are the only compounds that form complex monomers that consist of silver trimers. Coordination of the ditetrazolylmethane ligands with only one of their rings in **6** and **7** is a literature-known issue.[22] In complexes **4** and **8**, tetrameric clusters of silver are present, which build up 2D polymeric layers via Ag–Ag and Ag–O bonding. The additional linking of the ligand in **8** is connecting the layers and leads to the formation of a 3D polymeric network. Contrary to **8**, formation of the 3D structure in **3** is caused by 4-fold coordination of the ligand to different silver atoms, preventing the formation of Ag–O bonds. All ECC were analyzed regarding their physicochemical properties, and their sensitivities toward various external stimuli were determined and are summarized in Table 1. Whereas pure SF does not possess no-fire limits for friction and electrostatic discharge sensitivities, in every case, the incorporation of nitrogen-rich ligands leads to stabilization. Considering the friction sensitivity, it becomes clear that it corresponds with the SF to ligand ratio. Therefore, complexes **3** and **8** are the most sensitive ones, with values close to those of lead styphnate (LS). The incorporation of water molecules creates compounds that are completely insensitive and therefore safe to handle. All ECC show lower thermal stabilities compared to pure SF, except compound **3**, which exceeds 200 °C. Interestingly, the incorporation of bridging ligands (**2**, **3**, and **8**) causes higher exothermic decomposition temperatures, whereas monodentate acting ligands (**4**–**7**) lead to lower thermal stabilities.

Hot plate and hot needle tests reveal the energetic character of the complexes, which all show deflagrations or even detonations (Figures 2 and S13–S20). Whereas none of the ECCs can detonate nitropenta in classical initiation tests, the energetic performances of complexes **3** and **8** are similar to that of LS, making them potential lead-free replacements. Scanning electron microscopy (SEM) was performed to examine the morphology of some of the compounds and compare it with that of pure SF (Figures 2 and S21–S24). Interestingly, SF is the first primary explosive in our research group that is too sensitive to be investigated using SEM. During the sample

https://dx.doi.org/10.1021/acs.inorgchem.0c03027
Inorg. Chem. 2020, 59, 17875−17879

preparation, the substances have to be sputtered using a high-voltage pulse. Most likely, it is the high electrostatic discharge sensitivity of **1** that causes decomposition during the process. In contrast, the ECC show different crystal morphologies with differing crystal sizes, demonstrating their improved stability.

In conclusion, we successfully synthesized seven new SF complexes based on different neutral nitrogen-rich azole ligands. All ECC show fascinating coordination behavior with cluster formation and argentophilic interactions close to the shortest reported Ag−Ag distances. The resulting compounds possess manageable sensitivities, and ligands with bridging character increased the thermal stability up to 215 °C. The possible synthesis of complex **8** in a one-pot reaction from elemental silver, ethanol, nitric acid, and ligand in high yields avoids the isolation of pure SF and opens the field to a safe synthesis of SF complexes, which could be used as a potential replacement for LS.

■ ASSOCIATED CONTENT

Supporting Information

The Supporting Information is available free of charge at https://pubs.acs.org/doi/10.1021/acs.inorgchem.0c03027.

Experimental part and general methods, IR spectroscopy, XRD, differential thermal analysis and thermogravometric analysis plots, hot plate and hot needle tests, and SEM (PDF)

Accession Codes

CCDC 2021064−2021070 contain the supplementary crystallographic data for this paper. These data can be obtained free of charge via www.ccdc.cam.ac.uk/data_request/cif, or by emailing data_request@ccdc.cam.ac.uk, or by contacting The Cambridge Crystallographic Data Centre, 12 Union Road, Cambridge CB2 1EZ, UK; fax: +44 1223 336033.

■ AUTHOR INFORMATION

Corresponding Author

Jörg Stierstorfer − *Department of Chemistry, University of Munich, 81377 München, Germany;* orcid.org/0000-0002-2105-1275; Email: jstch@cup.uni-muenchen.de

Authors

Maximilian H. H. Wurzenberger − *Department of Chemistry, University of Munich, 81377 München, Germany*

Michael S. Gruhne − *Department of Chemistry, University of Munich, 81377 München, Germany*

Marcus Lommel − *Department of Chemistry, University of Munich, 81377 München, Germany*

Vanessa Braun − *Department of Chemistry, University of Munich, 81377 München, Germany*

Norbert Szimhardt − *Department of Chemistry, University of Munich, 81377 München, Germany;* orcid.org/0000-0001-6722-2562

Complete contact information is available at: https://pubs.acs.org/10.1021/acs.inorgchem.0c03027

Notes

The authors declare no competing financial interest.

■ ACKNOWLEDGMENTS

The authors are grateful for financial support of this work by Ludwig-Maximilian University. The authors want to thank Prof. Dr. Thomas M. Klapötke for scientific input and for providing research infrastructure and Prof. Dr. Wolfgang Beck for inspiring discussions. Furthermore, we are very grateful to Moritz Kofen and Jasmin Lechner for providing 1,5-DMT and graphical support and to Lisa Eichacker for proofreading.

■ REFERENCES

(1) Kurzer, F. Fulminic Acid in the History of Organic Chemistry. *J. Chem. Educ.* **2000**, *77*, 851−857.

(2) Iqbal, Z.; Yoffe, A. D. Electronic structure and stability of the inorganic fulminates. *Proc. R. Soc. London A* **1967**, *302*, 35−49.

(3) Martin, W. R.; Ball, D. W. Small organic fulminates as high energy materials. Fulminates of acetylene, ethylene, and allene. *J. Energ. Mater.* **2019**, *37*, 70−79.

(4) Beck, W.; Evers, J.; Göbel, M.; Oehlinger, G.; Klapötke, T. M. The Crystal and Molecular Structure of Mercury Fulminate (Knallquecksilber) [1]. *Z. Anorg. Allg. Chem.* **2007**, *633*, 1417−1422.

(5) Moss, A. J. Introductory Note to Alfred Nobel's Will. *Ann. Noninvasive Electrocardiol.* **2007**, *12*, 79−80.

(6) Matyáš, R.; Pachman, J. *Primary Explosives*, 1st ed.; Springer: Berlin, 2013.

(7) Beck, W. The First Chemical Achievements and Publications by Justus von Liebig (1803−1873) on Metal Fulminates and Some Further Developments in Metal Fulminates and Related Areas of Chemistry. *Eur. J. Inorg. Chem.* **2003**, *24*, 4275−4288.

(8) Nef, J. U. *Ann. Chem.* **1894**, *280*, 263−342.

(9) Wöhler, L.; Martin, F. Über neue Fulminate und Azide. *Ber. Dtsch. Chem. Ges.* **1917**, *50*, 586−596.

(10) Wieland, H. Die Polymerisation der Knallsäure. Isocyanilsäure und Erythro-cyanilsäure. VII. Mitteilung über die Knallsäure. *Justus Liebigs Ann. Chem.* **1925**, *444*, 7−40.

(11) Beck, W. Komplexe Metallfulminate. *Organometal. Chem. Rev. A* **1971**, *7*, 159−190.

(12) Beck, W.; Swoboda, P.; Feldl, K.; Schuierer, E. Neue komplexe Metallfulminate. *Chem. Ber.* **1970**, *103*, 3591−3604.

(13) Myers, T. W.; Bjorgaard, J. A.; Brown, K. E.; Chavez, D. E.; Hanson, S. K.; Scharff, R. J.; Tretiak, S.; Veauthier, J. M. Energetic Chromophores: Low-Energy Laser Initiation in Explosive Fe(II) Tetrazine Complexes. *J. Am. Chem. Soc.* **2016**, *138*, 4685−4692.

(14) Zhang, Q.; Shreeve, J. M. Metal-Organic Frameworks as High Explosives: A New Concept for Energetic Materials. *Angew. Chem., Int. Ed.* **2014**, *53*, 2540−2542.

(15) Wurzenberger, M. H. H.; Szimhardt, N.; Stierstorfer, J. Copper(II) Chlorate Complexes: The Renaissance of a Forgotten and Misjudged Energetic Anion. *J. Am. Chem. Soc.* **2018**, *140*, 3206−3209.

(16) Ilyushin, M. A.; Kotomin, A. A.; Dushenok, S. A. Energy-Saturated Metal Complexes. *Russ. J. Phys. Chem. B* **2019**, *13*, 119−138.

(17) Sun, Q.; Li, X.; Lin, Q.; Lu, M. Dancing with 5-substituted monotetrazoles, oxygen-rich ions, and silver: toward primary explosives with positive oxygen balance and excellent energetic performance. *J. Mater. Chem. A* **2019**, *7*, 4611−4618.

(18) Nguyen, T.-A. D.; Veauthier, J. M.; Angles-Tamayo, G. F.; Chavez, D. E.; Lapsheva, E.; Myers, T. W.; Nelson, T. R.; Schelter, E. J. Correlating Mechanical Sensitivity with Spin Transition in the Explosive Spin Crossover Complex [Fe(Htrz)3]n[ClO4]2n. *J. Am. Chem. Soc.* **2020**, *142*, 4842−4851.

(19) Gruhne, M. S.; Lommel, M.; Wurzenberger, M. H. H.; Szimhardt, N.; Klapötke, T. M.; Stierstorfer, J. OZM Ball Drop Impact Tester (BIT-132) vs. BAM Standard Method-a Comparative Investigation. *Propellants, Explos., Pyrotech.* **2020**, *45*, 147−153.

(20) Brigas, A. F. Product class 30: tetrazoles. *Sci. Synth.* **2004**, *13*, 861−915.

(21) Kirilchuk, A. A.; Yurchenko, A. A.; Vlasenko, Yu. G.; Kostyuk, A. N.; Rozhenko, A. B. Synthesis and Structure of Phosphanylated Bis-Triazoles as Potential Ligands for Chiral Catalysts. *Chem. Heterocycl. Compd.* **2015**, *50*, 1559−1566.

(22) Wurzenberger, M. H. H.; Braun, V.; Lommel, M.; Klapötke, T. M.; Stierstorfer, J. Closing the Gap: Synthesis of Three Isomeric *N,N*-Ditetrazolymethane Ligands and Their Coordination Proficiency in Adaptable Laser Responsive Copper(II) and Sensitive Silver(I) Complexes. *Inorg. Chem.* **2020**, *59*, 10938−10952.
(23) Britton, D.; Dunitz, J. D. The Crystal Structure of Silver Fulminate. *Acta Crystallogr.* **1965**, *19*, 662−668.
(24) Gao, G.-G.; Cheng, P.-S.; Mak, T. C. W. Acid-Induced Surface Functionalization of Polyoxometalate by Enclosure in a Polyhedral Silver-Alkynyl Cage. *J. Am. Chem. Soc.* **2009**, *131*, 18257−18259.
(25) Schmidbaur, H.; Schier, A. Argentophilic Interactions. *Angew. Chem., Int. Ed.* **2015**, *54*, 746−784.
(26) Mistry, L.; El-Zubir, O.; Dura, G.; Clegg, W.; Waddell, P. G.; Pope, T.; Hofer, W. A.; Wright, N. G.; Horrocks, B. R.; Houlton, A. Addressing the properties of "Metallo-DNA" with a Ag(i)-mediated supramolecular duplex. *Chem. Sci.* **2019**, *10*, 3186−3195.
(27) Wang, Q.-Y.; Wang, J.; Wang, S.; Wang, Z.-Y.; Cao, M.; He, C.-L.; Yang, J.-Q.; Zang, S.-Q.; Mak, T. C. W.; Mak, T. C. W. o-Carborane-Based and Atomically Precise Metal Clusters as Hypergolic Materials. *J. Am. Chem. Soc.* **2020**, *142*, 12010−12014.
(28) Ai, P.; Danopoulos, A. A.; Braunstein, P.; Monakhov, K. Yu. A novel, rigid diphosphine with an active NHC spacer; di- and trinuclear complexes of d10 coinage metals. *Chem. Commun.* **2014**, *50*, 103−105.
(29) Selected X-ray data: **3**, *Ccca*, a = 11.8399(9) Å, b = 20.8348(16) Å, c = 5.8163(3) Å, V = 1434.78(17) Å^3, Z = 8, ρ = 3.406 g cm^{-3}; **4**, *P6*^{3}*/m*, a = 15.0648(5) Å, c = 6.1186(4) Å, V = 1202.57(13) Å^3, Z = 2, ρ = 2.204 g cm^{-3}; **5**, *C2/c*, a = 32.653(3) Å, b = 5.4602(5) Å, c = 12.9896(11) Å, β = 97.805(3)°, V = 2294.5(4) Å^3, Z = 8, ρ = 2.454 g cm^{-3}; **8**, *P2/c*, a = 12.5173(11) Å, b = 5.6400(4) Å, c = 12.8877(10) Å, β = 100.146(8)°, V = 895.61(12) Å^3, Z = 2, ρ = 2.891 g cm^{-3}.
(30) Klapötke, T. M. *Energetic Materials Encyclopedia*, 1st ed.; De Gruyter: Berlin, 2018.

https://dx.doi.org/10.1021/acs.inorgchem.0c03027
Inorg. Chem. 2020, 59, 17875−17879

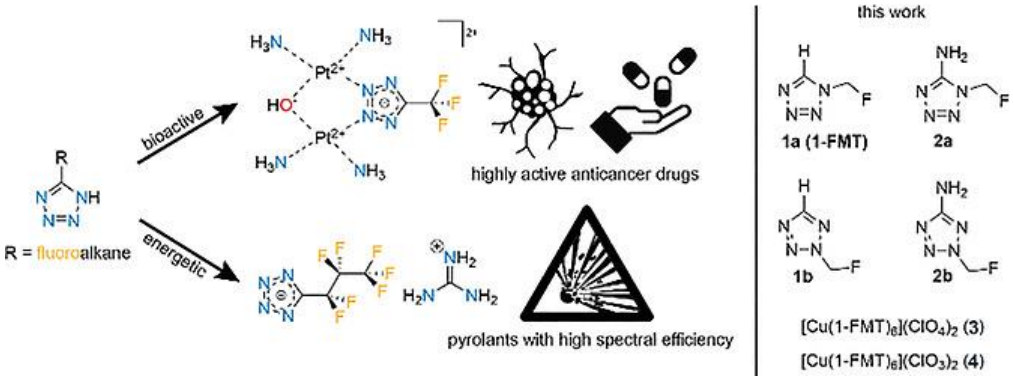
Appendix 20

N-Fluoromethylated (Amino)Tetrazoles: Manipulating Thermal and Energetic Properties

M. Reichel, M. H. H. Wurzenberger, M. Lommel, M. Kofen, B. Krumm, J. Stierstorfer, K. Karaghiosoff

Z. Anorg. Allg. Chem. **2021**, 647, 341–349.

https://doi.org/10.1002/zaac.202000341



Supplementary Information:
https://onlinelibrary.wiley.com/action/downloadSupplement?doi=10.1002%2Fzaac.202000341&file=zaac202000341-sup-0001-SupMat.pdf

Journal of Inorganic and General Chemistry
ZAAC
Zeitschrift für anorganische und allgemeine Chemie
DOI: 10.1002/zaac.202000341
ARTICLE

N-Fluoromethylated (Amino)Tetrazoles: Manipulating Thermal and Energetic Properties

Marco Reichel,[a] Maximilian H. H. Wurzenberger,[a] Marcus Lommel,[a] Moritz Kofen,[a] Burkhard Krumm,*[a] Jörg Stierstorfer,*[a] and Konstantin Karaghiosoff*[a]

Dedicated to Prof. Dr. Thomas M. Klapötke on the Occasion of his 60th Birthday

Abstract. Fluoroiodomethane was allowed to react with the sodium salts of 5*H*-tetrazole and 5-aminotetrazole to give in each case the two corresponding isomers 1-fluoromethyl-5*H*-tetrazole (**1a**) and 2-fluoromethyl-5*H*-tetrazole (**1b**), as well as 1-fluoromethyl-5-aminotetrazole (**2a**) and 2-fluoromethyl-5-aminotetrazole (**2b**). The new tetrazoles were isolated and characterized by spectroscopic methods (IR, Raman, multinuclear NMR), mass spectrometry, and in the case of fluoromethyl-5-aminotetrazole the crystal structures of both isomers were obtained and discussed. Differential thermal analysis (DTA) gave insight in how a FCH_2 moiety attached to a tetrazole effects the thermal behavior compared to its CH_3 analog. In addition, the detonation parameters were calculated and compared to those of the corresponding methyltetrazoles. In addition, the preparation of energetic copper complexes of the new ligands was attempted. Complexes of copper(II) perchlorate and chlorate are crystallographically described and their energetic properties discussed.

Introduction

Tetrazoles, whose discovery dates back to the year 1885,[1] are well investigated long known substances and can be easily synthesized. There are numerous ways to obtain substituted tetrazoles.

The most common and applied protocols nowadays either use a [3+2] cycloaddition of nitriles and azides in presence of a proton source or a [3+1+1] cyclization starting from an amine, triethyl orthoformate and sodium azide with acetic acid as reaction medium.[1] Another approach those of the substitution reactions of 1*H*-tetrazoles to introduce functional groups such as amines,[2] alkanes,[3] or even *N*-oxides[4] to the nitrogen atoms of the heterocycle. This synthetic pathway allows the preparation of 2*N*-substituted tetrazoles, which are often obtained as isomeric mixtures with the 1*N*-substituted compound. Since tetrazoles are bioisoster to carboxylate groups, they are mostly used as pharmaceutical agents and show central nervous system-, anti-inflammatory-, anti-allergic-, anti-microbial-, cardiovascular- and miscellaneous activity.[1,5] Furthermore, it is well known that tetrazoles can be used for the synthesis of coordination compounds with various metal ions, and there has been a growing interest over the last years.[6] The resulting complexes further expand the field of possible applications for tetrazole-based substances (e.g. metal-organic frameworks (MOFs) with unique properties,[7] spin crossover systems,[8] and energetic materials[9]). It is also well-known, that most tetrazole derivatives are melting above 150 °C and exhibit explosive properties when heated above their melting points or touched with a hot wire.[10] Furthermore, the impact sensitive behavior of tetrazole cycle linked to nitrogen atoms and the explosive nature of heavy metal salts of 5-monosubstituted tetrazoles were mentioned in literature before.[10] However, *Klapötke* and co-workers were the first who recognized, that tetrazoles are good starting materials for the synthesis of new highly energetic nitrogen-rich materials.[11]

Because tetrazoles combine the desired endothermicity with kinetic stability, forming non-toxic reaction products, producing a high temperature and having a high burning rate during decomposition,[11] *Klapötke* and co-workers investigated tetrazole derivatives as green[12] high performance explosive replacements.[13] Therefore, this class of compounds was applied in primary explosives,[14] secondary explosives,[11,13] and pyrotechnics.[11,15] Fluorine containing tetrazoles are especially interesting as oxidizers in magnesium based flare compositions (decoy flares)[15] (Figure 1) or in agent defeat weapons, as fluorine containing payloads are effective in destroying biological threats like anthrax.[11] More recent investigations showed that the replacement of a CH_3 with a FCH_2 moiety can lead to a drastic change in the physical- and sensitivity properties of a compound.[16]

However, until very recently this year, the first and only fluoromethyl containing tetrazole, 5-fluoromethyl-tetrazole[17] and one non-energetic complex[18] were reported. Since a large number of fluoromethylating agents for various nucleophiles are available until now[19] and only *N*-methylated but no *N*-fluoromethylated tetrazoles are known up to date, this

* Dr. B. Krumm
E-Mail: bkr@cup.uni-muenchen.de
* Dr. J. Stierstorfer
E-Mail: jstch@cup.uni-muenchen.de
* Prof. Dr. K. Karaghiosoff
E-Mail: klk@cup.uni-muenchen.de
[a] Department of Chemistry
Ludwig–Maximilian University of Munich
Butenandtstr. 5–13 (D)
81377 Munich, Germany
Supporting information for this article is available on the WWW under **http://dx.doi.org/10.1002/zaac.202000341** or from the author.

© 2020 Wiley-VCH GmbH

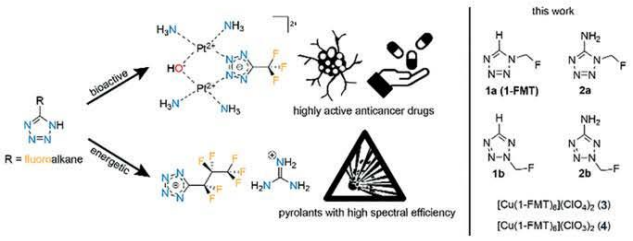
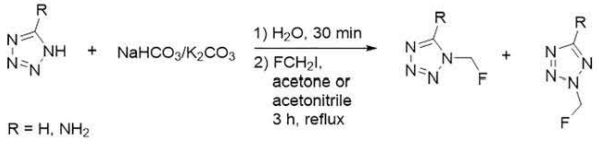


Figure 1. Selected fluorine containing tetrazoles.

prompted us to synthesize fluoromethylated tetrazoles und investigate their thermal-, energetic- and complexation behavior.

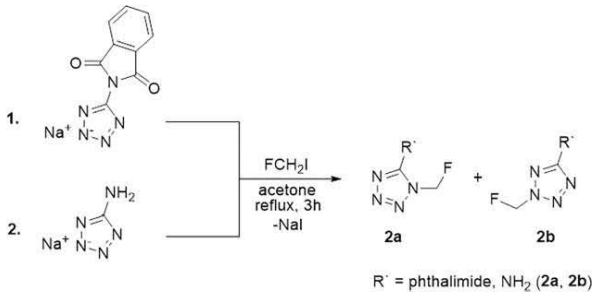
Results and Discussion

N-Fluoromethylated tetrazoles were obtained in a simple, mild and high yield synthesis from the reaction of the corresponding sodium or potassium tetrazolate salts with fluoroiodomethane in acetone or acetonitrile (Scheme 1). Unlike for the reaction of sodium 5-aminotetrazolate (NaAT) with CH_3I or $(CH_3O)_2SO_2$, water[20] or ethanol[21] should be avoided as solvent for the synthesis, since such use did cause extensive decomposition during the reaction.



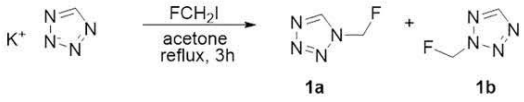
Scheme 1. Synthesis of *N*-fluoromethylated tetrazoles.

This synthetic pathway leads to the formation of two isomers which have to be specially purified. In contrast to their methyl analogs, special synthetic routes *via* their phthalimides[22] resulting exclusively in the formation of only one isomer, were not successful here by employing fluoroiodomethane. Here also both corresponding fluoromethyl isomers were formed (Scheme 2).



Scheme 2. Synthesis of fluoromethylated 5-aminotetrazoles.

The reaction of potassium tetrazolate with FCH_2I gave 85 % of a mixture of 1-fluoromethyl-5*H*-tetrazole (**1a**) and 2-fluoromethyl-5*H*-tetrazole (**1b**) (Scheme 3).



Scheme 3. Synthesis of *N*-fluoromethylated 5*H*-tetrazoles.

From this mixture the isomers were separated as colorless oils via distillation with 10 % (**1a**) and 40 % (**1b**) yield. Both compounds can easily be distinguished by multinuclear NMR spectroscopy in $CDCl_3$. In the ^1H NMR spectrum, the FCH_2 resonance for **1a** is observed at δ = 6.40 ppm with a coupling constant of $^2J(F,H)$ = 50.0 Hz and the resonance of C*H* hydrogen atom at δ = 8.90 ppm. In comparison with **1a**, the FCH_2 resonance of **1b** at δ = 6.55 ppm with a coupling constant of $^2J(F,H)$ = 49.7 and $^5J(H,H)$ = 0.4 Hz is shifted to higher frequencies and that of C*H* is shifted to lower frequencies (δ = 8.65 ppm). The ^{13}C NMR resonances of **1a** appear at δ = 82.8 ppm with a coupling constant of $^1J(F,C)$ = 209.5 Hz (CH_2F) and at δ = 143.7 ppm for the tetrazole carbon atom. Both resonances are shifted to lower frequencies compared to **1b**. Here, the FCH_2 resonance appears at δ = 86.1 ppm, having a coupling constant of $^1J(F,C)$ = 211.7 Hz and that of C*H* is detected at δ = 154.1 ppm. Similarly, both isomers can easily be distinguished by their ^{19}F NMR resonances. Here, the triplet of **1a** is detected at δ = –169.4 ppm, whereas that of **1b** is found at δ = –171.4 ppm.

The tetrazole **1a** has a melting point of 19 °C. Compared to its methyl derivative (extrapolated boiling point of 259 °C at normal pressure, 110 °C/5 Torr; melting point 39 °C)[25] the thermal properties of **1a** are shifted to lower values. The same accounts for the isomer **1b**. With an extrapolated boiling point of 160 °C and a melting point of 0 °C this boils and melts lower as the corresponding methyl derivative, which has an extrapolated boiling point of 213 °C (145 °C/118 Torr) and a melting point of 10 °C.[25,29]

The reaction of NaAT with FCH_2I in acetone resulted in 83 % of a 2:1 mixture of 1-fluoromethyl-5-aminotetrazole **2a** and 2-fluoromethyl-5-aminotetrazole **2b**. From this mixture **2a** was isolated with 51 % and **2b** with 24 % yield (Scheme 2, reaction 2).

Both isomers are colorless solids and can be easily distinguished via multinuclear NMR spectroscopy in DMSO-D_6. In the ^1H NMR spectrum, the FCH_2 signal for **2a** is observed at δ = 6.25 ppm with a coupling constant of $^2J(F,H)$ = 51.9 Hz and the resonance of the amino group at δ = 7.32 ppm. In comparison with **2a**, the FCH_2 resonance of **2b** at δ = 6.46 ppm with a coupling constant of $^2J(F,H)$ = 50.8 Hz is shifted to higher frequencies and the resonance of the amino group is shifted to lower frequencies (δ = 6.45 ppm). The ^{13}C NMR resonances of **2a** appear at δ = 86.6 ppm with a coupling constant of $^1J(F,C)$ = 202.2 Hz (FCH_2) and at δ = 168.0 ppm. Both resonances are shifted to lower frequencies compared to **2b**. Here, the FCH_2 signal at δ = 81.2 ppm, having a coupling constant of $^1J(F,C)$ = 197.7 Hz differs clearly. However, final distinction of the two isomers in the ^{13}C NMR spectra is given by the CNH_2 resonance of **2b**, which splits into a doublet $^4J(F,C)$ = 1.4 Hz having a chemical shift of δ = 156.1 ppm. A

© 2020 Wiley-VCH GmbH

good distinction of the both isomers is possible by ^{19}F NMR spectroscopy. The triplet of **2a** is detected at δ = –170.8 ppm, and is shifted to lower frequencies, compared to that of **2b** with δ = –169.7 ppm. The ^{15}N NMR chemical shift of the NH_2 group is shifted to lower frequencies for **2b** compared to **2a**. The NCH_2F resonance in **2b** splits in a doublet with a coupling constant of $^2J(F,N)$ = 17.4 Hz. However, due to the low solubility of **2a** in DMSO, this resonance is not visible. Whereby only one long range coupling at δ = –23.8 ppm $J(F,N)$ = 1.1 Hz, forming a doublet is observed for **2a**, the isomer **2b** displays two long range couplings at δ = –71.6 and –120.7 ppm forming a doublet with $J(F,N)$ = 0.7 and 1.2 Hz. The slow isomerization of **2b** into **2a** is visible in the $^{15}N\{^1H\}$ NMR spectrum (Figure 2, marked with an asterisk).

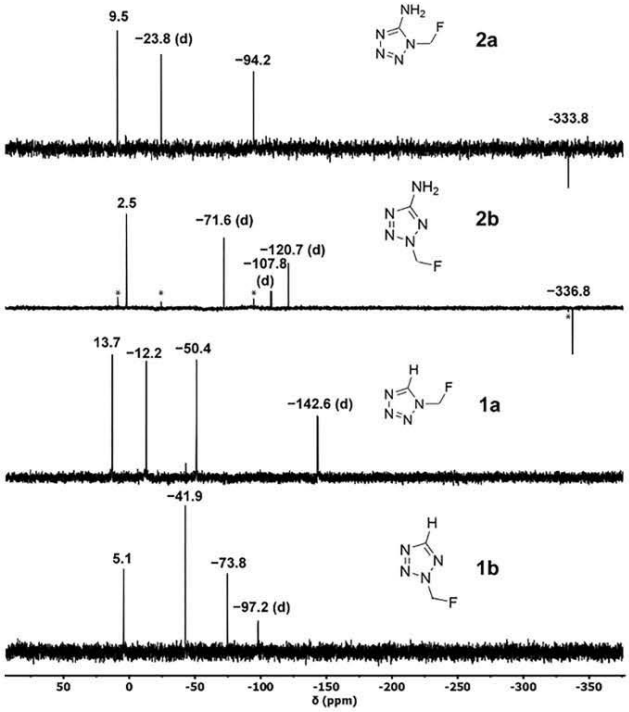


Figure 2. $^{15}N\{^1H\}$ NMR spectra of **1a/b** and **2a/b** (DMSO-D_6 or $CDCl_3$, 25 °C). Isomerization to **2a** is marked with an asterisk.

In contrast to aminotetrazoles **2a** and **2b**, no long range couplings in the ^{15}N NMR were observed for tetrazoles **1a** and **1b**. The NCH_2F group shows in **1a** a drastic shift to lower frequencies [δ = –142.6 ppm (**1a**) vs. δ = –97.2 ppm (**1b**)]. However, the coupling constant of the doublet with $^2J(F,N)$ = 17.5 Hz remains the same.

Single crystals of both aminotetrazoles were obtained by dissolving the products in water and cooling the solution to 3 °C for several days. The molecular structures of **2a** and **2b** in the crystal are shown in Figure 3.

The nitrogen atom bonded to the FCH_2 group in **2a** and **2b** displays a trigonal planar environment. The corresponding N1–C2 and N2–C2 bond lengths of 1.429(4) and 1.439(2) Å, respectively, compare well to each other and are shortened compared to the known $[Me_3NCH_2F]^+$[23a] moiety. The C2–F1 distance of 1.382(3) Å (**2a**) and 1.380(2) Å (**2b**) compare well

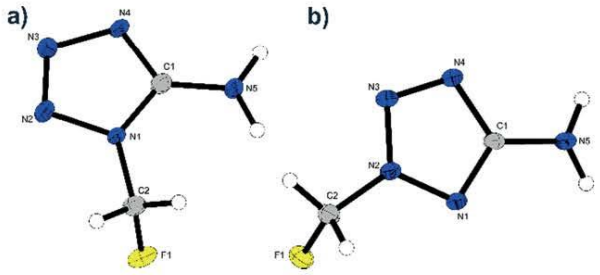


Figure 3. Molecular structure of **2a** (a) and **2b** (b) in the crystal. Selected bond lengths and angles of **2a**: F1–C2, 1.382(3); C2–N1, 1.429(4); F1–C2–N1, 109.3(2); F1–C2–N1–C1, –82.7(4). **2b**: F1–C2, 1.380(2); C2–N2, 1.439(2); F1–C2–N2, 108.6(2); F1–C2–N2–N1, –70.0(2).

with those reported for a FCH_2P phosphonium salt [1.379(5) Å],[19c] FCH_2I [1.380(17) Å][23b] and FCH_2Br [1.377(4) Å].[23b] Noteworthy is the different thermal behavior observed for **2a** and **2b**. The melting points of these two compounds differ by almost 60 °C. Analogous properties are reported for the methyl derivatives.[24]

In order to understand this behavior, intermolecular interactions in the crystal have to be investigated and a Hirshfeld analysis was performed on the crystal structures of **2a** and **2b** (Figure 4). The sum $d_i + d_e$ (d_i: distance from the Hirshfeld surface to the nearest atom interior; d_e: distance from the Hirshfeld surface to the nearest atom exterior) in the 2D plot of **2a** and **2b** reveals, that the spikes for N···H contacts are similarly wide for both compounds and only slightly longer for **2a**. Thus, for both compounds, the N···H contacts in this range are similarly strong and the strong interactions occur with a similar frequency. However, there are clear differences regarding the F···H contacts. These are clearly stronger for **2a** (distinct long spikes) than for **2b**, as indicated also by the

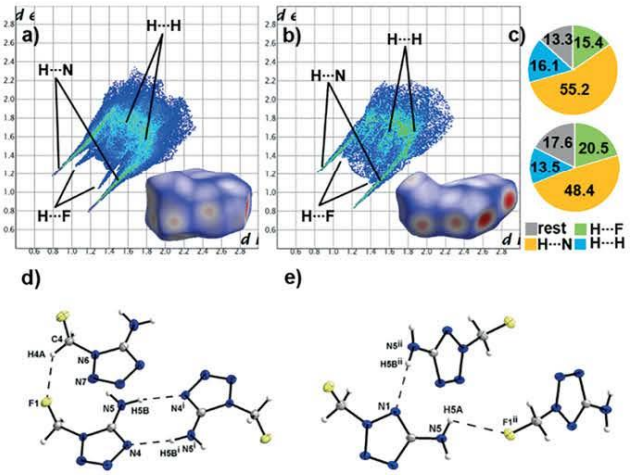


Figure 4. Two-dimensional fingerprint plot as well as the corresponding Hirshfeld surface (bottom right in 2D plot) of **2a** (a) and **2b** (b). Color coding: white, distance d equals VDW distance; blue, d exceeds VDW distance, red, d, smaller than VDW distance). Population of close contacts of **2a** (c) top and **2b** (c) bottom in crystal stacking. Strongest hydrogen bonds in **2a** (d) and **2b** (e). Symmetry codes: *i*) 2–x, 1–y, –z; *ii*) 0.5+x, 0.5–y, 0.5+z; *iii*) 0.5–x, 0.5+y, 0.5–z.

© 2020 Wiley-VCH GmbH

shorter hydrogen bridges in the crystal structure. With H···F contact distances of 2.37(3) Å (**2a**) vs. 2.60(3) Å (**2b**) the attractive forces in the crystal of 1-fluoromethyl-5-aminotetrazole **2a** are clearly stronger than for **2b**. The sum of the attractive interactions for **2a** (70.6 %) and for **2b** (68.9 %) is almost the same. As consequence, the sum of all intermolecular interactions in the crystal of **2a** are stronger than in **2b**. This results in dramatic differences in the thermal behavior of the two isomers **2a** and **2b**. Aminotetrazole **2a** decomposes while melting at 131 °C, whereas the isomer **2b** melts at 75 °C and decomposes at 166 °C. It is interesting to compare these thermal properties with those of the corresponding methyl derivatives. The 1-methyl 5-aminotetrazole (m.p. 226 °C[24a]) and 2-methyl-5-aminotetrazole (m.p. 105 °C[24b]) show in both cases a higher melting point than their fluorine containing derivatives (Figure 5).

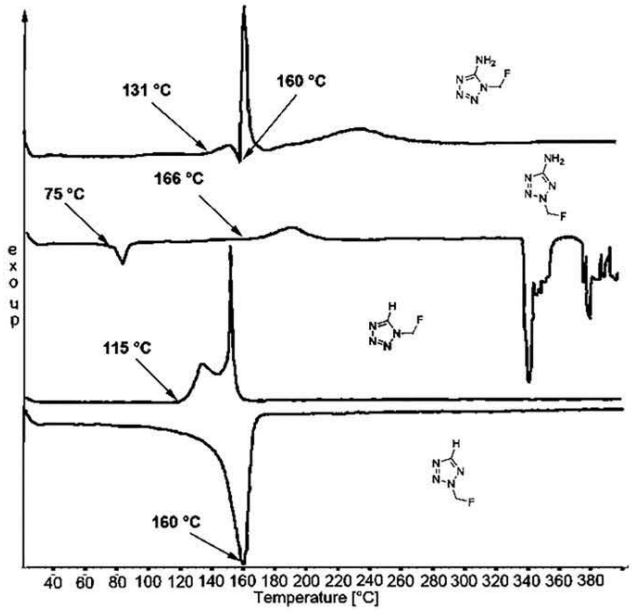


Figure 5. DTA of fluoromethyl tetrazoles **1**–**2**.

Similar as for aminotetrazoles **2**, the fluorine effects the thermal properties of tetrazoles **1**, compared to their methyl analogs in a similar manner.

Energetic Properties

The sensitivities towards friction and impact of **1** and **2** were determined experimentally according to standards of the German Federal Institute for Material Research and Testing (BAM). According to the UN recommendations on transport of dangerous goods, **1** and **2** have to be classified as insensitive towards impact and friction (Table 1). *Ab initio* calculations were carried out to compute the heat of formation for **1**, **2** and the corresponding methyl derivatives, using the optimized geometry of the molecules starting from the X-ray diffraction experiment.

In general, the methyl derivatives show a higher heat of formation than their fluoromethyl derivatives. Further, compounds **1a** and **2a** show a higher heat of formation than for the isomers (**1b**, **2b**) thereof, which is also the case for the methyl derivatives. Based on the heats of formation and the corresponding densities determined from the X-ray experiments or calculations, the detonation parameters were calculated using the EXPLO5 V6.03 code. The detonation parameters were calculated at the Chapman-Jouguet (C-J) point with the help of a stationary detonation model using a modified Becker-Kistiakowski-Wilson state equation for the system. The C-J point was located using the first derivative of the Hugoniot curve of the system. Interestingly the heat of detonation of the methyl derivatives exceeds – except for **1-MATz** – those of the fluoromethyl compounds. However, the detonation temperature and pressure show better performance parameters for the fluoromethyl compounds than for their methyl derivatives. Whereas the detonation velocity is always higher for the fluoromethyl compounds (except for **1a**), the volume of detonation gases varies. In summary, the conversion of a CH_3 to a FCH_2 group seems to increase the performance parameters in most cases. Further regarding the fluoromethyl compounds, as a general trend, the 1N-isomers exhibit better performance parameters, than the 2N-isomers.

N-Fluoromethylated Tetrazoles as Ligands

For investigating the complexation behavior of the nitrogen-rich molecules and comparison with their fluorine-free analogs, attempts were made to synthesize complexes according to literature procedures.[30] Various combinations of the ligands **1a**–**2b** with various metals (Ag^+, Mn^{2+}, Fe^{2+}, Fe^{3+}, Cu^{2+}, and Zn^{2+}) and anions (Cl^-, NO_3^-, ClO_3^-, ClO_4^-) were investigated (Scheme 4). In the cases of **1b** and **2b** only starting material was recovered regardless of the used solvent systems (water, methanol, ethanol, acetonitrile, and mixtures). Most of the silver salt solutions showed signs of decomposition and deposition of elemental silver within hours or days, which also occurred when stored in the dark. When applying **1a** for the synthesis of complexes **3** and **4**, it is possible to achieve hexa-coordination to copper(II) central metals as with 1-methyl-5*H*-tetrazole.[30c] Combining 1-fluoromethyl-5-aminotetrazole with silver(I), iron(II), or copper(II) salts led to the immediate formation of viscid brownish precipitates. However, it was possible to pick one single crystal out of the reaction of copper(II) chlorate with **2a**. The single-crystal diffraction experiment revealed a copper(I) chlorate complex (**5**), as a product of a redox process. To the best of our knowledge, **5** is the first copper(I) chlorate complex described in literature, but unfortunately impossible for straightforward synthesis, due to the non-existence of a copper(I) chlorate source. Consequently, tetrakis(acetonitrile)copper(I) perchlorate was synthesized from a standard procedure in acetonitrile and further reacted with **2a**. This synthetic approach led to the analog perchlorate complex **6** (identified by X-ray crystallography, see Supporting Information), showing almost the identical coordination as

© 2020 Wiley-VCH GmbH

Table 1. Energetic parameters of **1a–2b** compared to their methyl analogs.

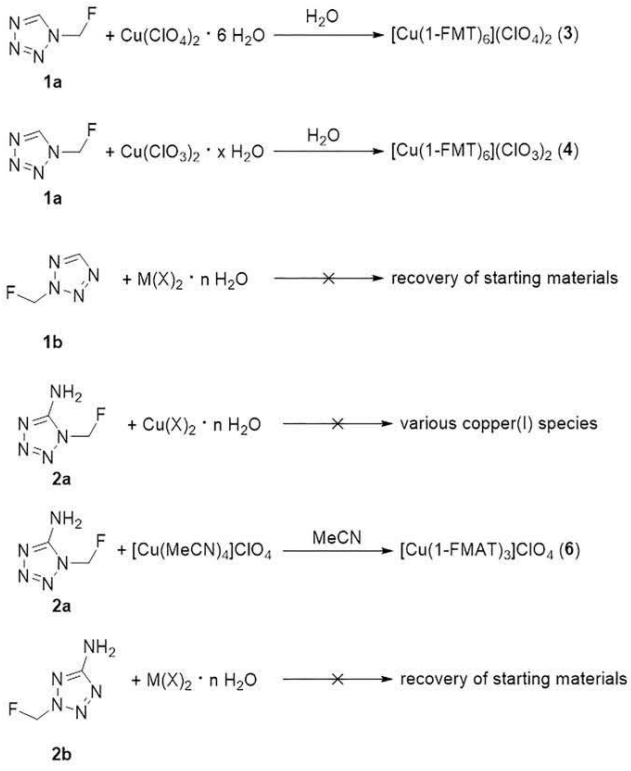
	1a	**1b**	**2a**	**2b**	1-MATz	2-MATz	1-MHTz	2-MHTz
Formula	$C_2H_3FN_4$	$C_2H_3FN_4$	$C_2H_4FN_5$	$C_2H_4FN_5$	$C_2H_5N_5$	$C_2H_5N_5$	$C_2H_4N_4$	$C_2H_4N_4$
M /g·mol^{-1}	102.03	102.03	117.04	117.04	99.10	99.10	84.08	84.08
IS [a] /J	>40	>40	>40	>40	>40[14a]	>40[14a]	>40[14a]	>40[14a]
FS [b] /N	>360	>360	>360	>360	>360[14a]	>360[14a]	>360[14a]	>360[14a]
N [c] /%	54.89	54.89	59.81	59.81	70.67	70.67	66.63	66.63
Ω_{CO} [d] /%	–47.0	–47.0	–47.8	–47.8	–72.6	–72.6	–76.1	–76.1
Ω_{CO2} [d] /%	–78.4	–78.4	–75.2	–75.2	–104.9	–104.9	–114.2	–114.2
T_{melt} [e] /°C	19	0	131	75	225[14a]	104[14a]	39[14a]	9[25]
ρ_{293K} [f] /g·cm^{-3}	1.593	1.581	1.648	1.638	1.42[26]	1.341[27]	1.432[28]	1.31[26]
ΔH_f^0 [g] /kJ·mol^{-1}	71.0	56.3	44.5	34.4	210.2	206.3	244.1	227.9
EXPLO5 V 6.03								
ΔU_f^0 [h] /kJ·kg^{-1}	–3235	–3096	–2773	–2691	–2725	–2713	–3316	–3210
T_{C-J} [i] /K	2533	2465	2220	2184	1967	1974	2225	2227
P_{C-J} [j] /GPa	17.8	17.1	20.4	19.8	16.5	14.0	16.7	13.8
V_{det} [k] /ms^{-1}	7221	7105	7677	7589	7313	6897	7321	6876
V_o [l] /dm^3·kg^{-1}	826	826	858	859	864	872	817	825

a) Impact sensitivity (BAM drop-hammer, method 1 of 6). b) Friction sensitivity (BAM friction tester, method 1 of 6). c) Nitrogen content. d) Absolute oxygen balance assuming the formation of CO or CO_2 and HF. e) Melting point. f) Density at 293 K. g) Heat of formation calculated at the CBS-4M level of theory. h) Detonation energy. i) Detonation temperature. j) Detonation pressure. k) Detonation velocity. l) Volume of detonation gases at standard temperature and pressure conditions.

found for the chlorate **5**. Both compounds **5** and **6** are highly unstable under ambient conditions.

In contrast to **5** and **6**, the complexes **3** and **4** when using copper(II) perchlorate and chlorate as starting material are stable in air.

The bond lengths and angles of the tetrazole ligands are in all complexes similar to those of **1a** and **2a**. The perchlorate **3** with a hexacoordination around the copper(II) center, crystallizes in the monoclinic space group $P2_1/c$ with two formula units per unit cell and a calculated density of 1.911 g·cm^{-3} (107 K). The molecular unit consists of one copper(II) cation octahedrally coordinated by six tetrazole ligands and two non-coordinating perchlorate anions (Figure 6). The Cu-N bond lengths are in the typical range of octahedrally coordinated copper(II) centers showing a Jahn-Teller distortion.



Scheme 4. Reactivity of **1a–2b** towards metal salts.

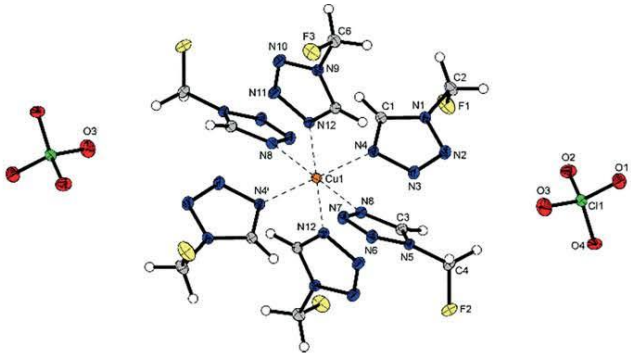


Figure 6. Molecular unit of perchlorate **3**. Selected bond lengths and angles of **3**: Cu1–N4 2.0489(12), Cu1–N8 2.4377(13), Cu1–N12 2.0133(12), N4–Cu1–N8 90.94(5), N4–Cu1–N8 90.71(5), N4–Cu1–N4^i 180.00. Symmetry code: *i*) –x, 1–y,1–z.

Chlorate complex **4** shows a similar buildup like perchlorate compound **3** and crystallizes in the trigonal space group $R\bar{3}$ with three formula units per unit cell and a calculated density of 1.752 g·cm^{-3} (298 K) (Figure 7; for energetic parameters of **3** and **4**, see Table 2).

The chlorate **5** crystallizes in the hexagonal space group $P6_3$ with two formula units per unit cell and a calculated density of 1.895 g·cm^{-3} (133 K). The molecular unit consists of one copper(I) cation coordinated by three tetrazole ligands in trigonal-planar fashion and one non-coordinating chlorate anion (Figure 8). The Cu–N bond lengths are in the typical range of trigonal-planar copper(I) complexes.[31]

© 2020 Wiley-VCH GmbH

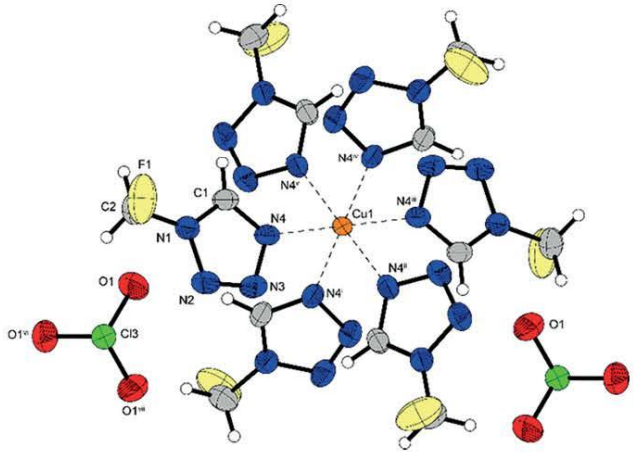


Figure 7. Molecular unit of chlorate **4**. Selected bond length and angle of **4**: Cu1–N4 2.135(2), N4–Cu1–N4^{i} 92.03(9). Symmetry codes: *i*) 1–y, x–y, z; *ii*) 1–x+y, 1–x, z; *iii*) 4/3–x, 2/3–y, 2/3–z; *iv*) 1/3 + y,2/3–x+y, 2/3–z; *v*) 1/3 + *x*–y, –1/3 + *x*, 2/3–z.

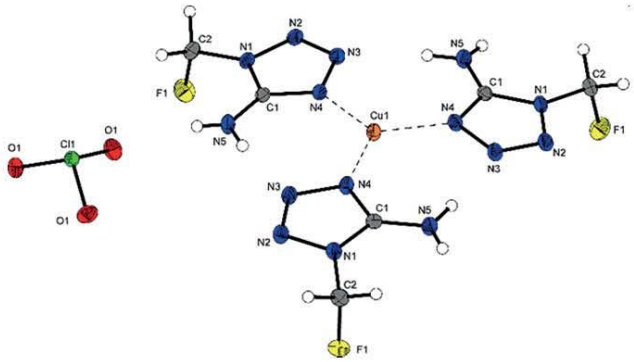


Figure 8. Molecular unit of chlorate **5**. Selected bond length and angle of **5**: Cu1–N4 1.952(3), N4–Cu1–N4^{i} 119.95(12). Symmetry codes: *i*) 2–y, 1+x–y, z; *ii*) 1–x+y, 2–x, z.

Conclusions

In summary, new fluoromethylated tetrazoles were synthesized, which can act as versatile interesting ligands, especially in energetic complexes. Single crystal X-ray diffraction reveals structural information of a nitrogen connected to a FCH_2 moiety in heterocycles, the first of its kind. The NCH_2F moiety has a shortened N–C and C–F bond length compared to the $[Me_3NCH_2F]^+$ moiety. Only weak fluorine hydrogen interactions were observed. Using Hirshfeld analysis, it could be demonstrated that in 2-fluoromethyl-5-aminotetrazole the reduced number of stronger N···H contacts – replaced by weaker F···H contacts is the main reason for the drastically changed thermal behavior between the isomers. As a general trend, thermal properties are influenced in such manner, that a FCH_2 group lowers the boiling and melting point compared to a CH_3 group. Whereas the fluoromethyl derivatives lead to a lower heat of formation, the detonation parameters exhibit in most cases better performance. Interestingly the coordination ability of the new tetrazoles **1a**, **1b**, **2a** and **2b** towards copper centers seems to be moderate. While the 2N-isomers did not yield any pure and crystalline material, the 5-aminotetrazole derivatives act as reducing agents yielding mostly amorphous Cu(I) species. However, **1a** (1-FMT) was successfully incorporated as a ligand in the highly energetic complexes $[Cu(1\text{-}FMT)_6](ClO_4)_2$ (**4**) and $[Cu(1\text{-}FMT)_6](ClO_3)_2$ (**4**). While the change from the perchlorate anion (**3**) to chlorate (**4**) has no significant effect on the sensitivity towards external stimuli, a drastically lower thermal stability for **4** (87 °C) than **3** (186 °C) is observed. Furthermore, the crystal structures of the unstable Cu^{I} fluoromethyl 5-aminotetrazole complexes $[Cu(1\text{-}FMAT)_3]ClO_3$ (**5**) and $[Cu(1\text{-}FMAT)_3]ClO_4$ (**6**) was determined.

Experimental Section

Fluoroiodomethane was distilled prior use. All other chemicals were commercially available from ABCR. For NMR spectroscopy the solvents were dried using 3 Å molecular sieve. Spectra were recorded on a Bruker Avance III spectrometer operating at 400.1 MHz (^{1}H), 100.6 MHz (^{13}C), 376.4 MHz (^{19}F), and 40.6 MHz (^{15}N). Chemical shifts are referred to TMS (^{1}H, ^{13}C), $CFCl_3$ (^{19}F) and $MeNO_2$ (^{15}N). The ^{19}F NMR spectra were also recorded in the ^{1}H decoupled mode. Raman spectra were recorded with a Bruker MultiRam FT Raman spectrometer using a neodymium doped yttrium aluminum garnet (Nd:YAG) laser (λ = 1064 nm) with 1074 mW. The samples for Infrared spectroscopy were placed under ambivalent conditions onto an ATR unit using a Perkin–Elmer Spectrum BX II FT-IR System spectrometer. Melting and / or decomposition points were detected with a OZM DTA 552-Ex. The scanning temperature range was set from 293 K to 673 K at a scanning rate of 5 K·min^{-1}. Elemental analysis was done with a Vario EL instrument and a Metrohm 888 Titrando device. The mass spectrum was recorded on a Thermos Fischer GC/MS instrument. Crystallographic Data collection was performed with an Oxford Xcalibur 3 diffractometer equipped with a Spellman generator (50 kV, 40 mA) and a Kappa CCD detector, operating with Mo–K_α radiation (λ = 0.71073 Å). Data collection and data reduction were performed with the CrysAlisPro software[32] Absorption correction using the multiscan method[33] was applied. The structures were solved

Table 2. Energetic parameters of **3** and **4** compared to their methyltetrazole analogs.

Compound	T_{endo} /°C [a]	T_{exo} /°C [b]	IS /J [c]	FS /N [d]	ESD /mJ [e]
$[Cu(1\text{-}FMT)_6](ClO_4)_2$ (**3**)	–	184	≤ 1	24	181
$[Cu(1\text{-}FMT)_6](ClO_3)_2$ (**4**)	–	87	≤ 1	24	224
$[Cu(1\text{-}MTZ)_6](ClO_4)_2$ [7]	178	211	2.5	54	80
$[Cu(ClO_3)_2(1\text{-}MTZ)_4]$ [7]	–	159	3	7	100

a) Endothermic peak, which indicates melting or dehydration. Onset temperature at a heating rate of 5 K·min^{-1} measured by DTA. b) Exothermic peak, which indicates decomposition. Onset temperature at a heating rate of 5 K·min^{-1} measured by DTA. c) Impact sensitivity according to the BAM drop hammer (method 1 of 6). d) Friction sensitivity according to the BAM friction tester (method 1 of 6). e) Electrostatic discharge sensitivity (OZM Electric Spark XSpark10).

© 2020 Wiley-VCH GmbH

with SHELXS-97[34] refined with SHELXL-97[34] and finally checked using PLATON[35] All thermal ellipsoids are shown at 50 % probability level.

Crystallographic data (excluding structure factors) for the structures in this paper have been deposited with the Cambridge Crystallographic Data Centre, CCDC, 12 Union Road, Cambridge CB21EZ, UK. Copies of the data can be obtained free of charge on quoting the depository numbers CCDC-2020838, CCDC-2020839, CCDC-2020905, CCDC-2020906, CCDC-2020907, and CCDC-2020908. (Fax: +44-1223-336-033; E-Mail: deposit@ccdc.cam.ac.uk, http://www.ccdc.cam.ac.uk)

Details for data collection and structure refinement are summarized in the Supporting Information.

2-Fluoromethyl-5H tetrazole (1b): 5*H*-Tetrazole (0.83 mg, 11.8 mmol) was solved in acetone (35 mL) and potassium carbonate (0.82 g, 5.70 mmol) was added in one portion. After 30 min, fluoroiodomethane (0.8 mL, 11.8 mmol) was added dropwise and refluxed overnight. After the precipitate was filtered, the solvent was removed by distillation. The residue was dissolved in water and extracted with ethyl acetate (3 × 50 mL). The combined organic phases were washed with brine, dried with anhydrous magnesium sulfate, and the solvent was removed at reduced pressure. The crude liquid product was distilled in high vacuum to obtain tetrazole **1b** as a colorless liquid (0.48 g, 40 %). 0 °C (m.p.), 160 °C (b.p.). **^{1}H NMR** (400 MHz, $CDCl_3$): δ = 8.65 (s, 1 H), 6.55 (dd, J = 49.7, J = 0.4 Hz, 2 H) ppm. ^{19}F NMR (376 MHz, $CDCl_3$): δ = –171.4 (t, J = 50.0 Hz) ppm. **^{13}C{^{1}H} NMR** (101 MHz, $CDCl_3$): δ = 151.1, 86.1 (d, J = 211.7 Hz) ppm. **^{15}N{^{1}H} NMR** (40.6 MHz, $CDCl_3$): δ = 5.1 (s), –41.9 (s), –73.8 (s), –97.2 (d, J = 17.5 Hz) ppm. **IR** (ATR): $\tilde{\nu}$ = 3150 (w), 3058 (w), 3000 (w), 2404 (w), 2361 (w), 2129 (w), 1704 (w), 1545 (w), 1461 (w), 1403 (m), 1367 (s), 1323 (w), 1283 (s), 1224 (m), 1184 (s), 1118 (m), 1046 (s), 1019 (s), 995 (s), 890 (m), 768 (s), 707 (s), 680 (s) cm^{-1}. **Raman** (1074 mW): $\tilde{\nu}$ = 3153 (m), 3056 (w), 3001 (s), 2921 (w), 1461 (m), 1403 (m), 1370 (m), 1320 (m), 1285 (s), 1226 (m), 1186 (m), 1120 (w), 1053 (w), 1023 (m), 998 (s), 772 (m), 683 (m), 440 (m), 156 (s) cm^{-1}. **HRMS** (GC/EI) *m/z*: [M]$^+$ Calcd for $C_2H_4FN_4$ 102.0342; Found: 102.0336.

1-Fluoromethyl-5*H*-tetrazole (1a): The 1-fluoromethyl-5*H*-tetrazole **1a** remained in the distillation flask after **1b** was separated by distillation. Therefore, the remaining residue was dissolved in acetone (50 mL) and filtered through a silica plug. After removing the solvent at reduced pressure, tetrazole **1a** was obtained as colorless liquid (0.42 g, 35 %). 115 °C (dec). **^{1}H NMR** (400 MHz, $CDCl_3$): δ = 8.90 (s, 1 H), 6.40 (d, J = 50.0 Hz, 2 H) ppm. **^{19}F NMR** (376 MHz, $CDCl_3$): δ = –169.4 (t, J = 50.0 Hz) ppm. **^{13}C{^{1}H} NMR** (101 MHz, $CDCl_3$): δ = 143.7, 82.8 (d, J = 209.5 Hz) ppm. **^{15}N{^{1}H} NMR** (40.6 MHz, $CDCl_3$): δ = 13.7 (s), –12.2 (s), –50.4 (s), –142.6 (d, J = 17.5 Hz) ppm. **IR** (ATR): $\tilde{\nu}$ = 3139 (w), 1487 (m), 1460 (w), 1431 (w), 1403 (w), 1370 (w), 1312 (w), 1274 (w), 1205 (w), 1170 (s), 1102 (m), 1025 (s), 993 (m), 947 (w), 881 (w), 754 (s), 716 (w), 656 (m), 440 (w) cm^{-1}. **Raman** (1074 mW): $\tilde{\nu}$ = 3142 (m), 3053 (m), 3003 (s), 2966 (w), 2916 (w), 2794 (w), 1488 (w), 1482 (m), 1433 (m), 1404 (w), 1315 (s), 1276 (m), 1204 (w), 1173 (m), 1104 (w), 1036 (m), 998 (m), 948 (w), 759 (m), 717 (w), 660 (w), 440 (w), 336 (w), 211 (w), 159 (s), 93 (s) cm^{-1}. **HRMS** (GC/EI) *m/z*: [M]$^+$ Calcd for $C_2H_4FN_4$ 102.0342; Found: 102.0337.

1-Fluoromethyl-5-aminotetrazole (2a): 5-Aminotetrazole (10.2 g, 120 mmol) was dissolved in water (50 mL) and sodium hydrogen carbonate (10.8 g, 120 mmol) was added slowly in small portions. After the solution was stirred for 30 min, the solvent was removed. The obtained sodium 5-aminotetrazolate (12.6 g, 117 mmol), was slurried in acetone (50 mL) and fluoroiodomethane (7.94 mL, 117 mmol) was added dropwise. After the reaction mixture was refluxed for 3 h, the solvent was removed in vacuo. The beige crude product slurried in water (70 mL), was filtered and washed with diethyl ether (200 mL), and pure aminotetrazole **2a** was obtained (7.05 g, 51 %). 131 °C (m.p.), 160 (dec). **^{1}H NMR** (400 MHz, DMSO-D_6): δ = 7.32 (s, 2 H), 6.25 (d, J = 51.9 Hz, 2 H) ppm. **^{19}F NMR** (376 MHz, DMSO-D_6): δ = –170.8 (t, J = 51.8 Hz) ppm. **^{13}C{^{1}H} NMR** (101 MHz, DMSO-D_6): δ = 168.0 (d, J = 1.1 Hz), 86.6 (d, J = 202.2 Hz) ppm. **^{15}N{^{1}H} NMR** (40.6 MHz, DMSO-D_6): δ = 9.5 (s), –23.8 (d, J = 1.1 Hz), –94.2 (s), –333.8 (s) ppm. **IR** (ATR): $\tilde{\nu}$ = 3319 (w), 3137 (w), 2798 (w), 2750 (w), 1652 (m), 1591 (m), 1485 (w), 1459 (w), 1400 (w), 1342 (w), 1305 (w), 1284 (w), 1183 (w), 1104 (w), 1007 (m), 960 (m), 805 (m), 752 (w), 720 (m), 472 (m) cm^{-1}. **Raman** (1074 mW): $\tilde{\nu}$ = 3057 (w), 2996 (w), 1593 (w), 1464 (w), 1403 (w), 1342 (w), 1309 (w), 1141 (w), 1100 (w), 1011 (w), 964 (w), 807 (s), 753 (w), 722 (w), 480 (w), 443 (w), 299 (w), 164 (w), 143 (m), 102 (s) cm^{-1}. $C_2H_4FN_5$: C, 20.52; H, 3.44. Found: C, 20.30; H, 3.45. HRMS (DEI) *m/z*: [M] Calcd for $C_2H_4FN_5$ 117.0451; Found: 117.0446.

2-Fluoromethyl-5-aminotetrazole (2b): The solvent of the received filtrate from the synthesis of **2a**, was removed in vacuo. The obtained solid was dissolved in water (100 mL) and extracted with diethyl ether (100 mL). The aminotetrazole **2b** was obtained as a white solid (3.32 g, 24 %). 75 °C (m.p.), 166 °C (dec). **^{1}H NMR** (400 MHz, (DMSO-D_6): δ = 6.46 (d, J = 50.8 Hz, 2 H), 6.45 (s, 2 H) ppm. ^{19}F NMR (376 MHz, DMSO-D_6): δ = –169.7 (t, J = 50.9 Hz) ppm. **^{13}C{^{1}H} NMR** (101 MHz, DMSO-D_6): δ = 156.1 (d, J = 1.4 Hz), 81.2 (d, J = 197.7 Hz) ppm. **^{15}N{^{1}H} NMR** (40.6 MHz, DMSO-D_6): δ = 2.5 (s), –71.6 (d, J = 0.7 Hz), –107.8 (d, J = 17.4 Hz), –120.7 (d, J = 1.2), –336.8 (s) ppm. **IR** (ATR): $\tilde{\nu}$ = 3387 (w), 3310 (w), 3237 (w), 3177 (w), 3049 (w), 2996 (w), 2005 (w), 1633 (w), 1565 (w), 1442 (w), 1409 (w), 1369 (w), 1213 (w), 1027 (w), 983 (w), 820 (w), 759 (w), 711 (w), 533 (w) 464 (w) cm^{-1}. **Raman** (1074 mW): $\tilde{\nu}$ = 3310 (w), 3047 (w), 2994 (m), 1544 (w), 1463 (w), 1410 (w), 1234 (w), 1212 (w), 1105 (w), 1088 (w), 1022 (w), 986 (s), 713 (w), 661 (w), 467 (m), 339 (w), 294 (w), 142 (s), 115 (m) 102 (s) cm^{-1}. $C_2H_4FN_5$: calcd. C, 20.52; H, 3.44 %; found: C, 20.21; H, 3.34 %. **HRMS** (DEI) *m/z*: [M] Calcd for $C_2H_4FN_5$ 117.0451; found: 117.0443.

[Hexakis(1-fluoromethyl-tetrazole) copper(II)] perchlorate (3): **1a** (0.273 g, 2.7 mmol) was added dropwise to a stirring solution of copper(II) perchlorate hexahydrate (0.17 g, 0.45 mmol) in water (10 mL). The reaction mixture was heated to 100 °C for 10 min and filtered while hot. After solvent evaporation, the complex **3** was obtained in the form of dark blue crystals (0.27 g, 70 %). 184 °C (dec). **IR** (ATR): $\tilde{\nu}$ = 3152 (w), 3114 (w), 3014 (vw), 2022 (vw), 1503 (m), 1490 (w), 1462 (w), 1450 (w), 1406 (m), 1395 (w), 1329 (w), 1290 (w), 1205 (w), 1177 (s), 1107 (s), 1082 (s), 1042 (vs), 1032 (vs), 998 (s), 983 (s), 960 (m), 938 (w), 921 (w), 905 (m), 882 (m), 756 (vs), 714 (m), 656 (s), 624 (vs) cm^{-1}. $C_{12}H_{18}Cl_2CuF_6N_{24}O_8$: calcd. C, 16.47; H, 2.07; N, 38.42 %; found: C, 16.60; H, 1.87; N, 38.32 %. BAM drophammer: ≤ 1 J; BAM friction tester: 24 N; ESD: 181 mJ (grain size 100–500 µm).

[Hexakis(1-fluoromethyl-tetrazole) copper(II)] chlorate (4): Copper(II) chlorate (0.11 g, 0.45 mmol) was prepared via metathesis reaction of copper sulfate pentahydrate and barium chlorate monohydrate. **1a** (279 mg, 2.7 mmol) was added dropwise to the stirring solution of copper chlorate in water (5 mL). The reaction mixture was heated to 100 °C for 10 min and filtered while hot. After solvent evaporation, the complex **4** was obtained as greenish turquoise crystals (0.26 g, 67 %). 87 °C (dec). **IR** (ATR): $\tilde{\nu}$ = 3106 (m), 3061 (w), 2997 (vw),

© 2020 Wiley-VCH GmbH

1504 (m), 1469 (w), 1447 (w), 1408 (m), 1334 (w), 1209 (m), 1183 (s), 1108 (m), 1039 (s), 993 (m), 960 (vs), 934 (s), 909 (s), 758 (vs), 714 (s), 657 (s), 604 (m), 479 (s) cm^{-1}. $C_{12}H_{18}Cl_2CuF_6N_{24}O_6$: calcd. C, 17.10; H, 2.15; N, 39.88%, found: C, 17.37; H, 2.02; N, 39.64%. BAM drophammer: ≤ 1 J; BAM friction tester: 24 N; ESD: 226 mJ (grain size <100 µm).

[Tris(1-fluoromethyl-5-aminotetrazole) copper(I)] perchlorate (6): Tetra(acetonitrile)copper(I) perchlorate (0.33 g, 1.0 mmol) was prepared according to the literature and dissolved in dry acetonitrile (10 mL) under nitrogen atmosphere.[36] Amino tetrazole **2a** (0.35 g, 3.0 mmol) was dissolved in acetonitrile (10 mL) separately and dropwise added to the acetonitrile complex solution at 80 °C. A color change to yellow indicated product formation and the opaque solution was filtered. The solvent was removed in vacuo, yielding a yellow microcrystalline solid **6** (0.32 g, 62%). At ambient conditions the complex decomposed rapidly, accompanied with a color change to dark brown.

Supporting Information (see footnote on the first page of this article): NMR details; crystallographic data; calculation details.

Acknowledgements

Financial support by the Ludwig-Maximilian University is grateful acknowledged. We are also thankful to F-Select GmbH for a generous donation of fluoroiodomethane.

Keywords: Fluoromethylation; Energetic materials; Tetrazoles; Spectroscopy; Fluorine effect

References

[1] S. Wittenberger, *Org. Prep. Proced. Int.* **1994**, *26*, 499–531.
[2] R. Raap, *Can. J. Chem.* **1969**, *47*, 3677–3681.
[3] P. L. Franke, J. G. Haasnoot, A. Zuur, *Inorg. Chim. Acta* **1982**, *59*, 5–9.
[4] M. A. C. Härtel, T. M. Klapötke, D. G. Piercey, J. Stierstorfer, *Z. Anorg. Allg. Chem.* **2012**, *638*, 2008–2014.
[5] a) A. Warrilow, C. M. Hull, J. E. Parker, E. P. Garvey, W. J. Hoekstra, W. R. Moore, R. J. Schotzinger, D. E. Kelly, S. L. Kelly, *Antimicrob. Agents Chemother.* **2014**, *58*, 7121–7127; b) S. R. Lockhart, A. W. Fothergill, N. Iqbal, C. B. Bolden, N. T. Grossman, E. P. Garvey, S. R. Brand, W. J. Hoekstra, R. J. Schotzinger, E. Ottinger, T. F. Patterson, N. P. Wiederhold, *Antimicrob. Agents Chemother.* **2016**, *60*, 2528–2531.
[6] V. A. Ostrovskii, E. A. Popova, R. E. Trifonov, *Adv. Heterocycl. Chem.* **2017**, *123*, 1–62.
[7] J.-S. Qin, S.-J. Bao, P. Li, W. Xie, D.-Y. Du, L. Zhao, Y.-Q. Lan, Z.-M. Su, *Chem. Asian J.* **2014**, *9*, 749–753.
[8] A. Rudavskyi, R. W. A. Havenith, R. Broer, C. de Graaf, C. Sousa, *Dalton Trans.* **2013**, *42*, 14702–14709.
[9] S. Li, Y. Wang, C. Qi, X. Zhao, J. Zhang, S. Zhang, S. Pang, *Angew. Chem.* **2013**, *125*, 14281–14285; *Angew. Chem. Int. Ed.* **2013**, *52*, 14031–14035.
[10] F. R. Benson, *Chem. Rev.* **1947**, *41*, 1–61.
[11] T. M. Klapötke, *Chemie der hochenergetischen Materialien*, De Gruyter, **2009**.
[12] T. M. Klapötke, J. Stierstorfer, *Green Energetic Materials*, John Wiley & Sons Ltd., **2014**, pp. 133–177.
[13] N. Fischer, K. Karaghiosoff, T. M. Klapötke, J. Stierstorfer, *Z. Anorg. Allg. Chem.* **2010**, *636*, 735–749.
[14] a) L. Zeisel, N. Szimhardt, M. H. H. Wurzenberger, T. M. Klapötke, J. Stierstorfer, *New J. Chem.* **2019**, *43*, 609–616; b) M. H. H. Wurzenberger, M. S. Gruhne, M. Lommel, N. Szimhardt, T. M. Klapötke, J. Stierstorfer, *Chem. Asian J.* **2019**, *14*, 2018–2028; c) M. H. H. Wurzenberger, B. R. G. Bissinger, M. Lommel, M. S. Gruhne, N. Szimhardt, J. Stierstorfer, *New J. Chem.* **2019**, *43*, 18193–18202; d) N. Szimhardt, M. H. H. Wurzenberger, P. Spiess, T. M. Klapötke, J. Stierstorfer, *Propellants Explos. Pyrotech.* **2018**, *43*, 1203–1209; e) M. H. H. Wurzenberger, N. Szimhardt, J. Stierstorfer, *Inorg. Chem.* **2018**, *57*, 7940–7949; f) M. H. H. Wurzenberger, N. Szimhardt, J. Stierstorfer, *J. Am. Chem. Soc.* **2018**, *140*, 3206–3209; g) N. Szimhardt, M. H. H. Wurzenberger, T. M. Klapötke, J. T. Lechner, H. Reichherzer, C. C. Unger, J. Stierstorfer, *J. Mater. Chem. A* **2018**, *6*, 6565–6577; h) N. Szimhardt, M. H. H. Wurzenberger, L. Zeisel, M. S. Gruhne, M. Lommel, J. Stierstorfer, *J. Mater. Chem. A* **2018**, *6*, 16257–16272; i) N. Szimhardt, M. H. H. Wurzenberger, A. Beringer, L. J. Daumann, J. Stierstorfer, *J. Mater. Chem. A* **2017**, *5*, 23753–23765.
[15] E.-C. Koch, A. Hahma, T. M. Klapötke, H. Radies, *Propellants Explos. Pyrotech.* **2010**, *35*, 248–253.
[16] a) M. Reichel, B. Krumm, Y. V. Vishnevskiy, S. Blomeyer, J. Schwabedissen, H.-G. Stammler, K. Karaghiosoff, N. W. Mitzel, *Angew. Chem.* **2019**, *131*, 18730–18734; *Angew. Chem. Int. Ed.* **2019**, *58*, 18557–18561; b) M. Reichel, B. Krumm, K. Karaghiosoff, *J. Fluorine Chem.* **2019**, *226*, 109351–109355.
[17] H. Yoneyama, N. Oka, Y. Usami, S. Harusawa, *Tetrahedron Lett.* **2020**, *61*, 151517–151520.
[18] S. Komeda, H. Yoneyama, M. Uemura, T. Tsuchiya, M. Hoshiyama, T. Sakazaki, K. Hiramoto, S. Harusawa, *J. Inorg. Biochem.* **2019**, *192*, 82–86.
[19] a) M. Reichel, K. Karaghiosoff, *Angew. Chem.* **2020**, *132*, 12364–12377; *Angew. Chem. Int. Ed.* **2020**, *59*, 12268–12281; b) M. Reichel, M. Egenhöfer, B. Krumm, K. Karaghiosoff, *Z. Anorg. Allg. Chem.* **2020**, *646*, 328–331; c) M. Reichel, J. Martens, E. Woellner, L. Huber, A. Kornath, K. Karaghiosoff, *Eur. J. Inorg. Chem.* **2019**, 2530–2534; d) M. Reichel, J. Martens, C. C. Unger, K. Karaghiosoff, *Phosphorus Sulfur Silion Relat. Elem.* **2019**, *194*, 467–468.
[20] C. Stadler, J. Daub, J. Koehler, R. W. Saalfrank, V. Coropceanu, V. Schuenemann, C. Ober, A. X. Trautwein, S. F. Parker, M. Poyraz, T. Inomata, R. D. Cannon, *J. Chem. Soc., Dalton Trans.* **2001**, 3373–3383.
[21] E. Vieira, J. Huwyler, S. Jolidon, F. Knoflach, V. Mutel, J. Wichmann, *Bioorg. Med. Chem. Lett.* **2005**, *15*, 4628–4631.
[22] T. M. Klapötke, C. M. Sabate, A. Penger, M. Rusan, J. M. Welch, *Eur. J. Inorg. Chem.* **2009**, 880–896.
[23] a) X. Hua, W. Liao, Y. Tang, P. Li, P. Shi, D. Zhao, R. Xiong, *J. Am. Chem. Soc.* **2018**, *140*, 12296–12302; b) M. Feller, K. Lux, A. Kornath, *Eur. J. Inorg. Chem.* **2015**, 5357–5362.
[24] a) K. Karaghiosoff, T. M. Klapötke, P. Mayer, C. M. Sabate, A. Penger, J. M. Welch, *Inorg. Chem.* **2008**, *47*, 1007–1019; b) R. A. Henry, W. G. Finnegan, *J. Am. Chem. Soc.* **1954**, *76*, 923–926; c) T. M. Klapötke, N. K. Minar, J. Stierstorfer, *Polyhedron* **2009**, *28*, 13–26.
[25] O. Gryszkiewicz-Trochimowski, *Compt. Rend.* **1958**, *246*, 2627–2629.
[26] M. Jafari, K. Ghani, M. H. Keshavarz, F. Derikvandy, *Propellants Explos. Pyrotech.* **2018**, *43*, 1236–1244.
[27] J. H. Bryden, *Acta Crystallogr.* **1956**, *9*, 874–878.
[28] M. H. Palmer, S. Parsons, *Acta Crystallogr., Sect. C: Cryst. Struct. Commun.* **1996**, *52*, 2818–2822.
[29] E. Oliveri-Mandala, T. Passalacqua, *Gazz. Chim. Ital.* **1914**, *44*, 465–475.
[30] a) L. Zeisel, N. Szimhardt, M. H. H. Wurzenberger, T. M. Klapötke, J. Stierstorfer, *New J. Chem.* **2019**, *43*, 609–616; b) P. N. Gaponik, M. M. Degtyarik, A. S. Lyakhov, V. E. Matulis, O. A. Ivashkevich, M. Quesada, J. Reedijk, *Inorg. Chim. Acta* **2005**, *358*, 3949–3957; c) N. Szimhardt, M. H. H. Wurzenberger, A. Beringer, L. J. Daumann, J. Stierstorfer, *J. Mater. Chem. A* **2017**, *5*, 23753–23765; d) M. H. H. Wurzenberger, M. Lommel, M. S. Gruhne, N. Szimhardt, J. Stierstorfer, *Angew. Chem.* **2020**,

© 2020 Wiley-VCH GmbH

132, 12466–12469; *Angew. Chem. Int. Ed.* **2020**, *59*, 12367–12370; e) M. H. H. Wurzenberger, N. Szimhardt, J. Stierstorfer, *J. Am. Chem. Soc.* **2018**, *140*, 3206–3209.
[31] a) V. A. K. Adiraju, J. A. Flores, M. Yousufuddin, H. V. R. Dias, *Organometallics* **2012**, *31*, 7926–7932; b) T. Chavez-Gil, J. Lugo, D. L. Cedeño, C. G. Hamaker, *J. Chem. Crystallogr.* **2015**, *45*, 189–192.
[32] Program package CrysAlisPro 1.171.38.46 Rigaku OD, **2015**.
[33] G. M. Sheldrick, SHELXS-97, Program for Crystal Structure Solution, University of Göttingen, Germany, **1997**.
[34] G. M. Sheldrick, SHELXL-97, Program for the Refinement of Crystal Structures, University of Göttingen, Germany, **1997**.
[35] A. L. Spek, PLATON: A Multipurpose Crystallographic Tool, Utrecht University, Utrecht, Netherlands, **1999**.
[36] P. Hemmerich, C. Sigwart, *Experientia* **1963**, *19*, 488–489.

Received: September 17, 2020
Published Online: November 9, 2020

© 2020 Wiley-VCH GmbH

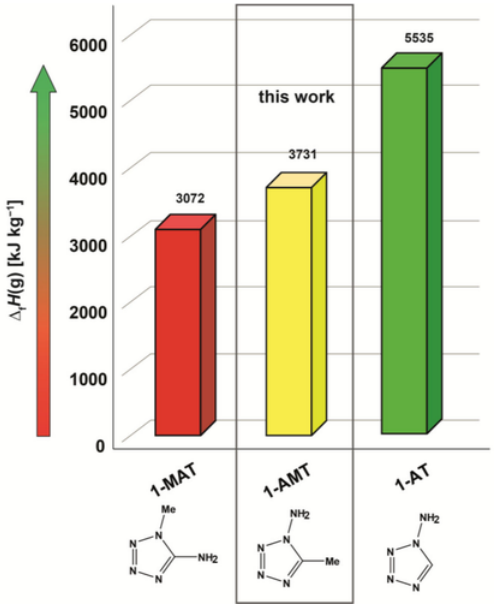
Appendix 21

1-Amino-5-methyltetrazole in Energetic 3d Transition Metal Complexes – Ligand Design for Future Primary Explosives

M. H. H. Wurzenberger, M. S. Gruhne, M. Lommel, J. Stierstorfer

Propellants Explos. Pyrotech. **2021**, *46*, 207–213.

https://doi.org/10.1002/prep.202000179



Supplementary Information:
https://onlinelibrary.wiley.com/action/downloadSupplement?doi=10.1002%2Fprep.202000179&file=prep202000179-sup-0001-misc_information.pdf

Full Paper

Propellants, Explosives, Pyrotechnics

DOI: 10.1002/prep.202000179

1-Amino-5-methyltetrazole in Energetic 3 d Transition Metal Complexes – Ligand Design for Future Primary Explosives

Maximilian H. H. Wurzenberger,[a] Michael S. Gruhne,[a] Marcus Lommel,[a] and Jörg Stierstorfer[a]

Dedicated to Prof. Thomas M. Klapötke on the Occasion of his 60th Birthday

Abstract: New lead-free primary explosives are needed for safe future ignition and initiation applications. Especially, ignition by low-energy laser irradiation has been demonstrated to be a valuable method. For this technology, primary explosives with safer sensitivities are needed. In order to adjust the desired properties of the neat primary explosives, we follow the concept of "energetic coordination compounds" (ECC) in which the ligand significantly alters the final properties. As the result of a study where 1-amino-5*H*-tetrazole (1-AT) was used as one of the most endothermic ligands, yielding materials with outstanding performance but very high sensitivities, in this work its 5-methyl analogue 1-amino-5-methyltetrazole (1-AMT, **1**) was synthesized and applied as ligand. For a short evaluation, metal perchlorate complexes $[M(1\text{-}AMT)_6](ClO_4)_2$ of manganese(II), iron(II), and zinc(II) as well as $[Cu(1\text{-}AMT)_4(H_2O)](ClO_4)_2$ were prepared. All compounds were intensively characterized e.g., by XRD, IR, EA, TGA, DTA as well as sensitivity measurements (impact, friction, BDIS, and ESD). The obtained materials show reduced performance but they are safer to handle than the corresponding 1-AT derivatives. Moreover, the satisfactory performances of ECC **3** and **4** were impressively demonstrated by PETN initiation and laser ignition experiments.

Keywords: Energetic Coordination Compounds · Primary Explosives · Tetrazoles · Transition Metals · Laser Ignition

1 Introduction

Primary Explosives are one of the most exciting compounds within the large area of energetic materials due to their immediate reaction towards outer stimuli such as flame, heat, or impact. They are used to initiate or ignite secondary charges. Without knowing, many people are in daily contact with them. Depending on the application, primary explosives are either used for creating a shock wave that transfers a detonation (detonators) or for providing a flame (igniters) and can be found in various civil and military devices, such as gas generators or ammunition cartridges [1]. Mercury fulminate (MF), known since the 17th century, represents the first substance ever to be used as primary explosive. Initiators based on MF were already patented in 1807 [2,3]. Although lead azide (LA) was known since the end of the 19th century [4] and postulated as a MF replacement with numerous improvements, the production of mercury fulminate further enhanced until World War I [5,6]. The most serious drawbacks of MF compared to LA are its relatively slow deflagration-to-detonation transition as well as initiation efficiency, dead-pressing, long-term stability when exposed to humidity, and most importantly, its very toxic decomposition products [1]. The latter fact and the resulting harms for operators were already recognized as significant issues back then, but the higher sensitivities of LA and several tragic accidents with it prevented a comprehensive implementation [6]. External circumstances like the imminent occupation of mercury mines during World War I have led to extensive production of lead azide among the Central Powers, and soon after the war, other nations also began to produce LA [7]. Due to the superior characteristics of both LA and lead styphnate (LS), as well as their very low production costs, concerns regarding their only slightly lower toxicity compared to MF were almost completely put aside. However, their long-term use caused considerable contaminations in training grounds that can highly affect human health [8]. Again, it seems that external circumstances, represented by governmental regulations, are necessary to force the next step towards less toxic primary explosives. Therefore, LA and LS are listed on the candidate list of authorization (substances of very high concern, An-

[a] *M. H. H. Wurzenberger, M. S. Gruhne, M. Lommel, J. Stierstorfer*
Department of Chemistry, Ludwig-Maximilian University of Munich
81377
Butenandtstr. 5–13
Munich
Germany

Supporting information for this article is available on the WWW under https://doi.org/10.1002/prep.202000179

© 2021 The Authors. Propellants, Explosives, Pyrotechnics published by Wiley-VCH GmbH. This is an open access article under the terms of the Creative Commons Attribution License, which permits use, distribution and reproduction in any medium, provided the original work is properly cited.

$[Fe(1\text{-}AMT)_6](ClO_4)_2$ (3)

ECC **3** was obtained after 4 days as off-white crystals. Yield: 845 mg (0.99 mmol, 99 %).

DTA (5 °C min^{-1}): 177 °C (exo.); IR (ATR, cm^{-1}): ṽ= 3342 (m), 3293 (w), 3237 (w), 3155 (vw), 2033 (vw), 1635 (w), 1525 (w), 1487 (w), 1431 (w), 1411 (w), 1387 (vw), 1374 (vw), 1333 (vw), 1320 (w), 1271 (m), 1076 (vs), 1046 (s), 1003 (m), 916 (m), 744 (w), 721 (w), 675 (m), 624 (s), 590 (vw), 560 (vw), 544 (vw), 499 (vw), 476 (w), 435 (w), 414 (w), 404 (w); EA ($C_{12}H_{30}Cl_2FeN_{30}O_8$, 849.32) calcd.: C 16.97, H 3.56, N 49.48 %, found: C 17.26, H 3.46, N 48.47 %; BAM drophammer: < 1 J, friction tester: 0.45 N, ESD: 250 mJ, BDIS: 16 mJ (at grain size 100–500 µm).

$[Cu(1\text{-}AMT)_4(H_2O)](ClO_4)_2$ (4)

Aqua complex **4** crystallized within one day in the form of blue blocks. Yield: 575 mg (0.85 mmol, 85 %).

DTA (5 °C min^{-1}): 163 °C (endo followed by decomposition); IR (ATR, cm^{-1}): ṽ= 3482 (vw), 3357 (w), 3324 (vw), 3296 (w), 3248 (w), 2004 (vw), 1633 (w), 1533 (w), 1489 (vw), 1432 (w), 1411 (w), 1383 (w), 1318 (w), 1282 (w), 1099 (vs), 1086 (vs), 933 (m), 740 (w), 717 (w), 676 (m), 622 (s), 589 (w), 576 (w), 530 (w), 518 (w), 509 (w), 496 (w), 480 (m), 468 (w), 459 (w), 439 (w), 426 (w), 421 (w), 414 (w), 407 (w); EA ($C_8H_{22}Cl_2CuN_{20}O_9$, 676.84) calcd.: C 14.20, H 3.28, N 41.39 %, found: C 14.46, H 3.17, N 41.31 %; BAM drophammer: < 1 J, friction tester: 0.75 N, ESD: 270 mJ, BDIS: 14 mJ (at grain size 100–500 µm).

$[Zn(1\text{-}AMT)_6](ClO_4)_2$ (5)

Zinc compound **5** was received within 9 days as colorless single-crystals suitable for X-ray diffraction experiments. Yield: 295 mg (0.34 mmol, 34 %).

DTA (5 °C min^{-1}): 198 °C (exo.); IR (ATR, cm^{-1}): ṽ= 3342 (m), 3295 (w), 3237 (m), 1635 (m), 1525 (m), 1488 (w), 1431 (w), 1411 (w), 1374 (w), 1320 (w), 1271 (m), 1074 (vs), 1046 (s), 1006 (m), 915 (m), 744 (w), 720 (w), 675 (m), 624 (s); EA ($C_{12}H_{30}Cl_2N_{30}O_8Zn$, 858.86) calcd.: C 16.78, H 3.52, N 48.93 %, found: C 16.78, H 3.31, N 48.63 %; BAM drophammer: < 1 J, friction tester: 5 N; ESD: 630 mJ, BDIS: 30 mJ (at grain size 100–500 µm).

3 Results and Discussion

3.1 Synthesis

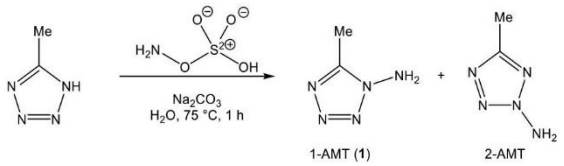
The nitrogen-rich ligand 1-amino-5-methyltetrazole (1-AMT, **1**) was prepared according to a literature procedure by the amination of 5-methyltetrazole [19]. Because the reactivity of the aminating reagent, hydroxylamine-*O*-sulfonic acid (HOSA) strongly depends on the reaction conditions, it is vital to monitor the pH-value of the reaction solution. Constantly readjusting the pH to a value between 7 and 8, utilizing a saturated solution of sodium bicarbonate, enables the nucleophilic substitution of the hydrogen sulfate leaving group by the tetrazole anion that is generated *in situ* (Scheme 1). The obtained isomeric mixture of 1- and 2-amino-5-methyltetrazole (2-AMT) was separated by flash column chromatography with an eluent mixture of ethyl acetate/isohexane (1:1). 1-AMT (**1**) was obtained in a yield of 33 % and 2-AMT as a side product (Yield: 25 %).

For the synthesis of the ECC **2**–**5**, the corresponding metal(II) perchlorates were reacted with the respective equivalents of 1-AMT in acetonitrile and left in air for crystallization (Scheme 2). The complexes were obtained within 1–9 days in decent to very good yields. While in the case of **2**, **3**, and **5** a hexa-coordination around the central metals could be achieved, it was impossible to increase the number of 1-AMT ligands around the Cu^{2+} cation in **4**. Even if the equivalents of 1-AMT were increased during the reaction, solely the aqua species was obtained.

Interestingly, when applying 2-AMT as ligand for the synthesis of 3d perchlorate complexes, crystalline materials could only be obtained *in vacuo*. The products are highly hygroscopic and become slushy under ambient conditions.

3.2 Crystal Structures

All ECC were analyzed by low-temperature single-crystal X-ray diffraction experiments and the crystal structures were uploaded to the CSD database (CCDC number 2014298 (**2**),



Scheme 1. Amination of 5-methyltetrazole leading to an isomeric mixture of 1-AMT and 2-AMT.

$Mn(ClO_4)_2 \cdot 6\,H_2O \xrightarrow[\text{MeCN, 70 °C}]{\text{1-AMT}} [Mn(1\text{-}AMT)_6](ClO_4)_2$ (**2**)

$Fe(ClO_4)_2 \cdot 6\,H_2O \xrightarrow[\text{MeCN, 70 °C}]{\text{1-AMT}} [Fe(1\text{-}AMT)_6](ClO_4)_2$ (**3**)

$Cu(ClO_4)_2 \cdot 6\,H_2O \xrightarrow[\text{MeCN, 70 °C}]{\text{1-AMT}} [Cu(1\text{-}AMT)_4(H_2O)](ClO_4)_2$ (**4**)

$Zn(ClO_4)_2 \cdot 6\,H_2O \xrightarrow[\text{MeCN, 70 °C}]{\text{1-AMT}} [Zn(1\text{-}AMT)_6](ClO_4)_2$ (**5**)

Scheme 2. Synthesis of the complexes **2**–**5**.

 © 2021 The Authors. Propellants, Explosives, Pyrotechnics published by Wiley-VCH GmbH

nex XIV) for the REACH (Registration, Evaluation, Authorization, and Restriction of Chemicals) regulations as well as the EPA list of 17 toxic chemicals, which will sooner or later lead to their prohibition [9].

Within the last few years, various different concepts for the synthesis of lead-free primary explosives were published, including neutral [10], ionic [11], or energetic coordination compounds (EEC) [12]. Latter one gained increasing attention for the synthesis of new energetic compounds during the last years: The desired properties can be tuned by exchanging one of the three different building blocks (metal center, anion, ligand) [13]. Particularly suitable for the synthesis of energetic coordination compounds (ECC) are monotetrazoles (Figure 1). They can be modified both by substitution at the carbon as well as at one of the nitrogen atoms and act as either neutral or anionic ligands in complexes. The energetic properties of many ECC based on different substituted monotetrazoles, e.g., 1,5-diamino-tetrazole [14], 2-methyl-5-aminotetrazole [15], or 5-nitrotetrazole [16] were investigated within the last few years. Considering recent results of the performance of perchlorate complexes based on either 1-aminotetrazole (1-AT) [17] or 1-methyl-5-amino-tetrazole (1-MAT) [18], it becomes clear that for some applications they are either too sensitive or not powerful enough. We decided to address this problem by applying 1-amino-5-methyltetrazole as a ligand, which is an isomer of 1-MAT. Thereby the system can be tamed (compared to 1-AT) through the additional methyl group while at the same time the amino substituent at the N1 position ensures a higher energy input (in comparison with 1-MAT, see Figure 1).

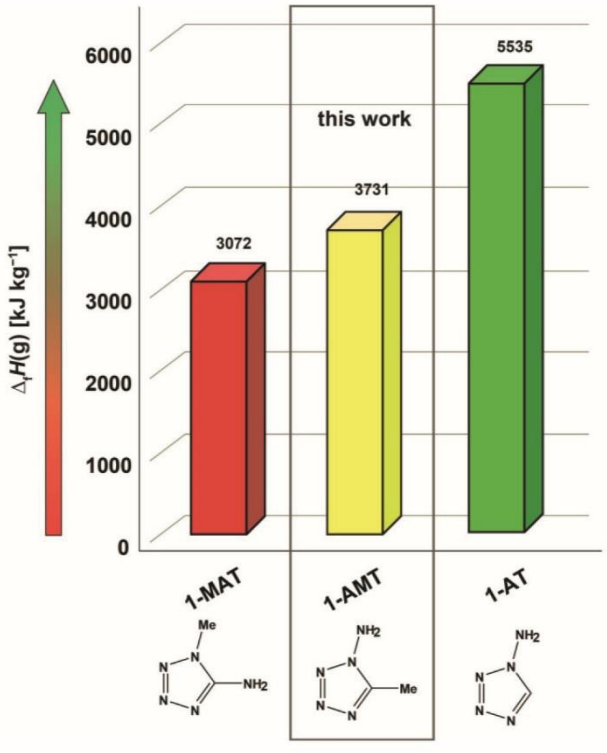


Figure 1. Overview of calculated gas-phase enthalpies of formation for three substituted monotetrazoles. Enthalpies of formation were calculated using the atomization method ($\Delta_f H^0_{(g,M)} = H(M) - \Sigma H^0_{(A)} + \Sigma \Delta_f H^0_{(A)}$) using Gaussian09 computed CBS-4 M electronic enthalpies.

Therefore, in this work, 3d transition metal perchlorate complexes based on 1-amino-5-methyltetrazole as nitrogen-rich ligand are presented. The sensitivities and performance are compared with recently published energetic complexes.

2 Experimental Section

Caution! *All investigated compounds are energetic materials and the ECC show sensitivities in the range of primary explosives. Although no incidents took place, proper security precautions (safety glasses, face shield, earthed equipment and shoes, leather jacket, Kevlar sleeves, and earplugs) have to be worn while handling the coordination compounds.*

1-Amino-5-methyltetrazole (1)

Nitrogen-rich ligand **1** was synthesized according to a literature procedure [19].

General procedure for the synthesis of ECC 2–5

For synthesizing the complexes, 1.00 mmol of the corresponding metal(II) perchlorate (**2**: 362 mg $Mn(ClO_4)_2 \cdot 6\ H_2O$, **3**: 363 mg $Fe(ClO_4)_2 \cdot 6\ H_2O$, **4**: 370 mg $Cu(ClO_4)_2 \cdot 6\ H_2O$, **5**: 372 mg $Zn(ClO_4)_2 \cdot 6\ H_2O$) and 1-AMT (**2**: 6.00 mmol, 595 mg; **3**: 6.00 mmol, 595 mg; **4**: 4.00 mmol, 396 mg; **5**: 6.00 mmol, 595 mg) were each dissolved in 5 mL acetonitrile and combined while stirring. The resulting reaction mixtures were heated to 70 °C, stirred for 5 min, and left in air for crystallization.

$[Mn(1\text{-}AMT)_6](ClO_4)_2$ (2)

Coordination compound **2** crystallized after 7 days. Yield: 702 mg (0.83 mmol, 83 %).

DTA (5 °C min^{-1}): 199 °C (exo.); IR (ATR, cm^{-1}): $\tilde{\nu}$= 3341 (m), 3293 (w), 3238 (m), 3161 (vw), 1635 (m), 1526 (m), 1488 (w), 1431 (w), 1412 (w), 1373 (w), 1318 (m), 1272 (m), 1071 (vs), 1046 (s), 1001 (s), 914 (s), 744 (m), 720 (w), 674 (s), 623 (s); EA ($C_{12}H_{30}Cl_2MnN_{30}O_8$, 848.41) calcd.: C 16.99, H 3.56, N 49.53 %, found: C 17.22, H 3.53, N 49.33 %; BAM drop-hammer: 2 J, friction tester: 9 N, ESD: 323 mJ, BDIS: 25 mJ (at grain size > 1000 µm).

 © 2021 The Authors. Propellants, Explosives, Pyrotechnics published by Wiley-VCH GmbH

$[Fe(1\text{-}AMT)_6](ClO_4)_2$ (3)

ECC **3** was obtained after 4 days as off-white crystals. Yield: 845 mg (0.99 mmol, 99 %).

DTA (5 °C min^{-1}): 177 °C (exo.); IR (ATR, cm^{-1}): ṽ= 3342 (m), 3293 (w), 3237 (w), 3155 (vw), 2033 (vw), 1635 (w), 1525 (w), 1487 (w), 1431 (w), 1411 (w), 1387 (vw), 1374 (vw), 1333 (vw), 1320 (w), 1271 (m), 1076 (vs), 1046 (s), 1003 (m), 916 (m), 744 (w), 721 (w), 675 (m), 624 (s), 590 (vw), 560 (vw), 544 (vw), 499 (vw), 476 (w), 435 (w), 414 (w), 404 (w); EA ($C_{12}H_{30}Cl_2FeN_{30}O_8$, 849.32) calcd.: C 16.97, H 3.56, N 49.48 %, found: C 17.26, H 3.46, N 48.47 %; BAM drophammer: < 1 J, friction tester: 0.45 N, ESD: 250 mJ, BDIS: 16 mJ (at grain size 100–500 µm).

$[Cu(1\text{-}AMT)_4(H_2O)](ClO_4)_2$ (4)

Aqua complex **4** crystallized within one day in the form of blue blocks. Yield: 575 mg (0.85 mmol, 85 %).

DTA (5 °C min^{-1}): 163 °C (endo followed by decomposition); IR (ATR, cm^{-1}): ṽ= 3482 (vw), 3357 (w), 3324 (vw), 3296 (w), 3248 (w), 2004 (vw), 1633 (w), 1533 (w), 1489 (vw), 1432 (w), 1411 (w), 1383 (w), 1318 (w), 1282 (w), 1099 (vs), 1086 (vs), 933 (m), 740 (w), 717 (w), 676 (m), 622 (s), 589 (w), 576 (w), 530 (w), 518 (w), 509 (w), 496 (w), 480 (m), 468 (w), 459 (w), 439 (w), 426 (w), 421 (w), 414 (w), 407 (w); EA ($C_8H_{22}Cl_2CuN_{20}O_9$, 676.84) calcd.: C 14.20, H 3.28, N 41.39 %, found: C 14.46, H 3.17, N 41.31 %; BAM drophammer: < 1 J, friction tester: 0.75 N, ESD: 270 mJ, BDIS: 14 mJ (at grain size 100–500 µm).

$[Zn(1\text{-}AMT)_6](ClO_4)_2$ (5)

Zinc compound **5** was received within 9 days as colorless single-crystals suitable for X-ray diffraction experiments. Yield: 295 mg (0.34 mmol, 34 %).

DTA (5 °C min^{-1}): 198 °C (exo.); IR (ATR, cm^{-1}): ṽ= 3342 (m), 3295 (w), 3237 (m), 1635 (m), 1525 (m), 1488 (w), 1431 (w), 1411 (w), 1374 (w), 1320 (w), 1271 (m), 1074 (vs), 1046 (s), 1006 (m), 915 (m), 744 (w), 720 (w), 675 (m), 624 (s); EA ($C_{12}H_{30}Cl_2N_{30}O_8Zn$, 858.86) calcd.: C 16.78, H 3.52, N 48.93 %, found: C 16.78, H 3.31, N 48.63 %; BAM drophammer: < 1 J, friction tester: 5 N; ESD: 630 mJ, BDIS: 30 mJ (at grain size 100–500 µm).

3 Results and Discussion

3.1 Synthesis

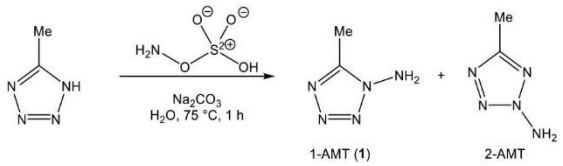
The nitrogen-rich ligand 1-amino-5-methyltetrazole (1-AMT, **1**) was prepared according to a literature procedure by the amination of 5-methyltetrazole [19]. Because the reactivity of the aminating reagent, hydroxylamine-*O*-sulfonic acid (HOSA) strongly depends on the reaction conditions, it is vital to monitor the pH-value of the reaction solution. Constantly readjusting the pH to a value between 7 and 8, utilizing a saturated solution of sodium bicarbonate, enables the nucleophilic substitution of the hydrogen sulfate leaving group by the tetrazole anion that is generated *in situ* (Scheme 1). The obtained isomeric mixture of 1- and 2-amino-5-methyltetrazole (2-AMT) was separated by flash column chromatography with an eluent mixture of ethyl acetate/isohexane (1:1). 1-AMT (**1**) was obtained in a yield of 33 % and 2-AMT as a side product (Yield: 25 %).

For the synthesis of the ECC **2**–**5**, the corresponding metal(II) perchlorates were reacted with the respective equivalents of 1-AMT in acetonitrile and left in air for crystallization (Scheme 2). The complexes were obtained within 1–9 days in decent to very good yields. While in the case of **2**, **3**, and **5** a hexa-coordination around the central metals could be achieved, it was impossible to increase the number of 1-AMT ligands around the Cu^{2+} cation in **4**. Even if the equivalents of 1-AMT were increased during the reaction, solely the aqua species was obtained.

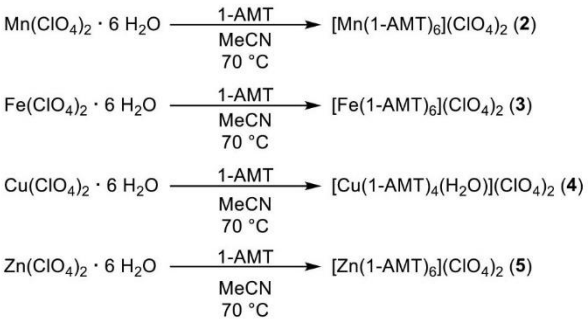
Interestingly, when applying 2-AMT as ligand for the synthesis of 3d perchlorate complexes, crystalline materials could only be obtained *in vacuo*. The products are highly hygroscopic and become slushy under ambient conditions.

3.2 Crystal Structures

All ECC were analyzed by low-temperature single-crystal X-ray diffraction experiments and the crystal structures were uploaded to the CSD database (CCDC number 2014298 (**2**),



Scheme 1. Amination of 5-methyltetrazole leading to an isomeric mixture of 1-AMT and 2-AMT.



Scheme 2. Synthesis of the complexes **2**–**5**.

 © 2021 The Authors. Propellants, Explosives, Pyrotechnics published by Wiley-VCH GmbH

2014297 (**3**), 2014296 (**4**), and 2014295 (**5**)). Details on the measurement and refinement data of all structures are given in the Supporting Information (Table S1). The crystal structure of the free ligand **1** is already known in the literature and the bond lengths and angles of the coordinating tetrazole molecules are comparable to those of the parent one and are therefore not part of the crystal discussion [19].

Complexes **2**, **3**, and **5** all crystallize isotypically in the trigonal space group $P-3$ with comparable cell axes and one molecule per unit cell. They are built up by octahedrally coordinated central metals with non-coordinating perchlorate anions (Figures 2–4). While the density is increasing with the atomic number (**2**: 1.689 g cm^{-3}; **3**: 1.711 g cm^{-3}; **5**: 1.734 g cm^{-3} at 143 K) the metal-nitrogen bond lengths are decreasing (Mn–N ⌀ 228 pm; Fe–N ⌀ 222 pm; Zn–N ⌀ 220 pm).

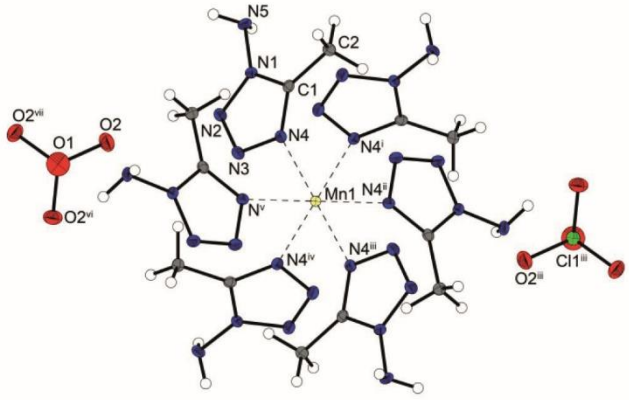


Figure 2. Molecular structure of **2**. Thermal ellipsoids of non-hydrogen atoms in all structures are set to the 50 % probability level. Selected bond length (pm): Mn1–N4 228.23(13). Selected bond angles (°): N4–Mn1–N4^{iii} 180.00, N4–Mn1–N4^{iv} 89.78(5), N4–Mn1–N4^{v} 90.22(5). Symmetry codes: i) y, −x + y, 1−z; ii) −x + y, −x, z; iii) −x, −y, 1−z; iv) −y, x−y, z; v) x−y, x, 1−z; vi) −x + y, 1−x, z; vii) 1−y, 1 + x−y, z.

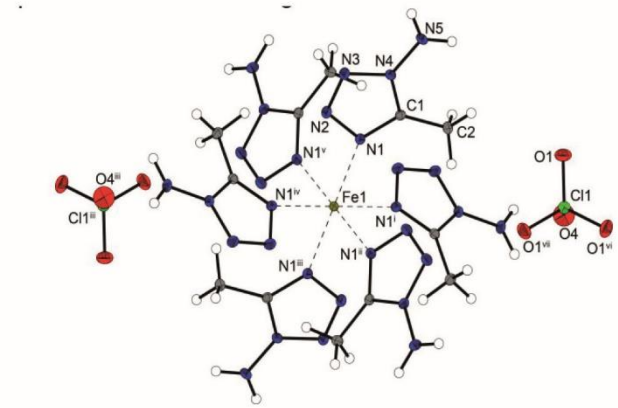


Figure 3. Molecular structure of **3**. Selected bond length (pm): Fe1–N1 220.5(14). Selected bond angles (°): N1–Fe1–N1^{i} 90.90(6), N1–Fe1–N1^{iii} 180.00, N1–Fe1–N1^{iv} 89.10(6). Symmetry codes: i) y, −x + y, −z; ii) −x + y, −x, z; iii) −x, −y, −z; iv) −y, x−y, z; v) x−y, x, −z; vi) 1−x + y, 1−x, z; vii) 1−y, x−y, z.

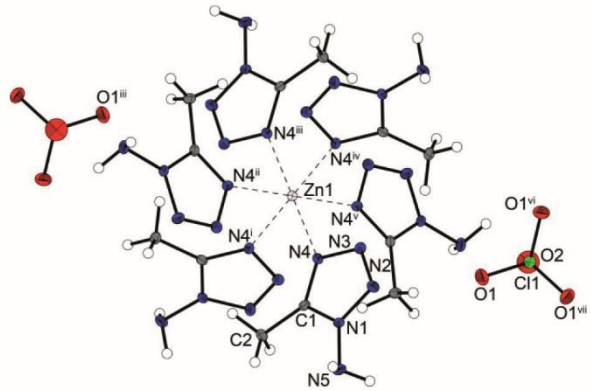


Figure 4. Molecular structure of **5**. Selected bond length (pm): Zn1–N4 220.4(3). Selected bond angles (°): N4–Zn1–N4^{iii} 180.00, N4–Zn1–N4^{iv} 89.70(13), N4–Zn1–N4^{v} 90.30(12). Symmetry codes: i) y, −x + y, −z; ii) −x + y, −x, z; iii) −x, −y, −z; iv) −y, x−y, z; v) x−y, x, −z; vi) −x + y, 1−x, z; vii) 1−y, 1 + x−y, z.

In contrast to the octahedral coordination of **2**, **3**, and **5**, copper(II) compound **4** shows a rather uncommon pentacoordination around the central metal. It crystallizes in the monoclinic space group $P2_1/c$ with four formula units per unit cell and a calculated density of 1.787 g cm^{-3} at 143 K. The coordination sphere is built up of four 1-AMT and one aqua ligand, forming a square pyramidal geometry (Figure 5). The base of the pyramid, made up of the tetrazole molecules, is almost planar with a torsion angle of N4–N9–N14–N19 = 7.04°.

The Cu1–O1 bond (219.8(4) pm) is slightly longer than any of the Cu–N bonds (199.7(3)–200.3(3) pm). Opposing pairs of 1-AMT ligands face the same way and are twisted against each other. Again, the perchlorate anions are non-coordinating.

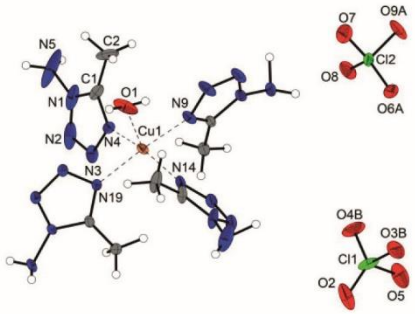


Figure 5. Molecular structure of **4**. Selected bond lengths (pm): Cu1–N4 200.3(3), Cu1–N9 199.7(4), Cu1–N14 199.7(3), Cu1–N19 200.2(4). Selected bond angles (°): O1–Cu1–N4 98.77(18), O1–Cu1–N14 100.00(18), N4–Cu1–N9 89.97(16), N4–Cu1–N14 161.21(15).

© 2021 The Authors. Propellants, Explosives, Pyrotechnics published by Wiley-VCH GmbH

Table 1. Thermal stability measurements by DTA[a] as well as sensitivities towards impact, friction, ESD, and ball drop impact sensitivity of **1–5** compared to LA and some recently published monotetrazole complexes.

	T_{dec}[b] (°C)	IS[c] (J)	FS[d] (N)	ESD[e] (mJ)	$BDIS$[f] (mJ)	HP[g]	HN[g]
1-AMT [18] (**1**)	190	> 40	360	n.d.	n.d.	n.d.	n.d.
$[Mn(1\text{-}AMT)_6](ClO_4)_2$ (**2**)	199	2	9	323	25	def.	def.
$[Fe(1\text{-}AMT)_6](ClO_4)_2$ (**3**)	177	< 1	0.45	250	16	det	det.
$[Cu(1\text{-}AMT)_4(H_2O)](ClO_4)_2$ (**4**)	163	< 1	0.75	270	14	def.	det.
$[Zn(1\text{-}AMT)_6](ClO_4)_2$ (**5**)	198	< 1	5	630	30	def.	def.
$[Mn(1\text{-}AT)_6](ClO_4)_2$ [16]	195	< 1	0.5	11	14	det.	det.
$[Fe(1\text{-}AT)_6](ClO_4)_2$ [16]	187	< 1	< 0.1	12	25	det.	det.
$[Cu(1\text{-}AT)_6](ClO_4)_2$ [16]	174	< 1	< 0.1	5	< 4	det.	det.
$[Zn(1\text{-}AT)_6](ClO_4)_2$ [16]	189	< 1	0.5	12	16	det.	det.
$[Cu(1\text{-}MAT)_4(H_2O)_2](ClO_4)_2$ [17]	106	2.7	> 360	n.d.	n.d.	n.d.	n.d
$Pb(N_3)_2$ [21]	320–360	2.5–4	0.1–1.0	7	37	det.	det.

[a] Onset temperatures at a heating rate of 5 °C min^{-1}. [b] First exothermic or endothermic peak, which indicates decomposition. [c] Impact sensitivity according to the BAM drop hammer (method 1 of 6). [d] Friction sensitivity according to the BAM friction tester (method 1 of 6). [e] Electrostatic discharge sensitivity (OZM ESD tester); [f] Ball drop impact sensitivity determined with the 1 of 6 method in accordance with the MIL-STD 1751A (method 1016). [g] def.: deflagration; det.: detonation.

3.3 Physicochemical Properties

The physicochemical properties of compounds **2–5** were investigated by measuring thermal stabilities and determining their sensitivities towards external stimuli. The determined sensitivities have been used to classify the compounds in accordance with the "UN Recommendations on the Transport of Dangerous Goods" (Impact: insensitive > 40 J, less sensitive≥ 35 J, sensitive≥ 4 J, very sensitive≥ 3 J. Friction: insensitive > 360 N, less sensitive= 360 N, sensitive < 360 N and > 80 N, very sensitive≥ 80 N, extremely sensitive≥ 10 N). Furthermore, the values were compared to similar monotetrazole-based complexes.

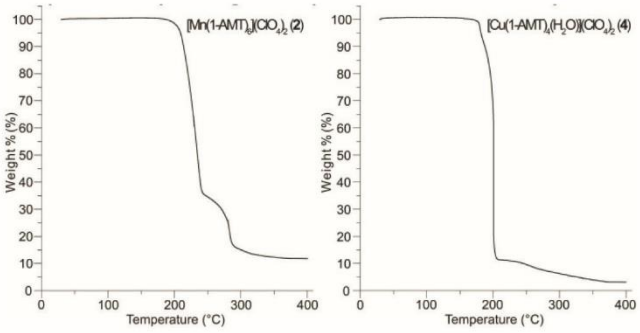


Figure 6. TGA measurements of ECC **2** and **4**.

3.3.1 Thermal Analysis

Table 1 summarizes the decomposition temperatures determined via differential thermal analysis (DTA) together with the obtained sensitivity values. The DTA measurements were performed with a linear heating rate of β= 5 °C min^{-1} from 30 °C to 400 °C and critical events are given as onset temperatures (Figure S2). Manganese(II) and zinc(II) complexes **2** and **5** show decomposition temperatures close to 200 °C even exceeding the one of the free 1-AMT ligand. Compounds **3** and **4** possess good thermal stabilities above 150 °C (177 and 163 °C, respectively) and interestingly the aqua ligand in $[Cu(1\text{-}AMT)_4(H_2O)](ClO_4)_2$ is leaving the coordination sphere far above 100 °C, which is proven by TGA measurements (Figure 6). In contrast, ECC **2** shows no mass loss until its exothermic decomposition temperature, proving its superior thermal stability.

Comparing the AMT complexes with the analogous AT and MAT compounds it becomes clear that they possess similar decomposition temperatures like the 1-amino-5*H*-tetrazole compounds. The only difference is represented by $[Cu(1\text{-}MAT)_4(H_2O)_2](ClO_4)_2$ which already loses its two aqua ligands at 106 °C leading to the formation of a new complex that has never been investigated until now.

3.3.2 Sensitivities and Energetic Properties

The ECC were investigated concerning their sensitivities against impact, friction, and ball drop impact as well as electrostatic discharge (Table 1). They are all in the range of primary explosives with sensitivities comparable to lead azide. Compared to the 1-AT complexes, the additional methyl group of 1-AMT is increasing the stability, which can especially be seen when considering the sensitivities against friction and ESD of the corresponding complexes. While $[Cu(1\text{-}AT)_6](ClO_4)_2$ and $[Fe(1\text{-}AT)_6](ClO_4)_2$ do not possess a no-fire-limit towards friction stimuli, compounds **2–5** could successfully be improved. The stability increases in the following order: $Fe^{2+} < Cu^{2+} < Mn^{2+} < Zn^{2+}$ – which is in accordance with our previous findings [20]. While the

 © 2021 The Authors. Propellants, Explosives, Pyrotechnics published by Wiley-VCH GmbH

aqua ligand in **4** does not seem to strongly affect the stability of the complex, the two aqua ligands in $[Cu(1\text{-}MAT)_4(H_2O)_2](ClO_4)_2$ have a highly stabilizing effect.

Hot needle (HN) and hot plate (HP) tests of ECC **2**–**5** lead in every case to either deflagrations or detonations (Figures 7 and S3–6), proving their energetic character. Especially iron(II) compound **3** is impressive with its strong energy output in both tests.

Hence, it was tested in classical initiation tests using penthrite (PETN) as secondary charge for determining its capability as potential lead azide replacement. Details on the test setup can be found in the Supporting Information (Figure S7). An amount of 50 mg primary explosive was able to transfer the detonation towards 200 mg PETN which is proven by the hole in the copper witness plate (Figure 8). Of the four tested complexes, ECC **3** was the only one capable of initiating PETN. Latter result proves the potential use of complex **3** as lead-free and less toxic primary explosive for classical initiation setups. Furthermore, compounds **3** and **4** were tested towards their ignitability when irradiated using a near-infrared laser diode. Both ECC showed violent detonations with light energy inputs of only 0.17 and 1.70 mJ, respectively (Figure 9).

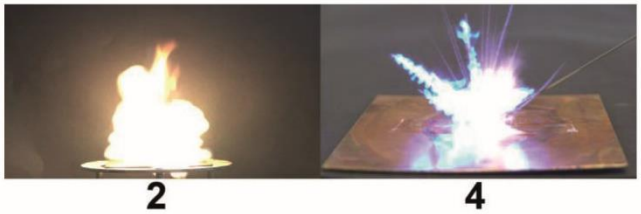


Figure 7. Deflagration of compound **2** (left) during HP and detonation of ECC **4** (right) during HN test.



Figure 8. Positive initiation capability test towards PETN of iron(II) complex **3**.

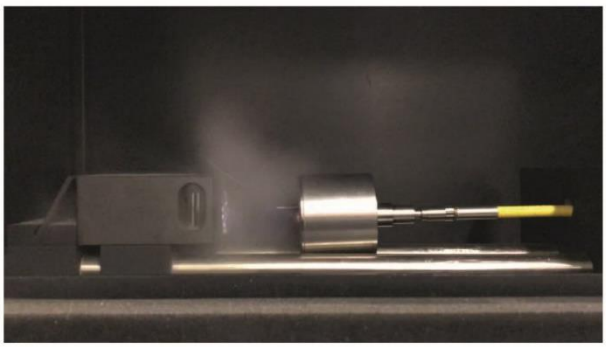


Figure 9. Moment of detonation of complex **4** during the laser initiation experiments.

4 Conclusion

By means of four new 3d metal(II) perchlorate complexes based on 1-amino-5-methyltetrazole as nitrogen-rich ligand, it was possible to stabilize the compounds while at the same time maintaining their energetic performance compared to analogous 1-AT coordination compounds. All ECC show good to very good thermal stabilities up to 199 °C and possess sensitivities in the range of primary explosives. Complex **3**, based on non-toxic iron(II) as central metal shows characteristics of a potential lead azide replacement and was successfully tested in classical initiation tests with PETN. Furthermore, it can be ignited, just like copper(II) compound **4**, with low-energy laser irradiation, which further extends their potential field of applications. It was fortunately obtained with a yield of 99%. It is suggested that the novel compound can be part of future energetic investigations.

Acknowledgements

For financial support of this work by Ludwig Maximilian University (LMU). Besides our congratulations, we also would like to thank Prof. Thomas M. Klapötke for his constant support and scientific input. The authors would also like to thank Mr. Benjamin Bissinger and Mr. Valentin Bockmaier for their great contribution to this work. Open access funding enabled and organized by Projekt DEAL.

Data Availability Statement

No data available.

References

[1] R. Matyáš, J. Pachman, *Primary Explosives*, 1st ed., Springer, Berlin, Heidelberg, **2013**.

 © 2021 The Authors. Propellants, Explosives, Pyrotechnics published by Wiley-VCH GmbH

[2] W. Beck, J. Evers, M. Göbel, G. Oehlinger, T. M. Klapötke, The Crystal and Molecular Structure of Mercury Fulminate (Knallquecksilber), *Z. Anorg. Allg. Chem.* **2007**, *633*, 1417–1422.
[3] U. Brede, R. Hagel, K. H. Redecker, W. Weuter, Primer compositions in the course of time: from black powder and SINOXID to SINTOX compositions and SINCO booster, *Propellants Explos. Pyrotech.* **1996**, *21*, 113–117.
[4] T. Curtius, Neues vom Stickstoffwasserstoff, *Ber. Dtsch. Chem. Ges.* **1891**, *24*, 3341–3349.
[5] T. Curtius, R. Radenhauser, Zur Kenntniss der Stickstoffwasserstoffsäure, *J. prakt. Chem.* **1891**, *43*, 207–208.
[6] T. Urbański, *Chemistry, and Technology of Explosives*, 1st ed., Pergamon, Oxford, **1984**.
[7] L. F. Audrieth, Hydrazoic acid and its inorganic derivates, *Chem. Rev.* **1934**, *15*, 169–224.
[8] T. M. Klapötke, *Chemistry of High-Energy Materials*, 5th ed., De Gruyter, Berlin, Boston, **2019**.
[9] a) https://echa.europa.eu/de/candidate-list-table, (accessed June 2020); b) https://archive.epa.gov/oppt/3350/web/pdf/3350-fnl.pdf, (accessed June 2020).
[10] a) K. Karaghiosoff, T. M. Klapötke, A. Michailovski, H. Nöth, M. Suter, G. Holl, 1,4-Diformyl-2,3,5,6-Tetranitratopiperazine: A New Primary Explosive Based on Glyoxal, *Propellants Explos. Pyrotech.* **2003**, *28*, 1–6; b) W. Huang, Y. Tang, G. H. Imler, D. A. Parrish, J. M. Shreeve, Nitrogen-Rich Tetrazolo[1,5-b]pyridazine: Promising Building Block for Advanced Energetic Materials, *J. Am. Chem. Soc.* **2020**, *142*, 3652–3657.
[11] a) T. Musil, R. Matyáš, R. Vala, A. Růžička, M. Vlček, Silver Salt of 4,6-Diazido-*N*-nitro-1,3,5-triazine-2-amine – Characterization of this Primary Explosive, *Propellants Explos. Pyrotech.* **2014**, *39*, 251–259; b) D. Fischer, T. M. Klapötke, J. Stierstorfer, Potassium 1,1′-Dinitramino-5,5′-bistetrazolate: A Primary Explosive with Fast Detonation and High Initiation Power, *Angew. Chem. Int. Ed.* **2014**, *53*, 8172–8175.
[12] a) M. Krawiec, S. R. Anderson, P. Dubé, D. D. Ford, J. S. Salan, S. Lenahan, N. Mehta, C. R. Hamilton, Hydronium Copper(II)-tris (5-nitrotetrazolate) Trihydrate – A Primary Explosive, *Propellants Explos. Pyrotech.* **2015**, *40*, 457–459; b) M. A. Ilyushin, I. V. Tselinsky, I. A. Ugryumov, V. Y. Dolmatov, I. V. Shugalei, Study of submicron structured energetic coordination metal complexes for laser initiation systems, *Cent. Eur. J. Energ. Mater.* **2005**, *2*, 21–33.
[13] a) T.-A. D. Nguyen, J. M. Veauthier, G. F. Angles-Tamayo, D. E. Chavez, E. Lapsheva, T. W. Myers, T. R. Nelson, E. J. Schelter, Correlating Mechanical Sensitivity with Spin Transition in the Explosive Spin Crossover Complex $[Fe(Htrz)_3]_n[ClO_4]_{2n}$, *J. Am. Chem. Soc.* **2020**, *142*, 4842–4851; b) S. Seth, A. J. Matzger, Coordination Polymerization of 5,5′-Dinitro-2*H*,2*H*′-3,3′-bi-1,2,4-triazole Leads to a Dense Explosive with High Thermal Stability, *Inorg. Chem.* **2017**, *56*, 561–565; c) M. H. H. Wurzenberger, S. M. J. Endraß, M. Lommel, T. M. Klapötke, J. Stierstorfer, Comparison of 1-Propyl-5*H*-tetrazole and 1-Azidopropyl-5*H*-tetrazole as Ligands for Laser Ignitable Energetic Materials, *ACS Appl. Energy Mater.* **2020**, *3*, 3798–3806; d) J.-G. Xu, S.-J. Lin, X.-Z. Li, H.-F. Wu, J. Lu, W.-F. Wang, J. Chen, F.-K. Zheng, G.-C. Guo, Energetic azide-based coordination polymers: Sensitivity tuning through diverse structural motifs, *Chem. Eng. J.* **2020**, *390*, 124587.
[14] V. P. Sinditskii, V. Y. Egorshev, T. Y. Dutova, M. D. Dutov, T.-L. Zhang, J.-G. Zhang, Combustion of Derivatives of 1,5-Diaminotetrazole, *Combust. Explos. Shock Waves* **2011**, *47*, 36–44.
[15] L. Zeisel, N. Szimhardt, M. H. H. Wurzenberger, T. M. Klapötke, J. Stierstorfer, 2-Methyl-substituted monotetrazoles in copper (ii) perchlorate complexes: manipulating coordination chemistry and derived energetic properties, *New J. Chem.* **2019**, *43*, 609–616.
[16] A. S. Tverjanovich, A. O. Aver'yanov, M. A. Ilyshin, Y. S. Tverjanovich, Decomposition of cobalt(III) nitrotetrazolato amminates under the action of laser light, *Russ. J. Appl. Chem.* **2015**, *88*, 226–231.
[17] N. Szimhardt, M. H. H. Wurzenberger, L. Zeisel, M. S. Gruhne, M. Lommel, J. Stierstorfer, Maximization of the energy capability level in transition metal complexes through application of 1-amino- and 2-amino-5H-tetrazole ligands, *J. Mater. Chem. A* **2018**, *6*, 16257–16272.
[18] H. Tang, Z. Zhou, Z. Li, S. Chen, L. Wang, T. Zhang, Copper (II) complexes of 1-methyl-5-aminotetrazole with different energetic anions: syntheses, crystal structures and properties, *J. Energ. Mater.* **2020**, doi.org/10.1080/07370652.2020.1748763.
[19] M. H. H. Wurzenberger, B. R. G. Bissinger, M. Lommel, M. S. Gruhne, N. Szimhardt, J. Stierstorfer, Synthesis and comparison of copper(II) complexes with various *N*-aminotetrazole ligands involving trinitrophenol anions, *New J. Chem.* **2019**, *43*, 18193–18202.
[20] M. H. H. Wurzenberger, M. S. Gruhne, M. Lommel, N. Szimhardt, T. M. Klapötke, J. Stierstorfer, Comparison of 1-Ethyl-5*H*-tetrazole and 1-Azidoethyl-5*H*-tetrazole as Ligands in Energetic Transition Metal Complexes, *Chem. Asian J.* **2019**, *14*, 2018–2028.
[21] a) J. Köhler, R. Meyer, A. Homburg, *Explosivstoffe*, 10th ed., Wiley-VCH, Weinheim, **2008**; b) T. M. Klapötke, *Energetic Materials Encyclopedia*, 1st ed., De Gruyter: Berlin/Boston, **2018**; c) M. S. Gruhne, M. Lommel, M. H. H. Wurzenberger, N. Szimhardt, T. M. Klapötke, J. Stierstorfer, OZM Ball Drop Impact Tester (BIT-132) vs. BAM Standard Method – a Comparative Investigation, *Propellants Explos. Pyrotech.* **2020**, *45*, 147–153.

Manuscript received: July 15, 2020
Revised manuscript received: August 11, 2020

 © 2021 The Authors. Propellants, Explosives, Pyrotechnics published by Wiley-VCH GmbH

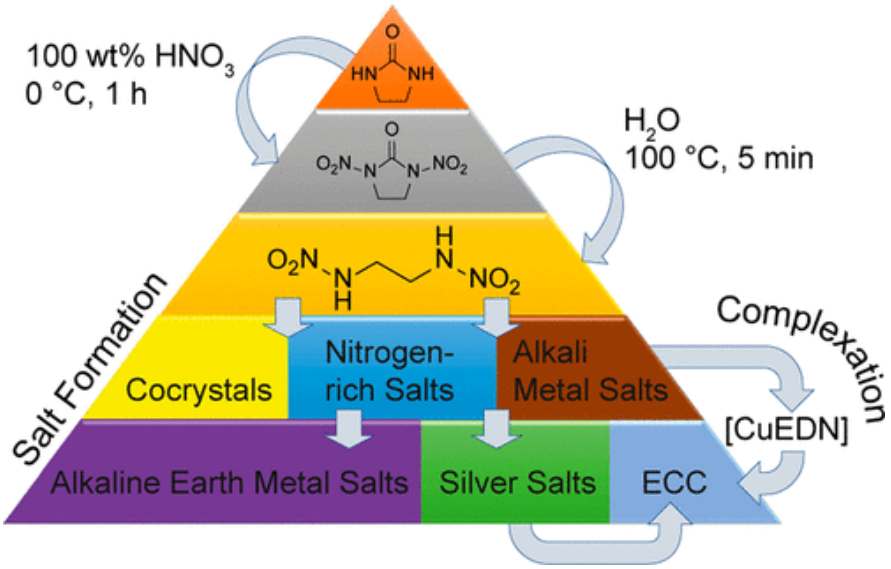
Appendix 22

Investigation of Ethylenedinitramine as a Versatile Building Block in Energetic Salts, Cocrystals, and Coordination Compounds

M. S. Gruhne, M. Lommel, M. H. H. Wurzenberger, T. M. Klapötke, J. Stierstorfer

Inorg. Chem. **2021**, *60*, 4816−4828.

https://doi.org/10.1021/acs.inorgchem.0c03752



Supplementary Information:
https://pubs.acs.org/doi/suppl/10.1021/acs.inorgchem.0c03752/suppl_file/ic0c03752_si_001.pdf

Inorganic Chemistry

pubs.acs.org/IC Article

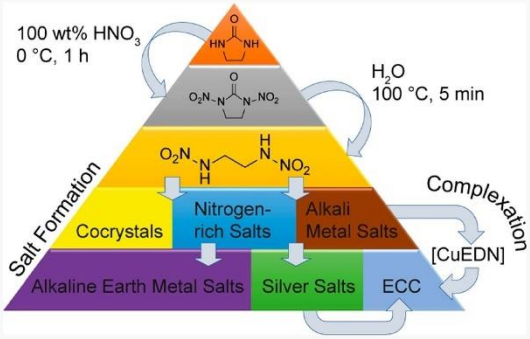
Investigation of Ethylenedinitramine as a Versatile Building Block in Energetic Salts, Cocrystals, and Coordination Compounds

Michael S. Gruhne,[‡] Marcus Lommel,[‡] Maximilian H. H. Wurzenberger,[‡] Thomas M. Klapötke,[‡] and Jörg Stierstorfer*[,‡]

Cite This: *Inorg. Chem.* 2021, 60, 4816−4828 Read Online

ACCESS | Metrics & More | Article Recommendations | Supporting Information

ABSTRACT: Ethylenedinitramine (H_2EDN, **1**) was prepared in a simple manner and with a high overall yield by direct nitration of 2-imidazolidinone using 100% HNO_3 at 0 °C and subsequent hydrolysis in water at 100 °C. The versatility of **1** allows its application as starting material for a broad range of different materials. It was used for the preparation of both various salts and cocrystalline materials incorporating varying amounts of the TATOT moiety. Furthermore, H_2EDN was successfully applied in the concept of energetic coordination compounds (ECCs) resulting in five copper(II) and two silver(I) complexes. A reaction path for the direct precipitation or slow crystallization of 17 different salts, including several alkali, alkaline earth, silver, and nitrogen-rich samples, is presented. The substances were extensively characterized by low-temperature single-crystal X-ray diffraction, elemental analysis (EA), IR spectroscopy, differential thermal analysis (DTA), and thermogravimetric analysis (TGA), proving their high thermal stability, especially of the alkali salts. In addition, **1** and all salts were characterized by ^{1}H, ^{13}C, and ^{14}N NMR, whereas **1** was also investigated using the beneficial $^{1}H-^{15}N$ HMBC NMR spectroscopy. The sensitivities toward various mechanical stimuli according to BAM standard methods, as well as ball drop impact and electrostatic discharge (ESD) were determined using the BAM 1-out-6 method. Hot plate and hot needle tests were performed, followed by further characterization of the copper(II)-based ECCs through laser ignition experiments and UV−vis spectroscopy, offering new candidates for nontoxic, less sensitive laser-ignitable materials. Several detonation parameters were calculated using EXPLO5 (V6.05.02).



Downloaded via LMU MUENCHEN on February 16, 2022 at 08:08:56 (UTC).
See https://pubs.acs.org/sharingguidelines for options on how to legitimately share published articles.

1. INTRODUCTION

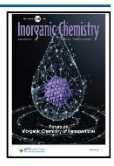
In the growing field of energetic materials, the oxidation of the carbon backbone, the introduction of cage strain, or the synthesis of nitrogen-rich compounds are still the main approaches for the preparation of new molecules (Figure 1).[1] In addition to the synthesis of new materials, the reinvestigation of known materials according to current standards should also be considered. Ethylenedinitramine (H_2EDN) is interesting for this purpose, because its known moderate impact sensitivity at high detonation velocity meets the requirements for energetic materials.[2]

The molecule's history dates to the late 1930s with the investigation of its application in composite-based explosives. One of the most common compositions found during those times was the so-called "Composition B", consisting of about 60% RDX and 40% TNT.[2] Besides the use in fuses of landmines or rockets, it was also implemented as an explosive charge in the first nuclear weapons (Chart 1).[3] Because of its highly sensitive character, replacement had already begun before World War II.[4]

One of those substitutes is called Ednatol and was investigated by the US Army in 1935 at the Picatinny Arsenal. It consists of 40−50% TNT and 50−60% ethylenedinitramine H_2EDN.[5] Although Ednatol was widely used during World War II, today it can be found only in unexploded war ammunition.

However, ethylenedinitramine was not completely forgotten at the end of the war, and first attempts were made to re-examine its salts. These were primarily intended for civilian use, for example as fertilizers in agriculture.[6] There have also been more recent developments, aiming at the use of ethylenedinitramine as an energetic component. For this purpose, the compound's energetic properties were improved by cocrystallization, which is a currently popular method,

Received: December 22, 2020
Published: March 16, 2021



ACS Publications

© 2021 The Authors. Published by American Chemical Society

https://dx.doi.org/10.1021/acs.inorgchem.0c03752
Inorg. Chem. 2021, 60, 4816−4828

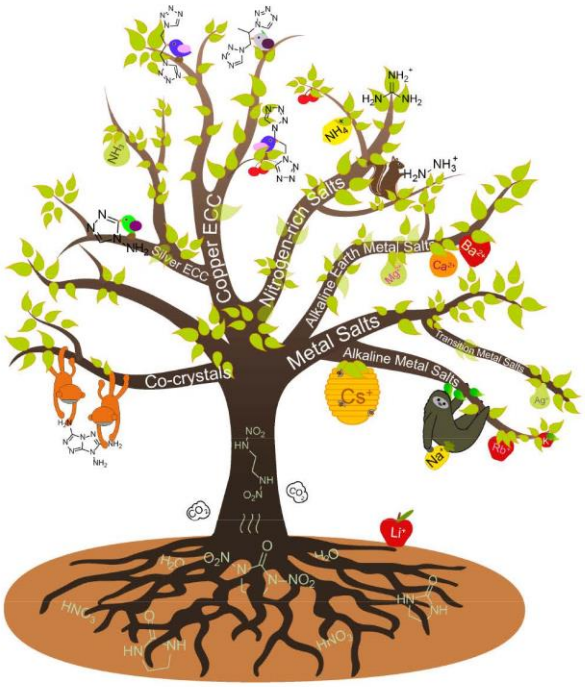


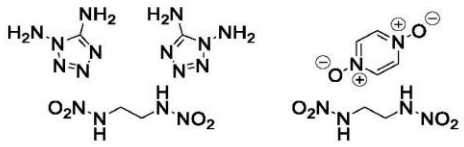
Figure 1. Overview of the versatility of ethylenedinitramine.

Chart 1. Common Energetic Components of Plastic Explosives



especially for well-known substances like HMX and Cl-20.[7] Hussein *et al.* reported in 2018 the preparation of a cocrystal incorporating ethylenedinitramine and 1,5-diaminotetrazole (Chart 2).[8] This compound was also extensively investigated

Chart 2. Molecular Units of Literature-Known Ethylenedinitramine-Based Cocrystals[8,9]



with regard to its detonation parameters, thermal stability, and sensitivity to impact. A crystal structure was not published by the authors, and the structure was justified by powder XRD diffractograms. Therefore, it is not certain whether a salt or a cocrystal was formed. Aakeröy *et al.* on the other hand used solely nonenergetic components for cocrystallization.[9] These were mainly nitrogen- or oxygen-containing heterocycles, which act as proton acceptors for the formation of hydrogen bonds.

Only little effort was made in studying the energetic parameters of the salts of ethylenedinitramine.[10,11] Worth mentioning is the reported impact sensitivity of the silver and the lead salts. Further information on their behavior is not described. However, a procedure for the preparation of the lead and copper(II) salts and their utilization in explosive compositions can also be found in the literature.[12] Besides the neutral compound, the sodium and hydrazinium as well as the corresponding 1,3-diaminopropane and 1,4-diaminobutane salts were examined crystallographically.[13−16] Only the last two structures where determined at low-temperature conditions. In addition, vibrational spectra and quantum chemical calculations predicting the structure of several salts can be found.[17]

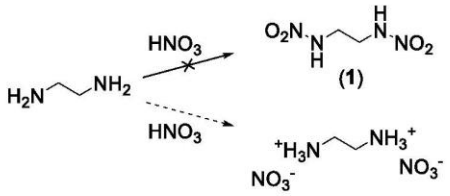
In addition to those salts, a small number of complexes, which include the ethylene dinitramide moiety as an anion, are described in the literature. Apart from the crystal structure of a diammine complex, the crystal structure of an ethylenediamine coordination compound based on copper(II) has been published.[18] Furthermore, a diammine palladium(II) and a hexaaqua nickel(II) complex are known, whereas all of the structures reported have been determined only at room temperature.[18] Only the compound based on ethylenediamine together with a 1,2-diaminopropane complex, which was not investigated crystallographically, were examined for their kinetics of thermal decomposition. The authors also discuss the thermal decomposition of the corresponding diammine silver complex, which, to the best of the authors' knowledge, is the only known silver complex based on this anion.[18] Effort was also made in the crystallization and characterization of the *N*-halo nitramides. Parts of this work have already been published at the 23rd international seminar "New Trends in Research of Energetic Materials".[19]

In order to fill the gaps and to classify the substances using the current state-of-the-art technology, the forgotten molecule, its salts, cocrystals, and coordination compounds were synthesized and examined in more detail for this work.

2. RESULTS AND DISCUSSION

2.1. Synthesis. There are many known ways in the literature to prepare ethylenedinitramine.[20,21] However, the simplest conceivable option, the direct nitration of ethylenediamine, is not possible and leads only to the dinitrate salt of the starting material (Scheme 1).[22]

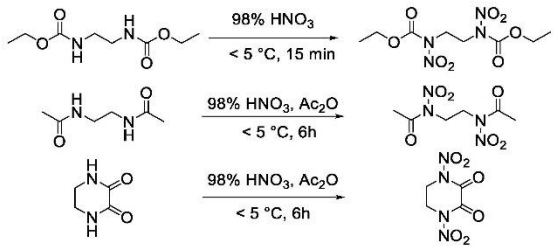
Scheme 1. Direct Nitration of Ethylenediamine[22]



Instead, derivatives of the diamino compound have to be used for obtaining the desired dinitramine. Bachman *et al.* presented several ways, for example starting from ethylene bisurethan, the diacetyl derivative or by nitration of 2,3-piperazinedione monohydrate using acetic anhydride and 98% nitric acid with subsequent ammonolysis.[20] The nitrations shown in Scheme 2 are followed by a reaction with aqueous ammonia solution. The major disadvantages behind these synthetic pathways are the long reaction times and the commercial availability of the reactants. Although the starting materials for the latter two reactions can be purchased, their

https://dx.doi.org/10.1021/acs.inorgchem.0c03752
Inorg. Chem. 2021, 60, 4816−4828

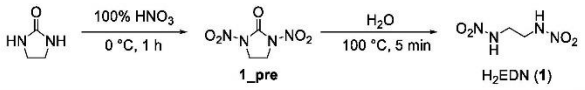
Scheme 2. Outline of Different Precursors for the Preparation of Ethylenedinitramine (1)



prices prevent cost-effective syntheses and make a further reaction step necessary.

For this reason, another attempt presented by Aakeröy *et al.* was chosen.[9] Cheap and commercially available 2-imidazolidinone was nitrated with fuming nitric acid at 0 °C to obtain the precursor 1,3-dinitroimidazolidin-2-one (**1_pre**) in almost quantitative amounts. After hydrolysis in boiling water, ethylenedinitramine (**1**, H_2EDN) was obtained in an almost excellent overall yield of 88% (Scheme 3).

Scheme 3. Preparation of Compound 1 Starting from 2-Imidazolidinone



The $^1H-^{15}N$ HMBC NMR spectrum of ethylenedinitramine was recorded in DMSO-d_6 (Figure 2). The nitro moiety was

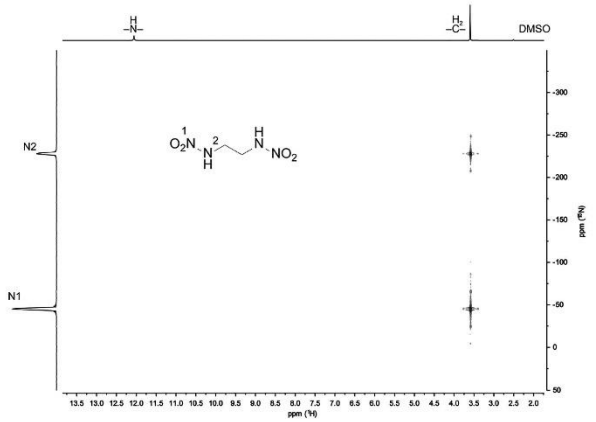
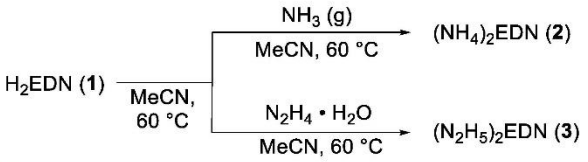


Figure 2. $^1H-^{15}N$ HMBC NMR spectrum of ethylenedinitramine (**1**).

observed at a chemical shift of −45.2 ppm, whereas the nitramide moiety is shifted to −227.9 ppm. A coupling between the proton of the nitramide moiety and the nitro group was not observed.

In addition, several nitrogen-rich salts were synthesized (Schemes 4–6). For the preparation of the ammonium salt **2**, gaseous ammonia was passed through a solution of ethylenedinitramine (**1**) in acetonitrile at 60 °C for 5 min (yield: 88%). The only poorly characterized hydrazinium compound (**3**) was prepared by addition of stoichiometric amounts of hydrazine hydrate to a solution of **1** in acetonitrile at 60 °C

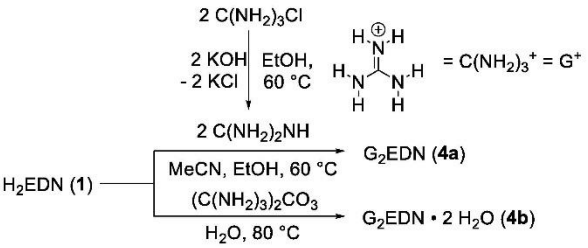
Scheme 4. Overview of the Preparation of Nitrogen-Rich Salts 2 and 3



(yield: 96%). Recrystallization from water gave single crystals of every nitrogen-rich compound suitable for X-ray determination. Unfortunately, the isolation of an elemental analysis-pure hydroxylammonium salt was not possible.

Reaction of an aqueous guanidine carbonate solution with **1** at 80 °C afforded the dihydrate salt **4b** (yield: 73%). The anhydrous species **4a** was obtained by reacting **1** with *in situ* prepared guanidinium (G^+) in ethanol in a yield of 65% (Scheme 5). The latter was obtained by reacting guanidinium

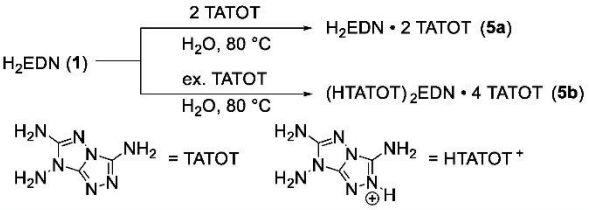
Scheme 5. Preparation of the Guanidinium Salts 4a and 4b



hydrochloride with potassium hydroxide in ethanol. A reaction of *in situ* formed triaminoguanidine with ethylenedinitramine (**1**) yielded only starting material.

When using two equivalents of 3,6,7-triamino-[1,2,4]-triazolo[4,3-*b*][1,2,4]triazole (TATOT) for the salt formation, solely a cocrystal consisting of one ethylenedinitramine and two neutral TATOT moieties (**5a**) was obtained (yield: 76%). As shown in Scheme 6, an excess of TATOT was added to a

Scheme 6. Preparation of Compounds 5a and 5b Incorporating the TATOT Moiety

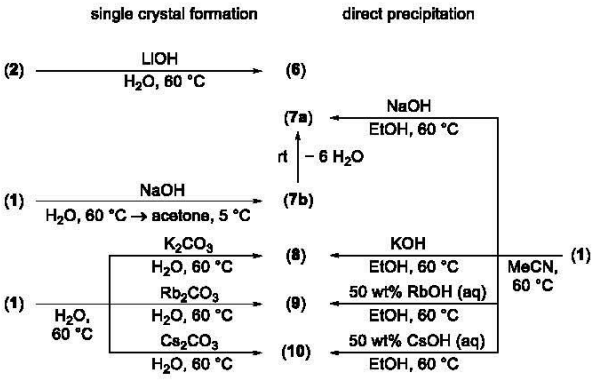


hot solution of compound **1** in water to forcefully obtain a compound possessing a 6,7-triamino-[1,2,4]triazolo[4,3-*b*]-[1,2,4]triazolium cation ($HTATOT^+$). This approach proved to be successful as a salt **5b** was obtained in sufficient yields of 69%. However, the excess also led to a cocrystallization of four additional neutral TATOT molecules. Single crystals of **5a** and **5b** suitable for X-ray determination were both obtained within 1 day directly from the mother liquor. With respect to the possible formation of traces of compound **5b** during the synthesis of compound **5a**, powder X-ray diffraction was used to ensure the purity. Details can be found in the experimental section of the Supporting Information (Figure S11).

https://dx.doi.org/10.1021/acs.inorgchem.0c03752
Inorg. Chem. 2021, 60, 4816−4828

The alkali salts (**6**–**10**) were prepared by simple acid base reactions, where the corresponding carbonate or hydroxide was dissolved in water and reacted with ethylenedinitramine (**1**) or the respective ammonium salt **2** at 80 °C (Scheme 7). As

Scheme 7. Overview of the Different Preparation Methods of Salts 6–10

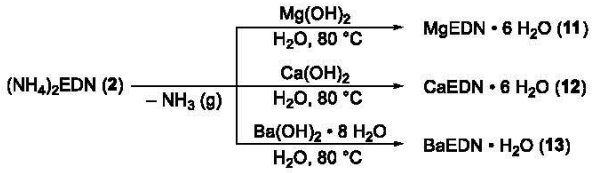


already stated, compound **7a** is known in the literature but poorly characterized.[14] Because it is a compound of the rare class of anhydrous sodium salts, reinvestigations were performed. Single crystals suitable for X-ray diffraction of all alkali salts were obtained after a few days directly from the mother liquors (yields: 73–86%). It was not possible to reproduce single crystals suitable for X-ray diffraction for **7a**. Instead, a hexahydrate (**7b**) was obtained when adding an aqueous solution of compound **7a** to acetone with subsequent cooling. The compound loses all of its hydrate water within an hour, leading to compound **7a** unsuitable for X-ray determination.

The direct precipitation of the alkali salts (**7a** and **8**–**10**) can be achieved by changing the solvent (Scheme 7). Ethylenedinitramine (**1**) was dissolved in acetonitrile at 60 °C, and subsequently the corresponding hydroxide dissolved in ethanol was added. As both cesium and rubidium hydroxide are commercially available only as 50 wt % aqueous solutions, stoichiometric amounts of these solutions were mixed with ethanol and added. A precipitation of the lithium salt (**6**) was not possible because of its high solubility.

Because of the rather bad solubility of the alkaline earth carbonates in water or their respective hydroxides in alcohols, together with the low acidity of the neutral compound **1** (pK_{a1} = 5.31, pK_{a2} = 6.64), a different synthetic approach was chosen for the preparation of compounds **11**–**13**.[9] The ammonium salt **2** was reacted with the respective hydroxides in water at 80 °C with the formation of ammonia as the driving force (Scheme 8). After the reaction mixture was stirred for 30 min at 80 °C, it was possible to filter off a precipitate which was

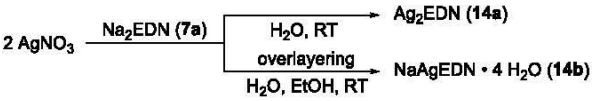
Scheme 8. Reaction of Ammonium Ethylenedinitramide with Various Alkaline Earth Hydroxides



assumed to consist of carbonates formed by the reaction with carbon dioxide from the ambient air. The crystallization of the salts started within a few hours (yield: 61–71%), affording single crystals of **11** and **12**.

Silver ethylenedinitramide (**14a**) was prepared in high yields of 88% by reacting sodium ethylenedinitramide (**7a**) with silver nitrate in aqueous solution at ambient temperature (Scheme 9). As the product readily precipitates during the

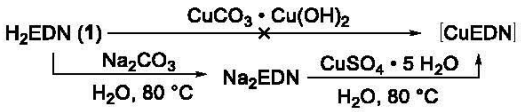
Scheme 9. Preparation of the Silver Salts 14a and 14b



reaction, layering experiments were attempted to obtain single crystals suitable for X-ray diffraction. However, layering of an aqueous solution of compound **7a** with an ethanolic solution of silver nitrate, separated by a layer of water and ethanol in equal amounts, gave the sodium silver salt **14b**.

Because of ethylenedinitramine's low acidity a reaction with carbonates of the 3d transition metal series was not possible (Scheme 10).[9] Neither a synthesis via the neutral compound

Scheme 10. *In Situ* Preparation of Copper(II) Ethylenedinitramide

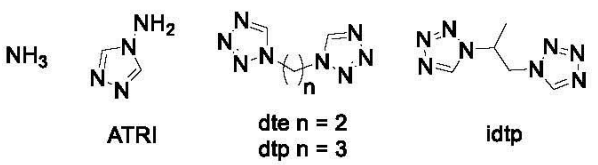


nor approaches using an alkali salt yielded any of the 3d salts. It is assumed that a reaction of the sodium salt with manganese(II), iron(II), copper(II) or zinc(II) salts results in the formation of the corresponding hydroxides or possibly also basic ethylenedinitramide salts because of the basicity of the sodium salt. This would correspond to the preparation of copper(II) azide from sodium azide and a soluble copper salt. Here, because of the azide anion's p*K* value of 4.92, basic copper azides are precipitated first.[23]

However, through sufficient dilution and ambient temperatures, the *in situ* formation of the copper(II) salt, by reacting ethylenedinitramine (**1**) with sodium carbonate in water and subsequent reaction with copper(II) sulfate pentahydrate, was achieved (Scheme 10).

This enables the preparation of the copper(II) complexes **15**–**19** by the reaction of a solution of copper(II) ethylenedinitramide and stoichiometric amounts of the corresponding ligands displayed in Chart 3. With the exception of the commercially available 4-amino-1,2,4-triazole (ATRI), all

Chart 3. Overview of the Ligands Used for the Complexation of Copper(II) and Silver(I) Ethylenedinitramide

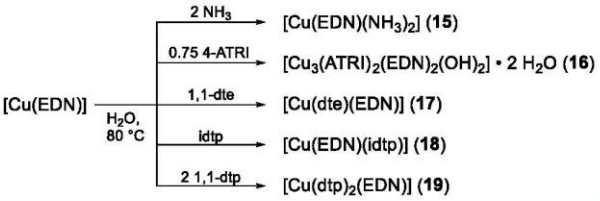


https://dx.doi.org/10.1021/acs.inorgchem.0c03752
Inorg. Chem. 2021, 60, 4816–4828

ligands displayed in Chart 3 were prepared from the corresponding alkyl diamines or dibromides.[24]

The nitrogen-rich endothermic ligands dissolved in water or an aqueous solution of ammonia were added in stoichiometric amounts directly to the solution (Scheme 11). The mother liquor was left for crystallization at ambient conditions.

Scheme 11. Preparation of the ECCs 15–19



All compounds were obtained in decent yields up to 94%. Single crystals of the compounds **15** and **17–19** were obtained directly from the solution. ECC **16** precipitates directly when the ligand is added. The crystals obtained for **16** therefore were of too poor quality to be examined directly by X-ray diffraction. Therefore, layering experiments were performed, successfully yielding suitable single crystals of **16**. A solution of *in situ* prepared copper(II) ethylenedinitramide in water was layered with a 50/50 mixture of ethanol and water followed by an ethanolic solution of the respective ligand in stoichiometric amounts.

The diammine silver complex (**20**) was prepared by dissolving silver ethylenedinitramide (**14a**) in a concentrated aqueous solution of ammonia (Scheme 12) in very high yields

Scheme 12. Preparation of the ECCs 20 and 21



(96%). The solution was left for crystallization, giving single crystals suitable for X-ray determination within a day. Because it is assumed that the compound decomposes slowly under the exposure to light, the drying process and storage were carried out under exclusion of light. The addition of stoichiometric amounts of the nitrogen-rich ligands to the solution of compound **14a** in aqueous ammonia yielded the corresponding ECC **21**, which also represents one of the rare water-containing silver coordination compounds. Single crystals were obtained directly from the solution within a day.

Further attempts to synthesize complexes based on commonly used monotetrazole ligands were unsuccessful for both investigated central metals. In contrast to ATRI, monotetrazoles are monodentate ligands, and it is assumed that they are not able to replace the ammine ligands in the *in situ* prepared compound **20**. Furthermore, ditetrazoles such as 1,1-di(tetrazol-1-yl)ethane were also not able to react with ECC **20** to form complexes.

2.2. Crystal Structures. The crystal structures of compounds **1**, **2**, **3**, **4b**, **5a**, **5b**, **6**, **7b**, **8–12**, **14b**, and **15–21** were determined by low-temperature single-crystal X-ray diffraction. In the case of compound **18** the measurements allow an indication of the most likely composition, but finalization of the data sets was not possible because of the highly disordered ligand moieties. Further information on the structures of the compounds **4b**, **6**, **7b**, **8**, **11**, **12**, **14b**, **15**, **16**, **18**, and **20** together with the measurement and the refinement data of all crystallographic investigated compounds are given in the Supporting Information (Tables S1–S6 and Figures S1–S10). The crystal data sets were uploaded to the CSD database and can be obtained free of charge with the CCDC Nos. 2047743 (**1**), 2047748 (**2**), 2047757 (**3**), 2047761 (**4b**), 2047751 (**5a**), 2047750 (**5b**), 2047755 (**6**), 2047752 (**7b**), 2047746 (**8**), 2047745 (**9**), 2047753 (**10**), 2047758 (**11**), 2047749 (**12**), 2047756 (**14b**), 2047754 (**15**), 2047765 (**16**), 2047759 (**17**), 2047760 (**19**), 2047744 (**20**), 2047747 (**21**).

The crystal structure of the neutral compound **1** is already known in the literature but has been determined only at room temperature.[13] It crystallizes in the form of colorless blocks in the orthorhombic space group *Pbca* with four formula units per unit cell. The compound possesses a density of 1.768 g cm^{-3} at 110 K and shows a roto inversion center on the C1–C1′ axis (Figure 3). All single bonds are in typical ranges.

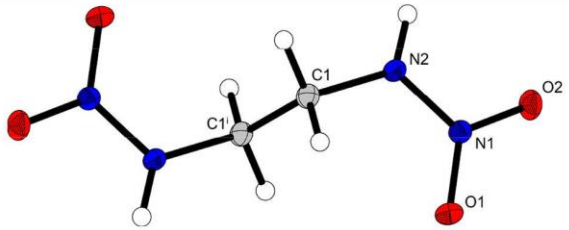


Figure 3. Molecular structure of ethylenedinitramine (**1**). Selected bond lengths (Å): C1–C1^{i}, 1.5273(17); N2–C1, 1.4521(14); O1–N1, 1.2434(13); O2–N1, 1.2366(13); N1–N2, 1.3230(14). Selected bond angles (deg): N2–C1–C1^{i}, 110.85(9); N1–N2–C1, 121.87(10); O1–N1–O2, 123.31(9). Symmetry code: (i) $-x$, $1-y$, $-z$.

The geometry of the ethylenedinitramine unit found in compound **1** can only be observed in cocrystal **5a**, which also contains a unit of the neutral compound. In most of the other structures the roto inversion center is transformed into a classic inversion center (**2**, **3**, **4b**, **5b**, **6**, **7b**, **8–11**, **15**, and **17–21**). This resulted in even shorter N–N bond distances, whereas the remaining bond lengths and angles are all in the typical range. Nevertheless, both configurations have the same conformation in terms of their C–C bond. With an N2–C1–C1^{i}–N2^{i} respectively N1–C1–C1^{i}–N1^{i} dihedral angle of 180°, both structure types exhibit an *anti*-conformation (Figure 4). In addition to these structural types, two compounds were discovered in whose structure a *gauche*-conformation can be observed (**12**: N2–C1–C2^{i}–N3^{i} = 78.767(8); **14b**: N2–C1–C2–N3 = 67.960(3)), as well as one ECC which possesses an anion whose methylene units are approximately arranged in *cis*-conformation (**16**: N5–C4–C3–N7 = 37.6477(18)°).

Bis(ammonium) ethylenedinitramide (**2**) crystallizes in the monoclinic space group $P2_1/c$, and the unit cell is built up by two formula units. The observed density of 1.514 g cm^{-3} (115 K) is lower than that of **1**. As illustrated in Figure 5, all protons of the ammonium cations participate in hydrogen bonds resulting in a 3D layered structure. In detail, an ammonium cation is coordinated here by five anions, forming a total of nine H-bonds. The N–N bond length of 1.2775(3) Å is significantly lower than in compound **1**. This is to be expected, because deprotonation forms a delocalized electron system from N2 via N1 to the oxygen atoms of the nitro group. As a

https://dx.doi.org/10.1021/acs.inorgchem.0c03752
Inorg. Chem. 2021, 60, 4816–4828

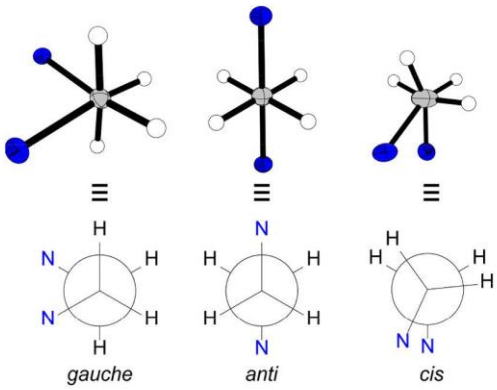


Figure 4. Different conformations for the methylene groups of the ethylene dinitramide moiety observed, displayed along the C−C bond.

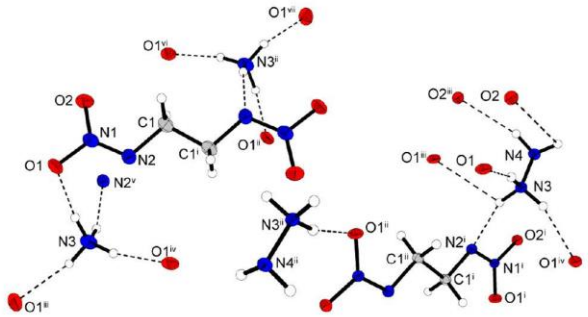


Figure 5. Extended molecular structure of compound **2** (top left) and compound **3** (bottom right). Symmetry codes of **2**: (i) $-x, 1-y, 1-z$; (ii) $1-x, 1-y, 1-z$; (iii) $1-x, 0.5+y, 0.5-z$; (iv) $x, 1.5-y, 0.5+z$; (v) $1+x, y, z$; (vi) $1-x, -0.5+y, 0.5-z$; (vii) $x, 0.5-y, 0.5+z$. Symmetry codes of **3**: (i) $-1+x, -1+y, z$; (ii) $1-x, 1-y, 1-z$; (iii) $x, -1+y, z$; (iv) $-1+x, y, z$.

result, the bond has a slight double-bonding character and is thus shorter.

The crystal structure of the hydrazinium salt **3** was already determined in 1996.[15] Remeasurement at low temperature confirmed the monoclinic space group $P2_1/n$. The unit cell consists of two formula units, leading to a calculated density of 1.615 g cm^{-3} at 131 K. The N−N bond length 1.27549(8) Å in this case is again significantly shorter than in the neutral compound **1**. Hydrogen bonds are mainly formed between the oxygen atoms of the nitro groups and the protons of the hydrazinium ion. In addition, each cation is bound by another hydrogen bridge, which is located between the amide nitrogen of the anion and a proton of the cation (Figure 5). The hydrogen bonds formed by the protons of the N4 nitrogen are much longer (~ 2.3 Å) than those formed by the protons of the N3 (1.9−2.0 Å). These are therefore probably more unstable because of their length. A total of five H-bonds can be recognized. Because the ammonium salt (**2**) forms a clearly more complex network of nine hydrogen bonds, the network formed is probably more stable than that of compound **3**.

The cocrystalline compounds **5a** and **5b** both crystallize in the triclinic space group $P\bar{1}$ in the form of colorless blocks. The unit cells each consist of one formula unit and possess similar calculated densities of 1.681 g cm^{-3} at 106 K (**6a**) and 1.693 g cm^{-3} at 107 K (**5b**). In contrast to compound **5a**, the TATOT unit in **5b** was successfully protonated, leading to the formation of two HTATOT$^+$ cations, one ethylenedinitramide moiety, and four cocrystallizing molecules of neutral TATOT (Figure 6). A comparison of the two compounds shows clear

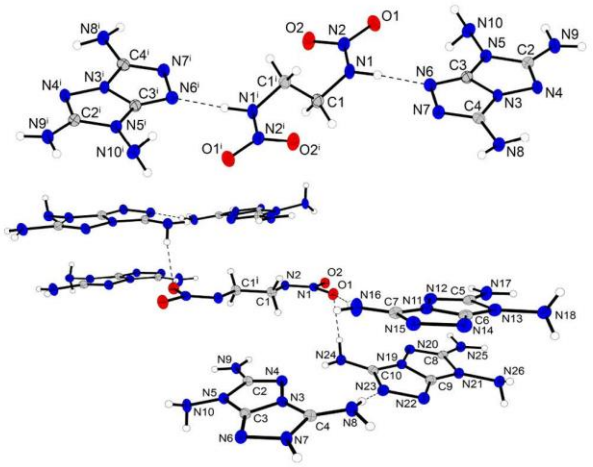


Figure 6. Molecular structures of compound **5a** (top) and compound **5b** (bottom). Symmetry code of **5a**: (i) $-x, -y, -z$. Symmetry code of **5b**: (i) $-x, -y, -z$.

structural differences in the respective packing of the molecules. In both cases, layers are formed that are interconnected by H-bonds. These are mainly formed between the oxygen atoms of the anions and the amino groups of the TATOT units, as well as between TATOT molecules themselves. In addition to that, in compound **5a** a bond of the N1−H group to the N6 nitrogen of the neutral TATOT is found. The bond is not found in compound **5b** because of the deprotonation of the ethylenedinitramine moiety. Therefore, a H-bond between the N7−H group of the HTATOT+ cation and the N2 of the anion is formed. Also worth mentioning is the arrangement of the layers. In the case of compound **5a**, alternating layers of neutral TATOT moieties and ethylenedinitramine can be found. Those layers are solely interconnected via H-bonds formed by oxygen atoms of the methylene groups and the anions. To form this linking, the anions' torsion angle between the C1−C1^i and the N2−N1 bonds is 82.66°. For compound **5b**, the torsion angle is 177.89°. In this case, however, a layer consisting entirely of neutral TATOT molecules follows. The interconnections of the layers to each other are also not exclusively built up by anion interactions. In addition to H-bonds between anions and neutral TATOT units, interactions between neutral TATOTs of different planes can also be observed.

All crystallographically investigated alkali metal salts crystallize in monoclinic or orthorhombic space groups (**6**, **7b**, **8**, and **9**: $P2_1/c$; **10**: *Pbam*). There also appears to be a general trend for the alkali metals, except for compound **7b**, to possess densities increasing with ascending atomic number (**6**, 1.746 g cm^{-3}; **7b**, 1.688 g cm^{-3}; **8**, 1.864 g cm^{-3}; **9**, 2.641 g cm^{-3}; **10**, 3.170 g cm^{-3}). The coordination spheres around the respective metal cations grow according to the same pattern (**6**, 4-fold; **7b**, 6-fold; **8**, 8-fold; **9**, 9-fold; **10**, 10-fold). In any case, the unit cell consists of two formal units (Figures 7 and S2−S4).

https://dx.doi.org/10.1021/acs.inorgchem.0c03752
Inorg. Chem. 2021, 60, 4816−4828

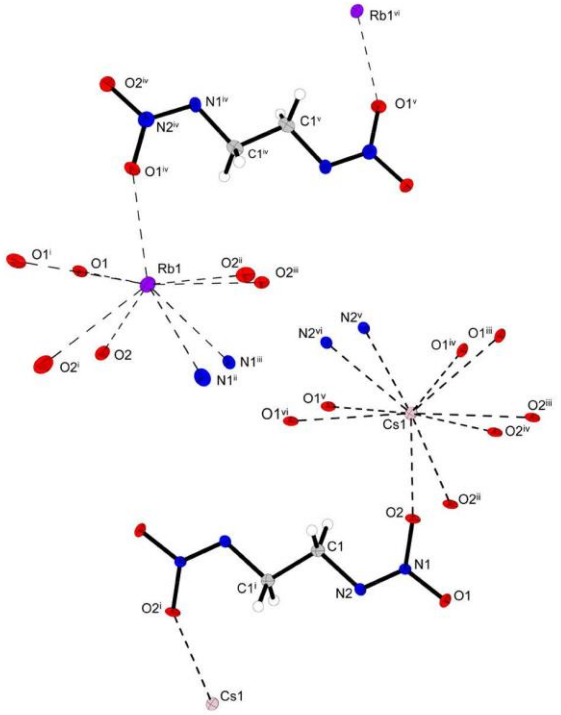


Figure 7. Extended molecular structures of **9** (left) and **10** (right). Selected bond lengths (Å) of **9**: Rb1–O1, 3.0378(3); Rb1–O2, 2.9629(3); Rb1–O2^{i}, 3.1357(4); Rb1–N1^{ii}, 3.3266(3). Selected bond lengths (Å) of **10**: Cs1–O2, 3.1855(19); Cs1–O1^{iii}, 3.219(2); Cs1–N2^{v}, 3.2241(19). Symmetry codes of **9**: (i) $-1 + x, y, z$; (ii) $-1 + x, 0.5 - y, -0.5 + z$; (iii) $x, 0.5 - y, -0.5 + z$; (iv) $1 - x, -y, -z$; (v) $x, y, -1 + z$; (vi) $1 - x, -y, 1 - z$. Symmetry codes of **10**: (i) $2 - x, 1 - y, z$; (ii) $x, y, 1 + z$; (iii) $1 - x, 1 - y, 1 + z$; (iv) $1 - x, 1 - y, z$; (v) $1.5 - x, 0.5 + y, 2 - z$; (vi) $1.5 - x, 0.5 + y, 1 - z$.

Coordination compounds **17** and **19** crystallize in the triclinic space group $P\bar{1}$. The unit cells are formed by one formal unit and show a calculated density differing only slightly. (**17**, 1.794 g cm^{-3} at 126 K; **19**, 1.702 g cm^{-3} at 103 K). Both complexes possess an octahedral coordination sphere built up by the anion in equatorial, as well as in axial positions and the respective ligand in the remaining unoccupied equatorial positions. As observed for the copper diammine complex **15**, the anion again coordinates via one of its oxygen atoms and the nitrogen atom of the nitramide group (Figure 8). Both complexes possess a Jahn–Teller distortion along their O–Cu–O bond axes. The octahedral coordination sphere is also strongly distorted by the steric properties of the anions, resulting in the axial bonds not being perpendicular to the equatorial bonds at all. The big difference between both complexes is the polymeric network formed by the ligand applied. Whereas the bridging di(tetrazolyl)ethane ligands in compound **17** lead to the formation of two-dimensional layers, the nonbridging character of di(tetrazolyl)propane results in 1D chains (**19**). This behavior is very unusual for ditetrazole ligands but was already observed on some rare occasions in our group.[25]

In general, the ligands of **17** and **19** differ only in the length of their respective carbon bridge. The ethylene bridged ligand of compound **17** is found in an *anti*-conformation resulting in a ligand forming two-dimensional networks (Figure 9). Extending the carbon bridge by another carbon atom leads to a *gauche*

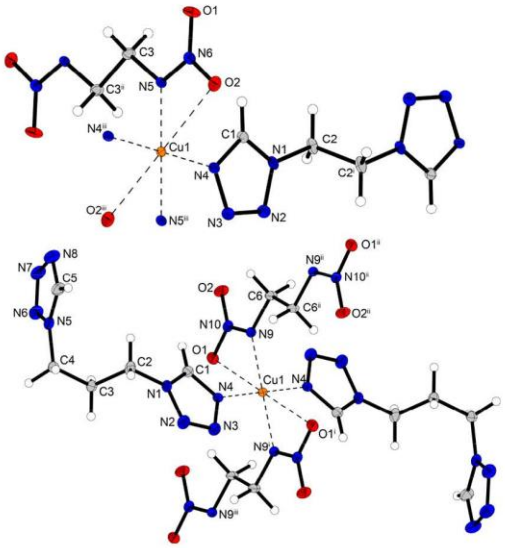


Figure 8. Extended molecular structures of the ECCs **17** (top) and **19** (bottom). Selected bond lengths (Å) of **17**: Cu1–N4, 2.0149(18); Cu1–N5, 1.9632(19); Cu1–O2, 2.5610(14). Selected bond lengths (Å) of **19**: Cu1–O1, 2.6150(16); Cu1–N4, 2.0122(18); Cu1–N9, 1.9697(19). Selected bond angles (deg) of **17**: O2–Cu1–N4, 90.27(6); O2–Cu1–N5, 55.56(7); N4–Cu1–N5, 90.37(8). Selected bond angles (deg) of **19**: O1–Cu1–N4, 92.32(6); O1–Cu1–N9, 54.40(7); N4–Cu1–N9, 90.38(8). Symmetry codes of **17**: (i) $1 - x, 2 - y, -z$; (ii) $2 - x, 1 - y, 1 - z$; (iii) $2 - x, 2 - y, -z$. Symmetry codes of **19**: (i) $1 - x, -y, 2 - z$; (ii) $2 - x, -y, 2 - z$; (iii) $x, -1 + y, z$.

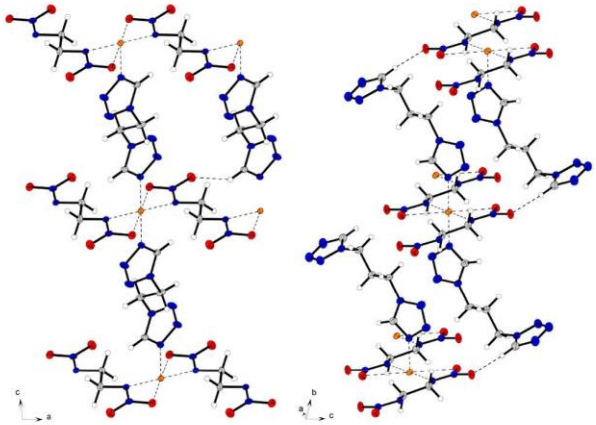


Figure 9. Segments of the polymeric networks of the ECCs **17** (left) and **19** (right), formed by tetrazole ligands linking between different copper centers.

conformation. The resulting rotation of the ligand does further coordination to another metal center. In both cases hydrogen bonds are formed between the proton of the tetrazole unit and the noncoordinating oxygen atom of the nitro group. Only the distance between the respective oxygen and hydrogen atoms is slightly longer in the case of compound **19**, making the packing less dense (**17**, O1–H1 = 2.1925(18) Å; **19**, O2–H5 = 2.259(2) Å).

The silver coordination compound **21** crystallizes as colorless blocks in the monoclinic space group $P2_1/c$ with two formula units per unit cell. The calculated density of 2.432

https://dx.doi.org/10.1021/acs.inorgchem.0c03752
Inorg. Chem. 2021, 60, 4816–4828

g cm^{-3} at 110 K is higher than the ones observed for the copper-based ECCs but lower than the density observed for complex **20**. The silver cation is arranged in a very rare trigonal planar manner, with the metal ion coordinated via two ATRI ligands and one of the amide nitrogen atoms of the ethylenedinitramide moiety. As shown in Figure 10 the two ligands are each bridging via the N3 or N4 atoms between the same two silver atoms, resulting in the formation of dimers. These pairs are then linked to form 1D polymeric chains via the ethylene dinitramide units. Because of the hydrogen bridge bonding of the proton to C2 with O1, the polymer chain is almost perfectly planar (O1−N1−N3−C2 = 2.2968(4)°). The trigonal coordination sphere is slightly distorted as the silver cation is moved out of the center by 0.0116(17) Å. Hydrogen bonds form a bridge between water molecules in the structure and the 1D polymeric chains, leading to a complex 3D structure.

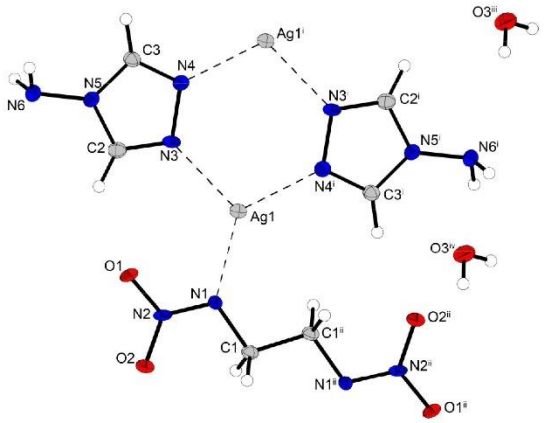


Figure 10. Molecular structure of $[Ag_2(ATRI)_2(EDN)]\cdot 2\ H_2O$ (**21**). Selected bond lengths (Å): Ag1−N1, 2.219(4); Ag1−N3, 2.3098(4); Ag1−N4^i, 2.246(4). Selected bond angles (deg): N1−Ag1−N4^i, 129.51(14); N3−Ag1−N4^i, 108.84(15), N1−Ag1−N3, 121.64(13). Symmetry codes: (i) $1-x, -y, 1-z$; (ii) $2-x, -y, -z$; (iii) $x, y, -1+z$; (iv) $-1+x, y, z$.

2.3. Compound Sensitivities and Thermal Stability. Differential thermal analysis (DTA) at a linear heating rate of 5 °C min^{-1} in the range of 50−400 °C was applied for every compound except **7b** and **14b**. Because it was not possible to isolate these substances, this measurement was forgone. The observed decomposition temperatures as well as endothermic events (melting or loss of crystal water) are listed in Table 1. All DTA plots can be found in the Supporting Information (Figures S18−S23). Thermogravimetric (TG) measurements at a heating rate of 5 °C min^{-1} in the temperature range of 50−400 °C were performed for compounds **1**−**4a**, **4b**, **6**, **8**, **11**−**13**, **20**, and **21** (Figures 11, S24, and S25). For the neutral compound **1**, an endothermic event was observed at 178 °C, indicating a melting of the compound according to TG. The compound decomposes at 183 °C, which is consistent with the literature data.[2,9] With the exception of bis(ammonium) ethylenedinitramide (**2**, T_{exo} = 177 °C), all nitrogen-rich salts

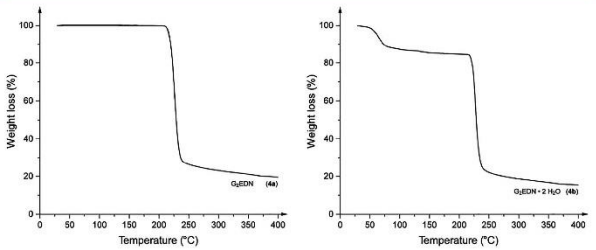


Figure 11. Thermogravimetric measurements of the bisguanidinium salts **4a** and **4b**.

Table 1. Overview of the Compounds' (1−7a, 8−14a, and 15−21) Thermal Stability,[a] Sensitivities toward Various External Stimuli and Results of Hot Plate (HP) as Well as Hot Needle (HN)

	1	2	3	4a	4b	5a	5b	6	7a	8	9
IS[b] (J)	5	>40	25	>40	>40	>40	>40	>40	3	5	3
BDIS[c] (mJ)	>200	>200	>200	>200	>200	>200	>200	>200	194	>200	152
FS[d] (N)	240	>360	324	>360	>360	>360	>360	>360	240	>360	288
ESD[e] (mJ)	960	1080	450	1500	1500	1500	1350	>1500	1350	>1500	>1500
HP[f]	defl.	defl.	defl.	dec.	dec.	dec.	dec.	dec.	defl.	defl.	defl.
HN[f]	dec.	dec.	defl.	dec.	dec.	dec.	dec.	dec.	defl.	defl.	defl.
T_{endo}[g] (°C)	178, 183	156, 177	141	208	63, 111, 211	–	–	103	–	54, 85	–
T_{exo}[h] (°C)	183	177	191	208	211	223	234	276	304	329	342

	10	11	12	13	14a	15	16	17	18	19	20	21
IS[b] (J)	9	>40	>40	>40	2	3	2	10	<1	10	9	>40
BDIS[c] (mJ)	28	>200	>200	69	28	111	>200	200	28	83	>200	>200
FS[d] (N)	216	>360	>360	>360	72	180	360	48	64	60	>360	>360
ESD[e] (mJ)	203	>1500	>1500	123	368	>1500	227	106	106	250	840	540
HP[f]	defl.	dec.	dec.	defl.	defl.	defl.	defl.	defl.	defl.	defl.	defl.	defl.
HN[f]	defl.	dec.	dec.	dec.	defl.	dec.	dec.	dec.	dec.	dec.	dec.	dec.
T_{endo}[g] (°C)	–	131	70, 100	179	–	–	–	–	–	–	98, 171	72
T_{exo}[h] (°C)	349	131	285	268	211	212	194	203	180	177	237	222

[a]Onset temperature at a heating rate of 5 °C min^{-1} measured by DTA. [b]Impact sensitivity according to the BAM drop hammer (method 1 of 6).[26,27] [c]Ball drop impact sensitivity determined with the 1 of 6 method in accordance with MIL-STD 1751A (method 1016).[28,29] [d]Friction sensitivity according to the BAM friction tester (method 1 of 6).[26,29,30] [e]Electrostatic discharge sensitivity (OZM Electric Spark XSpark10, method 1 of 6).[29] [f]def., deflagration; dec., decomposition. [g]Endothermic peak, which indicates melting or dehydration. [h]Exothermic peak, which indicates decomposition.

https://dx.doi.org/10.1021/acs.inorgchem.0c03752
Inorg. Chem. 2021, 60, 4816−4828

are thermally more stable than ethylenedinitramine (**1**). Endothermic events were observed for all these compounds except the cocrystalline compounds **5a** and **5b**. According to TG measurement, each of those endothermic events indicate the compound's melting point. In addition to that, compound **4b** exhibits additional two endothermic events, each representing a loss of crystal water.

The alkali salts (**5**, **7a**, and **8**–**10**) all exhibit significantly higher exothermic events than the starting compound **1**. With the exception of the lithium salt (**6**) all compounds' decomposition temperatures exceed the 300 °C mark and shift to higher temperatures with increasing atomic number. Endothermic events were detected only for compounds **6** and **8** containing crystal water. For the anhydrous sodium salt **7a**, neither endothermic signals during DTA measurements nor a loss of mass during TG measurements were observed. Because the IR spectrum of the compound does not show any bands indicating the presence of water, this confirms the previous assumptions that salt **7b** loses all of its six crystal waters and is converted to salt **7a**. The trend observed for alkali metals cannot be applied to the series of alkaline earth metals investigated.

The low decomposition temperature of compound **11** is due to the broad endothermic signal directly followed by the exothermic event. The decomposition temperatures of the remaining alkaline earth metal salts all exceed 250 °C. Endothermic events were detected for every compound indicating a loss of crystal water. The silver salt **14a** exhibits an exothermic event at 211 °C, making it the metal salt with the lowest thermal stability.

All compounds' sensitivity toward various mechanical stimuli as well as electrostatic discharge were evaluated (Table 1). Further details on the performed measurements can be found in the experimental section in the Supporting Information. Furthermore, all substances have been classified according to UN recommendations on the transport of dangerous goods.[31] BAM friction sensitivity measurements[26,29,30] showed that every salt except the sodium (**7a**), cesium (**10**), and silver salt (**14a**) are less sensitive than the neutral compound (**1**, **7a**: FS = 240 N; **10**: FS = 216 N, **14a**: FS = 72 N). An analysis of the salts with regard to their BAM impact sensitivity[26,27] showed that the sodium (**7a**) the rubidium salt (**9**) and the silver salt (**14a**) are more sensitive toward impact than ethylenedinitramine (**1**, **8**: IS = 5 J; **7a**, **9**: IS = 3 J, **14a**: IS = 2 J). The potassium salt (**8**) shows the same impact sensitivity as compound **1** (Figure 12). This is surprising because the compound contains two water molecules, and it is also insensitive toward friction (**8**: FS > 360 N). It was also recognized that both the water-containing (**4b**) and anhydrous guanidinium salts' (**4a**) sensitivities toward mechanical stimuli are identical (**4a**, **4b**: FS > 360 N, IS > 40 J). Therefore, IR spectra of the substances were recorded before and after each series of measurements to ensure substance **4a** had not absorbed water while standing in air. However, these tests did not indicate any change of the products. An analysis of the cocrystalline compounds **5a** and **5b** showed a clear desensitization of both compounds, with both being insensitive toward mechanical stimuli (**5a**, **5b**: IS > 40 J, FS > 360 N). Overall, the majority of the salts can be classified as insensitive (**2**, **4a**, **4b**, **5a**, **5b**, **6**, **11**, **12**, and **13**), with some substances that are sensitive (**1**, **3**, **8**, and **10**) and three salts that are even classified as very sensitive (**7a**, **9**, and **14a**).

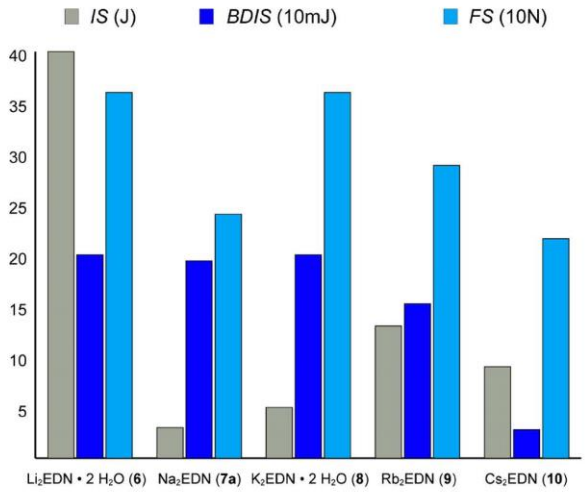


Figure 12. Selected sensitivities of the alkali metal salts **6**, **7a**, and **8**–**10**.

In addition, measurements of the salts' sensitivity toward ball drop impact according to MIL-STD 1751A (method 1016) were carried out.[28,29] This type of impact test is intended to produce more realistic results, because a combination of friction and impact is applied to the substance.[32] It was found that substances less sensitive toward friction were also less sensitive toward the ball drop impact test. The strongest exception is compound **13** (FS > 360 N, BDIS = 69 mJ) together with compound **9** (FS = 288 N; BDIS = 152 mJ). Both salts exhibit low sensitivities toward friction while being quite sensitive toward ball drop impact.

The complex possessing the highest thermal stability is the diammine coordination compound **20** (T_{exo} = 237 °C). Among the azole-based coordination compounds, complex **17** shows the highest thermal stability (T_{exo} = 203 °C), which is due to the bridging character of anion and ligand. Compound **16**, which shows a polymeric structure, decomposes at a temperature of 194 °C. Only complex **18**, structured similarly to **17**, showed a rather low thermal stability (T_{exo} = 180 °C). With the exception of ECCs **18** and **19** all of the investigated coordination compounds are thermally more stable than the neutral ethylenedinitramine (**1**, T_{exo} = 183 °C). In addition, the sensitivity of all ECCs toward mechanical stimuli and electrostatic discharge was investigated, as previously carried out for the metal salts. Details on the procedure can be found in the Supporting Information as already described for the metal salts. Of all complexes investigated, **18** was found to be the most sensitive toward impact (IS <1 J). Compounds **15** and **16** both possess impact sensitivities ≤3 J. In the case of compound **16** this fact is quite astonishing, as this compound contains two molecules of water, which usually make a compound less sensitive. The more impact-sensitive ECCs **15**, **16**, and **18** are less sensitive toward friction (**15**, FS = 180 N; **16**, FS = 360 N; **18**, FS = 64 N).

The lowest sensitivity among the complexes was observed for compound **17**, being rather insensitive toward impact (FS = 48 N, IS = 10 J). Overall, all compounds except **21** must be classified as sensitive according to the UN recommendations on the transport of dangerous goods. Compounds **15**, **16**, and **18** can even be considered very sensitive because of their low impact sensitivity. A slight correlation between ball drop

https://dx.doi.org/10.1021/acs.inorgchem.0c03752
Inorg. Chem. 2021, 60, 4816–4828

impact sensitivity and BAM impact sensitivity was observed in the case of compound **18** (BDIS = 28 mJ, IS ≤ 1 J) but not for the only slightly less sensitive complexes **16** (BDIS > 200 mJ, IS = 2 J), **17** (BDIS = 200 mJ, IS = 2 J), and **20** (BDIS > 200 mJ, IS = 9 J) (Figure 13). A correlation between sensitivity toward friction was also not observed in the case of the ECCs, which is contrary to our earlier findings.[32]

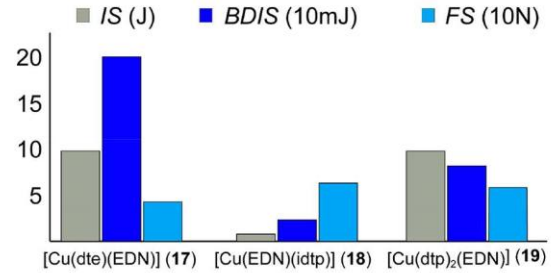


Figure 13. Selected sensitivities of the ECCs **17**–**19**.

A comparison of the ECCs **15**–**21** with compounds **1**–**7a** and **8**–**14a** indicates that their sensitivities toward mechanical stimuli, as well as the thermal stability, are much more widely scattered and generally correlate with the ligand applied. This supports the concept of energetic coordination compounds, by which a prediction of the properties of the resulting complex can be made.

2.4. Primary Explosive Suitability Evaluation and Laser Ignition Experiments. Hot plate and hot needle tests were performed to gain insight into each compounds' deflagration-to-detonation transition (DDT). The hot plate test shows the behavior of a compound during fast heating (Figure 14). The substance is placed on a copper plate which is



Figure 14. Deflagration reactions of silver ethylenedinitramide (**14a**) during hot plate (right and middle) and hot needle test (left).

heated by a Bunsen burner. Hot needle tests indicate the behavior of a sample during slight confinement. It is performed by fixation of the compound on a copper plate using adhesive tape. Subsequently, a needle, which has been heated up glowing red, is held on the sample (Figure 14). The outcome of each test is illustrated in Table 1. Further high-speed recording can be found in the Supporting Information (Figures S26–S46). The behavior of substances **1**–**7a** and **8**–**14a** during these tests is typical for high explosives and was expected because of their sensitivity data. While the reaction of silver salt **14a** indicates a possible use as a lead azide substitute, the burning of complexes **15**–**19** indicates a possible use as a laser-ignitable explosive.

In addition to ignition caused by heat and classic initiation by impact energy or friction force, optical ignition is becoming increasingly important. For a classical ignition, a substance is required which exhibits sensitivity parameters that are within a range that allows ignition by mechanical stimulation. This is not necessary for laser-based systems because the substance only has to react to the irradiation. Less sensitive substances result in advantages for application, because the energetic materials are considerably safer to handle. This circumstance facilitates not only the application but also production, storage, and transport. For this reason, the field of optical ignition is strongly researched.[33] As already mentioned, the coordination compounds **15**–**21** are of interest to be studied by irradiation with a laser. Because solely colored compounds are known to react in this setup, other compounds were not investigated. The outcome of each test is shown in Table 2 and Figure 15. Details on the process as well as on the used setup can be found in the experimental section of the Supporting Information.

Table 2. Results of the Laser Ignition Experiments of the ECCs 15–19[a]

	energy E (mJ)			
compound	3.4	4.5	51	67.5
15	dec.	dec.	–	–
16	–	dec.	dec.	–
17	defl.	–	defl.	–
18	–	–	defl.	–
19	–	–	defl.	defl.

[a]dec., decomposition; defl., deflagration; –, not tested. Operating parameters: current I = 10–15 A; voltage U = 4 V; theoretical maximal output power P_{max} = 45 W; theoretical energy E_{max} = 4.5–126 mJ; wavelength λ = 915 nm; pulse length τ = 1–15 ms.

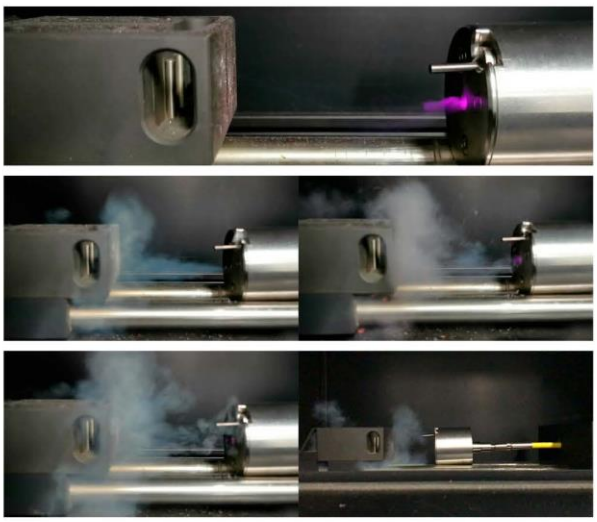


Figure 15. High-speed images of the laser ignition experiments of the ECCs **15**–**19**. Decomposition of compound **15** (top, 15 ms, 12 A). Decomposition reaction of complex **16** in the center, left (15 ms, 10 A). Deflagration of coordination compound **17** in the center, right (1 ms, 10 A). Deflagration reactions of ECCs **18** (bottom left, 15 ms, 10 A) and **19** (bottom right, 15 ms, 12 A).

All complexes showed a reaction toward the laser irradiation. For the compounds **17**, **18**, and **19** deflagrations were observed (Figure 15). Therefore, further investigations on the ability of the investigated compounds to replace the toxic tetraammine *cis*-bis(5-nitro-2*H*-tetrazolato-N^2)cobalt(III) perchlorate (BNCP) are of interest.[34] Compounds **15** and **16** showed only decomposition reactions. Despite the deflagrations during hot plate tests of **15** and **16**, this outcome was to be expected.

https://dx.doi.org/10.1021/acs.inorgchem.0c03752
Inorg. Chem. 2021, 60, 4816–4828

The results of the tests, like all parameters of the ECCs, depend on the ligand−metal−anion system used. Complexes **15** and **19** are limited in their performance by their ligands applied, and compound **16** is limited by its crystal water molecules.

At present, the mechanism behind the laser-based ignition of energetic materials is not fully understood. An attempt to gain more precise insight into this mechanism is the measurement of solid-state UV−vis spectra. This method has turned into a standard analytical method for coordination compounds, because it can also be used to obtain information on ligand−central metal bonding. For this reason, solid-state UV−vis measurements were performed for every colored compound investigated during laser ignition experiments. The spectrum (Figure S47) together with details on the measurement can be found in the Supporting Information (Table S10).

2.5. Detonation Parameters. The calculations for compounds **1** and **3** were performed with the EXPLO5 V6.05.02 computer code by using the room-temperature density data obtained from the X-ray structures as described in the literature.[35] For a better comparison, the data for 1,3,5-trinitro-1,3,5-triazinane (RDX) was recalculated using the EXPLO5 code in the same version (Table 3).

Table 3. Detonation Parameters of Compounds 1 and 3 Compared to Those of RDX

	1	3	RDX
formula	$C_2H_4N_4O_4$	$C_2H_{14}N_8O_4$	$C_3H_6N_6O_6$
Ω_{CO_2}[a] (%)	−31.98	−52.29	−21.61
ρ[b] (g cm^{-3})	1.720	1.576	1.800
$\Delta_f H°$[c] (kJ mol^{-1})	−364	102	317
EXPLO5 6.05.02[33]			
$\Delta_{ex}H°$[d] (kJ kg^{-1})	−5443	−5297	−5740
T_{det}[e] (K)	3397	2937	3745
$P_{C\text{-}J}$[f] (GPa)	30.1	30.5	33.6
$V_{det.}$[g] (m s^{-1})	8634	9239	8801
V_0[h] (dm^3 kg^{-1})	865	1038	1045

[a]Oxygen balance ($\Omega = (xO - 2yC - (1/2)zH)M/1600$). [b]Density at 298 K. [c]Calculated enthalpy of formation. [d]Heat of explosion. [e]Detonation temperature. [f]Detonation pressure. [g]Detonation velocity. [h]Volume of detonation gases (assuming only gaseous products).

The densities range from 1.576 g cm^{-3} (**3**) to 1.720 g cm^{-3} (**1**). Both compounds possess good calculated detonation parameters with detonation velocities (V_{det}) between 8600 and 9200 m s^{-1} and detonation pressures ($P_{C\text{-}J}$) of about 30 GPa. The hydrazinium salt **3** shows the highest calculated detonation velocity (9239 m s^{-1}) and detonation pressure (30.5 GPa), even outperforming RDX in means of detonation velocity.

3. CONCLUSIONS

Ethylenedinitramine (**1**) was prepared by nitration of 2-imidazolidinone and subsequent hydrolysis in boiling water, resulting in highly satisfying yields up to 88%. The reaction is easily scalable and based on low-cost, commercially available, and nontoxic starting materials. Based on this compound, 16 energetic, heavy metal-free salts and two cocrystalline compounds were prepared. Almost all of these compounds can easily be precipitated in high yields. During this process, only green solvents such as ethanol and acetonitrile or even water were used. In addition, five copper(II) and three silver(I) ECCs based on ethylenedinitramide as an anion and nitrogen-rich ligands were prepared. With the exception of hydrate-free guanidinium (**4a**), and sodium salts (**7a**), together with the barium salt (**13**), and the silver salt (**14a**), the crystal structure of every compound was determined, or in the case of compounds **1**, **3**, and **15** redetermined, at low temperature. Furthermore, compound **7a** is one of the rare anhydrous sodium salts. During its synthesis in aqueous medium a hexahydrate (**7b**) is formed first, which could also be examined crystallographically. This compound then loses all its crystal water at room temperature without any further application of energy. DTA and TG measurements together with IR spectroscopy proved this finding. Apart from the ammonium salt (**2**), all nitrogen-rich salts exceed ethylenedinitramine with respect to their thermal stability. This has also been observed for all metal salts except for the magnesium salt (**11**). Except for the silver salt (**14a**, T_{exo} = 211 °C), all of these salts exceed the 250 °C mark; four of the alkali metal salts even exceed the 300 °C mark culminating in the decomposition temperature of the cesium salt (**10**) at T_{exo} = 349 °C. At the same time, sensitivity measurements for most of the substances showed a high stability against mechanical manipulation. Besides four compounds, which are classified as sensitive, only the anhydrous sodium salt (**7a**), rubidium (**9**) and silver salt (**14a**), and the copper-based ECCs **15**, **16**, and **18** are considered very sensitive according to UN Recommendations on the Transport of Dangerous Goods. Also of interest are the two cocrystalline compounds **5a** and **5b**, which contain up to four units of cocrystallizing TATOT. Sensitivity measurements indicated that the substances are insensitive to the mechanical stress tested. This, together with the hydrazinium salt **3**, which has a detonation speed of more than 9000 m s^{-1} calculated with the EXPLO5 code (V6.05.02), makes them possibly promising high explosives.

For every substance investigated toward their sensitivities, additional hot plate and hot needle tests were performed. While the hot plate tests resulted in deflagration of the substance for almost all compounds, decomposition reactions were mainly observed during the hot needle tests. However, this behavior is to be expected, because most of the compounds tend to be in the high explosive range and this is a typical behavior of this substance class. Laser ignition experiments of the copper complexes also indicate a possible use as laser-ignitable ECCs because most of the substances show deflagrations during these tests.

In conclusion, it can be noted that this comprehensive study underlines the many ways in which the ethylenedinitramide moiety can be used as a building block in energetic materials. The extraordinarily high thermal stability of the majority of alkali metal salts by itself shows that in a world of energetic materials that appears to be almost fully explored from a chemical point of view, a re-examination of known compounds like ethylenedinitramine can be useful.

■ ASSOCIATED CONTENT

Supporting Information

The Supporting Information is available free of charge at https://pubs.acs.org/doi/10.1021/acs.inorgchem.0c03752.

Compounds overview; crystallographic data of **1**−**3**, **4b**, **5**−**12**, **14b**, **15**−**17**, and **19**−**21**; structures of **4b**, **6**, **7b**, **8**, **11**, **12**, **14b**, **15**, **16**, and **20** and PowderXRD of **5a**; computations and detonation parameters of **1** and **3**; IR

https://dx.doi.org/10.1021/acs.inorgchem.0c03752
Inorg. Chem. 2021, 60, 4816−4828

spectroscopy of **1**–**7a**, **8**–**14a**, and **15**–**21**; DTA plots of **1**–**7a**, **8**–**14a**, and **15**–**21**; TGA plots of **1**–**4**, **8**, **12**, **13**, and **21**; high-speed recordings of hot plate, and hot needle tests of **1**–**5b**, **7a**, **8**–**14a**, and **15**–**20**; laser ignition experiments, and UV–vis spectra of **15**–**19**; experimental section and general methods (PDF)

Accession Codes

CCDC 2047743–2047761 and 2047765 contain the supplementary crystallographic data for this paper. These data can be obtained free of charge via www.ccdc.cam.ac.uk/data_request/cif, or by emailing data_request@ccdc.cam.ac.uk, or by contacting The Cambridge Crystallographic Data Centre, 12 Union Road, Cambridge CB2 1EZ, UK; fax: +44 1223 336033.

AUTHOR INFORMATION

Corresponding Author

Jörg Stierstorfer – *Department of Chemistry, Ludwig-Maximilian University Munich, 81377 Munich, Germany;* orcid.org/0000-0002-2105-1275; Email: jstch@cup.uni-muenchen.de

Authors

Michael S. Gruhne – *Department of Chemistry, Ludwig-Maximilian University Munich, 81377 Munich, Germany*

Marcus Lommel – *Department of Chemistry, Ludwig-Maximilian University Munich, 81377 Munich, Germany*

Maximilian H. H. Wurzenberger – *Department of Chemistry, Ludwig-Maximilian University Munich, 81377 Munich, Germany*

Thomas M. Klapötke – *Department of Chemistry, Ludwig-Maximilian University Munich, 81377 Munich, Germany;* orcid.org/0000-0003-3276-1157

Complete contact information is available at: https://pubs.acs.org/10.1021/acs.inorgchem.0c03752

Author Contributions

‡All authors contributed equally to this work.

Notes

The authors declare no competing financial interest.

ACKNOWLEDGMENTS

The financial support of this work by Ludwig-Maximilian University (LMU), the Office of Naval Research (ONR) under Grant No. ONR N00014-19-1-2078, and the Strategic Environmental Research and Development Program (SERDP) under Contract No. W912HQ19C0033 is gratefully acknowledged. The authors thank Prof. Dr. Konstantin Karaghiosoff for the measurement of the ^{15}N NMR spectra and Prof. Dr. Jürgen Evers for the measurements of the powder X-ray diffraction experiments and Rietveld calculations.

REFERENCES

(1) Klapötke, T. M. *Chemistry of High-Energy Materials*, 4th ed.; De Gruyter: Berlin/Boston, 2017.

(2) Köhler, J.; Meyer, R.; Homburg, A. *Explosivstoffe*, 10th ed.; Wiley-VCH: Weinheim, 2008.

(3) Coster-Mullen, J. *Atom Bombs: The Top Secret Inside Story of Little Boy and Fat Man*, 1st ed.; 2003.

(4) Doll, D. W.; Hanks, J. M.; Niles, J. H. Insensitive Composition B Replacement. *Proc. of 1999 Insensitive Munitions and Energetic Materials Technology Symposium*, Tampa, FL, USA, Nov 29–Dec 2, 1999; p. 264.

(5) United States Department of the Army. *Military explosives*, 1st ed.; Headquarters, Department of the Army, Washington, 1989.

(6) (a) Rottink, B. A. N,N'-dinitroethylenediamine Stimulates Height Growth of Kentucky Coffeetree. *For. Sci.* **1971**, *17*, 313. (b) Leasure, J. K.; Mussell, D. R. Plant growth altering. US 3,356,483, December 5, 1967. (c) Borer, K.; Hardy, R. J.; Lindsay, W. S.; Spratt, D. A.; Mees, G. C. Ethylenebisnitrourethan. Investigation of the plant growth stimulant action of analogous compounds. *J. Exp. Bot.* **1966**, *17*, 378–389.

(7) (a) Landenberger, K. B.; Matzger, A. J. Cocrystals of 1,3,5,7-Tetranitro-1,3,5,7-tetrazacyclooctane (HMX). *Cryst. Growth Des.* **2012**, *12*, 3603–3609. (b) Bolton, O.; Simke, L. R.; Pagoria, P. F.; Matzger, A. J. High Power Explosive with Good Sensitivity: A 2:1 Cocrystal of CL-20:HMX. *Cryst. Growth Des.* **2012**, *12*, 4311–4314. (c) Liu, K.; Zhang, G.; Luan, J.; Chen, Z.; Su, P.; Shu, Y. Crystal structure, spectrum character and explosive property of a new cocrystal CL-20/DNT. *J. Mol. Struct.* **2016**, *1110*, 91–96.

(8) Hussein, A. K.; Zeman, S.; Elbeih, A. Crystal structure, spectrum character and explosive property of a new cocrystal CL-20/DNT. *Z. Anorg. Allg. Chem.* **2018**, *644*, 430–437.

(9) Aakeröy, C. B.; Wijethunga, T. K.; Desper, J. Crystal Engineering of Energetic Materials: Co-crystals of Ethylenedinitramine (EDNA) with Modified Performance and Improved Chemical Stability. *Chem. - Eur. J.* **2015**, *21*, 11029–11037.

(10) (a) Carignan, Y. P.; Satriana, D. R. Differential Thermal Analysis of Nitramines, Amine Salts, and Guanidine Derivatives. *J. Org. Chem.* **1967**, *32*, 285–289. (b) Matyushin, Y. N.; Konkova, T. S.; Miroshnichenko, E. A. Thermochemical characteristics of salts of MEDINA and EDNA. *Proceedings of the 32nd International Annual Conference of ICT*, Karlsruhe, July 3–6, **2001**.

(11) Ficheroulle, H. Study of explosives. Ethylenedinitramine, ammonium ethylenedinitramate. Binary mixtures with ammonium nitrate. Preparation-properties. *Mem. Poudres* **1948**, *30*, 98–100.

(12) (a) Arvel, O. F.; Cartersville, G. Explosive compound, process of making same and a composition thereof. US 2,708,623, May 17, 1995. (b) Millar, R. W. *Lead-Free Initiator Materials for Small Electro-Explosive Devices for Medium Caliber Munitions: Final Report 04 June 2003*; QinetiQ Ltd: Farnborough, Hampshire, United Kingdom, 2004. (c) Okazaki, K.; Hasue, K.; Shimazu, M. Leadsalts of ethylenedinitramine. *Rikogaku Kenkyu Hokoku - Boei Daigakko* **1980**, *18*, 349–354.

(13) Turley, J. W. A refinement of the crystal structure of *N,N'*-dinitroethylenediamine. *Acta Crystallogr., Sect. B: Struct. Crystallogr. Cryst. Chem.* **1968**, *24*, 942–946.

(14) Allentoff, N.; Wright, G. F. Disodium ethane-bisnitraminate. *Acta Crystallogr.* **1953**, *6*, 1–8.

(15) Bircher, H.-R.; Ochsenbein, P.; Hauser, J.; Burgi, H.-B. Bis(hydrazinium) N,N'-Dinitroethylenediaminate(2 -). *Acta Crystallogr., Sect. C: Cryst. Struct. Commun.* **1996**, *52*, 2002–2004.

(16) Roodt, G. T.; Uprety, B.; Levendis, D. C.; Arderne, C. Energetic propane-1,3-diaminium and butane-1,4-diaminium salts of *N,N'*-dinitroethylenediazanide: syntheses, crystal structures and thermal properties. *Acta Crystallogr., Sect. C: Struct. Chem.* **2019**, *75*, 54–60.

(17) (a) Cherskaya, N. O.; Shlyapochnikov, V. A.; Ivshin, V. P.; Ivshina, T. N. Vibrational spectra and structure of salts of N,N'-dinitroalkylenediamines. *B. Acad. Sci. USSR Ch.* **1986**, *7*, 1533–1537. (b) Shlyapochnikov, V. A.; Cherskaya, N. O.; Ivshin, V. P.; Levchenkov, D. V.; Kharitonkin, A. B. Spectra and structure of mercury derivatives of primary nitramines. *Russ. Chem. Bull.* **2002**, *51*, 1071–1074.

(18) Palopoli, S. F.; Geib, S. J.; Rheingold, A. L.; Brill, T. B. Synthesis and modes of coordination of energetic nitramine ligands in copper(II), nickel(II), and palladium(II) complexes. *Inorg. Chem.* **1988**, *27*, 2963–2971.

(19) Gruhne, M. S.; Lommel, M.; Wurzenberger, M. H. H.; Klapötke, T. M.; Stierstorfer, J. *Proceedings of the 23rd seminar on New trends in research of energetic materials*, Czech Republic, April 1–3, 2020, *1*, 74–79.

(20) Bachmann, W. E.; Horton, W. J.; Jenner, E. L.; MacNaughton, N. W.; Maxwell, C. E. The Nitration of Derivatives of Ethylenediamine.1. *J. Am. Chem. Soc.* **1950**, *72*, 3132−3134.
(21) Zharkov, M. N.; Kuchurov, I. V.; Fomenkov, I. V.; Tartakovsky, V. A.; Fedyanin, I. V.; Zlotin, S. G. Safe and Convenient Synthesis of Primary N-Nitramines in the Freon Media. *Synthesis* **2017**, *49*, 1103−1108.
(22) McKenney, R. L.; Struck, S. R.; Hildreth, R. A.; Fryling, J. A. Synthesis and properties of selected energetic organodi- and polyammonium nitrate salts. *J. Energ. Mater.* **1987**, *5*, 1−25.
(23) Holleman, A. F.; Wiberg, N.; Krieger-Hauwede, M.; Chang, J. *Anorganische Chemie Band 1: Grundlagen und Hauptgruppenelemente*, 103rd ed.; De Gruyter: Berlin, 2017.
(24) (a) Gaponik, P. N.; Karavai, V. P.; Grigor'ev, Yu. V. Synthesis of 1-substituted tetrazoles by heterocyclization of primary amines, orthoformic ester, and sodium azide. *Chem. Heterocycl. Compd.* **1985**, *21*, 1255−1258. (b) Kamiya, T.; Saito, Y. Process for preparing 1h-tetrazole compounds. US 3,767,667, October 7, 1971. (c) Szimhardt, N.; Wurzenberger, M. H. H.; Klapötke, T. M.; Lechner, J. T.; Reichherzer, H.; Unger, C. C.; Stierstorfer, J. Highly functional energetic complexes: stability tuning through coordination diversity of isomeric propyl-linked ditetrazoles. *J. Mater. Chem. A* **2018**, *6*, 6565−6577.
(25) (a) Wurzenberger, M. H. H.; Szimhardt, N.; Stierstorfer, J. Nitrogen-Rich Copper(II) Bromate Complexes: an Exotic Class of Primary Explosives. *Inorg. Chem.* **2018**, *57*, 7940−7949. (b) Wurzenberger, M. H. H.; Braun, V.; Lommel, M.; Klapötke, T. M.; Stierstorfer, J. *Inorg. Chem.* **2020**, *59*, 10938−10952.
(26) BAM. http://www.bam.de, accessed December 2020.
(27) (a) NATO standardization agreement (STANAG) on explosives, impact sensitivity tests, no. 4489, 1st ed.; Sept. 17, 1999. (b) WIWEB-Standardarbeitsanweisung 4−5.1.02, Ermittlung der Explosionsgefährlichkeit, hier der Schlagempfindlichkeit mit dem Fallhammer, Nov. 8, 2002.
(28) Military Standard 1751A (MIL-STD-1751A): safety and performance tests for qualification of explosives (high explosives, propellants and pyrotechnics), method 1016; Dec. 11, 2001.
(29) OZM Research. http://www.ozm.cz, accessed December 2020.
(30) (a) NATO standardization agreement (STANAG) on explosive, friction sensitivity tests, no. 4487, 1st ed.; Aug. 22, 2002. (b) WIWEB-Standardarbeitsanweisung 4−5.1.03, Ermittlung der Explosionsgefährlichkeit oder der Reibeempfindlichkeit mit dem Reibeapparat; Nov. 8, 2002.
(31) (a) UN Model Regulation: Recommendations on the Transport of Dangerous Goods − Manual of Tests and Criteria, section 13.4.2.3.3, 2015. (b) Impact: insensitive > 40 J, less sensitive ≥ 35 J, sensitive ≥ 4 J, very sensitive ≤ 3 J; Friction: insensitive > 360 N, less sensitive = 360 N, sensitive < 360 N and > 80 N, very sensitive ≤ 80 N, extremely sensitive ≤ 10 N. According to the UN Recommendations on the Transport of Dangerous Goods, 5th ed., 2009.
(32) Gruhne, M. S.; Lommel, M.; Wurzenberger, M. H. H.; Szimhardt, N.; Klapötke, T. M.; Stierstorfer, J. OZM Ball Drop Impact Tester (BIT-132) vs. BAM Standard Method − a Comparative Investigation. *Propellants, Explos., Pyrotech.* **2020**, *45*, 147−153.
(33) Ilyushin, M. A.; Kotomin, A. A.; Dushenok, S. A. Energy-Saturated Metal Complexesz. *Russ. J. Phys. Chem. B* **2019**, *13*, 119−138.
(34) Zhilin, A. Yu.; Ilyushin, M. A.; Tselinskii, I. V.; Kozlov, A. S.; Lisker, I. S. High-Energy-Capacity Cobalt(III) Tetrazolates. *Russ. J. Appl. Chem.* **2003**, *76*, 572−576.
(35) Sućeska, M. *EXPLO5 Version 6.05 User's Guide*; OZM: Zagreb, Croatia, 2018.

https://dx.doi.org/10.1021/acs.inorgchem.0c03752
Inorg. Chem. 2021, 60, 4816−4828

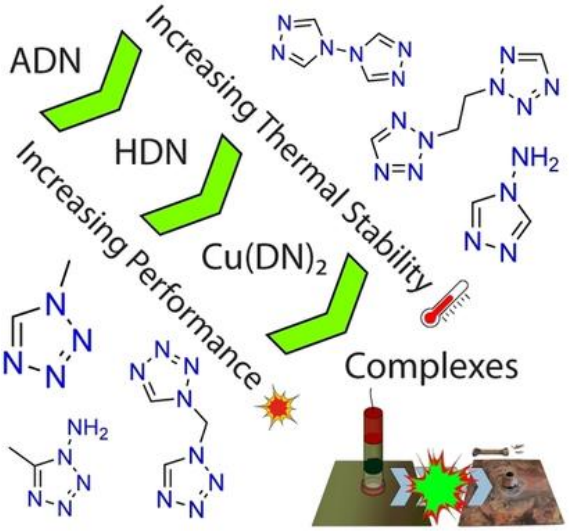
Appendix 23

A Smart Access to the Dinitramide Anion – The Use of Dinitraminic Acid for the Preparation of Energetic Coordination Compounds

M. S. Gruhne, M. H. H. Wurzenberger, M. Lommel, J. Stierstorfer

Chem. Europ. J. **2021**, 27, 9112–9123.

https://doi.org/10.1002/chem.202100747



Supplementary Information:
https://chemistry-europe.onlinelibrary.wiley.com/action/downloadSupplement?doi=10.1002%2Fchem.202100747&file=chem202100747-sup-0001-misc_information.pdf

Full Paper
doi.org/10.1002/chem.202100747
Check for updates
Chemistry Europe
European Chemical Societies Publishing

A Smart Access to the Dinitramide Anion – The Use of Dinitraminic Acid for the Preparation of Nitrogen-Rich Energetic Copper(II) Complexes

Michael S. Gruhne,[a] Maximilian H. H. Wurzenberger,[a] Marcus Lommel,[a] and Jörg Stierstorfer*[a]

Dedicated to Professor Jürgen Evers on the occasion of his 80th birtday

Abstract: Dinitraminic acid ($HN(NO_2)_2$, HDN) was prepared by ion exchange chromatography and acid-base reaction with basic copper(II) carbonate allowed the *in situ* preparation of copper(II) dinitramide, which was reacted with twelve nitrogen-rich ligands, for example, 4-amino-1,2,4-triazole, 1-methyl-5*H*-tetrazole, di(5*H*-tetrazolyl)-methane/-ethane/-propane/-butane. Nine of the complexes were investigated by low-temperature X-ray diffraction. In addition, all compounds were investigated by infrared spectroscopy (IR), differential thermal analysis (DTA), elemental analysis (EA) and thermogravimetric analysis (TGA) for selected compounds. Furthermore, investigations of the materials were carried out regarding their sensitivity toward impact (IS), friction (FS), ball drop impact (BDIS) and electrostatic discharge (ESD). In addition, hot plate and hot needle tests were performed. Complex $[Cu(AMT)_4(H_2O)](DN)_2$, based on 1-amino-5-methyltetrazole (AMT), is most outstanding for its detonative behavior and thus also capable of initiating PETN in classical initiation experiments. Laser ignition experiments at a wavelength of 915 nm were performed for all substances and solid-state UV-Vis spectra were recorded to apprehend the ignition mechanism.

Introduction

The so-called ammonium perchlorate composite propellants (APCP) are ammonium perchlorate (AP, NH_4ClO_4) (mostly mixed with HTPB and aluminum) based fuels in solid rocket motors.[1] At temperatures above 200 °C, AP decomposes mostly into gaseous chlorine, oxygen, nitrogen, and water due to the reducing effect of the ammonia cation, while the perchlorate anion acts as an oxidizing species.[2] Despite the toxicity of the perchlorate anion and its decomposition products, these mixtures are still widely used, mainly because of their cheap and easy preparation. Nevertheless, much research is being carried out on halogen-free rocket propellants and burn rate catalysts,[3] with some approaches to replacing AP already well advanced.[1]

Besides liquid fuel mixtures based on cryogenic or hypergolic reactions, ammonium dinitramide (ADN) is considered as a compound with high potential.[1] It was first synthesized in 1971 at the Zelinsky Institute of Organic Chemistry in Moscow.[4] However, information was kept under seal and published later in the course of time in the form of some publications.[4,5] Therefore, the anion was discovered by US scientists in the late 1980s, independently of the Russians.[6] Since the salt contains no carbon or halogens, its decomposition products are mostly environmentally friendly.[7] This makes the dinitramide anion also a promising candidate for the use in halogen-free energetic coordination compounds (ECC). These materials could act not only as sensitive explosives but also as low carbon and oxygen-rich burn rate catalysts, for example, in airbags. Implementing the dinitramide function in 3d transition metal coordination compounds is not a new concept, for example Klapötke *et al.* published some dinitramide complexes based on 3-amino-1-nitroguanidines.[5b,8]

To the best of our knowledge, only three azole-based transition metal complexes are known, two of which have been published by the Klapötke group.[9] Both show octahedral coordination geometries, although the one based on 5-(1-methylhydrazinyl)-1*H*-tetrazole is more clearly distorted (Figure 1). Furthermore, an aminoguanidine-based complex is known, which exhibits a square planar coordination geometry rare for copper(II) compounds.[10]

The low thermal stability of dinitramine-based compounds (e.g., ADN = 135 °C) is a known issue and a significant aspect that must be taken into account when designing new energetic materials based on this anion.[11] At this point, the concept of ECC is applied, since the adaptation of the properties, such as performance and thermal stability, of the formed coordination

[a] M. S. Gruhne, Dr. M. H. H. Wurzenberger, M. Lommel, Dr. J. Stierstorfer
Energetic Materials Research, Department of Chemistry
University of Munich (LMU)
Butenandtstr. 5–13, 81377 München (Germany)
E-mail: jstch@cup.uni-muenchen.de

Supporting information for this article is available on the WWW under https://doi.org/10.1002/chem.202100747

© 2021 The Authors. Chemistry - A European Journal published by Wiley-VCH GmbH. This is an open access article under the terms of the Creative Commons Attribution License, which permits use, distribution and reproduction in any medium, provided the original work is properly cited.

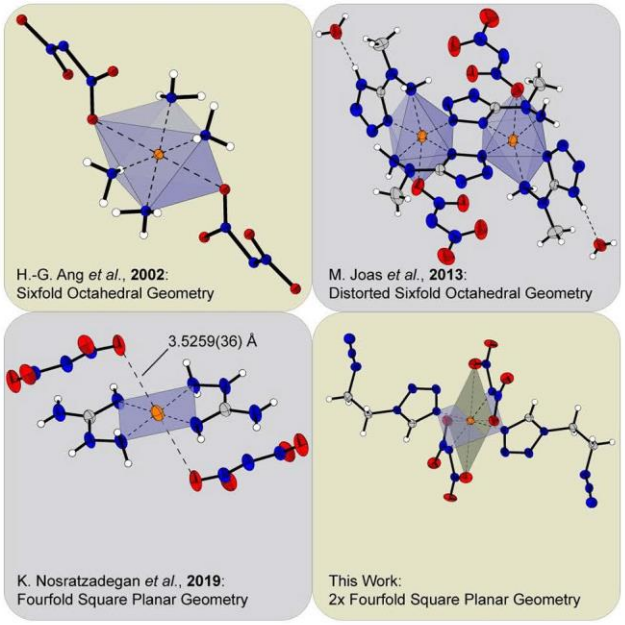


Figure 1. Overview of literature known copper(II) dinitramide ECC and their coordination environments compared to coordination compound **6** of this work.

compounds can be readily tuned by changing the central metal, anion, or ligand.[12,13] Szimhardt *et al.* already showed that the implementation of propylene bridged ditetrazoles in complexes can increase thermal stability through the linking of the ligand between several metal centers.[9b] Furthermore, a comparison of the previously known complexes shows that probably none of them is able to successfully initiate PETN. Therefore, the focus should also lie on the incorporation of ligands that are known to enhance the performance of the complexes by their high positive heat of formation.[13b,14]

The major task that needs to be dealt with when synthesizing dinitramine complexes can be explained by the corresponding tetraammine copper(II) compound (**2**) presented in Figure 1. The coordination compound was already described in 2002 and, due to the impossible isolation of an elemental pure sample, was only examined by X-ray diffraction, ^{14}N NMR, and vibrational spectroscopy.[15] The reason for this is probably the reaction that precedes the formation of the complex. Typically, a mixture of ammonium dinitramide with any copper(II) salt is reacted with the respective ligand.[9b] Alternatively, a copper(II) complex with any anion and the desired ligand is formed in solution and a dinitramide salt is added.[8] Thus, in every case, ions are left behind which can contaminate the sample or lead to a wrong composition of the complex. In this work the problem was solved using ion exchangers, which enables the simple production of dinitraminic acid (HDN). Reaction with metal carbonates allows the preparation of pure metal dinitramide salts without interfering anions *in situ*, which was already shown by Lukyanov *et al.* by reacting HDN with silver carbonate.[5b] However, the dinitraminic acid was preferably obtained by the injection of hydrogen chloride into a solution of KDN. The idea of an alternative preparation of an aqueous HDN solution was already shown by Bottaro *et al.* though the authors did not perform reactions with metal carbonates of the 3d series.[6]

The complexes synthesized in this way can be used in a wide range of applications. The easily accessible anion is not only extending the field of ECC with this method, but the resulting complexes can also serve as burn rate catalysts in solid propellants and as halogen- and lead-free explosives. In addition to this, the complexes can also be used in the field of laser-ignitable compounds.[16]

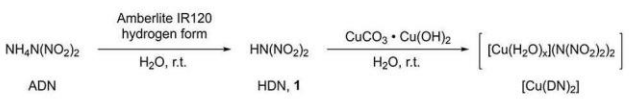
Results and Discussion

Synthesis

As already mentioned above, the synthesis of dinitramide-based coordination compounds in particular has some drastic disadvantages. Until now, in every case ammonium dinitramide (ADN) or potassium dinitramide (KDN) was used as a starting material together with water-soluble copper(II) salts.[8–10,15] This leads to the possible formation of complexes without the integration of dinitramide anions. In the case of chloride anions, which is known to act as a bridge between metal centers, the formation of such complexes may even be facilitated.[17] To avoid such side reactions, ion exchange techniques were used. Ammonium dinitramide was thus converted into a highly clean aqueous solution of dinitraminic acid. The solution obtained should be practically free of interfering anions and can be applied for the *in situ* formation of transition metal dinitramides when reacted with the corresponding carbonates (Scheme 1).

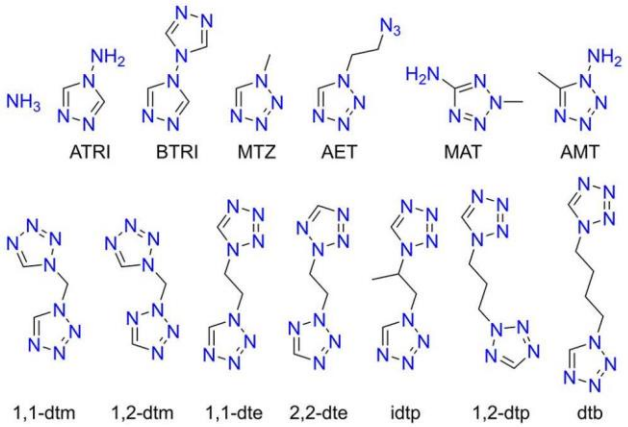
Due to the instability of pure dinitraminic acid at ambient conditions special attention is required during the preparation of the acid and an isolation of the pure compound has to be avoided.[18] Concentrations in the range of 7–10 wt% can be safely prepared in aqueous solution. At a concentration of about 20 wt% the solution is still stable for several days. Higher concentrations should be avoided as decomposition can occur explosively.[5b] In addition to photocatalyzed decomposition of the dinitramide anion in aqueous solution, low stability in acids must be taken into account.[18,19] It is reported that the decomposition of HDN acid is catalyzed in 8 M sulfuric acid. In 10 M sulfuric acid the decomposition takes place within minutes.[18] This could be an important fact as ion exchange materials can be regenerated by acids.

In order to provide a general proof of concept, the ammine ligand was chosen as the resulting complex could not be obtained in a clean manner by the common methodology (Scheme 2).[15] The use of nitrogen-rich endothermic tri- and

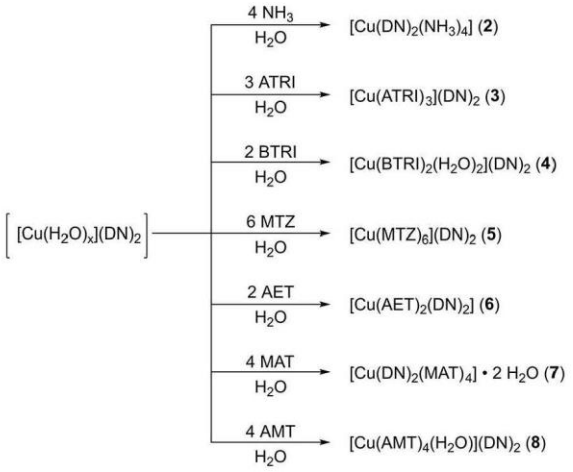


Scheme 1. Preparation of an aqueous solution of copper(II) dinitramide.

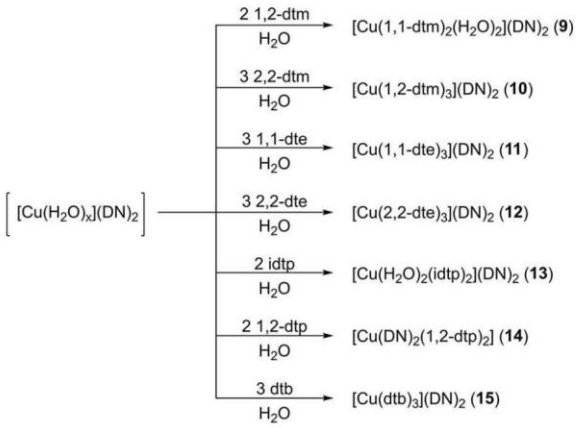
© 2021 The Authors. Chemistry - A European Journal published by Wiley-VCH GmbH



Scheme 2. Ligands used for the complexation of copper(II) dinitramide.



Scheme 3. Overview of the prepared ECC **2**–**8**.



Scheme 4. Overview of the prepared ditetrazole based copper(II) dinitramide coordination compounds **9**–**15**.

tetrazole ligands increases the energetic character of the ECC and, therefore, several different mono- and ditetrazoles were selected.[13,14,20] Since dinitramide-based compounds are known to suffer from low thermal stability,[11] the main focus was on bridging molecules, such as 1,2,4-triazoles and ditetrazoles.[12] Since the further aim of this work was to increase the energetic character of the complexes, focus was also put on ligands like 1-AT, 1-AMT, 1,5-DAT, as well as with different dtm isomers (Scheme 2). These ligands possess the highest calculated gas phase enthalpies of formation and are therefore known to yield the most powerful coordination compounds.[13,14]

All used ligands (Scheme 2) were either purchasable (NH_3, ATRI) or synthesized using literature known procedures. Tetrazole derivatives were either prepared by the reaction of alkyl halides (MAT, dtm, 2,2-dte, 1,2-dtp) or dimethyl sulfate (1-MTZ) with 1,5*H*-tetrazole[9b,13a,14,20a,21] and through ring closure reactions using sodium azide, triethyl orthoformate, and the respective alkyl amine or diamine (AET, AMT, 1,1-dte, idtp, dtb).[13b,22] For the syntheses of the complexes, freshly prepared aqueous solutions of copper(II) dinitramide as well as stochiometric amounts of the respective ligands were combined (Scheme 3 & Scheme 4) and the resulting reaction mixtures were left for crystallization at ambient conditions.

All coordination compounds were directly obtained from the mother liquors and crystallized in moderate to excellent yields (55–92%). Single crystals, suitable for X-ray diffraction were directly obtained except for **3**, **4**, and **14**. Regarding compounds **3** and **14**, the complex' composition was determined by elemental analysis. Sufficient single crystals of ECC **4** were obtained through layering experiments.

The crystalline materials were filtered off, washed with a small amount of ice-cold water when necessary and dried in air overnight. The use of other common monotetrazoles such as 1-amino-5*H*-tetrazole,[17] 1,5-dimethyltetrazole,[23] 1,5-diaminotetrazole,[24] and 1-methyl-5-aminotetrazole[25] or ditetrazoles such as di(tetrazol-2-yl)propane,[9b] which have already been successfully used as ligands, did not result in isolable crystalline ECC. One factor that could play a crucial role here is that in our synthesis we were limited to the solvent water because of the ion exchange and could not use organic solvents such as acetonitrile.

Crystal structures

All compounds, with the exception of complex **2**, whose crystal structure is already known in the literature, and compounds **3** and **14**, where it was impossible to obtain crystals of sufficient quality, were characterized by low temperature X-ray diffraction. In case of compounds **5** and **7** the measurements allow an indication of the most likely composition, but finalization of the data sets was not possible due to the highly disordered dinitramide moieties. The complexes' composition was finally confirmed by elemental analysis. Copper atoms are displayed as orange ellipsoids, nitrogen atoms blue, oxygen atoms red, carbon atoms grey and hydrogen atoms white. Further information on the structures of the compounds **8**, **10**, and **11** together with the measurement and refinement data of all

© 2021 The Authors. Chemistry - A European Journal published by Wiley-VCH GmbH

crystallograpically investigated compounds are given in the Supporting Information (Tables S1–3, and Figures S1–3). The crystal datasets were uploaded to the CSD database[26] and can be obtained free of charge. The bond lengths and angles of the coordinating ligands in the crystallographically investigated complexes are within the typical range of tetrazole and triazole ligands and nearly the same as in the non-coordinating molecules.[9b,13b,14,21,22,27] Therefore, they are not part of the discussion in any of the following coordination compounds. All copper(II) dinitramide coordination compounds except ECC **6** and **8** show an octahedral coordination sphere around the central metal with typical Jahn-Teller distortions along the axial axis.

The triazole-based coordination compound **4** crystallizes in the monoclinic space group $P2_1/n$ in the form of blue blocks. The unit cell is built up by two formula units and possesses a calculated density of 1.945 g cm^{-3} at 120 K. The octahedral coordination sphere consists of two BTRI in equatorial and two aqua ligands in axial position (Figure 2). The triazoles are linking between two different copper centers, building up 2D polymeric layers.

Dinitramide complex **6** shows a very uncommon coordination geometry around the copper(II) central metal and crystallizes in the monoclinic space group $P2_1/c$ in the form of blue needles. The unit cell is built up by two formula units and possesses a calculated density of 1.932 g cm^{-3} at 102 K. The complex monomers are formed by two neutral AET molecules and two dinitramide anions bounded to the metal cation (Figure 3). The tetrazole ligands and the deprotonated amide moieties form a square planar coordination sphere with bond lengths below 2 Å. The very unusual fourfold coordination around the Cu^{2+} cation is stabilized by another square planar plane formed by four oxygens of the nitro groups with very weak Cu–O interactions in the range of ~2.7–2.8 Å. Both coordination tiers are perfectly planar (N4–N4^{i}–N8–N8^{i} = 0°, O1–O1^{i}–O3–O3^{i} = 0°) and almost perpendicular to each other. This results in an eightfold coordination sphere, which is to be

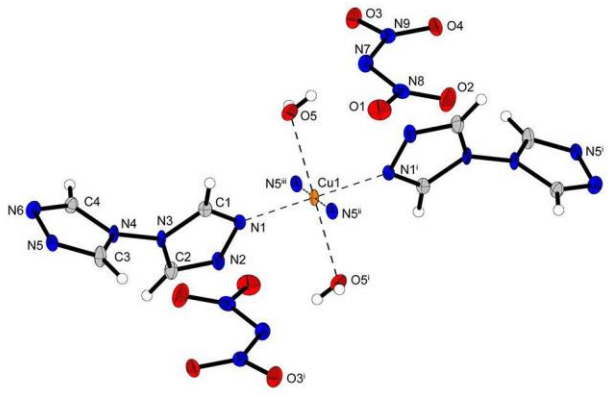


Figure 2. Coordination environment of $[Cu(BTRI)_2(H_2O)_2](DN)_2$ (**4**). Selected bond lengths (Å): Cu1–N1 2.003(2), Cu1–N5^{ii} 2.034(2), Cu1–O5 2.356(3); selected bond angles (°): O5–Cu1–N1 89.77(9), O5–Cu1–N5^{ii} 94.57(10), N1–Cu1–N5^{ii} 88.87(10). Symmetry codes: (i) −x, −y, −z; (ii) −0.5 + x, −0.5 − y, −0.5 + z; (iii) 0.5 − x, 0.5 + y, 0.5 − z.

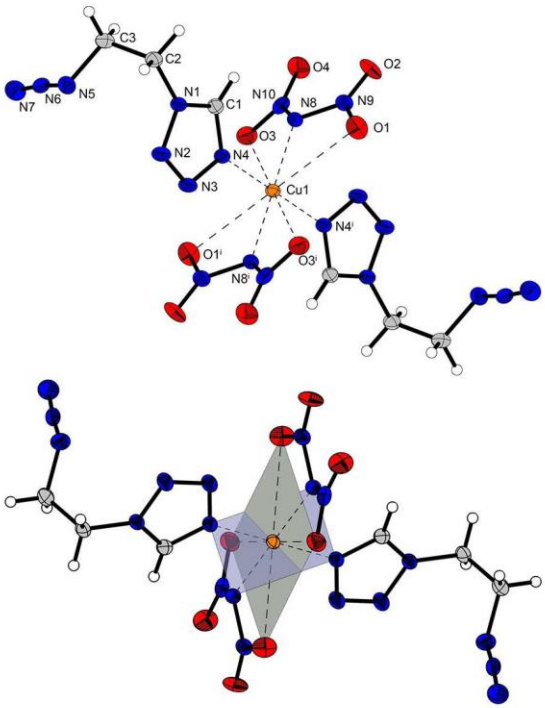


Figure 3. Molecular unit of $[Cu(AET)_2(DN)_2]$ (**6**) (top) and illustration of the double square planar coordination sphere around the central metal (bottom). Selected bond lengths (Å): Cu1–N4 1.975(2), Cu1–N8 1.999(2), Cu1–O1 2.782(2); selected bond angles (°): O1–Cu1–O3 98.23(6), O1–Cu1–N4 86.47(7), O3–Cu1–N8 49.22(7), N4–Cu1–N8 90.76(8). Symmetry code: (i) 1−x, 1−y, 1−z.

expected for metals of the 4d series but is very rare within the 3d metals. This is most likely made possible by the additional square planar coordination by the oxygen atoms of the dinitramido ligands mentioned earlier. The Cu1–O3, bond is therefore with a length of 2.858(2) Å rather long compared to the other bonds. It is difficult to determine exactly which complexes are present in solution, but it is likely that the complex formed here is the most thermodynamically stable in the solid state.

Energetic coordination compound **9** crystallizes in the monoclinic space group $P2_1/n$ in the form of blue blocks. The unit cell is built up by two formula units and possesses a calculated density of 2.017 g cm^{-3} at a temperature of 123 K. The coordination sphere is arranged similarly to complex **4**, consisting of two bridging ligand units in equatorial positions and two aqua ligands in axial position (Figure 4). Despite this correlation, the polymeric structure of both complexes is different due to the different binding behavior of the triazole-based ligand (**4**) compared to the tetrazole derivative in ECC **9**. Since two 1,1-dtm ligands each bind to the same metal center, only chains are formed instead of 2D layers. The occupation of the axial positions by the water molecules is most likely made possible by the steric hindrance of the ligands caused by the methylene bridge, which prevents coordination of further ligand moieties. Nevertheless, anhydrous copper(II) complexes based on 1,1-dtm have recently been discovered by our

© 2021 The Authors. Chemistry - A European Journal published by Wiley-VCH GmbH

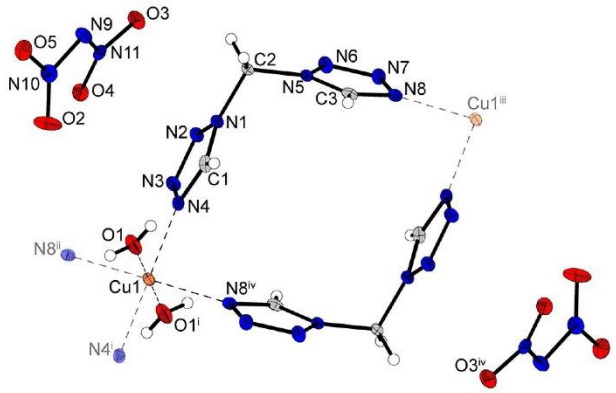


Figure 4. Extended coordination environment of $[Cu(1,1\text{-dtm})_2(H_2O)_2](DN)_2$ (**9**). Selected bond lengths (Å): Cu1–N4 2.0289(19), Cu1–O1 2.2484(19) Cu1–N8 2.051(2); selected bond angles (°): N4–Cu1–N8 89.54(8), N4–Cu1–O1 89.32(8), N8–Cu1–O1 92.56(8). Symmetry codes: (i) −x, 2−y, 1−z; (ii) −1+x, y, z; (iii) 1+x, y, z; (iv) 1−x, 2−y, 1−z.

research group.[14] This requires the use of organic solvents, such as acetonitrile, to prevent the coordination of aqua ligands but is impossible in this case due to the use of aqueous HDN solution.

The copper(II) dinitramide complex **12** crystallizes as blue blocks in the monoclinic space group *C*2/*m* with one formula unit per unit cell and a calculated density of 1.815 g cm^{-3} at 123 K. The coordination sphere is built up analogous to compound **11**. Three (2,2-ditetrazolyl)ethane ligands, each linking between two copper centers are part of the molecular unit (Figure 5). The Jahn-Teller distortion is located along the N8–Cu1–N8 axes.

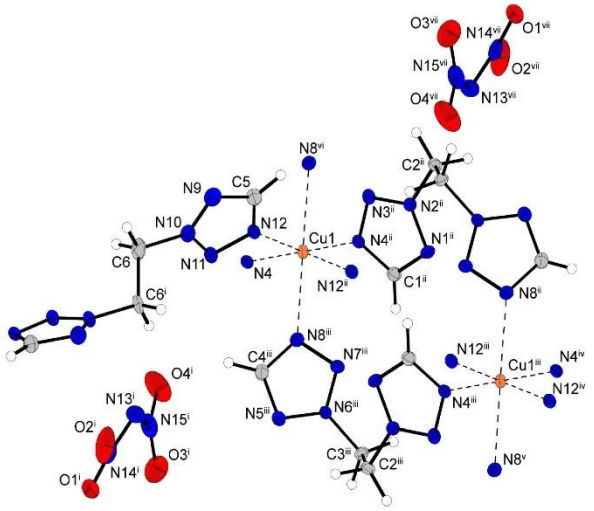


Figure 5. Extended coordination environment of $[Cu(2,2\text{-dte})_3](DN)_2$ (**12**). Selected bond lengths (Å): Cu1–N4 2.0320(18), Cu1–N8 2.3833(18), Cu1–N12 2.0260(17); selected bond angles (°): N12–Cu1–N8 88.42(7), N4–Cu1–N12 88.88(7), N4–Cu1–N8 88.99(7), selected torsion angles (°): N2–C2–C3–N6 71.87(18), N10–C6–C6ⁱ–N10ⁱ 178.146(2). Symmetry codes: (i) 1−x, y, 1.5−z; (ii) 0.5−x, 0.5−y, 1−z; (iii) −0.5+x, −0.5+y, z; (iv) −x, −y, 1−z; (v) −1+x, −1+y, z; (vi) 1−x, 1−y, 1−z; (vii) −0.5+x, 0.5−y, −0.5+z.

Two different bonding types of the ditetrazole ligand can be observed in the two similar crystallizing complexes **11** and **12**. Each coordination compound possesses two ligands in *anti*-conformation, together with one ligand arranged linearly in *gauche* conformation (Figures 6 and 7). In every case investigated, the Jahn-Teller distortion is found between ligands in *anti*-conformation and the copper center.

The two ligands arranged in *gauche*-conformation bridge between the same copper centers and thus form 1D polymeric chains (Figure 6). These networks are linked further by the ligands in *anti*-conformation. However, the type of substitution of the ligands plays a crucial role in the type of organometallic framework formed. The 1,1-substitution in **11** leads to the formation of two-dimensional sheets, whereas the 2,2-substitution in **12** results in the formation of a three-dimensional structure (Figure 7).

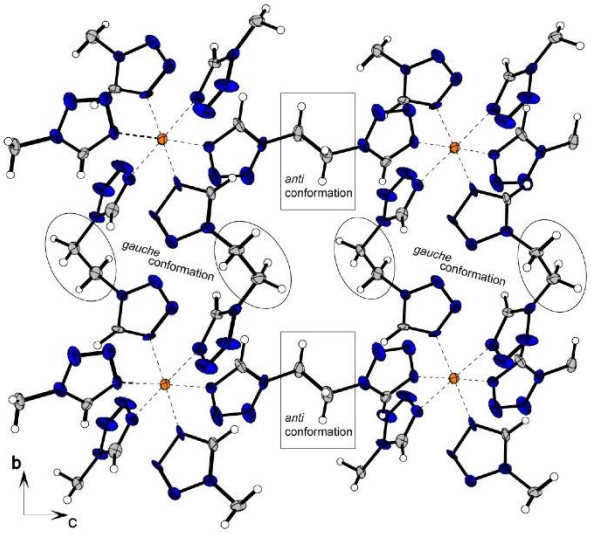


Figure 6. Two-dimensional layers of compound **11** along the *a* axis.

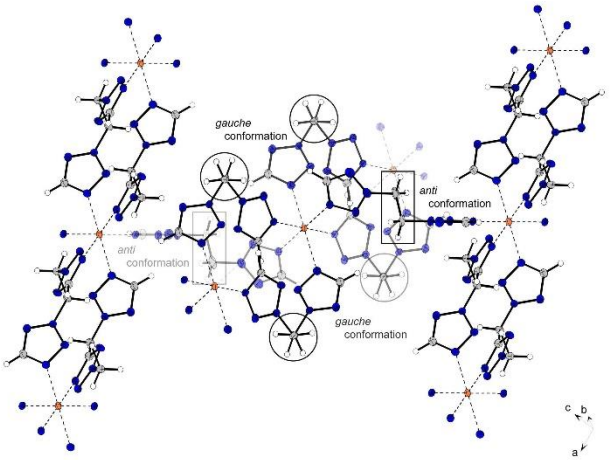


Figure 7. Polymeric chains formed by ligands in *gauche*-conformation and linked to form a 3D network by ligands showing an *anti*-arrangement in compound **12**.

© 2021 The Authors. Chemistry - A European Journal published by Wiley-VCH GmbH

Coordination compound **13** crystallizes as blue rods in the monoclinic space group $P2_1/n$ with two formula units per unit cell. The complex possesses a calculated density of 1.753 g cm^{-3} at 106 K, which is the second lowest density observed among all crystallographically investigated coordination compounds in this work. The coordination sphere is built up similar to the one observed for compound **9**. The *gauche* conformation of the ligand's carbon chains is showing the same effect, as already found in the structures of complexes **10** and **11**. Two ligand moieties are linking between the same copper centers, forming one-dimensional chains (Figure 8).

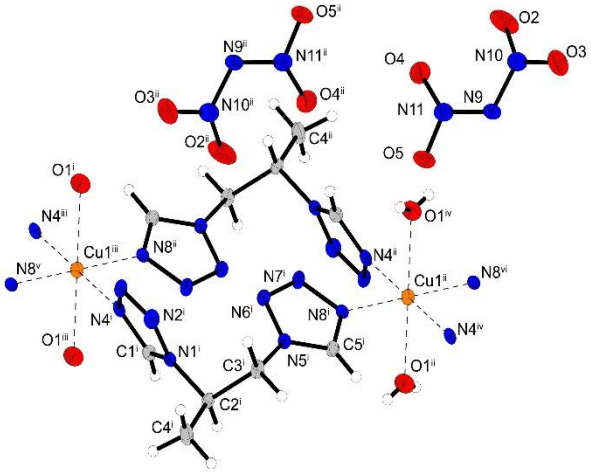


Figure 8. Section of the coordination environment of compound **13**. Selected bond lengths (Å): Cu1^{ii}–N4^{ii} 2.02595(12), Cu1^{ii}–N8^{i} 2.01064(14), Cu1^{ii}–O1^{iv} 2.36080(16); selected bond angles (°): N4^{ii}–Cu1^{ii}–O1^{iv} 94.223(5), N4^{ii}–Cu1^{ii}–N8^{i} 89.992(7), N8^{i}–Cu1^{ii}–O1^{iv} 87.337(5). Symmetry codes: (i) −x, 1−y, −z; (ii) −0.5+x, 1.5−y, −0.5+z; (iii) −1+x, y, z; (iv) 1−x, 1−y, −z; (v) −1.5+x, 1.5−y; (vi) 1.5−x, 0.5+y, 0.5−z.

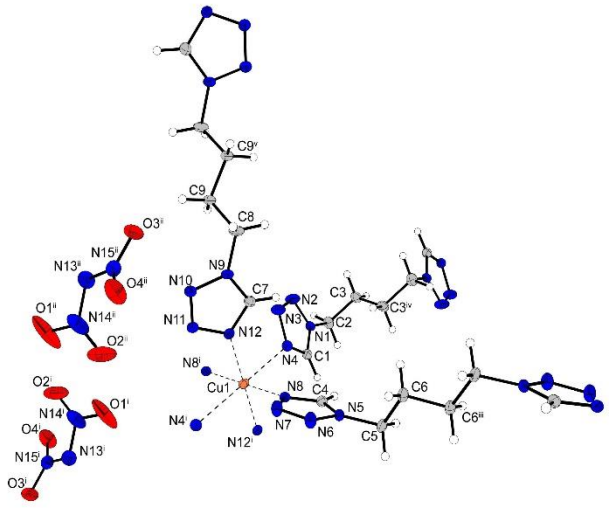


Figure 9. Extended coordination environment of compound **15**. Selected bond lengths (Å): Cu1–N4 2.4811(17), Cu1–N8 1.9967(14), Cu1–N12 2.032(2); selected bond angles (°): N4–Cu1–N12 90.71(7), N4–Cu1–N8 90.18(6), N8 Cu1 N12 89.98(7). Selected torsion angles (°): N1 C2 C3 C3^{i} 60.1(3), C2–C3–C3^{i}–C2^{i} 180.0(3), C3–C3^{i}–C2^{i}–N1^{i} 60.1(3). Symmetry codes: (i) −x, 2−y, 1−z; (ii) 1−x, 1−y, 2−z.

Complex **15** crystallizes in the triclinic space group $P\bar{1}$ in the form of blue blocks. The unit cell consists of one formula unit and with a density of 1.663 g cm^{-3} at 108 K it is the least dense of all compounds crystallographically investigated during this study. The octahedral coordination sphere is built up by six di(tetrazolyl)butane units, each bridging to another copper center (Figure 9).

Unlike coordination compounds **11** and **12**, two ligands are arranged in *anti*-conformation, forming planar 2D polymeric layers. The C3–C3^{i} bond of the remaining ligand also shows an *anti*-conformation. However, the ligand's remaining carbon bonds (C2–C3, C3^{i}–C2^{i}) are in a *gauche* pattern. Due to the length of the carbon chain this leads to a linearly aligned ditetrazole, which links between the two-dimensional layers and builds up a three-dimensional polymeric network (Figure 10).

Sensitivities and thermal stability

Every coordination compound was investigated by differential thermal analysis (DTA) at a linear heating rate of 5 °C min^{-1} in the range of 25–400 °C. The observed decomposition temperatures as well as endothermic events (melting or loss of aqua ligands and crystal water) are listed in Table 1. In addition,

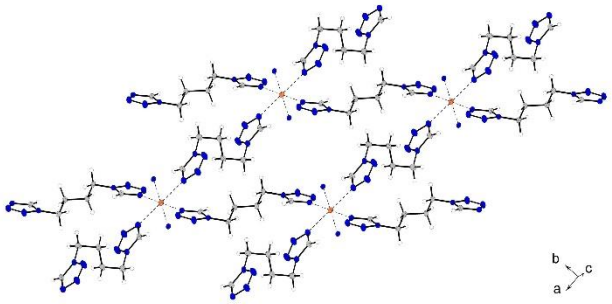


Figure 10. Section of the framework, which is formed in complex **15**. The ligands, not displayed for simplicity, are also aligned in *anti*-conformation and form 2D layers.

Table 1. Overview on the compounds' thermal stability[a] according to DTA.

No.	T_{endo} [°C][b]	T_{exo} [°C][c]	No.	T_{endo} [°C][b]	T_{exo} [°C][c]
2	66	179	**9**	97	165
3	–	203	**10**	–	147
4	129	195	**11**	–	164
5	114	159	**12**	–	150
6	–	106	**13**	113	152
7	65	114	**14**	–	141
8	89*	89*	**15**	97	147

[a] Onset temperature at a heating rate of 5 °C min^{-1} measured by DTA; [b] Endothermic peak, which indicates melting or loss of aqua ligands; [c] Exothermic peak, which indicates decomposition; * Endothermic event followed by exothermic event.

© 2021 The Authors. Chemistry - A European Journal published by Wiley-VCH GmbH

thermogravimetric (TGA) measurements at the same heating rate and temperature range were carried out for compounds **2**, **4**, **5**, **8**, **9**, **13**, and **15** (Figures 11, S10–S11) in order to investigate the behavior of the complexes on heating in more detail. The DTA plots of compounds **2**–**15** as well as additional information regarding the thermal stabilities can be found in the in the Supporting Information (Figures S7–S9).

Endothermic events were observed for eight of the fourteen investigated compounds. As verified by TGA, the endothermic events of **4**, **9**, and **13** represent the loss of aqua ligands or, in the case of compound **7**, the loss of crystal water. Thermogravimetric measurements of the compounds **2**, **5**, **8**, and **15** indicated no loss of mass before reaching the decomposition temperature of the complexes. This indicates that the endothermic events only represent melting points of the ECC **2**, **5**, and **15**. The DTA measurement of complex **8** has an endothermic event immediately followed by an exothermic event, thus it is assumed that the loss of the aqua ligand (T_{endo} = 89 °C) simultaneously results in the decomposition of the complex. The reason for this is probably a square planar complex resulting from the loss of the ligand. Its stability is so low that decomposition occurs immediately after dehydration. In consequence, no mass loss prior to decomposition could be detected during the TG measurement since both events occur simultaneously.

The complex possessing the highest thermal stability is the ATRI based ECC **3** (T_{exo} = 203 °C). This is due to the bridging effect of the triazole ligands, each linking between two copper (II) centers. Similar effects can be observed for complexes **4** (T_{exo} = 195 °C), **9** (T_{exo} = 165 °C), and **11** (T_{exo} = 164 °C), although less evident. The remaining complexes with a bridging ligand motif show no signs of increased thermal stability. In fact, the exothermal events of complexes **2** (T_{exo} = 179 °C) and **5** (T_{exo} = 159 °C), both based on non-bridging ligands, are higher. On the one hand, this is due to a known effect whereby complexes based on ditetrazoles exhibit decreasing thermal stability as the alkyl chain becomes longer.[9c] This effect can also be observed in the comparison of the ditetrazoles prepared in this work (Figure 12). On the other hand, effects such as the low decomposition temperature of the ligand itself (ECC **10**), or the lower stability of the dehydrated species (compound **13**) are reasons for lower thermal stabilities.[14] Nevertheless, the exothermic decomposition temperature of compound **3** clearly proofed, that a tuning of the compounds' thermal stability is possible through the choice of the suitable ligand.

In addition, every compounds' sensitivity toward mechanical stimuli according to BAM standard methods[28] and electrostatic discharge were investigated and ranked in accordance with the UN recommendations on the transport of dangerous goods (Table 2).[29] Interestingly, complex **8** is one the most sensitive complex studied in terms of its sensitivity toward friction (*FS* = 3 N). This is surprising, because usually the presence of water in energetic materials leads to desensitization, which seems to be equalized by the strong endothermic character of the ligand.[13] Similar sensitivities were observed for complexes **8**, **9**, and **10**. The di(tetrazolyl)methane ligands (1,1-dtm & 1,2-dtm) used in these complexes are known to form powerful but sensitive coordination compounds, which is why ECC **10** is the third most sensitive (*FS* = 15 N), closely followed by coordination compound **9** (*FS* = 40 N).[14] The high friction sensitivity of the compound is unusual, as noted for complex **8**, because of the two aqua ligands. Regarding the other coordination compounds containing water ligands, it becomes clear that these are the least sensitive compounds besides complex **15** (*FS* = 240 N). The high stability of the latter is due to the complex's high carbon content compared to the other ones. Also, worth mentioning is complex compound **6**, which is the second most sensitive of the compounds tested regarding friction sensitivity or thermal stability (T_{exo} = 106 °C; *FS* = 5 N, *IS* = 2 J). The reason for this is probably the unusual structure of the complex and its anionic dinitramido ligands, which are bonded to the central metal via a nitrogen atom. Since this is the first case of a

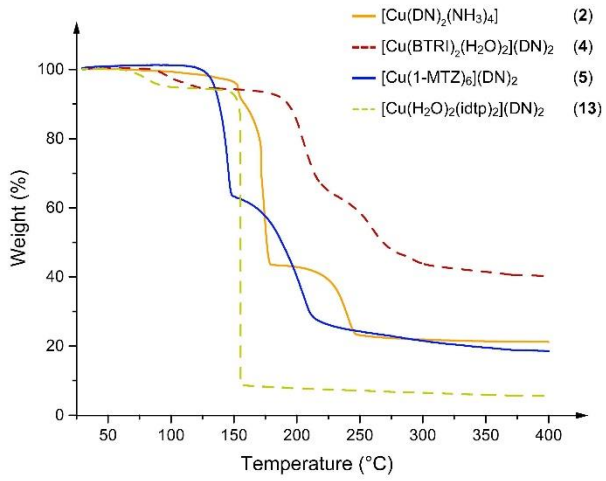


Figure 11. TGA spectra of the coordination compounds **2**, **4**, **5**, and **13** in the range of 30 °C to 400 °C at a heating rate of 5 °C min $^{-1}$.

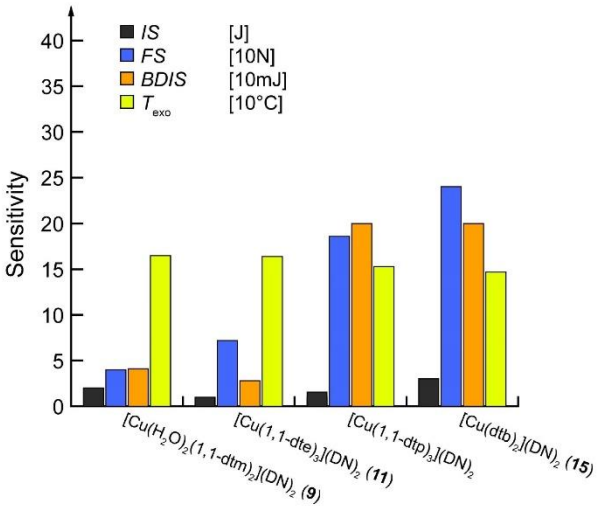


Figure 12. Graphical representation of the thermal stability together with the sensitivity toward various mechanical stimuli of compounds **9**, **11**, **15**, and [Cu(1,1-dtp)$_3$](DN)$_2$.[9b]

© 2021 The Authors. Chemistry - A European Journal published by Wiley-VCH GmbH

Table 2. Overview of the compounds' sensitivities toward various stimuli.

	No.	*IS* (J)[a]	*BDIS* (mJ)[b]	*FS* (N)[c]	*ESD* (mJ)[d]
$[Cu(DN)_2(NH_3)_4]$	**(2)**	2	> 200	50	1080
$[Cu(ATRI)_3](DN)_2$	**(3)**	8	20	80	14
$[Cu(BTRI)_2(H_2O)_2](DN)_2$	**(4)**	7	83	144	181
$[Cu(MTZ)_6](DN)_2$	**(5)**	8	> 200	120	203
$[Cu(AET)_2(DN)_2]$	**(6)**	2	28	5	250
$[Cu(DN)_2(MAT)_4]\cdot 2\ H_2O$	**(7)**	4	> 200	80	> 1500
$[Cu(AMT)_4(H_2O)](DN)_2$	**(8)**	2	28	3	250
$[Cu(1,1\text{-dtm})_2(H_2O)_2](DN)_2$	**(9)**	2	41	40	> 1500
$[Cu(1,2\text{-dtm})_3](DN)_2$	**(10)**	2	28	15	270
$[Cu(1,1\text{-dte})_3](DN)_2$	**(11)**	≤ 1	28	72	76
$[Cu(2,2\text{-dte})_3](DN)_2$	**(12)**	2	25	30	250
$[Cu(H_2O)_2(idtp)_2](DN)_2$	**(13)**	2	180	120	317
$[Cu(DN)_2(1,2\text{-dtp})_2]$	**(14)**	2	> 200	60	840
$[Cu(dtb)_3](DN)_2$	**(15)**	3	> 200	240	> 1500

[a] Impact sensitivity acc. to the BAM drop hammer (method 1 of 6).[28,30] [b] Ball drop impact sensitivity (method 1 of 6) acc. to MIL-STD 1751 A (method 1016).[31] [c] Friction sensitivity acc. to the BAM friction tester (method 1 of 6).[28,32] [d] Electrostatic discharge sensitivity (OZM Electric Spark XSpark10, method 1 of 6).[31b]

complex showing such coordination geometry known to the authors, a proof of this assumption by literature data is unfortunately not possible at this time.

The effect of the carbon content on the properties of a complex, especially the stability against mechanical stimuli, can be illustrated using the example of dinitramide complexes investigated in this work. Together with the complex already published by Szimhardt *et al.*, the complete series of copper dinitramide ECC based on ditetrazole ligands from di(tetrazol-1-yl)methane to 1,4-di(tetrazol-1-yl)butane is known.[9b]

The trends shown in Figure 12 represent a fundamental concept of ECC. As the length of the carbon chain increases, sensitivity toward impact and friction decreases, whilst thermal stability drops. However, the effect of the different coordination geometry in compound **9**, compared to the other complexes, should be noted. A comparison of the sensitivity to electrostatic discharge is less meaningful since this is extremely dependent on the grain size. Ball drop impact sensitivity of $[Cu(1,1\text{-dtp})_3](DN)_2$ was determined and impact and friction sensitivity were redetermined using the same batch to reduce grain size influences.

Apart from the trend shown in Figure 12, there are no other significant sensitivity patterns with respect to impact sensitivity. According to the UN recommendations on the transport of dangerous goods, every compound except **3**, **4**, **5**, and **7** are ranked as very sensitive regarding impact sensitivity.[29] The remaining compounds must only be considered as sensitive. In terms of sensitivity toward friction, compounds **3** and **7** are also considered very sensitive, with ECC **6** and **8** being even extremely sensitive. The complexes **13** and **15** are only considered sensitive.

In addition to BAM sensitivities, the ball drop impact sensitivity (BDIS) according to MIL-STD 1751 A (method 1016) was investigated.[31a] The aim was to obtain measured values which are more realistic than data obtained mainly with the BAM drop hammer. This method is known to suffer from some weaknesses, for example, the ignition of the substance by forming hotspots within the shells.[33] In the ball drop test, however, a steel ball with a defined spin is dropped onto an unconfined sample, spread over a thin layer of defined height (Figure 13).[31a]

Experiments were carried out for every coordination compound. The outcome is displayed in Table 2. The sensitivities obtained for compounds **5** (*IS* = 8 J, *BDIS* > 200 mJ, *FS* = 120 N), **6** (*IS* = 2 J, *BDIS* = 28 mJ, *FS* = 5 N), **7** (*IS* = 2 J, *BDIS* > 28 mJ, *FS* = 3 N), **13** (*IS* = 2 J, *BDIS* = 180 mJ, *FS* = 120 N), and **15** (*IS* = 3 J, *BDIS* > 200 mJ, *FS* = 240 N) are either very low, or very high, which is consistent with our earlier findings.[34] It is assumed that there is a strong correlation between low sensitivity toward friction and ball drop impact. However, in the case of compounds **2**, **3**, and **11** the results do not match our previous results. ECC **3** (*IS* = 8 J, *BDIS* = 20 mJ, *FS* = 80 N) was not considered sensitive during BAM sensitivity measurements but was tested the most sensitive compound during ball drop testing. Whilst the tetrammine complex **2** (*IS* = 2 J, *BDIS* > 200 mJ, *FS* = 50 N) was much more insensitive than expected the ball drop impact sensitivity on **11** (*IS* = 1 J, *BDIS* = 28 mJ, *FS* = 72 N) correlates more with the BAM impact rating than with the friction sensitivity. This shows that the system of ball drop impact sensitivity has not yet been completely understood and that there are other substances that need to be investigated using this method in order to further expand our knowledge about this method and sensitivities of energetic materials in general. For safety reasons, different and unknown sensitivity values from external devices must be evaluated carefully.



Figure 13. High-speed image of the moment of detonation of complexes **6** (left) and **9** (right) during the ball drop impact test.

 © 2021 The Authors. Chemistry - A European Journal published by Wiley-VCH GmbH

Table 3. Results of hot plate, hot needle and PETN Initiation experiments.[a]

	Initial Testing HP	HN	PETN Initiation Experiment		Initial Testing HP	PETN Initiation Experiment HN	
2	dec.	dec.	–	**9**	defl.	defl.	negative
3	defl.	dec.	–	**10**	defl.	defl.	negative
4	defl.	dec.	–	**11**	defl.	defl.	negative
5	defl.	defl.	–	**12**	defl.	defl.	–
6	defl.	defl.	negative	**13**	defl.	defl.	–
7	defl.	defl.	–	**14**	defl.	defl.	–
8	defl.	det.	positive	**15**	dec.	dec.	–

[a] –: not tested, dec.: decomposition, defl.: deflagration, det.: detonation.

A comparison of the complexes of this work with earlier work of our group on this area is difficult in most cases. Since strongly coordinating anions such as fulminate, azide, or various trinitrophenolates lead to significantly different coordination geometries, a comparison here is almost impossible. Therefore, the best way of making meaningful comparisons is probably with other oxidizing, weakly coordinating anions such as nitrate, chlorate, bromate or perchlorate. In the case of complexes **2**, **4**, **6**, **9**, **12**, and **15**, this is also not possible, since either no similarly structured complexes are known in the literature or have not been sufficiently investigated for their energetic parameters. In the cases in which a comparison was useful, it was found that apart from compound **11**, which is 0.5 J more sensitive than the respective chlorate and perchlorate complexes, all dinitramide based ECCs are less sensitive than the analogous chlorate, bromate or perchlorate complexes. The only suitable nitrate complex $[Cu(MTZ)_6](NO_3)_2$ on the other side is less sensitive than ECC **5**.

Primary explosive suitability evaluation

Hot plate and hot needle tests were performed as an initial test to get an insight into each compounds' deflagration to detonation transition (DDT), which is a very important property of primary explosives. Investigations on DDT allow conclusions to be drawn on how well a primary is capable of initiating a booster charge such as PETN. The hot plate test displays the behavior of a compound during fast heating (Figure 14, left). Hot needle tests indicate the performance of a sample during slight confinement (Figure 14, right).

Details on the process and further high-speed images of the experiments can be found in the General Methods in the Supporting Information (Figures S7–S19). The outcome of each test is summarized in Table 3. With the exception of **2**, **3**, **4**, and **15**, all ECC examined showed at least a deflagration in both initial experiments. These are very promising findings and the basis for further tests such as the initiation of pentaerythritol tetranitrate (PETN) or laser-based ignitions. Since complex **8** detonated during the hot needle test and the complexes **6**, **9**, **10** and **11** showed very strong deflagrations, those compounds were investigated as lead azide (LA, $Pb(N_3)_2$) substitutes.

To carry out the initiation experiments, 200 mg of PETN were pressed into a copper shell and initiated with 50 mg of the substance to be investigated using a Type A electric igniter. A positive result, as observed in the case of ECC **8**, is indicated by a hole in the copper plate (Figure 15). This clearly proved that by choosing the appropriate ligand, the power of the complex can be increased to a level capable of initiating PETN. A test of compound **11** indicated that this compound is close to being capable of initiating PETN. A modification of the test, for example, a variation of the particle size or quantity, could resolve this problem. Further details on the procedure can be found in the General Methods of the Supporting Information.

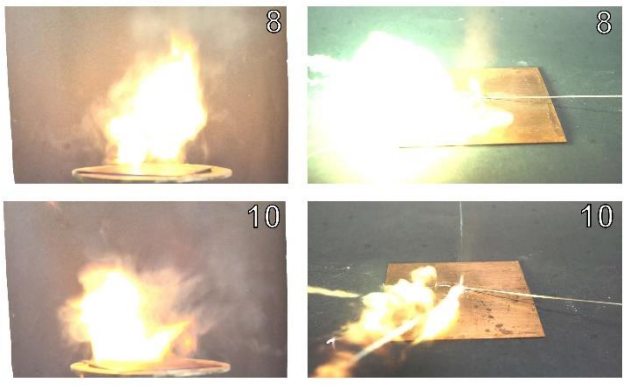


Figure 14. High-speed images of deflagration reactions of compounds **8** and **10** during the hot plate test (left) and detonation in the hot needle test (right).

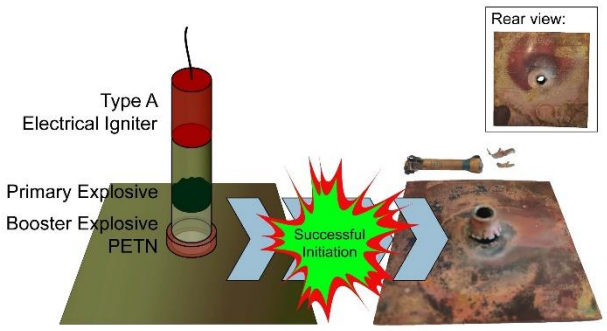


Figure 15. Positive initiation test result of compound **8**, together with a graphical representation of the test setup used.

© 2021 The Authors. Chemistry - A European Journal published by Wiley-VCH GmbH

Table 4. Results of laser ignition experiments.

	Laser Ignition Experiments, E (mJ)[a,b]					Laser Ignition Experiments, E (mJ)[a,b]		
	4.5	30	51	126		30	51	67.5
2	–	–	dec.	–	**9**	defl.	–	–
3	–	–	defl.	defl.	**10**	defl.	–	–
4	–	–	dec.	–	**11**	–	defl.	defl.
5	defl.	–	defl.	–	**12**	dec.	–	–
6	–	defl.	–	–	**13**	–	dec.	dec.
7	–	defl.	–	–	**14**	dec.	–	–
8	–	det.	–	–	**15**	defl.	–	–

[a] Operating parameters: current I=7–15 A; voltage U=4 V; theoretical maximal output power P_{max}=45 W; theoretical energy E_{max}=4.5–126 mJ; wavelength λ=915 nm; pulse length τ=1–15 ms. [b] –: not tested, dec.: decomposition, defl.: deflagration, det.: detonation.

Laser ignition experiments

Besides the classical ignition methods by flame, as used in initiation experiments, or by mechanical stimuli, as found in percussion caps, more and more research is performed in the field of alternative ignition methods. One of these fields where ECC are already established are laser-based ignitions.[16] Especially regarding the dinitramide anion as part of ECC, there is evidence that copper(II) complexes based on this system respond to laser radiation.[9a–c]

The principle of laser-based ignition of primary explosives and priming mixtures has a great advantage over classical mechanical ignition. For a mechanical initiation, an impact or for primers frictional force must be generated. The substances used for this must therefore have a suitable mechanical sensitivity. For the most commonly used primary explosives lead azide (LA RD-1333) and lead styphnate (LS) these sensitivities were determined to 0.45–1 N and 7–8 J (LS) as well as $\leq$0.1 N and 4 J (LA RD-1333).[34,35] For explosives ignited by laser irradiation, however, less sensitive substances are also suitable, which drastically reduces the risk potential during production, processing, and storage of the respective energetic materials.

In this work, every compound was investigated for its behavior when irradiated with a laser beam. The outcome of each test, together with the applied energy, is shown in Table 4. Further information on the test setup and procedure can be found in the General Methods in the Supporting Information. With the exception of compound **12**, all complexes showed a reaction toward the laser irradiation. The result of such examination, in this case the result of the testing of compound **5**, is shown in Figure 16. Further high-speed recordings of all compounds can be found in the Supporting Information (Figures S20–26).

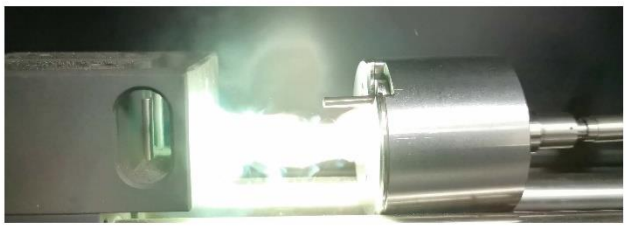


Figure 16. Deflagration of $[Cu(MTZ)_6](DN)_2$ (**5**) during laser irradiation.

The outcome of each investigation differed significantly due to the applied ligand. Thus, especially complexes **2**, **3**, **13**, **14**, and **15** showed only weak reactions, which, considering the respective hot plate and hot needle tests of the substances, is within the expectations. Coordination compounds **5**, **6**, **8**, **9**, and **10**, which are based on ligands known to form powerful complexes, showed significantly stronger reactions when irradiated by the laser, up to a detonation in the case of compound **8**. However, based on these expectations, compound **12** in particular disappointed in terms of output upon laser irradiation.

As mentioned earlier, the complex based on 2,2-dte did not respond at all to radiation despite promising hot plate and hot needle tests. Only minimal decomposition was detected in the primer cap after completion of the test, with a bulk of the complex remaining unreacted. This is worth mentioning because complex **11**, based on the isomeric ligand 1,1-dte, which has the same molecular formula, underwent strong deflagration during laser irradiation. Assuming that the decomposition of the sample in the laser is thermal in nature, the two-step slow decomposition observed during the DTA measurement could be a reason for the behavior (Figure S9).

Except for compound **12**, these results suggest a possible use as potential laser-ignitable explosives and demonstrates again that by utilizing the concept of ECC, the performance of the dinitramide anion in complexes can be adjusted by selecting the appropriate ligand system. As the mechanisms behind laser ignition (most probably thermal ignition) are still not fully understood, UV-Vis spectra were recorded in the solid state for selected compounds. Particular emphasis was placed on the wavelength range corresponding to that of the laser when evaluating the spectra. Details on this, as well as all spectra, can be found in the Supporting Information (Table S4, Figure S27–S28).

Conclusion

Dinitraminic acid (HDN, **1**) was successfully prepared by ion exchange techniques using an acidified Amberlite IR 120 and an aqueous ADN solution as eluent. The dinitraminic acid was

 © 2021 The Authors. Chemistry - A European Journal published by Wiley-VCH GmbH

further reacted with copper(II) carbonate for the *in situ* preparation of highly clean copper(II) dinitramide. The combination of the obtained solution with different ligands led to 13 new copper complexes of which nine were crystallographically investigated. To the best of our knowledge, it is also the first time that the tetraammine complex of the copper dinitramide has been isolated elemental pure. The complexes were analyzed in detail regarding their thermal and mechanical stability as well as their sensitivity to electrostatic discharge. The thermal stability could thus be increased to over 200 °C (**3**) using the bridging and commercially available 4-amino-triazole ligand. Only three compounds were less thermally stable than ADN. The systematic series of ditetrazole ligands from a methylene to a butylene bridge in copper dinitramide complexes was also completed by this work. Here, with the lengthening of the alkyl chain, a nearly halving of the sensitivity was observed. This trend contributes significantly to the concept of ECC to estimate the properties of the following complexes. In addition, all complexes were investigated in laser initiation experiments. During these, only one complex did not show a response to the irradiation, whereas compound **4** even deflagrated at an energy of 51 mJ and **8** detonated at an energy of 30 mJ. Furthermore, the concept of ECC was successfully applied to increase the compounds performance, leading to one complex (**8**) even being capable of initiating PETN. Furthermore, ditetrazole-based complexes **11–15** should be considered for further testing as burn rate catalysts due to their low water solubility and decomposition temperature of about 150 °C.

Acknowledgements

For financial support of this work by Ludwig-Maximilian University (LMU). The authors would like to thank Professor Dr. Thomas M. Klapötke for his scientific support as well as for providing his research facilities. Also, the authors would like to thank Markus Rösch for his great contribution to this work. Open access funding enabled and organized by Projekt DEAL.

Conflict of Interest

The authors declare no conflict of interest.

Keywords: burn rate catalyst · dinitramide · dinitraminic acid · laser ignition · primary explosives

[1] T. M. Klapötke, *Chemistry of High-Energy Materials*, 5th ed., De Gruyter, Berlin, Boston, **2019**.
[2] A. G. Keenan, R. F. Siegmund, *Q. Rev. Chem. Soc.* **1969**, *23*, 430–452.
[3] a) D. E. Chavez, B. C. Tappan, B. A. Mason, D. Parrish, *Propellants Explo. Pyrotech.* **2009**, *34*, 475–479; b) B. C. Tappan, D. E. Chavez, *Propellants Explos. Pyrotech.* **2015**, *40*, 13–15; c) H. Gao, C. Ye, O. D. Gupta, J.-C. Xiao, M. A. Hiskey, B. Twamley, J. n. M. Shreeve, *Chem. Eur. J.* **2007**, *13*, 3853–3860; d) T. T. Vo, D. A. Parrish, J. n. M. Shreeve, *J. Am. Chem. Soc.* **2014**, *136*, 11934–11937.
[4] O. A. Luk'yanov, V. P. Gorelik, V. A. Tartakovskii, *Russ. Chem. Bull.* **1994**, *43*, 89–92.
[5] a) O. A. Luk'yanov, A. R. Agevnin, A. A. Leichenko, N. M. Seregina, V. A. Tartakovsky, *Russ. Chem. Bull.* **1995**, *44*, 108–112; b) O. A. Luk'yanov, O. V. Anikin, V. P. Gorelik, V. A. Tartakovsky, *Russ. Chem. Bull.* **1994**, *43*, 1457–1461; c) O. A. Luk'yanov, O. V. Anikin, V. A. Tartakovsky, *Russ. Chem. Bull.* **1996**, *45*, 433–440; d) O. A. Luk'yanov, Y. V. Konnova, T. A. Klimova, V. A. Tartakovsky, *Russ. Chem. Bull.* **1994**, *43*, 1200–1202; e) O. A. Luk'yanov, I. K. Kozlova, O. P. Shitov, Y. Y. Konnova, I. V. Kalinina, Y. A. Tartakovsky, *Russ. Chem. Bull.* **1996**, *45*, 863–867; f) O. A. Luk'yanov, N. I. Shlykova, V. A. Tartakovsky, *Russ. Chem. Bull.* **1994**, *43*, 1680–1683; g) O. A. Luk'yanov, S. N. Shvedova, E. V. Shepelev, O. N. Varfolomeeva, N. N. Malkina, V. A. Tartakovsky, *Russ. Chem. Bull.* **1996**, *45*, 1497–1498; h) V. A. Shlyapochnikov, N. O. Cherskaya, O. A. Luk'yanov, O. V. Anikin, V. A. Tartakovsky, *Russ. Chem. Bull.* **1996**, *45*, 430–432; i) V. A. Shlyapochnikov, M. A. Tafipolsky, I. V. Tokmakov, E. S. Baskir, O. V. Anikin, Y. A. Strelenko, O. A. Luk'yanov, V. A. Tartakovsky, *J. Mol. Struct.* **2001**, *559*, 147–166.
[6] J. C. Bottaro, P. E. Penwell, R. J. Schmitt, *J. Am. Chem. Soc.* **1997**, *119*, 9405–9410.
[7] P. Kumar, *Def. Technol.* **2018**, *14*, 661–673.
[8] N. Fischer, M. Joas, T. M. Klapötke, J. Stierstorfer, *Inorg. Chem.* **2013**, *52*, 13791–13802.
[9] a) M. Joas, T. M. Klapötke, J. Stierstorfer, N. Szimhardt, *Chem. Eur. J.* **2013**, *19*, 9995–10003; b) N. Szimhardt, M. H. H. Wurzenberger, T. M. Klapötke, J. T. Lechner, H. Reichherzer, C. C. Unger, J. Stierstorfer, *J. Mater. Chem. A* **2018**, *6*, 6565–6577; c) M. B. Joas, PhD thesis, Ludwig-Maximilians University Munich, **2014**; d) J. Zhang, Y. Du, K. Dong, H. Su, S. Zhang, S. Li, S. Pang, *Chem. Mater.* **2016**, *28*, 1472–1480.
[10] K. Nosratzadegan, M. Mahdavi, K. Ghani, K. Barati, *Propellants Explos. Pyrotech.* **2019**, *44*, 830–836.
[11] R. M. J. Köhler, A. Homburg, *Explosivstoffe*, 10th ed., Wiley-VCH, Weinheim, **2008**.
[12] N. Szimhardt, M. H. H. Wurzenberger, L. Zeisel, M. S. Gruhne, M. Lommel, T. M. Klapötke, J. Stierstorfer, *Chem. Eur. J.* **2019**, *25*, 1963–1974.
[13] a) N. Szimhardt, M. H. H. Wurzenberger, A. Beringer, L. J. Daumann, J. Stierstorfer, *J. Mater. Chem. A* **2017**, *5*, 23753–23765; b) M. H. H. Wurzenberger, B. R. G. Bissinger, M. Lommel, M. S. Gruhne, N. Szimhardt, J. Stierstorfer, *New J. Chem.* **2019**, *43*, 18193–18202.
[14] M. H. H. Wurzenberger, V. Braun, M. Lommel, T. M. Klapötke, J. Stierstorfer, *Inorg. Chem.* **2020**, *59*, 10938–10952.
[15] H. G. Ang, W. Fraenk, K. Karaghiosoff, T. M. Klapötke, P. Mayer, H. Nöth, J. Sprott, M. Warchhold, *Z. Anorg. Allg. Chem.* **2002**, *628*, 2894–2900.
[16] M. A. Ilyushin, A. A. Kotomin, S. A. Dushenok, *Russ. J. Phys. Chem. B* **2019**, *13*, 119–138.
[17] N. Szimhardt, M. H. H. Wurzenberger, L. Zeisel, M. S. Gruhne, M. Lommel, J. Stierstorfer, *J. Mater. Chem. A* **2018**, *6*, 16257–16272.
[18] J. S. M. P. A. Politzer, *Theoretical and Computational Chemistry, Vol. 12: Energetic Materials Part 1: Decomposition, Crystal and Molecular Properties*, 1st ed., Elsevier B. V., Amsterdam, **2003**.
[19] A. I. Kazakov, Y. I. Rubtsov, G. B. Manelis, *Propellants Explos. Pyrotech.* **1999**, *24*, 37–42.
[20] a) L. Zeisel, N. Szimhardt, M. H. H. Wurzenberger, T. M. Klapötke, J. Stierstorfer, *New J. Chem.* **2019**, *43*, 609–616; b) M. H. H. Wurzenberger, M. S. Gruhne, M. Lommel, N. Szimhardt, T. M. Klapötke, J. Stierstorfer, *Chem. Asian J.* **2019**, *14*, 2018–2028.
[21] R. Bronisz, *Inorg. Chim. Acta* **2002**, *340*, 215–220.
[22] a) J. Schweifer, P. Weinberger, K. Mereiter, M. Boca, C. Reichl, G. Wiesinger, G. Hilscher, P. J. van Koningsbruggen, H. Kooijman, M. Grunert, *Inorg. Chim. Acta* **2002**, *339*, 297–306; b) C. Baldé, M. S. Sylla, C. Desplanches, G. Chastanet, *Polyhedron* **2019**, *159*, 84–92; c) P. J. van Koningsbruggen, Y. Garcia, H. Kooijman, A. L. Spek, J. G. Haasnoot, O. Kahn, J. Linares, E. Codjovi, F. Varret, *J. Chem. Soc. Dalton Trans.* **2001**, 466–471.
[23] L. S. Ivashkevich, A. S. Lyakhov, A. N. Shmakov, V. V. Efimov, O. A. Ivashkevich, S. I. Tyutyunnikov, *Phys. Part. Nucl. Lett.* **2008**, *5*, 62–65.
[24] Y.-G. Bi, Y.-A. Feng, Y. Li, B.-D. Wu, T.-L. Zhang, *J. Coord. Chem.* **2015**, *68*, 181–194.
[25] K. Karaghiosoff, T. M. Klapötke, C. Miró Sabaté, *Chem. Eur. J.* **2009**, *15*, 1164–1176.
[26] Deposition numbers 2063682 (**4**), 2063676 (**6**), 2063681 (**8**), 2063679 (**9**), or 2063675 (**10**) 2063677 (**11**), 2063680 (**12**), 2063678 (**13**) and 2063674 (**15**) contain the supplementary crystallographic data for this paper. These data are provided free of charge by the joint Cambridge

 © 2021 The Authors. Chemistry - A European Journal published by Wiley-VCH GmbH

Crystallographic Data Centre and Fachinformationszentrum Karlsruhe Access Structures service (accessed February **2021**).
[27] a) M. Daszkiewicz, M. K. Marchewka, *J. Mol. Struct.* **2012**, *1017*, 90–97; b) P. Domiano, *Cryst. Struct. Commun.* **1977**, *6*, 503; c) J. Bryden, *Acta Crystallogr.* **1956**, *9*, 874–878; d) M. H. Palmer, S. Parsons, *Acta Crystallogr. Sect. C* **1996**, *52*, 2818–2822.
[28] BAM, www.bam.de, (accessed February **2021**).
[29] Impact sensitivity: insensitive > 40 J, less sensitive ≥ 35 J, sensitive ≥ 4 J, very sensitive 3 J; Friction sensitivity: insensitive > 360 N, less sensitive = 360 N, sensitive < 360 N and > 80 N, very sensitive 80 N, extremely sensitive 10 N. According to the UN Recommendations on the Transport of Dangerous Goods – Manual of Tests and Criteria, section 13.4.2.3.3, **2015**.
[30] a) NATO standardization agreement (STANAG) on explosives, impact sensitivity tests, no. 4489, 1st ed., Sept. 17, **1999**; b) WIWEB-Standardarbeitsanweisung 4–5.1.02, Ermittlung der Explosionsgefährlichkeit, hier der Schlagempfindlichkeit mit dem Fallhammer, Nov. 8, **2002**.
[31] a) United States Military Standard 1751 A (MIL-STD-1751 A), Safety and performance tests for qualification of explosives (high explosives, propellants and pyrotechnics), Method 1016, **2001**; b) OZM, www.ozm.cz, (accessed February **2021**).
[32] a) NATO standardization agreement (STANAG) on explosive, friction sensitivity tests, no. 4487, 1st ed., Aug. 22, **2002**; b) WIWEB-Standardarbeitsanweisung 4–5.1.03, Ermittlung der Explosionsgefährlichkeit oder der Reibeempfindlichkeit mit dem Reibeapparat, Nov. 8, **2002**.
[33] a) J. G. Reynolds, P. C. Hsu, G. A. Hust, S. A. Strout, H. K. Springer, *Propellants Explos. Pyrotech.* **2017**, *42*, 1303–1308; b) S. M. Walley, J. E. Field, R. A. Biers, W. G. Proud, D. M. Williamson, A. P. Jardine, *Propellants Explos. Pyrotech.* **2015**, *40*, 351–365.
[34] M. S. Gruhne, M. Lommel, M. H. H. Wurzenberger, N. Szimhardt, T. M. Klapötke, J. Stierstorfer, *Propellants Explos. Pyrotech.* **2020**, *45*, 147–153.
[35] T. M. Klapötke, *Energetic Materials Encyclopedia*, 2nd ed., De Gruyter, Berlin, Boston, **2021**.

Manuscript received: March 1, 2021
Accepted manuscript online: April 26, 2021
Version of record online: June 10, 2021

© 2021 The Authors. Chemistry - A European Journal published by Wiley-VCH GmbH

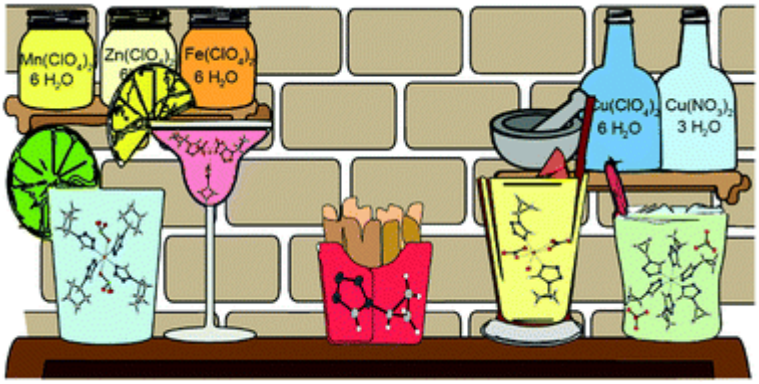
Appendix 24

Tailoring the properties of 3d transition metal complexes with different N-cycloalkyl-substituted tetrazoles

M. Wurzenberger, V. Braun, V. Weippert, J. Stierstorfer

New J. Chem. **2021**, *45*, 11042–11050.

https://doi.org/10.1039/D1NJ01675J



Supplementary Information:
https://www.rsc.org/suppdata/d1/nj/d1nj01675j/d1nj01675j1.pdf

Published on 29 April 2021. Downloaded by Ludwig Maximilians Universitaet Muenchen on 3/6/2022 8:27:05 AM.

NJC

ROYAL SOCIETY OF CHEMISTRY

PAPER

View Article Online
View Journal | View Issue

Check for updates

Cite this: *New J. Chem.*, 2021, **45**, 11042

Tailoring the properties of 3d transition metal complexes with different *N*-cycloalkyl-substituted tetrazoles†

Vanessa Braun, Maximilian H. H. Wurzenberger, Valentin Weippert and Jörg Stierstorfer *

Received 6th April 2021,
Accepted 27th April 2021

DOI: 10.1039/d1nj01675j

rsc.li/njc

Three ligands, 1-cyclopropyl-5*H*-tetrazole (C_3tz, **1**), 1-cyclobutyl-5*H*-tetrazole (C_4tz, **2**), and 1-cyclopentyl-5*H*-tetrazole (C_5tz, **3**), were synthesized and used for the design of 19 new energetic coordination compounds (ECC) based on 3d transition metal complexes. By the varying the metal(II) centres (Mn^{2+}, Fe^{2+}, Cu^{2+}, and Zn^{2+}), the corresponding anions (nitrates, azides, chlorates, and perchlorates), and the ligands, the characteristics and properties of the ECC could be perfectly tailored to the desired values. All ligands and coordination compounds were extensively characterized regarding their sensitivities towards various influences, such as impact, friction, and electrostatic discharge, and their thermal stabilities were determined. Furthermore, single-crystal X-ray diffraction experiments, infrared spectroscopy (IR), and elemental analysis (EA) were applied for their investigation. Additionally, ligands **1–3** were examined using the superior two-dimensional ^{1}H–^{15}N-HMBC NMR spectroscopy. The iron(II) spin-crossover (SCO) complex **19** was investigated by a temperature-dependent magnetic study, allowing the mapping of the spin transition in a temperature-dependent susceptibility curve.

Introduction

Explosives can be distinguished based on their sensitivity, as primary or secondary explosives; primary explosives can be easily detonated *via* a simple initiating impulse, such as impact or heat, and they are used to transfer shockwaves to the less-sensitive secondary explosives.[1] The synthesis of the most common primary explosive, lead azide (LA), was first published by Curtius in 1891.[2] LA, together with lead styphnate, is still dominating the field of ignition and initiation systems and causes serious environmental problems, for instance, heavy metal contamination of shooting ranges.[3] Due to their high toxicity, both were included in the candidate list of authorization (substances of very high concern, Annex XIV) for the REACH (Registration, Evaluation, Authorization and Restriction of Chemicals) regulations in 2011, impending a ban on their use.[4] Furthermore, the most commonly used high explosives, such as TNT and RDX, also has a toxic influence towards the environment.[1] Hence, the replacement of both, the toxic primary and secondary explosives, by the so-called "green" substances is one of the major worldwide interests in modern energetic material research.[5–12] The new energetic materials must fulfil basic criteria, including high thermal and chemical stability, as well as high energy and density.[13] Building blocks with high nitrogen content, such as tri- and tetrazoles, are particularly promising for the development of new highly energetic materials. This unique class of compounds owes its energetic properties to the very high heat of formation, which is directly proportional to the number of energetic N–N and C–N bonds (Fig. 1). In addition to the high heat of formation, another added advantage of the ring system is the decomposition into harmless molecular nitrogen accompanied by the release of an enormous amount of energy.[14]

In oxidation state +I and, especially, in oxidation state +II, copper as the metal centre offers a multitude of possible coordination compounds. These complexes with predominantly oxygen- and nitrogen-rich ligands represent an important group of new energetic materials.[16–18] In particular, endothermic tetrazole ligands have been of interest in recent years, which is due to their good kinetic and thermal stabilities.[19–21] Besides the use as ligands for energetic materials, tetrazole and its derivatives are also important structural motifs in medical research and can be found in several pharmaceuticals.[22]

External stimuli, such as specific temperature, pressure or light irradiation, can cause the so-called spin-crossover in transition

Department of Chemistry, Ludwig Maximilian University Munich, Butenandtstr. 5-13, 81377 Munich, Germany. E-mail: jstch@cup.uni-muenchen.de

† Electronic supplementary information (ESI) available. CCDC 2061069 (**1**), 2061078 (**4**), 2061087 (**5**), 2061071 (**6**), 2061075 (**7**), 2061086 (**8**), 2061084 (**9**), 2061085 (**10**), 2061081 (**11**), 2061079 (**12**), 2061076 (**13**), and 2061073 (**14**), 2061074 (**15a**), 2061089 (**15b**), 2061072 (**16**), 2061077 (**17**), 2061080 (**18**), 2061070 (**19**), 2061082 (**20**), 2061088 (**21**), 2061083 (**22**). For ESI and crystallographic data in CIF or other electronic format see DOI: 10.1039/d1nj01675j

 This journal is © The Royal Society of Chemistry and the Centre National de la Recherche Scientifique 2021

Published on 29 April 2021. Downloaded by Ludwig Maximilians Universitaet Muenchen on 3/6/2022 8:27:05 AM.

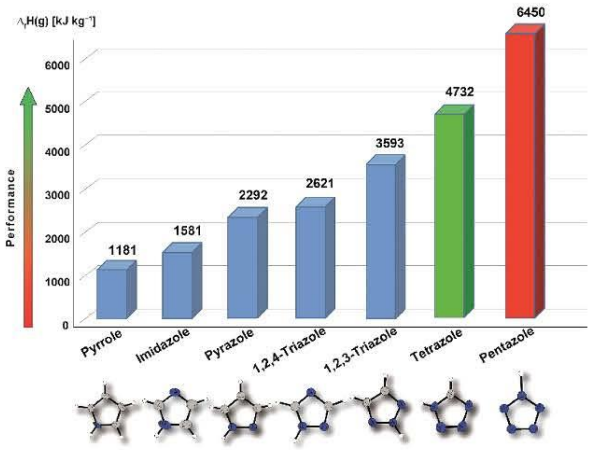


Fig. 1 Increasing gas phase heat of the formation of azole-based heterocycles.[15]

metal coordination compounds with d^4 to d^7 electron configuration. This phenomenon is based on the interaction between the electron–electron repulsion and the dependence of the ligand-field strength on the distance of metal to ligand. The basic requirement of this attribute of 3d transition metals is the ground state exhibiting a lower spin than the temporarily occupied metastable state.[23,24] This effect leads to a change in the properties of the solid materials resulting in many new, possible applications of spin-crossover materials, for example, nano-materials, memory devices, sensors, or displays.[25,26] Since the first reported iron(II) spin-crossover (SCO) complex in the 1960s,[27] this research area is a growing field and many transition metals with various counterions (*e.g.*, BF_4^-, ClO_4^-) were investigated.[28] In particular, octahedrally coordinated iron(II) complexes with a diamagnetic low-spin state are affected by the spin-crossover phenomenon and also many tetrazole-based coordination compounds were examined. 1-Cyclopropyl-5*H*-tetrazole (C_3tz) was already used to prepare a new iron(II) SCO complex with tetrafluoroborate as the anion (Fig. 2) and Soliman *et al.* published other octahedrally coordinated

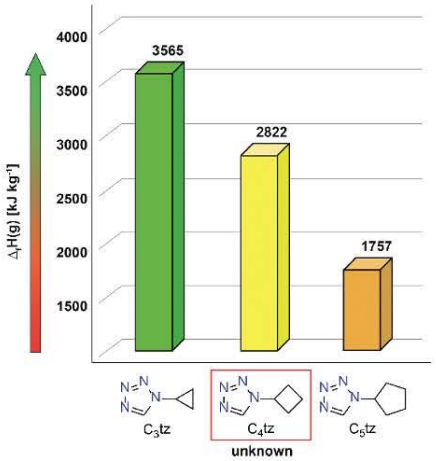


Fig. 2 Cyclically substituted tetrazole ligands and their gas phase heat of formation.[15]

complexes with C_3tz, including $[Cu(C_3tz)_6](BF_4)_2$, $[Ni(C_3tz)_6](BF_4)_2$, and $[Fe(C_3tz)_6](PF_6)_2$.[29]

In 2009, Hassan *et al.* reported further cyclically substituted tetrazole ligands for SCO complexes. 1-Cyclopentyl-5*H*-tetrazole (C_5tz) and 1-cyclohexyl-5*H*-tetrazole were converted with iron(II) tetrafluoroborate to form octahedrally coordinated complex compounds showing the SCO phenomenon.[30] Due to the potential of cyclically substituted tetrazoles for multiple application possibilities, this work focusses on the implementation of 1-cyclopropyl-5*H*-tetrazole, 1-cyclobutyl-5*H*-tetrazole, and 1-cyclopentyl-5*H*-tetrazole for the design of new ECC and the perfect taming of the sensitivities of the complexes. A comparison with the non-stained open 1-propyl-5*H*-tetrazole ligand, which was also implemented in energetic complexes,[31,32] is drawn. Furthermore, the influence of the different ring sizes on the energetic properties and coordination geometry was investigated in detail.

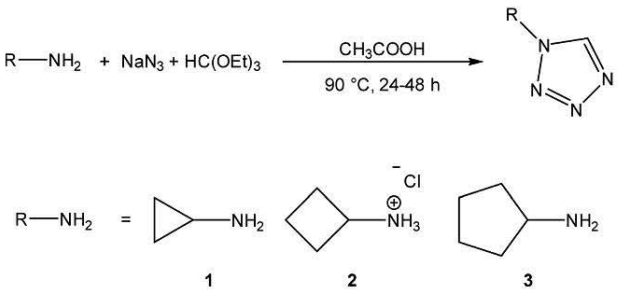
Results and discussion

Synthesis

According to the modified literature procedures,[29,30] ligands **1**–**3** were prepared in a simple one-step [3+1+1] ring closure reaction starting from commercially available materials (Scheme 1).

To a suspension of the corresponding amines or amine hydrochlorides and sodium azide in triethyl orthoformate, glacial acetic acid was added dropwise. The mixture was heated up for 24 h or in the case of compounds **2** and **3** for 48 h, cooled to ambient temperature and extracted with ethyl acetate. After purification of the organic layer with water, sodium bicarbonate solution, and brine, the solvent was evaporated under reduced pressure to obtain C_4tz (**2**) as a yellow oil in 57% yield and C_5tz (**3**) as an orange oil in 80% yield. It was not possible to obtain pure compound **1** without acetic acid, and distillation destroyed the product. Recrystallization from methanol yielded pure C_3tz (**1**) as colourless crystals in 49% yield. All ligands were investigated by elemental analysis, differential thermal analysis (DTA), infrared spectroscopy (IR), and ^{1}H and ^{13}C NMR spectroscopies. Furthermore, the superior two-dimensional ^{1}H–^{15}N-HMBC NMR measurements can be easily applied to characterize and distinguish the different tetrazole ligands (Fig. 3 and Fig. S4 and S5, ESI†).

Most of the reactions for the synthesis of the coordination compounds were carried out in ethanol, and due to solubility issues, a few of the obtained products had to be recrystallized in



Scheme 1 Synthesis of ligands **1**–**3**.

Published on 29 April 2021. Downloaded by Ludwig Maximilians Universitaet Muenchen on 3/6/2022 8:27:05 AM.

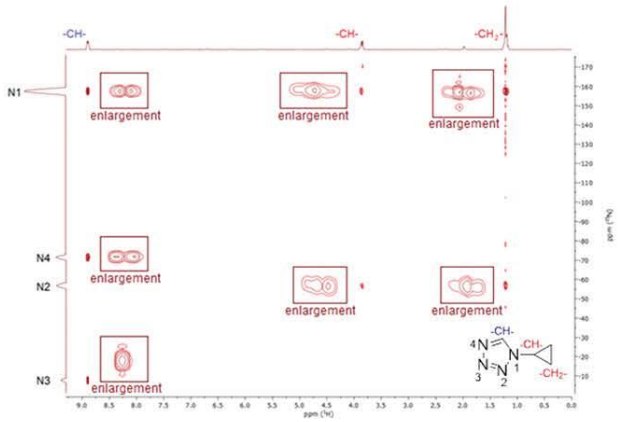


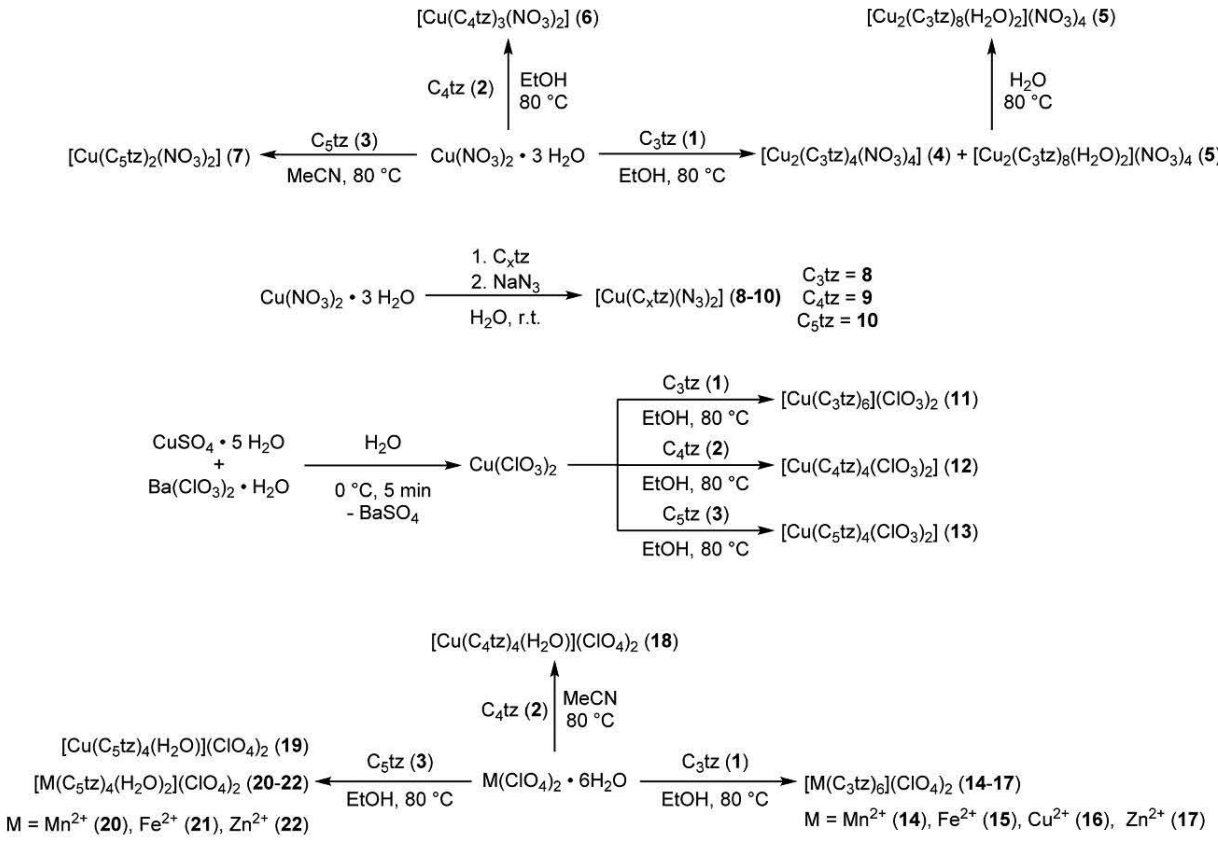
Fig. 3 $^{1}H-^{15}N$-HMBC NMR spectrum of ligand C_3tz (**1**).

different solvents for purification. All complexes were obtained in acceptable to very good yields (23–89%) and crystallized within minutes up to 14 days. Copper(II) nitrate compounds **4**–**7** were synthesized in organic solvents and due to the instability of $[Cu(C_3tz)_3(NO_3)_2]$ (**4**) against moisture, it was solely obtained as mixtures with **5**. Recrystallisation from water yielded pure $[Cu_2(C_3tz)_8(H_2O)_2](NO_3)_4$ (**5**) as medium blue crystals in 89% yield (Scheme 2). Copper(II) azide ECC **8**–**10** were prepared according to a modified literature procedure.[31] While the preparation with C_4tz only required one equivalent, an excess of two equivalents of the ligand had to be used in the case of C_3tz and C_5tz to obtain pure products for elemental analysis. Copper(II) chlorate coordination compounds were synthesized starting with a metathesis reaction of copper(II) sulphate and barium chlorate. The *in situ* formed copper(II) chlorate was further reacted with **1**–**3** in ethanol at elevated temperatures to give complexes $[Cu(C_3tz)_6](ClO_3)_2$ (**11**), $[Cu(C_4tz)_4(ClO_3)_2]$ (**12**), and $[Cu(C_5tz)_4(ClO_3)_2]$ (**13**).

Due to the extreme hygroscopicity of compound **13**, it was impossible to investigate it in more detail, except with X-ray diffraction experiments. Perchlorate complexes **14**–**19** were synthesized by reacting metal(II) perchlorate and the corresponding ligand in organic solvents under elevated conditions. Similar to azide complexes **8**–**10**, it is possible to precipitate (per)chlorate compounds **11** and **15**–**19** by using a minimum amount of solvent during the reaction. While the reaction of **2** with manganese(II), zinc(II), and iron(II) perchlorates did not lead to the formation of single crystals, it was possible to successfully incorporate ligand **3**. Nevertheless, it was not feasible to obtain pure samples of **20**–**22** for elemental analysis and they were only investigated using X-ray diffraction experiments.

Crystal structures

All ECC (**4**–**22**) and the ligand 1-cyclopropyl-5*H*-tetrazole (**1**) were characterized by low-temperature X-ray diffraction experiments. Due to the liquid state of **2** and **3** under ambient conditions,



Scheme 2 Synthesis of coordination compounds **4**–**22**.

 This journal is © The Royal Society of Chemistry and the Centre National de la Recherche Scientifique 2021

Published on 29 April 2021. Downloaded by Ludwig Maximilians Universitaet Muenchen on 3/6/2022 8:27:05 AM.

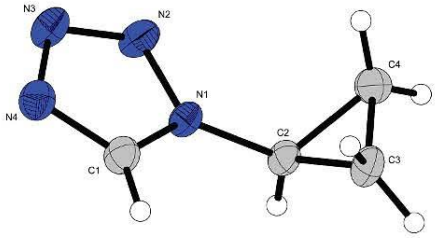


Fig. 4 Crystal structure of 1-cyclopropyl-5*H*-tetrazole (**1**). Selected bond lengths (Å): N1–N2 1.354(3), N2–N3 1.304(3), N3–N4 1.373(3), N1–C1 1.334(3), N1–C2 1.448(3), N4–C1 1.315(3), C2–C4 1.491(4), and C3–C4 1.500(4). Selected bond angles (°): N2–N1–C1 108.32(19), N2–N1–C2 122.2(2), C1–N1–C2 129.4(2), N1–N2–N3 106.2(2), N2–N3–N4 110.63(19), N3–N4–C1 105.3(2), N1–C1–N4 109.6(2), N1–C2–C4 118.5(2), and C2–C3–C4 59.76(18).

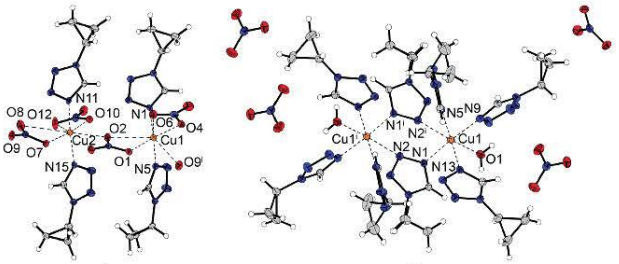


Fig. 5 Dimeric units of **4** and **5**. Selected bond lengths of **4** (Å): Cu1–O1 1.973(4), Cu1–O2 2.687(4), Cu1–N1 1.984(5), Cu1–N5 1.991(5), Cu1–O9^{i} 2.543(4). Selected bond angles of **4** (°): O1–Cu1–O2 52.93(15), O1–Cu1–O4 170.72(18), O1–Cu1–O6 133.52(18), O1–Cu1–N1 89.3(2), O1–Cu1–N5 91.9(2), O1–Cu1–O9^{i} 81.90(15), O2–Cu1–O4 135.97(16), O2–Cu1–N1 88.41(19), N1–Cu1–N5 174.6(2), O9^{i}–Cu1–N1 110.0(2). Symmetry code of **4**: (i) 0.5 + *x*, 1.5 − *y*, *z*. Selected bond lengths of **5** (Å): Cu1–O1 2.2353(17), Cu1–N1 2.023(2), Cu1–N13 1.991(2), Cu1–N2^{i} 2.5321(18). Selected bond angles of **5** (°): O1–Cu1–N1 87.62(8), O1–Cu1–N2^{i} 176.18(7), N1–Cu1–N5 91.01(8), N1–Cu1–N9 175.32(7), N1–Cu1–N13 89.49(8). Symmetry code of **5**: (i) 1 − *x*, 1 − *y*, −*z*.

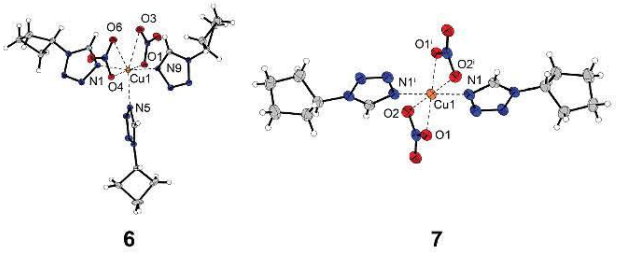


Fig. 6 Molecular units of **6** and **7**. Selected bond lengths of **6** (Å): Cu1–O1 1.998(2), Cu1–O3 2.702(2), Cu1–N5 2.216(2), Cu1–N9 2.011(2). Selected bond angles of **6** (°): O1–Cu1–O3 52.46(7), O1–Cu1–O4 177.24(8), O1–Cu1–O6 128.80(7), O1–Cu1–N1 90.24(9), O3–Cu1–O6 76.34(7), O3–Cu1–N1 85.49(8), O3–Cu1–N5 141.15(7), N1–Cu1–N5 95.63(9), N1–Cu1–N9 168.66(9). Selected bond lengths of **7** (Å): Cu1–O1 1.996(3), Cu1–O2 2.588(2), Cu1–N1 1.964(3). Selected bond angles of **7** (°): O1–Cu1–O2 54.89(8), O1–Cu1–N1 89.08(11), O1–Cu1–O2^{i} 125.11(8). Symmetry code of **7**: (i) 1 − *x*, 1 − *y*, −*z*.

no single crystals could be obtained. Additionally, the SCO compound $[Fe(C_3tz)_6](ClO_4)_2$ was measured at low temperature (**15a**) as well as room temperature (**15b**) to further investigate the influence of electron multiplicity. The measurement and refinement data of all compounds together with details on the crystal structures of compounds **9**, **10**, **14**–**17**, **21**, and **22** are given in the ESI† (Tables S1–S6 and Fig. S6–S14) and all crystal datasets were deposited with the CSD database.[33] CCDC 2061069 (**1**), 2061078 (**4**), 2061087 (**5**), 2061071 (**6**), 2061075 (**7**), 2061086 (**8**), 2061084 (**9**), 2061085 (**10**), 2061081 (**11**), 2061079 (**12**), 2061076 (**13**), and 2061073 (**14**), 2061074 (**15a**), 2061089 (**15b**), 2061072 (**16**), 2061077 (**17**), 2061080 (**18**), 2061070 (**19**), 2061082 (**20**), 2061088 (**21**), and 2061083 (**22**).†

Ligand **1** crystallizes as colourless platelets in the monoclinic space group $P2_1$ with two formula units per unit cell and a calculated density of 1.409 g cm^{-3} at 112 K (Fig. 4). Comparing the crystal structure of **1** with the one of cyclopropylamine reveals similar bond lengths and angles within the cyclopropane ring and the attached nitrogen atom (Table S7, ESI†).[34]

Bond lengths and bond angles of the coordinating ligands are in the same range as in the noncoordinating C_3tz and are therefore not a part of the discussion in any of the following complex compounds. In general, ligands **1**–**3** show no bridging behaviour in transition metal complexes and coordinate exclusively *via* the nitrogen atom at the 4th position of the ring. The only exceptions are copper(II) complex compounds **5**, **15**, and **16** in which the tetrazole ring additionally binds *via* the N atom of the 3rd position of the ring.

Comparing the crystal structures of copper(II) nitrate complexes **4**–**7** reveals very diverse and interesting coordination geometries. While the anions are non-binding in compound **5**, they are didentate in **6** as well as in **7**, and in **4** they form up to three bonds with two central metals. The bridging of the nitrato ligands in complex **4** leads to polymeric chains, whereas in **5** two tetrazole ligands form a link between the same two copper(II) centres forming dimers (Fig. 5).

The complex monomer of ECC **7** shows a strongly distorted octahedron, while in compound **6** it is an intensely twisted pentagonal bipyramid (Fig. 6) similar to complex **4**. They crystallize in monoclinic (**6** and **7**), orthorhombic (**4**), or triclinic (**5**) space groups and show densities between 1.585 and 1.775 g cm^{-3}.

All copper(II) azide complexes show a six-fold coordination around the metal centre. While **9** crystallizes in the monoclinic space group $P2_1/c$, **8** and **10** are present in the triclinic space group $P\bar{1}$. The density of the coordination compounds decreases with increasing carbon content in the complex (**8**: 1.863 g cm^{-3} at 102 K, **9**: 1.797 g cm^{-3} at 106 K, **10**: 1.775 g cm^{-3} at 112 K). The molecular units of the copper(II) azide complexes **8**–**10** all show an octahedral environment consisting of one copper(II) atom which is surrounded by five azides and one coordinating ligand (Fig. 7 and Fig. S6, S7, ESI†). The 1,1-bridging azides form polymeric copper chains, which are further cross-linked by the 1,1,3-azides leading to 2D layers. The binding nitrogen atoms of 1,1,3-azides underlay a Jahn–Teller distortion and in all complexes the *z*-axis is elongated to about 0.4–0.7 Å (**8**: Cu1–N7^{iii} 2.6322(15) Å; **9**: Cu1–N8^{ii} 2.686(3) Å, **10**: Cu1–N20 2.579(7) Å) compared to the remaining Cu–N bonds.

Published on 29 April 2021. Downloaded by Ludwig Maximilians Universitaet Muenchen on 3/6/2022 8:27:05 AM.

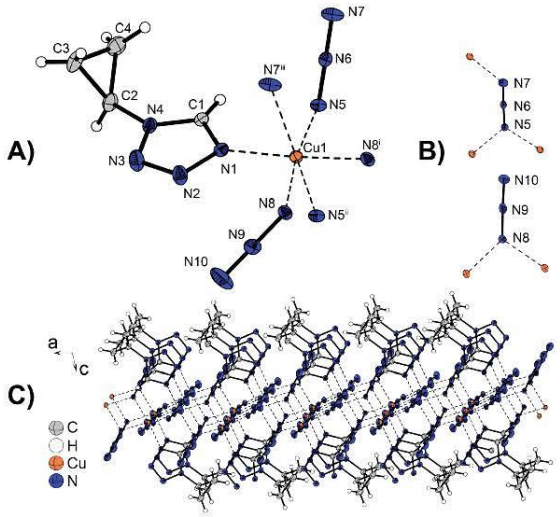


Fig. 7 (A) Coordination sphere around the copper(II) centre in **8**. Selected bond lengths (Å): Cu1–N1 2.0026(15), Cu1–N5 1.9812(16), Cu1–N5 2.216(2), Cu1–N9 2.011(2). Selected bond angles (°): N1–Cu1–N5 90.38(6), N1–Cu1–N8 97.86(6), N1–Cu1–N8^{i} 171.38(6), 84.11(6), N8–Cu1–N8^{i} 79.01(6). Symmetry codes: (i) $-x$, $1-y$, $1-z$, (ii) $1-x$, $1-y$, $1-z$, (iii) $1-x$, $2-y$, $1-z$. (B) Different coordination modes of the azide anion. (C) Polymeric layer of compound **8** viewed along the *b*-axis.

The (per)chlorate complexes of C_3tz (**11** and **14**–**17**) all crystallize isotypically in the trigonal space group $R\bar{3}$ showing similar cell axes, volumes, and densities preventing the Jahn–Teller distortion in the copper(II) compounds. In all structures, the central metals are octahedrally coordinated by six tetrazole ligands and the counterions are non-coordinating (Fig. 8 and Fig. S8–S12, ESI†). The metal–nitrogen bond lengths only differ slightly (**11** and **16**: Cu–N 2.13 Å; **14**: Mn–N 2.25 Å; **15b**: Fe–N 2.19 Å; **17**: Zn–N 2.16 Å;) and are almost identical to the literature values of *N*-hexacoordinated 3d metals with six equal bonds.[21,35]

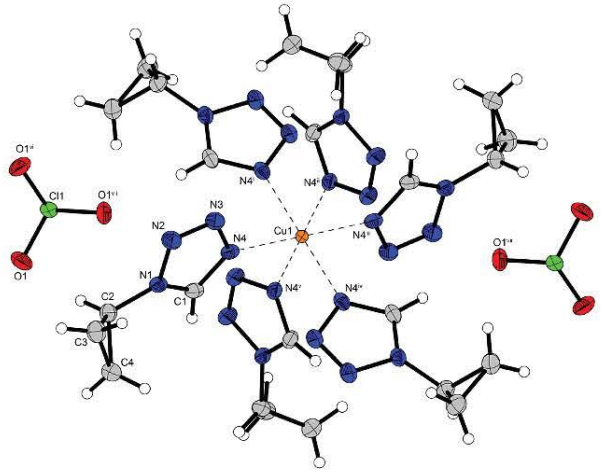


Fig. 8 Molecular unit of **11**. Selected bond length (Å): Cu1–N4 2.1277(17). Selected bond angles (°): N4–Cu1–N4^{ii} 91.09(6), N4–Cu1–N4^{iii} 180.00, N4–Cu1–N4^{v} 88.91(6). Symmetry codes: (i) y, $-x+y$, $1-z$, (ii) $-x+y$, $-x$, z, (iii) $-x$, $-y$, $1-z$, (iv) $-y$, $x-y$, z, (v) $x-y$, x, $1-z$, (vi) $1-x+y$, $1-x$, z, (vii) $1-y$, $x-y$, z, (viii) $-1+y$, $-x+y$, $1-z$.

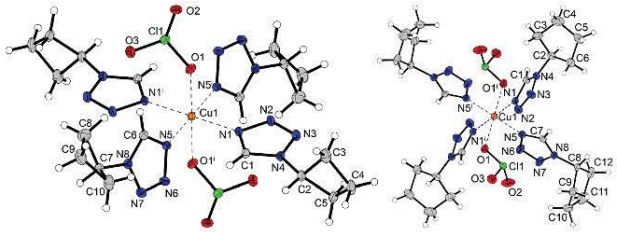


Fig. 9 Molecular units of **12** and **13**. Selected bond lengths of **12** (Å): Cu1–O1 2.4202(14), Cu1–N1 2.0274(18), Cu1–N5 2.0047(19). Selected bond angles of **12** (°): O1–Cu1–N1 88.87(7), O1–Cu1–N5 87.11(7), O1–Cu1–O1^{i} 180.00, O1–Cu1–N1^{i} 91.13(7). Symmetry code of **12**: (i) $2-x$, $1-y$, $1-z$. Selected bond lengths of **13** (Å): Cu1–O1 2.3700(13), Cu1–N1 2.0046(14), Cu1–N5 2.0231(15). Selected bond angles of **13** (°): O1–Cu1–N1 93.52(5), O1–Cu1–N5 90.44(5), O1–Cu1–O1^{i} 180.00, O1–Cu1–N1^{i} 86.49(5). Symmetry code of **13**: (i) $1-x$, $1-y$, $1-z$.

The shortening in the iron complex at lower temperatures (**15a**: Fe–N 2.01 Å) is a typical evidence for the SCO systems, revealing the high spin state under ambient conditions.[25,35]

Compared to chlorate complex **11**, the octahedrons in **12** and **13** are formed by four neutral tetrazole and two coordinating chlorato ligands (Fig. 9). Both ECC crystallize in the monoclinic space groups ($P2_1/c$ and $I2/a$, respectively) and the Jahn–Teller distortion can be found along the O–Cu–O axes. Despite the difference in the built-up of the octahedral coordination sphere, all three chlorate complexes have comparable densities (**11**: 1.527 g cm^{-3} at 127 K, **12**: 1.582 g cm^{-3} at 100 K, **13**: 1.534 g cm^{-3} at 127 K).

All other perchlorate ECC **18**–**22** based on ligands **2** and **3** are present as aqua species. Copper(II) complexes **18** and **19** show a similar coordination geometry to nitrate compound **5**. They consist of a dimeric unit of central atoms coordinated by four monodentate as well as two bidentate tetrazoles, and two aqua molecules (Fig. 10). They have a slightly higher density compared to **16** (**16**: 1.543 g cm^{-3} at 115 K, **18**: 1.576 g cm^{-3} at 111 K, **19**: 1.558 g cm^{-3} at 103 K). The O1–Cu1 bond (**18**: ~2.25 Å; **19**: ~2.35 Å) is elongated, as well as the opposing bond to the bridging tetrazole ligand (**18**: ~2.76 Å; **19**: ~2.50 Å), which can be explained by the Jahn–Teller distortion typical for copper(II) complexes.

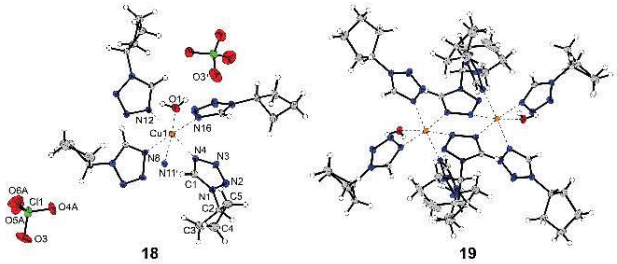


Fig. 10 Coordination sphere around the copper(II) centre in **18** and representation of the cationic dimeric unit of **19**. Selected bond lengths of **18** (Å): Cu1–O1 2.249(3), Cu1–N4 1.996(3), Cu1–N12 2.012(3), Cu1–N11^{i} 2.762(3). Selected bond angles of **18** (°): O1–Cu1–N4 97.52(13), O1–Cu1–N12 85.39(13), O1–Cu1–N16 91.69(13), O1–Cu1–N11^{i} 175.70(11). Symmetry code of **18**: (i) $1-x$, $-y$, $-z$.

 This journal is © The Royal Society of Chemistry and the Centre National de la Recherche Scientifique 2021

Published on 29 April 2021. Downloaded by Ludwig Maximilians Universitaet Muenchen on 3/6/2022 8:27:05 AM.

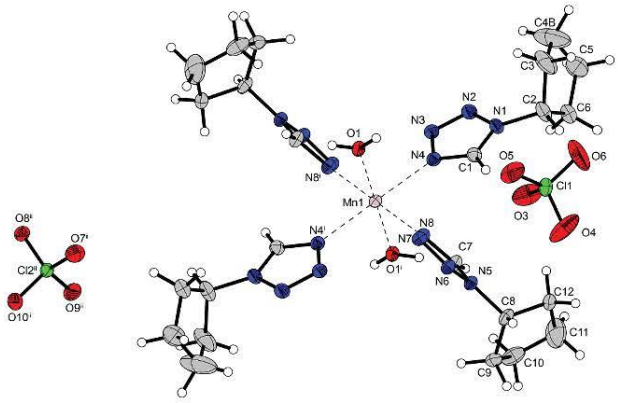


Fig. 11 Molecular unit of **20**. Selected bond lengths (Å): Mn1–O1 2.157(2), Mn1–N4 2.249(3), Mn1–N8 2.276(3). Selected bond angles (°): O1–Mn1–N4 88.01(10), O1–Mn1–N8 93.97(10), O1–Mn1–O1^{i} 180.00, O1–Mn1–N8^{i} 86.03(10). Symmetry codes of **18**: (i) $-x, 2-y, -z$, (ii) $2-x, 1-y, -z$.

While the Jahn–Teller distortion in **18** and **19** allows the formation of dimeric units, the manganese(II), zinc(II), and iron(II) complexes **20**–**22** with C_5tz ligands crystallize as dihydrates and show an identical structural built-up. Four tetrazole ligands and two coordinating water molecules form an octahedral environment around the metal centre and the complex monomers are completed by two noncoordinating perchlorate anions (Fig. 11 and Fig. S13, S14, ESI†).

The higher hydrophilicity of the manganese, iron, and zinc compounds could also be a reason for the failed synthesis of elemental pure complexes with C_4tz and C_5tz.

Sensitivities and thermal stability

All compounds, except **4**, **13**, and **20**–**22**, were investigated with regard to their temperature stability by differential thermal analysis (DTA) experiments with a heating rate of $\beta = 5$ °C min^{-1} in the range of 25–400 °C (Fig. S15–S19, ESI†). Critical points, such as melting, dehydration, or exothermic decomposition, are given as onset temperatures. Endothermic events were verified by using thermal gravimetric analysis (TGA) (Fig. S20–S22, ESI†). For initial safety testing, the impact (IS) and friction sensitivities (FS) as well as the sensitivities towards electrostatic discharge (ESD) of all ECC were examined according to BAM standards. All detailed values are listed in Table 1 together with the outcome of the compounds in hot plate and hot needle tests. All three ligands show similar thermal stabilities with decomposition temperatures close to 200 °C (**1**: 200 °C; **2** and **3**: 202 °C) and only **1** possesses an endothermic event at 42 °C, which is attributed to its melting point. Furthermore, the uncoordinated ligands are insensitive towards both impact (>40 J) and friction (>360 N). Compound **1** is also quite insensitive towards electrostatic discharge with 750 mJ. Since **2** and **3** are liquids, ESD measurements could not be performed.

In general, the sensitivities of the complexes can be perfectly tailored by using different combinations of cations and oxidizing or endothermic anions as well as the carbon content of the ligands.

Table 1 Stability of compounds against external stimuli and results of the hot plate and hot needle tests compared to ECC based on 1-propyl-5*H*-tetrazole (Ptz) and LA as well as RDX[1,31,32]

	IS[a] [J]	FS[b] [N]	ESD[c] [J]	T_{endo}[d] [°C]	T_{exo}[d] [°C]	HP[e]	HN[e]
C_3tz (**1**)	>40	>360	750	42	200	inf.	dec.
C_4tz (**2**)	>40	>360	—	—	202	inf.	dec.
C_5tz (**3**)	>40	>360	—	—	202	inf.	dec.
$[Cu_2(C_3tz)_8(H_2O)_2](NO_3)_4$ (**5**)	>40	>360	1000	71	150	def.	def.
$[Cu(C_4tz)_3(NO_3)_2]$ (**6**)	9	>360	90	—	160	dec.	dec.
$[Cu(C_5tz)_2(NO_3)_2]$ (**7**)	>40	>360	750	—	165	dec.	dec.
$[Cu(C_3tz)(N_3)_2]$ (**8**)	<1	5	37	—	149	def.	def.
$[Cu(C_4tz)(N_3)_2]$ (**9**)	2	60	50	—	148	def.	def.
$[Cu(C_5tz)(N_3)_2]$ (**10**)	5	216	76	—	145	def.	def.
$[Cu(C_3tz)_6](ClO_3)_2$ (**11**)	2	32	100	138	156	def.	dec.
$[Cu(C_4tz)_4(ClO_3)_2]$ (**12**)	5	36	200	126	153	def.	dec.
$[Mn(C_3tz)_6](ClO_4)_2$ (**14**)	5	216	90	188	206	def.	def.
$[Fe(C_3tz)_6](ClO_4)_2$ (**15**)	3	54	90	—	192	def.	def.
$[Cu(C_3tz)_6](ClO_4)_2$ (**16**)	4	80	480	174	183	def.	dec.
$[Zn(C_3tz)_6](ClO_4)_2$ (**17**)	6	144	250	188	201	def.	def.
$[Cu(C_4tz)_4(H_2O)](ClO_4)_2$ (**18**)	8	84	250	151	191	def.	dec.
$[Cu(C_5tz)_4(H_2O)](ClO_4)_2$ (**19**)	4	160	250	—	207	def.	dec.
$[Cu(N_3)_2(Ptz)]$[31]	2.5	10	112	—	148	n.d.	n.d.
$[Cu(Ptz)_6](ClO_3)_2$[32]	>40	168	960	111	152	dec.	dec.
$[Fe(Ptz)_6](ClO_4)_2$[32]	25	192	1220	—	202	dec.	dec.
$[Cu(Ptz)_6](ClO_4)_2$[32]	30	240	>1500	174	209	dec.	dec.
LA (RD-1333)	4	<0.1	5	—	315	det.	det.
RDX	7.4	120	200		204	def.	dec.

[a] Impact sensitivity according to BAM drop hammer test (method 1 of 6): insensitive > 40 J, less sensitive ≥ 35 J, sensitive ≥ 4 J, very sensitive ≤ 3 J. [b] Friction sensitivity according to BAM friction tester (method 1 of 6): insensitive > 360 N, less sensitive = 360 N, sensitive < 360 N and > 80 N, very sensitive ≤ 80 N, extremely sensitive ≤ 10 N. [c] Electrostatic discharge sensitivity (OZM Electric Spark XSpark10; method 1 of 6). [d] DTA onset temperatures at a heating rate of $\beta = 5$ °C min^{-1}; endothermic peak indicating melting or dehydration; exothermic peak indicating decomposition. [e] HP: hot plate test; HN: hot needle test; inf.: inflammation; dec.: decomposition; def.: deflagration; det.: detonation.

Water containing compound **5** as well as the other copper(II) nitrate coordination compounds **6** and **7** can be categorized as insensitive towards both friction (>360 N) and impact (>40 J), except $[Cu(C_4tz)_3(NO_3)_2]$ (**6**), which is sensitive towards both impact (9 J) and electrostatic discharge (90 mJ). The decomposition temperature increases from **5** to **7**. Water containing compound **5** shows the lowest exothermic event (**5**: 150 °C, **6**: 160 °C, **7**: 165 °C) and also shows an endothermic event at 71 °C, which is explained by the loss of crystal water. The trend of decreasing sensitivity with the increasing number of carbon atoms can be perfectly observed in the most sensitive and structurally identical copper(II) azide complexes **8**–**10** (Fig. 12). All of them are "very sensitive" towards impact (**8**: <1 J, **9**: 2 J, **10**: 5 J). $[Cu(C_3tz)(N_3)_2]$ (**8**) is

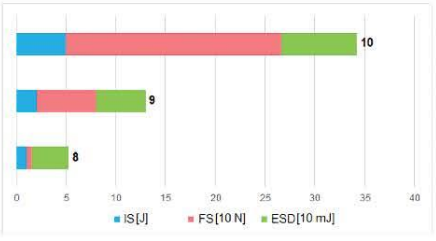


Fig. 12 Comparison of the sensitivities of the copper(II) azide complexes.

Published on 29 April 2021. Downloaded by Ludwig Maximilians Universitaet Muenchen on 3/6/2022 8:27:05 AM.

also "extremely sensitive" towards friction (5 N), whereas its C_4tz analog is "very sensitive" (60 N) and the C_5tz analog is solely "sensitive" (216 N). This observation continued in the ESD measurements (**8**: 37 mJ < **9**: 50 mJ < **10**: 76 mJ). Among the transition metal complexes, ECC **8** is the most sensitive one. Unlike the rising trend in sensitivity examinations, the decomposition temperature of the azide complexes decreases (**8**: 149 °C > **9**: 148 °C > **10**: 145 °C) with the increasing ring size of the alkyl substituent, and **10** shows the lowest exothermic decomposition temperature among all examined compounds.

Chlorate complexes **11** and **12** show relatively similar properties and can be classified as sensitive towards friction (**11**: 32 N, **12**: 36 N) and vary from sensitive to very sensitive towards impact (2–5 J). Their sensitivity towards electrostatic discharge differs by 100 mJ. The melting point (**11**: 138 °C > **12**: 126 °C) as well as the decomposition temperature (**11**: 156 °C > **12**: 153 °C) decreases from **11** to **12**. Except iron(II) perchlorate complex **15**, which is very sensitive against impact (3 J) and friction (54 N), all other perchlorate complexes can be considered as sensitive (4–8 J; 80 N–160 N). Most of the copper(II) coordination compounds show exothermic decomposition events in the range of 145–165 °C. The copper(II) perchlorates show the highest thermal stability with 183 °C (**16**) and 191 °C (**18**), whereby compound **19** (207 °C) has the highest decomposition temperature of all ECC, exceeding 200 °C. While ECC **16** (melting) and **18** (loss of aqua ligand) show endothermic events during the DTA experiments, monohydrate **19** solely shows an exothermic one. Nevertheless, investigations by TGA prove the loss of the aqua ligands in **18** and **19** as well as presence of a melting event in **16** (Fig. 13). Furthermore, the endothermic events of **14** and **17** at 188 °C proceed without loss of weight which was also verified by thermal gravimetric analysis (TGA). The thermal stabilities of metal(II) C_3tz perchlorate complexes increase in the following order: Cu^{2+} (183 °C) < Fe^{2+} (192 °C) < Zn^{2+} (201 °C) < Mn^{2+} (206 °C), which is in accordance with our previous findings,[21,36] the cyclopropyl complexes **8**, **11**, **15**, and **16** can be compared to the analogous ECC based on the open chain ligand 1-propyl-5*H*-tetrazole (PTz), $[Cu(N_3)_2(Ptz)]$, $[Cu(Ptz)_6](ClO_3)_2$, $[Fe(Ptz)_6](ClO_4)_2$, and $[Cu(Ptz)_6](ClO_4)_2$, which were all already investigated in the literature.[31,32] It becomes clear that the additional ring strain of the ligand C_3tz drastically increases the energetic properties, which can be seen from the sensitivities as well as the hot plate and hot needle tests. Furthermore, the thermal stability is similar (**8** and **11**) or only slightly decreased (**15** and **16**) compared to the compounds based on Ptz (Table 1).

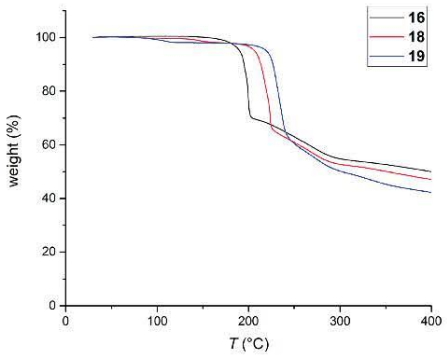


Fig. 13 TGA curves of copper(II) perchlorate complexes **16**, **18**, and **19**.

Energetic properties

To investigate the behaviour of the complexes towards fast heating with and without confinement, hot plate and hot needle tests were performed for all prepared ECC, except **4**, **13**, and **20–22**. Hot needle tests were performed by fixing a small amount of the product on a copper plate with tape and touching it with the tip of a hot needle. Detonation of the compound is an indicator of its capability as a primary explosive. The hot-plate test is a good method to investigate the behaviour of the unconfined product towards heating on a hot plate. However, this test does not necessarily give conclusion about the suitability as primary explosives. Most of the complexes show deflagrations with varying intensities during both test setups (Fig. S23–S30, ESI†). The most vigorous reaction can be observed in the case of azide complex **8** (Fig. 14), which is also the most sensitive compound.

Again, the energetic properties can be adapted through the different combinations of the building blocks and the performance slightly decreases with the increasing amounts of carbon content, which can be seen in nitrate compounds **5–7**. While **5**, based on the ligand C_3tz, shows deflagrations during both HN and HP tests, **6** and **7** only decompose. Nevertheless, none of the ECC possess a deflagration-to-detonation transition, which would make it a suitable primary explosive.

Magnetic properties

Compound **15** exhibits a thermochromic effect upon cooling with liquid nitrogen as demonstrated in Fig. S31 (ESI†). To investigate the exact nature of the underlying mechanism, we investigated its magnetic properties. Fig. 15 indicates the paramagnetic behaviour of $[Fe(C_3tz)_6](ClO_4)_2$ with an effective magnetic moment of μ_{eff} = 5.389(3) μ_B for T > 225 K. This is somewhat in line with an expected HS-Fe^{2+} with a theoretical value of μ_{eff} = 4.90 μ_B.

This discrepancy is explained by a slow oxidation process of the sample towards HS-Fe^{3+} (μ_{eff} = 5.92 μ_B) as well as an incomplete extinction of the angular momentum. A fully contributing angular momentum would result in μ_{eff} = 6.70 μ_B for Fe^{2+}. For temperatures T < 225 K, the magnetic susceptibility deviates from the Curie–Weiss law which is facilitated through a spin-crossover from the HS state ($t_{2g}^4 e_g^2$, $^5T_{2g}$, S = 2) to the diamagnetic LS state ($t_{2g}^6 e_g^0$, $^1A_{1g}$, S = 0). The turning point of the curve at 172 K is defined as the onset of the spin-crossover with a maximum extent reached at T = 100 K ($\chi_{mol} \approx 0$). An analogous behaviour has been observed *via* temperature-dependent PXRD in the



Fig. 14 Hot plate (left) and hot needle (right) tests of azide complex **8**.

 This journal is © The Royal Society of Chemistry and the Centre National de la Recherche Scientifique 2021

Published on 29 April 2021. Downloaded by Ludwig Maximilians Universitaet Muenchen on 3/6/2022 8:27:05 AM.

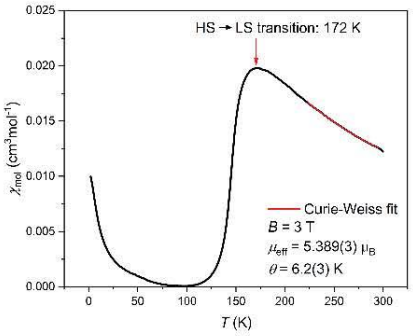


Fig. 15 Molar magnetic susceptibility of $[Fe(C_3tz)_6](ClO_4)_2$ as a function of temperature at a field strength of B = 3 T. The Curie–Weiss fit (red) indicates an effective magnetic moment of μ_{eff} = 5.389(3) μ_B for T > 225 K.

related compound $[Fe(Ptz)_6](BF_4)_2$, although at lower temperatures (130 K).[37] The subsequent increase in magnetic susceptibility is again attributed to some proportion of Fe^{3+}. The magnetization isotherms shown in Fig. S32 (ESI†) exhibit purely paramagnetic behaviour at 300 K and a reduced magnetic moment at 2 K most likely originating from Fe^{3+} with some hint of saturation.

Conclusions

In this research work, the synthesis of the three 5*H*-tetrazole-based ligands, 1-cyclopropyl-5*H*-tetrazole (C_3tz, **1**), 1-cyclobutyl-5*H*-tetrazole (C_4tz, **2**), and 1-cyclopentyl-5*H*-tetrazole (C5tz, **3**), is described. For the first time, the previously unknown synthesis of C_4tz (**2**) is presented in this work, which completes the series of *N*-cycloalkyl-substituted tetrazole ligands, and it was possible to obtain the single crystal structure of C_3tz. The tetrazole derivatives were characterized by various analytical methods, including elemental analysis, ^1H and ^{13}C as well as superior ^1H–^{15}N-HMBC NMR spectroscopies and infrared spectroscopy. Furthermore, the thermal stability of the heterocycles was determined by DTA analysis ($T_{exo} \geq$ 200 °C), and sensitivity measurements according to BAM standards were used to classify them as insensitive. In order to tune the energetic properties of new energetic coordination compounds, the ligands were incorporated in 19 complexes based on various central metal atoms (Cu^{2+}, Fe^{2+}, Mn^{2+}, Zn^{2+}) and a variety of anions, such as nitrates, azides, and (per)chlorates. The ECC were thoroughly characterized and all coordination compounds were investigated by low-temperature single-crystal experiments revealing very diverse and fascinating coordination geometries highly depending on the used ligand and anion systems. In general, **1**–**3** coordinate solely *via* the N4 atoms of their tetrazole ring, whereas in the case of copper(II) complexes **5**, **18**, and **19**, they additionally bind *via* the N3 atom, leading to the formation of dimers of two copper(II) centres. Furthermore, $[Cu_2(C_3tz)_4(NO_3)_4]$ (**4**) and $[Cu(C_4tz)_3(NO_3)_2]$ (**6**) show very unusual and strongly distorted pentagonal-bipyramidal coordination spheres. The different assemblies of the three building blocks allow for the synthesis of anhydrous energetic materials with a full range of sensitivities. While copper azide complex **8** ($[Cu(C_3tz)(N_3)_2]$) shows sensitivities of a primary explosive (extremely sensitive), nitrate compound **7** is completely insensitive against impact and friction. Furthermore, the stability against external stimuli can be optimized by the carbon content of the ligands. The investigated complexes possess thermal stabilities above 145 °C, and $[Mn(C_3tz)_6](ClO_4)_2$ (**14**) and $[Cu(C_5tz)_4(H_2O)](ClO_4)_2$ (**19**) show exothermic decomposition temperatures above 200 °C even exceeding the one for the pure ligand. Compared to the open chain ligand, 1-propyl-5*H*-tetrazole, the C_3tz-based complexes show increased energetic properties while at the same time similar thermal stabilities. These results prove the benefits of cycloalkyl-substituted tetrazole ligands with higher ring strain and their ability to adjust the properties of the resulting complexes. Furthermore, a new iron(II) SCO complex was synthesized and investigated with regard to the correlation between the spin-state change of a transition metal complex and its crystal structure. At $T_{1/2}$ = 172 K, an HS-LS spin-crossover transition could be observed accompanied by a visible colour change from violet to colourless. The successful characterization of **15** revealed an interesting candidate for future SCO research, and it was possible to determine the crystal structure of both the HS and the LS species.

Conflicts of interest

There are no conflicts to declare.

Acknowledgements

The authors are grateful for the financial support of this work by Ludwig Maximilian University Munich. The authors want to thank Prof. Dr Thomas M. Klapötke for providing research infrastructure and for his scientific input, as well as Prof. Dr Dirk Johrendt for his support with the magnetic measurements.

References

1 T. M. Klapötke, *Chemistry of High-Energy Materials*, De Gruyter, Berlin, 5th edn, 2019.
2 T. Curtius, *Chem. Ber.*, 1891, **24**, 3345–3346.
3 T. M. Klapötke and N. Mehta, *Propellants, Explos., Pyrotech.*, 2014, **39**, 7–8.
4 http://echa.europa.eu/de/candidate-list-table, (accessed January 2021).
5 J. W. Fronabarger, M. D. Williams, W. B. Sanborn, J. G. Bragg, D. A. Parrish and M. Bichay, *Propellants, Explos., Pyrotech.*, 2011, **36**, 541–550.
6 Y. Tang, K. Li, A. K. Chinnam, R. J. Staples and J. M. Shreeve, *Dalton Trans.*, 2021, **50**, 2143–2148.
7 A. A. Larin, D. M. Bystrov, L. L. Fershtat, A. A. Konnov, N. N. Makhova, K. A. Monogarov, D. B. Meerov, I. N. Melnikov, A. N. Pivkina, V. G. Kiselev and N. V. Muravyev, *Molecules*, 2020, **25**, 5836.
8 R. V. Kent, T. P. Vaid, J. A. Boissonnault and A. J. Matzger, *Dalton Trans.*, 2019, **48**, 7509–7513.

Published on 29 April 2021. Downloaded by Ludwig Maximilians Universitaet Muenchen on 3/6/2022 8:27:05 AM.

9 M. L. Gettings, M. T. Thoenen, E. F. C. Byrd, J. J. Sabatini, M. Zeller and D. G. Piercey, *Chem. – Eur. J.*, 2020, **26**, 14530–14535.
10 M. H. H. Wurzenberger, J. T. Lechner, M. Lommel, T. M. Klapötke and J. Stierstorfer, *Propellants, Explos., Pyrotech.*, 2020, **45**, 898–907.
11 N. Lease, L. M. Kay, G. W. Brown, D. E. Chavez, P. W. Leonard, D. Robbins and V. W. Manner, *Cryst. Growth Des.*, 2019, **19**, 6708–6714.
12 R. Haiges, G. Belanger-Chabot, S. M. Kaplan and K. O. Christe, *Dalton Trans.*, 2015, **44**, 7586–7594.
13 G. Singh and S. P. Felix, *J. Hazard. Mater.*, 2002, **90**, 1–17.
14 Q. Sun, X. Li, C. Bamforth, Q.-H. Lin, M. Murugesu and M. Lu, *Sci. China Mater.*, 2020, **63**, 1779–1787.
15 Gas phase enthalpies of formation were calculated using the atomization method $\{\Delta_f H_{(g,M)}{}^0 = H_{(M)} - \Sigma H_{(A)}{}^0 + \Sigma \Delta_f H_{(A)}{}^0\}$ using Gaussian09 computed CBS-4M electronic enthalpies.
16 H. Tang, Z. Zhou, Z. Li, S. Chen, L. Wang and T. Zhang, *J. Energ. Mater.*, 2021, **39**, 23–32.
17 K. Nosratzadegan, M. Mahdavi, K. Ghani and K. Barati, *Propellants, Explos., Pyrotech.*, 2019, **44**, 830–836.
18 M. H. H. Wurzenberger, B. R. G. Bissinger, M. Lommel, M. S. Gruhne, N. Szimhardt and J. Stierstorfer, *New J. Chem.*, 2019, **43**, 18193–18202.
19 J.-G. Xu, S.-J. Lin, X.-Z. Li, H.-F. Wu, J. Lu, W.-F. Wang, J. Chen, F.-K. Zheng and G.-C. Guo, *Chem. Eng. J.*, 2020, **390**, 124587.
20 Q. Sun, X. Li, Q. Lin and M. Lu, *J. Mater. Chem. A*, 2019, **7**, 4611–4618.
21 N. Szimhardt, M. H. H. Wurzenberger, A. Beringer, L. J. Daumann and J. Stierstorfer, *J. Mater. Chem. A*, 2017, **5**, 23753–23765.
22 S. V. Voitekhovich, A. N. Vorobev, P. N. Gaponik and O. A. Ivashkevich, *Chem. Heterocycl. Compd.*, 2005, **41**, 999–1004.
23 T. Boonprab, S. J. Lee, S. G. Telfer, K. S. Murray, W. Phonsri, G. Chastanet, E. Collet, E. Trzop, G. N. L. Jameson, P. Harding and D. J. Harding, *Angew. Chem., Int. Ed.*, 2019, **58**, 11811–11815.
24 G. Aromí, L. A. Barrios, O. Roubeau and P. Gamez, *Coord. Chem. Rev.*, 2011, **255**, 485–546.
25 O. Roubeau, M. Evangelistia and E. Natividad, *Chem. Commun.*, 2012, **48**, 7604–7606.
26 G. Molnár, L. Salmon, W. Nicolazzi, F. Terkib and A. Bousseksou, *J. Mater. Chem. C*, 2014, **2**, 1360–1366.
27 K. Madeja and E. König, *J. Inorg. Nucl. Chem.*, 1963, **25**, 377–385.
28 G. Aromí, L. A. Barrios, O. Roubeau and P. Gamez, *Coord. Chem. Rev.*, 2011, **255**, 485–546.
29 A. A. Soliman, M. M. Khattab, M. Reissner, P. Weinberger, F. Werner and W. Linert, *Inorg. Chim. Acta*, 2007, **360**, 3987–3996.
30 N. Hassan, P. Weinberger, F. Kubel, G. Molnar, A. Bousseksou, L. Dlhan, R. Boča and W. Linert, *Inorg. Chim. Acta*, 2009, **362**, 3629–3636.
31 M. H. H. Wurzenberger, M. Lommel, M. S. Gruhne, N. Szimhardt and J. Stierstorfer, *Angew. Chem., Int. Ed.*, 2020, **59**, 12367–12370.
32 M. H. H. Wurzenberger, S. M. J. Endraß, M. Lommel, T. M. Klapötke and J. Stierstorfer, *ACS Appl. Energy Mater.*, 2020, **3**, 3798–3806.
33 Crystallographic data for the structures has been deposited with the Cambridge Crystallographic Data Centre.
34 P. Lozano-Casal, D. R. Allan and S. Parsons, *Acta Crystallogr., Sect. B: Struct. Sci.*, 2005, **61**, 717–723.
35 R. Eßmann, G. Kreiner, A. Niemann, D. Rechenbach, A. Schmieding, T. Sichla, U. Zachwieja and H. Jacobs, *Z. Anorg. Allg. Chem.*, 1996, **622**, 1161–1166.
36 M. H. H. Wurzenberger, M. S. Gruhne, M. Lommel and J. Stierstorfer, *Propellants, Explos., Pyrotech.*, 2021, **46**, 207–213.
37 L. Wiehl, H. Spiering, P. Guetlich and K. Knorr, *J. Appl. Crystallogr.*, 1990, **23**, 151–160.

 This journal is © The Royal Society of Chemistry and the Centre National de la Recherche Scientifique 2021

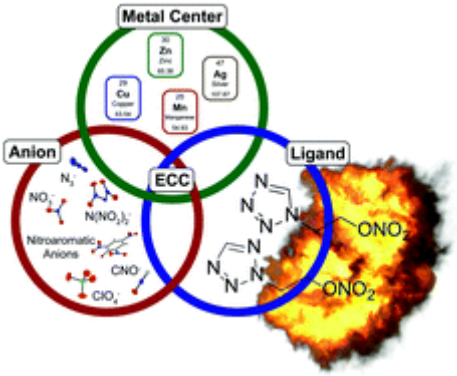
Appendix 25

Nitratoethyl-5H-tetrazoles: Improving Oxygen Balance through Application of Organic Nitrates in Energetic Coordination Compounds

M. Gruhne, T. Lenz, M. Rösch, M. Lommel, M. H. H. Wurzenberger, T. M. Klapötke, J. Stierstorfer

Dalton Trans. **2021**, *50*, 10811–10825,

https://doi.org/10.1039/D1DT01898A



Supplementary Information:
https://www.rsc.org/suppdata/d1/dt/d1dt01898a/d1dt01898a1.pdf

Published on 29 June 2021. Downloaded by Ludwig Maximilians Universitaet Muenchen on 2/16/2022 8:09:47 AM.

Ermittlung der Explosionsgefährlichkeit, hier der Schlagempfindlichkeit mit dem Fallhammer, Nov. 8th, 2002; (*d*) NATO standardization agreement (STANAG) on explosive, friction sensitivity tests, no. 4487, 1st edn., Aug. 22nd, 2002; (*e*) WIWEB-Standardarbeitsanweisung 4-5.1.03, Ermittlung der Explosionsgefährlichkeit oder der Reibeempfindlichkeit mit dem Reibeapparat, Nov. 8th, 2002.

23 (*a*) M. J. Turner, J. J. McKinnon, S. K. Wolff, D. J. Grimwood, P. R. Spackman, D. Jayatilaka and M. A. Spackman, *CrystalExplorer17*, University of Western Australia, 2017; (*b*) M. A. Spackman and D. Jayatilaka, *CrystEngComm*, 2009, **11**, 19–32.

24 (*a*) C. Zhang, X. Xue, Y. Cao, Y. Zhou, H. Li, J. Zhou and T. Gao, *CrystEngComm*, 2013, **15**, 6837–6844; (*b*) Y. Ma, A. Zhang, X. Xue, D. Jiang, Y. Zhu and C. Zhang, *Cryst. Growth Des.*, 2014, **14**, 6101–6114.

25 J. G. Reynolds, P. C. Hsu, G. A. Hust, S. A. Strout and H. K. Springer, *Propellants, Explos., Pyrotech.*, 2017, **42**, 1303–1308.

26 M. Sućeska, *EXPLO5 Version 6.05 User's Guide*, OZM, Zagreb, Croatia, 2018.

27 N. Szimhardt, M. H. H. Wurzenberger, A. Beringer, L. J. Daumann and J. Stierstorfer, *J. Mater. Chem. A*, 2017, **5**, 23753–23765.

28 N. Szimhardt, M. H. H. Wurzenberger, L. Zeisel, M. S. Gruhne, M. Lommel and J. Stierstorfer, *J. Mater. Chem. A*, 2018, **6**, 16257–16272.

29 M. H. H. Wurzenberger, B. R. G. Bissinger, M. Lommel, M. S. Gruhne, N. Szimhardt and J. Stierstorfer, *New J. Chem.*, 2019, **43**, 18193–18202.

30 M. S. Gruhne, M. H. H. Wurzenberger, M. Lommel and J. Stierstorfer, *Chem. Eur. J.*, 2021, **27**, 9112–9123.

31 M. H. H. Wurzenberger, N. Szimhardt and J. Stierstorfer, *J. Am. Chem. Soc.*, 2018, **140**, 3206–3209.

32 M. H. H. Wurzenberger, M. Lommel, M. S. Gruhne, N. Szimhardt and J. Stierstorfer, *Angew. Chem.*, 2020, **59**, 12367–12370.

33 M. H. H. Wurzenberger, M. S. Gruhne, M. Lommel, V. Braun, N. Szimhardt and J. Stierstorfer, *Inorg. Chem.*, 2020, **59**, 17875–17879.

34 Crystallographic data for the structures have been deposited with the Cambridge Crystallographic Data Centre.

35 T. Lenz, T. M. Klapötke, M. Mühlemann and J. Stierstorfer, *Propellants, Explos., Pyrotech.*, 2021, **46**, 723–731.

36 T. Ohtake, S. Date, K. Ikeda and Y. Shiraishi, *Sci. Technol. Energ. Mater.*, 2015, **76**, 39–41.

37 (*a*) L. M. Foroughi, R. A. Wiscons, D. R. Du Bois and A. J. Matzger, *Chem. Commun.*, 2020, **56**, 2111–2114; (*b*) M. K. Bellas and A. J. Matzger, *Angew. Chem., Int. Ed.*, 2019, **58**, 17185–17188.

38 T. M. Klapötke, *Energetic Materials Encyclopedia*, De Gruyter, Berlin, Boston, 2nd edn, 2021.

39 OZM Research, http://www.ozm.cz/en, (accessed May 2021).

40 Military Standard 1751A (MIL-STD-1751A): safety and performance tests for qualification of explosives (high explosives, propellants and pyrotechnics), method 1016, Dec. 11st, 2001.

41 M. S. Gruhne, M. Lommel, M. H. H. Wurzenberger, N. Szimhardt, T. M. Klapötke and J. Stierstorfer, *Propellants, Explos., Pyrotech.*, 2020, **45**, 147–153.

42 T. W. Myers, J. A. Bjorgaard, K. E. Brown, D. E. Chavez, S. K. Hanson, R. J. Scharff, S. Tretiak and J. M. Veauthier, *J. Am. Chem. Soc.*, 2016, **138**, 4685–4692.

43 M. A. Ilyushin, A. A. Kotomin and S. A. Dushenok, *Russ. J. Phys. Chem. B*, 2019, **13**, 119–138.

Published on 29 June 2021. Downloaded by Ludwig Maximilians Universitaet Muenchen on 2/16/2022 8:09:47 AM.

Dalton Transactions

ROYAL SOCIETY OF CHEMISTRY

PAPER

View Article Online
View Journal | View Issue

Check for updates

Cite this: *Dalton Trans.*, 2021, **50**, 10811

Nitratoethyl-5*H*-tetrazoles: improving the oxygen balance through application of organic nitrates in energetic coordination compounds†

Michael S. Gruhne, Tobias Lenz, Markus Rösch, Marcus Lommel, Maximilian H. H. Wurzenberger, Thomas M. Klapötke and Jörg Stierstorfer *

1- and 2-Nitratoethyl-5*H*-tetrazole (1-NET and 2-NET) were prepared through nitration of the respective alkyl alcohol using 100% nitric acid. A mixture of 1- and 2-hydroxyethyl-5*H*-tetrazole was obtained after alkylation of 1,5*H*-tetrazole. Also, a one-pot synthesis of 1-hydroxyethyl-5*H*-tetrazole was developed enabling the selective preparation of 1-NET. Both organic nitrates were characterized by ^{1}H, ^{13}C, and ^{1}H–^{15}N HMBC NMR spectroscopy. In addition, calculations using the Hirshfeld method and the EXPLO5 code were performed. Principally, 20 energetic coordination compounds involving the d-metals Mn, Cu, Zn, and Ag, each structurally characterized by low temperature single crystal X-ray diffraction, were prepared based on 1-NET and 2-NET. Of these complexes, 18 were obtained as pure bulk materials, and therefore, characterized for impact, friction, and ball drop impact sensitivity, as well as electrostatic discharge and thermal stability using differential thermal analysis. Hot plate and hot needle tests were performed mostly showing strong deflagrations making the complexes candidates for green combustion catalysts. Furthermore, successful PETN initiation experiments were carried out for several complexes and all ECCs were investigated by laser ignition experiments.

Received 9th June 2021,
Accepted 29th June 2021

DOI: 10.1039/d1dt01898a

rsc.li/dalton

Introduction

Ever since the first energetic materials were discovered, research is focused on the improvement of their properties. The explosives widely used today are tailored to specific applications in terms of power, sensitivity, and stability while being cost efficient.[1] In recent years, there has been a worldwide increase in the demand for environmentally friendly and sustainable materials in every area, including the field of energetic materials.[2] Additionally, regulations such as the REACH directive of the European Union or similar regulations of the US Environmental Protection Agency put pressure on the search for suitable substitutes. In the field of primary explosives commonly used, heavy metal-based lead azide and lead styphnate are harming users and the environment especially when utilized over a long time.[3] These two lead salts are therefore classified as substances of very high concern (SVHCs).[4]

In the search for new compounds, great attention is now paid to an environmentally friendly production chain while still having a cost-efficient synthesis and long-term stability.[5] The nitrogen-rich tetrazole moiety has proven to be a chameleon for energetic materials.[6] The simplest representative, 1,5*H*-tetrazole, shows sensitivity toward impact due to its high nitrogen content of 80%, but is also a common reactant due to its straightforward preparation.[7] Regarding its derivatives, 1-ethyl-5*H*-tetrazole[8] has proven to be a suitable building block. This structural element has already been successfully used for the introduction of various energetic groups, such as an azido[9] or trinitromethyl group.[10] The synthesis of haloethyl[11] and hydroxyethyl[9] tetrazole has also been described. An overview on the 1-ethyl-5*H*-tetrazole derivatives, already known in the literature together with unknown representatives of this group, is presented in Chart 1.

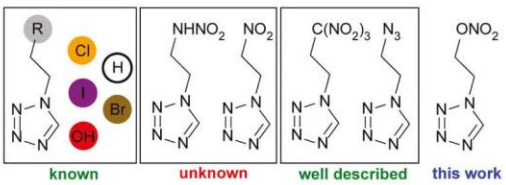


Chart 1 Outline on the tetrazole derivatives based on 1-ethyl-5*H*-tetrazole.[8–11] Corresponding 2-ethyl-5*H*-tetrazoles and especially 2-nitratoethyl-5*H*-tetrazole, which is also a part of this work, are not shown here.

Department of Chemistry, Ludwig-Maximilian University of Munich, Butenandtstr. 5-13, D-81337 Munich, Germany. E-mail: jstch@cup.uni-muenchen.de; Fax: +49-89-2180-77007http://www.hedm.cup.uni-muenchen.de

† Electronic supplementary information (ESI) available. CCDC 2080666–2080685. For ESI and crystallographic data in CIF or other electronic format see DOI: 10.1039/d1dt01898a

Published on 29 June 2021. Downloaded by Ludwig Maximilians Universitaet Muenchen on 2/16/2022 8:09:47 AM.

The ethylene group is favourable because of its easy accessibility from ethylamine hydrochlorides or halides. These starting materials are usually available for purchase at low cost and, with the exception of the trinitromethyl derivative, make the compounds shown in Chart 1 easily accessible.[8–11]

The reason for the preparation of functionalized tetrazoles is not just to fulfil the need for more nitrogen-rich compounds. They also help to further explore the concept of energetic coordination compounds (ECCs). The aim here is to adjust the properties of the resulting complex as desired by varying the parameters of the central metal, anion, or ligand.[12] A variation of the substitute on the alkyl chain of the 1-ethyl-5*H*-tetrazole building block, for example, affects the solubility, performance, and thermal stability of ECCs. In every case, the anion and central metal (here Mn, Cu, Zn, and Ag) also influence the complex's behaviour. However, in this work, focus is placed on the introduction of an organic nitrate function into the building block to study its effects on the coordination compound.

Organic nitrates are useful for lowering the water solubility of compounds, while increasing the oxygen balance.[13] As of today, only two tetrazole derivatives with a nitratoethyl group at the N1 position are known.[14,15] Both molecules, displayed in Chart 2, are not suitable for use as ligands in promising ECCs. The amino group in the structure on the left, for example, leads to sterically demanding coordination geometries likely leading to the inclusion of aqua ligands and lowering the performance.[16] Nitrimino groups on the other hand are highly acidic, making them more likely to serve as anionic ligands.[15,17]

Therefore, in this work, focus was placed on the preparation of 1- and 2-nitratoethyl-5*H*-tetrazole (1-NET and 2-NET). The resulting coordination compounds show an increased oxygen balance, making them interesting for use as energetic combustion catalysts in air bag systems or solid rocket propellants as a potential alternative to basic copper nitrate (BCN).[18]

Results and discussion

CAUTION! All investigated compounds are potentially explosive energetic materials (the majority of the compounds lie in the range of primary explosives!), which show increased sensitivities toward various stimuli (*e.g.*, elevated temperatures, impact, friction, or electrostatic discharge). Therefore, proper security precautions (safety glasses, face shield, earthed equipment and shoes, leather jacket, Kevlar gloves, Kevlar sleeves, and ear plugs) have to be taken while synthesizing and handling the described compounds.

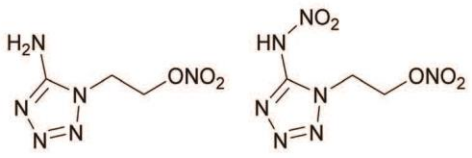


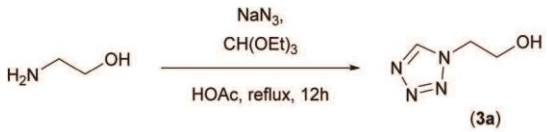
Chart 2 Literature known 1-nitratoethyltetrazole derivatives.[14,15]

Synthesis of the ligands

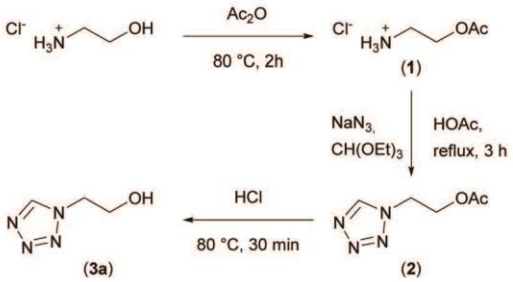
Like most tetrazole derivatives, the ligands can be synthesized in two ways. The first strategy, already described by Gaponik *et al.*, involves the reaction of 2-aminoethanol or the respective hydrochloride together with triethyl orthoformate and sodium azide, yielding only the 1*H*-substituted derivative **3a** (Scheme 1).[8] However, workup by complexation and subsequent breakdown of the complex with hydrogen sulphide is suggested.

Since the complicated processing of the raw material makes an industrial scale synthesis less promising, the authors have worked out another synthetic pathway toward 1-hydroxyethyl-5*H*-tetrazole (**3a**). As it is assumed that the use of alcohol derivatives together with triethyl orthoformate leads to undesired alkylation products, a modified synthesis of Bays *et al.* was applied.[19] Here, the introduction of a protective group prevents the formation of by-products (Scheme 2). The reaction of 2-aminoethanol hydrochloride with acetic anhydride gave **1** in good yields up to 75%. Subsequently a ring closure reaction was performed resulting in compound **2** in the form of colourless crystals (yield: 61%). This contradicts literature data, describing the substance as a pale-yellow oil.[19] After reacting compound **2** with concentrated hydrochloric acid, 1-hydroxyethyltetrazole (**3**) was obtained in the form of a colourless solid (yield: 93%).

The steps can be carried out sequentially (overall yield: 26%), or by an industrially valuable one-pot synthesis, resulting in an overall yield of 75%. For this purpose, acetic acid formed during the reaction of 2-ethanolamine and acetic anhydride was not removed in the first step. The reaction was cooled down to 40 °C and triethyl orthoformate followed by



Scheme 1 Synthesis of compound **3a** starting from 2-aminoethanol.



Scheme 2 Synthesis of 1-hydroxyethyltetrazole (**3a**) using acetic anhydride.

This journal is © The Royal Society of Chemistry 2021

Published on 29 June 2021. Downloaded by Ludwig Maximilians Universitaet Muenchen on 2/16/2022 8:09:47 AM.

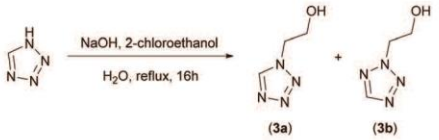
sodium azide was added. After the addition of further acetic acid, the mixture was refluxed. Subsequently, concentrated hydrochloric acid was added to the hot solution and heating was continued for 30 min. All solvents were removed under reduced pressure and the remaining residue was extracted with hot acetone. The solvent was removed under reduced pressure and the product was dried under high vacuum affording compound **3a** as colourless crystals.

To also obtain 2-hydroxyethyl-5*H*-tetrazole, a classic alkylation, as the second synthetic strategy for the derivatization of tetrazoles, was applied. A reaction of chloroethanol with 1,5*H*-tetrazole involving a base resulted in a mixture of two isomers **3a** and **3b** (Scheme 3) in a 1 : 1 ratio (yield: 88%).[20] No separation of the products was carried out.

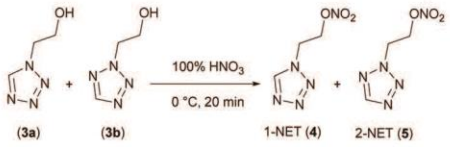
The nitration of both the isomeric mixture and pure compound **3a** was carried out by adding the alcohol to fuming nitric acid. The reaction of the pure 1-isomer with neutralization and extraction yielded compound **4** (yield: 73%). In the case of the isomeric mixture column chromatography with a solvent gradient was used to separate ligands **4** and **5** (yield **4**: 45%, yield **5**: 43%) (Scheme 4). Compound **5** can be further purified by sublimation, but separation of the isomers is not possible with this method.

Analysis of the ligands

The isomers, thus obtained, were distinguished by infrared spectroscopy (IR) as well as by proton, carbon, and nitrogen NMR spectroscopy. The isomer distribution can easily be followed by integration of the ^{1}H resonances. Furthermore, ^{1}H–^{15}N-HBMC spectra were measured. In the two-dimensional coupled spectra of tetrazole derivatives **4** and **5**, ^2J and ^3J couplings between nitrogen and hydrogen were measured. This allows a clear assignment of the isomers (Fig. 1 & 2). In advance, compound **5** was analyzed by one dimensional ^{15}N NMR to clarify the superimposed shifts at about −62 ppm (Fig. 2, top). The HMBC method used is only showing nitrogen atoms that have a finite ^{1}H–^{15}N coupling (>1 Hz) to an immobile hydrogen atom. This is the case here for all nitrogen



Scheme 3 Reaction of 1,5*H*-tetrazole with 2-chloroethanol.



Scheme 4 Nitration of 1-hydroxyethyl-5*H*-tetrazole (**3a**) and 2-hydroxyethyl-5*H*-tetrazole (**3b**).

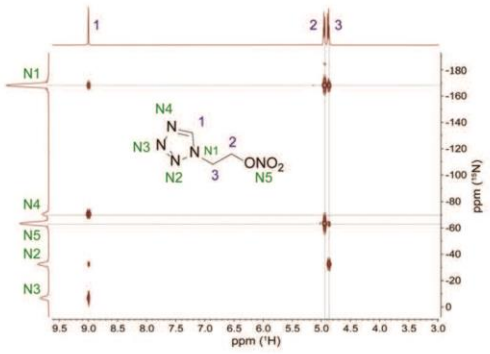


Fig. 1 Two-dimensional ^{1}H–^{15}N-HMBC NMR spectra of **4** (MeCN-d_3, 25 °C): δ (ppm) = −7.0 (N3), −32.4 (N2), −63.4 (N5), −70.5 (N4), −168.2 (N1).

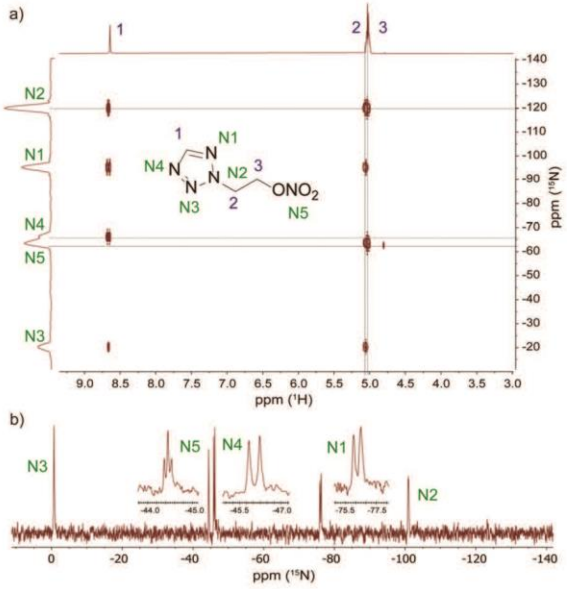


Fig. 2 (a) Two-dimensional ^{1}H–^{15}N-HMBC NMR spectra of **5** (acetone-d_6, 25 °C): δ (ppm) = −2.0 (N3), −63.5 (N5), −66.4 (N4), −95.3 (N1), −120.1 (N2); (b) ^{15}N NMR spectra of **5** (acetone-d_6, 25 °C).

atoms. In addition to the simpler atom assignment due to the coupling, the measurement time is many times shorter than that for traditional ^{15}N NMR measurements. Additional ^{14}N NMR shifts can be found in the ESI.†

The crystal structures of precursor **2** (Fig. S1, ESI†) together with the structures of both nitratoethyl-5*H*-tetrazoles were determined using low temperature single crystal X-ray diffraction (Fig. 3). Compound **4** crystallizes in the monoclinic space group $P2_1/n$ and possesses an asymmetric unit of two slightly different ordered molecules of 1-NET. Therefore, the unit cell is built up by eight formula units and shows a calculated density of 1.619 g cm^{-3} at 105 K. In contrast, isomeric compound **5** crystallizes in the orthorhombic space group $Pna2_1$. The unit cell contains only four formula units and shows a

Published on 29 June 2021. Downloaded by Ludwig Maximilians Universitaet Muenchen on 2/16/2022 8:09:47 AM.

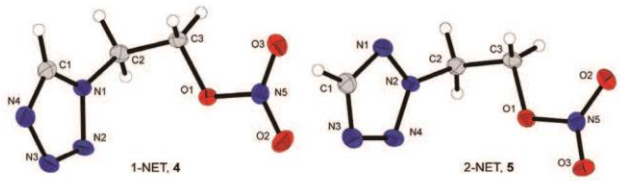


Fig. 3 Formula units of 1-NET (4) displayed on the left and 2-NET (5) on the right. Selected bond lengths (Å) of 4: N1–C1 1.334(2), N3–N2 1.2978(19), N4–N3 1.359(2), O1–C3 1.4576(17), O1–N5 1.3927(17), O2–N5 1.2038(18). Selected bond lengths (Å) of 5: N1–C1 1.327(4), N3–N2 1.326(4), N4–N3 1.318(4), O1–C3 1.456(4), O1–N5 1.394(3), O2–N5 1.216(4). Selected bond angles (°) of 4: N4–C1–N1 109.32(14), N4–N3–N2 111.18(12), N1–C2–C3 111.19(12), C3–O1–N5 113.22(10), O1–N5–O2 113.09(13), O2–N5–O3 128.78(15). Selected bond angles (°) of 5: N4–C1–N1 113.2(3), N4–N3–N2 106.1(3), N2–C2–C3 111.5(3), C3–O1–N5 114.1(2), O1–N5–O2 118.0(3), O2–N5–O3 129.2(3).

slightly lower density of 1.584 g cm^{-3} at a temperature of 128 K. The bond distances and angles are similar in both molecules and comparable to those of literature known tetrazole derivates and organic nitrates.

The crystalline material of the ligands was analysed for their sensitivity toward impact and friction according to the "UN declaration of dangerous goods" with a BAM drop hammer and friction tester.[21,22] The hard and brittle crystals of 5 (IS = 2 J) are more sensitive toward impact than the plate like and ductile crystals of 4 (IS = 10 J). Both ligands are insensitive towards friction (FS > 360 N).

Hirshfeld surfaces of 1-NET (4) and 2-NET (5) were generated, and the intermolecular atom interactions were calculated based on the crystallographic data and are visualized in Fig. S8 (ESI†).[23] Attractive and repulsive interactions are comparable for both molecules and therefore the exact location of the interactions in the crystal is of more importance. To investigate the location of the respective interaction, structural elements were investigated (Fig. 4). The strong interactions, visible as red dots on the Hirshfeld surface (Fig. S8, ESI†), were analysed and the interactions are visualized in the structural elements. It becomes clear that compound 4 is arranged in layers. These

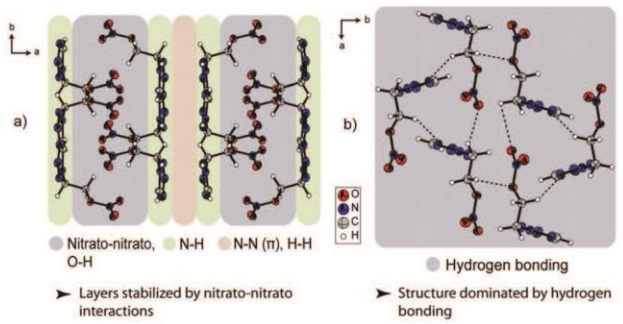


Fig. 4 (a) Structural elements of 1-NET (4) along the c-axis; (b) structural elements of 2-NET (5) along the c-axis. The areas showing the same interactions are marked and the type of interaction is noted below the respective structure.

layers have an outer part (green, N–H) and a rigid inner part (grey, nitrato–nitrato, O–H). The layers among themselves are only weakly connected (orange, N–N (π), H–H). It is assumed that these properties are responsible for the ductile, layered physical character. In contrast, compound 5 is largely dominated by hydrogen bonding in every direction and cannot be divided into layers.

The crystal is thus fixed in all spatial directions and is clearly more rigid, which is also consistent with the physical properties. With this information, one could explain the lower sensitivity of compound 4, through its layer like structure.[24] Regarding the low sensitivity toward friction we believe that the heat generated through the applied frictional force leads to melting and therefore desensitizing of the samples (the liquid samples are often less sensitive towards friction).[6] It is questionable if the impact is causing the solid sample to detonate or if a melting process occurs beforehand.[25]

The heat of formation of 4 and 5 was calculated using the atomization method (Gaussian CBS-4M electronic enthalpies) and the detonation parameters were calculated using the EXPLO5 V6.05 code (Table 1).[26] Additional information on the calculations is given in the ESI (Tables S7 & 8†). The heat of formation of 1-NET (4) is 27 kJ mol^{-1} which is higher than that of 2-NET (5). This leads to a detonation velocity of 7583 m s^{-1} for compound 4, and a slightly lower value of 7420 m s^{-1} for compound 5. In Table 1 the most important physicochemical and calculated properties of 4, 5, and TNT are compared. Although the melting points of 4 and 5 are too close to room temperature to classify the energetic materials as suitable melt castable materials, it proves the compatibility of the tetrazole and the nitrate ester moiety.

Synthesis of the ECCs

Many complexes based on monotetrazole ligands are already known in the literature.[27–29] However, in addition to their

Table 1 Physico chemical and calculated properties of 4, 5, and TNT

Compound	4	5	TNT
IS[a] [J]	10	2	15
FS[b] [N]	>360	>360	>360
Ω_{CO_2}[c] [%]	−55.31	−55.31	−73.96
T_{endo}[d]/T_{exo}[e] [°C]	25/168	24/188	80/290
ρ[f] [g cm^{-3}]	1.55	1.57	1.65
$\Delta_f H_m^\circ$[g] [kJ mol^{-1}]	174	147	−59
Detonation parameters calculated with the EXPLO5 V6.05 code			
$-\Delta_E U^{\circ h}$ [kJ kg^{-1}]	4861	4689	4406
T_E[i] [K]	3336	3268	3176
p_{C-J}[j] [GPa]	21.5	20.4	18.3
V_{det}[k] [m s^{-1}]	7583	7420	6798
V_0[l] [L kg^{-1}]	815	818	640

[a] Impact sensitivity, (BAM drop hammer, 1 of 6). [b] Friction sensitivity, (BAM friction tester, 1 of 6). [c] Oxygen balance toward CO_2. [d] Endothermic peak, which indicates melting. [e] Exothermic peak, which indicates decomposition. [f] Calculated density at 298 K. [g] Calculated enthalpy of formation at 298 K. [h] Heat of explosion. [i] Detonation temperature. [j] Detonation pressure. [k] Detonation velocity. [l] Volume of detonation gases (assuming only gaseous products).

This journal is © The Royal Society of Chemistry 2021

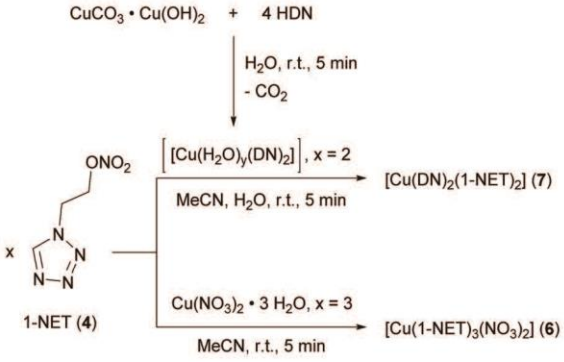
Published on 29 June 2021. Downloaded by Ludwig Maximilians Universitaet Muenchen on 2/16/2022 8:09:47 AM.

good performance, these usually exhibit very good water solubility, which is generally not desired in the field of energetic materials. To address this problem, a variety of ECCs containing organic nitrate-based ligands 1-NET (**4**) and 2-NET (**5**) were prepared. The resulting complexes should not only exhibit a reduced solubility, but also at the same time maintain their performance.

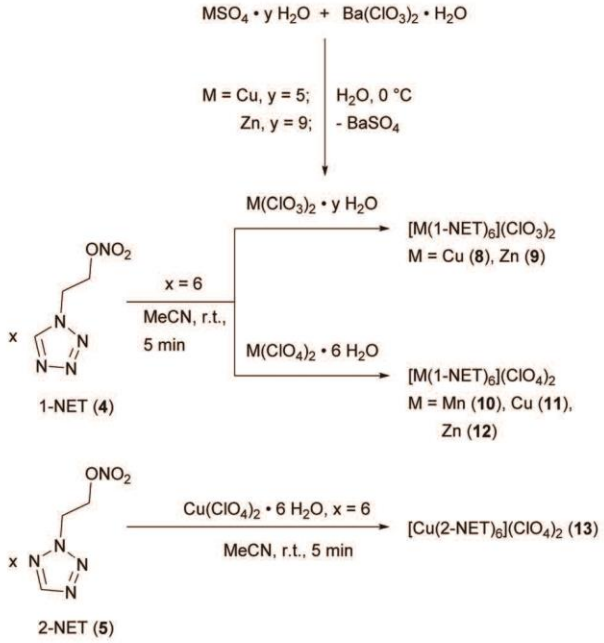
In the first step, several neutral or cationic coordination compounds based on oxidizing anions like nitrate, dinitramide, chlorate, or perchlorate were formed. The role of the ligand is to tune the energy content and sensitivity of the complex. Due to the bad solubility of the ligand, the sole use of water as a green solvent was not possible. Therefore, acetonitrile, or a combination of water and acetonitrile, was applied for the preparation of coordination compounds **6–13**. Besides rather easily accessible nitrate anions, the dinitramide anion was made accessible using basic copper carbonate and dinitraminic acid, as published in our previous work (Scheme 5).[30] Both metal salts were reacted with stoichiometric amounts of the ligand and crystallized within several days in decent yields up to 96% in the form of single crystals suitable for X-ray diffraction.

Furthermore, the strongly oxidizing chlorate anion was used, as it is also less toxic than the perchlorate anion.[31] In addition to copper(II) chlorate (**8**), the less investigated zinc(II) chlorate (**9**) was also incorporated in an ECC. The respective metal chlorate was made accessible by a reaction of barium chlorate with the respective sulphate salts (Scheme 6).[31] Both complexes were obtained in the form of single crystals in high yields (80–84%).

Compounds **10–13** were prepared analogous to copper(II) nitrate complex **6** by combining the solutions of the respective metal salt and stoichiometric amounts of the ligand, each dissolved in acetonitrile (Scheme 6). Whereas the use of manganese(II) and zinc(II) perchlorate only led to the isolation of a few single crystals, applying 1-NET (**4**) to copper(II) perchlorate gave ECC **11** in a satisfying yield (76%). Using 2-NET (**5**) solely resulted in copper(II) perchlorate complex **13** (yield: 89%). Single crystals suitable for X-ray diffraction were not obtained. Applying 2-NET (**5**) to copper(II)nitrate, dinitramide or



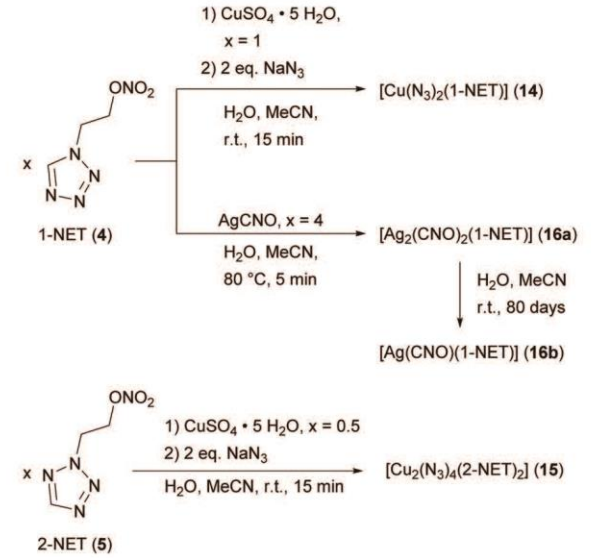
Scheme 5 Preparation of copper(II) complexes **6** and **7**.



Scheme 6 Synthesis of coordination compounds **8–13**.

different perchlorate salts like manganese(II) or zinc(II), was not successful. The use of iron(II) perchlorate as a building block also did not result in any isolable complexes in either case.

Besides the use of neutral nitrogen-rich ligands as a means of enhancing the performance in nitrate or perchlorate complexes, the concept of ECCs also allows a stabilization of highly sensitive metal salts like copper(II) azide or silver(I) fulminate (Scheme 7). Both synthetic strategies were recently pub-



Scheme 7 Stabilization of copper(II) azide and silver(I) fulminate using 1-NET and 2-NET.

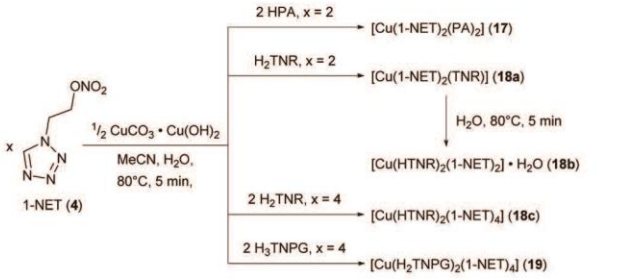
Published on 29 June 2021. Downloaded by Ludwig Maximilians Universitaet Muenchen on 2/16/2022 8:09:47 AM.

lished by our group.[32,33] To obtain the copper(II) azide complex **14**, the respective copper(II) sulphate complex is formed *in situ* and further reacted with an aqueous solution of sodium azide. Since the coordination positions remain occupied by the ligands, the formation of pure copper azide is avoided. The complex is formed immediately and precipitates directly and can be filtered off in a very good yield (82%). An elemental analysis pure preparation of compound **15** was not possible using this method, as most likely a side species is formed. Single crystal growth of **14** and **15** was achieved by performing layering experiments. Whereas handling of an extremely sensitive species could be avoided during the preparation of **14** and **15**, pure silver fulminate must be used for obtaining ECC **16a**. The silver salt was dissolved in a warm mixture of water and acetonitrile and an excess of ligand in acetonitrile was added. Single crystals suitable for X-ray diffraction were obtained after two days (yield: 43%). Leaving compound **16a** in its mother liquor for four weeks is resulting in single crystals of the thermodynamic product **16b**.

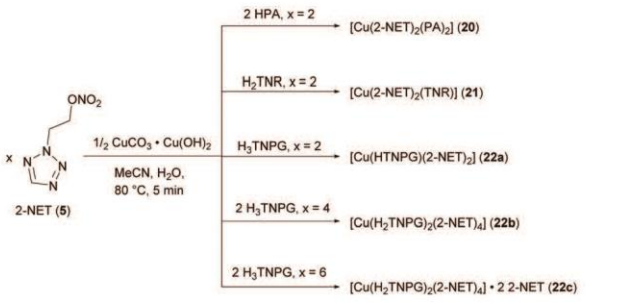
Another well-studied system is that of trinitrophenolate anions, each of which provides different properties to the respective complex depending on the number of hydroxy groups.[29] Compounds **17–22** were prepared in a straight forward manner by the reaction of basic copper carbonate with stoichiometric amounts of the respective acid in boiling water (Schemes 8 & 9). Subsequently, the ligand dissolved in small amounts of acetonitrile was added. Single crystal formation started within one day, depending on the amount of water used, in sufficient to high yields (68–88%). In the case of compound **18a** no single crystals suitable for X-ray diffraction were obtained but its composition could be verified by elemental analysis. Instead, recrystallization from hot water afforded single crystals of **18b**. Unfortunately, an elemental analysis pure isolation of **18b** was not possible.

By variation of the number of anions added to one equivalent of basic copper carbonate different states of deprotonation of styphnate ($HTNR^-$ and TNR^{2-}, Scheme 8) or trinitrophloroglucinate (H_2TNPG^- and $HTNPG^{2-}$, Scheme 9) anions could be obtained. In the case of compound **22c**, the addition of 6 equivalents of 2-NET led to the formation of a co-crystalline species, resulting in a total of three different species based on trinitrophloroglucinol. Each of these ECCs was obtained pure according to elemental analysis.

Except side species **18b**, all coordination compounds crystallized without the inclusion of water and were isolated directly from the mother liquor. The crystalline materials were filtered off, washed with small quantities of ice-cold ethanol, and then dried in air overnight.



Scheme 8 Preparation of copper(II) picrate (PA), styphnate (HTNR/TNR) and 2,4,6-trinitrophloroglucinol-based (HTNPG/H_2TNPG) complexes of 1-nitratoethyltetrazole (1-NET, **4**).



Scheme 9 Reaction of basic copper(II) carbonate with several trinitrophenole derivatives and subsequent applications of 2-NET (**5**).

Crystal structures of the ECCs

ECCs **6–12** and **14–22** were examined by low-temperature single crystal X-ray diffraction. In the case of compounds **9** and **22b** the measurements allow an indication of the most likely composition, but finalization of the data sets was not possible due to the highly disordered nitratoethyl moieties. Together with compounds **13** and **18a** in which case no single crystals were obtained, the complexes' composition was finally confirmed by elemental analysis. Details of the structures of compounds **2**, **10**, **12**, **15**, **18b**, **18c**, **19**, **21**, **22a**, and **22c** (Fig. S1–7, ESI†) are given in the ESI,† together with the measurement and refinement data of all experiments (Tables S1–S6, ESI†). The crystal datasets were uploaded in the CSD database and can be obtained free of charge.[34] All copper(II) complexes, except the nitrato (**6**), and dinitramido (**7**) ECCs, show octahedral coordination spheres around the copper(II) centers. Therefore, typical Jahn–Teller distortions along the respective O–Cu–O or N–Cu–N axes can be observed. Except for ECC **16b**, the ligands are solely coordinating *via* the N4 nitrogen atom of the tetrazole rings.

The copper(II) nitrate complex **6** crystallizes in the monoclinic space group $P2_1/c$ with four formula units per unit cell. The compound possesses a calculated density of 1.888 g cm^{-3} at 99 K. The coordination sphere could either be interpreted as distorted fivefold trigonal bipyramidal (N9–Cu1–O10 147.87 (10)°, O10–Cu1–O13 80.22(8)°), or as distorted seven fold pentagonal bipyramidal (N9–Cu1–O11 96.37(9)°, O11–Cu1–O10 51.93(8)°) depending on whether the longer Cu–O bonds between the central metal and nitrato ligands are included (Cu1–O11 2.695(2) Å, Cu1–O14 2.583(2) Å). In every case, the equatorial positions are occupied by the anionic nitrato ligands, and one ligand moiety (Fig. 5).

The dinitramide complex **7** crystallizes in the monoclinic space group $P2_1/n$ with two formula units per unit cell. The

 This journal is © The Royal Society of Chemistry 2021

Published on 29 June 2021. Downloaded by Ludwig Maximilians Universitaet Muenchen on 2/16/2022 8:09:47 AM.

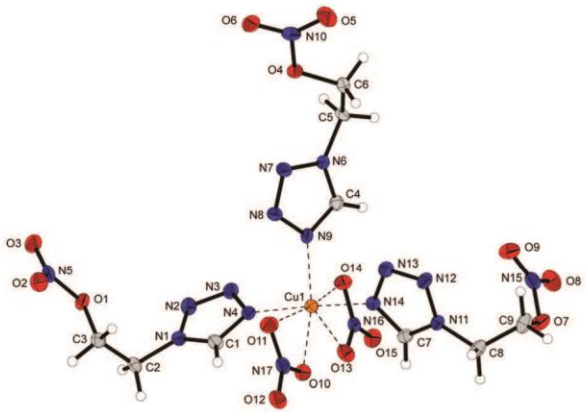


Fig. 5 Formula unit of $[Cu(1\text{-NET})_3(NO_3)_2]$ (**6**). Selected bond lengths (Å): Cu1–N9 2.028(3), Cu1–N4 1.973(3), Cu1–N14 1.987(3), Cu1–O10 2.117(2), Cu1–O13 2.268(2). Selected bond angles (°): N9–Cu1–N4 93.87 (10), N9–Cu1–N14 89.14(10), N14–Cu1–N4 174.78(11), N4–Cu1–O11 86.03(9).

complex shows a high density of 1.953 g cm^{-3} at 102 K, with only the copper azide and silver fulminate complexes possessing higher densities. The coordination sphere is built up by two ligand moieties and two coordinating dinitramido anions (Fig. 6). This rather uncommon built up was already observed one time by our group employing 1-azidoethyl-5*H*-tetrazole as the ligand.[30] One way of explaining the complexes' coordination geometry is by using two square planar spheres by either the oxygen atoms of the anion or the nitrogen atoms of the anion and ligand. Another possible coordination geometry might be distorted hexagonal bipyramidal. Also, it should be pointed out that in each case the extremely long Cu–O bonds were included. (Cu1–O1 2.8715(17) Å, Cu1–O4 2.8287(17) Å). Therefore, no clear Jahn–Teller distortion can be observed, but a strongly distorted dinitramide anion is evident (O7–N8–N7–O5 25.19(17)°, O6–N8–N6–N7 150.45(16)°).

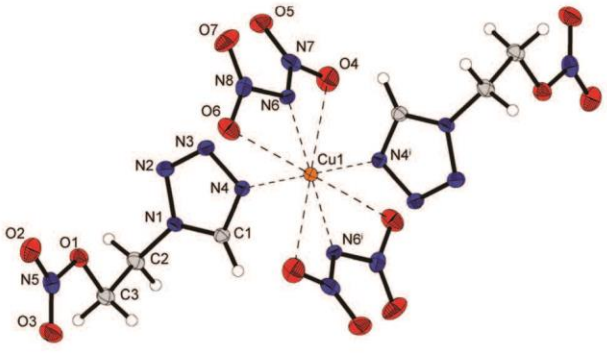


Fig. 6 Coordination environment of $[Cu(DN)_2(1\text{-NET})_2]$ (**7**). Selected bond lengths (Å): Cu1–N6 1.9978(17), Cu1–N4 1.9735(17). Selected bond angles (°): N4–Cu1–N6 90.02(7), O4–Cu1–N4 90.33(6), O6–Cu1–N4 102.57(6), O6–Cu1–N6 49.13(6), O4–Cu1–N6 49.33(6), N6–N8–O6 111.96(17), N6–N7–O4 110.25(17). Symmetry code: (i) 1 – *x*, 1 – *y*, 1 – *z*.

The copper(II) chlorate complex **8** crystallizes in the monoclinic space group *Cc* and the unit cell consists of four formula units. The compound's density of 1.689 g cm^{-3} (at 100 K) is slightly lower than the density observed for the corresponding perchlorate complex **11**. The octahedral coordination sphere is built up by six ligand moieties, whereas some nitrato-groups had to be split due to disorder and are therefore not refined to be anisotropic. The metal perchlorate complexes **10–12** crystallize isotypically in the triclinic space group $P\bar{1}$ with one formula unit per unit cell. The observed densities differ only slightly, with the copper coordination compound showing the highest value (**10** (Mn): 1.681 g cm^{-3} at 123 K; **11** (Cu): 1.727 g cm^{-3} at 114 K; **12** (Zn): 1.719 g cm^{-3}). Each compound shows an octahedral coordination sphere built up by six moieties of 1-NET (**4**), whereas only **11** shows a Jahn–Teller distortion due to its d^9 configuration (Fig. 7).

Copper(II) azide complex **14** crystallizes in the form of brown plates in the triclinic space group $P\bar{1}$. The asymmetric unit consists of two molecular units, whereas the molecular unit is built up by one tetrazole moiety per copper(II) azide. This coordination geometry has already been observed in previous studies.[32] The unit cell contains four formula units and shows the highest density of all investigated copper complexes (1.985 g cm^{-3} at 173 K). Each copper centre is surrounded by a strongly distorted octahedral coordination sphere (N11–Cu1–$N11^i$ 77.11(13)) with the 1-NET ligands in the equatorial positions (Fig. 8, part A). The remaining coordination sites are occupied by azido ligands. In addition to that the azide anion shows a bridging behaviour, further linking the copper centres in various ways. Two of the anions show the same binding behaviour and bridge exclusively to the same neighbouring copper centres. This binding behaviour, shown in part C of Fig. 8, leads to the formation of dimers. The remaining equatorial coordinating azide ion, and both moieties in the axial position, exhibit a bridging behaviour as shown in part B of Fig. 8. This further linking of the metal centres leads to the formation of a two-dimensional polymeric network, as displayed in part D (Fig. 8).

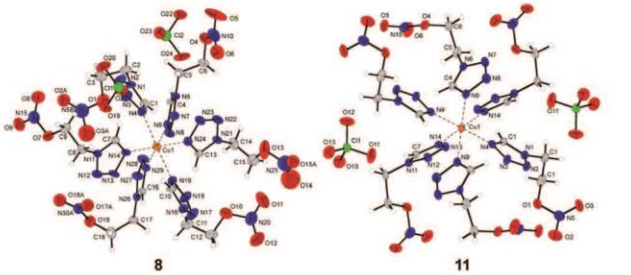


Fig. 7 Formula units of $[Cu(1\text{-NET})_6](ClO_3)_2$ (**8**) and $[Cu(1\text{-NET})_6](ClO_4)_2$ (**11**). Selected bond lengths (Å) of **8**: Cu1–N4 2.371(8), Cu1–N9 2.048(8), Cu1–N14 2.046(7). Selected bond lengths (Å) of **11**: Cu1–N4 2.022(3), Cu1–N14 2.035(3), Cu1–N9 2.338(3). Selected bond angles (°) of **8**: N4–Cu1–N9 86–1(3), N4–Cu1–N14 92.8(3), N9–Cu1–N14 88.7(3). Selected bond angles (°) of **11**: N9–Cu1–N4 89.48(11), N9–Cu1–N14 88.66(10), N14–Cu1–N4 91.60(11). Symmetry codes of **11**: (i) 1 – *x*, 1 – *y*, 1 – *z*.

Published on 29 June 2021. Downloaded by Ludwig Maximilians Universitaet Muenchen on 2/16/2022 8:09:47 AM.

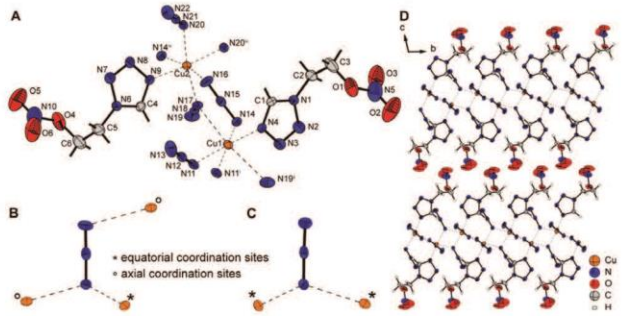


Fig. 8 A: Coordination environment of the copper(II) azide dimer **14**. Selected bond lengths (Å): Cu1–N17 2.497(3), Cu1–N19^{ii} 2.683(3), Cu2–N14^{iv} 2.534(3), Cu2–N16 2.715(3). Selected bond angles (°): N14–Cu1–N19^{ii} 84.62(10), N11^{i}–Cu1–N4 95.86(11), N11–Cu1–N14 94.55(12), N9–Cu2–N20 95.15(11), N17–Cu2–N16 86.55(10), N16–Cu2–N20 86.85(19), N16–Cu2–N14^{iv} 170.95(10), N20–Cu2–N17 169.31(11). Symmetry codes: (i) 1 – *x*, 1 – *y*, 1 – *z*; (ii) –1 + *x*, *y*, *z*; (iii) 2 – *x*, 2 – *y*, 1 – *z*; (iv) 1 + *x*, *y*, *z*. B & C: Coordination modes of the azide anions. D: Polymeric structure of compound **14**.

Silver complex **16a** crystallizes in the form of colourless plates in the monoclinic space group *I*2/*a*. The unit cell consists of eight formula units and shows the highest density of all investigated compounds with 2.718 g cm^{-3} at 104 K. The molecular unit consists of one 1-NET per two silver fulminate moieties. In addition to the formation of argentophilic Ag–Ag interactions, all centres within the cluster are further linked to each other by the fulminate anions. Two identical cations are bridged by two anions, one *via* the carbon of one fulminate ligand and the other *via* the oxygen atom of the other fulminate ligand, in an alternating order forming twofold coordinated silver chains. This 1D polymeric chain is further coordinated by 1-NET ligands which shifts the linear 2-fold coordination of the silver atoms to a distorted tetrahedral coordination. The resulting fourfold coordination environment around each silver cation has already been observed for silver(I) fulminate complexes based on monotetrazole ligands.[33]

Fulminato complex **16b**, based on the same ligand as complex **16a**, on the other hand crystallizes in the monoclinic space group $P2_1/c$ with four formula units. The calculated density of 2.337 g cm^3 at 173 K is lower than the one determined for **16a**. The molecular formula in this case consists of only one silver fulminate moiety per 1-NET ligand. Also, the silver atoms are coordinated differently (Fig. 9, bottom). In compound **16b** each silver atom shows only a six-fold coordination sphere, whereas no Ag–O bonds were found. Instead, bridging tetrazole ligands were observed. Every moiety of 1-NET is binding *via* its N4 nitrogen atom together with its N3 position, which is a rather uncommon behaviour of tetrazoles in ECCs. This linking is further connecting the Ag–Ag chains formed by the fulminato ligands, leading to the formation of 2D polymeric sheets.

Overall, both silver fulminate complexes based on 1-NET (**4**) form two dimensional polymeric networks, while the sum formula and the structure of these networks are very different.

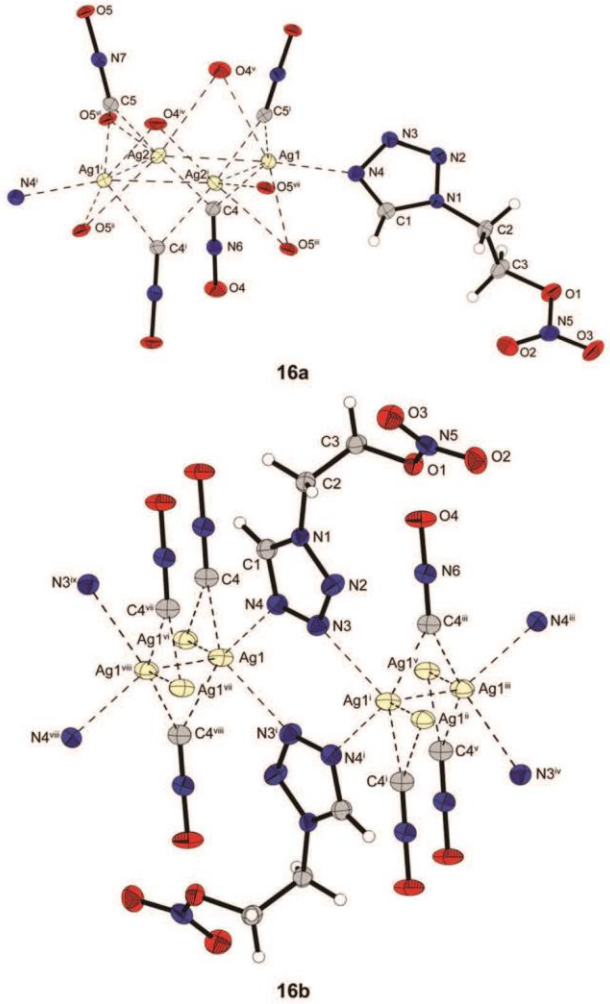


Fig. 9 Extended molecular units of [$Ag_2(CNO)_2$(1-NET)] (**16a**) and [Ag(CNO)(1-NET)] (**16b**). Selected bond lengths (Å) of **16a**: Ag1–N4 2.291(3), Ag2–O5 2.501(3), Ag1–C4 2.236(3), Ag2–C4 2.195(4), Ag1–O4 2.893(3), Ag2–O4 2.846(3), Ag1–C5 2.242(4), Ag2–C5 2.200(4), Ag1–O5 2.698(2), Ag2–O5 2.703(2). Selected bond lengths (Å) of **16b**: Ag1–Ag1^{vi} 3.0106 (2), Ag1–C4 2.184(2), Ag1^{vi}–C4 2.247(2), Ag1–N4 2.4260(18), Ag1–N3 2.4692(19). Selected bond angles (°) of **16a**: Ag2–Ag1–N4 161.47(8), Ag1–Ag2–O5 126.02(6), Ag2–Ag1–Ag2 67.284(13), Ag1–Ag2–Ag1 112.694(13), Ag2–C4–Ag1 77.89(11), Ag1–O5–Ag2 64.53(5). Selected bond angles (°) of **16b**: Ag1^{vi}–Ag1–C4 48.10(6), Ag1–C4–Ag1^{vi} 85.59(7), N4–Ag1–N3^{i} 103.46(6), N4–Ag1–C4^{viii} 106.50(7), N3–Ag1–C4^{viii} 82.16 (7). Symmetry codes of **16a**: (i) 1.5 – *x*, *y*, 1 – *z*; (ii) *x*, –1 + *y*, *z*; (iii) 1.5 – *x*, –1 + *y*, 1 – *z*; (iv) 1.5 – *x*, 1 + *y*, 1 – *z*; (v) *x*, 1 + *y*, *z*; (vi) 2 – *x*, 2 – *y*, 1 – *z*; (vii) –0.5, 2 – *y*, *z*. Symmetry codes of **16b**: (i) 1 – *x*, 1 – *y*, 1 – *z*; (ii) *x*, 1.5 – *y*, –0.5 + *z*; (iii) *x*, 0.5 – *y*, –0.5 + *z*; (iv) 1*x*, –0.5 + *y*, 0.5 – *z*; (v) 1 – *x*, –*y*, 1*z*; (vi) 1 – *x*, –0.5 + *y*, 1.5 – *z*; (vii) *x*, 1 + *y*, *z*; (viii) 1 – *x*, 0.5 + *y*, 1.5 – *z*; (ix) *x*, 1.5 – *y*, 0.5 + *z*.

Both complexes **17** and **20** based on the picrate anion crystallize with the same molecular formula in the form of green plates and blocks, respectively. However, since both complexes crystallize in different space groups (**17**: monoclinic $P2_1/c$; **20**: triclinic $P\bar{1}$), the unit cell of compound **17** consists of four formula units and the one of **20** is made of one unit. Despite

This journal is © The Royal Society of Chemistry 2021

Published on 29 June 2021. Downloaded by Ludwig Maximilians Universitaet Muenchen on 2/16/2022 8:09:47 AM.

this fact, the densities of both complexes are very similar (**17**: 1.852 g cm^{-3} at 173 K, **20**: 1.890 g cm^{-3} at 132 K). The distorted octahedral coordination sphere is, for picrate-based complexes, structured in the expected manner.[27,29] Two ligand moieties are arranged in the equatorial positions together with Cu–O bonds formed by the deprotonated hydroxy groups of the anion (Fig. 10). The axial positions are occupied by the oxygen atoms of picrate's nitro group next to its hydroxy group.

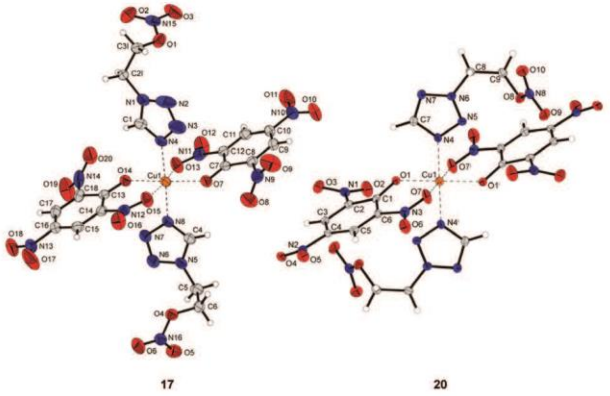


Fig. 10 Molecular units of ECCs **17** and **20**. Selected bond lengths (Å) of **17**: Cu1–N4 1.999(3), Cu1–N8 2.000(3), Cu1–O14 1.919(2), Cu1–O7 1.931(2), Cu1–O13 2.296(2), Cu1–O15 2.412(3). Selected bond lengths (Å) of **20**: Cu1–O1 1.9193(18), Cu1–N4 2.001(2), Cu1–O7 2.430(2). Selected bond angles (°) of **17**: O7–Cu1–O13 81.58(9), O13–Cu1–O14 94.72(9), O14–Cu1–O15 77.39(9), O13–Cu1–N4 88.02(11), N4–Cu1–O15 92.32, N4–Cu1–O14 85.29(10), O14–Cu1–N8 91.67(10). Selected bond angles (°) of **20**: O7–Cu1–O1 76.34(7), O7–Cu1–N4 89.49(8), N4–Cu1–O1 87.10(8). Symmetry code of **20**: (i) 1 – *x*, 2 – *y*, 1 – *z*.

Thermal stability and sensitivity data of the ECCs

Each coordination compound, which could be obtained elemental analysis pure, was investigated by differential thermal analysis (DTA) in the range from 25 to 400 °C at a heating rate of 5 °C min^{-1}. The resulting endothermic processes indicating a melting of the respective compound, a loss of ligand, or a phase transition, together with the exothermic processes, indicating a decomposition, are listed in Table 2. Plots of every DTA spectrum measured can be found in the ESI (Fig. S20–24†). When endothermic processes occurred during DTA measurements, thermogravimetry (TG) analysis was applied at a heating rate of 5 °C min^{-1} in the range from 30 to 400 °C to ensure that only melting of the respective compound occurred. The TG plots of the chlorate and perchlorate complexes **8**, **9**, **11**, and **13** are illustrated in Fig. 11. Further spectra can be found in the ESI (Fig. S25 & 26†). In the case of **16a**, the second endothermic process indicates a loss of the ligand according to TG measurements. Since no mass loss has been detected for compound **11**, a phase transformation probably takes place here.

Except the nitrate (**6**, T_{exo} = 196 °C) and the trinitrophenolate based complexes **17** (T_{exo} = 197 °C) and **18a** (T_{exo} = 195 °C), none of the compounds' thermal stability exceeds the free ligands' stability. Furthermore, quite low melting points were observed especially for the chlorate and perchlorate complexes **8**, **9**, **11**, and **13**. This is most likely due to the low melting temperatures of the respective ligands (**4**, **5**: $T_{endo} \leq 25$ °C).

Table 2 Thermal stability measurements[a] and sensitivities toward various mechanical stimuli[b]

Compound		T_{endo}[c] (°C)	T_{exo}[d] (°C)	IS[e] (J)	FS[f] (N)	ESD[g] (mJ)	BDIS[h] (mJ)
1-NET	**4**	25	168	10	>360	n.d.	n.d.
2-NET	**5**	24	188	2	>360	n.d.	n.d.
[Cu(1-NET)$_3$(NO$_3$)$_2$]	**6**	121	196	5	48	1080	14
[Cu(DN)$_2$(1-NET)$_2$]	7	—	110	2	7	1080	14
[Cu(1-NET)$_6$](ClO$_3$)$_2$	**8**	54	149	2	15	250	55
[Zn(1-NET)$_6$](ClO$_3$)$_2$	**9**	71	154	7	14	750	69
[Cu(1-NET)$_6$](ClO$_4$)$_2$	**11**	70, 117	165	3	25	480	>200
[Cu(2-NET)$_6$](ClO$_4$)$_2$	**13**	65	143	2	5	1080	55
[Cu(N$_3$)$_2$(1-NET)]	**14**	—	122	3	1	14	≤4
[Ag$_2$(CNO)$_2$(1-NET)]	**16a**	96	123	≤1	20	250	8
[Ag(CNO)(1-NET)]	**16b**	67, 102[i]	102[i]	9	60	250	83
[Cu(1-NET)$_2$(PA)$_2$]	**17**	—	197	20	>360	480	>200
[Cu(1-NET)$_2$(TNR)]	**18a**	—	195	2	96	480	111
[Cu(HTNR)$_2$(1-NET)$_4$]	**18c**	—	167	5	96	>1500	>200
[Cu(H$_2$TNPG)$_2$(1-NET)$_4$]	**19**	—	108	2	96	1080	>200
[Cu(2-NET)$_2$(PA)$_2$]	**20**	165[i]	165[i]	3	192	1080	>200
[Cu(2-NET)$_2$(TNR)]	**21**	—	161	≤1	80	750	138
[Cu(HTNPG)(2-NET)$_2$]	**22a**	—	112	4	324	750	>200
[Cu(H$_2$TNPG)$_2$(2-NET)$_4$]	**22b**	—	105	4	324	750	>200
[Cu(H$_2$TNPG)$_2$(2-NET)$_4$] · 2 2-NET	**22c**	92	105	4	60	750	>200
Pb(TNR)·H$_2$O	—	—	260–310 (ref. 38)	8 (ref. 41)	0.45 (ref. 41)	0.04–1 (ref. 38)	15 (ref. 41)
Pb(N$_3$)$_2$ (RD-1333)	—	—	320–350 (ref. 38)	4 (ref. 41)	≤0.1 (ref. 41)	5–8 (ref. 38)	37 (ref. 41)

[a] Onset temperatures at a heating rate of 5 °C min^{-1}. [b] Determined by 1 of 6 methods. [c] Endothermic peak, which indicates melting, phase transition, or loss of ligands. [d] Exothermic peak, which indicates decomposition. [e] Impact sensitivity (BAM drophammer test).[22] [f] Friction sensitivity (BAM friction tester).[22] [g] Electrostatic discharge sensitivity (OZM XSpark10).[39] [h] Ball drop impact sensitivity (OZM BIT-132).[39,40] [i] Endothermic signal followed by exothermic signal; n.d.: not determined.

Published on 29 June 2021. Downloaded by Ludwig Maximilians Universitaet Muenchen on 2/16/2022 8:09:47 AM.

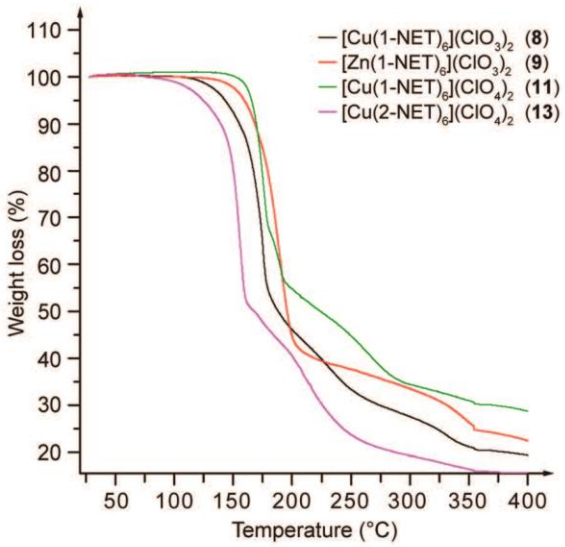


Fig. 11 Thermogravimetric measurements of the copper(II) and zinc(II) chlorate complexes **8** and **9** together with the copper(II) perchlorate complexes **11** and **13** in the range from 30 to 400 °C at a heating rate of 5 °C min^{-1}.

The complexes' low decomposition temperatures are on the one hand again caused by the ligand's properties. Organic nitrates in general are known to possess decomposition temperatures rarely exceeding 180 °C.[35] Therefore, it is expected that the compounds' exothermic processes are within this range. On the other hand, catalytic effects might play a crucial role in the decomposition of the ECCs, further limiting the compounds' thermal stability. Thus, similar effects like those observed in the catalytic decomposition of guanidinium nitrate using BCN, probably occur when the complexes are heated.[18,36]

A detailed look at the compounds' exothermic processes reveals some trends already observed for ECCs in the past. For example, complex **11** (T_{exo} = 165 °C) based on the perchlorate anion is among the most thermally stable compounds, whereas the respective copper(II) chlorate **8** complex (T_{exo} = 149 °C) is less stable.[9]

Also, the decrease in the thermal stability of complexes **20** (T_{exo} = 165 °C) to **22c** (T_{exo} = 105 °C) with an increasing number of hydroxy groups is expected.[29] The expected trend of improved thermal stability caused by bridging anions (such as TNR^{2-} and $HTNPG^{2-}$) was only observed for complexes **18a** (T_{exo} = 195 °C), **21** (T_{exo} = 161 °C), and **22a** (T_{exo} = 112 °C).[9,29] Previous results suggest that the thermal stability of these complexes should be significantly higher than that of the picrate complexes. The drastically lower decomposition temperature of **13** (T_{exo} = 143 °C) was also surprising. Literature data showed rather similar decomposition temperatures for copper(II) perchlorate complexes based on the respective isomers. The reason for this again appears to be the catalytic effects of the central metal on the stability of the organic nitrate of the ligand. Hence, the latest exothermic processes were observed for compounds **6**, **17**, and **18a**. Compounds **16b** (T_{exo} = 102 °C), **22b** (T_{exo} = 105 °C), and **22c** (T_{exo} = 105 °C) showed the lowest thermal stability of all complexes investigated.

In addition to the compound's thermal stability, great emphasis was placed on the determination of the compounds' sensitivity toward various external stimuli (*e.g.*, impact, friction, ball drop impact sensitivity, and electrostatic discharge). The classification of the compounds regarding the "UN Recommendations on the Transport of Dangerous Goods" should ensure a safe handling of every ECC investigated. Sensitivity measurements were carried out for complexes **6–9**, **11**, **13**, **14**, and **16–22** and ligands **4** and **5**. Further characterization of coordination compounds which could not be isolated elemental analysis pure was waived. Friction sensitivity (FS) measurements showed that, except picrate complex **17**, every ECC is more sensitive than the respective ligand by itself. Copper azide **14** is the most sensitive complex (FS = 1 N), followed by copper(II) perchlorate complex **13** (FS = 5 N), and copper(II) dinitramide complex **7** (FS = 7 N). This is surprising as compound **13** at the same time possesses one of the lowest melting points. In the case of compounds **8** (FS = 15 N), **9** (FS = 14 N), and **11** (FS = 25 N) the low melting point is clearly reducing the compounds' friction sensitivity. Also, it is worth mentioning that the effect of the co-crystallizing 2-NET moieties in compound **22c** on the compound's higher sensitivity toward friction is observed (FS = 60 N). Compared to **22b** (FS = 324 N), lacking the co-crystallizing 2-NET units, the sensitivity is drastically higher. This contradicts the common assumption that energetic materials are less sensitive by introducing co-crystallizing compounds.[37]

Regarding impact sensitivity (IS) measurements, the effects caused by the low melting points are not as severe as those observed during friction sensitivity measurements. This is reflected by the general impact sensitivity of ≤4 J observed for most of the compounds (except **6**, **9**, and **17**). A reason for this might be the ignition of the sample through adiabatic compression or hot spot formation within the setup.[25] Also, it is worth mentioning that during impact sensitivity measurements some complexes are tested to be less sensitive than ligand **5** (IS = 2 J). The highest impact sensitivity was observed for styphnate **21** (IS ≤ 1 J), whereas compound **17** (IS = 20 J) showed the lowest sensitivity toward impact.

The low sensitivity of complex **17**, especially compared to ECC **20** based on the same anion, is likely caused by grain size effects. While **17** (FS > 360 N, IS = 20 J) was investigated at a roughly determined grain size <100 μm, the particle size distribution of **20** (FS = 192 N, IS = 3 J) was about 500–1000 μm, possibly making the sample more sensitive. Similar effects are assumed to be responsible for the difference in the sensitivity data for compounds **19** (IS = 2 J, FS = 96 N) and **22b** (IS = 4 J, FS = 324 N). The difference in the sensitivity between the two silver fulminate complexes is due to the content of fulminate in each complex. While in ECC **16a** two fulminate moieties are observed on one ligand, in **16b** only one moiety is found per ligand. Therefore, complex **16a** is clearly more sensitive than **16b**.

Regarding the "UN Recommendations on the Transport of Dangerous Goods", except ECCs **4**, **6**, **9**, and **17**, every com-

This journal is © The Royal Society of Chemistry 2021

Published on 29 June 2021. Downloaded by Ludwig Maximilians Universitaet Muenchen on 2/16/2022 8:09:47 AM.

pound must at least be classified as sensitive because of impact sensitivity measurements.[21] Complexes **5**, **7**, **8**, **11**, **13**, **14**, **16a**, and **19–21** even must be considered as very sensitive. The remaining compounds **4**, **9**, and **17** are classified as less sensitive. Taking into account the sensitivity toward friction, the zinc(II) chlorate complex **9** must be rated as very sensitive, with the compounds **7**, **13**, and **14** being extremely sensitive.

The synthesis of several complexes based on 1-NET has again extended the series of ECCs based on alkyl tetrazoles. This suggests a comparison of the complexes with each other, whereby the copper chlorate and perchlorate complexes probably appear to be the most suitable ones, since these, except for the chlorate complex based on 1-methyl-5*H*-tetrazole (MTZ), have the same structure. For this purpose, the data of different complexes known in the literature were compiled and are plotted with the data of ECCs **8** and **13** obtained from this work in the bar charts shown in Fig. 12.[9,27,31]

The charts generally indicate that a longer carbon chain without an additional energetic group leads to compounds being less sensitive. This is represented through the ECCs based on 1-ethyl-5*H*-tetrazole (ETZ). By adding an energetic group, like an azide (AET) or nitrate (NET), the effect becomes less imminent, and the resulting coordination compounds are even more sensitive than those based on 1-methyl-5*H*-tetrazole, having a shorter carbon chain. Regarding friction sensitivity another general trend can be observed, stating that chlorate complexes are always more sensitive than the ones based on perchlorate. When it comes to impact sensitivity, this tendency is less clear. It must be noted that the different structure of the methyl tetrazole chlorate complex might influence these findings. Comparing the complexes based on NET and AET shows that with the exception of $[Cu(AET)_6](ClO_3)_2$ (IS = 2.5 J), the complexes based on 1-azidoethyl-5*H*-tetrazoel are more sensitive.

Because of the already mentioned problems regarding BAM standard impact measurements, in this work, also ball drop impact sensitivity (BDIS) measurements were performed. The device is said to deliver results closer to realistic conditions due to a combination of spin and impact onto the sample.[41] Earlier works of our group showed that there are coherences between the friction and ball drop impact. This work generally supports this thesis, with compounds **7**, **8**, **9**, **14**, **15**, and **21** being tested sensitive during both measurement types. However, the chlorate and perchlorate complexes are less sensitive toward BDIS which is likely due to the compounds' melting point, resulting in crystals absorbing a lot of impact energy. Major exceptions also are compounds **11**, **19b**, and **22c**, which were tested less sensitive than expected. A reason explaining this behaviour might again be the particle size distribution or crystal shape. A high-speed image of the moment of impact of compounds **13** and **14** is displayed in Fig. 13.

Hot plate and hot needle experiments

To get an insight into the compounds' behaviour when exposed to fast heating, hot plate tests were performed for every ECC obtained elemental analysis pure. To run the test, the sample was placed on a copper plate and heated with a Bunsen burner until decomposition. An evaluation of the compounds' reaction when ignited under light confinement was made by performing hot needle tests. For this test the sample was fixed onto a copper plate by using an adhesive tape. Subsequently the compound was penetrated with a red glowing hot needle. Usually, a detonation in at least one of the tests is desired, as this outcome indicates a fast deflagration to detonation transition (DDT), which is an important property of a primary explosive. The DDT is said to allow conclusions to be drawn on how well a primary explosive is capable of igniting pentaerythritol tetranitrate (PETN). Since the substances are intended to rather serve as combustion catalysts than as primary explosives, deflagration or decomposition reactions are desired. The outcome of each test is displayed in Table 3;

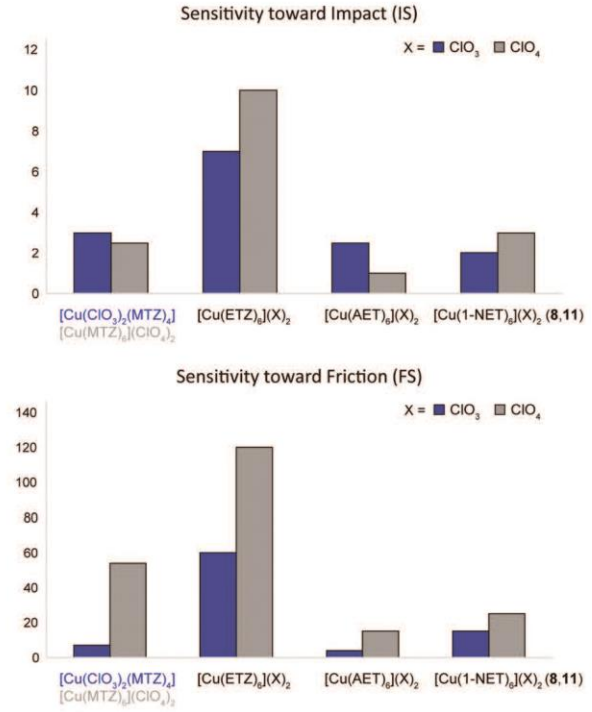


Fig. 12 Bar charts displaying the impact sensitivity (top) and friction sensitivity (bottom) of selected copper(II) chlorate and perchlorate complexes based on various alkyl tetrazoles known in the literature.[9,27,31]

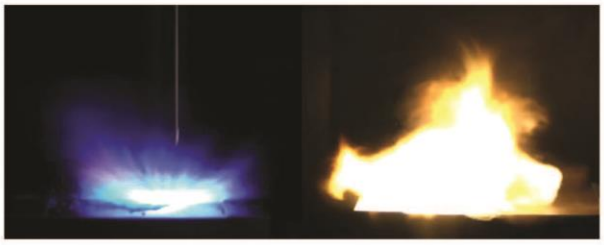


Fig. 13 Moment of detonation during ball drop impact sensitivity measurements of the copper(II) perchlorate (**13**) and copper(II) azide complexes (**14**).

Published on 29 June 2021. Downloaded by Ludwig Maximilians Universitaet Muenchen on 2/16/2022 8:09:47 AM.

Table 3 Results of hot plate and hot needle experiments[a]

Compound	No.	HP	HN	PETN initiation	Laser energy, E^b (mJ) 1.7	25.5	51.0
$[Cu(1\text{-}NET)_3(NO_3)_2]$	**6**	defl.	defl.	—	dec.	defl.	—
$[Cu(DN)_2(1\text{-}NET)_2]$	**7**	defl.	defl.	Negative	det.	det.	—
$[Cu(1\text{-}NET)_6](ClO_3)_2$	**8**	defl.	defl.	—	—	dec.	—
$[Zn(1\text{-}NET)_6](ClO_3)_2$	**9**	defl.	dec.	—	—	—	—
$[Cu(1\text{-}NET)_6](ClO_4)_2$	**11**	defl.	defl.	—	—	dec.	—
$[Cu(2\text{-}NET)_6](ClO_4)_2$	**13**	defl.	defl.	—	—	dec.	—
$[Cu(N_3)_2(1\text{-}NET)]$	**14**	det.	det.	Positive	—	det.	—
$[Ag_2(CNO)_2(1\text{-}NET)]$	**16a**	det.	defl.	Negative	—	—	—
$[Ag(CNO)(1\text{-}NET)]$	**16b**	det.	dec.	—	—	—	—
$[Cu(1\text{-}NET)_2(PA)_2]$	**17**	defl.	dec.	—	—	comb.	comb.
$[Cu(1\text{-}NET)_2(TNR)]$	**18a**	defl.	defl.	—	—	comb.	comb.
$[Cu(H_2TNR)_2(1\text{-}NET)_4]$	**18c**	defl.	defl.	—	—	dec.	dec.
$[Cu(H_2TNPG)_2(1\text{-}NET)_4]$	**19**	defl.	dec.	—	—	comb.	comb.
$[Cu(2\text{-}NET)_2(PA)_2]$	**20**	defl.	defl.	—	—	dec.	dec.
$[Cu(2\text{-}NET)_2(TNR)]$	**21**	defl.	defl.	—	—	comb.	comb.
$[Cu(HTNPG)(2\text{-}NET)_2]$	**22a**	defl.	defl.	—		comb.	comb.
$[Cu(H_2TNPG)_2(2\text{-}NET)_4]$	**22b**	defl.	dec.	—	dec.	dec.	dec.
$[Cu(H_2TNPG)_2(2\text{-}NET)_4] \cdot 2\ 2\text{-}NET$	**22c**	defl.	defl.	—	det.	comb.	dec.

[a] Not tested, comb.: combustion, dec.: decomposition, defl.: deflagration, det.: detonation. [b] Operating parameters: current $I = 7$ A; voltage $U = 4$ V; theoretical maximal output power $P_{max} = 45$ W; theoretical energy $E_{max} = 1.7$–51.0 mJ; wavelength $\lambda = 915$ nm; pulse length $\tau = 1$–30 ms.

further high-speed images of the tests and details on the setup can be found in the general information in the ESI.†

Deflagration reactions were observed for the majority of the investigated ECCs (Table 3). Only exceptions were copper(II) azide complex **14** (Fig. 14), and silver(I) fulminate **16a**, which detonated during at least one of the experiments, together with compounds **9**, **17**, **19**, and **22b**, only decomposing during at least one of these experiments. Excluding ECCs **14** and **16a** this behaviour indicates their possible use as combustion catalysts. Based on these results, laser ignition experiments, and in the case of **14**, **16a** and because of its strong deflagration, also complex **7**, PETN initiation experiments are of interest. Compound **16b** showed a significant weaker reaction than ECC **16a** due to the lower fulminate content in the complex.



Fig. 14 High-speed images of the results of the hot plate (left and middle) and hot needle tests (the right picture) of the copper(II) dinitramide complex **7** (top) and the copper(II) azide coordination compound **14** (bottom).

PETN initiation experiments

The compounds which showed the most powerful behaviour during hot plate and hot needle tests have been found to be dinitramide coordination compound **7**, copper(II) azide complex **14**, and silver fulminate ECC **16a**. These complexes showed either sharp deflagrations or even detonations during hot plate and hot needle tests. For their potential use as lead-free primary explosives, the compounds were tested for their capability of initiating PETN. Therefore, 200 mg of the booster explosive was loaded into a copper shell and 50 mg of the test substance was filled on top (Fig. 15, left). More details of the test setup can be found in the general methods of the ESI.† A positive DDT from the primary explosive towards PETN is indicated by a hole in the copper witness plate and the fragmentation of the shell. As illustrated in Fig. 15 on the right, compound **14** successfully initiates PETN. In the case of compounds **7**, and **16a** only negative results were obtained.

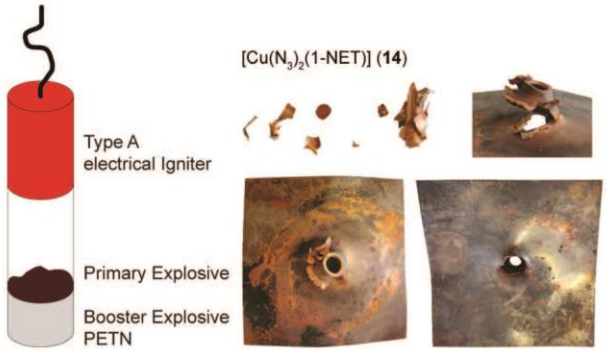


Fig. 15 Left: Initiation test setup without a copper witness plate. Right: Result of the initiation experiment of compound **14** toward PETN.

Laser ignition experiments

Particularly in the field of primary explosives, the safe handling of materials is still severely limited since the mechanical action is in many cases necessary for ignition.[1] For example,

 This journal is © The Royal Society of Chemistry 2021

Published on 29 June 2021. Downloaded by Ludwig Maximilians Universitaet Muenchen on 2/16/2022 8:09:47 AM.

the pyrotechnic charges used in the percussion caps are ignited by the frictional force generated by impact with the anvil. Therefore, the used energetic materials need to possess high sensitivities toward external stimuli like impact and friction. The sensitivity data of the most common primary explosives lead azide and lead styphnate monohydrate are displayed in Table 2. The sensitivity not only affects the safe preparation of the energetic materials, but also makes processing and distribution more difficult.

However, new ways of ignition, which do not require mechanical stimuli, enable the use of less sensitive materials. One method that has received great attention in recent years is ignition through laser irradiation.[27,42,43] In order to make use of this new technique, every elemental analysis pure ECC prepared in this work was tested for its ignitability by using a laser. Since only coloured compounds are known to react during these experiments, testing of the zinc and silver complexes **9**, and **16** was waived. The outcome of each test and the respective energy used for ignition are displayed in Table 3. Further information on the test setup and the procedure can be found in the general information in the ESI.†

Interestingly not every compounds investigated showed positive results during the laser experiments. A decomposition (Table 3) indicates that no output was observed in the laser setup during laser irradiation. An inspection of the primer cap only showed changes in the colour within the sample. A combustion (Fig. 16, bottom right) was observed for most of the complexes based on trinitrophenolate anions. This is likely caused by the compounds' higher carbon content, resulting in lower energetic compounds. Detonations were observed for compounds **7** and **14**, which was expected with respect to the corresponding hot plate and hot needle tests (Fig. 16, top right & bottom left). However, the results of complexes **8**, **11**, and **13** were surprising in terms of outcome. In previous experiments, chlorate, and perchlorate complexes proved to exhibit the strongest performance.[27,28,31] In this case only a slight decomposition within the primer cap was observed after the irradiation. This reinforces the theory that thermal ignition may be the reason for initiation and that the substances' low melting point may be a hindrance to this. Furthermore, pressing the substance into the caps also showed melting because of the force applied during compression. Therefore, these substances are likely to find applications as laser-ignitable energetic components, only as a component of a mixture and not as a neat substance.

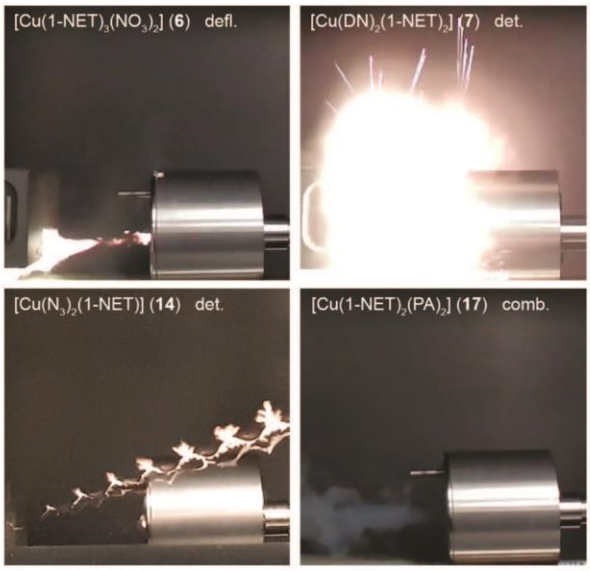


Fig. 16 Single pictures of a high-speed movie of the reaction of ECCs **6**, **7**, **14**, and **17** during laser ignition experiments at an energy of 25.5 mJ.

Conclusions

A one pot synthesis of 1-hydroxyethyl-5*H*-tetrazole was established in good overall yields by taking advantage of acetyl protection. A mixture of the 1- and 2-hydroxyethyl isomers was prepared by alkylation and after nitration with 100% nitric acid the mixture was separated by chromatographic methods. Both compounds 1-NET (1-nitratoethyl-5*H*-tetrazole) and 2-NET (2-nitratoethyl-5*H*-tetrazole), further used as ligands, were investigated by single crystal XRD and various NMR techniques, including ^{1}H, ^{13}C, ^{14}N, and ^{1}H ^{15}N HMBC. 2-NET was additionally investigated through ^{15}N NMR to clarify the atom assignment in the HMBC spectrum. BAM sensitivity measurements showed equal values for the friction sensitivity; however much higher impact sensitivities for the 2-isomer were observed. Molecular interactions were investigated to shed light on the sensitivity data. On the basis of Hirshfeld analysis, structural elements were investigated concluding that the rigid structure of 2-NET is likely to cause the increased sensitivity. The tetrazole derivatives were subsequently used for the preparation of 22 different metal (Mn, Cu, Zn, and Ag) complexes. Only acetonitrile and water were used as green solvents, with both the ligands and the resulting ECCs exhibiting a desirable poor solubility in water. Each of these, with the exception of compound **13**, was investigated using low temperature single crystal X-ray diffraction. Thus, 18 of these complexes were obtained elemental analysis pure and subsequently characterized with respect to their sensitivity toward impact, friction, ball drop impact, and electrostatic discharge. In particular, nitrate complex **6** (196 °C) and trinitrophenolate based complexes **17** (197 °C) and **18a** (195 °C) showed very good thermal stabilities, which are outstanding especially for organic nitrates. The improved oxygen balance due to this functional group and the deflagration reactions of the compounds during hot plate and hot needle tests reveal that these compounds can be considered as burn rate catalysts like basic copper nitrate (BCN). However, due to their energetic properties, they simultaneously improve the performance of the mixture. The laser ignition experiments showed that non-classical routes of initiation are also possible for the majority of these additives. Furthermore, these experiments indicate that the dinitramide

Published on 29 June 2021. Downloaded by Ludwig Maximilians Universitaet Muenchen on 2/16/2022 8:09:47 AM.

complex 7 and azide complex **14** in particular are promising candidates as substitutes for BNCP. Because of a positive PETN initiation test, the latter compound is also interesting as a substitute for lead azide or lead styphnate.

Author contributions

The manuscript was written through contributions of all authors. All authors have given approval to the final version of the manuscript.

Conflicts of interest

There are no conflicts to declare.

Acknowledgements

The financial support of this work by the Ludwig-Maximilian University (LMU), the Office of Naval Research (ONR), under grant no. ONR N00014-19-1-2078, and the Strategic Environmental Research and Development Program (SERDP) under contract no. W912HQ19C0033 is gratefully acknowledged. Furthermore, the authors would like to thank Professor Dr Konstantin Karaghiosoff for the measurement of the ^{1}H–^{15}N NMR spectra, and Dr Burkhard Krumm for the measurement of the ^{15}N NMR spectrum.

Notes and references

1 T. M. Klapötke, *High Energy Materials*, De Gruyter, Berlin, Boston, 5th edn, 2019.

2 (*a*) D. Kumar, G. H. Imler, D. A. Parrish and J. M. Shreeve, *J. Mater. Chem. A*, 2017, **5**, 10437–10441; (*b*) Y. Tang, K. Li, A. K. Chinnam, R. J. Staples and J. M. Shreeve, *Dalton Trans.*, 2021, **50**, 2143–2148; (*c*) L. M. Barton, J. T. Edwards, E. C. Johnson, E. J. Bukowski, R. C. Sausa, E. F. C. Byrd, J. A. Orlicki, J. J. Sabatini and P. S. Baran, *J. Am. Chem. Soc.*, 2019, **141**, 12531–12535; (*d*) J. Ma, H. Yang, J. Tang, G. Zhang, Z. Yi, S. Zhu and G. Cheng, *Dalton Trans.*, 2020, **49**, 4675–4679; (*e*) N. Lease, L. M. Kay, G. W. Brown, D. E. Chavez, D. Robbins, E. F. C. Byrd, G. H. Imler, D. A. Parrish and V. W. Manner, *J. Org. Chem.*, 2020, **85**, 4619–4626.

3 M. A. S. Laidlaw, G. Filippelli, H. Mielke, B. Gulson and A. S. Ball, *Environ. Health*, 2017, **16**, 34.

4 (*a*) Candidate List of substances of very high concern for Authorisation, https://echa.europa.eu/de, (accessed May 2021); (*b*) D. C. Dorman, S. H. Benoff, E. C. Bishop, M. L. Bleecker, L. M. Brosseau, R. H. Goldman, J. H. Graziano, S. A. Milz, S. K. Park and M. A. Roberts, *National Research Council Report: Potential Health Risks to DOD Firing-Range Personnel from Recurrent Lead Expo-sure*, National Academies Press, Washington, DC, USA, 2012.

5 T. Brinck, *Green Energetic Materials*, John Wiley & Sons Ltd., New York, 1st edn, 2014.

6 (*a*) M. L. Gettings, M. T. Thoenen, E. F. C. Byrd, J. J. Sabatini, M. Zeller and D. G. Piercey, *Chem. – Eur. J.*, 2020, **26**, 14530–14535; (*b*) N. Fischer, D. Fischer, T. M. Klapötke, D. G. Piercey and J. Stierstorfer, *J. Mater. Chem.*, 2012, **22**, 20418–20422; (*c*) S. Manzoor, Q. Tariq, X. Yin and J. Zhang, *Def. Technol.*, 2021, DOI: 10.1016/j.dt.2021.02.002; (*d*) R. Meyer, J. Köhler and A. Homburg, *Explosives*, Wiley-VCH, Weinheim, 7th edn, 2016.

7 J. Roh, K. Vávrová and A. Hrabálek, *Eur. J. Org. Chem.*, 2012, 6101–6118.

8 P. N. Gaponik and V. P. Karavai, *Chem. Heterocycl. Compd.*, 1985, **21**, 1172–1174.

9 (*a*) P. N. Gaponik, V. P. Karavai and Yu. V. Grigor'ev, *Chem. Heterocycl. Compd.*, 1985, **21**, 1255–1258; (*b*) M. H. H. Wurzenberger, M. S. Gruhne, M. Lommel, N. Szimhardt, T. M. Klapötke and J. Stierstorfer, *Chem. – Asian J.*, 2019, **14**, 2018–2028.

10 T. M. Klapötke, B. Krumm, T. Reith and C. C. Unger, *J. Org. Chem.*, 2018, **83**, 10505–10509.

11 (*a*) M. S. Ghasemzadeh and B. Akhlaghinia, *ChemistrySelect*, 2020, **5**, 6440–6452; (*b*) A. F. Stassen, M. Grunert, E. Dova, H. Schenk, G. Wiesinger, M. Müller, P. Weinberger, W. Linert, J. G. Haasnoot and J. Reedijk, *Eur. J. Inorg. Chem.*, 2003, **2003**, 2273–2282.

12 (*a*) K. A. McDonald, S. Seth and A. J. Matzger, *Cryst. Growth Des.*, 2015, **15**, 5963–5972; (*b*) Q. Zhang and J. M. Shreeve, *Angew. Chem., Int. Ed.*, 2014, **53**, 2540–2542; (*c*) H. Gao, Q. Zhang and J. M. Shreeve, *J. Mater. Chem. A*, 2020, **8**, 4193–4216.

13 R. N. Roberts and R. H. Dinegar, *J. Phys. Chem.*, 1958, **62**, 1009–1011.

14 N. Fischer, T. M. Klapötke, J. Stierstorfer and C. Wiedemann, *Polyhedron*, 2011, **30**, 2374–2386.

15 J. Stierstorfer, K. R. Tarantik and T. M. Klapötke, *Chem. – Eur. J.*, 2009, **15**, 5775–5792.

16 L. Zeisel, N. Szimhardt, M. H. H. Wurzenberger, T. M. Klapötke and J. Stierstorfer, *New J. Chem.*, 2019, **43**, 609–616.

17 T. M. Klapötke, J. Stierstorfer and B. Weber, *Inorg. Chim. Acta*, 2009, **362**, 2311–2320.

18 K. Shiota, H. Matsunaga and A. Miyake, *J. Therm. Anal. Calorim.*, 2015, **121**, 281–286.

19 (*a*) D. E. Bays, *Eu. Pat*, EP0117368A1, 1982; (*b*) T. M. Klapötke and S. M. Sproll, *Eur. J. Org. Chem.*, 2010, 1169–1175.

20 W. G. Finnegan and R. A. Henry, *J. Org. Chem.*, 1959, **24**, 1565–1567.

21 UN Model Regulation: Recommendations on the Transport of Dangerous Goods – Manual of Tests and Criteria, section 13.4.2.3.3, 2015.

22 (*a*) BAM, http://www.bam.de, (accessed April May); (*b*) NATO standardization agreement (STANAG) on explosives, impact sensitivity tests, no. 4489, 1st edn., Sept. 17th, 1999; (*c*) WI-WEB-Standardarbeitsanweisung 4-5.1.02,

This journal is © The Royal Society of Chemistry 2021

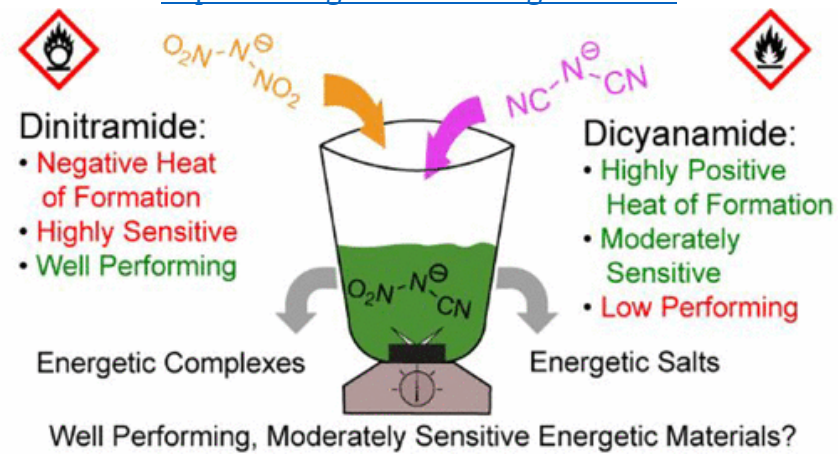
Appendix 26

Hybridization of Dinitramide and Dicyanamide: Evaluation of Nitrocyanamide in Energetic Salts and Coordination Compounds

M. Gruhne, M. Benz, T. Lorenzen, T. Lenz, T. M. Klapötke, J. Stierstorfer

Cryst. Growth Des., **2022**, *22*, 200–212.

https://doi.org/10.1021/acs.cgd.1c00858



Supplementary Information:
https://pubs.acs.org/doi/suppl/10.1021/acs.cgd.1c00858/suppl_file/cg1c00858_si_001.pdf

CRYSTAL GROWTH & DESIGN

pubs.acs.org/crystal

Article

Hybridization of Dinitramide and Dicyanamide: Evaluation of Nitrocyanamide in Energetic Salts and Coordination Compounds

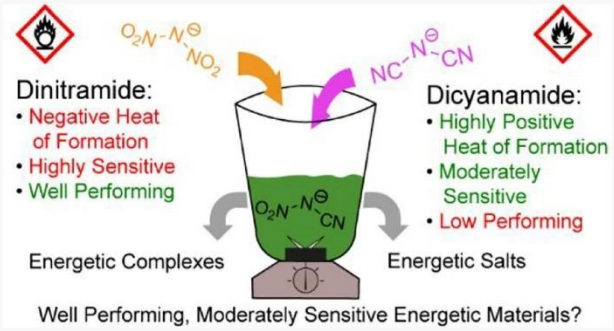
Michael Gruhne,[‡] Maximilian Benz,[‡] Tizian Lorenzen, Tobias Lenz, Thomas M. Klapötke, and Jörg Stierstorfer*

Cite This: *Cryst. Growth Des.* 2022, 22, 200−212

Read Online

ACCESS | Metrics & More | Article Recommendations | Supporting Information

ABSTRACT: In this work, the anion nitrocyanamide (NCA^-), as a cross between the dinitramide and the dicyanamide anion, was investigated as a building block in various energetic materials. Apart from nonenergetic complexes, only the use in ionic liquids has been investigated so far. Consequently, the focus in this work was on the synthesis of energetic coordination compounds (ECC) involving tetrazole ligands as well on nitrogen-rich salts, which includes not only ammonium but also hydrazinium, hydroxylammonium, and triaminoguanidinium. During the formation of the salts, particular focus was also put on the possible formation of adducts with nitrogen bases. This was proven with the help of IR and NMR spectroscopy. The complexation resulted in two silver(I) and nine copper(II) complexes, which were studied not only in terms of their coordination geometries but also in terms of their energetic properties. Each compound was checked on purity using CHNO elemental analysis. In some cases, X-ray diffraction experiments were carried out to become clear about their final composition. Thermal stability measurements were carried out using differential thermal analysis (DTA) and, for selected substances, thermogravimetric analysis (TGA). The sensitivities toward impact and friction were determined according to BAM (Bundesanstalt für Materialforschung and -prüfung) standard methods, together with measurements regarding sensitivity toward electrostatic discharge. Hot plate and hot needle tests were conducted for every metal salt and complex, whereas the detonation parameters of every nitrogen-rich salt were calculated using the EXPLO5 code.



Downloaded via LMU MUENCHEN on February 16, 2022 at 08:11:05 (UTC).
See https://pubs.acs.org/sharingguidelines for options on how to legitimately share published articles.

1. INTRODUCTION

The nitrocyanamide anion (NCA^-) was discovered rather accidentally in 1950 by McKay.[1] During the preparation of diazomethane from *N*-methyl-*N*′-nitro-*N*-nitrosoguanidine under alkaline conditions, he isolated the corresponding potassium salt as a byproduct. To date, further pathways for accessing the anion have already been examined. Thus, the reaction of various *N*-alkyl-*N*′-nitro-*N*-nitrosoguanidine derivatives results in the formation of nitrocyanamide salts.[2,3] Furthermore, syntheses starting from 1-alkyl-1,3-dinitroguanidines and *S*-methyl-*N*-nitroisothiourea are described.[4,5] The first energetic investigations of salts based on the nitrocyanamide anion were already carried out by Harris in 1957, i.e. shortly after its discovery.[6] At that time, he already emphasized the initiation capacity of silver and barium salts.[6]

The main research on this anion, however, focused on the reaction of nitrocyanamide as a nucleophile,[7−9] resulting in isocyanates, and later the implementation of the anion into transition metal complexes.[10−24] These were mainly based on pyrazole[10−12] and imidazole[10,13−17] ligands and were largely part of spectroscopic studies. Further energetic investigations were carried out rather recently, focusing on nitrocyanamide as part of ionic liquids used in hypergolic mixtures.[25−32] In this area, the group of Shreeve has been leading the way, whereas mostly dialkylated imidazolium cations[25,27,32] or other alkylammonium salts[25,28−32] were used. However, some energetic salts, such as aminoguanidnium or triaminoguanidinium, which are solids at ambient temperature, have also been investigated.[27]

In this work, the focus is again on the energetic properties of the anion. In general, the previous investigations are to be supplemented in terms of its use in nitrogen-rich salts. Furthermore, the anion is to be examined as a building block in energetic coordination compounds (ECC). The latter point is particularly interesting with respect to the earlier work of our group about energetic complexes. Thus, the dicyanamide (DCA^-) and more recently the dinitramide anion (DN^-) have

Received: July 29, 2021
Revised: November 11, 2021
Published: November 23, 2021



ACS Publications

© 2021 The Authors. Published by American Chemical Society

already been studied excessively in copper complexes.[33,34] The nitrocyanamide anion is therefore of particular interest in this context because of its structure. Since half of it consists of the oxidizing dinitramide anion due to its nitro group and the other half of the endothermic dicyanamide anion due to the nitrile unit. Accordingly, the heat of formation for the centerpiece is between that of the two anions (Figure 1).

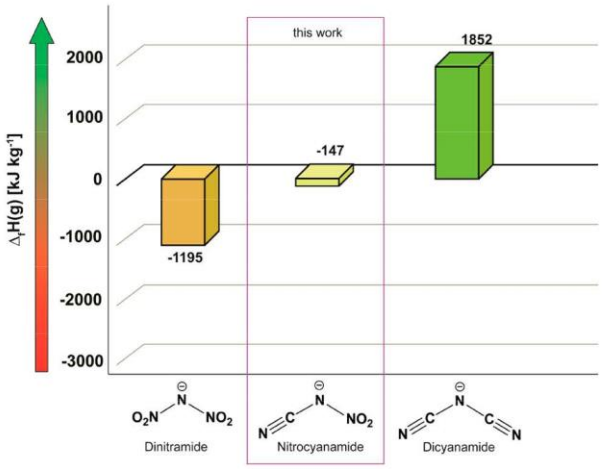


Figure 1. Calculated gas phase heats of formation for the scope of related anions dinitramide (DN^-), nitrocyanamide (NCA^-), and dicyanamide (DCA^-).

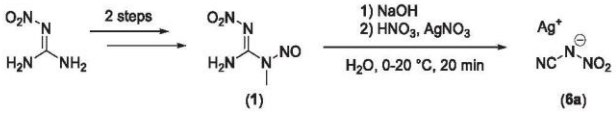
In the preceding studies, the dicyanamide complexes in particular showed only weak performance with sufficient thermal stabilities. The sensitivity of the compounds examined, however, was in rather low. Improved performances were observed for the dinitramide complexes. Nevertheless, the complexes were very sensitive and showed, with exceptions, too low thermal stabilities. However, since the centerpiece consists in part of the two anions, it was expected that the good performance of the complexes could be maintained. The sensitivity, on the other hand, should be within an acceptable range.

Thermal stability of DCA complexes is also partly based on the bridging character of the anion. This behavior is not to be expected especially in copper NCA complexes according to complexes described in the literature, the thermal stability must be influenced in other ways. In contrast to energetic salts, for which only the cation can be varied (*e.g.*, hydrazinium, hydroxylammonium), the concept of energetic coordination compounds offers further possibilities for adjusting the properties. In several studies, for example in copper dinitramide complexes, the thermal stability of the compounds has already been significantly increased by the introduction of bridging ligands.[34]

2. RESULTS AND DISCUSSION

2.1. Synthesis. As already mentioned earlier, the nitrocyanamide anion was discovered rather accidentally as a side product during the preparation of diazomethane from *N*-methyl-*N*′-nitro-*N*-nitrosoguanidine (**1**, MNNG).[2] The reaction equation for the formation of silver nitrocyanamide is displayed in Scheme 1. Compound **1** can easily be prepared in a two-step synthesis starting from commercially available nitroguanidine.[1] The silver salt of nitrocyanamide (**6a**) was

Scheme 1. Preparation of Silver Nitrocyanamide (6a)



then obtained directly through alkali promoted cleavage of MMNG (**1**) and subsequent precipitation by silver nitrate under nitric acid conditions in 86% yield.[6]

A suggested mechanism is displayed in Scheme 2.[35] The reaction is basic catalyzed and involves the intermediate formation of methyldiazotate. Proton rearrangement and the cleavage of water leads to the generation of diazomethane and nitrocyaniamide, which is precipitated as its silver salt **6a**.

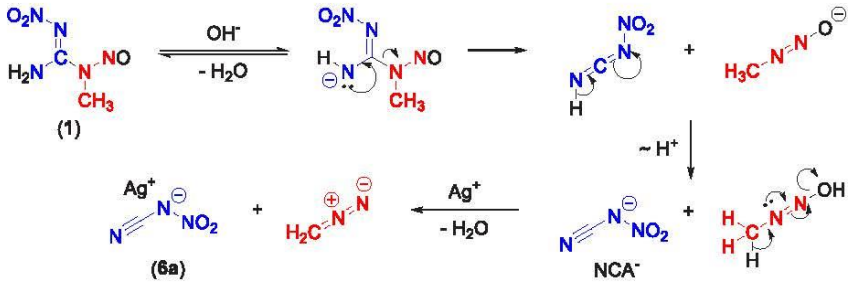
Several salts of nitrocyanamide including alkaline, alkaline earth, and transition metal salts are already known in the literature,[6] as well as nitrogen-rich derivatives including ammonium, and the already mentioned guanidinium, aminoguanidinium, and triaminoguanidium (TAG^+) salts,[6,27] as well as several ionic liquids.[25−32] Since the series of nitrogen-rich derivatives of NCA anions has not been fully investigated, we have focused on the synthesis and investigation thereof, as they tend to be promising compounds, which emerges from the structural hybridization of DCA and DN. Moreover, there are no energetic calculations or crystallographic studies on the known structures of nitrogen-rich NCA salts.[27] Therefore, compound **6a** was used as a basis for the preparation of the nitrogen-rich salts **2**, **3a**, **4a**, **5a**, and **5b**.[6] A metathesis reaction using the respective chloride or hydrochloride salts of nitrogen-rich cations, yielding silver chloride and the respective salt was performed enabling the convenient preparation of the desired salts in good yields of 74−90% (Scheme 3).[6] As green solvents, a mixture of methanol and acetonitrile (**3a**, **4a**, **5a**, and **5b**) or acetonitrile (**2**) and water was used, affording single crystals of each salt except compound **4a**, which is a liquid at room temperature. Applying an excess of the silver salt **6a** to triaminoguanidinium hydrochloride led to the formation of single crystals of compound **5b** (Scheme 3). Unfortunately, an elemental analysis pure isolation of the triaminoguanidinium nitrocyanamide argentat(I) complex was not possible.

Further reactions of nitrocyanamide anions as nucleophiles with alkyl halides, e.g., forming isocyanates and nitrous oxide, are already known in the literature.[7−9] In this work, however, reaction sequences of NCA^- anions, acting as electrophiles, were also investigated. Addition reaction of nitrocyanamine (HNCA) with hydroxylamine or hydrazine at elevated temperatures (100 °C) leads to the formation of the guanidine derivative products displayed in Scheme 4. Both compounds, 1-amino-3-nitroguanidine (**3b**) and 1-hydroxy-3-nitroguanidine (**4b**), are already known in the literature but only the hydrazinium adduct is sufficiently characterized.[36,37] A proposed mechanism for the formation of these adducts is shown in Scheme 4.

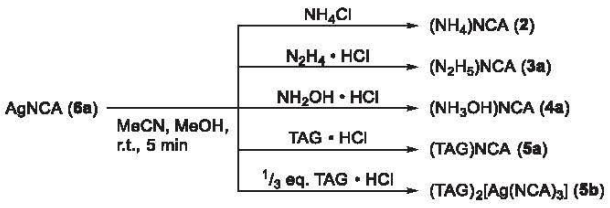
The examination whether an addition reaction or a salt formation has been taken place was analyzed according to the characteristic CN oscillation in the IR spectrum. As shown in Figure 2, the nitrile band at 2193 cm^{-1} clearly indicates whether the investigated substance is a cyanamide salt or guanidium derivative. Further IR spectra of the remaining compounds can be found in the Supporting Information (Figures S1−S4). The shift of the carbon signal in the

https://doi.org/10.1021/acs.cgd.1c00858
Cryst. Growth Des. 2022, 22, 200−212

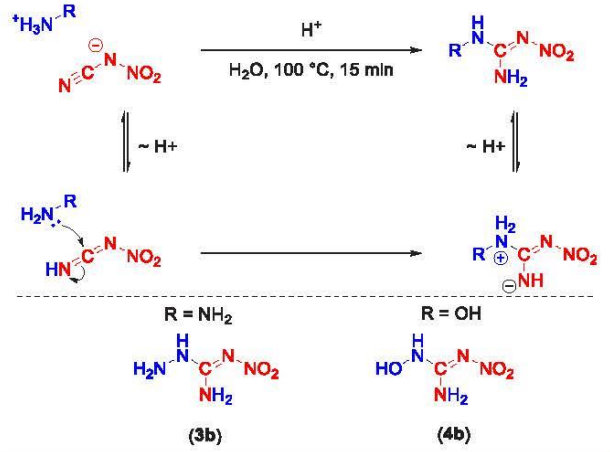
Scheme 2. Proposed Mechanism of the Formation of Silver Nitrocyanamide (6a) and Diazomethane from MNNG (1)[35]



Scheme 3. Formation of the Nitrogen-Rich Salts 2−5 of Nitrocyanamide from Silver Nitrocyanamide (6a)



Scheme 4. Formation of the Guanidine Derivatives for Hydrazinium (3a) and Hydroxylammonium (4a) Addition under Acidic Conditions



respective ^{13}C NMR spectrum is also a possible marker of addition product formation.

Addition reactions of cyanamide derivatives with nucleophiles under higher temperature are intensively described in the literature. For example, the reaction of guanidinium dicyanamide salts leads to the formation of melamine,[38,39] or the reaction of nitrocyanamide and strong acid to nitrourea.[3]

Besides the formation of energetic salts, the investigation of nitrocyanamide as an anion in energetic coordination compounds (ECCs) is a main aim of this work. Since the NCA^- anion is the center piece between the dinitramide (DN^-) and the dicyanamide anions (DCA^-), it is expected that the complexes properties lie in between those of the two anions. In the best case, the poor solubility as well as the good sensitivity data of the DCA complexes are thus achieved together with the performance of the DN complexes.[33,34]

Some transition metal complexes, mainly based on pyrazoles[10−12] and imidazoles[10,13−17] and other nitrogen-containing hetrocycles are already known in the literature.[18,19] Nearly all of them were not investigated toward a potential use as energetic material, however, they leave an indication how the complexes most likely built up. With the exception of some triphenylphosphine complexes,[20−22] as well as a trimethyltin complex,[23] only two complexes are known possessing a formula differing from the general $[M(L)_4(A)_2]$ pattern (M = central metal; L = ligand; A = anion).[13,24]

The complexes presented in this work were prepared by first reacting an aqueous solution of copper(II) chloride dihydrate with two equivalents of silver nitrocyanamide (**6a**) in acetonitrile (Scheme 5). Evaporation of the solvent gave the tetraaqua copper(II) nitrocyanamide complex (**7a**), which was already described by Harris.[6] Unfortunately, no single crystals could be obtained of the compound. Instead, a reaction with an aqueous solution of ammonia afforded single crystals of the similarly structured tetraammine complex **7b**. Dissolving the silver salt **6a** in aqueous ammonia afforded single crystals of the second silver complex **6b** obtained in this work (Scheme 5). Applying nitrogen-rich tetrazole ligands to the solution of copper nitrocyanamide instead of aqueous ammonia results in the formation of several ECCs (**8**−**12**) displayed in Scheme 5 (yields: 63−92%). The nitrogen-rich tetrazole ligands used in this work are shown in Chart 1. Some ligands were excluded (e.g., 1-amino-5*H*-tetrazoles) due to failed reactions.

Each ligand used for the preparation of energetic coordination compounds is known in the literature and can easily be prepared either through a substitution reaction of 1,5*H*-tetrazole and an alkyl halide,[40] the amination of 5-methyl-1*H*-tetrazole,[41] or a ring closure reaction of an alkyl amine or diamine with sodium azide and triethyl orthoformate.[42] The nitrogen-rich monotetrazole ligands 1-methyl-5*H*-tetrazole (MTZ) and 1-amino-5-methyltetazole (AMT) were chosen as both ligands are known to form powerful coordination compounds.[41,43] The ditetrazoles 1,1-ditetrazolylmethane (1,1-dtm) and 1,2-ditetrazolylmethane (1,2-dtm) and 1,1-ditetrazolylethane (dte) were selected because these ligands are showing a bridging behavior, known to increase a coordination compounds' thermal stability.[24,40]

The direct addition of the ditetrazolylethane ligand to copper NCA solution results in a mixture of complexes **12a**−**c**, depending on the amount of ligand used. However, if the acetonitrile is evaporated, or copper(II) NCA (**7a**) is isolated beforehand, it is possible to obtain the complexes **12b** and **12c** in pure form (yield: 76−77%). Both complexes were already described by Joas et al. but were prepared using a different protocol.[44] The side species **12a** could not be obtained elemental analysis pure. The complex **12c** obtained here and the ECC **9** are also the only coordination compounds that exhibit a composition that rejects from $[M(L)_2(A)_2]$.

https://doi.org/10.1021/acs.cgd.1c00858
Cryst. Growth Des. 2022, 22, 200−212

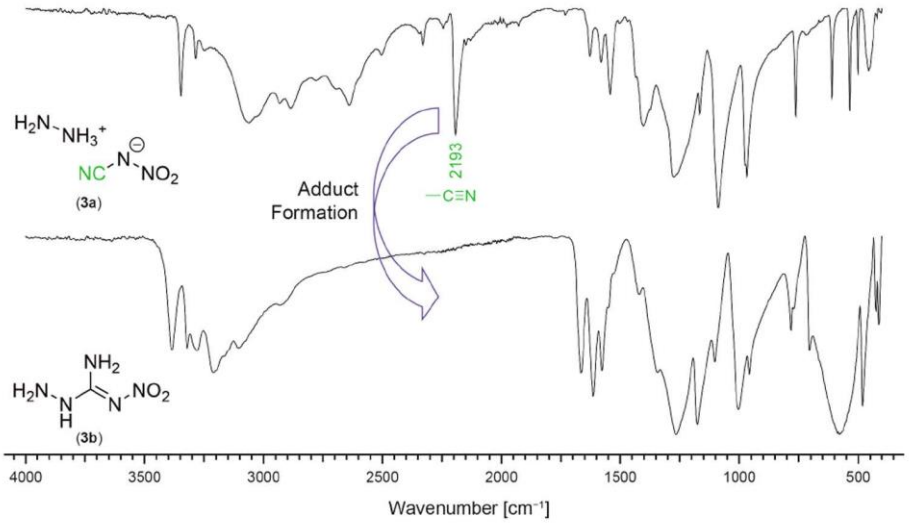


Figure 2. Comparison of the IR spectra of the hydrazinium salt (**3a**) and its respective addition product (**3b**).

Scheme 5. Overview of the Energetic Coordination Compounds based on the Nitrocyanamide Anion Prepared in this Work

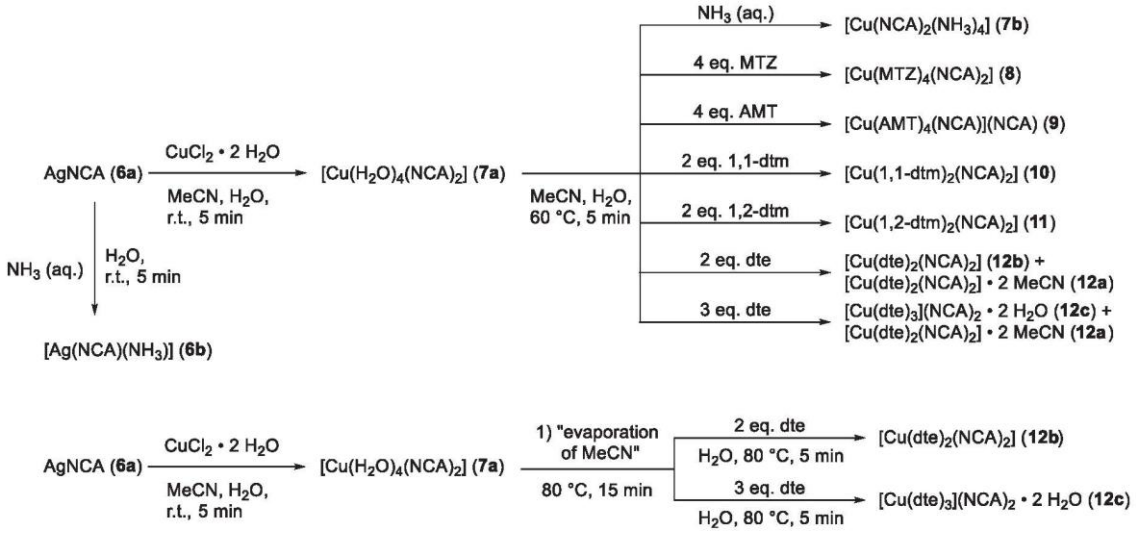
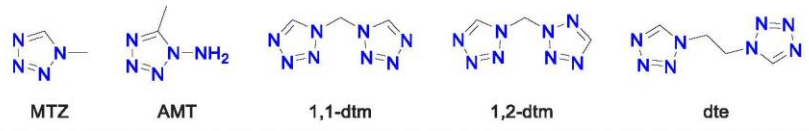


Chart 1. Overview on the Nitrogen-Rich Ligands Used for the Formation of the ECCs 8−12



As already mentioned, it was unfortunately not possible to obtained further coordination compounds with a silver central metal. Furthermore, the use of 1-aminotetrazole, or 1,5-diaminotetrazole, which are known to form some of the best performing ECCs only resulted in decomposition. This behavior was already observed during the investigation of copper(II) dinitramide ECCs and therefore most likely caused by an unwanted interaction with the nitramide moiety of the anion.[34]

2.2. Crystal Structures. Low temperature single crystal X-ray diffraction experiments were carried out for every solid compound except for **1**, **3b**, **4a**, and **6a** because the respective structures are already described in the literature,[45] and **7a**, of which unfortunately no single crystals could be obtained. In case of compound **12c** the measurement indicates the compounds' structure, but a finalization of the data set was not possible due to a strong disordered nitrocyanamide moiety. The complexes' composition was finally proved through CHNO elemental analysis. Details on the measurement and refinement data for every crystallographically investigated compound are listed in the Supporting Information (Tables S1−S4). The crystal data sets were uploaded to the CSD database with the CCDC numbers 2099366 (**2**), 2099365 (**3a**), 2099362 (**5a**), 2099357 (**5b**), 2099360 (**6b**), 2099356

https://doi.org/10.1021/acs.cgd.1c00858
Cryst. Growth Des. 2022, 22, 200−212

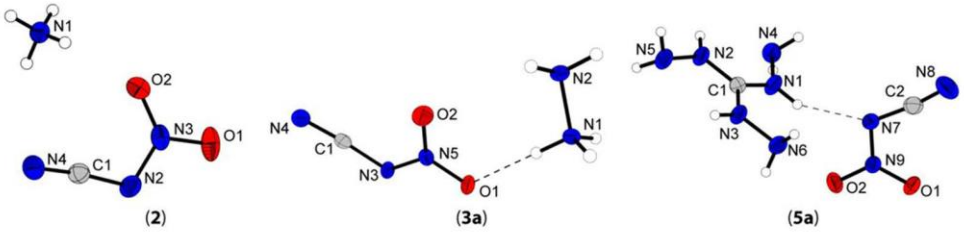


Figure 3. Crystal structures of the ammonium (**2**), hydrazinium (**3a**), and triaminoguanidinium (**5a**) salts of nitrocyanamide.

(**7b**), 2099361 (**8**), 2099363 (**9**), 2099364 (10), 2099355 (**11**), 2099359 (**12a**), and 2099358 (**12b**) and can be accessed free of charge.[46]

When it comes to the nitrogen-rich salts **2**, **3a**, and **4a**, the ammonium as well as the triaminoguanidinium salt have already been prepared but not structurally investigated yet.[6,27] Therefore, their structures were determined together with that of the hydrazinium salt (Figure 3). Every of the three salts crystallize in the monoclinic space group $P2_1/c$ with four formula units per unit cell. Hydrazinium salt **3a** possesses the highest density (1.606 g cm^{-3} at 123 K), followed by ammonium salt **2** (1.561 g cm^{-3} at 173 K), and finally by the triaminoguanidinium salt **5a** with density of 1.457 g cm^{-3} at 102 K. When it comes to the formation of a network of hydrogen bonds compound **5a** shows the strongest network. Intermolecular bonds are formed by each hydrogen atom of the cation. The NCA anion is participating with both of its oxygen atoms of the nitro group as well as with the nitramide and the nitrile nitrogen atoms. In case of the ammonium salt **2**, the cation is again forming hydrogen bonds with every of its hydrogen atoms. The anion, however, is only interacting throughout its amide and nitrile nitrogen atoms. For the hydrazinium salt **3a**, only the NH_3 group of the cation is forming bonds through their hydrogen atoms. The NH_2 group is only participating via its electron pair with a NH_3 group of another nearby hydrazinium cation. The anion is also solely interacting over one of its oxygen and its nitramide nitrogen atom.

The structurally investigated coordination compounds showed various coordination geometries including two- and trifold for both silver(I) complexes, as well as 5- and 6-fold for the copper(II) complexes. The hexacoordinated copper complexes show a classic Jahn–Teller distortion along the axial positions. Except for the silver complexes **5b** and **6b** and the copper complexes **9** and **12c**, in every case the anion is solely coordinating over its nitrile moiety. Of the coordination modes shown in Figure 4, **C** is the only mode known to date,

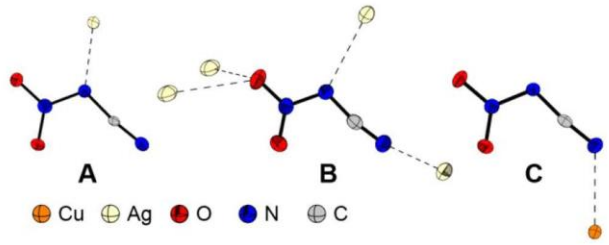


Figure 4. Overview on the Interactions of the NCA^- Anion with the Central Metals in the Coordination Compounds. Mode **A**: **5b**. Mode **B**: **6b**. Mode **C**: **7b**–**12b**.

with two other modes described in the literature not observed as part of this work.[19] For the structurally similar dinitramido ligand, a binding behavior via one of the oxygens is mainly known in copper complexes.[47,48] Recently, however, coordination via the nitramide nitrogen has also been observed by our group.[34] For the equally similar dicyanamide anion, a wide variety of coordination modes have been discovered in copper complexes.[33] Because of the nitrile moiety, one or more bonds originate from this unit in each case, with additional bonds via the amide nitrogen is also possible. In any case, it is interesting to note that the dinitramide anion does not coordinate in most cases, but DCA always does in the complexes described in the literature. Based on this information, it can be concluded that noncoordinating dicyanamide anions are probably not stable.

The tetrazole ligands, except for complex **10**, coordinate in the usual way via the N4 nitrogen. Since the bond lengths and angles in the nonbinding ligands are like those, found in the complexes, they are not part of the discussion.[40,41,49,50]

The argentat(I) complex **5b** crystallizes in the trigonal space group $P3_1c$ with six formula units per unit cell. The molecular unit consists of one silver, two triaminoguanidinium cations and three nitrocyanamide anions (Figure 5). The density of 1.933 g cm^{-3} (at 123 K) is higher than the ones of the other structurally investigated nitrogen-rich salts but significantly lower than the density published for the neat silver salt **6a** (3.251 g cm^{-3} at 293 K).[45] Hydrogen bonds are, as already observed in the TAG salt **5a**, formed by every hydrogen atom of the cation. The anion, however, is interacting with hydrogen atoms solely via both of its oxygen atoms and the nitrile moiety. The nitramide nitrogen atom is coordinating the silver atoms, leading to slightly distorted trigonal planar coordinated metal cations (Figure 4, mode A). The angles are close to the perfect 120° (N16–Ag3–N16 = 118.98(6)°), but the silver atom is displaced about 0.226(6) Å out of the plane.

Furthermore, a one-dimensional network is built up through argentophilic interactions of the silver cations (Ag2–Ag3 = 3.3083(10) Å). The NCA^- anions are arranged here in an alternating order. The TAG^+ cations arrange themselves between the strands and stabilize them by hydrogen bonds (Figure 6).

Both ammine complexes crystallize in the monoclinic space groups $P2_1/c$ (**6b**) and $C2/c$ (**7b**) with four formula units per unit cell, respectively. The silver(I) complex consists of one ammine and one nitrocyanamide ligand (Figure 7). The ligands are arranged almost perfectly linear (N1–Ag1–N4 = 174.77(10)°), whereas the anion is solely coordinating over its nitrile moiety. In addition to that, several stabilizing ionic interactions are formed between the silver center and nearby NCA^- anions as displayed in Figure 4 (mode **B**). The copper center in the ECC **7b** is coordinated by four ammine ligands in equatorial positions and two NCA^- anions (Figure 4, mode **C**) in the axial positions. A structural comparison with ammine

https://doi.org/10.1021/acs.cgd.1c00858
Cryst. Growth Des. 2022, 22, 200–212

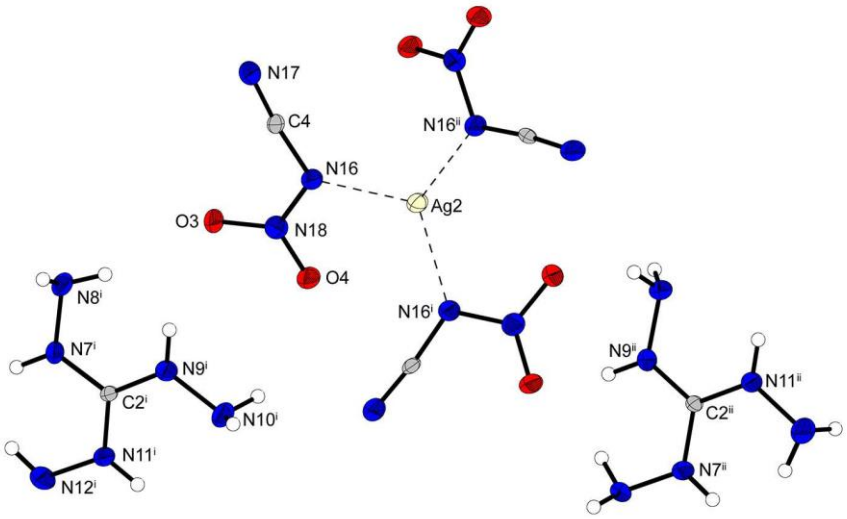


Figure 5. Molecular unit of compound **5b**. Selected bond length (Å): Ag1–N16 2.213(5). Symmetry codes: (i) $1 - y, x - y, z$; (ii) $1 - x + y, 1 - x, z$.

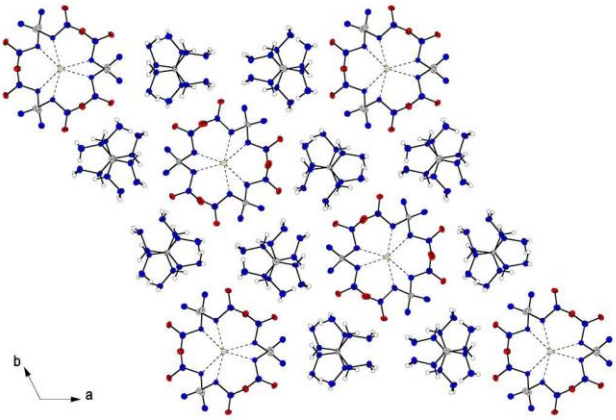
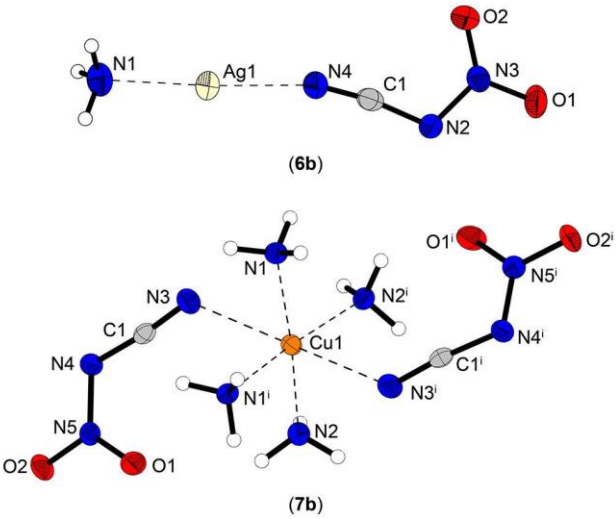


Figure 6. Packing of compound **5b** displayed along the *c* axis.



(7b)

Figure 7. Molecular units of the ammine complexes [Ag(NCA)-(NH_3)] (**6b**) and $[Cu(NCA)_2(NH_3)_4]$ (**7b**). Selected bond lengths (Å) of **6b**: Ag1–N1 2.153(3); Ag1–N4 2.135(3). Selected bond lengths (Å) of **7b**: Cu1–N1 2.013(2); Cu1–N3 2.610(3). Selected bond angles (deg) of **7b**: N3–Cu1–N2 90.44(9); N1–Cu1–$N2^i$ 90.08(8). Symmetry code of **7b**: $1 - x, y, 0.75 - z$.

complexes based on the dinitramide anion indicates a similar coordination geometry for the copper(II) complex, whereby the anion is coordinating via an oxygen atom.[47] The respective silver(I) complex was not crystallographically investigated, but the composition indicates a 2-fold coordinated diammine complex.[51] This is to be expected, since in this case the dinitramide anion has no coordination possibility via a nitrile group.

The copper(II) ECC **8**, based on the MTZ ligand, crystallizes in the form of blue platelets in the monoclinic space group $P2_1/c$ with four formula units per unit cell and a calculated density of 1.715 g cm^{-3} at 100 K. The central metal is coordinated very similar to the copper(II) ammine complex **7b**. Four ligands are arranged in the equatorial sites and anions in the remaining axial spots (Figure 8). The Jahn–Teller distortion (Cu1–N22 = 2.380(2) Å; Cu1–N19 = 2.390(2) Å) is not as distinct as in complex **7b** (Cu1–N3 = 2.610(3) Å).

The copper complex **9** crystallizes in the orthorhombic space group *Pbca*. The unit cell consist of eight formula units and possesses a calculated density of 1.635 g cm^{-3} (at 173 K). The compound is the only copper(II) complex of this work not showing a 6-fold geometry around its central metal (Figure 9). Instead, a slightly distorted square planar pyramidal conformation is observed (N4–N19–N14–N9 = 4.98(8)°). The AMT ligands are forming the basis, with one nitrocyanamido ligand at its tip (Figure 4, mode **C**). The remaining NCA^- anion is located on the bottom of the pyramid, whereby the distance between nitrile moiety and copper center is too long to be considered as any kind of interaction (Cu1–N26 = 5.375(3) Å). This is most likely caused by the sterically demanding disubstituted monotetrazole ligands and was therefore already observed in earlier studies.[34]

The copper(II) complexes **10** and **11** based on the isomeric dtm ligands crystallize with similar sum formulas in the monoclinic space groups $P2_1/n$ (**10**) and $P2_1/c$ (**11**). Both compounds' unit cells consist of two formula units with slightly differing calculated densities of 1.880 g cm^{-3} (**10**, at 103 K) and 1.932 g cm^{-3} (**11**, at 102 K). In both cases, the complexes'

https://doi.org/10.1021/acs.cgd.1c00858
Cryst. Growth Des. 2022, 22, 200–212

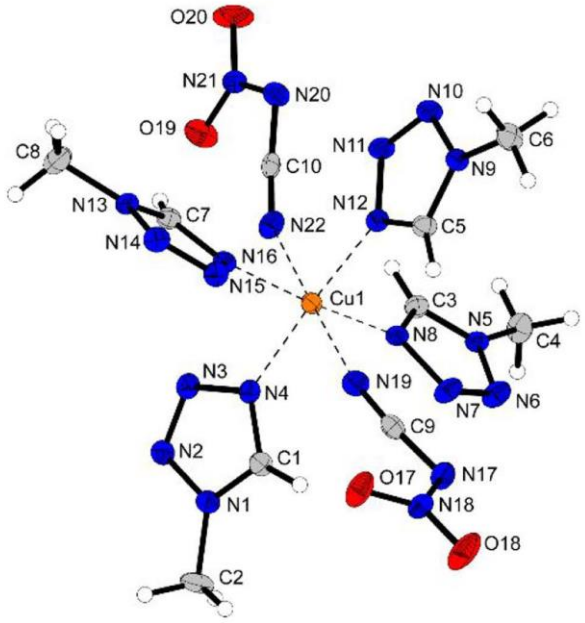


Figure 8. Molecular unit of $[Cu(MTZ)_4(NCA)_2]$ (**8**). Selected bond lengths (Å): Cu1−N4 2.024(2); Cu1−N8 2.030(2). Selected bond angles (deg): N12−Cu1−N16 89.18(8); N16−Cu1−N22 87.31(8); N12−Cu1−N22 91.33(8).

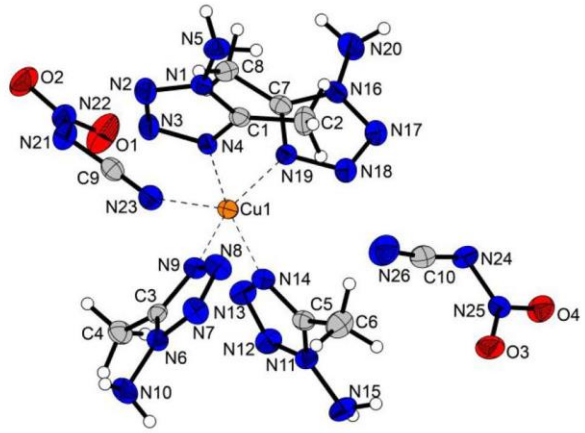


Figure 9. Molecular unit of $[Cu(AMT)_4(NCA)](NCA)$ (**9**). Selected bond lengths (Å): Cu1−N4 2.017(2); Cu1−N23 2.156(2). Selected bond angles (deg): N23−Cu1−N9 100.48(8); N23−Cu1−N4 96.61(8); N9−Cu1−N14 88.35(8); N9−Cu1−N19 159.84(8).

equatorial coordination sites are occupied by dtm ligands of which each links to a different metal center (Figures 10 and 11). This leads to the formation of two-dimensional polymeric layers. The nitrocyanamido ligands are located in the axial positions and are coordinating via the coordination mode **C** displayed in Figure 4.

Despite the similar built-up nature of both complexes, differently arranged polymeric layers are formed by each ligand (Figure 12). This is not only caused by the different substituted tetrazoles in the different ligands. As already mentioned earlier, complex **10** is the only compound possessing ligands which are not solely coordinating via its N4/N8 nitrogen atoms but also via the N3/N7 nitrogen.

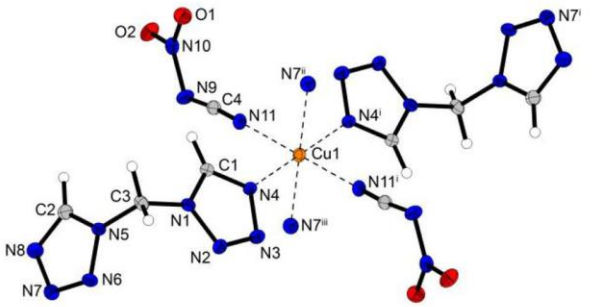


Figure 10. Molecular unit of $[Cu(1,1\text{-dtm})_2(NCA)_2]$ (**10**). Selected bond lengths (Å): Cu1−N4 2.005(2); Cu1−N7 2.414(2); Cu1−N11 1.982(2). Selected bond angles (deg): N4−Cu1−N11 89.44(9); N4−Cu1−N7ⁱⁱ 88.41(8); N7ⁱⁱ−Cu1−N11 92.18(8). Symmetry codes: (i) $2-x, 1-y, 1-z$; (ii) $0.5+x, 1.5-y, -0.5+z$; (iii) $1.5-x, -0.5+y, 1.5-z$.

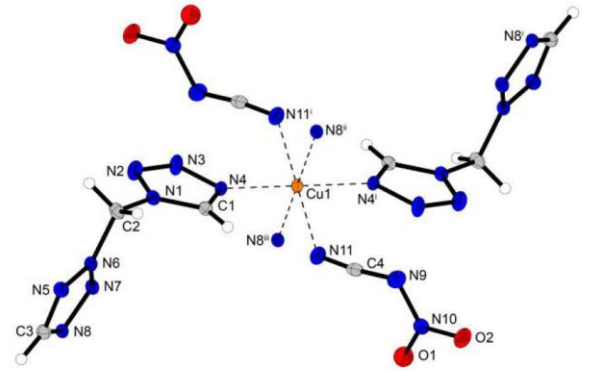


Figure 11. Extended molecular $[Cu(1,2\text{-dtm})_2(NCA)_2]$ (**11**). Selected bond lengths (Å): Cu1−N4 2.0217(18); Cu1−N8 2.0307(17); Cu1−N11 2.3216(19). Selected bond angles (deg): N8−Cu1−N11 91.29(7); N4−Cu1−N8 88.47(7); N4−Cu1−N11 93.23(7). Symmetry codes: (i) $2-x, 1-y, 1-z$; (ii) $x, 0.5-y, -0.5+z$; (iii) $2-x, 0.5+y, 1.5-z$.

The complexes **12a** and **12b**, both consisting of 2 equiv of the dte ligand, crystallize in the triclinic space group $P\bar{1}$ with only one formula unit per unit cell. The measurement data of **12b** is consistent with the data obtained by Joas et al.[24] The crystallographic density of complex **12b** (1.824 g cm^{-3} at 102 K) is significantly higher than the one calculated for **12a** (1.666 g cm^{-3} at 102 K). The general formula $[M(L)_2(A)_2]$ derived from the coordination sphere of each complex is like the ones of the complexes **10** an **11**. This is because all the complexes are based on ditetrazole ligands in equatorial positions, which exhibit a linking behavior (Figure 13). In complexes **12a** and **12b**, however, the complexes do not bridge to different metal centers, but instead bridge in pairs to the same metal center. Therefore, instead of a two-dimensional network, 1D polymeric chains are formed. The remaining axial positions are again occupied by NCA^- anions coordination via their nitrile moiety (Figure 4, mode **C**).

However, since complex **12a**, unlike **12b**, has two cocrystallizing acetonitrile molecules, the polymer network formed is slightly different (Figure 14). Caused by the interaction with the solvent molecules, the anion is slightly differently arranged in the coordination sphere. This can be represented best by the N8−Cu1−N11−C5 torsion angle in **12a**. This, with a value of 113.43° is considerably different from the respective angle in

https://doi.org/10.1021/acs.cgd.1c00858
Cryst. Growth Des. 2022, 22, 200−212

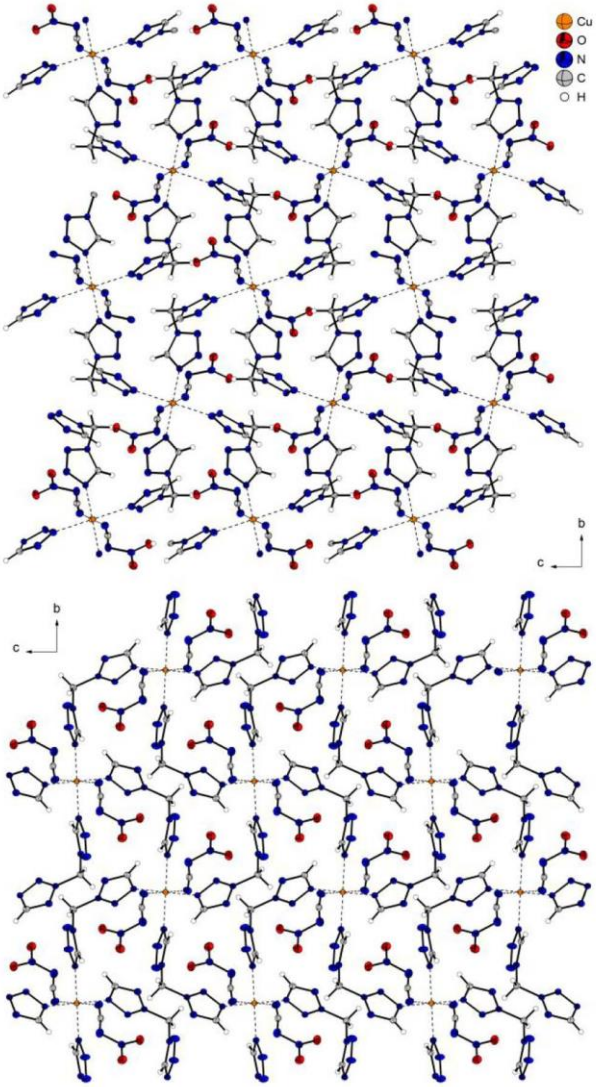


Figure 12. Detail of the packing of complexes **10** (top) and **11** (bottom) displayed along the *a* axis.

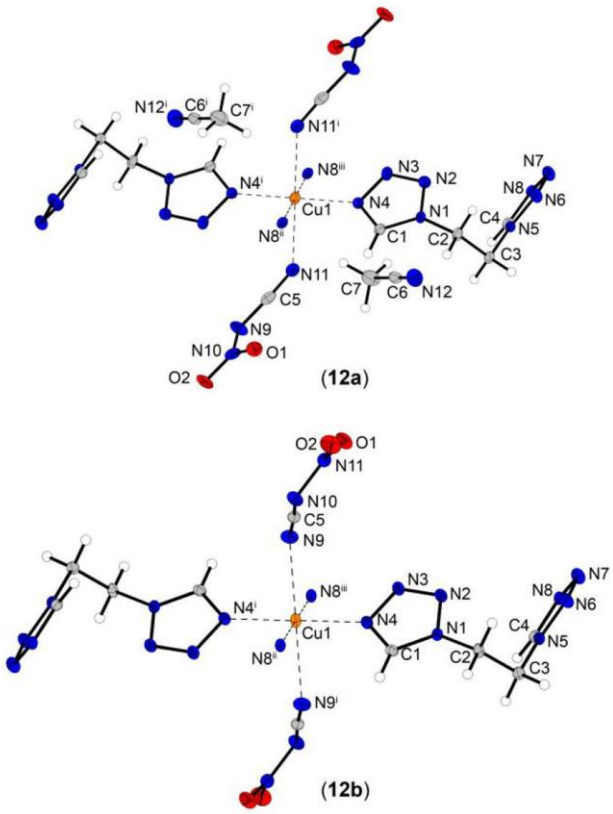


Figure 13. Extended Molecular Units of $[Cu(dte)_2(NCA)_2]\cdot 2$ MeCN (**12a**) and $[Cu(dte)_2(NCA)_2]$ (**12b**). Selected bond lengths (Å) of **12a**: Cu1–N4 2.0217(18), Cu1–N8 2.047(3), Cu1–N11 2.401(3). Selected bond lengths (Å) of **12b**: Cu1–N4 2.019(2), Cu1–N8 2.0308(15), Cu1–N9 2.4139(18). Selected bond angles (deg) of **12a**: N8–Cu1–N11 87.91(10), N4–Cu1–N8 91.19(10), N4–Cu1–N11 88.33(10). Selected bond angles (deg) of **12b**: N8–Cu1–N9 87.45(6), N4–Cu1–N8 90.21(6), N4–Cu1–N9 91.82(6). Symmetry codes of **12a**: (i) $2-x, 1-y, 1-z$; (ii) $1+x, y, z$; (iii) $1-x, 1-y, 1-z$. Symmetry codes of **12b**: (i) $-x, -y, 1-z$; (ii) $x, -1+y, z$; (iii) $-x, 1-y, 1-y$.

complex **12b** (N4–Cu1–N9–C5 = 69.25°). In addition to the packing shown in Figure 14, this also results in a lower density for **12a**.

As mentioned earlier, the structure of ECC **12c**, initially described by Joas et al.,[24] could not be finalized due to a heavily disordered anion. However, it is evident from the data obtained that each copper center is coordinated by three bridging dte ligands. This results in a three-dimensional network in which two crystal waters are intercalated. Furthermore, since all coordination sites are occupied, to the best of our knowledge this is the first NCA complex with two noncoordinating anions.

2.3. Evaluation of Physicochemical Properties. Besides the cost efficient synthesis and processing, the physicochemical properties are key factors for the developement of new energetic materials.[52] These include the thermal stability, the sensitivity toward various mechanical stimuli and electrostatic discharge as well as detonation parameters and an evaluation of the compounds' performance. The compounds **2**, **3a**, **3b**, **4a**, **5a**, **6a**, **7a**, **8**–**11**, **12a**, and **12c** were selected for further characterization since these substances were obtained elemental analysis pure and are expected to be the most promising materials regarding their energetic properties in this work.

Thermal stability measurements were carried out using differential thermal analysis (DTA) at a heating rate of 5 °C min^{-1} in the range 25–400 °C. The outcomes are listed in Tables 1 and 2. The endothermic events observed either indicate a melting (**2**, **3a**, **4a**, **5a**, and **8**), or, if present, a loss of hydrate water (**12c**) or aqua ligands (**7a**). Exothermic events usually indicate a decomposition of the material. In addition to DTA measurements, both aqua molecules containing complexes **7a** and **12c** were further investigated using thermogravimetry (TG) in the range of 30 to 400 °C at a heating rate of 5 °C min^{-1}. The TG plots are displayed in Figure 15. Plots of the DTA spectra together with full size versions of the TG plots can be found in the Supporting Information (Figures S4–S7).

The most significant properties due to their safety relevance are the sensitivities toward external mechanical stimuli.

https://doi.org/10.1021/acs.cgd.1c00858
Cryst. Growth Des. 2022, 22, 200–212

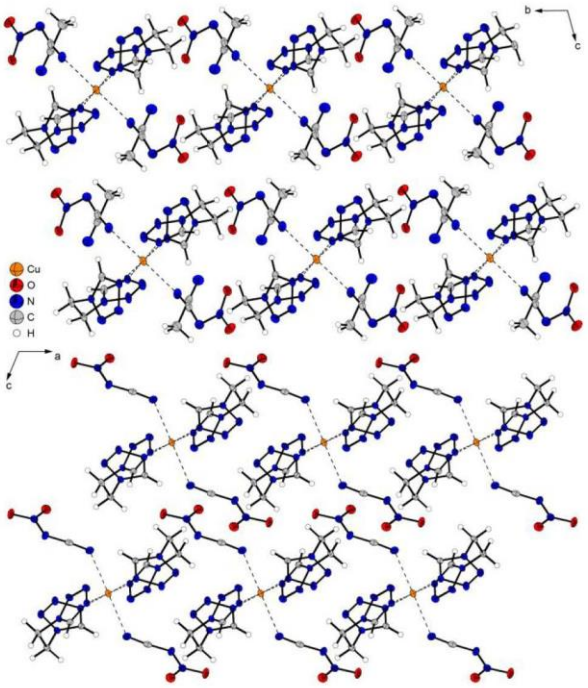


Figure 14. Detail of the packing of complexes **12a** (top) displayed along the *b* axis and **12b** (bottom) shown along the *a* axis.

Therefore, the substances were examined regarding their impact sensitivity (IS) and friction sensitivity (FS) according to BAM (Bundesanstalt für Materialforschung and -prüfung) standard measure methods. In addition, measurements evaluating the compounds' stability toward electrostatic discharge (ESD) were performed. The results are summarized in Tables 1 and 2.

Since it is rather difficult to compare energetic salts with complexes with respect to their stability or the stability trends occurring, the nitrogen-rich salts together with the poorly characterized compound **4b** were discussed first followed by the ECCs. First, the ammonium and hydroxylamine salts **2** and **4a** are classified as insensitive toward friction (FS > 360 N). All other derivatives are friction sensitive in the range of 360 N (for **5a**) to 80 N (for **3a**). The triaminoguanidinium derivative **5a** has the highest impact sensitivity (IS = 6 J), followed by **4b** with an impact sensitivity of 10 J. All other compounds (**2**–**4**) are insensitive toward impact (IS > 40 J). The compounds **4a** and **4b** mainly differ in their sensitivity toward impact, which is reasonable due to the different aggregate state. The ammonium and TAG salt **2** and **5a** show the highest decomposition temperature with 177 and 173 °C, respectively. The thermally most instable compound is ionic liquid **4a**, which sharply decomposes at 94 °C. Explosive properties of the ionic derivatives **2**–**5a** and the hydroxylamine adduct **4b** were calculated using the EXPLO5 code. The resulting parameters were then compared to those of ammonium dinitramide (ADN). Therefore, the heats of formation were calculated based on the CBS-4 M basis set, and the respective densities from crystallographic measurements were used. In case of compound **4a**, which is a room temperature ionic liquid, the density was estimated according to related molecular structures. The highest densities of the compounds investigated also result in the highest calculated detonation parameters for the hydroxylamine-containing compounds **4a** and **4b**. The detonation velocity and the detonation pressure are approximately equal (**4a**, V_{det} = 8915 m s^{-1}, P_{CJ} = 329 kbar; **4b**, V_{det} = 8878 m s^{-1}, P_{CJ} = 332 kbar) which is in the range of hexogen, and easily outperform ADN (V_{det} = 8502 m s^{-1}, P_{CJ} =

Table 1. Summary on the Compounds' (2, 3a, 4a, 4b and 5a) Thermal Stability,[a] Sensitivities Toward Various External Stimuli, and Detonation Parameters (compared with ADN)

	$(NH_4)NCA$ (**2**)	$(N_2H_5)NCA$ (**3a**)	$(NH_3OH)NCA$ (**4a**)	**4b**	(TAG)NCA (**5a**)	$(NH_4)DCA$[53]	ADN[54]
formula	$CH_4N_4O_2$	$CH_5N_5O_2$	$CH_4N_4O_3$	$CH_4N_4O_3$	$CH_9N_9O_2$	$C_2H_4N_4$	$N_4H_4O_4$
M [g mol^{-1}]	104.07	119.09	120.07	120.07	191.16	84.08	124.06
IS [J][b]	>40	>40	>40	10	6	>40	4
FS [N][c]	>360	80	>360	240	360	>360	72
ESD [J][d]	>1500	750	–	750	>1500	–	0.45
ρ [g cm^{-3}][e]	1.532	1.565	1.68*	1.752	1.415	1.284	1.812
N [%][f]	53.8	58.8	46.7	46.7	66.0	66.6	45.2
Ω [%][g]	−15.4/−30.7	−20.2/−33.6	0/−13.3	0/−13.3	−31.3/−40.2	114.2/−76.1	25.8/25.8
T_{endo} [°C][h]	88	101	–	–	73	–	92
T_{exo} [°C][i]	177	129	94	144	173	127	135
$\Delta_f H°$ [kJ mol^{-1}][j]	30.0	186.1	112.1	−25.0	367.1	264.7	−125.3
$\Delta_f U°$ [kJ mol^{-1}][k]	42.4	201.0	125.7	−94.6	391.9	274.61	–
			EXPLO5 V6.05.02				
$-\Delta_{Ex}U°$ [kJ kg^{-1}][l]	4606	5509	6216	5161	4673	3572	2784
T_{det} [K][m]	3159	3469	3961	3414	3009	2502	2319
V_0 [L kg^{-1}][n]	937	965	891	877	972	824	984
P_{CJ} [kbar][o]	229	273	329	332	213	161	270
V_{det} [m s^{-1}][p]	7956	8620	8915	8878	7956	6823	8502

[a]Onset temperature at a heating rate of 5 °C min^{-1} measured by DTA. [b]Impact sensitivity according to the BAM drophammer (method 1 of 6). [c]Friction sensitivity according to the BAM friction tester (method 1 of 6). [d]Electrostatic discharge sensitivity (OZM Electric Spark XSpark10, method 1 of 6). [e]Crystallographic density recalculated to 298 K. [f]Nitrogen content. [g]Oxygen balance with respect to CO/CO_2. [h]Endothermic peak, which indicates melting. [i]Exothermic peak, which indicates decomposition. [j]Calculated enthalpy of formation. [k]Calculated energy of formation. [l]Energy of explosion. [m]Detonation temperature. [n]Volume of detonation products (assuming only gaseous products). [o]Detonation pressure at the Chapman Jouguet point. [p]Detonation velocity.

https://doi.org/10.1021/acs.cgd.1c00858
Cryst. Growth Des. 2022, 22, 200−212

Table 2. Overview on the Compounds' (6a, 7a, 8−11, 12b, 12c) Thermal Stability,[a] Sensitivities Toward Various External Stimuli and Results of Hot Plate (HP) and Hot Needle (HN) Tests

compound	no.	T_{endo} [°C][b]	T_{exo} [°C][c]	IS [J][d]	FS [N][e]	ESD [mJ][f]	HP[g]	HN[g]
AgNCA	**6a**	–	158	3	10	51	defl.	defl.
$[Cu(H_2O)_4(NCA)_2]$	**7a**	89	108	>40	>360	1500	dec.	dec.
$[Cu(MTZ)_4(NCA)_2]$	**8**	110	159	40	240	750	dec.	dec.
$[Cu(AMT)_4(NCA)](NCA)$	**9**	124[h]	124[h]	≤1	20	250	defl.	defl.
$[Cu(1,1\text{-dtm})_2(NCA)_2]$	**10**	–	191	7	112	750	defl.	dec.
$[Cu(1,2\text{-dtm})_2(NCA)_2]$	**11**	–	157	2	80	480	defl.	dec.
$[Cu(dte)_2(NCA)_2]$	**12b**	–	174	6	180	>1500	dec.	dec.
$[Cu(dte)_3](NCA)_2 \cdot 2\ H_2O$	**12c**	103, 119	168	≤1	160	>1500	dec.	dec.

[a]Onset temperature at a heating rate of 5 °C min^{-1} measured by DTA. [b]Endothermic peak, which indicates melting, or dehydration; [c]Exothermic peak, which indicates decomposition. [d]Impact sensitivity according to the BAM drophammer (method 1 of 6). [e]Friction sensitivity according to the BAM friction tester (method 1 of 6). [f]Electrostatic discharge sensitivity (OZM Electric Spark XSpark10, method 1 of 6). [g]Key: –, not tested; def., deflagration; dec., decomposition. [h]Endothermic closely followed by exothermic event.

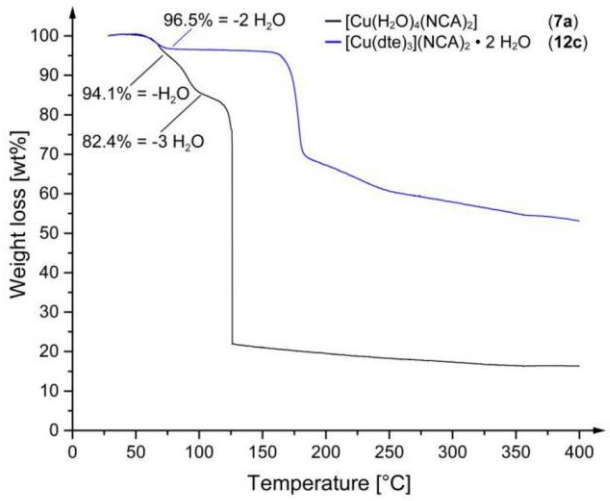


Figure 15. TG plots of $[Cu(H_2O)_4(NCA)_2]$ (**7a**) and $[Cu(dte)_3](NCA)_2 \cdot 2\ H_2O$ (**12c**).

270 kbar), which is also the case for the hydrazinium derivative **3a**. The ammonium and triaminoguanidinium derivatives **2** and **5a** feature a detonation velocity of around 8000 m s^{-1} (V_{det}(**2**, **5**) = 7956 m s^{-1}). For the ammonium derivative **2**, a clear trend is observed by comparing it with the respective ammonium salt of dicyanamide ((NH_4)DCA) and dinitramide (AND). The density increases by about 0.25 g cm^{-3} for the replacement of each cyano group by a nitro group from the dicyaniamide anion to the dinitramide anion. A similar trend is oberved for the resulting detonation velocity. This increases proportionally from the DCA$^-$ via the NCA$^-$ to the DN$^-$ derivative. The sensitivities, on the other hand, increase in the same order from the insensitive (NH_4)DCA and (NH_4)NCA to the moderately sensitive AND.

The thermal stability data determined for the ammonium salt (**2**) are consistent with the literature data.[6] Higher values were measured for the TAG salt (**5a**), but a higher heating rate of 10 °C min^{-1}, as used in this case, is known to result in higher decomposition temperatures of the products.[27] The sensitivity data for **5a** are consistent with the values reported in the literature.[27]

Comparing the ammonium salts of NCA$^-$ and dinitramide, the enthalpy of formation is significantly increased by the exchange of a nitro group of the ADN on the anion to a cyano group on the NCA ($\Delta_f H^0$ (**2**) = 30.0 kJ mol^{-1}; $\Delta_f H^0$(ADN) = −125.3 kJ mol^{-1}). On the other hand, this also significantly reduces the crystallographic density, which generally leads to a significant loss of performance. ADN is clearly superior in all detonation parameters. However, the relatively sensitive ADN (IS = 4 J, FS = 72 N) is opposed by the completely insensitive (NH_4)NCA (**2**).

The endothermic events of the complexes **8** and **9** indicate a melting of the compound, whereby in case of **9** the endothermic signal is directly followed by an exothermic signal. In case of compounds **7a** and **12c**, the endothermic signals represent a loss of hydrate water or aqua ligands (Figure 15).

A comparison of the thermal stabilities of the ECCs shows that the majority of the complexes exceed 150 °C (**6a**, **8**, **9**, **11**, and **12c**) with complex **10** even exceeding 190 °C. Furthermore, the effect of bridging ligands on temperature stability becomes clear. The most stable complex **10** in this context possesses bridging 1,1-dtm ligands. Complexes **11** and **12c** follow closely, but their composition causes a slight reduction in stability. Thus, on the one hand, the thermal stability of the ligands and the resulting complexes reduces when, in the case of dtm, the substitution pattern is changed from 1,1- (**10**) to 1,2- (**11**). On the other hand, it is assumed that complex **12c** loses significant stability after the loss of its hydrate water and therefore decomposes earlier. The same is expected as a reason for the decomposition temperature of the tetraaquacopper(II) complex **7a** after loss of its aqua ligands.

The metal salts and ECCs investigated in this work are almost all significantly more sensitive than the nitrogen-rich salts. The most sensitive compounds are neat silver nitrocyanamide (**5a**, IS = 3 J, FS = 10 N) together with the copper(II) complexes $[Cu(AMT)_4(NCA)](NCA)$ (**9**, IS ≤ 1 J, FS = 20 N) and $[Cu(dte)_3](NCA)_2 \cdot 2H_2O$ (**12c**, IS ≤ 1 J, FS = 160 N). In the case of pure silver nitrocyanamide (**5a**), these results are not surprising, as the compound is described as sensitive, but no BAM sensitivities were reported.[6] Similar findings apply to complexes based on the AMT ligand.[34,55] For example, $[Cu(AMT)_4(H_2O)](DN)_2$, which also has a pyramidal structure and has an aqua ligand instead of coordinating anions, is extremely sensitive to IS and FS (IS = 2 J, FS = 3 N).[34] In this context, the low impact sensitivity of **12c** is no longer surprising. Generally, it is assumed that aqua ligands or hydrated water led to less sensitive compounds. However, the measurements indicate that powerful ligands can compensate this influence. Both the AMT ligand used in complexes **9** and $[Cu(AMT)_4(H_2O)](DN)_2$ and the dite-

https://doi.org/10.1021/acs.cgd.1c00858
Cryst. Growth Des. 2022, 22, 200−212

trazolyl ligand showed very high gas phase enthalpies of formation. However, since the respective FS with a value of 160 N is in a completely different dimension, effects influencing the result, like ignition through hot spot formation, should also be considered.[56] Furthermore, based on previous observations of our group, it would be expected that complex **12b** would have to be significantly more sensitive than **12c**, since coordinating anions have led to extremely sensitive complexes in previous work.[24]

However, in this study, opposite values were measured. An analysis of the tetraaqua copper(II) complex (**7a**), for example, shows a clear desensitization due to the water ligands. Other trends already known include, for example, the higher sensitivity of 1,2-dtm (**11**, IS = 2 J, FS = 80 N) complexes compared to 1,1-dtm (**10**, IS = 7 J, FS = 112 N), and AMT (**9**, IS ≤ 1 J, FS = 20 N) compared to MTZ (**8**, IS = 40 J, FS = 240 N). Only the assumption that dtm complexes (**10**, **11**), because of their lower carbon content, are more sensitive than similar structured dte complexes (**12b**, IS = 6 J, FS = 180 N) could not be confirmed in this case. The sensitivity data for **12b** and **12c** are only roughly consistent with the values reported in the literature which is most likely due to a difference in the grain size of the investigated samples.

For a proper examination of the substances, a classification according to the UN Recommendation for the Transport of Dangerous Goods was carried out for every material. Accordingly, the earlier mentioned compounds **6a**, **9**, and **12c** are ranked as very sensitive, with pure silver nitrocyanamide (**6a**) being even extremely sensitive. Because of its friction sensitivity of 80 N, coordination compound **11** is also evaluated as a very sensitive material. The remaining compounds were less sensitive (**4b**, **5a**, **8**, **10**, **12b**) and therefore classified as sensitive only or even insensitive et all (**2**, **4a**, **7a**). It must also be added that silver nitrocyanamide exhibits a considerable sensitivity toward electrostatic discharge (ESD = 51 mJ).

Performance evaluations were examined for the metal salts and complexes **6a**, **7a**, **8**–**11**, **12b**, and **12c** through hot plate (HP) and hot needle (HN) tests. To perform a hot plate test, the investigated sample is placed on a copper plate and subsequently heated with a Bunsen burner. During a hot needle test, the sample is fixed on a copper plate using adhesive tape. Subsequently, the substance is penetrated with a red heated needle. The experiments are intended to provide insights into the behavior of the substances, respectively, under rapid heating or under light confinement. The outcomes of each investigation were recorded with a high-speed camera and the outcome of each test is displayed in Table 1. The reactions of silver NCA during these experiments are shown in Figure 16. Further high-speed images can be found in the Supporting Information (Figures S8–S11).

These experiments are of particular interest for perspective primary explosives. The outcome, in the best case is a detonation, is assumed to give insights into the compounds deflagration to detonation transition (DDT). A fast DDT is required for the initiation of PETN through primary explosives like lead azide. During the investigation of the metal salts and complexes in this work, the main outcomes were deflagrations for the hot plate tests and decompositions reactions during hot needle tests. Since most of the substances were investigated to be less or insensitive, this outcome was expected. Thus, the more sensitive compounds **6a**, **9**, **10**, and **11** showed deflagrations during at least one of both tests. At this point,

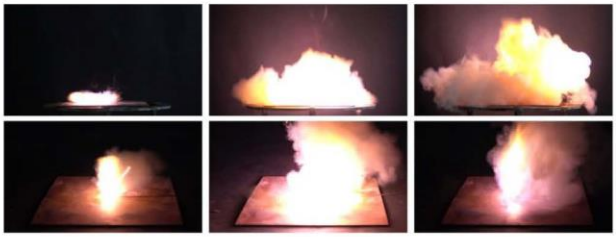


Figure 16. Deflagration of silver nitrocyanamide (**5a**) during hot plate (left) and hot needle tests (right).

laser ignition experiments would be discussed, but these tests were not performed due to the results of the HP and HN tests.

3. CONCLUSIONS

The main objective of this work was to investigate the nitrocyanamide anion (NCA^-)as a building block combining the properties of the dicyanamide and dinitramide anions. This was accomplished through the preparation of the insensitive ammonium, hydrazinium and hydroxylammonium salts. Both the hydrazinium and the hydroxylammonium salts showed impressive detonation parameters. Furthermore, the reactivity of the nitrocyanamide moiety toward hydroxylamine and hydrazine was investigated, which revealed a further method for accessing nitroguanidine derivatives.

As a further application, the anion was incorporated into various transition metal ECCs. Especially here, the aim was to combine the good properties of copper dinitramide and dicyanamide complexes. However, the comparisons proved difficult because the structure was strongly influenced by the coordination behavior of the anions. Regardless of structure and composition, it is apparent that the copper dinitramide complexes are in any case the most sensitive, followed by nitrocyanamide complexes and finally dicyanamide complexes, whereby the majority of complexes are still insensitive or less sensitive only. The thermal stability of the complexes was also greatly increased, especially by the introduction of bridging ditetrazoles up to 191 °C, outperforming the dicyanamide and dinitramide complexes based on such ligands. When it comes to performance, it also becomes clear that the complexes studied in this work could not surpass dinitramide-based copper complexes but are eventually more powerful than copper dicyanamide complexes. Consequently, the nitrocyanamide anion with regard to the energetically relevant properties of its copper complexes is in many aspects between the dinitramide and the dicyanamide anion.

■ ASSOCIATED CONTENT

Supporting Information

The Supporting Information is available free of charge on the ACS Publications Web site. The Supporting Information is available free of charge at https://pubs.acs.org/doi/10.1021/acs.cgd.1c00858.

Compound overview; crystallographic data of **2**, **3a**, **4a**, **5a**, **5b**, **6b**, **7b**, **8**–**11**, **12a**, and **12b**; computations and detonation parameters of **2**, **3a**, **4a**, **4b**, and **5a**; IR Spectroscopy of **2**–**4**, **5a**, **6**–**11**, **12b**, and **12c**; DTA plots of **2**, **3a**, **4a**, **5a**, **6a**, **7a**, **8**–**11**, **12b**, and **12c**; TGA plots of **7a** and **12c**; high speed recordings of hot plate, and hot needle tests of **2**, **3a**, **4a**, **5a**, **6a**, **7a**, **8**–**11**, **12b**,

https://doi.org/10.1021/acs.cgd.1c00858
Cryst. Growth Des. 2022, 22, 200−212

and **12c**; and experimental part and general methods (PDF)

Accession Codes

CCDC 2099355−2099366 contain the supplementary crystallographic data for this paper. These data can be obtained free of charge via www.ccdc.cam.ac.uk/data_request/cif, or by emailing data_request@ccdc.cam.ac.uk, or by contacting The Cambridge Crystallographic Data Centre, 12 Union Road, Cambridge CB2 1EZ, UK; fax: +44 1223 336033.

AUTHOR INFORMATION

Corresponding Author

Jörg Stierstorfer − *Department of Chemistry, Ludwig-Maximilian University of Munich, D-81377 Munich, Germany;* orcid.org/0000-0002-2105-1275; Email: jstch@cup.uni-muenchen.de; Fax: +49 89 2180 77007

Authors

Michael Gruhne − *Department of Chemistry, Ludwig-Maximilian University of Munich, D-81377 Munich, Germany*

Maximilian Benz − *Department of Chemistry, Ludwig-Maximilian University of Munich, D-81377 Munich, Germany*

Tizian Lorenzen − *Department of Chemistry, Ludwig-Maximilian University of Munich, D-81377 Munich, Germany*

Tobias Lenz − *Department of Chemistry, Ludwig-Maximilian University of Munich, D-81377 Munich, Germany*

Thomas M. Klapötke − *Department of Chemistry, Ludwig-Maximilian University of Munich, D-81377 Munich, Germany;* orcid.org/0000-0003-3276-1157

Complete contact information is available at: https://pubs.acs.org/10.1021/acs.cgd.1c00858

Author Contributions

‡M.G. and M.B. contributed equally. The manuscript was written through contributions of all authors. All authors have given approval to the final version of the manuscript.

Notes

The authors declare no competing financial interest.

ACKNOWLEDGMENTS

The financial support of this work by Ludwig-Maximilian University (LMU) is acknowledged. The Office of Naval Research (ONR) under Grant No. ONR N00014-19-1-2078 and the Strategic Environmental Research and Development Program (SERDP) under Contract No. W912HQ19C0033 are gratefully acknowledged. Jasmin Lechner is thanked for several TG measurements.

REFERENCES

(1) McKay, A. F.; Wright, G. F. Preparation and Properties of N-Methyl-N-nitroso-N'-nitroguanidine. *J. Am. Chem. Soc.* **1947**, *69* (12), 3028−3030.

(2) McKay, A. F.; Ott, W. L.; Taylor, G. W.; Buchanan, M. N.; Crooker, J. F. Diazohydrocarbons. *Can. J. Res., Sect. B* **1950**, *28B*, 683−688.

(3) Astrat'ev, A. A.; Kuznetsov, L. L. Formation and Decomposition of Nitrocyanamide in Strong Mineral Acids. *Russ. J. Org. Chem.* **2002**, *38* (9), 1252−1259.

(4) Meen, R. H.; Wright, G. F. The scission of new 1-alkyl-1,3-dinitroguanidines and an analog. *J. Am. Chem. Soc.* **1952**, *74*, 2077−2079.

(5) Astachov, A. M.; Kruglyakova, L. A.; Gelemurzina, I. V.; Vasiliev, A. D.; Stepanov, R. S. In *Simple method of synthesis and characterization of some nitrocyanamide salts*; University of Pardubice: 2003; p 36.

(6) Harris, S. R. Some salts of nitrocyanamide and their efficiency as primary explosives. *J. Am. Chem. Soc.* **1958**, *80*, 2302−2305.

(7) Boyer, J. H.; Manimaran, T. Isocyanates from alkyl and aralkyl halides. *Synthesis* **1987**, *1987*, 907.

(8) Boyer, J. H.; Manimaran, T.; Wolford, L. T. Alkylation of nitrocyanamide. A new synthesis of isocyanates. *J. Chem. Soc., Perkin Trans. 1* **1988**, 2137−2140.

(9) Manimaran, T.; Wolford, L. T.; Stevens, E. D.; Boyer, J. H.; Klein, C. N-alkoxy-N'-cyanodiazene N-oxides. *J. Chem. Res., Synop.* **1989**, No. 11, 330.

(10) Hvastijová, M.; Boča, R.; Kohout, J.; Jäger, L.; Císařová, I.; Kožíšek, J. Cyanamidonitrate-cobalt(II) complexes of pyrazole and imidazole ligands.: X-ray structure of $[Co(NO_2NCN)_2(pyrazole)_4]$ and $[Co(2\text{-methylimidazole})_4](NO_2NCN)_2$. *Inorg. Chim. Acta* **2003**, *343*, 217−223.

(11) Hvastijová, M.; Kohout, J.; Díaz, J. G.; Kožíšek, J.; Buchler, J. W. X-ray structural and spectroscopic investigation of cyanamidonitrate nickel(II) complexes with pyrazole type ligands. *Transition Met. Chem.* **2001**, *26* (4), 430−434.

(12) Diaz, J. G.; Kozisek, J.; Langer, V. Bis(cyanamidonitrato-κ*N*)[tris(3,5-dimethylpyrazole)copper(II). *Acta Crystallogr., Sect. E: Struct. Rep. Online* **2003**, *59* (5), m241−m243.

(13) Kozisek, J.; Garcia Diaz, J.; Hvastijova, M.; Jager, L. *trans*-Bis(cyanamidonitrato-*N*:*O*)bis(imidazole-N^3)copper(II), $[Cu(CN_3O_2)_2(C_3H_4N_2)_2]$. *Acta Crystallogr., Sect. C: Cryst. Struct. Commun.* **1997**, *53* (6), 703−705.

(14) Hvastijová, M.; Kohout, J.; Kožíšek, J.; Jäger, L.; Díaz, J. G. a. Cyanamidonitrate−nickel(II) and − cobalt(II) complexes of imidazole ligands: X-ray crystallography and spectroscopic investigation. *Polyhedron* **2000**, *19* (8), 1021−1027.

(15) Kohout, J.; Hvastijová, M.; Kožíšek, J.; Garcia Díaz, J.; Valko, M.; Jäger, L.; Svoboda, I. Cyanamidonitrate−copper(II) complexes of imidazole ligands: X-ray crystallography and physical investigation. *Inorg. Chim. Acta* **1999**, *287* (2), 186−192.

(16) Diaz, J. G.; Kozisek, J.; Fronc, M.; Gatial, A.; Svoboda, I.; Langer, V. Pseudo-merohedrally twinned tetrakis(1*H*-imidazole-κN^3)-bis(*N*-nitrocyanamidato-κ*N*)copper(II). *Acta Crystallogr., Sect. C: Cryst. Struct. Commun.* **2005**, *61* (4), m180−m182.

(17) Boča, R.; Hvastijová, M.; Kožíšek, J.; Valko, M.; Ehrenberg, H.; Fuess, H.; Haase, W.; Svoboda, I.; Werner, R. A trinuclear cyanamidonitrate−copper(II) complex bridged by imidazolato ligands. *Inorg. Chem. Commun.* **2005**, *8* (6), 548−551.

(18) Vahovska, L.; Vitushkina, S.; Potocnak, I.; Travnicek, Z.; Herchel, R. Effect of linear and non-linear pseudohalides on the structural and magnetic properties of Co(II) hexacoordinate single-molecule magnets. *Dalton Trans.* **2018**, *47* (5), 1498−1512.

(19) Kutasi, A. M.; Turner, D. R.; Jensen, P.; Moubaraki, B.; Batten, S. R.; Murray, K. S. Coordination polymers of nitrocyanamide, O−NNCN$^-$: synthesis, structure and magnetism. *CrystEngComm* **2009**, *11* (10), 2089−2095.

(20) Jager, L.; Tretner, C.; Hartung, H.; Biedermann, M. Pseudoelement compounds. Part 10. Synthesis and crystal structure of new complexes of the type *trans*-$[Pt(H)X(PPh_3)_2]$ with cyanamide and cyanomethanide ligands. *Chem. Ber.* **1997**, *130* (7), 1007−1012.

(21) Jäger, L.; Tretner, C.; Hartung, H.; Biedermann, M. Pseudoelementverbindungen. XI. [1] Untersuchungen zum Komplexbildungsverhalten von Cyanamidonitrat $[NO_2NCN]^-$. *Z. Anorg. Allg. Chem.* **1997**, *623* (8), 1299−1305.

(22) Jäger, L.; Tretner, C.; Hartung, H.; Biedermann, M. Pseudoelement Compounds, X Synthesis and Crystal Structure of New Complexes of the Type *trans*-$[Pt(H)X(PPh_3)_2$ with Cyanamide and Cyanomethanide Ligands. *Chem. Ber.* **1997**, *130* (7), 1007−1012.

(23) Jäger, L.; Tretner, C.; Biedermann, M.; Hartung, H. Pseudoelementverbindungen IX. Organostannylierung von Cyanamidonitrat — Molekül- und Kristallstruktur von *N*-Trimethylstannyl-*N'*-nitro-carbodiimid. *J. Organomet. Chem.* **1997**, *530* (1), 13−17.
(24) Joas, M. B. *Investigations concerning the laser ignition of energetic coordination compounds*. Ph.D. Thesis; Ludwig-Maximilian University Munich: 2014.
(25) Zhang, Y.; Gao, H.; Joo, Y.-H.; Shreeve, J. M. Ionic liquids as hypergolic fuels. *Angew. Chem., Int. Ed.* **2011**, *50* (41), 9554−9562.
(26) Drake, G. W.; Hawkins, T.; Tollison, K. *Energetic ionic salts*. US7,745,635, 16th July, 2010.
(27) He, L.; Tao, G.-H.; Parrish, D. A.; Shreeve, J. M. Nitrocyanamide-Based Ionic Liquids and Their Potential Applications as Hypergolic Fuels. *Chem. - Eur. J.* **2010**, *16* (19), 5736−5743.
(28) Joo, Y.-H.; Gao, H.; Zhang, Y.; Shreeve, J. M. Inorganic or Organic Azide-Containing Hypergolic Ionic Liquids. *Inorg. Chem.* **2010**, *49* (7), 3282−3288.
(29) Zhang, Y.; Gao, H.; Guo, Y.; Joo, Y.-H.; Shreeve, J. M. Hypergolic N,N-Dimethylhydrazinium Ionic Liquids. *Chem. - Eur. J.* **2010**, *16* (10), 3114−3120.
(30) Wang, Z.; Pan, G.; Wang, B.; Zhang, L.; Zhao, W.; Ma, X.; Zhang, J.; Zhang, J. Synthesis and Properties of Azide-Functionalized Ionic Liquids as Attractive Hypergolic Fuels. *Chem. - Asian J.* **2019**, *14* (12), 2122−2128.
(31) Schneider, S.; Hawkins, T.; Ahmed, Y.; Deplazes, S.; Mills, J. Ionic liquid fuels for chemical propulsion. *ACS Symp. Ser.* **2012**, *1117*, 1−25.
(32) McCrary, P. D.; Chatel, G.; Alaniz, S. A.; Cojocaru, O. A.; Beasley, P. A.; Flores, L. A.; Kelley, S. P.; Barber, P. S.; Rogers, R. D. Evaluating Ionic Liquids as Hypergolic Fuels: Exploring Reactivity from Molecular Structure. *Energy Fuels* **2014**, *28* (5), 3460−3473.
(33) Wurzenberger, M. H. H.; Lechner, J. T.; Stierstorfer, J. Copper(II) Dicyanamide Complexes with *N*-Substituted Tetrazole Ligands − Energetic Coordination Polymers with Moderate Sensitivities. *ChemPlusChem* **2020**, *85* (4), 769−775.
(34) Gruhne, M. S.; Wurzenberger, M. H. H.; Lommel, M.; Stierstorfer, J. A Smart Access to the Dinitramide Anion − The Use of Dinitraminic Acid for the Preparation of Energetic Coordination Compounds. *Chem. - Eur. J.* **2021**, *27* (35), 9112−9123.
(35) Galtress, C. L.; Morrow, P. R.; Nag, S.; Smalley, T. L.; Tschantz, M. F.; Vaughn, J. S.; Wichems, D. N.; Ziglar, S. K.; Fishbein, J. C. Mechanism for the solvolytic decomposition of the carcinogen *N*-methyl-*N'*-nitro-*N*-nitrosoguanidine in aqueous solutions. *J. Am. Chem. Soc.* **1992**, *114* (4), 1406−1411.
(36) Fischer, N.; Klapötke, T. M.; Stierstorfer, J. 1-Amino-3-nitroguanidine (ANQ) in High-performance Ionic Energetic Materials. *Z. Naturforsch., B: J. Chem. Sci.* **2012**, *67* (6), 573−588.
(37) Petrie, M. A.; Bottaro, J. C.; Penwell, P. E.; Dodge, A. L. *N-hydroxy-N'-nitrourea and related compounds as high energy density materials*. US20090139618A1, 6th August, 2002.
(38) Lotsch, B. V.; Schnick, W. Thermal Conversion of Guanylurea Dicyanamide into Graphitic Carbon Nitride via Prototype CN_x Precursors. *Chem. Mater.* **2005**, *17* (15), 3976−3982.
(39) Lotsch, B. V.; Schnick, W. Towards novel C−N materials: crystal structures of two polymorphs of guanidinium dicyanamide and their thermal conversion into melamine. *New J. Chem.* **2004**, *28* (9), 1129−1136.
(40) Wurzenberger, M. H. H.; Braun, V.; Lommel, M.; Klapötke, T. M.; Stierstorfer, J. Closing the Gap: Synthesis of Three Isomeric *N,N*-Ditetrazolylmethane Ligands and Their Coordination Proficiency in Adaptable Laser Responsive Copper(II) and Sensitive Silver(I) Complexes. *Inorg. Chem.* **2020**, *59* (15), 10938−10952.
(41) Wurzenberger, M. H. H.; Bissinger, B. R. G.; Lommel, M.; Gruhne, M. S.; Szimhardt, N.; Stierstorfer, J. Synthesis and comparison of copper(ii) complexes with various N-aminotetrazole ligands involving trinitrophenol anions. *New J. Chem.* **2019**, *43* (46), 18193−18202.
(42) Gaponik, P. N.; Karavai, V. P.; Grigor'ev, Y. V. Synthesis of 1-substituted tetrazoles by heterocyclization of primary amines, orthoformic ester, and sodium azide. *Chem. Heterocycl. Compd.* **1985**, *21* (11), 1255−1258.
(43) Szimhardt, N.; Wurzenberger, M. H. H.; Beringer, A.; Daumann, L. J.; Stierstorfer, J. Coordination chemistry with 1-methyl-5*H*-tetrazole: cocrystallization, laser-ignition, lead-free primary explosives − one ligand, three goals. *J. Mater. Chem. A* **2017**, *5* (45), 23753−23765.
(44) Joas, M.; Klapötke, T. M.; Szimhardt, N. Photosensitive Metal(II) Perchlorates with 1,2-Bis[5-(1-methylhydrazinyl)tetrazol-1-yl]ethane as Ligand: Synthesis, Characterization and Laser Ignition. *Eur. J. Inorg. Chem.* **2014**, *2014* (3), 493−498.
(45) Jäger, L.; Tretner, C.; Hartung, H.; Biedermann, M.; Wagner, C. Kristallstrukturen von Kalium- und Silbercyanamidonitrat. *Z. Anorg. Allg. Chem.* **1998**, *624* (9), 1558−1562.
(46) Crystallographic data for the structures have been deposited with the Cambridge Crystallographic Data Centre. Copies of the data can be obtained free of charge on application to The Director, CCDC, 12 Union Road, Cambridge CB2 1EZ, UK (Fax: int.code_(1223)336-033; e-mail for inquiry: fileserv@ccdc.cam.ac.uk; e-mail for deposition: (depos-it@ccdc.cam.ac.uk).
(47) Ang, H.-G.; Fraenk, W.; Karaghiosoff, K.; Klapötke, T. M.; Mayer, P.; Nöth, H.; Sprott, J.; Warchhold, M. Synthesis, Characterization, and Crystal Structures of Cu, Ag, and Pd Dinitramide Salts. *Z. Anorg. Allg. Chem.* **2002**, *628* (13), 2894−2900.
(48) Joas, M.; Klapötke, T. M.; Stierstorfer, J.; Szimhardt, N. Synthesis and Characterization of Various Photosensitive Copper(II) Complexes with 5-(1-Methylhydrazinyl)-1*H*-tetrazole as Ligand and Perchlorate, Nitrate, Dinitramide, and Chloride as Anions. *Chem. - Eur. J.* **2013**, *19* (30), 9995−10003.
(49) Schweifer, J.; Weinberger, P.; Mereiter, K.; Boca, M.; Reichl, C.; Wiesinger, G.; Hilscher, G.; van Koningsbruggen, P. J.; Kooijman, H.; Grunert, M.; Linert, W. *catena*-[μ-Tris(1,2-bis(tetrazol-1-yl)ethane-N4,N4')iron(II)] bis(tetrafluoroborate): synthesis, structure, spectroscopic and magnetic characterization of a chain-type coordination polymer spin-crossover compound. *Inorg. Chim. Acta* **2002**, *339*, 297−306.
(50) Palmer, M. H.; Parsons, S. 4-Methyl-1,2,4-triazole and 1-Methyltetrazole. *Acta Crystallogr., Sect. C: Cryst. Struct. Commun.* **1996**, *52* (11), 2818−2822.
(51) Luk'yanov, O. A.; Anikin, O. V.; Gorelik, V. P.; Tartakovsky, V. A. Dinitramide and its salts. *Russ. Chem. Bull.* **1994**, *43* (9), 1457−1461.
(52) Klapötke, T. M. *Chemistry of High-Energy Materials*, 5th ed.; De Gruyter: Berlin and Boston, MA, 2019.
(53) Lotsch, B. V.; Senker, J.; Schnick, W. Characterization of the Thermally Induced Topochemical Solid-State Tranformation of $NH_4[N(CN)_2]$ into NCN = $C(NH_2)_2$ by Means of X-ray and Neutron Diffraction as Well as Rama and Solid-State NMR Spectroscopy. *Inorg. Chem.* **2004**, *43*, 895−904.
(54) Klapötke, T. M. *Energetic materials Encyclopedia*, 2nd ed.; DeGruyter: Berlin and Boston, MA, 2021.
(55) Wurzenberger, M. H. H.; Gruhne, M. S.; Lommel, M.; Stierstorfer, J. 1-Amino-5-methyltetrazole in Energetic 3d Transition Metal Complexes − Ligand Design for Future Primary Explosives. *Propellants, Explos., Pyrotech.* **2021**, *46* (2), 207−213.
(56) Reynolds, J. G.; Hsu, P. C.; Hust, G. A.; Strout, S. A.; Springer, H. K. Hot Spot Formation in Mock Materials in Impact Sensitivity Testing by Drop Hammer. *Propellants, Explos., Pyrotech.* **2017**, *42* (11), 1303−1308.

https://doi.org/10.1021/acs.cgd.1c00858
Cryst. Growth Des. 2022, 22, 200−212

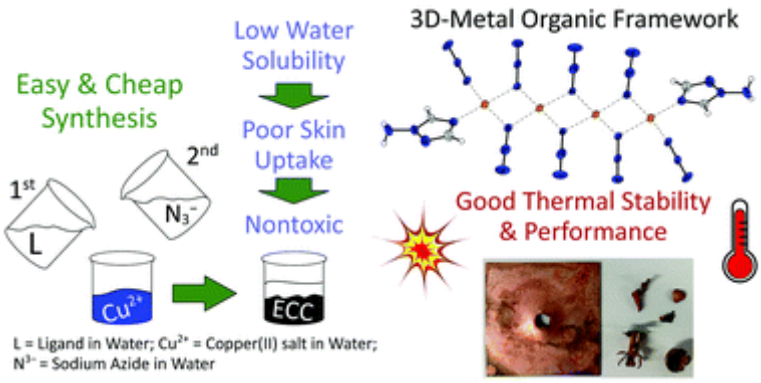
Appendix 27

Advancement and Stabilization of Copper(II) Azide by the Use of Triazole- and Tetrazole Ligands – Enhanced Primary Explosives

M. H. H. Wurzenberger, M. Gruhne, N. Szimhardt, M. Lommel, J. Stierstorfer

Mater. Adv. **2022**, *3*, 579–591.

https://doi.org/10.1039/D1MA00588J



Supplementary Information:
https://www.rsc.org/suppdata/d1/ma/d1ma00588j/d1ma00588j1.pdf

Materials Advances

ROYAL SOCIETY OF CHEMISTRY

PAPER

View Article Online
View Journal | View Issue

Open Access Article. Published on 11 November 2021. Downloaded on 2/16/2022 8:09:20 AM.
This article is licensed under a Creative Commons Attribution 3.0 Unported Licence.

Check for updates

Cite this: *Mater. Adv.*, 2022, 3, 579

Advancement and stabilization of copper(II) azide by the use of triazole- and tetrazole ligands – enhanced primary explosives†‡

Maximilian H. H. Wurzenberger, Michael S. Gruhne, Marcus Lommel, Norbert Szimhardt and Jörg Stierstorfer *

Received 7th July 2021,
Accepted 4th November 2021

DOI: 10.1039/d1ma00588j

rsc.li/materials-advances

Copper(II) (cupric) and copper(I) (cuprous) azide are both very powerful primary explosives with good thermal stabilities. However, both suffer from extreme sensitivities, which makes them unsuitable for any application. One brilliant concept for the synthesis of new ecofriendly, non-water soluble, and very powerful primary explosives is the assembly of ligands in the coordination sphere of copper(II) azide. Blocking of possible coordination sites through endothermic azoles allows the desensitization of copper(II) azide and leads to compounds with manageable sensitivities. 13 different nitrogen-rich tri- and tetrazole derivatives were used for the synthesis of energetic copper(II) azide complexes. The water insoluble compounds are highly promising candidates for the replacement of lead and perchlorate containing primary explosives. For the characterization, the complexes were analyzed by single crystal X-ray diffraction, elemental analysis (EA), infrared (IR) spectroscopy, and differential thermal analysis (DTA) measurements with heating rates of 5 °C min^{-1}. The bulk material purity of selected complexes was confirmed by X-ray powder diffraction. The sensitivities toward impact (IS), friction (FS), and electrostatic discharge (ESD) of all synthesized compounds were tested and determined according to BAM (Bundesanstalt für Materialforschung und -prüfung) standards. The most promising compounds were investigated in copper shell initiation experiments with PETN as main charge.

Introduction

Metal azides are widely used chemicals in industry and daily applications. The most important one is sodium azide with an annual production of around 250 t worldwide.[1] In former times NaN_3 was mainly used for the synthesis of lead azide, whereas today's utilization is widespread and ranges from a broad spectrum of organic synthesis reactions,[2–4] to gas generating mixtures in airbags and bacteriostatic preservatives.[5] Heavy metal azides are sensitive toward friction and impact and are used as important ingredients in detonators.[6] While lead azide is still among today's most commonly utilized primary explosives in detonators or primer mixtures, other azides such as AgN_3, CuN_3, and $Cu(N_3)_2$ have only limited use in special applications due to their high cost (silver azide) or sensitivity (copper azides).[7]

However, the use of lead azide has many disadvantages, which are outweighed by its advantages such as an exceptionally high thermal stability of 330 °C, high density, low cost, and many more.[8] The incorporation of lead has disastrous effects to the human body. Already small amounts of lead are toxic and cause annual costs of $43.5 billion alone in the US.[9] Various studies show that chronic lead uptake is responsible for a higher autism risk, late puberty onset of 6–8 months, and a reduced IQ score up to 9 points.[10] "Green" alternatives for lead containing primer mixtures were introduced onto the market in the past, using DDNP as primary explosive and tetrazene as sensitizer.[11] Since then, countless numbers of diverse energetic compounds, including organic compounds, organic salts, and metastable interstitial composites have been investigated as lead replacements but none of them could be established in the market.[12–17] Furthermore; the alternatives, DDNP and tetrazene, again suffer from long term stability issues or sensitivity toward light (DDNP).[18,19] In the last years many efforts were put in the investigation of new energetic complex compounds (ECCs) with nitrogen-rich ligands, non-toxic or less toxic 3d metal cations, and diverse anions.[20–25] One outstanding class of coordination compounds consists of copper(II) azide and nitrogen rich ligands. Cuprous and cupric azide show high decompositions

Department of Chemistry, Ludwig Maximilian University of Munich, Butenandtstr. 5–13, D-81377 Munich, Germany. E-mail: jstch@cup.uni-muenchen.de; Web: http://www.hedm.cup.uni-muenchen.de; Fax: 49-89-2180-77007

† Dedicated to Professor Dr Wolfgang Beck on the Occasion of his 90th Birthday.

‡ Electronic supplementary information (ESI) available. CCDC 2081730–2081740 and 2084455. For ESI and crystallographic data in CIF or other electronic format see DOI: 10.1039/d1ma00588j

© 2022 The Author(s). Published by the Royal Society of Chemistry

Open Access Article. Published on 11 November 2021. Downloaded on 2/16/2022 8:09:20 AM.
This article is licensed under a Creative Commons Attribution 3.0 Unported Licence.

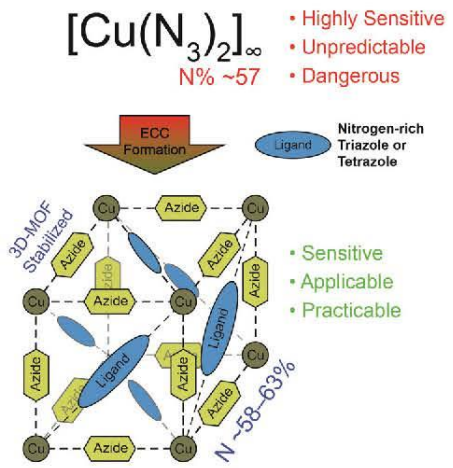


Fig. 1 Stabilization of cupric azide using nitrogen-rich triazole and tetrazole ligands.

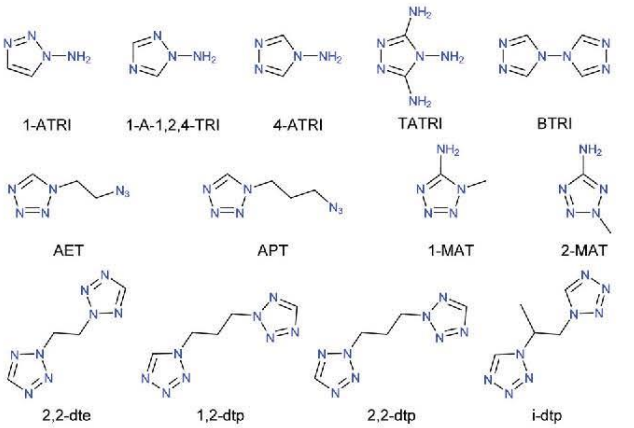


Chart 1 Overview of used nitrogen-rich ligands: 1-ATRI: 1-amino-1,2,3-triazole; 1-A-1,2,4-TRI: 1-amino-1,2,4-triazole; 4-ATRI: 4-amino-1,2,4-triazole; TATRI: 3,4,5-triamino-1,2,4-triazole; BTRI: 4,4′-bi(1,2,4-triazole); AET: 1-azidoethyl-5*H*-tetrazole; APT: 1-azidopropyl-5*H*-tetrazole; 1-MAT: 1-methyl-5-aminotetrazole; 2-MAT: 2-methyl-5-aminotetrazole; 2,2-dte: 1,3-di(tetrazol-2-yl)ethane; 1,2-dtp: 1-(tetrazol-1-yl)-3-(tetrazol-2-yl)propane; 2,2-dtp: 1,3-di(tetrazol-2-yl)propane; i-dtp: 1,2-di(tetrazol-1-yl)propane.

temperatures above 200 °C but are unfortunately way too sensitive for any application.[8] The latter also tends to form basic copper azides (*e.g.*, Cu(OH)N_3) under basic conditions. However, this is precisely where the ECC concept demonstrates its advantages. The aim here is to stabilize the copper azide with nitrogen-rich ligands while maintaining performance and thermal stability of neat cupric azide (Fig. 1).[25–28]

This has already been demonstrated with 1-methyl/1-ethyl and 1-propyl-5*H*-tetrazole in a previous work of our group.[29] The corresponding complexes are of high interest for industrial application and have been successfully incorporated into primer mixtures.[29] Furthermore, several patents were issued on this topic.[30,31] However, the concept of complexation of cupric azide is not new. Simple ECCs of copper(II) azide and primary amines have been known since the early 20th century and were already investigated toward their explosive character.[32] In more recent times researcher all over the world focused rather on the magnetic behaviour and the structural diversity of copper(II) azide complexes.[33–35] But since the scope of coordination compounds containing nitrogen-rich ligands expanded in recent years, ranging from simple diamino alkanes to more complex triazole derivatives, the synthesis of further copper azide complexes has become feasible.[36–38] However, the energetic complexes used in the previous work[29] showed weaknesses especially when it comes to thermal stability. In the current study, we present a large number of enhanced copper(II) azide complexes which were stabilized and tuned with different bridging nitrogen-rich ligands, thus further increasing the compounds' thermal stability.

Results and discussion

Synthesis

In every case, literature known, or commercially available ligands were used for the preparation of the ECCs.[39–47] First of all, layering experiments were performed to obtain single crystals. For this purpose, sodium azide and the respective ligand (Chart 1) were dissolved in water and carefully layered with a mixture of water and ethanol. This was followed by a solution of copper(II) chloride or nitrate in ethanol.

Using AET as a ligand afforded the two species **6a** and **6b**. In every other case only one species was obtained during these experiments.

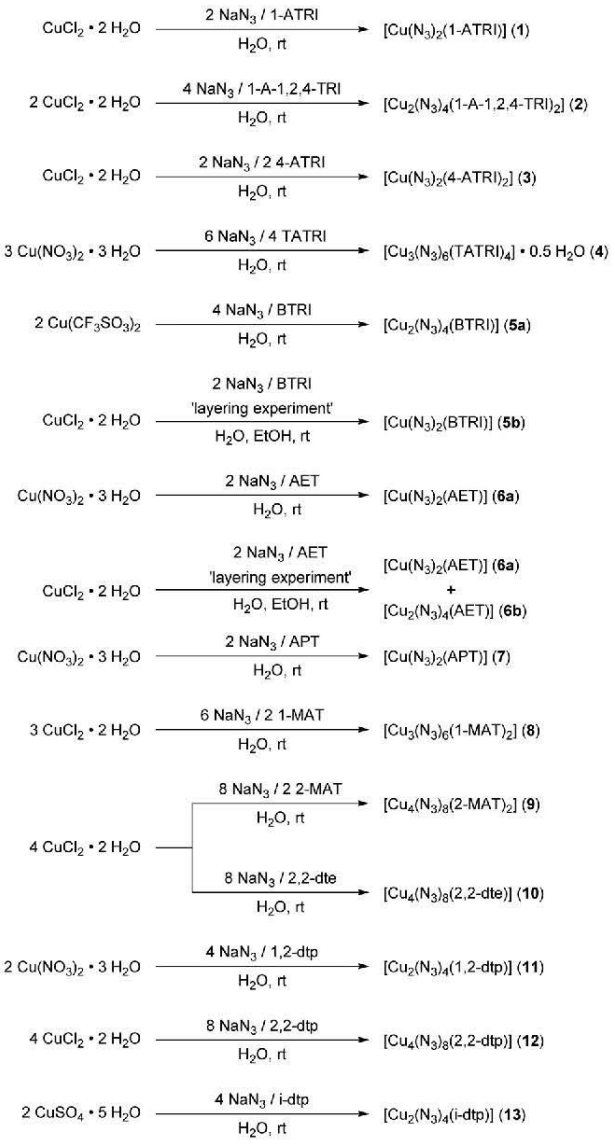
Subsequently, the ECCs were synthesized by the reaction of stoichiometric amounts of a soluble copper(II) salt with the respective ligand (Chart 1 and Scheme 1) in water and the addition of an aqueous solution of sodium azide, which leads to the precipitation of the complexes. For compound **5a** the found elemental analysis fits well to a complex with bridging ligand. In case of the AET ligand, only species **6a** could be isolated elemental analysis pure. Additional purity checks were performed using powder X-ray diffraction (Fig. S4–S9, ESI‡). The complexes **2**, **5b**, **6b**, and **8** could not be obtained pure and were therefore not further characterized. However, this is to be expected since the formation of by-products is a general problem regarding copper azide chemistry. All complexes were obtained in good yields (44–86%).

Crystal structures

All complexes were characterized by low temperature single crystal X-ray diffraction. Measurement and refinement data of all experiments can be found in the (Tables S1–S3, ESI‡). The crystal datasets were uploaded to the CSD database and can be obtained free of charge.[48] The bond lengths and angles of the coordinating ligands in the analysed complexes are in the typical range of tetrazole and triazole ligands and nearly the same as in the non-coordinating ligands.[41–43,47,49–54] The ligands are therefore not part of the discussion in any of the following coordination compounds. All copper(II) azide complexes show an octahedral coordination around the central

© 2022 The Author(s). Published by the Royal Society of Chemistry

Open Access Article. Published on 11 November 2021. Downloaded on 2/16/2022 8:09:20 AM.
This article is licensed under a Creative Commons Attribution 3.0 Unported Licence.



Scheme 1 Preparation of various copper(II) azide coordination compounds based on nitrogen-rich azole ligands.

metal with a Jahn–Teller (JT) distortion along the axial coordination sphere. In addition, every complex is forming polymeric structures, whereas the type of polymerization (1D, 2D, 3D) highly depends on the combination of coordination modes of the azido and azole ligands. The investigated complexes show six different types of coordinated azide

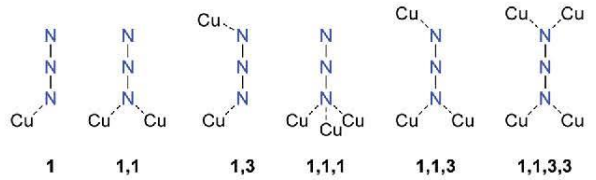


Chart 2 The six occurring coordination modes of the azide anions in compounds **1-13**.

moieties (Chart 2). An overview on the bridging types observed in each structure is given in Table 1.

Pure cupric azide ($Cu(N_3)_2$) without any ligands shows two different types of coordinating azide anions (Chart 2: 1,1,1; 1,1,3) leading to very long axial Cu–N-bonds (2.54 Å, 2.71 Å) and the formation of 2-D polymeric layers.[55] Single crystals of azide complex **11** and **13** were measured and allowed a determination of the most likely appearance of the structure. Finalizations of the datasets were not possible due to the highly disordered moieties and the related weak diffractions.

Complex compound **1** crystallizes in the form of brown rods in the monoclinic space group $P2_1/c$ with four formula units per unit cell and a calculated density of 2.093 g cm^{-3} at 100 K. The metal centre is coordinated (Fig. 2) by one 1-amino-1,2,3-triazole molecule in equatorial position and five azide ligands. One equatorial and one axial azide are bridging to two different metals (Chart 2: 1, 1) and the remaining three anions (one axial, two equatorial) are linking between three copper(II) atoms (Chart 2: 1, 1, 1), building up linear chains with two parallel copper strands in one plane (Fig. 5).

Complex **2** possess one of the highest densities of all complexes in this work (2.226 g cm^{-3} @ 143 K) and crystallizes in the form of brown blocks in the triclinic space group $P\bar{1}$ with two formula unit per unit cell. The molecular unit is formed by two differently coordinated copper(II) cations (Fig. 3). The Cu1 cation is solely coordinated by 1,1,1 and 1,1 bridging azido ligands. This leads to the formation of strands of four copper atoms. Additionally, the Cu2 atoms are coordinated by amino-triazole ligands and 1,1,3 bridging azido anions. The azide moieties are linking two Cu2 cations, connecting the copper strands and further leading to a 2D polymeric network.

Complex **3** possess a high density (1.952 g cm^{-3} @ 143 K) and crystallizes in the form of green needles in the triclinic space group $P\bar{1}$ with one formula unit per unit cell. The molecular unit consists of one copper(II) cation (Fig. 4) coordinated by two 1-amino-1,2,4-triazoles in equatorial position and four bridging azide anions. Each pair of one axial and one equatorial azide is linking between the same two copper(II) atoms (Chart 2: 1,3), which leads to the formation of 1D-chains. It is the only complex where all anions show the same bridging mode.

Comparing the polymeric structures of **1** and **3**, it becomes clear that the different coordination modes of the azide moieties are leading to a double strand in the case of **1** whereas in **3** single strands are formed (Fig. 5). In both structures, intermolecular interactions between anions and triazole ligands of neighbouring chains are stabilizing the structures.

The only water containing coordination compound $[Cu_3(N_3)_6(TATRI)_4]\cdot 0.5\ H_2O$ (**4**) crystallizes in the form of green blocks in the triclinic space group $P\bar{1}$ with one formula unit per unit cell and a density of 1.975 g cm^{-3} at 123 K. The molecular unit is built up by a trimer of copper(II) cations (Fig. 6) with two different coordination spheres. Two of the triazole ligands are linking between two copper(II) ions, which is leading to a fourfold binding of the middle cation to neutral ligands all in equatorial position. This is the highest number of azole ligands

© 2022 The Author(s). Published by the Royal Society of Chemistry

Open Access Article. Published on 11 November 2021. Downloaded on 2/16/2022 8:09:20 AM.
This article is licensed under a Creative Commons Attribution 3.0 Unported Licence.

Table 1 Overview on selected crystallographic data of the compounds examined by single crystal X-ray diffraction

Compound		Space group	ρ^a [g cm^{-3}]	T^b [K]	Colour^c	Bridging modes of azido ligands^d		
$[Cu(N_3)_2(1\text{-ATRI})]$	**1**	$P2_1/c$	2.093	100	Brown	1,1	1,1,1	
$[Cu_2(N_3)_4(1\text{-A-}1,2,4\text{-TRI})_2]$	**2**	$P\bar{1}$	2.226	143	Brown	1,1	1,1,1	1,1,3
$[Cu(N_3)_2(4\text{-ATRI})_2]$	**3**	$P\bar{1}$	1.952	143	Green	1,3		
$[Cu_3(N_3)_6(\text{TATRI})]\cdot 0.5\ H_2O$	**4**	$P\bar{1}$	1.975	123	Green	1	1,1	1,3
$[Cu_2(N_3)_4(\text{BTRI})]$	**5a**	$P2_1/c$	2.065	173	Red	1,1	1,1,3	
$[Cu(N_3)_2(\text{AET})]$	**6a**	$I2/a$	2.003	143	Brown	1,1	1,1,3	
$[Cu_2(N_3)_4(\text{AET})]$	**6b**	$P2_1/c$	2.072	143	Brown	1,1	1,1,1	1,1,3
$[Cu(N_3)_2(\text{APT})]$	**7**	$P2_1/c$	1.897	109	Brown	1,1	1,1,3	
$[Cu_3(N_3)_6(1\text{-MAT})_2]$	**8**	$P\bar{1}$	2.103	293	Red	1	1,1	1,1,3,3
$[Cu_4(N_3)_8(2\text{-MAT})_2]$	**9**	$P2_1/n$	2.188	173	Red	1,1	1,1,1	1,1,3
$[Cu_4(N_3)_8(2,2\text{-dte})]$	**10**	$P\bar{1}$	2.200	143	Brown	1,1	1,1,1	1,1,3
$[Cu_4(N_3)_8(2,2\text{-dtp})]$	**12**	$C2/c$	2.136	123	Brown	1,1	1,1,1	1,1,3

^{a} Crystallographic density at cell measurement temperature. ^{b} Cell measurement temperature. ^{c} Colour of the single crystal used for X-ray diffraction experiments. ^{d} Different types of bridging observed for the azido ligands in the respective crystal structure.

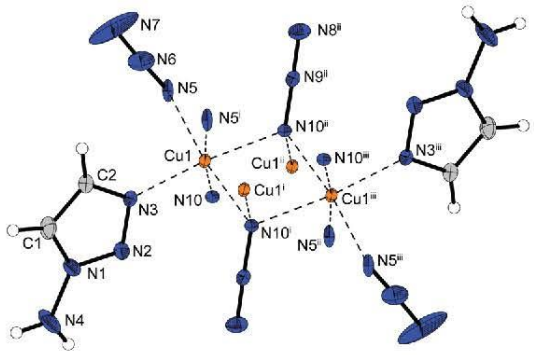


Fig. 2 Copper(II) coordination environment of $[Cu(N_3)_2(1\text{-ATRI})]$ (**1**). Selected bond lengths (Å): Cu1–N3 1.982(3), Cu1–N5 2.037(3), Cu1–N10 2.580(4); selected bond angles (°): N3–Cu1–N5 94.16(12), N3–Cu1–N10 95.47(12), N3–Cu1–N10ii 173.72(13), N5–Cu1–N10 83.55(12). Symmetry codes: (i) $-1+x, y, z$; (ii) $1-x, -y, 1-z$.

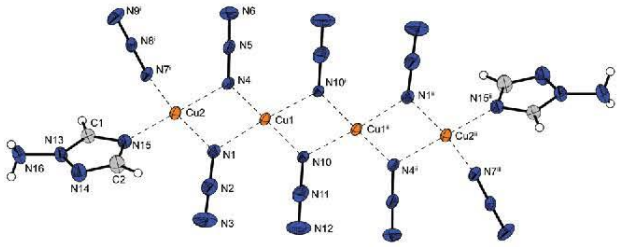


Fig. 3 Copper(II) coordination environment of $[Cu_2(N_3)_4(1\text{-A-}1,2,4\text{-TRI})_2]$ (**2**). Selected bond lengths (Å): Cu1–N1 2.005(3), Cu1–N4 2.001(3), Cu1–N7 2.409(3), Cu1–N4 2.878(3), Cu1–N10^{ii} 2.021(4), Cu1–N10 2.016(3), Cu2–N9 2.593(3), Cu2–N15 1.980(4), Cu2–N10 2.658(3); selected bond angles (°): N7–Cu1–N4^i 173.08(12), Cu1–N4–Cu2 101.37(14), N9^{iv}–Cu2–N7^i 96.27(11), N9^{iv}–Cu2–N15 85.61(13), N7–Cu1–N1 101.70(13). Symmetry codes: (i) $-1+x, y, z$; (ii) $2-x, 1-y, 1-z$; (iii) $3-x, 1-y, 1-z$; (iv) $2-x, -y, 1-z$; (v) $1-x, 1-y, 1-z$.

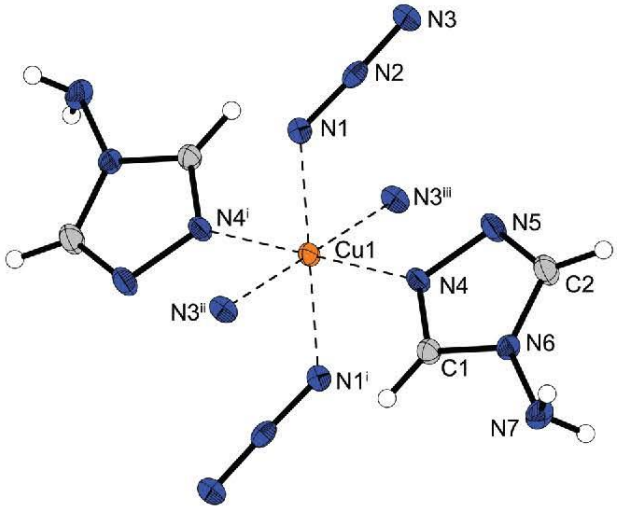


Fig. 4 Copper(II) coordination environment of $[Cu(N_3)_2(4\text{-ATRI})_2]$ (**3**). Selected bond lengths (Å): Cu1–N1 2.006(2), Cu1–N4 2.005(2), Cu1–N3^{ii} 2.523(2); selected bond angles (°): N1–Cu1–N4 92.30(9), N1–Cu1–N3^{ii} 88.78(8), N3^{ii}–Cu1–N4 85.61(8). Symmetry codes: (i) $-x, -y, -z$; (ii) $-1+x, y, z$; (iii) $1-x, -y, -z$.

around the central metal of the herein presented complexes. The coordination sphere around Cu1 is completed by two 1,1-linking azido anions in axial positions causing a typical Jahn–Teller distortion (Cu1–N13 2.355(4) Å). The azido ligands around Cu2 show two additional coordination modes, a rather unconventional monodentate binding (Chart 2: 1) and a 1,3-bridging similar to **3** leading to the formation of 1D polymeric chains. Interestingly, latter coordination mode can only be observed in these two compounds, which are the only green coloured ones. Whereas in **3** the JT-distortion of the 1,3-azido ligands is close to 2.5 Å, it is astonishingly long in complex **4** (Cu2–N21^{ii} = 2.825(6) Å). The crystal structure shows strong disordering effects in the monodentate azido ligand as well as in the crystal water molecule.

Complex compound **5b** crystallizes in the form of red platelets in the monoclinic space group $P2_1/c$. It possesses four formula units per unit cell and a calculated density of 2.065 g cm^{-3} at 173 K. Every copper(II) cation is octahedral coordinated by one bistriazole (BTRI) molecule and five azide anions (Fig. 7).

© 2022 The Author(s). Published by the Royal Society of Chemistry

Open Access Article. Published on 11 November 2021. Downloaded on 2/16/2022 8:09:20 AM.
This article is licensed under a Creative Commons Attribution 3.0 Unported Licence.

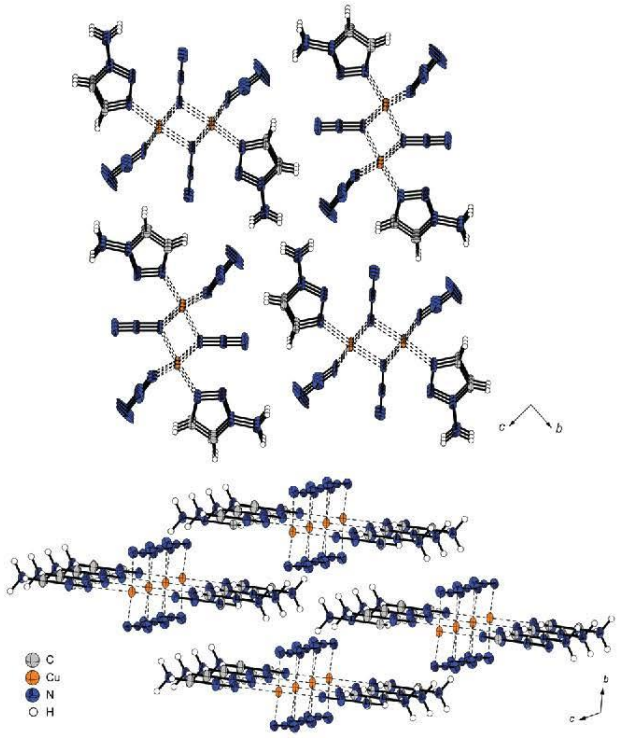


Fig. 5 1-D polymeric chains of **1** (top) and **3** (bottom) along the *a* axis.

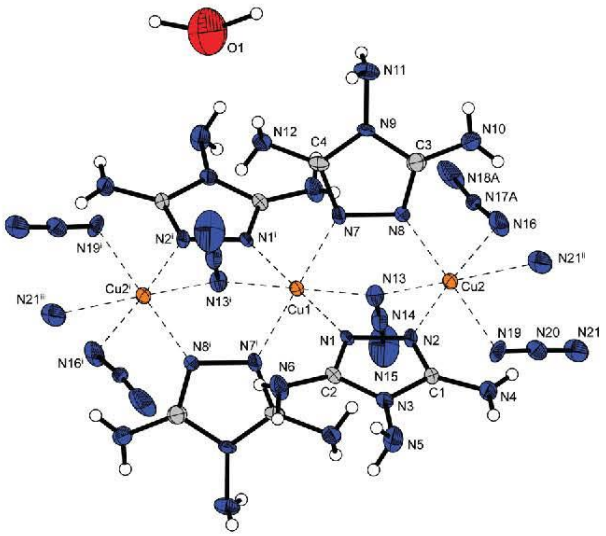


Fig. 6 Coordination environment of trinuclear unit of $[Cu_3(N_3)_6(TATRI)_4]\cdot 0.5\ H_2O$ (**4**). Selected bond lengths (Å): Cu1–N13 2.355(4), Cu1–N1 2.033(4), Cu1–N7 1.993(5), Cu2–N2 1.991(5), Cu2–N8 2.015(4), Cu2–N13 2.264(5), Cu2–N16 1.978(6), Cu2–N19 2.005(4); selected bond angles (°): N1–Cu1–N7 89.38(19), N7–Cu1–N7^{i} 180, N7–Cu1–N13 84.99(18), N2–Cu2–N8 89.18(18), N2–Cu2–N16 171.1(3), N2–Cu2–N21^{ii} 88.78(18), N8–Cu2–N16 90.7(2). Symmetry codes: (i) 2 − *x*, 1 − *y*, −*z*; (ii) 2 − *x*, 2 − *y*, 1 − *z*, (iii) *x*, −1 + *y*, −1 + *z*.

The polyhedrons are linked over the azide anions in two different ways forming two dimensional layers. (Chart 2: 1,1,3; 1,1).

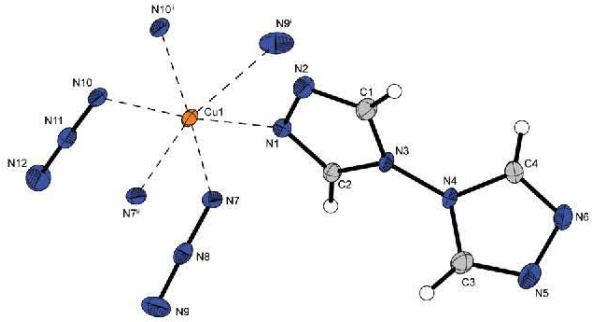


Fig. 7 Coordination environment of $[Cu(N_3)_2(BTz)]$ (**5b**). Selected bond lengths (Å): Cu1–N1 1.9858 (16), Cu1–N7 2.0016(16), Cu1–N10 1.9968(16), Cu1–N9^{i} 2.7764(19), Cu1–N7^{iii} 2.5212(19), Cu1–N10^{ii} 2.0083(17); selected bond angles (°): N1–Cu1–N9^{i} 79.83(7), N1–Cu1–N10^{ii} 97.42(7), N7–Cu1–N9^{i} 84.33(7), N7–Cu1–N7^{iii} 92.55(6). Symmetry codes: (i) −*x*, −0.5 + *y*, 0.5−*z*; (ii) −*x*, 0.5 + *y*, 0.5 − *z*; (iii) −*x*, 1 − *y*, −*z*.

Azide complex $[Cu(N_3)_2(AET)]$ (**6a**) crystallizes as brown plates in the monoclinic space group *I*2/*a* with eight formula units per unit cell and a calculated density of 2.003 g cm^{-3} at 143 K. The octahedral coordination sphere around the copper(II) centre of **6a** is made up of one molecule of AET and five azide anions and is Jahn–Teller distorted along N11^{i}–Cu1–N13^{iii} (Fig. 8). The metal centres form double strands, that extend through the structure, bridged by azide anions (Chart 2: 1,1). The different chains are linked by a second species of azido ligands (Chart 2: 1,1,3) leading to the formation of a 2D-polymeric network.

The by-product $[Cu_2(N_3)_4(AET)]$ (**6b**) crystallizes as brown rods in the monoclinic space group $P2_1/c$ with four formula units per unit cell and a calculated density of 2.072 g cm^{-3} at 143 K. Similar to **6a**, 1,1 and 1,1,3 bridging azido ligands are leading to the formation of 2D-polymeric networks. But, as already observed in compound **2**, the existence of azide anions in an additional 1,1,1 coordination mode is building up strands consisting of four copper ions (Fig. 9). The centrosymmetric unit is completed by two AET ligands, that coordinate to the

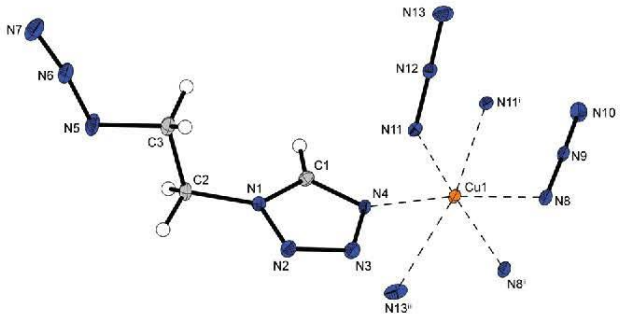


Fig. 8 Coordination environment of $[Cu(N_3)_2(AET)]$ (**6a**). Selected bond lengths (Å): Cu1–N4 1.985(2), Cu1–N8 1.995(2), Cu1–N8^{ii} 2.011(2), Cu1–N11 2.001(2), Cu1–N11^{i} 2.5095(19), Cu1–N13^{iii} 2.736(3). Selected bond angles (°): N4–Cu1–N8 173.22(8), N4–Cu1–N8^{ii} 97.39(8), N4–Cu1–N11 90.70(8), N4–Cu1–N11^{i} 90.70(7), N4–Cu1–N13^{iii} 79.21(8), N8^{ii}–Cu1–N11 169.61(8), N11^{i}–Cu1–N13^{iii} 169.29(7). Symmetry codes: (i) 1 − *x*, −0.5 + *y*, 0.5 − *z*; (ii) 1.5 − *x*, 0.5 − *y*, 0.5 − *z*; (iii) 1 − *x*, 0.5 + *y*, 0.5 − *z*.

© 2022 The Author(s). Published by the Royal Society of Chemistry

Open Access Article. Published on 11 November 2021. Downloaded on 2/16/2022 8:09:20 AM.
This article is licensed under a Creative Commons Attribution 3.0 Unported Licence.

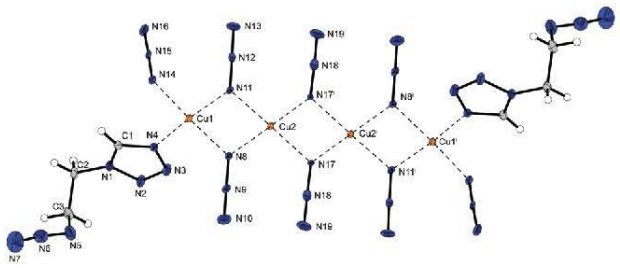


Fig. 9 Molecular unit of by-product $[Cu_2(N_3)_4(AET)]$ (**6b**). Selected bond lengths (Å): Cu1–N4 1.984(3), Cu1–N8 2.001(3), Cu1–N11 2.009(3), Cu1–N14 1.978(3), Cu2–N8 1.994(3), Cu2–N11 1.996(3), Cu2–N17 1.998(3). Selected bond angles (°): N4–Cu1–N8 96.38(12), N4–Cu1–N11 170.51(11), N4–Cu1–N14 92.36(12), N8–Cu1–N11 78.91(11), N8–Cu2–N11 79.39(11), N8–Cu2–N17 100.72(11). Symmetry code: (i) $2-x, -y, -z$.

outer copper centres on opposite sites, whereas the inner two cations are only bounded to azido ligands. All metal centres are Jahn–Teller distorted along the axis vertical to the plane shown in Fig. 9, bond lengths are partly notably longer than in other JT-distorted complexes, from 2.5 Å to even exceeding 2.7 Å.

In both copper(II) azide complexes of AET the 2D-polymeric networks are formed by the 1,1,3 coordinating azido ligands bridging between strands of copper ions (Fig. 10). While the existence of solely 1,1 binding azido ligands are building up double strands (**6a**) of cations, the combination of 1,1 and 1,1,1 anions is leading to quadruple strands (**6b**).

Compound **7**, based on the ligand 1-azidopropyl-5*H*-tetrazole, crystallizes as brown platelets in the monoclinic space group $P2_1/c$ with four formula units per unit cell and the lowest of all calculated densities (1.897 g cm^{-3} @ 109 K). The octahedral coordination sphere around the copper(II) centre of compound **7** shows an almost identical built up like

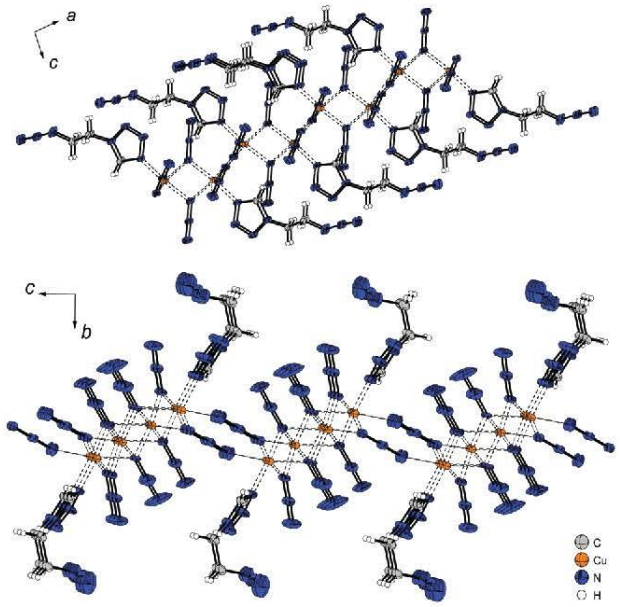


Fig. 10 Polymeric layers of **6a** (top) along the *b* axis and **6b** (bottom) along the *a* axis.

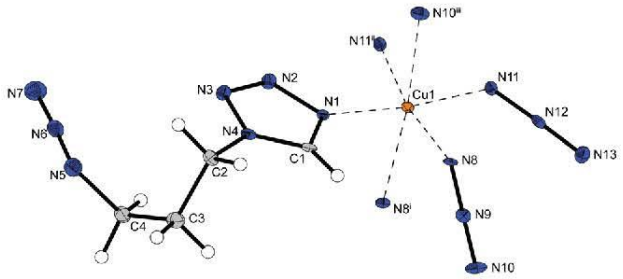


Fig. 11 Coordination environment of $[Cu(N_3)_2(APT)]$ (**7**). Selected bond lengths (Å): Cu1–N1 1.984(3), Cu1–N8 2.005(3), Cu1–N8i 2.519(3), Cu1–N10iii 2.702(4), Cu1–N11 2.006(3). Selected bond angles (°): N1–Cu1–N8 90.88(14), N1–Cu1–N11 173.33(14), N8–Cu1–N10iii 84.06(11), N8ii–Cu1–N11 169.61(8), N8–Cu1–N11ii 169.86(14), N11–Cu1–N11ii 77.54(13). Symmetry codes: (i) $1-x, -0.5+y, 1.5-z$; (ii) $1-x, 1-y, 1-z$; (iii) $1-x, 0.5+y, 1.5-z$.

compound **6a** and is made up of one molecule of APT and five azide anions with the same coordination modes as in **6a** (Chart 2: 1,1; 1,1,3) leading again to the formation of a 2D-polymeric network (Fig. 11).

The unique trinuclear complex **8** crystallizes as red platelets in the triclinic space group $P\bar{1}$ with one formula unit per unit cell and a calculated density of 2.103 g cm^{-3} at 293 K. The structure of **8** shows exceptional characteristics in many respects. It is the only compound which shows a bridging of single tetrazole rings between two different copper(II) atoms leading to the blocking of two coordination sites of Cu1. Furthermore, it prevents the linking of the N12–N13–N14 azide anion (comparable to **4**) causing a mono-bonded anion with the shortest Cu–N (Cu2–N12 1.9558(19) Å) bond of all observed

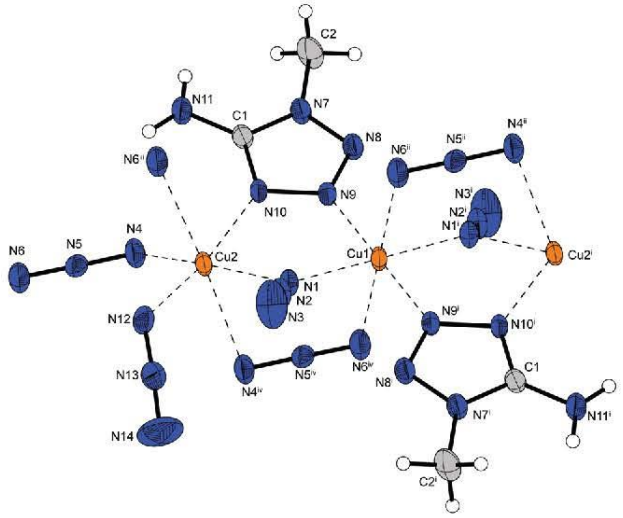


Fig. 12 Extended molecular unit of $[Cu_3(N_3)_6(1\text{-MAT})]$ (**8**). Selected bond lengths (Å): Cu1–N1 1.9903(18), Cu1–N6^{ii} 2.5836(18), Cu2–N1 2.0205(17) Cu2–N4 1.9922(17), Cu2–N4^{iv} 2.721(2). Selected bond angles (°): Cu1–N1–Cu2 120.65(8), N1–Cu1–N9 85.40(7), N1–Cu1–N1^{i} 180.00, N6^{iv}–Cu1–N9 84.47(7), N1–Cu2–N4 164.45(8), N4–Cu2–N4^{iv} 82.23(7), N4^{iv}–Cu2–N10 97.75(7). Symmetry codes: (i) $-x, -y, -z$; (ii) $x, -1+y, z$; (iii) $-1-x, 1-y, -z$; (iv) $-x, 1-y, -z$.

© 2022 The Author(s). Published by the Royal Society of Chemistry

Open Access Article. Published on 11 November 2021. Downloaded on 2/16/2022 8:09:20 AM.
This article is licensed under a Creative Commons Attribution 3.0 Unported Licence.

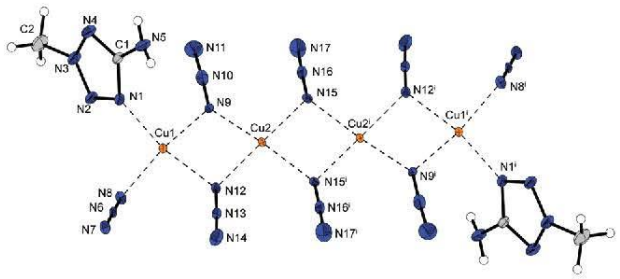


Fig. 13 Copper(II) coordination environment of $[Cu_4(N_3)_8(2\text{-MAT})_2]$ (**9**). Selected bond lengths (Å): Cu1–N1 1.998(3), Cu1–N8 1.983(3), Cu1–N9 1.974(3), Cu1–N12 2.032(3), Cu2–N9 1.964(3), Cu2–N12 2.024(3), Cu2–N15 2.018(3); selected bond angles (°): N1–Cu1–N8 96.98(12), N1–Cu1–N12 168.34(12), N1–Cu1–N9 90.49(12), N8–Cu1–N9 165.71(12), N9–Cu1–N12 78.84(12), N12–Cu2–N15 175.19(11), N9–Cu2–N12 79.28(12), N9–Cu2–N15 100.17(12), Cu1–N9–Cu2 102.55(14), Cu1–N12–Cu2 98.47(12). Symmetry code: (i) $-x, 1-y, -z$.

structures. The anions show three different coordination modes in the complex. While the 1,1-linking was already observed in many structures it shows another unique quadruple 1,1,3,3 (Chart 2) bridging of azide moieties between four different cations (Fig. 12).

The copper(II) azide complex **9** shows a high density (2.188 g cm^{-3} at 173 K) and crystallizes in the form of red rods in the monoclinic space group $P2_1/n$ with four formula units per unit cell. Two asymmetric unit cells build up the molecular unit (Fig. 13). The asymmetric unit of the compound contains two different copper(II) centres – both of them are coordinated octahedrally. Similar to **2** and **6b** the combination of three different bridging modes of the anions (Chart 2: 1,1; 1,1,1; 1,1,3) are leading the formation of polymeric 2D-structures with Cu1 coordinated by five azido anions and one 2-MAT ligand as well as Cu2 solely surrounded by six azido ligands.

Complex compound **10** crystallizes in the triclinic space group $P\bar{1}$ in from of brown needles, with a very high calculated density (2.200 g cm^{-3} at 143 K) and two formula units per unit cell.

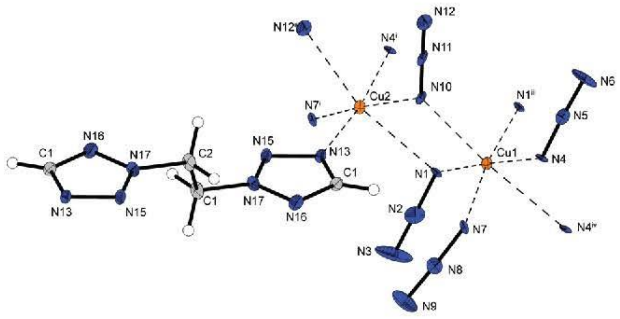


Fig. 14 Coordination environment of $[Cu_4(N_3)_8(2,2\text{-dte})]$ (**10**). Selected bond lengths (Å): Cu1–N1 1.991(5), Cu1–N4^{iv} 2.703(5), Cu1–N10 2.392(6), Cu2–N1 2.671(5), Cu2–N10 1.970(5), Cu2–N12^{ii} 2.530(6), Cu2–N13 1.988(6); selected bond angles (°): N1–Cu1–N10 84.5(2), N4–Cu1–N7 79.5(2), N4–Cu1–N4^{iv} 80.45(19), N1–Cu2–N10 77.7(2), N10–Cu2–N12^{ii} 94.9(2), N10–Cu2–N13 91.5(2), Cu1-N1-Cu2 93.7(2), Cu1–N10–Cu2 103.4(3). Symmetry codes: (i) $-1+x, y, z$; (ii) $1+x, y, z$; (iii) $-x, -y, 1-z$; (iv) $1-x, -y, 1-z$.

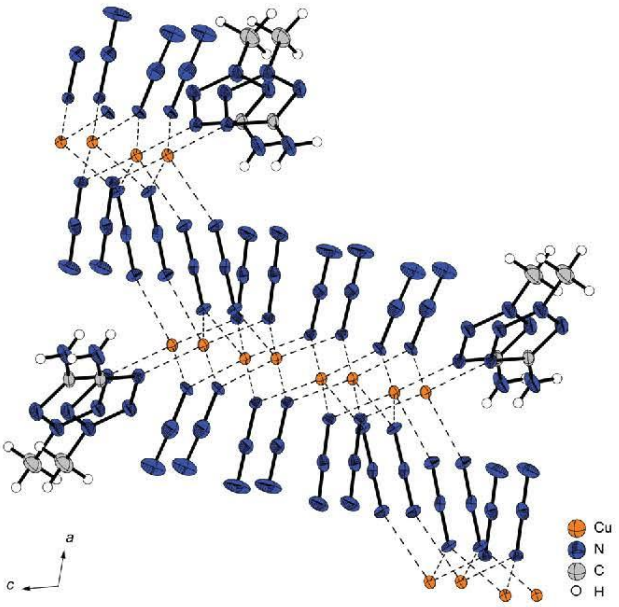


Fig. 15 Polymeric structures of **9** along the *b* axis.

The molecular unit cell is built up out of four copper centres, one ligand molecule, and eight azide anions (Fig. 14). Again, the presence of 1,1, 1,1,1, and 1,1,3 coordinating azido ligands is leading to quadruple strands of copper ions bridged to polymeric networks. In contrast to **2**, **6b**, and **9**, the use of a ditetrazole instead of a monotetrazole ligand is causing a further linkage of the polymeric layers leading to 3D structures.

Comparable to **2** and **6b**, in **9** and **10** quadruple strands of copper(II) ions are formed by 1,1,1-linking azido anions and further connected by 1,1,3-bridging ligands to polymeric networks (Fig. 15 and 16). While both ligands 2-MAT and 2,2-dte are only blocking one of the coordination sites of every second central metal, the later one is also combining the layers to 3D-networks, by binding to two copper(II) cations of different levels.

$[Cu_4(N_3)_8(2,2\text{-dtp})]$ (**12**) crystallizes in the form of brown needles in the monoclinic space group $C2/c$ with four formula units per unit cell and a calculated density of 2.136 g cm^{-3} at 123 K. Compound **12** shows almost the same consistency as **10**

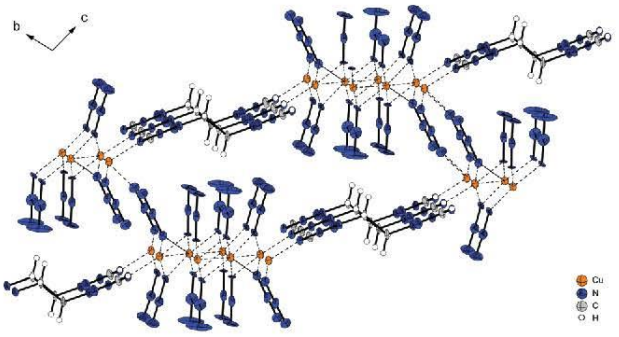


Fig. 16 Polymeric structures of **10** along the *a* axis.

© 2022 The Author(s). Published by the Royal Society of Chemistry

Open Access Article. Published on 11 November 2021. Downloaded on 2/16/2022 8:09:20 AM.
This article is licensed under a Creative Commons Attribution 3.0 Unported Licence.

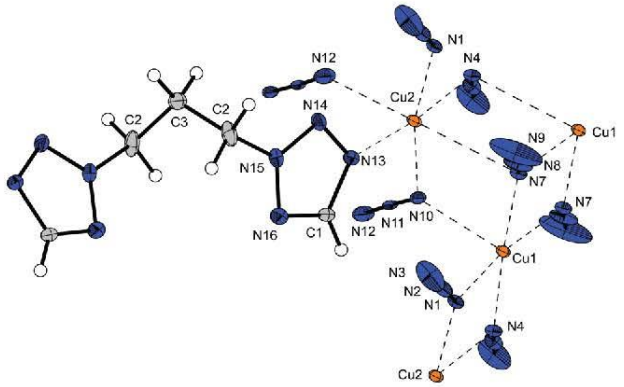


Fig. 17 Molecular unit of $[Cu_4(N_3)_8(2,2\text{-dtp})]$ (**12**). Selected bond lengths (Å): Cu1–N1 1.995(3), Cu1–N4 1.995(3), Cu1–N7 2.003(3), Cu1–N10 2.374(3), Cu2–N7 2.683(3), Cu2–N10 1.978(3), Cu2–N13 1.986(3); selected bond angles (°): N1–Cu1–N4 78.78(12), N1–Cu1–N7 101.45(12), N1–Cu1–N10 98.06(11), N4–Cu1–N7 176.02(12), N7–Cu2–N10 78.39(11), N7–Cu2–N13 100.76(10), Cu1–N7–Cu2 92.17(11), Cu1–N10–Cu2 102.74(12). Symmetry codes: (i) 0.5 − *x*, 0.5 − *y*, −*z*; (ii) *x*, 1 + *y*, *z*; (iii) −*x*, 1 − *y*, −*z*; (iv) *x*, −1 + *y*, *z*; (v) −*x*, *y*, 0.5 − *z*.

with a molecular unit built up of four copper(II) cations (Fig. 17), eight azide moieties, and one ditetrazole ligand. Whereas the outer two copper(II) atoms (Cu2) are coordinated to one tetrazole ring and five azide ligands, the inner two (Cu1) are only coordinating to anions.

The three different bridging modes (Chart 2: 1,1; 1,1,1; 1,1,3) of the anions along the *a* and *b* axis are leading to the formation of polymeric 2D-layers, only containing copper(II) and azide ions. The additionally linking of two copper(II) atoms by the ditetrazole ligand along the *c* axis (Fig. 18) is finalizing the development of a 3D-polymer with unique physical properties. Due to the strong steric hindrance, there is a large deviation of the ideal octahedral coordination sphere.

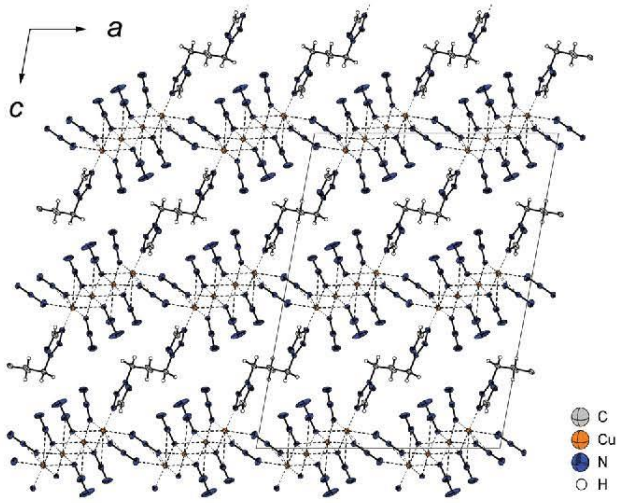


Fig. 18 Polymeric 3D-structure of **12** along the *b* axis. The ligand is bridging quadruple strands of copper(II) along the *c* axis with a small shift along the *a* axis.

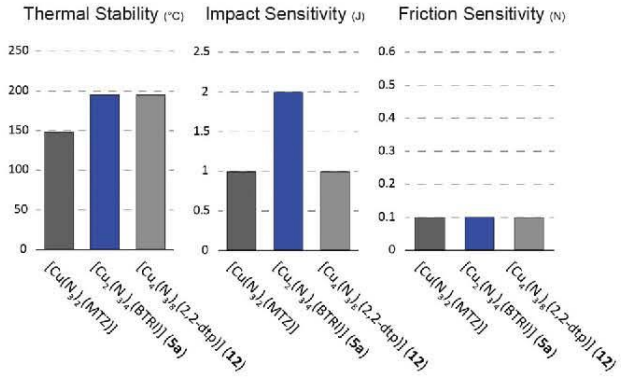


Fig. 19 Comparison of $[Cu(N_3)_2(MTZ)]$ with compound **5a** and **12**.

Thermal stability and sensitivity measurements

The complexes' thermal stability was investigated using differential thermal analysis (DTA) at a heating rate of 5 °C min $^{-1}$. The DTA curves, in the range from 50–400 °C can be found in the (Fig. S10–S12, ESI‡). Measurements of the compounds **2**, **5b**, **6b**, and **8** were waived as no elemental analysis pure samples could be obtained of these complexes.

Overall, the exothermic events of only four compounds are below 150 °C (**1**, **6a**, **7**, **11**). The majority of the compounds is exceeding 150 °C (**3**, **4**, **9**, **13**), with three ECCs even possessing very good thermal stabilities of at least 190 °C (**5a**, **10**, **12**). Those are significantly more stable than previously published $[Cu(N_3)_2(1\text{-methyl-5}H\text{-tetrazole})$[29] (Fig. 19). Endothermic events, which generally indicate a phase transition, melting, or a loss of ligand or hydrate water were observed only for $[Cu(N_3)_2(APT)]$ (**7**). Here, thermogravimetric measurements (TG) showed that upon heating, the ligand evaporates from the complex, indicating, that the ECC is not stable.

The decomposition points are in every case related to the complexes' structure. In case of the ditetrazoles based ECCs **10-13**, the high thermal stability is caused by the 3D polymeric structure formed by azido and tetrazole ligands. However, the complexes based on ligands like i-dtp and 1,2-dtp are known to possess lower thermal stabilities than the ECCs based on the respective 2,2-substituted isomers.[43,56] The assumption that $[Cu_2(N_3)_4(BTRI)]$ (**5a**) exhibits bridging BTRI ligands is supported by the thermal stability of the compound (T_{exo} = 195 °C).

Consequently, one would assume that the remaining complexes, which exhibit a 2D polymeric network, possess higher thermal stabilities than those which form only one-dimensional chains. However, the two complexes **6a** (T_{exo} = 131 °C) and **7** (T_{exo} = 132 °C) unfortunately do not follow this trend. In this case, accelerated decomposition catalysed by the copper cations is probably the reason for the earlier exothermic events. Thus, similar effects in copper complexes based on these ligands have already been observed in previous works of our group.[39,40] The third complex having a 2D structure, $[Cu_4(N_3)_8(2\text{-MAT})_2]$ (**9**), is showing a sufficient thermal stability of 161 °C, however measurements regarding compound **3** and **4**, only forming 1D polymeric chains, gave exothermic events at the same or even higher temperatures

© 2022 The Author(s). Published by the Royal Society of Chemistry

Open Access Article. Published on 11 November 2021. Downloaded on 2/16/2022 8:09:20 AM.
This article is licensed under a Creative Commons Attribution 3.0 Unported Licence.

Table 2 Overview of the compounds' thermal stability[a] and sensitivities toward various external stimuli compared to lead azide[b]

Compound		$T_{endo.}$[c] (°C)	$T_{exo.}$[d] (°C)	IS[e] (J)	FS[f] (N)	ESD[g] (mJ)
$[Cu(N_3)_2(1\text{-ATRI})]$	**1**	—	123	3	<5	5
$[Cu(N_3)_2(4\text{-ATRI})_2]$	**3**	—	161	10	>360	300
$[Cu_3(N_3)_6(TATRI)]\cdot 0.5\ H_2O$	**4**	—	170	15	>360	250
$[Cu_2(N_3)_4(BTRI)]$	**5a**	—	195	2	≤0.1	5
$[Cu(N_3)_2(AET)]$	**6a**	—	131	<1	≤0.1	1.1
$[Cu(N_3)_2(APT)]$	**7**	54	132	<1	4.5	2.5
$[Cu_4(N_3)_8(2\text{-MAT})_2]$	**9**	—	161	<1	<5	13
$[Cu_4(N_3)_8(2,2\text{-dte})]$	**10**	—	190	<1	<5	5
$[Cu_2(N_3)_4(1,2\text{-dtp})]$	**11**	—	146	3	<5	18
$[Cu_4(N_3)_8(2,2\text{-dtp})]$	**12**	—	195	1	≤0.1	5
$[Cu_2(N_3)_4(i\text{-dtp})]$	**13**	—	165	2	<5	5
$Pb(N_3)_2$ (RD-1333)[59,60]	—	—	320–350	4	≤0.1	0.007–5

[a] Onset temperatures at a heating rate of 5 °C min^{-1}. [b] Determined by 1 of 6 method.[57] [c] Endothermic peak, which indicates a loss of ligands. [d] Exothermic peak, which indicates decomposition. [e] Impact sensitivity (BAM drop hammer test).[61,62] [f] Friction sensitivity (BAM friction tester).[63,64] [g] Electrostatic discharge sensitivity (OZM XSpark10).[65]

(**3**: T_{exo} = 161 °C; **4**: T_{exo} = 170 °C). Accordingly, the hydrogen bonding specifically formed by the amino groups of the ligands in **3** and **4** are believed to counterbalance the effects of a 2D polymer on the thermal stabilities of a complex. The rather poor thermal stability of $[Cu(N_3)_2(1\text{-ATRI})]$ (**1**) is probably due to the double strand formed in the crystal structure by the azido ligands. Conclusively, it can be stated, that especially the use of bridging BTRI or ditetrazoles ligands leads to ECCs possessing a better thermal stability than those presented in our previous work.[29]

Since sensitivity data are some of the most important safety parameters in the field of energetic materials, especially when it comes to primary explosives, special emphasis was placed on it. For this purpose, sensitivity measurements with regard to impact (IS) and friction sensitivity (FS) were carried out according to BAM (Bundesamt für Materialforschung und -prüfung) standard methods.[57] Furthermore, the sensitivity toward electrostatic discharge was evaluated. For every parameter, the 1-in-6 method was applied to determine the lowest energy or force needed for an ignition. The data are summarized in Table 2. Conclusively, a classification of the compounds according to the UN Recommendation on the Transport of Dangerous Goods was made.[58]

Because the primary goal here was to find a substitute for lead azide (LA), its sensitivity data are also listed in Table 2. A comparison of the impact sensitivity with lead azide shows that the complexes presented in this work are for the most part more sensitive. However, this is irrelevant, since both LA as well as the copper azide ECCs are extremely sensitive materials and the danger of the substances is primarily due to their sensitivity toward friction and electrostatic discharge. Thus, similar sensitivity results were observed for the copper complexes of this work, and lead azide (LA ≤ 0.1 N).[59]

Measurements of friction sensitivity below 5 N were not performed in most cases. This is mainly due to the fact that a more precise determination in this range is usually less significant. In general, a friction sensitivity of below 5 N is already considered as extremely sensitive.

The only exceptions to this pattern are the compounds **3** (IS = 10 J, FS > 360 N) and **4** (IS = 15 J, FS > 360 N). The reason for this is difficult to explain. Both complexes are the only ones to show a distinct green colour. Furthermore, their crystal structure exhibits a unique coordination behaviour of an azido ligand, which coordinates in each case only simply *via* a nitrogen atom. Furthermore, the hydrate water in **4** leads to further desensitization.

It should also be noted that the majority of the ECCs in this work, analogous to lead azide, require an extremely low electrostatic discharge energy for ignition, which on the one hand facilitates ignition in detonators by electrostatic discharge, but on the other hand makes extreme caution necessary when handling these substances. The classification according to the UN Recommendation on the Transport of dangerous goods also results in the category extremely sensitive for all substances, except **3** and **4**. The remaining substances are considered sensitive only.[58,66]

Lead azide replacement suitability evaluation

In the following the suitability of selected ECCs to replace LA was investigated. The compounds **1**, **3**, **4**, and **7** examined further because they either exhibited poor thermal stability or poor performance in the sensitivity measurements, indicating a distinct lack of performance. This assumption is based on the observation that primary explosives are only sufficiently suitable below a certain sensitivity threshold.[67] The definition of a primary explosive here results from the position of the compound in the initiation chain. Consequently, an energetic material should be able to initiate a booster explosive such as pentaerythritol tetranitrate (PETN) to be classified as a primary explosive.[67]

An important property of a suitable primary explosive is the deflagration to detonation transition (DDT) of a compound.[67] In order to gain insight into this behaviour, hot plate and especially hot needle tests are performed with the respective substances. To perform the hot plate tests the evaluated substance is placed on a copper plate and subsequently heated with a Bunsen burner until a conversion was observed (Fig. 20, left). Especially the behaviour of the compound under fast heating is investigated with this experiment. Hot needle tests on the other hand, are carried out to investigate the substances' reaction when ignited under slight confinement. Therefore, the complex is taped to a copper plate with adhesive tape and penetrated with a red glowing needle subsequently (Fig. 20, right).

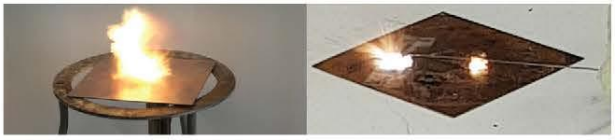


Fig. 20 Detonation of compound **5a** during hot plate test (right side) and detonation of complex **10** (left side).

© 2022 The Author(s). Published by the Royal Society of Chemistry

Open Access Article. Published on 11 November 2021. Downloaded on 2/16/2022 8:09:20 AM.
This article is licensed under a Creative Commons Attribution 3.0 Unported Licence.

Table 3 Results of hot plate and hot needle tests together with PETN initiation experiments of the compounds **5a**, **6a**, and **9–13**

Compound		HP[a]	HN[a]	PETN initiation	Laser ignition energy[b] 0.17 mJ	0.20 mJ	1.7 mJ	25.5 mJ	Detonation velocity[c] [km s^{-1}]
$[Cu_2(N_3)_4(BTRI)]$	**5a**	det.	det.	positive	—	det.	—	—	8.28
$[Cu(N_3)_2(AET)]$	**6a**	det.	det.	positive	defl.	—	—	defl.	7.98
$[Cu_4(N_3)_8(2\text{-MAT})_2]$	**9**	det.	det.	positive	—	—	det.	det.	8.02
$[Cu_4(N_3)_8(2,2\text{-dte})]$	**10**	det.	det.	positive	—	det.	—	—	8.07
$[Cu_2(N_3)_4(1,2\text{-dtp})]$	**11**	det.	det.	positive	det.	—	det.	—	7.90
$[Cu_4(N_3)_8(2,2\text{-dtp})]$	**12**	det.	det.	positive	det.	—	—	-	7.83
$[Cu_2(N_3)_4(i\text{-dtp})]$	**13**	det.	det.	positive	defl.	—	defl.	—	7.79

[a] defl.: deflagration; det.: detonation. [b] Operating parameters: current I = 7–8 A; voltage U = 4 V; theoretical maximal output power P_{max} = 45 W; theoretical energy E_{max} = 0.17–25.5 mJ; wavelength λ = 915 nm; pulse length τ = 1–15 ms. [c] Details can be found in the ESI.

In any case, the preferred test results are "detonations". The results are summarized in Table 3.

Due to the high detonation velocity of the remaining compounds, it was not possible to capture further images of the detonations during hot plate and hot needle tests with the setup used. However, these highly positive results enable testing the compounds in PETN initiation experiments. These studies provide further insight into the extent to which copper(II) azide ECCs are capable of replacing LA. For this purpose, 200 mg of PETN was pressed into a copper shell and 50 mg of the compound to be tested was loosely filled on top. Subsequently, the shell was placed on a copper witness plate and ignited with a type A electrical igniter. Parts of the setup are shown in Fig. 21. A positive DDT is indicated by a hole in the witness plate. Further details on the process and setup can be found in the ESI.‡

For all of the compounds tested in this setup the initiation was positive (Table 3). This is quite impressive as these are more than half of the compounds presented in the work.

A positive initiation of compound **5a** is exemplarily displayed in Fig. 21. Further images of the positive results can be found in the ESI.‡

Another feature of ECCs is laser ignitability. The field is attracting great interest, as it is anticipated that laser ignition will make mechanical ignition irrelevant.[22,68–70] Therefore, an extreme sensitivity toward mechanical stimuli is no longer required for energetic materials and thus safe handling becomes easier.

The compounds presented in this work are not suitable insensitive laser ignitable substances as they are as sensitive as the cobalt perchlorate complex BNCP which they are supposed to replace.[8] Nevertheless, the superior performance of the copper azide complexes, especially with respect to their simple synthesis and poor water solubility, makes a brief analysis of their behaviour in laser experiments interesting. The results of these experiments are displayed in Table 3. An example of a positive laser ignition result is shown in Fig. 22.



Fig. 22 Detonation of complex **9** during laser ignition experiments.

Further details on the laser setup can be found in the Supporting Information. As with the hot plate and hot needle tests, it was unfortunately not possible to record all detonations due to their high velocity. Overall, all complexes showed a reaction toward the laser irradiation. Interestingly the compounds **6a** and **13** only showed deflagration, even at higher energies. This is particularly surprising because both compounds showed powerful detonations during preliminary hot plate and hot needle tests and successfully initiated PETN. Nevertheless, the majority of the coordination compounds



Fig. 21 Test setup for PETN Ignition experiments shown without the copper witness plate (left) and positive initiation experiment of compound **5a** (right).

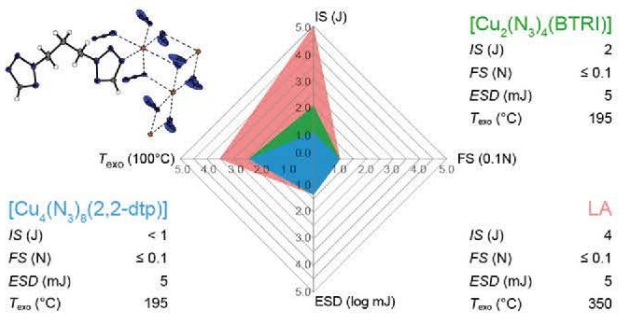


Fig. 23 Comparison of lead azide (LA) with the ECCs $[Cu_2(N_3)_4(BTRI)]$ (**5a**) and $[Cu_4(N_3)_8(2,2\text{-dtp})]$ (**12**) in terms of thermal stability (T_{exo}) and sensitivity toward friction (*FS*), impact (IS), and electrostatic discharge (*ESD*). The friction sensitivity was only determined to <5 N but is assumed to be within the range of LA.

© 2022 The Author(s). Published by the Royal Society of Chemistry

showed strong detonations at energies of 0.17–0.20 mJ, again proving that copper azide complexes are powerful initiators in diverse application fields. Detonation velocities of the ECC was estimated according to a method, outlined in theESI.‡

The experiments performed in this section demonstrate that the copper complexes in this work not only have the thermal stability and sensitivity, but also the required performance to successfully replace lead azide finally (Fig. 23).

Conclusions

In this work we have prepared 15 copper azide complexes based on nitrogen-rich triazole and tetrazole ligands. A special feature is the simple synthesis, which leads to a direct precipitation of the complexes. The poor water solubility drastically reduces the toxicity of the resulting complexes as well as enable their desensitization by moistening. The majority of the complexes was investigated using single crystal X-ray crystallography, unveiling unique coordination geometries caused by the interaction of azido ligands with tri- and tetrazoles. The main aim of this work was the stabilization of neat copper azide while keeping its useful properties like performance and thermal stability. This was achieved especially through the application of bridging ligands like BTRI, 2,2-dte, and 2,2-dtp with the resulting three-dimensional metalorganic frameworks exhibiting a thermal stability exceeding 190 °C. Furthermore, PETN initiation tests have successfully demonstrated that the performance of copper azide has also been retained. Overall, the excellent initiation capability of these ECCs was not only shown in PETN initiation experiments, but also during laser ignition experiments. Consequently, the energetic coordination compounds presented in this work are worth considering as lead azide substitutes not only because of their simple synthesis, low toxicity, excellent thermal stability, but also because of their superior initiation ability.

Author contributions

The manuscript was written through contributions of all authors. All authors have given approval to the final version of the manuscript.

Conflicts of interest

There are no conflicts to declare.

Acknowledgements

For financial support of this work Ludwig Maximilian University of Munich (LMU) is gratefully acknowledged. The authors would like to thank Professor Dr Thomas M. Klapötke for his scientific support as well as for providing his research facilities. Furthermore, the authors would like to thank Benjamin Bissinger, Marina Schönherr, and Lukas Zeisel for their great contribution to this work.

Notes and references

1 H. H. Jobelius and H.-D. Scharff, *Ullmann's Encyclopedia of Industrial Chemistry*, Wiley-VCH, Weinheim, 6th edn, 2002.
2 M. Breugst and H.-U. Reissig, The Huisgen Reaction: Milestones of the 1,3-Dipolar Cycloaddition, *Angew. Chem., Int. Ed.*, 2020, **59**, 12293–12307.
3 H. C. Kolb, M. G. Finn and K. B. Sharpless, Click Chemistry: Diverse Chemical Function from a Few Good Reactions, *Angew. Chem., Int. Ed.*, 2001, **40**, 2004–2021.
4 H. Staudinger and J. Meyer, Über neue organische Phosphorverbindungen III. Phosphinmethylenderivate und Phosphinimine, *Helv. Chim. Acta*, 1919, **2**, 635–646.
5 J. Haase, in *Organic Azides*, ed. S. Bräse and K. Banert, John Wiley & Sons, Ltd, Hoboken, New Jersey, 2009, pp. 29–51.
6 J. J. Jobelius and H.-D. Scharff, *Ullmann's Encyclopedia of Industrial Chemistry*, Wiley VCH, Weinheim, 7th edn, 2012.
7 H. D. Fair and R. F. Walker, in *Physics and Chemistry of the Inorganic Azides*, ed. H. D. Fair and R. F. Walker, Plenum Press, New York, 1st edn, 1977, vol. 1.
8 R. Matyás and J. Pachman, *Primary Explosives*, Springer Verlag, Berlin, 2013.
9 P. J. Landrigan, C. B. Schechter, J. M. Lipton, M. C. Fahs and J. Schwartz, Environmental pollutants and disease in American children: estimates of morbidity, mortality, and costs for lead poisoning, asthma, cancer, and developmental disabilities, *Environ. Health Perspect.*, 2002, **110**, 721–728.
10 A. D. Woolf, R. Goldman and D. C. Bellinger, Update on the Clinical Management of Childhood Lead Poisoning, *Pediatr. Clin. North Am.*, 2007, **54**, 271–294.
11 R. Hagel and K. Redecker, Sintox - A New, Non-Toxic Primer Composition by Dynamit Nobel AG, *Propellants, Explos., Pyrotech.*, 1986, **11**, 184–187.
12 C. He and J. M. Shreeve, Potassium 4,5-Bis(dinitromethyl) furoxanate: A Green Primary Explosive with a Positive Oxygen Balance, *Angew. Chem., Int. Ed.*, 2016, **55**, 772–775.
13 W. Huang, Y. Tang, G. H. Imler, D. A. Parrish and J. M. Shreeve, Nitrogen-Rich Tetrazolo[1,5-b]pyridazine: Promising Building Block for Advanced Energetic Materials, *J. Am. Chem. Soc.*, 2020, **142**, 3652–3657.
14 J. W. Fronabarger, M. D. Williams, W. B. Sanborn, J. G. Bragg, D. A. Parrish and M. Bichay, DBX-1 – A Lead Free Replacement for Lead Azide, *Propellants, Explos., Pyrotech.*, 2011, **36**, 541–550.
15 J. Tang, D. Chen, G. Zhang, H. Yang and G. Cheng, A "Green" Primary Explosive: Design, Synthesis, and Testing, *Synlett*, 2019, 885–892.
16 M. L. Gettings, M. T. Thoenen, E. F. C. Byrd, J. J. Sabatini, M. Zeller and D. G. Piercey, Tetrazole Azasydnone ($C_2N_7O_2H$) And Its Salts: High-Performing Zwitterionic Energetic Materials Containing A Unique Explosophore, *Chem. – Eur. J.*, 2020, **26**, 14530–14535.
17 L. M. Foroughi, R. A. Wiscons, D. R. Du Bois and A. J. Matzger, Improving stability of the metal-free primary energetic cyanuric triazide (CTA) through cocrystallization, *Chem. Commun.*, 2020, **56**, 2111–2114.

Open Access Article. Published on 11 November 2021. Downloaded on 2/16/2022 8:09:20 AM. This article is licensed under a Creative Commons Attribution 3.0 Unported Licence.

Open Access Article. Published on 11 November 2021. Downloaded on 2/16/2022 8:09:20 AM.
This article is licensed under a Creative Commons Attribution 3.0 Unported Licence.

18 L. Havlíková, R. Matyáš, L. Ihnát, L. Nováková and D. Šatínský, Degradation study of nitroaromatic explosives 2-diazo-4,6-dinitrophenol and picramic acid using HPLC and UHPLC-ESI-MS/MS, *Anal. Methods*, 2014, **6**, 4761–4768.
19 J. W. Fronabarger, M. D. Williams, A. G. Stern and D. A. Parrish, MTX-1 - a potential replacement for tetrazene in primers, *Cent. Eur, J. Energ. Mater.*, 2016, **13**, 33–52.
20 M. Joas, T. M. Klapötke and N. Szimhardt, Photosensitive Metal(II) Perchlorates with 1,2-Bis[5-(1-methylhydrazinyl)tetrazol-1-yl]ethane as Ligand: Synthesis, Characterization and Laser Ignition, *Eur. J. Inorg. Chem.*, 2014, 493–498.
21 Z. Mi, S. Chen, Z. Jing, L. Yang and T. Zhang, Innovative Concept of Designing Primary Explosives by IntroducingPolymers: Preparation and Investigation of {[Ca(CHZ)2](ClO4)2}n (CHZ = carbohydrazide), *Eur. J. Inorg. Chem.*, 2016, 3978–3983.
22 T. W. Myers, J. A. Bjorgaard, K. E. Brown, D. E. Chavez, S. K. Hanson, R. J. Scharff, S. Tretiak and J. M. Veauthier, Energetic Chromophores: Low-Energy Laser Initiation in Explosive Fe(II) Tetrazine Complexes, *J. Am. Chem. Soc.*, 2016, **138**, 4685–4692.
23 M. H. V. Huynh, M. D. Coburn, T. J. Meyer and M. Wetzler, Green primary explosives: 5-Nitrotetrazolato-N2-ferrate hierarchies, *Proc. Natl. Acad. Sci. U. S. A.*, 2006, **103**, 10322–10327.
24 Q. Zhang and J. M. Shreeve, Metal–Organic Frameworks as High Explosives: A New Concept for Energetic Materials, *Angew. Chem., Int. Ed.*, 2014, **53**, 2540–2542.
25 J.-G. Xu, X.-Z. Li, H.-F. Wu, F.-K. Zheng, J. Chen and G.-C. Guo, Substitution of Nitrogen-Rich Linkers with Insensitive Linkers in Azide-Based Energetic Coordination Polymers toward Safe Energetic Materials, *Cryst. Growth Des.*, 2019, **19**, 3934–3944.
26 R. Haiges, R. J. Buszek, J. A. Boatz and K. O. Christe, Preparation of the First Manganese(III) and Manganese(IV) Azides, *Angew. Chem., Int. Ed.*, 2014, **53**, 8200–8205.
27 R. Haiges, P. Deokar and K. O. Christe, Coordination Adducts of Niobium(v) and Tantalum(v) Azide M(N3)5 (M = Nb, Ta) with Nitrogen Donor Ligands and their Self-Ionization, *Angew. Chem., Int. Ed.*, 2014, **53**, 5431–5434.
28 R. Haiges, J. Skotnitzki, Z. Fang, D. A. Dixon and K. O. Christe, The Molybdenum(v) and Tungsten(VI) Oxoazides $[MoO(N_3)_3]$, $[MoO(N_3)_3{\cdot}2CH_3CN]$, $[(bipy)MoO(N_3)_3]$, $[MoO(N_3)_5]2-$, $[WO(N_3)_4]$, and $[WO(N_3)_4{\cdot}CH_3CN]$, *Angew. Chem., Int. Ed.*, 2015, **54**, 15550–15555.
29 M. H. H. Wurzenberger, M. Lommel, M. S. Gruhne, N. Szimhardt and J. Stierstorfer, Refinement of Copper(II) Azide with 1-Alkyl-5*H*-tetrazoles: Adaptable Energetic Complexes, *Angew. Chem., Int. Ed.*, 2020, **59**, 12367–12370.
30 H. Zöllner, M. Joas, R. Schirra and K. Kaplan, Lead-free initiating agents or initiating agent mixtures, *WO Pat.*, WO 2018011134A1, 2018.
31 T. M. Klapötke, J. Stierstorfer, M. H. H. Wurzenberger and N. Szimhardt, Use of a copper(II) azide complex as a primary explosive, *WO Pat.*, 2019134867A1, 2019.
32 A. Cirulis, Das Kupferazid und dessen Komplexe, *Naturwissenschaften*, 1939, **27**, 583.
33 Z.-G. Gu, J.-L. Zuo and X.-Z. You, A three-dimensional ferromagnet based on linked copper–azido clusters, *Dalton Trans.*, 2007, 4067–4072.
34 S. Mukherjee and P. S. Mukherjee, CuII–azide polynuclear complexes of Cu4 building clusters with Schiff-base co-ligands: synthesis, structures, magnetic behavior and DFT studies, *Dalton Trans.*, 2013, **42**, 4019–4030.
35 Y.-B. Xie, L. Gan, E. Carolina Sañudo, H. Zheng, J. Zhao, M. Zhao, B. Wang and J.-R. Li, Tetrazolate-azido-copper(II) coordination polymers: tuned synthesis, structure, and magnetic properties, *CrystEngComm*, 2015, **17**, 4136–4142.
36 X. Qu, L. Zhai, B. Wang, Q. Wei, G. Xie, S. Chen and S. Gao, Copper-based energetic MOFs with 3-nitro-1H-1,2,4-triazole: solvent-dependent syntheses, structures and energetic performances, *Dalton Trans.*, 2016, **45**, 17304–17311.
37 B.-D. Wu, Y.-G. Bi, F.-G. Li, L. Yang, Z.-N. Zhou, J.-G. Zhang and T.-L. Zhang, A Novel Stable High-Nitrogen Energetic Compound: Copper(II) 1,2–Diaminopropane Azide, *Z. Anorg. Allg. Chem.*, 2014, **640**, 224–228.
38 J. Zhang, Y. Du, K. Dong, H. Su, S. Zhang, S. Li and S. Pang, Taming Dinitramide Anions within an Energetic Metal–Organic Framework: A New Strategy for Synthesis and Tunable Properties of High Energy Materials, *Chem. Mater.*, 2016, **28**, 1472–1480.
39 M. H. H. Wurzenberger, M. S. Gruhne, M. Lommel, N. Szimhardt, T. M. Klapötke and J. Stierstorfer, Comparison of 1-Ethyl-5*H*-tetrazole and 1-Azidoethyl-5*H*-tetrazole as Ligands in Energetic Transition Metal Complexes, *Chem. – Asian J.*, 2019, **14**, 2018–2028.
40 M. H. H. Wurzenberger, S. M. J. Endraß, M. Lommel, T. M. Klapötke and J. Stierstorfer, Comparison of 1-Propyl-5*H*-tetrazole and 1-Azidopropyl-5*H*-tetrazole as Ligands for Laser Ignitable Energetic Materials, *ACS Appl. Energy Mater.*, 2020, **3**, 3798–3806.
41 P. J. van Koningsbruggen, Y. Garcia, O. Kahn, L. Fournès, H. Kooijman, A. L. Spek, J. G. Haasnoot, J. Moscovici, K. Provost, A. Michalowicz, F. Renz and P. Gütlich, Synthesis, Crystal Structure, EXAFS, and Magnetic Properties of Catena [μ-Tris(1,2-bis(tetrazol-1-yl)propane-N1,N1′)iron(II)] Bis(perchlorate). First Crystal Structure of an Iron(II) Spin-Crossover Chain Compound, *Inorg. Chem.*, 2000, **39**, 1891–1900.
42 N. Szimhardt, M. H. H. Wurzenberger, L. Zeisel, M. S. Gruhne, M. Lommel, T. M. Klapötke and J. Stierstorfer, 1-AminoTriazole Transition-Metal Complexes as Laser-Ignitable and Lead-Free Primary Explosives, *Chem. – Eur. J.*, 2019, **25**, 1963–1974.
43 N. Szimhardt, M. H. H. Wurzenberger, T. M. Klapötke, J. T. Lechner, H. Reichherzer, C. C. Unger and J. Stierstorfer, Highly functional energetic complexes: stability tuning through coordination diversity of isomeric propyl-linked ditetrazoles, *J. Mater. Chem. A*, 2018, **6**, 6565–6577.
44 F. Lu, E. Wang, J. Huang, M. Huang, F. Nie and F.-X. Chen, The synthesis, property and reduction of high-nitrogen compound 3,3′,5,5′-tetraazido-4,4′-bis(1,2,4-triazole), *Polyhedron*, 2016, **117**, 445–452.

© 2022 The Author(s). Published by the Royal Society of Chemistry

Open Access Article. Published on 11 November 2021. Downloaded on 2/16/2022 8:09:20 AM.
This article is licensed under a Creative Commons Attribution 3.0 Unported Licence.

45 R. A. Henry and W. G. Finnegan, Mono-alkylation of Sodium 5-Aminotetrazole in Aqueous Medium, *J. Am. Chem. Soc.*, 1954, **76**, 923–926.
46 R. G. Child, A new synthesis of 3,4,5-triamino-4H-1,2,4-triazole (guanazine), Synthesis and structure of {[Zn(1,2-di(1,2,3,4-tetrazol-2-yl)ethane)3](ClO4)2}n. The first coordination polymer based on 2-substituted tetrazole, *J. Heterocycl. Chem.*, 1965, **2**, 98–99.
47 R. Bronisz, Synthesis and structure of $\{[Zn(1,2\text{-di}(1,2,3,4\text{-tetrazol-2-yl})ethane)_3](ClO_4)_2\}_n$. The first coordination polymer based on 2-substituted tetrazole, *Inorg. Chim. Acta*, 2002, **340**, 215–220.
48 ESI‡.
49 R. C. Seccombe and C. H. L. Kennard, Bonding in 1,2,4-triazoles. Part II. Crystal structure of 3,4,5-triamino-1,2,4-triazole hydrobromide (guanazine hydrobromide), *J. Chem. Soc., Perkin Trans. 2*, 1973, 1–3.
50 J. Bryden, The crystal structure of 2-methyl-5-aminotetrazole, *Acta Crystallogr.*, 1956, **9**, 874–878.
51 M. Aouial, P. Viallefont and L. El Ammari, Etude conformationnelle du bi(triazole-1,2,4)-3,4', *Acta Crystallogr., Sect. C: Cryst. Struct. Commun.*, 1991, **47**, 1866–1868.
52 J. Bryden, The unit-cell dimensions and space groups of some tetrazole compounds, *Acta Crystallogr.*, 1953, **6**, 669–670.
53 M. Daszkiewicz and M. K. Marchewka, Crystal structure, vibrational and theoretical studies of bis(4-amino-1,2,4-triazolium) hexachloridostannate(IV), *J. Mol. Struct.*, 2012, **1017**, 90–97.
54 G. Kaplan, G. Drake, K. Tollison, L. Hall and T. Hawkins, Synthesis, characterization, and structural investigations of 1-amino-3-substituted-1,2,3-triazolium salts, and a new route to 1-substituted-1,2,3-triazoles, *J. Heterocycl. Chem.*, 2005, **42**, 19–27.
55 R. Soderquist, Studies on explosives. I. The crystal structure of copper(II) oxide, catena-diazidocopper(II), *Acta Crystallogr., Sect. B: Struct. Crystallogr. Cryst. Chem.*, 1968, **24**, 450–455.
56 M. S. Gruhne, M. H. H. Wurzenberger, M. Lommel and J. Stierstorfer, A Smart Access to the Dinitramide Anion – The Use of Dinitraminic Acid for the Preparation of Energetic Coordination Compounds, *Chem. – Eur. J.*, 2021, **27**, 9112–9123.
57 BAM, www.bam.de, accessed June, 2021.
58 UN Model Regulation: Recommendations on the Transport of Dangerous Goods – Manual of Tests and Criteria, section 13.4.2.3.3, 2015.
59 M. S. Gruhne, M. Lommel, M. H. H. Wurzenberger, N. Szimhardt, T. M. Klapötke and J. Stierstorfer, OZM Ball Drop Impact Tester (BIT-132) vs. BAM Standard Method – a Comparative Investigation, *Propellants, Explos., Pyrotech.*, 2020, **45**, 147–153.
60 T. M. Klapötke, *Energetic materials Encyclopedia*, DeGruyter, Berlin, Boston, 2nd edn, 2021.
61 NATO standardization agreement (STANAG) on explosives, impact sensitivity tests, no. 4489, 1st edn., Sept. 17th, 1999.
62 WIWEB-Standardarbeitsanweisung 4-5.1.02, Ermittlung der Explosionsgefährlichkeit, hier der Schlagempfindlichkeit mit dem Fallhammer, Nov. 8th, 2002.
63 OZM Research, www.ozm.cz/en, accessed June, 2021.
64 NATO standardization agreement (STANAG) on explosive, friction sensitivity tests, no. 4487, 1st edn., Aug. 22nd, 2002.
65 WIWEB-Standardarbeitsanweisung 4-5.1.03, Ermittlung der Explosionsgefährlichkeit oder der Reibeempfindlichkeit mit dem Reibeapparat, Nov. 8th, 2002.
66 Impact: insensitive $>$ 40 J, less sensitive $\geq$ 35 J, sensitive $\geq$ 4 J, very sensitive $\leq$ 3 J; Friction: insensitive $>$ 360 N, less sensitive = 360 N, sensitive $<$ 360 N and $>$ 80 N, very sensitive $\leq$ 80 N, extremely sensitive $\leq$ 10 N. According to the UN Recommendations on the Transport of Dangerous Goods, 5th edn, 2009.
67 T. M. Klapötke, *Chemistry of High-Energy Materials*, De Gruyter, Berlin, Boston, 5th edn, 2019.
68 T. W. Myers, K. E. Brown, D. E. Chavez, R. J. Scharff and J. M. Veauthier, Laser Initiation of Fe(II) Complexes of 4-Nitro-pyrazolyl Substituted Tetrazine Ligands, *Inorg. Chem.*, 2017, **56**, 2297–2303.
69 A. Y. Zhilin, M. A. Ilyushin, I. V. Tselinskii, A. S. Kozlov and I. S. Lisker, High-Energy-Capacity Cobalt(III) Tetrazolates, *Russ. J. Appl. Chem.*, 2003, **76**, 572–576.
70 M. A. Ilyushin, A. S. Tver'yanovich, Y. S. Tver'yanovich, G. O. Abdrashitov, A. O. Aver'yanov and M. D. Bal'makov, Laser Initiation of Photo- and Thermal Processes on a Pentaammine (5-Nytrotetrazolato-N_2) Cobalt(III) Perchlorate Example, *Glass Phys. Chem.*, 2018, **44**, 120–122.

© 2022 The Author(s). Published by the Royal Society of Chemistry

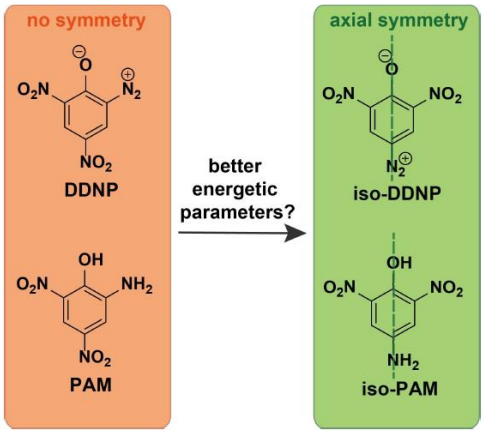
Appendix 28

Synthesis, Characterization and Derivatives of Iso-Picramic Acid

J. T. Lechner, T. M. Klapötke, J. Stierstorfer

Propellants. Explos. Pyrotech. **2022**, *47*, e2021002.

https://doi.org/10.1002/prep.202100205



Supplementary Information:
https://onlinelibrary.wiley.com/action/downloadSupplement?doi=10.1002%2Fprep.202100205&file=prep202100205-sup-0001-misc_information.pdf

Research Article

Propellants, Explosives, Pyrotechnics

doi.org/10.1002/prep.202100205

pep.wiley-vch.de

Synthesis, Characterization and Derivatives of Iso-Picramic Acid

Thomas M. Klapötke,[a] Jasmin T. Lechner,[a] and Jörg Stierstorfer*[a]

Abstract: Comparing the sensitive explosives DDNP (2-diazonium-4,6-dinitrophenolate) with iso-DDNP (para-DDNP, 4-diazonium-2,6-dinitrophenolate), it seems obvious that with increasing symmetry in the molecule, the energetic parameters also increase. This work therefore investigates whether the same trend can be applied for the isomers picramic acid (2-amino-4,6-dinitrophenol) and iso-picramic acid (para picramic acid, 4-amino-2,6-dinitrophenol). For this purpose, iso-picramic acid was synthesized and compared with the properties of picramic acid. In addition, selected ionic and other energetic derivatives such as 2,6-dinitro-4-(5*H*-tetrazol-1-yl)phenol were synthesized. The compounds were extensively studied by XRD, IR, EA, DTA and TGA. Further, their sensitivities towards impact and friction were investigated and the energetic properties were computed using the EXPLO5 code.

Keywords: Nitrophenols · Energtic Materials · NMR spectroscopy · Isomers · Structure Elucidation

1 Introduction

The structures of energetic molecules are diverse, as are their uses. They reaches from covalent compounds like TNT (trinitrotoluene), over (mostly) ionic compounds like lead azide up to coordination compounds like BNCP (tetraamine-cis-bis(5-nitro-2*H*-tetrazolato) cobalt(III) perchlorate). On the other hand, it reaches from very small molecules like mercury fulminate to large molecules e.g. HNS (hexanitrostilbene). Beyond that, there are various applications in the military sector, such as in munitions, and in the civil sector, e.g. in the mining industry [1–7].

However, all energetic compounds have in common that, as the name suggests, there is a high energy release when used. This energy in the molecule is related based on their composition and constitution. An energetic material can be achieved through nitration of a carbon backbone, which combines a fuel (carbon) and an oxidizer (NO_2) in one molecule. A subgroup of these compounds are nitroaromatics where an aromatic ring, such as a benzene ring, constitutes the carbon backbone and nitro groups the oxidizing part. The most common nitroaromatics are shown in Figure 1 [6–9].

TNT, one of the most known and widely used representatives, is synthesized by nitration of toluene using mixed acid. It is used as a melt-castable explosive due to its melting point at around 80 °C [7,10]. Picric acid (PA) replaced black powder in almost all applications at the end of the 19th century [11,12]. It is synthesized similarly to trinitroresorcinol (TNR), also known as sytphnic acid. After initial disulfonation of phenol or resorcinol by sulfuric acid, nitric acid is used for nitration [13,14]. The lead salt of styphnic acid has application as a primary explosive e.g. in primer mixtures. Together with lead azide, it is the most commonly used primary explosive today [7,15]. However, there are problems with the decomposition products due to the use of the toxic heavy metal lead. For example, there is strong lead contamination on military training grounds or firing ranges [1]. Due to the problems with the heavy metal lead, there is a constant search for heavy metal-free primary explosives. One substitute that is used in some primer mixtures is the zwitterionic compound diazodinitrophenol

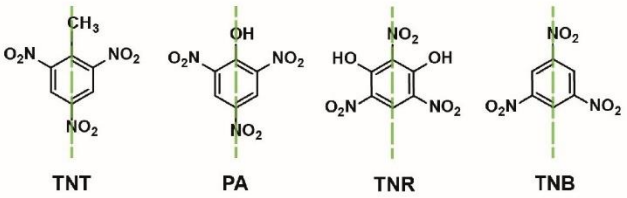


Figure 1. Molecular structure of 2,4,6-trinitrotoluene (TNT), 2,4,6-trinitrophenol (PA), 2,4,6-trinitroresorcinol (TNR), 1,3,5- trinitrobenzene (TNB). Dashed green lines indicate a symmetry element.

[a] *T. M. Klapötke, J. T. Lechner, J. Stierstorfer*
Department of Chemistry
Ludwig-Maximilian University of Munich
Butenandtstr. 5–13, 81377 Munich (Germany)
**e-mail: jstch@cup.uni-muenchen.de*
Homepage: http://www.hedm.cup.uni-muenchen.de

Supporting information for this article is available on the WWW under https://doi.org/10.1002/prep.202100205

© 2022 The Authors. Propellants, Explosives, Pyrotechnics published by Wiley-VCH GmbH. This is an open access article under the terms of the Creative Commons Attribution License, which permits use, distribution and reproduction in any medium, provided the original work is properly cited.

© 2022 The Authors. Propellants, Explosives, Pyrotechnics published by Wiley-VCH GmbH

(DDNP). DDNP is synthesized by diazotization of picramic acid (PAM) [1,7,16]. Picramic acid can be synthesized by partial reduction of picric acid with sodium hydrogen sulfide or ammonium sulphide [12].

Inspecting the structures of the nitroaromatics shown in Figure 1, it is noticeable that TNT, picric acid, styphnic acid and trinitrobenzene have a (nearly) axial symmetry. In Figure 1 the molecules are drawn one-dimensionally, but in reality the nitro groups are slightly twisted (at ~0 K, or in the rendering provided by an X-ray structure). Neglecting this fact, in the following discussion an axial symmetry is assumed for these molecules.

In DDNP and PAM, however, no axial symmetry can be found. The axially symmetric isomers, iso-DDNP and iso-PAM are also shown in Figure 2. Therefore the question arises, how the symmetrical isomers differ from the asymmetrical ones and if the symmetry might have an influence on the energetic character of these compounds. The symmetric isomer of DDNP was already synthesized by Preimesser *et al.* in 2015 and was recently reinvestigated by Wang *et al.* [17]. Comparing the densities of the two isomers, the density of the symmetrical isomer (1.79 g cm^{-3}) is higher than that one of DDNP (1.73 g cm^{-3}), as well as the heat of formation for isoDDNP (184.1 kJ mol^{-1}) is higher than that of DDNP (142.4 kJ mol^{-1}). When calculating energetic properties, the calculations mainly depends on the enthalpy of formation of the molecules and moreover on the density of the compounds. Therefore, slightly higher energetic parameters are obtained for iso-DDNP. Thus it is interesting, as shown in Figure 2, whether this trend is also visible for picramic acid and iso-picramic acid.

The energetic and molecular properties of picramic acid and its salts are also already described in the literature [12,18]. Iso-picramic acid, in contrast, is very poorly described in literature until now and its properties have not been investigated at all [19]. Therefore, in this work, the symmetric isomer of picramic acid was synthesized and the two isomers were compared with each other in terms of their properties. In addition salts of iPAM were synthesized and compared with the newly synthesized corresponding 2,6-dinitro-4-(5*H*-tetrazol-1-yl)phenolates.

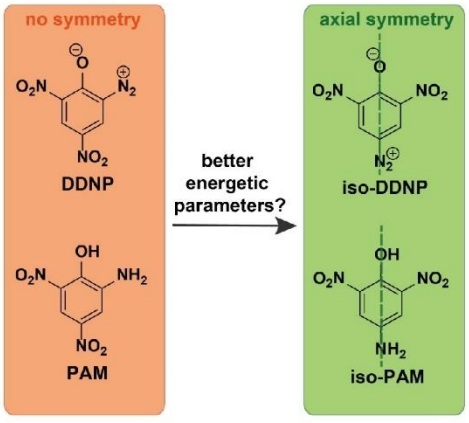


Figure 2. Figure illustrating the symmetric isomers of DDNP and PAM.

2 Experimental Section

Caution! *All investigated compounds are energetic materials and some of them show sensitivities towards various stimuli (e.g. elevated temperature). Although no hazards occurred, proper security precautions (safety glasses, face shield, earthed equipment and shoes, leather jacket, Kevlar sleeves, and earplugs) have to be worn while synthesizing and handling the described compounds.*

The synthesis of **1** and **2** was carried out according to a well working procedure released recently [20].

2.1 4-Acetamino-2,6-Dinitrophenol (1)

4-Acetaminophenol (15.0 g, 0.10 mol, 1.0 eq) was dissolved in concentrated sulfuric acid (96%, 75 mL) at 0°C. A solution of ammonium nitrate (19.8 g, 0.25 mol, 2.5 eq) in sulfuric acid (96%, 30 mL) was slowly added while cooling to 0°C. After stirring the reaction mixture for 5 hours at 0°C it was quenched on ice (500 mL). The precipitation was filtered and washed with a small amount of cold water. 4-Acetamino-2,6-dinitrophenol (**1**, 19.5 g, 0.08 mol, 81%) was obtained as yellow powder. Crystals, suitable for X-Ray diffraction, could be obtained by recrystallization in ethanol.

DTA (5°C min^{-1}) onset: 171°C(endo.), 223°C (dec.); ^{1}H NMR (400 MHz, DMSO-d_6) δ 10.42 (s, 1H), 8.41 (s, 2H), 2.06 (s, 3H); ^{13}C NMR (101 MHz, DMSO-d_6) δ 169.2, 141.7, 139.5, 130.5, 120.0, 23.9; IR (ATR, cm^{-1}): $\tilde{\nu}$= 3359 (m), 3175 (w), 3112 (w), 3076 (w), 1685 (m), 1646 (w), 1588 (m), 1551 (s), 1538 (vs), 1519 (s), 1467 (m), 1405 (m), 1364 (m), 1338 (s), 1316 (s), 1279 (s), 1249 (vs), 1147 (s), 1026 (m), 989 (w), 948 (w), 930 (w), 914 (s), 914 (s), 906 (s), 827 (m), 818 (s), 773 (m), 756 (w), 730 (s), 705 (w); EA ($C_8H_7N_3O_6$, 241.16): calcd: C 39.84, H 2.93, N 17.42%; found: C 39.91, H 2.96, N17.21%.

2.2 Iso-Picramic Acid (4-Amino-2,6-Dinitrophenol) (2)

4-Acetamino-2,6-dinitrophenol (**1**, 19.5 g, 80.0 mmol, 1.0 eq) was dissolved in sulfuric acid (96%, 30 mL) at 0°C. The mixture was heated up to 100°C and kept at this temperature for one hour. After that, aqueous ammonia (25%, 100 mL) was added at ice cooling conditions. Then sulfuric acid (conc.) was added again until the reaction mixture reached a pH value of 5. The solution was extracted with toluene (3×300 mL), the combined organic phases were dried over magnesium sulfate and the solvent was removed *in vacuo*. After recrystallization from ethanol iso-picramic acid (**2**,

© 2022 The Authors. Propellants, Explosives, Pyrotechnics published by Wiley-VCH GmbH

0.97 g, 0.005 mol, 6%) was obtained as golden yellow crystals suitable for X-Ray diffraction.

DTA (5 °C min^{-1}) onset: 158 °C (endo.), 183 °C (dec.); ^{1}H NMR (400 MHz, DMSO-d_6) δ (ppm) = 7.43 (s, 2C*H*); ^{13}C NMR (101 MHz, DMSO) δ (ppm) = 140.3, 114.0; ^{14}N NMR (29 MHz, DMSO-d_6) δ −13; IR (ATR, cm^{-1}): ṽ = 3185 (w), 3162 (w), 3098 (w), 2789 (m), 2746 (m), 2518 (m), 2511 (m), 2446 (m), 1980 (m), 1935 (w), 1817 (w), 1620 (m), 1534 (m), 1499 (s), 1482 (vs), 1421 (s), 1364 (m), 1333 (s), 1253 (s), 1226 (s), 1190 (s), 1145 (m), 1120 (m), 1102 (m), 966 (m), 913 (m), 896 (s), 828 (s), 799 (s), 779 (vs); EA ($C_6H_5N_3O_5$, 199.12): calcd: C 36.49, H 2.53, N 21.10%; found: C 36.35, H 2,43, N 20.88%; BAM drophammer: > 40 J; friction tester: > 360 N; ESD: 500 mJ (at grain size < 100 µm).

2.3 2,6-Dinitro-4-(5*H*-Tetrazol-1-yl)Phenol (3)

Iso-picramic acid (**2**, 500 mg, 2.50 mmol, 1.0 eq) was dissolved in triethyl orthoformate (3 mL) and sodium azide (195 mg, 3.00 mmol, 1.2 eq) was added to the reaction mixture. Over a period of 30 minutes, acetic acid (8 mL) was added dropwise and afterwards it was heated up to 90 °C for 12 hours. The solvent was removed *in vacuo* and the residue was then suspended in water (50 mL) again. After hydrochloric acid (2 M, 10 mL) was added, it was stirred at room temperature for 10 minutes and filtered. 2,6-Dinitro-4-(5*H*-tetrazol-1-yl)phenol (**3**, 377 mg, 1.50 mmol, 60%) was obtained as orange solid. Crystals, suitable for X-Ray diffraction, could be obtained by recrystallization in ethanol.

DTA (5 °C min^{-1}) onset: 175 °C (dec.);^{1}H NMR (400 MHz, DMSO-d_6) δ (ppm) = 11.26 (s, 1H), 10.07 (s, 1H), 8.73 (s, 2H); ^{13}C NMR (101 MHz, DMSO- d_6) δ (ppm) = 147.4, 142.2, 140.7, 123.5, 122.9; ^{14}N NMR (29 MHz, DMSO) δ (ppm) = −17; ^{15}N NMR (41 MHz, DMSO-d_6) δ (ppm) = 11.8 (d, *J* = 3.4 Hz), −15.5 (dd, *J* = 1.4 Hz), −19.4 (s), −51.8 (d, *J* = 12.1 Hz), −140.9 (dt, *J* = 9.3, 1.9 Hz); IR (ATR, cm^{-1}): ṽ = 3151 (w), 3089 (w), 3080 (w), 1843 (vw), 1820 (vw), 1790 (vw), 1720 (vw), 1645 (w), 1597 (w), 1561 (m), 1531 (vs), 1489 (s), 1455 (s), 1391 (m), 1373 (m), 1357 (s), 1318 (vs), 1291 (m), 1261 (vs), 1218 (s), 1162 (s), 1089 (s), 1077 (s), 1077(s), 1016 (s), 961(m), 922 (vs), 895 (s), 862 (s), 775 (s), 757 (m); EA ($C_7H_4N_6O_5$, 252.15): calcd: C 33.34, H 1.60, N 33.33%; found: C 33.21, H 1.49, N 32.70%; BAM drophammer: 30 J; friction tester: > 360 N; ESD: 380 mJ (at grain size < 100 µm).

2.4 4-(5*H*-Tetrazol-1-yl)Phenol (3a)

4-Aminophenol (546 mg, 5.0 mmol, 1 eq) was suspended in triethyl orthoformate (2 mL, 1.8 g, 12.0 mmol, 2.4 eq). Then, sodium azide (488 mg, 7.5 mmol, 1.5 eq) was added followed by the dropwise addition of glacial acetic acid (12 mL). The reaction mixture was refluxed at 100 °C for 5 hours. After slowly cooling to room temperature the resulting precipitation was filtered. The residue was suspended in a mixture of ethanol (25 mL) and water (5 mL). After stirring the suspension for 10 minutes hydrochloric acid (2 M, 5 mL) was added and the mixture was left over night for crystallization. The solid was filtered and washed with a small amount of cold water to yield 4-(5*H*-tetrazol-1-yl)phenol (**3a**, 318 mg, 2.0 mmol, 40%) as colorless crystals suitable for X-Ray diffraction.

DTA (5 °C min^{-1}) onset: 209 °C (dec.), 270 °C(endo.); ^{1}H NMR (400 MHz, DMSO-d_6) δ (ppm) = 10.12 (s, 1H), 9.90 (s, 1H), 7.71–7.63 (m, 2H), 7.02–6.93 (m, 2H); ^{13}C NMR (101 MHz, DMSO-d_6) δ (ppm) = 158.6, 142.1, 125.6, 123.1, 116.2; IR (ATR, cm^{-1}): ṽ = 3119 (m), 2837 (w), 2704 (w), 2603 (w), 2495 (w), 1886 (w), 1780 (vw), 1602 (m), 1519 (s), 1480 (m), 1469 (m), 1401 (m), 1374 (m), 1318 (w), 1268 (m), 1237 (s), 1209 (s), 1170 (s), 1110 (w), 1088 (s), 1043 (m), 1014 (m), 1000 (m), 972 (m), 952 (w), 894 (m), 830 (vs), 814 (m), 720 (s), 674 (s); EA ($C_7H_6N_4O$, 162.15): calcd: C 51.85, H 3.73, N 34.55%; found: C 51.54, H 3.83, N 34.59%.

2.5 2,6-Dinitro-4-(5*H*-Tetrazol-1-yl)Phenol (3) (Alternative Synthesis)

Under ice cooling conditions, fuming nitric acid (3 mL) was added slowly to concentrated sulfuric acid (6 mL). 4-(1*H*-tetrazol)phenol (**3a**, 300 mg, 1.85 mmol) was added to the mixture at 0 °C and after complete addition the mixture was allowed to warm up to room temperature and was further stirred for 1 h at this temperature. Then the reaction mixture was quenched on ice water (25 mL) and the precipitate was filtered. 2,6-Dinitro-4-(5*H*-tetrazol-1-yl)phenol (**3**, 307 mg, 1.22 mmol, 66%) was obtained as orange crystals suitable for X-Ray diffraction.

EA ($C_7H_4N_6O_5$, 252.15): calcd: C 33.34, H 1.60, N 33.33%; found: C 33.14, H 1.69, N 33.17%.

The synthesis of the following ionic compounds are described in the SI.

2.6 Sodium Iso-Picramate·H_2O (4)

DTA (5 °C min^{-1}) onset: 270 °C (dec.), 139 °C (endo.); IR (ATR, cm^{-1}): ṽ = 3589 (m), 3403 (s), 3139 (m), 1636 (s), 1562 (s), 1550 (vs), 1510 (s), 1475 (m), 1437 (s), 1413 (m), 1336 (vs), 1288 (s), 1251 (vs), 1215 (vs), 1176 (m), 1101 (m), 1079 (s), 1021 (m), 979 (w), 907 (s), 885 (w), 782 (s), 714 (m); EA ($C_6H_6N_3NaO_6$, 239.12): calcd: C 30.14, H 2.53, N 17.57%; found: C 30.10, H 2.46, N17.63%; BAM drophammer: > 40 J; friction tester: > 360 N (at grain size < 100 µm).

2.7 Potassium Iso-Picramate (5)

DTA (5 °C min^{-1}) onset: 270 °C (dec.); IR (ATR, cm^{-1}): ṽ = 3439 (m), 3362 (m), 3221 (w), 3081 (w), 2886 (w), 2723 (w), 1768 (vw), 1650 (m), 1621 (m), 1539 (s), 1520 (vs), 1436 (s), 1420

© 2022 The Authors. Propellants, Explosives, Pyrotechnics published by Wiley-VCH GmbH

(s), 1375 (w), 1325 (s), 1292 (w), 1253 (m), 1175 (vs), 1147 (vs), 1119 (vs), 991 (s), 902 (s), 873 (s), 822 (s), 796 (s), 779 (vs), 757 (m), 715 (m), 704 (m), 673 (s), 635 (m), 615 (m); EA ($C_6H_4KN_3O_5$, 237.21): calcd: C 30.38, H 1.70, N 17.71%; found: C 30.42, H 1.72, N 17.75%; BAM drophammer: 40 J; friction tester: > 360 N (at grain size < 100 µm).

2.8 Barium Iso-Picramate·1.5 H_2O (6)

DTA (5 °C min^{-1}) onset: 277 °C (dec.), 175 °C(endo.); IR (ATR, cm^{-1}): ṽ= 3406 (m), 3316 (w), 3301 (w), 3202 (w), 3085 (vw), 2881 (vw), 1635 (w), 1524 (s), 1503 (s), 1490 (s), 1427 (m), 1375 (w), 1334 (s), 1236 (vs), 1152 (m), 1100 (w), 985 (w), 915 (s), 898 (m), 865 (m), 830 (w), 775 (s), 744 (m), 744 (m), 724 (m), 646 (vw); EA ($C_{24}H_{22}Ba_2N_{12}O_{23}$, 1121.16): calcd: C 25.71, H 1.98, N 14.99%; found: C 25.74, H 1.77, N14.91%; BAM drophammer: > 40 J; friction tester: > 360 N (at grain size < 100 µm).

2.9 Guanidinium Iso-Picramate (7)

DTA (5 °C min^{-1}) onset: 250 °C (dec.); IR (ATR, cm^{-1}): ṽ= 3411 (vs), 3350 (vs), 3173 (s), 3009 (m), 3001 (m), 1659 (vs), 1635 (m), 1620 (s), 1616 (s), 1563 (m), 1557 (s), 1549 (s), 1539 (s), 1521 (vs), 1489 (m), 1447 (m), 1421 (s), 1335 (s), 1310 (w), 1187 (vs), 1149 (vs), 1119 (vs), 992 (s), 992 (s), 906 (s), 870 (m), 828 (m), 794 (w), 776 (s), 741 (m), 735 (m), 693 (m), 678 (m); EA ($C_7H_{10}N_6O_5$, 258.19): calcd: C 32.56, H 3.90, N 32.55%; found: C 32.56, H 3.98, N 32.25%; BAM drophammer: 40 J; friction tester: > 360 N (at grain size < 100 µm).

2.10 Sodium 2,6-Dinitro-4-(5*H*-Tetrazol-1-yl)Phenolate·4 H_2O (8)

DTA (5 °C min^{-1}) onset: 242 °C (dec.), 54/ 115 °C(endo.); IR (ATR, cm^{-1}): ṽ= 3547 (w), 3477 (w), 3470 (w), 3404 (m), 3376 (m), 3310 (m), 3288 (m), 3277 (m), 3259 (m), 3214 (w), 3087 (w), 1663 (w), 1646 (w), 1529 (vs), 1494 (s), 1448 (w), 1427 (m), 1333 (s), 1249 (s), 1160 (m), 1103 (m), 993 (w), 907 (s), 888 (m), 826 (m), 803 (m), 775 (s), 745 (m), 729 (m), 657 (w); EA ($C_7H_{11}N_6NaO_9$, 364.19): calcd: C 24.29, H 3.20, N 24.28%; found: C 23.95, H 3.16, N 24.60%; BAM drophammer: > 40 J; friction tester: > 360 N (at grain size < 100 µm).

2.11 Potassium 2,6-Dinitro-4-(5*H*-Tetrazol-1-yl)Phenolate·H_2O (9)

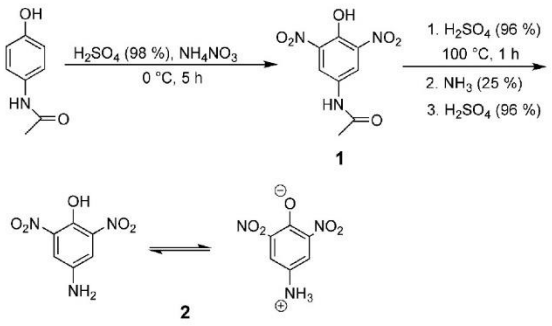
DTA (5 °C min^{-1}) onset: 260 °C (dec.), 88 °C(endo.); IR (ATR, cm^{-1}): ṽ= 3624 (w), 3532 (w), 3483 (w), 3131 (m), 3092 (w), 3039 (w), 1836 (vw), 1637 (s), 1560 (s), 1541 (s), 1536 (s), 1491 (m), 1470 (s), 1438 (s), 1414 (m), 1335 (s), 1288 (s), 1247 (s), 1219 (s), 1190 (s), 1170 (s), 1111 (m), 1097 (s), 1097 (s), 1084 (s), 1021 (m), 972 (m), 906 (vs), 886 (s), 852 (m), 820 (m), 779 (s), 728 (s), 717 (m), 713 (m), 695 (m), 676 (w), 661 (m), ; EA ($C_7H_5KN_6O_6$, 308.25): calcd: C 27.28, H 1.64, N 27.26%; found: C 27.17, H 1.84, N27.05%; BAM drophammer: > 40 J; friction tester: > 360 N (at grain size < 100 µm).

2.12 Copper(II) 2,6-Dinitro-4-(5*H*-Tetrazol-1-yl)Phenolate·6 H_2O (10)

DTA (5 °C min^{-1}) onset: 249 °C (dec.), 114 °C(endo.); IR (ATR, cm^{-1}): ṽ= 3541 (m), 3380 (s), 3129 (s), 3056 (m), 1836 (vw), 1775 (vw), 1756 (vw), 1636 (m), 1621 (m), 1539 (vs), 1509 (s), 1474 (m), 1454 (s), 1404 (m), 1351 (s), 1332 (s), 1309 (s), 1259 (s), 1226 (s), 1195 (s), 1178 (s), 1118 (m), 1097 (s), 1097 (s), 1086 (s), 1031 (m), 1014 (s), 915 (m), 897 (s), 881 (m), 826 (w), 781 (s), 732 (m), 712 (s), 698 (s), 660 (m); EA ($C_{14}H_{18}CuN_{12}O_{16}$, 673.91): calcd: C 24.95, H 2.69, N 24.94%; found: C 24.84, H 2.53, N39.81%; BAM drophammer: > 40 J; friction tester: > 360 N (at grain size < 100 µm).

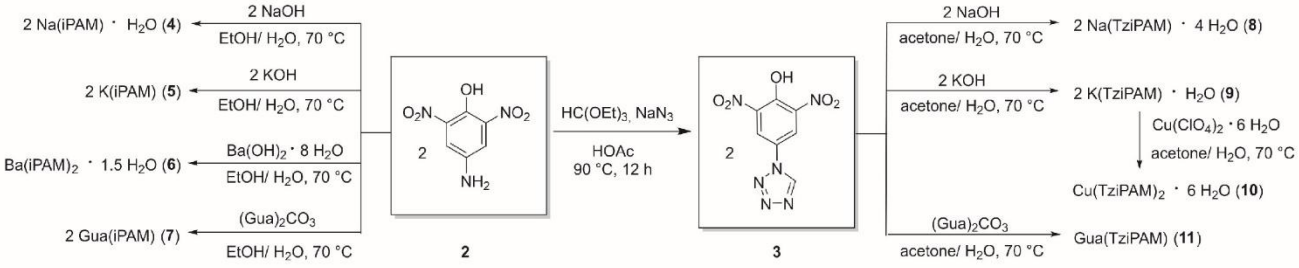
2.13 Guanidinium 2,6-Dinitro-4-(5*H*-Tetrazol-1-yl)Phenolate (11)

DTA (5 °C min^{-1}) onset: 258 °C (dec.); IR (ATR, cm^{-1}): ṽ= 3441 (m), 3414 (m), 3349 (s), 3340 (s), 3302 (m), 3295 (m), 3276 (m), 3182 (s), 3145 (s), 3114 (s), 3093 (s), 2945 (m), 2791 (m), 2438 (m), 2206 (m), 2166 (m), 1820 (vw), 1656 (vs), 1632 (s), 1542 (vs), 1536 (vs), 1503 (s), 1490 (s), 1459 (s), 1438 (s), 1408 (m), 1356 (m), 1330 (vs), 1285 (s), 1232 (vs), 1214 (vs), 1185 (s), 1124 (s), 1106 (s), 1081 (s), 1035 (m), 1006 (m), 987 (m), 941 (w), 904 (s), 890 (m), 858 (s), 821 (w), 781 (s), 770 (s), 712 (s), 659 (w); EA ($C_8H_9N_9O_5$, 311.21): calcd: C 30.87, H 2.91, N 40.51%; found: C 40.48, H 30.77, N 2.90%; BAM drophammer: 40 J; friction tester: > 360 N (at grain size < 100 µm).



Scheme 1. Synthesis route of iso-picramic acid (**2**) and equilibrium thereof.

© 2022 The Authors. Propellants, Explosives, Pyrotechnics published by Wiley-VCH GmbH



Scheme 2. Synthesis of ionic compounds **4**–**11** of iso-picramic acid (**2**) and 2,6-dinitro-4-(5*H*-tetrazol-1-yl)phenol (**3**).

3 Results and Discussion

3.1 Synthesis

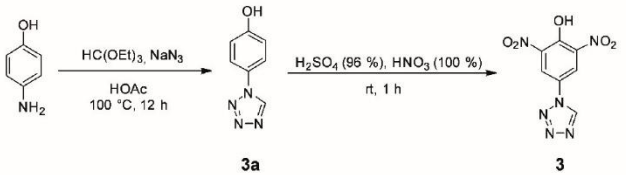
The synthesis of iso-picramic acid was first described by Dabney in 1884 [19]. In this procedure, 5-benzamido-2-hydroxybenzoic acid was used as starting material and was nitrated with a mixture of nitric acid and acetic acid. By splitting off the carboxyl group at the position 2 directly next to the hydroxy group, 4-benzamido-2,6-dinitrophenol was obtained. The benzoyl group was removed and the free amine was obtained by heating in concentrated hydrochloric acid.

In this work, iso-picramic acid (**2**) was prepared according to a different synthetic route (Scheme 1) [20].

Paracetamol is used as starting material, which in contrast to the starting molecule of Dabney does not have a carboxyl group on the benzene ring and in which the amino group is acetyl-protected. Nitration of the two positions next to the hyrdoxyl group with a mixture of concentrated sulfuric acid and ammonium nitrate yields 4-acetamino-2,6-dinitrophenol (**1**). Deprotection to the free amine is achieved by heating in concentrated sulfuric acid. Ammonium iso-picramate precipitates by the addition of ammonia. Treatment with sulfuric acid again yields the neutral compound. Scheme 1 shows the investigated reaction route for iso-picramic acid, an demonstrates that iso-picramic acid (**2**) exists in equilibrium as a zwitterionic compound.

The obtained iso-picramic acid (**2**) was reacted with triethyl orthoformate and sodium azide in acetic acid yielding of 2,6-dinitro-4-(5*H*-tetrazol-1-yl)phenol (**3**). The reaction pathway is shown in Scheme 2.

In addition, an alternative synthesis of 2,6-dinitro-4-(5*H*-tetrazol-1-yl)phenol (**3**) was developed which does not proceed via iso-picramic acid (**2**). Therefore, para-aminophenol was used as starting material. In this route, the tetrazole ring closure with triethyl orthoformate and sodium azide in acetic acid was performed first, whereby 4-(5*H*-tetrazol-1-yl)phenol (**3a**) was obtained. Since the amino group has already reacted to form the tetrazole and is thus blocked, no further protective group chemistry is required and the nitration process can be continued directly. **3a** was then reacted in a nitration reaction with mixed acid to obtain 2,6-dinitro-4-(5*H*-tetrazol-1-yl)phenol (**3**), shown in Scheme 3.

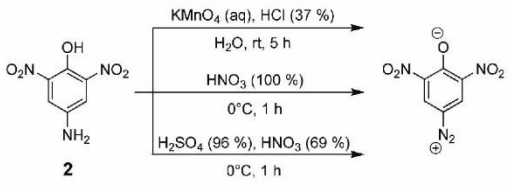


Scheme 3. Alternative synthesis of 2,6-dinitro-4-(5*H*-tetrazol-1-yl)phenol (**3**).

The two synthesis routes differ in the order of functionalization. In route 1 (Scheme 2), nitration is carried out first and then the tetrazole ring is closed, in route 2 (Scheme 3) it is the other way round. In route 1, the amine must be protected before nitration can take place and it must be deprotected after nitration. Therefore, route 2 is faster and easier because the tetrazole ring is able to resist the nitration conditions and thus two reaction steps can be saved.

Furthermore, oxidation and azo-coupling of iso-picramic acid was tried. For this purpose, **2** was reacted e. g. with potassium permanganate in hydrochloric acid. Nevertheless, the azo-coupled compound was not obtained, but rather 4-diazo-2,6-dinitrophenol (iso-DDNP) as can be seen in Scheme 4. Also, when trying to nitrate iso-picramic acid (**2**) with different mixed acids or pure nitric acid, again iso-DDNP was obtained.

In addition, various ionic compounds of compound **2** and **3** were synthesized as shown in Scheme 2.



Scheme 4. Synthesis of iso-DDNP starting from iso-picramic acid (**2**).

© 2022 The Authors. Propellants, Explosives, Pyrotechnics published by Wiley-VCH GmbH

3.2 Characterization

The synthesized neutral compounds **1**–**3** and **3a** were characterized by ^{1}H and $^{13}C\{^{1}H\}$ NMR spectroscopy. Additionally compound **3** was characterized by proton coupled ^{15}N and two dimensional ^{1}H, ^{15}N HMBC NMR spectroscopy. The measured two dimensional ^{1}H, ^{15}N HMBC spectrum of compound **3** is depicted in Figure 3.

More detailed information about the NMR spectra can be found in the SI.

In addition to NMR spectroscopy compounds **1**–**3** were analysed by IR spectroscopy. The spectra of all compounds can be found in the SI in Figure S1–S3. Comparison of the spectra of picramic acid and iso-picramic acid (**2**) are shown in Figure 4.

Iso-PAM exists as a zwitterionic compound. Thus, a hydroxy group is not present and therefore cannot be found in the IR spectrum. The signals of the stretching vibration of the amino group is slightly shifted compared to PAM but can be assigned to the peaks at 3185 cm^{-1} and 3098 cm^{-1}.

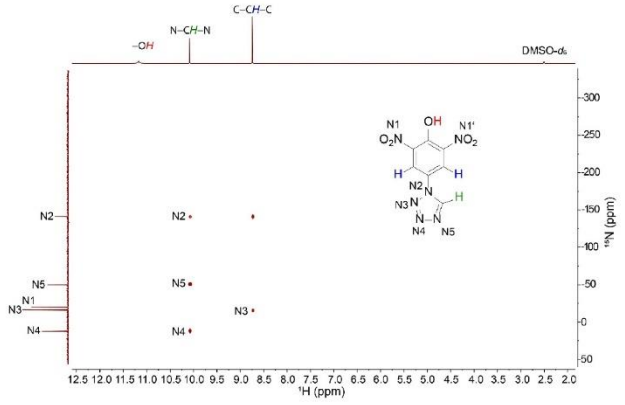


Figure 3. Two dimensional ^{1}H, ^{15}N HMBC NMR spectrum of compound **3**.

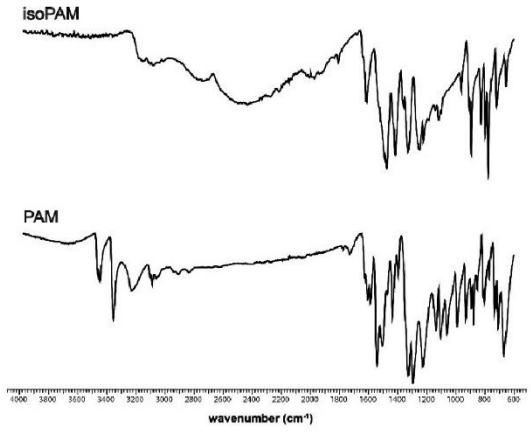


Figure 4. IR spectra of iso-picramic acid (**2**) (top) and picramic acid (bottom) [12].

3.3 Crystal Structures

Single crystal X-ray diffraction experiments of compounds **1**–**3** and **8**–**11** were performed. The crystal structures have been uploaded to the CSD database and are available under the CCDC number 2094681 (**1**), 2094679 (**2**), 2094677 (**3a**), 2094674 (**3**), 2094680 (**8**), 209467 (**9**), 2094676 (**10**) and 2094678 (**11**). Details of the measurement and refinement of the crystal structures can be found in the SI in Table S1–S4.

The crystal structure of 4-acetamino-2,6-dinitrophenol (**1**) can be seen in Figure 5 (left). It crystallizes as a yellow-orange block in the monoclinic space group $P2_1/c$ with a recalculated density of 1.65 g cm^{-3} at 298 K and four molecules per unit cell.

Figure 5 (right) shows the crystal structure of iso-picramic acid (**2**). Here, the compound is presented as a zwitterionic compound with a deprotonated hydroxyl group and a protonated amino group. Iso-PAM (**2**) crystallizes as orange rods in the monoclinic space group $P2_1/c$ with four molecules per unit cell and a density recalculated to room temperature of 1.78 g cm^{-3}. The crystals of iso-picramic acid (**2**) have a golden color and shine viewing without magnification, which can be seen in the microscope images in Figure S8.

Comparing the bond lengths of C4–N3 in **1** (1.408(2) Å) and C4–N2 in **2** (1.453(3) Å), it can be seen that the carbon -nitrogen bond is 0.05 Å longer. The main effect therefore is the acetyl deprotection of the amino group. The bond lengths between the four carbons of the benzene ring and the nitrogen atoms of the nitro groups are in both compounds almost the same between 1.455 Å and 1.465 Å (**1**: 1.459(2) Å, 1.465(2) Å; **2**: 1.458(3) Å, 1.457(3) Å). The bond length C1–O1 is 0.05 Å shorter for the deprotonated oxy-

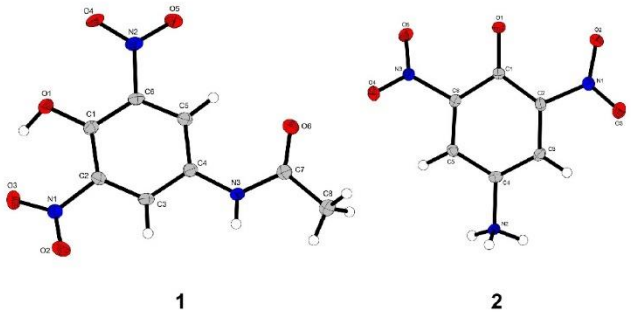


Figure 5. Molecular structure of **1** (left) and **2** (right). Thermal ellipsoids of non-hydrogen atoms in all structures are set to the 50% probability level. Selected bond lengths for **1** (Å): C1–O1 1.3287(18), C4–N3. Selected bond lengths for **2** (Å): C1–O1 1.283(3), C4–N2 1.453(3).

© 2022 The Authors. Propellants, Explosives, Pyrotechnics published by Wiley-VCH GmbH

15214087, 2022, 3, Downloaded from https://onlinelibrary.wiley.com/doi/10.1002/prep.202100205 by Ludwig-Maximilians-Universität, Wiley Online Library on [29/12/2022]. See the Terms and Conditions (https://onlinelibrary.wiley.com/terms-and-conditions) on Wiley Online Library for rules of use; OA articles are governed by the applicable Creative Commons License

gen of iso-picramic acid (**2**: 1.283(3) Å) than for compound **1** (1.3287(18) Å). The bond angles of compounds **1** and **2** show that the angle between C–C–O of the deprotonated hydroxyl group in iso-picramic acid (123.0(2)°) becomes slightly smaller compared to the protonated hydroxyl group of compound **1** (125.40(14)°). The angle C–C–N to the protonated amino group in **2** (119.3(2)°), on the other hand, becomes slightly larger compared to the protected amino group in **1** (117.46(13)°). Because of the sp^2-hybridization, in compound **2**, the benzene ring, the aromatic protons, the hydroxyl oxygen and all nitrogens are in one plane, only the amino group protons and the oxygens of the nitro groups extend out of the plane.

The crystal structure of 4-(5*H*-tetrazol-1-yl)phenol (**3a**) is shown in Figure 6 (left). It crystallizes as colorless needles in the orthorhombic space group $P2_12_12_1$ with a density of 1.48 g cm^{-3} at 298 K and four molecules per unit cell.

In compound **3a**, the benzene ring and the oxygen of the hydroxy group are in one plane, the tetrazole ring in contrast, turns out of this plane by 38.6(5)° (C3–C4–N1–N2).

Figure 6 (right) shows the crystal structure of compound **3**. 2,6-Dinitro-4-(5*H*-tetrazol-1-yl)phenol (**3**) crystallizes as colorless needles in the orthorhombic space group $P2_12_12_1$ with a density of 1.78 g cm^{-3} recalculated to 298 K and four molecules per unit cell.

In compound **3** again, the tetrazole ring and nitro groups turns out of the benzene plane (C5–C4–N2–N3 16.2(4)°, C5–C6–N6–O4 33.8(4)°, C3–C2–N1–O 34.7(4)°). Comparing the structures of **3a** and **3**, the bond length C–O of the hydroxyl group do not differ enormously (**3a**: 1.369(4) Å; **3**: 1.337(4) Å). The bond angle of C2–C1–O1 for the same position, however, becomes slightly larger due to the introduction of the nitro groups in compound **3** (**3a**: 117.8(3)°, **3**: 124.8(3)°). The bond lengths of the tetrazole ring of the two compounds are also comparable (**3a**: 1.359(4) Å, 1.285(4) Å, 1.362(4) Å, 1.320(4) Å, 1.328(5) Å; **3**: 1.361(3) Å, 1.295(4) Å, 1.374(4) Å, 1.314(4) Å, 1.342(4) Å).

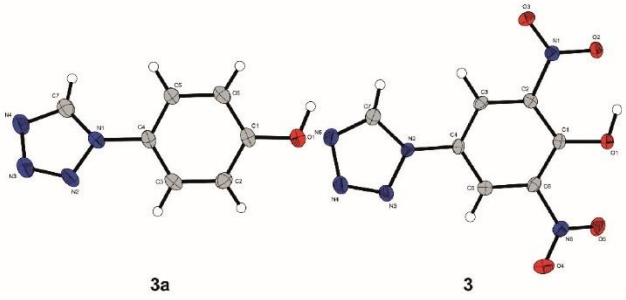


Figure 6. Molecular structure of **3a** (left) and **3** (right). Selected bond lengths for **3a** (Å): C1–O1 1.369(4), C4–N1 1.436(4), N1–N2 1.359(4), N2–N3 1.285(4), N3–N4 1.362(4), N4–C7 1.320(4), C7–N1 1.328(5). Selected bond lengths for **3** (Å): C1–O1 1.337(4), C2–N1 1.467(4), N1–O2 1.246(3), N1–O3 1.217(3), C4–N2 1.426(4), N2–N3 1.361(3), N3–N4 1.295(4), N4–N5 1.374(4), N5–C7 1.314(4), C7–N2 1.342(4).

Comparing the angles C–C–N to the nitro groups of compound **2** and **3**, they are in a similar range (**2**: 120.2(2)°, 118.2(2)°, 115.8(2)°, 116.5(2)°; **3**: 120.3(3)°, 119.6(3)°, 116.6(3)°, 116.9(3)°).

Figure 7 (left) shows the molecular structure of the potassium salt **9** from compound **3**. Compound **9** crystallizes as a monohydrate in the orthorhombic space group *Pnma* with a density of 1.878 g cm^{-3} at 102 K. The guanidinium salt **11** of compound **3** is shown in Figure 7 (right). It crystallizes anhydrously in the triclinic space group *P*-1 with a density of 1.735 g cm^{-3} at 106 K.

3.4 Thermal Analysis

For thermal characterization, differential thermal analysis (DTA) was performed for all compounds using a heating rate of 5°/min. In addition, thermogravimetric analysis (TGA) was performed for **1**, **2** and **3**.

The endothermic and exothermic onset points of all compounds and picramic acid in comparison are shown in Table 1. In addition, the DTA plots of the compounds **1**–**11** are shown in the SI in Figure S4–S6.

For the neutral compounds **1** and **2** both, endothermic and exothermic, signals are detected in the DTA measurement. To determine whether the endothermic signals are due to solvent evaporation or a melting point, additional TGA measurements were carried out and can be found in Figure 8 and Figure S3.

Both compounds **1** and **2** show no loss of weight in the TGA at the temperatures (**1**: 171 °C, **2**: 158 °C) of the respective endothermic signals. Therefore, the endothermic signals can be identified as the melting points of the respective compounds. The exothermic signals from the DTA measurement and the visible mass loss in the TGA agree in temperature (**1**: 223 °C, **2**: 183 °C), so this considers as the decomposition temperature of the compounds. A broadened second exothermic signal at 273 °C can be seen in the DTA plot of iso-picramic acid (**2**). This is probably the decomposition of a previously formed decomposition product. For compounds **3** and **3a**, no endothermic signals are detected in the DTA measurement. The exothermic signals

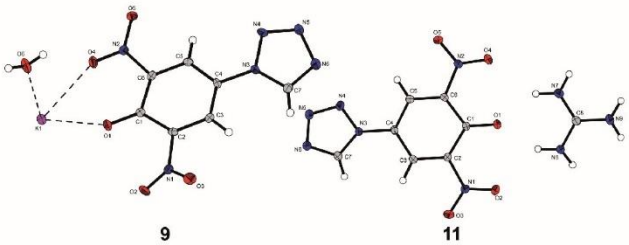


Figure 7. Molecular structure of **9** (left) and **11** (right). Selected bond lengths for **9** (Å): K1–O1 2.8459(12), K1–O4 2.7340(12), K1–O6 2.850(2).

© 2022 The Authors. Propellants, Explosives, Pyrotechnics published by Wiley-VCH GmbH

Table 1. Thermal stability as well as sensitivities towards impact, friction and ESD of compounds **1**–**11** and picramic acid for comparison.

	T_{endo} [a] [°C]	T_{exo} [b] [°C]	IS [J][c]	FS [N][d]
Acetaminodinitrophenol (**1**)	171	223	> 40	> 360
Iso-picramic acid (**2**)	158	183	> 40	> 360
4-Tetrazolylphenol (**3a**)	–	209	> 40	> 360
2,6-Dinitro-4-(5*H*-tetrazol-1-yl)phenol (**3**)	–	175	30	> 360
Na(iPAM)·H_2O (**4**)	139	270	> 40	> 360
K(iPAM) (**5**)	–	270	> 40	> 360
$Ba(iPAM)_2$·1.5 H_2O (**6**)	175	277	> 40	> 360
Gua(iPAM) (**7**)	–	250	> 40	> 360
Na(TziPAM)·4 H_2O (**8**)	54/115	242	> 40	> 360
K(TziPAM)·H_2O (**9**)	88	260	> 40	> 360
$Cu(TziPAM)_2$·6 H_2O (**10**)	114	249	> 40	> 360
Gua(TziPAM) (**11**)	–	258	> 40	> 360
PAM [12]	178	217	> 40	> 360

[a] Onset point of the endothermic event; [b] Onset point of the exothermic event; [c] impact sensitivity according to the BAM drop-hammer (method 1 of 6); [d] friction sensitivity according to the BAM friction tester (method 1 of 6).

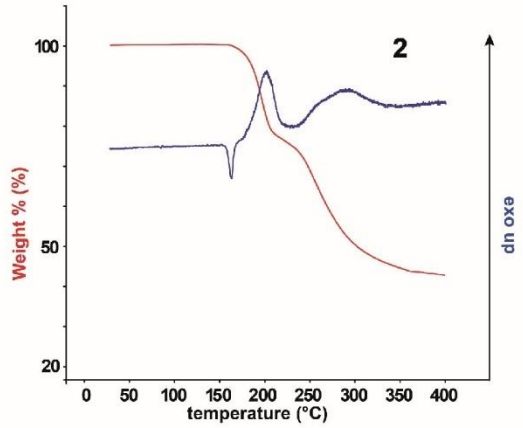


Figure 8. TGA measurement of compound **2**.

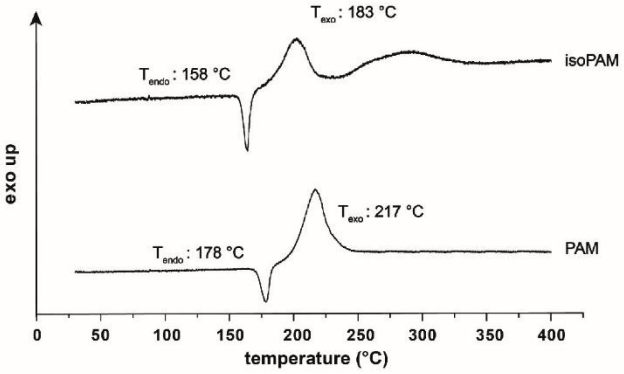


Figure 9. DTA measurement of iso-picramic (**2**, top) acid and picramic acid (bottom) [12].

therefore represent the decomposition temperature of the compounds.

To compare the thermal stability of picramic acid and iso-picramic acid (**2**), their DTA plots are shown in Figure 9.

Here, a melting point for both compounds can be observed. However, the melting point of iso-picramic acid (**2**) is 20 °C lower than that of PAM. The decomposition temperature of iso-picramic acid (**2**) is 34 °C lower than the one of picramic acid. Thus, the symmetric isomer is thermally less stable.

For the ionic compounds, all hydrates (**4**, **6**, **8**, **9**, **10**) show an endothermic signal indicating water loss. All anhydrous ionic compounds (**5**, **7**, **11**) have only an exothermic signal.

3.5 Sensitivities and Energetic Properties

To determine the sensitivities of all compounds **1**–**11**, the sensitivities toward impact (IS) and friction (FS) were tested. The determined values of **1**–**11** and picramic acid for comparison are shown in Table 2.

Considering the impact sensitivities, all compounds, except **3**, with values of > 40 J are classified as insensitive according to the UN Recommendations on the Transport of Dangerous Goods [21]. Compound **3** with an impact sensitivity of 30 J is classified as sensitive. All values for friction sensitivity are > 360 N and are therefore classified as friction insensitive.

The energetic properties were calculated using the EXPLO5 code version 6.05.04[22] and can be found in Table 2. EXPLO5 calculations are based on the density of the compounds as well as their enthalpy of formation.

The calculated detonation velocity for compound **3** is 7300 $m\,s^{-1}$, which is between HNS (7132 $m\,s^{-1}$) and picric acid (7426 $m\,s^{-1}$) and is higher than the values for TNT (6797 $m\,s^{-1}$) and DDNP (6864 $m\,s^{-1}$).

Comparing compounds **2** and **3**, it can be seen that both compounds have the same density of 1.78 $g\,cm^{-3}$ at

© 2022 The Authors. Propellants, Explosives, Pyrotechnics published by Wiley-VCH GmbH

Table 2. Energetic properties of compounds **2**, **3** and picramic acid.

	2	**3**	PAM [12]
Formula	$C_6H_5N_3O_5$	$C_7H_4N_6O_5$	$C_6H_5N_3O_5$
FW [g mol^{-1}]	199.12	252.15	199.12
N [%][a]	21.10	33.33	21.10
$1_{calc.}$ (298 K) [g cm^{-3}] [b]	1.78	1.78	1.69
$T_{dec.}$ [°C][c]	183	175	217
$\Delta_f H°$ [kJ mol^{-1}][d]	−0.5	159.4	−262.4
Ω_{CO} [%][e]	−28.1	−25.4	−28.1
EXPLO5 version	V6.05.04	V6.05.04	V6.05.04
$P_{C\text{-}J}$ [GPa][f]	22.5	21.0	16.2
V_{det} [m s^{-1}][g]	7458	7300	6553
$-\Delta_{ex}U°$ [kJ kg^{-1}][h]	4568	4072	3347
T_{det} [K][i]	3139	3047	2543
V_0 [L kg^{-1}][j]	638	635	643

[a] Nitrogen content; [b] X-ray density converted to RT; [c] temperature of decomposition indicated by exothermic event according to DTA (onset temperatures at a heating rate of 5 °C min^{-1}); [d] calculated (CBS-4M) heat of formation; [e] Oxygen balance; [f] detonation pressure; [g] detonation velocity; [h] Energy of explosion; [i] Explosion temperature; [j] Assuming only gaseous products.

Table 3. Values for the calculation of the energetic parameters in comparison.

	iPAM zwitterionic exp.	iPAM neutral calc.	PAM neutral exp.	PAM neutral calc.	PAM zwitterionic cal.
$\Delta_f H°$ [kJ mol^{-1}][a]	−0.5	−214.3	−262.4 [12]	−262.4 [12]	−139.2
$1_{X\text{-}Ray}$ [g cm^{-3}] [b]	1.78	–	1.69 [12]	–	–
1_{Holden} [g cm^{-3}] [c]	–	1.68	–	1.68	1.67
EXPLO5 version	V6.05.04	V6.05.04	V6.05.04	V6.05.04	V6.05.04
$P_{C\text{-}J}$ [GPa][d]	22.5	16.6	16.3	16.0	17.5
V_{det} [m s^{-1}][e]	7458	6607	6546	6513	6716

[a] calculated (CBS-4M) heat of formation; [b] X-ray density converted to 298 K; [c] calculated density according to Holden; [d] detonation pressure; [e] detonation velocity.

298 K, but compound **2** has a better calculated detonation velocity of 7458 m s^{-1}.

Comparing the isomers iso-picramic acid (**2**) and picramic acid, it can be seen that the zwitterionic compound **2** has a significantly higher enthalpy of formation (−0.5 kJ mol^{-1} vs −262.4 kJ mol^{-1}) as well as a higher density (1.78 g cm^{-3} vs 1.69 g cm^{-3}) than PAM. This results in a calculated detonation velocity of 7458 m s^{-1} and in a detonation pressure of 22.5 GPa, these values are very similar to the values of picric acid (V_{det}: 7426 m s^{-1}, $P_{C\text{-}J}$: 23.2 GPa).

In order to draw a conclusion from the calculated parameters with regard to the initial theory that higher symmetry leads to better energetic properties, calculations were also carried out for the neutral iso-picramic acid (see Scheme 1) and hypothetical zwitterionic picramic acid. For this purpose, the enthalpy of formation and the densities according to Holden [23] of the hypothetical isomers were calculated, which can be seen in Table 3. The obtained calculated density for neutral iso-PAM is 1.68 g cm^{-3}, which is the same for PAM (calculated) due to the same binding increments. However, since the CBS-4M heat of formation with −214.3 kJ mol^{-1} for the neutral iso-PAM is higher than that of PAM (−262.4 kJ mol^{-1}), we also obtain better energetic parameters for the neutral iso-PAM (6607 m s^{-1} and 16.6 GPa) than for PAM (6513 m s^{-1} and 16.0 GPa with Holden density 1.68 g cm^{-3}). A hypothetical zwitterionic PAM shows the same trend in having a higher heat of formation.

4 Conclusion

In this work, iso-picramic acid (**2**), an isomer of picramic acid, was synthesized and characterized. Moreover, the trend that symmetric isomers have better energetic properties could be proofed.

For the symmetric zwitterionic isomer of picramic acid, **2**, a density of 1.78 g cm^{-3} (298 K) was obtained and in addition higher performance parameters than that of PAM can also be determined.

Because iso-picramic acid shows a zwitterionic structure, most of the reactions to transform the -NH_3 group failed and oftentimes iso-DDNP was obtained as the product. The amine could successfully converted to a 5*H*-tetrazole substituent which shows very similar energetic parameters.

Moreover some selected ionic compounds of **2** and **3** were synthesized, investigated and compared but mostly showing poor energetic characteristics.

Acknowledgements

For financial support of this work by Ludwig Maximilian University (LMU), the Office of Naval Research (ONR) under grant no. ONR N00014-19-1-2078 and the Strategic Environmental Research and Development Program (SERDP) under contract no. W912HQ19C0033 are gratefully acknowledged. Moreover, the authors would like to thank Dr. Peter Mayer for helping with X-ray crystal structure analysis and Dr. Burkhard Krumm for NMR measurements. Open Access funding enabled and organized by Projekt DEAL.

Data Availability Statement

No data are available.

 © 2022 The Authors. Propellants, Explosives, Pyrotechnics published by Wiley-VCH GmbH

References

[1] T. M. Klapötke, Chemistry of High-Energy Materials, 5th ed., DE GRUYTER, Berlin/Boston **2019**.
[2] P. F. Pagoria, G. S. Lee, A. R. Mitchell, R. D. Schmidt, A review of energetic materials synthesis, *Thermochim. Acta* **2002**, *384*, 187–204.
[3] L. E. Fried, M. R. Manaa, P. F. Pagoria, R. L. Simpson, Design and Synthesis of Energetic Materials, *Annu. Rev. Mater. Sci.* **2001**, *31*, 291–321.
[4] D. M. Budgujar, M. B. Talawar, S. N. Asthana, P. P. Mahulikar, Advances in science and technology of modern energetic materials: An overview, *J. Hazard. Mater.* **2008**, *151*, 289–305.
[5] A. K. Skider, N. Skider, A review of advanced high performance, insensitive and thermally stable energetic materials emerging for military and space applications, *J. Hazard. Mater.* **2004**, *112*, 1–15.
[6] J. P. Agrawal, R. D. Hodgson, Organic Chemistry of Explosives, 1st ed., Wiley-VCH, Weinheim **2006**.
[7] J. Köhler, R. Meyer, A. Homburg, Explosivstoffe, 10th ed., Wiley-VCH, Weinheim **2008**.
[8] S. S. Talmage, D. M. Opresko, C. J. Maxwell, C. J. E. Welsh, F. M. Cretella, P. H. Reno, F. B. Daniel, Nitroaromatic munition compounds: environmental effects and screening values, *Rev. Environ. Contam. Toxicol.* **1999**, *161*, 1–156.
[9] T. B. Brill, K. J. James, Kinetics and mechanisms of thermal decomposition of nitroaromatic explosives, *Chem. Rev.* **1993**, *93*, 2667–2692.
[10] E. de Vries, Advances in the Explosive Industry, *Chem.-Ztg.* **1908**, *32*, 765–781.
[11] H. Sprengel, The Discovery of Picric Acid, 2nd ed., Eyre & Spottiswoode, London **1903**.
[12] M. H. H. Wurzenberger, J. T. Lechner, M. Lommel, T. M. Klapötke, J. Stierstorfer, Salts of Picramic Acid-Nearly Forgotten Temperature-Resistant Energetic Materials, *Propellants Explos. Pyrotech.* **2020**, *45*, 898–907.
[13] K. M. Aitken, R. A. Aitken, Nitroarenes, *Sci. Synth.* **2007**, *31*, 1183–1320.
[14] V. Merz, G. Zetter, Ueber einige Derivate des Resorcins und Orcins, *Ber. Dt. Chem. Ges.* **1879**, *12*, 2035–2049.
[15] R. Matyáš, J. Pachman, Primary Explosives, 1st ed., Springer, Berlin, Heidelberg **2013**.
[16] Z. Yang, Y. Liu, D. Liu, L. Yan, J. Chen, Synthesis and characterization of spherical 2-diazo-4,6-dinitrophenol (DDNP), *J. Hazard. Mat.* **2010**, *177*, 938–943.
[17] a) T. M. Klapötke, A. Preimesser, J. Stierstorfer, Synthesis and Energetic Properties of 4-Diazo-2,6-dinitrophenol and 6-Diazo-3-hydroxy-2,4-dinitrophenol, *Eur. J. Org. Chem.* **2015**, *2015*, 4311–4315; b) J.-I. Wang, C. Cao, J.-Y. Cao, Y.-M. Yan, L.-Z. Chen, D.-L. Cao, Synthesis, Characterization and Decomposition of 4-Diazo-2,6-dinitrophenol, *Propellants Explos. Pyrotech.* **2021**, *46*, 1–10.
[18] a) S. P. Agrawal, J. P. Agrawal, Chemistry of metal picramates. I. Picramates of iron, *Indian J. Chem.* **1969**, *7*, 1264–1267; b) S. P. Agrawal, J. P. Agrawal, Chemistry of Metal Picramates, *Def. Sci. J.* **1970**, *20*, 237–248; c) S. P. Agrawal, B. D. Agrawal, Chemistry of zinc, cadmium, and mercury picramates, *Indian J. Chem.* **1972**, *10*, 1106–1107; d) R. S. Srivastava, S. P. Agrawal, H. N. Bhargava, Chemistry of Titanium, Zirconium and Thorium Picramates , *Propellants Explos. Pyrotech.* **1976**, *1*, 101–103.
[19] C. W. Dabney, An Isopicramic Acid, *Am. Chem. J.* **1884**, *5*, 20–38.
[20] www.sciencemadness.org/whisper/viewthread.php?action=printable&tid=439&page=5, accessed 12.2020.
[21] Impact: insensitive > 40 J, less sensitive≥ 35 J, sensitive≥ 4 J, very sensitive≥ 3 J; Friction: insensitive > 360 N, less sensitive= 360 N, sensitive < 360 N and > 80 N, very sensitive≥ 80 N, extremely sensitive≥ 10 N. According to the UN Recommendations on the Transport of Dangerous Goods, (+) indicates not safe for transport.
[22] M. Sućeska, Explo5V6.05.04, Zagreb (Croatia), **2020**.
[23] a) D. A. Cichra, J. R Holden. C. Dickinson, NSWC TR-79-273, **1979**; b) R. L. Willer, Calculation of the Density and Detonation Properties of C, H, N, O and F Compounds: Use in the Design and Synthesis of New Energetic Materialss, *J. Mex. Chem. Soc.* **2009**, *53*, 108–119; c) S. Wahler, Rose Boom 2.0, Munich (Germany), **2021**.

Manuscript received: July 14, 2021
Revised manuscript received: December 10, 2021
Version of record online: January 27, 2022

© 2022 The Authors. Propellants, Explosives, Pyrotechnics published by Wiley-VCH GmbH

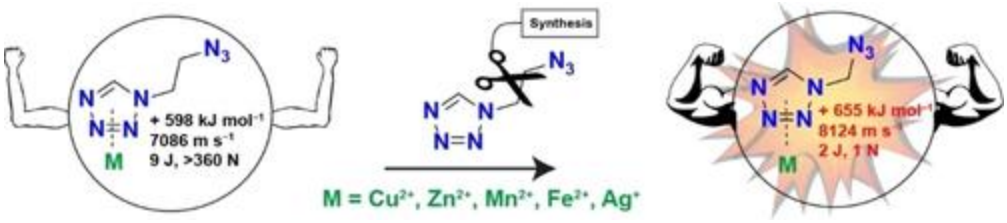
Appendix 29

1-(Azidomethyl)-5H-Tetrazole: A Powerful New Ligand for Highly Energetic Coordination Compounds

M. Kofen, M. Lommel, M. H. H. Wurzenberger, T. M. Klapötke, J. Stierstorfer

Chem. Eur. J. **2022**, *28*, e202200492

https://doi.org/10.1002/chem.202200492



Supplementary Information:
https://chemistry-europe.onlinelibrary.wiley.com/action/downloadSupplement?doi=10.1002%2Fchem.202200492&file=chem202200492-sup-0001-misc_information.pdf

Chemistry–A European Journal
Research Article
doi.org/10.1002/chem.202200492
Chemistry Europe
European Chemical Societies Publishing
www.chemeurj.org

1-(Azidomethyl)-5*H*-Tetrazole: A Powerful New Ligand for Highly Energetic Coordination Compounds

Moritz Kofen,[a] Marcus Lommel,[a] Maximilian H. H. Wurzenberger,[a] Thomas M. Klapötke,[a] and Jörg Stierstorfer*[a]

Dedicated to Professor Dr. Wolfgang Beck on the occasion of his 90th birthday.

Abstract: Highly energetic 1-(azidomethyl)-5*H*-tetrazole (AzMT, **3**) has been synthesized and characterized. This completes the series of 1-(azidoalkyl)-5*H*-tetrazoles represented by 1-(azidoethyl)-5*H*-tetrazole (AET) and 1-(azidopropyl)-5*H*-tetrazole (APT). AzMT was thoroughly analyzed by single-crystal X-ray diffraction experiments, elemental analysis, IR spectroscopy and multinuclear (^{1}H, ^{13}C, ^{14}N, ^{15}N) NMR measurements. Several energetic coordination compounds (ECCs) of 3d metals (Mn, Fe, Cu, Zn) and silver in combination with anions such as (per)chlorate, mono- and dihydroxytrinitrophenolate were prepared, giving insight into the coordination behavior of AzMT as a ligand. The synthesized ECCs were also analyzed by X-ray diffraction experiments, elemental analysis, and IR spectroscopy. Differential thermal analysis for all compounds was conducted, and the sensitivity towards external stimuli (impact, friction, and ESD) was measured. Due to the high enthalpy of formation of AzMT (+654.5 kJ mol^{-1}), some of the resulting coordination compounds are extremely sensitive, yet are able to undergo deflagration-to-detonation transition (DDT) and initiate pentaerythritol tetranitrate (PETN). Therefore, they are to be ranked as primary explosives.

Introduction

The design of novel energetic materials is mostly subjected to a purely synthetic approach, generally delimited by the same synthetic strategies. While some of those strategies are known and have been applied since the early 19th century, such as the introduction of several nitro groups to a molecular framework,[1–5] the concept of using energetic materials as ligands for energetic coordination compounds (ECCs) is relatively new.[6,7] By combining a variety of metal cations (Cu^{2+}, Fe^{2+}, Zn^{2+}, Mn^{2+}, Ag^{+}) with energetic anions (e.g., NO_3^-, ClO_3^-, ClO_4^-, N_3^-, and nitrophenolates) as well as a practically unlimited number of energetic ligands, ECCs offer a great adjustability and tuning of the energetic properties. It therefore expands the traditional approaches of synthesizing energetic materials, now used as ligands, by the possibility of further tuning the properties by the formation of coordination compounds.

While the tetrazole moiety, with its high nitrogen content, has been introduced in several recent high-performing energetic materials[8–14] as well as potential pharmaceuticals[15–17] several 1 *N*-functionalised tetrazoles[18] such as 1-methyl-5*H*-tetrazole[19] (1-MTZ) and 1-amino-5*H*-tetrazole[20] (1-AT) promoted the range of adjustability of energetic properties of ECCs. 1-MTZ is able to stabilize sensitive materials (e.g., AgCNO), thus performs well when desensitizing an energetic coordination compound, whereas 1-AT drastically increases the sensitivity. Due to the exceptional high enthalpy of formation (5059 kJ kg^{-1})[21] and low oxidative resistance of the 1-AT molecule, the corresponding ECCs are among the most sensitive compounds, some being on par with pure copper(II) azide in terms of sensitivity. Efforts to find the perfect balance between performance and sensitivity has led to the formation of ECCs with 1-(azidopropyl)-5*H*-tetrazole[22] and 1-(azidoethyl)-5*H*-tetrazole[23] as ligands. Both compounds exhibit lower gas-phase enthalpies of formation (APT: 3990 kJ kg^{-1}, AET: 4616 kJ kg^{-1}) and lower sensitivities (APT: >40 J, >360 N; AET: 9 J, >360 N) towards impact and friction than pure 1-AT (<1 J, 64 N). By comparing ECCs of copper(II) and iron(II) perchlorate of 1-AT, AET, and APT, a clear success in lowering the sensitivities can be demonstrated. The high sensitivities of both metal perchlorate complexes with 1-AT (<1 J, <0.1 N), can be decreased by applying AET (1–3 J, 4–15 N) or APT (3 J, 24–28 N) as ligand.

Another promising ligand is di-(tetrazol-1,1′-yl)-methane (1,1′-DTM), being structurally similar to 1-MTZ, having one proton substituted by another tetrazole moiety (Figure 1). 1,1′-DTM validated the concept of adjustability of energetic coordination compounds by selecting appropriate metal cations

[a] M. Kofen, M. Lommel, Dr. M. H. H. Wurzenberger, Prof. Dr. T. M. Klapötke, Dr. J. Stierstorfer
Department of Chemistry
Ludwig-Maximilian University of Munich
Butenandtstrasse 5–13, 81377 Munich (Germany)
E-mail: jstch@cup.uni-muenchen.de
Homepage: www.hedm.cup.uni-muenchen.de

Supporting information for this article is available on the WWW under https://doi.org/10.1002/chem.202200492

© 2022 The Authors. Chemistry - A European Journal published by Wiley-VCH GmbH. This is an open access article under the terms of the Creative Commons Attribution License, which permits use, distribution and reproduction in any medium, provided the original work is properly cited.

© 2022 The Authors. Chemistry - A European Journal published by Wiley-VCH GmbH

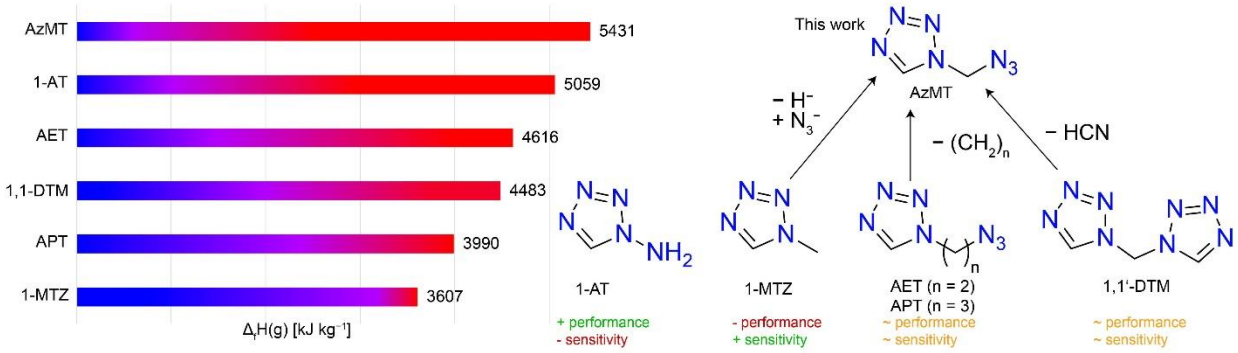


Figure 1. Molecular structures of 1-methyl-5*H*-tetrazole (1-MTZ), di(tetrazol-1-yl)-methan (1,1′-DTM), 1-(azidopropyl)-5*H*-tetrazole (APT), 1-(azidoethyl)-5*H*-tetrazole (AET), 1-amino-5*H*-tetrazole (1-AT) and 1-(azidomethyl)-5*H*-tetrazole (AzMT). The structural relationship between 1-MTZ, 1,1-DTM and AET/APT is indicated (right), and a comparison of the calculated gas-phase enthalpies of formation of all six ligands is shown on the left.

and energetic anions, as can be seen from the different sensitivities of the copper(II) perchlorate (< 1 *J*, < 1 N) and the copper(II) picrate (6 *J*, > 360 N) coordination compounds.

Considering the molecular structures of 1-MTZ, AET, and 1,1′-DTM, a structurally similar, yet missing compound is 1-(azidomethyl)-5*H*-tetrazole. It is formally obtained by substitution of one hydrogen atom of 1-MTZ by an azide functionality, as well as formally removing hydrogen cyanide from 1,1′-DTM (Figure 1). More obvious, it can be obtained by formally further decreasing the alkyl chain from AET to a methylene moiety. Independent from the synthesis, the resulting 1-(azidomethyl)-5*H*-tetrazol represents the smallest tetrazole with an *N*-azidoalkyl functionality, having a drastically increased gas-phase enthalpy of formation (5431 kJ kg^{-1}), compared to its three parent compounds (Figure 1), even surpassing 1-AT. Although methylene bridged functional groups on the tetrazole moiety can be found in literature,[24–26] especially 5-(azidomethyl)-1*H*-tetrazole,[27] they always show 5-substitution of the tetrazole ring.[28–29] Sadly, all 5-substituted derivatives still exhibit acidic protons, making them unsuitable for use as ligands in energetic coordination compounds.

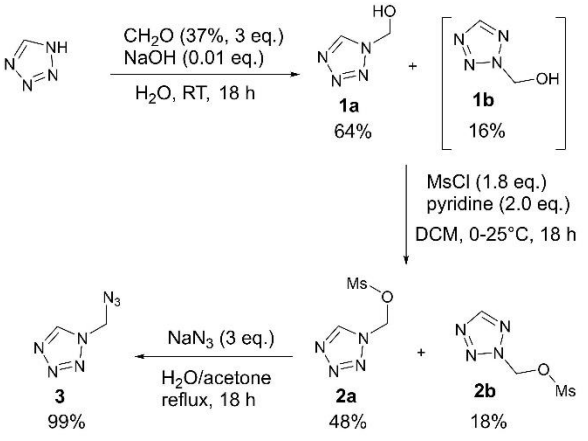
Independent of the synthesis, the resulting 1-(azidomethyl)-5*H*-tetrazol represents the smallest tetrazole with an *N*-azidoalkyl functionality, having a drastically increased gas-phase enthalpy of formation (5431 kJ kg^{-1}), compared to its three parent compounds (Figure 1), only surpassed by 1-AT. Therefore, we opted to synthesize the highly energetic and hardly accessible 1-(azidomethyl)-5*H*-tetrazole (**3**) for the first time. Here, next to the synthesis and characterization of highly energetic 1-(azidomethyl)-5*H*-tetrazole, several energetic coordination compounds of the new ligand were synthesized. Single-crystal X-ray diffraction experiments were conducted, and all compounds were analyzed by elemental analysis and IR spectroscopy. The ligand was characterized by multinuclear NMR (^{1}H, ^{13}C, ^{14}N, and ^{15}N) spectroscopy, and the thermal and physicochemical properties of all compounds were determined.

Results and Discussion

Synthesis

CAUTION! The synthetic work described in this section involves the handling of very sensitive intermediates such as 1-(azidomethyl)-5*H*-tetrazole (**3**) and ECCs **5**–**14**. Proper protective measurements and equipment must be used!

The synthesis of 1-(azidomethyl)-5*H*-tetrazol (**3**) is shown in Scheme 1. The known literature[30] hydroxy methylation of 1,5*H*-tetrazole with formaldehyde (37%) in aqueous solution was optimized towards a 66% shorter reaction time with an improved yield of 80% (over 65%). An isomeric mixture of 1- and 2-(hydroxymethyl)-5*H*-tetrazole (**1a**, **1b**) was obtained as a colorless oil. Due to the polarity of the alcohol functionality, a separation of the isomers by column chromatography was not possible at this stage. The isomeric mixture **1** was mesylated by methanesulfonyl chloride in CH_2Cl_2 at room temperature with a good overall yield of 64%. After the reaction solution had been



Scheme 1. Synthesis of 1-(azidomethyl)-5*H*-tetrazole (AzMT, **3**), starting from 1,5*H*-tetrazole.

© 2022 The Authors. Chemistry - A European Journal published by Wiley-VCH GmbH

quenched in water, pure 1-(methanesulfonyl-methyl)-5*H*-tetrazole (**2a**) precipitated and was filtered off. Compound **2a** was obtained as a colorless solid in moderate yield (48%). The organic layer was separated, washed with hydrochloric acid (2 M) and water, and the solvent was removed in vacuo to obtain crude 2-(methanesulfonyl-methyl)-5*H*-tetrazole (**2b**) in poor yield (18%). After refluxing **2a** with an excess of sodium azide in a water/acetone mixture (1:1) overnight, the reaction solution was extracted with CH_2Cl_2 and the organic-phase was washed with water and dried over magnesium sulfate. By removing the solvent in vacuo, 1-(azidomethyl)-5*H*-tetrazole (**3**) was obtained as colorless solid in quantitative yield. Crystals suitable for single-crystal X-ray diffraction experiments were obtained by recrystallization from acetone.

NMR spectroscopy

The ^{1}H NMR of the crude isomeric mixture **1** in [D_6]DMSO shows two signals at $\delta = 9.31$ and 8.77 ppm attributed to the tetrazole protons of **1a** and **1b** isomers, respectively. Integration of the signals reveals a distribution of 4/1 favoring **1a** over **1b**. The two signals at $\delta = 6.11$ and 6.03 ppm are attributed to the respective CH_2 group of **1a** and **1b**. The ^{1}H NMR of **2a** in [D_6]acetone shows three signals at $\delta = 9.43$, 6.67, and 3.27 ppm attributed to the CH, the CH_2 and the CH_3 group, respectively. The ^{1}H NMR of compound **3** in [D_6]DMSO shows two signals at $\delta = 9.60$ and 6.02 ppm attributed to the CH and CH_2 group. Compared to **1a**, the tetrazole CH is downfield shifted by 0.29 ppm whereas the upfield shift of the CH_2 unit (0.01 ppm) is negligible. The ^{13}C NMR spectrum also shows two signals at $\delta =$ 144.2 and 60.5 ppm, marking the tetrazole and the methylene carbon atoms, respectively. ^{14}N NMR measurement of **3** in [D_6]DMSO shows two broadened signals at $\delta = -135.6$ and -160.4 ppm corresponding to the N_β atom of the azide moiety and to the N_γ atom of the tetrazole.

Due to the invisibility of the missing nitrogen atoms, proton coupled ^{15}N NMR measurement (Figure 2) was performed. The resonances for the azide at $\delta = -302.1$ (N_α), -158.9 (N_γ), and -136.3 (N_β) are in the same range as comparable azido-methyl compounds. The signal at $\delta = -136.3$ splits into a triplet due to ^3J coupling to the methylene protons. The signals for the tetrazole at $\delta = 14.4$ (N_3), -14.0 (N_2), -50.4 (N_4), and -141.9 ppm (N_1) are also in the typical range of 1 *N*-subsituted tetrazoles.[22] Whereas the signal at $\delta = -14.0$ (N_2) appears as a singlet, the remaining resonances appear as doublets with coupling constants of 3.3 Hz (14.4 ppm), 12.7 Hz (-50.4 ppm), and 9.5 Hz (-50.4 ppm) due to ^3J and ^2J coupling with the tetrazole proton.

Detonation properties

The detonation performance parameters of **3** were calculated with the EXPLO5 program code,[31] for which the enthalpy of formation was determined by applying the atomization method using room temperature CBS-4M enthalpy. As the performance

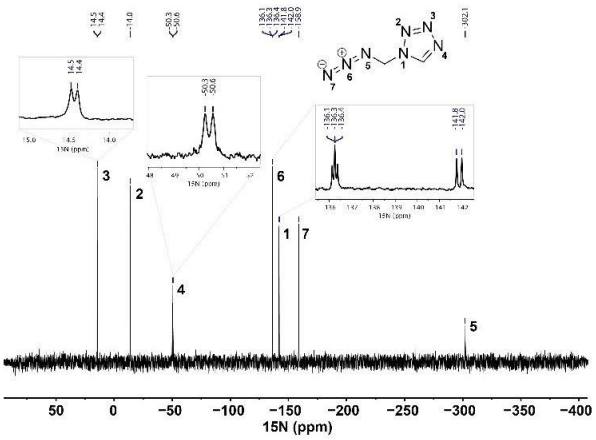


Figure 2. ^{15}N NMR spectrum of 1-(azidomethyl)-5*H*-tetrazole (**3**) in [D_6]acetone.

properties for AET and APT are not reported in literature, their enthalpies of formation were also calculated to further obtain their detonation performances. Table 1 compares all calculated values for **3**, AET and APT. A small increase in density of 0.06 g cm^{-3} (Table 1) is observed by decreasing the alkyl-chain by one CH_2 group from APT to AET, whereas further shortening the alkyl chain by a second CH_2 group to AzMT causes a more drastic increase in density by 0.24 g cm^{-3}. The higher increase in density can be explained due to the liquid state of APT and AET at room temperature, whereas AzMT is already a solid at room temperature. Additionally, the enthalpy of formation from **3** (654.5 kJ mol^{-1}) to APT (568.4 kJ mol^{-1}) also decreases drastically. As the performance of energetic compounds depends on their enthalpy of formation and their densities, combining both

Table 1. Energetic properties of AzMT (**3**), compared to AET[23] and APT.[22]

	AzMT (3)	AET[23]	APT[22]
Formula	$C_2H_3N_7$	$C_3H_5N_7$	$C_4H_7N_7$
M [g mol^{-1}]	125.1	139.1	153.2
ρ [g cm^{-3}]	1.545[a]	1.31[b]	1.25[b]
N [%][c]	78.38	70.48	64.02
Ω_{CO} [%][d]	−70.34	−97.75	−120.13
$\Delta_f H°$ [kJ mol^{-1}][e]	655	598	568
$\Delta_f H°$ [kJ kg^{-1}][f]	5232	4427	3853
$\Delta_f H°$ [J cm^{-3}] [g]	8110	5630	4639
EXPLO5 V6.05.04			
$-\Delta_{ex}U°$ [kJ kg^{-1}][h]	5127	4449	4121
T_{det} [K][i]	3473	3169	2609
V_0 [L kg^{-1}][j]	502	540	620
P_{CJ} [kbar][k]	229	192	130
V_{det} [m s^{-1}][l]	8124	7086	6757

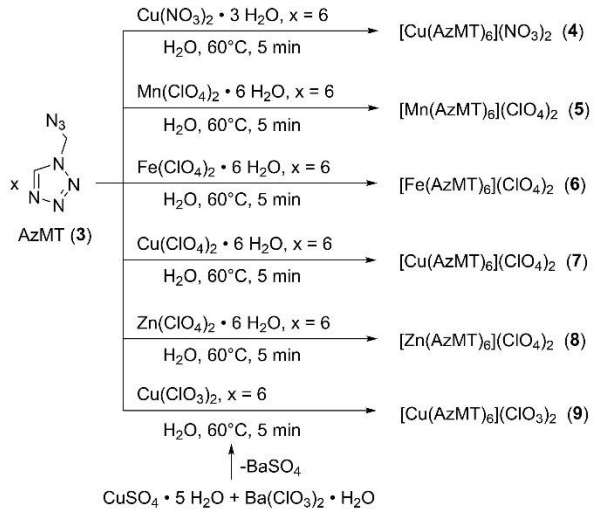
[a] From single-crystal X-ray diffraction analysis recalculated to room temperature. [b] Measured with a gas pycnometer. [c] Nitrogen content. [d] Oxygen balance towards the formation of CO. [e] Calculated enthalpy of formation. [f] Calculated mass related enthalpy of formation. [g] Calculated volume related enthalpy of formation. [h] Energy of explosion. [i] Detonation temperature. [j] Volume of detonation products (assuming only gaseous products). [k] Detonation pressure at Chapman-Jouguet point. [l] Detonation velocity.

© 2022 The Authors. Chemistry - A European Journal published by Wiley-VCH GmbH

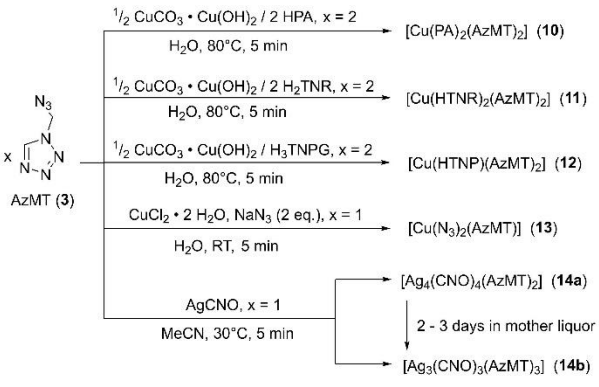
into an enthalpy density offers an appropriate value to quickly elucidate the differences. Here, AzMT shows a very high enthalpy density of 8110 J cm ^{3}, followed by AET (5630 J cm ^{3}) and APT (4639 J cm^{-3}). Therefore, the calculated detonation performances show a drastic increase in performance from APT (6757 m s^{-1}) to AzMT (8124 m s^{-1}), hence a significantly higher performance of the corresponding ECCs can also be estimated.

Energetic coordination compounds

Due to the absence of acidic protons in compound **3**, it can be used as a well-suited neutral ligand for ECCs. The application of several oxidizing anions such as nitrate, chlorate, perchlorate, fulminate, picrate, styphnate, and trinitro phloroglucinol, and reducing anions such as azide, enables the tuning of the energetic properties of the resulting coordination compound. The energetic coordination compounds **4**–**9** were obtained by dissolving the corresponding metal(II) salts in water at elevated temperatures (60–80 °C) and adding **3** in stoichiometric amounts (Scheme 2). Due to the commercial unavailability of copper(II) chlorate, it was synthesized according to a previously published procedure.[23]



Scheme 2. Synthesis of energetic coordination compounds of copper(II) nitrate (**4**), 3d-metal perchlorates (**5**–**8**) and copper(II) chlorate (**9**) with 1-(azidomethyl)-5*H*-tetrazole.



Scheme 3. Synthesis of nitroaromatic coordination compounds **10**–**12**, as well as the coordination compounds of copper(II) azide (**13**) and silver(I) fulminate (**14a/b**) with AzMT.

The copper(II) nitroaromatic salts for compounds **10**–**12** were synthesized by dissolving basic copper(II) carbonate in water and adding stoichiometric amounts of the free acids of the corresponding nitroaromatic anion (Scheme 3). Compound **13** was synthesized by dissolving copper(II) chloride dihydrate in water, adding one equivalent of **3**, followed by adding two equivalents of sodium azide dissolved in water. Immediately after the addition of the azide, a brown precipitate of **13** formed, was filtered off and washed with little hot water.

Compound **14a/b** was obtained by dissolving silver(I) fulminate in acetonitrile at 30 °C and adding one equivalent of ligand. Crystals of compound **14a** start to form in the mother liquor after one day. By filtering off the platelets, crystals suitable for single-crystal X-ray diffraction are obtained. When leaving the mother liquor for several days, white needles, suitable for X-ray diffraction, of compound **14b** start to crystallize on top of the crystals of **14a**, ultimately completely turning **14a** into **14b**. Crystallization of the coordination compounds **4**–**12** was achieved by slowly evaporating the mother liquor for 1–2 days, and collecting the formed solids by filtration with subsequent drying in air. Single crystals suitable for X-ray diffraction experiments were also obtained from the mother liquor for compounds **4**, **9**, and **10**. Single crystals of compound **13** were obtained by a three-layered crystallization approach. Sodium azide together with **3** was dissolved in water and added to a test tube. A second layer consisting of a 1:1 mixture of water and ethanol was layered on top, and the third layer of copper(II) chloride dissolved in ethanol was slowly added. The test tube was carefully stoppered as not to mix the three layers and was set aside. After several days, crystals of compound **13** had formed and were collected by filtration and washed with little hot water. It was not possible to obtain crystals suitable for single-crystal X-ray diffraction of compounds **5**–**8**, **11**, and **12**; their composition was analyzed and proven by elemental analysis. Generally, all energetic coordination compounds were fully characterized by elemental analysis, infrared spectroscopy, differential thermal analysis, as well as their sensitivity towards impact (IS), friction (FS), and electrostatic discharge (ESD) were tested. Hot needle (HN) and hot plate (HP) tests were performed to obtain insight into their initiation capabilities, which were then tested for several chosen compounds.

Crystal structures

Solid-state crystal structures of compounds **3**, **4**, **9**, **10**, and **14a/b** were determined by using low-temperature single-crystal X-ray diffraction. All of the data and parameters of the measurements as well as of the refinements are given in Table S1 in the

© 2022 The Authors. Chemistry - A European Journal published by Wiley-VCH GmbH

Supporting Information. All crystal densities were recalculated to their respective room temperature crystal density.

Deposition Numbers 2124092 (for **3**), 2124093 (for **10**), 2124094 (for **9**), 2124095 (for **13**), 2124096 (for **14b**), 2124097 (for **4**), 2144883 (for **14a**) contain the supplementary crystallographic data for this paper. These data are provided free of charge by the joint Cambridge Crystallographic Data Centre and Fachinformationszentrum Karlsruhe Access Structures service.

Compound **3** crystallizes in the orthorhombic space group *Pbca* with eight formula units in the unit cell and a density of 1.55 g cm^{-3} (Figure 3). All bond lengths are in the typical range for C–N, N–N single and double bonds. The tetrazole moiety forms a nearly perfectly level plane (C1-N1-N2-N3 = 0.3°) from which the methylene group protrudes slightly by an angle of C1-N1-N2-N3 = 1.4°. Typical for covalently bound azides, the $-N_3$ unit protrudes from the tetrazole plane with an angle of N1-C2-N5 = 111° as shown in Figure 3.

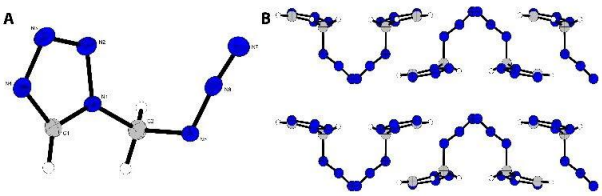


Figure 3. A) Crystal structure of 1-(azidomethyl)-5*H*-tetrazole. B) Crystal packing along the *a*-axis; ellipsoids in all structures are shown with a probability of 50%; Selected bond lengths [Å]: N1-N2 1.35(2), N1-C1 1.33(3), N1-C2 1.46(3), N2-N3 1.29(3), N3-N4 1.37(3), N4-C1 1.31(3), N5-C2 1.47(4), N5-N6 1.25(3), N6-N7 1.12(3); angles [°]: N2-N1-C1 108.0(15), N1-C2-N5 111.6(2), N2-N1-C2 120.8(18), N1-C1-H1 125.3(13), C1-N1-C2 131.2(18), N4-C1-H1 124.8(13), N1-N2-N3 106.1(17), N1-C2-H2 A 107.9(12), N2-N3-N4 111.0(18), N1-C2-H2B 106.1(13), N3-N4-C1 105.0(19), N5-C2-H2 A 112.4(13), N6-N5-C2 113.9(19), N5-C2-H2B 107.3(13), N5-N6-N7 172.6(3), H2A-C2-H2B 111.4(18), N1-C1-N4 109.9(19).

Compound **4** crystallizes in the monoclinic space group *Cc* with four formula units in the unit cell and a density of 1.66 g cm^{-3} (Figure 4). The copper(II) cation is sixfold coordinated by 1-(azidomethyl)-5*H*-tetrazole ligands whereas the two nitrate anions are non-coordinating. While the bond lengths within the six ligands are equivalent as for pure compound **3**, the bond lengths towards the copper(II) center range between 2.02–2.33 Å with angles of nearly perfect 180° between opposing ligands. Two of them (N4 and N25) show a longer bond distance towards the copper(II) cation than the four other ligands. Hence, the copper(II) cation is coordinated in a square bipyramidal conformation, caused by a typical Jahn–Teller-like distortion, due to the electron configuration of [Ar]3d^9 of the copper(II) cation.

The chlorate complex **9** crystallizes in the triclinic space group $P\bar{1}$ with two formula units in the unit cell and a density of 1.71 g cm^{-3} (Figure 5). The copper(II) cation is sixfold coordinated by AzMT ligands, all binding via their respective N4-nitrogen atom. Like in **4**, the coordination sphere is a square bipyramid due to Jahn–Teller-like distortion along the N1-Cu1-N1^{i} axis. The change of anion from nitrate (**4**) to chlorate (**9**) does not induce a change of bond lengths within the ligands. The bond lengths between the ligands and the copper(II) center are in the same range as in **4** (2.02–2.36 Å). The two chlorate anions are also non-coordinating.

Copper(II) picrate **10** (Figure 6) crystallizes in the monoclinic space group $P2_1/c$ with two formula units in the unit cell and a density of 1.83 g cm^{-3}. The copper(II) cation is coordinated by two equatorial AzMT ligands and two coordinating picrate anions, acting as bidentate ligands. The two picrates coordinate via their deprotonated hydroxy group as well as a second oxygen atom of one of the *ortho*- nitro groups. The bond lengths between the copper(II) and the AzMT ligands (2.01 Å) are in the same range as for the copper(II) nitrate (**4**) and

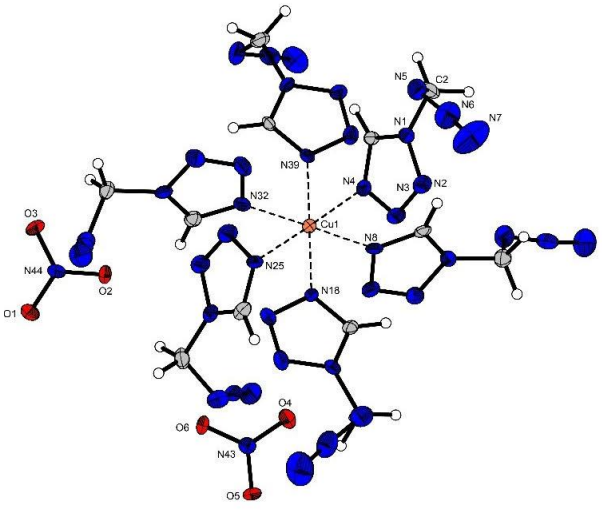


Figure 4. Molecular unit of $[Cu(AzMT)_6](NO_3)_2$ (**4**); Selected bond lengths [Å]: Cu1-N4 2.30(6), Cu1-N8 2.07(6), Cu1-N18 2.02(6), Cu1-N25 2.33(6), Cu1-N32 2.07(6), Cu1-N39 2.03(6); angles [°]: N4-Cu1-N8 89.5(2), N4-Cu1-N18 91.6(2), N4-Cu1-N25 178.3(2), N4-Cu1-N32 93.5(2), N4-Cu1-N39 87.9(2).

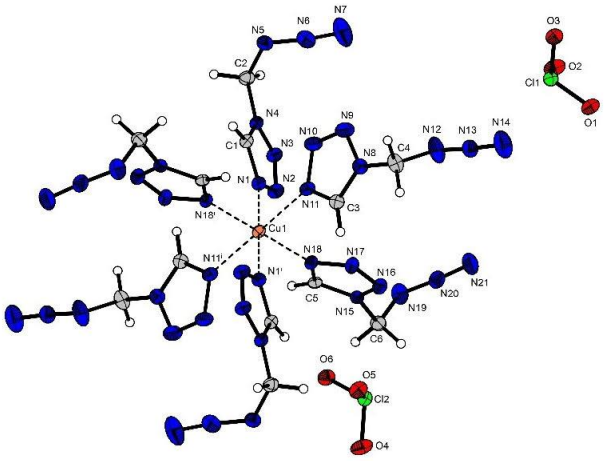


Figure 5. Molecular unit of $[Cu(AzMT)_6](ClO_3)_2$ (**9**); Selected bond lengths [Å]: Cu1-N1 2.05(2), Cu1-N11 2.36(2), Cu1-N18 2.02(2); angles [°]: N1-Cu1-N11 91.2(9), N1-Cu1-N18 91.6(8), N11-Cu1-N11^{i} 180.0.

© 2022 The Authors. Chemistry - A European Journal published by Wiley-VCH GmbH

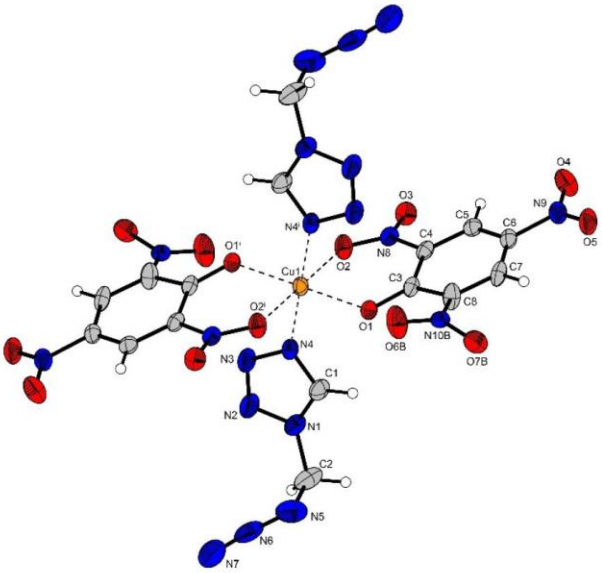


Figure 6. Molecular unit of $[Cu(PA)_2(AzMT)_2]$ (**10**); Selected bond lengths [Å]: Cu1-O1 1.92(2), Cu1-O2 2.35(2), Cu1-N4 2.01(2); angles [°]: O1-Cu1-O2 78.9(7), O1-Cu1-N4 86.8(7), O2-Cu1-N4 90.13(7).

chlorate (**9**). The deprotonated hydroxy groups also coordinate in the equatorial plane, whereas the nitro groups oxygen atoms are axial standing with a bond length of 2.35 Å, resulting in a typical Jahn-Teller-like distortion along the O2-Cu1-O2^{i} axis.

The copper(II) azide complex **13** crystallizes in the monoclinic space group $P2_1/c$ with four formula units in the unit cell and a density of 1.93 g cm^{-3}. The copper(II) cation is coordinated by five azide anions as well as one AzMT (**3**) ligand (Figure 7) forming a strongly distorted octahedron due to high deviations from the 90° coordination angles, observed in compounds **4**, **9**, and **10**. The deviation of up to 13.5° (N1-Cu1-N11^{ii}) from a linear arrangement of two opposing coordinating compounds is caused by two different bridging modes of the azide anions. Two of the coordinating azide anions bridge between two copper cations, thereby forming strands that are interconnected by the other three anions, which bridge between three copper cations.

Interestingly, the coordination of the copper(II) cation, as well as the two different bridging modes of the azide anions, are nearly identical to those of the 1-MTZ analogous, proving the structural similarity of the 1-MTZ and AzMT ligand.[32] For the silver(I) fulminate complexes, crystallization in two different space groups was observed. The initially formed platelets (**14a**) crystallized in the monoclinic space group *I*2/*a* with eight formula units in the unit cell and a density of 2.71 g cm^{-3}, the highest of all herein investigated compounds (Figure 8). The molecular unit consists of a tetrameric cluster of silver fulminate (SF), with the silver cations forming a nearly planar rhombus with angles of 75.72° (Ag2^{i}-Ag1-Ag2) and 104.28° (Ag1-Ag2-Ag1^{i}), and a torsion angle of 3.32°. The fulminate anions bridge between the silver cations with their terminal carbon and oxygen atoms, having shorter Ag-C (2.17–2.27 Å) interactions than Ag–O interactions (2.50–2.73 Å). Like in previously reported silver fulminate complexes,[33] the carbon atoms of the fulminate anions bridge between two silver cations of a tetramer. While the same bridging between two silver cations of the tetramer is observed for the oxygen atoms, a third interaction with a silver cation of a second tetrameric unit causes the formation of an extended three-dimensional structure. Due to the bridging character of the fulminate anions, Ag–Ag interactions (Figure 8) are observed within the tetrameric unit. Comparable to previously reported coordination compounds of SF with monodentate ligands,[33] the bond lengths of these argentophilic interactions (2.91–2.77 Å) are in the range to be classified as sub-van der Waals contacts (< 3.44 Å).[34] Additionally, the shortest argentophilic interaction observed has a distance of 2.7675(7) Å, being close to the shortest reported distance of 2.746(1) Å.[34]

After the mother liquor had stood for several days, white crystalline needles started to form on top of the platelets. These crystalline needles were also suitable for single-crystal X-ray diffraction experiments, showing compound **14b** crystallizing in the triclinic space group $P\bar{1}$ with two formula units in the unit cell and a density of 2.30 g cm^{-3}. In contrast to **14a**, the

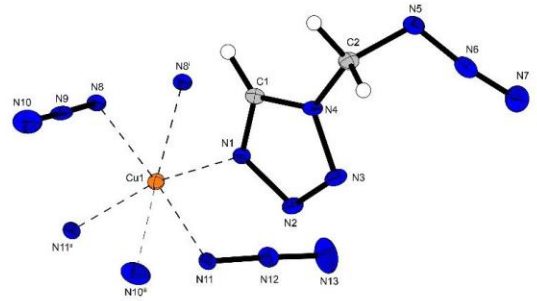


Figure 7. Molecular unit of $[Cu(N_3)_2(AzMT)]$ (**13**); Selected bond lengths [Å]: Cu1-N1 2.01(2), Cu1-N8 1.97(2), Cu1-N11 2.00(2), Cu1-N10^{iii} 2.65(3), Cu1-N11^{ii} 2.02(2), Cu1-N8^{i} 2.43(2); angles [°]: N1-Cu1-N11^{ii} 166.5(9), N8-Cu1-N11 172.8(9), N8^{i}-Cu1-N10^{iii} 169.4(8), N1-Cu1-N8 91.7(9), N1-Cu1-N11 95.2(9).

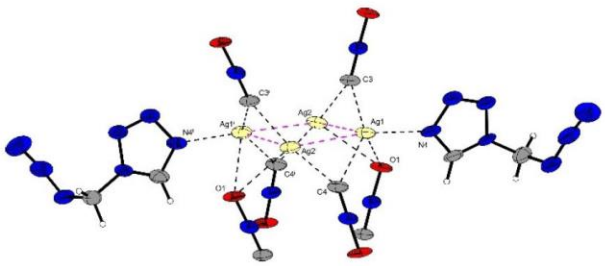


Figure 8. Molecular unit of $[Ag_4(CNO)_4(AzMT)_2]$ (**14a**); Selected bond lengths [Å]: Ag1-Ag2 2.91(8), Ag1-Ag2^{i} 2.77(7), Ag1-N4 2.29(5), Ag1-C3 2.27(5), Ag1-O2 2.66(3), Ag2-C3 2.17(5); angles [°]: Ag2-Ag1-N4 121.92(12), N4-Ag1-C3 100.34(18), Ag2-C3-Ag1 81.94(20), Ag2-Ag1-O2 129.02(11), Ag2^{i}-Ag1-O2 66.85(10), Ag1-Ag2^{i}-C3^{i} 93.11(13), Ag2^{i}-Ag1-C3 74.66(11); Torsion angles [°] Ag2^{i}-Ag1-Ag2-Ag1^{i} 3.32(2).

© 2022 The Authors. Chemistry - A European Journal published by Wiley-VCH GmbH

molecular unit consists of a trimeric cluster of silver fulminate coordinated by three AzMT ligands (Figure 9). Here, the fulminate anions also bridge between silver cations, but in contrast to **14a**, only by their terminal carbon atom, forming monomers with argentophilic interactions between the silver cations, slightly longer (2.81–2.87 Å) than those in the tetrameric structure.

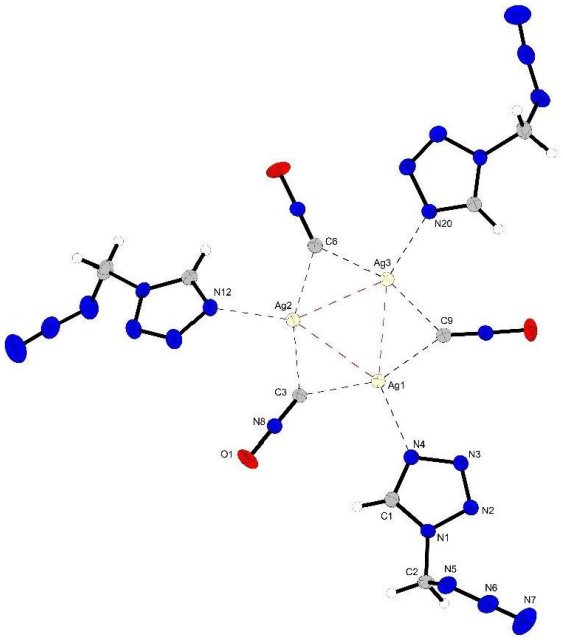


Figure 9. Molecular unit of $[Ag_3(CNO)_3(AzMT)_3]$ (**14b**); Selected bond lengths [Å]: Ag1-Ag2 2.87(7), Ag1-Ag3 2.84(7), Ag2-Ag3 2.81(7), Ag1-N4 2.31(2), Ag2-N12 2.31(2), Ag3-N20 2.31(2), Ag1-C3 2.22(3), Ag1-C9 2.20(2), Ag2-C3 2.17(2), Ag2-C6 2.19(2), Ag3-C6 2.18(3), Ag3-C9 2.20(3); angles [°]: Ag1-Ag2-Ag3 59.9(1), Ag2-Ag1-Ag3 58.9(1), Ag1-Ag3-Ag2 61.2(1), Ag1-C3-Ag2 81.7(8), Ag2-C6-Ag3 79.7(9), Ag1-C9-Ag3 80.4(9), C3-Ag1-C9 155.2(9), C3-Ag2-C6 159.1(10), C6-Ag3-C9 159.3(9).

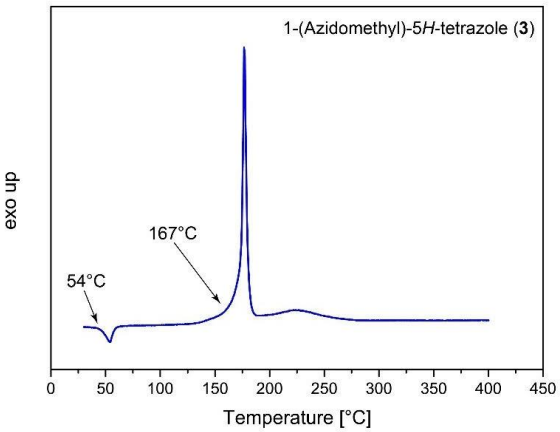


Figure 10. Differential thermal analysis of compound **3** with a heating rate of 5 °C min^{-1}.

As in the tetrameric structure, the silver fulminate cluster is nearly planar with a torsion angle of 7.8° (C6-Ag2-Ag1-C9). Interestingly, a different protrusion for every AzMT ligand from the plane, formed by the SF trimer, is observed. While the first AzMT (via N4) is nearly perpendicular with the plane, the AzMT ligands (coordinated via N12 and N20) protrude from the plane by 8.0° and 46.5°, respectively.

Physicochemical properties

Thermal behavior

Differential thermal analyses of compounds **3**–**14** are shown in Figures 10 and 11. DTA plots for compounds **4**, **9** and **12** are shown in the Supporting Information. Compound **3** shows an endothermic event at 54 °C, due to a melting of the compound, and an exothermic decomposition temperature of 167 °C, lower than the comparable 1-(azidoethyl)-5*H*-tetrazole (AET) derivative (193 °C).[23] All energetic coordination compounds show

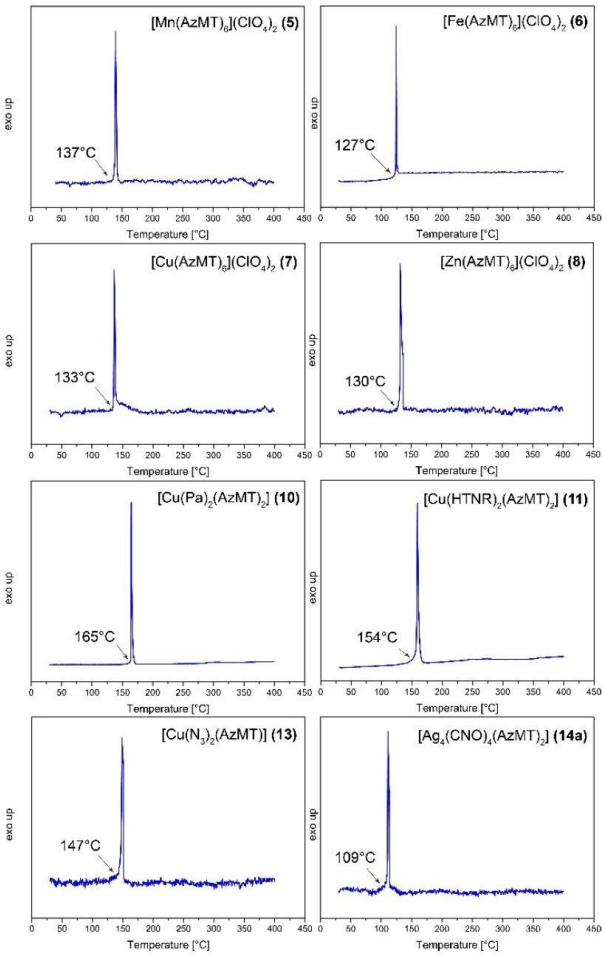


Figure 11. Differential thermal analysis of compounds **5**–**8**, **10**–**11**, and **13**–**14a**, with a heating rate of 5 °C min^{-1}.

© 2022 The Authors. Chemistry - A European Journal published by Wiley-VCH GmbH

lower thermal stability, which is also observed for ECCs of AET. Compound **4** shows a small endothermic event at 60 °C, attributing a melting of the compound, with a first exothermic event happening already at 123 °C contributing to explosive decomposition. The same behavior is observed for compound **9**, showing an endothermic event at 112 °C, immediately evolving into an exothermic event at 123 °C. The metal perchlorate compounds **5–8** exhibit exothermic decompositions between 127 (**6**) and 137 °C (**5**) where all four compounds violently detonate. The nitroaromatic compounds **10** (165 °C), **11** (154 °C), and **12** (151 °C) exhibit slightly higher thermal stabilities, yet they are less stable than pure **3**. The coordination compounds of copper(II) azide (**13**) and silver(I) fulminate (**14 b**) are thermally stable up to 147 and 109 °C, respectively. Here the formation of complexes with 1-(azidomethyl)-5*H*-tetrazole (**3**) leads to a more drastic drop in thermal stability compared to their parent salts copper(II) azide (205 °C) and silver(I) fulminate (196 °C).

Sensitivities

1-(Azidomethyl)-5*H*-tetrazole (**3**) is a very sensitive compound with an impact and friction sensitivity of 2 J and 1 N (Table 2). (Both values are considered as very sensitive.) Although it is not sensitive (540 mJ) towards electrostatic discharge (ESD), due to its mechanical sensitivities, it has to be ranked as a primary explosive. By applying **3** as ligand in ECCs of copper(II) nitrate (**4**), picrate, (**10**), styphnate (**11**), and trinitrophloroglycinolate (**12**), it is possible to stabilize the friction sensitivity of **3**. While **4** is only slightly less sensitive (15 N) than pure **3**, compound **10** is completely insensitive (360 N). With an increasing amount of hydroxy groups, **11** shows a higher sensitivity (192 N) and **12** the highest friction sensitivity of 45 N. Yet all nitroaromatic compounds are far less sensitive than the copper(II) nitrate complex **4**. When changing from copper(II) nitrate to perchlorate (**7**) or chlorate (**9**) the resulting coordination compounds exhibits drastically increased sensitivities (< 1 J, < 0.1 N) compared to pure **3**. Changing to manganese(II) (**5**), iron(II) (**6**), or zinc(II) perchlorate (**8**) the same increase in sensitivities is observed. While all compounds show very high sensitivities towards impact (< 1 J), compound **5** towards friction (0.5 N) than **6**, **7**, and **8** (< 0.1 N). Compound **13** also shows a very high mechanical sensitivity of < 1 J and < 0.1 N. Yet it seems to be more stable than pure copper(II) azide, derived from the fact that we had no problems handling compound **13**, while several minor explosions happened when handling pure copper(II) azide. The coordination compound of silver(I) fulminate with **3** leads to an increase in impact sensitivity (< 1 J) compared to pure silver fulminate (5 J), whereas the friction sensitivity is approximately equal to pure SF (< 0.1 N). The same trends of stabilization or destabilization as for the mechanical sensitivities of the ligand (**3**) is observed comparing the ESD sensitivities. Compounds **4**, **10**, and **11** are completely insensitive towards ESD (> 1500 mJ), while compound **12** (1220 mJ) is nearly insensitive. Changing to metal perchlorates or chlorates the ESD sensitivity of the resulting complex (**6**: 380 mJ; **7**: 480 mJ; **8**: 380 mJ; **9**: 380 mJ) is increased compared to the pure ligand (540 mJ). Here, only compound **5**, the manganese perchlorate complex shows a slightly lower sensitivity (740 mJ) than **3**. The highest sensitivity towards ESD is observed for the silver(I) fulminate complex **14 b** (10 mJ), followed by the copper(II) azide complex **13** (38 mJ). Here, the addition of **3** to the corresponding salt results in a stabilization of the otherwise sensitive parent compound. Due to the high sensitivities of the metal (per-)chlorates, as well as **14 b** towards impact (< 1 J), ball drop impact measurements were performed, allowing a more detailed differentiation of the compounds. For compounds **5** and **7** (Table 1) a ball drop impact sensitivity (BDIS) of 25 mJ was observed, while compounds **8**, and **14 b** are slightly more sensitive (20 mJ) and iron(II) perchlorate (**6**), as well as the copper(II) chlorate (**9**) showed the highest sensitivity (16 mJ).

Table 2. Thermal stability[a] as well as sensitivities to mechanical and electrical stimuli of compounds **3**–**14**, compared to copper azide and silver fulminate.

Compound	T_{endo}[b] [°C]	T_{exo}[c] [°C]	IS[d] [J]	FS[e] [N]	ESD[f] [mJ]	BDIS[g] [mJ]	HP	HN
AzMT (**3**)	54	167	2	1	540		Det	Def
$[Cu(AzMT)_6](NO_3)_2$ (**4**)	60	123	2	15	> 1500		Def	Def
$[Mn(AzMT)_6](ClO_4)_2$ (**5**)		137	< 1	0.5	740	25	Def	Det
$[Fe(AzMT)_6](ClO_4)_2$ (**6**)		127	< 1	< 0.1	380	16	Det	Det
$[Cu(AzMT)_6](ClO_4)_2$ (**7**)		133	< 1	< 0.1	480	25	Det	Det
$[Zn(AzMT)_6](ClO_4)_2$ (**8**)		130	< 1	< 0.1	380	20	Def	Def
$[Cu(AzMT)_6](ClO_3)_2$ (**9**)	112	123	< 1	< 0.1	380	16	Det	Def
$[Cu(Pa)_2(AzMT)_2]$ (**10**)		165	< 1	360	> 1500		Def	Dec
$[Cu(HTNR)_2(AzMT)_2]$ (**11**)		154	< 1	192	> 1500		Dec	Dec
$[Cu(HTNPG)(AzMT)_2]$ (**12**)		151	< 1	45	1220		Def	Def
$[Cu(N_3)_2(AzMT)]$ (**13**)		147	< 1	< 0.1	38		Det	Det
$[Ag_4(CNO)_4(AzMT)_2]$ (**14 a**)		109	< 1	< 0.1	10	20	Det	Det
$Cu(N_3)_2$		205	≪ 1	≪ 0.1	≤ 0.28			
AgCNO[33]		196	5	≤ 0.1	≤ 0.28			

[a] DTA onset temperatures at a heating rate of 5 °Cmin $^{-1}$. [b] Oset temperature of endothermic event in the DTA, indicating a melting of the compound. [c] Onset temperature of exothermic event in the DTA. [d] Impact sensitivity (BAM drop hammer (1 of 6)). [e] Friction sensitivity (BAM friction tester (1 of 6)). [f] Electrostatic discharge device (OZM XSpark10). [g] Ball drop impact sensitivity (OZM BIT-132) determined with the 1-of-6 method in accordance with the MIL-STD 1751 A (method 1016).

© 2022 The Authors. Chemistry - A European Journal published by Wiley-VCH GmbH

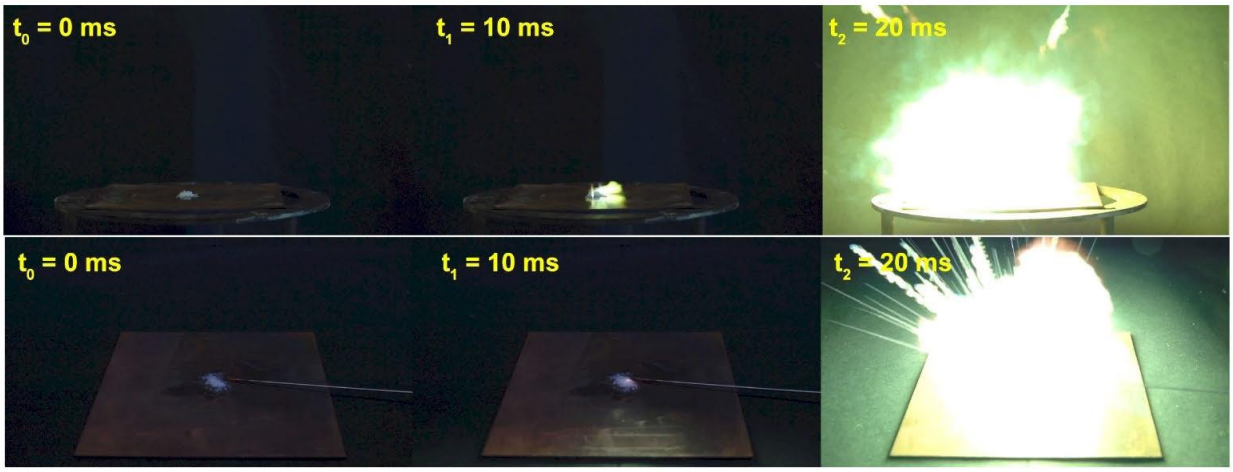


Figure 12. Top row: Hot-plate test of $[Mn(AzMT)_6](ClO_4)_2$ (**5**); Bottom row: Hot-needle test of 5; The time between each frame is 10 ms and shows the moment before (t_0), at the onset of (t_1) and during (t_2) decomposition.

Initiation capabilities

To get a further insight on the behavior upon fast heating with and without confinement, hot plate (HP) and hot needle (HN) tests were carried out. This also allows for a first evaluation of the applicability of the tested compounds as primary explosives. Detailed experimental procedures are given in the Supporting Information, the results are summarized in Table 1. Pure compound **3** showed a detonation in the HP test and a deflagration in the HN test. While the copper(II) nitrate (**4**) and the nitroaromatic compounds **10**, **11**, and **12** show deflagration or decomposition (**10**, **11**), the (per)chlorate metal complexes show a violent detonation (**6**, **7**, and **9**) or sharp deflagration (**5** and **8**) in the HP test (Figure 12). The complexes of copper(II) azide (**13**) and silver(I) fulminate (**14**) detonate both in the HP and HN test.

For compounds **3**, **5**, **7**, **8**, and **12** initiation tests were performed. The detailed testing setup and procedure are given in the Supporting Information. Compounds **3** and **12** showed no positive initiation of PETN, which is indicated by the still intact witness plate (Figure 13). Therefore, neither compound was able to undergo deflagration to detonation transition (DDT) in this setup, which is a necessary characteristic for a compound to be used as a primary explosive. Nonetheless, the perchlorates **5**, **7**, and **8** were able to undergo DDT and initiate the PETN sample, indicated by a perforation of the copper witness plate (Figure 14).

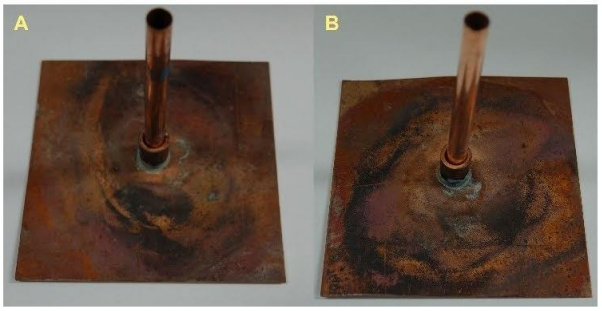


Figure 13. Intact witness plates and copper tubes after the initiation testing of compounds **3** and **12**.

Conclusion

Successful hydroxymethylation of 1,5*H*-tetrazole with aqueous formalin solution can only be achieved by the addition of

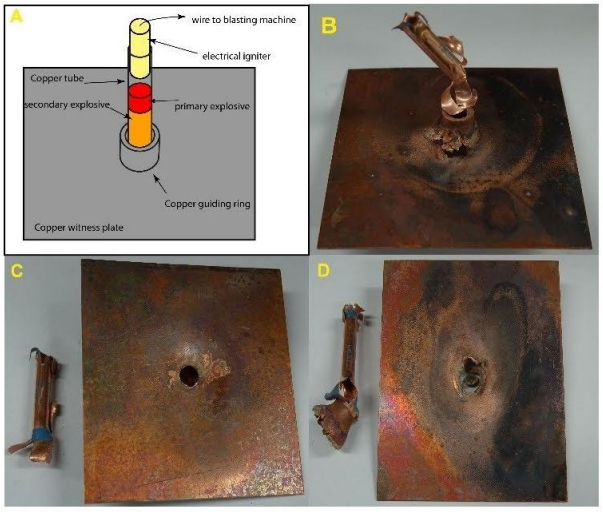


Figure 14. A) Schematic test setup for initiation testing. Positive initiation of PETN by B) $[Mn(AzMT)_6](ClO_4)_2$ (**5**), C) $[Cu(AzMT)_6](ClO_4)_2$ (**7**), and D) $[Zn(AzMT)_6](ClO_4)_2$ (**8**), indicating a DDT for all three compounds. The positive initiation of PETN is indicated by the perforation of the copper witness plate.

© 2022 The Authors. Chemistry - A European Journal published by Wiley-VCH GmbH

catalytic amounts (3–5 wt%) of sodium hydroxide to the reaction solution. Subsequent protection of the alcohol by methanesulfonyl chloride provided the precursor compound needed to successfully synthesize the highly energetic 1-(azidomethyl)-5*H*-tetrazole (**3**) for the first time. While its structural isomer 5-(azidomethyl)-1*H*-tetrazole has already been reported, **3** represents the smallest tetrazole derivate with the shortest *N*-alkyl-azide functionality reported, showing a very high positive heat of formation. Single-crystal X-ray analysis of **3** was supplemented by elemental analysis, infrared spectroscopy as well as multinuclear NMR (^{1}H, ^{13}C, ^{14}N, and ^{15}N) spectroscopy. The thermal behavior was determined by DTA measurement, and the sensitivities towards external stimuli were determined. Like other azido alkyl-tetrazoles, it performs well as a ligand in the formation of energetic coordination compounds. Here, the ECCs of copper(II) nitrate (**4**), chlorate (**9**), perchlorate (**7**), azide (**13**), manganese(II) (**5**), iron(II) (**6**), and zinc(II) perchlorate (**8**) were synthesized. The ECCs of copper(II) nitroaromatic salts (**10–12**), as well as that of silver(I) fulminate (**14a/b**) were prepared. Suitable crystals were analyzed by single-crystal X-ray diffraction experiments, giving insight into the molecular structure of the ligand itself, as well as its coordination behavior towards 3d and 4d metals. The successful syntheses of the ECCs are supported by elemental analysis as well as infrared spectroscopy. Analysis of the sensitivities towards external stimuli showed the high sensitivity (impact: 2 J, friction: 1 N) of the ligand, which is generally increased by the formation of ECCs. While the impact sensitivity of the ligand was increased by the formation of ECCs (<1 J (**5–14**)), the friction sensitivity can be decreased by forming the copper(II) picrate (360 N), styphnate (192 N), and trinitrophloroglycinolate (45 N) complexes. The same trend was observed for the thermal stability of **3** (177 °C). Analyzing the thermal stabilities of the ECCs by DTA, showed decreasing thermal stabilities of the ECCs compared to the ligand itself. Initiation testing of the ligand itself and the ECC of copper(II) trinitrophloroglycinolate (**12**) showed no DDT, thus no initiation of the PETN sample. Testing the perchlorate salts of manganese, copper, and zinc showed a DDT with a positive initiation of PETN.

Experimental Section

CAUTION! This paper contains a large amount of extremely sensitive compounds. Full-body protection containing Kevlar® gloves, Kevlar® sleeves, face shield, leather coat and ear protection must be worn when manipulating those compounds! The equipment used must be earthed!

1-(2-Hydroxymethyl)-5*H*-tetrazole[30] (**1**): 1,5*H*-tetrazole (20 g, 285 mmol), synthesized according to literature,[35–36] and sodium hydroxide (0.5 g, 12.5 mmol) were dissolved in water (200 mL), and formalin solution (37%, 66 mL, 917 mmol) was added. The reaction mixture was stirred over night at room temperature and was extracted into ethyl acetate (3x400 mL). The organic phase was dried over $MgSO_4$, and the solvent was removed in vacuo, resulting in crude isomeric mixture **1** as a colorless oil in good yield (22.1 g, 221 mmol, 80%). ^{1}H NMR ([D$_6$]DMSO, 25 °C): **1a** δ = 9.45 (s, *CH*), 5.77 (s, CH_2); **1b** δ = 8.97 (s, *CH*), 5.92 (s, CH_2).

(Tetrazol-1-yl)methyl methanesulfonate (**2a**): Crude isomeric mixture **1** (5.0 g, 50 mmol) was suspended in CH_2Cl_2 (100 mL), cooled to 0 °C. Methanesulfonyl chloride (6.87 g, 60 mmol, 1.2 equiv.) was added, the reaction mixture was stirred for 1 h while cooling, and pyridine (5.93 g, 75 mmol, 1.5 equiv.) was added, keeping the temperature below 5 °C. The reaction mixture was allowed to slowly warm and was stirred for 18 h at room temperature. The reaction mixture was then transferred to a separatory funnel and washed with water (100 mL), hydrochloric acid (2 M, 50 mL), and water (50 mL). Colorless crystals of compound **2a** slowly start to crystallize from the aqueous phase in moderate yield (3.12 g, 17.5 mmol, 35%). The organic phase was dried over $MgSO_4$, and the solvent was removed in vacuo, leaving a colorless oil consisting of compounds **2a** and **2b**, which were separated by flash column chromatography over silica with *n*-hexane/ethyl acetate (50:50) as the eluting solvent. After removing the solvent in vacuo, additional compound **2a** was obtained in a yield of 13%, whereas crude compound **2b** was still obtained. ^{1}H NMR ([D$_6$]acetone, 25 °C): **2a** δ = 9.43 (s, *CH*), 6.66 (s, CH_2), 3.27 ppm (s, CH_3); **2b** δ = 8.95 (s, *CH*), 6.77 (s, CH_2), 3.24 ppm (s, CH_3). ^{13}C NMR ([D$_6$]acetone, 25 °C): **2a** δ = 145.5 (s, *CH*), 72.7 (s, CH_2), 39.0 ppm (s, CH_3).

1-(Azidomethyl)-5*H*-tetrazole (AzMT, 3): Compound **2a** (350 mg, 1.96 mmol) and sodium azide (383 g, 5.89 mmol) were dissolved in a mixture of water (10 mL) and acetone (10 mL), and the mixture was refluxed for 18 h at 75 °C. After cooling to room temperature, water (40 mL) was added, and the mixture was extracted into CH_2Cl_2 (3×50 mL). The organic phase was dried over $MgSO_4$, the solvent was removed in vacuo, and 1-(azidomethyl)-5*H*-tetrazole (**3**) was obtained as an off-white solid in quantitative yield (243 mg, 1.94 mmol, 99%). ^{1}H NMR ([D$_6$]DMSO, 25 °C): δ = 9.60 (s, *CH*), 6.02 ppm (s, CH_2); ^{13}C NMR ([D$_6$]DMSO, 25 °C): δ = 144.2 (s, *CH*), 60.5 ppm (s, CH_2); ^{14}N NMR ([D$_6$]DMSO, 25 °C): δ = −135.6.2 (brs, N_β), −160.4 ppm (brs, N_γ); ^{15}N NMR ([D$_6$]DMSO, 25 °C): δ = 14.4 (d, $N_{(3)}$), −14.0 (s, $N_{(2)}$), −50.4 (d, $N_{(4)}$), −136.3 (t, $N_{(\alpha)}$), −141.9 (d, $N_{(1)}$), −158.9 (s, N_γ), −302.1 ppm (s, N_β); elemental analysis calcd. (%) for $C_2H_3N_7$ (125.10): C 19.20, H 2.42, N 78.38; found C 19.02, H 2.32, N 76.00; DTA (5 °C min^{-1}): 54 °C (T_{endo}), 177 °C (T_{exo}); BAM drop hammer: 2 J; BAM friction tester: 1 N; ESD: 540 mJ; IR (ATR, cm^{-1}): 3154 (m), 3048 (w), 2979 (w), 2460 (w), 2236 (w), 2153 (s), 2106 (vs), 1819 (vw), 1762 (w), 1478 (s), 1443 (m), 1428 (m), 1370 (w), 1317 (w), 1294 (s), 1263 (m), 1230 (vs), 1161 (vs), 1100 (vs), 1026 (w), 1000 (w), 951 (m), 911 (s), 881 (s), 754 (s), 716 (s), 655 (vs), 562 (s), 416 (w).

Synthesis of energetic coordination compounds

General procedure: Compound **3** (125 mg, 1 mmol) was dissolved in water at 60–80 °C. In a second container, the corresponding equivalents of metal salt (**4–9**: 0.16 mmol, **10–12**: 0.5 mmol, **13** and **14**: 1 mmol) was dissolved in water (**4–13**) or acetonitrile (**14**) at 60–80 °C. After all solids dissolved, the solution containing compound **3** was added to the metal salt solution with stirring. After stirring for 5 min at 60 °C, any undissolved solids were filtered off, and the solution was left to crystallize for compounds **4–12**, and **14a/b**. After the solvent was evaporated, the remaining solids were dried under high vacuum for 1 h. Compound **13** was obtained by combining the two solutions, stirring for 5 min at 60 °C, filtering off the precipitate and washing with cold water.

[Cu(AzMT)$_6$](NO$_3$)$_2$ (**4**): Obtained as blue platelets in good yield (124.6 mg, 0.133 mmol, 83%). Elemental analysis calcd. (%) for $C_{12}H_{18}CuN_{44}O_6$ (938.12): C 15.36, H 1.93, N 65.70; found C 15.46, H 1.94, N 62.97; DTA (5 °C min^{-1}): 60 °C (T_{endo}), 123 °C (T_{exo}); BAM drop hammer: 2 J; BAM friction tester: 15 N; ESD: >1500 mJ. IR (ATR, cm^{-1}): 3086 (m), 3043 (m), 2984 (m), 2454 (w), 2394 (w), 2352 (w), 2315 (w), 2156 (s), 2106 (s), 1588 (m), 1501 (m), 1447 (m), 1342 (vs),

© 2022 The Authors. Chemistry - A European Journal published by Wiley-VCH GmbH

1290 (s), 1277 (s), 1230 (s), 1169 (s), 1162 (s), 1100 (vs), 1043 (m), 997 (m), 913 (s), 829 (m), 781 (m), 748 (s), 716 (m), 648 (s), 561 (m), 421 (w), 413 (w).

[Mn(AzMT)$_6$](ClO$_4$)$_2$ (5): Obtained as white platelets in quantitative yield (160.5 mg, 0.16 mmol, 100%). Elemental analysis calcd. (%) for $C_{12}H_{18}Cl_2MnN_{42}O_8$ (1004.40): C 14.35, H 1.81, N 58.87; found C 14.79, H 1.91, N 58.01; DTA (5 °C min^{-1}): 137 °C (T_{exo}); BAM drop hammer: < 1 J; ball drop impact: 25 mJ; BAM friction tester: 0.5 N; ESD: 740 mJ; IR (ATR, cm^{-1}): 3128 (m), 3096 (m), 3038 (m), 2982 (m), 2157 (s), 2105 (s), 1586 (m), 1497 (s), 1448 (m), 1373 (m), 1311 (m), 1283 (m), 1232 (s), 1174 (s), 1100 (vs), 1041 (m), 978 (s), 935 (s), 913 (s), 747 (s), 713 (m), 647 (s), 622 (s), 604 (m), 561 (m), 479 (m), 425 (w), 420 (w).

[Fe(AzMT)$_6$](ClO$_4$)$_2$ (6): Obtained as an orange-brown solid in very good yield (149.6 mg, 0.149 mmol, 99%). Elemental analysis calcd. (%) for $C_{12}H_{18}Cl_2FeN_{42}O_8$ (1005.31): C 14.34, H 1.80, N 58.52; found C 15.10, H 2.02, N 58.86; DTA (5 °C min^{-1}): 127 °C (T_{exo}); BAM drop hammer: < 1 J; ball drop impact: 16 mJ; BAM friction tester: < 0.1 N; ESD: 380 mJ; IR (ATR, cm^{-1}): 3135 (w), 3043 (vw), 2986 (vw), 2163 (m), 2106 (s), 1497 (m), 1440 (w), 1375 (w), 1314 (m), 1285 (m), 1237 (s), 1172 (m), 1075 (vs), 1039 (m), 983 (m), 914 (s), 896 (m), 746 (m), 712 (m), 655 (s), 651 (s), 622 (s), 560 (m), 425 (vw), 413 (w), 407 (vw).

[Cu(AzMT)$_6$](ClO$_4$)$_2$ (7): Obtained as blue platelets in quantitative yield (162 mg, 0.16 mmol, 100%). Elemental analysis calcd. (%) for $C_{12}H_{18}Cl_2CuN_{42}O_8$ (1013.01): C 14.23, H 1.79, N 58.07; found C 14.33, H 1.97, N 57.50; DTA (5 °C min^{-1}): 133 °C (T_{exo}); BAM drop hammer: < 1 J; ball drop impact: 25 mJ; BAM friction tester: < 0.1 N; ESD: 480 mJ; IR (ATR, cm^{-1}): 3136 (m), 3045 (w), 2992 (w), 2155 (m), 2106 (s), 1591 (vw), 1556 (vw), 1503 (m), 1447 (w), 1375 (w), 1284 (m), 1236 (m), 1175 (m), 1100 (s), 1074 (vs), 992 (m), 909 (m), 747 (m), 711 (m), 655 (s), 647 (s), 622 (vs), 560(m).

[Zn(AzMT)$_6$](ClO$_4$)$_2$ (8): Obtained as white solid in good yield (141.3 mg, 0.139 mmol, 87%). Elemental analysis calcd. (%) for $C_{12}H_{18}Cl_2N_{42}O_8Zn$ (1014.84): C 14.20, H 1.79, N 57.97; found C 14.60, H 1.86, N 57.37; DTA (5 °C min^{-1}): 130 °C (T_{exo}); BAM drop hammer: < 1 J; ball drop impact: 20 mJ; BAM friction tester: < 0.1 N; ESD: 380 mJ; IR (ATR, cm^{-1}): 3136 (w), 3048 (vw), 2986 (vw), 2163 (m), 2108 (s), 1793 (vw), 1498 (m), 1442 (w), 1375 (w), 1315 (w), 1284 (m), 1238 (m), 1175 (m), 1074 (vs), 1040 (m), 985 (m), 915 (m), 897 (m), 746 (m), 711 (m), 656 (m), 647 (m), 622 (s), 560 (m), 416 (w).

[Cu(AzMT)$_6$](ClO$_3$)$_2$ (9): Obtained as light-blue blocks in good yield (146 mg, 0.149 mmol, 93%). Elemental analysis calcd. (%) for $C_{12}H_{18}Cl_2CuN_{42}O_6$ (981.01): C 14.69, H 1.85, N 59.97; found C 14.94, H 2.04, N 58.84; DTA (5 °C min^{-1}): 112 °C (T_{endo}), 123 °C (T_{exo}); BAM drop hammer: < 1 J; BAM friction tester: < 0.1 N; ESD: 380 mJ; IR (ATR, cm^{-1}): 3098 (s), 3039 (m), 2985 (m), 2458 (w), 2227 (w), 2155 (s), 2104 (s), 1588 (w), 1499 (m), 1448 (m), 1373 (m), 1310 (m), 1292 (m), 1281 (m), 1230 (s), 1176 (s), 1163 (s), 1100 (vs), 1042 (m), 958 (vs), 935 (s), 912 (vs), 775 (m), 747 (m), 715 (m), 646 (s), 603 (s), 562 (m), 479 (s), 426 (w), 411 (w).

[Cu(PA)$_2$(AzMT)$_2$] (10): Obtained as green platelets in good yield (338.8 mg, 0.44 mmol, 88%). Elemental analysis calcd. (%) for $C_{16}H_{10}CuN_{20}O_{14}$ (769.93): C 24.96, H 1.31, N 36.39; found C 24.84, H 1.29, N 35.97; DTA (5 °C min^{-1}): 165 °C (T_{exo}); BAM drop hammer: < 1 J; BAM friction tester: > 360 N; ESD: > 1500 mJ. IR (ATR, cm^{-1}): 3147 (w), 3094 (w), 3060 (w), 2158 (m), 2106 (s), 1608 (s), 1574 (s), 1542 (s), 1517 (s), 1493 (s), 1420 (m), 1349 (s), 1321 (s), 1276 (s), 1239 (s), 1163 (vs), 1092 (s), 1037 (m), 1012 (m), 988 (m), 941 (m), 933 (m), 910 (s), 899 (s), 847 (m), 825 (m), 788 (s), 741 (s), 707 (vs), 659 (s), 542 (s), 515 (m), 460 (m), 427 (m), 418 (m).

[Cu(HTNR)$_2$(AzMT)$_2$] (11): Obtained as dark green blocks in moderate yield (312.8 mg, 0.39 mmol, 78%). Elemental analysis calcd. (%) for $C_{16}H_{10}CuN_{20}O_{16}$ (801.93): C 23.96, N 1.26, N 34.93,; found C 24.01, H 1.60, N 34.78; DTA (5 °C min^{-1}): 154 °C (T_{exo}); BAM drop hammer: < 1 J; BAM friction tester: 192 N; ESD: > 1500 mJ. IR (ATR, cm^{-1}): 3135 (w), 3052 (w), 2149 (m), 2098 (m), 1627 (m), 1561 (s), 1520 (s), 1490 (m), 1477 (m), 1456 (s), 1443 (m), 1368 (s), 1334 (s), 1321 (m), 1307 (s), 1274 (vs), 1247 (s), 1222 (s), 1204 (s), 1173 (s), 1160 (s), 1094 (vs), 1037 (m), 987 (s), 948 (m), 931 (m), 915 (s), 891 (s), 829 (w), 783 (m), 775 (m), 763 (m), 747 (m), 734 (s), 705 (s), 697 (vs), 646 (vs), 578 (m), 562 (m), 527 (m), 464 (m), 456 (m), 421 (m).

[Cu(HTNPG)(AzMT)$_2$] (12): Obtained as dark brown blocks in moderate yield (203.4 mg, 0.36 mmol, 71%). Elemental analysis calcd. (%) for $C_{10}H_7CuN_{17}O_9$ (572.82): C 20.97, H 1.23, N 41.57; found C 21.00, H 1.66, N 39.33; DTA (5 °C min^{-1}): 151 °C (T_{exo}); BAM drop hammer: < 1 J; BAM friction tester: 45 N; ESD: 1220 mJ. IR (ATR, cm^{-1}): 3142 (m), 3043 (w), 2984 (w), 2163 (m), 2112 (s), 2105 (s), 1645 (m), 1589 (m), 1569 (s), 1521 (s), 1515 (s), 1503 (s), 1494 (s), 1447 (m), 1436 (m), 1404 (m), 1375 (m), 1337 (s), 1318 (s), 1288 (s), 1237 (s), 1164 (vs), 1092 (vs), 1032 (m), 1008 (m), 1001 (m), 984 (m), 916 (s), 905 (m), 872 (w), 833 (m), 820(m), 805 (m), 786 (m), 760 (m), 740 (m), 710 (s), 694 (s), 645 (s), 559 (m), 503 (m), 493 (m), 457 (w), 418 (w).

[Cu(N$_3$)$_2$(AzMT)] (13): Obtained as brown powder in moderate yield (171.8 mg, 0.63 mmol, 63%). Elemental analysis calcd. (%) for $C_2H_3CuN_{13}$ (272.68): C 8.81, H 1.11, N 66.78; found C 8.92, H 1.46, N 63.60; DTA (5 °C min^{-1}): 147 °C (T_{exo}); BAM drop hammer: < 1 J; BAM friction tester: < 0.1 N; ESD: 38 mJ. IR (ATR, cm^{-1}): 3104 (m), 3047 (w), 2463 (w), 2158 (m), 2080 (vs), 2047 (vs), 1501 (s), 1447 (m), 1377 (m), 1340 (m), 1309 (m), 1286 (s), 1239 (s), 1171 (vs), 1101 (s), 1039 (m), 1024 (m), 993 (m), 909 (s), 895 (s), 759 (s), 713 (m), 689 (m), 654 (vs), 597 (m), 587 (s), 562 (m), 403 (s).

[Ag$_4$(CNO)$_4$(AzMT)$_2$] (14a): Obtained as colorless platelets in moderate yield (280.4 mg, 0.66 mmol, 66%). Elemental analysis calcd. (%) for $C_4H_3Ag_2N_9O_2$ (424.87): C 11.31, H 0.71, N 29.67; found C 11.37, H 0.86, N 29.90; DTA (5 °C min^{-1}): 109 °C (T_{exo}); BAM drop hammer: < 1 J; BAM friction tester: < 0.1 N; ESD: 10 mJ; IR (ATR, cm^{-1}): 3220 (w), 3134 (m), 3032 (w), 2960 (w), 2458 (w), 2303 (w), 2292 (w), 2246 (w), 2154 (m), 2104 (vs), 2090 (vs), 1818 (w), 1487 (m), 1449 (m), 1439 (w), 1376 (w), 1301 (m), 1276 (m), 1235 (s), 1152 (vs), 1130 (vs), 1099 (s), 1035 (m), 1008 (m), 976 (m), 909 (s), 885 (s), 767 (w), 746 (m), 710 (m), 654 (s), 563 (m), 498 (w), 481 (m), 462 (m), 418 (w), 405 (w).

Acknowledgements

Financial support of this work by the Ludwig Maximilian University of Munich (LMU), the Office of Naval Research (ONR) under grant no. N00014-19-1-2078 as well as the Strategic Environmental Research and Development Program (SERDP) under grant no. WP19-1287 is gratefully acknowledged. Open Access funding enabled and organized by Projekt DEAL.

Conflict of Interest

The authors declare no conflict of interest.

© 2022 The Authors. Chemistry - A European Journal published by Wiley-VCH GmbH

Data Availability Statement

The data that support the findings of this study are available in the supplementary material of this article.

Keywords: alkylazides · energetic coordination compounds · initiation · primary explosives · tetrazole

[1] J. Wilbrand, *Justus Liebigs Ann. Chem.* **1863**, *128*, 178–179.
[2] A. Cahours, A. Sobrero *Justus Liebigs Ann. Chem.* **1848**, *64*, 396–398.
[3] D. Kumar, Y. Tang, C. He, G. H. Imler, D. A. Parrish, J. n. M. Shreeve, *Chem. Eur. J.* **2018**, *24*, 17220–17224.
[4] E. C. Johnson, T. A. Reid, C. W. Miller, J. J. Sabatini, R. C. Sausa, E. F. C. Byrd, J. A. Orlicki, *ChemPlusChem* **2021**, *86*, 875–878.
[5] E. C. Johnson, J. J. Sabatini, D. E. Chavez, L. A. Wells, J. E. Banning, R. C. Sausa, E. F. C. Byrd, J. A. Orlicki, *ChemPlusChem* **2020**, *85*, 237–239.
[6] J. Fronabarger, A. Schuman, R. Chapman, W. Fleming, W. Sanborn, T. Massis, in *31st Joint Propulsion Conference and Exhibit*, AIAA, July **1995**..
[7] T. W. Myers, K. E. Brown, D. E. Chavez, R. J. Scharff, J. M. Veauthier, *Inorg. Chem.* **2017**, *56*, 2297–2303.
[8] M. L. Gettings, M. T. Thoenen, E. F. C. Byrd, J. J. Sabatini, M. Zeller, D. G. Piercey, *Chem. Eur. J.* **2020**, *26*, 14530–14535.
[9] S. Manzoor, Q.-u.-n. Tariq, X. Yin, J.-G. Zhang, *Def. Tech.* **2021**, *17*, 1995–2010.
[10] A. A. Larin, L. L. Fershtat, *Energ. Mater. Front.* **2021**, *2*, 3–13.
[11] A. A. Larin, N. V. Muravyev, A. N. Pivkina, K. Y. Suponitsky, I. V. Ananyev, D. V. Khakimov, L. L. Fershtat, N. N. Makhova, *Chem. Eur. J.* **2019**, *25*, 4225–4233.
[12] Q. Wu, Q. Li, K. Li, H. Li, B. Kou, Z. Hang, W. Zhu, *Can. J. Chem.* **2018**, *96*, 459–465.
[13] S. R. Yocca, M. Zeller, E. F. C. Byrd, D. G. Piercey, *J. Mater. Chem. A* **2022**, *10*, 1876–1884.
[14] P. He, J.-G. Zhang, X. Yin, J.-T. Wu, L. Wu, Z.-N. Zhou, T.-L. Zhang, *Chem. Eur. J.* **2016**, *22*, 7670–7685.
[15] K. Y. Titenkova, A. V. Shaferov, A. A. Larin, M. A. Epishina, A. S. Kulikov, I. V. Ananyev, L. L. Fershtat, *Tetrahedron* **2022**, *103*, 132563.
[16] T. Liu, Y.-G. Ji, L. Wu, *Org. Biomol. Chem.* **2019**, *17*, 2619–2623.
[17] A. Qian, Y. Zheng, R. Wang, J. Wei, Y. Cui, X. Cao, Y. Yang, *Bioorg. Med. Chem. Lett.* **2018**, *28*, 344–350.
[18] T. M. Klapötke, M. Kofen, L. Schmidt, J. Stierstorfer, M. H. H. Wurzenberger, *Chem. Asian J.* **2021**, *16*, 3001–3012.
[19] N. Szimhardt, M. H. H. Wurzenberger, A. Beringer, L. J. Daumann, J. Stierstorfer, *J. Mater. Chem. A* **2017**, *5*, 23753–23765.
[20] N. Szimhardt, M. H. H. Wurzenberger, L. Zeisel, M. S. Gruhne, M. Lommel, J. Stierstorfer, *J. Mater. Chem. A* **2018**, *6*, 16257–16272.
[21] M. H. H. Wurzenberger, B. R. G. Bissinger, M. Lommel, M. S. Gruhne, N. Szimhardt, J. Stierstorfer, *New J. Chem.* **2019**, *43*, 18193–18202.
[22] M. H. H. Wurzenberger, S. M. J. Endraß, M. Lommel, T. M. Klapötke, J. Stierstorfer, *ACS Appl. Energ. Mater.* **2020**, *3*, 3798–3806.
[23] M. H. H. Wurzenberger, M. S. Gruhne, M. Lommel, N. Szimhardt, T. M. Klapötke, J. Stierstorfer, *Chem. Asian J.* **2019**, *14*, 2018–2028.
[24] G. Bélanger-Chabot, S. M. Kaplan, P. Deokar, N. Szimhardt, R. Haiges, K. O. Christe, *Chem. Eur. J.* **2017**, *23*, 13087–13099.
[25] R. Haiges, K. O. Christe, *Dalton Trans.* **2015**, *44*, 10166–10176.
[26] A. R. Katritzky, C. N. Fali, I. V. Shcherbakova, S. V. Verin, *J. Heterocycl. Chem.* **1996**, *33*, 335–339.
[27] O. N. Verkhozina, V. N. Kizhnyaev, L. I. Vereshchagin, A. V. Rokhin, A. I. Smirnov, *Russ. J. Org. Chem.* **2003**, *39*, 1792–1796.
[28] D. A. Chaplygin, A. A. Larin, N. V. Muravyev, D. B. Meerov, E. K. Kosareva, V. G. Kiselev, A. N. Pivkina, I. V. Ananyev, L. L. Fershtat, *Dalton Trans.* **2021**, *50*, 13778–13785.
[29] L. Y. Peng Lei, Y. Yuzhang, L. Wei, Z. Xuejiao, P. Siping, *Chin. J. Org. Chem.* **2012**, *32*, 667–676.
[30] I. V. Tselinskii, A. A. Mel'nikov, L. G. Varyagina, I. G. Zhigadlova, *Chem. Heterocycl. Compd.* **1983**, *19*, 341–343.
[31] M. Sućeska, *EXPLO5 Version 6.05 User's Guide*, Zagreb, **2018**.
[32] M. H. H. Wurzenberger, M. Lommel, M. S. Gruhne, N. Szimhardt, J. Stierstorfer, *Angew. Chem. Int. Ed.* **2020**, *59*, 12367–12370; *Angew. Chem.* **2020**, *132*, 12466–12469.
[33] M. H. H. Wurzenberger, M. S. Gruhne, M. Lommel, V. Braun, N. Szimhardt, J. Stierstorfer, *Inorg. Chem.* **2020**, *59*, 17875–17879.
[34] H. Schmidbaur, A. Schier, *Angew. Chem. Int. Ed.* **2015**, *54*, 746–784; *Angew. Chem.* **2015**, *127*, 756–797.
[35] R. Bronisz, *Inorg. Chim. Acta* **2002**, 215–220.
[36] T. M. Klapötke, M. Stein, J. Stierstorfer, *Z. Anorg. Allg. Chem.* **2008**, *634*, 1711–1723.

Manuscript received: February 15, 2022
Accepted manuscript online: May 3, 2022
Version of record online: May 25, 2022

© 2022 The Authors. Chemistry - A European Journal published by Wiley-VCH GmbH

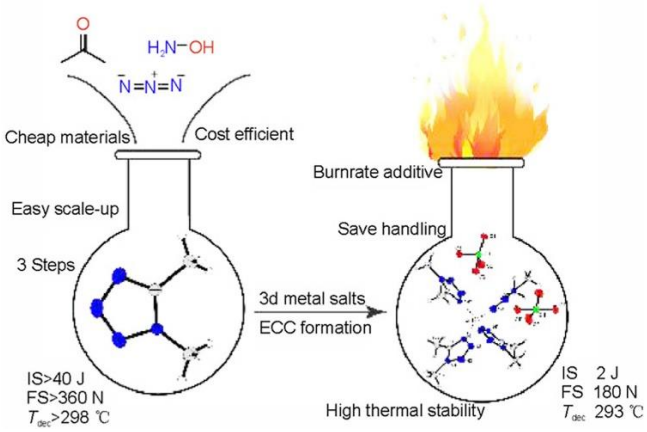
Appendix 30

1,5-Dimethyltetrazole as a ligand in energetic 3d5 to 3d10-metal coordination compounds

M. Kofen, A. G. Harter, T. M. Klapötke, J. Stierstorfer

Energetic Materials Frontiers, **2022**, 3, 111–121.

https://doi.org/10.1016/j.enmf.2022.07.004



Supplementary Information:
https://ars.els-cdn.com/content/image/1-s2.0-S2666647222000586-mmc1.docx

Energetic Materials Frontiers 3 (2022) 111–121

Contents lists available at ScienceDirect

Energetic Materials Frontiers

journal homepage: www.keaipublishing.com/en/journals/energetic-materials-frontiers

1,5-Dimethyltetrazole as a ligand in energetic $3d^5$ to $3d^{10}$-metal coordination compounds

Moritz Kofen, Alexander G. Harter, Thomas M. Klapötke, Jörg Stierstorfer *

Department of Chemistry, Ludwig Maximilian University of Munich, Butenandtstr, 5-13, D-81377, Munich, Germany

ARTICLE INFO

Keywords:
Transition metal
N-ligand
Energetic coordination compound
Tetrazole
Structure elucidation

ABSTRACT

During the last decade, energetic coordination compounds gained considerable attention due to the simple adjustments in their physicochemical properties. By combining different metal cations, energetic anions, and ligands, those compounds can be adapted for their intended use. This study used 1,5-dimethyltetrazole (**3**) as a highly endothermic, easily accessible, and insensitive ligand. It is a structural isomer to 1-ethyl-5*H*-tetrazole (1-ETZ), which was recently described as a suitable ligand. 1,5-Dimethyltetrazole was synthesized using two different methods: (1) reaction of acetone with azido (trimethyl) silane and (2) reaction of acetoxime benzenesulfonate with sodium azide. Subsequently, 1,5-dimethyltetrazole was reacted with the perchlorate salts of different 3*d* metals (e.g., Mn, Fe, Co, Ni, Cu, Zn) to obtain new energetic coordination compounds (ECCs). In addition, copper (II) complexes with 2,4,6-trinitro-phenolate anions were synthesized. The resultant complexes were investigated through low-temperature, single crystal diffraction experiments complemented by elemental analysis, infrared spectroscopy, and differential thermal analysis. Moreover, sensitivities towards impact and friction were investigated. In this study, all ECCs exhibited impact sensitivities between 2 and 10 J, friction sensitivities between 128 and 360 N, and thermal stabilities of up to 360 °C.

1. Introduction

Owing to their physical and chemical properties, coordination compounds are critical to various applications, such as spin-crossover systems,[1,2] metal-organic frameworks,[3] and energetic materials.[4] Most specifically, metal-organic frameworks have recently gained significant attention as hypergolic solid fuels for aerospace applications.[5–7] ECCs typically contain a 3*d* metal cation, are coordinated by a nitrogen-rich ligand, and gain charge balance with an oxidizing (e.g., ClO_4^-, ClO_3^-) or reducing (e.g., N_3^-) anion. Additionally, the concept of ECC formation expands many traditional synthetic approaches into new energetic materials, offering a broad range of further tuning the energetic properties towards their intended applications.[8,9] Nevertheless, the synthesis of ligands themselves is subjected to the introduction of explosophores,[10,11] increasing enthalpy of formation by incorporating high amounts of nitrogen or oxygen in the molecule[11] or introducing a high strain.[11,12] The use of azoles[13,14] as ligands is highly desirable as they provide broad chemical diversity with high energy content due to their endothermic enthalpy of formation.[11] Furthermore, tetrazoles[15–18] have been proven to be promising energetic compounds that are suitable to be applied as ligands in energetic coordination compounds.[19,20] Their energetic properties can be easily modified by altering their functional groups or substitution patterns, as shown in Fig. 1. 1,5-Dimethyltetrazole (DMT, **3**) is an easily accessible, small, neutral, and nitrogen-rich molecule, which makes it a potent candidate as an energetic ligand. Although the compound looks trivial, it has never been used as a ligand; however, it offers a surprisingly high positive heat of formation. In this study, **3** was synthesized using different procedures from existing literature and further reacted with different 3*d* metal (e.g., Mn, Fe, Co, Ni, Cu, Zn) salts to form energetic coordination compounds. Besides their energetic properties, the change in the coordination of the ligand around the central metal was investigated. Finally, the influence of structural isomers was studied by comparing the ligands 1,5-dimethyltetrazole and 1-ethyl-5*H*-tetrazole.

2. Results and discussion

2.1. Synthesis

1,5-Dimethyltetrazole (DMT, **3**) can be synthesized by different routes according to relevant literature[27–29] (Scheme 1). A straightforward method is the reaction of acetone with azidotrimethylsilane, which yields **3** in a one-step synthesis.[30] Another synthesis route starts with the

* Corresponding author.
E-mail address: jstch@cup.uni-muenchen.de (J. Stierstorfer).

https://doi.org/10.1016/j.enmf.2022.07.004
Received 29 April 2022; Received in revised form 25 May 2022; Accepted 21 July 2022
Available online 5 August 2022
2666-6472/© 2022 The Authors. Publishing services by Elsevier B.V. on behalf of KeAi Communications Co. Ltd. This is an open access article under the CC BY license (http://creativecommons.org/licenses/by/4.0/).

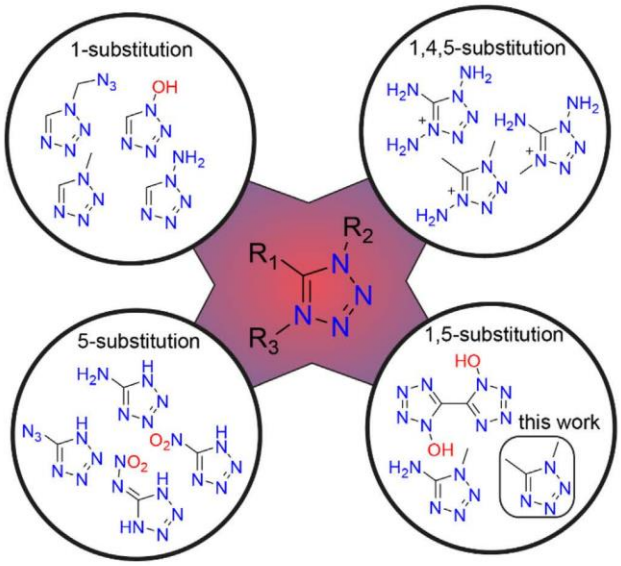
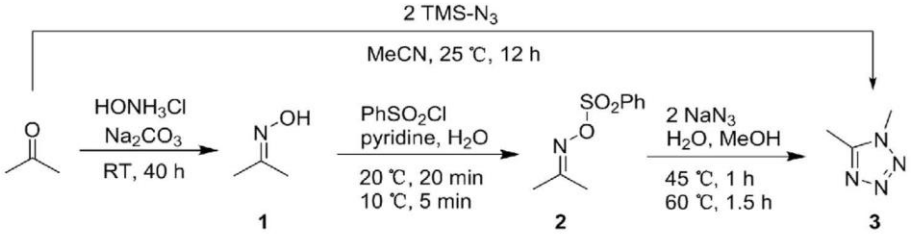


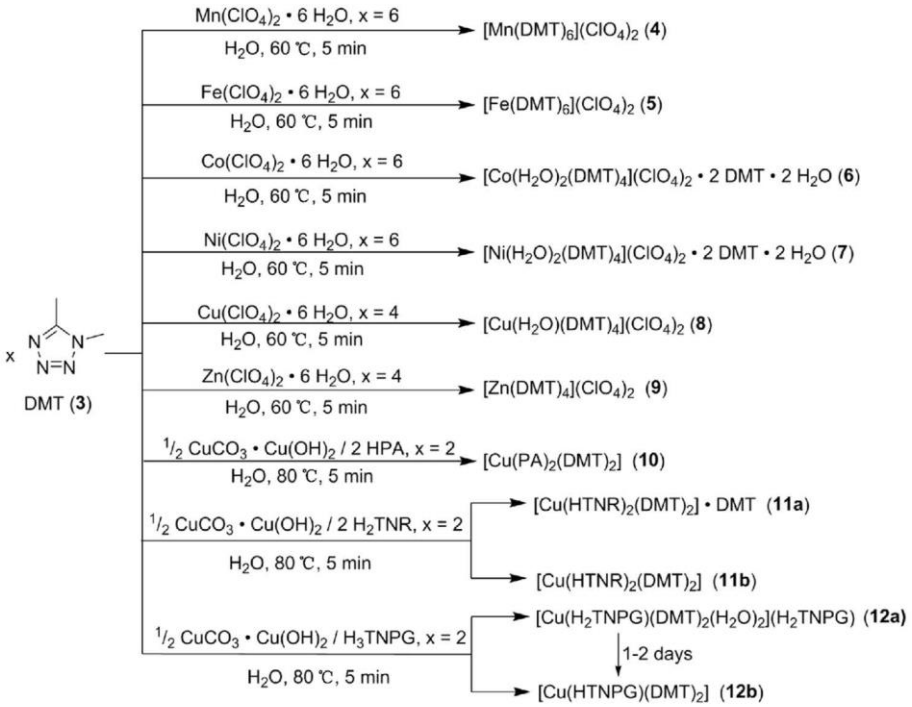
Fig. 1. Possible substitution patterns of 1,2,3,4-tetrazole, which highlight the chemical diversity.[17,18,21–26]

reaction of acetone with hydroxylamine hydrochloride in water to form acetone oxime, followed by the reaction of acetone oxime with benzene sulfonyl chloride to form acetoxime benzenesulfonate, which acts as a leaving group in the final step of the reaction with sodium azide. The ring closure starts with a nucleophilic attack of the azide on the imine, accompanied by a [1,2]-rearrangement of one methyl group. Although the first synthesis procedure of applying trimethylsilylazide is more economical in terms of atoms, reaction time, and cost, the second procedure was preferred for the synthesis of **3** on a 10–20 g scale since it has a slightly higher yield of 42% than the first one (34%). **3** can be obtained as a colorless solid in the form of blocky crystals through recrystallization from water.

ECCs **4**–**12** were synthesized by combining aqueous solutions of corresponding metal salts with stoichiometric amounts of **3** at elevated temperatures (60–80 °C; Scheme 2). Because of the unavailability of copper (II) nitroaromatic salts, their aqueous solutions were obtained by suspending basic copper (II) carbonate in water, adding corresponding free acid, and stirring at high temperatures until the solids dissolved. For compounds **4**, **8**, **9**, **10**, **11**, and **12**, crystals suitable for single crystal X-ray diffraction experiments were obtained. For compounds **5**–**7**, the evaporation of the solvent resulted in glass-like residues, from which single crystals started to grow under a high vacuum. After crystal structures of these compounds were obtained, further analysis was impossible – even by recrystallization from different solvents. When the aqueous



Scheme 1. Synthetical routes of 1,5-DMT (**3**) starting with acetone.



Scheme 2. Synthesis of energetic coordination compounds **4**–**12**.

solution of **3** was combined with that of copper (II) styphnate, solids began to precipitate immediately. This solid was insoluble and filtered off, and the resulting clear solution was left to crystallize. The growing crystals were collected and analyzed through single crystal X-ray diffraction as compound **11a**. Elemental analysis proved that the solid formed initially was compound **11b**, for which single crystals cannot be obtained. In the synthesis of compound **12**, needle-like (**12a**) and block-like (**12b**) crystals began to precipitate, and **12a** was consumed due to the formation of **12b** after several days. Therefore, **12b** was the main product. Complex **12a** contained deprotonated nitrophenol anions, one of which was coordinating and one was non-coordinating. The copper (II) cation in complex **12a** was further coordinated by two aqua ligands and two molecules of **3**. By contrast, the copper (II) cation in **12b** was coordinated by two double deprotonated anions, bridging different metal centers. Each center was also coordinated by two molecules of **3**, with no inclusion of water.

2.2. Crystal structures

Compound **3** and all ECCs were characterized through low-temperature single-crystal X-ray diffraction. The crystal density of all structures was recalculated to values at room temperature (298 K) for the sake of comparison. The datasets of all compounds (except for **7**) were uploaded to the CSD database and can be accessed for free with CCDC 2169296 (**3**), 2163674 (**4**), 2163667 (**5**), 2163668 (**6**), 2163673 (**8**), 2163675 (**9**), 2163671 (**10**), 2163670 (**11a**), 2163672 (**12a**), and 2163669 (**12b**). The obtained crystals of **7** had poor quality, rendering proper measurement and refinement impossible. Nonetheless, an insight into the compound's composition and the coordination of the nickel (II) cation can be obtained. The depiction of the obtained structure is provided in the supporting information (Fig. S1). Compound **3** crystallizes in the orthorhombic space group *Pnma* with four formula units per cell and a density of 1.31 g·cm^{-3}. While the bond lengths are in the same range as those of comparable 1- or 5-methyltetrazoles, **3** exhibits a mirror axis (σ_v) due to a C/N disorder (Fig. 2). This causes a difficult distinction between the C1 and N1 atoms, which is intensified by a simultaneous sharing of the atoms' positions. The crystal packing of **3** along the *b* axis (Fig. 2b) represents the stacking in sets of perpendicular but rotated against molecules of **3** (red/blue). The packing along the *c* axis (Fig. 2b) shows that these sets exhibit an offset and are not face-on with each other, thereby presenting a screw-axis of **3** along the *b* axis.

Compounds **4** and **5** crystallize in the triclinic space group, *P*–3, and their calculated density is 1.53 g·cm^{-3} and 1.55 g·cm^{-3}, respectively, with one formula unit per cell. The manganese (II) cation of **4** (Fig. 3, top) shows sixfold coordination by 1,5-DMT ligands, forming a nearly perfect octahedron. Thus, only minor deviation angles of 0.06° from the perfect octahedron and M–L bond lengths of 2.303 Å for all six ligands can be observed. Accordingly, the manganese (II) cation with an electron configuration of [Ar]3$d^5$4s^0 is in its high-spin state. Additionally, the iron cation of **5** (Fig. 3, bottom) also shows sixfold coordination by 1,5-DMT ligands, forming an octahedron with an angle deviation of only 0.65° from the perfect octahedron. The distortion is caused by the electron configuration of [Ar]3d^6 for a high-spin (hs) Fe (II) cation, leading to one fully filled t_{2g} orbital (Fig. 4). Since the t_{2g} orbitals do not participate in the building of σ-bonds and the π-back bonding is weak, the overall M–L bond lengths are not influenced by this distortion. Accordingly, a bond length of 2.238 Å is found in all six ligands, which is comparable to that of other hs-Fe (II) coordination compounds. By comparing the ion radii of hs-Mn (0.830 Å[31]) with hs-Fe (0.780 Å[31]) cations, the difference of 0.050 Å is found to suit the observed change in M–L bond length of −0.065 Å from Mn (II) to Fe (II), supporting the assumption of a *high spin* Fe (II) compound. Furthermore, unlike previously reported ECCs of iron (II) perchlorate,[32] compound **5** shows no thermochromic effect, which would derive from a change from hs-Fe (II) to low spin (ls)-Fe (II) when cooling crystals for low-temperature X-ray diffraction experiments. This effect is known for coordination compounds exhibiting sufficient ligand field

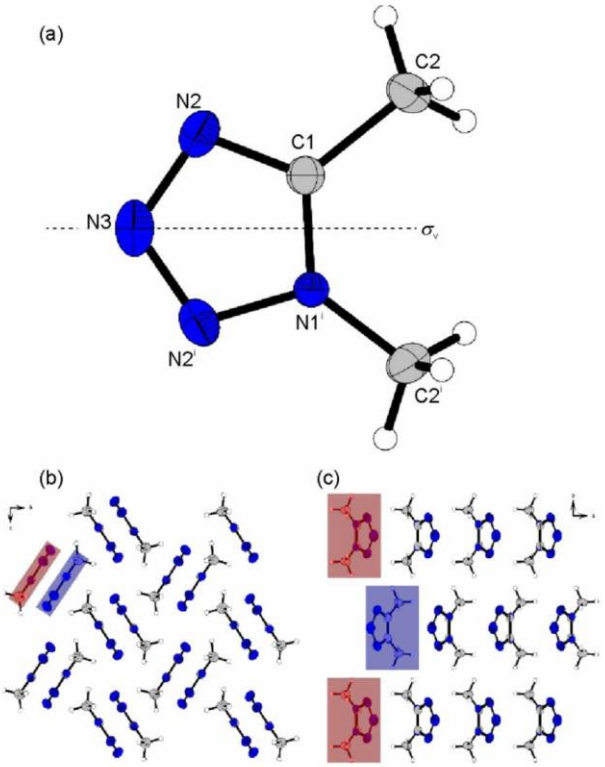


Fig. 2. (a) Molecular structure of 1,5-dimethyltetrazole (**3**); (b) crystal packing of **3** along *b*-axis; (c) crystal packing of **3** along *c*-axis. Selected bond lengths [Å]: N1–N2 1.350 (6), N1–C2 1.414 (6), N2–N3 1.325 (14), N2–C1 1.319 (7), C1–C2 1.529 (7); All ellipsoids are depicted with a probability of 50%. Symmetry codes: i) $+x$, $3/2-y$, $+z$.

splitting of *d*-orbitals. Cooling such coordination compounds results in an increase in ligand field splitting of the *d*-orbitals, ultimately enabling a spin-crossover from hs-to ls-state.[32] Overall, this observation leads to the classification of 1,5-DMT as a weak field ligand.

Compounds **6** (Fig. 5) and **7** (Fig. S1) crystallize in the monoclinic space group $P2_1/n$ and have calculated densities of 1.54 g·cm^{-3} and 1.55 g. cm^{-3}, respectively. The cobalt cation in **6** is coordinated by four molecules of 1,5-DMT and two water molecules, forming a slightly distorted octahedron co-crystallized by one additional 1,5-DMT and one water molecule. The angle deviations from the perfect octahedron are smaller than those in **5** due to three different M–L bond lengths. Besides the M − O bond of the axial standing aqua ligands, there are two different M − N bonds built by two pairs of 1,5-DMT ligands. One pair of opposite standing ligands coordinate via N4 of the tetrazole ring, whereas the other pair coordinate via N3 of the tetrazole ring. Among all the ligands, the highest difference in bond length is found between Co1–O6 and Co1–N7, with a Δ of 0.12 Å, which appears to be too small for *Jahn Teller*-like [33] distortions. Since oxygen atoms have π-basic character due to their lone pair and thus do not increase the gap difference of the t_{2g}- and e_g-orbitals, the cobalt (II) cation is in its high spin state, where significant *Jahn-Teller* effects are not expected. Consequently, steric effects between the DMT ligands and maintenance of a good π-orbital overlap cause the deviation from a perfect octahedron. Compound **7** shows the same coordination around the Ni (II) cation (Fig. S1) while being co-crystallized by two 1,5-DMT and two water molecules. Since the nickel cation has an electronic configuration of [Ar]3d^8 and the e_g orbital does not degrade, the slight deviations from the perfect octahedron are also caused by steric effects.

Like in compound **6**, the nickel cation of **7** is coordinated by two pairs of opposite standing DMT ligands and coordinates via N3 and N4 of the

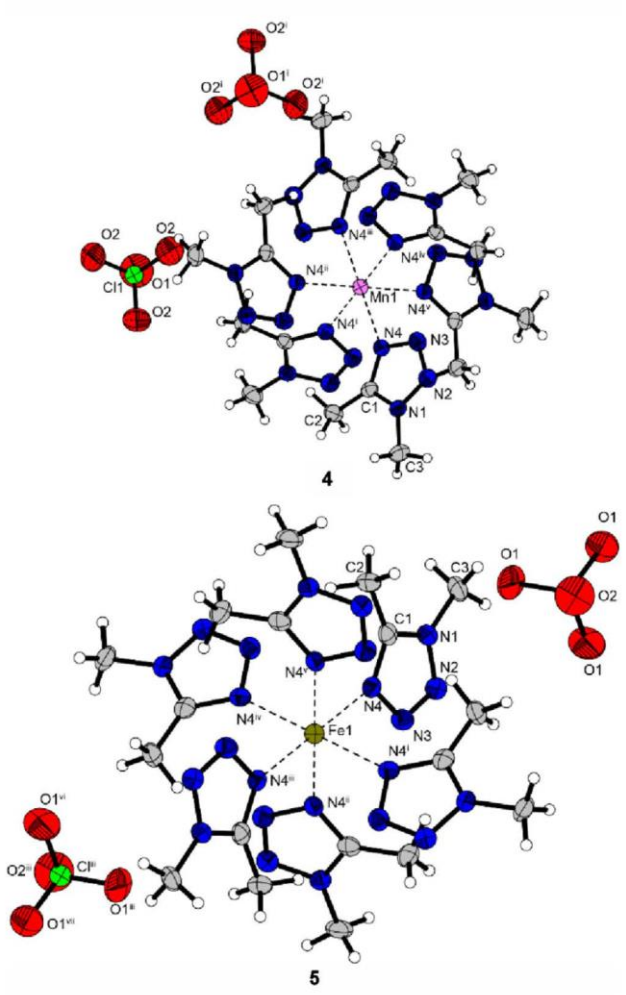


Fig. 3. Molecular structures of ECCs **4** and **5** in the crystalline state, displaying the coordination of the metal cation centers by 1,5-DMT. Selected bond lengths [Å]: Mn1–N4 2.303 (2), Fe1–N4: 2.238 (5).

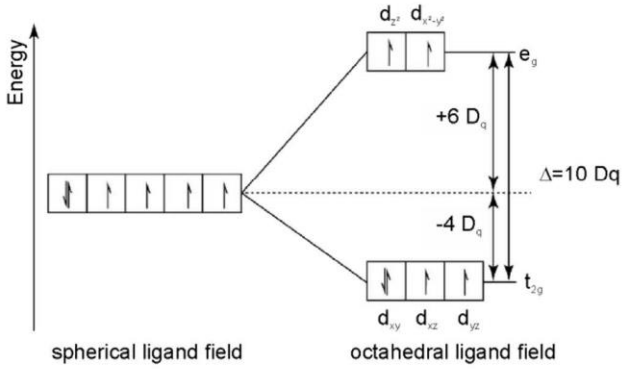


Fig. 4. Electronic configuration of a Fe (II) cation and the splitting of *d*-orbitals due to an octahedral coordination.

tetrazole rings, resulting in small differences in the M–L bond lengths. Compound **8** (Fig. 6) crystallizes in the orthorhombic space group *Pbca* and has a calculated density of 1.67 g·cm^{-3}.

The copper (II) cation is coordinated and distorted pentagonal by four 1,5-DMT ligands and one aqua ligand. All four M – N bond lengths are

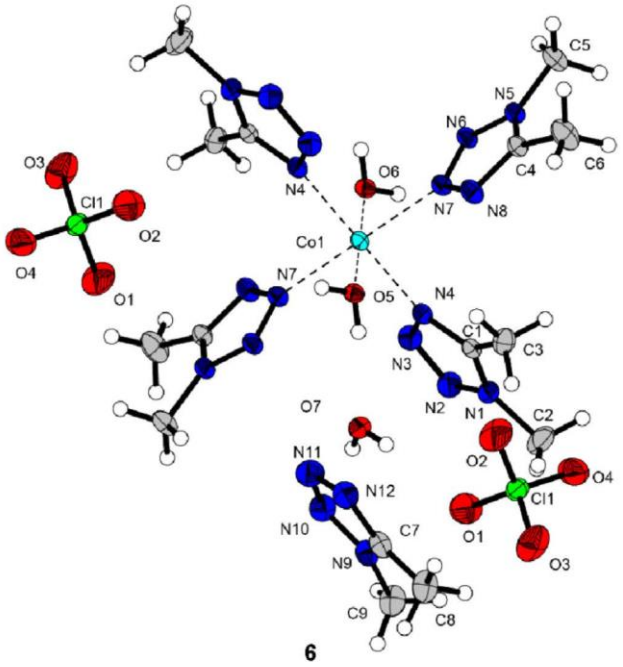


Fig. 5. Crystal structures of ECC **6** representing the coordination of the cobalt cation by four molecules of 1,5-DMT and two aqua ligands. Selected bond lengths [Å]: Co1 – N4 2.139 (2), Co1 – N7 2.176 (2).

equal within the error interval, with a value of around 2.00 Å. The M – O bond length of 2.144 Å can be explained by the degradation of the z^2-over the x^2–y^2-orbital for a d^9-metal in a square-pyramidal ligand field. This structure perfectly aligns with a previously suggested square-pyramidal coordination of Cu (II) cations in an aqueous solution[34] rather than the more classical *Jahn-Teller* distorted octahedral sixfold coordination. Compound **9** (Fig. 6, bottom) crystallizes in the tetragonal space group $P4_12_12$ with a density of 1.63 g cm^{-3}. The zinc (II) cation is coordinated by four molecules of **3**, forming a nearly perfect tetrahedron with M–L bond lengths of 1.990 Å for all four ligands. Throughout the series of first-row transition metals (**4**–**9**), a decrease in the metal-ligand bond length from 2.30 (2) Å to 1.99 (2) Å was observed, thus causing a strong contraction of the polyhedron and disfavoring the octahedral coordination of Cu (II) and Zn (II) cations by **3**. Additionally, the decreasing metal-ligand bond length indicates a decreasing radius of the corresponding metal cation. Fig. 7 shows the cation radii for first-row transition metals starting from manganese according to *Shannon & Prewitt*.[31,35] As shown in this figure, the radii of the cations, which have a coordination number (CN) of six, decrease from Mn (II) to Ni (II) and then increase (blue dotted line) for Cu (II) and Zn (II). However, this phenomenon was not observed in this study. Owing to the change in the coordination number for Cu (II) (CN = 5) and Zn (II) (CN = 4), the effective ion radii do not follow this trend. As concluded by *Shannon & Prewitt*, Cu (II) and Zn (II) cations exhibit a decreasing effective ion radius with a decrease in the coordination number. Therefore, the change in coordination, due to a decreased metal-ligand bond length, leads to a steady decrease in cation radii throughout the whole series of **4**–**9**.

Compound **10** (Fig. 8) crystallizes in the monoclinic space group $P2_1/n$ with eight formula units per cell and a calculated density of 1.67 g·cm^{-3}. Like in comparable ECCs,[9] the picrate anions coordinate. Therefore, the copper (II) cation in compound **10** is sixfold coordinated by two picrate anions and two molecules of **3**, forming a highly distorted square bipyramid. Ultimately, the deprotonated hydroxy groups and the 1,5-DMT ligands are positioned in the equatorial plane with bond lengths between 1.935 (3) Å (Cu1–O1) and 1.995 (3) Å (Cu1–N8). Additionally, the oxygen atoms of the two coordinating nitro groups are in axial position with bonds

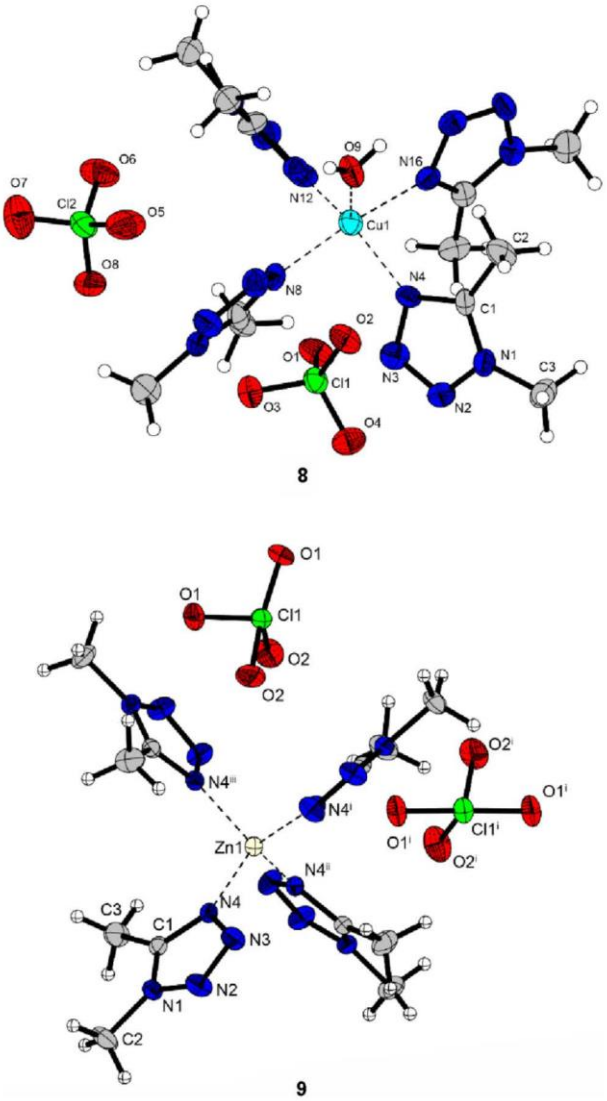


Fig. 6. Crystal structures of ECCs **8** and **9**, showing the coordination of the metal cation centers by 1,5-DMT. Selected bond lengths [Å]: Cu1–N4 1.995 (7), Cu1–N8 2.016 (7), Cu1–N12 1.991 (6), Cu1–N16 2.010 (7), Zn1–N4 1.990 (2).

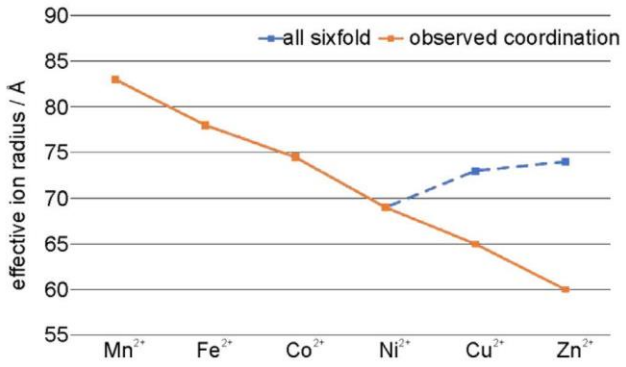


Fig. 7. Effective ion radii of first row transition metals from Mn (II) to Zn (II). The dotted blue line shows the effective ion radii for all sixfold coordination of the metal cations. The orange line shows the effective ion radii while considering their coordination numbers.

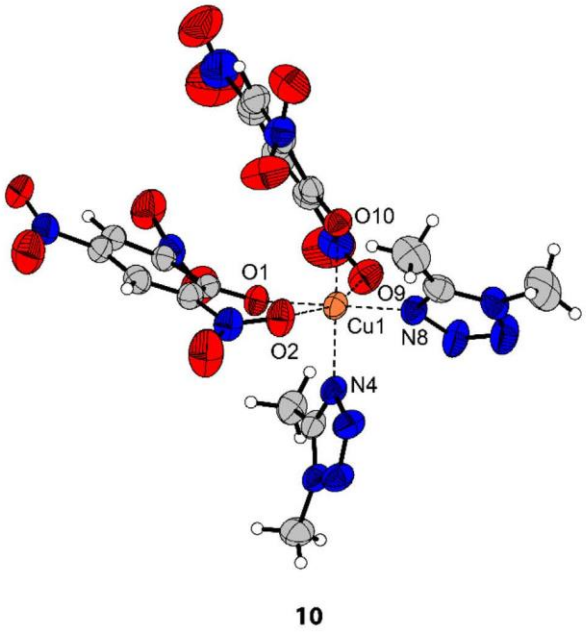


Fig. 8. Crystal structure of [Cu(PA)$_2$ (DMT)$_2$] (**10**), showing two coordination picrate anions and two 1,5-DMT ligands.

Cu1–O9 and Cu1–O8 with lengths of 2.372 (3) Å 2.420 (3), respectively. While the angles within the equatorial plane differ only marginally (0.781°) from a perfect 90°, the axial positions are bent by 17.015° from the perfect 180° due to the rigidity of the anions. Compound **11a** (Fig. 9) crystallizes in the triclinic space group *P*−1 with one formula unit per unit cell and a density of 1.65 g·cm^{-3}. Like in **10**, the copper (II) cation in compound **11a** is also sixfold coordinated. The deprotonated hydroxy groups and the nitrogen atoms of the 1,5-DMT ligands are positioned in an equatorial plane, and the oxygen atoms of the coordinating nitro groups are axially positioned. Like those in **10**, the bond lengths and angles of compound **11a** range between 1.941 Å (Cu1–O9) and 2.014 Å (Cu1–N4) within the equatorial plane and 2.286 Å (Cu1–O13) and 2.301 Å (Cu1–O3) at axial positions. Additionally, the axial positions are strongly bent by 17.5° from the perfect 180° also due to the high rigidity of the anions. Compound **12a** (Fig. 10) crystallizes in the monoclinic space group $P2_1/c$ with four formula units per cell and a calculated density of 1.77 g·cm^{-3}—the highest among all investigated compounds. Like in **10** and **11a**, the copper (II) cation in **12a** is sixfold coordinated by two molecules of **3**, two aqua ligands, and one deprotonated trinitro phloroglucinolate anion. Owing to the rigidity of the anion occupying two coordination sites, a strongly distorted square bipyramid is formed. Meanwhile, an equatorial plane is formed by the deprotonated hydroxy group, the two 1,5-DMT ligands, and one aqua ligand with bond lengths between 1.983 (1) Å (Cu1–O3) and 2.025 (1) Å (Cu1–O1). Unlike to **10** and **11a**, the bond lengths of the axially positioned atoms of **12a** are 2.210 (1) Å (Cu1–O2) and 2.433 (1) Å (Cu1–O7), ultimately distorting the bipyramid in its axial expansion. Interestingly, **12a** is the only nitroaromatic compound in which the 1,5-DMT ligands are in a *trans* position towards each other, while they are in a cis position in **10** and **11a**. Additionally, the axis O1–Cu1–O7 in **12a** is strongly bent to an angle of 168.65°, which is comparable to that of axes in **10** and **11a**. Compound **12b** (Fig. 11) crystallizes in the monoclinic space group $P2_1/n$ with four formula units per cell and a calculated density of 1.72 g·cm^{-3}. The copper (II) cation in **12b** is sixfold coordinated by two 1,5-DMT molecules and two deprotonated trinitro phloroglucinolate anions, which bridge two copper centers. While compound **12b** is free of water, the ligands form a distorted square bipyramid like in **12a**. Like all other nitroaromatic compounds (**10**, **11a**, and **12a**), the equatorial plane of **12b** is formed by the deprotonated hydroxy groups together with the 1,

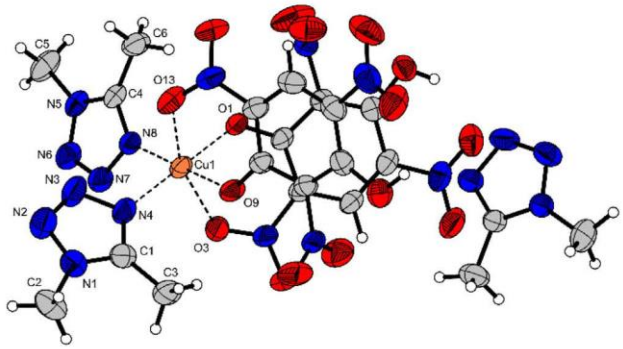


Fig. 9. Crystal structure of [Cu(HTNR)$_2$ (DMT)$_2$] • DMT (**11a**), showing two coordination picrate styphnate and two 1,5-DMT ligands with one co-crystallized 1,5-DMT molecule.

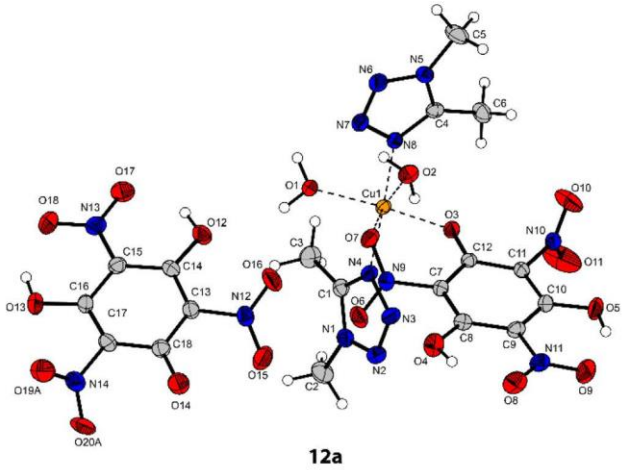


Fig. 10. Crystal structure of [Cu(H$_2$TNPG) (DMT)$_2$(H$_2$O)$_2$](H$_2$TNPG) (**12a**), showing one coordinating trinitro-phloroglucinolate anion, two 1,5-DMT, and two aqua ligands coordinating the copper (II) cation.

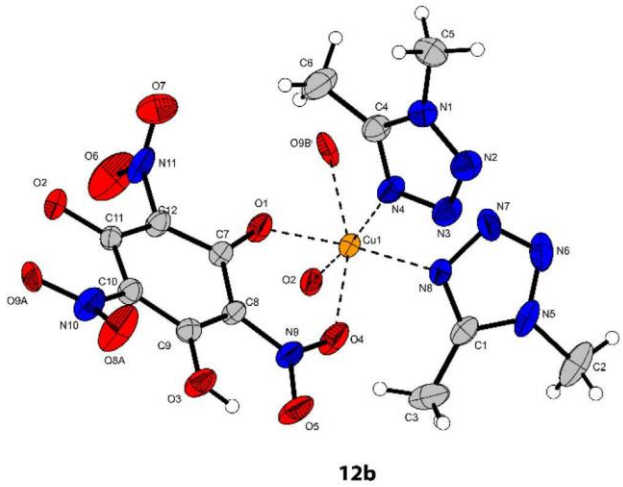


Fig. 11. Crystal structure of [Cu(HTNPG)$_2$ (DMT)$_2$] (**12b**), showing two coordination trinitro-phloroglucinolate anions and two 1,5-DMT ligands. The anions bridge two copper (II) centers.

5-DMT ligands, with bond lengths between 1.922 (2) Å (Cu1–O1) and 2.007 (2) Å (Cu1–N4) and minor angle deviations (<2.5°) from the ideal 90°. The axial positions of **12b** are also coordinated by the nitro groups of the anions, with different bond lengths (2.249 Å (Cu1–O4) and 2.407 (3) Å (Cu1–O9B)) and an angle deviation of 18.5° from the perfect 180°—the highest distortion of the ideal axis observed in this study.

2.3. Infrared spectroscopy

The infrared spectra of compounds obtained as single crystals are depicted in Fig. 12 (**3**), Fig. 13 (**4**, **8**, and **9**), and S7 (**10**, **11b**, and **12b**). The spectra of the obtained ECCs pure samples were recorded according to the initially conducted elemental analysis. The IR spectra of batches produced later were compared to those of the pure batch. They were used without further purification if consensus was above 98%. The spectrum of pure compound **3** shows asymmetric stretching vibration of the methyl groups at 2960 cm^{-1}. The broad range of 3500–3000 cm^{-1} was derived from small amounts of residual water. Additionally, strong bands at 1097, 728 cm^{-1} and 657 cm^{-1} can be attributed to the deformation vibrations of the tetrazole ring.

Fig. 13 depicts the IR spectra of the obtained perchlorate containing ECCs **4**, **8**, and **9**. Compound **4** shows a weak band at 2968 cm^{-1}, attributing to the asymmetric stretching vibration of the methyl groups that are slightly shifted due to coordination compared to pure **3**. The deformation vibrations of the tetrazole rings are represented by the IR bands at 729 cm^{-1} and 663 cm^{-1}. The characteristic bands of the perchlorate anions are observed at 1079 cm^{-1} and 622 cm^{-1}, which greatly agrees with the published values of non-coordinating perchlorate anions (1100 cm^{-1} and 600–700 cm^{-1}).[36] These bands are slightly split, indicating weak hydrogen bonds between the anions and the 1,5-DMT ligands. Compounds **8** and **9** have no characteristic bands of methyl groups due to a very weak IR activity, as was already observed in pure compound **3**. Both compounds exhibit strong bands for the deformation vibrations of the tetrazole rings and the perchlorate anions, with the same range as **4**. Additionally, ECC **8** shows a broadened band with a maximum of 3421 cm^{-1}, corresponding to the vibration of the aqua ligand. Owing to the substantial overlap of bands between the ligands and the nitroaromatic anions (Fig. S7) in the fingerprint regions below 1500 cm^{-1} for compounds **10**, **11b**, and **12b**, the assignment of characteristic vibrations is quite elaborate and is not necessary for this study.

2.4. Thermal behavior and sensitivities

The physiochemical properties of **3** and the complexes obtained as bulk materials are summarized in Table 1. The reported melting point of **3** at 73 °C[37] was confirmed through DTA measurements. A second endothermic event occurred at 298 °C, which was identified as the boiling point of **3** (Fig. 14). The conducted TGA measurement showed a

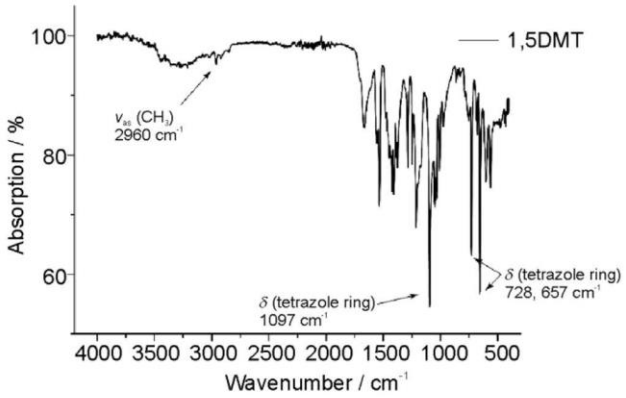


Fig. 12. IR spectrum of pure 1,5-dimethyltetrazole (**3**).

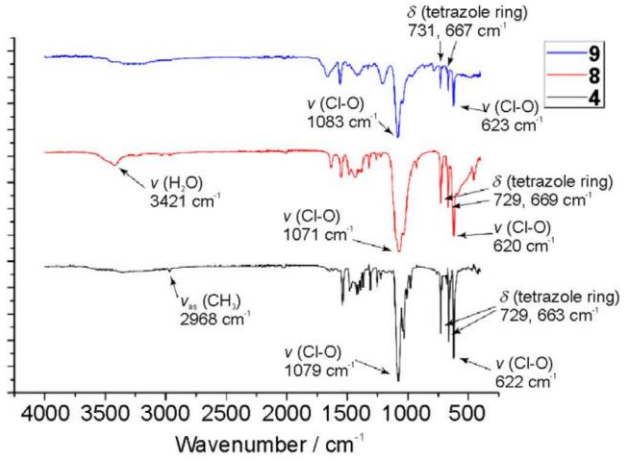


Fig. 13. IR spectra of ECCs **4**, **8**, and **9**.

Table 1
Sensitivities and thermal behavior of compounds **4**, **8**, **9**, and **10**–**12**.

Compound	IS[a]/J	FS[b]/N	$T_{endo.}$[c]/°C	$T_{exo.}$[d]/°C
3	>40	>360	73	>293
4	10	>360	171	307
8	3	128	106	226
9	2	180	293	321
10	8	>360	–	250
11b	2	>360	–	184
12b	2	360	–	192

[a] Impact sensitivity according to the BAM drop hammer[43] (method 1 of 6).
[b] Friction sensitivity according to the BAM friction tester[43] (method 1 of 6).
[c] Temperature of endothermic events (onset temperatures at a heating rate of 5 °C·min^{-1}).
[d] Temperature of decomposition indicated by exothermic event according to DTA (onset temperatures at a heating rate of 5 °C·min^{-1}).

mass loss of 96.8% between 100 °C and 214 °C, which is related to the slow evaporation of **3** already starting at 100 °C, suggesting high vapor pressure of **3** when melting. An exothermic decomposition was not observed in **3**. Therefore, the thermal stability of 1,5-DMT is presumably above 293 °C.

The thermal behavior of ECCs **4**, **8**, **9**, **10**, **11b**, and **12b** were investigated through DTA measurements at a heating rate of $\beta = 5$ °C·min^{-1} (Fig. 15). As shown by DTA and TGA measurements, an endothermic

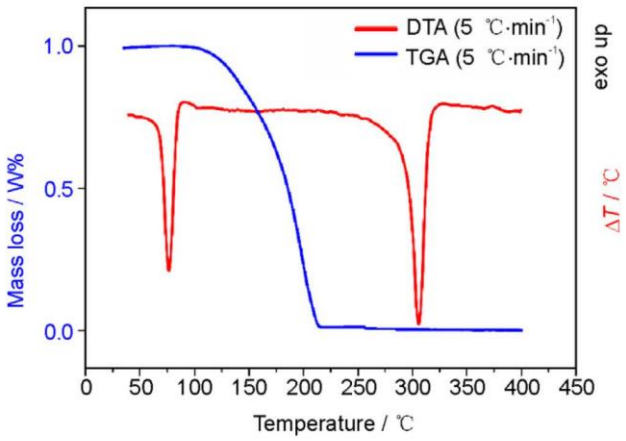


Fig. 14. DTA (red) and TGA (blue) analyses of 1,5-DMT (**3**) at a heating rate of 5 °C·min^{-1}.

event was observed in compound **4** at 171 °C as a loss of ligands (weight loss: 38.8 wt%; Fig. 15), while an endothermic event was observed in **8** at 106 °C, corresponding to a loss of aqua ligands (weight loss: 2.68 wt%). Moreover, compound **9** showed an endothermic event at 292 °C, shortly followed by an exothermic event starting at 321 °C, exhibiting the highest stability observed in this study. The conducted TGA measurement (Fig. 15) did not show weight loss until 293 °C. Therefore, the endothermic peak of the DTA measurement corresponded to the decomposition temperature of **9**, which is extraordinarily high for ECCs.[38–41] As the same behavior of an endothermic event immediately evolved into an exothermic event during the DTA measurements of **10** and **11b**, no further TGA measurement was conducted for these two compounds. Additionally, since no thermal event was observed prior to the exothermic decomposition of compound **12b**, no TGA analysis was conducted. Generally, compound **10** showed a very high thermal stability of 250 °C, while **11b** and **12b** showed drastically lower yet adequate thermal stabilities of 184 °C (**11b**) and 192 °C (**12b**). Although the direct influence of anions on thermal stability cannot be deduced, the perchlorate containing ECCs (**4**, **8**, and **9**) exhibited their exothermic decomposition reaction at higher temperatures than those containing nitroaromatic anions. Indeed, it must be kept in mind that compounds **4** and **8** exhibited endothermic decompositions due to the loss of ligands before any exothermic event happened. Furthermore, the measured thermal stabilities of nitroaromatic ECCs **10**–**12b** do not allow the deduction of the direct influence of nitroaromatic anions compared to each other. Nonetheless, they agree well with previously reported ECCs,[9] which also have no direct influence of anions on thermal stabilities. According to BAM standards, the sensitivities of the compounds to impact and friction have been determined and classified according to the UN recommendations on the transport of dangerous goods.[42] Accordingly, it was determined that **3** was completely insensitive to mechanical stimuli (>40 J, > 360 N), ECCs **4**, **10**, **11b**, and **12b** were not sensitive to friction, while **5** and **6** were slightly sensitive to friction, with friction sensitivity (FS) of 128 N and 180 N, respectively. All compounds were sensitive to impact, with **4** (10 J) and **10** (8 J) showing lower impact sensitivities than **8** (3 J), **9** (3 J), **11b** (2 J), and **12b** (2 J). Therefore, ECCs **8**, **9**, **11b**, and **12b** exhibited impact sensitivities in the range of a primary explosive, whereas **4** and **10** exhibited sensitivities as typical secondary explosives, such as hexogen.[24] Although the direct influence of anions on thermal stability could not be previously deduced, their influence can be determined by comparing sensitivities. Even though the differences in sensitivities between nitroaromatic compounds are not as prominent as those between other ligand systems,[8,33] compound **10**, which incorporated the picrate anions, exhibited the lowest sensitivities, followed by compounds **11b** and **12b**. Generally, the increasing number of hydroxy functionalities from picrate to trinitrophloroglucinate also increases the sensitivities to impact and friction. Furthermore, the sensitivities of the perchlorate-containing ECCs (**4**, **8**, and **9**) are higher than those of the nitroaromatic compounds, yet they are still moderately sensitive at least to friction. Owing to their poor crystallizability, enough compounds **5**, **6**, and **7** could not be obtained. Therefore, their thermal and energetic behavior was not explored. To further investigate the energetic properties, hot plate (HP) and hot needle (HN) tests of compounds **4** and **9** were performed (Fig. 16). HP tests were conducted to determine the performance of the samples under fast heating on a copper plate, during which both compounds showed deflagration without detonation. While HP tests do not necessarily allow any conclusions on the compound's capability as a primary explosive, the HN tests can be used to correlate deflagration with the detonation transition (DDT) capability of a compound. Therefore, HN tests were performed by fixing the sample underneath adhesive tape on a copper plate, followed by penetration with a red heated needle. A compound possesses rapid DDT if detonation occurs, which was not the case for the tested compounds.

Interestingly, there is a reported energetic coordination compound based on copper (II) perchlorate with 1-ethyl-5-tetrazole (1-ETZ) as ligand.[4] Given that 1,5-DMT and 1-ETZ are structural isomers and have

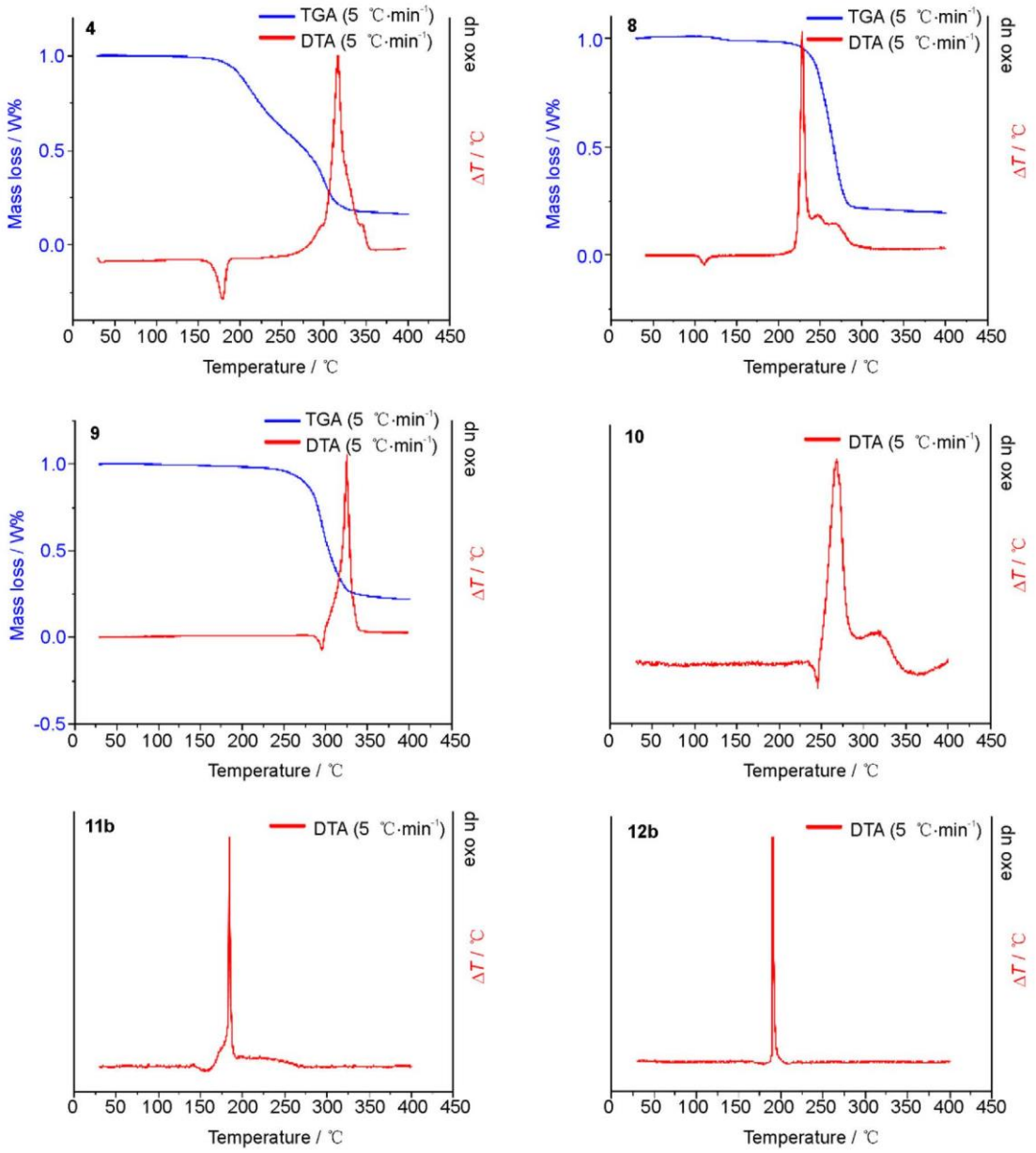


Fig. 15. Combined DTA and TGA measurements of ECCs **4**, **8**, and **9** and DTA of ECCs **10**, **11b**, and **12b** at a heating rate of 5 °C·min^{-1}.

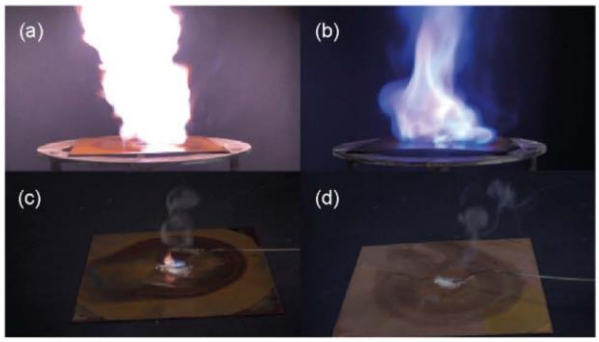


Fig. 16. HP and HN tests of compounds **4** and **9**. **a**: HP test of **4**; **b**: HP test of **9**; **c**: HN test of **1**; **d**: HN test of **6**.

the same empirical formula of $C_3H_6N_4$, it seems reasonable to compare both compounds as ligands. This, unfortunately, was impossible in this study since no isomeric complexes were obtained. All reported coordination compounds with 1-ETZ as ligand exhibit octahedral coordination of the copper (II) cation, whereas the obtained copper (II) complex displayed different coordination in this study. This results from higher steric demand of **3** compared to 1-ETZ. Specifically, the ethyl functionalization can easily minimize steric repulsion by rotation of the C–C bond for **3**, which is impossible for 1,5-DMT. Besides their coordinative behavior, the major difference between both compounds is their thermal behavior. 1-ETZ is a liquid at room temperature with thermal stability of up to 208 °C. Therefore, it is by far inferior to **3** in terms of thermal stability. This is also accompanied by a slight decrease in enthalpy of formation of **3** (184.1 kJ·mol^{-1}) compared to 1-ETZ (224.1 kJ·mol^{-1}). Thereby, higher stability of the resulting ECCs can be assumed.

3. Conclusion

1,5-DMT (**3**) was synthesized using a three-step procedure starting with acetone and hydroxylamine. This route was observed to be more economical than the one-step synthesis using TMS-N_3. 1,5-DMT (**3**) was fully characterized as a completely insensitive (>360 N, > 40 J) and highly thermally stable (>293 °C) compound with an astonishing high positive HOF of 184.1 kJ·mol^{-1}. Therefore, **3** was applied as a nitrogen-rich (N = 57.1%) ligand to 11 new energetic coordination compounds of the $3d^5$–$3d^{10}$ metal (e.g., Mn, Fe, Co, Ni, Cu, Zn) perchlorate salts. The change from a sixfold (**4**, **5**) to a fourfold (**9**) coordination of the central metal cation was observed. This change was caused by a decreasing metal-ligand bond length throughout the first-row transition metals, which decreased the coordination number and ultimately led to steadily decreasing cation radii. The additional increase in steric repulsion of the ligands favors the decrease in the coordination number, supporting the change in coordination. All measured ECCs exhibited exothermic decomposition events above 184 °C (**11b**). For compound **9**, an extraordinarily high decomposition temperature of 293 °C was measured, representing the highest thermal stability investigated in this study. Hot plate tests of the most promising compounds showed a complete decomposition without detonation, while the hot needle tests indicated that none of the compounds can be classified as applicable primary explosives since no rapid DDT was observed. However, the compounds are ideal candidates for burning rate catalysts in propellant charges due to their simple and cheap syntheses and great stability.

4. Experimental section

Acetone Oxime (1): Sodium carbonate (28.6 g, 0.27 mol) was added to a solution of hydroxyl ammonium chloride (15.6 g, 0.23 mol) and acetone (8.7 g, 0.15 mol) in water (300 mL). The mixture was stirred for 40 h at room temperature, and the residue was extracted with diethyl ether (4 × 100 mL). After washing with a saturated sodium chloride solution and drying over sodium sulfate, the solvent was removed under reduced pressure, and acetone oxime (7.7 g, 0.11 mol, 70%) was obtained as a colorless solid.

^{1}H NMR (400 MHz, $CDCl_3$): $\delta = 1.89$ (3H, CH_3), 1.90 (3H, CH_3), 7.77 (1H, O*H*); ^{13}C NMR (101 MHz, $CDCl_3$): $\delta = 14.8$, 21.9, 155.9.

Acetoxime Benzenesulfonate (2): Acetone oxime (6 g, 0.08 mol) was dissolved in pyridine (6.5 mL, 0.08 mol), and water (16 mL) and benzene sulfonyl chloride (10.2 mL, 0.08 mol) was added dropwise with the temperature kept at 15–20 °C. A colorless solid precipitated, and the suspension was cooled to 10 °C. After filtration and washing with cold water, the solid was dried, yielding acetoxime benzenesulfonate in quantitative amounts.

^{1}H NMR (400 MHz, CDCl3)δ: 1.93 (3H, CH_3), 1.98 (3H, CH_3), 7.54 (2H, C*H*(3, 5)), 7.65 (1H, C*H*(4)), 7.97 (2H, CH(2, 6)); ^{13}C NMR (101 MHz, $CDCl_3$)δ: 17.1 (*C*H_3), 21.8 (*C*H_3), 128.9 (2 *C*H), 129.0 (2 *C*H), 133.9 (*C*H), 165.2 (H_3CC(N)CH_3).

1,5-Dimethyltetrazole (3): Sodium azide (4.6 g, 0.07 mol) was dissolved in water (15 mL) and was added to a solution of acetoxime benzenesulfonate (15 g, 0.07 mol) in methanol (60 mL). The mixture was stirred for 1 h at 45 °C and later for 1.5 h at 60 °C. The solvent was removed under reduced pressure and the residue was extracted with hot benzene (4 × 30 mL). After evaporation of the solvent, 1,5-dimethyltetrazole (3.3 g, 0.033 mol, 48%) was obtained as a colorless solid. Recrystallization from water yields **3** as colorless block-shaped crystals.

DTA (5 °C·min^{-1}) onset: 73 °C (T_{endo}), 298 °C (T_{endo}); ^{1}H NMR (400 MHz, DMSO-d_6)δ: 2.49 (3H, CH_3), 3.96 (3H, CH_3); ^{13}C NMR (101 MHz, DMSO-d_6)δ: 8.1 (CCH_3), 33.2 (NCH_3), 152.4 (N_4C); IR: ($\tilde{\nu}$/cm^{-1}) (rel. int.) = 2961 (w), 1655 (w), 1533 (s), 1481 (m), 1451 (m), 1436 (m), 1423 (m), 1409 (m), 1386 (m), 1380 (m), 1374 (m), 1285 (m), 1248 (m), 1212 (m), 1097 (s), 1048 (m), 1034 (m), 1008 (m), 976 (w), 728 (s), 678 (w), 657 (vs), 605 (w), 565 (w).

Alternatively, acetone (1 g, 17 mmol, 1 eq.) was mixed with trimethylsilyl azide (5.87 g, 51 mmol, 3 eq.) and tin (II)chloride (0.322 g, 1.7 mmol, 0.1 eq.) and were stirred at 55 °C for 20 h. Extraction with benzene followed by evaporation yielded 1,5-dimethyltetrazole (0.66 g, 7.14 mmol, 42%) as a white solid.

^{1}H NMR (400 MHz, DMSO-d_6)δ: 2.49 (3H, CH_3), 3.96 (3H, CH_3); ^{13}C NMR (101 MHz, DMSO-d_6)δ: 8.1 (CCH_3), 33.3 (NCH_3), 152.4 (N_4C).

General procedure for the preparation of complexes **4–9**:

Stoichiometric amounts of the corresponding metal (II) perchlorate and **3** were individually dissolved in water, combined, and stirred for a short period at elevated temperatures. The product was obtained after crystallization at ambient conditions.

[Mn(DMT)$_6$](ClO$_4$)$_2$ (4): Compound **4** was isolated as a colorless crystalline precipitate.

DTA (5 °C·min^{-1}) onset: 171 °C (T_{endo}), 307 °C (T_{exo}); IR (ATR, $\tilde{\nu}$/cm^{-1}): 3346 (vw), 1540 (m), 1481 (w), 1408 (w), 1390 (m), 1370 (m), 1311 (w), 1254 (w), 1224 (w), 1079 (s), 1033 (s), 1009 (m), 979 (w), 729 (m), 678 (s), 663 (s), 622 (s); Elemental Analysis calcd. [%] for $C_{18}H_{36}Cl_2MnN_{24}O_8$ (842.48): C 25.66, H 4.31, N 39.90; found: C 25.31, H 4.09, N 38.93; BAM drop hammer: 10 J; BAM friction tester: >360 N.

[Fe(DMT)$_6$](ClO$_4$)$_2$ (5): Compound **5** was obtained as a brown glass-like solid. Crystals suitable for X-ray determination were obtained by subjecting a small amount to a high vacuum for several days.

[Co(H$_2$O)$_2$(DMT)$_4$](DMT)(H$_2$O)(ClO$_4$)$_2$ (6): Out of the oily red product, crystals suitable for X-ray determination of complex **6** were obtained. Owing to its consistency, only X-ray determination was possible.

[Ni(DMT)$_4$(H$_2$O)$_2$](DMT)$_2$(H$_2$O)$_2$(ClO$_4$)$_2$ (7):

Inhomogeneous solids were formed after evaporation of the solvent. From these inhomogeneous solids, small crystals of 7 suitable for X-ray determination were picked using a light microscope.

[Cu(H$_2$O)(DMT)$_4$](ClO$_4$)$_2$ (8): Complex **8** crystallized as deep blue needles suitable for X-ray determination.

DTA (5 °C·min^{-1}) onset: 106 °C (loss of water), 226 °C (T_{exo}); IR (ATR, $\tilde{\nu}$/cm^{-1}): 3425 (w), 1554 (w), 1434 (w), 1070 (s), 727 (m), 668 (m), 619 (s); Elemental Analysis calcd. [%] for $C_{12}H_{26}Cl_2CuN_{16}O_{10}$ (672.89): C 21.42, H 3.69, N 33.31; found: C 21.50, H 3.74, N 33.32; BAM drop hammer: 3 J; friction tester: 128 N.

[Zn(DMT)$_4$](ClO$_4$)$_2$ (9): Complex **9** was obtained as colorless crystals suitable for X-ray determination.

DTA (5 °C·min^{-1}) onset: 293 °C (T_{endo}), 321 °C (T_{exo}); IR (ATR, $\tilde{\nu}$/cm^{-1}): 1561 (w), 1500 (w), 1331 (w), 1265 (w), 1084 (s), 1042 (m), 731 (m), 678 (w), 666 (m), 623 (s); Elemental Analysis calcd. [%] for $C_{12}H_{24}Cl_2ZnN_{16}O_8$ (656.71): C 21.95, H 3.68, N 34.13; found: C 21.84, H 3.46, N 33.88; BAM drop hammer: 2 J; friction tester: 180 N).

[Cu(PA)$_2$(DMT)$_2$] (10): Basic copper (II) carbonate (50 mg, 226 mmol) was suspended in water (10 mL), and picric acid (104 mg, 452 mmol) was added. The mixture was stirred until all solids were dissolved and **3** (44 mg, 452 mmol) was added. After stirring for 5 min at 80 °C, the solution was left to crystallize. Compound **10** was obtained as green needles with a high yield (268 mg, 375 mmol, 83%).

DTA (5 °C·min^{-1}) onset: 250 °C ($T_{exo.}$); IR (ATR, $\tilde{\nu}$/cm^{-1}): 3087 (w), 1741 (w), 1616 (s), 1612 (s), 1576 (s), 1533 (s), 1507 (s), 1480 (s), 1418 (s), 1361 (s), 1326 (vs), 1269 (vs), 1168 (s), 1110 (m), 1083 (m), 1047 (m), 941 (m), 916 (s), 846 (w), 824 (w), 785 (m), 743 (m), 728 (m), 704 (vs), 679 (m), 666 (s), 551 (m), 517 (m), 455 (w), 428 (w), 416 (w); Elemental Analysis calcd. [%] for $C_{18}H_{16}CuN_{14}O_{14}$ (715.96): C 30.20, H 2.25, N 27.39; found: C 30.31, H 2.25, N 27.58; BAM drop hammer: 8 J; BAM friction tester: >360 N.

[Cu(HTNR)$_2$(DMT)$_2$] (11b): Basic copper (II) carbonate (50 mg, 226 mmol) was suspended in water (10 mL), and trinitro resorcinol (110 mg, 452 mmol) was added. The solution was heated to 80 °C and **3** (44 mg, 452 mmol) was added. After stirring for 5 min at 80 °C, the formed precipitate of **11b** was filtered out with a high yield (267 mg, 357 mmol, 79%). The remaining solution was left to crystallize for several days, from

which a few crystals of **11a** were obtained.

DTA (5 °C·min $^{-1}$) onset: 184 °C (T_{exo}); IR (ATR, $\tilde{\nu}$/cm $^{-1}$): 3096 (w), 1628 (s), 1561 (s), 1535 (s), 1528 (s), 1476 (s), 1453 (s), 1377 (s), 1353 (s), 1319 (s), 1284 (vs), 1194 (s), 1175 (s), 1088 (s), 1049 (s), 930 (s), 828 (w), 781 (m), 762 (m), 727 (s), 713 (s), 698 (s), 681 (s), 666 (s), 641 (m), 543 (m), 462 (w), 427 (m), 417 (m); Elemental Analysis calcd. [%] for $C_{18}H_{16}CuN_{14}O_{16}$ (747.95): C 28.91, H 2.16, N 26.22; found: C 28.79, H 2.27, N 28.76; BAM drop hammer: 2 J; BAM friction tester: >360 N.

[Cu(HTNPG) (DMT)$_2$] (12b): Basic copper (II) carbonate (50 mg, 226 mmol) was suspended in water (10 mL), and trinitro phloroglucinol (118 mg, 452 mmol) were added. The solution was heated to 80 °C and **3** (44 mg, 452 mmol) was added. After stirring for 5 min at 80 °C, the solution was left standing to crystallize. After 1–2 d, crystals in the form of needles (**12a**) and blocks (**12b**) started to form. The initially formed **12a** started to be consumed as blocks of **12b** continued to grow. After 3–4 d, crystals of **12b** were the main product of crystallization and then were filtered out and dried. **12b** was obtained as dark blocks with a high yield (197 mg, 379 mmol, 84%).

DTA (5 °C·min $^{-1}$) onset: 192 °C (T_{exo}); IR (ATR, $\tilde{\nu}$/cm $^{-1}$): 1736 (w), 1588 (s), 1538 (s), 1520 (vs), 1486 (s), 1455 (s), 1399 (s), 1345 (s), 1284 (vs), 1255 (vs), 1192 (s), 1175 (s), 1158 (s), 1134 (vs), 1109 (s), 1048 (s), 1027 (m), 929 (s), 837 (m), 825 (m), 806 (m), 792 (s), 708 (vs), 681 (s), 665 (vs), 642 (s), 456 (m), 434 (s), 413 (s), 408 (s); Elemental Analysis calcd. [%] for $C_{12}H_{13}CuN_{11}O_9$ (518.85): C 27.78, H 2.53, N 29.70; found: C 27.47, H 2.53, N 28.42; BAM drop hammer: 2 J; BAM friction tester: 360 N.

Declaration of competing interest

The authors declare that they have no known competing financial interests or personal relationships that could have appeared to influence the work reported in this paper.

Acknowledgements

This work was funded by the Ludwig Maximilian University of Munich (LMU), the Office of Naval Research (ONR) under Grant No. ONR. N00014-16-1-2062. The authors would like to thank Stefan Huber for sensitivity measurements.

Appendix A. Supplementary data

Supplementary data to this article can be found online at https://doi.org/10.1016/j.enmf.2022.07.004.

References

1. Pritchard R, Kilner CA, Barrett SA, Halcrow MA. Two new 4,4′-disubstituted dipyrazolylpyridine derivatives, and the structures and spin states of their iron(II) complexes. *Inorg Chim Acta*. 2009;362:4365 4371.
2. Mohammed R, Chastanet G, Tuna F, et al. Synthesis of 2,6-Di(pyrazol-1-yl)pyrazine derivatives and the spin-state behavior of their iron(II) complexes. *Eur J Inorg Chem*. 2013;2013:819 831.
3. Cook TR, Zheng YR, Stang PJ. Metal organic frameworks and self-assembled supramolecular coordination complexes: comparing and contrasting the design, synthesis, and functionality of metal organic materials. *Chem Rev*. 2013;113: 734 777.
4. Wurzenberger MHH, Gruhne MS, Lommel M, Szimhardt N, Klapötke TM, Stierstorfer J. Comparison of 1-ethyl-5*H*-tetrazole and 1-azidoethyl-5*H*-tetrazole as ligands in energetic transition metal complexes. *Chem Asian J*. 2019;14:2018 2028.
5. Titi HM, Marrett JM, Dayaker G, et al. Hypergolic zeolitic imidazolate frameworks (ZIFs) as next-generation solid fuels: unlocking the latent energetic behavior of ZIFs. *Sci Adv*. 2019;5, eaav9044.
6. Wang QY, Wang J, Wang S, et al. *o*-Carborane-Based and atomically precise metal clusters as hypergolic materials. *J Am Chem Soc*. 2020;142:12010 12014.
7. Wang C, Wang YJ, He CL, Wang QY, Zang SQ. Assembling silver cluster-based organic frameworks for higher-performance hypergolic properties. *JACS Au*. 2021;1: 2202 2207.
8. Wurzenberger MHH, Gruhne MS, Lommel M, Braun V, Szimhardt N, Stierstorfer J. Taming the dragon: complexation of silver fulminate with nitrogen-rich azole ligands. *Inorg Chem*. 2020;59:17875 17879.
9. Wurzenberger MHH, Bissinger BRG, Lommel M, Gruhne MS, Szimhardt N, Stierstorfer J. Synthesis and comparison of copper(ii) complexes with various N-aminotetrazole ligands involving trinitrophenol anions. *New J Chem*. 2019;43: 18193 18202.
10. Wilbrand J. Notiz über Trinitrotoluol. *Justus Liebigs Ann Chem*. 1863;128:178 179.
11. Klapötke TM. *Chemistry of High-Energy Materials*. fifth ed. Berlin/Boston: De Gruyter; 2019.
12. Simpson RL, Urtiew PA, Ornellas DL, Moody GL, Scribner KJ, Hoffman DM. CL-20 performance exceeds that of HMX and its sensitivity is moderate. *Propellants, Explos Pyrotech*. 1997;22:249 255.
13. Verkhozina ON, Kizhnyaev VN, Vereshchagin LI, Rokhin AV, Smirnov AI. Synthesis of polynuclear nonfused azoles. *Russ J Org Chem*. 2003;39:1792 1796.
14. Kumar D, Tang Y, He C, Imler GH, Parrish DA, Shreeve JnM. Multipurpose energetic materials by shuffling nitro groups on a 3,3′-bipyrazole moiety. *Chem Eur J*. 2018;24: 17220 17224.
15. Gettings ML, Thoenen MT, Byrd EFC, Sabatini JJ, Zeller M, Piercey DG. Tetrazole azasydnone ($C_2N_7O_2H$) and its salts: high-performing zwitterionic energetic materials containing A unique explosophore. *Chem Eur J*. 2020;26:14530 14535.
16. Wozniak DR, Zeller M, Byrd EC, Piercey DG. An improved synthesis of bromotetrazole. *Z Anorg Allg Chem*. 2022;648, e202100333.
17. Szimhardt N, Wurzenberger MHH, Zeisel L, Gruhne MS, Lommel M, Stierstorfer J. Maximization of the energy capability level in transition metal complexes through application of 1-amino- and 2-amino-5*H*-tetrazole ligands. *J Mater Chem*. 2018;6: 16257 16272.
18. Klapötke TM, Kofen M, Schmidt L, Stierstorfer J, Wurzenberger MHH. Selective synthesis and characterization of the highly energetic materials 1-hydroxy-5*H*-tetrazole (CHN_4O), its anion 1-oxido-5*H*-tetrazolate (CN_4O^-) and bis(1-hydroxytetrazol-5-yl)triazene. *Chem Asian J*. 2021;16:3001 3012.
19. Wurzenberger MHH, Endraß SMJ, Lommel M, Klapötke TM, Stierstorfer J. Comparison of 1-propyl-5*H*-tetrazole and 1-azidopropyl-5*H*-tetrazole as ligands for laser ignitable energetic materials. *ACS Appl Energy Mater*. 2020;3:3798 3806.
20. Fronabarger J, Schuman A, Chapman R, Fleming W, Sanborn W, Massis T. Chemistry and development of BNCP, a novel DDT explosive (deflagration-to-detonation). In: *31st Joint Propulsion Conference and Exhibit*. AIAA; July, 1995.
21. Moderhack D, Noreiks M. *Tetrazolium N-Aminides. Heterocycles*. 2004;63:2605 2614.
22. Klapötke TM, Piercey DG, Stierstorfer J. The 1,4,5-triaminotetrazolium cation ($CN_7H_6^+$): a highly nitrogen-rich moiety. *Eur J Inorg Chem*. 2012;2012:5694 5700.
23. Sharon P, Afri M, Mitlin S, et al. Preparation and characterization of bis(guanidinium) and bis(aminotetrazolium)dodecahydroborate salts: green high energy nitrogen and boron rich compounds. *Polyhedron*. 2019;157:71 89.
24. Klapötke TM. *Energetic Materials Encyclopedia*. second ed. Berlin/Boston: De Gruyter; 2021.
25. Fischer N, Fischer D, Klapötke TM, Piercey DG, Stierstorfer J. Pushing the limits of energetic materials the synthesis and characterization of dihydroxylammonium 5,5′-bistetrazole-1,1′-diolate. *J Mater Chem*. 2012;22:20418 20422.
26. Klapötke TM, Stierstorfer J. The CN_7^- anion. *J Am Chem Soc*. 2009;131:1122 1134.
27. Langhals H, Range G, Wistuba E, Rüchardt C. Alkylwanderungen bei Sextettumlagerungen. *Chem Ber*. 1981;114:3813 3830.
28. Kamuf M, Rominger F, Trapp O. Investigation of the rearrangement in alkyl-bridged bis(carbamoyldiaziridine) derivatives. *Eur J Org Chem*. 2012;2012:4733 4739.
29. Knoll AG, Reich Deutsches. *Verfahren zur Darstellung von Tetrazolen*. 1926.
30. El-Ahl AAS, Elmorsy SS, Soliman H, Amer FA. A facile and convenient synthesis of substituted tetrazole derivatives from ketones or α,β-unsaturated ketones. *Tetrahedron Lett*. 1995;36:7337 7340.
31. Shannon R. Revised effective ionic radii and systematic studies of interatomic distances in halides and chalcogenides. *Acta Crystallogr A*. 1976;32:751 767.
32. Braun V, Wurzenberger MHH, Weippert V, Stierstorfer J. Tailoring the properties of 3d transition metal complexes with different N-cycloalkyl-substituted tetrazoles. *New J Chem*. 2021;45:11042 11050.
33. Kofen M, Lommel M, Wurzenberger MHH, Klapötke TM, Stierstorfer J. 1-(Azidomethyl)-5*H*-tetrazole a powerful new ligand for highly energetic coordination compounds. *Chem Eur J*. 2022, e202200492.
34. Frank P, Benfatto M, Szilagyi RK, D'Angelo P, Della Longa S, Hodgson KO. The solution structure of $[Cu(aq)]^{2+}$ and its implications for rack-induced bonding in blue copper protein active sites. *Inorg Chem*. 2005;44:1922 1933.
35. Shannon RD, Prewitt CT. Effective ionic radii in oxides and fluorides. *Acta Crystallogr B*. 1969;25:925 946.
36. Lewis DL, Estes ED, Hodgson DJ. The infrared spectra of coordinated perchlorates. *J Mol Struct*. 1975;5:67 74.
37. Xie A, Zhang Q, Liu Y, Feng L, Hu X, Dong W. An environmentally friendly method for N-methylation of 5-substituted 1*H*-tetrazoles with a green methylating reagent: dimethyl carbonate. *J Heterocycl Chem*. 2015;52:1483 1487.
38. Szimhardt N, Gruhne MS, Lommel M, et al. 2,2-Bis(5-tetrazolyl)propane as ligand in energetic 3d transition metal complexes. *Z Anorg Allg Chem*. 2019;645:354 361.
39. Szimhardt N, Stierstorfer J. Methylsemicarbazide as a ligand in late 3d transition metal complexes. *Chem Eur J*. 2018;24:2687 2698.
40. Szimhardt N, Wurzenberger MHH, Klapötke TM, et al. Highly functional energetic complexes: stability tuning through coordination diversity of isomeric propyl-linked ditetrazoles. *J Mater Chem*. 2018;6:6565 6577.
41. Joas M, Klapötke TM, Szimhardt N. Photosensitive metal(II) perchlorates with 1,2-Bis[5-(1-methylhydrazinyl)tetrazol-1-yl]ethane as ligand: synthesis, characterization and laser ignition. *Eur J Inorg Chem*. 2014;2014:493 498.
42. UN. *In Recommendations on the Transport of Dangerous Goods: Model Regulations*. nineteenth ed. 2015. New York.
43. BAM (accessed April 2022) http://www.bam.de.



Moritz Kofen began studying chemistry at LMU in 2012 and joined the Group of Prof. Klapötke in 2018 for his master thesis on "Synthesis and Characterization of New Energetic Compounds Based on 1-Hydroxytetrazole". He obtained his Master's degree in 2019 and continued working in the Klapötke group for his Ph.D. His current research includes the synthesis and characterization of primary explosives, focusing on new highly energetic substituted tetrazoles as ligands in energetic coordination compounds. Orcid.org/0000-0001-8522-2582; Email: mokoch@cup.uni-muenchen.de



Jörg Stierstorfer began studying chemistry at LMU in 2000 and joined the group of Prof. Klapötke in 2006 after his post- and undergraduate studies. He obtained his Ph.D. in Chemistry in 2009 with his Ph.D. thesis about "Advanced Energetic Materials based on 5-Aminotetrazole – Synthesis, Characterization, Scale-up, and Testing." After his post-doc at the LMU and the University of Maryland, USA, he continued his work in the Klapötke group in 2010. In 2017 he started his habilitation in chemistry with his research focusing on the synthesis, characterization, and application of energetic coordination compounds as primary explosives. As of 2018, he is the managing director of the EMTO Ltd., which he founded together with Prof. Thomas Klapötke. Orcid.org/0000-0002-2105-1275; Email: jst@cup.uni-muenchen.de

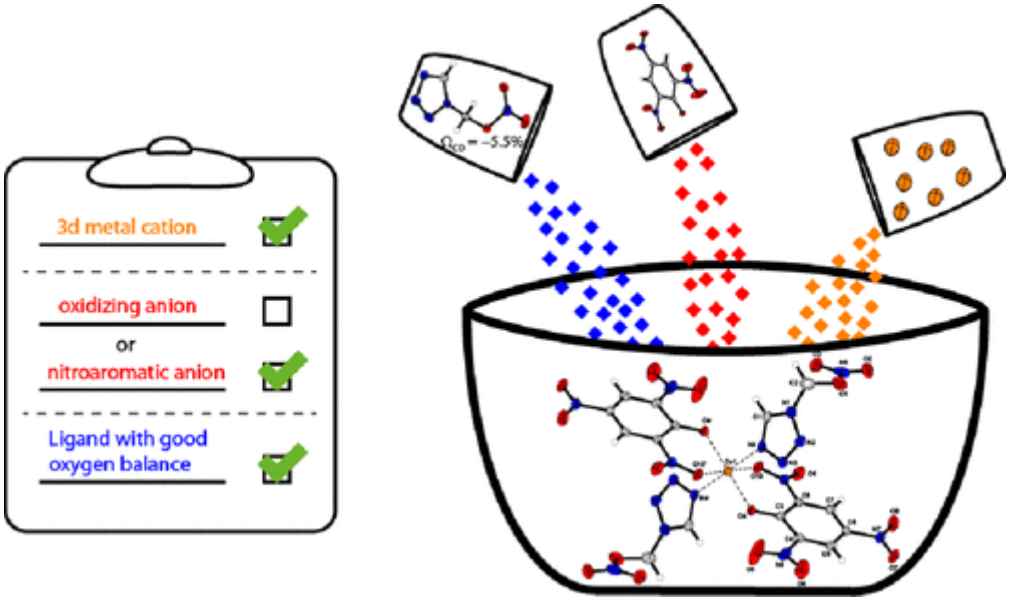
Appendix 31

1-(Nitratomethyl)-5H-tetrazole: A Highly Sensitive Ligand with Improved Oxygen Balance for Laser-Ignitable Coordination Compounds

M. Kofen, V. Braun, S. M. J. Endraß, T. M. Klapötke, J. Stierstorfer

Inorg. Chem. **2022,** *61*, 17212–17225.

https://doi.org/10.1021/acs.inorgchem.2c02805



Supplementary Information:
https://pubs.acs.org/doi/10.1021/acs.inorgchem.2c02805.

Inorganic Chemistry

pubs.acs.org/IC Article

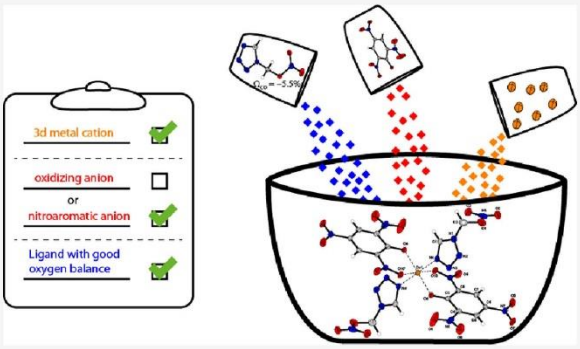
1-(Nitratomethyl)-5*H*-tetrazole: A Highly Sensitive Ligand with Improved Oxygen Balance for Laser-Ignitable Coordination Compounds

Moritz Kofen, Vanessa Braun, Simon M. J. Endraß, Thomas M. Klapötke, and Jörg Stierstorfer*

Cite This: *Inorg. Chem.* 2022, 61, 17212−17225 Read Online

ACCESS | Metrics & More | Article Recommendations | Supporting Information

ABSTRACT: For the first time, the highly sensitive 1-(nitratomethyl)-5*H*-tetrazole (1-NAMT) was synthesized, representing the shortest possible 1-(nitratoalkyl)-5*H*-tetrazole with a combined nitrogen and oxygen content of 81.4%. Compared to its related ethyl derivative, 1-(nitratoethyl)-5*H*-tetrazole, it exhibits improved oxygen balance, resulting in higher detonation parameters. 1-NAMT was thoroughly analyzed by single-crystal diffraction experiments accompanied by elemental analysis, IR spectroscopy, and multinuclear (^{1}H, ^{13}C, and ^{14}N) NMR measurements. The thermal behavior of 1-NAMT was analyzed by differential thermal analysis supported by thermogravimetric analysis. Furthermore, energetic coordination compounds (ECCs) of Cu with different inorganic (*e.g.*, nitrate, chlorate, and perchlorate) and nitroaromatic anions (*e.g.*, picrate and styphnate) were synthesized and thoroughly analyzed. It is shown that the formation of ECCs with nitroaromatic anions (T_{dec} ~ 180 °C) is a suitable strategy to improve the rather low thermal stability of 1-NAMT (125 °C).



INTRODUCTION

Since the elucidation of DNA structure by Crick and Watson,[1] the importance of *N*-heterocyclic compounds cannot be known for building hemes, the most prominent being heme B, the oxygen-transporting iron coordination compound of blood.[2] The application of heterocycles as ligands in coordination compounds offers a nearly infinite amount of possible compounds whose chemical and physical properties can be tuned toward their intended use. Prominent examples of heterocycles applied as ligands are found in Grubbs I[3] and Grubbs II[4] catalysts as well as in B vitamins, with their most prominent representative being vitamin B_{12}.[5] A recently emerged, closely related field of research is that of energetic coordination compounds (ECCs) used in pyrotechnic mixtures,[6] burn rate modifiers,[7] and primary explosives.[8] Here, energetic and nitrogen-rich heterocycles are combined with transition-metal salts of oxidizing (*e.g.*, nitrate, chlorate, and perchlorate) or reducing (*e.g.*, azide) anions. Promising ligands for ECCs should exhibit several characteristics. Like for any energetic material, a high endothermic enthalpy of formation is favorable. Furthermore, the sensitivities of the pure ligand should be approximately in the range that is

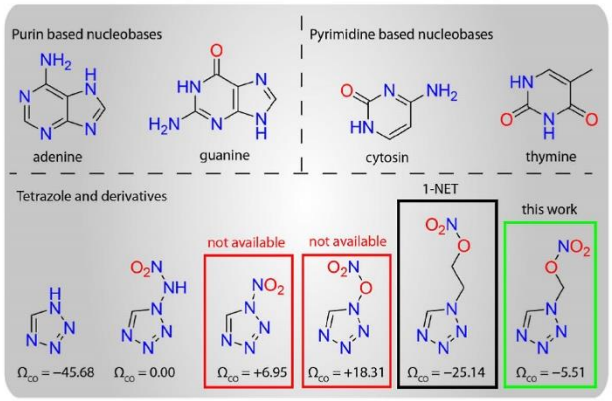
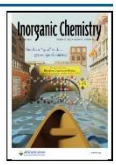


Figure 1. Comparison of oxygen balance between 1,5*H*-tetrazole and derivatives with different substitution patterns.

questioned. The four nucleobases adenine, guanine, cytosine, and thymine (Figure 1) that were found to build up the double-helical DNA strands are key examples of *N*-heterocyclic compounds. Other representatives of important heterocyclic compounds are based on the porphyrin scaffold, which are

Received: August 5, 2022
Published: October 17, 2022



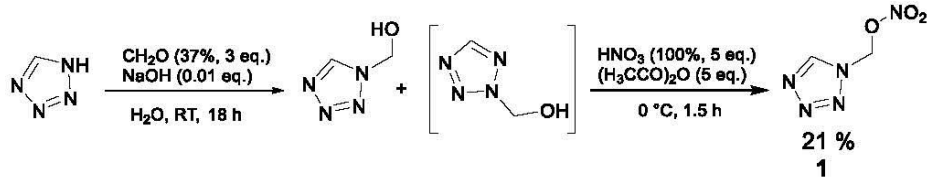
Downloaded via LMU MUENCHEN on November 4, 2022 at 10:51:32 (UTC).
See https://pubs.acs.org/sharingguidelines for options on how to legitimately share published articles.

ACS Publications

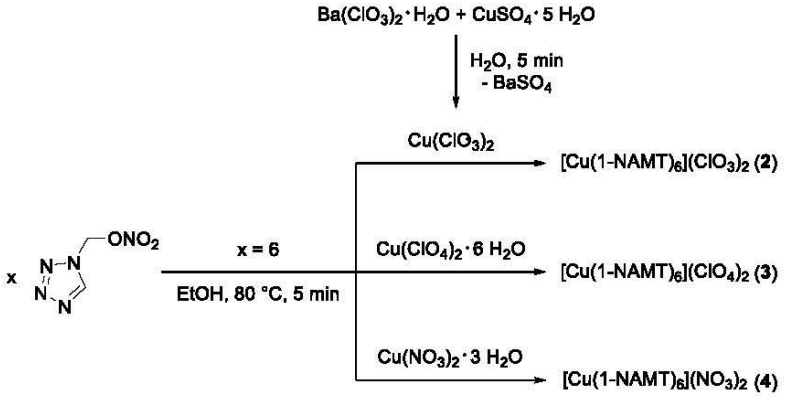
© 2022 The Authors. Published by American Chemical Society

https://doi.org/10.1021/acs.inorgchem.2c02805
Inorg. Chem. 2022, 61, 17212−17225

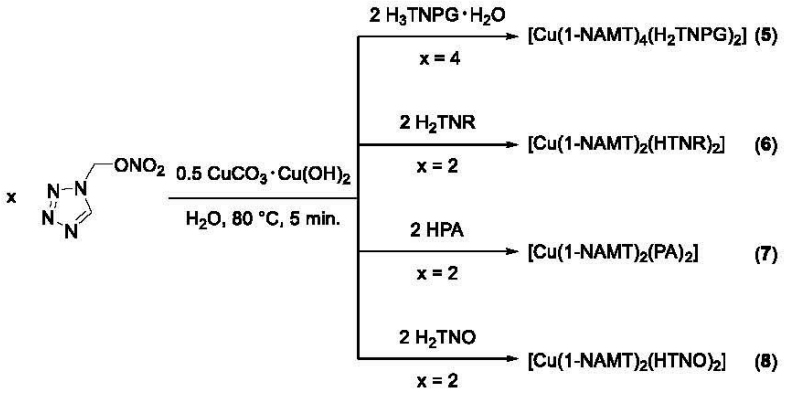
Scheme 1. Synthesis of 1-NAMT (1) with Hydroxymethylation of 1,5*H*-Tetrazole



Scheme 2. Preparation of $[Cu(1\text{-}NAMT)_6](ClO_3)_2$ (2), $[Cu(1\text{-}NAMT)_6](ClO_4)_2$ (3), and $[Cu(1\text{-}NAMT)_6](NO_3)_2$ (4)



Scheme 3. Preparation of Several Copper Trinitrophenolate Complexes of 1 and Nitroaromatic Acids: Trinitrophloroglucinol Monohydrate, $H_3TNPG{\cdot}H_2O$; Styphnic Acid, H_2TNR; Picric Acid, HPA; and Trinitro Orcinol, H_2TNO



desired for intended use of the resulting ECC. As the formation of ECCs most often leads to an increase in sensitivity,[9] it is easily possible to overstate the sensitivities of the resulting ECCs as seen in the work on 1-amino-5*H*-tetrazole[10] (1-AT) or 1-azidomethyl-5*H*-tetrazole[11] (AzMT). Among the nitrogen-rich heterocyclic compounds, those based on the 1,5*H*-tetrazole (Figure 1) moiety are promising substances to be applied as ligands. Due to a wide variety of possible substitutions of the tetrazole scaffold, a huge amount of (highly) energetic neutral compounds are feasible.[12] This enables a broad spectrum of potential applications such as antitumor drugs, low-toxic antifungal drugs, and also as green ECCs, depending on the size and type of substituents.[13−15] Additionally, the tetrazole scaffold offers a highly endothermic enthalpy of formation (1,5*H*-tetrazole: 4732 kJ kg^{-1}) due to a very high nitrogen content of the underlying tetrazole moiety (N = 79.98%). Besides the drawback of an acidic proton of 1,5*H*-tetrazole, the absence of oxygen atoms in the molecular structure leads to incomplete decomposition into gaseous products as elemental carbon may be produced upon exothermic decomposition. Therefore, increasing the amount of oxygen within the molecular structures improves the overall oxygen balance ($OB_{CO} = [d - a - b/2]*1600/M$; M = molar mass; formula for $C_aH_bN_cO_d$), which also generally increases the performance of an energetic material. This can be achieved by functionalization with explosophores such as nitro, nitramino, and nitrate ester moieties that all introduce oxygen to the molecular structure (Figure 1). While the direct functionalization of tetrazoles at the 1*N* position is generally easy, substitution by a nitro group or nitrate ester is not reported yet. Only the nitramino derivative is known to be reported in the literature.[16]

Due to the inaccessibility of a direct substitution at the 1*N* position of tetrazole by a nitrate ester, the introduction of alkyl bridges between the azole and nitrate ester is necessary. Recently, Klapötke *et al.* published a derivative containing a bridging ethyl chain, namely, 1-(nitratoethyl)-5*H*-tetrazole[17] (1-NET). This compound exhibits a decreased nitrogen content of 44.0% compared to pure tetrazole and an oxygen content of 30.2%. 1-NET therefore possesses oxygen balance

https://doi.org/10.1021/acs.inorgchem.2c02805
Inorg. Chem. 2022, 61, 17212−17225

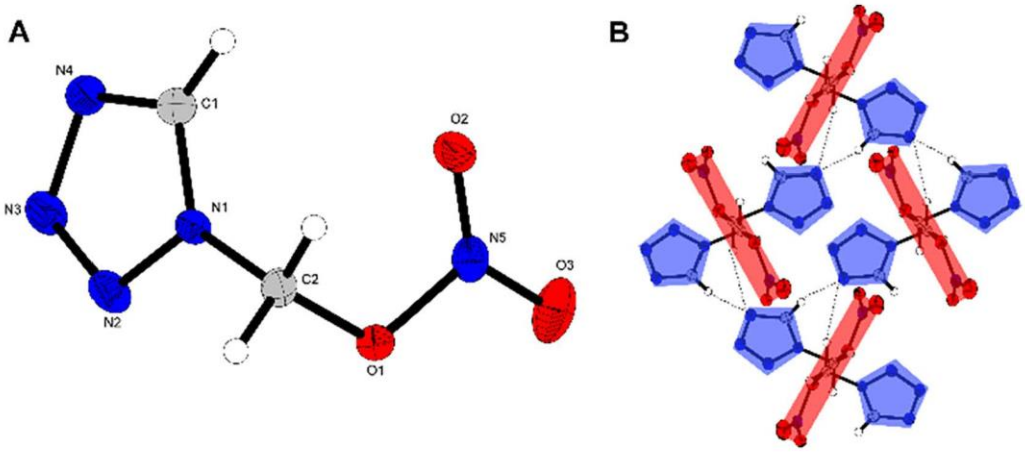


Figure 2. (A) Molecular structure of 1-(nitratomethyl)-5*H*-tetrazole (**1**). (B) Crystal packing of **1** along the *c* axis, highlighting areas of stacked nitro groups (red) and tetrazole moieties (blue). All ellipsoids are shown with a probability of 50%. Selected bond lengths [Å]: N1−C2, 1.44(2); O1−C2, 1.43(2); O1−N5, 1.42(2); O2−N5, 1.20(2); O3−N5, 1.20(2); angles [°]: O1−C2−N1, 111.00(15); N5−O1−C2, 113.46(14); O1−N5−O2, 117.83(16); O1−N5−O3, 111.50(16). Torsion angles [°]: N1−N2−N3−N4, −0.3(2); C2−O1−N5−O2, −6.0(2).

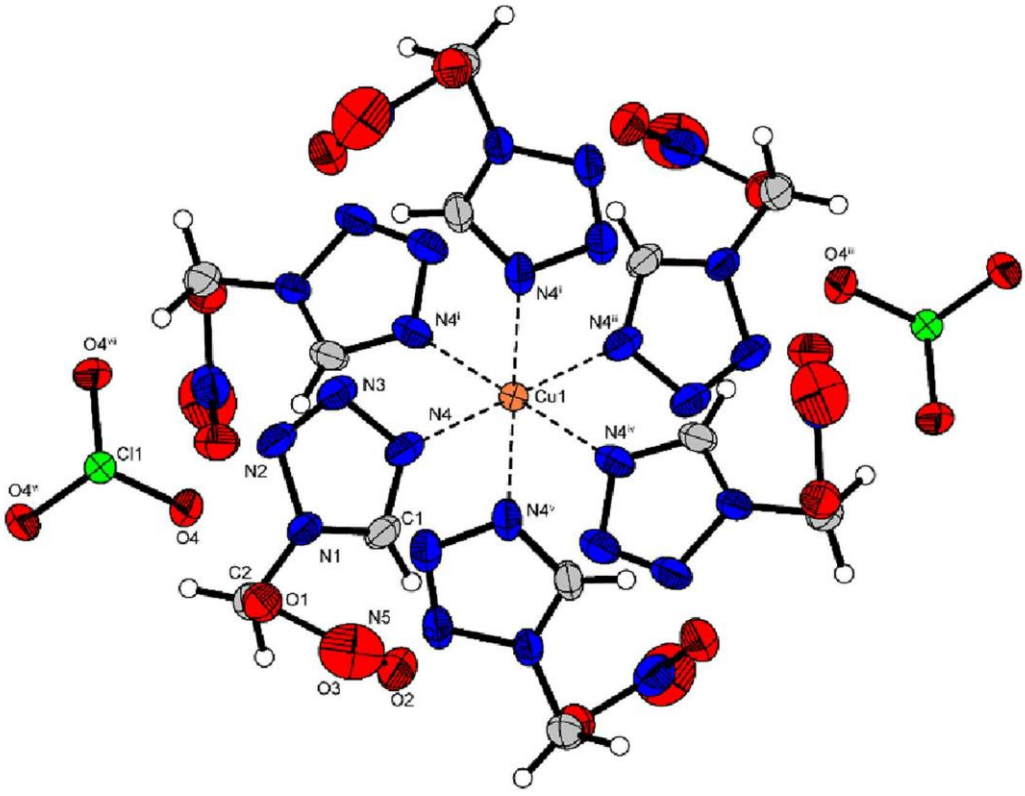


Figure 3. Molecular structure of $[Cu(1\text{-}NAMT)_6](ClO_3)_2$ (**2**). Selected bond length [Å]: Cu1−N1, 2.13(2). Selected bond angles [°]: N1−Cu1−$N1^{iii}$, 92.49(9); N1−Cu1−$N1^{v}$, 180.00; N1−Cu1−$N1^{vi}$, 87.51(9).

toward the formation of CO of $\Omega_{CO} = -25.1\%$. This drastically increased the oxygen balance compared to 1,5*H*-tetrazole ($\Omega_{CO} = -45.7\%$). Additionally, the introduction of oxygen atoms in 1-NET (1.55 g cm^{-3}) also increases the density of pure 1,5*H*-tetrazole (1.41 g cm^{-3}), even though a more sterically demanding substituent is introduced. This increase in density would noticeably be more drastic when comparing 1,5*H*-tetrazole to the methyl-bridged derivative, which is not published yet. Interestingly, there are only a few examples of methylene-bridged explosophores published,[18−20] and even less when focusing solely on 1*N* substitution.[21] While the introduction of an ethylene moiety is synthetically rather easy, the challenge to introduce a methylene moiety is to find a suitable starting material that is chemically inert enough to be functionalized further. We recently published a procedure for the synthesis of 1-(hydroxymethyl)-5*H*-tetrazole (1-HMT), which is at least stable enough to be smoothly converted to the mesylated derivative. Since 1-HMT also represents a suitable precursor for 1-(nitratomethyl)-5*H*-tetrazole (1-NAMT), we opted to synthesize it for the first time and apply it as a ligand

https://doi.org/10.1021/acs.inorgchem.2c02805
Inorg. Chem. 2022, 61, 17212−17225

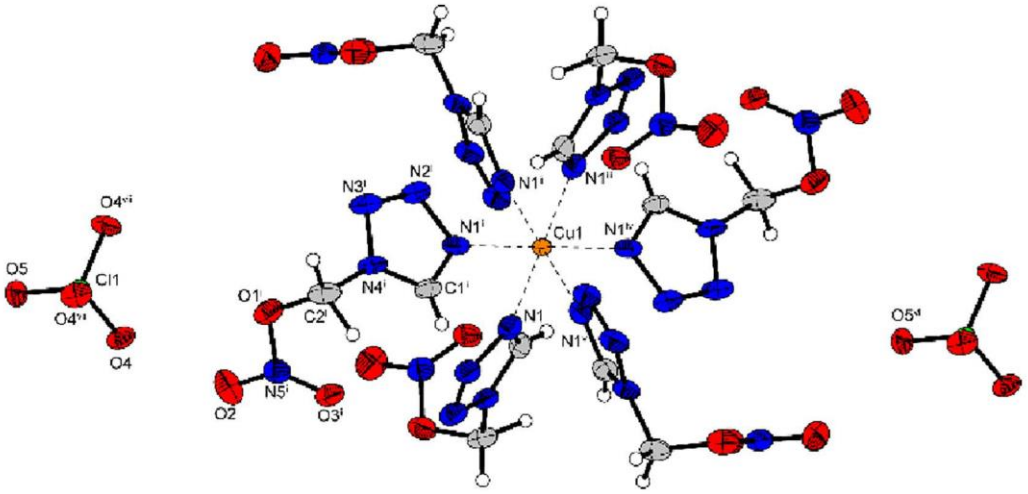


Figure 4. Molecular structure of $[Cu(1\text{-}NAMT)_6](ClO_4)_2$ (**3**). Selected bond lengths [Å]: Cu1–N1, 2.12(5). Selected bond angles [°]: N1–Cu1–N1^{iv}, 91.83(17); N1–Cu1–N1^{vii}, 88.16(17); N1–Cu1–N1^{v}, 180.00.

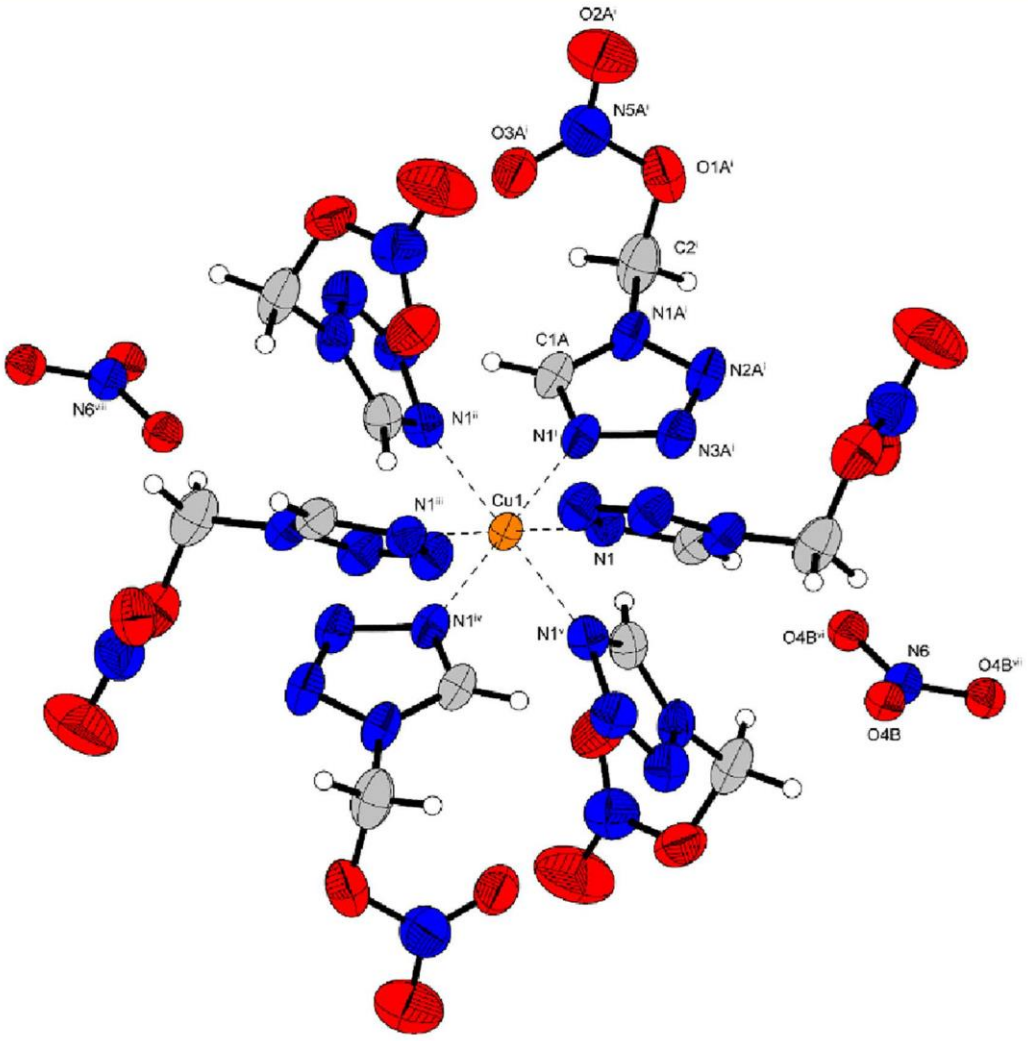


Figure 5. Molecular structure of $[Cu(1\text{-}NAMT)_6](NO_3)_2$ (**4**). Selected bond lengths (Å): Cu1–N1, 2.12(3). Selected bond angles (°): N1–Cu1–N1^{i}, N1–Cu1–N1^{ii}, N1–Cu1–N1^{iii}, N1–Cu1–N1^{iv}, and N1–Cu1–N1^{v}.

https://doi.org/10.1021/acs.inorgchem.2c02805
Inorg. Chem. 2022, 61, 17212–17225

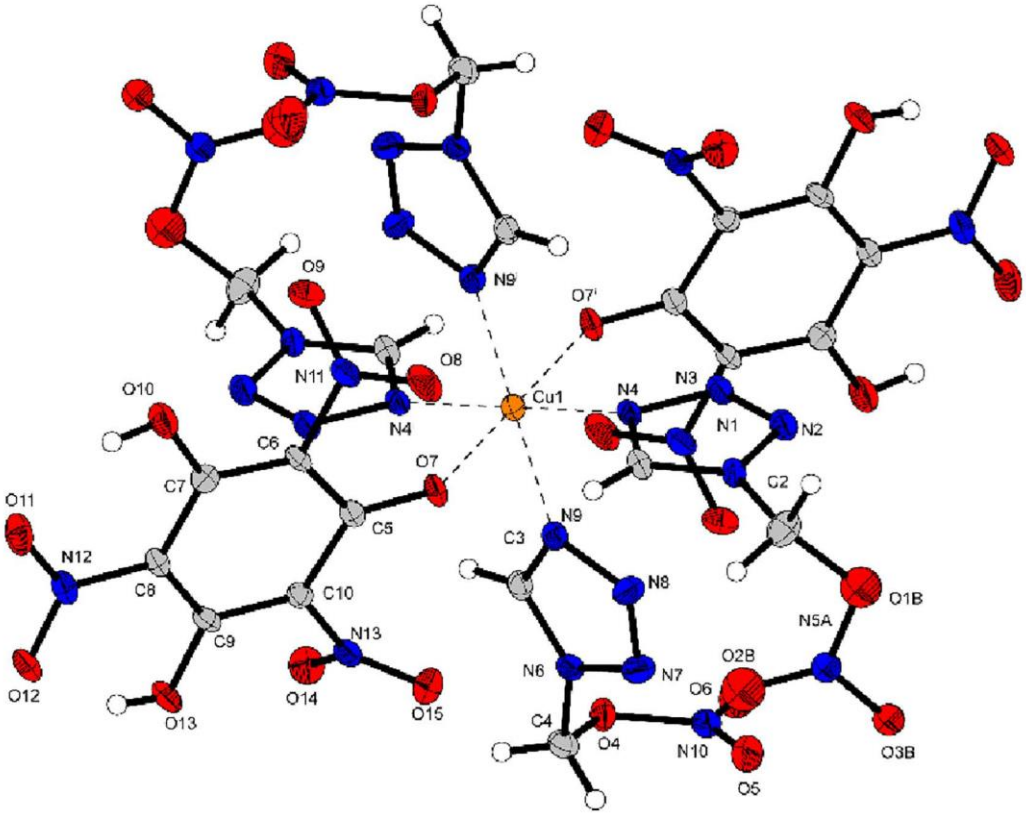


Figure 6. Octahedral coordination in $[Cu(1\text{-NAMT})_4(H_2TNPG)_2]$ (**5**). Selected bond lengths [Å]: Cu1–O7, 2.32(19); Cu1–N4, 2.00(3); Cu1–N9, 2.03(2). Selected bond angles [°]: O7–Cu1–N4, 85.05(8); O7–Cu1–N9, 89.14(8); N4–Cu1–N9, 88.60(10).

for new ECCs. In this work, we present the synthesis of 1-NAMT, as well as several new ECCs of 1-NAMT. The ligand was analyzed by multinuclear NMR spectroscopy, and all compounds were analyzed by single-crystal X-ray diffraction experiments. Additionally, the physico-chemical properties of all compounds were determined.

Synthesis of 1-NAMT. *Warning!* The synthetic work described includes the handling of very sensitive compounds such as 1-NAMT (**1**) and ECCs (**2**–**8**). Appropriate protective equipment (leather coat, face shield, Kevlar wrist protectors, and hearing protection) must be worn at all times when handling these materials!

The synthesis of 1-NAMT (**1**) is shown in Scheme 1. The crude isomeric mixture of 1- and 2-(hydroxymethyl)-5*H*-tetrazole was synthesized according to the literature.[11] The isomeric mixture was added to a stirring mixture of acetic anhydride and fuming nitric acid precooled to 5 °C. Preliminary separation of the isomers is not necessary due to a complete decomposition of the 2*N* isomer during nitration. The target molecule 1-NAMT (**1**) was obtained as a colorless solid by stirring at 5 °C for 1.5 h, quenching on ice, adjusting the pH to 6, and extracting into ethyl acetate. To remove trace amounts of spent acid, **1** was purified *via* column chromatography with a mixture of iso-hexane/ethyl acetate (1/1) as the eluting solvent. After removing the solvent *in vacuo*, the resulting oil (**1**) started to solidify after standing undisturbed for 1–2 h. **1** was obtained as a colorless solid in a moderate yield of 21%.

Synthesis of ECCs. Several ECCs with 1-NAMT as a ligand were synthesized according to Schemes 2 and 3. Due to the commercial unavailability of Cu(II) chlorate, it was freshly produced according to the literature.[22] Generally, compounds **2**–**4** (Scheme 2) were produced by adding the corresponding Cu(II) salt to a solution of **1** in ethanol at elevated temperatures. After stirring for several minutes, the solutions were left to crystallize for up to 3 days. Before complete evaporation of the solvent, the compounds were filtered off and washed with little ice-cold ethanol. The compounds thus obtained were suitable for single-crystal X-ray diffraction experiments without the need for any further recrystallization.

Compounds **5**–**8** were synthesized by adding the corresponding free nitroaromatic acid to a suspension of basic copper carbonate in water and stirring at 80 °C until a clear solution was obtained (Scheme 3). The solutions were left alone for crystallization for several days.

Crystal Structures. The obtained compounds were further analyzed by low-temperature single-crystal X-ray diffraction analysis. The low-temperature densities of all compounds were recalculated [$d_{298K} = dT/1 + \alpha_V(298 - T_0)$; $\alpha_V = 1.5*10^{-4}$ K^{-1}] to their respective densities at room temperature. The data and parameters of the measurements as well as the refinements are given in Supporting Information Table S1.

Compound **1** crystallizes as colorless platelets in the orthorhombic space group $P2_12_12_1$, with a density of 1.68 g cm^{-3} and four formula units in the unit cell (Figure 2A). The bond lengths within the tetrazole moiety are in the expected range for 1*N*-substituted tetrazoles.[17,23] The tetrazole unit forms a nearly perfect level plane together with the methylene moiety, which is marginally protruding by 0.3°. A second plane is also constructed by the methylene carbon atom with the

https://doi.org/10.1021/acs.inorgchem.2c02805
Inorg. Chem. 2022, 61, 17212–17225

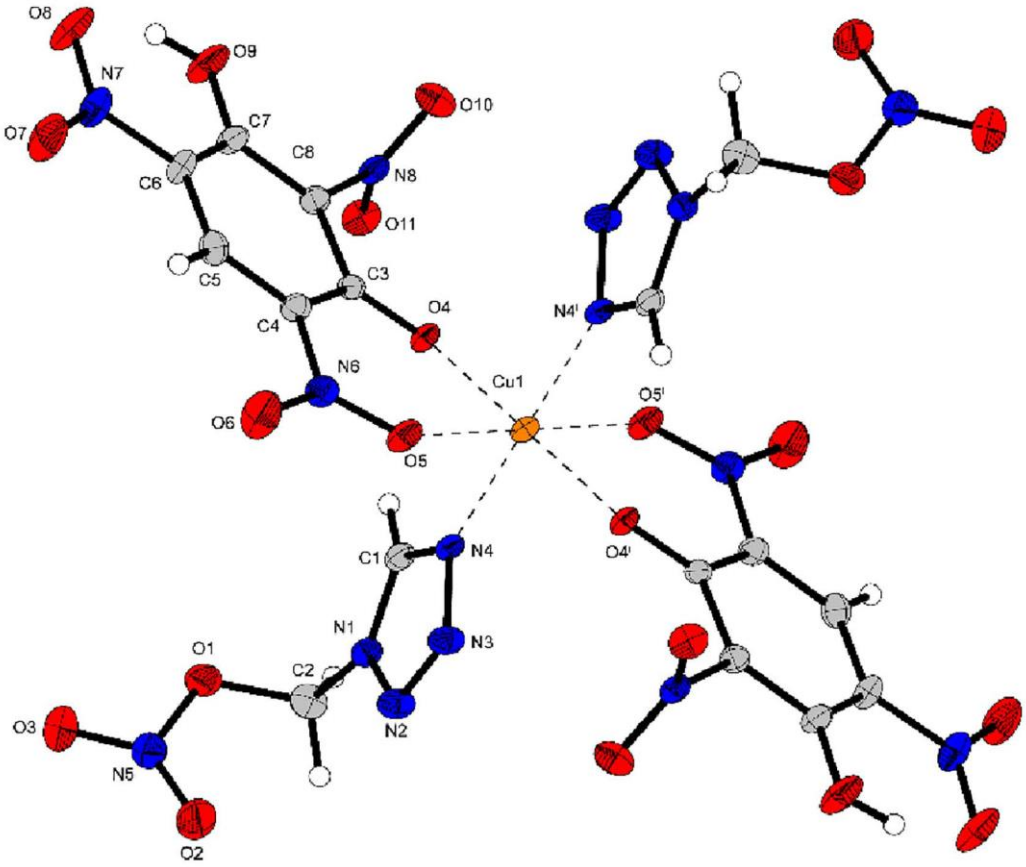


Figure 7. Molecular structure of $[Cu(1\text{-}NAMT)_2(HTNR)_2]$ (**6**) showing a Jahn–Teller-like distorted coordination sphere. Selected bond lengths [Å]: Cu1–O4, 1.93(16); Cu1–O5, 2.33(2); Cu1–N4, 2.00(2). Selected bond angles [°]: O4–Cu1–O5, 81.77(7); O4–Cu1–N4, 89.48(7); O5–Cu1–N4, 86.14(7).

planar nitrate group. Both planes are intersecting at an angle of 111°, which derives from the sp^3-hybridization of the methylene carbon atom. The bond lengths within the nitrate group are similar to comparable nitrate esters[19,24] with an elongated bond of 1.42 Å between O1–N5, and two nearly equivalent bonds of 1.20 Å between O2–N5 and O3–N5. Figure 2B shows the crystal packing of **1** along the *c* axis. This highlights the screw axis along *c*, which leads to a slight offset of the methylene groups of two stacked molecules of **1**. This results in a clear distinction of areas of stacked but twisted nitrate units (red blocks) and tetrazole moieties (blue pentagons). Interestingly, there are only non-classical hydrogen bonds between two tetrazole rings without any participation in hydrogen bonding of the nitrate moieties. For all ECCs, octahedral coordination of the Cu(II) centers is observed. All three ECCs crystallize isotypically in the trigonal space group $R\bar{3}$ with calculated densities of 1.77 g cm^{-3} (**2**) 1.80 g cm^{-3} (**3**), and 1.76 g cm^{-3} (**4**) as well as three units per unit cell. In the molecular structures, **2**–**4** (Figures 3, 4, 5) show almost perfect octahedral coordination of the Cu(II) cation with only slightly tilted axes but Cu–N distance of 2.12 Å. Due to the symmetry, the expected Jahn–Teller distortion (always present for Cu^{2+} d^9 systems) cannot be allocated.

Compound **5** crystallizes in the triclinic space group $P\bar{1}$ with a density of 1.88 g cm^{-3} and one molecular formula in the unit cell (Figure 6). The Cu(II) cation is sixfold coordinated by two single deprotonated trinitrophloroglucinate anions as well as four molecules of **1** forming a distorted octahedron. The four ligands of **1** are positioned in the equatorial plane with bond lengths of 2.00 Å (Cu1–N4) and 2.03 Å (Cu1–N9), with a minor deviation of 1.4° (N4–Cu1–N9) from the ideal 90°. The anions are positioned in the axial position with a bond length of 2.32 Å. This distortion is caused by a high steric demand of the anions together with Cu(II) being a d^9 cation with an electronic configuration of $t_{2g}^6e_g^3$, ultimately leading to a degradation of the z^2-orbital. This causes a Jahn–Teller-like distortion. As displayed in Figure 6, the trinitrophloroglucinate anions form intermolecular hydrogen bonds between the two hydroxy groups and the para-positioned nitro group, which is hence nearly perfectly planar with the aromatic ring. This ultimately leads to a rotation of the two remaining nitro groups out of plane, positioning them in an orientation disfavoring a coordination of the metal center by the nitro groups, as is observed in comparable compounds.[11]

Compound **6** (Figure 7) crystallizes in the triclinic space group $P\bar{1}$ with a density of 1.88 g cm^{-3} and one formula unit in the unit cell. The Cu(II) cation is sixfold coordinated by two single deprotonated anions as well as two molecules of **1** in the form of a Jahn–Teller-like distorted octahedron, like in compound **5**. The equatorial plane is built by the two ligands of **1** with a bond length of 2.00 Å and the two deprotonated hydroxy groups of the anions with a bond length of 1.93 Å. The absence of a third hydroxy group, like in the anions of **5**, leads to only one nitro group being rotated out of the aromatic ring plane, which now enables the remaining level nitro group (N6) to additionally coordinate to the metal cation. This

https://doi.org/10.1021/acs.inorgchem.2c02805
Inorg. Chem. 2022, 61, 17212–17225

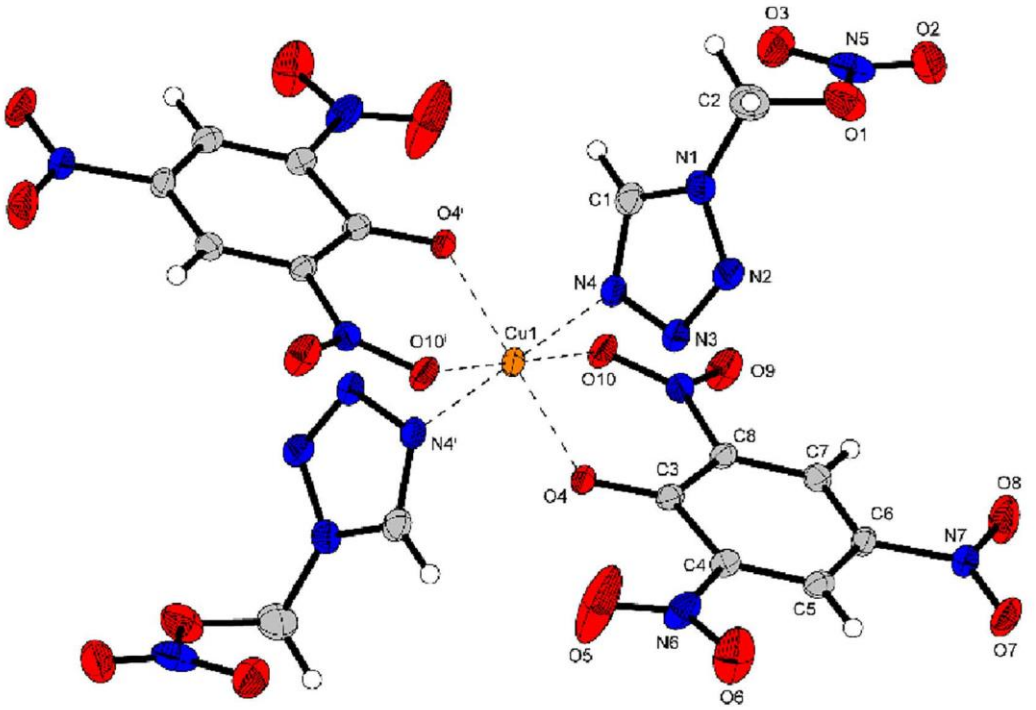


Figure 8. Coordination center of $[Cu(1\text{-}NAMT)_2(PA)_2]$ (**7**). Selected bond lengths [Å]: Cu1–O4, 1.93(2); Cu1–O10, 2.30(3); Cu1–N4, 2.01(3). Selected bond angles [°]: O4–Cu1–O10, 80.27(11); O4–Cu1–N4, 92.29(11); O10–Cu1–N4, 90.92(12).

results in the occupation of four coordination sites of the Cu(II) cation by the anions; thus, only two sites remain to be coordinated by molecules of **1**.

Compound **7** (Figure 8) crystallizes in the monoclinic space group $P2_1/c$ with two formula units in the unit cell and a density of 1.91 g cm^{-3}, the highest of all herein investigated compounds. Like in **6**, the Cu(II) cation is coordinated in a Jahn–Teller-like distorted octahedron, with an equatorial plane built by two ligands of **1** and the two deprotonated hydroxy groups of the picrate anions. Here, the bond lengths are similar to those previously observed with lengths of 1.90 and 2.01 Å, respectively, for the deprotonated hydroxy groups and the tetrazole ligands. Like for the styphnate anions, the absence of hydroxy groups leads to a nearly perfectly planar anion, again enabling the additional coordination of the Cu(II) cation by the nitro groups.

Compound **8** crystallizes in the triclinic space group $\bar{P}1$ with a density of 1.87 g cm^{-3} and one formula unit in the unit cell. Like in the previously discussed nitroaromatic ECCs, the Cu(II) cation is sixfold coordinated in the form of a distorted octahedron. The equatorial plane is again built by two molecules of **1** as well as the deprotonated hydroxy groups, whereas the coordinating nitro groups are positioned in the axial position. Here, the bond lengths toward all coordinating atoms are in the same range as previously observed (Figure 9). Interestingly, the introduction of one methyl group to the styphnate anion leads to a slight rotation (14.6°) of the nitro group (N1), which is normally planar to the aromatic ring due to stabilization by the hydroxy group. A more drastic change is observed for the coordinating nitro group (N2) which is now clearly twisted out of the plane (36.4°) compared to the coordinating nitro group of the styphnate anions of **6**. Nevertheless, this rotation lead to a slightly decreased Cu(II)–NO_2 (κO) bond length of 2.28 Å compared to that of compounds **6** (2.32 Å) and **7** (2.30 Å).

Physicochemical Properties. *Characterization of 1-NAMT.* Table 1 compares the physical and energetic properties of compound **1** with its structurally related compounds 1-(azidomethyl)-5*H*-tetrazole (AzMT) and 1-(nitratoethyl)-5*H*-tetrazole (1-NET). Here, an increase in density of +0.13 g cm^{-3} is observed when changing from the explosophoric azide (AzMT) functionalization to a nitrate ester. A more drastic change is observed when comparing the enthalpies of formation, where **1** (187 kJ mol^{-1}) is a significantly less endothermic compound than AzMT (655 kJ mol^{-1}), which directly derives from the lack of two N–N double bonds found in the azide functionality. Comparing the energetic properties of all three compounds, calculated with the EXPLOS[25,26] program code, a clear increase in performance is observed for the methyl-containing (**1** and AzMT) compounds over the ethyl-containing 1-NET. Compound **1** exhibits a detonation velocity of 8294 m s^{-1}, slightly outperforming AzMT with a detonation velocity of 8124 m s^{-1}, whereas 1-NET does not reach a detonation velocity of over 8000 m s^{-1}. Overall, the nitrate ester **1** outperforms its structurally analogous azides (AzMT), expressing the high importance of a high theoretical maximum density (TMD), which is even able to compensate the lack of enthalpy of formation. Interestingly, 1-NET is completely insensitive toward friction (>360 N) and moderately sensitive toward impact (10 J). By shortening the alkyl chain, the sensitivities are drastically increased, as compound **1** (<1 J, 9 N) exhibits sensitivities in the range of a primary explosive. Even higher sensitivities were reported for AzMT (<1 J, 2 N).

Hirshfeld surface analysis of compound **1** and AzMT (Figure 10) shows the intermolecular contacts for each type of atoms within the molecules. Here, generally destabilizing N···N, N···

https://doi.org/10.1021/acs.inorgchem.2c02805
Inorg. Chem. 2022, 61, 17212–17225

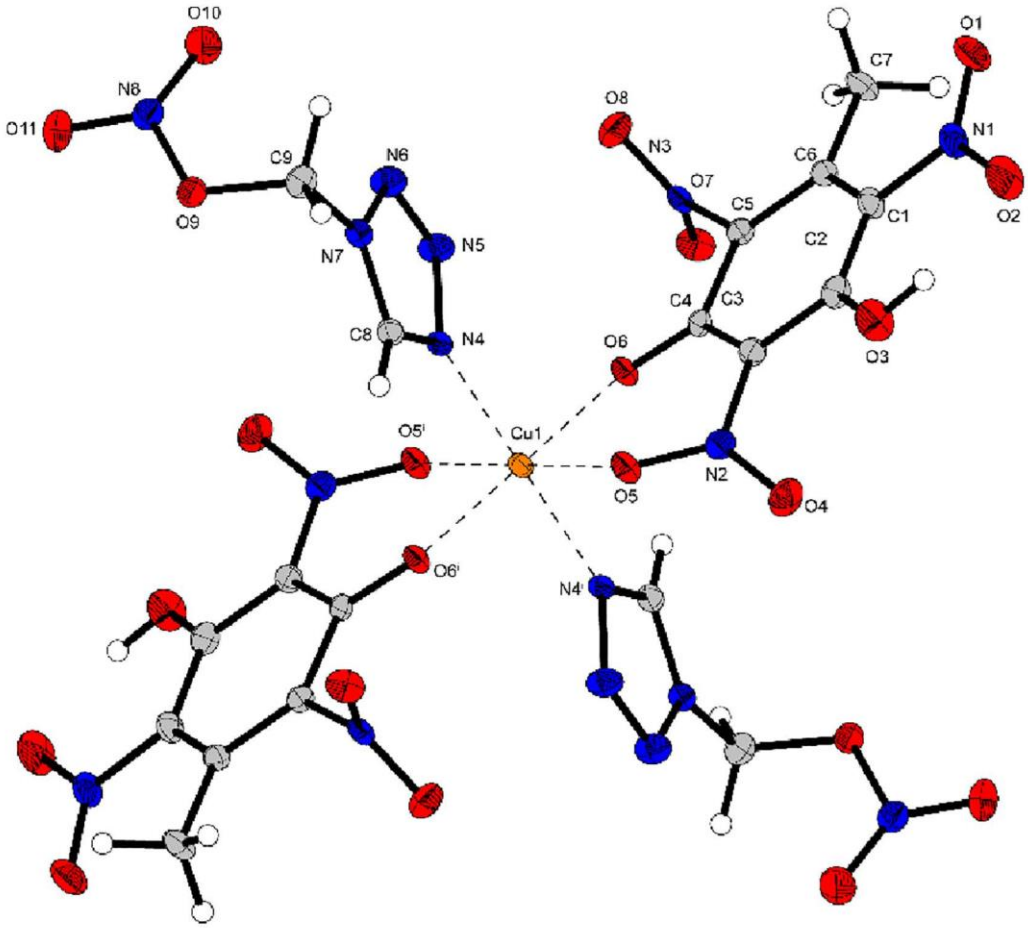


Figure 9. Molecular structure of $[Cu(1\text{-}NAMT)_2(HTNO)_2]$ (**8**). Selected bond lengths [Å]: Cu1–O5, 2.28 (14); Cu1–O6, 1.92(14); Cu1–N4, 2.02(18). Selected bond angles [°]: O5–Cu1–O6, 83.60(5); O5–Cu1–N4, 90.72(6); O6–Cu1–N4, 90.37(7).

O, and O···O contacts are observed for compound **1**, contributing to the surface by 40%. Contrarily, stabilizing contacts such as O···H and N···H make up 50% of the Hirshfeld surface, showing a nearly equal distribution of destabilizing to stabilizing contacts for compound **1**. Additionally, all repulsive interactions exhibit very long distances of over 2.9 Å, while for the stabilizing interactions, a distance of 2.2 Å is observed. For AzMT, the Hirshfeld surface consists of 29% destabilizing contacts, whereas attractive N···H contacts alone build up 63% of the surface. Here, also long contact distances of over 3.0 Å are observed for the destabilizing contacts, with a distance of 2.4 Å for the destabilizing contacts. Therefore, the stabilizing interactions in **1** seem to be a little stronger than in AzMT, which is correlating with the measured friction sensitivities, showing a more sensitive AzMT (2 N) than 1-NAMT (9 N). The same correlation is not observed for impact sensitivity (IS), which is mostly because both compounds exhibit sensitivities below the limit of measurement of 1 J. Therefore, no distinction between both compounds can be concluded based on their IS. Differential thermal analysis (DTA) of compound **1** indicated an endothermic event at 57 °C (Figure 11), which was confirmed as a melting point by thermal gravimetric analysis (TGA). The exothermic event happening in the DTA at 119 °C correlates with the decomposition temperature, confirmed by the TGA measurement, showing a major mass loss of 58.6% between 123 and 174 °C. Therefore, 1-NAMT is significantly less thermally stable compared to its analogous azide (167 °C) as well as to 1-NET (168 °C).

Characterization of ECC. The thermal stabilities of all ECCs were analyzed by DTA measurements (Figure 12) with a heating rate of $\beta = 5$ °C min^{-1}. Additionally, the sensitivities toward impact, friction, and electrostatic discharge were measured according to BAM[27] standards (Table 2). Compound **2** exhibits exothermic decomposition at 145 °C, while **3** and **4** exhibit an exothermic decomposition temperature of about 120 °C, which is equivalent to that of pure ligand **1**. Additionally, the DTA of **4** shows an endothermic event happening at 102 °C, which derives from a melting of the compound shortly before decomposition, which is confirmed by Büchi melting point analysis. For all nitroaromatic ECCs (**5**–**8**), exothermic decomposition, without any endothermic events happening before, was observed. Generally, a significant increase in stability of the ECCs compared to the pure ligand is observed for compounds **6**, **7**, and **8**. Compound **5** exhibits a thermal stability of 135 °C, which is rather low compared to those of **6** (176 °C), **7** (181 °C), and **8** (161 °C). This can be explained by the higher ligand to metal salt ratio of **5** (4:1) compared to the other nitroaromatic compounds (2:1). Therefore, the overall low thermal stability of **1** is inherited to the resulting ECC. On the other hand, the more balanced (2:1) ligand to metal salt ratio of compounds **6**–**8** leads to

https://doi.org/10.1021/acs.inorgchem.2c02805
Inorg. Chem. 2022, 61, 17212–17225

Table 1. Energetic Properties of 1-NAMT (1) Compared to AzMT and 1-NET

	1-NAMT (1)	AzMT	1-NET
formula	$C_2H_3N_5O_3$	$C_2H_3N_7$	$C_3H_5N_5O_3$
M [g mol^{-1}]	145.08	125.1	159.1
ρ [g cm^{-3}]	1.68[a]	1.55[a]	1.55[b]
N/N + O [%][c]	48.27/81.35	78.38/78.38	44.02/74.19
Ω_{CO} [%][d]	−5.51	−70.34	−25.14
IS [J][e]	<1	<1	10
FS [N][f]	9	2	>360
ESD [mJ][g]	150	540	n.d.
T_{exo} [°C][h]	119	167	168
$\Delta_f H°$ [kJ mol^{-1}][i]	187	655	174
$\Delta_f H°$ [kJ kg^{-1}][j]	1398	5232	1094
EXPLOS V6.05.04			
$-\Delta_{ex}U°$ [kJ kg^{-1}][k]	5301	5127	4861
T_{det} [K][l]	3789	3473	3336
V_0 [L kg^{-1}][m]	451	502	815
P_{CJ} [kbar][n]	280	229	215
V_{det} [m s^{-1}][o]	8294	8124	7583

[a]From single-crystal X-ray diffraction analysis recalculated to room temperature. [b]Measured with a gas pycnometer. [c]Nitrogen and combined nitrogen + oxygen content. [d]Oxygen balance toward the formation of CO. [e]Impact sensitivity (BAM drop hammer test). [f]Friction sensitivity (BAM friction tester). [g]Electrostatic discharge sensitivity (OZM XSpark10). [h]DTA onset temperature of exothermic decomposition at a heating rate of 5 °C min^{-1}. [i]Calculated enthalpy of formation (CBS-4M + atomization method). [j]Calculated mass related enthalpy of formation. [k]Energy of explosion. [l]Detonation temperature. [m]Volume of detonation products (assuming only gaseous products). [n]Detonation pressure at the Chapman-Jouguet point. [o]Detonation velocity.

stabilization of the low thermal stability of **1** by the nitroaromatic anions, which is contrary to previous findings.[11,23,28] While a stabilizing effect was previously observed for some cases,[28] it was never as significant as it is in this study. The drastic increase in thermal stability is most likely due to the low thermal stability of **1**, resulting in high relative differences between the pure ligand and the resulting ECCs.

Following an increment method by Ilyushin,[29] it was possible to estimate the detonation velocities of all ECCs, except for **2**, due to the unavailability of data for chlorate anions (Table 2). Detailed information can be found in the Supporting Information. Overall, a slight decrease in detonation velocity compared to the pure ligand is observed. Compounds **3** and **4** exhibit velocities between 7800 and 7900 m s^{-1}, which is about 300 m s^{-1} slower than pure **1**. Generally, for the nitroaromatic ECCs **5**−**8**, a more distinct decrease is observed. Compounds **6** and **7** have estimated detonation velocities of below 7800 m s^{-1}, while for **8**, a velocity of 7500 m s^{-1} was calculated. Interestingly, **5** shows the highest estimated detonation velocity (7918 m s^{-1}) by far surpassing the other nitroaromatic ECCs. Due to the incremental method, a higher contribution of ligand **1** to the detonation velocity is introduced, since the ligand-to-metal salt ratio differs between **5** (4:1) and **6**−**8** (2:1). Overall, all herein synthesized compounds outperform lead azide (LA) (6187 m s^{-1}) as well as lead styphnate (LS) (6137 m s^{-1}) by at least 21%.

Sensitivities. According to the UN Recommendation on the Transport of Dangerous Goods,[30] compound **1** has to be classified as extremely sensitive with an IS of <1 J and a friction sensitivity (FS) of 9 N. It is significantly more sensitive toward an electrostatic discharge (150 mJ) compared to AzMT (540 mJ) but less sensitive than typical primaries such as lead azide (Table 2). Compounds **2**−**8** are also extremely sensitive toward impact, all exhibiting a sensitivity <1 J, except compound **3**, having an IS of 2 J. Therefore, all ECCs exhibit a higher IS than lead azide or lead styphnate. While no clear trend in stability is derived from ISs, the formation of ECCs **2**−**4** results in compounds distinctively more sensitive toward friction than to pure compound **1**. While all three compounds are classified as extremely sensitive toward friction, the nitrate compound **4** (5 N) is less sensitive than the chlorate (**2**, 0.4 N) and perchlorate (**3**, 0.75 N) compounds, which are on a par with LA and LS. The ECCs containing nitroaromatic anions, on the other hand, show a stabilization of **1**, as their friction sensitivities are lowered compared to pure **1**. Interestingly, compound **5** (72 N) is less sensitive than compound **6** (40 N), which is contrary to the higher amount of 1-NAMT in compound **5** than in **6**. While compound **8** exhibits a FS (84 N) comparable to that of **5**, compound **7** (120 N) exhibits the lowest FS of all herein analyzed compounds, highlighting the high stability of the picrate anion. All ECCs exhibit an ESD sensitivity (90−160 mJ) comparable to pure **1** (150 mJ), the only exception being compound **4** exhibits a sensitivity of 13 mJ. Nonetheless, all compounds are less sensitive than LA (5−8 mJ) or LS (0.04−1 mJ).[31,32]

Initiation Capabilities. To get an insight into the behavior of the sample toward fast heating with and without confinement, hot plate (HP) and hot needle (HN) tests were performed. These tests allow for a first evaluation of their capability to be applied as primary explosives. Detailed procedures for HP and HN tests are given in the Supporting Information. While the HP reflects on the behavior toward fast heating without confinement, the HN test allows for an assessment of the compound's behavior upon fast heating with confinement. Table 3 summarizes the results from HN and HP tests of all compounds. Here, all compounds showed deflagration, except compound 2 showing detonation. Thus, only **2** exhibits detonation behavior, which is crucial to be applied as detonating primary explosives. While HP and HN tests assess the susceptibility toward initiation by heat and flame, the possibility of ignition by laser impulse cannot be concluded and was additionally tested (Table 4).

All ECCs were directly irradiated by a single-pulsed 45 W InGaAs laser diode. About 25 mg of each compound was pressed into a transparent polycarbonate percussion cap and sealed with UV curing adhesive. The sample was placed in the focused beam path and irradiated with a single laser pulse with a wavelength of 915 nm, a voltage of 4 V, a current of 6−7 A, and pulse lengths of 0.1, 1.0, 15, or 30 ms. The results of these experiments are listed in Table 4.

While compounds **2**−**4** exhibited no ignition at the lowest tested energy of 0.1 mJ, strong detonations were observed for all compounds already at 1.7 mJ, strong enough to destroy parts of the laser setup. The moment of detonation of compound **2** is shown in Figure 13A. Compound **5** showed no ignition at the lowest tested energy, and therefore, this energy was not tested for all other nitroaromatic compounds. Nevertheless, **5** and **6** showed deflagrations already at 17 mJ (Figure 13B,C), as well as at 255 and 510 mJ. Compound **7** shows no ignition at any of the tested energies (17, 255, and 510 mJ), which derives from the lower energetic character of the picrate anions compared to the styphnate and trinitrophloroglucinate anions. Compound **8** shows a slow burning of

https://doi.org/10.1021/acs.inorgchem.2c02805
Inorg. Chem. 2022, 61, 17212−17225

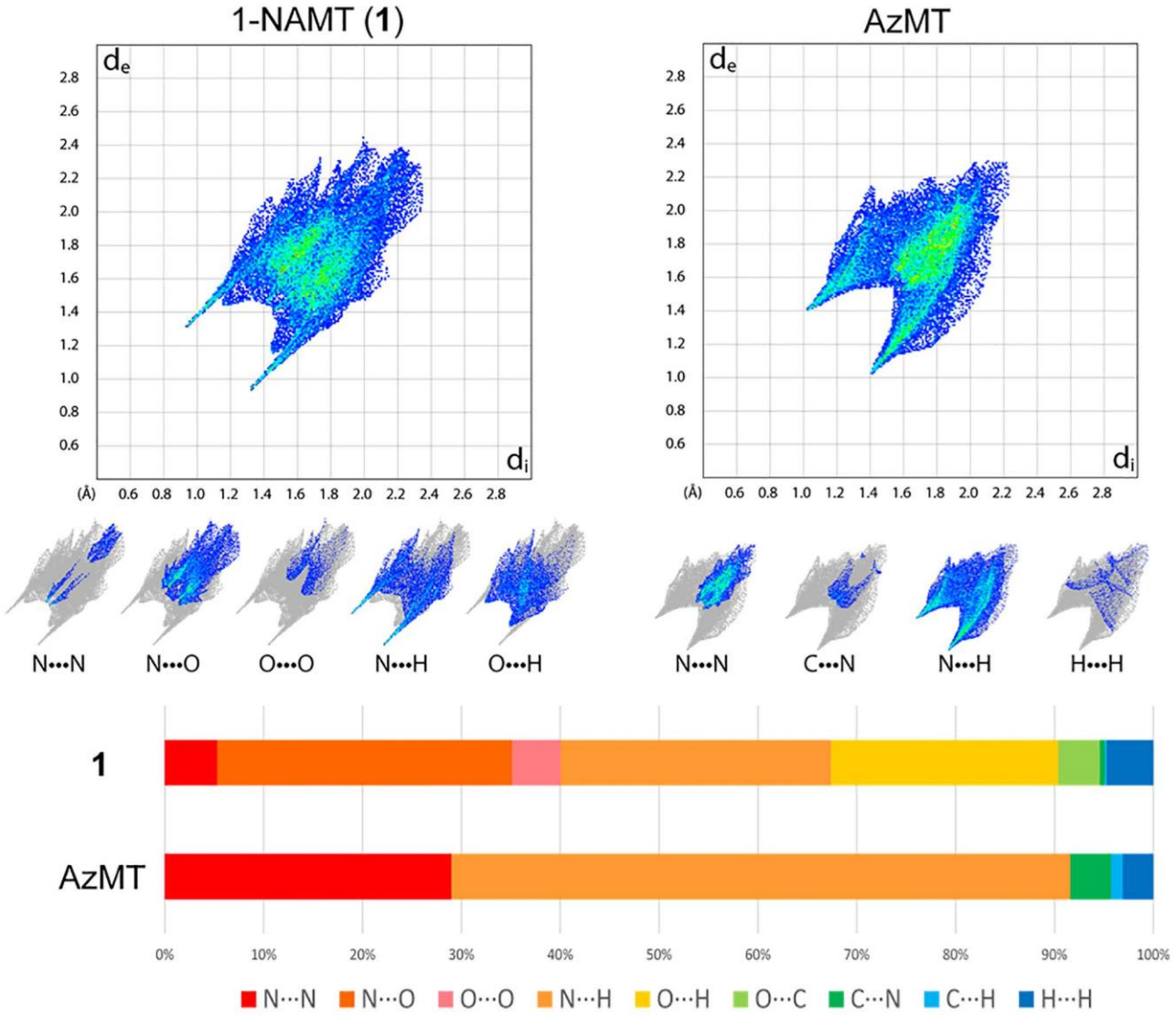


Figure 10. Hirshfeld analysis of compound **1** compared to AzMT. Stabilizing interactions observed in **1** are shorter and hence stronger than in AzMT.

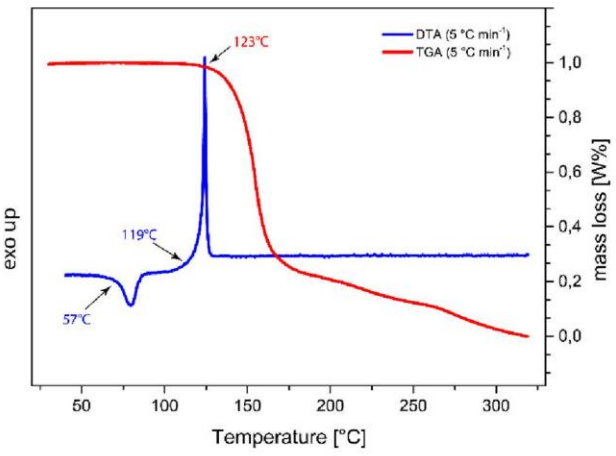


Figure 11. Combined DTA and TGA measurements of compound **1** with a heating rate of 5 °C min^{-1}, exhibiting melting of **1** at 57 °C and an exothermic decomposition at 119 °C.

the material at all tested energies (Figure 13D). Due to the substitution of one hydroxy group of each trinitrophloroglucinate anion by methylene groups, the resulting ECC is lacking energetic performance; thus, a self-sustained deflagration is not observed, which is additionally accompanied by the formation of soot.

■ CONCLUSIONS

The synthesis of 1-NAMT (**1**) was possible by nitration of the literature-known isomeric mixture of 1- and 2-(hydroxymethyl)-5*H*-tetrazole with acetyl nitrate in a moderate yield (21%). 1-NAMT was investigated by low-temperature single-crystal X-ray diffraction experiments, multinuclear ^{1}H, ^{13}C, and ^{14}N NMR spectroscopy techniques, as well as elemental analysis and infrared spectroscopy. Differential thermal analysis showed a rather low thermal stability of **1** (119 °C), while BAM sensitivity measurements revealed a high IS (<1 J) and FS (9 N), both in the range of typical primary explosives. The comparison of the molecular interactions of **1** with its structurally analogous azide (AzMT) on the basis of Hirshfeld

https://doi.org/10.1021/acs.inorgchem.2c02805
Inorg. Chem. 2022, 61, 17212−17225

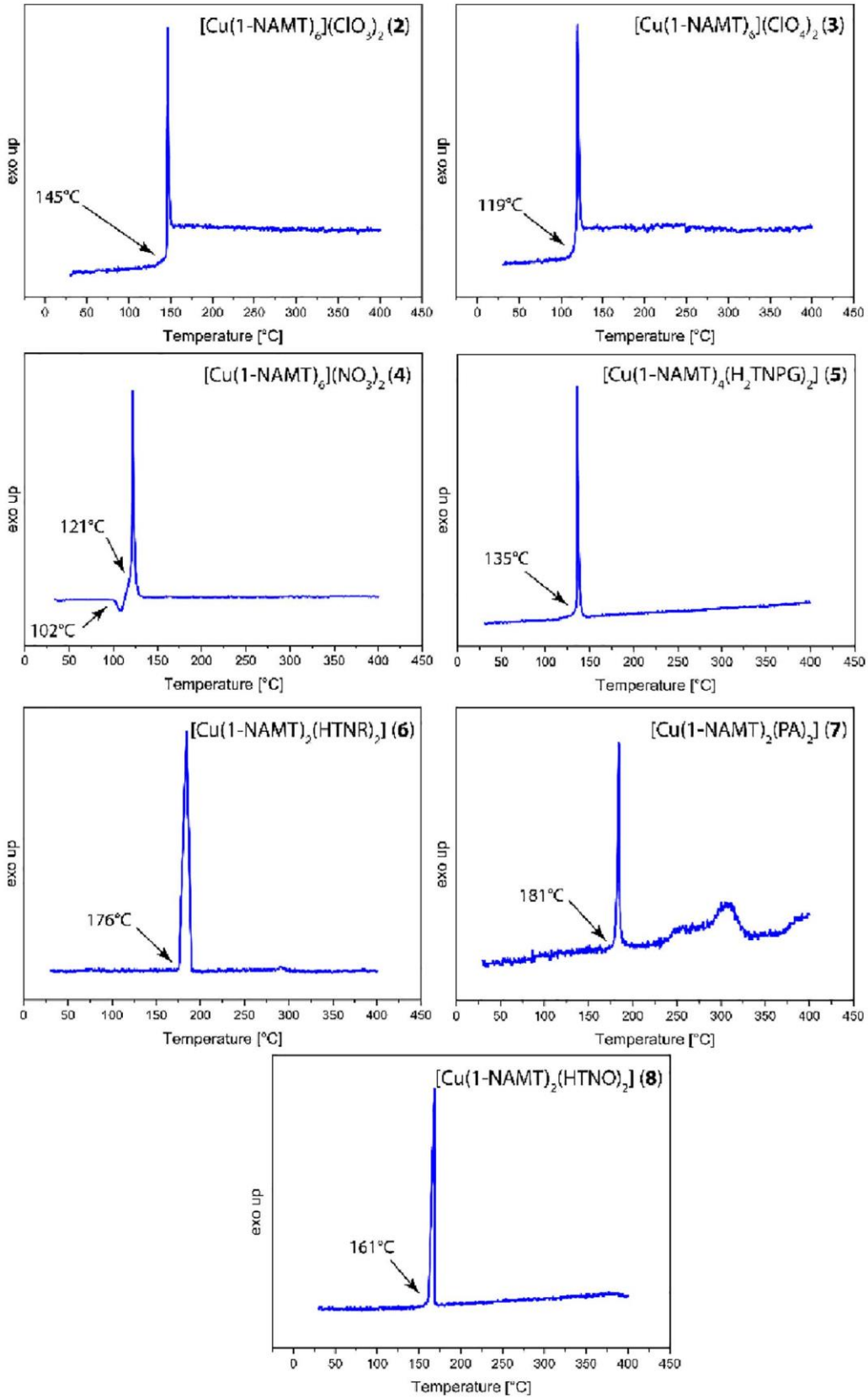


Figure 12. Differential thermal analysis of ECCs **2**–**8** with a heating rate of 5 °C min^{-1}.

https://doi.org/10.1021/acs.inorgchem.2c02805
Inorg. Chem. 2022, 61, 17212−17225

Table 2. Overview of the Thermal Stability and Sensitivity toward External Stimuli

compound		$T_{endo.}$ [°C][a]	$T_{exo.}$ [°C][b]	IS [J][c]	FS [N][d]	ESD [mJ][e]	V_{det} [m s^{-1}][f]
1-NAMT	**1**	57	119	<1	9	150	8294
$[Cu(1\text{-}NAMT)_6](ClO_3)_2$	**2**		145	<1	0.4	139	-[h]
$[Cu(1\text{-}NAMT)_6](ClO_4)_2$	**3**		119	2	0.75	13	7910[h]
$[Cu(1\text{-}NAMT)_6](NO_3)_2$	**4**	102	121	<1	5	90	7865[h]
$[Cu(1\text{-}NAMT)_4(H_2TNPG)_2]$	**5**		135	<1	72	160	7918[h]
$[Cu(1\text{-}NAMT)_2(HTNR)_2]$	**6**		176	<1	40	140	7715[h]
$[Cu(1\text{-}NAMT)_2(PA)_2]$	**7**		181	<1	120	90	7767[h]
$[Cu(1\text{-}NAMT)_2(HTNO)_2]$	**8**		161	<1	84	90	7507[h]
LA[33,34]			320−350	4	≤0.1	5−8	6187[g]
LS[33,34]			260−310	8	0.45	0.04−1	6138[g]

[a]Endothermic peak, which indicates melting of the substance. [b]Exothermic peak, which indicates decomposition. [c]Impact sensitivity (BAM drop hammer test). [d]Friction sensitivity (BAM friction tester). [e]Electrostatic discharge sensitivity (OZM XSpark10). [f]Details can be found in the Supporting Information. [g]Calculated with EXPLO5_V6.05. [h]Estimated via the incremental method by Ilyushin.[29]

Table 3. Results of HN, HP, and Initiation Tests[a]

compound	HP	HN
2	def.	det.
3	def.	def.
4	def.	def.
5	def.	def.
6	def.	def.
7	def.	def.
8	def.	def.

[a]def. = deflagration; det. = detonation.

analysis showed stronger stabilizing interactions for **1**, ultimately explaining the differences in friction sensitivities. **1** was further used as a ligand for the formation of seven ECCs of copper(II) chlorate (**2**), perchlorate (**3**), nitrate (**4**), trinitrophloroglucinolate (**5**), styphnate (**6**), picrate (**7**), and trinitro-orcinolate (**8**). All ECCs were obtained in a pure form, according to elemental analysis, and were further analyzed by low-temperature single-crystal X-ray diffraction experiments, accompanied by DTA, infrared spectroscopy, and their sensitivities toward external stimuli (IS, FS, and ESD) measured according to BAM standards. For all ECCs, an extremely high IS of <1−2 J was observed, while compounds **2**−**4** exhibited increased FSs (0.4−5 N) compared to pure **1**. The nitroaromatic-containing ECCs **5**−**8** exhibited FSs (40−120 N) in the range of a booster explosive. The thermal stabilities of **2**−**5** are in the same range (119−145 C) as that of **1**. Interestingly, the formation of ECCs **6**−**8** led to a drastic increase of the thermal stability of **1**. Hot plate and needle tests revealed deflagration of all compounds, except for **2** showing a violent detonation in the hot needle test. Thus, only **2** exhibits

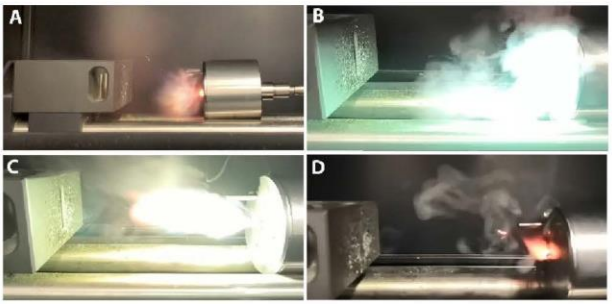


Figure 13. (A) Moment of detonation of compound **2** at 1.7 mJ; (B,C) moments of deflagration of compounds **5** and **6**; (D) burning of compound **8**.

a fast DDT, which makes it necessary to discuss its use as a primary explosive. Further assessment of laser initiation showed positive for compounds **2**−**4** already at low energies (1.7 mJ), while the nitroaromatic compounds showed deflagration or burning at all tested energies. Lastly, detonation velocity predictions suggested velocities of up to 7900 m s^{-1} for all ECCs investigated in this study.

■ ASSOCIATED CONTENT

Supporting Information

The Supporting Information is available free of charge at https://pubs.acs.org/doi/10.1021/acs.inorgchem.2c02805.

Overview of compounds; single-crystal X-ray diffraction; computations; NMR spectroscopy; IR spectroscopy; hot plate and hot needle testing; general methods;

Table 4. Results of Laser Initiation of Compounds 2−8[a]

compound	6 A	7 A		
2	τ = 0.1 ms x	τ = 0.1 ms det.	τ = 1 ms det.	
3		τ = 0.1 ms det.		
4	τ = 0.1 ms x	τ = 0.1 ms det.		
5	τ = 0.1 ms x	τ = 1 ms def.	τ = 15 ms def.	τ = 30 ms def.
6		τ = 1 ms def.	τ = 15 ms def.	T = 30 ms def.
7		τ = 1 ms x	τ = 15 ms x	τ = 30 ms x
8		τ = 1 ms dec.	τ = 15 ms dec.	τ = 30 ms dec.

[a]Operating parameters: current I = 6 and 7 A; voltage U = 4 V; theoretical maximum output power P_{max} = 45 W; theoretical energy E_{max} = 0.1−17 mJ; wavelength λ = 915 nm; pulse length τ = 0.1−1 ms. (− = not tested; x = no ignition; dec. = decomposition; def. = deflagration; det. = detonation).

https://doi.org/10.1021/acs.inorgchem.2c02805
Inorg. Chem. 2022, 61, 17212−17225

detonation velocity estimations; and experimental part (PDF)

Accession Codes

CCDC 2176029−2176036 contain the supplementary crystallographic data for this paper. These data can be obtained free of charge via www.ccdc.cam.ac.uk/data_request/cif, or by emailing data_request@ccdc.cam.ac.uk, or by contacting The Cambridge Crystallographic Data Centre, 12 Union Road, Cambridge CB2 1EZ, UK; fax: +44 1223 336033.

AUTHOR INFORMATION

Corresponding Author

Jörg Stierstorfer − *Department of Chemistry, Ludwig Maximilian University Munich, 81377 Munich, Germany;* orcid.org/0000-0002-2105-1275; Email: jstch@cup.uni-muenchen.de

Authors

Moritz Kofen − *Department of Chemistry, Ludwig Maximilian University Munich, 81377 Munich, Germany;* orcid.org/0000-0001-8522-2582

Vanessa Braun − *Department of Chemistry, Ludwig Maximilian University Munich, 81377 Munich, Germany*

Simon M. J. Endraß − *Department of Chemistry, Ludwig Maximilian University Munich, 81377 Munich, Germany;* orcid.org/0000-0003-1489-2380

Thomas M. Klapötke − *Department of Chemistry, Ludwig Maximilian University Munich, 81377 Munich, Germany;* orcid.org/0000-0003-3276-1157

Complete contact information is available at: https://pubs.acs.org/10.1021/acs.inorgchem.2c02805

Notes

The authors declare no competing financial interest.

ACKNOWLEDGMENTS

The Ludwig Maximilian University of Munich (LMU), the Office of Naval Research (ONR), is gratefully acknowledged for providing financial support for this work under grant no. N00014-19-1-2078. The authors want to further thank Stefan Huber for sensitivity measurements.

REFERENCES

(1) Watson, J. D.; Crick, F. H. C. Molecular Structure of Nucleic Acids: A Structure for Deoxyribose Nucleic Acid. *Nature* **1953**, *171*, 737−738.

(2) Thews, G. Atemgastransport und Säure-Basen-Status des Blutes. In *Physiologie des Menschen*; Springer Berlin Heidelberg: Berlin, Heidelberg, 1993.

(3) Schwab, P.; Grubbs, R. H.; Ziller, J. W. Synthesis and Applications of $RuCl_2(CHR')(PR_3)_2$: The Influence of the Alkylidene Moiety on Metathesis Activity. *J. Am. Chem. Soc.* **1996**, *118*, 100−110.

(4) Scholl, M.; Ding, S.; Lee, C. W.; Grubbs, R. H. Synthesis and Activity of a New Generation of Ruthenium-Based Olefin Metathesis Catalysts Coordinated with 1,3-Dimesityl-4,5-dihydroimidazol-2-ylidene Ligands. *Org. Lett.* **1999**, *1*, 953−956.

(5) Hodgkin, D. C.; Kamper, J.; Mackay, M.; Pickworth, J.; Trueblood, K. N.; White, J. G. Structure of Vitamin B12. *Nature* **1956**, *178*, 64−66.

(6) Klapötke, T. M. *Chemistry of High-Energy Materials*; De Gruyter, 2019.

(7) Ilyushin, M. A.; Tselinsky, I. V.; Bachurina, I. V.; Novoselova, L. O.; Konyushenko, E. N.; Kozlov, A. S.; Gruzdev, Y. A. Application of Energy-Saturated Complex Perchlorates. *AIP Conf. Proc.* **2006**, *849*, 213−217.

(8) Klapötke, T. M.; Kofen, M.; Schmidt, L.; Stierstorfer, J.; Wurzenberger, M. H. H. Selective Synthesis and Characterization of the Highly Energetic Materials 1-Hydroxy-5H-tetrazole (CHN_4O), its Anion 1-Oxido-5H-tetrazolate ($CN4O^-$) and Bis(1-hydroxytetrazol-5-yl)triazene. *Chem.−Asian J.* **2021**, *16*, 3001−3012.

(9) Kofen, M.; Lommel, M.; Stierstorfer, J.; Klapötke, T. M. Adjustability of Energetic Coordination Compounds: Comparison of three 1-(Azidoalkyl)-5H-tetrazole ligands and their Energetic Coordination Compounds. *New Trends in Research of Energetic Materials*; Pardubice, Czech Republic, 2022; pp 114−118.

(10) Szimhardt, N.; Wurzenberger, M. H. H.; Zeisel, L.; Gruhne, M. S.; Lommel, M.; Stierstorfer, J. Maximization of the energy capability level in transition metal complexes through application of 1-amino- and 2-amino-5H-tetrazole ligands. *J. Mater. Chem. A* **2018**, *6*, 16257−16272.

(11) Kofen, M.; Lommel, M.; Wurzenberger, M. H. H.; Klapötke, T. M.; Stierstorfer, J. 1-(Azidomethyl)-5H-Tetrazole: A Powerful New Ligand for Highly Energetic Coordination Compounds. *Chem. Eur J.* **2022**, *28*, No. e202200492.

(12) Ostrovskii, V. A.; Trifonov, R. E.; Popova, E. A. Medicinal chemistry of tetrazoles. *Russ.Chem.Bull., Int.Ed.* **2012**, *61*, 768−780.

(13) Popova, A. E.; Protas, V. A.; Trifonov, E. R. Tetrazole Derivatives as Promising Anticancer Agents. *Anti-Cancer Agents Med. Chem.* **2018**, *17*, 1856−1868.

(14) Wang, S.-Q.; Wang, Y.-F.; Xu, Z. Tetrazole hybrids and their antifungal activities. *Eur. J. Med. Chem.* **2019**, *170*, 225−234.

(15) Szimhardt, N.; Wurzenberger, M. H. H.; Beringer, A.; Daumann, L. J.; Stierstorfer, J. Coordination chemistry with 1-methyl-5H-tetrazole: cocrystallization, laser-ignition, lead-free primary explosives − one ligand, three goals. *J. Mater. Chem. A* **2017**, *5*, 23753−23765.

(16) Ilyushin, M. A.; Terpigorev, A. N.; Tselinskii, I. V. Effect of Isomeric Strucutre of (N-Nitramino)tetrazoles on the Properties of Theirs Salts. *Russ. J. Gen. Chem.* **1999**, *69*, 1645−1657.

(17) Gruhne, M. S.; Lenz, T.; Rösch, M.; Lommel, M.; Wurzenberger, M. H. H.; Klapötke, T. M.; Stierstorfer, J. Nitratoethyl-5*H*-tetrazoles: improving the oxygen balance through application of organic nitrates in energetic coordination compounds. *Dalton Trans.* **2021**, *50*, 10811−10825.

(18) Verkhozina, O. N.; Kizhnyaev, V. N.; Vereshchagin, L. I.; Rokhin, A. V.; Smirnov, A. I. Synthesis of Polynuclear Nonfused Azoles. *Russ. J. Org. Chem.* **2003**, *39*, 1792−1796.

(19) Klapötke, T. M.; Kofen, M.; Stierstorfer, J. N-Functionalisation of 5,5′-bistetrazole providing 2,2′-di(azidomethyl)bistetrazole: a melt-castable metal-free green primary explosive. *Dalton Trans.* **2021**, *50*, 13656−13660.

(20) Li, Y.; Liu, W.; Pang, S. Synthesis and Characterization of 5-Nitro-2-nitratomethyl-1,2,3,4-tetrazole: A High Nitrogen Energetic Compound with Good Oxygen Balance. *Molecules* **2012**, *17*, 5040−5049.

(21) Katritzky, A. R.; Fali, C. N.; Shcherbakova, I. V.; Verin, S. V. 1-(Azidomethyl)benzotriazole and -5-phenyl-1,2,3,4-tetrazole as 1, 3-dipolar cycloaddition components. *J. Heterocycl. Chem.* **1996**, *33*, 335−339.

(22) Wurzenberger, M. H. H.; Szimhardt, N.; Stierstorfer, J. Copper(II) Chlorate Complexes: The Renaissance of a Forgotten and Misjudged Energetic Anion. *J. Am. Chem. Soc.* **2018**, *140*, 3206−3209.

(23) Wurzenberger, M. H. H.; Gruhne, M. S.; Lommel, M.; Szimhardt, N.; Klapötke, T. M.; Stierstorfer, J. Comparison of 1-Ethyl-5H-tetrazole and 1-Azidoethyl-5H-tetrazole as Ligands in Energetic Transition Metal Complexes. *Chem.−Asian J.* **2019**, *14*, 2018−2028.

(24) Johnson, E. C.; Sabatini, J. J.; Chavez, D. E.; Sausa, R. C.; Byrd, E. F. C.; Wingard, L. A.; Guzmàn, P. E. Bis(1,2,4-oxadiazole)bis-(methylene) Dinitrate: A High-Energy Melt-Castable Explosive and Energetic Propellant Plasticizing Ingredient. *Org. Process Res. Dev.* **2018**, *22*, 736−740.

(25) Sućeska, M. Calculation of the Detonation Properties of CHNO explosives. *Propellants, Explos. Pyrotech.* **1991**, *16*, 197−202.
(26) Sućeska, M. *Explo5 V6.05.02*; Zagreb (Croatia), 2018.
(27) BAM. www.bam.de (accessed March 2022).
(28) Wurzenberger, M. H. H.; Bissinger, B. R. G.; Lommel, M.; Gruhne, M. S.; Szimhardt, N.; Stierstorfer, J. Synthesis and comparison of copper(ii) complexes with various N-aminotetrazole ligands involving trinitrophenol anions. *New J. Chem.* **2019**, *43*, 18193−18202.
(29) Ilyushin, M. A.; Smirnov, A. V.; Kotomin, A. A.; Tselinskii, I. V. Energy-Saturated Metal Complexes. *Russ. J. Phys. Chem. B* **2019**, *13*, 119−138.
(30) Beck, W.; Evers, J.; Göbel, M.; Oehlinger, G.; Klapötke, T. M. The Crystal and Molecular Structure of Mercury Fulminate (Knallquecksilber). *Z. Anorg. Allg. Chem.* **2007**, *633*, 1417−1422.
(31) Talawar, M. B.; Agrawal, A. P.; Anniyappan, M.; Wani, D. S.; Bansode, M. K.; Gore, G. M. Primary explosives: Electrostatic discharge initiation, additive effect and its relation to thermal and explosive characteristics. *J. Hazard Mater.* **2006**, *137*, 1074−1078.
(32) Raha, K.; Chhabra, J. S. Static charge development and impact sensitivity of high explosives. *J. Hazard Mater.* **1993**, *34*, 385−391.
(33) Klapötke, T. M. *Energetic Materials Encyclopedia*; 2nd ed.; DeGruyterBerlin/Boston, 2021; Vol. *1*−3.
(34) Gruhne, M. S.; Lommel, M.; Wurzenberger, M. H. H.; Szimhardt, N.; Klapötke, T. M.; Stierstorfer, J. OZM Ball Drop Impact Tester (BIT-132) vs. BAM Standard Method—a Comparative Investigation. *Propellants, Explos. Pyrotech.* **2020**, *45*, 147−153.

Recommended by ACS

Plutonium Hybrid Materials: A Platform to Explore Assembly and Metal–Ligand Bonding
Robert G. Surbella III, Christopher L. Cahill, *et al.*
OCTOBER 28, 2022
INORGANIC CHEMISTRY
READ

Structural and Spectroscopic Characterization of a Zinc-Bound *N*-Oxyphthalimide Radical
Miguel Á. Baeza Cinco, Trevor W. Hayton, *et al.*
AUGUST 16, 2022
INORGANIC CHEMISTRY
READ

Combination of 3-Aminofurazan-4-carboxylic Acid and Transition Metals to Prepare Functional Energetic Catalysts for Catalyzing the Decomposition of Ammonium Perchlorate
Tao Huang, Rufang Peng, *et al.*
JULY 06, 2022
CRYSTAL GROWTH & DESIGN
READ

Activation of Ammonia by a Carbene-Stabilized Dithiolene Zwitterion
Yuzhong Wang, Gregory H. Robinson, *et al.*
AUGUST 29, 2022
JOURNAL OF THE AMERICAN CHEMICAL SOCIETY
READ

Get More Suggestions >

https://doi.org/10.1021/acs.inorgchem.2c02805
Inorg. Chem. 2022, 61, 17212−17225

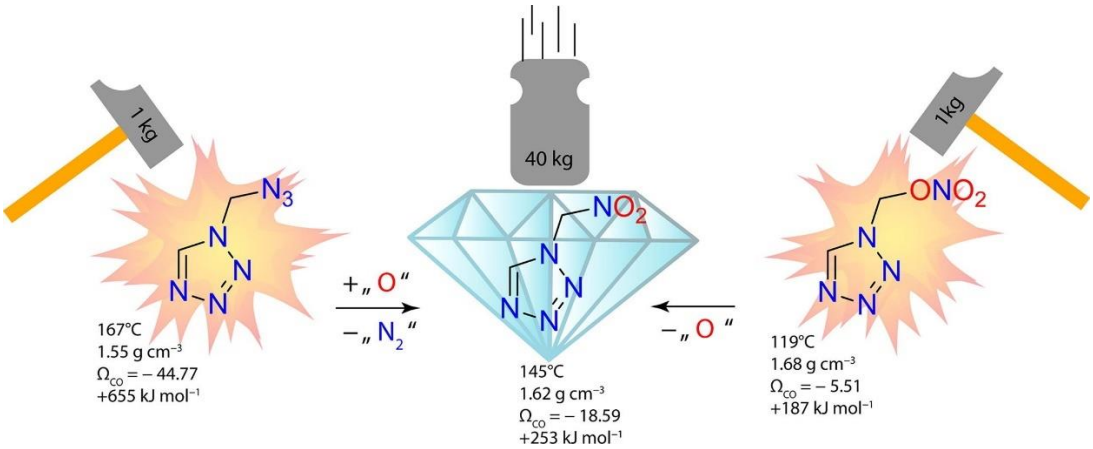
Appendix 32

Energetic Coordination Compounds of late 3d metals with 1N-(Nitromethyl)-5H-tetrazole, a ligand with astonishing properties from the rare class of N-nitromethyl azoles

M. Kofen, T. M. Klapötke, J. Stierstorfer

Chemical Engineering Journal, **2022**, *452*, 139375.

https://doi.org/10.1016/j.cej.2022.139375



Supplementary Information:
https://www.sciencedirect.com/science/article/pii/S1385894722048549

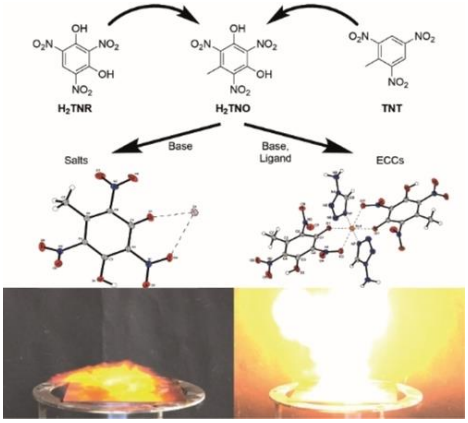
Appendix 33

Trinitro-orcinolate and Trinitro-resorcinate – Sensitivity Trends in Nitroaromatic Energetic Materials

S. M. J. Endraß, A. Neuer, T. M. Klapötke, J. Stierstorfer

ChemistrySelect, **2022**, 7, e202203140.

https://doi.org/10.1002/slct.202203140



Supplementary Information:
https://chemistry-europe.onlinelibrary.wiley.com/action/downloadSupplement?doi=10.1002%2Fslct.202203140&file=slct202203140-sup-0001-misc_information.pdf

ChemistrySelect

Research Article
doi.org/10.1002/slct.202203140

Chemistry Europe
European Chemical Societies Publishing

www.chemistryselect.org

Trinitro-orcinolate and Trinitro-resorcinate – Sensitivity Trends in Nitroaromatic Energetic Materials**

Simon M. J. Endraß, Andreas Neuer, Thomas M. Klapötke, and Jörg Stierstorfer*[a]

5-Methyl-2,4,6-trinitrobenzene-1,3-diol (trinitro-orcinol, H_2TNO) as a close structural relative to the well-known energetic materials trinitroresorcinol (styphnic acid) and trinitrotoluene (TNT) is prepared in high purity and analyzed concerning its vapor pressure using the transpiration method. Several energetic coordination compounds (ECCs) of its respective anion were produced and compared with structurally close styphnate complexes to give an insight into physiochemical trends of the ECC. The synthesized compounds were further analyzed by elemental analysis, IR spectroscopy, differential thermal analysis and low temperature X-ray diffraction analysis. To classify the reported compounds among the energetic materials, they were tested for their sensitivities towards mechanical stimuli such as impact, friction and electrostatic discharge as well as their behavior towards flame.

Introduction

Nitroaromatic compounds can be found in multiple industries and applications for example as drugs, dyes, pesticides and energetic materials.[1,2] Therefore, these compounds are distributed throughout the whole ecosystem and by various sources despite their well-known structure-toxicity relationship.[3–5] This is problematic as many compounds of this kind have been proven to be persistent in soil and are degraded within long time spans by different species.[6–8] Within the field of energetic materials, various nitroaromatic compounds have been studied and commonly found application as the oxidation of the carbon backbone can create interesting physiochemical properties.[9–11] By variation of the structural motifs and formation of salts and coordination compounds (Figure 1), different fields of application of the energetic materials have been achieved depending on the performance and sensitivities of the compounds.[12–14] However, this structural variety also leads to the necessity of methods for detection in order to provide safety precautions to civilians and military.[15,16]

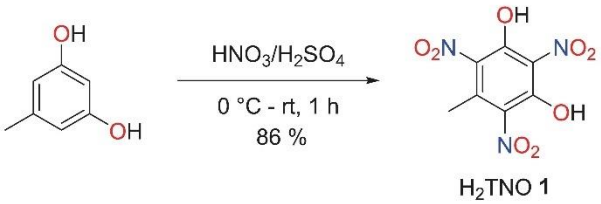
Often, the detection and possibilities for sample processing are limited by the type of design and exact way of application of the ordnance which might only allow measurement of the vapor pressure.[19,20] Trinitro-orcinol (H_2TNO) has been known since the 1870s but despite its structural similarities with styphnic acid (H_2TNR) and trinitro-toluene (TNT) it was not considered a potential energetic material.[21,22] This changed when in 2016 this group published first results of H_2TNO and the formation of its energetic salt Cs_2TNO.[23,24] Preliminary flame tests and the information that H_2TNO could serve as a potential starting material for primary explosives was described. However, no information on the initiation performance and potential application were given. In order to provide possible trends of energetic salts and coordination compounds the goal of this work was to synthesize and characterize several compounds and compare them with literature known styphnate compounds. Furthermore, neat trinitro-orcinol was evaluated concerning its vapor pressure to deliver an additional safety aspect of detection.

Results and Discussion

Synthesis

Trinitro-orcinol (1) was prepared by nitration of commercially available orcinol (5-methylbenzene-1,3-diol) as described in the literature (Scheme 1).[25] The nitration can be performed under relatively mild conditions leading to high yields due to the activating effect of the hydroxy groups.[26]

The obtained H_2TNO was further reacted in acid-base reactions (Scheme 2) which led to aqueous solutions of the respective salts (basic copper carbonate, zinc carbonate, cesium



H_2TNO 1

Scheme 1. Preparation of trinitro-orcinol (H_2TNO).

[a] S. M. J. Endraß, A. Neuer, Prof. Dr. T. M. Klapötke, Dr. J. Stierstorfer
Energetic Materials Research, Department of Chemistry
Ludwig Maximilian University Munich
Butenandtstr. 5–13, 81377
Munich, Germany
E-mail: jstch@cup.uni-muenchen.de
Homepage: www.hedm.cup.uni-muenchen.de/index.html

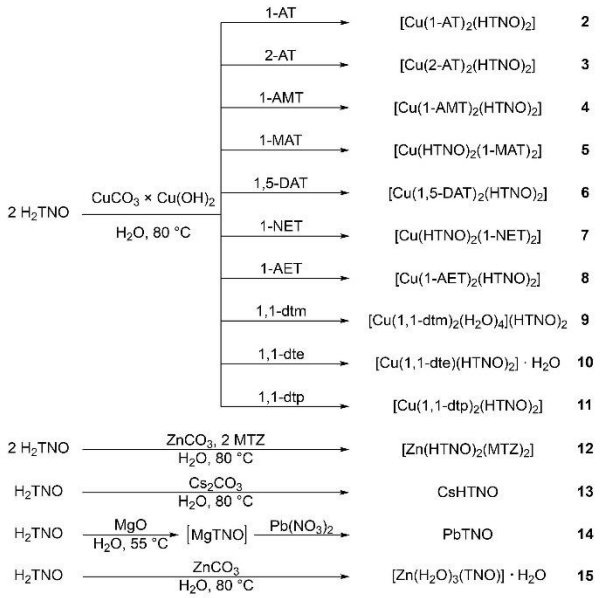
[**] *Parts of this work were published on the NTREM 2022 conference.*[44,45]

Supporting information for this article is available on the WWW under https://doi.org/10.1002/slct.202203140

© 2022 The Authors. ChemistrySelect published by Wiley-VCH GmbH. This is an open access article under the terms of the Creative Commons Attribution License, which permits use, distribution and reproduction in any medium, provided the original work is properly cited.

© 2022 The Authors. ChemistrySelect published by Wiley-VCH GmbH

23656549, 2022, 34, Downloaded from https://chemistry-europe.onlinelibrary.wiley.com/doi/10.1002/slct.202203140 by Ludwig-Maximilians-Universität, Wiley Online Library on [04/11/2022]. See the Terms and Conditions (https://onlinelibrary.wiley.com/terms-and-conditions) on Wiley Online Library for rules of use; OA articles are governed by the applicable Creative Commons License

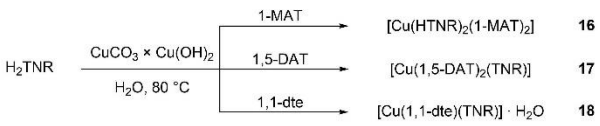


Scheme 2. Complexation and formation of salts of H_2TNO.

carbonate or magnesium oxide). These solutions were left to crystallize at room temperature to obtain the salts or used for complexation. Apart from compounds **4**, **9**, **10**, **12** and **14** single crystals suitable for X-ray diffraction analysis were obtained from the mother liquor. Compounds **9** and **12** were recrystallized from EtOH at room temperature to isolate single crystals of the compounds.

In the case of PbTNO, the synthetic approach of the commonly used β-lead styphnate was applied.[27] For this matter, MgO was added to a suspension of H_2TNO in water at 55 °C. The resulting solution was filtered off and lead(II) nitrate was added, which led to precipitation of the product.

In addition, three previously unknown styphnate complexes were prepared to compare them with trinitro-orcinolate complexes that carry the same ligand. In the case of the 1,5-diaminotetrazole (1,5-DAT) ligand, a styphnate complex was described in the literature, however the sensitivity determination was carried out according to a different standard which is not comparable.[28] Instead of the literature-known [Cu(1,5-DAT)$_2$(HTNR)$_2$], the double deprotonated styphnate species [Cu(1,5-DAT)$_2$(TNR)] was obtained in all attempts of preparation. An overview over the prepared styphnate complexes is given in Scheme 3.



Scheme 3. Preparation of styphnate complexes **16**–**18**.

Vapor pressure

The experimental vapor pressures p_{sat} as well as the thermochemical properties such as molar enthalpies of sublimation $\Delta^g_{cr}H^\circ_m(T)$ and molar entropies of sublimation $\Delta^g_{cr}S^\circ_m(T)$ of H_2TNO was determined using the transpiration method with coupled quantification via high pressure liquid chromatography assisted by an UV-diode array detector (HPLC-DAD) and was categorized in the existing literature of related nitroaromatics (H_2TNR, TNT).[29,30] Here, the data acquisition was obtained from a complete *p-T* dataset with an elaborate calculation based on the *Clausius-Clapeyron* equation.[31] The extrapolation to the standard temperature T_{ref} was carried out by the application of the modified *Clarke-Glew* fit function (see Supporting Information).

This technique allowed the determination of the sublimation behavior of H_2TNO in the temperature range of 332.4–380.7 K (for further information see Supporting Information). The absolute vapor pressures p_{sat} and thermodynamic properties of sublimation including the *Clark-Glew* fit function were presented in Table S8 of the ESI. From these results, the molar enthalpy of sublimation was found to be 122.7 ± 1.7 kJ mol^{-1} and the extrapolated vapor pressure at reference temperature of 298.15 K was derived to be 7.27 μPa.

Since this work determined the appointed thermochemical properties for the first time, the substance H_2TNO was contextualized to the related compounds H_2TNR and TNT. To enable a suitable comparison, the existing literature data were processed in the same manner as described in this paper. For this purpose, the revised properties were presented in Table 1 and Figure 2.

The vaporization behavior of H_2TNR was measured by *Cundall* in the temperature range of 330.2–440.9 K.[30] The molar enthalpy of sublimation was found to be 124.5 kJ mol^{-1} and from these findings the vapor pressure at reference temperature of 298.15 K (6.66×10^{-4} μPa) was extrapolated based on a calculated *p-T* data set via the published *Clausius-Clapeyron* equation and the application of the *Clark-Glew* fit function together with the calculated molar heat capacity (see Table S7).

In addition, the vaporization behavior of TNT was measured by *Cundall* and revised by *Östmark*.[29,30] The reported *Antoine* equation was determined in the temperature range of 285.1–353.4 K and converted into the *Clarke-Glew* fit function considering the molar heat capacity (see Table S7). The molar enthalpy of sublimation was found to be 114.1 kJ mol^{-1} and from these findings the vapor pressure at reference temperature of 298.15 K (714 μPa) were extrapolated.

By contrasting H_2TNO, the volatility was found to settle in between the two comparative substances H_2TNR and TNT. Thus, H_2TNO has a volatility four orders of magnitude higher than H_2TNR and a volatility two orders of magnitude lower than TNT. In addition, the sublimation enthalpy changes marginally compared to H_2TNR and by around 10 kJ mol^{-1} compared to TNT. Also, the illustrated fit function (see Figure 2) indicates that the slope of the fit functions approximates and the offset decreases from TNT over H_2TNO to H_2TNR. This classification corroborates our research results, since in an

© 2022 The Authors. ChemistrySelect published by Wiley-VCH GmbH

23656549, 2022, 34, Downloaded from https://chemistry-europe.onlinelibrary.wiley.com/doi/10.1002/slct.202203140 by Ludwig-Maximilians-Universität, Wiley Online Library on [04/11/2022]. See the Terms and Conditions (https://onlinelibrary.wiley.com/terms-and-conditions) on Wiley Online Library for rules of use; OA articles are governed by the applicable Creative Commons License

Table 1. Comparison of thermodynamic properties of the compounds H_2TNR, H_2TNO and TNT: Vapor pressure p_{sat} and molar enthalpies of sublimation $\Delta^g_{cr}H^{\circ}_m$ at 298.15 K.

Experiment	*T*-Range K	$\Delta^g_{cr}H^{\circ}_m$(298.15 K)[a] kJ mol^{-1}	p_{sat}[b] µPa
H_2TNO	332.4–380.7	122.7 ± 1.7 [c]	7.27
H_2TNR[30]	330.2–440.9	124.5	6.66×10^{-4}
TNT [29]	285.1–353.4	114.1	714

[a] Molar enthalpies of sublimation were adjusted according to *Chickos et al.* [32] with values of $\Delta^g_{cr}C^{\circ}_{p,m}$, $C^{\circ}_{p,m}$(cr) stated in Table S7. [b] Vapor pressure at 298.15 K extrapolated from the *p-T*-data. [c] Uncertainties for molar enthalpies of sublimation at reference temperatures are expressed as expanded uncertainties with confidence level of 0.95 ($k = 2$).

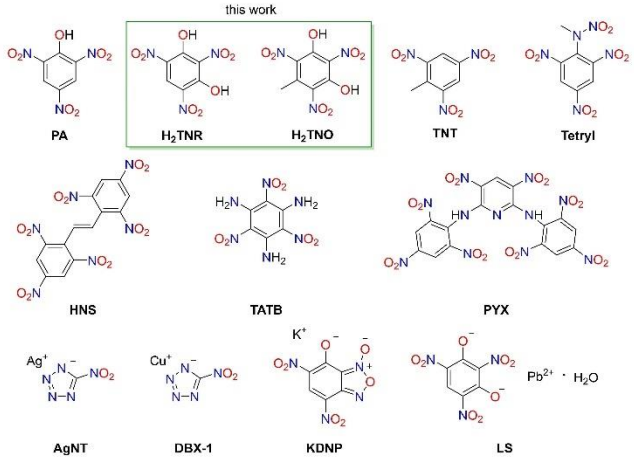


Figure 1. Overview of few examples of nitroaromatic energetic materials for different fields of application:[17,18] PA: picric acid, H_2TNR: styphnic acid, TNT: trinitrotoluene, HNS: hexanitrostilbene, TATB: 1,3,5-triamino-2,4,6-trinitrobenzene, PYX: 2,6-Bis(picrylamino)-3,5-dinitropyridine, AgNT: silver(I) 5-nitrotetrazolate, DBX-1: copper(I) 5-nitrotetrazolate, KDNP: potassium 5,7-dinitro-[2,1,3]-benzoxadiazol-4-olate 3-oxide, LS: lead styphnate.

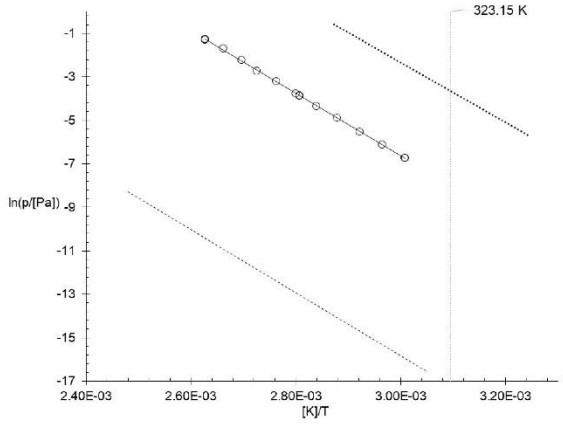


Figure 2. Comparison of the experimental vapor pressure values with the *Clausius-Clapeyron* fit function of the investigated H_2TNO with the corresponding published fit function of H_2TNR and TNT. Here ○ and solid line is H_2TNO; dashed line is H_2TNR; dotted line is TNT. The vertical dotted line serves merely as a guide.

analogous way as the volatility, polarity can also be lined up: H_2TNR has the highest polarity in comparison and TNT the lowest. Since a higher polarity has a direct demeaning effect on the volatility, it can be argued that the particular volatility of H_2TNO is plausible. Moreover, it can be observed that a similar fit function slope can be expected for related substances. Based on these considerations and the assured reproducibility of the measured values (procedure described in previous publications), we have a high degree of confidence in the determined values and have gained access to the thermochemical properties for the first time.

Detonation properties

The energetic properties of compound **1** are calculated with EXPLO5 program code and are displayed in Table 2.[33] Therefore, the enthalpy of formation was determined by applying the atomization method using room temperature CBS-4 M enthalpy and the experimentally determined molar enthalpy of sublimation. For better comparability, the properties of styphnic acid and TNT were recalculated using the same version of EXPLO5. Additionally, CBS-4 M results of all three substances are given in the Supplementary Information. Especially the detonation pressure at the *Chapman-Jouguet* point and the

© 2022 The Authors. ChemistrySelect published by Wiley-VCH GmbH

23656549, 2022, 34, Downloaded from https://chemistry-europe.onlinelibrary.wiley.com/doi/10.1002/slct.202203140 by Ludwig-Maximilians-Universität, Wiley Online Library on [04/11/2022]. See the Terms and Conditions (https://onlinelibrary.wiley.com/terms-and-conditions) on Wiley Online Library for rules of use; OA articles are governed by the applicable Creative Commons License

26565649, 2022, 34, Downloaded from https://chemistry-europe.onlinelibrary.wiley.com/doi/10.1002/slct.202203140 by Ludwig-Maximilians-Universität, Wiley Online Library on [04/11/2022]. See the Terms and Conditions (https://onlinelibrary.wiley.com/terms-and-conditions) on Wiley Online Library for rules of use; OA articles are governed by the applicable Creative Commons License

Table 2. Energetic properties of H_2TNO compared to H_2TNR and TNT.

	H_2TNO (1)	H_2TNR [34]	TNT [34]
Formula	$C_7H_5N_3O_8$	$C_6H_3N_3O_8$	$C_7H_5N_3O_6$
M [g mol^{-1}]	259.13	245.10	227.13
ρ [g cm^{-3}]	1.71[a]	1.83	1.65
N [%][b]	16.22	17.14	18.50
Ω_{CO} [%][c]	−9.3	3.3	−24.7
$\Delta_f H°$ [kJ mol^{-1}][d]	−436.7[j,k]	−374.3[j]	−59.3
Explo5 V6.05.04			
$-\Delta_{Ex}U$ [kJ kg^{-1}][e]	4024	4509	4406
$T_{det.}$ [K][f]	3026	3391	3177
V_0 [L kg^{-1}][g]	637	626	640
P_{CJ} [kbar][h]	198	252	183
$V_{det.}$ [m s^{-1}][i]	6987	7668	6798

[a] From X-Ray diffraction analysis recalculated to 298 K. [b] Nitrogen content. [c] Oxygen balance with respect to CO. [d] Enthalpy of formation. [e] Energy of explosion. [f] Detonation temperature. [g] Volume of detonation products (assuming only gaseous products). [h] Detonation pressure at the *Chapman-Jouguet* point. [i] Detonation velocity. [j] calculated by CBS-4M and atomization method; [k] corrected by gas-phase measurement.

detonation velocity correspond very well to the structural similarities of the compounds.

Crystal Structures

Compounds **2**, **3**, **5–9**, **11–13** and **15** were further examined by low-temperature X-ray diffraction analysis. The data and parameters of the measurements as well as the refinements are given in the supporting information Tables S1–4. $[Cu(1\text{-}AT)_2(HTNO)_2]$ crystallizes in the monoclinic space group $P2_1/c$ with a calculated density of 1.90 g cm^{-3} at 101 K and two formula units per unit cell. The compound shows the typical *Jahn-Teller*-like distortion (Figure 3) of a d^9-metal center in octahedral coordination as expected for Cu^{2-}. The distorted axis is formed by the coordinating nitro groups of the trinitro-orcinolate anions, while the coordination bonds, that are formed by the deprotonated hydroxy group and the 1-amino-5*H*-tetrazole ligand are significantly shorter.

The comparison of this coordination pattern, however, reveals a significant difference compared to the styphnate anions that is displayed in Figure 4. While the styphnate anions are known to coordinate via the nitro groups in *ortho*-position to the remaining proton of the carbon backbone, nitro group that is involved in the coordination of trinitro-orcinolate, is in *para*-position to the methyl group. This coordination pattern is also observed for the ECCs **3**, **5**, **6**, **7**, **8** and **12**. The crystal structures of compounds **3** and **5–8** can be found in the Supplementary Information.

$[Cu(1,1\text{-}dtm)_2(H_2O)_4](HTNO)_2$ crystallizes in the triclinic space group $P-1$ with a density of 1.78 g cm^{-3} at 173 K. Unlike in the literature known styphnate complex $[Cu(1,1\text{-}dtm)(TNR)]\cdot H_2O$ neither the anion nor the 1,1-dtm ligand showed bridging behavior in the case of compound **9**.[36] Instead, a composition close to the respective picrate complex was observed as displayed in Figure 5. The $HTNO^-$ anion is pushed out of the

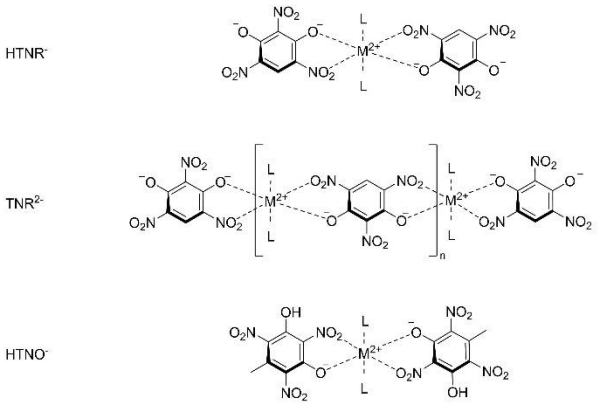


Figure 4. Typical coordination pattern of the styphnate anions $HTNR^-$ and TNR^{2-} in ECCs compared to $HTNO^-$.[35]

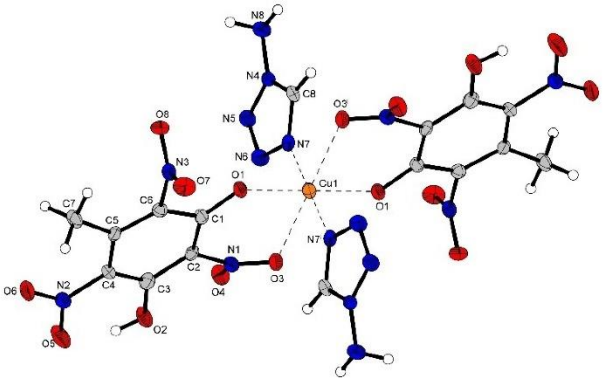


Figure 3. Crystal Structure of $[Cu(1\text{-}AT)_2(HTNO)_2]$ with typical structural motif. Selected bond lengths (Å): Cu1–O1 1.959(3), Cu1–O3 2.355(3), Cu1–N7 2.002(4); selected bond angles (°): O1–Cu1–O3 79.61(12), O1–Cu1–N7 88.98(15), O3–Cu1–N7 94.64(14); symmetry codes: (i) 1 − x, 1 − y, 1 − z.

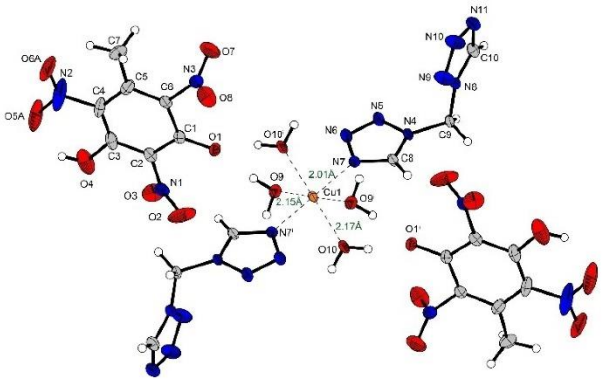


Figure 5. Crystal Structure of $[Cu(1,1\text{-}dtm)_2(H_2O)_4](HTNO)_2$. Selected bond lengths (Å): Cu1–O9 2.153(3), Cu1–O10 2.177(3), Cu1–N7 2.007(3); selected bond angles (°): O9–Cu1–O10 90.60(11), O9–Cu1–N7 91.08(13), O10–Cu1–N7 86.76(13); symmetry codes: (i) 1 − x, 1 − y, 1 − z.

© 2022 The Authors. ChemistrySelect published by Wiley-VCH GmbH

coordination sphere of the copper(II) center and replaced by four molecules of water. Therefore, the metal center is still coordinated octahedrally, but unlike expected without the more common *Jahn-Teller*-like elongation distortion of the coordination sphere. Instead, the four molecules of water are close to evenly distributed with coordination bond lengths of 2.15–2.17 Å and a compressed axis with a Cu^{2+}-ligand distance of 2.01 Å resulting in a *Jahn-Teller*-like compression distortion.

The X-ray diffraction analysis of compound **11** (Figure 6) reveals the distorted octahedral coordination of the copper(II) center by two molecules of ligand and anion each. The elongated axis is taken up by the deprotonated hydroxide of the trinitro-orcinolate, while the xy-level of the octahedra is occupied by the lateral nitrogen atoms of both tetrazole rings. Therefore, no coordination by the nitro group is possible. The compound crystallizes in the monoclinic space group $P2_1/c$ with a density of 1.77 g cm ^{3} at 173 K and two formula units per unit cell.

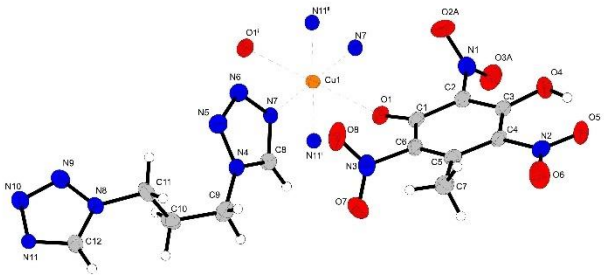


Figure 6. Asymmetric unit of $[Cu(1,1\text{-dtp})_2(HTNO)_2]$. Selected bond lengths (Å) O1–Cu1 2.3426(17), N7–Cu1 1.9956(15), N11–Cu1 2.0232(15); selected bond angles (°): N7–Cu1–N11^{ii} 90.54(6), N7–Cu1–O1 86.65(6), O1–Cu1–N11^{ii} 85.72(6); symmetry codes: (i) 2 − x, 1 − y, 1 − z; (ii) 1 + x, 1/2 − y, 1/2 + z; (iii) 1 − x, 1/2 + y, 1/2 − z.

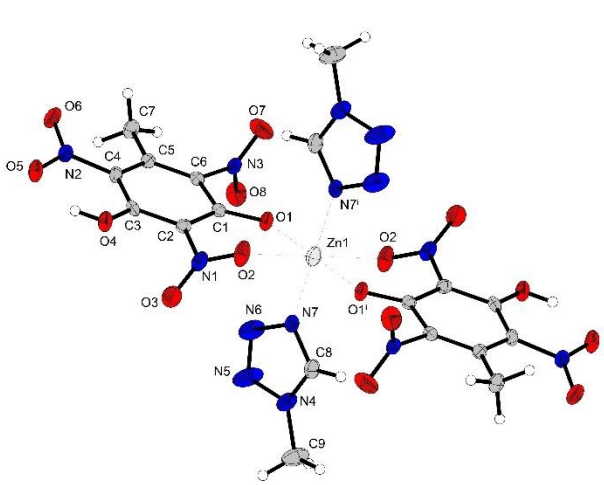


Figure 7. Crystal structure of $[Zn(HTNO)_2(MTZ)_2]$. Selected bond lengths (Å) Zn1–O1 1.940 (2), Zn1–O2 2.371(3), Zn1–N7 1.995(3); selected bond angles (°): O1–Zn1–O2 81.31(9), O1–Zn1–N7 89.32(11), O2–Zn1–N7 88.66(11); symmetry codes: (i) 1 − x, 1 − y, 2 − z.

As displayed in Figure 7, $[Zn(HTNO)_2(MTZ)_2]$ shows the typical coordination pattern of the trinitro-orcinolate anion that was shown earlier. The compound crystallizes in the triclinic space group *P*-1 with a density of 1.83 g cm^{-3} at 98 K.

Figure 8 shows a representative of the double deprotonated anion TNO^{2-} in form of the coordination compound $[Zn(H_2O)_3(TNO)]\cdot H_2O$. The crystal structure indicates, that unlike the styphnate anion TNR^{2-}, no 1D-polymeric chains are formed by TNO^{2-}. Instead of a symmetric coordination by both hydroxides, the torsion angles of the nitro groups lead to a low symmetry coordination pattern. While the coordinating nitro group in *ortho*-position to methyl group shows a torsion angle of −28.4(4)° (O5–N2–C4–C3), the noncoordinating nitro group in *ortho*-position is twisted further to an angle of 67.2(4)° (O8–N3–C6–C1).

Physiochemical properties

The thermal behavior of all compounds was investigated via differential thermal analysis (DTA) in a range of 25–400 °C with a heating rate of 5 °C min^{-1}. The observed events were given as onset temperatures. Endothermic events (e.g. melting point, loss of water or ligand, phase transition) were further investigated by thermogravimetric analysis (TGA) at a similar heating rate in the range 30–400 °C. Plots of every DTA measurement as well as TGA can be found in the supporting information. Detail on the cause of the endothermic events as well as the exothermic decomposition temperatures are briefly given in Table 3. The reported sensitivities classify all com-

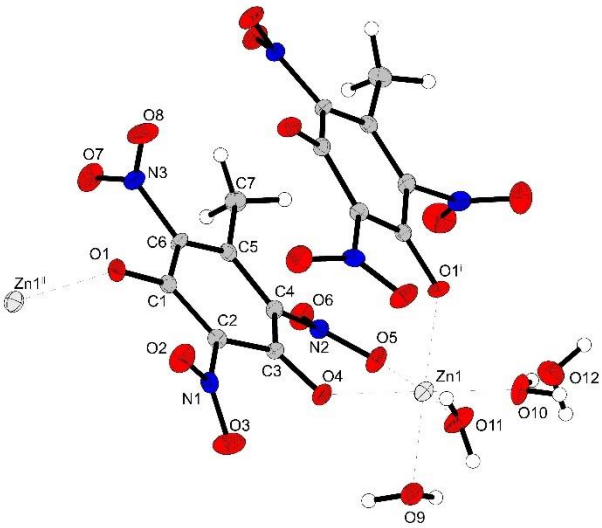


Figure 8. Crystal structure of compound **15**. Selected bond lengths (Å): Zn1–O1^{i} 2.073(2), Zn1–O4 2.028(2), Zn1–O5 2.123(3), Zn1–O9 2.123(2), Zn1–O10 2.039(3), Zn1–O11 2.062(3); selected bond angles (°): O1^{i}–Zn1–O9 175.07(12), O1^{i}–Zn1–O4 94.55(9), O1^{i}–Zn1–O5 92.13(11), O1^{i}–Zn1–O10 89.09(10), O1^{i}–Zn1–O11 86.57(11), O9–Zn1–O488.45(9), O9–Zn1–O5 84.50(11), O9–Zn1–O10 87.36(10), O9–Zn1–O11 97.19(12), O4–Zn1–O5 80.32(9), O4–Zn1–O11 93.09(10), O5–Zn1–O12 90.8(1), O11–Zn1–O12 95.89(11), O4–Zn1–O10 170.5(1), O5–Zn1–O11 173.17(10); symmetry codes: (i) 1/2 + x, 1/2 − y, z, (ii) −1/2 + x, 1/2 − y, z.

© 2022 The Authors. ChemistrySelect published by Wiley-VCH GmbH

23656549, 2022, 34, Downloaded from https://chemistry-europe.onlinelibrary.wiley.com/doi/10.1002/slct.202203140 by Ludwig-Maximilians-Universitäts, Wiley Online Library on [04/11/2022]. See the Terms and Conditions (https://onlinelibrary.wiley.com/terms-and-conditions) on Wiley Online Library for rules of use; OA articles are governed by the applicable Creative Commons License

Table 3. Thermal Stability[a] and sensitivities to mechanical and electrical stimuli of compounds **2**–**14**, compared to literature known styphnates.

Compound	T_{endo}[b] [°C]	T_{exo}[c] [°C]	IS[d] [J]	FS[e] [N]	ESD[f] [mJ]	HP[g]	HN[h]
$[Cu(1\text{-}AT)_2(HTNO)_2]$ **2**	–	185	<1	96	50	def.	dec.
$[Cu(1\text{-}AT)_2(HTNR)_2]$[35]	–	186	1.5	48	16	def.	def.
$[Cu(2\text{-}AT)_2(HTNO)_2]$ **3**	–	182	<1	80	50	def.	def.
$[Cu(2\text{-}AT)_2(HTNR)_2]$[35]	–	206	3	48	20	def.	def.
$[Cu(1\text{-}AMT)_2(HTNO)_2]$ **4**	–	192	<1	60	250	def.	dec.
$[Cu\ (1\text{-}AMT)_2(TNR)]$[35]	–	212	2	16	6.3	def.	def.
$[Cu(HTNO)_2(1\text{-}MAT)_2]$ **5**	–	220	2	>360	90	def.	dec.
$[Cu(HTNR)_2(1\text{-}MAT)_2]$ **16**	–	249	2	>360		def.	dec.
$[Cu(1,5\text{-}DAT)_2(HTNO)_2]$ **6**	–	220	<1	360	200	def.	dec.
$[Cu(1,5\text{-}DAT)_2(HTNR)_2]$[28]	–	242	1.5[i]	–[i]	n.d.	n.d.	n.d.
$[Cu(1,5\text{-}DAT)_2(TNR)]$ **17**	–	229	<1	45	160	def.	dec.
$[Cu(HTNO)_2(1\text{-}NET)_2]$ **7**	–	159	<1	192	90	def.	dec.
$[Cu(1\text{-}NET)_2(TNR)]$ [38]	–	195	2	96	480	def.	def.
$[Cu(1\text{-}AET)_2(HTNO)_2]$ **8**	–	191	<1	>360	90	def.	dec.
$[Cu(1\text{-}AET)_2(TNR)]$[39]	–	177	<1	240	123	def.	def.
$[Cu(1,1\text{-}dtm)_2(H_2O)_4](HTNO)_2$ **9**	100[j]	197	<1	360	160	dec.	dec.
$[Cu(TNR)(1,1\text{-}dtm)]\cdot H_2O$[36]	–	236	2	192	188	def.	dec.
$[Cu(1,1\text{-}dte)(HTNO)_2]\cdot H_2O$ **10**	–	252	>40	192	200	def.	dec.
$[Cu(1,1\text{-}dte)(TNR)]\cdot H_2O$ **18**	–	264	20	360	200	def.	def.
$[Cu(1,1\text{-}dtp)_2(HTNO)_2]$ **11**	–	184	<1	240	200	def.	dec.
$[Cu(1,1\text{-}dtp)(TNR)]\cdot H_2O$[40]	88 ($-H_2O$)	248	10	>360	500	n.d.	n.d.
$[Zn(HTNO)_2(MTZ)_2]$ **12**	–	229	2	168	33	def.	dec.
$[Zn(HTNR)_2(MTZ)_2]$[41]	–	214	4	240	800	n.d.	n.d.
CsHTNO **13**	–	233	<1	>360	50	def.	det.
$[Cs_2(H_2O)(HTNR)(OH)]_n$[42]	74 ($-2\ H_2O$)	292	–	–	–	n.d.	n.d.
PbTNO **14**	–	240	<1	<0.1	0.54	det.	det.
LS [34,43]	–	282	8	0.45	0.9	det.	det.

[a] DTA onset temperatures at a heating rate of 5 °C min^{-1}. [b] Onset temperature of endothermic event in the DTA, indicating a melting point of the compound. [c] Onset of exothermic event in the DTA. [d] Impact sensitivity (BAM drophammer (1 of 6)). [e] Friction sensitivity (BAM friction tester (1 of 6)). [f] Electrostatic discharge devise (OZM XSpark10). [g] Hot plate test (det.: detonation, def.: deflagration, dec.: decomposition, n.d.: not determined). [h] Hot needle test (det.: detonation, def.: deflagration, dec.: decomposition, n.d.: not determined). [i] according to China National Military Standard.[28] [j] gradual loss of mass.

pounds except of **10** (insensitive) and **18** (sensitive) as very sensitive towards impact according to the "UN Recommendations on the Transport of Dangerous Goods".[37] Furthermore, compounds **5**, **8**, **13** are considered insensitive towards friction, while **6**, **9**, **18** are less sensitive. Compounds **2**, **7**, **10**, **11** and **12** have been tested to be sensitive, **3**, **4**, **17** are very sensitive and only compound **14** is characterized as extremely sensitive towards friction. The general trend seems to be an increased impact sensitivity as well as lowered friction sensitivity and thermal stability of the trinitro-orcinolate complexes compared to the respective styphnates.

Conclusion

This work has provided 17 new compounds, among which 11 were characterized by low-temperature X-ray diffraction analysis. This analysis gave an interesting insight in the coordination behavior of trinitro-orcinolate compared to the anions of styphnic acid. Surprisingly, the investigation of the physiochemical properties showed, that despite the lower enthalpy of formation, trends towards an increased impact sensitivity and lower thermal stability of the trinitro-orcinolates can be observed. The sensitivities towards friction, in contrast, seem followed to be lower compared to the respective styphnates. In addition, the experimental vapor pressure of H_2TNO was determined, using the transpiration method. This crucial parameter for explosives' detection was put in context by comparison with literature values of the close structural relatives trinitroresorcinol and trinitrotoluene. The observed similarities of the fit function slopes as well as the overall placement of the volatility in between the literature values plausibly represent the shared structural similarities. While the high sensitivities towards impact, that were observed for most trinitro-orcinolates, excludes them from application as a primary explosive, utilization as a replacement of lead styphnate or as a sensitizer in priming mixtures might be considered.

Supporting information

Supplementary data on synthesis, purity assessment of the compounds and details of the quantification methods are provided in the Supporting information.

Deposition Number(s) 2191773 (for **2**), 2191776 (for **3**), 2191775 (for **5**), 2191782 (for **6**), 2191777 (for **7**), 2191778 (for **8**), 2191779 (for **9**), 2191774 (for **11**), 2191783 (for **12**), 2191781 (for **13**) and 2191780 (for **15**) contain the supplementary crystallographic data for this paper. These data are provided

© 2022 The Authors. ChemistrySelect published by Wiley-VCH GmbH

23656549, 2022, 34, Downloaded from https://chemistry-europe.onlinelibrary.wiley.com/doi/10.1002/slct.202203140 by Ludwig-Maximilians-Universität, Wiley Online Library on [04/11/2022]. See the Terms and Conditions (https://onlinelibrary.wiley.com/terms-and-conditions) on Wiley Online Library for rules of use; OA articles are governed by the applicable Creative Commons License

23656549, 2022, 34, Downloaded from https://chemistry-europe.onlinelibrary.wiley.com/doi/10.1002/slct.202203140 by Ludwig-Maximilians-Universität, Wiley Online Library on [04/11/2022]. See the Terms and Conditions (https://onlinelibrary.wiley.com/terms-and-conditions) on Wiley Online Library for rules of use; OA articles are governed by the applicable Creative Commons License

free of charge by the joint Cambridge Crystallographic Data Center and Fachinformationszentrum Karlsruhe Access Structures service.

Acknowledgements

For financial support of this work by Ludwig-Maximilian University (LMU), the Office of Naval Research (ONR) under grant no. ONR N00014-19-1-2078 and the Strategic Environmental Research and Development Program (SERDP) under contract no. W912HQ19C0033 and the DAAD (German Academic Exchange Service) [grant no. 57299294] are gratefully acknowledged. The authors would like to thank Dr. Burkhard Krumm for NMR measurements and Kay Chen for proofreading. Open Access funding enabled and organized by Projekt DEAL.

Conflict of Interest

The authors declare no conflict of interest.

Data Availability Statement

The data that support the findings of this study are available in the supplementary material of this article.

Keywords: Crystal Engineering · Energetic Coordination Compounds · Energetic Materials · Experimental Vapor Pressure · Structure Elucidation

[1] K.-S. Ju, E. Parales Rebecca, *Microbiol. Mol. Biol. Rev.* **2010**, *74*, 250–272.
[2] C. Kannigadu, D. D. N'Da, *Curr. Pharm. Des.* **2020**, *26*, 4658–4674.
[3] O. Isayev, B. Rasulev, L. Gorb, J. Leszczynski, *Mol. Diversity* **2006**, *10*, 233–245.
[4] H. Stucki, *Chimia* **2004**, *58*, 409–413.
[5] P. Kovacic, R. Somanathan, *J. Appl. Toxicol.* **2014**, *34*, 810–824.
[6] M. Megharaj, B. Ramakrishnan, K. Venkateswarlu, N. Sethunathan, R. Naidu, *Environ. Int.* **2011**, *37*, 1362–1375.
[7] J. C. Spain, *Annu. Rev. Microbiol.* **1995**, *49*, 523–555.
[8] J. S. Strehse, M. Brenner, M. Kisiela, E. Maser, *Arch. Toxicol.* **2020**, *94*, 4043–4054.
[9] M. H. H. Wurzenberger, J. T. Lechner, M. Lommel, T. M. Klapötke, J. Stierstorfer, *Propellants Explos. Pyrotech.* **2020**, *45*, 898–907.
[10] J. W. Fronabarger, M. D. Williams, W. B. Sanborn, D. A. Parrish, M. Bichay, *Propellants Explos. Pyrotech.* **2011**, *36*, 459–470.
[11] T. M. Klapötke, J. T. Lechner, J. Stierstorfer, *Propellants Explos. Pyrotech.* **2022**, *47*, e202100205.
[12] T. M. Klapötke, J. Stierstorfer, M. Weyrauther, T. G. Witkowski, *Chem. Eur. J.* **2016**, *22*, 8619–8626.
[13] J. W. Fronabarger, M. D. Williams, W. B. Sanborn, J. G. Bragg, D. A. Parrish, M. Bichay, *Propellants Explos. Pyrotech.* **2011**, *36*, 541–550.
[14] T. M. Klapötke, P. Mayer, C. Miró Sabaté, J. M. Welch, N. Wiegand, *Inorg. Chem.* **2008**, *47*, 6014–6027.
[15] A. W. Czarnik, *Nature* **1998**, *394*, 417–418.
[16] M. E. Germain, M. J. Knapp, *J. Am. Chem. Soc.* **2008**, *130*, 5422–5423.
[17] T. M. Klapötke, *Chemistry of High-Energy Materials*, 5th ed., De Gruyter, Berlin, Boston, **2019**.
[18] K. D. Oyler, in *Green Energetic Materials*, **2014**, pp. 103–132.
[19] S. J. Toal, W. C. Trogler, *J. Mater. Chem.* **2006**, *16*, 2871–2883.
[20] D. S. Moore, *Rev. Sci. Instrum.* **2004**, *75*, 2499–2512.
[21] V. Merz, G. Zetter, *Ber. Dtsch. Chem. Ges.* **1879**, *12*, 2035–2049.
[22] J. Stenhouse, C. E. Groves, *Ber. Dtsch. Chem. Ges.* **1880**, *13*, 1305–1308.
[23] A. Drechsel, T. M. Klapoetke, T. G. Witkowski, *J. J. Inorg. Chem.* **2016**, *1*, 1–8.
[24] T. G. Witkowski, Dissertation thesis, LMU Munich **2017**.
[25] A. J. Birch, R. A. Massy-Westropp, R. W. Rickards, H. Smith, *J. Chem. Soc.* **1958**, 360–365.
[26] A. P. Marchand, G. M. Reddy, *Synthesis* **1992**, *1992*, 261–262.
[27] M. A. Pierce-Butler, *Acta Crystallogr. Sect. B* **1982**, *38*, 3100–3104.
[28] Y.-G. Bi, Y.-A. Feng, Y. Li, B.-D. Wu, T.-L. Zhang, *J. Coord. Chem.* **2015**, *68*, 181–194.
[29] H. Östmark, S. Wallin, H. G. Ang, *Propellants Explos. Pyrotech.* **2012**, *37*, 12–23.
[30] R. B. Cundall, T. Frank Palmer, C. E. C. Wood, *J. Chem. Soc. Faraday Trans. 1* **1978**, *74*, 1339–1345.
[31] M. Härtel, Dissertation thesis, LMU München **2017**.
[32] W. Acree, J. S. Chickos, *J. Phys. Chem. Ref. Data* **2010**, *39*, 043101.
[33] M. Suceska, *EXPLO5 version V6.05 User's guide*, Zagreb, **2018**.
[34] T. M. Klapötke, *Energetic Materials Encyclopedia, Vol. 1–3*, 2nd ed., DeGruyter, Berlin/Boston, **2021**.
[35] M. H. H. Wurzenberger, B. R. G. Bissinger, M. Lommel, M. S. Gruhne, N. Szimhardt, J. Stierstorfer, *New J. Chem.* **2019**, *43*, 18193–18202.
[36] M. H. H. Wurzenberger, V. Braun, M. Lommel, T. M. Klapötke, J. Stierstorfer, *Inorg. Chem.* **2020**, *59*, 10938–10952.
[37] Impact: insensitive > 40 J, less sensitive ≥ 35 J, sensitive ≥ 4 J, very sensitive ≤ 3 J; Friction: insensitive > 360 N, less sensitive = 360 N, sensitive < 360 N and > 80 N, very sensitive ≤ 80 N, extremely sensitive ≤ 10 N, According to: *Recommendations on the Transport of Dangerous Goods, Manual of Tests and Criteria*, 4th. ed., United Nations, New York-Geneva, **1999**.
[38] M. S. Gruhne, T. Lenz, M. Rösch, M. Lommel, M. H. H. Wurzenberger, T. M. Klapötke, J. Stierstorfer, *Dalton Trans.* **2021**, *50*, 10811–10825.
[39] M. H. H. Wurzenberger, M. S. Gruhne, M. Lommel, N. Szimhardt, T. M. Klapötke, J. Stierstorfer, *Chem. Asian J.* **2019**, *14*, 2018–2028.
[40] N. Szimhardt, M. H. H. Wurzenberger, T. M. Klapötke, J. T. Lechner, H. Reichherzer, C. C. Unger, J. Stierstorfer, *J. Mater. Chem. A* **2018**, *6*, 6565–6577.
[41] N. Szimhardt, M. H. H. Wurzenberger, A. Beringer, L. J. Daumann, J. Stierstorfer, *J. Mater. Chem. A* **2017**, *5*, 23753–23765.
[42] J.-G. Zhang, K. Wang, Z.-M. Li, H. Zheng, T.-L. Zhang, L. Yang, *Main Group Chem.* **2011**, *10*, 205–213.
[43] M. S. Gruhne, M. Lommel, M. H. H. Wurzenberger, N. Szimhardt, T. M. Klapötke, J. Stierstorfer, *Propellants Explos. Pyrotech.* **2020**, *45*, 147–153.
[44] S. M. J. Endraß, T. M. Klapötke, J. Stierstorfer, *New Trends in Research of Energetic Materials* Pardubice, Czech Republic, 06–08 April, **2022**, 311–317.
[45] A. Neuer, G. Bikelyté, S. M. J. Endraß, T. M. Klapötke, J. Stierstorfer, *New Trends in Research of Energetic Materials* Pardubice, Czech Republic, 06–08 April, **2022**, 440–448.

Submitted: August 11, 2022
Accepted: August 15, 2022

© 2022 The Authors. ChemistrySelect published by Wiley-VCH GmbH

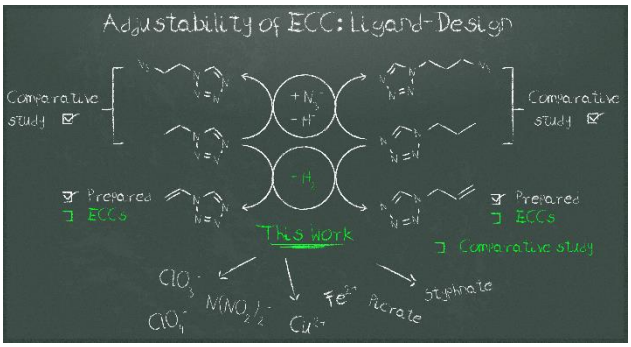
Appendix 34

The Adjustability of Physicochemical Properties: Comparison of 1-Vinyl-5*H*-tetrazole and 1-Allyl-5*H*-tetrazole as Ligands in 3d Metal Energetic Coordination Compounds (ECC)

Markus Rösch, Michael S. Gruhne, Marcus Lommel, Simon M. J. Endraß, and Jörg Stierstorfer

Inorg. Chem. **2023**, *in press*

https://doi.org/10.1021/acs.inorgchem.2c03624



Supplementary Information:

Inorganic Chemistry

pubs.acs.org/IC Article

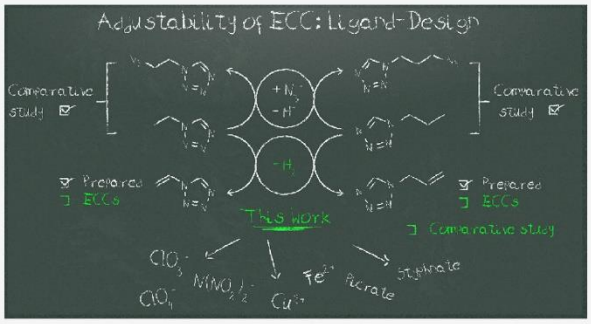
The Adjustability of Physicochemical Properties: Comparison of 1-Vinyl-5H-tetrazole and 1-Allyl-5H-tetrazole as Ligands in 3d Metal Energetic Coordination Compounds

Markus Rösch,[‡] Michael S. Gruhne,[‡] Marcus Lommel, Simon M. J. Endraß, and Jörg Stierstorfer*

Cite This: https://doi.org/10.1021/acs.inorgchem.2c03624 Read Online

ACCESS | Metrics & More | Article Recommendations | Supporting Information

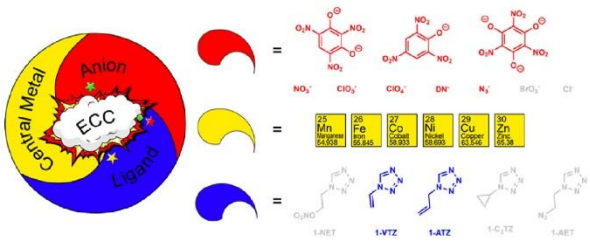
ABSTRACT: Energetic coordination compounds (ECCs) show promising properties to be used as potential substitutes for highly toxic lead-containing primary explosives. The concept is to combine the three building blocks: (i) ligand, (ii) transition metal, and (iii) anion, acting as (i) fuel, (ii) matrix, and (iii) oxidizer (e.g., ClO_4^-, NO_3^-, ClO_3^-) or energetic component (e.g., DN^-, N_3^-, picrate, styphnate, trinitrophloroglucinate). By variation of the ligands, the complexes' properties can be adjusted toward their desired performance and sensitivities. In the present study, 1-vinyl-5*H*-tetrazole (1-VTZ, **1**) and 1-allyl-5*H*-tetrazole (1-ATZ, **2**) were used as nitrogen-rich endothermic ligands to form 3d metal (Mn^{2+}, Fe^{2+}, Cu^{2+}, Zn^{2+}, Co^{2+}, Ni^{2+})-based ECCs. The influence of the introduction of an unsaturated C−C bond (**1**-ETZ *vs* 1-VTZ and **1**-PTZ *vs* 1-ATZ) on the performance and sensitivity of the complexes is discussed, as is the lengthening of the alkenyl chain (1-VTZ *vs* 1-ATZ). For further insights, the novel complexes were compared to literature-known complexes based on N1-substituted C2- and C3-derived tetrazole ligands, respectively. The ligand 1-VTZ (**1**) was prepared by elimination of hydrogen chloride from 1-(2-chloroethyl)-5*H*-tetrazole in methanolic KOH solution. 1-ATZ (**2**) was obtained by a heterocyclization reaction of allylamine with triethyl orthoformate and sodium azide in an acetic acid medium. All compounds were intensively characterized with analytical methods such as XRD, IR, EA, DTA, TGA, and sensitivity measurements (IS and FS). The energetic performances were visibly evaluated in fast heating experiments. Furthermore, PETN initiation and laser ignition experiments were carried out for promising ECCs.



1. INTRODUCTION

In the field of energetic materials, the main challenges remain to create compounds that have high performance and thermal stability with low toxicity, in addition to low-cost synthesis.[1] For primary explosives, the main substances to be replaced are lead styphnate (LS) and lead azide (LA). In the past, tetrazoles as endothermic nitrogen-rich compounds with a high positive heat of formation have emerged as suitable building blocks for energetic materials.[2−8] Notably, this class of compounds combines the desired properties of endothermicity with kinetic stability as well as forms non-toxic reaction products during decomposition.[1] To date, tetrazole-containing compounds are therefore in particular used as 'green' primary[2,7,9−11] and secondary explosives,[3,12] but also binders[13−15] and energy-rich additives can be found in the literature.[16] Besides these sufficiently known uses, tetrazoles have also found use as ligands in the research of ECCs (Chart 1).[17−19] In particular, the numerous possibilities to tailor the coordination compounds' chemical and physicochemical properties by varying the central metal, ligand, and anion make this substance class interesting for various purposes.[20]

Chart 1. Preliminary (Gray Colored) and Current Work Using Energetic *N*1-Substituted Tetrazoles in Energetic Coordination Compounds (ECCs)



Received: October 12, 2022

ACS Publications © XXXX The Authors. Published by American Chemical Society

The introduction of an *N*-substituent onto the tetrazole ring prevents acidic protons and allows to build up neutral complexes with oxidizing anions to synthesize more promising energetic materials. Among others, several monosubstituted[21−24] and disubstituted tetrazoles[25,26] were investigated as ligands in ECCs.

Noteworthily, the energetic character of tetrazole-based ligands is thereby tuned by alteration of the functional groups or their substitution pattern (*N*1-substituted *vs N*2-substituted *vs* C5-substituted). In addition to explosophoric groups (e.g., $-NO_2$, $-ONO_2$, $-N_3$), which enhance the density, nitrogen content, and oxygen balance, alkyl chains are introduced to desensitize the complexes. The main challenge is to design ECCs with a high heat of detonation as well as low sensitivity (impact, friction, and heat) especially required for special applications in industry (e.g., mining and oil drilling). Unfortunately, there is often a tradeoff between this contradictory relationship. In this context, the ethyl group has proven itself to be very versatile.[27−30] This is not only because of their low-cost availability but also because of the simplicity of implementation.[27]

2. RESULTS AND DISCUSSION

2.1. Comparison of the Ligands' $\Delta_f H°_{(g)}$. Every one of the tetrazole derivatives displayed in Figure 1 is known in the literature[27,31,32] and was partly used as a ligand in ECCs[33] with especially 1-ethyl-5*H*-tetrazole (1-ETZ)[23] and 1-propyl-5*H*-tetrazole (1-PTZ)[24] showing a lack of performance or having not been investigated toward their energetic parameters at all.[34−40] In the present work, 1-VTZ (**1**) and 1-ATZ (**2**) are used as ligands in energetic 3d transition metal complexes. The gas phase enthalpy of formation was chosen as a comparative criterion for the tetrazole derivatives. The results of the calculations are shown as per unit mass enthalpies of formation in the bar chart in Figure 1.

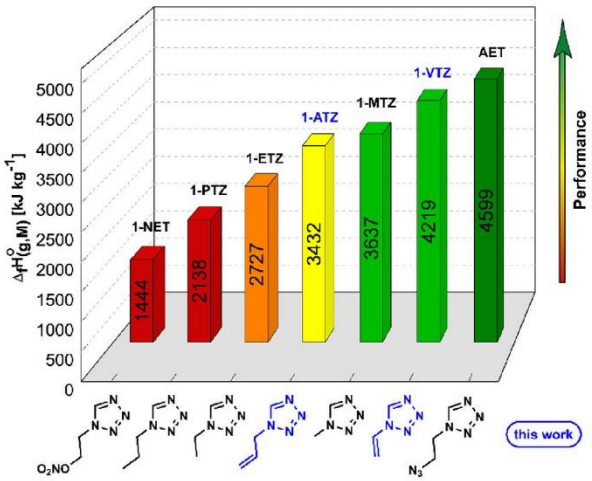


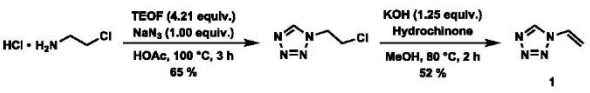
Figure 1. Comparison of the calculated gas-phase enthalpies of formation for various monotetrazole derivatives. Enthalpies of formation were calculated using the atomization method ($\Delta_f H°_{(g,M)} = H_{(M)} - \Sigma H°_{(A)} + \Sigma \Delta_f H°_{(A)}$) using Gaussian09 computed CBS-4M electronic enthalpies.

As shown in Figure 1, the formal reduction of the terminal C−C bond in 1-ETZ ($\Delta_f H°_{(g)}$ = 2727 kJ kg^{-1}) and 1-PTZ ($\Delta_f H°_{(g)}$ = 2138 kJ kg^{-1}) leads to an increase in the gas phase enthalpies of formation in 1-VTZ ($\Delta_f H°_{(g)}$ = 4219 kJ kg^{-1}) and 1-ATZ ($\Delta_f H°_{(g)}$ = 3432 kJ kg^{-1}), respectively.

For 1-VTZ, this should, in accordance with hexanitrostilbene (HNS), due to the larger π system not only result in a higher energetic performance but also higher thermal stability and lower sensitivity of the corresponding ECCs.[41] Throughout the sophisticated combination of anion, central metal, and *N*-vinyl or *N*-allyl ligand, the preparation of green ECCs, capable of replacing LA or LS, is aimed. Noteworthily, the polymerization of 1-ATZ and 1-VTZ has already been investigated in the early 1960s in an attempt to develop promising energetic polymers.[42]

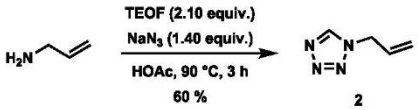
2.2. Synthesis of the Ligands. Initially, the nitrogen-rich heterocycle 1-vinyl-5*H*-tetrazole (**1**) was readily prepared *via* a convenient two-step reaction starting from commercially available 2-chloroethylamine hydrochloride (Scheme 1). In the first step, the primary amine salt was converted in a [3 + 1 + 1] cyclization to the corresponding 1-substituted alkyl tetrazole upon treatment with an excess of triethyl orthoformate and sodium azide in glacial acetic acid at 100 °C for 3 h.[43] Subsequent elimination of hydrogen chloride from the isolated intermediate 1-(2-chloroethyl)-5*H*-tetrazole (1-ClET) under basic conditions and elevated temperature led to the desired product 1-VTZ (**1**, Scheme 1). An alternative sequence for the preparation of 1-ClET has been published independently by Finnegan *et al.*[32] and Gaponik *et al.*[31] and involves the formation of 1-(2-hydroxyethyl)-5*H*-tetrazole (1-HET) followed by subsequent chlorination. However, since both approaches require a higher number of reaction steps, the synthesis in Scheme 1 was preferred.

Scheme 1. Synthesis of 1-Vinyl-5*H*-tetrazole (1, 1-VTZ)



1-Allyl-5*H*-tetrazole (**1**) was prepared by adapting a literature-known procedure starting from commercially available allylamine (Scheme 2).[27] In analogy to the first reaction step of the 1-VTZ (**1**) synthesis (Scheme 1), a three-component heterocyclization reaction of the free amine with triethyl orthoformate and sodium azide was carried out in an acetic acid medium. The resulting crude product was isolated by column chromatography (EtOAc/hexanes 1:1), yielding the target compound as a pale-yellow liquid (60%).

Scheme 2. Synthesis of 1-Allyl-5*H*-tetrazole (2, 1-ATZ)



Retrosynthetically, 1-ATZ (**2**) can also be synthesized starting from 3-chloropropylamine hydrochloride. Following the same synthesis strategy as for 1-VTZ (**1**, Scheme 2), ring closure with subsequent cleavage of hydrogen chloride from the resulting chloropropyltetrazole is possible under basic conditions and elevated temperatures. An alternative approach described in the literature is the substitution reaction of 1*H*-

https://doi.org/10.1021/acs.inorgchem.2c03624
Inorg. Chem. XXXX, XXX, XXX−XXX

tetrazole and alkyl halides, after which the formed 1- and 2-isomers are separated and purified by vacuum distillation.[44]

Notably, the solid–liquid crude product 1-VTZ (**1**) could be purified by sublimation *in vacuo* (40 °C/10 mbar) on a cooling finger with solid carbon dioxide-ethanol as coolant. Here, we obtained single crystals of 1-VTZ (**1**), which had already been synthesized in 1958 (Figure 2).[38,45]

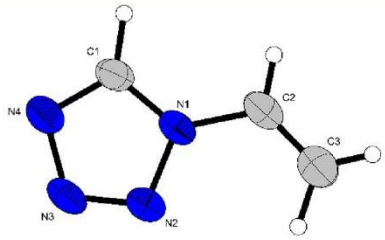
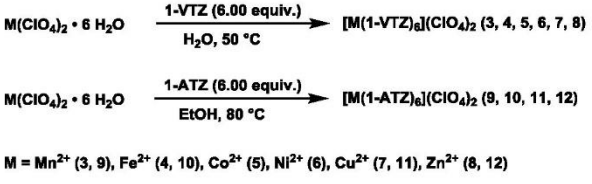


Figure 2. Crystal structure of 1-vinyl-5*H*-tetrazole (1-VTZ). Thermal ellipsoids of non-hydrogen atoms in all structures are set to the 50% probability level. Selected bond lengths (Å): N1–N2 1.353 (4), N1–C1 1.337 (4), N1–C2 1.435 (5), N2–N3 1.299 (4), N3–N4 1.373 (4), N4–C1 1.309 (4), C2–C3 1.283 (6). Selected bond angles (°): N2–N1–C1 107.9 (3), N2–N1–C2 123.4 (3), C1–N1–C2 128.7 (3), N1–N2–N3 106.0 (2), N2–N3–N4 111.2 (2), N3–N4–C1 104.7 (3), N1–C1–N4 110.2 (3), N1–C2–C3 122.8 (3).

2.3. Synthesis of the ECCs. To date, several complexes based on 1-VTZ (**1**) and 1-ATZ (**2**) utilizing chloride, nitrate, and thiocyanate as counterion have been reported in the literature but were neither energetically nor structurally investigated.[35−37,46] Apart from structural elucidation, we aimed to investigate the energetic properties of 1-VTZ (**1**) and 1-ATZ (**2**) in various novel transition metal complexes and their potential use as primary explosives, especially aiming for an increase in performance through the implementation of the vinyl or allyl moiety.

As neutral N-substituted tetrazoles, the ligands 1-VTZ (**1**) and 1-ATZ (**2**) were incorporated in ECCs with anionic oxidizing agents (e.g., perchlorate, chlorate, nitrate, dinitramide), powerful anionic azido ligands or nitrophenolate anions derived from picric acid (HPA), styphnic acid (H_2TNR), or trinitrophloroglucinol (TNPG), leading to powerful energetic materials. The alteration of both the metal(II) center and the counter anion results in ECCs with adjustable sensitivity, solubility, and performance parameters.[21] For the preparation of all coordination compounds, water or ethanol was chosen as environmentally friendly solvents. The perchlorate transition metal 1-VTZ complexes **3**–**8** were prepared by slowly adding stoichiometric amounts of liquid 1-VTZ (**1**) to an aqueous solution of the respective metal(II) salt at room temperature (Scheme 3, top). In case of a suspension formed, the reaction mixture was heated until complete dissolution. Both water and ethanol are suitable solvent systems for the preparation of the ECCs **3**–**8**, whereby the use of ethanol accelerates the crystallization process at room temperature. All perchlorate 1-VTZ complexes **3**–**8** were obtained as frequently observed hexacoordinated metal(II) centers without the inclusion of water.

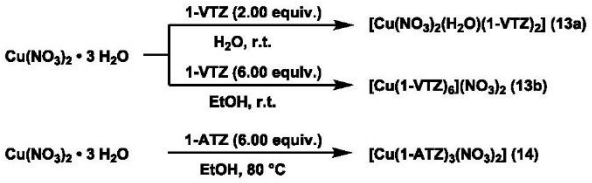
Scheme 3. Synthesis of Metal(II) Perchlorate-Based 1-VTZ (3–8) and 1-ATZ (9–12) Complexes



For the synthesis of 1-ATZ (**2**)-based perchlorate ECCs **9**–**12**, the ligand 1-ATZ (**2**) was added to an ethanolic solution of the corresponding metal(II) salt at elevated temperature (Scheme 3, bottom). All 1-ATZ-based complexes **9**–**12** precipitated from the ethanolic solution, at the least when cooled on ice or by precipitation with an antisolvent in decent to very good yields (49–87%). For crystal growth, small amounts of water were added to the hot ethanolic suspensions until complete dissolution occurred at 80 °C. However, it was difficult to obtain single crystals suitable for X-ray diffraction (XRD), as **9**–**12** show hexagonal plates that are already bent on growing. It was not possible to cut crystals into smaller pieces without introducing many defects. The same phenomenon was reported for hexakis(1-methyltetrazole)iron(II) bis(perchlorate).[47] While crystal structures could be obtained for $[Fe(1\text{-}ATZ)_6](ClO_4)_2$ (**10**) and $[Cu(1\text{-}ATZ)_6](ClO_4)_2$ (**11**), $[Mn(1\text{-}ATZ)_6](ClO_4)_2$ (**9**) and $[Zn(1\text{-}ATZ)_6](ClO_4)_2$ (**12**) were highly disordered and a complete refinement of the data was not feasible. It was nevertheless possible to get an insight into their composition, which was confirmed by elemental analysis (EA).

The copper(II) coordination compound $[Cu(NO_3)_2(H_2O)(1\text{-}VTZ)_2]$ (**13a**) was prepared by applying ligand **1** to an aqueous solution of $Cu(NO_3)_2$, providing the nitrato complex **13a** in 81% yield after 7 days of crystallization (Scheme 4). To prevent the incorporation of aqua ligands, the reaction conditions were adapted. Using ethanol as the reaction medium led to the formation of the nitrate complex $[Cu(1\text{-}VTZ)_6](NO_3)_2$ (**13b**). Unfortunately, only a few single crystals suitable for XRD could be isolated. It is assumed that a slow conversion from complex $[Cu(1\text{-}VTZ)_6](NO_3)_2$ to the monohydrate species $[Cu(NO_3)_2(H_2O)(1\text{-}VTZ)_2]$ (**13a**) is taking place. Due to its instability against moisture, no elemental analysis pure sample of **13b** was obtained. In particular, the copper(II) nitrate complex known in the literature with the composition $[Cu(NO_3)_2(1\text{-}VTZ)_4]\cdot H_2O$ was not obtained in our experiments.[36] As for the complexes of copper(II) nitrate with 1-ATZ, $[Cu(NO_3)_2(1\text{-}ATZ)_2]$ and $[Cu(1\text{-}ATZ)_6](NO_3)_2$ have already been reported by Lavrenova *et al.*[39] By applying the reaction conditions (solvent system, ligand concentration, temperature) as shown in Scheme 4, another species $[Cu(1\text{-}ATZ)_3(NO_3)_2]$ (**14**) could be obtained after 2 days of crystallization. However, probably due to the co-crystallization of the abovementioned species, no elemental analysis pure sample of **14** was obtained.

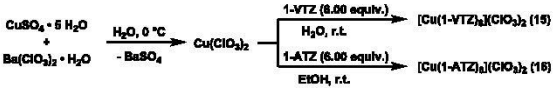
Scheme 4. Synthesis of Selected Copper(II) Nitrate-Based 1-VTZ (13a, 13b) and 1-ATZ (14) Complexes



https://doi.org/10.1021/acs.inorgchem.2c03624
Inorg. Chem. XXXX, XXX, XXX–XXX

Besides the perchlorate, the less toxic, highly oxidizing chlorate anion was used in ECCs. In correspondence to a recently published protocol,[48] $[Cu(1\text{-}VTZ)_6](ClO_3)_2$ (**15**) and $[Cu(1\text{-}ATZ)_6](ClO_3)_2$ (**16**) were synthesized by reacting a freshly prepared aqueous solution of copper(II) chlorate with the respective stoichiometric amounts of the nitrogen-rich ligand 1-VTZ (**1**) or 1-ATZ (**2**) (Scheme 5). $Cu(ClO_3)_2$ is

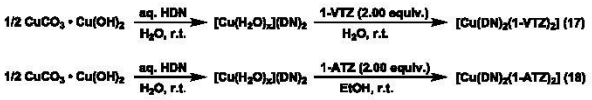
Scheme 5. Formation of the Copper(II) 1-VTZ (15) and 1-ATZ (16) Chlorate Complex



formed *in situ* by a metathesis reaction of copper(II) sulfate and barium chlorate. Both complexes were obtained in the form of single crystals in moderate yields (34−60%).

In the case of the copper(II) dinitramide complexes $[Cu(DN)_2(1\text{-}VTZ)_2]$ (**17**) and $[Cu(DN)_2(1\text{-}ATZ)_2]$ (**18**), stoichiometric amounts of the respective ligand 1-VTZ (**1**) or 1-ATZ (**2**) were combined with a freshly prepared aqueous solution of copper(II) dinitramide (Scheme 6). The mother

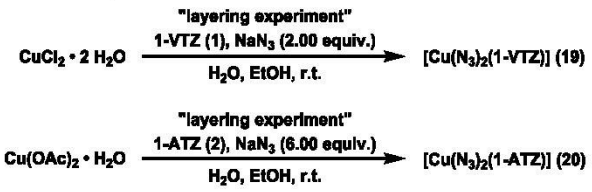
Scheme 6. Synthesis of the Energetic Copper(II) Dinitramide Complexes 17 and 18



liquor was left for crystallization at room temperature. Within 13 days, **17** and **18** were obtained as blue crystals in yields of 57% and 72%, respectively. For the *in situ* preparation of $[Cu(H_2O)_x](DN)_2$, dinitraminic acid (HDN) was reacted with basic copper(II) carbonate.

Based on our previously published work, the corresponding copper(II) azide complexes **19** and **20** were prepared. Thus, layering experiments were performed resulting in single crystals of the respective ECCs (Scheme 7). The bulk synthesis was

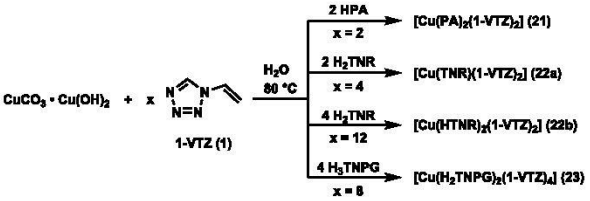
Scheme 7. Single Crystal Formation of the Copper(II) Azide Complex 19 and 20



attempted by slowly adding an aqueous solution of sodium azide to *in situ*-generated complexes of soluble $CuCl_2 \cdot 2\ H_2O$ with **1** or **2** as the ligand.[49] Unfortunately, no elemental analysis pure material could be obtained, most likely because of the formation of various unidentified side species.

The commercially unavailable metal(II) precursors for complexes **21**−**23** were prepared by reacting basic copper(II) carbonate with the corresponding acid.[50] To the *in situ*-obtained copper(II) trinitrophenolates, the ligand was added dropwise at elevated temperatures and the solutions were left for crystallization at room temperature (Scheme 8). Within several hours or days, all complexes were obtained without aqua ligands or inclusion of crystal water in decent yields (71−84%).

Scheme 8. Synthesis of the Trinitrophenolate-Based Coordination Compounds 21−23



All transition metal complexes were obtained directly from the mother liquor or the solvent layer experiment either by crystallization (**3**−**8**, **13**−**23**) or precipitation (**9**−**12**). The crystals obtained by slow evaporation were filtered, washed with small amounts of cold ethanol, and dried in air overnight, not requiring further purification.

2.4. Crystal Structures. All ECCs **3**−**23** and the ligand 1-vinyl-5*H*-tetrazole (**1**, 1-VTZ) were characterized by low-temperature XRD experiments. In the case of **9** and **12**, the measurements allow an indication of the most likely composition, but finalization of the data sets was not possible because of the highly intergrown compounds. Measurement and refinement data are provided in the Supporting Information (Tables S1−S6). The crystal datasets were uploaded to the CSD database and can be obtained free of charge with the CCDC Nos. 2207191 (**1**), 2207187 (**3**), 2207189 (**4**), 2207252 (**5**), 2207251 (**6**), 2207190 (**7**), 2207194 (**8**), 2207200 (**10a**), 2207254 (**10b**), 2207206 (**11**), 2207205 (**13a**), 2207192 (**13b**), 2207203 (**14**), 2207193 (**15**), 2207199 (**16**), 2207201 (**17**), 2207202 (**18**), 2207204 (**19**), 2207253 (**20**), 2207198 (**21**), 2207207 (**22a**), 2207195 (**22b**), and 2207197 (**23**). Due to the liquid state of 1-allyl-5*H*-tetrazole (**2**, 1-ATZ) under ambient conditions, no single crystals could be obtained.

Ligand 1-VTZ (**1**) crystallizes in the form of colorless blocks in the monoclinic space group $P2_1/c$ with four formula units per unit cell (Figure 2). The calculated density of 1-VTZ (**1**, 1.372 g cm^{-3} at 115 K) is higher than the pycnometrically determined density of 1-ATZ (**2**, 1.117 g cm^{-3} at 298 K). The bond lengths and angles of 1-VTZ (**1**) agree well with the geometry of similar literature known *N*1-substituted tetrazole derivatives. All non-hydrogen atoms of ligand 1-VTZ (**1**) are almost perfectly planar (torsion angle N2−N1−C2−C3: −0.1 (5)°), indicating a possible interaction between the π system of the tetrazole ring and the vinyl unit. An insight into the structure of 1-ATZ (**2**) is provided by its transition metal complexes with perchlorate (**10**, **11**), nitrate (**14**), chlorate (**16**), and dinitramide (**18**). In all complexes, the allyl moiety at the *N*1 position is rotated out of the plane (torsion angle N2−N1−C2−C3: −77.7 (4)° (**11**), 84.3 (3)° (**10**), 92.2 (3)° (**14**), −86.2 (5)° (**16**), and 122.5 (2)° (**18**)).

In the case of 1-VTZ (**1**), the bond lengths and angles of the coordinating ligands in the crystallographically investigated complexes are in the same range as in the non-coordinating molecule. Therefore, they are not part of the discussion in any of the following coordination compounds. However, the torsion angle at which the vinyl group is arranged away from the tetrazole ring system changes with complexation. The

https://doi.org/10.1021/acs.inorgchem.2c03624
Inorg. Chem. XXXX, XXX, XXX−XXX

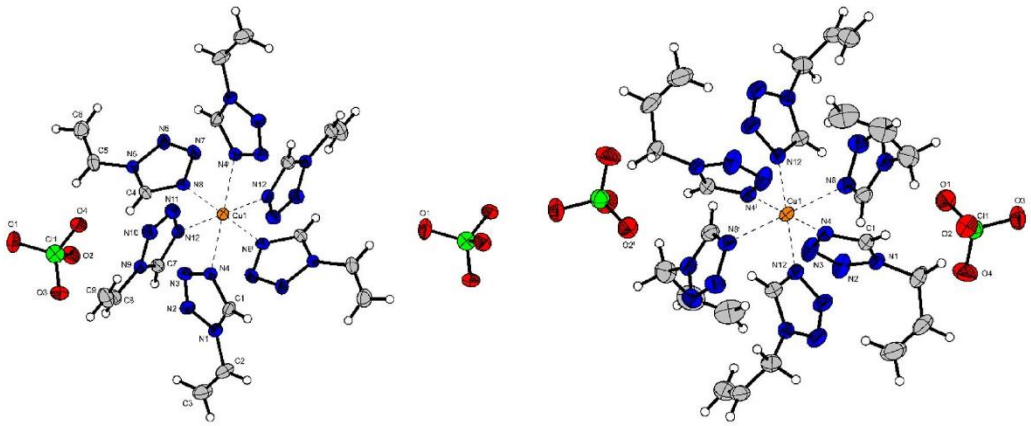


Figure 3. Left: Molecular structure of $[Cu(1\text{-}VTZ)_6](ClO_4)_2$ (**7**). Selected bond lengths (Å): Cu1−N4 2.378 (3), Cu1−N8 2.031 (3), Cu1−N12 2.048 (2). Selected bond angles (°): N4−Cu1−N8 88.67 (10), N4−Cu1−N12 88.34 (9), N8−Cu1−N12 92.17 (10). Symmetry code: (i) $1-x$, $1-y$, $1-z$. Right: Molecular structure of $[Cu(1\text{-}ATZ)_6](ClO_4)_2$ (**11**). Selected bond lengths (Å): Cu1−N3 2.030 (2), Cu1−N8 2.331 (3), Cu1−N12 2.060 (3). Selected bond angles (°): N3−Cu1−N8 89.54 (10), N3−Cu1−N12 89.53 (10), N8−Cu1−N12 91.37 (11). Symmetry code: (i) $-x$, $-y$, $-z$.

relevant torsion angles N2−N1−C2−C3 in the perchlorate complexes **3**−**8** are within 9.4−18.2° and an angle of 5.5° can be found in the chlorate complex $[Cu(1\text{-}VTZ)_6](ClO_3)_2$ (**15**). On the other hand, an angle of 165.5° is found for the dinitramide complex $[Cu(DN)_2(1\text{-}VTZ)_2]$ (**17**). While the torsion angle between the tetrazole plane and the −C≡C− plane differ by a maximum of ∼7.0° within the perchlorate complexes, the angles in the nitrate complex $[Cu(1\text{-}VTZ)_6](NO_3)_2$ (**13b**) differ significantly from each other (10.2−175.2°).

All copper(II) coordination compounds except the dinitramido (**17**, **18**), nitrato (**14**), and chlorate (**15**, **16**) complexes show an octahedral coordination sphere around the central metal with typical Jahn-Teller distortions along the axial axis. The ligands 1-VTZ (**1**) and 1-ATZ (**2**) show no bridging behavior in transition metal complexes and coordinate exclusively *via* the nitrogen atom at the 4th position of the ring. All prepared 1-VTZ perchlorate complexes **3**−**8** express an octahedral environment, where the central metal is surrounded by six 1-VTZ ligands and two non-coordinating anions (Figure 3, left and Figures S1−S5). All six ECCs, except $[Ni(1\text{-}VTZ)_6](ClO_4)_2$ (**6**) (*R*−3), crystallize isotypically in the orthorhombic space group *Pbca* with similar cell volumes (**3**: 3514.3 (2) Å;[3] **4**: 3476.8 (4) Å^3; **5**: 3454.7 (4) Å^3; **7**: 3475.5 (4) Å^3; **8**: 3488.2 (2) Å^3) and parameters (Tables S1 and S2, SI).

The unit cell consists of four formula units and the complexes' densities almost increase with increasing atomic number (**3**: 1.570 g cm^{-3} at 111 K; **4**: 1.588 g cm^{-3} at 109 K; **5**: 1.604 g cm^{-3} at 100 K; **6**: 1.552 g cm^{-3} at 96 K; **7**: 1.604 g cm^{-3} at 100 K; **8**: 1.601 g cm^{-3} at 103 K).

Like their 1-VTZ analogs, 1-ATZ-based perchlorate complexes $[Fe(1\text{-}ATZ)_6](ClO_4)_2$ (**10**) and $[Cu(1\text{-}ATZ)_6](ClO_4)_2$ (**11**) show an octahedral coordination sphere formed by a six-fold coordination of the metal center by tetrazole ligands (Figure 3, right and Figure S6). Only the copper perchlorate complex $[Cu(1\text{-}ATZ)_6](ClO_4)_2$ (**11**) shows a Jahn-Teller distortion with a typical copper(II) d^9 electronic configuration.

When cooled in liquid nitrogen, the color of $[Fe(1\text{-}ATZ)_6](ClO_4)_2$ (**10**) changes from light beige into light purple (Figure S39), indicating a spin-crossover that changes the ground state from $^5T_{2g}$ to $^1A_{1g}$.[51] Like alkylated tetrazole ligands (MTZ,[52] PTZ,[53] C_3tz,[54] *etc.*) 1-ATZ thus belongs to the compounds of the type $[Fe(R\text{-}TZ)_6]X_2$ (*R*-TZ = 1-alkyl/alkenyl-1*H*-tetrazole, *X* = BF_4, ClO_4, PF_6, CF_3SO_3) as some of the most investigated spin-crossover systems.[47] Therefore, single crystals were measured both at low (**10a**, ρ = 1.588 g cm^{-3} (100 K)) and room temperature (**10b**, ρ = 1.410 g cm^{-3} (297 K)). While the angles hardly change, the HS → LS transition is accompanied by a contraction of the Fe−N4 bond distance (**10a**: ∼2.03 Å; **10b**: ∼2.18 Å; Figure S6) and an increase in density (**10a**: 1.485 g cm^{-3}; **10b**: 1.410 g cm^{-3}). Particularly noteworthy is that the corresponding $[Fe(1\text{-}VTZ)_6](ClO_4)_2$ (**4**) complex shows no such behavior. This again proves the strong interdependence between crystal structure and spin-transition features, which both vary drastically with the substituent *R* of the monodentate ligands.[55] All the non-opposing ligands in $[Fe(1\text{-}ATZ)_6](ClO_4)_2$ (**10a**) span angles close to 90° to each other and all the metal−ligand bonds have the same lengths (∼2.03 Å), leading to a nearly perfect octahedral environment. Compared to the respective perchlorate complexes of 1-VTZ, $[Cu(1\text{-}ATZ)_6](ClO_4)_2$ (**11**, 1.481 g cm^{-3} at 173 K) and $[Fe(1\text{-}ATZ)_6](ClO_4)_2$ (**10a**, 1.485 g cm^{-3} at 100 K) possess a lower calculated density (∼0.1 g cm^{-3}). This is due to the lengthening of the alkenyl chain and the associated higher cell volume of the 1-ATZ ligand.

The copper nitrate complex **13a** crystallizes in the orthorhombic space group *Pbcn*. The unit cell consists of four formula units and possesses a calculated density of 1.801 g cm^{-3} at a temperature of 103 K. The coordination sphere of the compound is distorted fivefold square pyramidal (O1−N4−O1^i−N4^i = 15.40 (13) °) with an aqua ligand at its tip (Figure 4). The nitrato ligands are shielding the lower coordination position and prevent the formation of an octahedral coordination. Including the very long bond of the nitrato ligands toward the copper center ((O3−Cu1 = 2.815 (2) Å) results in a sevenfold coordination sphere. This has already been observed for an alkyl tetrazole-based complex. The anhydrous copper(II) nitrate complex $[Cu(1\text{-}VTZ)_6](NO_3)_2$ (**13b**) also crystallizes as blue blocks in an

https://doi.org/10.1021/acs.inorgchem.2c03624
Inorg. Chem. XXXX, XXX, XXX−XXX

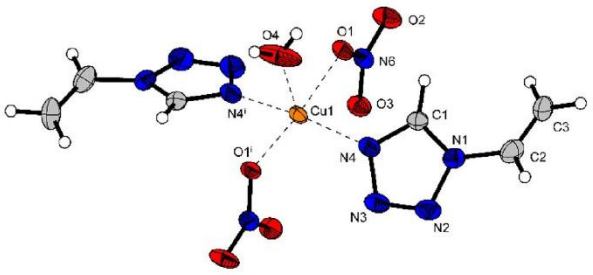


Figure 4. Molecular unit of $[Cu(H_2O)(NO_3)_2(1\text{-}VTZ)_2]$ (**13a**). Selected bond lengths (Å): Cu1–N4 1.985 (2), Cu1–O1 1.9787 (18), Cu1–O4 2.256 (4). Selected bond angles (°): O1–Cu1–N4 89.55 (9), N4–Cu1–O4 95.78 (8), O4–Cu1–O1 84.86 (6), O1–Cu1–O3 50.41 (7). Symmetry code: (i) $1 - x, y, 0.5 - z$.

orthorhombic space group (*Pbca*) with four formula units per unit cell (Figure 5).

However, the density of 1.580 g cm^{-3} at 102 K is significantly lower than the one of compound **13a**. Like the perchlorate $[Cu(1\text{-}VTZ)_6](ClO_4)_2$ (**7**), the nitrate $[Cu(1\text{-}VTZ)_6](NO_3)_2$ (**13b**) shows the same built-up with six 1-VTZ ligands around the central metal and two noncoordinating anions. The bond distance of the coordinating nitrogen and the metal center is nearly the same ($d_{eq} \approx 2.04$ Å, $d_{ax} \approx 2.38$ Å). The elongation of the N8–Cu1–$N8^i$ axis is caused by a Jahn-Teller distortion along the *z* axis of the complex.

In contrast to $[Cu(1\text{-}VTZ)_6](NO_3)_2$ (**13b**), the coordination sphere of $[Cu(1\text{-}ATZ)_3(NO_3)_2]$ (**14**) consists of three coordinating tetrazole and two nitrato ligands (Figure 5, right). The copper(II) nitrate complex $[Cu(1\text{-}ATZ)_3](NO_3)_2$ (**14**) crystallizes in the monoclinic space group $P2_1/c$ with four formula units per unit cell and a calculated density of 1.568 g cm^{-3} at 173 K. The coordination sphere could either be interpreted as a distorted fivefold trigonal bipyramidal (O1–Cu1–O4 127.58 (6)°, O4–Cu1–N12 89.35 (7)°) or as a distorted seven-fold pentagonal bipyramidal depending on whether the longer Cu–O bonds between the central metal and nitrato ligands are included (Cu1–O2 2.6213 (17) Å, Cu1–O6 2.916 (2) Å). In every case, the equatorial positions are occupied by the anionic nitrato ligands and one ligand moiety (Figure 5, right). This coordination geometry has already been observed for $[Cu(1\text{-}NET)_3(NO_3)_2]$[33] and $[Cu(C_4tz)_3(NO_3)_2]$.[54]

Like the $[Cu(1\text{-}ETZ)_6](ClO_3)_2$ complex (CCDC 1898541),[23] the copper chlorate complex $[Cu(1\text{-}VTZ)_6](ClO_3)_2$ (**15**) crystallizes in the hexagonal space group $R\bar{3}$ with three formula units per unit cell (Figure 6). The compound's calculated density of 1.499 g cm^{-3} at 101 K is significantly lower than the densities observed for the corresponding perchlorate complex $[Cu(1\text{-}VTZ)_6](ClO_4)_2$ (**7**). The coordination sphere is built up octahedrally by six ligand moieties, whereas no Jahn-Teller distortion is observed because of the compound's hexagonal space group. Deviating therefrom, the 1-ATZ-based complex $[Cu(1\text{-}ATZ)_6](ClO_3)_2$ (**16**) crystallizes in the monoclinic space group No. 15 (*C2/c*) with four formula units per unit cell and a calculated density of 1.455 g cm^{-3} at 173 K (Figure 6).

Both copper(II) dinitramide coordination compounds $[Cu(DN)_2(1\text{-}VTZ)_2]$ (**17**) and $[Cu(DN)_2(1\text{-}ATZ)_2]$ (**18**) crystallize isotypically in the monoclinic space group No. 14 ($P2_1/c$, $P2_1/n$) with two formula units per unit cell. The coordination sphere is built up of two ligand moieties and two coordinating dinitrimido anions (Figure 7). The calculated density of 1.842 g cm^{-3} at 103 K (**17**) and 1.774 g cm^{-3} at 101 K (**18**) are among the highest observed for coordination compounds based on ligands 1-VTZ and 1-ATZ. The rather uncommon coordination geometry has already been observed for $[Cu(DN)_2(1\text{-}NET)_2]$[33] and can either be interpreted as eightfold, considering the very long Cu–O bonds (**17**: Cu1–O3 = 2.911 (2) Å, Cu1–O1 = 2.736 (2) Å; **18**: Cu1–O1 = 2.8041 (18) Å, Cu1–O4 = 2.845 (2) Å), or as double square planar coordination.

Copper azide complex **19** crystallizes in the form of brown platelets in the orthorhombic space group *Pbca* with eight formula units per unit cell and shows the highest density of all investigated complexes (1.992 g cm^{-3} at 123 K), whereas $[Cu(N_3)_2(1\text{-}ATZ)]$ (**20**) crystallizes in the monoclinic space group $P2_1/c$ with four formula units per unit cell and a calculated density of 1.768 g cm^{-3} at 173 K. The molecular

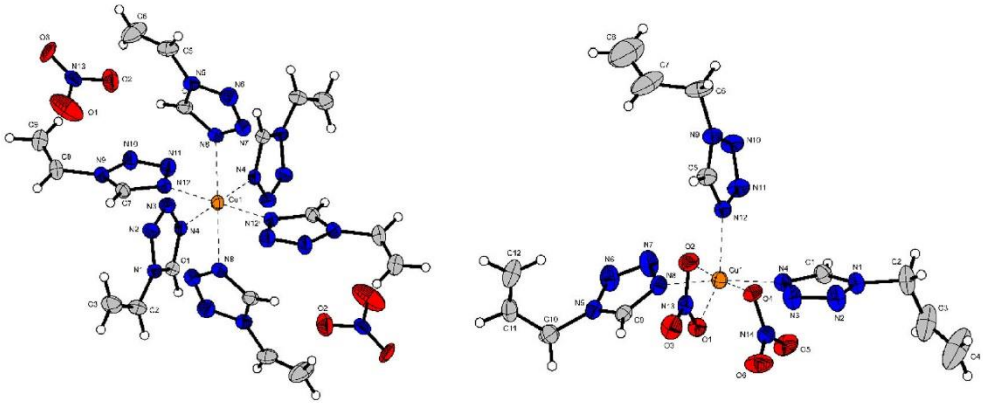


Figure 5. Left: Molecular structure of $[Cu(1\text{-}VTZ)_6](NO_3)_2$ (**13b**). Selected bond lengths (Å): Cu1–N4 2.017 (2), Cu1–N8 2.379 (2), Cu1–N12 2.054 (2). Selected bond angles (°): N4–Cu1–N8 89.52 (8), N4–Cu1–N12 91.34 (9), N8–Cu1–N12 90.35 (8). Symmetry code: (i) $1 - x, 1 - y, 1 - z$. Right: Molecular structure of $[Cu(1\text{-}ATZ)_3(NO_3)_2]$ (**14**). Selected bond lengths (Å): Cu1–O1 2.0192 (16), Cu1–O2 2.6213 (17), Cu1–O4 2.1805 (15), Cu1–O6 2.916 (2), Cu1–N4 1.998 (2), Cu1–N8 1.978 (2), Cu1–N12 2.0712 (18), Cu1–N13 2.711 (2). Selected bond angles (°): O1–Cu1–O2 54.04 (6), O1–Cu1–O4 127.58 (6), O1–Cu1–O6 80.78 (6), O1–Cu1–N4 89.99 (8), O1–Cu1–N8 87.96 (8), O1–Cu1–N12 143.04 (7), O1–Cu1–N13 27.25 (6).

https://doi.org/10.1021/acs.inorgchem.2c03624
Inorg. Chem. XXXX, XXX, XXX–XXX

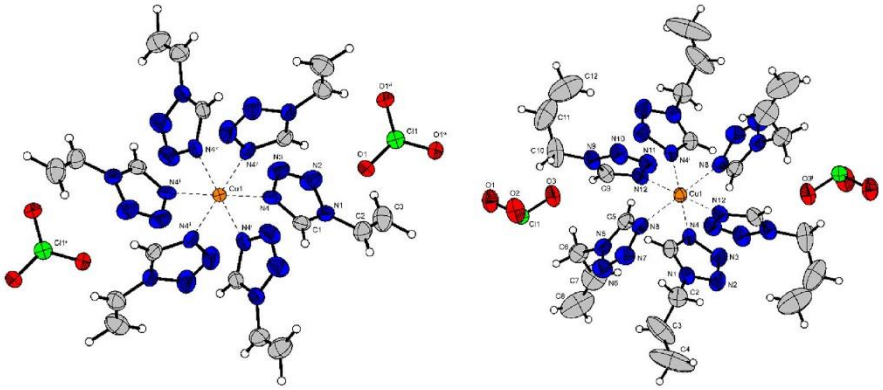


Figure 6. Left: Molecular structure of $[Cu(1\text{-}VTZ)_6](ClO_3)_2$ (**15**). Selected bond lengths (Å): Cu1–N4 2.128 (3). Selected bond angles (°): N4–Cu1–N4^{i} 90.81 (13), N4–Cu1–N4^{iv} 89.19 (13). Symmetry code: (i) $-y, x - y, z$; (ii) $-x + y, -x, z$; (iii) $-x, -y, 1 - z$; (iv) $y, -x + y, 1 - z$; and (v) $x - y, x, 1 - z$. Right: Molecular structure of $[Cu(1\text{-}ATZ)_6](ClO_3)_2$ (**16**). Selected bond lengths (Å): Cu1–N4 2.083 (2), Cu1–N8 2.179 (3), Cu1–N12 2.143 (3). Selected bond angles (°): N4–Cu1–N8 90.56 (11), N4–Cu1–N12 88.67 (11), N8–Cu1–N12 89.60 (11). Symmetry code: (i) $1 - x, 1 - y, 1 - z$.

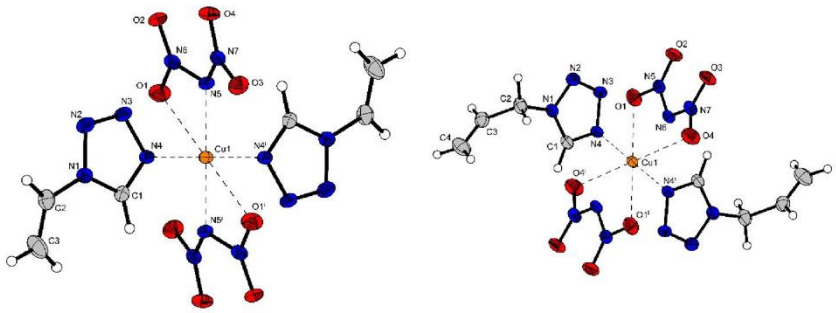


Figure 7. Left: Molecular structure of $[Cu(DN)_2(1\text{-}VTZ)_2]$ (**17**). Selected bond lengths (Å): Cu1–O1 2.736 (2), Cu1–O3 2.911 (2), Cu1–N4 1.986 (3), Cu1–N5 1.992 (2). Selected bond angles (°): O1–Cu1–O3 98.52 (7), O1–Cu1–N4 90.98 (9), O1–Cu1–N5 51.32 (8), O3–Cu1–N4 79.84 (8), O3–Cu1–N5 47.98 (8), N4–Cu1–N5 89.92 (11). Symmetry code: (i) $1 - x, 1 - y, 1 - z$. Right: Molecular structure of $[Cu(DN)_2(1\text{-}ATZ)_2]$ (**18**). Selected bond lengths (Å): Cu1–O1 2.8041 (18), Cu1–O4 2.845 (2), Cu1–N4 1.976 (2), Cu1–N6 1.9830 (17). Selected bond angles (°): O1–Cu1–O4 98.26 (6), O1–Cu1–N4 88.25 (6), O1–Cu1–N6 50.03 (7), O4–Cu1–N4 83.77 (7), O4–Cu1–N6 48.77 (7), N4–Cu1–N6 89.84 (8). Symmetry code: (i) $1 - x, 1 - y, 1 - z$.

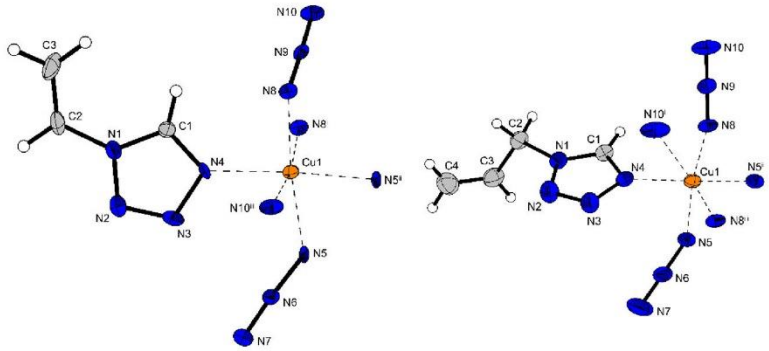


Figure 8. Left: Molecular structure of $[Cu(N_3)_2(1\text{-}VTZ)]$ (**19**). Selected bond lengths (Å): Cu1–N4 1.997 (7), Cu1–N5 2.005 (7), Cu1–N8 2.014 (7), Cu1–N5^{ii} 1.983 (7), Cu1–N10^{iii} 2.557 (8), Cu1–N8^{i} 2.568 (7). Selected bond angles (°): N4–Cu1–N8 90.4 (3), N10^{iii}–Cu1–N5^{ii} 92.9 (3), N10^{iii}–Cu1–N8 85.8 (3). Symmetry codes: (i) $0.5 + x, 0.5 - y, -z$; (ii) $2 - x, 1 - y, -z$; (iii) $-0.5 + x, 0.5 - y, -z$. Right: Molecular structure of $[Cu(N_3)_2(1\text{-}ATZ)]$ (**20**). Selected bond lengths (Å): Cu1–N4 2.0024 (15), Cu1–N5 1.9982 (12), Cu1–N8 1.9782 (12), Cu1–N5^{ii} 2.0105 (14), Cu1–N10^{i} 2.6546 (17), Cu1–N8^{iii} 2.4401 (13). Selected bond angles (°): N4–Cu1–N8 90.83 (6), N10^{i}–Cu1–N5^{ii} 89.56 (6), N10^{i}–Cu1–N8 94.11 (5). Symmetry codes: (i) $1 - x, -0.5 + y, 1.5 - z$; (ii) $1 - x, -y, 1 - z$; (iii) $1 - x, 1 - y, 1 - z$.

units of both are built up similar to copper(II) azide coordination compounds based on 1-alkyl tetrazoles.[33,49,54] It consists of one copper(II) central metal coordinated by one vinyl tetrazole ligand in the equatorial position and five azido anions (Figure 8). Overall, two different coordination modes of azido ligands are observed in the structure. The N5 nitrogen

https://doi.org/10.1021/acs.inorgchem.2c03624
Inorg. Chem. XXXX, XXX, XXX–XXX

atoms bridge between the same copper centers, while the N7 nitrogen atoms do not coordinate at all. The remaining anion bridges twice *via* the N8 nitrogen and once *via* the N10 nitrogen to different copper centers. These two different bridging modes lead to the formation of 2D layers (Figure 9).

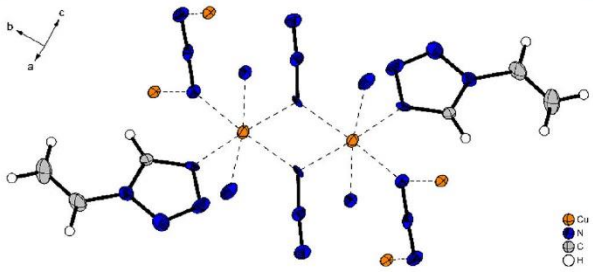


Figure 9. Coordination environment of the copper(II) azide complex **19**.

The coordination compounds $[Cu(PA)_2(1\text{-}VTZ)_2]$ (**21**) and $[Cu(HTNR)_2(1\text{-}VTZ)_2]$ (**22a**) crystallize in the monoclinic space group $P2_1/c$ and the triclinic space group $P\bar{1}$, respectively. Despite the compounds' different space groups, the densities of both ECCs are roughly the same (**21**: 1.801 g cm^{-3} at 123 K; **22a**: 1.862 g cm^{-3} at 123 K). A reason for this is most likely the similar coordination geometry both compounds possess. The copper center in complex **21** is coordinated by two picrato ligands with the Cu1–O1 bond (1.9294 (1) Å) formed by the hydroxy group of the anion, in the equatorial positions (Figure 10, left). The Cu1–O7 bond (2.3809 (2) Å) between the central metal and a nitrate group of the anion is located in the axial positions. The remaining equatorial binding sites are occupied by 1-VTZ moieties.

This coordination pattern has already been observed for several tetrazole complexes based on copper picrate.[50,56] The coordination sphere of **22a** (Figure 10, right) is arranged in the same way as that of **21**, the major difference here being the O1–Cu1–N4–C1 torsion angle (**21**: 68.1 (4)°, **22a**: −13.3 (3)°). The copper styphnate complex **22b** crystallizes in the orthorhombic space group *Fddd* with 16 formula units per unit cell. The observed density of 1.804 g cm^{-3} (at 103 K) is in the middle range of the values obtained for the trinitrophenolate ECC. The copper cation is coordinated by two 1-VTZ ligands and two bridging styphnate moieties. The tetrazole ligands and the anions are in this case *cis* arranged (Figure 11).

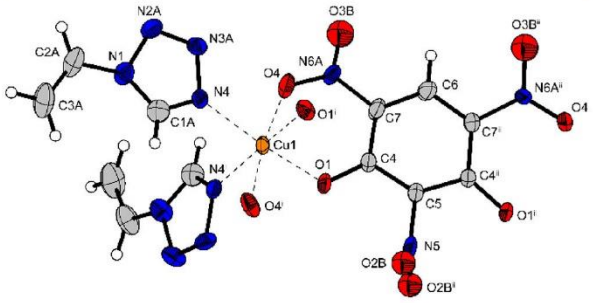


Figure 11. Coordination environment of $[Cu(TNR)(1\text{-}VTZ)_2]$ (**22b**). Selected bond lengths (Å): Cu1–N4 2.008 (3), Cu1–O1 1.944 (2), Cu1–O4 2.272 (3). Selected bond angles (°): O1–Cu1–O4 81.82 (10), O4–Cu1–N4 89.25 (10), N4–Cu1–O1 170.79 (11). Symmetry codes: (i): 0.75 − *x*, 0.75 − *y*, *z*; (ii) 1.25 − *x*, *y*, 1.25 − *z*.

The bridging character of the TNR^{2-} anion leads to the formation of 1D polymeric chains (Figure 12).

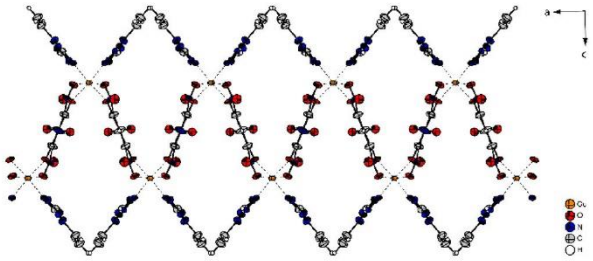


Figure 12. One-dimensional polymeric chains built up by compound **22b**, displayed along the *b* axis.

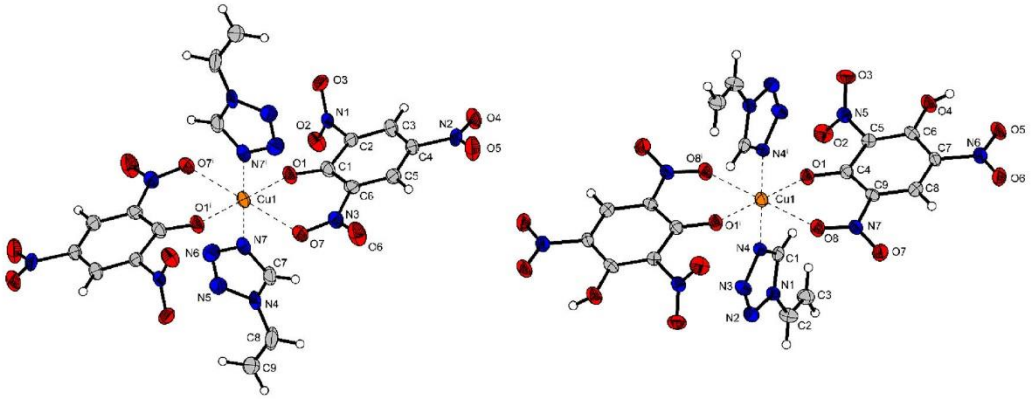


Figure 10. Left: Molecular unit of the picrate ECC $[Cu(PA)_2(1\text{-}VTZ)_2]$ (**21**). Selected bond lengths (Å): Cu1–O1 1.9294 (1), Cu1–O7 2.3809 (2), Cu1–N7 2.0005 (2). Selected bond angles (°): N7–Cu1–O7 86.99 (15), O1–Cu1–O7 78.51 (12). Symmetry code: (i) −*x*, 1*y*, 1 − *z*. Right: Molecular unit of the styphnate complex $[Cu(HTNR)_2(1\text{-}VTZ)_2]$ (**22a**). Selected bond lengths (Å): Cu1–O1 1.9238 (2), Cu1–O8 2.3427 (2), Cu1–N4 2.0071 (2). Selected bond angles (°): O1–Cu1–N4 89.27 (9), O1–Cu1–O8 81.20 (8), O8–Cu1–N4 92.05 (9). Symmetry code: (i) 1 − *x*, 1 − *y*, −*z*.

https://doi.org/10.1021/acs.inorgchem.2c03624
Inorg. Chem. XXXX, XXX, XXX−XXX

The ECC $[Cu(H_2TNPG)_2(1\text{-}VTZ)_4]$ (**23**) crystallizes in the form of green prisms in the triclinic space group $P\bar{1}$ with a calculated density of 1.767 g cm^{-3} (at 112 K). The unit cell consists of only one formula unit. The octahedral coordination sphere is arranged in a typical manner for the H_2TNPG^- anion.[50] Four 1-VTZ ligands are occupying the equatorial positions, whereas the anions are located in the axial position (Figure 13).

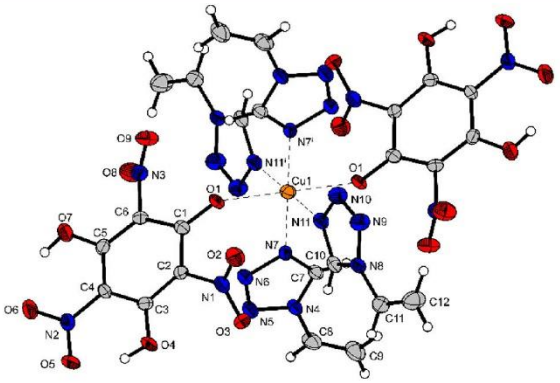


Figure 13. Molecular unit of $[Cu(H_2TNPG)_2(1\text{-}VTZ)_4]$ (**23**). Selected bond lengths (Å): Cu1–N7 2.0100 (2), Cu1-N11 2.0201 (3), Cu1-O1 2.3331 (2). Selected bond angles (°): N7–Cu1–N11 91.224 (8), N7–Cu1–O1 94.998 (6), O1–Cu1–N11 90.673 (6). Symmetry code: (i): $1-x, 1-y, 1-z$.

2.5. Thermal Stability and Sensitivity Data of the ECC.

Thermal stability measurements were carried out using differential thermal analysis (DTA) in the range from 25 to 400 °C at a heating rate of 5 °C min^{-1}. The ligands 1-VTZ (**1**) and 1-ATZ (**2**) together with the compounds **3**–**13a**, **15**–**18**, and **21**–**23** were investigated regarding their stability toward heat. Compounds **13b**, **14**, **19**, and **20**, which could not be obtained elemental analysis pure, were not further analyzed. Endothermic events indicating melting, phase transition, or dehydration, together with exothermic events indicating decomposition, are given as the extrapolated onset temperatures. The results of the DTA measurements are summarized in Table 1. Plots of every DTA spectrum measured can be found in the Supporting Information (Figures S13–S15).

To further verify endothermic processes that occurred during DTA measurements, thermogravimetric (TG) analysis was applied at a heating rate of 5 °C min^{-1} in the range from 30 to 400 °C. The TG plots of complexes **3**, **5**, and **9**–**12** can be found in the SI (Figures S16 and S17).

For all metal(II) perchlorate 1-ATZ complexes **9**–**12**, the first endothermic process indicates phase transitions, as no mass loss was observed during TGA and melting could be ruled out visually with a BÜCHI Melting Point B-540 instrument (Figure S17). In contrast to $[Fe(1\text{-}ATZ)_6](ClO_4)_2$ (**10**), which decomposes exothermically over a narrow temperature range, thermal decomposition of **9**, **11**, and **12** proceeds endothermically at first, directly followed by an exothermic event (Figure S15). This endothermic stage is characterized by a continuous mass loss (**9**: 45%, **11**: 37%, **12**: 41%), indicating the elimination of volatile 1-ATZ from the melt (Figure S17). This is confirmed by the weight loss being close to that calculated for the removal of 1-ATZ equivalents (**9**: 48%, **11**: 36%, **12**: 36%). For $[Fe(1\text{-}ATZ)_6](ClO_4)_2$ (**10**), the TG plot exhibits a continuous mass loss (25%) followed by a sharp disintegration event accompanied by complete decomposition (residual mass of 0.2%) (Figure S17).

Table 1. Summary of the Compounds' Thermal Stability[a] as Well as Sensitivities toward Various External Stimuli[i]

compound	no.	$T_{endo.}$ (°C)[b]	$T_{exo.}$ (°C)[c]	IS (J)[d]	FS (N)[e]	ESD (mJ)[f]	BDIS (mJ)[g]
1-VTZ	1	18	173	15	>360	n.d.	n.d.
1-ATZ	2		207	>40	>360	n.d.	n.d.
$[Mn(1\text{-}VTZ)_6](ClO_4)_2$	3	115[h]	115[h], ~250	2	20	1080	>200
$[Fe(1\text{-}VTZ)_6](ClO_4)_2$	4	120	165	4	3	480	41
$[Co(1\text{-}VTZ)_6](ClO_4)_2$	5	118	196	n.d.	n.d.	n.d.	n.d.
$[Ni(1\text{-}VTZ)_6](ClO_4)_2$	6		207	n.d.	n.d.	n.d.	n.d.
$[Cu(1\text{-}VTZ)_6](ClO_4)_2$	7	154[h]	154[h]	2	7	317	194
$[Zn(1\text{-}VTZ)_6](ClO_4)_2$	8	100, 174[h]	174[h]	6	10	1500	>200
$[Mn(1\text{-}ATZ)_6](ClO_4)_2$	9	61, 187	222	20	216	1500	n.d.
$[Fe(1\text{-}ATZ)_6](ClO_4)_2$	10	77	201	5	96	480	n.d.
$[Cu(1\text{-}ATZ)_6](ClO_4)_2$	11	76, 176[h]	176[h]	5	72	420	n.d.
$[Zn(1\text{-}ATZ)_6](ClO_4)_2$	12	89, 194[h]	194[h]	25	168	1500	n.d.
$[Cu(NO_3)_2(H_2O)(1\text{-}VTZ)_2]$	13a	78, 110[h]	110[h]	6	160	>1500	>200
$[Cu(1\text{-}VTZ)_6](ClO_3)_2$	15	79	107	4	2	480	≤4
$[Cu(1\text{-}ATZ)_6](ClO_3)_2$	16	58	113	3	36	600	n.d.
$[Cu(DN)_2(1\text{-}VTZ)_2]$	17		115	≤1	9	250	28
$[Cu(DN)_2(1\text{-}ATZ)_2]$	18		127	2	48	480	n.d.
$[Cu(PA)_2(1\text{-}VTZ)_2]$	21		191	10	288	750	>200
$[Cu(HTNR)_2(1\text{-}VTZ)_2]$	22a		184	2	96	1080	>200
$[Cu(TNR)(1\text{-}VTZ)_2]$	22b		191	2	144	750	180
$[Cu(H_2TNPG)_2(1\text{-}VTZ)_4]$	23		158	3	84	1080	>200

[a]Onset temperature at a heating rate of 5 °C min^{-1} measured by DTA. [b]Endothermic peak, which indicates melting, dehydration, loss of aqua ligands, or phase transition. [c]Exothermic peak, which indicates decomposition. [d]Impact sensitivity according to the BAM drop hammer (method 1 out of 6). [e]Friction sensitivity according to the BAM friction tester (method 1 out of 6). [f]Electrostatic discharge sensitivity (OZM XSpark10, method 1 out of 6). [g]Ball drop impact sensitivity (OZM BIT-132).[58] [h]Endothermic signal followed by an exothermic signal. [i]n.d.: not determined.

https://doi.org/10.1021/acs.inorgchem.2c03624
Inorg. Chem. XXXX, XXX, XXX–XXX

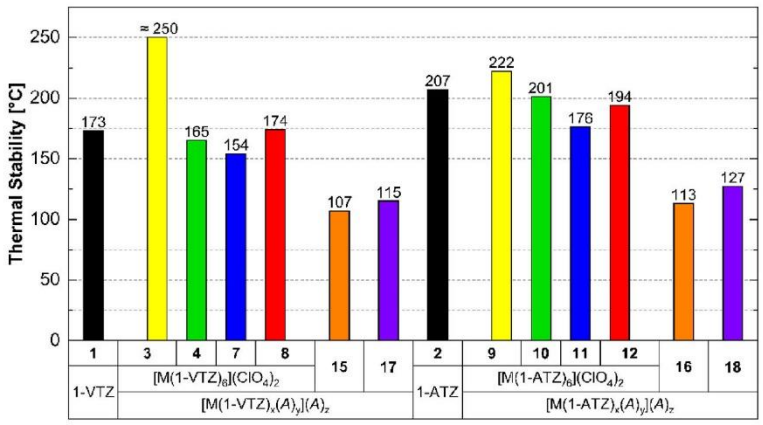


Figure 14. Comparison of the thermal stability of 1-VTZ (**1**) and 1-ATZ (**2**)-based complexes with different anions (A) and transition metals (M), confirming the lower stability of $[M(1\text{-}ATZ)_x(A)_y](A)_z$ analogs toward heat.

As verified by TGA and BÜCHI experiments, the endothermic event of $[Co(1\text{-}VTZ)_6](ClO_4)_2$ (**5**) at 118 °C represents its phase transition (Figure S16). Before compound **5**'s complete decomposition (196 °C), the detected mass loss during the TG measurement can be assumed to be the loss of one molecule of 1-VTZ (Figure S16). Consistent with the observed hygroscopicity of **3** under ambient conditions, the observed mass loss starting at 98 °C (5.07%) can be assigned to dehydration (Figure S16). Thereafter, **3** exhibits distinct disintegration events. One major step of decomposition is identified by an exothermic event at 250 °C.

The melting point of 1-VTZ (**1**, T_{endo} = 18 °C) is slightly higher than given in the literature (15−16 °C).[31] Overall, most of the coordination compounds based on oxidizing anions (**3**−**13a**, **15**−**18**) hardly exceed the thermal stability of the ligand they are based on (Table 1). When it comes to coordination compounds based on trinitrophenolate anions, compounds **21**, **22a**, and **22b** possess better thermal stabilities. According to the literature,[20,21,23,33] the exothermic events of the nitrate (**13a**), dinitramide (**17**, **18**), and chlorate[48] complexes (**15**, **16**) at rather low temperatures are caused by the anion. Another effect of the anion on the complexes' thermal stability described in the literature is seen in compounds **21** (T_{exo} = 191 °C) to **23** (T_{exo} = 158 °C). With an increasing number of hydroxy groups, the thermal stability is decreasing.[50] ECC **22b** (T_{exo} = 191 °C) is an exception because of its structure. The double deprotonated styphnate anion is bridging two copper centers and therefore increasing the stability of the complex. Concluding, the thermal stability within the $[Cu(1\text{-}VTZ)_x(A)_y](A)_z$ complexes decrease in the following sequence: PA^- (191 °C) = TNR^{2-} (191 °C) > $HTNR^-$ (184 °C) > H_2TNPG^- (158 °C) > ClO_4^- (154 °C) > $N(NO_2)_2^-$ (115 °C) > ClO_3^- (107 °C). As expected, the same order is found within the $[Cu(1\text{-}ATZ)_x(A)_y](A)_z$ coordination compounds: ClO_4^- (176 °C) > $N(NO_2)_2^-$ (127 °C) > ClO_3^- (113 °C). It can be stated that the perchlorate complexes **3**−**8** (T_{exo} = 154−207 °C) and **9**−**12** (T_{exo} = 176−222 °C) possess good exothermic decomposition temperatures.

By variation of the central metal in $[M^{II}(1\text{-}VTZ)_6](ClO_4)_2$ complexes **3**−**8**, the thermal stability increases in the following order (Table 1): Cu^{2+} (154 °C) < Fe^{2+} (165 °C) < Zn^{2+} (174 °C) < Co^{2+} (196 °C) < Ni^{2+} (207 °C) < Mn^{2+} (250 °C).

The same tunability is observed in the row of $[M^{II}(1\text{-}ATZ)_6](ClO_4)_2$ complexes **9**−**12** (Figure 14): Cu^{2+} (176 °C) < Fe^{2+} (201 °C) < Zn^{2+} (194 °C) < Mn^{2+} (222 °C). A similar trend has already been reported for 1-MTZ-,[21] 1,1-dtp-,[57] and 1-AT[22]-based perchlorate complexes.

Varying the ligand also affects thermal stability. Comparing the $[M^{II}(1\text{-}VTZ)_6](ClO_4)_2$ (**4**, **7**, **8**) with the corresponding $[M^{II}(1\text{-}ATZ)_6](ClO_4)_2$ complexes (**10**−**12**), the elongation of the *N*1-substituted alkenyl moiety leads to higher thermal stability (Figure 14). Thus, an increase in decomposition temperature is observed from 1-VTZ to 1-ATZ in the respective $[M^{II}(L)_6](ClO_4)_2$ compounds (ΔT_{dec} for Fe^{2+}: 36 °C, Cu^{2+}: 22 °C, Zn^{2+}: 20 °C), which corresponds approximately to the decomposition temperature difference of the free ligands (ΔT_{dec} = 34 °C) (Figure 14). A comparison of the analogs **3** and **9** is difficult due to their different decomposition behavior. Within $[Cu(L)_6](ClO_3)_2$ analogs, the introduction of an additional carbon atom at the ligands' *N*1 position increased the thermal stability (**15**: 107 °C, **16**: 113 °C).

Similarly, an increase in decomposition temperature from 1-VTZ (**17**: 115 °C) to 1-ATZ (**18**: 127 °C) is observed for the $[Cu(DN)_2(L)_2]$ cognates. A similar study on the influence of the alkyl-bridge carbon content in ditetrazole ligands (1,1-dte, 1,1-dtp, 1,1-dtp) supports these findings.[59]

One of the most important parameters for energetic materials, apart from thermal stability and performance, is their sensitivity to mechanical stimuli as well as electrostatic discharge. Therefore, all pure analytical substances obtained (except the most toxic **5** and **6**) were comprehensively characterized in terms of their sensitivities toward impact, friction, and also electrostatic discharge (Table 1). For the energetically more promising 1-VTZ complexes, the sensitivity toward ball drop impact was additionally measured (Table 1). For BAM friction,[60−62] BAM impact,[63−65] and BAM electrostatic discharge[66] sensitivity measurements, the BAM 1-out of-6 method was applied to determine the lowest ignition force or energy.

For the ligands 1-VTZ (**1**) and 1-ATZ (**2**), a characterization of ball drop impact (OZM BIT-132) and electrostatic discharge (OZM XSpark10) was waived because of the compounds' low melting point (**1**) or liquid state (**2**).

Considering the sensitivities of the *N*1-alkenylated tetrazoles **1** (IS = 15 J, FS ≥ 360 N) and **2** (IS ≥ 40 J, FS ≥ 360 N), the lengthening of the alkenyl chain decreases sensitivity toward impact. While the *N*1-allyl-substituted tetrazole **2** can be

https://doi.org/10.1021/acs.inorgchem.2c03624
Inorg. Chem. XXXX, XXX, XXX−XXX

categorized as insensitive toward both friction and impact, **1** is sensitive to impact.[67] In either case, subsequent complexation leads to more sensitive compounds than with the neutral ligands.

Amid the 1-VTZ-based ECC, the dinitramide complex **17** ($IS \leq 1$ J) is the most impact sensitive compound with no-fire-level being determined (Table 2 and Figure 15). This is followed by most of the chlorate and perchlorate complexes with impact sensitivities between 2 and 4 J as well as the styphnate and trinitrophloroglucinate complexes **22**–**23** (Tab. 1). The zinc perchlorate **8** (IS = 6 J), copper nitrate **13a** (IS = 6 J), and ultimately the copper picrate complex **20** (IS = 10 J) possess the lowest sensitivities. The friction sensitivity measurements on the other hand indicated that the copper chlorate complex **15** is the most sensitive compound (FS = 2 N) (Table 1 and Figure 16).

Table 2. Physicochemical and Calculated Properties for Compounds 1 and 2 Compared to TNT

	1	2	TNT
ρ (298 K) [g cm^{-3}][a]	1.34	1.12[32]	1.65
N [%][b]	58.3	50.9	18.5
Ω_{CO2} [%][c]	−133.2	−159.8	−74.0
Ω_{CO} [%][d]	−83.3	−101.7	−24.7
T_{endo}[e]/T_{exo}[f] [°C]	18/173	(-)/207	80/290
$\Delta_f H°$ [kJ mol^{-1}][g]	350.6	334.8	−59.3
Calculated detonation parameters (EXPLO V6.05.04)			
$-\Delta_{Ex}U°$ [kJ kg^{-1}][h]	3712	3472	4406
T_{det} [K][i]	2584	2189	3177
P_{CJ} [kbar][j]	154	82.4	183
V_{det} [m s^{-1}][k]	6503	5702	6798
V_0 [L kg^{-1}][l]	725	751	640

[a]Measured X-ray densities converted to RT. [b]Nitrogen content. [c]Oxygen balance with respect to CO_2 ($\Omega_{CO2} = ((xO - 2yC - 1/2zH)\cdot 1600)/M$). [d]Oxygen balance with respect to CO ($\Omega_{CO} = ((xO - yC - 1/2zH)\cdot 1600)/M$). [e]Endothermic peak, which indicates melting. [f]Exothermic peak, which indicates decomposition. [g]Calculated enthalpy of formation at 298.15 K. [h]Energy of explosion. [i]Detonation temperature. [j]Detonation pressure at the Chapman–Jouguet point. [k]Detonation velocity. [l]Volume of detonation products (assuming only gaseous products).

Nevertheless, the dinitramide complex (**17**, FS = 9 N) together with the copper (**7**, FS = 7 N) and iron perchlorate complexes (**4**, FS = 3 N) is still among the most sensitive compound regarding friction sensitivity. Worth mentioning is the higher frictional sensitivity of the manganese perchlorate coordination compound **3** (FS = 20 N) and the trinitrophenolate complexes **22**–**23**, which are ranked among the most sensitive compounds regarding impact sensitivity. In terms of sensitivity to electrostatic discharge, the dinitramide compound **17** (ESD = 250 mJ) is again the most sensitive of the ECC studied (Table 1 and Figure 17). With copper and iron being more sensitive than manganese and zinc in the transition metal complexes $[M^{II}(1\text{-VTZ})_6](ClO_4)_2$ (Figure 17), the sensitivity of **4** (ESD = 480 mJ) and **7** (ESD = 317 mJ) are in the same order of magnitude as the chlorate complex **15** (ESD = 480 mJ). This is followed by ECCs with oxidizing anions like picrate, trinitroresorcinates or trinitrophloroglucinate (**21**–**23**, ESD = 780–1080 mJ), subsequent to $[Mn^{II}(1\text{-VTZ})_6](ClO_4)_2$ (**3**, ESD = 1080 mJ) and $[Zn^{II}(1\text{-VTZ})_6](ClO_4)_2$ (**8**, ESD = 1500 mJ) as the least sensitive compounds.

When it comes to 1-ATZ-based ECCs, the perchlorate complexes **9**–**12** are sensitive toward impact (5–25 J) and vary from sensitive to very sensitive against friction (72–216 N). Among the $[M^{II}(1\text{-ATZ})_6](ClO_4)_2$ complexes, the impact sensitivity increases in the order Zn^{2+} (25 J) < Mn^{2+} (20 J) < Cu^{2+} (5 J) = Fe^{2+} (5 J) and in the following order toward friction Mn^{2+} (216 N) < Zn^{2+} (168 N) < Fe^{2+} (96 N) < Cu^{2+} (72 N). Similar trends have been observed in the literature for $[M(L)_6](ClO_4)_2$ (*e.g.*, L: 1-MTZ,[21] 1-AT,[22] 1-APT,[24] 1-AMT,[68] 1,1-dtp[57]) complexes, with manganese(II) and copper(II) being less sensitive than iron(II) and copper(II) coordination compounds. Compared to the perchlorate complexes **9**–**12** (Figures 15 and 16), the chlorate (**16**, IS = 3 J, FS = 36 N) and dinitramide complexes (**18**, IS = 2 J, FS = 48 N) show an increased sensitivity toward impact and friction, after which they can be classified as very sensitive. ESD sensitivity measurements (Figure 17) showed comparable values for the copper and iron perchlorate (**10**: 480 mJ; **11**: 420 mJ), chlorate (**16**: 600 mJ), and dinitramide complexes (**18**: 480 mJ). Manganese(II) and zinc(II) in $[M^{II}(1\text{-ATZ})_6](ClO_4)_2$ again seem to less catalyze the compounds' decomposition, leading to a lower sensitivity (**9**, **12**: 1500 mJ).

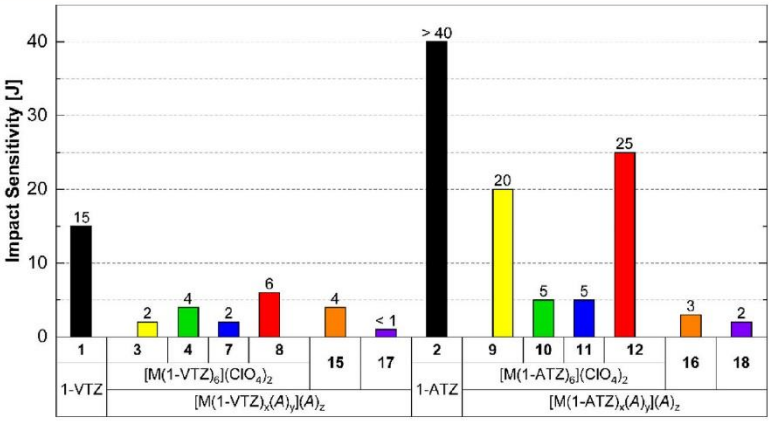


Figure 15. Comparison of the impact sensitivity of 1-VTZ (**1**) and 1-ATZ (**2**)-based complexes with different anions (A) and transition metals (M), confirming the lower stability of $[M(1\text{-ATZ})_x(A)_y](A)_z$ analogs toward impact.

https://doi.org/10.1021/acs.inorgchem.2c03624
Inorg. Chem. XXXX, XXX, XXX−XXX

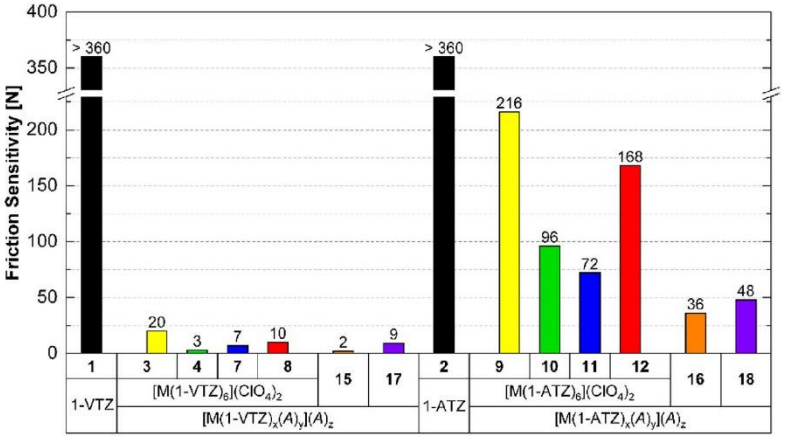


Figure 16. Comparison of the friction sensitivity of 1-VTZ (**1**) and 1-ATZ (**2**)-based complexes with different anions (A) and transition metals (M), confirming the lower stability of $[M(1\text{-}ATZ)_x(A)_y](A)_z$ analogs toward friction.

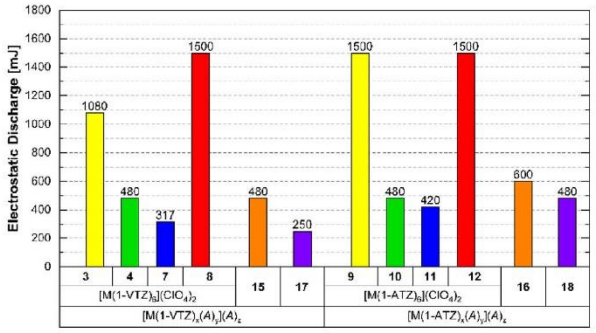


Figure 17. Comparison of the electrostatic discharge sensitivity of 1-VTZ (**1**) and 1-ATZ (**2**)-based complexes with different anions (A) and transition metals (M), confirming the lower stability of $[M(1\text{-}ATZ)_x(A)_y](A)_z$ analogs toward electrostatic discharge.

Comparing analogous complexes based on the different ligands 1-VTZ (**1**) and 1-ATZ (**2**), there is a clear trend of higher stability (IS, FS, ESD) for $[M(1\text{-}ATZ)_x(A)_y](A)_z$ correlates (Figures 15−17). While the free nitrogen-rich ligands show an impact sensitivity difference of about 25 J (Figure 15), the greatest difference within the perchlorate complexes after formal ligand exchange is observed for manganese(II) (**9** → **3**: ΔIS = 18 J) and zinc(II) (**12** → **8**: ΔIS = 19 J). Compared to the thermal behavior, the elongation of the alkenyl chain has the least influence on the impact sensitivity of the iron(II) (**10** → **4**: ΔIS = 1 J) and copper(II) (**11** → **7**: ΔIS = 3 J) complexes. With chlorate and dinitramide as a counter anion, almost no difference in sensitivity can be observed (**16** → **15**: ΔIS = −1 J; **18** → **17**: ΔIS = 1 J). The same correlations between carbon content (1-VTZ *vs* 1-ATZ) and desensitization of the complexes can be drawn with regard to friction sensitivity and sensitivity to electrostatic discharge: (i) Manganese(II) (**9** → **3**: ΔFS = 196 N, ΔESD = 420 mJ) and zinc(II) perchlorate complexes (**12** → **8**: Δ*FS* = 158 N) are more desensitized than the iron(II) (**10** → **4**: ΔFS = 93 N, ΔESD = 0 mJ) and copper(II) analogues (**11** → **7**: ΔFS = 65 N, ΔESD = 103 mJ). (ii) Independent of the varied anions (DN^-, ClO_3^-, ClO_4^-) the copper complexes show desensitization of similar magnitude (ΔFS: 65 N (**11** → **7**), 34 N (**16** → **15**), 39 N (**18** → **17**); ΔESD: 103 mJ (**11** → **7**), 120 mJ (**16** → **15**), 230 mJ (**18** → **17**)), indicating the important role of the central metal. As a consequence, according to the UN Recommendations on the Transport of Dangerous Goods,[67] 1-VTZ complexes (**3**, **4**, **7**, **8**) can be classified as very to extremely sensitive, while 1-ATZ compounds (**9**−**12**) are rated sensitive and are therefore not suitable as future primary explosives.

In general, the trends found for both the 1-VTZ and 1-ATZ-based ECCs are largely expected and are therefore described in the literature. This is especially relevant for the chlorate complexes, which are known to be among the most sensitive compounds, especially compared to perchlorates (Figure 14).[33,48] Also extensively studied are the perchlorate monosubstituted tetrazole complexes of the 3d metals manganese, iron, copper, and zinc. In these extensive studies,[21,22,24] the iron and copper perchlorates were found to be more sensitive than the respective manganese and zinc analogs. This tendency also applies predominantly to the compounds $[M^{II}(1\text{-}VTZ)_6](ClO_4)_2$ and $[M^{II}(1\text{-}ATZ)_6](ClO_4)_2$ (Figures 15−17). Deviations in impact sensitivity are less significant, as the drop hammer test is known to suffer from inadequacies such as hotspot formation.[69]

Among other things, because of these limitations, an alternative method of impact sensitivity determination, the ball drop impact sensitivity (BDIS),[58] was used in this work to investigate the more sensitive 1-VTZ-based ECC (Tab. 2). The resulting data are in large part in accordance with our previous work, indicating that a high sensitivity toward friction also comes with high sensitivity toward ball drop impact.[23,33,70] It is also worth mentioning that again no correlations can be drawn between BAM IS and BDIS. Good examples of the correlation between friction and ball drop impact are the copper chlorate complex **15** (FS = 2 N; BDIS ≤ 4 mJ) and the copper dinitramide ECC **17** (FS = 9 N; BDIS = 28 mJ). Both compounds were tested extremely sensitive during both measurement types. Furthermore, the trinitrophenolate-based ECC also show a correlation. In these cases, the complexes tend to be less sensitive toward both methods, as in the case of picrate **21** (FS = 288 N; BDIS > 200 mJ). Of course, there are exceptions again in this study, especially in the area of perchlorate complexes (**7**, FS = 7 N; BDIS = 194 mJ). However, since these primary explosives cannot be sieved

https://doi.org/10.1021/acs.inorgchem.2c03624
Inorg. Chem. XXXX, XXX, XXX−XXX

before testing due to their sensitivity, grain size effects are significantly involved in a reduction in sensitivity here.

Conclusively, every compound was ranked according to the UN Recommendations on the Transport of Dangerous Goods.[67] According to this document, every 1-VTZ-based coordination compound has to be either classified as very sensitive (**3**, **7**, **17**, **22a**, **22b**, **23**) or sensitive (**4**, **8**, **15**, **21**, **13a**) to impact. The 1-ATZ-based transition metal complexes can also be rated as very sensitive (**16**, **18**) or sensitive (**9**−**12**). When it comes to friction sensitivity, only the neutral ligands **1** and **2** are tested to be insensitive. The compounds based on 1-VTZ as ligand are classified at least as sensitive (**13a**, **21**−**23**), very sensitive (**3**), or in the majority even as extremely sensitive (**4**, **7**, **8**, **15**, **17**). With 1-ATZ as the ligand the complexes can be only rated very sensitive (**11**, **16**, **18**) or sensitive (**9**, **10**, **12**).

2.6. Hot Plate (HP) and Hot Needle (HN) Experiments. The enthalpies of formation of 1-VTZ (**1**), 1-ATZ (**2**), and TNT were calculated at the CBS-4M level of theory for a better comparison, using the atomization energy method and utilizing experimental data. The results are summarized in Table 2.

Both *N*1-alkenyl substituted tetrazoles exhibit highly endothermic enthalpies of formation (**1**: 350.6 kJ mol^{-1}; **2**: 334.6 kJ mol^{-1}), by far surpassing TNT (−59.3 kJ mol^{-1}). To estimate the detonation performances of the prepared ligands, selected key parameters were calculated using EXPLO5 (version 6.05.04),[71] and compared to TNT. The program is based on the chemical equilibrium steady-state model of detonation. It uses the Becker−Kistiakowsky−Wilson equation of state (BKW EOS) for gaseous detonation products and the Cowan−Fickett equation of state for solid carbon. For these calculations, the low-temperature XRD density of 1-VTZ was converted to a room temperature value with the equation $\rho_{298K} = \rho_T/(1 + \alpha_V(298 - T_0))$; $\alpha_V = 1.5 \times 10^{-4}\ K^{-1}$ and the density of liquid 1-ATZ was measured with a helium gas pycnometer at room temperature, which is equivalent to the literature value.[32] Noteworthily, a high density is vital for the performance of an energetic material, as the detonation pressure is proportional to the square of its density.[72] Therefore, **1** (6503 m s^{-1}) and **2** (5702 m s^{-1}) both show lower detonation velocity values compared to TNT (6798 m s^{-1}). Having both a higher enthalpy of formation as well as a higher density, 1-VTZ (**1**) shows better detonation parameters than 1-ATZ (**2**).

The 1-VTZ (**3**, **4**, **7**, **8**) and 1-ATZ (**7**−**10**)-based perchlorate complexes were tested for their capability of being primary explosives by applying some basic heating tests. A small amount (~5 mg) of the respective ECC was therefore heated on a spatula by a lighter without direct flame contact. All prepared compounds deflagrated upon reaching their ignition temperatures.

Next, HP tests were performed for every coordination compound by heating an unconfined sample (again ~30 mg) on a copper plate with a Bunsen burner (Figure 18). The results are supposed to give insights into a compound's behavior during fast heating. All four 1-ATZ complexes melt before their deflagration. This can also be observed for almost all 1-VTZ analogs, except for $[Fe(1\text{-}VTZ)_6](ClO_4)_2$ (**4**), which deflagrates without melting first. The results are summarized in Table 3. Additional images can be found in the Supporting Information (Figures S18−S34). Finally, a small sample (again ~30 mg) was fixed and confined onto a surface (copper plate)

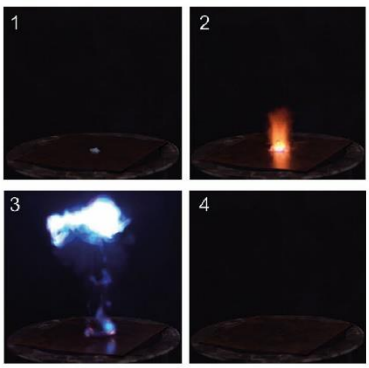


Figure 18. Hot plate test of compound **9** shown as a sequence.

with a bit of transparent tape and poked by a preheated needle (HN test). The result, preferably a detonation, shows the compound's behavior under slight confinement and is intended to indicate the deflagration-detonation transition (DDT). Only decomposition can be observed with the thermally stable (176−222 °C) 1-ATZ perchlorate complexes. A possible reason is the rapid cooling of the needle below the necessary ignition temperature. In contrast, the corresponding thermally more unstable (154−174 °C) 1-VTZ compounds show either deflagration or detonation.

During HP tests every compound showed deflagration reactions. However, when it comes to HN tests also detonations were observed for compounds **4**, **17**, and **18**. Because of this behavior, these particular compounds are of considerable interest in pentaerythritol tetranitrate (PETN) initiation experiments.

Compounds **7** and **15** were also selected for further characterization concerning their initiation capability, as their overall performance during hot needle testing, despite the lack of detonation, was also satisfying.

2.7. PETN Initiation Experiments. Following on from the preliminary tests (HP, HN), the most promising compounds were tested to ascertain whether they could ignite a secondary explosive and thus be considered as a potential substitute for lead azide. Showing either sharp deflagrations or even detonations during hot plate and hot needle tests, the dinitramide coordination compounds **17** and **18**, the ECCs **4** and **7**, and the copper(II) chlorate complex **15** were tested for their capability of initiating PETN. For this purpose, a 200 mg booster charge of PETN was loaded into a copper shell and 50 mg of the potential primary explosive to be tested was filled on top. More detailed information on the test setup can be found in the general methods of the ESI.† In case of a positive DDT from the primary explosive toward PETN a hole in the copper witness plate and the fragmentation of the copper shell is evident. Of the five tested complexes, none of them were able to initiate PETN. An overview of the test results can be found in Table 3. However, in the case of $[Cu(DN)_2(1\text{-}VTZ)_2]$ (**17**) fragmentation of the shell was observed (S38†).

2.8. Laser Ignition Experiments. Besides classic ignition through heat, mechanical stimuli, or electric discharge, laser ignition is getting increased attention over the last few years.[73−75] This is especially because of the ignition itself. One of the most common ignition methods for pyrotechnic mixtures are primer caps. These are ignited by a hit from the firing pin and the ignition, in the end, is caused by friction within the primer cap. Using laser irradiation for ignition

https://doi.org/10.1021/acs.inorgchem.2c03624
Inorg. Chem. XXXX, XXX, XXX−XXX

Table 3. Results of the Hot Plate, Hot Needle, and PETN Initiation Tests as Well as of Laser Ignition Experiments[a]

Compound	No.	HP	HN	PETN initiation	Laser energy, E^b (mJ)		
					1.7	25.5	51.0
$[Mn(1\text{-}VTZ)_6](ClO_4)_2$	**3**	defl.	defl.	—	—	—	—
$[Fe(1\text{-}VTZ)_6](ClO_4)_2$	**4**	defl.	det.	negative	—	—	—
$[Cu(1\text{-}VTZ)_6](ClO_4)_2$	**7**	defl.	defl.	negative	det.	det.	—
$[Zn(1\text{-}VTZ)_6](ClO_4)_2$	**8**	defl.	defl.	—	—	—	—
$[Mn(1\text{-}ATZ)_6](ClO_4)_2$	**9**	defl.	dec.	—	—	—	—
$[Fe(1\text{-}ATZ)_6](ClO_4)_2$	**10**	defl.	dec.	—	—	—	—
$[Cu(1\text{-}ATZ)_6](ClO_4)_2$	**11**	defl.	dec.	—	✗	✗	✗
$[Zn(1\text{-}ATZ)_6](ClO_4)_2$	**12**	defl.	dec.	—	—	—	—
$[Cu(NO_3)_2(H_2O)(1\text{-}VTZ)_2]$	**13a**	defl.	defl.	—	—	dec.	dec.
$[Cu(1\text{-}VTZ)_6](ClO_3)_2$	**15**	defl.	defl.	negative	det.	det.	—
$[Cu(1\text{-}ATZ)_6](ClO_3)_2$	**16**	defl.	dec.	—	✗	dec.	dec.
$[Cu(DN)_2(1\text{-}VTZ)_2]$	**17**	defl.	det.	negative	det.	defl.	—
$[Cu(DN)_2(1\text{-}ATZ)_2]$	**18**	defl.	det.	negative	defl.	defl.	defl.
$[Cu(PA)_2(1\text{-}VTZ)_2]$	**21**	defl.	dec.	—	—	dec.	dec.
$[Cu(HTNR)_2(1\text{-}VTZ)_2]$	**22a**	defl.	defl.	—	—	dec.	comb.
$[Cu(TNR)(1\text{-}VTZ)_2]$	**22b**	defl.	dec.	—	—	comb.	comb.
$[Cu(H_2TNPG)_2(1\text{-}VTZ)_4]$	**23**	defl.	dec.	—	—	dec.	comb.

[a]—: not tested, cross: no ignition, dec.: decomposition, defl.: deflagration, det.: detonation, comb.: combustion. [b]Operating parameters: current I = 7 A; voltage U = 4 V; theoretical maximal output power P_{max} = 45 W; theoretical energy E_{max} = 1.7−51.0 mJ; wavelength λ = 915 nm; pulse length τ = 1.0−30 ms.

makes the compound's sensitivity toward friction, which is needed for classic ignition, obsolete, and is simultaneously opening the field for less sensitive compounds. This has implications not only for safety but also for the processing and storage of the mixtures and compounds.

Laser ignition experiments were carried out for the copper 1-VTZ and 1-ATZ complexes only. The manganese (**3**, **9**), iron (**4**, **10**), and zinc (**8**, **12**) complexes were waived, as only colored complexes are known to react toward laser irradiation.[22,23] Details on the experiment and setup can be found in the experimental section of the Supporting Information. The outcome of each test is summarized in Table 3.

The most convincing results were obtained for the ECCs **7**, **15**, and **17**, showing detonations at an energy level of 1.7 mJ. High-speed images of selected experiments are shown in Figure 19. As already known from former investigations,[21−23,33] these results again underpin the special suitability of the anions ClO_4^-, ClO_3^-, and DN^- in future laser ignitable ECCs. Unsurprisingly, the compounds based on trinitrophenolate anions (**21**−**23**) or the complex of type $[Cu(NO_3)_2(H_2O)(1\text{-}VTZ)_2]$ mainly show decomposition reactions and are therefore rather not interesting as laser ignitable energetic materials. Nevertheless, this behavior indicates a correlation between the compounds' performance during HN tests and laser ignition experiments. ECCs that exhibit detonation or strong deflagration tend to detonate during laser experiments, while weaker reacting or water-containing compounds usually only decompose. A reason for this correlation is most likely that both experiments were carried out under the confinement of the samples.

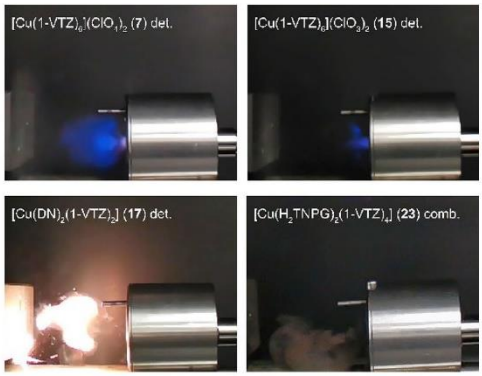


Figure 19. High-speed images of the detonations (det.) of the ECCs **7**, **15**, and **17** together with the combustion (comb.) of complex **23** during laser ignition experiments.

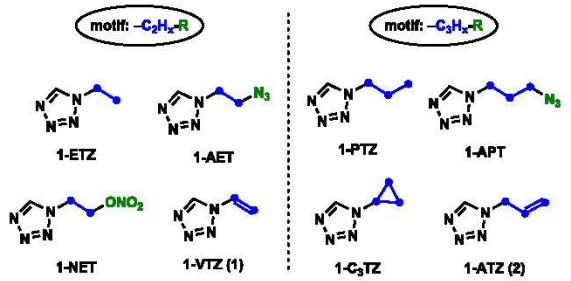
The formal introduction of an additional CH_2-group when replacing the *N*1-vinyl with an *N*1-allyl moiety is accompanied by a significant increase in the initiation threshold. While the coordination compounds based on the more energetic ligand **1** detonate at 1.7 mJ (**7**, **15**, **17**), the complementary complexes based on ligand **2** (**11**, **16**, **18**) show either no or only weak reactions, which is within expectations considering the corresponding HN tests.

2.9. Comparison of 1-Ethyl-5*H*-tetrazole Based ECCs and 1-Propyl-5*H*-tetrazole-Based ECCs. A main target of this work was not only to incorporate vinyl or allyl tetrazoles in energetic coordination compounds but also to investigate the complexes' properties. These properties have been discussed in

https://doi.org/10.1021/acs.inorgchem.2c03624
Inorg. Chem. XXXX, XXX, XXX−XXX

detail in the sections above; however, these results should be put in relation to already known, similarly arranged complexes. For this purpose, the ligands of this work (**1**, **2**) were subdivided according to their *N*1-substitution pattern and compared with three ligands of the same carbon number (Chart 2). Exactly these ligands, recently published by our group, were chosen on purpose, as it can be assumed that all experiments were performed similarly.

Chart 2. Overview of the Ligands Used for Comparison Subdivided According to Their Structural Motif (C_2/C_3-Chain/Ring)



Unfortunately, we are restricted to a comparison of the ligands themselves and copper as the central metal and chlorate, perchlorate, dinitramide, and picrate as anions. This is mainly because, for example, nitrate or styphnate complexes in many cases have a different composition or coordination geometry, and in many cases, the complexes cannot be isolated when metals other than copper were used. Thermal stability and also sensitivity to BAM drop hammer and friction tester were chosen as comparative variables. Since hot plate and hot needle tests are considered important preliminary tests for primary explosives, they were used to visualize the compounds' performance. The sensitivity data of the respective ligands and ECCs is summarized in Table 4.

Starting with the ligands of the *N*1 substitution pattern -C_2H_x-R, every molecule is insensitive toward friction, which is most likely caused by the liquid state of the compounds. Therefore, no conclusions about ECCs can be drawn from this point. The thermal stability on the other hand is the lowest for 1-NET and is again limited by the energetic group (-ONO_2). Consequently, the complexes based on the 1-NET ligand should have the lowest thermal stability. However, it is found that for the dinitramide and picrate complexes, the thermal stability is similar (Figure 20). The same applies to the perchlorate complexes except for the 1-ETZ complex (T_{exo} =

Table 4. Thermal Stability[a], BAM Impact, and Friction Sensitivity Together with a Hot Plate and Hot Needle Test Outcome for Several ECCs Based on 1-Ethyl-5*H*-tetrazole and 1-Propyl-5*H*-tetrazole Ligand Derivatives

N1 subst. pattern[b]	compound	no.	T_{exo} (°C)[c]	IS (J)[d]	FS (N)[e]	HP[f]	HN[f]	ref
$-C_2H_x-R$	1-ETZ		208	>40	>360	n.d.	n.d.	23
	1-AET		193	9	>360	n.d.	n.d.	23
	1-NET		168	10	>360	n.d.	n.d.	33
	1-VTZ	1	172	15	>360	n.d.	n.d.	
	$[Cu(1\text{-}ETZ)_6](ClO_4)_2$		210	10	120	defl.	defl.	23
	$[Cu(1\text{-}AET)_6](ClO_4)_2$		158	<1	15	defl.	det.	23
	$[Cu(1\text{-}NET)_6](ClO_4)_2$		165	3	25	defl.	defl.	33
	$[Cu(1\text{-}VTZ)_6](ClO_4)_2$	7	154	2	7	defl.	defl.	
	$[Cu(1\text{-}ETZ)_6](ClO_3)_2$		158	7	60	defl.	defl.	23
	$[Cu(1\text{-}AET)_6](ClO_3)_2$		146	2.5	4	defl.	det.	23
	$[Cu(1\text{-}NET)_6](ClO_3)_2$		149	2	15	defl.	defl.	33
	$[Cu(1\text{-}VTZ)_6](ClO_3)_2$	15	107	4	2	defl.	defl.	
	$[Cu(1\text{-}AET)_2(DN)_2]$		106	2	5	defl.	defl.	76
	$[Cu(1\text{-}NET)_2(DN)_2]$		110	2	7	defl.	defl.	33
	$[Cu(1\text{-}VTZ)_2(DN)_2]$	17	115	1	9	defl.	det.	
	$[Cu(PA)_2(1\text{-}AET)_2]$		183	3	252	defl.	defl.	23
	$[Cu(PA)_2(1\text{-}NET)_2]$		197	20	>360	defl.	dec.	33
	$[Cu(PA)_2(1\text{-}VTZ)_2]$	21	191	10	288	defl.	dec.	
$-C_3H_x-R$	1-PTZ		206	>40	>360	n.d.	n.d.	24
	1-APT		195	>40	>360	n.d.	n.d.	24
	1-C_3TZ		200	>40	>360	inf.	dec.	54
	1-ATZ	2	207	>40	>360	n.d.	n.d.	
	$[Cu(1\text{-}PTZ)_6](ClO_4)_2$		209	30	240	dec.	dec.	24
	$[Cu(1\text{-}APT)_6](ClO_4)_2$		165	2.5	32	defl.	defl.	24
	$[Cu(1\text{-}C_3TZ)_6](ClO_4)_2$		183	4	80	defl.	dec.	54
	$[Cu(1\text{-}ATZ)_6](ClO_4)_2$	11	176	5	72	defl.	dec.	
	$[Cu(1\text{-}PTZ)_6](ClO_3)_2$		152	>40	168	dec.	dec.	24
	$[Cu(1\text{-}APT)_6](ClO_3)_2$		151	2.5	24	defl.	defl.	24
	$[Cu(1\text{-}C_3TZ)_6](ClO_3)_2$		156	2	32	defl.	dec.	54
	$[Cu(1\text{-}ATZ)_6](ClO_3)_2$	16	113	3	36	defl.	dec.	

[a]Onset temperature at a heating rate of 5 °C min^{-1} measured by DTA. [b]R = H, ONO_2, N_3. [c]Exothermic peak, which indicates decomposition. [d]Impact sensitivity according to the BAM drop hammer (method 1 out of 6). [e]Friction sensitivity according to the BAM friction tester (method 1 out of 6). [f]dec.: decomposition; inf.: inflammation; defl.: deflagration; det.: detonation; n.d.: not determined.

https://doi.org/10.1021/acs.inorgchem.2c03624
Inorg. Chem. XXXX, XXX, XXX−XXX

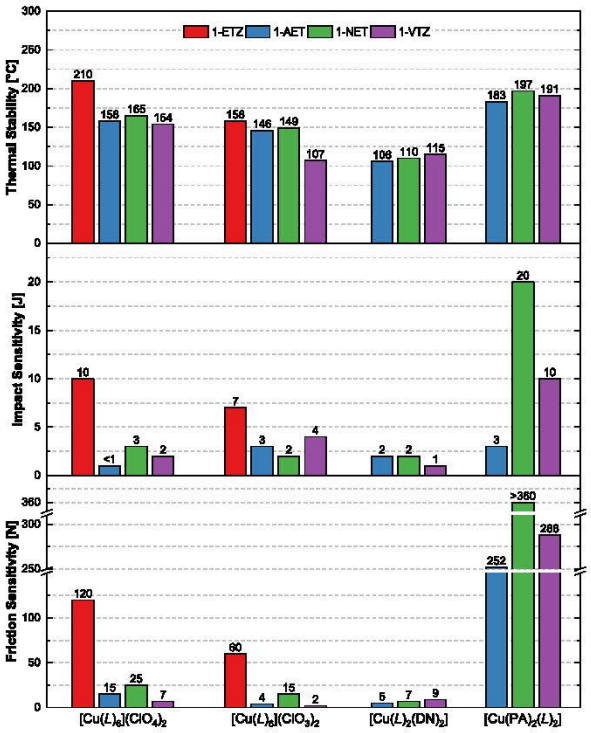


Figure 20. Comparison of the sensitivities and thermal stability of several ECCs based on different *N*1-substituted C_2-derived ligands (L).

210 °C). Only in the case of $[Cu(1\text{-}VTZ)_6](ClO_3)_2$ (**15**, T_{exo} = 107 °C), a significantly lower thermal stability was observed compared to the other complexes.

When it comes to impact sensitivity, the perchlorate, chlorate, and dinitramide ECCs based on 1-nitratoehyl-5*H*-tetrazole, 1-azidoethyl-5*H*-tetrazole, and 1-vinyl-5*H*-tetrazole are roughly within the same area of about 1−4 J. Only the coordination compounds having 1-ethyl-5*H*-tetrazole as a ligand are less sensitive (7−10 J). The picrate anion does not allow such a clear pattern since the sensitivities are much more widely scattered. A comparison of the friction sensitivity data indicates that ECCs based on 1-ETZ are the least sensitive complexes.

This is followed by the 1-NET complexes, with the dinitramide complexes being a slight exception here. 1-AET and 1-VTZ coordination compounds together form the most sensitive of the investigated complexes. The fact that in some cases no patterns are discernible or exceptions occur is probably due to grain size effects.

The HP and HN data of all complexes based on *N*1-substituted C_2-derived ligands indicate sufficient performance, except the picrate compounds. Deflagrations were observed in the majority of the tests carried out. However, the best results (detonations) were observed for 1-AET-based coordination compounds and in one case for the 1-VTZ-based complex (**17**). Overall, it can be stated, that the ECC based on 1-vinyl-5*H*-tetrazole possesses comparable or better thermal stability than the ECC based on 1-AET or 1-NET as the ligand. In most of the cases, the compounds' friction and impact sensitivity is lower than the ones for 1-AET complexes, while having comparable performance data.

Focusing on the tetrazoles with a C_3-based substitution pattern at *N*1, 1-PTZ as the least endothermic ligand forms both the most thermally stable and the least sensitive (IS, FS) perchlorate complex (Figure 21). As the endothermicity of the ligands increases, the complexes' thermal stability decreases and their sensitivity increases: 1-C_3TZ (T_{exo} = 183 °C, IS = 4 J, FS = 80 N) > 1-ATZ (T_{exo} = 176 °C, IS = 5 J, FS = 72 N) > 1-APT (T_{exo} = 165 °C, IS = 2.5 J, FS = 32 N). In terms of performance, the HP tests state that starting from the parent 1-PTZ structural motif, formal cyclization (1-C_3TZ), or reduction (1-ATZ) is sufficient for the perchlorate complexes to deflagrate, whereas HN experiments need the azide-substituted ligand (1-APT) for the same outcome.

This observation also applies to the complementary chlorate complexes (Figure 22). Accordingly, it is not surprising that $[Cu(1\text{-}APT)_6](ClO_3)_2$ is the most friction-sensitive ECC, although it should be mentioned that the sensitivities for 1-C_3TZ and 1-ATZ-based chlorate complexes are also of approximately the same order of magnitude. Only $[Cu(1\text{-}PTZ)_6](ClO_3)_2$ exhibits a significantly lower sensitivity (IS ≥ 40 J, FS = 168 N). Contrary to expectations, however, the thermal stabilities of the chlorate complexes based on 1-PTZ (T_{exo} = 152 °C), 1-APT (T_{exo} = 151 °C), and 1-C_3TZ (T_{exo} = 156 °C) are almost identical, while the decomposition temperature for **16** (T_{exo} = 113 °C) is significantly lower. When looking at the uncoordinated *N*1-substituted C_3-derived

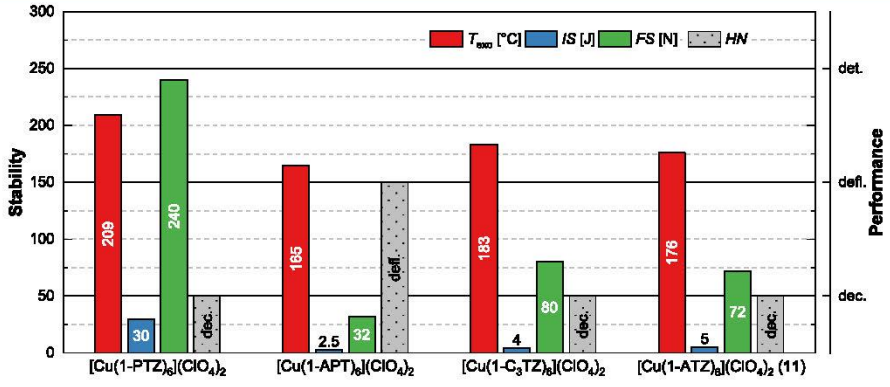


Figure 21. Comparison of the stabilities (T_{exo}, IS, FS) and performance (HN) of the copper(II) perchlorate complexes based on different *N*1-substituted C_3-derived tetrazole ligands.

https://doi.org/10.1021/acs.inorgchem.2c03624
Inorg. Chem. XXXX, XXX, XXX−XXX

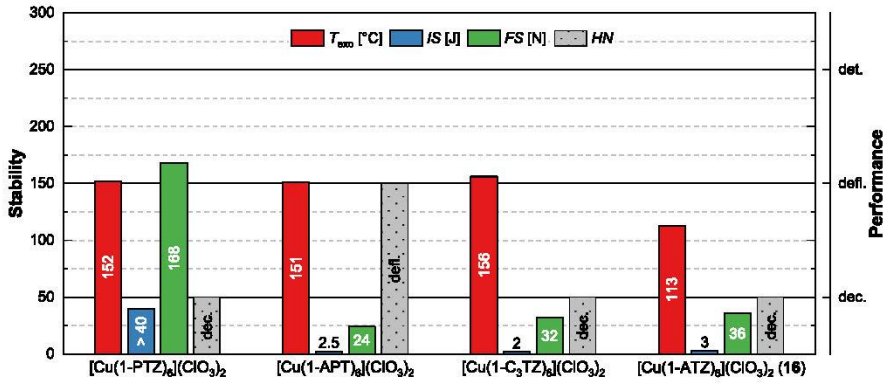


Figure 22. Comparison of the stabilities (T_{exo}, IS, FS) and performance (HN) of the copper(II) chlorate complexes based on different *N*1-substituted C_3-derived tetrazole ligands.

tetrazole ligands themselves, all of them can be classified as insensitive to mechanical stimuli. On the whole, this comparative study illustrates (Figures 21 and 22) that – as is often the case – higher performance goes hand in hand with higher sensitivity.

If we compare the 1-VTZ-based copper perchlorate complex [Cu(1-VTZ)$_6$](ClO$_4$)$_2$ (**5**) with the corresponding [Cu(1-ETZ)$_6$](ClO$_4$)$_2$, we observe that the introduction of an unsaturated bond leads to an increase in the sensitivities (IS, FS, ESD) on the one hand and to lower thermal stability on the other (Figure 23). The same applies to the comparison of

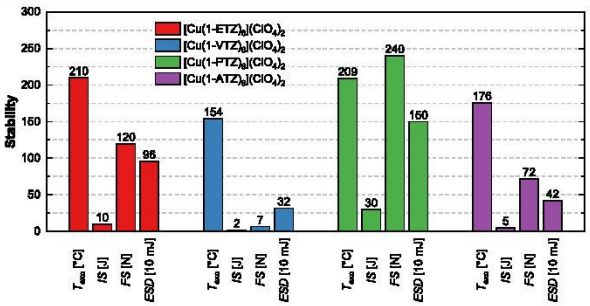


Figure 23. Graphical representation of the influence of the introduction of an unsaturated C–C bond.

the 1-ATZ-based energetic coordination compound [Cu(1-ATZ)$_6$](ClO$_4$)$_2$ (**9**) with the respective 1-PTZ complex (Figure 23). This fact is consistent with the higher heat of formation of the unsaturated compounds.

3. CONCLUSIONS

The goal of the present study has been the preparation of the nitrogen-rich neutral ligands 1-VTZ (**1**) and 1-ATZ (**2**) and their incorporation into ECCs aiming for green primary explosives capable of replacing LA and LS. Of particular interest was the investigation of the influence of the alkenyl chain lengthening by comparing analogous ECCs based on 1-VTZ (**1**) and 1-ATZ (**2**). Additionally, the influence of the increased endothermicity by introducing an unsaturated C–C bond (1-ETZ *vs* 1-VTZ and 1-PTZ *vs* 1-ATZ) is discussed. Starting from commercially available precursors, the ligand 1-vinyl-5*H*-tetrazole (**1**, 1-VTZ) was synthesized in a two-step reaction with an overall yield of 34%, whereas ligand 1-allyl-5*H*-tetrazole (**2**, 1-ATZ) was accessible in a straightforward one-step synthesis (yield: 60%). For characterization of the tetrazole derivatives, various analytical methods, including EA, NMR spectroscopy, and IR spectroscopy as well as DTA and sensitivity measurements (IS, FS, ESD, and BDIS), were used. As expected, the lengthening of the alkenyl chain leads to increased thermal stability (**1**: 173 °C (T_{dec}), **2**: 207 °C (T_{dec})) and decreased impact sensitivity (**1**: 15 J, **2**: > 40 J) of the uncoordinated ligands. For the first time, it was possible to obtain a single crystal structure of 1-VTZ.

The ligands were successfully applied for the synthesis of 23 new coordination compounds based on toxic (Co, Ni) and less or nontoxic 3d transition metals (Mn, Fe, Cu, and Zn) and oxidizing anions (perchlorate, nitrate, chlorate, and dinitramide) or trinitrophenolate anions. In the present work, a comprehensive comparative study of the physicochemical properties of the obtained 1-VTZ and 1-ATZ-based ECCs was conducted, which were partly also tested for their capability of initiating PETN or being laser ignitable. In all cases, the introduction of an additional carbon atom increased the thermal stability and decreased the complex sensitivity toward various mechanical stimuli.

Furthermore, the synthesized ligands 1-VTZ (**1**) and 1-ATZ (**2**) and their ECCs are put in relation to already published *N*1-substituted C_2-derived and C_3-derived tetrazole-based ECCs, respectively. Comparison of [Cu(1-VTZ)$_6$](ClO$_4$)$_2$ (**7**) with the literature-known [Cu(1-ETZ)$_6$](ClO$_4$)$_2$ proves that the introduction of an unsaturated bond leads to more sensitive and less thermally stable ECCs. The same observation is made in the case of [Cu(1-ATZ)$_6$](ClO$_4$)$_2$ (**11**) and [Cu(1-PTZ)$_6$](ClO$_4$)$_2$.

■ ASSOCIATED CONTENT

Supporting Information

The Supporting Information is available free of charge at https://pubs.acs.org/doi/10.1021/acs.inorgchem.2c03624.

Compound overview; mechanistic proposal for the synthesis of 1-ClET; X-ray diffraction; NMR spectroscopy of 1-ClET, 1-VTZ (**1**), and 1-ATZ (**2**); IR spectroscopy of **1**–**12**, **13a**, **15**–**18**, **21**–**23**; DTA plots of **1**–**12**, **13a**, **15**–**18**, **21**–**23**; TGA plots of **3**, **5**, **9**–**12**; hot plate & hot needle tests of **3**, **4**, **7**-**13a**, **15**–**18**, **21**–**23**; laser initiation tests of **16**, **18**, **22b**; initiation capability tests; magnetic properties; experimental part and general methods; references (PDF)

Accession Codes

CCDC 2207187, 2207189−2207195, 2207197−2207207, and 2207251−2207254 contain the supplementary crystallographic data for this paper. These data can be obtained free of charge via www.ccdc.cam.ac.uk/data_request/cif, or by emailing data_request@ccdc.cam.ac.uk, or by contacting The Cambridge Crystallographic Data Centre, 12 Union Road, Cambridge CB2 1EZ, UK; fax: +44 1223 336033.

CCDC 2207187−2207207 and 2207251−2207254 contain the supplementary crystallographic data for this paper. These can be obtained free of charge via www.ccdc.cam.ac.uk/data_request/cif, or by emailing data_request@ccdc.cam.ac.uk, or by contacting The Cambridge Crystallographic Data Centre, 12 Union Road, Cambridge CB2 1EZ, UK; fax: +441,223 336,033.

■ AUTHOR INFORMATION

Corresponding Author

Jörg Stierstorfer − *Department of Chemistry, Ludwig Maximilian University Munich, Munich D-81377, Germany;* orcid.org/0000-0002-2105-1275; Email: jstch@cup.uni-muenchen.de

Authors

Markus Rösch − *Department of Chemistry, Ludwig Maximilian University Munich, Munich D-81377, Germany*

Michael S. Gruhne − *Department of Chemistry, Ludwig Maximilian University Munich, Munich D-81377, Germany*

Marcus Lommel − *Department of Chemistry, Ludwig Maximilian University Munich, Munich D-81377, Germany*

Simon M. J. Endraß − *Department of Chemistry, Ludwig Maximilian University Munich, Munich D-81377, Germany;* orcid.org/0000-0003-1489-2380

Complete contact information is available at: https://pubs.acs.org/10.1021/acs.inorgchem.2c03624

Author Contributions

‡M.R. and M.G. contributed equally and are the first authors. All authors have approved the final version of the manuscript.

Notes

The authors declare no competing financial interest.

■ ACKNOWLEDGMENTS

Financial support of this work by Ludwig-Maximilian University (LMU), the Office of Naval Research (ONR) under grant no. ONR N00014-19-1-2078 and the Strategic Environmental Research and Development Program (SERDP) under contract no. W912HQ19C0033 is gratefully acknowledged.

■ REFERENCES

(1) Klapötke, T. M. *Chemistry of High-Energy Materials, 5th*; Walter de Gruyter, 2019.

(2) Fronabarger, J. W.; Williams, M. D.; Sanborn, W. B.; Bragg, J. G.; Parrish, D. A.; Bichay, M. DBX-1 - A Lead Free Replacement for Lead Azide. *Propellants Explosives Pyrotechnics* **2011**, *36*, 541−550.

(3) Fischer, N.; Fischer, D.; Klapötke, T. M.; Piercey, D. G.; Stierstorfer, J. Pushing the limits of energetic materials − the synthesis and characterization of dihydroxylammonium 5,5′-bistetrazole-1,1′-diolate. *J. Mater. Chem.* **2012**, *22*, 20418−20422.

(4) Wei, H.; Zhang, J.; Shreeve, J. M. Synthesis, Characterization, and Energetic Properties of 6-Amino-tetrazolo[1,5-b]-1,2,4,5-tetrazine-7-*N*-oxide: A Nitrogen-Rich Material with High Density. *Chem. − Asian J.* **2015**, *10*, 1130−1132.

(5) Yu, Q.; Imler, G. H.; Parrish, D. A.; Shreeve, J. M. Challenging the Limits of Nitro Groups Associated with a Tetrazole Ring. *Org. Lett.* **2019**, *21*, 4684−4688.

(6) Chavez, D. E.; Parrish, D. A.; Mitchell, L.; Imler, G. H. Azido and Tetrazolo 1,2,4,5-Tetrazine *N*-Oxides. *Angew. Chem., Int. Ed.* **2017**, *56*, 3575−3578.

(7) Gettings, M. L.; Thoenen, M. T.; Byrd, E. F. C.; Sabatini, J. J.; Zeller, M.; Piercey, D. G. Tetrazole Azasydnone (C2N7O2H) And Its Salts: High-Performing Zwitterionic Energetic Materials Containing A Unique Explosophore. *Chem. − Eur. J.* **2020**, *26*, 14530−14535.

(8) Kent, R. V.; Wiscons, R. A.; Sharon, P.; Grinstein, D.; Frimer, A. A.; Matzger, A. J. Cocrystal Engineering of a High Nitrogen Energetic Material. *Cryst. Growth Des.* **2018**, *18*, 219−224.

(9) Zhang, Q.; Chen, D.; Jing, D.; Fan, G.; He, L.; Li, H.; Wang, W.; Nie, F. Access to green primary explosives *via* constructing coordination polymers based on bis-tetrazole oxide and non-lead metals. *Green Chem.* **2019**, *21*, 1947−1955.

(10) Fischer, D.; Klapötke, T. M.; Stierstorfer, J. Potassium 1,1′-Dinitramino-5,5′-bistetrazolate: A Primary Explosive with Fast Detonation and High Initiation Power. *Angew. Chem., Int. Ed.* **2014**, *53*, 8172−8175.

(11) Huang, W.; Tang, Y.; Imler, G. H.; Parrish, D. A.; Shreeve, J. M. Nitrogen-Rich Tetrazolo[1,5-*b*]pyridazine: Promising Building Block for Advanced Energetic Materials. *J. Am. Chem. Soc.* **2020**, *142*, 3652−3657.

(12) Wang, Q.; Shao, Y.; Lu, M. Amino-tetrazole functionalized fused triazolo-triazine and tetrazolo-triazine energetic materials. *Chem. Commun.* **2019**, *55*, 6062−6065.

(13) Cheng, T. Review of novel energetic polymers and binders - high energy propellant ingredients for the new space race. *Des. Monomers Polym.* **2019**, *22*, 54−65.

(14) Betzler, F. M.; Boller, R.; Grossmann, A.; Klapötke, T. M. Novel Insensitive Energetic Nitrogen-rich Polymers Based on Tetrazoles. *Z. Naturforsch. B* **2013**, *68*, 714−718.

(15) Huang, M.-R.; Li, X.-G.; Li, S.-X.; Zhang, W. Resultful synthesis of polyvinyltetrazole from polyacrylonitrile. *React. Funct. Polym.* **2004**, *59*, 53−61.

(16) Lempert, D. B.; Kazakov, A. I.; Soglasnova, S. I.; Dalinger, I. L.; Sheremetev, A. B. Energetic abilities of nitro derivatives of isomeric (pyrazol-3-yl)tetrazoles as components of solid composite propellants. *Russ. Chem. Bull.* **2018**, *67*, 1580−1588.

(17) Nguyen, T.-A. D.; Veauthier, J. M.; Chavez, D. E.; Tappan, B. C.; Mueller, A. H.; Scott, B. L.; Parrish, D. A. Lanthanide Complexes of Bis(tetrazolato)amine: A Route to Lanthanide Nitride Foams. *Inorg. Chem.* **2020**, *59*, 16109−16116.

(18) Joas, M.; Klapötke, T. M.; Szimhardt, N. Photosensitive Metal(II) Perchlorates with 1,2-Bis[5-(1-methylhydrazinyl)tetrazol-1-yl]ethane as Ligand: Synthesis, Characterization and Laser Ignition. *Eur. J. Inorg. Chem.* **2014**, *2014*, 493−498.

(19) Ilyushin, M. A.; Tver'yanovich, A. S.; Tver'yanovich, Y. S.; Abdrashitov, G. O.; Aver'yanov, A. O.; Bal'makov, M. D. Laser Initiation of Photo- and Thermal Processes on a Pentaammine (5-Nytrotetrazolato-N^2) Cobalt(III) Perchlorate Example. *Glass Phys. Chem.* **2018**, *44*, 120−122.

(20) Sinditskii, V. P.; Serushkin, V. V. Design and Combustion Behaviour of Explosive Coordination Compounds. *DSJ* **1996**, *46*, 371−383.

(21) Szimhardt, N.; Wurzenberger, M. H. H.; Beringer, A.; Daumann, L. J.; Stierstorfer, J. Coordination chemistry with 1-methyl-5*H*-tetrazole: cocrystallization, laser-ignition, lead-free primary explosives − one ligand, three goals. *J. Mater. Chem. A* **2017**, *5*, 23753−23765.

(22) Szimhardt, N.; Wurzenberger, M. H. H.; Zeisel, L.; Gruhne, M. S.; Lommel, M.; Stierstorfer, J. Maximization of the energy capability level in transition metal complexes through application of 1-amino- and 2-amino-5*H*-tetrazole ligands. *J. Mater. Chem. A* **2018**, *6*, 16257−16272.

(23) Wurzenberger, M. H. H.; Gruhne, M. S.; Lommel, M.; Szimhardt, N.; Klapötke, T. M.; Stierstorfer, J. Comparison of 1-Ethyl-

5H-tetrazole and 1-Azidoethyl-5H-tetrazole as Ligands in Energetic Transition Metal Complexes. *Chem. – Asian J.* **2019**, *14*, 2018–2028.
(24) Wurzenberger, M. H. H.; Endraß, S. M. J.; Lommel, M.; Klapötke, T. M.; Stierstorfer, J. Comparison of 1-Propyl-5*H*-tetrazole and 1-Azidopropyl-5*H*-tetrazole as Ligands for Laser Ignitable Energetic Materials. *ACS Appl. Energy Mater.* **2020**, *3*, 3798–3806.
(25) Freis, M.; Klapötke, T. M.; Stierstorfer, J.; Szimhardt, N. Di(1H-tetrazol-5-yl)methane as Neutral Ligand in Energetic Transition Metal Complexes. *Inorg. Chem.* **2017**, *56*, 7936–7947.
(26) Evers, J.; Gospodinov, I.; Joas, M.; Klapötke, T. M.; Stierstorfer, J. Cocrystallization of photosensitive energetic copper(II) perchlorate complexes with the nitrogen-rich ligand 1,2-Di(1H-tetrazol-5-yl)-ethane. *Inorg. Chem.* **2014**, *53*, 11749–11756.
(27) Gaponik, P. N.; Karavai, V. P.; Grigorev, Y. V. Synthesis of 1-Substituted Tetrazoles by Heterocyclization of Primary Amines, Orthoformic Ester And Sodium Azide. *Khim. Geterotsikl. Soedin.* **1985**, *11*, 1521–1524.
(28) Fischer, N.; Klapötke, T. M.; Stierstorfer, J.; Wiedemann, C. 1-Nitratoethyl-5-nitriminotetrazole derivatives – Shaping future high explosives. *Polyhedron* **2011**, *30*, 2374–2386.
(29) Stierstorfer, J.; Tarantik, K. R.; Klapötke, T. M. New Energetic Materials: Functionalized 1-Ethyl-5-Aminotetrazoles and 1-Ethyl-5-nitriminotetrazoles. *Chem. – Eur. J.* **2009**, *15*, 5775–5792.
(30) Klapötke, T. M.; Krumm, B.; Reith, T.; Unger, C. C. Synthetic Routes to a Triazole and Tetrazole with Trinitroalkyl Substitution at Nitrogen. *J. Org. Chem.* **2018**, *83*, 10505–10509.
(31) Gaponik, P. N.; Karavai, V. P. Synthesis and Properties of 1-(2-hydroxyethyl)tetrazole. *Chem. Heterocycl. Compd.* **1985**, *21*, 1172–1174.
(32) Finnegan, W.; Henry, R. *N*-Vinyltetrazoles. *J. Org. Chem.* **1959**, *24*, 1565–1567.
(33) Gruhne, M. S.; Lenz, T.; Rösch, M.; Lommel, M.; Wurzenberger, M. H. H.; Klapötke, T. M.; Stierstorfer, J. Nitratoethyl-5*H*-tetrazoles: improving the oxygen balance through application of organic nitrates in energetic coordination compounds. *Dalton Trans.* **2021**, *50*, 10811–10825.
(34) Shvedenkov, Y.; Bushuev, M.; Romanenko, G.; Lavrenova, L.; Ikorskii, V.; Gaponik, P.; Larionov, S. Magnetic Anisotropy of New Layered Copper(II) Bromide Complexes of 1-Substituted Tetrazoles. *Eur. J. Inorg. Chem.* **2005**, *2005*, 1678–1682.
(35) Kizhnyaev, V. N.; Kruglova, V. A. Complexation of Vinyltetrazoles and Their Polymers with Divalent-Metal Chlorides. *J. Appl. Chem. USSR* **1992**, *65*, 1523–1527.
(36) Lavrenova, L. G.; Bogatikov, A. N.; Ikorskii, V. N.; Sheludyakova, L. A.; Boguslavskii, E. G.; Gaponik, P. N.; Larionov, S. V. Complexes of Co(II), Ni(II), and Cu(II) with 1-Vinyltetrazole and 1-Allyltetrazole. *Russ. J. Inorg. Chem.* **1996**, *41*, 406–409.
(37) Gaponik, P. N.; Ivashkevich, O. A.; Degtyarik, M. M. Synthesis and Complexation Properties of 1-Vinyltetrazole. *Chem. Informationsdienst* **1985**, *28*, 43–46.
(38) Kizhnyaev, V. N.; Vereshchagin, L. I. Vinyltetrazoles: synthesis and properties. *Russ. Chem. Rev.* **2003**, *72*, 143–164.
(39) Lavrenova, L. G.; Bogatikov, A. N.; Sheludyakova, L. A.; Ikorskii, V. N.; Larionov, S. V.; Gaponik, P. N. Complexes of transition metals with *N*-derivatives of tetrazole. *Russ. J. Inorg. Chem.* **1991**, *36*, 693–696.
(40) Lavrenova, L. G.; Ikorskii, V. N.; Larionov, S. V.; Bogatikov, A. N.; Gaponik, P. N. A New Ferromagnet – Dichlorobis(1-allyltetrazole)copper Complex Compound. *Russ. J. Inorg. Chem.* **1993**, *38*, 1416–1417.
(41) Agrawal, J. P. Past, Present & Future of Thermally Stable Explosives. *Cent. Eur. J. Energ. Mater.* **2012**, *9*, 273–290.
(42) Finnegan, W. G.; Henry, R. A.; Sol, S. Polymers of Substituted Tetrazoles US3,004,959A, 1959.
(43) Stassen, A. F.; Dova, E.; Ensling, R.; Schenk, H.; Gutlich, P.; Haasnoot, J. G.; Reedijk, J. Spin crossover in hexakis(1-(2-chloroethyl)-tetrazole)iron(II) complexes; synthesis and magnetic properties. *Inorg. Chim. Acta* **2002**, *335*, 61–68.
(44) Gaponik, P. N.; Ivashkevich, O. A.; Bubel, O. N.; Degtyarik, M. M.; Naumenko, V. N. Spectroscopic and Quantum-Chemical Investigation of Alkyl- and Alkenyltetrazoles. *Theor. Exp. Chem.* **1989**, *25*, 33–36.
(45) Finnegan, W. G.; Henry, R. A.; Sol, S. *Substituted Tetrazoles.*
(46) Gaponik, P. N.; Voitekhovich, S. V.; Ivashkevich, O. A. Metal derivatives of tetrazoles. *Russ. Chem. Rev.* **2006**, *75*, 569–603.
(47) Wiehl, L. Structures of Hexakis(1-propyltetrazole)iron(II) Bis(tetrafluoroborate), $[Fe(CHN_4C_3H_7)_6](BF_4)_2$, Hexakis(1-methyltetrazole)iron(II) Bis(tetrafluoroborate), $[Fe(CHN_4CH_3)_6](BF_4)_2$, and the Analogous Perchlorates. Their Relation to Spin Crossover Behaviour and Comparison of Debye–Waller Factors from Structure Determination and Mössbauer Spectroscopy. *Acta Crystallogr., Sect. B: Struct. Sci.* **1993**, *49*, 289–303.
(48) Wurzenberger, M. H. H.; Szimhardt, N.; Stierstorfer, J. Copper(II) Chlorate Complexes: The Renaissance of a Forgotten and Misjudged Energetic Anion. *J. Am. Chem. Soc.* **2018**, *140*, 3206–3209.
(49) Wurzenberger, M. H. H.; Lommel, M.; Gruhne, M. S.; Szimhardt, N.; Stierstorfer, J. Refinement of Copper(II) Azide with 1-Alkyl-5*H*-tetrazoles: Adaptable Energetic Complexes. *Angew. Chem., Int. Ed. Engl.* **2020**, *59*, 12367–12370.
(50) Wurzenberger, M. H. H.; Bissinger, B. R. G.; Lommel, M.; Gruhne, M. S.; Szimhardt, N.; Stierstorfer, J. Synthesis and comparison of copper(II) complexes with various *N*-aminotetrazole ligands involving trinitrophenol anions. *New J. Chem.* **2019**, *43*, 18193–18202.
(51) Gütlich, P.; Hauser, A.; Spiering, H. Thermal and Optical Switching of Iron(II) Complexes. *Angew. Chem., Int. Ed. Engl.* **1994**, *33*, 2024–2054.
(52) Stassen, A. F.; Roubeau, O.; Ferrero Gramage, I.; Linarès, J.; Varret, F.; Mutikainen, I.; Turpeinen, U.; Haasnoot, J. G.; Reedijk, J. Physical properties of the spin-crossover compound hexakis(1-methyltetrazole-N4)iron(II) triflate, steady state and relaxation studies, X-ray structure of the isomorphic Ni(II) compound. *Polyhedron* **2001**, *20*, 1699–1707.
(53) Franke, P. L.; Haasnoot, J. G.; Zuur, A. P. Tetrazoles as Ligands, Part IV. Iron(II) Complexes of Monofunctional Tetrazole Ligands, Showing High-Spin Low Spin Transitions. *Inorg. Chim. Acta* **1982**, *59*, 5–9.
(54) Braun, V.; Wurzenberger, M. H. H.; Weippert, V.; Stierstorfer, J. Tailoring the properties of 3d transition metal complexes with different *N*-cycloalkyl-substituted tetrazoles. *New J. Chem.* **2021**, *45*, 11042–11050.
(55) Hauser, A.; Gütlich, P.; Hinek, R.; Spiering, H.; Schollmeyer, D. The $[Fe(etz)_6](BF_4)_2$ Spin-Crossover System—Part One: High-Spin ⇌ Low-Spin Transition in Two Lattice Sites. *Chem. – Eur. J.* **1996**, *2*, 1427–1434.
(56) Bi, Y.-G.; Feng, Y.-A.; Li, Y.; Wu, B.-D.; Zhang, T.-L. Synthesis, structure, and thermal decomposition of two copper coordination compounds [Cu(DAT) 2 (PA) 2] and [Cu(DAT) 2 (HTNR) 2] with nitrogen rich 1,5-diaminotetrazole (DAT). *J. Coord. Chem.* **2015**, *68*, 181–194.
(57) Szimhardt, N.; Wurzenberger, M. H. H.; Klapötke, T. M.; Lechner, J. T.; Reichherzer, H.; Unger, C. C.; Stierstorfer, J. Highly functional energetic complexes: stability tuning through coordination diversity of isomeric propyl-linked ditetrazoles. *J. Mater. Chem. A* **2018**, *6*, 6565–6577.
(58) DOD *Military Standard 1751A (MIL-STD-1751A): safety and performance tests for the qualification of explosives (high explosives, propellants, and pyrotechnics);* method 1016, Dec 11, 2001.
(59) Joas, M. B. *Investigations Concerning the Laser Ignition of Energetic Coordination Compounds* Dissertation, Ludwig-Maximilians-Universität, 2014.
(60) NATO *Standardization Agreement (STANAG): explosives, friction sensitivity tests;* no. 4487, 2nd ed., Oct 29, 2009.
(61) UN *Manual of Tests and Criteria;* 7th ed.; United Nations Publication: New York and Geneva, 2019. ISBN: 978–92–1-130394-0; section 13.5.1 Test 3 (b) (i) BAM friction apparatus.

https://doi.org/10.1021/acs.inorgchem.2c03624
Inorg. Chem. XXXX, XXX, XXX–XXX

(62) WIWEB *Standardarbeitsanweisung 4−5.1.03: Ermittlung der Explosionsgefährlichkeit oder der Reibeempfindlichkeit mit dem Reibeapparat,* Nov 8, 2002.
(63) NATO *Standardization Agreement (STANAG): explosives, impact sensitivity tests;* no. 4489, 1st ed., Sep 17, 1999.
(64) UN *Manual of Tests and Criteria*; 7th ed.; United Nations Publication: New York and Geneva, 2019. ISBN: 978−92−1-130394-0; section 13.4.2 Test 3 (a) (ii) BAM Fallhammer.
(65) WIWEB *Standardarbeitsanweisung 4−5.1.02: Ermittlung der Explosionsgefährlichkeit, hier der Schlagempfindlichkeit mit dem Fallhammer,* Nov 8, 2002.
(66) NATO *Standardization Agreement (STANAG): explosives, electrostatic discharge sensitivity tests;* no. 4490, 1st ed., Feb 19, 2001.
(67) UN *Manual of Tests and Criteria*; 7th ed.; United Nations Publication: New York and Geneva, 2019. ISBN: 978−92−1-130394-0; Impact: insensitive > 40 J, less sensitive ≥ 35 J, sensitive ≥ 4 J, very sensitive ≤ 3 J; Friction: insensitive > 360 N, less sensitive = 360 N, sensitive < 360 N and > 80 N, very sensitive ≤ 80 N, extremely sensitive ≤ 10 N.
(68) Wurzenberger, M. H. H.; Gruhne, M. S.; Lommel, M.; Stierstorfer, J. 1-Amino-5-methyltetrazole in Energetic 3 d Transition Metal Complexes − Ligand Design for Future Primary Explosives. *Propellants, Explos., Pyrotech.* **2021**, *46*, 207−213.
(69) Reynolds, J. G.; Hsu, P. C.; Hust, G. A.; Strout, S. A.; Springer, H. K. Hot Spot Formation in Mock Materials in Impact Sensitivity Testing by Drop Hammer. *Propellants, Explos., Pyrotech.* **2017**, *42*, 1303−1308.
(70) Gruhne, M. S.; Lommel, M.; Wurzenberger, M. H. H.; Szimhardt, N.; Klapotke, T. M.; Stierstorfer, J. OZM Ball Drop Impact Tester (BIT-132) vs. BAM Standard Method-a Comparative Investigation. *Propellants, Explos., Pyrotech.* **2020**, *45*, 147−153.
(71) Sućeska, M. *EXPLO5 V6.05.04 program*; Brodarski Institute: Zagreb, Croatia, 2014.
(72) Fendt, T.; Fischer, N.; Klapötke, T. M.; Stierstorfer, J. *N*-rich Salts of 2-Methyl-5-nitraminotetrazole: Secondary Explosives with Low Sensitivities. *Inorg. Chem.* **2011**, *50*, 1447−1458.
(73) Myers, T. W.; Bjorgaard, J. A.; Brown, K. E.; Chavez, D. E.; Hanson, S. K.; Scharff, R. J.; Tretiak, S.; Veauthier, J. M. Energetic Chromophores: Low-Energy Laser Initiation in Explosive Fe(II) Tetrazine Complexes. *J. Am. Chem. Soc.* **2016**, *138*, 4685−4692.
(74) Myers, T. W.; Brown, K. E.; Chavez, D. E.; Scharff, R. J.; Veauthier, J. M. Laser Initiation of Fe(II) Complexes of 4-Nitropyrazolyl Substituted Tetrazine Ligands. *Inorg. Chem.* **2017**, *56*, 2297−2303.
(75) Ilyushin, M. A.; Kotomin, A. A.; Dushenok, S. A. Energy-Saturated Metal Complexes. *Russ. J. Phys. Chem. B* **2019**, *13*, 119−138.
(76) Gruhne, M. S.; Wurzenberger, M. H. H.; Lommel, M.; Stierstorfer, J. A Smart Access to the Dinitramide Anion - The Use of Dinitraminic Acid for the Preparation of Nitrogen-Rich Energetic Copper(II) Complexes. *Chem. − Eur. J.* **2021**, *27*, 9112−9123.

https://doi.org/10.1021/acs.inorgchem.2c03624
Inorg. Chem. XXXX, XXX, XXX−XXX

Curriculum Vitae



DR. JÖRG STIERSTORFER

Akademischer Oberrat & Habilitant

Geburtsdatum	Adresse	Telefon	Email
29.11.1979	Taubenweg 16, 82237 Wörthsee	0170 4708191	jstch@cup.uni-muenchen.de

ÜBER MICH

In meiner Funktion als akademischer Oberrat (verbeamtet auf Lebenszeit) am Department Chemie der LMU München strebe ich eine Habilitation an. Mit der damit verbundenen Lehrbefähigung möchte ich den Fachbereich der Anorganischen Chemie – sowohl in der Lehre als auch in der Forschung – qualifiziert unterstützen.
Als geborener Münchner mit 2 Kindern (2&4 Jahre), verheiratet mit einer Patentprüferin (RDir) am DPMA, möchte ich auch im Anschluß an die Habilitation der LMU München treu bleiben.

AUSBILDUNG

(2000 – 2005)

Dipl.-Chemiker

Chemiestudium an der LMU München
Diplomarbeit: Chemistry of Bistetrazolylamine
Abschluss: Dipl-Chemiker (Note 1.2)

(1990 – 1999)

Abitur

Christoph-Probst Gymnasium Gilching

BERUFSERFAHRUNG

(2010 – heute)

Akademischer Oberrat

in der Arbeitsgruppe von Prof. Dr. T. M. Klapötke am Department Chemie der LMU München

(2018 – heute)

Geschäftsführender Gesellschafter

EMTO (Energetic Materials Technology) GmbH

(Okt – Dez 2009)

Postdoktorand

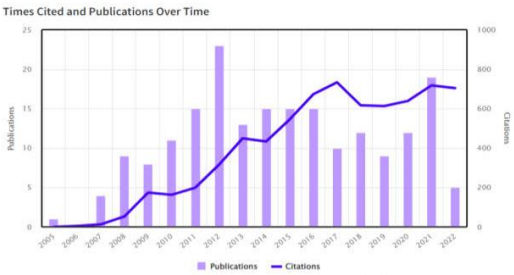
University of Maryland (USA), Installation eines Explosivstofflabors und Ausbildung von Studenten

PUBLIKATIONEN

Publikationen: 204

Patente: 7

ResearcherID: B-5261-2015



Gesamtzitierungen: 7085
H-Index: 45
Verified Reviews: 49
orcid.org/0000-0002-2105-1275

AUSGEWÄHLTE PUBLIKATIONEN

M. Benz, T. M. Klapötke, J. Stierstorfer, M. Voggenreiter, 2,2'-Azobis-5-Azidotetrazole (C_2N_{16}), *J. Am. Chem. Soc.* **2022**, 144, 6143–6147. https://pubs.acs.org/doi/10.1021/jacs.2c00995

D. Fischer, T. M. Klapötke, J. Stierstorfer, Tetranitratoethane, *Chem. Commun.* **2016**, *52*, 916–918. https://doi.org/10.1039/C5CC09010E

D. Fischer, T. M. Klapötke, J. Stierstorfer, 1,5-Dinitraminotetrazole, *Angew. Chem. Int. Ed.* **2015**, *54*, 10299–10302. https://doi.org/10.1002/ange.201502919

D. Fischer, T. M. Klapötke, J. Stierstorfer, Potassium 1,1'-Dinitramino-5,5'-bistetrazolate: A Primary Explosive with Fast Detonation and High Initiation Power, *Angew. Chem. Int. Ed.* **2014**, *53*, 8172–8175. https://doi.org/10.1002/anie.201404790

T. M. Klapötke, J. Stierstorfer, et al. Pushing the limits of energetic materials – the synthesis and characterization of dihydroxylammonium 5,5'-bistetrazole-1,1'-diolate, *J. Mater. Chem.* **2012**, **22**, 20418–20422. https://doi.org/10.1039/C2JM33646D

(2006 – 2009)

Doktorand

Wissenschaftlicher Mitarbeiter an der LMU München der AG von Prof. Dr. T. M. Klapötke,
Abschluss: Dr. rer. nat (summa cum laude, 0.57)

(2000&2002)

Praktika

Praktikum (2000) und Werkstudent (2002) bei der 3M Espe AG, R&D, chemische Analytik

EIGENSTÄNDIGE PUBLIKATIONEN: 34

u.a.

M. S. Gruhne, M. H. H. Wurzenberger, M. Lommel, J. Stierstorfer, A Smart Access to the Dinitramide Anion – The Use of Dinitraminic Acid for the Preparation of Energetic Coordination Compounds, *Chem. Europ. J.* **2021**, *27*, 9112–9123. https://doi.org/10.1002/chem.202100747

M. H. H. Wurzenberger, M. Lommel, M. S. Gruhne, N. Szimhardt, J. Stierstorfer, Refinement of Copper(II) Azide with 1-Alkyl-5H-tetrazoles: Adaptable Energetic Complexes, *Angew. Chem. Int. Ed.* **2020**, *59*, 12367–12370 https://doi.org/10.1002/anie.202002823.

M. H. H. Wurzenberger, N. Szimhardt, J. Stierstorfer, Copper(II) Chlorate Complexes – the Renaissance of a Forgotten and Misjudged Energetic Anion, *J. Am. Chem. Soc.* **2018**, *140*, 3206–3209. https://doi.org/10.1021/jacs.7b13230

AUSZEICHNUNGEN

Römer Preis der LMU München (Post-Doc), **2011**.

Römer Preis der LMU München (Promotion), **2007**.

Awards for best oral presentations, 11th and 12th NTREM Conference in Pardubice, Czech Republic **2008** and **2009**.

Awards for best and excellent poster presentation, 9th and 10th NTREM Conference in Pardubice, Czech Republic, **2006** and **2007**.

EHRENAMT

Münchener Chemische Gesellschaft

Schatzmeister (2016-2019), Kassenprüfer (2011-2015)

Sportclub Weßling

Abteilungs- und Übungsleiter Active(2012 -) & Triathlon (2005-2011), Schriftführer Vorstand (2011-2015)

INTERESSEN

Berg- und Wassersport, Musik, Garten

Wörthsee, 12.04.2022



Dr. Jörg Stierstorfer

Bibliography

PUBLICATIONS (PEER-REVIEWED)

1. M. Hiskey, A. Hammerl, G. Holl, T. M. Klapötke, K. Polborn, J. Stierstorfer, J. J. Weigand, Azidoformamidinium and Guanidinium 5,5'-Azotetrazolate Salts, *Chem. Mater.* **2005**, *17*, 3784–3793. https://doi.org/10.1021/cm050684f

2. V. Ernst, T. M. Klapötke, J. Stierstorfer, Alkali Salts of 5-Aminotetrazole - Structures and Properties, *Z. Anorg. Allg. Chem.* **2007**, *633*, 879–887. https://doi.org/10.1002/zaac.200700013

3. G. Geisberger, T. M. Klapötke, J. Stierstorfer, Copper Bis(1-methyl-5-nitriminotetrazolate): A Promising New Primary Explosive, *Europ. J. Inorg. Chem.* **2007**, *30*, 4743–4750. https://doi.org/10.1002/ejic.200700395

4. T. M. Klapötke, J. Stierstorfer, Nitration Products of 5-Amino-1*H*-tetrazole and Methyl-5-amino-1*H*-tetrazoles – Structures and Properties of Promising Energetic Materials, *Helv. Chim. Acta* **2007**, *90*, 2132–2150. https://doi.org/10.1002/hlca.200790220

5. T. M. Klapötke, H. Radies, J. Stierstorfer, Alkali Salts of 1-Methyl-5-nitriminotetrazole – Structures and Properties, *Z. Naturforschung* **2007**, *62b*, 1343–1352. https://doi.org/10.1515/znb-2007-1101

6. T. M. Klapötke, H. A. Laub, J. Stierstorfer, Synthesis and Characterization of a New Class of Energetic Compounds – Ammonium Nitriminotetrazolates, *Propellants Explos. Pyrotech.* **2009**, *33*, 421–430. https://doi.org/10.1002/prep.200700226

7. T. M. Klapötke, J. Stierstorfer, Synthesis and Characterization of the Energetic Compounds Aminoguanidinium-, Triaminoguanidinium and Azidoformamidinium Perchlorate, *Centr. Europ. J. Energ. Mat.* **2008**, *5*, 13–30. http://wydawnictwa.ipo.waw.pl/cejem/1-2008/Klapotke.pdf

8. R. D. Chapman, A. Hammerl, T. M. Klapötke, J. Stierstorfer, 5-Azido-1*H*-tetrazole – Improved Synthesis, Crystal Structure and Sensitivity Data, *Z. Anorg. Allg. Chem.* **2008**, *634*, 1051–1057. https://doi.org/10.1002/zaac.200800003

9. T. M. Klapötke, J. Stierstorfer, Triaminoguanidinium dinitramide - calculations, synthesis and characterization of a promising energetic compound, *Phys. Chem. Chem. Phys.* **2008**, *10*, 4340–4346. https://doi.org/10.1039/B804504F

10. T. M. Klapötke, J. Stierstorfer, The New Energetic Compounds 1,5-Diaminotetrazolium and 5-Amino-1-methyltetrazolium Dinitramide – Synthesis, Characterization and Testing, *Eur. J. Inorg. Chem.* **2008**, *26*, 4055–4062.

11. T. M. Klapötke, J. Stierstorfer, A. U. Wallek, Nitrogen-Rich Salts of 1-Methyl-5-nitrimino-tetrazolate: An Auspicious Class of Thermally Stable Energetic Materials, *Chem. Mater.* **2008**, *20*, 4519–4530. https://doi.org/10.1002/ejic.200800261

12. T. M. Klapötke, M. Stein, J. Stierstorfer, Salts of 1*H*-Tetrazole - Synthesis, Characterization and Properties, **2008**, *634*, 1711–1723. https://doi.org/10.1002/zaac.200800139

13. T. M. Klapötke, P. Mayer, J. Stierstorfer, J. J. Weigand, Bistetrazolylamines - synthesis and characterization, *J. Mat. Chem.* **2008**, *18*, 5248–5258. https://doi.org/10.1039/B811273H

14. T. M. Klapötke, J. Stierstorfer, Azidoformamidinium and 5-Aminotetrazolium Dinitramide – Two Highly Energetic Isomers with a Balanced Oxygen Content, *Dalton Transactions*, **2008**, *4*, 643–653. https://doi.org/10.1039/B811767E

15. T. M. Klapötke, C. M. Sabaté, J. Stierstorfer, Hydrogen-bonding Stabilization in Energetic Perchlorate Salts: 5-Amino-1*H*-tetrazolium Perchlorate and its Adduct with 5-Amino-1*H*-tetrazole, *Z. Anorg. Allg. Chem.* **2008**, *634*, 1867–1874. https://doi.org/10.1002/zaac.200800228

16. T. M. Klapötke, J. Stierstorfer, K. R. Tarantik, I. Thoma, Strontium Nitriminotetrazolates - Suitable Colorants in Smokeless Pyrotechnic Compositions, *Z. Anorg. Allg. Chem.* **2008**, *634*, 2777–2784. https://doi.org/10.1002/zaac.200800171

17. N. Fischer, T. M. Klapötke, S. Scheutzow, J. Stierstorfer, Hydrazinium 5-aminotetrazolate: An insensitive energetic material containing 83.72 % nitrogen, *Centr. Europ. J. Energ. Mater.* **2008**, *5*, 3–18. http://wydawnictwa.ipo.waw.pl/cejem/Number-3-4-2008/Klapotke.pdf

18. T. M. Klapötke, C. M. Sabaté, J. Stierstorfer, Neutral 5-nitrotetrazoles: easy initiation with low pollution, *New J. Chem.* **2009**, *33*, 136–147. https://doi.org/10.1039/B812529E

19. T. M. Klapötke, N. Minar, J. Stierstorfer, Investigations of *bis*(Methyl-tetrazolyl)triazenes as Nitrogen-Rich Ingredients in Solid Propellant Charges: Synthesis, Characterization and Properties, *Polyhedron*, **2009**, *28*, 13–26. https://doi.org/10.1016/j.poly.2008.09.015

20. T. M. Klapötke, J. Stierstorfer, B. Weber, New energetic materials: Synthesis and characterization of copper 5-nitriminotetrazolates, *Inorg. Chim. Acta* **2009**, *362*, 2311–2320. https://doi.org/10.1016/j.ica.2008.10.014

21. T. M. Klapötke, J. Stierstorfer, K. R. Tarantik, Pyrotechnically Relevant Salts of 1-(2-Chloroethyl)-5-nitriminotetrazole – Synthesis and Coloring Properties, *J. Pyrotech.* **2009**, *28*, 61–77. https://doi.org/10.1016/j.ica.2008.10.014

22. T. M. Klapötke, P. Mayer, J. Stierstorfer, Crystal Structures of Mono-, Di- and Triamino-guanidinium Sulfate as well as Azidoformamidinium Sulfate: Important Precursors for Syntheses of Nitrogen Rich Ionic Compounds. *Phosphorus, Sulfur Silicon Relat. Elem.* **2009**, *184*, 2393–2407. https://doi.org/10.1080/10426500802479877

23. T. M. Klapötke, J. Stierstorfer, The CN_7^--Anion, *J. Am. Chem. Soc.* **2009**, *131*, 1122–1134. https://doi.org/10.1021/ja8077522

24. T. M. Klapötke, J. Stierstorfer, K. Tarantik, New Energetic Materials: Functionalized 1-Ethyl-5-aminotetrazoles and 1-Ethyl-5-nitriminotetrazoles, *Chem. - Europ. J.* **2009**, *15*, 5775–5792. https://doi.org/10.1002/chem.200802203

25. N. Fischer, T. M. Klapötke, J. Stierstorfer, New Nitriminotetrazoles - Synthesis, Structures and Characterization, *Z. Anorg. Allg. Chem.* **2009**, *635*, 271–281. https://doi.org/10.1002/zaac.200800430

26. N. Fischer, K. Karaghiosoff, T. M. Klapötke, J. Stierstorfer, New Energetic Materials feat. Tetrazoles and Nitramines - Synthesis, Characterization and Properties, *Z. Anorg. Allg. Chem.* **2010**, *636*, 735–749. https://doi.org/10.1002/zaac.200900521

27. N. Fischer, T. M. Klapötke, J. Stierstorfer, Calcium 5-Nitriminotetrazolate – A new green replacement for lead azide in priming charges, *J. Energ. Mater.* **2011**, *29*, 61–74.

28. R. Damavarapu, T. M. Klapötke, J. Stierstorfer, K. R. Tarantik, Barium Salts of Tetrazole Derivatives – Synthesis and Characterization, *Propellants Explos. Pyrotech.* **2010**, *35*, 395–406. https://doi.org/10.1002/prep.200900058

29. G. Chen, T. M. Klapötke, A. Nagori, H. Radies J. Stierstorfer, K. R. Tarantik, Coloring Properties of Various High-Nitrogen Compounds in Pyrotechnic Compositions, *Propellants Explos. Pyrotech.* **2010**, *35*, 213–219. https://doi.org/10.1002/prep.201010018

30. T. Altenburg, T. M. Klapötke, A. Penger, J. Stierstorfer, Two Outstanding Explosives Based On 1,2-Dinitroguanidine: Ammonium- dinitroguanidine and 1,7-Diamino-1,7-dinitrimino-2,4,6-trinitro-2,4,6-triazaheptane, *Z. Anorg. Allg. Chem*. **2010**, *636*, 463–471. https://doi.org/10.1002/zaac.200900560

31. T. M. Klapötke, D. G. Piercey, J. Stierstorfer, The Facile Synthesis and Energetic Properties of an Energetic Furoxan Lacking Traditional 'Explosophore' Moieties: (E,E)-3,4-bis(oximomethyl)furoxan (DPX1), *Propellants, Explos. Pyrotech.* **2011**, *36*, 160–167. https://doi.org/10.1002/prep.201000057

32. N. Fischer, T. M. Klapötke, D. Piercey, S. Scheutzow, J. Stierstorfer, Diaminouronium Nitriminotetrazolates – Thermally Stable Explosives, *Z. Anorg. Allg. Chem.* **2010**, *636*, 2357–2363. https://doi.org/10.1002/zaac.201000231

33. T. M. Klapötke, F. A. Martin, N. T. Mayr, J. Stierstorfer, Synthesis and Characterization of 3,5-Diamino-1,2,4-triazolium Dinitramide, *Z. Anorg. Allg. Chem.* **2010**, *636*, 2555–2564. https://doi.org/10.1002/zaac.201000298

34. M. Göbel, K. Karaghiosoff, T. M. Klapötke, D. G. Piercey, J. Stierstorfer, Nitrotetrazolate-2*N*-oxides and the Strategy of *N*-Oxide Introduction, *J. Am. Chem. Soc.* **2010**, *132*, 17216–17226. https://doi.org/10.1021/ja106892a

35. D. Fischer, T. M. Klapötke, D. G. Piercey, J. Stierstorfer, Copper salts of halo tetrazoles: laser-ignitable primary explosives, *J. Energ. Mater.* **2011**, *30*, 40–54. https://doi.org/10.1080/07370652.2010.539998

36. T. Fendt, N. Fischer, T. M. Klapötke, J. Stierstorfer, N-rich Salts of 2-Methyl-5-nitraminotetrazole – Secondary Explosives with Low Sensitivities, *Inorg. Chem.* **2011**, *50*, 1447–1458. https://doi.org/10.1021/ic1019923

37. D. Fischer, T. M. Klapötke, J. Stierstorfer, Synthesis and Characterization of Guanidinium Difluoroiodate,$[C(NH_2)_3]^+[IF_2O_2]^-$ and its Evaluation as an Ingredient in Agent Defeat Weapons, *Z. Anorg. Allg. Chem.* **2011**, *637*, 660–665. https://doi.org/10.1002/zaac.201100052

38. N. Fischer, T. M. Klapötke, J. Stierstorfer, Explosives based on Diaminourea, *Propellants Explos. Pyrotech.* **2011**, *36*, 225–232.

39. T. M. Klapötke, F. A. Martin, J. Stierstorfer, C_2N_{14} – ein energetisches und höchst empfindliches binäres Azidotetrazol. *Angew. Chem.* **2011**, *123*, 4313-4316; C_2N_{14} - A new energetic and highly sensitive binary azidotetrazole *Angew. Chem. Int. Ed.* **2011**, *50*, 4227–4229. https://doi.org/10.1002/prep.201100001

40. N. Fischer, T.M. Klapötke, J. Stierstorfer, C. Wiedemann, 1-Nitratoethyl-5-nitriminotetrazole Derivatives – Shaping Future High Explosives, *Polyhedron* **2011**, *30*, 2374–2386. https://doi.org/10.1016/j.poly.2011.05.042

41. T. M. Klapötke, J. Stierstorfer, H. D. Brooke Jenkins, R. van Eldik, M. Schmeisser, Calculation of Some Thermodynamic Properties and Detonation Parameters of 1-Ethyl-3-Methyl-H-Imidazolium Perchlorate, [Emim][ClO_4], on the Basis of CBS-4M and CHEETAH Computations Supplemented by VBT Estimates *Z. Anorg. Allg. Chem.* **2011**, 637, 1308–1313. https://doi.org/10.1002/zaac.201100144

42. M. Schmeisser, P. Keil, J. Stierstorfer, A. König, T. M. Klapötke, R. van Eldik, An Ionic Liquid Designed for Coordination Chemistry Revisited: Synthetic Routes and Safety Tests for 1-Ethyl-3-methylimidazolium Perchlorate ([emim][ClO_4]), *Eur. J. Inorg. Chem.* **2011**, 4862–4868. https://doi.org/10.1002/ejic.201100529

43. D. Fischer, T. M. Klapötke, J. Stierstorfer, Salts of Tetrazolone – Synthesis and Properties of Insensitive Energetic Materials, *Propellants Explos. Pyrotech.* **2012**, *37*, 156–166. https://doi.org/10.1002/prep.201100108

44. N. Fischer, T. M. Klapötke, J. Stierstorfer, Hydrazinium 5-nitriminotetrazolates, *Z. Anorg. Allg. Chem.* **2011**, *637*, 1273–1276. https://doi.org/10.1002/zaac.201100149

45. N. Fischer, T. M. Klapötke, J. Stierstorfer, Energetic Nitrogen-rich Salts of 1-Hydroxyethyl Substituted 5-Nitriminotetrazole, *Eur. J. Inorg, Chem.* **2011**, *28*, 4471–4480. https://doi.org/10.1021/cm8004166

46. N. Fischer, T. M. Klapötke, K. Peters, M. Rusan, J. Stierstorfer, Alkaline earth metal salts of 5,5'-Bistetrazole – From academical interest to practical application, *Z. Anorg. Allg. Chem.* **2011**, *637*, 1784–178. https://doi.org/10.1002/zaac.201100263

47. T. M. Klapötke, D. Piercey, J. Stierstorfer, Taming of CN_7^- anion, *Chem. Eur. J.* **2011**, *17*, 5775–5792. https://doi.org/10.1002/chem.201102064

48. C. M. Sabaté, E. Jeanneau, J. Stierstorfer, Synthesis and Comprehensive Characterization of Hydrated Alkaline Earth Metal Salts of 5-Amino-1*H*-tetrazole, *Z. Anorg. Allg. Chem.* **2011** *637*, 1490–1501. https://doi.org/10.1002/zaac.201100193

49. T. M. Klapötke, F. A. Martin, J. Stierstorfer, N-bound primary Nitramines based on 1,5-Diaminotetrazole, *Chem. Eur.* J. **2012**, *18*, 1487–1501. https://doi.org/10.1002/chem.201102142

50. T. M. Klapötke, B. Krumm, F. A. Martin, J. Stierstorfer, New azidotetrazoles – structurally interesting and extremly sensitive, *Chem. Asian J.* **2012**, *7*, 214–224. https://doi.org/10.1002/asia.201100632

51. T. M. Klapötke, A. Nordheider, J. Stierstorfer, Synthesis and Reactivity of Unexpected Highly Sensitive 3-Diazonio-5-nitrimino-1,2,4-triazole, *New J. Chem.* **2012**, *36*, 1463–1468. https://doi.org/10.1039/C2NJ40044H

52. N. Fischer, E. D. Goddard-Borger, R. Greiner, T. M. Klapötke, J. Stierstorfer, Salts of Imidazole-1-sulfonyl azide – Insensitive and Efficient Diazo Transfer Reagents, *J. Org. Chem.* **2012**, *77*, 1760–1764. https://doi.org/10.1021/jo202264r

53. N. Fischer, T. M. Klapötke, D. G. Piercey, J. Stierstorfer, Hxdroxylammonium 5-nitriminotetrazolates, *Z. Anorg. Allg. Chem.* **2012**, *638*, 302–310. https://doi.org/10.1002/zaac.201100479

54. M. Härtel, T. M. Klapötke, D. G. Piercey, J. Stierstorfer, Synthesis and Characterization of Alkaline and Alkaline Earth Salts of the Nitrotetrazolate-2*N*-oxide Anion, *Z. Anorg. Allg. Chem.* **2012**, *638*, ,2008–2014. https://doi.org/10.1002/zaac.201200049

55. G. Laus, V. Kahlenberg, K. Wurst, H. Schottenberger, N. Fischer, J. Stierstorfer, T. M. Klapötke, Synthesis and Crystal Structures of New 5,5'-Azotetrazolates, *Crystals* **2012**, *2*, 127–136. https://doi.org/10.3390/cryst2010127

56. N. Fischer, D. Izsàk,T. M. Klapötke, S. Rappenglück, J. Stierstorfer, Nitrogen-Rich 5,5'-Bistetrazolates and their Potential Use in Propellant Systems: A Comprehensive Study, *Chem. Europ. J.* **2012**, *18*, 4051–4062. https://doi.org/10.1002/chem.201103737

57. T. M. Klapötke, D. G. Piercey, J. Stierstorfer, Amination of Energetic Anions: High-Performing Energetic Materials, *Dalton Trans.* **2012**, ***41***, 9451–9459. https://doi.org/10.1039/C2DT30684K

58. N. Fischer, T. M. Klapötke, S. Rappenglück, J. Stierstorfer, The Reactivity of 5-Cyano-tetrazole towards Water and Hydroxylamine, *ChemPlusChem.* **2012**, *77*, 877–888. https://doi.org/10.1002/cplu.201200136

59. D. Fischer, N. Fischer, T. M. Klapötke, D. G. Piercey, J. Stierstorfer, Pushing the Limits of Energetic Materials - The synthesis and characterization of hydroxylammonium bistetrazolate-N-oxide, *J. Mater. Chem.* **2012**, ***22***, 20418–20422. https://doi.org/10.1039/C2JM33646D

60. N. Fischer, T. M. Klapötke, K. Lux, F. A. Martin, J. Stierstorfer, Inorganic Amino-Nitro-Guanidinium Derivatives, *Crystals* **2012**, *2*, 675–689. https://doi.org/10.3390/cryst2020675

61. T. M. Klapötke, A. Preimesser, J. Stierstorfer, Energetic derivatives of 4,4',5,5'-Tetranitro-2,2'-bisimidazole, *Z. Anorg. Allg. Chem.* **2012**, *638*, 1278–1286. https://doi.org/10.1002/zaac.201200188

62. M. Joas, T.M. Klapötke, J. Stierstorfer, Preparation and Crystal Structure of Diaqua(μ-5,5'-bistetrazolato-κ^4*N*^{1},*N*^{2},*N*^{5},*N*^{6})copper(II), *Crystals*, **2012**, *2*, 958–966. https://doi.org/10.3390/cryst2030958

63. N. Fischer, K. Hüll, T. M. Klapötke, J. Stierstorfer, G. Laus, M. Hummel, C. Froschauer, K. Wurst, H. Schottenberger, 5,5'--Azoxytetrazolates – a new nitrogen-rich dianion and its comparison to 5,5′-azotetrazolate, *Dalton Trans.*, **2012**, ***41*, 11201–11211.** https://doi.org/10.1039/c2dt31217d.

64. N. Fischer, K. Hüll, T. M. Klapötke, J. Stierstorfer, Synthesis and Characterization of the New Heterocycle 5-(4-Amino-1,2,4-triazol-3-on-5´-yl)-1H-tetrazole and Some Ionic Nitrogen-Rich Derivatives, *J. Heterocycl. Chem.* **2014**, *51*, 85–95. https://doi.org/10.1002/jhet.1877

65. T. M. Klapötke, D. G. Piercey, F. Rohrbacher, J. Stierstorfer, Synthesis and Characterization of Energetic Salts of the ($C_4N_{12}^{2-}$) Dianion, *Z. Anorg. Allg. Chem.* **2012**, *638*, 2235–2242. https://doi.org/10.1002/zaac.201200363

66. J. Stierstorfer, Thomas M. Klapötke, Davin G. Piercey, The 1,4,5-Triaminotetrazolium Cation (CN7H6+): A Highly Nitrogen-Rich Moiety, *Eur. J. Inorg. Chem.* **2012**, *34*, 5694–5700. https://doi.org/10.1002/ejic.201200964

67. V. Verma, K. Singh, T. M. Klapötke, J. Stierstorfer, B. Narasimhan, A. Khurshid Qazi, A. Hamid, S. Jaglan, Synthesis, antimicrobial and cytotoxicity study of 1,3-disubstituted-1H-naphtho[1,2-e][1,3]oxazines, *Eur. J. Med. Chem.* **2012**, *56*, 195–202. https://doi.org/10.1016/j.ejmech.2012.08.018

68. N. Fischer, T. M. Klapötke, J. Stierstorfer, 1-Amino-3-nitroguanidine (ANQ) in High-performance Ionic Energetic Materials, *Z. Naturforsch.* **2012**, *67b*, 573–588. https://doi.org/10.5560/znb.2012-0066

69. T. M. Klapötke, D. G. Piercey, J. Stierstorfer, M. Weyrauther, The Synthesis and Energetic Properties of 5,7-Dinitrobenzo-1,2,3,4-tetrazine-1,3-dioxide (DNBTDO), *Propellants Explos. Pyrotech.* **2012**, *37*, 527–535. https://doi.org/10.1002/prep.201100151

70. J. Stierstorfer, Thomas M. Klapötke, Davin G. Piercey**,** The 1,3-Diamino-1,2,3-triazolium Cation: A Highly Energetic Moiety, *Eur. J. Inorg. Chem.* **2013**, 1509–1517. https://doi.org/10.1002/ejic.201201237

71. D. Fischer, N. Fischer, T. M. Klapötke, D. G. Piercey, J. Stierstorfer, Synthesis of 5-Aminotetrazole-1N-oxide and its Azo-Derivative – A Key Step in the Development of New Energetic Materials, *Chem. Eur. J.* **2013**, *19*, 4602–4613. https://doi.org/10.1002/chem.201203493

72. F. Boneberg, A. Kirchner, T. M. Klapötke, D. G. Piercey, M. J. Poller, J. Stierstorfer, A Study of Cyanotetrazole Oxides and Derivatives thereof, *Chem. Asian J.* **2013**, *8*, 148–159. https://doi.org/10.1002/asia.201200903

73. N. Fischer, T. M. Klapötke, M. Reymann, J. Stierstorfer, Nitrogen-Rich Salts of 5,5'-Bis(1-hydroxytetrazole) – Energetic Materials Combining Low Sensitivities with High Thermal Stability, *Europ. J. Inorg. Chem.* **2013**, 2167–2180. https://doi.org/10.1002/ejic.201201192

74. N. Fischer, L. Gao T. M. Klapötke, J. Sierstorfer, Energetic Salts of 5,5´-Bis(tetrazole-2-oxide) in a Comparison to 5,5´-Bis(tetrazole-1-oxide) Derivatives, *Polyhedron*, **2013**, *51*, 201–210. https://doi.org/10.1016/j.poly.2012.12.015

75. N. Fischer, M. Joas, T. M. Klapötke, J. Stierstorfer, Transition metal complexes of 3-amino-1-nitroguanidine as laser ignitible primary explosives – structures and properties, *Inorg. Chem.* **2013**, *52*, 13791–13802. https://doi.org/10.1021/ic402038x

76. N. Fischer, T. M. Klapötke, S. Marchner, M. Rusan, S. Scheutzow, J. Stierstorfer, A Selection of Alkali and Alkaline Earth Metal Salts of 5,5´-Bis(1-hydroxytetrazole) in Pyrotechnic Compositions *Propellants, Explos. Pyrotech*. **2013**, *38*, 448–459. https://doi.org/10.1002/prep.201200177

77. T. M. Klapötke, D. G. Piercey, J. Stierstorfer, The 1,3-bis(nitroimide)-1,2,3-triazolate anion, the N-nitroimide moiety, and the strategy of alternating positive and negative charges in the design of energetic materials, *J. Am. Chem. Soc.* **2012**, *134*, 20827−20836. https://doi.org/10.1021/ja310384y

78. N. Fischer, M. Feller, T. M. Klapötke, M. Kowalewski, S. Scheutzow, J. Stierstorfer, Spectroscopic Investigations of High-Nitrogen Compounds for Near-Infrared Illuminants, *Propellants, Explos. Pyrotech.* **2014**, *39*, 166–172. https://doi.org/10.1002/prep.201300092

79. T. M. Klapötke, A. Preimesser, S. Schedlbauer, J. Stierstorfer, Highly Energetic Salts of 3,6-Bishydrazino-1,2,4,5-tetrazine, *Centr. Europ. J. Energ. Mater.* **2013**, *10*, 151–170. http://yadda.icm.edu.pl/yadda/element/bwmeta1.element.baztech-0233a38e-b608-468c-b102-449e85e93322/c/Klapotke_cejem_2013_2.PDF

80. T. M. Klapötke, A. Penger, C. Pflüger, J. Stierstorfer, M. Suceska, Advanced Open-Chain Nitramines as Energetic Materials: Heterocyclic-Substituted 1,3-Dichloro-2-nitrazapropane, *Eur. J. Inorg. Chem.* **2013**, 4667–4678. https://doi.org/10.1002/ejic.201300382

81. M. Joas, T.M. Klapötke, J. Stierstorfer, N. Szimhardt, Synthesis and Characterization of Various Photosensitive Copper(II) Complexes with 5-(1-Methylhydrazinyl)-1*H*-tetrazole as Ligand and Perchlorate, Nitrate, Dinitramide, and Chloride as Anions, *Chem. Eur. J.* **2013**, *19*, 9995–10003. https://doi.org/10.1002/chem.201300688

82. D. Izsak, T. M. Klapötke, R. Scharf, J. Stierstorfer, Energetic Materials Based on the 5-Azido-3-nitro-1,2,4-triazolate Anion, *Z. Anorg. Allg. Chem.* **2013**, *639*, 1746–1755. https://doi.org/10.1002/zaac.201300203

83. T. M. Klapötke, A. Preimesser, J. Stierstorfer, Thermally Stable 3,6-Disubstituted 1,2,4,5-Tetrazines, *Z. Naturforsch. b* **2013**, *68b*, 1310–1320. https://doi.org/10.5560/znb.2013-3237

84. D. Fischer, T. M. Klapötke, J. Stierstorfer, Oxalylhydrazinium Nitrate - Efficiency meets Performance, *J. Energ. Mat.*, **2014**, *32*, 37–49. https://doi.org/10.1080/07370652.2012.750697

85. D. Fischer, T. M. Klapötke, M. Reymann, P. C. Schmid, J. Stierstorfer, M. Suceska, Synthesis of 5-(1H-Tetrazolyl)-1-hydroxy-tetrazole and Energetically Relevant Nitrogen-Rich Ionic Derivatives, *Propellants, Explos. Pyrotech*. **2014**, *39*, 550–557. https://doi.org/10.1002/prep.201300152

86. T. M. Klapötke, A. Preimesser, J. Stierstorfer, Energetic Derivatives of 2-Nitrimino-5,6-dinitro-benzimidazole, *Propellants, Explos. Pyrotech*. **2015**, *40*, 60–66. https://doi.org/10.1002/prep.201400045

87. T. M. Klapötke, T. G. Müller, M. Rusan, J. Stierstorfer, Metal Salts of 4,5-Dinitro-1,3-imidazole as Colorants in Pyrotechnic Compositions, *Z. Anorg. Allg. Chem.* **2014**, *640*, 1347–1354. https://doi.org/10.1002/zaac.201400082

88. D. Fischer, T. M. Klapötke, M. Reymann, J. Stierstorfer, Dense Energetic Nitraminofurazanes, *Chem. Eur. J.* **2014**, *20*, 6401–6411. https://doi.org/10.1002/chem.201400362

89. a) D. Fischer, T. M. Klapötke, J. Stierstorfer, Potassium 1,1'-Dinitramino-5,5'-bistetrazolate: A Primary Explosive with Fast Detonation and High Initiation Power, *Angew. Chem. Int. Ed.* **2014**, *53*, 8172–8175. https://doi.org/10.1002/anie.201404790 b) a) D. Fischer, T. M. Klapötke, J. Stierstorfer, Dikalium-1,1'-dinitramino-5,5'-bistetrazolat – ein Primärsprengstoff mit schneller Detonation und hoher Initiierungsleistung, *Angew. Chem.* **2014**, *126*, 8311–8314. https://doi.org/10.1002/ange.201404790

90. J. Glück, T. M. Klapötke, M. Rusan, J. Stierstorfer, Green Colorants Based on Energetic Azole Borates, *Chem. Europ. J.* **2014**, *20*, 15947–15960. https://doi.org/10.1002/chem.201403451

91. T. M. Klapötke, M. Rusan, J. Stierstorfer, Green Pyrotechnic Formulations Based on Metal-Free and Nitrogen-Rich Tetrazolylborate Salts, *J. Pyrotech.* **2014**, *33*, 24–38. http://www.jpyro.co.uk/?p=1698

92. T. M. Klapötke, M. Q. Kurz, R. Scharf , P. C. Schmid, J. Stierstorfer, M. Sucesca, 5-(1*H*-Tetrazolyl)-2-Hydroxy-Tetrazole: A Selective 2*N*-Monoxidation of Bis(1*H*-Tetrazole) *ChemPlusChem* 2**015**, *80*, 97–106. https://doi.org/10.1002/cplu.201402124

93. D. Chavez, T.M. Klapötke, D.Parrish, D. G. Piercey, J. Stierstorfer, The Synthesis and Energetic Properties of 3,4-Bis(2,2,2-trinitroethylamino)furazan (BTNEDAF), *Propellants Explos. Pyrotech.* **2014**, *39*, 641–648. https://doi.org/10.1002/prep.201300135

94. J. Evers, I. Gospodinov, M. Joas, T. M. Klapötke, and J. Stierstorfer, Cocrystallization of Photosensitive Energetic Copper(II) Perchlorate Complexes with the Nitrogen-rich Ligand 1,2-Di(1H-tetrazol-5-yl)ethane, *Inorg. Chem.* **2014**, *53*, 11749–11756. https://doi.org/10.1021/ic5020175

95. T. M. Klapötke, M. Q. Kurz, P. C. Schmid, J. Stierstorfer, Energetic Improvements by N-Oxidation: Insensitive Amino-Hydroximoyl-Tetrazole-2N-Oxides, *J. Energ. Mater.* **2015**, *33*, 191–201. https://doi.org/10.1080/07370652.2014.963743

96. D. Fischer, T. M. Klapötke, M. Reymann, J. Stierstorfer, M. B. R. Völkl, Energetic Alliance of Tetrazole-1-oxides and 1,2,5-Oxadiazoles, *New. J. Chem.* **2015**, *39*, 1619-1627. https://doi.org/10.1039/C4NJ01351D

97. D. G. Piercey, D. Chavez, S. B. Heimsch, C. Kirst, T. M. Klapötke, D. Parrish, J. Stierstorfer, An Energetic N-Oxide and N-Amino Heterocycle and its transformation to 1,2,3,4-Tetrazine-1-oxide, *Propellants Explos. Pyrotech.* **2015**, *40*, 491–497. https://doi.org/10.1002/prep.201400224

98. M. Joas, S. Kießling, T. M. Klapötke, P. C. Schmid, J. Stierstorfer, Energetic Complexes of 5-(4-Amino-1,2,4-triazol-3-on-5-yl)tetrazole and Ionic Derivatives of its 2*N*-Oxide, *Z. Anorg. Allg. Chem.* **2014**, *640*, 2759–2765. https://doi.org/10.1002/zaac.201400417

99. I. E. Drukenmüller, T. M. Klapötke*, Y. Morgenstern, M. Rusan, J. Stierstorfer, Metal Salts of Dinitro-, Trinitropyrazole, and Trinitroimidazole, *Z. Anorg. Allg. Chem.* **2014,** *640*, 2139–2148. https://doi.org/10.1002/zaac.201400233

100. D. Fischer, T. M. Klapötke, J. Stierstorfer, Synthesis and Characterization of Diaminobisfuroxane, *Eur. J. Inorg. Chem.* **2014**, 5808–5811. https://doi.org/10.1002/ejic.201402960

101. T. M. Klapötke, P. C. Schmid, J. Stierstorfer, Thermal stabilization of energetic materials by the aromatic nitrogen-rich 4,4′,5,5′-tetraamino-3,3′-bi-1,2,4-triazolium cation, *J. Mater. Chem. A*, **2015**, ***3***, 2658–2668. https://doi.org/10.1039/C4TA05964F

102. a) D. Fischer, T. M. Klapötke, J. Stierstorfer, 1,5-Dinitraminotetrazole, *Angew. Chem. Int. Ed.* **2015**, *54*, 10299–10302. https://doi.org/10.1002/anie.201502919; b) D. Fischer, T. M. Klapötke, J. Stierstorfer, 1,5-Dinitraminotetrazole, *Angew. Chem.* **2015**, *35*, 10438–10441. https://doi.org/10.1002/ange.201502919

103. T. M. Klapötke, P. C. Schmid, J. Stierstorfer, 3,6,7-Triamino-[1,2,4]triazolo[4,3-b][1,2,4]triazolium - a non-toxic, high performance energetic building block with excellent stabilities, *Chem. Europ. J.* **2015**, *21*, 9219–9228. https://doi.org/10.1002/chem.201500982

104. K. Hafner, T. M. Klapötke, P. C. Schmid, J. Stierstorfer, Synthesis and Characterization of the Asymmetric 1,2-Dihydroxy-5,5'-bitetrazole and Selected Nitrogen-Rich Derivatives, *Europ. J. Inorg. Chem.* **2015**, 2794–2803. https://doi.org/10.1002/ejic.201500338

105. T. M. Klapötke, A. Preimesser, J. Stierstorfer, Syntheses and Energetic Properties of 4-Diazo-2,6-dinitrophenol and 6-Diazo-3-hydroxy-2,4-dinitrophenol, *Europ. J. Org. Chem.* **2015**, 4311–4315. https://doi.org/10.1002/ejoc.201500465

106. N.-D. H. Gamage, B. Stiasny, J. Stierstorfer, P. D. Martin, T. M. Klapötke, C. H. Winter, Less sensitive oxygen-rich organic peroxides containing geminal hydroperoxy groups, *Chem. Commun*. **2015**, *51*, 13298–13300. https://doi.org/10.1039/C5CC05015D

107. T. M. Klapötke, B. Stiasny, J. Stierstorfer, C. H. Winter, Energetic Organic Peroxides - Synthesis and Characterization of 1,4-Dimethyl-2,3,5,6-tetraoxabicyclo[2.2.1]heptanes, *Europ. J. Org. Chem.* **2015**, *28*, 6237–6242. https://doi.org/10.1002/ejoc.201500919

108. N.-D. H. Gamage, B. Stiasny, J. Stierstorfer, P. D. Martin, T. M. Klapötke, C. H. Winter, Highly Energetic, Low Sensitivity Aromatic Peroxy Acids, *Chem. Eur. J.* **2016**, *22*, 2582–2585. (frontpicture). https://doi.org/10.1002/chem.201502989

109. T. M. Klapötke, M. Leroux, P. C. Schmid, J. Stierstorfer, Energetic Materials based on 5,5'-Diamino-4,4'-dinitramino-3,3'-bi(1,2,4-triazole), *Chem. Asian J.* **2016**, *11*, 844–851. https://doi.org/10.1002/asia.201500701

110. T. M. Klapötke, P. C. Schmid, J. Stierstorfer, Crystal Structures of Furazanes, *Crystals* **2015**, *5*, 418–432. https://doi.org/10.3390/cryst5040418

111. D. Fischer, T. M. Klapötke, J. Stierstorfer, 5-Nitriminotetrazole 1-Oxide: An Exciting Oxygen- and Nitrogen-Rich Heterocycle, *Europ. J. Inorg. Chem.* **2015**, 4628–4632. https://doi.org/10.1002/ejic.201500944

112. D. Fischer, T. M. Klapötke, J. Stierstorfer, N. Szimhardt, 1,1-Nitramino-5,5-bitetrazoles, *Chem. Eur. J.* **2016**, 22,4966–4970. https://doi.org/10.1002/chem.201600177

113. T. M. Klapötke, N. Mayr, J. Stierstorfer, M. Weyrauther, Maximum Compaction of Ionic Organic Explosives: Bis(hydroxylammonium) 5,5'-Dinitromethyl-3,3'-bis(1,2,4-oxadiazolate) and its Derivatives, *Chem. Eur. J.* **2014**, *20*, 1410–1417. https://doi.org/10.1002/chem.201303825

114. D. Fischer, T. M. Klapötke, J. Stierstorfer, Tetranitratoethane, *Chem. Commun.* **2016**, *52*, 916–918. https://doi.org/10.1039/C5CC09010E

115. D. Izsák, T. M. Klapötke, A. Preimesser, J. Stierstorfer, Synthesis and Initiation Capabilities of Energetic Diazodinitrophenols, *Z. Anorg. Allg. Chem.* **2016**, *642*, 48–55. https://doi.org/10.1002/zaac.201500703

116. Z. L. Chioato, T. M. Klapötke, F. Mieskes, J. Stierstorfer, M. Weyrauther, (Picrylamino)-1,2,4-triazole Derivatives – Thermally Stable Explosives, *Eur. J. Inorg. Chem.* **2016**, 956–962. https://doi.org/10.1002/ejic.201501435

117. T. M. Klapötke, F. Mieskes, J. Stierstorfer, M. Weyrauther, T. Witkowski, Synthesis and Investigation of 2,6-Bis(picrylamino)-3,5-dinitro-pyridine (PYX) and Its Salts, *Chem. Eur. J.* **2016**, *22*, 8619–8626. https://doi.org/10.1002/chem.201600769

118. T. M. Klapötke, P. C. Schmid, J. Stierstorfer, N. Szimhardt, Synthesis and Characterization of Tetrahedral Zinc(II) Complexes with 3, 6,7-Triamino-7H-[1, 2,4]triazolo[4, 3-b][1, 2,4]triazole as Nitrogen-Rich Ligand, *Z. Anorg. Allg. Chem.* 2016, *642*, 383–389. https://doi.org/10.1002/zaac.201600006

119. T. M. Klapötke, F. Mieskes, J. Stierstorfer, M. Weyrauther, Studies on Energetic Salts Based on (2,4,6-Trinitrophenyl)guanidine, *Propellants Explos. Pyrotech.* **2016**, *41*, 217–222. https://doi.org/10.1002/prep.201500338

120. N.-D. H. Gamage, B. Stiasny, E. G. Kratz, J. Stierstorfer, P. D. Martin, G. Andrés Cisneros, T. M. Klapötke, C. H. Winter, Energetic Materials Trends in 5- and 6-Membered Cyclic Peroxides Containing Hydroperoxy and Hydroxy Substituents, *Eur. J. Inorg. Chem.* **2016**, 5036–5043. https://doi.org/10.1002/ejic.201600767

121. T. M. Klapötke, T. Rotariu, B. Stiasny, J. Stierstorfer, S. Wiegmann, T. Zecheru, Azido(*tert*-butylperoxy)methyl Compounds – An Exceptional Class of Energetic Materials, *Eur. J. Org. Chem.* **2016**, 4382–4386. https://doi.org/10.1002/ejoc.201600717

122. T. M. Klapötke, A. Penger, C. Pflüger, J. Stierstorfer, Melt-cast materials: combining the advantages of highly nitrated azoles and open-chain nitramines, *New J. Chem.* **2016**, *40*, 6059–6069. https://doi.org/10.1039/C6NJ00202A

123. T. M. Klapötke, B. Stiasny, and J. Stierstorfer, Energetic Materials - Nitrated Phenyl Peroxy Anhydrides as Peroxide Based Explosives with Relatively High Densities and Thermal Stabilities, *ChemistrySelect* **2016**, *1*, 4057–4061. https://doi.org/10.1002/slct.201601114

124. T. M. Klapötke, B. Stiasny, J. Stierstorfer, Synthesis and Investigation of 1,3-Di(5-nitraminotetrazol-1-yl)-propan-2-ole and its Salts, *Z. Anorg. Allg. Chem.* **2017,** *643*, 228–234. https://doi.org/10.1002/zaac.201600389

125. D. Fischer, J. L. Gottfried, K. Karaghiosoff, T. M. Klapötke, J. Stierstorfer, T. Witkowski, Synthesis and Investigation of Advanced Energetic Materials Based on Bispyrazolylmethanes, *Angew. Chem. Int. Ed.* **2016**, 55, 16132–16135. https://doi.org/10.1002/ange.201609267

126. M. Born, M. A. C. Härtel, T. M. Klapötke, M. Mallmann, J. Stierstorfer, Investigation on the Sodium and Potassium Tetrasalts of 1,1,2,2-Tetranitraminoethane, *Z. Anorg. Allg. Chem.* **2016**, *642*, 1412–1418. https://doi.org/10.1002/zaac.201600339

127. T. Hermann, B. Krumm, T. M. Klapötke, J. Stierstorfer, The Reagent-depending Nitration of 1,3-Dihydroxyacetone Dimer, *Z. Anorg. Allg. Chem.* **2017**, *643*, 149–151. https://doi.org/10.1002/zaac.201600397

128. M. A. C. Härtel, T. M. Klapötke, J. Stierstorfer, L. Zehetner, Gas Phase Detectability by Vacuum Outlet GC/MS of Linear Nitrate Esters as Components in Improvised Explosive Devices, *Propellants Explos. Pyrotech.* **2019,** *44*, 484-492. https://doi.org/10.1002/prep.201800133

129. N. Szimhardt, M. F. Bölter, M. Born, T. M. Klapötke, J. Stierstorfer, Highly Energetic Metal Salts and Complexes of 1,1'-Dinitramino-5,5'-bitetrazole, *Dalton Transactions* **2017**, *46*, 5033–5040. https://doi.org/10.1039/C7DT00536A

130. M. A. C. Härtel, T. M. Klapötke, B. Stiasny, J. Stierstorfer, Gas-phase Concentration of Triacetone Triperoxide (TATP) and Diacetone Diperoxide (DADP), *Propellants Explos. Pyrotech.* **2017**, *42*, 623–634, https://doi.org/10.1002/prep.201700034

131. T. Hermann, B. Krumm, T. M. Klapötke, J. Stierstorfer, The Energetic 3-Trinitromethyl-5-nitramino-1H-1,2,4-triazole and Nitrogen-rich Salts, *New J. Chemistry* **2017**, *41*, 3068–3072, https://doi.org/10.1039/c7nj00695k

132. T. M. Klapötke, J. Stierstorfer, N. Szimhardt, Di(1H-tetrazolyl-5-yl)methane as Neutral Ligand in Energetic Transition Metal Complexes, *Inorg. Chem.* **2017,** 56, 7936–7947. https://doi.org/10.1021/acs.inorgchem.7b00432

133. G. Bikelytė, M. A. C. Härtel, J, Stierstorfer, T. M Klapötke, A. A Pimerzin, S. P. Verevkin, Benchmark properties of 2-, 3- and 4-nitrotoluene: evaluation of thermochemical data with complementary experimental

and computational methods, *J. Chem. Thermodynamics*. **2017**, *111*, 271–278; https://doi.org/10.1016/j.jct.2017.03.029

134. T. S. Hermann, K. Karaghiosoff, T. M. Klapötke, J. Stierstorfer, Synthesis and Characterization of 2,2'-Dinitramino-5,5'-bi(1-oxa-3,4-diazole) and Derivatives as Economic and Highly Dense Energetic Materials, *Chem. Eur. J.* **2017**, *23*, 12087-12091; https://doi.org/10.1002/chem.201702191

135. M. M. Puszynski, N. Mehta, G. Cheng, K. D. Oyler, D. Fischer, T. M. Klapötke, and J. Stierstorfer, M42 Primer Processing with Potassium and Copper Salt Formulations, *J. J. Inorg. Chem.* **2016**, *1(1)*, 003. https://www.academia.edu/37867371/M42_Primer_Processing_with_Potassium_and_Copper_Salt_Formulations

136. N. Szimhardt, Maximilian H. H. Wurzenberger, A. Beringer, Lena J. Daumann, J. Stierstorfer, Coordination chemistry with 1-methyl-5*H*-tetrazole: cocrystallization, laser-ignition, lead-free primary explosives - one ligand, three goals, *J. Mater. Chem. A*, **2017**, *5*, 23753–23765; https://doi.org/10.1039/C7TA07780G

137. a) J. Glück, M. Rusan, T. M. Klapötke, Jesse Sabatini, J. Stierstorfer, A Strontium- and Chlorine-Free Pyrotechnic Illuminant of High ColorPurity, *Angew. Chem. Int. Ed*. **2017**, *56*, 16507–16509, https://doi.org/10.1002/anie.201710746; b) J. Glück, M. Rusan, T. M. Klapötke, Jesse Sabatini, J. Stierstorfer, Ein Strontium- und Chlor-freies rotes pyrotechnisches Leuchtsignal mit hoher spektraler Reinheit, *Angew. Chem.* **2017**, *129*, 16733–16736. https://doi.org/10.1002/ange.201710746

138. N. Szimhardt, J. Stierstorfer, Methylsemicarbazide as Ligand in Late 3d Transition Metal Complexes, *Chem. Europ. J.* **2018**, *24*, 2687–2698. https://doi.org/10.1002/chem.201705030.

139. M. Wurzenberger, N. Szimhardt, J. Stierstorfer, Copper(II) Chlorate Complexes – the Renaissance of a Forgotten and Misjudged Energetic Anion, *J. Am. Chem. Soc.* **2018**, *140*, 3206–3209. https://doi.org/10.1021/jacs.7b13230

140. N. Szimhardt, M. H. H. Wurzenberger, T. M. Klapötke, J. T. Lechner, H. Reichherzer, C. C. Unger, J. Stierstorfer, Highly functional energetic complexes: stability tuning through coordination diversity of isomeric propyl-linked ditetrazoles, *Mater. Chem. A*, **2018**, *6*, 6565–6577. https://doi.org/10.1039/C8TA01412D

141. I. Gospodinov, T. Hermann, T. M. Klapötke, J. Stierstorfer, Energetic Compounds Based on 3,4-Bis(4-nitramino-1,2,5-oxadiazol-3-yl)-1,2,5-furoxan (BNAFF), *Propellants, Explosives, Pyrotech.*, **2018**, *43*, 355–363. https://doi.org/10.1002/prep.201700289

142. I. Gospodinov, T. M. Klapötke, J. Stierstorfer, Energetic Functionalization of the Pyridazine Scaffold: Synthesis and Characterization of 3,5-Diamino-4,6-dinitropyridazine-1-Oxide, *Europ. J. Org. Chem.* **2018**, 1004–1010. https://doi.org/10.1002/ejoc.201800068

143. T. S. Hermann, B. Krumm, T. M. Klapötke, J. Stierstorfer, Synthesis, Characterization, and Properties of Di- and Trinitromethyl-1,2,4-Oxadiazoles and Salts, *Asian J. Org. Chem.* **2018**, *7*, 739–750. https://doi.org/10.1002/ajoc.201700698

144. T. S. Hermann, B. Krumm, T. M. Klapötke, J. Stierstorfer, Synthesis, Characterization and Properties of Ureido-Furazan Derivatives, *J. Heterocyclic Chem.* **2018,** *55*, 852–862. https://doi.org/10.1002/jhet.3109

145. M. Wurzenberger, N. Szimhardt, J. Stierstorfer, Nitrogen-Rich Copper(II) Bromate Complexes: an Exotic Class of Primary Explosives, *Inorg. Chem.* **2018**, **57, 7940–7949.** https://doi.org/10.1021/acs.inorgchem.8b01045

146. M. F. Bölter, Thomas M. Klapötke, Tessa Kustermann, Tobias Lenz, Jörg Stierstorfer, Improving the Energetic Properties of Dinitropyrazoles by Utilization of Current Concepts, *Europ. J. Inorg. Chem.* **2018**, 4125–4132. https://doi.org/10.1002/ejic.201800781

147. M. F. Bölter, Alexander Harter, Thomas M. Klapötke, Jörg Stierstorfer, Isomers of Dinitropyrazoles: Synthesis, Comparison and Tuning of Their Physico-Chemical Properties, *ChemPlusChem*, **2018**, *83*, 804–811. https://doi.org/10.1002/cplu.201800318

148. K. V. Domasevitch, I. Gospodinov, H. Krautscheid, T. M. Klapötke, J. Stierstorfer Facile and selective polynitrations at the 4-pyrazolyl dual backbone: straightforward access to a series of high-density energetic materials, *New J. Chem.* **2019**, *43*, 1305–1312. https://doi.org/10.1039/c8nj05266b

149. N. Szimhardt, M. H. H. Wurzenberger, L. Zeisel, M.S. Gruhne, M. Lommel, Maximization of the Energy Capability Level in Transition Metal Complexes through Application of 1-Amino- and 2-Amino-5H-tetrazole Ligands *J. Mater. Chem. A*, **2018**, *6*, 16257–16272. https://doi.org/10.1039/C8TA06326E

150. J. Glück, I. Gospodinov, T. M. Klapötke, J. Stierstorfer, Metal Salts of 3,3_-Diamino-4,4_-dinitramino-5,5_-bi-1,2,4-triazole in Pyrotechnic Compositions, *Z. Anorg. Allg. Chem.* **2019,** *645*, 370–376. https://doi.org/10.1002/zaac.201800179

151. N. Szimhardt, M. S. Gruhne, M. Lommel, A. Hess, Maximilian H. H. Wurzenberger, T. M. Klapötke, J. Stierstorfer, 2,2-Bis(5-tetrazolyl)propane as Ligand in Energetic 3d Transition Metal Complexes, *Z. Anorg. Allg. Chem.* **2019**, *645*, 354–361. https://doi.org/10.1002/zaac.201800288

152. L. Zeisel N. Szimhardt, Maximilian H. H. Wurzenberger, T. M. Klapötke, J. Stierstorfer, 2-Methyl-substituted monotetrazoles in copper(II) perchlorate complexes: manipulating coordination chemistry and derived energetic properties, *New. J. Chem.* **2019**, *43*, 609–616. https://doi.org/10.1039/c8nj05375h

153. N. Szimhardt, M. H. H. Wurzenberger, P. Spieß, T. M. Klapötke, J. Stierstorfer, Potassium *N*-Nitramino-5*H*-tetrazolates - Powerful Green Primary Explosives with High Initiation Capabilities, *Propellants Explos. Pyrotech.* **2018**, *43*, 1203–1209. https://doi.org/10.1002/prep.201800221

154. Maximilian H. H. Wurzenberger, Michael S. Gruhne, Marcus Lommel, Norbert Szimhardt, Thomas M. Klapötke, Jörg Stierstorfer, Comparison of 1-Ethyl-5H-tetrazole and 1-Azidoethyl-5H-tetrazole as Ligands in Energetic Transition Metal Complexes, *Chem. Asian J.* **2019**, *14*, 2018–2028. https://doi.org/10.1002/asia.201900269.

155. N. Szimhardt, Maximilian H. H. Wurzenberger, L. Zeisel, M. S. Gruhne, M. Lommel, T. M. Klapötke, J. Stierstorfer, 1-AminoTriazole Transition-Metal Complexes as Laser-Ignitable and Lead-Free Primary Explosives, *Chem. Eur.J.* **2019**, *25*, 1963–1974. https://doi.org/10.1002/chem.201803372

156. M. H. H. Wurzenberger, B. R. G. Bissinger, M. Lommel, M. S. Gruhne, , N. Szimhardt, J. Stierstorfer, Synthesis and Comparison of Copper(II) Complexes with various N-Aminotetrazole Ligands Involving Trinitrophenol Anions, *New J. Chem.* **2019**, *43*, 18193–18202. https://doi.org/10.1039/C9NJ03937F.

157. M. S. Gruhne, M. Lommel, M. H. H. Wurzenberger, N. Szimhardt, T. M. Klapötke, J. Stierstorfer, OZM Ball Drop Impact Tester (BIT-132) vs. BAM Standard Method-a Comparative Investigation, *Propellants Explos. Pyrotech.* **2020**, *45*, 147–153. https://doi.org/10.1002/prep.201900286.

158. A. M. W. Dufter, T. M. Klapötke, M. Rusan, J. Stierstorfer, The Lithium Salts of Bis(azolyl)borates as Strontium- and Chlorine-free Red Pyrotechnic Colorants, *Z. Anorg. Allg. Chem.* **2019,** https://doi.org/10.1002/zaac.201900132

159. I. Gospodinov, T. M. Klapötke, J. Singer, J. Stierstorfer, The Pyridazine Scaffold as a Building Block for Energetic Materials: Synthesis, Characterization, and Properties, *Z. Anorg. Allg. Chem.* **2019**, *645*, 1247–1254. https://doi.org/10.1002/zaac.201900146

160. I. Gospodinov, K. V. Domasevitch, C.C. Unger, T. M. Klapötke, J. Stierstorfer, Midway between Energetic Molecular Crystals and High-Density Energetic Salts: Crystal Engineering with Hydrogen Bonded Chains of Polynitro Bipyrazoles, *Cryst. Growth Des.*, **2020**, *20*, 755–764. https://doi.org/10.1021/acs.cgd.9b01177

161. M. H. H. Wurzenberger, J. T. Lechner, M. Lommel, T. M. Klapötke, J. Stierstorfer, Salts of Picramic Acid – Nearly forgotten temperature-resistant energetic materials, *Propellants Explos. Pyrotech.* **2020**, *45*, 898–907. https://doi.org/10.1002/prep.201900402

162. M. H. H. Wurzenberger, S. M. J. Endraß, M. Lommel, T. M. Klapötke, J. Stierstorfer, Comparison of 1-Propyl-5*H*-tetrazole and 1-Azidopropyl-5*H*-tetrazole as Ligands for Laser Ignitable Complexes, *ACS Appl. Energy Mater.* **2020**, 3, 4, 3798–3806. https://doi.org/10.1021/acsaem.0c00229

163. M. H. H. Wurzenberger, J. T. Lechner, J. Stierstorfer, Copper(II) Dicyanamide Complexes with *N*-Substituted Tetrazole Ligands – Energetic Polymers with Moderate Sensitivities, *ChemPlusChem* **2020**, *85*, 769– 775. http://doi.org/10.1002/cplu.202000156.

164. T. M. Klapötke, R. Scharf, J. Stierstorfer, C. Unger, Toxicity Assessment of Energetic Materials by Using the Luminescent Bacteria Inhibition Test, *Propellants Explos. Pyrotech*. **2021**, *46*, 114–123. https://doi.org/10.1002/prep.202000044.

165. M. Benz, Thomas M. Klapötke, J. Stierstorfer, Combining Performance with Thermal Stability: Synthesis and Characterization of 5-(3,5-Dinitro-1*H*-pyrazol-4-yl)-1*H*-tetrazoleand its Energetic Derivatives *Z. Anorg. Allg. Chem.* **2020**, *646*, 1380–1388. DOI: 10.1002/zaac.202000123.

166. a) M. H. H. Wurzenberger, M. Lommel, M. S. Gruhne, N. Szimhardt, J. Stierstorfer, Refinement of Copper(II) Azide with 1-Alkyl-5H-tetrazoles: Adaptable Energetic Complexes, *Angew. Chem. Int. Ed.* **2020**, *59*, 12367–12370 https://doi.org/10.1002/anie.202002823. b) M. H. H. Wurzenberger, M. Lommel, M. S. Gruhne, N. Szimhardt, J. Stierstorfer, Veredelung von Kupfer(II)-azid mittels 1-Alkyl-5*H*-tetrazolen: Leistungsfähige energetische Komplexverbindungen, *Angew. Chem.* **2020**, *132*, 12466–12469. https://doi.org/10.1002/ange.202002823.

167. T. M. Klapötke, B. Krumm, C. Riedelsheimer, J. Stierstorfer, C. C. Unger, M. H. H. Wurzenberger, Urazine – a Long Established Heterocycle and Energetic Chameleon, *Eur. J. Org. Chem.* **2020**, 4916–4924. https://doi.org/10.1002/ejoc.202000886

168. M. H. H. Wurzenberger, V. Braun, M. Lommel, T. M. Klapötke, J. Stierstorfer, Closing the Gap: Synthesis of Three Isomeric N,N-Ditetrazolymethane Ligands and Their Coordination Proficiency in Adaptable Laser Responsive Copper(II) and Sensitive Silver(I) Complexes, *Inorg. Chem.* **2020**, *59*, 10938−10952. https://dx.doi.org/10.1021/acs.inorgchem.0c01403.

169. A. M. W. Dufter, T. M. Klapötke, M. Rusan, A. Schweiger, J. Stierstorfer, Comparison of Functionalized Lithium Dihydrobis(azolyl)borates with Their Corresponding Azolates as Environmentally Friendly Red Pyrotechnic Coloring Agents, *ChemPlusChem* **2020**, *85*, 2044–2050. https://doi.org/10.1002/cplu.202000427

170. M. H. H. Wurzenberger, M. Gruhne, M. Lommel, V. Braun, N. Szimhardt, J. Stierstorfer, Taming the Dragon: Complexation of Silver Fulminate with Nitrogen-Rich Azole Ligands, *Inorg. Chem.* **2020**, *59*, 17875–17879. https://doi.org/10.1021/acs.inorgchem.0c03027

171. M. Reichel, M. H. H. Wurzenberger, M. Lommel, M. Kofen, B. Krumm, J. Stierstorfer, K. Karaghiosoff, *N*-Fluoromethylated (Amino)Tetrazoles: Manipulating Thermal and Energetic Properties, *Z. Anorg. Allg. Chem.* **2021**, *Z. Anorg. Allg. Chem.* 2021, 647, 341–349. https://doi.org/10.1002/zaac.202000341

172. M. H. H. Wurzenberger, M. S. Gruhne, M. Lommel, J. Stierstorfer, 1-Amino-5-methyltetrazole in Energetic 3 d Transition Metal Complexes – Ligand Design for Future Primary Explosives, *Propellants Explos. Pyrotech.* **2021**, *46*, 207–213. https://doi.org/10.1002/prep.202000179

173. M. S. Gruhne, M. Lommel, M. H. H. Wurzenberger, T. M. Klapötke, J.Stierstorfer, Investigation of Ethylenedinitramine as a Versatile Building Block in Energetic Salts, Cocrystals, and Coordination Compounds, *Inorg. Chem.* **2021**, *60*, 4816−4828. https://doi.org/10.1021/acs.inorgchem.0c03752

174. A. Harter, T. M. Klapötke, C. Riedelsheimer, J. Stierstorfer, M. Voggenreiter, Synthesis and Characterization of Geminal Diazido Derivatives based on Diethyl Malonate, *Europ. J. Inorg. Chem.* **2021**, 2241–2247. https://doi.org/10.1002/ejic.202100212

175. T. Lenz, T. M. Klapötke, M. Mühlemann, J. Stierstorfer, About the Azido Derivatives of Pentaerythritol Tetranitrate, *Propellants Explos. Pyrotech*. **2021**, *46*, 723–731. https://doi.org/10.1002/prep.202000265

176. M. Born, T. C. Fessard, L. Göttemann, T. M. Klapötke, J. Stierstorfer, M. Voggenreiter, 3,3-Dinitratooxetane – an important leap towards energetic oxygen-rich monomers and polymers, *Chem. Commun.* **2021**, *57*, 2804–2807. https://doi.org/10.1039/D1CC00466B

177. L. Bauer, M. Benz, T. M. Klapötke, T. Lenz, J. Stierstorfer, Polyazido-methyl Derivatives of Prominent Oxadiazole and Isoxazole Scaffolds: Synthesis, Explosive Properties, and Evaluation, *J. Org. Chem.* **2021**, *86*, 9, 6371–6380 https://doi.org/10.1021/acs.joc.1c00216

178. M. Benz, T. M. Klapötke, B. Krumm, M. Lommel, J. Stierstorfer, Nitrocarbamoyl Azide $O_2NN(H)C(O)N_3$: A Stable but Highly Energetic Member of the Carbonyl Azide Family, *J. Am. Chem. Soc.* **2021**, *143*, 1323–1327. https://doi.org/10.1021/jacs.0c12507

179. T. M. Klapötke, A. G. Harter, J. Stierstorfer, M. Voggenreiter; X. Zeng, Synthesis, Characterization and Energetic Performance of Oxalyl Diazide, Carbamoyl Azide, and N,N'-Bis(azidocarbonyl)hydrazine, *ChemPlusChem*, **2021**, *86*, 870–874. https://doi.org/10.1002/cplu.202100214

180. M. S. Gruhne, M. H. H. Wurzenberger, M. Lommel, J. Stierstorfer, A Smart Access to the Dinitramide Anion – The Use of Dinitraminic Acid for the Preparation of Energetic Coordination Compounds, *Chem. Europ. J.* **2021**, 27, 9112–9123. https://doi.org/10.1002/chem.202100747

181. M. Wurzenberger, V. Braun, V. Weippert, J. Stierstorfer, Tailoring the properties of 3d transition metal complexes with different N-cycloalkyl-substituted tetrazoles, *New J. Chem.* **2021**, *45*, 11042–11050. https://doi.org/10.1039/D1NJ01675J

182. M. Gruhne, T. Lenz, M. Rösch, M. Lommel, M. H. H. Wurzenberger, T. M. Klapötke, J. Stierstorfer, Nitratoethyl-5H-tetrazoles: Improving Oxygen Balance through Application of Organic Nitrates in Energetic Coordination Compounds, *Dalton Trans*. **2021**, *50*, 10811–10825, https://doi.org/10.1039/D1DT01898A.

183. D. Shem-Tov, N. Petrutik , M. H. H. Wurzenberger, M. Meincke, E. Flaxer, B. Tumanskii, L. Zhang, R. Dobrovetsky, S. Fleischer, T. M. Klapötke, J. Stierstorfer, Low Power Laser Ignition of Antenna-type Secondary Energetic Copper Complex: Synthesis, Characterization, Evaluation and Ignition Mechanism studies, *Inorg Chem.* **2021**, *60*, 10909–10922. https://doi.org/10.1021/acs.inorgchem.1c00358

184. M. Benz, M. S. Gruhne, T. M. Klapötke, N. Krüger, T. Lenz M. Lommel, J. Stierstorfer, Evolving the Scope of 5,5'-Azobistetrazoles in the Search for High Performing Green Energetic Materials, *Eur. J. Org. Chem.* **2021**, 4388–4392. https://doi.org/10.1002/ejoc.202100747

185. M. Gruhne, M. Benz, T. Lorenzen, T. Lenz, T. M. Klapötke, J. Stierstorfer, Hybridization of Dinitramide and Dicyanamide: Evaluation of Nitrocyanamide in Energetic Salts and Coordination Compounds, *Cryst. Growth Des.*, **2022**, *22*, 200–212. https://doi.org/10.1021/acs.cgd.1c00858

186. T. M. Klapötke, M. Kofen, L. Schmidt, J. Stierstorfer, Maximilian H. H. Wurzenberger, Selective Synthesis and Characterization of the Highly Energetic Materials 1-Hydroxy-5H-tetrazole (CHN_4O), its Anion 1-Oxido-5H-tetrazolate (CN_4O^-) and Bis(1-hydroxytetrazol-5-yl)triazene, *Chemistry – Asian J.* **2021**, *16*, 3001–3012. https://doi.org/10.1002/asia.202100714.

187. M. H. H. Wurzenberger, M. Gruhne, N. Szimhardt, M. Lommel, J. Stierstorfer, Advancement and Stabilization of Copper(II) Azide by the Use of Triazole- and Tetrazole Ligands – Enhanced Primary Explosives, *Mater. Adv*. **2022**, *3*, 579–591. https://doi.org/10.1039/D1MA00588J

188. T. M. Klapötke, M. Kofen, J. Stierstorfer, N-Functionalisation of 5,5'-bistetrazole providing 2,2'-di(azidomethyl)bistetrazole: A melt-castable metal-free green primary explosive, *Dalton Trans.* **2021**, *50*, 13656–13660. https://doi.org/10.1039/D1DT02731J

189. J. Das, D. Shem-Tov, S. Wang, L. Zhang, E. Flaxer, S. Zhang, J. Stierstorfer, K. Wang, Q.-L. Yan, R. Dobrovetsky, M. Gozin, Hydride- and Boron-free Solid Hypergolic H_2O_2-Ignitophores. *Chem. Eng. J.* **2022**, in press. https://doi.org/10.1016/j.cej.2022.136246

190. J. T. Lechner, T. M. Klapötke, J. Stierstorfer, Synthesis, Characterization and Derivatives of Iso-Picramic Acid, *Propellants. Explos. Pyrotech.* **2022**, *47*, e2021002. https://doi.org/10.1002/prep.202100205

191. L. Bauer, M. Benz, T. M. Klapötke, C. Pignot, J. Stierstorfer, Combining the Most Suitable Energetic Tetrazole and Triazole Moieties: Synthesis and Characterization of 5-(1-Hydroxy-3-Nitro-1,2,4-Triazol-5-yl)-1-Hydroxy-Tetrazole and its Nitrogen-Rich Ionic Derivatives, *Materials Advances*, **2022,** 3, 3945-3951. https://doi.org/10.1039/D2MA00135G

192. A. M. W. Dufter-Münster, A. G. Harter, T. M. Klapötke, E. Reinhardt, J. Römer, J. Stierstorfer, Lithium Nitropyrazolates as Potential Red Pyrotechnic Colorants, *Eur. J. Inorg. Chem.* **2022**, e202101048-e202101048. https://doi.org/10.1002/ejic.202101048

193. T. M. Klapötke, M. Kofen, L. Schmidt, J. Stierstorfer, Maximilian H. H. Wurzenberger, 1-(Azidomethyl)-5H-tetrazole – a Powerful New Ligand for Highly Energetic Coordination Compounds, *Chemistry Eur. J.* **2022**, *28*, e2022004. https://doi.org/10.1002/chem.202200492

194. J. Das, D. Shem Tov, S. Zhang, C.-Z. Gao, L. Zhang, C. Yao, E. Flaxer, Eli, J. Stierstorfer, M. Wurzenberger, I. Rahinov, M. Gozin, Power of Sulfur – Chemistry, Properties and Laser Ignition Studies of Energetic Perchlorate-Free 1,3,4-Thiadiazole Nitramines, **2022**, *443*, 136246. https://doi.org/10.1016/j.cej.2022.136246

195. J. T. Lechner, A. Harter, T. M. Klapötke, J. Stierstorfer, Kinetic predictions concerning the long-term stability of TKX-50 and other common explosives using the NETZSCH Kinetics Neo software, *Propellants Explos. Pyrotech.* **2022**, e202200031. https://doi.org/10.1002/prep.202200031

196. M. Benz, T. M. Klapötke, J. Stierstorfer, Krapcho Decarboxylation of Ethyl-Carbazate: New Synthetic Approach toward 1,1'-Diamino-5,5'-Bistetrazole and its Utilization as High Performing Metal-free Primary Explosive, *Organic Letters***, 2022**, *24*, 1747–1751. https://doi.org/10.1021/acs.orglett.2c00430

197. A. Harter, T. M. Klapötke, C. Riedelsheimer, J. Stierstorfer, 2-Hydrazonyl-propandihydrazide - a versatile precursor for high-energy materials, *Eur. J. Inorg. Chem.* **2022**, e202200100. https://doi.org/10.1002/ejic.202200100

198. J. T. Lechner, T. M. Klapötke, B. Krumm, J. Stierstorfer, Investigation of deuterated FOX-7 – changes in structural behavior and energetic characteristics after deuteration under ambient conditions, *Dalton Trans*, **2022**, *51*, 5788–5791. https://doi.org/10.1039/D2DT00490A

199. M. Benz, T. Lenz, T. M. Klapötke, J. Stierstorfer, Tuning the Properties of 5-Azido and 5-Nitramino-tetrazoles by Diverse Functionalization - General Concepts for Future Energetic Materials, *Chem. Europ. J.* **2022**, *28*, e202200772. https://doi.org/10.1002/chem.202200772

200. M. Benz, T. M. Klapötke, J. Stierstorfer, M. Voggenreiter, Synthesis and Characterization of Binary, Highly Endothermic and Extremely Sensitive 2,2'-Azobis-5-Azidotetrazole (C_2N_{16}), *J. Am. Chem. Soc.* **2022**, *144*, 6143–6147. https://pubs.acs.org/doi/10.1021/jacs.2c00995

201. T. C. Fessard, I. Gospodinov, T. M. Klapötke, J. Stierstorfer, M. Voggenreiter, Energetic but insensitive spiro-tetrahydrotetrazines based on oxetane-3-one, *J. Heterocyclic Chem.*, **2022**, *59*, 1781–1789. https://doi.org/10.1002/jhet.4518

202. M. Kofen, A. G. Harter, T. M. Klapötke, J. Stierstorfer, 1,5-Dimethyltetrazole as a ligand in energetic 3d5 to 3d10-metal coordination compounds, *Energetic Materials Frontiers*, **2022**, *3*, 111–121. https://doi.org/10.1016/j.enmf.2022.07.004

203. M. Benz, T. M. Klapötke, J. Stierstorfer,1-Nitramino-5-aminotetrazole – A simple accessible highly energetic building block, *Energetic Materials Frontiers*, **2022**, *3*, 161–165. https://doi.org/10.1016/j.enmf.2022.08.003

204. J. T. Lechner, A. Neuer, V. Bockmair, J. Stierstorfer, T. M. Klapötke, Crystal Structures of the Commonly Used Plasticizers Ethylene Glycol Dinitrate, Diethylene Glycol Dinitrate, and Triethylene Glycol Dinitrate - Characterization and Discussion of Their Structural Behavior, *Cryst. Growth Des.* **2022**, *22*, 6215–6223. https://doi.org/10.1021/acs.cgd.2c00775

205. J. Bauer, M. Benz, T. M. Klapötke, J. Stierstorfer, Chemistry of 2,5-diaminotetrazole, *Dalton Trans.* **2022**, *51*, 11806–11813. https://doi.org/10.1039/D2DT01480G

206. M. Benz, T. M. Klapötke, J. Stierstorfer, M. Voggenreiter, 1-Amino-5-nitriminotetrazole: Effective Interaction of N-Nitro and N-Amino Functionalities for Outperforming and Applicable Energetic Materials, *ACS Appl. Eng. Mater.* **2023**, *1*, 3–6. https://doi.org/10.1021/acsaenm.2c00031

207. M. Kofen, V. Braun, S. M. J. Endraß, T. M. Klapötke, J. Stierstorfer, 1-(Nitratomethyl)-5H-tetrazole: A Highly Sensitive Ligand with Improved Oxygen Balance for Laser-Ignitable Coordination Compounds, *Inorg. Chem.* **2022,** *61*, 17212–17225. https://doi.org/10.1021/acs.inorgchem.2c02805

208 M. Kofen, T. M. Klapötke, J. Stierstorfer, Energetic Coordination Compounds of late 3d metals with 1N-(Nitromethyl)-5H-tetrazole, a ligand with astonishing properties from the rare class of N-nitromethyl azoles, *Chemical Engineering Journal*, **2022**, *452*, 139375. https://doi.org/10.1016/j.cej.2022.139375

209. S. M. J. Endraß, A. Neuer, T. M. Klapötke, J. Stierstorfer, Trinitro-orcinolate and Trinitro-resorcinate – Sensitivity Trends in Nitroaromatic Energetic Materials, *ChemistrySelect*, **2022**, *7*, e202203140. https://doi.org/10.1002/slct.202203140

210. T. M. Klapötke, G. Lemarchand, T. Lenz, M. Mühlemann, G. Lemarchand, R. Weber, ,J. Stierstorfer, Impact and Friction Sensitivities of PETN: I. Sensitivities of the Pure and Wetted Material, *Propellants Explos. Pyrotech.* **2022**, *47*, e202200150. https://doi.org/10.1002/prep.202200150

211. M. Rösch, M. Gruhne, M. Lommel, S.M. J. Endraß, J. Stierstorfer, The Adjustability of Physicochemical Properties: Comparison of 1-Vinyl-5H-tetrazole and 1-Allyl-5H-tetrazole as Ligands in 3d Metal Energetic Coordination Compounds (ECC), *Inorg. Chem.* **2023**, *62*, *1488–1507*. https://doi.org/10.1021/acs.inorgchem.2c03624

212. V.Fuchs, T. M. Klapötke, J. Stierstorfer, M. Voggenreiter, Nitrogen-Rich Oxetanes Based on the Combination of Azides and Tetrazoles, *Europ. J. Org. Chem.* **2023**, *e20220173*. https://doi.org/10.1002/ejoc.202201073

213. T. Lenz, M. Mühlemann, G. Lemarchand, F. Venetz, R. Weber, J. Wutke,T. M. Klapötke, J. Stierstorfer, Impact and Friction Sensitivities of PETN: II. Sensitivities of the Acidic Material During Manufacturing, *Propellants, Explos. Pyrotech.* **2023,** *in press*. https://doi.org/10.1002/prep.202200288

List of Lecture Activities

Lehrveranstaltungen Dr. Jörg Stierstorfer (laut LSF Vorlesungsverzeichnis Fakultät 18)

Wintersemester 2022/23

T1IA-M Anorganisch-chemisches Fortgeschrittenenpraktikum mit Oberseminar im Schwerpunktfach (16+2 SWS Blockpraktikum mit Vortrag in Gruppen, Haus D)

T1IZ-14 Daily chemistry (Vorlesung 2.0 SWS)

T1IC-P-ST Literaturseminar (Seminar 2.0 SWS)

Sommersemester 2022

T1BBB Anorganisch-chemisches Praktikum 1 (Praktikum, 7-stündig, 2x6 Wochenblöcke, Di.-Fr., 13-17 Uhr, Saal E-L)

T1IA-M Anorganisch-chemisches Fortgeschrittenenpraktikum mit Oberseminar im Schwerpunktfach (16+2 SWS Blockpraktikum mit Vortrag in Gruppen, Haus D)

T1IC-P-ST Literaturseminar (Seminar 2.0 SWS)

Wintersemester 2021/22

T1IA-M Anorganisch-chemisches Fortgeschrittenenpraktikum mit Oberseminar im Schwerpunktfach (16+2 SWS Blockpraktikum mit Vortrag in Gruppen, Haus D)

T1IZ-1-I Aktuelle Chemie der Nichtmetalle, Moderne Stickstoffchemie (Vorlesung 2.0 SWS)

T1IZ-14 Daily Chemistry (Vorlesung 1.0 SWS)

T1IC-P-ST Literaturseminar (Seminar 2.0 SWS)

Sommersemester 2021

T1BBB Anorganisch-chemisches Praktikum 1 (Praktikum, 7-stündig, 2x6 Wochenblöcke, Di.-Fr., 13-17 Uhr, Saal E-L)

T1IA-M Anorganisch-chemisches Fortgeschrittenenpraktikum mit Oberseminar im Schwerpunktfach (16+2 SWS Blockpraktikum mit Vortrag in Gruppen, Haus D)

T1IC-P-ST Literaturseminar (Seminar 2.0 SWS)

Wintersemester 2017-2020

T1IA-M Anorganisch-chemisches Fortgeschrittenenpraktikum mit Oberseminar im Schwerpunktfach (16+2 SWS Blockpraktikum mit Vortrag in Gruppen, Haus D)

T1IZ-1-I Aktuelle Chemie der Nichtmetalle, Moderne Stickstoffchemie (Vorlesung 2.0 SWS)

T1IC-P-ST Literaturseminar (Seminar 2.0 SWS)

Sommersemester 2017-2020

T1BBB Anorganisch-chemisches Praktikum 1 (Praktikum, 7-stündig, 2x6 Wochenblöcke, Di.-Fr., 13-17 Uhr, Saal E-L)

T1IA-M Anorganisch-chemisches Fortgeschrittenenpraktikum mit Oberseminar im Schwerpunktfach (16+2 SWS Blockpraktikum mit Vortrag in Gruppen, Haus D)

T1IC-P-ST Literaturseminar (Seminar 2.0 SWS)

Sowie diverse Vertretungen für Professoren Klapötke und Karaghiosoff in den Vorlesungen: Anorganische Molekülchemie I&II, HEDM, Fluorchemie, NMR Spektroskopie, Nichtmetallkationen, AC1 Grundvorlesung.